Development and Biological Evaluation of Selective Ligands and Pharmacological Tools Targeting Caspase-2, Histamine H$_2$ Receptors, and orphan GPR3 for the Treatment of Neurodegenerative Diseases

DISSERTATION

zur Erlangung des Doktorgrades der Naturwissenschaften (Dr. rer. nat.)

der Fakultät für Chemie und Pharmazie

der Universität Regensburg

vorgelegt von

Merlin Niklas Bresinsky

aus Regensburg

2023

Die vorliegende Arbeit entstand in der Zeit von September 2018 bis Februar 2023 unter der Leitung von Herrn PD Dr. Steffen Pockes am Institut für Pharmazie der Fakultät für Chemie und Pharmazie der Universität Regensburg.

Promotionsgesuch wurde eingereicht im März 2023.

Vorsitzender des Prüfungsausschusses: Prof. Dr. Achim Göpferich

Erstgutachter: PD Dr. Steffen Pockes

Zweitgutachter: Prof. Dr. Sigurd Elz

Drittprüfer: Prof. Dr. Jörg Heilmann

Per aspera ad astra

Für meine Eltern

Acknowledgment

An dieser Stelle möchte ich mich herzlich bei allen bedanken die zum Entstehen dieser Arbeit beigetragen und mich auf diesem Weg begleitet haben. Insbesondere möchte ich meinen Dank folgenden Personen aussprechen:

Meinem Doktorvater Herrn PD Dr. Steffen Pockes für die Vergabe des interessanten und herausfordernden Promotionsthemas, für seine wissenschaftliche Expertise, für seine intensive und ausgezeichnete Betreuung, für die Durchsicht der Arbeit, für das mir entgegengebrachte Vertrauen, sowie der Unterstützung in allen erdenklichen Bereichen. Des Weiteren möchte ich mich für die Erstellung des Erstgutachtens bedanken;

Herrn Prof. Dr. Sigurd Elz für die Aufnahme an seinem Lehrstuhl und für die Erstellung des Zweitgutachtens;

Herrn Prof. Dr. Jörg Heilmann für die Bereitschaft das Amt des Drittprüfers zu übernehmen sowie der Möglichkeit, die Zelllabore an seinem Lehrstuhl nutzen zu dürfen;

Herrn Prof. Dr. Achim Göpferich für die Übernahme des Vorsitzes der Promotionsprüfung;

Herrn Prof. Dr. Pierre Koch und Herrn PD Dr. Max Keller für die Erlaubnis, die Gerätschaften am Lehrstuhl für Pharmazeutische und Medizinische Chemie II nutzen zu dürfen.

My great gratitude goes to Michael Walters and Karen Ashe for including me into the caspase-2 project, for their scientific expertise, and for their warm welcome at the University of Minnesota during my research stay; to Kristen John for teaching me how to perform the caspase assay. I would also like to sincerely thank Mu Yang and Jessica Fuller for the friendly integration in Minneapolis, for all the help with organizational

things, and for the interesting conversations we had in the laboratory. I would like to thank Gunda Georg for inviting me to her wonderful parties.

Allen Studierenden die im Laufe der Jahre im Zuge von studentischen Laborpaktika am Entstehen der Arbeit mitgewirkt haben. Insbesondere hervorheben möchte ich: Bernadette Vallaster. Vielen Dank Bernadette für deine großartige Arbeit im Labor und der kulinarischen Versorgung unseres Lehrstuhls;

Vivien Czipper für ihre exzellente technische Hilfe im Labor. Vielen Dank Vivien, dass du uns eine so große Stütze im täglichen Laborbetrieb bist.

Uta Hasselmann für ihre schnelle Unterstützung bei jeglicher Art von organisatorischen Aufgaben;

Frau Christine Braun und Frau Kerstin Röhrl für die Durchführung der organpharmakologischen Testungen;

Allen Kooperationspartnern die im Verlauf der Jahre zum Entstehen der verschiedenen Publikationen und der Dissertation beigetragen haben. Besonders hervorzuheben sind: Dr. Katharina Tropmann, Dr. Sabrina Biselli, Dr. Lisa Forster, Dr. Andrea Straßer, Dr. Lukas Grätz, Dr. Katarzyna Szczepańska, Prof. Dr. Joachim Neumann, Dr. Ulrich Gergs, Dr. Gurpreet Singh, Dr. Hannes Schihada, Jessica Fuller, Jessica Strasser, Prof. Dr. Kathryn Nelson, Dr. William McCue, Prof. Dr. Barry Finzel und Prof. Dr. Peng Liu;

Meinem Chemielehrer und Oberstufenkoordinator Herrn Martin Gruber für einen exzellenten Chemieunterricht. Vielen Dank, dass Sie mich für die Aufnahme eines naturwissenschaftlichen Studiums begeistern konnten.

Bei Sandra Werther möchte ich mich für das Korrekturlesen der Arbeit bedanken;

Alexander Hubmann, Jonas Daschner und Constantin Lier möchte ich für unser wöchentliches Weißwurstfrühstück danken, für die gute Stimmung bei der Arbeit, für den exzellenten Musikgeschmack (Apache 207 und Tream) und für die gemeinsamen

Fußballabende. Danke, dass man mit und über euch so gut lachen kann. Alex, dir möchte ich nochmal besonders danken, dass du es mit mir im Labor ausgehalten hast; Mein Dank gilt auch allen weiteren Mitgliedern unseres Lehrstuhls Julia Blüml, Dr. Herwig Pongratz, Dr. Martin Nagl, Dr. Niklas Rosier, Sebastian Pitzl, Simon Scheuerer, Lukas Wirth, Denise Mönnich, Marlisa Ködel, Dr. Lisa Forster und Dr. Franziska Naporra für die gute Zusammenarbeit, für ihre Unterstützung und für die vielen schönen gemeinsamen Erlebnisse.

Lukas Voit und Florian Weigl möchte ich für ihre langjährige Freundschaft und für die unzähligen gemeinsamen Abende danken.

Mein tief empfundener Dank gilt meinen Eltern und meinen Brüdern, die mich in allen Bereichen meines Lebens stets bestärkt und unterstützt haben.

Zuletzt und vor allem möchte ich meiner Freundin Melanie danken. Vielen Dank für deine bedingungslose Unterstützung, die Aufmunterung und Ablenkung bei Misserfolgen, deine wissenschaftlichen Ratschläge, deine Geduld, dein Verständnis, die gemeinsamen Reisen als Ausgleich und dafür, dass du einfach immer für mich da bist.

Publications and Poster Presentations

Publications

Grätz, L.; Tropmann, K.; **Bresinsky, M.**; Müller, C.; Bernhardt, G.; Pockes, S. NanoBRET Binding Assay for Histamine H_2 Receptor Ligands Using Live Recombinant HEK293T Cells. *Scientific Reports* **2020**, *10* (1), 13288.

Szczepańska, K.; Pockes, S.; Podlewska, S.; Höring, C.; Mika, K.; Latacz, G.; Bednarski, M.; Siwek, A.; Karcz, T.; Nagl, M.; **Bresinsky, M.**; Mönnich, D.; Seibel, U.; Kuder, K. J.; Kotańska, M.; Stark, H.; Elz, S.; Kieć-Kononowicz, K. Structural Modifications in the Distal, Regulatory Region of Histamine H_3 Receptor Antagonists Leading to the Identification of a Potent Anti-Obesity Agent. *European Journal of Medicinal Chemistry* **2021**, *213*, 113041.

Biselli, S.; **Bresinsky, M.**; Tropmann, K.; Forster, L.; Honisch, C.; Buschauer, A.; Bernhardt, G.; Pockes, S. Pharmacological Characterization of a New Series of Carbamoylguanidines Reveals Potent Agonism at the H_2R and D_3R. *European Journal of Medicinal Chemistry* **2021**, *214*, 113190. (shared first authorship)

Tropmann, K.; **Bresinsky, M.**; Forster, L.; Mönnich, D.; Buschauer, A.; Wittmann, H.-J.; Hübner, H.; Gmeiner, P.; Pockes, S.; Strasser, A. Abolishing Dopamine D_{2long}/D_3 Receptor Affinity of Subtype-Selective Carbamoylguanidine-Type Histamine H_2 Receptor Agonists. *J. Med. Chem.* **2021**, *64* (12), 8684–8709.

Gergs, U.; Büxel, M. L.; **Bresinsky, M.**; Kirchhefer, U.; Fehse, C.; Höring, C.; Hofmann, B.; Marušáková, M.; Čináková, A.; Schwarz, R.; Pockes, S.; Neumann, J. Cardiac Effects of Novel Histamine H_2 Receptor Agonists. *J Pharmacol Exp Ther* **2021**, *379* (3), 223–234.

Bresinsky, M.; Strasser, J. M.; Vallaster, B.; Liu, P.; McCue, W. M.; Fuller, J.; Hubmann, A.; Singh, G.; Nelson, K. M.; Cuellar, M. E.; Wilmot, C. M.; Finzel, B. C.; Ashe, K. H.; Walters, M. A.; Pockes, S. Structure-Based Design and Biological Evaluation of Novel Caspase-2 Inhibitors Based on the Peptide AcVDVAD-CHO and the Caspase-2-Mediated Tau Cleavage Sequence YKPVD314. *ACS Pharmacol. Transl. Sci.* **2022**, *5* (1), 20–40.

Singh, G.; Liu, P.; Yao, K. R.; Strasser, J. M.; Hlynialuk, C.; Leinonen-Wright, K.; Teravskis, P. J.; Choquette, J. M.; Ikramuddin, J.; **Bresinsky, M.**; Nelson, K. M.; Liao, D.; Ashe, K. H.; Walters, M. A.; Pockes, S. Caspase-2 Inhibitor Blocks Tau Truncation and Restores Excitatory Neurotransmission in Neurons Modeling FTDP-17 Tauopathy. *ACS Chem. Neurosci.* **2022**, *13* (10), 1549–1557.

Bresinsky, M.; Strasser, J. M.; Hubmann, A.; Vallaster, B.; McCue, W. M.; Fuller, J.; Singh, G.; Nelson, K. M.; Cuellar, M. E.; Finzel, B. C.; Ashe, K. H.; Walters, M. A.; Pockes, S. Characterization of Caspase-2 Inhibitors Based on Specific Sites of Caspase-2-mediated Proteolysis. *Archiv der Pharmazie* **2022**, *355* (9), 2200095.

Bresinsky, M.; Shahraki, A.; Kolb, P.; Pockes, S.; Schihada, H. Development of fluorescent AF64394 analogs enables real-time binding studies for the orphan class A GPCR GPR3. *J. Med. Chem.* **2023**, in review.

Poster presentations

<u>Bresinsky M.</u>, Sadek B., Pockes S., Synthesis and pharmacological characterization of potent CNS-penetrating H_2R agonists as a new approach against neurodegenerative diseases, *Frontiers in Medicinal Chemistry, March 2019, Würzburg, Germany*

<u>Bresinsky M.</u>, Sadek B., Pockes S., Preparation of carbamoylated guanidines and their biological activity at the human and guinea pig histamine H_2 receptor*, DPhG-Jahrestagung (Annual meeting), September 2019, Heidelberg, Germany*

<u>Bresinsky M.</u>, Hubmann A., Strasser J., Nelson K., Ashe K.H., Walters M.A., Pockes S., Development of Selective Caspase-2 Inhibitors as a New Approach against Alzheimer's disease, *DPhG-Jahrestagung (Annual meeting), September 2021, Leipzig, Germany*

<u>Bresinsky M.</u>, Hubmann A., Strasser J., Nelson K., Ashe K.H., Walters M.A., Pockes S., Structure-Based Design and Biological Evaluation of Peptidic Caspase-2 Inhibitors based on Specific Protein Cleavage Sites and the Canonical Inhibitor AcVDVAD-CHO*, Frontiers in Medicinal Chemistry, March 2022, Freiburg, Germany*

<u>Bresinsky M.</u>, Singh G., A. Hubmann, Strasser J., Nelson K., Liao D., K.H. Ashe, Walters M.A., Pockes S., Design and Biological Evaluation of Selective Caspase-2 Inhibitors: Elucidating the Impact of Caspase-2 on Synpatic Functions, *Alzheimer's & Parkinson's Diseases Conference (ADPD), March 2022, Barcelona, Spain*

Table of Contents

Chapter 1

Alzheimer's Disease

1 Alzheimer's Disease

The German psychiatrist Alois Alzheimer first described Alzheimer's disease (AD) in 1907.[1] In 1901, he started investigating the case of 51-year-old Auguste Deter after her admission to a mental health hospital. The patient's condition was characterized by rapidly deteriorating memory and psychiatric disturbances like paranoia, aggressiveness, and disorientation.[1] After her death in 1906, the autopsy of the brain revealed significant histological deviations from the normal brain, later known as amyloid β plaques and neurofibrillary tangles.[1] Alzheimer associated these pathological variations as a cause of the until then unknown Alzheimer's disease.

Alzheimer's disease is a progressing neurodegenerative disease. It is symptomatically manifested by the loss of memory and cognitive impairments (e.g., forgetting recent events and people's names), behavioral changes (e.g., aggressiveness and paranoia), and the loss of functional abilities (e.g., increasing difficulty with communication and impaired mobility).[2,3] Even though the exact pathological cause is not yet fully clarified, it is characterized by two neuropathological hallmarks: extracellular deposition of amyloid β (Aβ) plaques and intracellular neurofibrillary tangles (NFTs).[2]

The prevalence rate of Alzheimer's disease in the population is about 3% in persons aged 65 to 74 years and 19% in persons aged 75 to 84 years. A prevalence of approximately 47% was found for the population over 84 years of age, revealing a strong correlation between the onset of the disease and the age of the affected persons.[4] Additional risk factors for the onset of the disease are smoking, alcohol abuse, overweight, high blood pressure, low educational attainment, social isolation, cognitive inactivity, and air pollution.[3] With about 60-70% of all cases, Alzheimer's disease is the leading cause of dementia affecting elderly individuals.[3,5] Other major dementia forms include vascular dementia, Lewy body dementia, dementia from physical injuries to the brain, and dementia resulting from strokes or from certain infections (e.g., HIV).[3] Worldwide, around 55 million people have dementia. Due to the rapidly aging population, the prevalence is expected to rise to 78 million cases in 2030 and 139 million cases in 2050, indicating a major impact on public health and the healthcare system.[3] The estimated total global societal cost of dementia in 2019 was

about 1.3 trillion US dollars. These costs are expected to reach 2.8 trillion US dollars by the year 2030.[3]

Only a limited number of drugs exist for the treatment of Alzheimer's disease. To date, the established treatments for the disease are only of symptomatic nature, all attempting to neutralize the neurotransmitter disturbance.[6] The approved treatments are not able to cure or prevent Alzheimer's disease and demonstrate solely minor improvements in the patient's condition.[6] The first group of drugs are the cholinesterase inhibitors with donepezil (Pfizer), rivastigmine (Novartis), and galantamine (Janssen) as approved drugs.[6,7] These drugs are authorized for the treatment of mild to moderate forms of AD and are referred to as the standard and first-line treatment.[6] The cholinesterase inhibitors are supposed to prevent the loss of acetylcholine neurons and the impairment of enzymatic function for acetylcholine synthesis and degradation. The loss of cholinergic neurons in the basal forebrain during the progression of AD has been associated with memory loss and the deterioration of several cognitive and non-cognitive functions.[6] Another pharmaceutical is memantine (Lundbeck), a N-methyl-D-aspartate receptor (NMDA) antagonist approved for the treatment of moderate to severe AD.[6,7] Memantine normalizes the increased activity of NMDA receptors reported for AD by acting as a non-competitive, fast off-rate NMDA receptor antagonist that binds to the open state of the NMDA receptor channel.[7] In addition, antidepressants (e.g., sertraline) and antipsychotics (e.g., risperidone) are used to treat depression and behavioral disorders of the patients.[6] Drugs that do not simply improve the patient's condition but stop or at least effectively modify the disease are referred to as disease-modifying drugs.[6] To halt progress, drugs must influence pathogenic processes responsible for the clinical symptoms of the disease. Namely, these are the deposition of extracellular amyloid β plaques and the formation of intracellular neurofibrillary tangles.[6] Aβ originates from the amyloid precursor protein (APP) by proteolytic processing through β-secretase in the extracellular domain and γ-secretase in the transmembrane region.[6] The amplified formation, accumulation, and aggregation of Aβ is identified as one of the factors of the clinical manifestation of Alzheimer's disease.[6,7] This was first described in 1992 by Hardy and Higgins in the so-called amyloid hypothesis.[8] Aβ is capable of forming oligomer clusters which are held responsible for neurotoxicity. The Aβ oligomers can form Aβ-fibrils and protofibrils, which are subsequently converted to amyloid plaques[6].

The amyloid plaques are considered as non-toxic. It is the Aβ oligomer that triggers the amyloid cascade, resulting in local inflammation, oxidation, excitotoxicity, and tau hyperphosphorylation. Subsequently, tau hyperphosphorylation leads to the formation of intraneuronal tangles causing cell death.[6] The advancing neuronal destruction leads to an imbalance of neurotransmitters (e.g., acetylcholine) and to the characteristic cognitive deficits.[6] Therefore, significant efforts have been made by the pharmaceutical industry to develop new drugs that can normalize the Aβ-level in the brain.[6,7,9] In 2021, aducanumab (Biogen) received accelerated approval by the US Food and Drug Administration (FDA) for the treatment of mild forms of AD.[10] It is the first approved drug on the market targeting the underlying pathophysiological processes of AD. Aducanumab is an Aβ directed human immunoglobulin gamma 1 (IgG1) monoclonal antibody that is capable of crossing the blood-brain barrier. Subsequently, aducanumab selectively targets and binds aggregated soluble oligomers and insoluble fibril conformations of Aβ plaques in the brain.[10] Aducanumab as a drug is controversially debated in the scientific community due to a lack of efficacy and safety reservations. The approval of the drug resulted in the resignation of three members of the FDA advisory committee, which advised against the authorization.[11] In January 2023, lecanemab (Biogen and Eisai) was approved as the second drug on the market, targeting and reducing the Aβ-levels in the brain.[12] However, several concerns remain regarding the actual clinical relevance and safety of this novel class of drugs.[13] Another promising approach is the development of β-secretase inhibitors (e.g., verubecestat (Merck) in clinical phase II/III)[2] or γ-secretase inhibitors (e.g., semagacestat (Eli Lilly) in clinical phase III)[2] that mediate the formation of Aβ from APP.[9] Nevertheless, there are still some enigmatic aspects left of the Aβ cascade, and additional findings on how Aβ aggregates cause AD might lead to new therapeutic approaches.[9] While most of the (candidate) drugs targeting Aβ could not demonstrate clinical efficacy, another encouraging approach can be found in the development of tau-targeting therapies. The tau protein can be more closely associated with cognitive decline than Aβ.[2] Promising therapeutic strategies targeting the tau protein are drugs that prevent the abnormal tau hyperphosphorylation (e.g., tideglusib (Noscira), failed in clinical phase II)[2] or the tau aggregation (e.g., methylthioninium chloride, improvement in cognitive performance was determined in clinical phase II)[2]. Further promising anti-tau agents in clinical phase II are the monoclonal antibodies gosuranemab (Biogen), tilavonemab (AbbVie),

semorinemab (Genentech/AC Immune), and zagotenemab (Eli Lilly) and the anti-tau vaccine AADvac1 (Axon Neuroscience).[2]

Even though great efforts have been made in the last decades to understand the pathology of Alzheimer's disease and to discover effective and safe drugs, there is still a long way to go to discover a treatment with high efficacy and clinical benefit. Another important challenge in this context is the search for a reliable (peripheral) biomarker, allowing the predictive diagnosis of AD. As of today, a biomarker that allows early identification of AD before symptoms onset has not been found yet.[14,15] A final histological examination of the brain is still required to make a definitive diagnosis.[14,15]

Chapter 2

Design and Biological Evaluation of Selective Caspase-2 Inhibitors

2   Design and Biological Evaluation of Selective Caspase-2 Inhibitors

Results of this chapter have been published in:

Bresinsky, M.; Strasser, J. M.; Vallaster, B.; Liu, P.; McCue, W. M.; Fuller, J.; Hubmann, A.; Singh, G.; Nelson, K. M.; Cuellar, M. E.; Wilmot, C. M.; Finzel, B. C.; Ashe, K. H.; Walters, M. A.; Pockes, S. Structure-Based Design and Biological Evaluation of Novel Caspase-2 Inhibitors Based on the Peptide AcVDVAD-CHO and the Caspase-2-Mediated Tau Cleavage Sequence YKPVD314. *ACS Pharmacol. Transl. Sci.* **2022**, *5* (1), 20–40.

Singh, G.; Liu, P.; Yao, K. R.; Strasser, J. M.; Hlynialuk, C.; Leinonen-Wright, K.; Teravskis, P. J.; Choquette, J. M.; Ikramuddin, J.; **Bresinsky, M.**; Nelson, K. M.; Liao, D.; Ashe, K. H.; Walters, M. A.; Pockes, S. Caspase-2 Inhibitor Blocks Tau Truncation and Restores Excitatory Neurotransmission in Neurons Modeling FTDP-17 Tauopathy. *ACS Chem. Neurosci.* **2022**, *13* (10), 1549–1557.

Bresinsky, M.; Strasser, J. M.; Hubmann, A.; Vallaster, B.; McCue, W. M.; Fuller, J.; Singh, G.; Nelson, K. M.; Cuellar, M. E.; Finzel, B. C.; Ashe, K. H.; Walters, M. A.; Pockes, S. Characterization of Caspase-2 Inhibitors Based on Specific Sites of Caspase-2-mediated Proteolysis. *Archiv der Pharmazie* **2022**, *355* (9), 2200095.

2.1 Introduction Caspases

2.1.1 Proteolytic Enzymes

Proteases (also referred to as peptidases) demonstrate several physiological functions such as general protein digestion or more specified functions like activation of zymogens, blood coagulation and the lysis of fibrin clots, hormone release, processing precursor of pharmacologically active peptides, and the transport of secretory proteins across membranes.[16] A variety of hormones and physiologically active proteins are synthesized as inactive precursors (zymogens) and are first activated by the corresponding protease (cf. Figure 2.001A and 2.001B). The activation is performed in either one step or in multiple steps (cascade) (cf. Figure 2.002B).
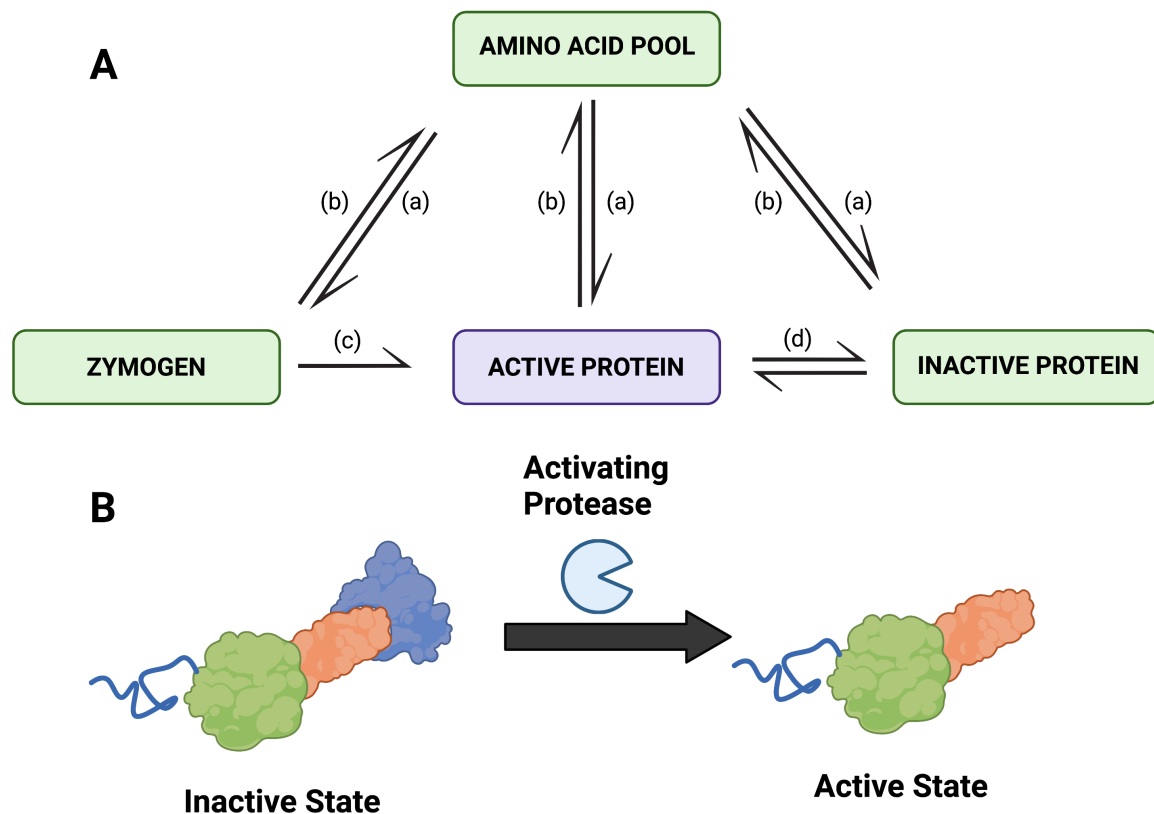
Figure 2.001. (**A**) Schematic diagram of the different pathways of protein formation: (a) Transcription and translation control the building of different proteins out of the amino acid pool. (b) Degradation of proteins to amino acids. (c) Zymogen activation mechanism to active proteins. (d) Reversible conformational changes that affect the activity of the protein (allosteric transition or covalent modification). Figure adapted from Figure 1 of Neurath and Walsh (1976)[17]. (**B**) Activation of zymogen (inactive state) to active proteins (active state) by the corresponding protease. Figures created with BioRender.com.

9

The promotion of zymogens is a vital control element that can initiate new physiological processes. Proteolytic cascades are enzymatic amplification systems where a small stimulus is converted to a major physiological response (e.g., blood coagulation). The investigation of specific zymogen reactions can be challenging because the precursor is activated prior to isolation.[17] The regulation of physiological functions is affected by the specificity and efficiency of the individual activation processes.[17]

A striking feature of proteases is that they exhibit a large variety of biological functions by employing solely basic mechanisms; they exert their functions by selectively catalyzing the truncation of specific proteins. Thereby the amide bond between two amino acids is hydrolyzed. The underlying physiological mechanism is characterized by the polarization of the peptide bond by a nucleophilic attack on the carbonyl group. This can occur either by a water molecule or directly by the protease. The process is accompanied by the donation of a proton to the neighboring nitrogen (cf. Figure 2.002A).[16,18]
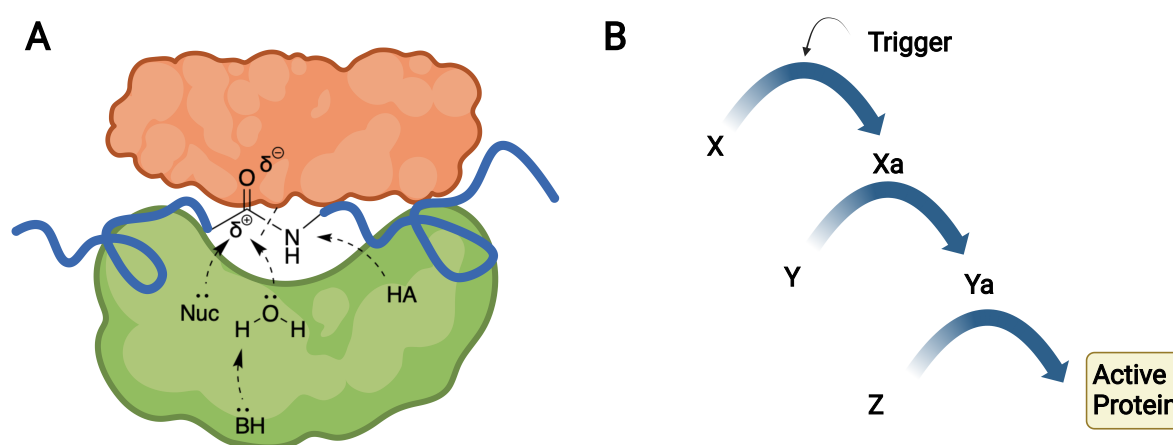
Figure 2.002. (**A**) Mechanisms of enzymatic cleavage of amide bonds. Nucleophiles (Nuc) or bases (BH) (indirectly by water) attack the carbonyl carbon atom. The process is supported by the donation of a proton through a donor (HA) to the neighboring nitrogen (**B**) Schematic demonstration of cascade activation of zymogens: Physiological signal (trigger) initiates the cascade by activating zymogen X, which results in the formation of protease intermediate Xa. Subsequently, zymogen Y is cleaved, and protease intermediate Ya is formed. These steps are repeated until the active protein is released. Figure **A** is adapted from Figure 1 of Neurath (1984)[16] and Figure **B** from Figure 1 of Neurath and Walsh (1976)[17]. Figures created with BioRender.com.

Specific functional residues in the binding site of the protease serve either as a nucleophilic group or as a proton donator. The proteases are distinguished according to specific functional groups in the active site of the enzyme, 3D structures, and the enzymatic reaction they execute (cf. Table 2.01). Every group of peptidases is characterized by specific amino acids or metals arranged in a particular configuration in the active site of the enzyme. Members of a protease group are descending from mutual ancestors by deviating evolutionary paths. The serin proteases and the metalloproteases comprise two families that have emerged from a separate predecessor.[16,17]

Table 2.01. Protease families, with corresponding examples and enzymes involved in the active site.[16,19–22]

Family	Representative proteases	Characteristic active site residues
Serine proteases I	Chymotrypsin	Asp^{102}, Ser^{195}, His^{57}
Serine proteases II	Subtilisin	Asp^{32}, Ser^{221}, His^{64}
Cysteine proteases	Caspase-1	Cys^{285}, His^{237}
Threonine proteases	20S proteasome	Thr^{1}, Asp^{17}, Lys^{33}
Aspartic proteases	Penicillopepsin	Asp^{33}, Asp^{213}
Glutamic proteases	Scytalidocarboxyl peptidase B	Gln^{53}, Glu^{136}
Metalloproteases I	Bovine carboxypeptidases A	Zn, Glu^{270}, Tyr^{248}
Metalloproteases II	Thermolysin	Zn, Glu^{143}, His^{231}
Asparagine peptide lyases	Tsh-associated self-cleaving domain	Asn^{1100}, Lys^{1201}, Tyr^{1227}

2.1.2 Caspases: A Family of Cysteine-Aspartic Proteases

Caspases (cysteine-dependent aspartate-directed proteases) are a family of protease enzymes that cleave target proteins on the C-terminal side of aspartic acid and are typically subdivided into three major groups: initiator caspases (e.g., caspase-2, -8, -9, -10), effector/executioner caspases (e.g., caspase-3, -6, -7), and inflammatory caspases (e.g., caspase-1, -4, -5) (cf. Figure 2.003).[23,24] Caspase-2 is classified differently depending on the literature, as it combines the functions of both initiator caspases and executioner caspases.[24,25] Therefore, it is also referred to as caspase being responsible for the cell cycle.[23] There are findings about 11 humans, 10 murine,

4 avians, 4 fish, 8 amphibians, 7 insects, and 3 nematode caspases. In total, 14 different mammalian caspases have been detected (cf. Figure 2.003).[26,27] In terms of structure, most caspases possess a prodomain (CARD or DED) at the N-terminal side that promotes the recruitment and activation of multiprotein complexes (cf. Figure 2.003). Inflammatory caspases (e.g., caspase-1, -4, -5) all possess a CARD domain (= caspase recruitment domain).
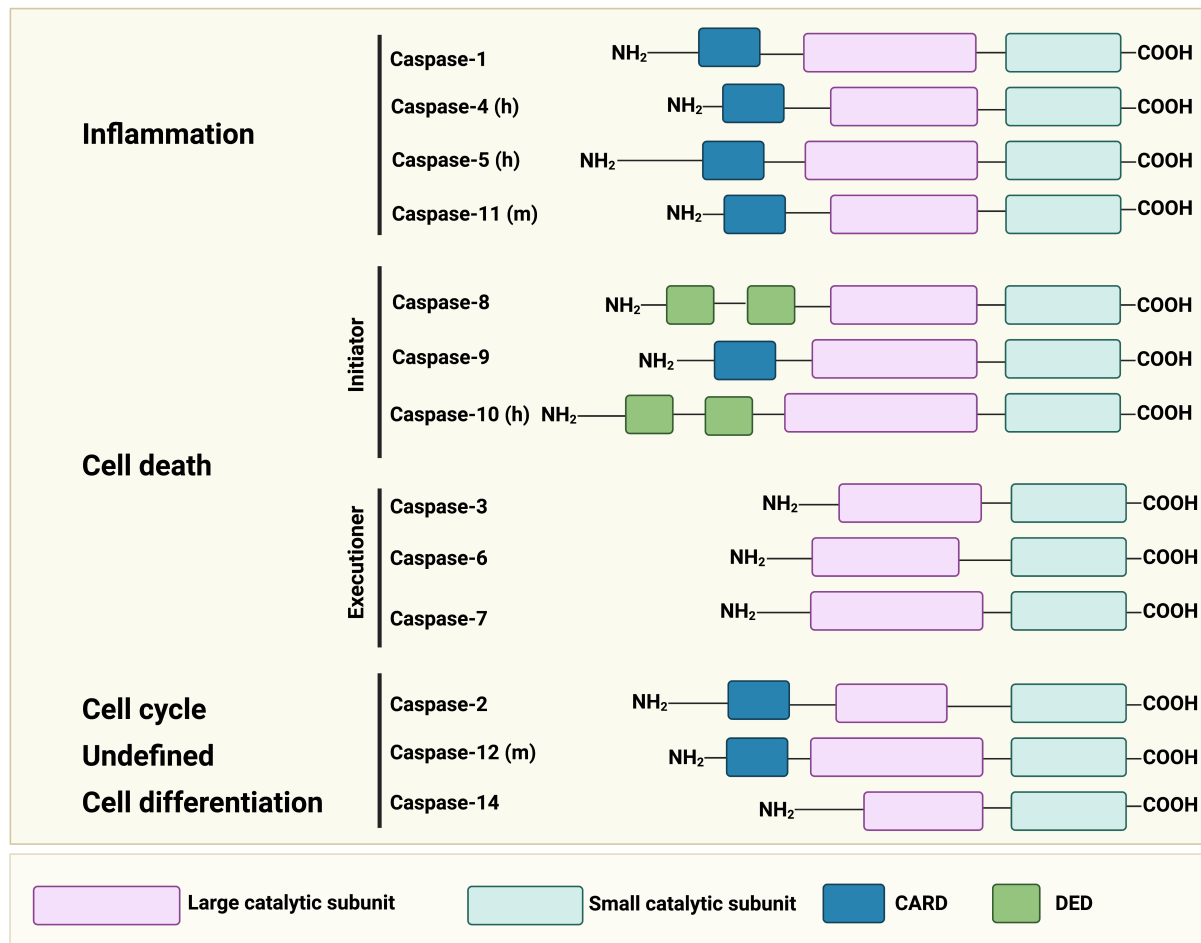
Figure 2.003. Functional classification and domain organization of murine and human caspases: The caspases are classified into three different groups, initiator caspases (e.g., caspase-2, -8, -9, -10), effector/executioner caspases (e.g., caspase-3, -6, -7), and inflammatory caspases (e.g., caspase-1, -4, -5). In total, 14 different mammalian caspases have been detected: within the human, there are 11 different caspases. m, murine and h, human. Figure adapted from Figure 1 of Opdenbosch and Lamkanfi (2019)[23]. Figure created with BioRender.com.

Within the initiator caspases caspase-8 and caspase-10 share a DED domain (= death effector domain) and caspase-9 a CARD domain. In contrast, executioner caspases do not exhibit a prodomain. Furthermore, all caspases have large (~20 kDa) and small (~10 kDa) catalytic subunit that together form the protease domain (cf. Figure 2.003).[23] Caspase zymogens are activated in active proteases by a proximity-induced autoactivation that is driven by a conformational change due to dimerization. This causes proteolytic cleavage of the flexible linker regions separating the prodomain from the large and small catalytic subunit. In contrast, effector caspases do not possess a prodomain and need to be activated by the cleavage of initiator caspases (cf. Figure 2.003).[28] All caspase catalytic domains share a similar dimeric quaternary structure, with two identical monomers associated about two-fold rotation axis to form one large beta sheet of twelve strands. The monomers adopt a highly homologous fold, with highly variable loops (L1-L4) that lead to the specific and varying substrate selectivity of the different caspases (cf. Figure 2.004). Following proteolytic cleavage in the L2 loop, a rearrangement of the L2 and L3 loops occurs resulting in a repositioning of the active site cysteine and enzyme activation. Substrates and inhibitors bind in a cleft formed atop the L3 loop, with L2 and L4 on either side of this cleft (cf. Figure 2.004).
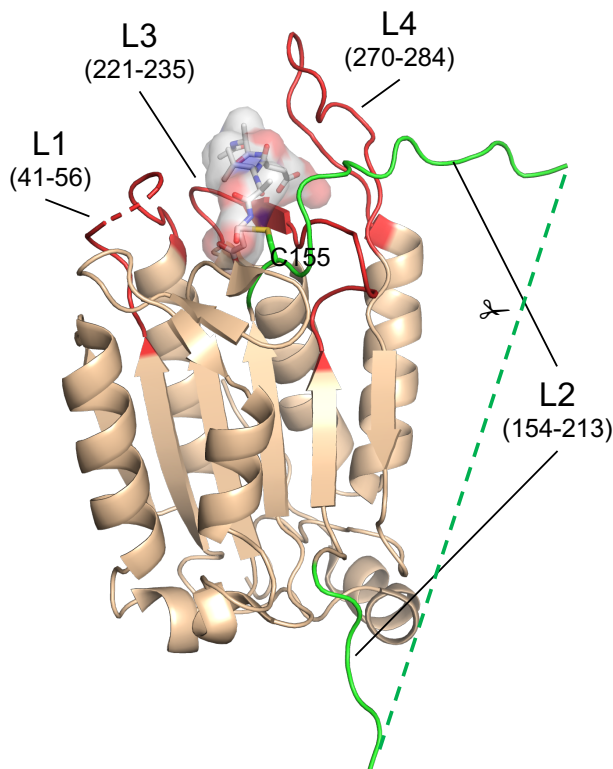
Figure 2.004. The Caspase folds. All caspase catalytic domains share a similar fold, with highly variable loops (L1-L4) that afford selectivity by different caspases. Rearrangement of L2 and L3 occurs following proteolytic cleavage in the L2 loop, resulting in enzyme activation.[29] Peptidic inhibitors bind cradled in the groove above L3 pinched between L2 and L4. The structure shown is the Casp2/AcVDVAD complex described by Tang et al. (PDBid:3r5j).[30]

2.1.3 Apoptotic Pathways of Caspases

Caspases are synthesized as zymogens and first have to be activated by a variety of internal and external triggers.[24,31] They are classically associated as an enzyme cascade during the initiation and execution of apoptotic cell death and the processing and maturation of inflammatory cytokines. After the perception of an apoptotic stimuli, initiator caspases (e.g., Casp2, Casp8, and Casp9) are enabled. The extrinsic pathway is triggered by the binding of extracellular death ligands (e.g., Fas L) to death receptors (e.g., Fas) (cf. Figure 2.005).[32–34] A death-inducing signaling complex (DISC) is formed by the binding of a death ligand to the death receptor and the recruitment of a death domain-containing adaptor protein. The death-inducing signaling complex recognizes death domains on the procaspases, initiates the recruitment of procaspases, and thereby activates the initiator caspases Casp8 and Casp10 (cf. Figure 2.005).[24] Those catalytically cleave effector caspases (e.g., Casp3, Casp6, and Casp7) out of the inactive precursor (procaspases). Effector caspases cleave a variety of substrates, which are responsible for inducing cell death (cf. Figure 2.005). Casp8 additionally can advance the intrinsic apoptotic pathway by the release of Bcl-2 homology 3 (BH3)-only protein Bid. This is further converted to truncated Bid (tBid), which activates the Bcl-2 proteins Bax and Bak. Mitochondrial outer membrane permeabilization (MOMP) is activated by the Bcl-2 proteins Bax and Bak, resulting in the release of proapoptotic mitochondrial messengers (e.g., cytochrome c) into the cytoplasm (cf. Figure 2.005).[35] The apoptotic pathway of the BH3-only protein Bid is in balance with anti-apoptotic Bcl-2 family proteins.[35] Cytochrome c leads to the oligomerization of the caspase recruitment domain-containing adaptor protein (Apaf-1), resulting in the activation of Casp9 by Apaf-1 from the zymogenic form (procaspase-9). Casp9 then again enables effector caspases.[24] The precise apoptotic mechanism of caspase-2 initiation remains largely unclear, but it is assumed that a variety of stress factors may be responsible.[24,36] Therefore, it is difficult to classify caspase-2 as an initiator or an executioner caspase as it demonstrates features of both.[25] Further intrinsic factors for caspase activation are endoplasmic reticulum (ER) stress, metabolic stress, response to DNA damage, and a variety of other factors.[36–40]
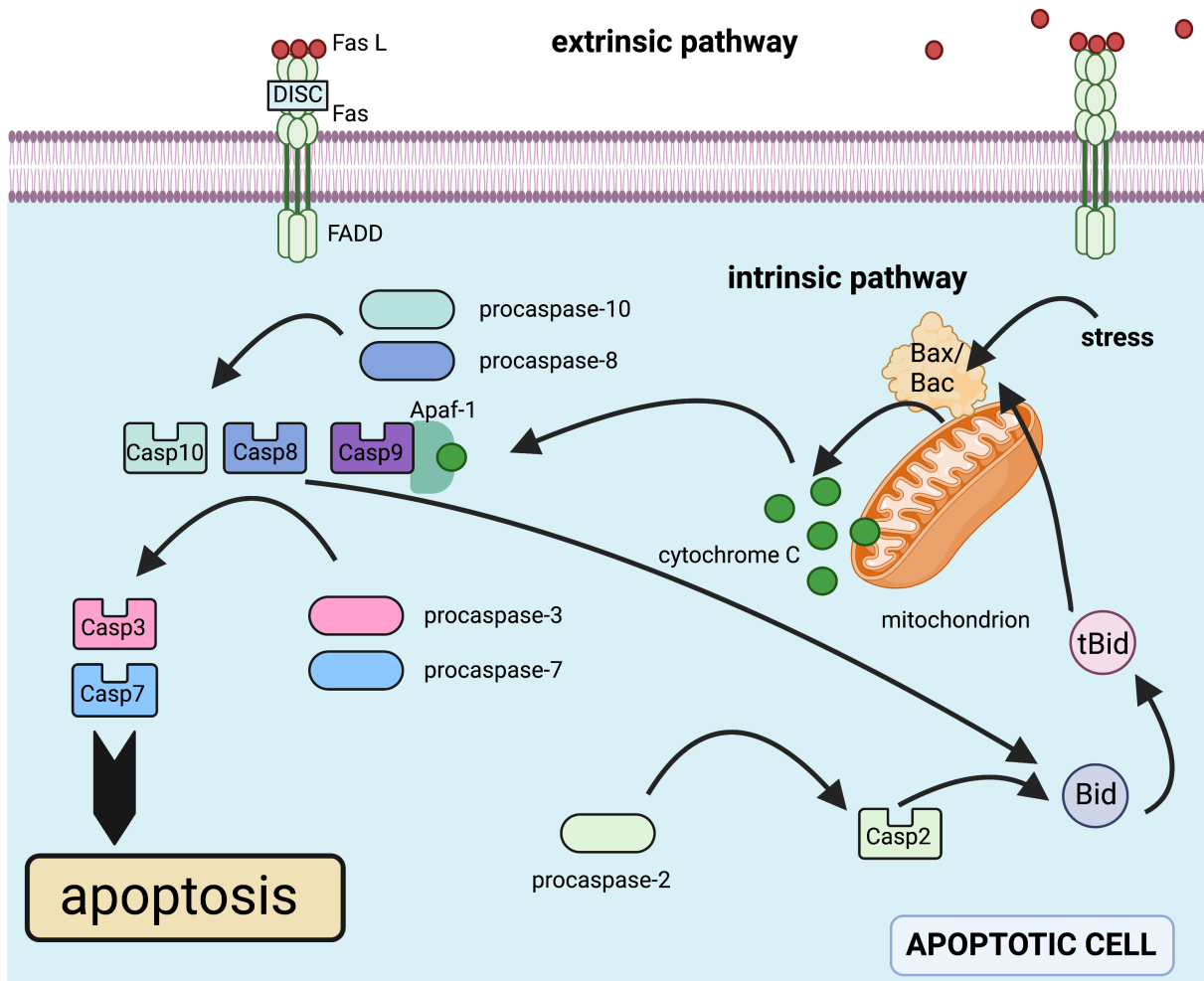
Figure 2.005. Extrinsic and intrinsic apoptotic pathways.[24,33] Extrinsic pathway: A death ligand (e.g., Fas L) binds to a death receptor (e.g., Fas). Thereby, a death-inducing signaling complex (DISC) is formed consisting of the death receptor and the death domain-containing adaptor protein (e.g., Fas-associated death domain (FADD)). This causes the activation of Casp8 and Casp10 from the procaspase-8 and procaspase-10. The active proteins Casp8 and Casp10 promote the activation of effector caspases (e.g., Casp3 and Casp7) and/or the BH3-only protein Bid. Casp3 and Casp7 are responsible for the initiation of apoptosis. Bid leads to the activation of the intrinsic apoptotic pathway. Intrinsic pathway: The intrinsic pathway is promoted by the BH3-only protein Bid (activated by Casp2 or Casp8). Bid is truncated to tBid, which causes the activation of Bax/Bak. The proapoptotic proteins Bax and Bak promote the release of cytochrome c from the mitochondria to the cytoplasm. Cytochrome c enables the adaptor protein Apaf-1, which recruits and activates caspase-9. Casp9, in turn, activates the effector caspases. Figure adapted from Figure 1 of Kurokawa et al. (2009)[24]. Figure created with BioRender.com.

2.1.4 Cellular Substrates of Caspase-2

To date, a variety of cellular substrates of Casp2 are known, as it is present in different organelles (e.g., nucleus, Golgi body, cytoplasm, and mitochondrion), even though a greater part of them is processed by multiple caspases (e.g., caspase-3).[41,42] The listing of all substrates is not sufficient to draw a conclusion about the actual preference. The crucial parameter is the catalytic efficiency for a more precise identification of the preference of substrate cleavage within the caspases. This was analyzed by Julien et al. (2016) in an extensive study.[43]

Table 2.02. Selected Casp2 substrates indicating their cleavage site, Casp2 selectivity, and cleavage efficiency. Table adapted from Table 1 of Miles et al. (2017)[41].

Substrate	Cleavage Site	Casp2 Selectivity	Cleavage Efficiency ($M^{-1} S^{-1}$)
CUX-1[44]	SEGD⎮S and/or DSCD⎮G	No	6.2×10^5
Prothymosin α[43]	M$^{(init)}$SD⎮A	Yes	1.5×10^5
Golgin-160[45]	ESPD⎮G	Yes	3.3×10^4
Nucleosome assembly protein 1-like 4 (NAP1L4)[43]	SFSD⎮G	Yes	1.3×10^4
Protein transport protein Sec16A[43]	VHPD⎮S	Yes	8.3×10^3
	DRAD⎮S	Yes	5.4×10^3
Bid[46,47]	LQTD⎮G	No	3.2×10^3
Rho GDI 2[43]	DTKD⎮G	No	2.6×10^3
Guanine nucleotide-binding protein-like 1[43]	DIND⎮G	Yes	2.0×10^3
Scaffold attachment factor B2[43]	DSRD⎮G	Yes	2.0×10^3
Runx1[47]	DVPD⎮G	Yes	1.8×10^3
BAG-6[43]	DEQD⎮G	Yes	1.6×10^3
Transcriptional regulating factor 1[43]	DTRD⎮G	Yes	1.3×10^3

Table 2.02 (continued)

Substrate	Cleavage Site	Casp2 Selectivity	Cleavage Efficiency $(M^{-1} S^{-1})$
eIF-4H[43]	DEPD⏐A	No	1.3×10^3
Histone deacetylase 6[43]	DMAD⏐S	No	1.3×10^3
Holliday junction recognition protein[43]	DRTD⏐G	No	1.2×10^3
Deubiquitinating protein VCIP135[43]	ETTD⏐G	Yes	1.2×10^3
Ubinuclein-1[43]	DESD⏐S	No	1.1×10^3
Scaffold attachment factor B2[43]	DGTD⏐G	Yes	1.1×10^3
Protein PRRC2B[43]	DQAD⏐S	Yes	1.1×10^3
Serine/arginine-related protein 53[43]	IESD⏐S	No	1.1×10^3
GEM-interacting protein[43]	DTSD⏐G	Yes	1.1×10^3
Ral GTPase-activating protein subunit alpha-1[43]	TVKD⏐G	Yes	1.1×10^3
C18orf25[43]	VQKD⏐G	Yes	1.0×10^3
eIF-4B[48]	DRKD⏐G	Yes	n.a
MDM-2[49]	DVPD⏐C	Yes	n.a
Tau[50,51]	KPVD⏐L	No	n.a

For many substrates, the physiological role of the cleavage remains obscure. The best-examined substrates are Bid (causing the release of cytochrome c of the mitochondrion), Golgin-160 (causing the Golgi body dissolution), and MDM-2 (causing cell cycle arrest and p53 stabilization).[50] Golgin-160 can also be cleaved by caspase-3 *in vitro* at a different site, but because of its localization in the Golgi organelle, Casp2 has better access to it.[41,52] Further notable substrates of caspase-2 are CUX-1, huntingtin (Htt), *α*II-spectrin, Rho kinases-2 (Rock-2), PKC*δ*, plakin, HDAC4, ICAD, PARP, DNp63a, and tau. Most of the substrates are processed by a variety of other proteases.[42,45,49] Table 2.02 shows a selection of known substrates, their cleavage site, cleavage efficiency, and the selectivity for caspase-2 over other caspases.

2.1.5 Physiological Functions of Caspase-2 and Associated Diseases

A variety of caspases also possess nonapoptotic physiological features such as cell cycle regulation and DNA repair.[40] Analysis of the Casp2 protein sequence revealed that it is the evolutionarily most conserved caspase.[53] Nevertheless, it is the most enigmatic member of the family.[52–56] While the exact biological role and mechanism of caspase-2 are still unclear, it is associated with various processes of cell death by cleaving BH3-only protein Bid.[41,57] Furthermore, it is linked with metabolic syndrome, obesity, and nonalcoholic fatty liver disease.[58] Metabolic benefits of Casp2 loss were demonstrated in a study by Machado et al. (2016)[58]. Casp2 deficient mice exhibit less susceptibility for dyslipidemia, diabetes mellitus, and hepatic steatosis.[58] This was impressively demonstrated by wild-type mice that were fed a high sugar/fat diet.[58] They had almost twice as much body fat as Casp2 deficient mice with the same diet or as wild-type mice that were fed ordinary food.[58] Additionally, wild-type mice showed impaired glucose tolerance compared to the Casp2-deficient mice.[41,58] Caspase-2 is known for the protection of retinal ganglion cells (RGCs), indicating that inhibitors can be used for the treatment of optic nerve injuries.[59] Optic nerve damage causes the apoptosis of RGCs.[59] Ahmed et al. (2011)[59] demonstrated that the clamping of the axon of rat RCGs led to a 60% reduction of retinal ganglion cells (RGCs) within seven days. However, this process was diminished by the intravitreal injection of siRNA targeting Casp2.[41,59] Besides, Casp2 is involved in cytoskeleton protein degradation during cell death.[42] Vakifahmetoglu-Norberg et al. (2013)[42] discovered four cytoskeleton proteins (tropomyosin, profilin, stathmin-1, and myotrophin) that were degraded during DNA damage, cytoskeleton disruption, or endoplasmic reticulum stress-induced apoptosis. Although the cleavage of this protein was not directly induced by Casp2, the degradation was prevented by using siRNA for downregulating caspase-2 or through pharmacological inhibition of Casp2.[41,42,60] Additionally, caspase-2 amplifies the harm to CNS neurons under stress, e.g., excitotoxicity, [61] increased ROS, exposure to Aβ or MPTP, neonatal stroke,[61] retinal ischemia and transgenic expression of mutant APP,[62] huntingtin[63] or tau[51]. This leads to the conclusion that targeting Casp2 may be beneficial for various neurological indications (cf. Table 2.03).[51,59,62–68] Casp2 −/− mice show no perceptible physiological abnormalities and the same life expectancy as their wild-type littermates, strengthening

the assumption that pharmacological inhibition of Casp2 could be a safe and effective therapeutic strategy.[69]

Table 2.03. CNS indications that may benefit from Casp2 inhibition.[51,59,62–68]

Indication	Model System
Alzheimer's disease (AD)	Transgenic mouse (J20)
Huntington disease (HD)	Transgenic mouse (YAC128)
Frontotemporal dementia (FTD)	Transgenic mouse (Tg4510)
Parkinson's disease (PD)	MPTP (mouse)
Excitotoxicity	Ibotenic acid (mouse)
Neuro-ophthalmology	Crush, glaucoma (rat)
Stroke	Neonatal (wt, Casp2 null)
Neuroblastoma	Transgenic mouse (TH-MYCN)

2.1.6 Truncation of Tau and Physiological Role of Caspase-2 in Tauopathies like Alzheimer's Disease

Two physiological functions for Casp2 are disclosed in the healthy brain: During development, Casp2 likely mediates neuronal apoptosis.[70,71] In the mature brain, Casp2 facilitates long-term depression, a synapse-weakening form of long-lasting synaptic plasticity.[72] However, in recent years, the caspase-2 (Casp2) enzyme has been increasingly associated with neurodegenerative diseases, in particular tauopathies like Alzheimer's disease (AD), Huntington's disease (HD), frontotemporal dementia (FTD), and Lewy body dementia (LBD).[51,62,63,73–75] Fibrillar tau has been dissociated from neuronal death and network dysfunction, implying the contribution of non-fibrillar species in the mediation of cognitive anomalies.[76,77] Post-translational modifications (PTMs) of tau, such as phosphorylation and acetylation, play a crucial role in the normal physiological conditions of neurons. Phosphorylation serves as a regulator of tau functions such as the stimulation and stabilization of microtubule assembly.[78,79] In AD and other tauopathies, the tau protein undergoes hyperphosphorylation, which promotes the accumulation and mistargeting of abnormal tau in dendritic spines (cf. Figure 2.006).[80,81] Casp2 cleavage of tau at Asp314 generates the cleavage product Δtau314 and leads to synaptic dysfunction and

impaired cognition by enabling tau to mislocalize to dendritic spines and dislocates glutamate receptors on the postsynaptic membrane (cf. Figure 2.006).
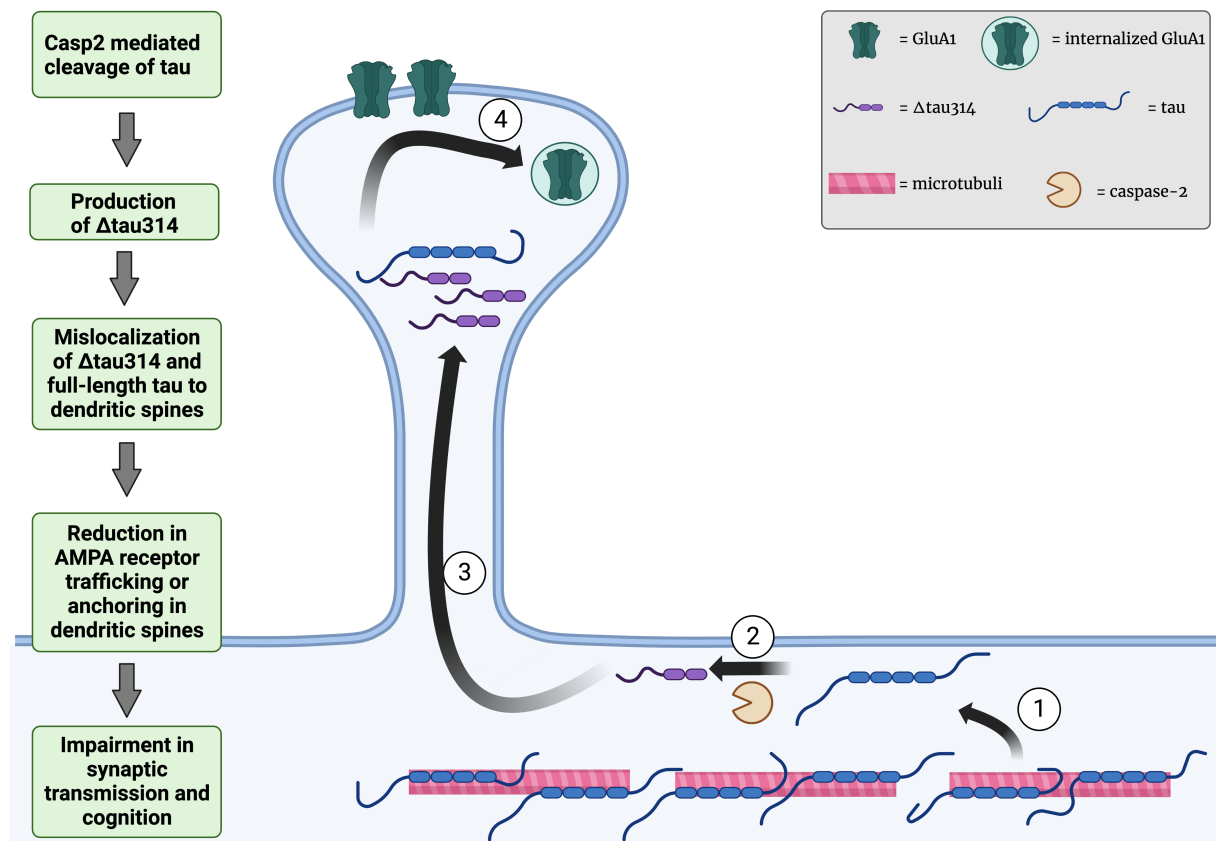
Figure 2.006. Mechanism for synaptic dysfunction and impaired cognition prompted by excessive Δtau314 accumulation.[51,80] (1) hyperphosphorylation and disassociation of tau from microtubules. (2) Casp2 mediated truncation of full-length tau to Δtau314 (3) mislocalization of Δtau314 and full-length tau to dendritic spines. (4) accumulated Δtau314 in dendritic spines impairs glutamatergic synaptic transmission by lowering the number of functional AMPA and NMDA receptors on the surface of the neuronal membrane by internalization and diminished anchoring of the glutamate receptors. Figure is adapted from Figure 2 of Pockes et al. (2022)[82]. Figure created with BioRender.com.

The synapses affected by this are referred to as "silent synapses" since the number is not decreasing. [51,80] The Δtau314 fragment may be a biomarker of impaired cognition, as Δtau314 was increased approximately threefold in brain samples from patients with mild cognitive impairment (MCI) and Alzheimer's disease (AD) compared to cognitively intact subjects.[51,74] Zhao et al. (2016)[51] revealed that mutant tau, not cleaved by caspase-2, hinders tau from hyperaccumulating into dendritic spines, dislocating glutamate receptors and impairing synaptic function in cultured neurons. It prevented memory deficits and neurodegeneration in mice. Furthermore, lowering the level of caspase-2 restored long-term memory in mice with existing deficits. Therefore,

blocking this truncation can be a promising therapeutic approach for AD or other tauopathies like Huntington's disease (HD) and Lewy body dementia.[51,75,83]

2.1.7 Lowering Casp2 Enhances Synaptic Function: Catalytical or Non-catalytical Pathway?

Most cellular events of caspases are of non-apoptotic nature,[84] albeit being discovered due to the search for genes that are responsible for apoptotic processes of cells.[85] Caspase-2 possesses biological activity through catalytical or non-catalytical cellular pathways. For instance, it has been proven that some non-apoptotic events are conducted via a non-catalytic process. Although the exact mechanism is unclear, dead Casp2 with its mutated catalytic active cysteine negatively impacts cellular autophagy.[86] One hypothesis is that catalytically dead Casp2 acts as a translational co-factor to produce cyclin-dependent kinase inhibitor p21[87]. This can verifiably downregulate autophagy in various cell types under stress conditions.[88,89] Zhao et al. (2016) demonstrated that lowering the level of Casp2 restored synaptic functions.[51] The basic assumption is that pathological effects of Casp2 on synaptic functions are caused by the catalytical pathway of Casp2. Casp2 hydrolyzes tau at Asp314. Thereby, Δtau314 is formed, which excessively accumulates in dendritic spines.[51] Nevertheless, it is also possible that a non-catalytical mechanism of dead Casp2 is the cause of impaired synaptic functions since there is proof of at least one relevant cellular process, i.e., autophagy by catalytical dead Casp2.[86] It might be possible to rescue neurotransmission by stimulating autophagy and thereby decreasing the amount of misfolded and aggregated forms of tau. In order to do so, it must be deciphered whether the pathological cellular processes of Casp2 on synaptic functions are due to its catalytic or non-catalytic properties to justify the potential use of selective Casp2 inhibitors as a treatment for tauopathies like Alzheimer's disease. The biological experiments in chapters **2.4.2.3**, **2.4.2.4**, and **2.4.2.5** are intended to verify whether Casp2 exerts synaptic dysfunction through catalytical or non-catalytical cellular processes.

2.1.8 Amino Acid Motif Preferences of Substrates within the Caspase Family

Extensive success in the structural biology of caspases has provided a wealth of information regarding enzyme architecture, activation, and the basis for selectivity of these enzymes for different substrates.[29] Within the caspase family, only Casp2 requires a motif of five amino acids, instead of four, as a specific recognition sequence for efficient substrate cleavage.[30,90] The closest similarities to the cleavage specificity of Casp2 are found with Casp3, 7, and 8 where an aspartic acid is also favored at position P1 and P4 for effective binding (cf. Figure 2.007). This close homology between Casp2 and Casp3 makes the design of selective Casp2 inhibitors challenging. All caspases conduct substrate cleavage by the same mechanism, using a catalytic Cys/His dyad architecture in their active site. The aspartic acid of substrates is deeply buried in the basic S1 pocket, where it interacts with two arginines and one glutamine residue (e.g., Arg202, Arg361, and Gln301 Casp2). Casp3, 6, and 7 are limited to smaller aliphatic residues at P2 (e.g., alanine and valine; cf. Figure 2.007), as their S2 binding sites show a narrower spatial shape recognition than other caspases. Notably, Casp2 accommodates larger substrates in S2, and also contains a negatively charged Glu52 as a unique structural feature.[32,91] Therefore, it was hypothesized that the introduction of sterically demanding P2 residues, as recently shown by Maillard et al. (2011)[92] , and/or the use of positively charged amino acids (e.g., lysine, arginine) at P3 could lead to enhanced potency at Casp2 over Casp3. The S3 binding site of all caspases is characterized by a conserved arginine which can provide ionic interactions with negatively charged amino acids (e.g., glutamic acid) of the substrates at P3 (cf. Figure 2.007).[91] Casp8 and Casp9 are characterized by a second arginine, allowing a tighter binding of ionic groups in its S3 pocket.[91] The S4 binding site of the caspase family can be subdivided into three groups.[91] Casp1, 4, 5, and 11 consist of an extended, shallow hydrophobic binding pocket, favorably engaging aromatic amino acids (e.g., tryptophan; cf. Figure 2.007).[32,91] In contrast, Casp2, 3, and 7 have a significantly smaller hydrophilic binding site, typically preferring an aspartic acid (cf. Figure 2.007).[32,91] Recent work has demonstrated that a homoglutamic acid P4 sidechain can confer excellent selectivity for Casp2 versus other caspases.[93] S4 structures of Casp6, 8, 9, and 10 show little selectivity toward specific amino acids and represent a hybrid between the two binding sites mentioned above.[91] Casp2 is the only caspase that prefers an occupied binding subsite S5 for activity, e.g., valine or

tryptophan.[93] This unique requirement for its substrate guarantees efficient substrate cleavage and a substrate-selectivity preference for Casp2 over other caspases.[32,94]
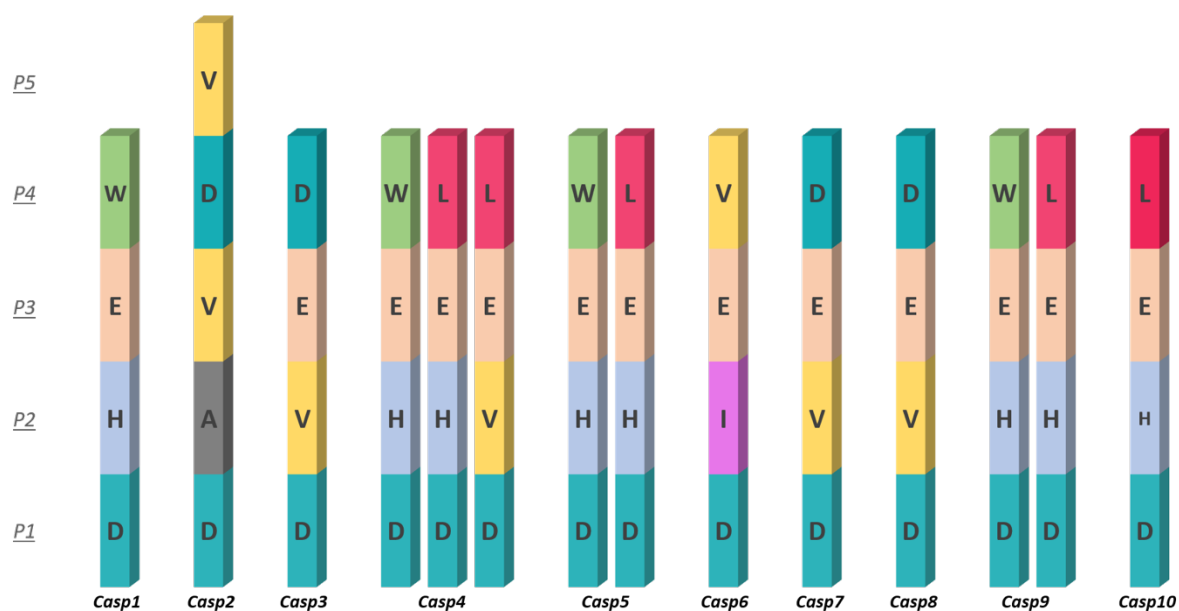
Figure 2.007. Peptide substrate preferences for Casp1, 2, 3, 4, 5, 6, 7, 8, 9, 10.[95,96] P1-P5 represent the respective amino acid position of the peptidic substrate or inhibitor. P1 always marks the position of the aspartic acid (D) cleavage site. P4 and P5 (for Casp2) represent the N-terminal position, respectively.

2.2 Scope and Objectives

Fibrillar tau has been dissociated from neuronal death and network dysfunction, implying the contribution of non-fibrillar species in the mediation of cognitive anomalies.[76,77] Δtau314, a 35-kDa tau cleavage product of tau, can reversibly impair cognitive and synaptic function in animal and cellular models of tauopathies.[51] Δtau314 is formed by truncation of tau at Asp314 by Casp2.[51] The accumulation of this cleavage product in the dendritic spines is being held responsible for synaptic dysfunction and impaired cognition by reducing AMPA receptors in the post-synaptic membrane.[51] Down-regulating or genetically shutting off the level of caspase-2 preserves synaptic functions in mouse models of frontotemporal dementia,[51] Alzheimer's disease,[62] and Huntington's disease.[63] Most *in vivo* studies revealed that Casp2 expression levels mediate neurodegeneration, but no certain proof of the exact mechanism was revealed. As Casp2 can process its biological functions, catalytically or non-catalytically, it is of great relevance to evolving selective Casp2 inhibitors to verify that the impaired cognitive and synaptic function is caused by catalytically hydrolyzing tau at Asp314 since catalytically dead caspase-2 is also capable of acting as a translational co-factor that downregulates autophagy in various cell types. Therefore, lowering caspase-2 in different models might also exhibit positive effects on synaptic functions due to enhanced autophagy.

The goal of this study was the exploration of the caspase-2 binding pocket to elucidate the interactions of Casp2 inhibitors and the target enzyme. This allows understanding the specific features of the active site to achieve the goal of discovering selective and potent Casp2 inhibitors. A particular focus was on the development of selective Casp2 inhibitors against Casp3, since the canonical inhibitor AcVDVAD-CHO (**2.016**) provides equally high affinities for Casp2 and Casp3 (cf. Table 2.06 & Maillard et al. (2011)[92]). A further reason is the high concentration of active Casp3, compared to other caspases, which is present in almost all tissues.[95] Ultimately, the neuroprotective effects of a Casp3 inhibitor have already been demonstrated in an HD model.[97] Therefore, strengthening the case for targeting Casp2-mediated proteolysis by developing a series of selective inhibitors is indispensable to prove the benefits of inhibiting Casp2 for synaptic functions. The high degree of homology observed between Casp2 and Casp3 makes the design of selective Casp2 inhibitors challenging.

The inhibitors are supposed to serve as pharmacological tools in planned *in vivo* studies and as lead compounds for the design of bioavailable and more drug-like small molecules that potentially can treat Alzheimer's disease and other tauopathies.

The design of the reversible covalent inhibitors is hereby influenced by previously published structure-activity-relationship (SAR) studies[92,93,98,99], computational docking methods, and the crystallographic examination of caspase/inhibitor co-crystals. The design strategy of the Casp2 inhibitors consists of three different concepts: 1) Structure-based design of Casp2 inhibitors evolved from natural proteolysis sequences and the canonical inhibitor AcVDVAD-CHO; 2) Addressing Glu52 in the binding site of Casp2 and introducing previously published structural features; 3) Improvement of the physicochemical properties of Casp2 inhibitors to increase bioavailability. After every series was synthesized and biologically evaluated the favored structural features were analyzed and used for the design of further Casp2 inhibitors.

2.3 Structure-Based Design of Casp2 Inhibitors Derived from Natural Proteolysis Sequences and the Canonical Inhibitor AcVDVAD-CHO

AcVDVAD-CHO
(non-selective canonical Casp2 inhibitor)

Structure-based design

- canonical inhibitor
- 8 specific sites of caspase-2 mediated proteolysis

Y-K-P-V-D314 | L-S-K
(Casp2-mediated tau cleavage sequence, D314 | L = cleavage site)

Sequence	Comp.	pK_i ± SEM				Selectivity ratios of K_i (Casp2: Casp3)
		Casp2	N	Casp3	N	
AcYKPVD-CHO	2.008	4.56 ± 0.22	3	4.73 ± 0.05	4	1:1
AcFDVPD-CHO	2.014	8.15 ± 0.09	2	8.52 ± 0.06	4	2:1
		8.03 ± 0.07	2			3:1
AcITVKD-CHO	2.015	6.40 ± 0.16	4	6.05 ± 0.06	4	1:2
AcVDVAD-CHO	2.016	7.85 ± 0.03	5	7.73 ± 0.04	5	1:1

Concentration-response curves at Casp2

- AcYKPVD-CHO
- AcGESPD-CHO
- AcWDRAD-CHO
- AcQDTRD-CHO
- AcADRTD-CHO
- AcLDVPD-CHO
- AcFDVPD-CHO
- AcITVKD-CHO

Since the discovery of the caspase-2 (Casp2)-mediated Δtau314 cleavage product and its associated impact on tauopathies such as Alzheimer's disease, the design of selective Casp2 inhibitors has become a focus in medicinal chemistry research. In the search for new lead structures with respect to Casp2 selectivity and drug-likeness, a promising approach is looking more closely at the specific sites of Casp2-mediated proteolysis and the canonical inhibitor AcVDVAD-CHO. Using eight selected protein cleavage sequences, a peptide series of 54 novel molecules was designed and investigated using *in vitro* pharmacology, molecular modeling, and crystallography.

2.3.1 Design Rationale

The first approach in the search for new lead structures with respect to Casp2 selectivity and drug-likeness is based on looking more closely at the specific sites of Casp2-mediated proteolysis (cf. Table 2.04) and the canonical inhibitor AcVDVAD-CHO (**2.016**). This enables the revealing of new peptide sequences that might offer clues to the structural elements that could be beneficial in the design of Casp2 enzyme inhibitors. A detailed examination of structural data describing complexes of AcVDVAD-CHO (**2.016**) bound to both Casp3 (PDBid; 2h65)[100] and Casp2 (PDBid:3r6g)[30] provides an excellent basis for understanding the high potency of this inhibitor scaffold toward both Casp2 and Casp3 and helps to identify some of the challenges and opportunities for selective inhibitor design. AcVDVAD-CHO (**2.016**) binds to Casp2 and Casp3 almost identically (cf. Figure 2.008). Reaction with the C-terminal aldehyde results in the formation of a covalent bond to the catalytic cysteine (Cys163 in Casp3; Cys155 in Casp2). The P1 aspartic acid is firmly anchored in the S1 subsite by H-bonds and ionic interactions with Arg207, Arg64, and Gln161 (Casp3 numbering). The remainder of the inhibitor lies stretched out over the L3 loop, with the peptide backbone of the P3 valine and P5 valine making H-bonds with the backbone of L3 at Arg207 and Ser209 that resemble those of an antiparallel β-sheet (cf. Figure 2.008C). All these interactions are largely conserved in complexes of most caspases with peptidic inhibitors and substrates; they confer broad potency but not selectivity. AcVDVAD-CHO (**2.016**) also exploits the P4 aspartic acid to increase affinity for Casp3 and Casp2. In both complexes, the Asp carboxylate forms a bridge connecting L3 to L4, with H-bonds to Asn208 of L3 and Phe250 of L4. The L4 loop is quite different in other caspases, and the L3 asparagine is only conserved in caspases-2, -3, and -8 in humans. A comparison of the binding sites of the two structures exposes other differences not exploited by the AcVDVAD-CHO (**2.016**) scaffold. The most noticeable difference noted by Tang et al. (2011)[30] is the presence of Glu52 in Casp2, which introduces a negatively charged functional group in the proximity of the S2 and S3 subsites (cf. Figure 2.008B). This amino acid is an uncharged threonine in Casp3 (cf. Figure 2.008A). Another significant difference is the presence of a much smaller alanine (Ala228) in Casp2 in place of the tyrosine (Tyr204) of Casp3. This difference results in a significant expansion of the S2 subsite, which potentially can be targeted with larger P2 substituents.
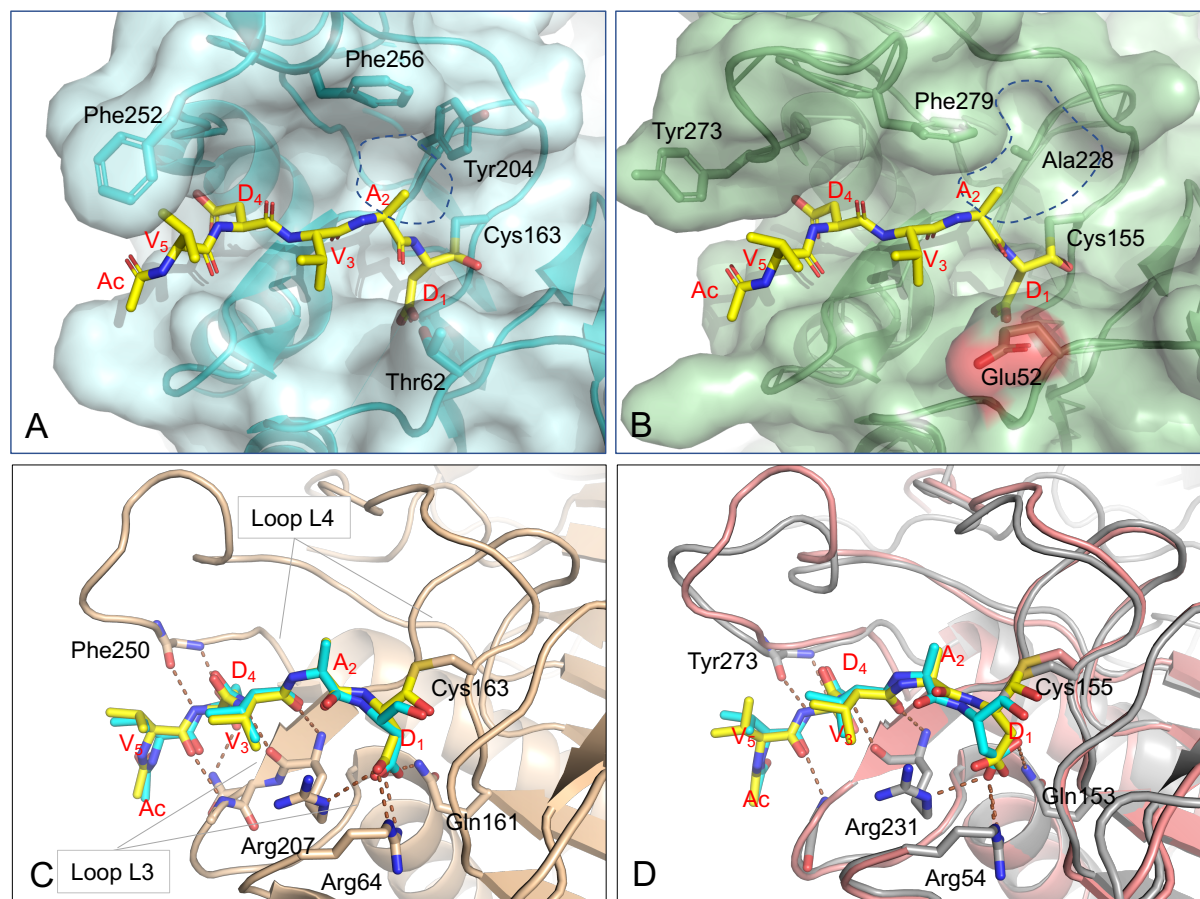
Figure 2.008. A comparison of experimentally determined Casp3 and Casp2 complexes with the same peptidic inhibitor (AcVDVAD-CHO). (**A**) The complex with Casp3 (PDB-id 2h65). (**B**) The complex with Casp2 (PDB-id 3r6g). Sequence differences Y204-A and T62-E result (Casp3 numbering) in an expansion of the P2 subsite (encircled with dashed line), and a change in the electrostatic environment there. (**C**) An overlay of AcVDVAD-CHO complexes with Casp3 (yellow) and Casp2 (cyan). Only the Casp3 backbone and sidechains are shown for clarity. Although most H-bonds are conserved in peptidic complexes with all caspases, H-bonds to the backbone of the L4 loop at Phe250 (Casp3 numbering) from the P4 aspartic acid are also present in Casp2 but are likely not conserved to any great extent. Both complexes are also stabilized by H-bonds from the P4 Asp carboxylate to L3 Asn208 (Asn232 in Casp2), and the P5 valine carbonyl O to the backbone of L3 at Ser209/Thr233. (**D**) An overlay of models of AcVDVAD-CHO binding derived by docking into Casp3 and Casp2. Peptidic inhibitors were docked into respective protein targets (Casp3, salmon, yellow inhibitor; Casp2-gray, cyan inhibitor). The RMS deviation in modeled vs experimentally observed ligand atom positions is 0.78 and 0.84 Å, respectively.

The design strategy arose out of consideration of the cleavage site of the tau protein (GSVQIVYKPVD|LSKVTSKCG-; D|L cleavage site), which creates the Δtau314 associated with Alzheimer's disease. Since Casp2 is the only caspase to catalyze this cleavage, it was anticipated that AcYKPVD-CHO (**2.008**) might be a selective inhibitor. Upon applying covdock protocols, however, AcYKPVD-CHO docking scores predict that binding to both Casp2 and Casp3 enzymes would be significantly weaker (-9.561

(Casp2), -10.126 (Casp3) than binding predicted for the canonical inhibitor AcVDVAD-CHO (**2.016**) (cf. Table 2.05). It was hoped that systematic investigation of hybrid pentapeptides that incorporate some features of **2.008** onto the potent scaffold of **2.016** could lead to more potent and selective inhibitors. AcYKPVD-CHO (**2.008**), AcVDVAD-CHO (**2.016**), and the hybrid molecule AcVDPVD-CHO (**2.017**) (cf. Figure 2.009) served as starting points in the design of a new pentapeptide series by which the gaps in SAR between the three lead compounds can be explored. A series was developed that provides the motifs $V_{(P5)}D_{(P4)}$, $Y_{(P5)}K_{(P4)}$, $V_{(P5)}K_{(P4)}$, or $Y_{(P5)}D_{(P4)}$ for the amino acid positions P5-P4 and the motifs $P_{(P3)}V_{(P2)}D_{(P1)}$, $K_{(P3)}V_{(P2)}D_{(P1)}$ or $V_{(P3)}K_{(P2)}D_{(P1)}$ for the positions P3-P1 (cf. Figure 2.009). To complete the series, individual changes were subsequently made at various positions.
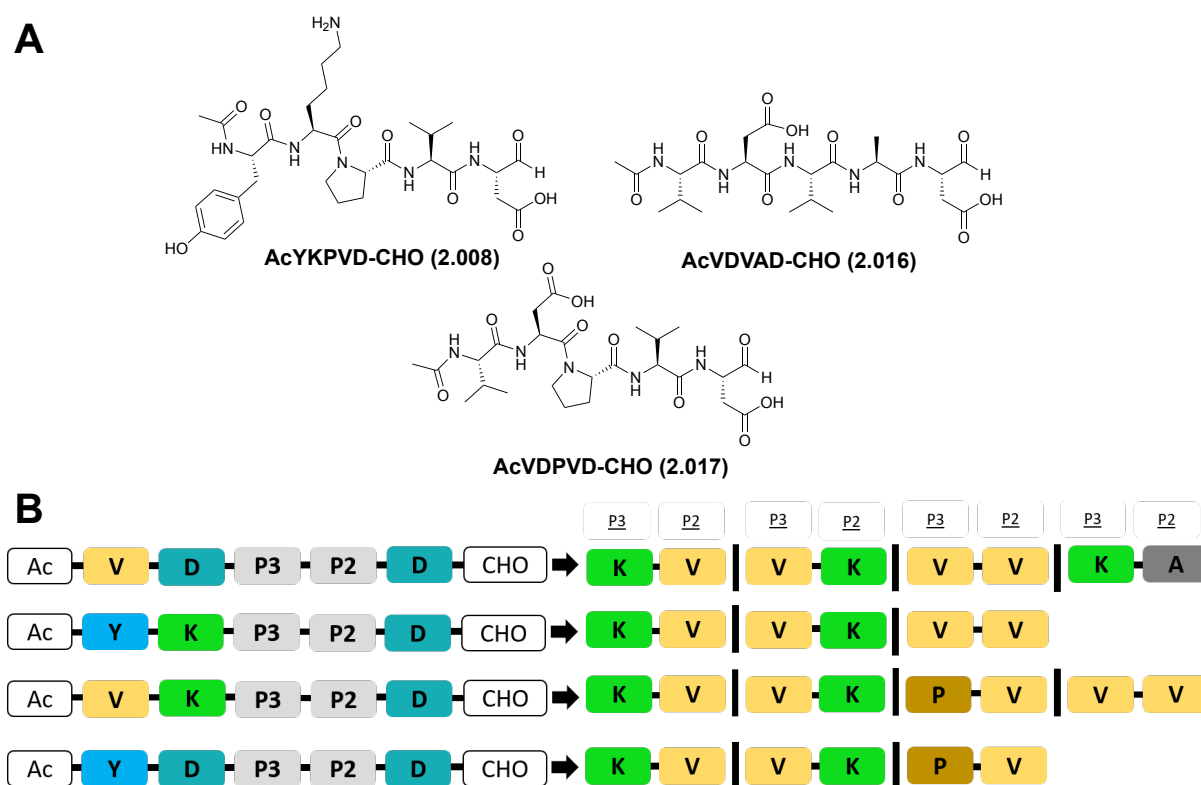
Figure 2.009. (**A**) Caspase-2 lead compounds AcYKPVD-CHO (**2.008**), AcVDVAD-CHO (**2.016**), and AcVDPVD-CHO (**2.017**). (**B**) Substitution pattern of the peptide series derived from AcYKPVD-CHO, AcVDVAD-CHO, and the hybrid peptide AcVDPVD-CHO.

Additionally, seven other selected protein cleavage sequences (cf. Figure 2.010), like Golgin-160[45], Protein transport protein Sec16A[43], Transcriptional-regulating factor 1[43], Ral GTPase-activating protein subunit alpha-1[43], Holliday junction recognition protein[43], and MDM2 (mice/human)[49] were used as starting point for the inhibitor development. The appearance of Casp2 within the nucleus, Golgi, and mitochondria

enables access to other cellular substrates located in these organelles.[52] Many of these cleavage events can also be mediated by Casp3 or other caspases, but some of these peptide sequences have also been reported to be cleaved under physiological conditions only or preferentially by Casp2.[41] These specific sites were selected because of three reasons: (1) specificity of Casp2 cleavage (except for Holliday junction recognition protein which will serve as a control and SAR point), (2) the interest in characterizing arginine-containing sequences since there is evidence due to computational methods that this basic amino acid will interact with Glu52 in the Casp2 binding site, and (3) non-canonical sequences (sequence ≠ -DXXD-) containing lysine at P2 (cf. Table 2.04). The strategy is to start with peptides that represent the cleavage sequences at these sites (cf. Figure 2.010) and modify them to exploit specific features in the Casp2 binding pocket. The presumption that the selected protein cleavage sequences are a good basis for the design of highly active inhibitors is supported by computational docking scores. All of them exhibit a better docking score for Casp2 relative to compound **2.008** (AcYKPVD-CHO). However, no significant trend of Casp2 selectivity can be predicted for the inhibitors (cf. Table 2.05). Shortening the pentapeptides to tetra- and tripeptides is supposed to give more information about the importance of the P5 and P4 positions and the possibility of decreasing molecular weight for small molecules. All inhibitors contain an aldehyde (-CHO) that serves as an electrophilic warhead that reacts with the proteolytic cysteine in the active site in a reversible covalent mechanism. These findings could be eligible to improve the peptide inhibitors with respect to selectivity and pharmacokinetic properties toward peptidomimetic structures.

Table 2.04. Cleavage sequences of selected substrates specifically and/or efficiently cleaved by Caspase-2 and initial synthetic targets.

Protein Name, *UniProt designation*	Sub-Sequence/Sequence **D|X** indicates cleavage site	Initial Synthetic Target	Casp2*	k_{cat}/K_m (M^{-1} s^{-1})**	Ref.
Tau *A0A024RA17* *(A0A024RA17_HUMAN)*	YKPV**D|L** GSVQIVYKPV**D|L**SKVTSKCGSLGNI	AcYKPVD-CHO (**2.008**)	YES	ND	51
Golgin subfamily A member 3 *Q08378 (GOGA3_HUMAN)*	GESP**D|G** NRASTEGESP**D|G**PGQGGLCQNGPTP	AcGESPD-CHO (**2.009**)	YES	3.3×10^4	45
Protein Transport Protein Sec16A *O15027 (SC16A_HUMAN)*	WDRA**D|S** SEAPPGWDRA**D|S**GPTQPPLSLSPAP	AcWDRAD-CHO (**2.010**)	YES	5.4×10^3	43
Transcriptional-regulating factor 1 *Q96PN7 (TREF1_HUMAN)*	QDTR**D|G** ISPHFPQDTR**D|G**LGLPVGSKNLGQM	AcQDTRD-CHO (**2.011**)	YES	1.3×10^3	43
Holliday junction recognition protein *Q8NCD3 (HJURP_HUMAN)*	ADRT**D|G** DSSMKPADRT**D|G**SVQAAAWGPELPS	AcADRTD-CHO (**2.012**)	Casp3 8.3×	1.2×10^3	43
E3 ubiquitin-protein ligase Mdm2 P23804 (MDM2_MOUSE)	LDVP**D|G** AQAEEGLDVP**D|G**KKLTENDAKEPCA	AcLDVPD-CHO (**2.013**)	YES	ND	49
E3 ubiquitin-protein ligase Mdm2 Q00987 (MDM2_HUMAN)	FDVP**D|C** TQAEEGFDVP**D|C**KKTIVNDSRESCV	AcFDVPD-CHO (**2.014**)	YES	ND	49
Ral GTPase-activating protein subunit alpha-1 *Q6GYQ0 (RGPA1_HUMAN)*	ITVK**D|G** NECLEDITVK**D|G**LSLQFKRFRETVP	AcITVKD-CHO (**2.015**)	YES	1.1×10^3	43

*Is the protein sequence cleaved specifically by casp2? **2.012** is cleaved by Casp2 but 8.3× more efficiently by Casp3. **k_{cat}/K_m represents the catalytic efficiency of Casp2. ND = not determined.
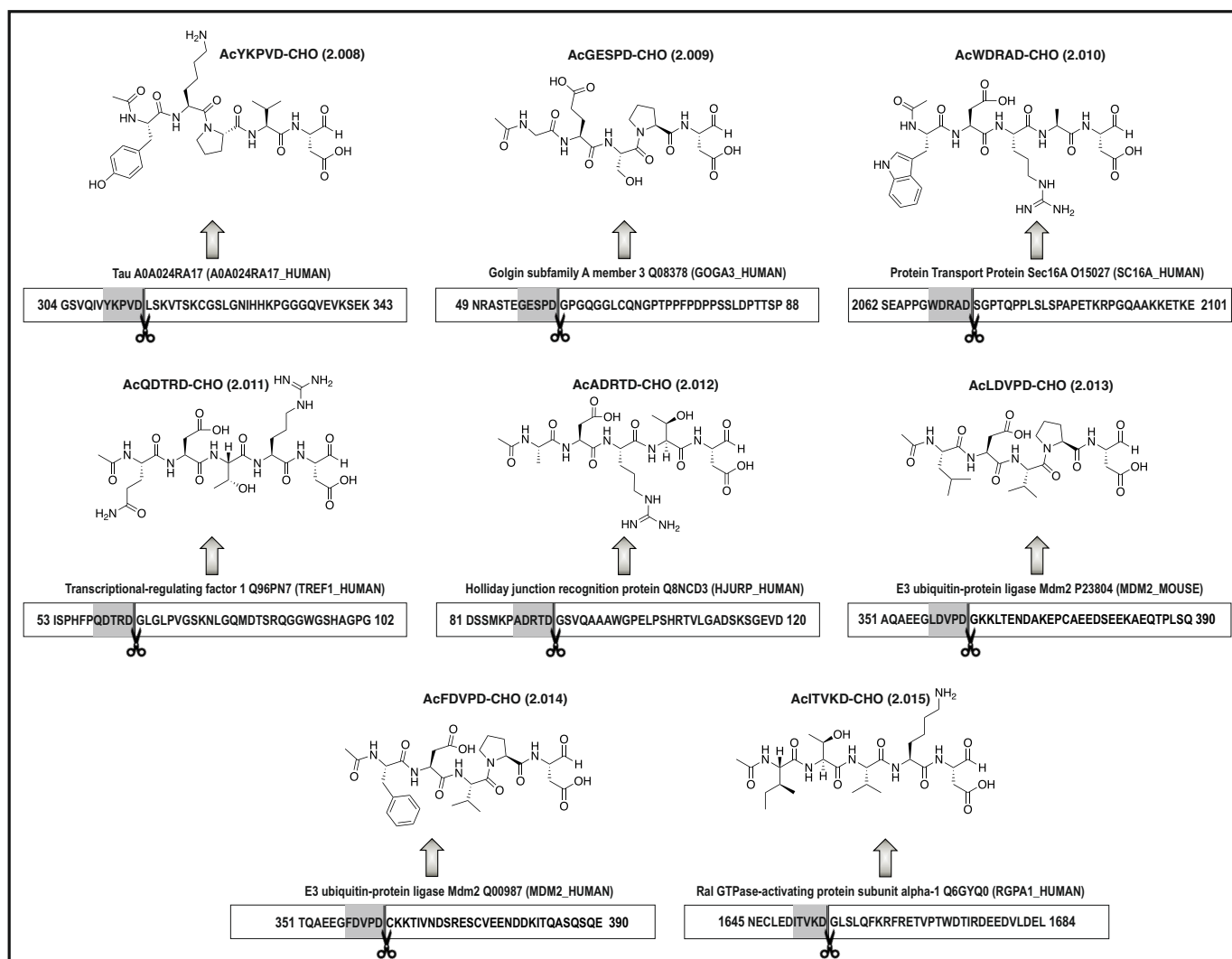
Figure 2.010. Specific Casp2 cleavage sequences of selected natural proteins and the proposed inhibitors: AcYKPVD-CHO (**2.008**), AcGESPD-CHO (**2.009**), AcWDRAD-CHO (**2.010**), AcQDTRD-CHO (**2.011**), AcADRTD-CHO (**2.012**), AcLDVPD-CHO (**2.013**), AcFDVPD-CHO (**2.014**), and AcITVKD-CHO (**2.015**).

Table 2.05. Molecular Modeling of Casp2 and Casp3 and the ligands **2.008-2.015**, **2.043**, **2.059**, and **2.060**.

Sequence	Comp.	Casp2 cdock affinity	Casp3 cdock affinity
AcYKPVD-CHO	**2.008**	-9.561	-10.126
AcGESPD-CHO	**2.009**	-13.073	-12.564
AcWDRAD-CHO	**2.010**	-13.771	-12.706
AcQDTRD-CHO	**2.011**	-15.376	-13.369
AcADRTD-CHO	**2.012**	-13.113	-12.475
AcLDVPD-CHO	**2.013**	-13.080	-13.271
AcFDVPD-CHO	**2.014**	-12.728	-13.634
AcITVKD-CHO	**2.015**	-15.328	-13.100
AcDVPD-CHO	**2.043**	-11.856	-11.896
AcVDKVD-CHO	**2.059**	-14.613	-13.274
AcDKVD-CHO	**2.060**	-12.641	-11.952
Reference compounds			
AcVDVAD-CHO	**2.016**	-13.614	-12.148
AcLDESD-CHO	**2.127**	-13.519	-13.369
AcDEVD-CHO	**2.128**	-13.439	-12.218

Calculation using covalent docking in Schrödinger 2021.3. Casp2 = PDBid: 1pyo, Casp3 = PDBid: 3edq. Proteins and ligands prepared as described in the section Computational Chemistry. cdock affinity = covalent docking affinity (kcals/mol).

2.3.2 Results and Discussion

2.3.2.1 Chemistry

Preparation of aspartic acid loaded semicarbazide amino-Merrifield resin

The synthesis of the aspartic acid loaded semicarbazide amino-Merrifield resin was realized according to the specifications of Marlowe et al. (1998)[101] and Black et al. (2001)[102] with minor modifications in the sequence of the synthesis steps in order to improve the yield (cf. Scheme 2.01).
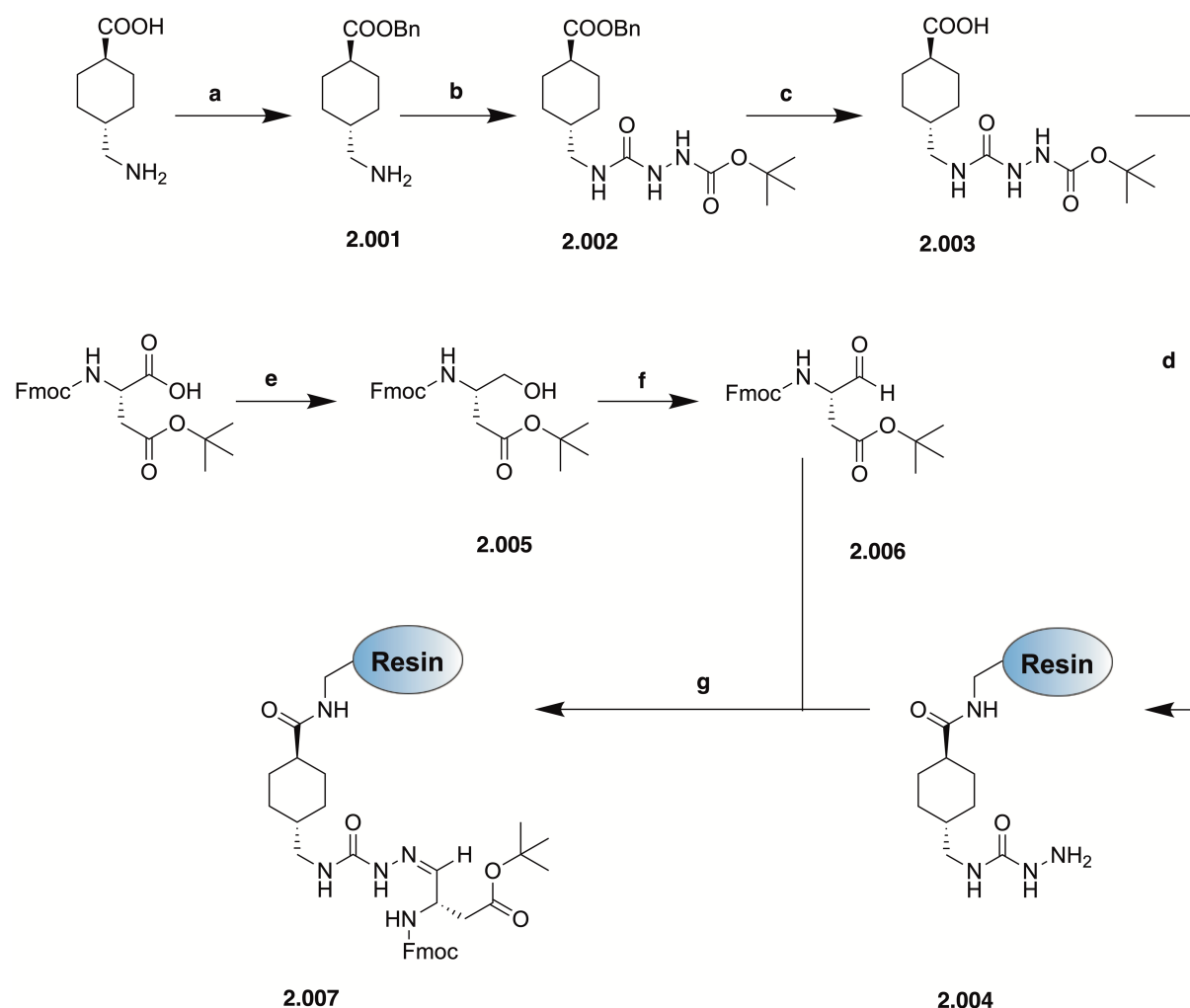
Scheme 2.01. Preparation of the resin: **(a)** Dean-Stark conditions, benzyl alcohol (7.6 eq), *p*-toluenesulfonic acid (2.3 eq), toluene, 150 °C, 3 h; **(b)** CDI (1.2 eq), tert-butylcarbazate (1.2 eq), triethylamine (4.2 eq), DMF, argon, 10 h, rt; **(c)** Pd/C (10%), H_2 (5 bar), MeOH, rt, 15 h; **(d)** (1) EDCI (1.2 eq), HOBt (1.2 eq), amino-Merrifield resin (0.6 eq), DMF, rt, 12 h; (2) trifluoroacetic acid/dichloromethane 1/2 v/v, rt, 2 h; **(e)** N-methylmorpholine (1.10 eq), isobutyl chloroformate (1.05 eq), sodium borohydride (2.10 eq), THF, MeOH, 0 °C → -78 °C; **(f)** oxalyl chloride (1.2 eq), dimethyl sulfoxide (2.2 eq), DIPEA (3.0 eq), DCM, -78 °C, 2 h; **(g)** acetic acid (0.6 eq), THF, rt, 12 h.

Initially, the carboxyl group of (1*r*,4*r*)-4-(aminomethyl)cyclohexane-1-carboxylic acid was esterified with benzyl alcohol using a Dean-Stark trap to collect water formed during the reaction. Subsequently, *tert*-butylcarbazat was coupled to **2.001** using 1,1′-carbonyldiimidazole, leading to the formation of the desired semicarbazide (**2.002**). After hydrogenation of the benzyl group, the semicarbazide linker (**2.003**) was coupled to the amino-Merrifield resin (chloromethylpolystyrene-resin) utilizing 1-ethyl-3-(3-dimethylaminopropyl)carbodiimid (EDCI) and 1-hydroxybenzotriazole (HOBt). Eventually, the *tert*-butyloxycarbonyl protecting group was eliminated from the semicarbazide partial structure by using a mixture of trifluoroacetic acid/dichloromethane. Subsequently, the semicarbazide amino-Merrifield resin (**2.004**) was loaded with an alpha-modified aspartic acid by acetic acid catalyzed reaction of the reactive aldehyde with the semicarbazide. The aldehyde at the alpha position was introduced by reducing aspartic acid to *tert*-butyl (*S*)-3-((((9*H*-fluoren-9-yl)methoxy)carbonyl)amino)-4-hydroxybutanoate (**2.005**) with sodium borohydride. This was followed by a Swern oxidation using oxalyl chloride and dimethyl sulfoxide to form *tert*-butyl (*S*)-3-((((9*H*-fluoren-9-yl)methoxy)carbonyl)amino)-4-oxobutanoate (**2.006**).

Solid-phase peptide synthesis (SPPS) of the penta-, tetra-, and tripeptides

The peptides were synthesized by manual solid-phase peptide synthesis (SPPS) on an aspartic acid-loaded amino-Merrifield resin in accordance with the standard Fmoc strategy (cf. Scheme 2.02). The Fmoc protection group of the N-terminal amino acid was deprotected with piperidine 20% in DMF (**a**). The amino acids were coupled to the amino-Merrifield resin by using HATU/DIPEA or Oxyma/DIC (**b**). The deprotecting and coupling steps were repeated until the desired tri-, tetra-, or pentapeptide was built up. Finally, the N-terminus was acetylated by using acetic anhydride (**c**). Subsequently, the peptides were cleaved from the resin, and the side chains of the amino acids were deprotected by treatment with trifluoroacetic acid (90%) in water (**d**). The chemical stability of selected peptides was analyzed at room temperature for 28 days and is illustrated in chapter **2.7.2.2** (cf. Figures 2.269-2.274).

tripeptides   **tetrapeptides**
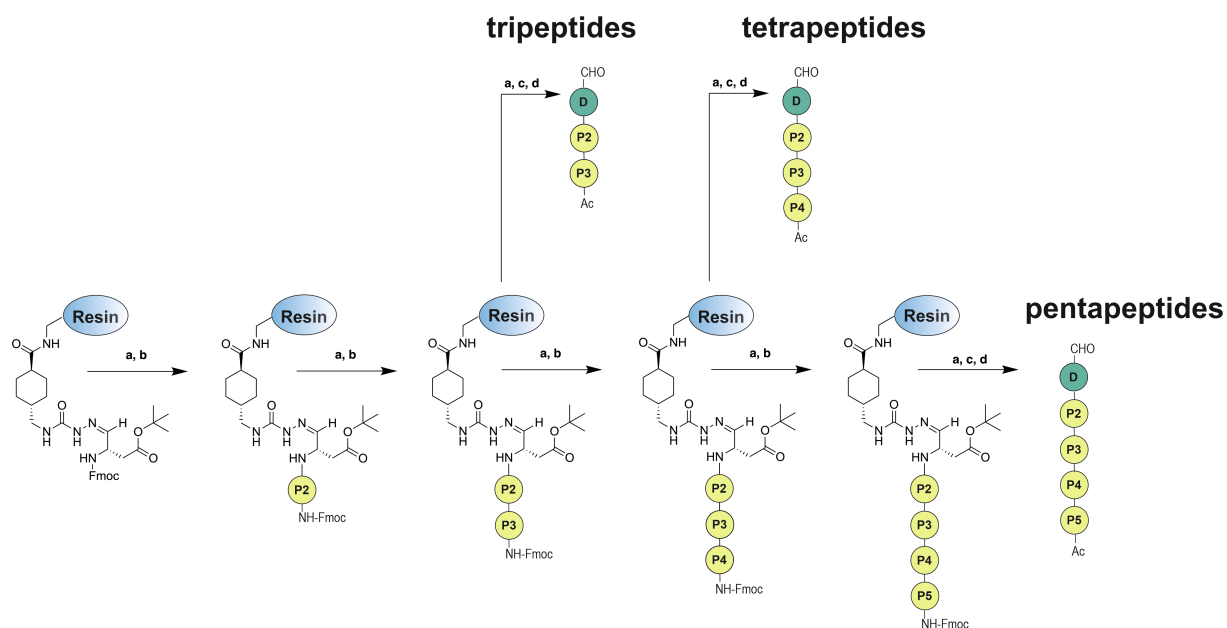
Scheme 2.02. Preparation of the peptides on the modified amino-Merrifield resin: **(a)** piperidine 20% in DMF, 35 °C ,15 min; **(b)** amino acid (5 eq), HATU/DIPEA (5/5 eq) or Oxyma/DIC (5/5 eq), DMF/NMP (8/2 v/v), 35 °C, 45 min (single coupling); **(c)** acetic anhydride (10 eq), DIPEA (10 eq), DMF, rt, 30 min; **(d)** trifluoroacetic acid (90% in water), rt, 1 h.

2.3.2.2 Inhibitory Affinity of Compound 2.008-2.062 in a Fluorometric Enzyme Assay

The peptide inhibitors were investigated in a fluorescence-based enzyme inhibition assay using Casp1, Casp2, Casp3, Casp6, Casp7, and Casp9 to elucidate their structure-activity relationships and selectivity profile. The results are presented as binding constants (pK_i values) in Table 2.06 and Table 2.07. The assumption that AcYKPVD-CHO (**2.008**), derived from the cleavage site of the tau protein (GSVQIVYKPVD|LSKVTSKCG-; D|L cleavage site), potentially is a highly active and selective inhibitor for Casp2 was disproved. **2.008** demonstrates no activity for Casp2 (pK_i: 4.56) and Casp3 (pK_i: 4.73). Further pentapeptide inhibitors based on natural proteins (cf. Figure 2.010) cleaved by Casp2 resulted in a series of inhibitors with distinct affinities. While the peptides AcLDVPD-CHO (**2.013**) and AcFDVPD-CHO (**2.014**) derived from the MDM2 protein (mouse/human) show high affinities for both Casp2 (pK_i: 7.88/7.66 and 8.15/8.03) and Casp3 (pK_i: 8.16 and 8.52), the inhibitors based on the protein Golgin subfamily A member 3 AcGESPD-CHO (**2.009**) and Ral GTPase-activating protein subunit alpha-1 AcITVKD-CHO (**2.015**) demonstrate lower affinities for Casp2 (pK_i: 5.23 and 6.40) and Casp3 (pK_i: 6.73 and 6.05) (cf. Table 2.06). Interestingly, **2.015** is the first Casp2 inhibitor within the series with the absence of

aspartic acid (Asp) at position 4, showing a moderate affinity for Casp2. The inhibitors AcWDRAD-CHO (**2.010**) (based on Protein Transport Protein Sec16A), AcQDTRD-CHO (**2.011**) (based on Transcriptional-regulating factor 1), and AcADRTD-CHO (**2.012**) (based on Holliday junction recognition protein) have a moderate inhibitory affinity for Casp2 (pK_i value of 6.73-7.34) with approximately the same affinity for Casp3 (pK_i value of 7.00-7.34) (cf. Table 2.06). All natural proteins were selected because of their specificity of Casp2 cleavage except for the Holliday junction recognition protein, which serves as a control and SAR point. Apart from this, compounds **2.009**-**2.014** show a lack of selectivity for Casp2 (selectivity ranging from 0.03 to 1.00), as already seen for the canonical inhibitor AcVDVAD-CHO (**2.016**, Casp2 pK_i: 7.85; Casp3 pK_i: 7.73) (cf. Table 2.06 and Figure 2.011). Only AcITVKD-CHO (**2.015**) exhibits a marginal tendency for Casp2 with a selectivity factor of 2 (cf. Table 2.06 and Figure 2.011).
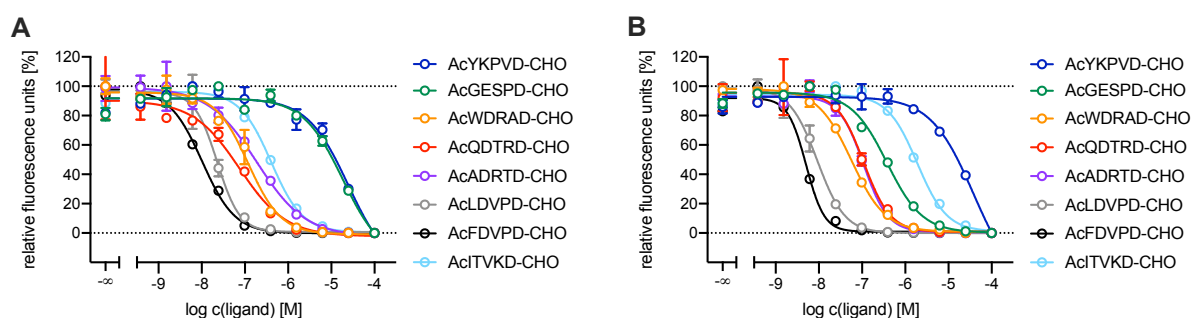
Figure 2.011. Concentration-response curves of AcYKPVD-CHO (**2.008**), AcGESPD-CHO (**2.009**), AcWDRAD-CHO (**2.010**), AcQDTRD-CHO (**2.011**), AcADRTD-CHO (**2.012**), AcLDVPD-CHO (**2.013**), AcFDVPD-CHO (**2.014**), and AcITVKD-CHO (**2.015**) at Casp2 (**A**) and Casp3 (**B**) in the fluorometric enzyme assay. Data points represent mean values ± SD from representative experiments, each performed in duplicate.

The alternation of valine in position 5, coming from the canonical inhibitor AcVDVAD-CHO (**2.016**), with tyrosine and isoleucine, resulted in a series of peptides that demonstrate no significant changes with respect to affinity. AcVDVKD-CHO (**2.061**), AcYDVKD-CHO (**2.028**), and AcIDVKD-CHO (**2.058**) have high inhibitory affinity at Casp2 (pK_i value of 7.63-7.83) with a slight tendency toward selectivity for Casp2 (selectivity ranging from a factor of 5.06-7.53) as opposed to Casp3. Furthermore, AcVDKVD (**2.059**) and AcYDKVD-CHO (**2.027**) show high affinity at Casp2 (pK_i: 7.40 and 7.39/7.18). However, they have a lack of selectivity (factor of 1.32 and 0.44/0.27) in comparison to the before mentioned peptides (cf. Table 2.06). This suggests that

valine at position 5 is not crucial for the inhibitor and can be exchanged with tyrosine and isoleucine, whereas the substitution of aspartic acid at position 4 by lysine, coming from the tau cleavage sequence YKPVD leads to a loss of affinity at Casp2 and Casp3 for all peptides. AcVKVVD-CHO (**2.022**), AcVKKVD-CHO (**2.023**), and AcVKVKD-CHO (**2.024**) show no affinity at Casp2 in comparison to AcVDVVD-CHO (**2.018**), AcVDKVD-CHO (**2.059**), and AcVDVKD-CHO (**2.061**) (cf. Table 2.06). The same applies to AcYKKVD-CHO (**2.020**) and AcYKVKD-CHO (**2.021**) in contrast to AcYDKVD-CHO (**2.027**) and AcYDVKD-CHO (**2.028**) (cf. Table 2.06). Moreover, the peptides AcYKVVD-CHO (**2.026**) and AcVKPVD-CHO (**2.025**) demonstrate no affinity for Casp2 (cf. Table 2.06). AcYDVVD-CHO (**2.036**) on the other hand, reveals a high affinity for Casp2 (pK_i: 7.50) and Casp3 (pK_i: 8.43), with no trend for Casp2 selectivity. The peptide AcYKPVD-CHO (**2.008**), emanated from the optimal cleavage sequence of Casp2 for the tau protein, as well as the peptides AcVDPVD-CHO (**2.017**), AcVKPVD-CHO (**2.025**), AcYDPVD-CHO (**2.029**), AcVDPPD-CHO (**2.034**), and AcVDPKD-CHO (**2.035**) indicate that proline at position 3 is also not tolerated at Casp2 and Casp3 (cf. Table 2.06). For example, AcVDKPD-CHO (**2.033**) (Casp2 pK_i: 7.66/7.38; Casp3 pK_i: 7.70) has a high affinity at Casp2 and Casp3, whereas AcVDPKD-CHO (**2.035**) (Casp2 pK_i: < 4; Casp3 pK_i: < 4) leads to a significant loss in affinity by switching proline from position 2 to position 3. In addition, it was unveiled that the exchange of valine at P2 and/or P5 by threonine, phenylalanine, alanine, and isoleucine of compound **2.059** is tolerated. AcTDKTD-CHO (**2.030**), AcVDKID-CHO (**2.031**), AcVDKAD-CHO (**2.019**), and AcVDKFD-CHO (**2.032**) exhibit high affinity at Casp2 and Casp3, without any notable trend toward selectivity (cf. Table 2.06).

The inhibitors derived from the natural cleavage sequences (except AcYKPVD-CHO (**2.008**) and AcGESPD-CHO (**2.009**)) were truncated to verify the extent to which this affects the affinities for Casp2 and Casp3. The purpose of shortening was to make the molecules more drug-like with respect to Lipinski's rule of 5[103] and to pave the way for future small molecules. Truncations of **2.010** resulted in the tetrapeptide AcDRAD-CHO (**2.037**) and the tripeptide AcRAD-CHO (**2.038**). While **2.037** continues to show affinity for Casp2 (pK_i: 6.39/5.97) and Casp3 (pK_i: 6.59), **2.038** evidenced a sharp loss in affinity for Casp2 (pK_i: < 4) and Casp3 (pK_i: < 4). The same can be observed for the tetrapeptides AcDTRD-CHO (**2.039**), AcDRTD-CHO (**2.041**), and AcDVPD-CHO (**2.043**) (Casp2 pK_i: 6.35/6.16, 5.80/5.60, and 6.44/6.33; Casp3 pK_i: 7.09, 7.09, and

8.18) and the respective tripeptides AcTRD-CHO (**2.040**), AcRTD-CHO (**2.042**), and AcVPD-CHO (**2.044**) (Casp2 pK_i: <4; Casp3 pK_i: < 4, 4.96, and 5.24) (cf. Table 2.06). The peptide AcTVKD-CHO (**2.045**) represents a slightly lower affinity for Casp2 (pK_i: 5.11) and Casp3 (pK_i: 4.95) compared to the other tetrapeptides, which can be explained by the absence of aspartic acid at position 4. In turn, the tripeptide AcVKD-CHO (**2.046**) completely loses its affinity for Casp2 (pK_i: < 4) and Casp3 (pK_i: < 4) (cf. Table 2.06). It can be summarized that the truncation of the pentapeptides by one amino acid is tolerated for all tetrapeptides (**2.037**, **2.039**, **2.041**, and **2.043**) containing an aspartic acid at position 4. The loss of affinity for Casp2 and Casp3 is somewhat greater for tetrapeptides having threonine at position 4 (e.g., AcTVKD-CHO (**2.045**)). However, the truncation by a further amino acid is accompanied by a sharp loss in affinity for all tripeptides (**2.038**, **2.040**, **2.042**, **2.044**, and **2.046**). Overall, a more significant decrease in Casp2 affinity (ranging from 0.67-1.70 logarithmic units) than Casp3 (ranging from 0.20-0.75 logarithmic units) can be observed for all tetrapeptides. In the case of AcDRTD-CHO (**2.041**) and AcDVPD-CHO (**2.043**) even a slight increase (ranging from 0.02-0.09 logarithmic units) in Casp3 affinity can be observed compared to AcADRTD-CHO (**2.012**) and AcLDVPD-CHO (**2.013**) (cf. Table 2.06). These observations go hand in hand with the assumption that a motif of five amino acids is required for efficient Casp2 inhibition. Regarding the tetrapeptide's selectivity between Casp2 and Casp3, it can be observed that **2.037**, **2.039**, **2.041**, and **2.043** are showing a trend toward Casp3 selectivity (2-71-fold), whereas **2.045** demonstrates no trend in selectivity (cf. Table 2.06). AcDVKD-CHO (**2.062**) and AcDKVD-CHO (**2.060**) are the corresponding tetrapeptides of the peptides AcVDVKD-CHO (Casp2 pK_i: 7.63; Casp3 pK_i: 6.91) and AcVDKVD-CHO (Casp2 pK_i: 7.40; Casp3 pK_i: 7.28). While AcDVKD-CHO (**2.062**) and AcDKVD-CHO (**2.060**) show a significant decrease in affinity for Casp2 (pK_i: 6.05 and 5.61/5.22), the affinity for Casp3 (pK_i: 6.61 and 7.79) conserves. In the case of **2.060**, the affinity for Casp3 even increases, making the tetrapeptide a selective Casp3 inhibitor with a selectivity factor of 151 or 371, respectively. Since AcITVKD-CHO (**2.015**) shows the best Casp2 selectivity profile within the inhibitors derived from natural proteolysis sequences of Casp2, further inhibitors based on **2.015** were developed to gain more insight into the structure-activity relationships between the inhibitors and the Casp2/Casp3 binding site. Moreover, **2.015** is the only reasonably active Casp2 inhibitor that does not contain an aspartic acid at the P4 position, which should be beneficial for its pharmacokinetic properties.

Valine at position P3 was replaced by glycine and alanine. At the same time, the peptides were shortened to tetra- and tripeptides. This resulted in AcITGKD-CHO (**2.049**), AcTGKD-CHO (**2.050**), AcGKD-CHO (**2.051**), AcITAKD-CHO (**2.052**), AcTAKD-CHO (**2.053**), and AcAKD-CHO (**2.054**). The pentapeptide **2.049** (Casp2 pK_i: 5.57; Casp3 pK_i: 5.75) shows slightly lower affinity for Casp2 and Casp3 than **2.015** (Casp2 pK_i: 6.40; Casp3 pK_i: 6.05), whereas the affinities maintained for **2.052** (Casp2 pK_i: 6.63; Casp3 pK_i: 6.27). Tetrapeptides **2.050** (Casp2 pK_i: 4.96; Casp3 pK_i: 5.47) and **2.053** (Casp2 pK_i: 5.79; Casp3 pK_i: 5.92) show lower affinities for Casp2 and Casp3 than the corresponding pentapeptides (cf. Table 2.06) but the affinity decrease is more pronounced for Casp2 (0.61 and 0.84) than for Casp3 (0.28 and 0.37). The tripeptides **2.051** and **2.054** demonstrate no affinity for Casp2 (pK_i: < 4) and Casp3 (pK_i: < 4). Furthermore, isoleucine at position P5 was replaced by alanine resulting in AcATVKD-CHO (**2.055**, Casp2 pK_i: 5.86; Casp3 pK_i: 5.93). Additionally, serine was installed at position P2, but the expected selectivity advantage for Casp2 described by Poreba et al. (2019)[93] could not be determined for AcITVSD-CHO (**2.056**, Casp2 pK_i: 6.01; Casp3 pK_i: 6.24) (cf. Table 2.06). To elucidate further structure-activity relationships, modifications starting from the canonical inhibitor AcVDVAD-CHO (**2.016**, Casp2 pK_i: 7.85; Casp3 pK_i: 7.73) were carried out. First, the pentapeptide was truncated to a tetra- and tripeptide, resulting in AcDVAD-CHO (**2.047**) and AcVAD-CHO (**2.048**). **2.047** demonstrates a massive loss of affinity for Casp2 (pK_i: 5.95) by 2 logarithmic units, while the affinity for Casp3 (pK_i: 7.37) is almost completely preserved (cf. Table 2.06). Thus, AcDVAD-CHO (**2.047**) shows a selectivity factor of 26 for Casp3 over Casp2. The tripeptide **2.048** completely loses its inhibitory affinity for Casp2 (pK_i: < 4) and Casp3 (pK_i: < 4). In another attempt to gain selectivity for Casp2, serine at position P2 of the canonical inhibitor was incorporated, but once again, the desired effect could not be detected for AcVDVSD-CHO (**2.057**, Casp2 pK_i: 7.26; Casp3 pK_i: 7.29) (cf. Table 2.06).

Table 2.06. Binding data (pK_i values) and selectivity ratios of peptides **2.008**-**2.062** at Casp2 and Casp3.

| Sequence | Comp. | pK_i ± SEM | | | | Selectivity ratios of K_i (Casp2: Casp3) |
		Casp2	N	Casp3	N	
AcYKPVD-CHO	**2.008**	4.56 ± 0.22[a]	3	4.73 ± 0.05	4	1:1
AcGESPD-CHO	**2.009**	5.23 ± 0.12[a]	4	6.73 ± 0.14	3	32:1
AcWDRAD-CHO	**2.010**	7.34 ± 0.04[a]	2	7.34 ± 0.05	4	1:1
		6.99 ± 0.05[b]	2			2:1
AcQDTRD-CHO	**2.011**	7.02 ± 0.06[a]	3	7.14 ± 0.16	3	1:1
AcADRTD-CHO	**2.012**	6.73 ± 0.05[a]	3	7.00 ± 0.09	3	2:1
AcLDVPD-CHO	**2.013**	7.88 ± 0.01[a]	2	8.16 ± 0.04	4	2:1
		7.66 ± 0.02[b]	2			3:1
AcFDVPD-CHO	**2.014**	8.15 ± 0.09[a]	2	8.52 ± 0.06	4	2:1
		8.03 ± 0.07[b]	2			3:1
AcITVKD-CHO	**2.015**	6.40 ± 0.16[a]	4	6.05 ±0.06	4	1:2
AcVDVAD-CHO	**2.016**	7.85 ± 0.03[a]	5	7.73 ± 0.04	5	1:1
AcVDPVD-CHO	**2.017**	4.82 ± 0.08[a]	2	5.70 ± 0.03	2	8:1
AcVDVVD-CHO	**2.018**	7.77 ± 0.06[a]	4	7.81 ± 0.07	4	1:1
AcVDKAD-CHO	**2.019**	7.35[a]	1	7.22 ± 0.13	3	1:1
		7.09 ± 0.08[b]	2			1:1
AcYKKVD-CHO	**2.020**	< 4[a]	2	< 4.5	2	-
AcYKVKD-CHO	**2.021**	< 4[a]	1	< 4	2	-
		< 4[b]	1			
AcVKVVD-CHO	**2.022**	< 4[b]	2	5.16 ± 0.04	2	> 14:1
AcVKKVD-CHO	**2.023**	< 4[a]	1	4.78 ± 0.02	2	> 6:1
		< 4[b]	1			
AcVKVKD-CHO	**2.024**	< 4[a]	2	< 4	2	-
AcVKPVD-CHO	**2.025**	< 4[a]	2	4.88 ± 0.03	2	> 8:1

Table 2.06 (continued)

Sequence	Comp.	pK$_i$ ± SEM				Selectivity ratios of K$_i$ (Casp2: Casp3)
		Casp2	N	Casp3	N	
AcYKVVD-CHO	**2.026**	< 4[b]	2	5.31 ± 0.05	2	> 20:1
AcYDKVD-CHO	**2.027**	7.39 ± 0.01[a]	2	7.75 ± 0.07	3	2:1
		7.18[b]	1			4:1
AcYDVKD-CHO	**2.028**	7.83 ± 0.02[a]	4	7.13 ± 0.01	4	1:5
AcYDPVD-CHO	**2.029**	< 4[a]	1	5.61 ± 0.03	2	> 40:1
		< 4[b]	1			
AcTDKTD-CHO	**2.030**	6.84 ± 0.12[a]	2	7.03 ± 0.04	3	1:2
		6.53[b]	1			3:1
AcVDKID-CHO	**2.031**	7.57 ± 0.03[a]	2	7.57 ± 0.11	3	1:1
		7.16[b]	1			3:1
AcVDKFD-CHO	**2.032**	7.24 ± 0.04[a]	2	7.34 ± 0.04	3	1:1
		6.78[b]	1			4:1
AcVDKPD-CHO	**2.033**	7.66 ± 0.02[a]	2	7.70 ± 0.14	3	1:1
		7.38[b]	1			2:1
AcVDPPD-CHO	**2.034**	< 4[a]	2	< 4.5	2	-
AcVDPKD-CHO	**2.035**	< 4[a]	1	< 4	2	-
		< 4[b]	1			
AcYDVVD-CHO	**2.036**	7.50 ± 0.02[b]	3	8.43 ± 0.04	3	8:1
AcDRAD-CHO	**2.037**	6.39[a]	1	6.67 ± 0.08	3	2:1
		5.99 ± 0.02[b]	2			5:1
AcRAD-CHO	**2.038**	< 4[a]	1	< 4	2	-
		< 4[b]	2			-
AcDTRD-CHO	**2.039**	6.35 ± 0.03[a]	2	7.09 ± 0.05	3	5:1
		6.32 ± 0.16[b]	2			5:1
AcTRD-CHO	**2.040**	< 4[a]	2	< 4	2	-
AcDRTD-CHO	**2.041**	5.80 ± 0.02[a]	2	7.09 ± 0.05	3	18:1
		5.49 ± 0.11[b]	2			39:1
AcRTD-CHO	**2.042**	< 4[b]	2	4.96 ± 0.09	2	> 9:1
AcDVPD-CHO	**2.043**	6.44 ± 0.01[a]	2	8.18 ± 0.12	4	55:1
		6.33 ± 0.03[b]	2			71:1
AcVPD-CHO	**2.044**	< 4[b]	2	5.24 ± 0.04	2	> 17:1
AcTVKD-CHO	**2.045**	5.11 ± 0.04[a]	2	4.95 ± 0.04	2	1:1

Table 2.06 (continued)

| Sequence	Comp.	pK_i ± SEM				Selectivity ratios of K_i (Casp2: Casp3)
		Casp2	N	Casp3	N	
AcVKD-CHO	**2.046**	< 4[a]	2	< 4	2	-
AcDVAD-CHO	**2.047**	5.95 ± 0.19[b]	3	7.37 ± 0.11	3	26:1
AcVAD-CHO	**2.048**	< 4[b]	2	< 4	2	-
AcITGKD-CHO	**2.049**	5.57 ± 0.01[a]	2	5.75 ± 0.22	2	2:1
AcTGKD-CHO	**2.050**	4.96 ± 0.03[a]	2	5.47 ± 0.02	2	3:1
AcGKD-CHO	**2.051**	< 4[a]	1	< 4	2	-
		< 4[b]	2			-
AcITAKD-CHO	**2.052**	6.63 ± 0.04[a]	3	6.27 ± 0.05	3	1:2
AcTAKD-CHO	**2.053**	5.79 ± 0.10[a]	2	5.92 ± 0.01	2	1:1
AcAKD-CHO	**2.054**	< 4[a]	1	< 4	2	-
		< 4[b]	2			-
AcATVKD-CHO	**2.055**	5.86 ± 0.03[b]	2	5.93 ± 0.05	2	1:1
AcITVSD-CHO	**2.056**	6.01 ± 0.10[b]	3	6.24 ± 0.04	3	2:1
AcVDVSD-CHO	**2.057**	7.26 ± 0.06[b]	3	7.29 ± 0.03	3	1:1
AcIDVKD-CHO	**2.058**	7.68 ± 0.02[a]	4	6.80 ± 0.05	4	1:8
AcVDKVD-CHO	**2.059**	7.40 ± 0.01[a]	5	7.28 ± 0.09	4	1:1
AcDKVD-CHO	**2.060**	5.61 ± 0.06[a]	2	7.79 ± 0.02	4	151:1
		5.22 ± 0.03[b]	2			371:1
AcVDVKD-CHO	**2.061**	7.63 ± 0.02[a]	4	6.91 ± 0.04	4	1:5
AcDVKD-CHO	**2.062**	6.05 ± 0.07[b]	3	6.61 ± 0.03	3	4:1

Data shown are mean values ± SEM of N independent experiments, each performed in duplicate or triplicate. Data were analyzed by nonlinear regression and and were best fitted to sigmoidal concentration−response curves using 4PL regression using GraphPad Prism. [a]Data represent pK_i values determined with Casp2. [b]Data represent pK_i values determined with cpCasp2. Saturation binding curves of the enzymes can be seen in chapter **2.7.5** (cf. Figures 2.286, 2.287, and 2.288).

Table 2.07. Binding data (pK_i values) of selected peptides (**2.008**-**2.016**, **2.018**, **2.028**, **2.043**, **2.052**, **2.058**, **2.059**, **2.060**, and **2.061**) at Casp1, Casp6, Casp7, and Casp9.

Sequence	Comp.	pK_i ± SEM							
		Casp1	*N*	*Casp6*	*N*	*Casp7*	*N*	*Casp9*	*N*
AcYKPVD-CHO	**2.008**	< 4	2	< 4	2	4.53 ± 0.14[a]	2	< 4.5[a]	2
AcGESPD-CHO	**2.009**	6.52 ± 0.10	2	< 4	2	5.72 ± 0.01	2	5.61 ± 0.11	2
AcWDRAD-CHO	**2.010**	6.48 ± 0.02	2	4.64 ± 0.03	2	6.83 ± 0.01	2	4.96 ± 0.05	2
AcQDTRD-CHO	**2.011**	5.51 ± 0.01	2	< 4	2	6.55 ± 0.03	2	< 4	2
AcADRTD-CHO	**2.012**	5.83 ± 0.07	2	< 4	2	6.93 ± 0.07	2	4.81 ± 0.14	2
AcLDVPD-CHO	**2.013**	7.30 ± 0.02	2	4.57 ± 0.08	2	7.68 ± 0.01	2	5.66 ± 0.10	2
AcFDVPD-CHO	**2.014**	7.34 ± 0.07	2	4.85 ± 0.04	2	8.07 ± 0.11	2	5.98 ± 0.57	2
AcITVKD-CHO	**2.015**	6.35 ± 0.06	2	5.48 ± 0.07	2	5.25 ± 0.14	2	4.46 ± 0.35	2
AcVDVAD-CHO	**2.016**	7.06 ± 0.04[a]	2	< 4[a]	2	7.08 ± 0.04[a]	2	5.57 ± 0.22[a]	2
AcVDVVD-CHO	**2.018**	6.61 ± 0.09	2	4.93 ± 0.01	2	7.63 ± 0.05	2	5.52 ± 0.51	2
AcYDVKD-CHO	**2.028**	6.34 ± 0.01	2	< 4	2	7.04 ± 0.01	2	4.72 ± 0.02	2
AcDVPD-CHO	**2.043**	7.15 ± 0.05	2	< 4	2	7.74 ± 0.07	2	6.32 ± 0.08	2
AcITAKD-CHO	**2.052**	5.84 ± 0.04	2	4.69 ± 0.02	2	5.48 ± 0.02	2	4.59 ± 0.12	2
AcIDVKD-CHO	**2.058**	6.05 ± 0.02	2	< 4	2	6.25 ± 0.08	2	< 4.5	2
AcVDKVD-CHO	**2.059**	5.97 ± 0.08	2	< 4	2	7.28 ± 0.07	2	4.77 ± 0.35	2
AcDKVD-CHO	**2.060**	6.17 ± 0.06	2	< 4	2	7.51 ± 0.10	2	5.41 ± 0.05	2
AcVDVKD-CHO	**2.061**	6.18 ± 0.14	2	< 4	2	6.25 ± 0.05	2	< 4.5	2

Data shown are mean values ± SEM of N independent experiments, each performed in duplicate or triplicate. Data were analyzed by nonlinear regression and were best fitted to sigmoidal concentration−response curves using 4PL regression using GraphPad Prism. Saturation binding curves of the enzymes can be seen in chapter **2.7.5** (cf. Figures 2.285 and 2.289-2.291).

In addition, a panel assay at Casp1, Casp6, Casp7, and Casp9 (cf. Table 2.07) was carried out for selected peptides (**2.008**-**2.016**, **2.018**, **2.028**, **2.043**, **2.052**, **2.058**, **2.059**, **2.060**, and **2.061**). The peptide AcYKPVD-CHO (**2.008**) shows no major affinity for Casp1, Casp6, Casp7, and Casp9, while the canonical inhibitor AcVDVAD-CHO (**2.016**) is active at Casp1 (pK_i: 7.06), Casp7 (pK_i: 7.08), and Casp9 (pK_i: 5.57) (cf. Table 2.07 and Figure 2.012). The pentapeptides AcGESPD-CHO (**2.009**) and AcADRTD-CHO (**2.012**) display moderate inhibitory affinities for Casp1 (pK_i: 6.52 and 5.83), Casp7 (pK_i: 5.72 and 6.93), and Casp9 (pK_i: 5.61 and 4.81) and no affinity for Casp6 (pK_i: < 4). AcWDRAD-CHO (**2.010**) and AcQDTRD-CHO (**2.011**) exhibit moderate affinities for Casp1 (pK_i: 6.48 and 5.51) and Casp7 (pK_i: 6.83 and 6.55) and low affinities for Casp6 (pK_i: 4.64 and < 4) and Casp9 (pK_i: 4.96 and < 4) (cf. Table 2.07 and Figure 2.012). AcLDVPD-CHO (**2.013**, Casp1 pK_i: 7.30; Casp6 pK_i: 4.57; Casp7 pK_i: 7.68; Casp9 pK_i: 5.66) and AcFDVPD-CHO (**2.014**, Casp1 pK_i: 7.34; Casp6 pK_i: 4.85; Casp7 pK_i: 8.07; Casp9 pK_i: 5.98) derived from the MDM2 protein (mouse/human) are highly active for Casp1 and Casp7. The affinity for Casp9 is lower, while for Casp6 no noticeable affinity can be observed (cf. Table 2.07 and Figure 2.012). The peptide AcITVKD-CHO (**2.015**) exhibits moderate to low affinity for Casp1 (pK_i: 6.35), Casp6 (pK_i: 5.48), Casp7 (pK_i: 5.25), and Casp9 (pK_i: 4.46). The tetrapeptide AcDVPD-CHO (**2.043**, Casp1 pK_i: 7.15; Casp6 pK_i: < 4; Casp7 pK_i: 7.74; Casp9 pK_i: 6.32) shows a similar affinity profile as AcLDVPD-CHO (**2.013**) and AcFDVPD-CHO (**2.014**) (cf. Table 2.07). Finally, AcITAKD-CHO (**2.052**) demonstrates moderate to low affinities for Casp1 (pK_i: 5.84), Casp6 (pK_i: 4.69), Casp7 (pK_i: 5.48), and Casp9 (pK_i: 4.59) (cf. Table 2.07 and Figure 2.012) and AcDKVD-CHO (**2.060**) displays high affinity for Casp7 (pK_i: 7.51), moderate affinity for Casp1 (pK_i: 6.17), Casp9 (pK_i: 5.41), and low affinity for Casp6 (pK_i: < 4) (cf. Table 2.07). AcVDKVD-CHO (**2.059**) and AcVDVKD-CHO (**2.061**) exhibit inhibitory affinity at Casp1 (pK_i: 5.97 and 6.18), Casp7 (pK_i: 7.28 and 6.25), and Casp9 (pK_i: 4.77 and < 4.5), and no affinity at Casp6 (pK_i: < 4). Further panel results are summarized in Table 2.07 Displacement curves from representative competition binding experiments (Casp1, Casp2, Casp3, Casp6, Casp7, and Casp9) are displayed in chapter **2.7.6** (cf. Figures 2.292-2.327).
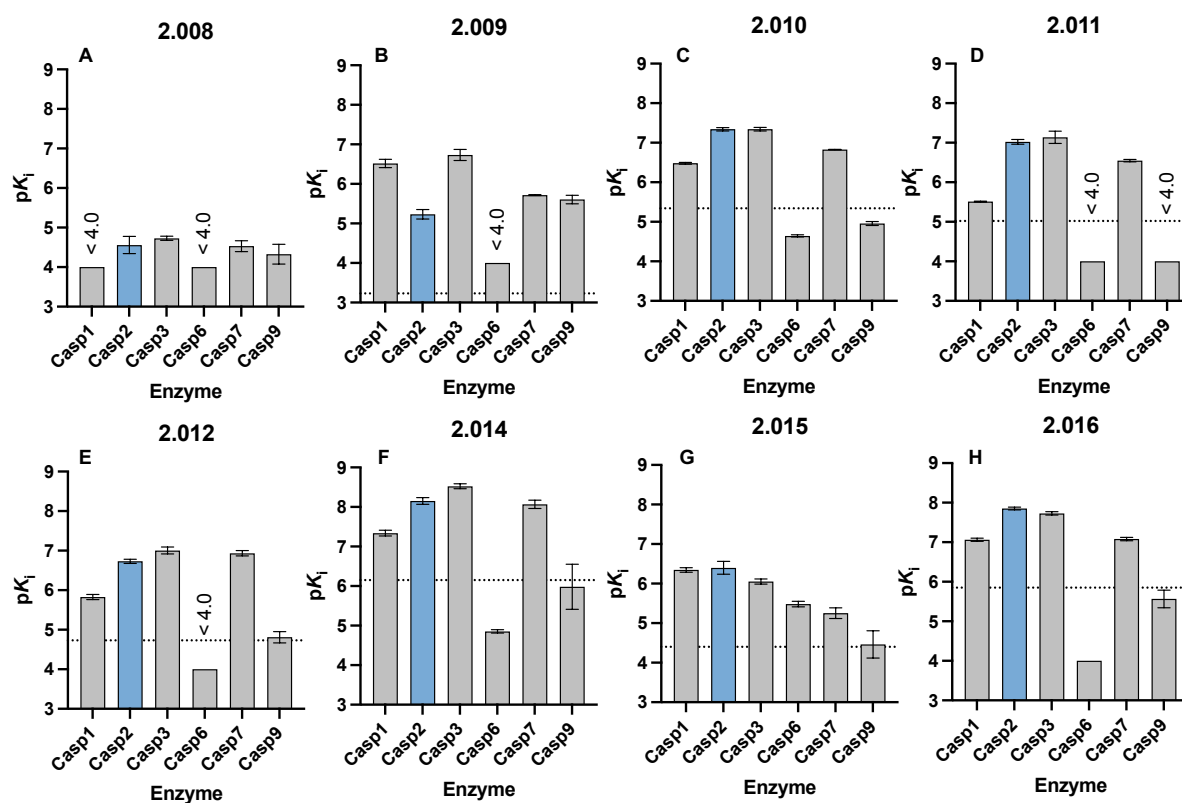
Figure 2.012. Selectivity profile within the caspase family (**A**) AcYKPVD-CHO (**2.008**), (**B**) AcGESPD-CHO (**2.009**), (**C**) AcWDRAD-CHO (**2.010**), (**D**) AcQDTRD-CHO (**2.011**), (**E**) AcADRTD-CHO (**2.012**), (**F**) AcFDVPD-CHO (**2.014**), (**G**) AcITVKD-CHO (**2.015**), and (**H**) AcVDVAD-CHO (**2.016**). The dashed line indicates an at least 100-fold selectivity for Casp2. No dashed line is displayed for the inhibitor **2.008** as the activity for all caspases is relatively low. Bars represent the mean ± SEM of at least two individual experiments each performed in duplicate or triplicate.

2.3.2.3 Site-Directed Mutagenesis of Tau Protein: The Role of P5-P2 Residues in Caspase-2-Mediated Tau Cleavage

The engineering and expression of a series of recombinant tau mutants in addition to the wild-type form are supposed to understand better the contributions of amino acid residues at P5, P4, P3, and P2 to caspase-2-catalyzed cleavage of tau, one of its naturally occurring substrates. The time-dependent *in vitro* cleavage assay demonstrates that while a K-to-D mutation at P4 or a P-to-V mutation at P3 is not altering tau cleavage, combining these two mutations leads to a 25-fold increase in the cleavage product after a 4 h reaction. Meanwhile, a triple mutation of tau at P5−P3 (i.e., YKP-to-VDV) results in a 6-fold increase in the cleavage product after a 4 h reaction (cf. Figure 2.013). These findings are consistent with the results of the *in vitro* characterization of peptidic inhibitors (cf. AcYKPVD-CHO (**2.008**), AcVDVAD-CHO

(**2.016**), AcVDVVD-CHO (**2.018**), AcYKVVD-CHO (**2.026**), AcYDPVD-CHO (**2.029**), and AcYDVVD-CHO (**2.036**)) observed in the pharmacological experiments.
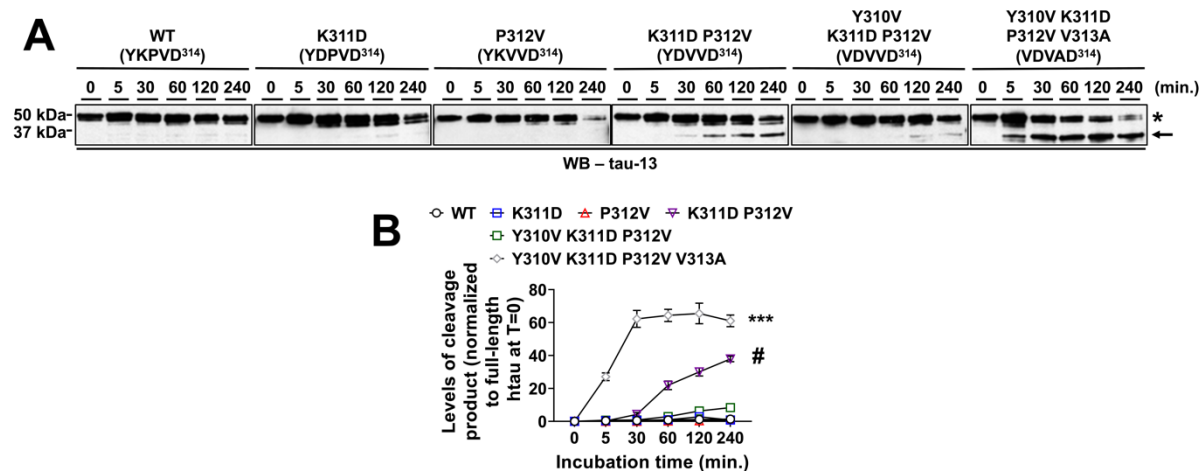
Figure 2.013. The contributions of P5-P2 residues to *in vitro* Casp2-catalyzed tau cleavage. (**A**) Representative Western blots (tau-13) showing *in vitro* Casp2-catalyzed cleavage of a variety of tau mutants in a time-dependent manner. The emergence and yield of the ~35-kDa cleavage product (ending at D314, arrow) differed among investigated tau mutants. (**B**) Quantification. Levels of the cleavage product were normalized to levels of full-length tau (asterisk in **A**) at T = 0; Experiments were performed in duplicates; Means (open symbols), and standard deviations (SDs, error bars) are shown; Repeated measures ANOVA was performed to compare effects of tau mutants ($F_{(5, 6)}$ = 279.60, $P < 0.0001$), followed by Tukey's *post hoc* test (***, $p < 0.001$, tau Y310V K311D P312V V313A vs. tau WT, tau K311D, or tau P213V; #, $p = 0.05$-0.06, tau K311D P312V vs. tau WT, tau K311D, or tau P213V).

2.3.2.4 Crystallography

Novel complexes of peptidic covalent inhibitors with Casp3 have been crystallographically characterized in the course of this work. These are complexes with compounds **2.008**, **2.017**, **2.043**, and **2.059**. Different unique crystal forms (space groups $P2_1$ and $P2_12_12_1$) arise from identical crystallization conditions. Each form includes an activated heterotetramer in the crystallographic asymmetric unit. Diffraction quality varies within this collection of structures from 2.11 to 2.73 Å. Even though the diffraction quality varies, unequivocal confirmation of the covalent bond between the C-terminal aspartic acid of the peptides and the catalytic cysteine (Cys163) exists.
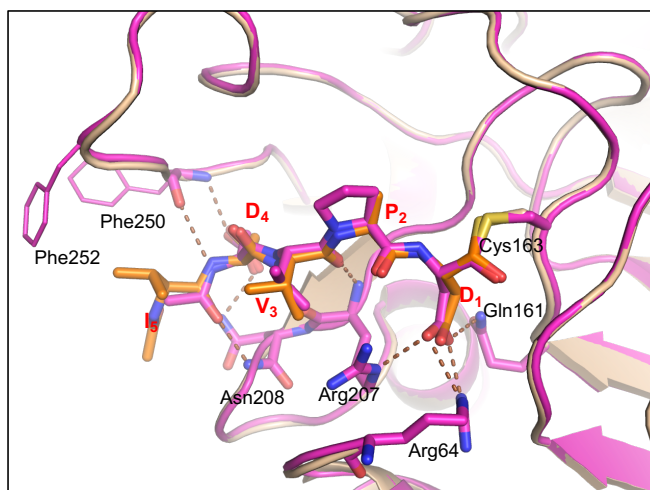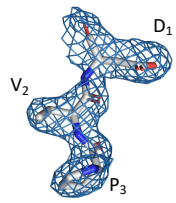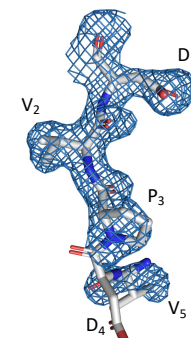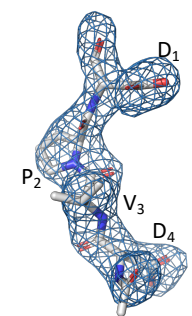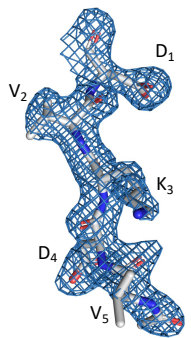
Figure 2.014. An overlay of AcDVPD-CHO (pink) and AcVDVAD-CHO. The P2 proline does not alter the conformation or H-bonding in subsites S1-S4.

In most structures, clear electron density identifies the position of each bound peptide across its entire length (see omit maps included in Table 2.08). The only exceptions are complexes with the peptides AcYKPVD-CHO (**2.008**) and AcVDPVD-CHO (**2.017**) containing proline at P2. For compound **2.008**, no density is present to permit the positioning of any of the peptides upstream of the P3 proline. From the absence of density, it can be inferred that the peptide has no preferred conformation for the AcYK moieties. Some density exists to allow for positioning of the P3 proline and P4 aspartic acid in the complex with **2.017**, but the P4 aspartic acid sidechain and the P5 valine backbone have exchanged places, presumably necessitated by conformational limitations imposed by the P3 proline. There is no density for the N-terminal acetate. The absence of order is not entirely unexpected, given the very low affinity (25−52 µM) of the peptides with the P3 proline. A comparison of the complex of compound AcDVPD-CHO (**2.043**) and the canonical inhibitor AcVDVAD-CHO is provided in Figure 2.014. Backbone H-bonds are conserved in both complexes, illustrating that truncation of pentapeptides to tetrapeptides does not affect the backbone binding conformation. Interestingly, a proline in the tetrapeptide sequence does not alter the backbone binding confirmation either, leading to the hypothesis that the ring in the proline structure locks the peptide into the binding confirmation. Limiting the number of possible binding confirmations creates a more favorable enthalpy of binding (Gibbs free energy of binding) and could help explain the increase in potency of compound AcDVPD-CHO (**2.043**) at both Casp2 and Casp3 as compared to other tetrapeptides

in the series (e.g., AcDVAD-CHO (**2.047**) and AcDVKD-CHO (**2.062**)). Further crystallographic data and refinement statistics are provided in Table 2.08.

Table 2.08. Crystallographic data and refinement statistics for Casp3 co-crystal Structures with compounds **2.008**, **2.017**, **2.043**, and **2.059**.

Data collection and processing				
Compound	**2.008**	**2.017**	**2.043**	**2.059**
Ligand	AcYKPVD-CHO	AcVDPVD-CHO	AcDVPD-CHO	AcVDKVD-CHO
PDB ID code	7rne	7rnd	7usq	7rnf
Omit Map (3s)				
Resolution range (Å)	63.38-2.73 (2.83-2.73)	40.9-2.15 (2.23-2.15)	36.28-2.71 (2.81-2.71)	33.54-2.11 (2.19-2.11)
Space group	$P\,2_12_12_1$	$P\,2_1$	$P\,2_1$	$P\,2_1$
a, b, c (Å)	68.10 84.16 96.33	50.31 68.61 81.80	50.171 67.821 82.641	50.34 67.08 82.18
a, b, g (°)	90 90 90	90 90.45 90	90 90.146 90	90 91.14 90
Observations	30366 (2948)	57475 (5421)	28232 (2039)	59043 (6105)
Unique reflections	15215 (1471)	29662 (2924)	14731 (1222)	30149 (3101)
Multiplicity	2.0 (2.0)	1.9 (1.9)	1.9 (1.7)	2.0 (2.0)
Completeness (%)	99.43 (99.59)	97.35 (96.79)	96.52 (79.70)	95.41 (99.81)
Mean I/s(I)	10.85 (2.95)	12.15 (4.49)	15.89 (3.10)	9.26 (2.28)
Wilson B-factor (Å^2)	42.48	26.45	46.99	30.85
R_{merge}	0.0387 (0.2103)	0.0383 (0.1936)	0.02661 (0.1783)	0.0450 (0.3021)
CC1/2	0.998 (0.946)	0.998 (0.931)	0.999 (0.926)	0.998 (0.861)
CC*	1.00 (0.986)	0.999 (0.982)	1 (0.981)	0.999 (0.962)

Table 2.08 (continued)

Structure Refinement				
Compound	**2.008**	**2.017**	**2.043**	**2.059**
Ligand	AcYKPVD-CHO	AcVDPVD-CHO	AcDVPD-CHO	AcVDKVD-CHO
Reflections used	15156 (1471)	29638 (2924)	14717 (1221)	30132 (3102)
R_{free} reflections (5%)	737 (76)	1421 (145)	721 (35)	1497 (179)
R_{work}	0.1904 (0.2870)	0.1687 (0.2033)	0.1633 (0.2252)	0.1782 (0.2066)
R_{free}	0.2535 (0.3852)	0.2218 (0.2778)	0.2410 (0.3343)	0.2368 (0.2630)
CC_{work}	0.961 (0.890)	0.965 (0.935)	0.958 (0.904)	0.966 (0.924)
CC_{free}	0.920 (0.796)	0.945 (0.806)	0.907 (0.750)	0.926 (0.814)
Non-hydrogen atoms	3798	4021	3905	3977
Solvent molecules	33	151	47	124
Protein residues	471	475	474	472
Bonds ($Å^2$)	0.008	0.007	0.009	0.008
Angles (°)	0.95	1.37	1.08	0.95
Ramachandran Analysis				
Favored (%)	96.95	97.41	96.32	97.61
Allowed (%)	3.05	2.16	3.68	2.39
Outliers (%)	0	0.43	0	0
Rotamer outliers	4	1	1.87	0
Clashscore	7.91	3.92	8.1	4.57
Mean B-factor ($Å^2$)	42.48	28.92	46.92	34.62

[#]Values in parenthesis refer to the highest resolution shell.

2.3.3 Conclusion

Within this approach, it was aimed to elucidate the caspase-2 binding site by a series of new peptides and the resulting SAR. In particular, the differences with respect to caspase-3 should be investigated to get closer to the goal of highly potent and selective caspase-2 inhibitors. Besides the classic key motif of caspase-2 inhibitors, consisting of five amino acids, the inhibitors were truncated to tetrapeptides and tripeptides, which should result in a better bioavailability and a more drug-like character of the ligands with respect to Lipinski's rule of 5 (Ro5).[103] For this purpose, 54 peptides were synthesized and tested for their inhibitory affinity at Casp2 and Casp3. Selected inhibitors were subjected to a panel assay screening to investigate affinities at Casp1, Casp6, Casp7, and Casp9 to get more information about the selectivity within the caspase family. The ligands are structurally derived from the canonical inhibitor AcVDVAD-CHO (**2.016**), the tau cleavage sequence YKPVD, and other specific sites of caspase-2-mediated proteolysis (e.g., Golgin-160 and Transcriptional-regulating factor 1). The inhibitor AcYKPVD-CHO (**2.008**) deriving from the optimal tau cleavage sequence has not shown to be an active Casp2 inhibitor. The same applies to all other inhibitors containing proline at position 3 (e.g., AcVDPVD-CHO (**2.017**) and AcVDPKD-CHO (**2.035**)) or lysine at position 4 (e.g., AcVKVKD-CHO (**2.024**) and AcYKVKD-CHO (**2.021**)). The best inhibitory affinity at Casp2 (pK_i value of 7.63-7.83) and selectivity over Casp3 (selectivity ranging from a factor of 5.06-7.53) is demonstrated by the hybrid peptides (combination of AcVDVAD-CHO and AcYKPVD-CHO), AcVDVKD-CHO (**2.061**), AcYDVKD-CHO (**2.028**), and AcIDVKD-CHO (**2.058**). Within the other cleavage sequences, the inhibitors AcLDVPD-CHO (**2.013**) and AcFDVPD-CHO (**2.014**) demonstrate the highest affinity for Casp2 (pK_i: 7.88/7.66 and 8.15/8.03). Nevertheless, it must be noted that **2.013** and **2.014** display no selectivity for Casp2 over Casp3. Truncation of **2.013** and **2.014** resulted in the tetrapeptide AcDVPD-CHO (**2.043**, Casp2 pK_i: 6.44/6.33; Casp3 pK_i: 8.18) with **2.043** showing Casp3 selectivity. Overall, the truncation of pentapeptides to tetra- and tripeptides do not lead to Casp2 selectivity. In the case of tripeptides, even a total collapse of Casp2 and Casp3 activities can be observed. These findings support the assumption that a motif of five amino acids is required for efficient Casp2 inhibition in this class of peptidic, reversible inhibitors. The pentapeptide AcITVKD-CHO (**2.015**, Casp2 pK_i: 6.40) is the only inhibitor derived from the natural cleavage sequences to show marginal selectivity for

caspase-2 (2-fold selectivity). Interestingly, it does not contain aspartic acid at position P4. Regarding Casp3 selectivity AcDKVD-CHO (**2.060**) (Casp2 pK_i: 5.61/5.22; Casp3 pK_i: 7.79), the corresponding tetrapeptide of AcVDKVD-CHO (**2.059**, Casp2 pK_i: 7.40; Casp3 pK_i: 7.28), proves to be the most selective Casp3 inhibitor in this series with a selectivity factor of 151 or 371, respectively. Furthermore, an *in vitro* cleavage assay with a series of recombinant tau mutants [e.g., K311D P312V (YDVVD314)] was performed and showed results that coincide with the results of the *in vitro* Casp2 binding data. In summary, the results of this study provide an extensive knowledge of the structure−activity relationships (SAR) of a large number of peptides with various activities and selectivities within the caspase family. These findings provide a reasonable basis for the development of selective Caspase-2 inhibitors.

2.4 Development of Highly Selective Casp2 Inhibitors by Introducing Basic Amino Acids at P2/P3 to Address Glu52 in the Binding Pocket of Casp2 and by Using Literature-known Structural Features that are Linked to Casp2 Selectivity

1) Targeting Glu52 in the Casp2 binding pocket

2) Literature-known structural features
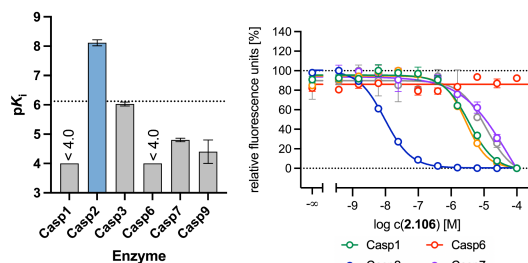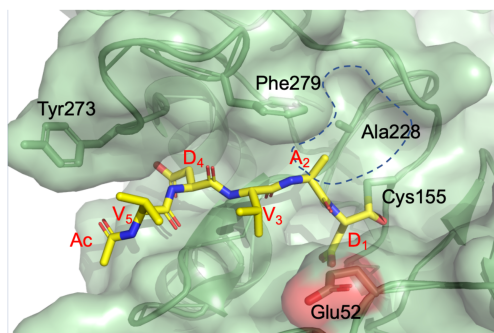
Structure-based design of 39 Casp2 inhibitors
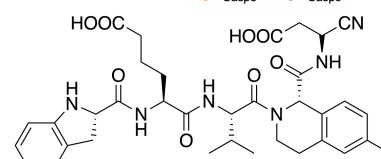
Idc(hE)V(S-Me-THIQ)D-CN
2.106

- Fluorescence-based enzyme inhibition assay (Casp1, Casp2, Casp3, Casp6, Casp7, and Casp9)

- *In vitro* cleavage assay: Measuring Δtau314 formation by Casp2

- Investigation of P301S tau accumulation in dendritic spines

- Efficacy of inhibitors on P301S tau-induced functional deficits in dendritic spines
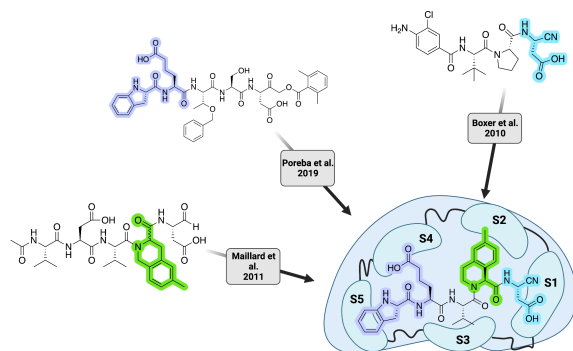
Casp2 is an essential component of a pathological cascade, causing synaptic and cognitive deficits by a disproportionate accumulation of the neuronal protein tau in dendritic spines. The design of highly selective and potent Casp2 inhibitors is of immense relevance to deciphering whether the pathological effects of Casp2 on synaptic function are due to its catalytic or noncatalytic properties. The peptides that have been developed in the course of this work did not demonstrate the desired selectivity so far. Hence, another series of peptides was developed by combining two design strategies. First of all, by targeting Glu52 in the binding pocket of Casp2. Secondly, by introducing literature-known structural features known for Casp2 activity and selectivity. This resulted in a series of highly selective and active Casp2 inhibitors (e.g., **2.101**, **2.106**, **2.107**, and **2.108**). In an *in vitro* assay based on Casp2-mediated cleavage of tau, compound **2.106** blocked the production of Δtau314. Moreover, compound **2.106** prevented tau from accumulating excessively in dendritic spines and rescued excitatory neurotransmission in cultured primary rat hippocampal neurons expressing the P301S tau variant linked to FTDP-17, a familial tauopathy.

2.4.1 Design Rationale

As already mentioned, Casp2 and Casp3 reveal structural differences in their binding site. Whereas Casp2 is characterized by the presence of Glu52 in proximity to the S2 and S3 subsite, Casp3 features an uncharged threonine instead. (see chapter **2.3.1**, Figure 2.008A and 2.008B).[30] This diversity is of particular interest because it allows addressing exclusively Casp2 over Casp3, by introducing basic amino acids at P2 and P3 of the peptide scaffold that interact with the negatively charged Glu52 in the binding pocket. To reinforce the hypothesis and to accelerate the lead optimization process, a covalent inhibitor docking protocol employing CovDock of the Schrödinger Software Suite was implemented. This aims to predict relative binding affinities for Casp2 and Casp3. To confirm that computational methods can recapitulate a reasonable binding pose, covalent docking studies were first performed with ligands AcVDVAD-CHO (**2.016**), AcLDESD-CHO (**2.127**), and AcDEVD-CHO (**2.128**), previously co-crystallized with caspases 2 and 3.[96,104] The resulting docking scores reflect the expected high affinity that these peptide inhibitors show experimentally for both caspases (cf. Table 2.09). Moreover, the predicted poses recapitulate the crystallographically determined structures with good fidelity (cf. Figure 2.008D). This docking protocol was then applied to pentapeptides related to AcVDVAD-CHO that include a positively charged amino acid in place of the P3 valine or the P2 alanine to virtually quantify any potential benefit in Casp2 affinity or selectivity of installing a group that can make a favorable ionic interaction with the Glu52 unique to Casp2 (cf. Figure 2.008A). The scoring suggests that AcVDKVD-CHO (**2.059**), but in particular AcVDRVD-CHO (**2.066**) and AcVDV(Dab)D-CHO (**2.069**) might have a higher affinity for Casp2 (cf. Table 2.09). Significant affinity enhancement was not predicted in modeling with Casp3, suggesting that this may indeed be a viable approach to achieve more selective inhibition. Therefore, peptides analogs of AcVDKVD-CHO (**2.059**), AcVDVKD-CHO (**2.061**), AcITVKD-CHO (**2.015**), and AcATVKD-CHO (**2.055**) (all synthesized in the first series) with amino acids arginine, ornithine, diaminobutyric acid (Dab), and diaminopropionic acid (Dap) were synthesized (cf. Figure 2.015). In order to test the hypothesis that the charge is beneficial and not just the larger sidechains, inhibitors AcVD(AcK)VD-CHO (**2.067**), AcVDV(AcK)D-CHO (**2.073**), and AcITV(AcK)D-CHO (**2.084**) were also synthesized as negative controls with a non-basic terminal amide (cf. Figure 2.015). All peptides

within this approach were shortened to tetra- and/or tripeptides to give insights into the SAR and to verify if a decrease of the molecular weight is feasible to make the molecules more drug-like with respect to Lipinski's rule of 5.[103]

Table 2.09. Molecular Modeling of Casp2 and Casp3 and the ligands **2.066**, **2.069**, **2.078**, and **2.081**.

Sequence	Comp.	Casp2 cdock affinity	Casp3 cdock affinity
AcVDRVD-CHO	**2.066**	-15.055	-12.768
AcVDV(Dab)D-CHO	**2.069**	-15.523	-13.871
AcITV(Dab)D-CHO	**2.078**	−12.972	−12.876
AcITV(Dap)D-CHO	**2.081**	−14.278	−12.721
Reference compounds			
AcVDVAD-CHO	**2.016**	-13.614	-12.148
AcLDESD-CHO	**2.127**	-13.519	-13.369
AcDEVD-CHO	**2.128**	-13.439	-12.218

Calculation using covalent docking in Schrödinger 2021.3. Casp2 = PDBid: 1pyo, Casp3 = PDBid: 3edq. Proteins and ligands prepared as described in the section Computational Chemistry. cdock affinity = covalent docking affinity (kcals/mol).

Figure 2.015. Substitution of AcVDVXD-CHO at P2, AcVDXVD-CHO at P3, and AcITVXD-CHO at P2 with various basic amino acids and interaction with Glu52 in the active site of Casp2; negative control with acetylated lysine.

In addition, known structural elements of previous structure-activity-relationship (SAR) studies that demonstrated good selectivity and activity were combined for a rational-design strategy (cf. Figure 2.017).[105] Maillard et al. (2011) modified the canonical inhibitor AcVDVAD-CHO (**2.016**) by installing the racemic 6-methyltetrahydroisoquinoline-1-carboxylic acid (6-Me-THIQ-COOH) at P2 position, resulting in an inhibitor with a slight selectivity trend toward Casp3.[92] The results of this study revealed that sterically demanding amino acids preferably fit into the S2 subunit of Casp2. Therefore, enantiopure (*R*)-6-Me-THIQ-COOH and (*S*)-6-Me-THIQ-COOH were introduced as structural features, leading to AcVDV(*S*-Me-THIQ)D-CHO (**2.093**) and AcVDV(*R*-Me-THIQ)D-CHO (**2.094**). This enables the evolution of even more selective and active peptides for Casp2. The *R*-enantiomer serves both as a negative control and to estimate the influence of the stereochemical properties of amino acids at P2. hL-glutamic acid (hE), with its extended side chain, accurately fits in the S4 subsite of Casp2, while the cyclic (*S*)-indoline-2-carboxylic acid (Idc) perfectly embeds in the S5 subsite. Casp2 inhibitors containing these structural features are characterized by a significantly increased selectivity over Casp3.[93] Taking AcVDV(*S*-Me-THIQ)D-CHO (**2.093**) as a lead compound, hL-glutamic acid (hE) and (*S*)-indoline-2-carboxylic acid (Idc) were introduced in P4 and P5, resulting in Idc(hE)V(*S*-Me-THIQ)D-CHO (**2.101**). In addition, quinaldic acid (derived from TRP601 of Chauvier et

al. (2011)[99]), another sterically demanding group, was incorporated in place of the N-acetyl moiety, leading to (Quin)VDV(*S*-Me-THIQ)D-CHO (**2.097**).

A
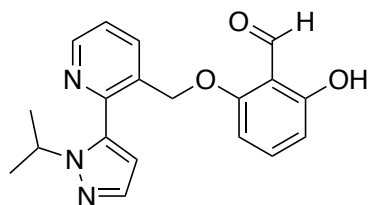
B
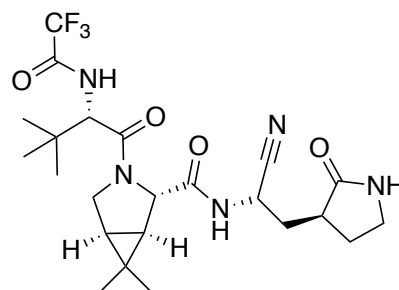
C
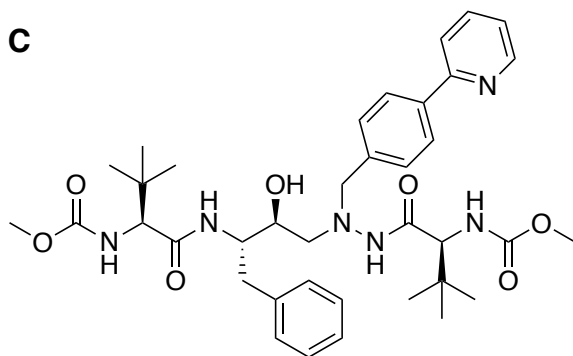
D
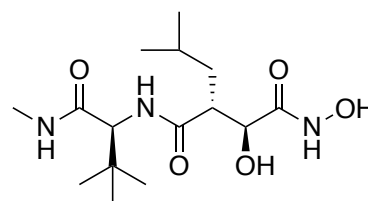
Figure 2.016. Structures of pharmaceutical drugs voxelotor (**A**), nirmatrelvir (**B**), atazanavir (**C**), and marimastat (**D**).

All of the previously mentioned Casp2 inhibitors are characterized by their reversible covalent mechanism containing an aldehyde (-CHO). Conducting early SAR studies using an aldehyde as a reactive group is popular because of the fast and easy accessibility of inhibitors using solid phase synthesis. Nevertheless, the R-CHO warhead is seen as unfavorable due to its high electrophilicity and its susceptibility to oxidative metabolism, even though there are approved drugs on the market as an exception (e.g., voxelotor, used for the treatment of sickle cell anemia (cf. Figure 2.016A)).[106] Featuring nitrile-based covalent inhibitors can eliminate these disadvantages. Moreover, they are clinically validated and known for their safety and efficacy in humans (e.g., nirmatrelvir, used as a covalent inhibitor of the SARS-CoV-2 main protease (cf. Figure 2.016B)).[107] Furthermore, Boxer et al. (2010) proved that a nitrile-based reactive group can be an excellent structural feature for the inhibition of caspases (NCGC00183434, inhibition of caspase-1).[98] Therefore, a nitrile was introduced to Idc(hE)V(S-Me-THIQ)D-CHO (**2.101**), leading to

Idc(hE)V(*S*-Me-THIQ)D-CN (**2.106**) (cf. Figure 2.017). In addition, position P2 (*S*)-6-Me-THIQ-COOH) was replaced by diaminobutyric acid (Dab), another amino acid that confers a selectivity advantage over caspase-3, resulting in Idc(hE)V(Dab)D-CHO (**2.107**). Further, valine at position P3 was replaced by L-α-*tert*-leucine (Tle), leading to Idc(hE)(Tle)(Dab)D-CHO (**2.108**). *Tert*-leucine (Tle), as a non-natural amino acid, may confer better stability toward drug-metabolizing enzymes due to its sizeable steric hindrance. L-α-*tert*-leucine is widely used as a structural feature of various pharmaceuticals, such as protease inhibitors for the treatment of HIV (e.g., atazanavir (cf. Figure 2.016C)), SARS-CoV-2 main protease (e.g., nirmatrelvir), or as tumor-fighting agents (e.g., marimastat (cf. Figure 2.016D)).[108] Finally, fine-tuning with respect to Casp2 activity and selectivity was performed by investigating the role of P3, resulting in Idc(hE)(BnT)(Dab)D-CHO (**2.109**).
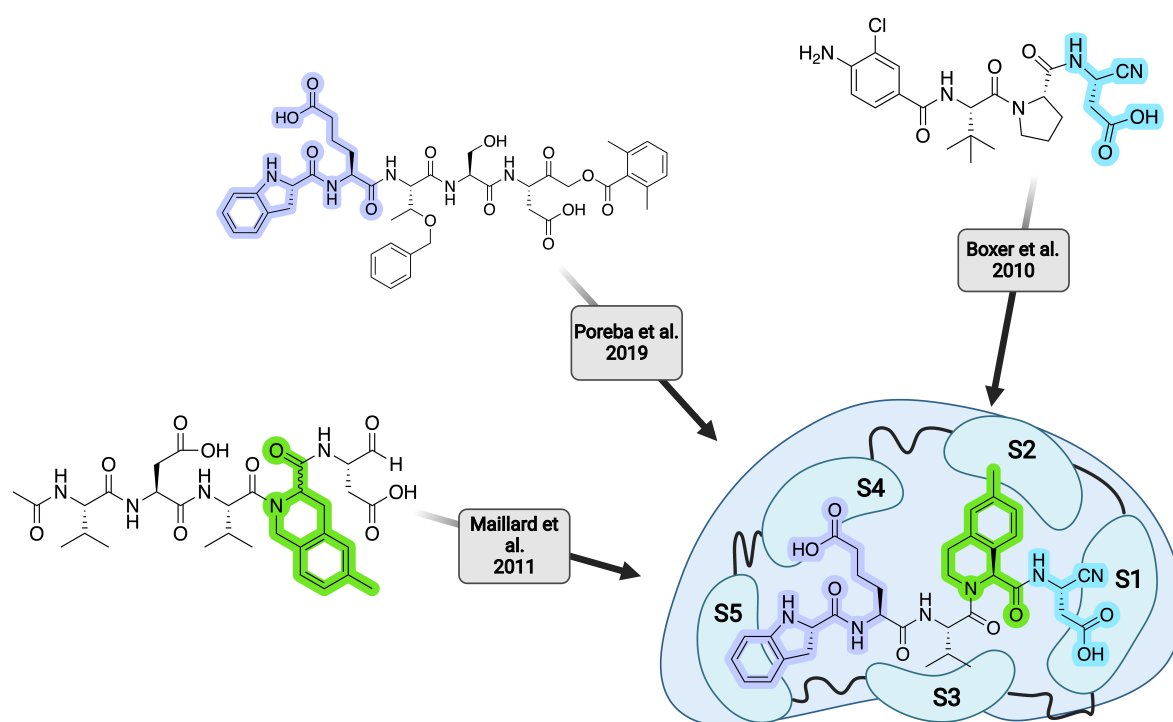
Figure 2.017. The rational design strategy of compound **2.106** (Idc(hE)V(S-Me-THIQ)D-CN). (*S*)-indoline-2-carboxylic acid (Idc) at P5 was introduced based on a publication from Poreba et al. (2019)[93]. A nitrile was established based on the publication of Boxer et al. (2010)[98] as a covalent reactive group (CRG) (also referred to as a warhead) due to stability advantages. Using enantiopure (*S*)-6-Me-THIQ-COOH at position P2 is supposed to enable Casp2 activity and selectivity due to the sterically demanding amino acid.[92] S1-S5 represents the respective subsite where the amino acids P1-P5 are embedded. Figure created with BioRender.com.

2.4.2 Results and Discussion

2.4.2.1 Chemistry

Preparation of aspartic acid loaded semicarbazide amino-Merrifield resin

For the synthetic route see chapter **2.3.2.1**.

Solid-phase peptide synthesis (SPPS) of the penta-, tetra-, and tripeptides

For the synthetic route see chapter **2.3.2.1**.

Peptides **2.101**, **2.107**, **2.108**, and **2.109** were not acetylated N-terminally but were cleaved from the resin directly after removing the N-Fmoc protecting group. Additionally, they were cleaved from the resin under milder conditions (trifluoroacetic acid (90%) in water, 15 minutes, room temperature).

Fmoc protection of (S)- and (R)-tetrahydrosioquinoline carboxylic acids

Racemic 6-methyl-tetrahydroisoquinoline-1-carboxylic acid (6-Me-THIQ-COOH) and 6-bromo-tetrahydroisoquinoline-1-carboxylic acid (6-Br-THIQ-COOH) were acquired from a commercial supplier and were outsourced for chiral resolution by supercritical fluid chromatography (SFC). The enantiopure amino acids P1 and P2 (see chapter **2.7.3**, Figures 2.279 and 2.280) were N-Fmoc protected with *N*-(Fluorenyl-9-methoxycarbonyloxy)-succinimide (Fmoc-OSu) in a mixture of tetrahydrofuran and 10% (aq.) sodium carbonate to obtain **2.089** (*R*-enantiomer) and **2.090** (*S*-enantiomer), as well as **2.091** (*R*-enantiomer) and **2.092** (*S*-enantiomer) (cf. Scheme 2.03). The absolute configurations of the amino acids were determined by comparison with reported specific rotation of the commercially available enantiopure N-Fmoc-tetrahydroisoquinoline-1-carboxylic acids.
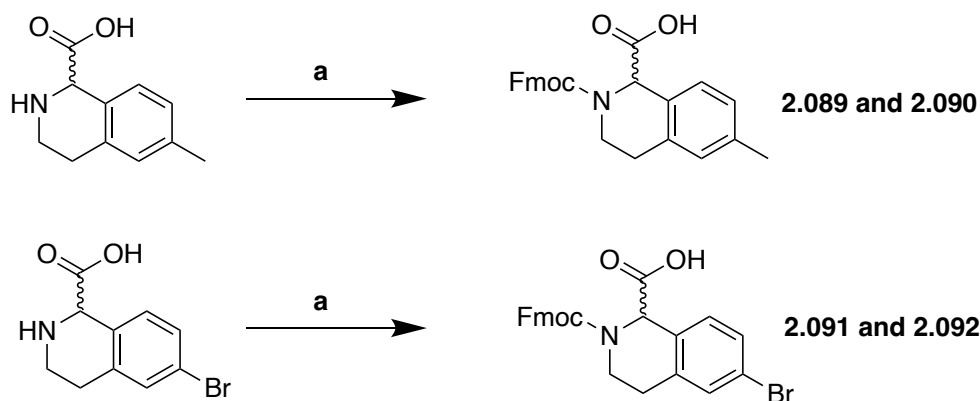
Scheme 2.03. Fmoc protection of (*S*)- and (*R*)-tetrahydrosioquinoline carboxylic acids: **(a)** Fmoc-OSu (1eq), THF, 10% (aq.), Na$_2$CO$_3$, rt, overnight.

Preparation of compound 2.016 through solid-phase and liquid-phase synthesis
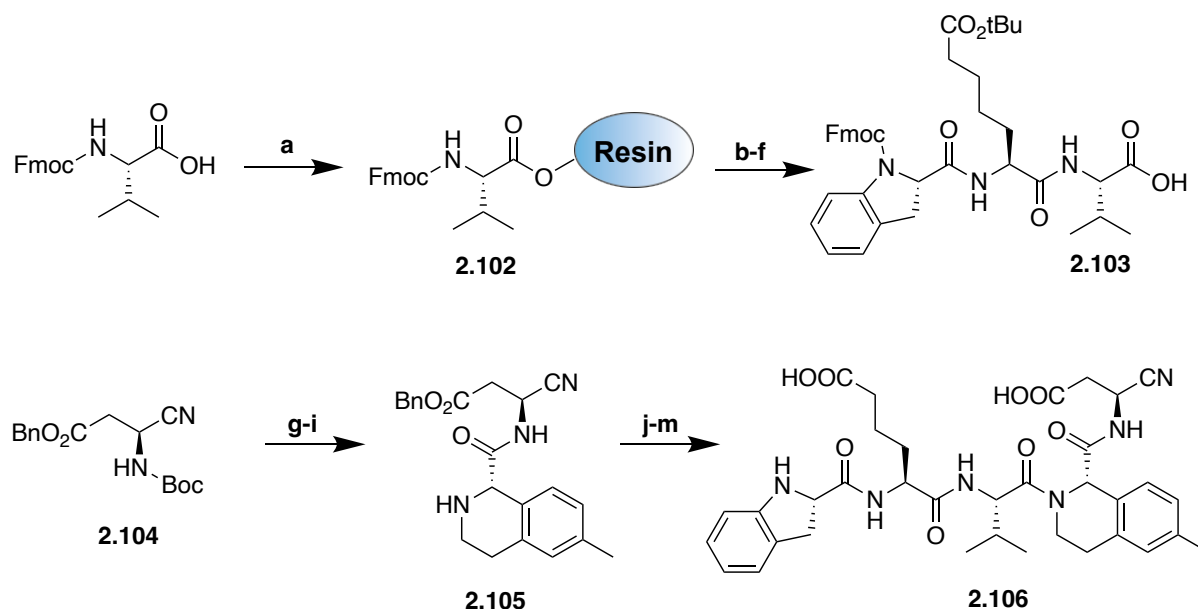
Scheme 2.04. Synthesis of caspase-2 Inhibitor **2.106**: **(a)** 2-Chlorotrityl chloride resin, collidine, DCM; **(b)** 20% piperidine in DMF; **(c)** Fmoc-hGlu(OtBu)-OH, HATU, DMF; **(d)** 20% piperidine in DMF; **(e)** (*S*)-Fmoc-IdcOH, HATU, DMF; **(f)** 20% HFIP in DCM; **(g)** H$_3$PO$_4$; DCM **(h)** Fmoc-(*S*)-6-Me-THIQ-COOH, HATU, collidine, acetonitrile; **(i)** 30% diethylamine in acetonitrile; **(j)** **2.103**, HATU, collidine; **(k)** H$_3$PO$_4$; DCM **(l)** 30% diethylamine in acetonitrile; **(m)** 10% Pd/C.

The synthesis of **2.106** (cf. Scheme 2.04) differs from that of all other peptides in this work, since a nitrile was introduced as a reactive group instead of an aldehyde. For this reason, a simple solid-phase peptide synthesis (SPPS) is not feasible for the design of the inhibitor. In the first step, tripeptide **2.103** was built up through a 2-chlorotrityl chloride resin. Initially, the resin was loaded with valine (**2.102**) using collidine in dichloromethane (**a**). The amino acid sequence was expanded with hL-

glutamic acid (**c**) and (*S*)-indoline-2-carboxylic acid (**e**). The coupling was performed with HATU and collidine in DMF, while the N-Fmoc deprotection was carried out with 20% piperidine in DMF (**b** and **d**). However, (*S*)-indoline remains Fmoc protected N-terminally. The cleavage of the tripeptide **2.103** from the resin was accomplished with 20% hexafluoroisopropanol (HFIP) in dichloromethane (**f**). The dipeptide **2.105**, consisting of the alpha-modified aspartic acid and (*S*)-6-methyltetrahydroisoquinoline-1-carboxylic acid was prepared using classical liquid-phase synthesis. **2.104** was N-Boc deprotected under mild conditions using phosphoric acid (85%) in dichloromethane to prevent hydrolyzation of the nitrile (**g**). Subsequently, **2.104** was coupled with (*S*)-6-methyltetrahydroisoquinoline-1-carboxylic acid by using HATU and collidine in acetonitrile (**h**). This resulted in the dipeptide **2.105**, which was N-Fmoc deprotected (**i**) with 30% diethylamine in acetonitrile and subsequently coupled (**j**) to the tripeptide **2.103.** The resulting pentapeptide was deprotected in a series of steps (N-Boc deprotection (**k**), N-Fmoc deprotection (**l**), and benzyl deprotection (**m**)), leading to Casp2-inhibitor **2.106**.

2.4.2.2 Inhibitory Affinity of Compound 2.063-2.088 and 2.093-2.109 in a Fluorometric Enzyme Assay

To characterize the potential Glu52 interaction in the subsite of Casp2 demonstrated by covalent docking, an additional peptide series based on AcVDKVD-CHO (**2.059**) and AcVDVKD-CHO (**2.061**) was designed. Starting with **2.059** (Casp2 pK_i: 7.40; Casp3 pK_i: 7.28), the chain length of the basic amino acid Lys was shortened piecewise. This resulted in AcVD(Orn)VD-CHO (**2.063**) and AcVD(Dab)VD-CHO (**2.064**), which show almost the same affinity as **2.059** for Casp2 (pK_i: 7.37/6.92 and 7.44) and Casp3 (pK_i: 7.52 and 7.54). In contrast, AcVD(Dap)VD-CHO (**2.065**) demonstrates a significantly lower affinity at Casp2 (pK_i: 6.53/6.18), while the affinity at Casp3 (pK_i: 7.38) remains. The exchange of Lys at position 3 by Arg resulted in AcVDRVD-CHO (**2.066**), which displays a similar affinity (Casp2 pK_i: 7.38, Casp3 pK_i: 7.21). Likewise, the acetylation of Lys in position 3, resulting in **2.067**, demonstrates no shift in affinity (Casp2 pK_i: 7.70/7.41; Casp3 pK_i: 7.96). The same variations of the chain length were performed with Lys at position 2 of compound **2.061**. AcVDV(Orn)D-CHO (**2.068**) (Casp2 pK_i: 7.45; Casp3 pK_i: 6.60) and AcVDV(Dab)D-CHO (**2.069**) (Casp2 pK_i: 7.26; Casp3 pK_i: 5.82) show comparable affinities at Casp2, while Casp3

affinity decreases with further shortening of the chain length (cf. Table 2.10 and Figures 2.018 and 2.019). In contrast, AcVDV(Dap)D-CHO (**2.071**) shows a loss in affinity at Casp2 (same as for **2.065**), while affinity at Casp3 slightly increases (Casp2 pK_i: 6.77; Casp3 pK_i: 6.14) in comparison to **2.069** (cf. Table 2.10 and Figures 2.018 and 2.019). Truncation of **2.069** led to AcDV(Dab)D-CHO (**2.070**), which shows a low affinity for Casp2 (pK_i: 4.93) and Casp3 (pK_i: 5.48) (cf. Table 2.10). Substitution of Lys by Arg resulted in **2.072**, which displays nearly the same affinity as **2.061** at Casp2 and Casp3 (cf. Table 2.10). Acetylation of the Lys side chain of **2.061** resulted in AcVDV(AcK)D-CHO (**2.073**), which shows the same affinity at Casp2 and a slightly higher affinity at Casp3 (Casp2 pK_i: 7.53/7.30; Casp3 pK_i: 7.60). Since the two peptides with acetylated lysine side chains (**2.067** and **2.073**) exhibit high affinity, both at Casp2 and at Casp3, the hypothesis of ionic interactions between Lys at position 2 or 3 and Glu52 in the subsite of Casp2 must be doubted. This was additionally confirmed by exchanging Lys with Phe, resulting in AcVDFVD-CHO (**2.074**) that displays no drastic loss in Casp2 affinity (pK_i: 7.00/6.50). Due to these negative controls, it must be assumed that the interactions in the S2 and S3 subsites of Casp2 are not mainly due to ionic interactions. The shift from Lys at position 3 to position 2 goes hand in hand with a moderate gain in Casp2 selectivity. Compound **2.061** demonstrates a selectivity ratio of 5.16, whereas **2.059** shows no selectivity (cf. Table 2.10). This effect increased with shorter chains, whereas **2.068** has a selectivity factor of 7.07 compared to **2.063** (0.70/0.25-fold). The maximum gain in selectivity was reached for **2.069** (27.7-fold) (cf. Table 2.10 and Figure 2.019), featuring diaminobutyric acid, at position P2. Further shortening leads to a loss of selectivity, as demonstrated for **2.071** (4.30-fold) (cf. Table 2.10 and Figure 2.019). Interestingly, the gain in selectivity is not achieved by an increase in Casp2 affinity, but by a steady decrease of Casp3 affinity (cf. Figure 2.019). In molecular modeling studies of Casp2 and Casp3, the trends for Casp2 selectivity are relatively well confirmed for **2.069** (cf. Table 2.09 and 2.10), whereas the docking scores for **2.059** and **2.066** are not entirely consistent with the *in vitro* data (cf. Table 2.05, 2.06, 2.09, and 2.10).
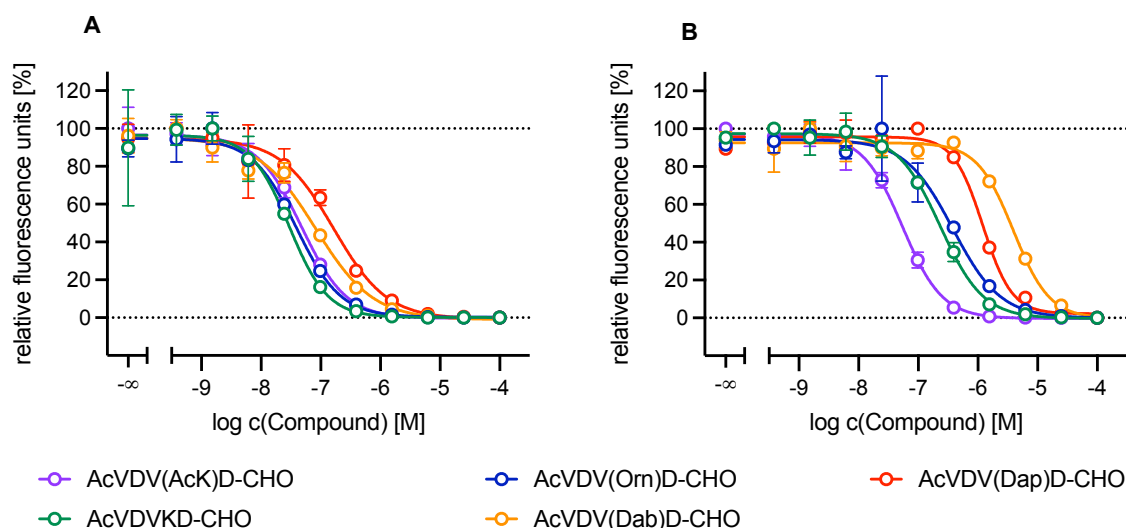
Figure 2.018. Concentration-response curves of AcVDVKD-CHO (**2.061**), AcVDV(Orn)D-CHO (**2.068**), AcVDV(Dab)D-CHO (**2.069**), AcVDV(Dap)D-CHO (**2.071**), and AcVDV(AcK)D-CHO-CHO (**2.073**) at Casp 2 (**A**) and Casp3 (**B**) in the fluorometric enzyme assay. Data points represent mean values ± SD from representative experiments, each performed in duplicate.
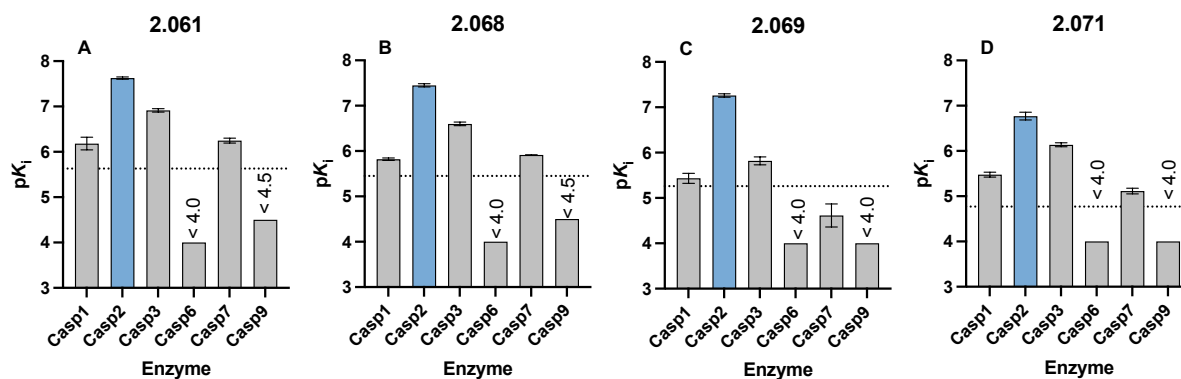
Figure 2.019. Selectivity profile within the caspase family (**A**) AcVDVKD-CHO (**2.061**), (**B**) AcVDV(Orn)D-CHO (**2.068**), (**C**) AcVDV(Dab)D-CHO (**2.069**), and (**D**) AcVDV(Dap)D-CHO (**2.071**). From left to right, the basic side chain of the amino acid at positon P2 (Lys, Orn, Dab, and Dap) is shortened piecewise. The dashed line indicates an at least 100-fold selectivity for Casp2. Bars represent the mean ± SEM of at least two individual experiments each performed in duplicate or triplicate.

In order to advance the finding that the introduction of diaminobutyric acid (Dab) at position P2 creates a selectivity advantage over Casp3, AcITVKD-CHO (**2.015**) and AcVDV(Dab)D-CHO (**2.069**) were used as a basis for the design of further Casp2 inhibitors. **2.015** demonstrates the best selectivity within the inhibitors derived from natural proteolysis sequences of Casp2. The aim was to gain selectivity over Casp3 by introducing Dab at position P2, as previously demonstrated with AcVDV(Dab)D-CHO (**2.069**). To get a further understanding of the importance of the length of the side chain, it was not only prepared inhibitors with diaminobutyric acid at P2 but also with

the amino acids arginine, ornithine (Orn), diaminopropionic acid (Dap), and acetylated lysine (AcK). This modifications led to the peptides AcITV(Orn)D-CHO (**2.075**; Casp2 pK_i: 6.14; Casp3 pK_i: 5.68), AcITV(Dab)D-CHO (**2.078**; Casp2 pK_i: 5.85/5.38; Casp3 pK_i: 5.04), AcITV(Dap)D-CHO (**2.081**; Casp2 pK_i: 5.93/5.48; Casp3 pK_i: 5.32), and AcITV(AcK)D-CHO (**2.084**; Casp2 pK_i: 6.30/6.24; Casp3 pK_i: 7.34), all of them showing lower affinities for Casp2 (cf. Table 2.10). While **2.075**, **2.078**, and **2.081** demonstrate lower affinities for Casp3, AcITV(AcK)D-CHO (**2.084**) has a higher affinity for Casp3 than the lead structure **2.015**. In terms of selectivity, a selectivity advantage for Casp2 over Casp3 can be detected due to the stepwise shortening of the lysine sidechain. While **2.015** (containing lysine) has a selectivity factor of 2, **2.075** (containing ornithine) exhibits a factor of 3, **2.078** (containing diaminobutyric acid) of 6 or 2, respectively, and **2.081** (containing diaminopropionic acid) of 4 or 1, respectively (cf. Table 2.10). The acetylation of lysine (AcITV(AcK)D-CHO, **2.084**) generates a selectivity shift toward Casp3 (Casp2/Casp3 selectivity 11-fold or 13-fold, respectively). The inhibitors **2.075**, **2.078**, **2.081**, and **2.084** were also truncated to get a deeper understanding of the structure-activity relationship of shortened peptides. This resulted in the tetrapeptides AcTV(Orn)D-CHO (**2.076**; Casp2 pK_i: 4.62; Casp3 pK_i: 4.77), AcTV(Dab)D-CHO (**2.079**; Casp2 pK_i: 4.21; Casp3 pK_i: 4.43), and AcTV(Dap)D-CHO (**2.082**; Casp2 pK_i: < 4; Casp3 pK_i: 4.43) which show slightly lower affinities for Casp2 and Casp3 relative to AcTVKD-CHO (**2.045**) (cf. Table 2.06 and 2.10). While AcTV(AcK)D-CHO (**2.085**, Casp2 pK_i: 4.70/4.68; Casp3 pK_i: 6.65) shows a low affinity for Casp2, the affinity for Casp3 remains almost unchanged. Thus, the peptide displays selectivity for Casp3 over Casp2 (Casp3/(cp)Casp2 selectivity 89-fold or 93-fold) (cf. Table 2.10). The corresponding tripeptides of this series AcV(Orn)D-CHO (**2.077**), AcV(Dab)D-CHO (**2.080**), AcV(Dap)D-CHO (**2.083**), and AcV(AcK)D-CHO (**2.086**) do not show notable affinity for Casp2 (pK_i values < 4) nor Casp3 (pK_i values < 4 - 5.02) (cf. Table 2.10). Furthermore, Dab was introduced in AcATVKD-CHO (**2.055**, Casp2 pK_i: 5.86; Casp3 pK_i: 5.93), leading to AcATV(Dab)D-CHO (**2.087**, Casp2 pK_i: 4.72; Casp3 pK_i: 4.68). However, **2.087** was an unsuccessful approach to gain selectivity for Casp2 by exchanging lysine at P2 with diaminobutyric acid (Dab). AcTDTAD-CHO (**2.088**) represents a precursor for stapled peptides. It demonstrates high affinities for Casp2 (pK_i: 7.48/7.04) and Casp3 (pK_i: 7.22) with no distinct selectivity trend.

Based on the canonical pentapeptide structure AcVDVAD-CHO (**2.016**, Casp2 pK_i: 7.85; Casp3 pK_i: 7.73), a new series of inhibitors was designed that included the best structural features of previously published structure-activity relationship studies. The canonical inhibitor shows high Casp2 potency but, unfortunately, no selectivity over Casp3. The integration of sterically demanding (*S*)-6-Me-THIQ-COOH, derived from Maillard et al. (2011)[92], at position P2 of the canonical pentapeptide structure resulted in compound AcVDV(*S*-Me-THIQ)D-CHO (**2.093**, Casp2 pK_i: 7.89; Casp3 pK_i: 6.04). AcVDV(*S*-Me-THIQ)D-CHO shows both high potency at caspase-2 and a reasonable selectivity over caspase-3 (Casp3/cpCasp2 selectivity 60-fold) (cf. Table 2.10 and Figures 2.020 and 2.021). The exchange of (*S*)-6-Me-THIQ-COOH to (*S*)-6-Br-THIQ-COOH at position P2 led to the peptide AcVDV(*S*-Br-THIQ)D-CHO (**2.095**, Casp2 pK_i: 7.96; Casp3 pK_i: 6.52). The caspase-2 activity is maintained with respect to pentapeptide **2.093**, while selectivity over caspase-3 is about half as high (Casp3/cpCasp2 selectivity 28-fold) (cf. Table 2.10). Starting from **2.093**, the sterically demanding quinaldic acid was incorporated in place of the N-acetyl group, leading to (Quin)VDV(*S*-Me-THIQ)D-CHO (**2.097**). The inhibitor demonstrates a slight deterioration with respect to caspase-2 activity (Casp2 pK_i: 7.50), while the activity at caspase-3 increases (Casp3 pK_i: 6.45) (cf. Table 2.10). (Quin)VDV(*S*-Br-THIQ)D-CHO (**2.099**, Casp2 pK_i: 7.41; Casp3 pK_i: 6.66) shows almost the same activity at Casp2/Casp3 and selectivity as **2.097**. As already anticipated, the peptides AcVDV(*R*-Me-THIQ)D-CHO (**2.094**), AcVDV(*R*-Br-THIQ)D-CHO (**2.096**), (Quin)VDV(*R*-Me-THIQ)D-CHO (**2.098**), and (Quin)VDV(*R*-Br-THIQ)D-CHO (**2.100**) containing an amino acid with R conformation ((*R*)-6-Me-THIQ-COOH or (*R*)-6-Br-THIQ-COOH) at position P2 are (almost) inactive against Casp2 and Casp3 (cf. Table 2.10). It must be concluded that the peptides cannot be embedded in the S2 subsite of Casp2 and Casp3 due to their inverted structural conformation.

The replacement of alanine at position P2 of the canonical inhibitor AcVDVAD-CHO (**2.016**) with (*S*)-Me-THIQ-COOH in comparison to (*S*)-Br-THIQ-COOH delivered more promising results in terms of caspase-2 activity and selectivity. Therefore, for the creation of further inhibitors, (*S*)-Me-THIQ-COOH was retained as a structural feature of the pentapeptides. The exchange of the N-acetyl at position P5 of the canonical inhibitor so far showed no increase in selectivity (e.g., (Quin)VDV(*S*-Me-THIQ)D-CHO (**2.097**)). In a recent study Poreba et al. (2019)[93], demonstrated a significant increase

of affinity and selectivity for Casp2 by the sterically demanding non-acylated indoline-2(*S*)-carboxylic acid at position P5. In addition, this publication revealed that the incorporation of h-L-glutamic acid at position P4 causes a great increase of potency and selectivity. These modifications ultimately resulted in the Casp2 inhibitor Idc(hE)V(*S*-Me-THIQ)D-CHO (**2.101**, Casp2 pK_i: 7.40; Casp3 pK_i: <4.5). **2.101** is characterized by high activity toward caspase-2, low activity toward caspase-3, and an excellent selectivity profile (Casp3/cpCasp2 selectivity 794-fold). Therefore, Idc(hE)V(*S*-Me-THIQ)D-CHO (**2.101**) served as a model for the optimization of the reactive warhead. As already mentioned, aldehydes are considered unfavorable due their high electrophilicity and their susceptibility to oxidative metabolism.[105] Idc(hE)V(*S*-Me-THIQ)D-CN (**2.106**, Casp2 pK_i: 8.12; Casp3 pK_i: 6.03) was created by the insertion of a nitrile as a reversible covalent reactive group in place of the aldehyde. Inhibitors featuring nitrile as a reactive warhead are clinically proven and known for their safety and efficacy in humans (e.g., nirmatrelvir).[105] Despite the exchange of the warhead, **2.106** demonstrates high potency for Casp2 and a good selectivity profile (Casp3/cpCasp2 selectivity 123-fold). In the course of this study Idc(hE)V(*S*-Me-THIQ)D-CN (**2.106**) was used for further biological experiments examining the pathophysiological role of Casp2 in the emergence of tauopathies like Alzheimer's disease and to find out whether the inhibition of Casp2 in the cellular cascade could be a potential treatment (see chapter **2.4.2.3**, **2.4.2.4**, and **2.4.2.5**).[105] Idc(hE)V(Dab)D-CHO (**2.107**, Casp2 pK_i: 7.18; Casp3 pK_i: < 4) was designed to examine whether the exchange of (*S*)-6-Me-THIQ with diaminobuyric acid (Dab) at position P2 of Idc(hE)V(*S*-Me-THIQ)D-CHO causes a loss of activity and selectivity for the Casp2 inhibitor. Fortunately, the activity (pK_i: 7.18 vs. pK_i: 7.40) and the selectivity (Casp3/cpCasp2 selectivity 1514-fold vs. 794-fold) for Casp2 are preserved. For the selectivity, it is even possible to observe a greater increase. The introduction of L-α-*tert*-leucine (Tle) for a better enzymatic stability of the peptide resulted in Idc(hE)(Tle)(Dab)D-CHO (**2.108**, Casp2 pK_i: 6.76; Casp3 pK_i: < 4). The affinity of **2.108** for Casp2 drops by 0.4 log units relative to **2.107**, while an affinity for Casp3 cannot be determined. In the inhibitor Idc(hE)(BnT)(Dab)D-CHO (**2.109**), *O*-benzyl-L-threonin (BnT) was implemented as a structural feature at position P3 to further elucidate structure-activity relationships for subsite 3 of Casp2. **2.109** shows a high affinity for Casp2 (pK_i: 7.40) and an excellent selectivity profile over Casp3 (Casp3/cpCasp2 selectivity 2512-fold). As postulated earlier, by inserting (*S*)-indoline-2-carboxylic acid

(Idc) at position P5 and hL-glutamic acid (hE) at position P4 in combination with diaminobutyric acid (Dab) or (*S*)-6-methyltetrahydroisoquinoline-1-carboxylic acid ((*S*)-Me-THIQ-COOH) at P2, a series of highly selective peptides (**2.101**-**2.109**) were synthesized. These insights are helpful for the ongoing efforts to design peptides with better drug-like properties, to pave the way for small molecule Casp2 inhibitors.
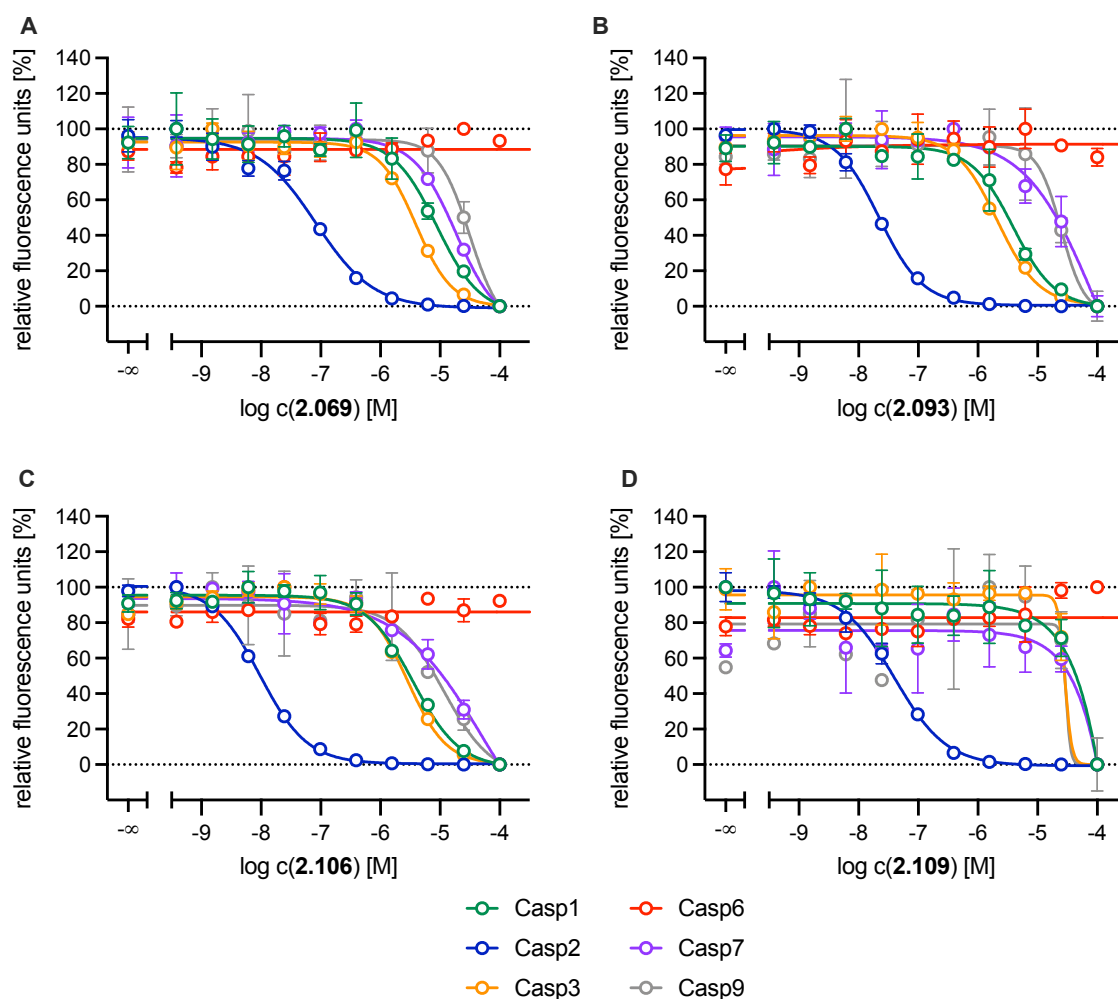
Figure 2.020. Concentration-response curves of (**A**) AcVDV(Dab)D-CHO-CHO (**2.069**), (**B**) AcVDV(*S*-Me-THIQ)D-CHO (**2.093**), (**C**) Idc(hE)V(*S*-Me-THIQ)D-CN (**2.106**), and (**D**) Idc(hE)(BnT)(Dab)D-CHO (**2.109**) at Casp1, Casp2, Casp3, Casp6, Casp7, and Casp9 in the fluorometric enzyme assay. Data points represent mean values ± SD from representative experiments, each performed in duplicate.

The peptides within this series were also subjected to a panel assay screening for Casp1, Casp6, Casp7, and Casp9 (cf. Table 2.11). As a reminder, the lead structures for the Glu52 engagement, AcVDKVD-CHO (**2.059**) and AcVDVKD-CHO (**2.061**), demonstrate a decent inhibitory affinity for Casp1 (pK_i: 5.97 and 6.18) and Casp7 (pK_i: 7.28 and 6.25), a low affinity for Casp9 (pK_i: 4.77 and < 4.5), and no affinity for Casp6

(pK_i: < 4) (cf. Table 2.07). AcVD(Dab)VD-CHO (**2.064**) shows almost the same affinities in the panel as the respective lead compound **2.059**, whereas AcVDV(Orn)D-CHO (**2.068**), AcVDV(Dab)D-CHO (**2.069**), and AcVDV(Dap)D-CHO (**2.071**) demonstrate lower affinities at Casp1, Casp6, Casp7, and Casp9 compared to lead compound **2.061** (Casp1 pK_i: 5.82, 5.43, and 5.48; Casp7 pK_i: 5.92, 4.61, and 5.12; Casp9 pK_i: < 4.5, < 4, and < 4) (cf. Table 2.07 and 2.11). Within the peptides targeting amino acid Glu52 in the Casp2 subsite, **2.069** shows the best selectivity profile for Casp2 (cf. Tables 2.10 and 2.11 and Figures 2.018 and 2.019), displaying a 27.7-fold selectivity over Casp3, 67.3-fold selectivity over Casp1, 444-fold selectivity over Casp7, and at least 1827-fold selectivity over Casp6 and Casp9. Idc(hE)V(S-Me-THIQ)D-CHO (**2.101**), Idc(hE)V(S-Me-THIQ)D-CN (**2.106**), and Idc(hE)(BnT)(Dab)D-CHO (**2.109**) are characterized by an excellent selectivity profile within the Caspase family (cf. Figures 2.020 and 2.021). **2.106** shows a > 2000-fold selectivity versus Casp1, Casp6, Casp7, and Casp9 (cf. Tables 2.10 and 2.11 and Figures 2.020 and 2.021), whereas **2.109** demonstrates a > 28-fold selectivity over Casp1 and > 2500-fold selectivity over Casp6, Casp7, and Casp9 (cf. Tables 2.10 and 2.11 and Figures 2.020 and 2.021). Further panel results are summarized in Table 2.11. Displacement curves from representative competition binding experiments (Casp1, Casp2, Casp3, Casp6, Casp7, and Casp9) are displayed in chapter **2.7.6** (cf. Figures 2.292-2.327).
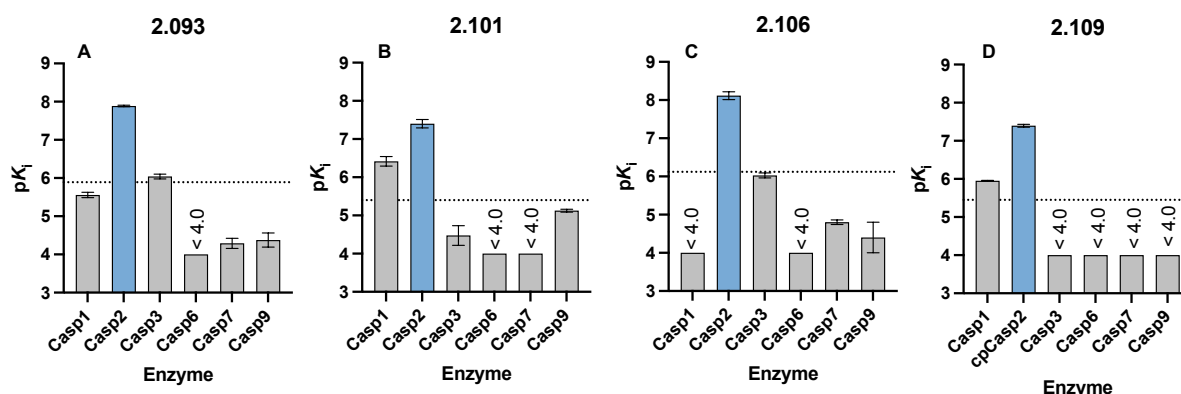
Figure 2.021. Selectivity profile within the caspase family (**A**) AcVDV(S-Me-THIQ)D-CHO (**2.093**), (**B**) Idc(hE)V(S-Me-THIQ)D-CHO (**2.101**), (**C**) Idc(hE)V(S-Me-THIQ)D-CN (**2.106**), and (**D**) Idc(hE)(BnT)(Dab)D-CHO (**2.109**). The dashed line indicates an at least 100-fold selectivity for Casp2. Bars represent the mean ± SEM of at least two individual experiments each performed in duplicate or triplicate.

Table 2.10. Binding data (pK_i values) and selectivity ratios of peptides **2.063**-**2.088** and **2.093**-**2.109** at Casp2 and Casp3.

Sequence	Comp.	pK_i ± SEM				Selectivity ratios of K_i (Casp2: Casp3)
		Casp2	N	Casp3	N	
AcVD(Orn)VD-CHO	**2.063**	7.37 ± 0.04[a]	2	7.52 ± 0.04	3	1:1
		6.92[b]	1			4:1
AcVD(Dab)VD-CHO	**2.064**	7.44 ± 0.04[a]	4	7.54 ± 0.01	4	1:1
AcVD(Dap)VD-CHO	**2.065**	6.53 ± 0.05[a]	2	7.38 ± 0.09	3	7:1
		6.18[b]	1			16:1
AcVDRVD-CHO	**2.066**	7.38 ± 0.07[a]	3	7.21 ± 0.05	3	1:1
AcVD(AcK)VD-CHO	**2.067**	7.70 ± 0.01[a]	2	7.96 ± 0.13	3	2:1
		7.41[b]	1			4:1
AcVDV(Orn)D-CHO	**2.068**	7.45 ± 0.04[a]	4	6.60 ± 0.04	4	1:7
AcVDV(Dab)D-CHO	**2.069**	7.26 ± 0.04[a]	4	5.82 ± 0.09	4	1:28
AcDV(Dab)D-CHO	**2.070**	4.93 ± 0.07[b]	2	5.48 ± 0.03	2	4:1
AcVDV(Dap)D-CHO	**2.071**	6.77 ± 0.09[a]	4	6.14 ± 0.04	4	1:4
AcVDVRD-CHO	**2.072**	7.37 ± 0.03[a]	2	7.12 ± 0.17	3	1:2
		7.07[b]	1			1:1
AcVDV(AcK)D-CHO	**2.073**	7.53 ± 0.13[a]	2	7.60 ± 0.12	3	1:1
		7.30[b]	1			2:1
AcVDFVD-CHO	**2.074**	7.00 ± 0.12[a]	2	8.02 ± 0.15	3	10:1
		6.50[b]	1			33:1
AcITV(Orn)D-CHO	**2.075**	6.14 ± 0.12[a]	2	5.68 ± 0.11	2	1:3
		6.14 ± 0.04[b]	2			1:3
AcTV(Orn)D-CHO	**2.076**	4.62 ± 0.14[a]	2	4.77 ± 0.01	2	1:1
AcV(Orn)D-CHO	**2.077**	< 4[a]	2	< 4	2	-
AcITV(Dab)D-CHO	**2.078**	5.85 ± 0.04[a]	2	5.04 ± 0.11	3	1:6
		5.38 ± 0.18[b]	2			1:2

Table 2.10 (continued)

Sequence	Comp.	pK$_i$ ± SEM				Selectivity ratios of K$_i$ (Casp2: Casp3)
		Casp2	N	Casp3	N	
AcTV(Dab)D-CHO	**2.079**	4.21 ± 0.11[a]	2	4.43 ± 0.21	2	2:1
AcV(Dab)D-CHO	**2.080**	4.28 ± 0.18[a]	2	< 4	2	> 1:2
AcITV(Dap)D-CHO	**2.081**	5.93 ± 0.58[a]	2	5.32 ± 0.17	3	1:4
		5.48 ± 0.01[b]	2			1:1
AcTV(Dap)D-CHO	**2.082**	< 4[a]	2	4.43 ± 0.21	2	3:1
AcV(Dap)D-CHO	**2.083**	< 4[a]	2	< 4	2	-
AcITV(AcK)D-CHO	**2.084**	6.30 ± 0.06[a]	2	7.34 ± 0.12	3	11:1
		6.24 ± 0.01[b]	2			13:1
AcTV(AcK)D-CHO	**2.085**	4.70 ± 0.18[a]	2	6.65 ± 0.10	3	89:1
		4.68 ± 0.03[b]	2			93:1
AcV(AcK)D-CHO	**2.086**	< 4[a]	2	5.02 ± 0.15	2	> 10:1
AcATV(Dab)D-CHO	**2.087**	4.72 ± 0.02[b]	2	4.68 ± 0.09	2	1:1
AcTDTAD-CHO	**2.088**	7.48 ± 0.14[a]	2	7.22 ± 0.12	3	1:2
		7.19 ± 0.15[b]	2			1:1
AcVDV(S-Me-THIQ)D-CHO	**2.093**	7.89 ± 0.02[a]	5	6.04 ± 0.06	5	1:60
AcVDV(R-Me-THIQ)D-CHO	**2.094**	4.98 ± 0.20[a]	5	< 4.0	4	> 1:9
AcVDV(S-Br-THIQ)D-CHO	**2.095**	7.96 ± 0.04[a]	3	6.52 ± 0.02	3	1:28
AcVDV(R-Br-THIQ)D-CHO	**2.096**	4.74 ± 0.50[a]	2	4.42 ± 0.17	2	1:2
(Quin)VDV(S-Me-THIQ)D-CHO	**2.097**	7.50 ± 0.07[a]	4	6.45 ± 0.09	4	1:11
(Quin)VDV(R-Me-THIQ)D-CHO	**2.098**	5.33 ± 0.54[a]	3	4.32 ± 0.32	3	1:10
(Quin)VDV(S-Br-THIQ)D-CHO	**2.099**	7.41 ± 0.05[a]	4	6.66 ± 0.08	4	1:6
(Quin)VDV(R-Br-THIQ)D-CHO	**2.100**	5.38 ± 0.04[a]	3	4.58 ± 0.14	3	1:6

Table 2.10 (continued)

Sequence	Comp.	pK_i ± SEM				Selectivity ratios of K_i (Casp2: Casp3)
		Casp2	*N*	*Casp3*	*N*	
Idc(hE)V(*S*-Me-THIQ)D-CHO	**2.101**	7.40 ± 0.11[a]	3	< 4.5	3	> 1:794
Idc(hE)V(*S*-Me-THIQ)D-CN	**2.106**	8.12 ± 0.10[a]	3	6.03 ± 0.06	3	1:123
Idc(hE)V(Dab)D-CHO	**2.107**	7.18 ± 0.04[b]	4	< 4	3	> 1:1514
Idc(hE)(Tle)(Dab)D-CHO	**2.108**	6.76 ± 0.04[b]	4	< 4	3	> 1:575
Idc(hE)(BnT)(Dab)D-CHO	**2.109**	7.40 ± 0.04[b]	3	< 4	3	> 1:2512

Data shown are mean values ± SEM of N independent experiments, each performed in duplicate or triplicate. Data were analyzed by nonlinear regression and were best fitted to sigmoidal concentration−response curves using 4PL regression using GraphPad Prism. [a]Data represent pK_i values determined with Casp2. [b]Data represent pK_i values determined with cpCasp2. Saturation binding curves of the enzymes can be seen in chapter **2.7.5** (cf. Figures 2.286, 2.287, and 2.288).

Table 2.11. Binding data (pK_i values) of selected peptides (**2.064**, **2.068**, **2.069**, **2.071**, **2.081**, **2.084**, **2.093**-**2.095**, **2.097**-**2.099**, **2.101**, **2.106**, and **2.109**) at Casp1, Casp6, Casp7, and Casp9.

Sequence	Comp.	pKi ± SEM							
		Casp1	*N*	*Casp6*	*N*	*Casp7*	*N*	*Casp9*	*N*
AcVD(Dab)VD-CHO	**2.064**	6.04 ± 0.01	2	< 4	2	7.34 ± 0.08	2	5.17 ± 0.14	2
AcVDV(Orn)D-CHO	**2.068**	5.82 ± 0.03	2	< 4	2	5.92 ± 0.01	2	< 4.5	2
AcVDV(Dab)D-CHO	**2.069**	5.43 ± 0.11	2	< 4	2	4.61 ± 0.26	2	< 4	2
AcVDV(Dap)D-CHO	**2.071**	5.48 ± 0.05	2	< 4	2	5.12 ± 0.06	2	< 4	2
AcITV(Dap)D-CHO	**2.081**	5.82 ± 0.29	2	4.42 ± 0.37	2	4.61 ± 0.47	2	4.68 ± 0.02	2
AcITV(AcK)D-CHO	**2.084**	6.74 ± 0.19	2	6.01 ± 0.39	2	6.65 ± 0.05	2	5.33 ± 0.04	2
AcVDV((*S*)-Me-THIQ)D-CHO	**2.093**	5.62 ± 0.05	3	< 4	3	4.37 ± 0.15	3	4.31 ± 0.25	3
AcVDV(*R*-Me-THIQ)D-CHO	**2.094**	< 4	3	< 4	3	< 4.0	3	< 4.0	3

Table 2.11 (continued)

Sequence	Comp.	pK$_i$ ± SEM							
		Casp1	*N*	*Casp6*	*N*	*Casp7*	*N*	*Casp9*	*N*
AcVDV(*S*-Br-THIQ)D-CHO	**2.095**	5.84 ± 0.03	2	< 4	2	4.84 ± 0.05	2	4.48 ± 0.05	2
(Quin)VDV(*S*-Me-THIQ)D-CHO	**2.097**	6.94 ± 0.11	2	< 4	2	5.12 ± 0.17	2	4.68 ± 0.34	2
(Quin)VDV(*R*-Me-THIQ)D-CHO	**2.098**	5.04	1	< 4	1	< 4	1	< 4	1
(Quin)VDV(*S*-Br-THIQ)D-CHO	**2.099**	6.85 ± 0.04	2	< 4	2	5.24 ± 0.03	2	4.83 ± 0.01	2
Idc(hE)V(*S*-Me-THIQ)D-CHO	**2.101**	6.41 ± 0.12	2	< 4	2	< 4.0	2	5.12 ± 0.04	2
Idc(hE)V(*S*-Me-THIQ)D-CN	**2.106**	< 4	2	< 4	2	4.80 ± 0.06	2	4.40 ± 0.40	2
Idc(hE)(BnT)(Dab)D-CHO	**2.109**	5.95 ± 0.01	2	< 4	2	< 4	2	< 4	2

Data shown are mean values ± SEM of N independent experiments, each performed in duplicate or triplicate. Data were analyzed by nonlinear regression and were best fitted to sigmoidal concentration−response curves using 4PL regression using GraphPad Prism. Saturation binding curves of the enzymes can be seen in chapter **2.7.5** (cf. Figures **2.285** and 2.289-2.291).

2.4.2.3 *In vitro* Cleavage Assay: Measuring the Enzyme-catalyzed Formation of Δtau314 by Casp2 in the Presence of 2.093, 2.094, and 2.106
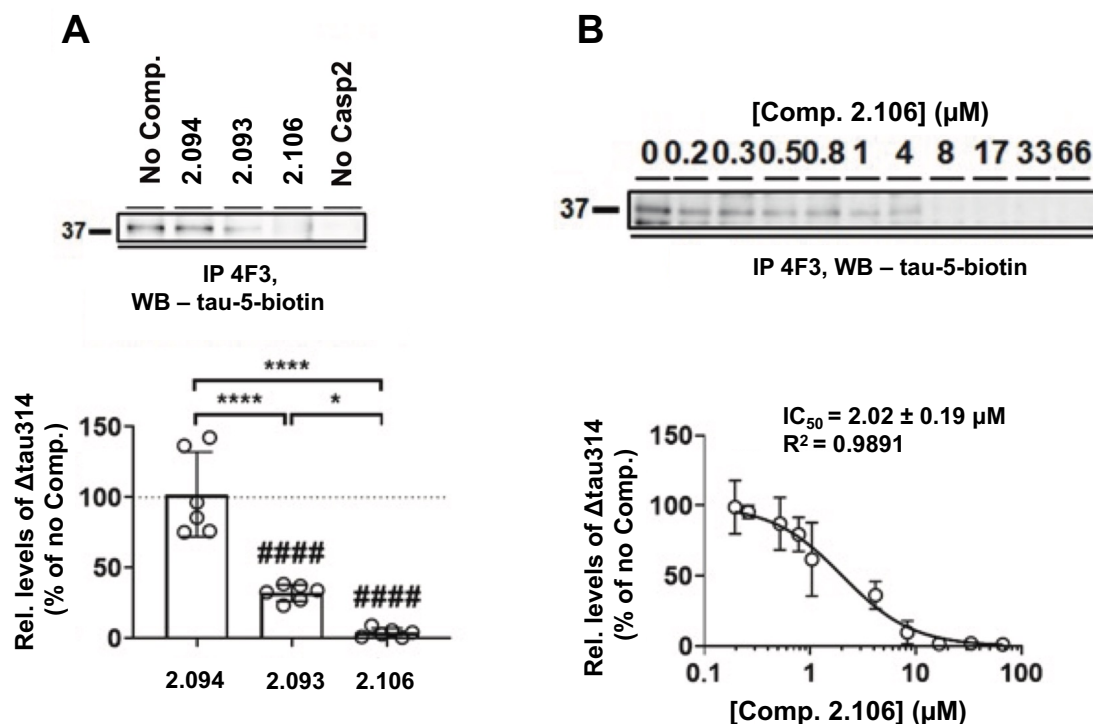
Figure 2.022. (**A**) *Lower panel:* Inhibitors **2.093**, **2.094**, and **2.106** were investigated in an *in vitro* cleavage assay, measuring the formation of Δtau314 by Casp2. Quantification of the inhibition of enzyme-catalyzed Δtau314 production by the peptides, reveals different efficacies of the inhibitors. The level of Δtau314 produced in the absence of any tested compound was defined as 100% (dotted line). Experiments were repeated six times. Individual values (open circles), means (histograms), and standard deviations (SDs, error bars) are shown. A single-sample *t*-test was performed to compare the effect of each compound to that of no compound (####, $p < 0.0001$). One-way ANOVA was performed to compare effects of tested compounds ($F_{(2, 15)} = 48.50$, $P < 0.0001$), followed by Tukey's *post hoc* test (*, $p < 0.05$; ****, $p < 0.0001$). *Upper panel*: A representative immunoprecipitation (IP, 4F3)/Western blotting (WB, tau-5-biotin) showing Δtau314 formation in the presence of inhibitors at 10 μM. Δtau314 formation in the absence of any compound (positive control) and a reaction in the absence of an enzyme (negative control). (**B**) *Lower panel*: Amount of Δtau314 formation (normalized to the no-compound control) in the presence of various concentrations of **2.106** were analyzed and fitted to a dose-response curve. Experiments were performed in duplicate. Means (open circles) and SDs (error bars) are shown. *Upper panel*: a representative IP (4F3)/WB (tau-5-biotin) showing Δtau314 in the presence of various concentrations of compound **2.106**.

Compounds **2.093**, **2.094** (served as negative control), and **2.106** were evaluated in an *in vitro* Casp2 cleavage assays using purified recombinant proteins.[105] Mass spectrometry (MS) was used to determine the formation of Δtau314, the soluble truncated tau fragment ending C-terminally at D314[51]. The level of Δtau314 produced

in the absence of any inhibitor is defined as 100%. At 10 µM, compounds AcVDV((*S*)-Me-THIQ)D-CHO (**2.093**) and Idc(hE)V((*S*)-Me-THIQ)D-CN (**2.106**) diminish tau cleavage by 68% and 96%, respectively. In comparison, the epimer of **2.093** AcVDV(*R*)-Me-THIQ)D-CHO (**2.094**) demonstrates no inhibition of Δtau314 formation (cf. Figure 2.022A). The level of Δtau314 formation by Casp2 was determined for various concentrations of compound **2.106**. The results were fitted to a dose-response curve to determine an IC_{50} of 2.02 µM for Idc(hE)V((*S*)-Me-THIQ)D-CN (cf. Figure 2.022B).

2.4.2.4 Preventing the Accumulation of P301S Tau in Dendritic Spines of Cultured Rat Hippocampal Neurons

Frontotemporal dementia with parkinsonism-17 (FTDP-17) is an autosomal tauopathy linked with a mutation in the tau gene.[109] The excessive accumulation in dendritic spines of mutant tau is linked to FTDP-17. This hyper-accumulation has been shown to depend on tau truncation by caspase-2.[51] A P301S tau mutation linked to FTDP-17[109,110] was performed to investigate whether **2.106** can prevent tau from accumulating in the spines. Dissociated hippocampal neurons from postnatal day 0-1 rat puppies were cultured. After 5-7 days *in vitro* (DIV) culturing, the neurons were co-transfected with plasmids encoding DsRed (to label neuronal morphology) and GFP-tagged wild-type or P301S mutant tau proteins.[80] Neurons at 17-18 DIV were incubated with 10 µM compound **2.106** for 3 days, and live neurons were imaged at 20-21 DIV. Only few dendritic spines of neurons co-expressing DsRed and wild-type tau contained GFP-tagged tau proteins (cf. Figure 2.023A, top row). In contrast, neurons co-expressing DsRed and GFP-tagged P301S tau accumulated GFP-tagged tau (cf. Figure 2.023A, middle row). Only a few dendritic spines of neurons co-expressing DsRed and GFP-tagged P301S tau accumulated GFP-tagged tau in the presence of Idc(hE)V((*S*)-Me-THIQ)D-CN (**2.106**). The amount of accumulated GFP-tagged tau in the dendritic spines of hippocampal neurons was 21.9% in neurons expressing wild-type tau. For neurons expressing P301S tau, the number increased to 75.5%. **2.106** is capable to normalize the amount of GFP-tagged tau in neurons expressing P301S tau (24.8% (with **2.106**) vs. 75.5% (no **2.106**)) (cf. Figure 2.023B).
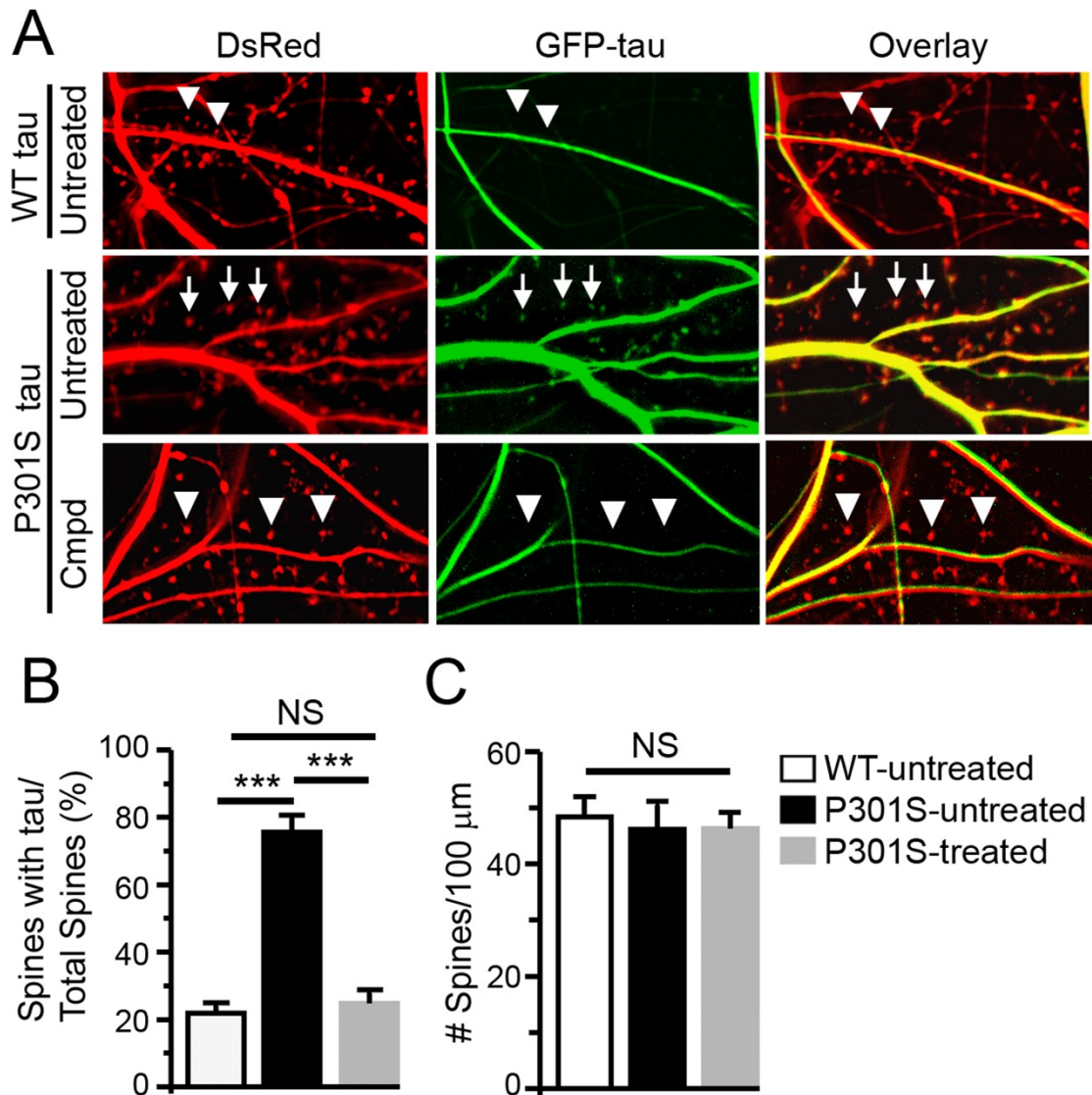
Figure 2.023. Inhibitor **2.106** blocks the hyper-accumulation of tau caused by the P301S mutation in dendritic spines. (**A**) Untreated neurons co-expressing DsRed and GFP-tagged wild-type tau (top row) were compared with neurons co-expressing DsRed and GFP-tagged P301S tau in the absence (middle row) or presence of compound **2.106** (bottom row). Arrows denote dendritic spines containing tau. Triangles denote spines without tau. (**B**) Comparison of the average percentage of dendritic spines labeled by DsRed containing GFP-tagged tau between the three groups. n = 8 neurons in each group; ANOVA, ***, p < 0.001. (**C**) Comparison of the density of dendritic spines (the number of DsRed-labeled dendritic spines/100 μm length of dendrites) between the three groups. n = 8 neurons in each group; ANOVA, NS (not significant), P > 0.05.

2.4.2.5 Efficacy of Casp2 Inhibitors 2.093, 2.094, and 2.106 on P301S Tau-induced Functional Deficits in Dendritic Spines
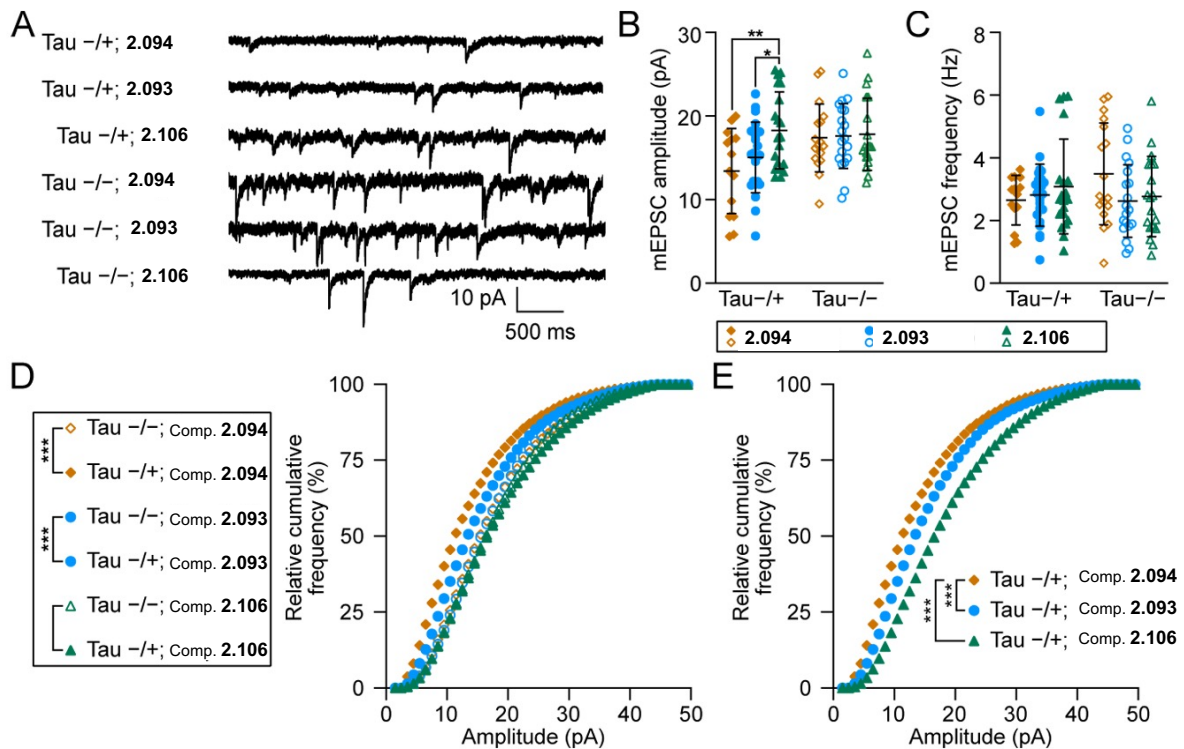
Figure 2.024. Treatment with **2.106** rescues synaptic dysfunction caused by the P301S mutation. (**A**) Representative traces of mEPSCs recorded in Tau−/+ and Tau−/− neurons that were treated with **2.093**, **2.094**, and **2.106**. **B** and **C**) Comparisons between the means of mEPSC amplitude (**B**) or frequency (**C**) between the abovementioned six groups. n = 31 neurons in Compound **2.106** treated groups (−/− and −/+); n = 41 in Compound **2.093** treated groups; n = 39 in Compound **2.094** treated groups; ANOVA, *, $p < 0.05$; **, $p < 0.01$. (**D**) Comparisons of cumulative curves of mEPSC amplitudes recorded in the abovementioned six groups. (**E**) Comparison of the rescuing efficacy between **2.106** and **2.093** in Tau −/+ neurons. For **D** and **E**: Mann-Whitney U Test, *, $p < 0.05$; ***, p, 0.001. For **B-E**, orange circles, blue circles, and blue triangles denote treatment with **2.093**, **2.094**, and **2.106**, respectively. Closed shapes denote Tau−/+ mice, and open shapes denote Tau−/− mice.

Models of various tauopathies revealed that hyper-accumulation of tau in dendritic spines is related to a reduction in postsynaptic excitatory neurotransmission due to the internalization of AMPA receptors.[51,80,111–114] **2.093**, **2.094**, and **2.106** were examined in order to find out whether they are able to rescue functional synaptic deficits in a cellular model of tauopathy. For these examinations, PS19 transgenic mice expressing P301S mutant tau were used. Primary hippocampal neurons from heterozygous transgenic mice overexpressing P301S[115,116] and littermate controls (labeled as Tau −/+ and Tau −/− respectively) (cf. Figure 2.024). To reveal functional deficits, miniature

excitatory synaptic currents (mEPSCs) of the neurons were recorded. The Casp2 inhibitors **2.093**, **2.094**, or **2.106** were added to the culture media in a final concentration of 10 µM and incubated for 3 days. The average amplitudes of mEPSC responses in Tau −/+ and Tau −/− neurons treated with **2.106** did not differ significantly, suggesting that the Casp2 inhibitor rescues impaired mEPSC amplitudes (ANOVA, F = 3.3, P > 0.05). In contrast, neurons treated with **2.094** (epimer of **2.093**, which serves as negative control) demonstrate a significantly smaller amplitude of mEPSC responses in Tau −/+ neurons than that in Tau −/− neurons (cf. Figure 2.024B, ANOVA, F = 3.3; Bonferroni post hoc test: P < 0.05). **2.093** cannot rescue post-synaptic neurotransmission in Tau −/+ to the same extent as **2.106**. This leads to the conclusion that the expression of P301S tau impaired postsynaptic function of the excitatory synapses by reducing the number of functional AMPA receptors on post-synaptic membranes and that **2.106** and **2.093** (significantly less) can compensate the decrease, while **2.094** is not able. The average amplitudes of mEPSC responses of Tau −/+ neurons treated with **2.106** are markedly larger than those treated with **2.094** (cf. Figure 2.024B, F = 3.3; Bonferroni after test: P < 0.01) or **2.093** (cf. Figure 2.024B, F = 3.3; Bonferroni post-hoc test: P < 0.05). To confirm the biological effects observed, the cumulative curves of mEPSC amplitudes were analyzed. The cumulative curve of mEPSC amplitudes of **2.106** treated neurons from Tau −/+ compared with Tau −/− mice is not significantly shifted (cf. Figure 2.024D, Mann-Whitney U test: P > 0.05). This implies that **2.106** completely blocks the synaptic impairment caused by the P301S mutation. Meanwhile, the cumulative curve of mEPSC amplitudes of **2.094** treated neurons from Tau −/+ compared with Tau −/− mice is shifted to the left (cf. Figure 2.024D, Mann-Whitney U test: P < 0.001), suggesting that the P301S mutation reduces the amplitudes of mEPSCs. The cumulative curve of mEPSC amplitudes of **2.093** treated neurons from Tau −/+ compared with Tau −/− mice is shifted to the left but less markedly (cf. Figure 2.024D, Mann-Whitney U test: P < 0.001), indicating that **2.093** partially blocks the synaptic impairment caused by the P301S mutation. Comparison of the cumulative curves of Tau −/+ neurons treated with each compound displays that **2.106** is the most active compound since it was eligible to shift the cumulative curve of mEPSC amplitudes more to the right than all other compounds (cf. Figure 2.024E, Mann-Whitney U test: P < 0.001). No changes in presynaptic functions were noticed since there were no significant differences in the average frequency of mEPSCs between the six groups (cf. Figure 2.024C, ANOVA, F = 0.6, P > 0.05).

2.4.2.6 Crystallography

While there has been some exploration of the structural consequences of variation of the P4 amino acid from the preferred aspartic acid in complexes with Casp3[117] and Casp7[118,119], these have been limited to tetrapeptide inhibitors, and none have specifically involved the P4 threonine found to be preferred in this series. In addition, the binding principle of the peptides designed for the Glu52 engagement, as well as the negative controls, should be determined. Motivated by curiosity regarding details of how the threonine substitutes for the well-characterized aspartic acid and how amino acids installed for the Glu52 engagement of Casp2 actually embed in the Casp3 binding site, crystallographic studies were initiated, and complexes of seven inhibitors with caspase-3 were obtained: one with compound AcVD(Orn)VD-CHO (**2.063**), AcVDRVD-CHO (**2.066**), AcVD(AcK)VD-CHO (**2.067**), AcVDV(Dab)D-CHO (**2.069**), AcVDFVD-CHO (**2.074**), AcITV(Orn)D-CHO (**2.075**), and one with AcITV(Dab)D-CHO (**2.078**). Various unique crystals (space groups $P2_1$, $P2_12_12_1$, and $P6_3$) resulted from identical crystallization conditions. Each form includes an activated heterotetramer in the crystallographic asymmetric unit. Diffraction quality varies within this collection of structures from 1.67 to 3.25 Å.

In the 1.9 Å complex with AcITV(Dab)D-CHO (**2.078**), the position of the N-terminal acetyl group is not resolved, whereas in other structures, the ligand backbone geometry is otherwise well-defined by electron density across the length of the pentapeptide. As to be expected, the -CHO leaving group is displaced, and a covalent bond joins the P1 Asp to Cys163. The P4 threonine sidechain occupies the same position and engages in similar H-bonding in all threonine-containing structures. A comparison of the complex of compound AcITV(Dab)D-CHO with the canonical inhibitor is provided in Figure 2.025. Backbone H-bonds observed in the two complexes are the same, but the lone hydroxyl group of the threonine sidechain (T4) is not capable of accepting hydrogen bonds from both Phe250 and Asn208 as can a D4 carboxylate. Only the hydrogen bond from the T4 OH to Phe250 NH is observed. It was imagined that this might cause either the inhibitor to slide away from L4 toward Asn208 and L3, or L4 to move in tighten packing against the inhibitor with a smaller footprint, but neither change has occurred. The threonine seems to be an isosteric substitute for aspartic acid in P4, albeit with a predictable loss in potency due to the loss of one H-bond.
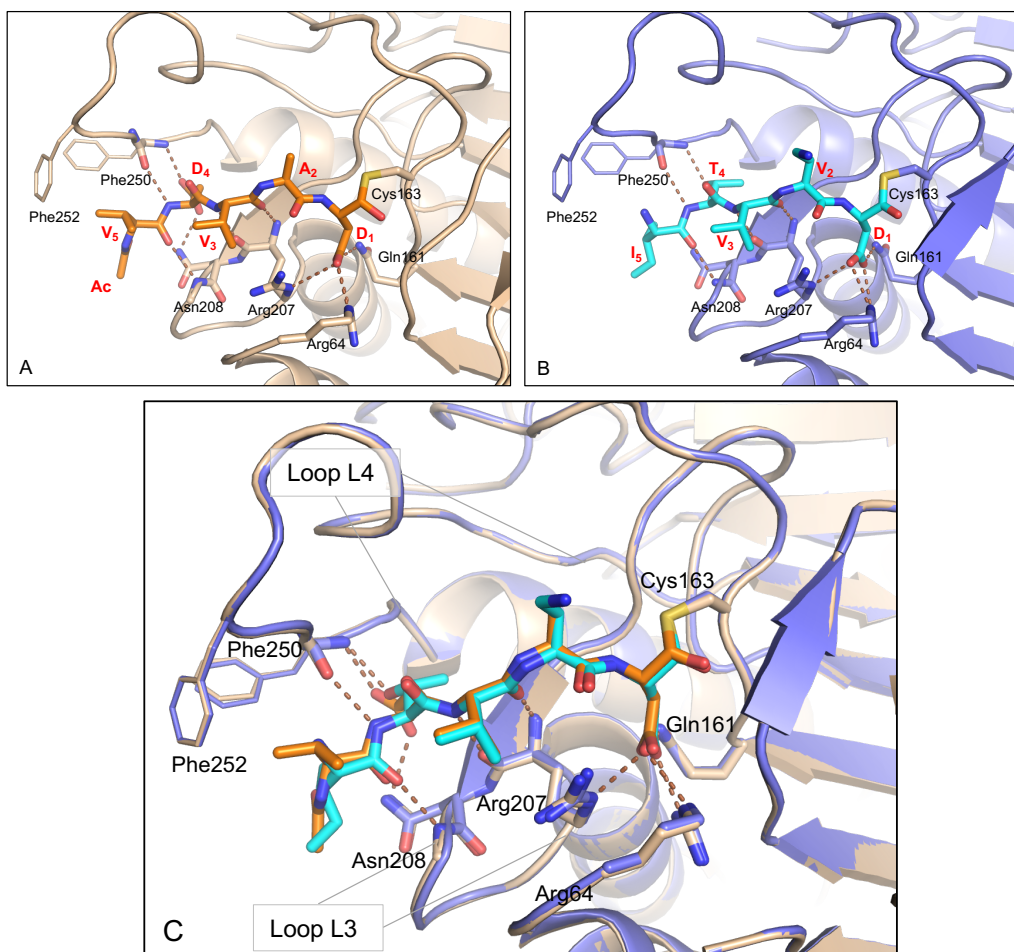
Figure 2.025. A comparison of experimentally determined Casp3 complexes with the canonical Casp2 inhibitor (AcVDVAD-CHO) and non-canonical inhibitor AcITV(Dab)D-CHO. (**A**) The complex with covalently bound AcVDVAD-CHO (PDB-id 2h65). Hydrogen bonding involving the P1 Asp (D_1) to Gln161, Arg64, and Arg207 is universally conserved in all caspase complexes with peptidic substrates, as are the antiparallel H-bonds between the P2 (A_2) and P3 (V_3) amino acids and the backbone of Arg207. In this and other Casp-2/3 structures, the sidechain carboxylate of the aspartic acid in P4 (D_4) generates H-bonds that span the gap between the L4 loop backbone at Phe250 and the sidechain amide of Asn207. The P5 amino acid also accepts an H-bond from the backbone amide of Ser209. (**B**) In the complex with AcITV(Dab)D-CHO (PDB-id 7rna), all the same H-bonds are preserved. However, the P4 threonine sidechain (T_4) can only accept the H-bond from the Phe250. An H-bond from this sidechain to Asn208 is not possible, perhaps accounting for the lower inhibitory potency. (**C**) An overlay of proteins and inhibitors involved in these two complexes reveals how little the protein conformation is altered upon binding of the different inhibitors (AcVDVAD-CHO orange, Casp3 tan; AcITV(Dab)D-CHO cyan, Casp3 blue). Peptidic inhibitors bind cradled in a groove above L3 (residues 209-213) and between L4 (residues 248-263) and L1 (residues 53-65; largely omitted for clarity). While the L4 loop has been shown to move in response to the binding of different inhibitors, little movement is revealed by the comparison of these two complexes.

The complexes with the basic structure AcVDXXD-CHO are all broadly similar, despite variations in the P3 or P2 amino acid. All complexes conserve the constellation of H-bonds around the P1 aspartic acid involving Arg64, Arg207, and Gln161. The anti-

parallel H-bonds between the peptide backbone at P3 and the Arg207 mainchain are exactly as seen in the complex with AcVDVAD-CHO (**2.016**, cf. Figure 2.025). As these peptides also preserve the P4 aspartic acid, H-bonds joining the P4 Asp to the backbone of the L4 loop at Phe250 are also strictly conserved. None of these interactions involve sidechains varied in the different inhibitors. The only significant difference in the complexes is a shift in a portion of the L4 loop of Casp3, specifically residues 251-255 (cf. Figure 2.025). The effect of this shift is to widen the cavity between the L3 and L4 loops where the S5 subsite resides. The shift was first observed in the complex with AcVDPVD-CHO (**2.017**), where it can be attributed to the absence of the H-bonds from P4 Asp to Phe250 and the need for a broader S5 pocket to accommodate the P5 valine in its place (cf. Figure 2.026). However, the L4 shift is actually most pronounced in the AcVDRVD-CHO (**2.066**) and AcVD(AcK)VD-CHO (**2.067**) complexes, where Phe252 has moved 1.6 Å from its position in the AcVDVAD-CHO complex (cf. Figure 2.026). The hydrophobic contacts between the P5 valine and Phe250 and Phe252 are lost with the movement, but hydrogen bonds to both Phe250 and Asn208 by the P4 aspartic acid of L3 are preserved (and even improved), as the P5 valine moves 1.6 Å in the opposite direction to more closely contact L3, which does not move. Two conclusions may be drawn from the examination of these complexes: (1) single amino acid substitution in the peptide inhibitors can induce changes in binding unrelated to direct contacts between the amino acid and the subsite in which it resides, and (2) the protein itself is at least as flexible and responsive to ligand binding as the ligands. This should serve as a cautionary tale when attempting to dock ligands into these proteins using protocols that essentially assume the protein conformation is fixed.
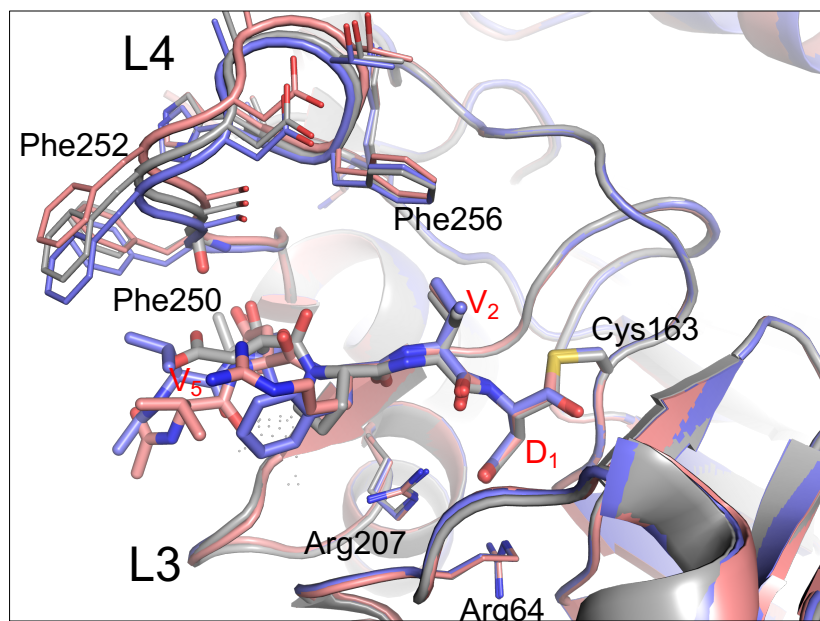
Figure 2.026. L4 loop movements in Casp3-inhibitor complexes. Three complexes are shown to represent the magnitude of the shift that occurs in L4 upon ligand binding (AcVDPVD-CHO (**2.017**), gray; AcVDRVD-CHO (**2.066**), salmon; AcVDFVD-CHO (**2.074**), blue). Inhibitors differ only in the P3 amino acid; although the P3 alpha-carbon position is essentially unchanged in these complexes, the L4 loop shifts significantly. Changes are also observed in P4-P5 of ligands as the gap between L3 and L4 loops widens; ligands seem to prefer to associate more closely with L3 as hydrophobic contacts with L4 are lost. None of the structures resulting during this study show significant movement in Phe256.

For compound (AcVD(AcK)VD-CHO (**2.067**), no density for the acetyl group at the end of the lysine sidechain of P2 can be observed (cf. Table 2.12). This group is essentially dangling into solvent and not held in any specific position. The complex with compound AcVDV(Dab)D-CHO (**2.069**) is interesting as it reveals a structural basis for the selectivity of this compound for Casp2 over Casp3. Diffraction data for this complex are the poorest of all those determined in this work (3.25 Å), but it is nevertheless sufficient to show that the inhibitor binds with the P1 aspartic acid anchored as expected, and the ligand backbone positioned as in all other complexes to make H-bonds along the entire length toward the valine at P5, but sidechains (Phe256 and Tyr204) lining the P2 subsite limit extension of the diaminobutyric acid (Dab), forcing it to adopt a strained conformation (cf. Figure 2.027). These findings are consistent with the Casp2 and Casp3 results from the fluorescence-based *in vitro* assay in chapter **2.4.2.2**. Further crystallographic data and refinement statistics are provided in Table 2.12 and 2.13.
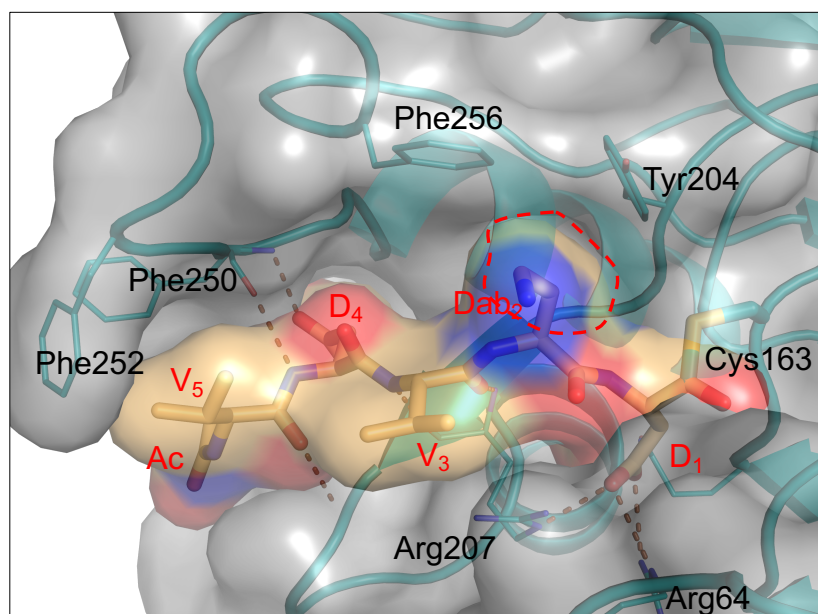
Figure 2.027. The Casp3/AcVDV(Dab)D-CHO (**2.069**) complex. Backbone interactions conserved throughout the peptide complexes anchor the ligand in the expected position, but sidechains (Phe256 and Tyr204) lining the P2 subsite limit extension of the Dab, forcing it to adopt a strained conformation. Solvent-accessible surfaces of both Casp3 (gray) and the ligand are shown to illustrate the tight packing that exists against the ceiling of the P2 subsite (dashed red line).

Table 2.12. Crystallographic data and refinement statistics for Casp3 co-crystal Structures with compounds **2.063**, **2.066**, **2.067**, and **2.069**.
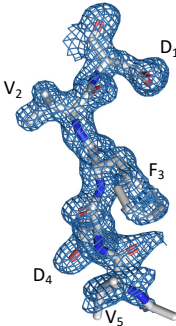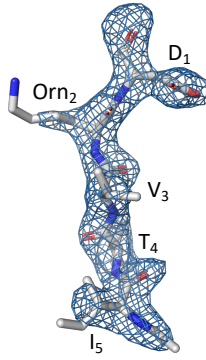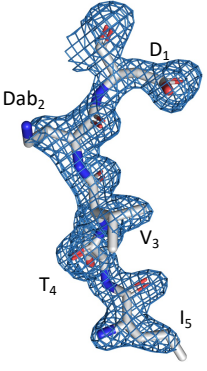
Data collection and processing				
Compound	**2.063**	**2.066**	**2.067**	**2.069**
Ligand	AcVD(Orn)VD-CHO	AcVDRVD-CHO	AcVD(AcK)VD-CHO	AcVDV(Dab)D-CHO
PDB ID code	7rn8	7rnb	7rn7	7seo
Omit Map (3s)				
Resolution range (Å)	43.28-2.4 (2.49-2.4)	56.22-1.75 (1.81-1.75)	43.28-2.4 (2.49-2.4)	19.90-3.25 (3.37-3.25)
Space group	P 2$_1$	P 6$_3$	P 2$_1$	P 2$_1$
a, b, c (Å)	50.51 68.04 82.49	129.83 129.83 60.42	50.51 68.04 82.49	50.46 66.13 83.47
a, b, g (°)	90 90.61 90	90 90 120	90 90.61 90	90 90.87 90
Observations	41458 (4026)	112174 (11468)	41458 (4026)	14243 (1147)

Table 2.12 (continued)

Data collection and processing				
Compound	**2.063**	**2.066**	**2.067**	**2.069**
Ligand	AcVD(Orn)VD-CHO	AcVDRVD-CHO	AcVD(AcK)VD-CHO	AcVDV(Dab)D-CHO
Unique reflections	21706 (2160)	56317 (5772)	21706 (2160)	8170 (702)
Multiplicity	1.9 (1.9)	2.0 (2.0)	1.9 (1.9)	1.7 (1.6)
Completeness (%)	98.36 (98.18)	95.92 (98.68)	98.36 (98.18)	92.41 (79.39)
Mean I/s(I)	4.44 (2.19)	17.08 (4.43)	4.44 (2.19)	5.33 (3.41)
Wilson B-factor (Å^2)	30.39	22.28	30.39	47.94
R_{merge}	0.1175 (0.3766)	0.0208 (0.1348)	0.1175 (0.3766)	0.0612 (0.1046)
CC1/2	0.965 (0.718)	0.999 (0.943)	0.965 (0.718)	0.993 (0.978)
CC*	0.991 (0.914)	1.00 (0.985)	0.991 (0.914)	0.998 (0.994)
Structure Refinement				
Reflections used	21693 (2161)	56310 (5772)	21693 (2161)	8144 (701)
R_{free} reflections (5%)	1107 (133)	2816 (284)	1107 (133)	432 (42)
R_{work}	0.1878 (0.2272)	0.1668 (0.1945)	0.1878 (0.2272)	01883 (0.1977)
R_{free}	0.2515 (0.3158)	0.2018 (0.2507)	0.2515 (0.3158)	0.2691 (0.3534)
CC_{work}	0.946 (0.877)	0.969 (0.916)	0.946 (0.877)	0.937 (0.936)
CC_{free}	0.919 (0.655)	0.959 (0.844)	0.919 (0.655)	0.875 (0.670)
Non-hydrogen atoms	3915	4150	3915	3931
Solvent molecules	105	260	105	59
Protein residues	473	478	473	478
Bonds (Å^2)	0.008	0.007	0.008	0.002
Angles (°)	1.09	0.95	1.09	0.55
Ramachandran Analysis				
Favored (%)	96.48	97.85	96.48	95.45
Allowed (%)	3.52	2.15	3.52	4.33
Outliers (%)	0	0	0	0.22
Rotamer outliers	0	0	0	0
Clashscore	5.18	3.37	5.18	8.33
Mean B-factor (Å^2)	30.12	24.96	30.12	48.5

[#]Values in parenthesis refer to the highest resolution shell.

Table 2.13. Crystallographic data and refinement statistics for Casp3 co-crystal Structures with compounds **2.074**, **2.075**, and **2.078**.

Data collection and processing			
Compound	**2.074**	**2.075**	**2.078**
Ligand	AcVDFVD-CHO	AcITV(Orn)D-CHO	AcITV(Dab)D-CHO
PDB ID code	7rn9	7usp	7rna
Omit Map (3s)			
Resolution range (Å)	42.35-1.67 (1.73-1.67)	43.2-2.85 (2.95-2.85)	43.2-1.9 (1.97-1.90)
Space group	$P\,2_1 2_1 2_1$	$P\,2_1$	$P\,2_1$
a, b, c (Å)	67.47 85.20 97.61	50.117 66.133 83.044	50.05 66.17 83.22
a, b, g (°)	90 90 90	90 90.881 90	90 90.93 90
Observations	127065 (10909)	22247 (1822)	68436 (6860)
Unique reflections	64162 (5853)	12015 (1080)	41044 (4176)
Multiplicity	2.0 (1.9)	1.9 (1.7)	1.7 (1.6)
Completeness (%)	97.13 (89.45)	93.38 (83.58)	95.42 (97.80)
Mean I/s(I)	14.75 (2.46)	13.18 (4.52)	11.02 (2.30)
Wilson B-factor (Å^2)	21.75	46.5	30.54
R_{merge}	0.0221 (0.2335)	0.03575 (0.1317)	0.0323 (0.419)
CC1/2	0.999 (0.921)	0.997 (0.964)	0.999 (0.731)
CC*	1.00 (0.979)	0.999 (0.991)	1.00 (0.919)
Structure Refinement			
Reflections used	64072 (5853)	12003 (1079)	41013 (4176)
R_{free} reflections (5%)	3259 (283)	616 (66)	1991 (186)
R_{work}	0.1831 (0.2943)	0.1776 (0.2338)	0.1945 (0.2817)
R_{free}	0.2099 (0.3383)	0.2539 (0.3660)	0.2099 (0.3268)
CC_{work}	0.969 (0.907)	0.948 (0.902)	0.963 (0.867)

Table 2.13 (continued)

Structure Refinement			
Compound	**2.074**	**2.075**	**2.078**
Ligand	AcVDFVD-CHO	AcITV(Orn)D-CHO	AcITV(Dab)D-CHO
CC$_{free}$	0.962 (0.844)	0.917 (0.664)	0.935 (0.789)
Non-hydrogen atoms	4130	3855	3945
Solvent molecules	289	16	130
Protein residues	472	473	475
Bonds (Å^2)	0.008	0.008	0.008
Angles (°)	0.93	1.05	1
Ramachandran Analysis			
Favored (%)	98.04	96.06	98.26
Allowed (%)	1.96	3.94	1.74
Outliers (%)	0	0	0
Rotamer outliers	0	0.71	1
Clashscore	4.99	11	5.94
Mean B-factor (Å^2)	24.23	40.9	34.56

[#]Values in parenthesis refer to the highest resolution shell.

2.4.3 Conclusion

Within this series of peptides, an attempt was made to exclusively target Casp2 over Casp3 by inserting basic amino acids as structural features in P2 and P3 of the peptides, which are supposed to interact with the negatively charged Glu52 in the binding pocket of Casp2. The presence of Glu52 in proximity to the S2 and S3 subsite of Casp2 is unique within the family of caspases. Casp3 is distinguished by an uncharged threonine at this site. Starting from AcVDKVD-CHO, AcVDKVD-CHO, and AcITVKD-CHO, various basic amino acids with different chain lengths were introduced at the position of lysine to improve affinity and selectivity for Casp2. In addition, different negative controls were implemented by introducing acetylated lysine and phenylalanine instead of basic amino acids to verify whether an ionic interaction is involved in the binding. AcVDV(Dab)D-CHO (**2.069**) (Casp2 pK_i: 7.26; Casp3 pK_i: 5.82) demonstrates the best results within the approach, displaying a 27.7-fold selectivity over Casp3, 67.3-fold selectivity over Casp1, 444-fold selectivity over Casp7, and at least 1827-fold selectivity over Casp6 and Casp9. Since AcVD(AcK)VD-CHO (**2.067**), AcVDV(AcK)D-CHO (**2.073**), AcITV(AcK)D-CHO (**2.084**), and AcVDFVD-CHO (**2.074**) demonstrate affinity, both at Casp2 and at Casp3, the hypothesis of ionic interactions between a basic amino acid at position 2 or 3 and Glu52 in the subsite of Casp2 must be doubted. Even if an ionic interaction between Glu52 and basic amino acids of the peptides can be excluded, this series provides important insights into amino acids (e.g., diaminobutyric acid (Dab)) that can offer a selectivity advantage over caspase-3. These findings and others from already published structure-activity relationship (SAR) studies served as a fundament for the rational design of optimized inhibitors with respect to affinity and selectivity. Poreba et al. (2019) reported the excellent properties of (*S*)-indoline-2-carboxylic acid (Idc) at position P5 and hL-glutamic acid (hE) at position P4.[93] (*S*)-6-Me-THIQ-COOH was installed at position 2 as a structural motif, derived from the findings of Maillard et al.[92] A nitrile was introduced as a reactive warhead, since Boxer et al. (2011)[98] proved, that they are an excellent structural feature for the inhibition of caspases. This resulted in highly active and selective Casp2 inhibitors such as Idc(hE)V(*S*-Me-THIQ)D-CHO (**2.101**, Casp2 pK_i: 7.40; Casp3 pK_i: <4.5), Idc(hE)V(*S*-Me-THIQ)D-CN (**2.106**, Casp2 pK_i: 8.12; Casp3 pK_i: 6.03), and Idc(hE)V(Dab)D-CHO (**2.107**, Casp2 pK_i: 7.18; Casp3 pK_i: < 4). An *in vitro* Casp2 cleavage assay proved that **2.106** inhibits the formation of Δtau314, the soluble

truncated tau fragment, by 96%. Compound **2.106** blocked the excessive accumulation of tau in the dendritic spines in a P301S tau mutation model linked to FTDP-17 (cf. Figure 2.023). Furthermore, Idc(hE)V(*S*-Me-THIQ)D-CN (**2.106**) restored excitatory neurotransmission in neurons modeling FTDP-17 tauopathy (cf. Figure 2.024). The tau-induced synaptic dysfunction by the excessive accumulation of tau in dendritic spines was proven to induce synaptic dysfunction in models of tauopathy like Alzheimer's disease, Lewy body dementia, FTDP-17, and chronic traumatic encephalopathy. The dysfunctional process is caused by the redistribution of tau from axons to dendrites, initiated by various pathological triggers.[120,121] The findings exhibit that Casp2 exerts its pathological effects on synaptic function catalytically by truncation of tau at aspartate-314. It can therefore be excluded that the rescue of synaptic functions by the lowering of Casp2, demonstrated by Zhao et al. (2016)[51] is caused by non-catalytically enhancing autophagy and thereby reducing the levels of misfolded and aggregated forms of tau. These are important results to strengthen the case for the development of bioavailable caspase-2 inhibitors for the treatment of tauopathies, such as Alzheimer's disease.

2.5 Design of Casp2 Inhibitors with Improved Physicochemical Properties by Introducing Spacer into the Peptide Backbone
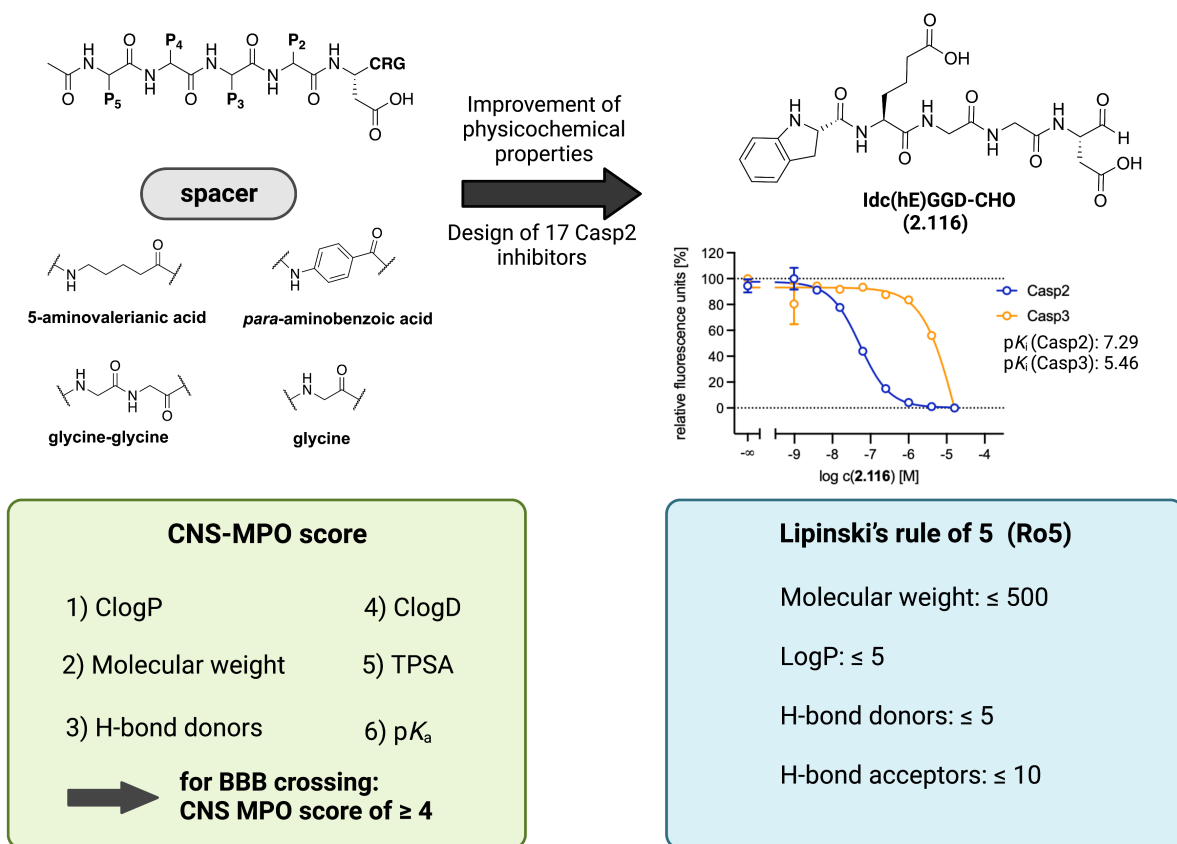
In previous investigations, highly selective and active caspase-2 inhibitors (e.g., **2.107**) have been developed. To tackle neurodegenerative diseases like Alzheimer's disease, it is essential that the drugs reach the desired target site. The blood-brain barrier (BBB) consists of the very dense brain capillary endothelium that is able to prevent the uncontrolled crossing of substances from the blood to the central nervous system (CNS). This study is aimed to improve the physiochemical properties of the Casp2 inhibitors to ensure drug-likeness and CNS penetration. To achieve this, various linkers (5-aminovalerianic acid, glycine, or *para*-aminobenzoic acid) were inserted into the peptide backbone in order to reduce the molecular weight and the number of hydrogen bonds with respect to Lipinski's rule of five. This resulted in a series of 17 peptides that were tested for their Casp2 activity and selectivity. Moreover, an *in silico* study predicting several crucial physicochemical and pharmacokinetic parameters of representative Casp2 inhibitors was carried out.

2.5.1 Design Rationale

The first two series of inhibitors provided essential insights into the influence of different peptide sequences on the selectivity and activity of Casp2 inhibitors. The approach of truncating the inhibitors to tetra- and tripeptides to improve the drug-likeness following Lipinski's rule of 5 (Ro5)[103] did not achieve the desired results in terms of activity for caspase-2.
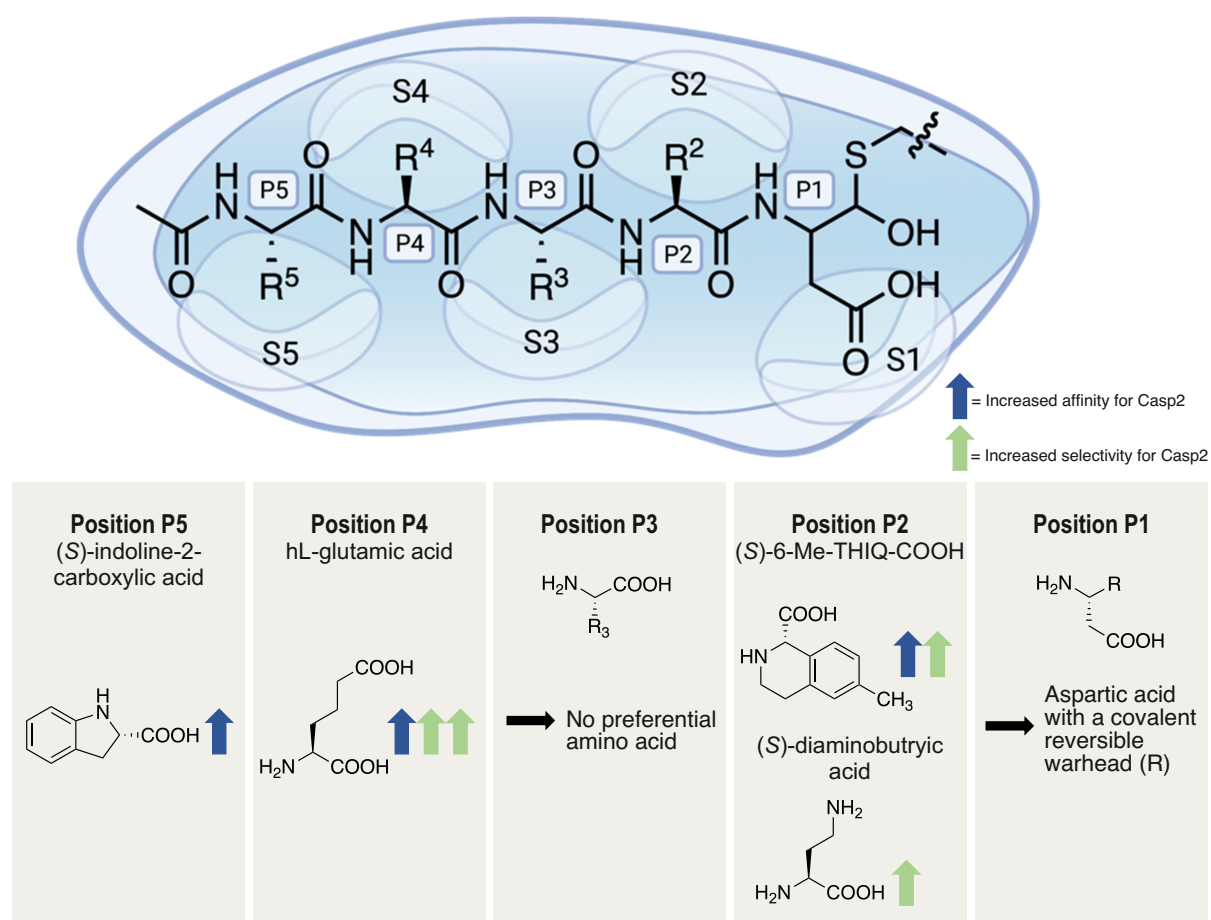
Figure 2.028. Schematic diagram of Casp2 binding site (created with BioRender.com).[122,123] P1-P5 represents the respective amino acid position of the Casp2 inhibitor. S1-S5 represents the respective subsite in the enzyme binding pocket at Casp2. The preferred amino acids for each position, as well as the effect on affinity or selectivity for Casp2 are shown. The blue arrow indicates an increase in affinity for Casp2. The green arrow indicates an increase in selectivity for Casp2.

The findings of the first two series are particularly supposed to facilitate the design of future inhibitors with improved drug-like properties. In the following, the findings are briefly summarized (cf. Figure 2.028): diaminobutyric acid (Dab) at position P2 increases selectivity over Casp3, while (S)-6-Me-THIQ-COOH is capable to enhance

selectivity and activity toward Casp2. h-L-glutamic acid (hE) as a structural feature at position P4 is responsible for a substantial increase in Casp2 selectivity. (S)-indoline-2-carboxylic acid (Idc) causes a sharp increase in potency. No specific amino acid preference can be determined for position P3. Hence, this position can be designed variable. An Aspartic acid with a reversible covalent warhead at position P1 is a prerequisite for active Casp2 inhibition.

The blood-brain barrier (BBB) consists of the brain capillary endothelium and can prevent the uncontrolled crossing of substances from blood to the central nervous system (CNS).[124] This distinctive feature makes it challenging to design drugs with sufficient blood-brain barrier penetration. The BBB is capable of excluding almost 100% of large-molecule neurotherapeutics and more than 98% of all small-molecule drugs. The challenges of designing blood-brain barrier permeable drugs lead to the situation that only a few effective treatments for the majority of CNS disorders are known. Due to their size, most large-molecule biotechnology products, like monoclonal antibodies, recombinant proteins, antisense, or gene therapeutics, are not capable of crossing the BBB. Small molecule drugs targeting CNS disorders are characterized by an average molecular mass of 357 Da.[125] This peptide series strives to design Casp2 inhibitors with superior physicochemical and pharmacokinetic properties, especially in terms of enhanced bioavailability, blood-brain barrier penetration, and cell penetration.

To accomplish this, lowering the molecular weight is a feasible choice since the literature relates poorer intestinal and blood-brain barrier permeability with higher molecular weight. The molecular mass for BBB penetrating drugs ought to be beneath the range of 400-500 Da. In addition, the compounds should display a high lipid solubility.[125] The crossing of the BBB reduces exponentially with the addition of every hydrogen bond donor/acceptor group to the scaffold of the drug.[125] Consequently, the number of amino acids with functional groups (NH and OH bonds) in the side chain must be kept to a minimum to guarantee permeability across a membrane bilayer.[103] The total number of hydrogen bonds should not exceed 8-10; otherwise, the crossing of the BBB is reduced to a minimum.[125] These rules are well summarized with the so-called rule of 5 (Ro5), which implies that for sufficient absorption or permeation, the structural features of the molecule should not exceed: more than 5 H-bond donors, more than 10 H-bond acceptors, a molecular weight of 500, a LogP of 5

(cf. Figure 2.031).[103] For a more precise prediction of the blood-brain barrier penetration of potential drugs the CNS MPO score can be applied. It is expected that the score will enable the prospective development of small-molecule drugs in medicinal chemistry with superior CNS properties. The algorithm of the tool combines six fundamental physicochemical properties. Namely, these are lipophilicity (ClogP), calculated partition coefficient at pH 7.4 (ClogD), molecular weight (MW), topological polar surface area (TPSA), number of hydrogen-bond donors (HBDs), and the most basic center (pK_a) (cf. Figure 2.029). Each parameter is weighted equally in the calculation. The score ranges from 0 to 6, whereby higher scores are preferred for good BBB crossing (MPO desirability score ≥ 4). The advantage of the tool is the use of a flexible, multiparameter approach as opposed to individual hard cutoffs (e.g., Lipinski's rule of 5) for individual physicochemical properties.[126,127]
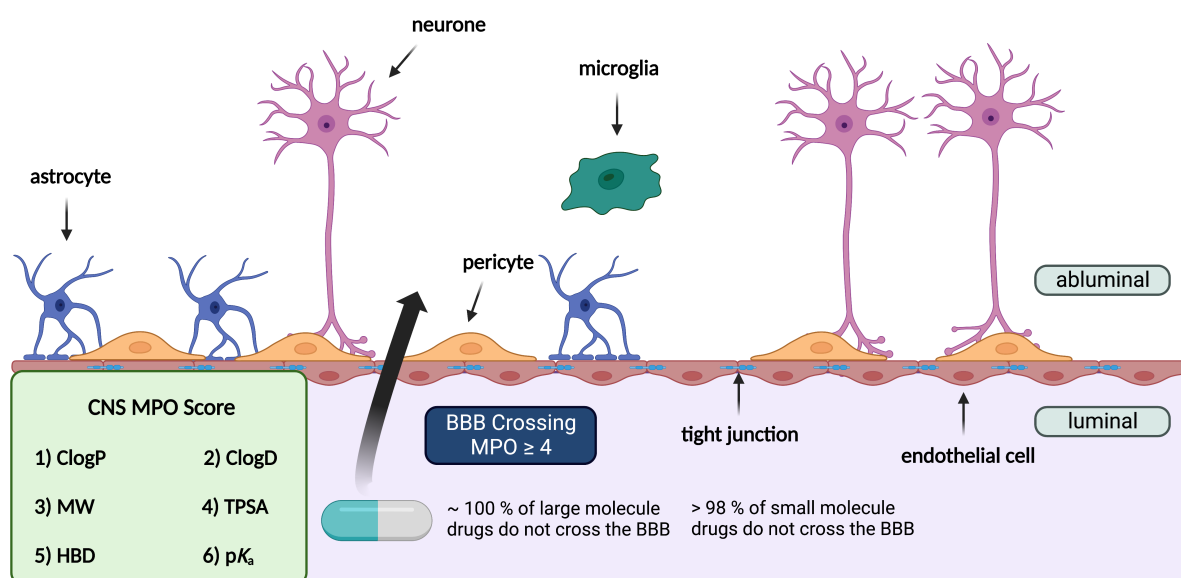
Figure 2.029. Structural overview of the blood-brain barrier (BBB) and the influences of the CNS MPO score. The ability of drugs to cross the BBB is characterized by the MPO score. The MPO score is a dynamic value which is influenced by lipophilicity (ClogP), calculated partition coefficient at pH 7.4 (ClogD), molecular weight (MW), topological polar surface area (TPSA), number of hydrogen-bond donors (HBDs), and the most basic center (pK_a). CNS MPO score of ≥ 4 is desired for BBB crossing. Figure adapted from Figure 1 of Pardridge (2005)[125] and Figure 1 of Arvanitis et al. (2020)[128]. Figure created with BioRender.com.
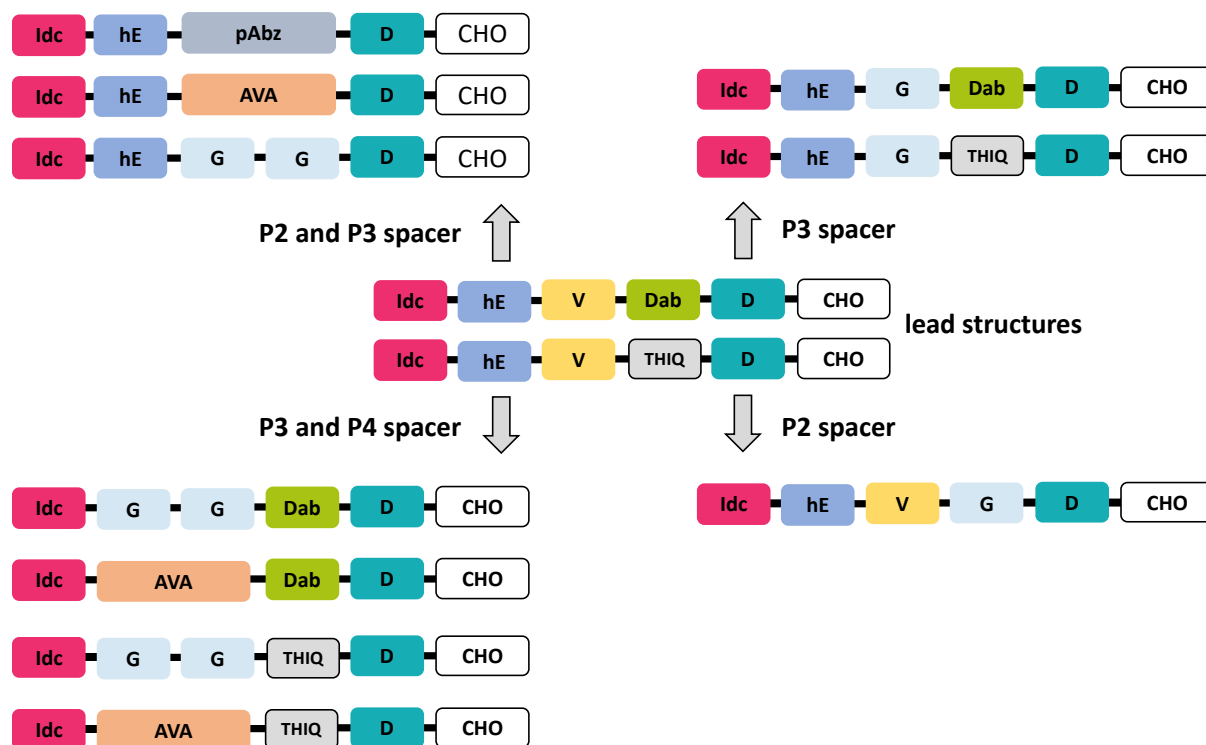
Figure 2.030. Schematic illustration of the implementation of spacers (G, GG, AVA, and pAbz) at several positions in the backbone of Idc(hE)V(*S*-Me-THIQ)D-CHO (**2.101**) and Idc(hE)V(Dab)D-CHO (**2.107**). Idc: (*S*)-indoline-2-carboxylic acid, Dab: diaminobutyric acid, THIQ: (*S*)-6-methyltetrahydroisoquinoline-1-carboxylic acid, pAbz: para-aminobenzoic acid, hE: hL-glutamic acid.

The starting point were Idc(hE)V(*S*-Me-THIQ)D-CHO (**2.101**) and Idc(hE)V(Dab)D-CHO (**2.107**), inhibitors that combine all essential structural features for effective Casp2 inhibition. The decrease of molecular weight and hydrogen bond donor/acceptor groups was achieved by bridging single or multiple amino acids in the backbone of the peptide. Spacers (5-aminovalerianic acid, glycine, or *para*-aminobenzoic acid) were successively inserted at specific positions of the peptide. Thus, it was determined at which sites of the backbone linkers are tolerated without losing Casp2 activity. Initially, amino acid P2 (diaminobutyric acid or (*S*)-6-methyltetrahydroisoquinoline-1-carboxylic acid) and P3 (valine) were bridged, resulting in the Casp2 inhibitors Idc(hE)GGD-CHO (**2.116**), Idc(hE)(AVA)D-CHO (**2.118**), and Idc(hE)(pAbz)D-CHO (**2.119**) (cf. Figure 2.030). The distinct spacers have approximately the same length (5-aminovalerianic acid: 7.4 Å, glycine-glycine: 7.3 Å, and *para*-aminobenzoic acid: 5.5 Å) but differ in their rigidity. The flexibility of 5-aminovalerianic acid is somehow greater than that of glycine-glycine or *para*-aminobenzoic acid. The rigidity could cause differing affinities for Casp2, by the varied arrangement of the inhibitors in the binding pocket of the target. Additionally, position

3 (valine) and position 4 (hL-glutamic acid) were bridged, resulting in the Casp2 inhibitors IdcGG(Dab)D-CHO (**2.110**), Idc(AVA)(Dab)D-CHO (**2.111**), IdcGG(*S*-Me-THIQ)D-CHO (**2.112**), and Idc(AVA)(*S*-Me-THIQ)D-CHO (**2.113**) (cf. Figure 2.030). The implementation of glycine at position P3 (valine) resulted in the peptides Idc(hE)G(Dab)D-CHO (**2.114**) and Idc(hE)G(*S*-Me-THIQ)D-CHO (**2.115**) (cf. Figure 2.030). Bridging only position P2 resulted in the Casp2 inhibitor Idc(hE)VGD-CHO (**2.117**) (cf. Figure 2.030). Bridging single or multiple amino acids directs to a decreased molecular weight (e.g., **2.107** (604.66) vs. **2.116** (519.50)) and a lower number of hydrogen bond donor/acceptor groups (e.g., **2.107** (H-bond donors: 8 and H-bond acceptors: 10) vs. **2.116** (H-bond donors: 7 and H-bond acceptors: 9)). Furthermore, for the bridged Casp2 inhibitor an enhancement of the CNS MPO score can be determined (cf. Table 2.15). The changes in the physicochemical properties of Idc(hE)V(Dab)D-CHO (**2.107**) and Idc(hE)GGD-CHO (**2.116**) are contrasted exemplarily for all bridged Casp2 inhibitors in Figure 2.031.
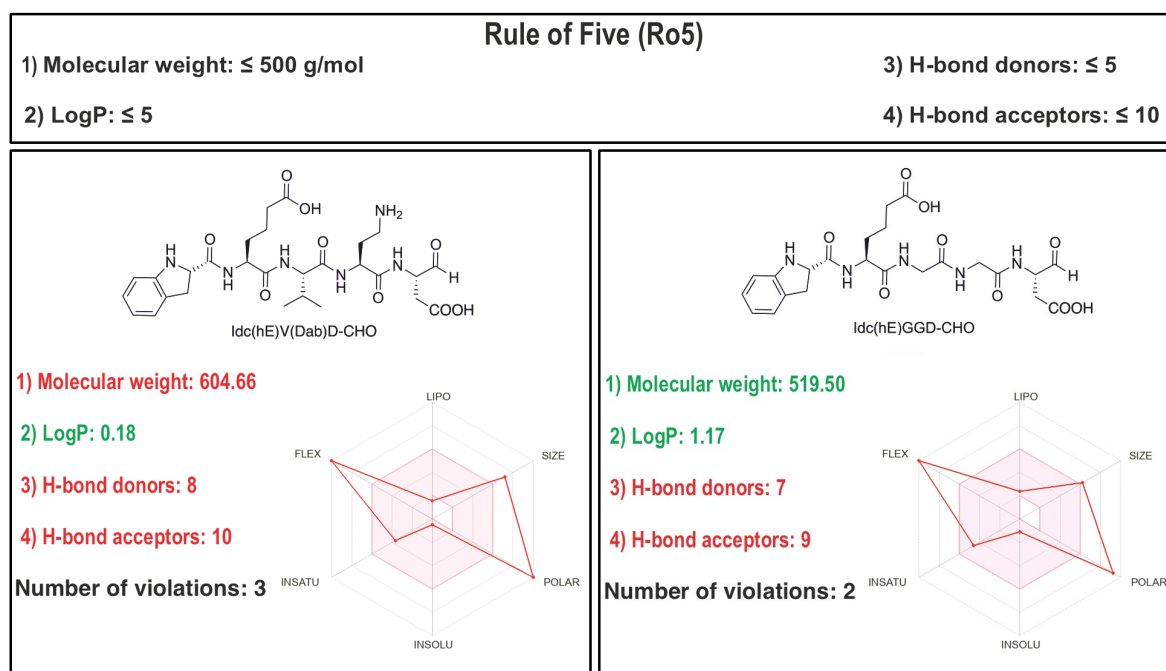
Figure 2.031. Relevant physicochemical properties for Lipinski's rule of 5 (Ro5).[103] *In silico* determined properties for Idc(hE)V(Dab)D-CHO (**2.107**) and Idc(hE)GGD-CHO (**2.116**) including bioavailability radars (calculated with SwissADME web tool).[129]

For Casp2 inhibitors containing indoline (e.g., **2.107** and **2.114**), a chemical instability due to oxidation was observed (for further information see chapter **2.5.2.2**). In this process, the indoline heterocycle is oxidized to indole. Hence, at position P5 (*S*)-5-fluoro-3,3-dimethylindoline-2-carboxylic acid (Idc*) was incorporated in place of (*S*)-indoline-2-carboxylic acid (Idc). The insertion of the 3,3-dimethyl group in the indoline heterocycle is believed to prevent aromatization due to the absence of hydrogens. These modifications led to the peptides Idc*(hE)G(Dab)D-CHO (**2.120**), Idc*(hE)V(Dab)D-CHO (**2.121**), Idc*(hE)GGD-CHO (**2.122**), Idc*(hE)VGD-CHO (**2.123**), Idc*(hE)(AVA)D-CHO (**2.124**), and Idc*(hE)(pAbz)D-CHO (**2.125**). In the case of Idc(hE)(BnT)(Dab)D-CHO (**2.109**), the degradation product Ind(hE)(BnT)(Dab)D-CHO (**2.126**, cf. Scheme 2.05B) was isolated and analytically characterized by mass spectrometry and HPLC purity control. **2.126** was then also investigated for its inhibitory affinity for Casp2 and Casp3.

2.5.2 Results and Discussion

2.5.2.1 Chemistry

Preparation of aspartic acid loaded semicarbazide amino-Merrifield resin

For the synthetic route see chapter **2.3.2.1**.

Solid-phase peptide synthesis (SPPS) of the penta-, tetra-, and tripeptides

For the synthetic route see chapter **2.3.2.1**.

Peptides **2.110**-**2.119** were not acetylated N-terminally but were cleaved from the resin directly after removing the N-Fmoc protecting group. Peptides **2.120**-**2.125** were directly cleaved from the resin after coupling (*S*)-5-fluoro-3,3-dimethylindoline-2-carboxylic acid. The N-Boc protecting group of amino acid P5 was removed through the cleavage from the resin. Peptides **2.110**-**2.125** were cleaved from the resin under milder conditions (trifluoroacetic acid (90%) in water, 15 minutes, room temperature).

2.5.2.2 Stability of (*S*)-Indoline-2-carboxylic Acid Containing Casp2 Inhibitors

Casp2 inhibitors with (*S*)-indoline-2-carboxylic acid (Idc) at position P5 demonstrated significant degradation within a few days. The exact same decomposition process was analyzed for all these peptides (e.g., **2.107** and **2.109**; cf. Scheme 2.05B). The indoline heterocycle at P5 tends to be oxidized to indole under various conditions (in solution or as dry powder; confirmed by mass spectrometry and NMR). Hence, the stability of several peptides containing Idc (dissolved in water (1 mM) or dimethyl sulfoxide (5 mM)) was tested over a period of 14 days at room temperature (e.g., **2.107**; cf. Figures 2.032A and 2.032C). Significant degradation was observed in both water and dimethyl sulfoxide, although in dimethyl sulfoxide degradation was slightly less pronounced. The trend that the peptides are more stable in dimethyl sulfoxide was confirmed by additional HPLC measurements (see chapter **2.7.2.3**; cf. Figures 2.275 and 2.276).
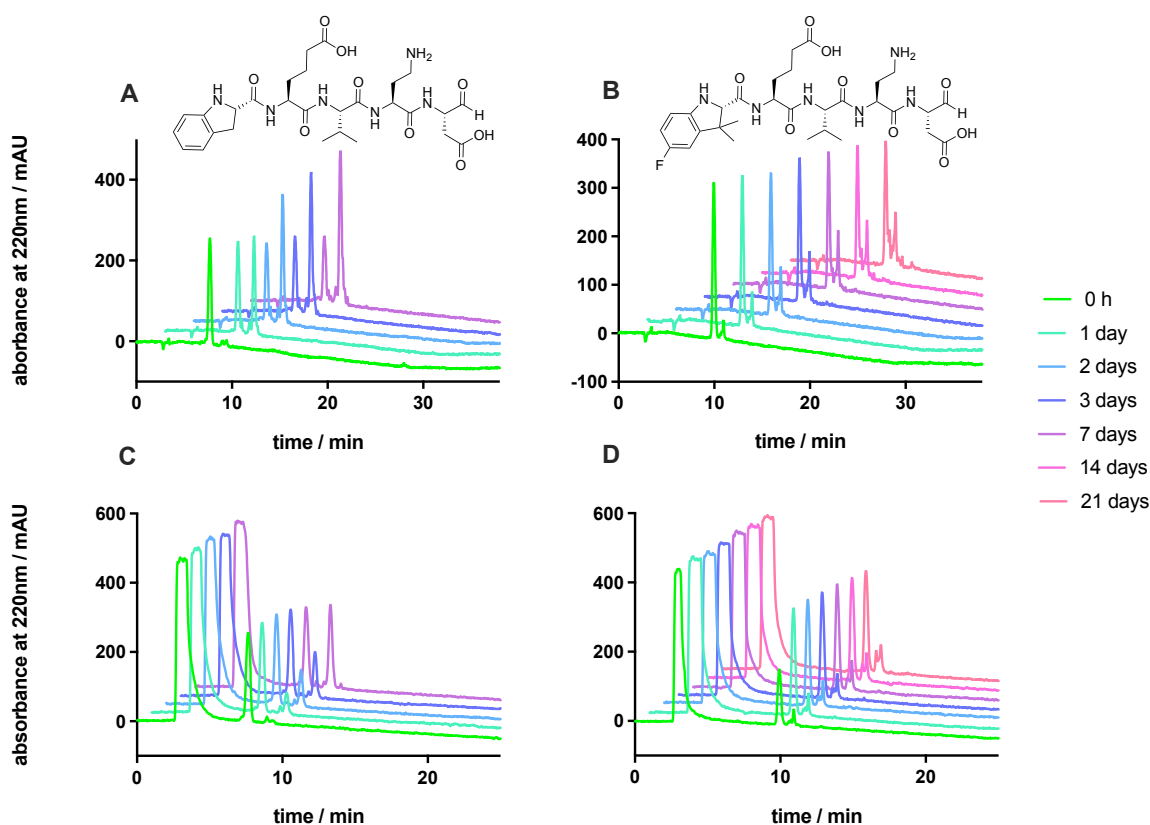
Figure 2.032. Chemical stability of indoline containing peptides in solution (DMSO or water). (**A**) RP-HPLC analysis (stability control) of peptide Idc(hE)V(Dab)D-CHO (**2.107**) in water (1 mM) at rt for 7 days. (**B**) RP-HPLC analysis (stability control) of peptide Idc*(hE)V(Dab)D-CHO (**2.121**) in water (1 mM) at rt for 21 days. (**C**) RP-HPLC analysis (stability control) of peptide Idc(hE)V(Dab)D-CHO (**2.107**) in DMSO (5 mM) at rt for 7 days. (**D**) RP-HPLC analysis (stability control) of peptide Idc*(hE)V(Dab)D-CHO (**2.121**) in DMSO (5 mM) at rt for 21 days. Intensities of the different HPLC measurements may differ due to inaccuracies of the HPLC during the injection of the sample.

Moreover, the stability of the peptides as dry powder was tested at several temperatures (room temperature, -20 °C, and -80 °C). At room temperature, it was observed that over a period of 114 days, a certain amount of the peptides **2.107** and **2.108** was oxidized to the corresponding indole-containing peptide (cf. Figures 2.033 and 2.034). In contrast, the stability of **2.107** and **2.108** at -20 °C and -80 °C was excellent; only a small amount of oxidation product was detected after 114 days.
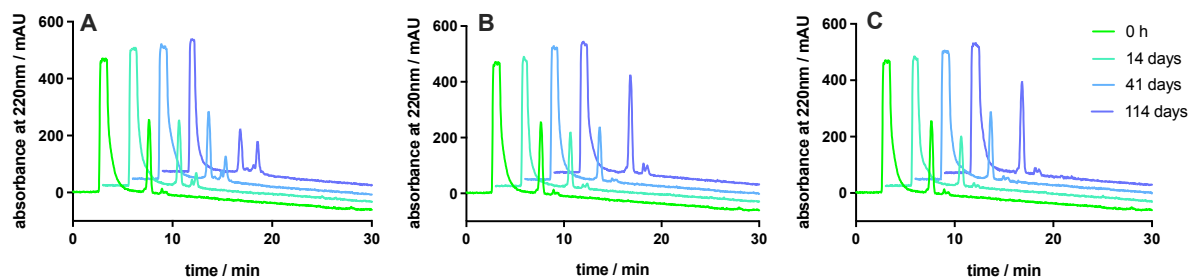
Figure 2.033. Chemical stability of Idc(hE)V(Dab)D-CHO (**2.107**) stored as dry powder at different temperatures. (**A**) Stored at room temperature in the dark. (**B**) Stored at -20 °C. (**C**) Stored at -80 °C. For each point in time (0 h, 14 days, 41, days, and 114 days) **2.107** was dissolved in DMSO (5 mM) for the HPLC measurements. Intensities of the different HPLC measurements may differ due to inaccuracies of the HPLC during the injection of the sample.
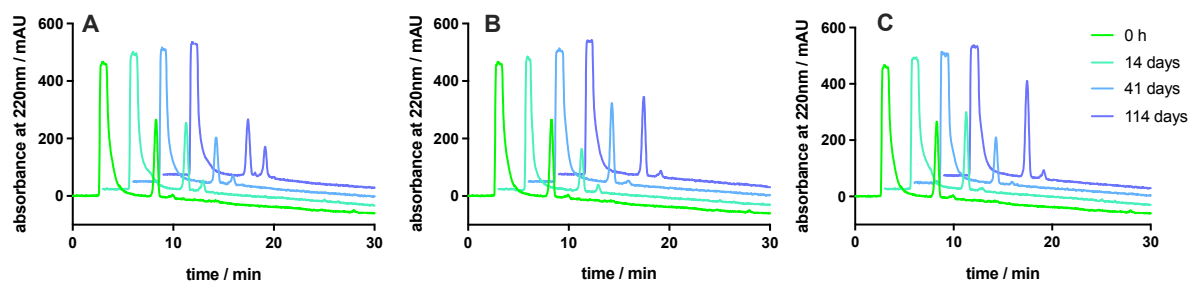
Figure 2.034. Chemical stability of Idc(hE)(Tle)(Dab)D-CHO (**2.108**) stored as dry powder at different temperatures. (**A**) Stored at room temperature in the dark. (**B**) Stored at -20 °C. (**C**) Stored at -80 °C. For each point in time (0 h, 14 days, 41, days, and 114 days) **2.108** was dissolved in DMSO (5 mM) for the HPLC measurements. Intensities of the different HPLC measurements may differ due to inaccuracies of the HPLC during the injection of the sample.

Finally, the stability of the frozen stock solutions (dissolved in water and stored at - 20 °C) was determined to guarantee the accuracy of the various *in vitro* assay results of the Casp2 inhibitors. Within 115 days, the stock solutions of peptides **2.107** and **2.108** were thawed and refrozen several times to mimic the procedures during the *in vitro* testing. Fortunately, the Casp2 inhibitors displayed good stability under these conditions, ensuring the accuracy and reproducibility of the *in vitro* results obtained (cf. Figure 2.035). Nonetheless, it was attempted to increase the stability of the Casp2

inhibitors to provide the basis for their use as pharmaceuticals. Thus, (*S*)-5-fluoro-3,3-dimethylindoline-2-carboxylic acid (Idc*) was incorporated in place of (*S*)-indoline-2-carboxylic acid (Idc). The insertion of the 3,3-dimethyl group into the indoline heterocycle at position 3 is believed to prevent oxidation due to the absence of hydrogens. This approach has proven to decrease the degradation of the peptides by measuring the stability of Casp2 inhibitor **2.121** over a period of 21 days at room temperature (cf. Figures 2.032B and 2.032D). Only a small amount of the degradation product was detected (confirmed by mass spectrometry and HPLC). The decomposition product of the Casp2 inhibitors bearing the 3,3-dimethyl group at the indoline ring was identified as 3,3-dimethyl-3*H*-indole (cf. Scheme 2.05A). Thus, it was confirmed that the oxidation of the indoline still occurs, although to a significantly lower extent. The introduction of (*S*)-2-methylindoline-2-carboxylic acid at position P5 is intended to eliminate this entirely (cf. Scheme 2.05A).
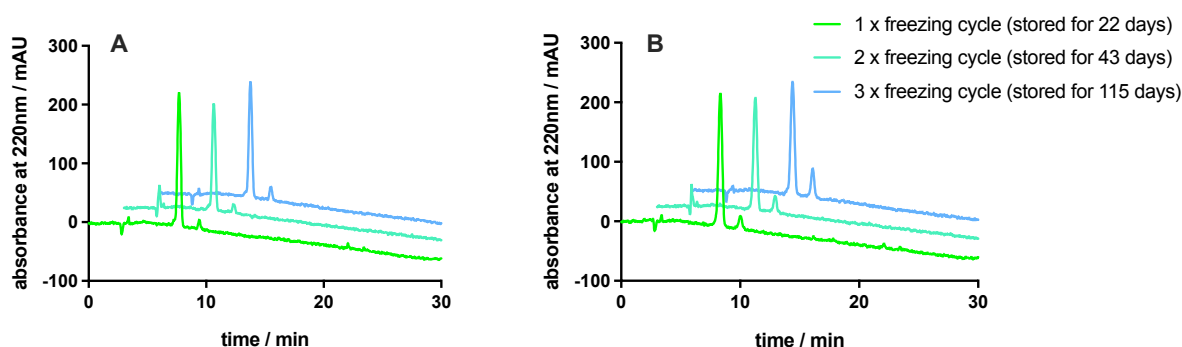
Figure 2.035. (**A**) Chemical stability of the stock solution (1 mM in water) of Idc(hE)V(Dab)D-CHO (**2.107**). (**B**) Chemical stability of the stock solution (1 mM in water) of Idc(hE)(Tle)(Dab)D-CHO (**2.108**). The stock solutions were stored at -20 °C. During the storage, the solution was thawed and refrozen several times (1 x freezing cylce (stored for 22 days at -20 °C), 2 x freezing cylce (stored for 43 days at -20 °C), 3 x freezing cylce (stored for 114 days at -20 °C)). Intensities of the different HPLC measurements may differ due to inaccuracies of the HPLC during the injection of the sample.
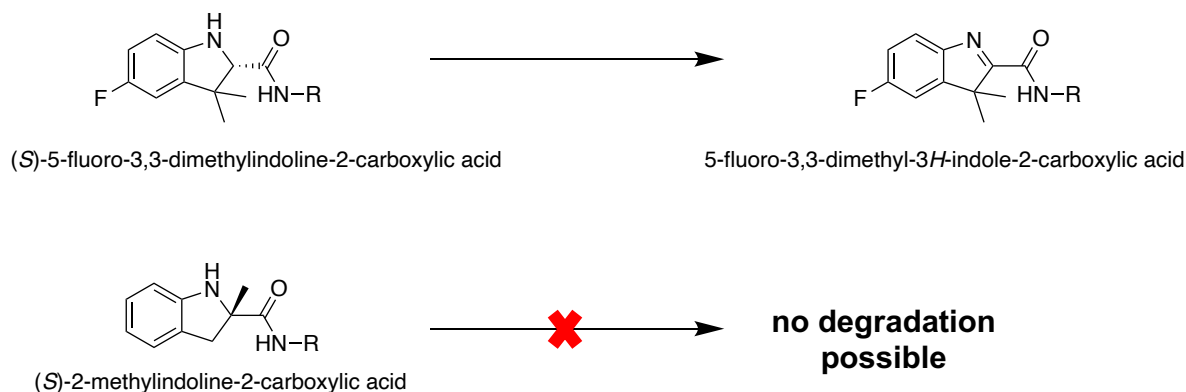
Scheme 2.05A. Chemical stability of (*S*)-5-fluoro-3,3-dimethylindoline-2-carboxylic acid and (*S*)-2-methylindoline-2-carboxylic acid at position P5 of the Casp2 inhibitors.

Idc(hE)(BnT)(Dab)D-CHO
2.109
Chemical Formula: $C_{34}H_{44}N_6O_{10}$
Molecular Weight: 696,7580

Ind(hE)(BnT)(Dab)D-CHO
2.126
Chemical Formula: $C_{34}H_{42}N_6O_{10}$
Molecular Weight: 694,7420

Idc(hE)V(Dab)D-CHO
2.107
Chemical Formula: $C_{28}H_{40}N_6O_9$
Molecular Weight: 604,6610

Ind(hE)V(Dab)D-CHO
Chemical Formula: $C_{28}H_{38}N_6O_9$
Molecular Weight: 602,6450
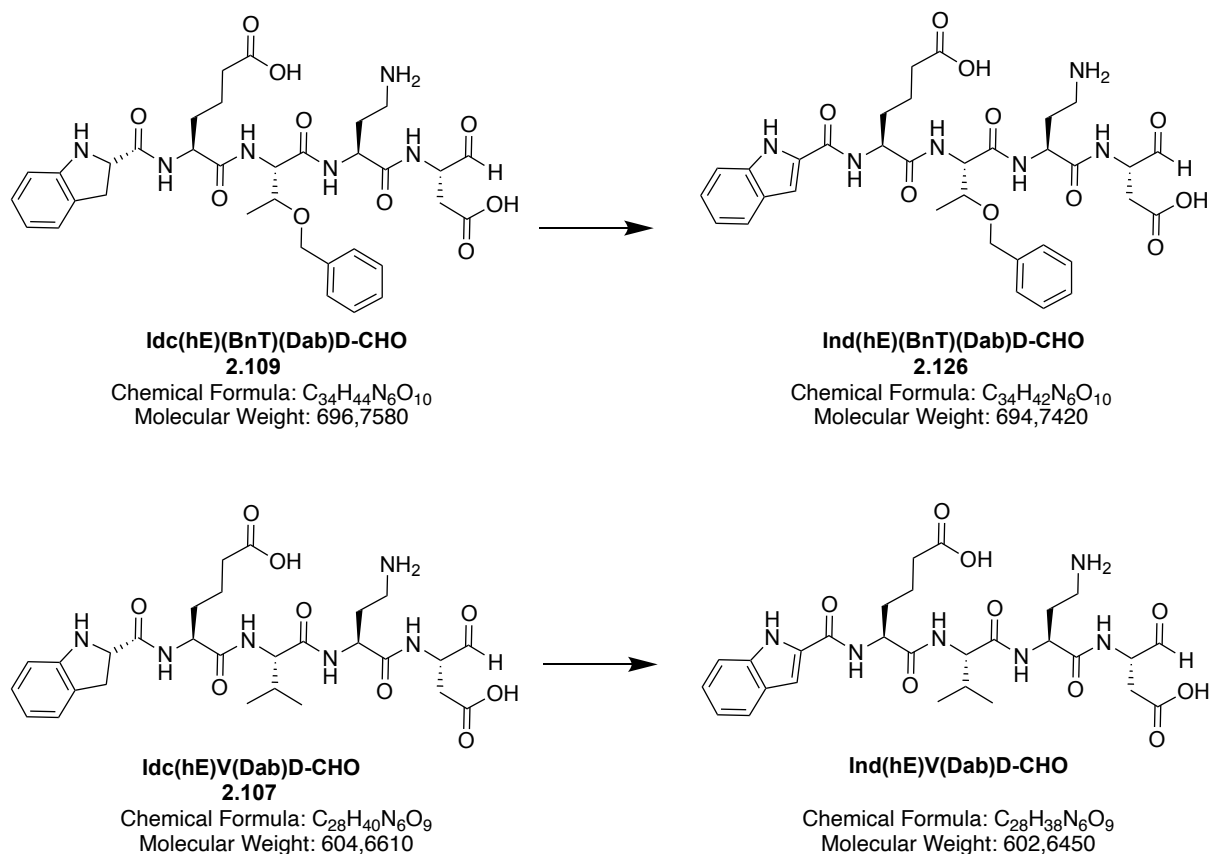
Scheme 2.05B. Chemical instability of Casp2 inhibitor Idc(hE)V(Dab)D-CHO (**2.107**) and Idc(hE)(BnT)(Dab)D-CHO (**2.109**). In solution (DMSO or water), the oxidation of indoline to indole occurs within a short period of time. The reactions are illustrated exemplarily for all Casp2 inhibitors containing indoline. Ind: degraded (S)-indoline-2-carboxylic acid = indole-2-carboxylic acid.

2.5.2.3 Inhibitory Affinity of Compound 2.110-2.126 in a Fluorometric Enzyme Assay

The insertion of spacers (5-aminovalerianic acid and glycine-glycine) at positions P3 and P4 into the backbone of Idc(hE)V(S-Me-THIQ)D-CHO (**2.101**) and Idc(hE)V(Dab)D-CHO (**2.107**) is not tolerated. The peptides IdcGG(Dab)D-CHO (**2.110**), Idc(AVA)(Dab)D-CHO (**2.111**), IdcGG(S-Me-THIQ)D-CHO (**2.112**), and Idc(AVA)(S-Me-THIQ)D-CHO (**2.113**) demonstrate no affinity for Casp2 ($pK_i < 4$) and Casp3 ($pK_i < 4$) (cf. Table 2.14). In contrast, if only valine at position P3 is bridged by glycine, the affinity for the target is preserved. Idc(hE)G(Dab)D-CHO (**2.114**) is characterized by a high affinity toward Casp2 (pK_i 7.51) and an excellent selectivity profile over Casp3 (Casp3/cpCasp2 selectivity 933-fold) (cf. Table 2.14). The same applies to Idc(hE)G(S-Me-THIQ)D-CHO (**2.115**, Casp2 pK_i: 7.77; Casp3 pK_i: 5.26; Casp3/cpCasp2 selectivity 324-fold). These findings indicate that position P4 (hL-

glutamic acid) is not bridgeable by a spacer, whereas position P3 (valine) of the peptide is not crucial for Casp2 affinity. Idc(hE)VGD-CHO (**2.117**, Casp2 pK_i: 7.39; Casp3 pK_i: 4.87) is characterized by the replacement of diaminobutyric acid/(*S*)-6-methyltetrahydroisoquinoline-1-carboxylic acid at position P2 by glycine. Contrary to expectations, the Casp2 inhibitor shows a high affinity for Casp2 and high selectivity over Casp3 (Casp3/cpCasp2 selectivity 331-fold) similar to the peptides Idc(hE)V(*S*-Me-THIQ)D-CHO (**2.101**, Casp2 pK_i: 7.40; Casp3 pK_i: < 4.5) and Idc(hE)V(Dab)D-CHO (**2.107**, Casp2 pK_i: 7.18; Casp3 pK_i: < 4) it was derived from (cf. Tables 2.10 and 2.14). Previously, it was assumed that diaminobutyric acid (Dab) or (*S*)-6-methyltetrahydroisoquinoline-1-carboxylic acid ((*S*)-6-Me-THIQ) at position P2 were indispensable for a high affinity and selectivity toward Casp2. The inhibitor **2.117** has disproved this assumption, thus allowing greater diversity in the design of upcoming peptides, in particular in terms of enhancing physicochemical properties. Hereafter, an effort was made to bridge positions P2 and P3 with glycine-glycine, *para*-aminobenzoic acid, and 5-aminovalerianic acid spacer. This resulted in Idc(hE)GGD-CHO (**2.116**), Idc(hE)(AVA)D-CHO (**2.118**), and Idc(hE)(pAbz)D-CHO (**2.119**). Idc(hE)GGD-CHO exhibits a high affinity for Casp2 with a pK_i value of 7.29, while the affinity for Casp3 (pK_i: 5.46) is consistently low (cf. Table 2.14). Idc(hE)(AVA)D-CHO is inactive for Casp2 and Casp3; the inhibitor possesses pK_i values of < 4 (Casp2) and < 4 (Casp3). Idc(hE)(pAbz)D-CHO likewise lacks activity for Casp2 and Casp3. As already hypothesized, **2.116**, **2.118**, and **2.119** differ in their inhibitory caspase-2 activity, which can be ascribed to the distinct rigidity of the spacers. Additionally, the glycine-glycine linker demonstrates a peptide character in contrast to *para*-aminobenzoic acid and 5-aminovalerianic acid. (*S*)-5-fluoro-3,3-dimethylindoline-2-carboxylic acid (Idc*) was inserted in place of (*S*)-indoline-2-carboxylic acid (Idc) to enhance the stability of the Casp2 inhibitors. This led to Idc*(hE)G(Dab)D-CHO (**2.120**), Idc*(hE)V(Dab)D-CHO (**2.121**), Idc*(hE)GGD-CHO (**2.122**), Idc*(hE)VGD-CHO (**2.123**), Idc*(hE)(AVA)D-CHO (**2.124**), and Idc*(hE)(pAbz)D-CHO (**2.125**). The stability of the indoline heterocycle was successfully increased (cf. Figure 2.032). Simultaneously, the activity and selectivity for caspase-2 was preserved (cf. Table 2.14). Idc*(hE)V(Dab)D-CHO (**2.121**, Casp2 pK_i: 7.18; Casp3 pK_i: < 4) demonstrates the same activity and selectivity for Casp2 as Idc(hE)V(Dab)D-CHO (**2.107**, Casp2 pK_i: 7.18; Casp3 pK_i: < 4). Idc*(hE)G(Dab)D-CHO (**2.120**, Casp2 pK_i: 6.99; Casp3 pK_i: 4.89) and Idc*(hE)VGD-CHO (**2.123**, Casp2 pK_i: 7.02; Casp3 pK_i: 5.34) demonstrate a slightly lower activity

for Casp2 than Idc(hE)G(Dab)D-CHO (**2.114**, Casp2 pK_i: 7.51; Casp3 pK_i: 4.54) and Idc(hE)VGD-CHO (**2.117**, Casp2 pK_i: 7.39; Casp3 pK_i: < 5) (cf. Figure 2.036). The most significant decrease in Casp2 activity by a logarithmic value of 0.7 can be determined for Idc*(hE)GGD-CHO (**2.122**, Casp2 pK_i: 6.59; Casp3 pK_i: 5.57) and Idc(hE)GGD-CHO (**2.116**, Casp2 pK_i: 7.29; Casp3 pK_i: 5.46) (cf. Figure 2.036). The peptides Idc*(hE)(AVA)D-CHO (**2.124**), Idc(hE)(AVA)D-CHO (**2.118**), and Idc(hE)(pAbz)D-CHO (**2.119**) all demonstrate no remarkable activity for Casp2 and Casp3. Idc*(hE)(pAbz)D-CHO (**2.125**, Casp2 pK_i: 5.66; Casp3 pK_i: < 4), in contrast to Idc(hE)(pAbz)D-CHO (**2.119**) displays a slight affinity for Casp2, while the affinity for Casp3 is consistently low. The degradation product Ind(hE)(BnT)(Dab)D-CHO (**2.126**; Casp2 pK_i: 5.97; Casp3 pK_i: 4.55) shows significantly reduced activity for Casp2 compared to Idc(hE)(BnT)(Dab)D-CHO (**2.109**; Casp2 pK_i: 7.40; Casp3 pK_i: < 4), while the low activity for Casp3 is maintained. Thus, the selectivity of the peptide over caspase-3 decreases substantially by two orders of magnitude compared to the original inhibitor (26-fold (**2.126**) vs. 2512-fold (**2.109**)). Displacement curves from representative competition binding experiments (Casp1, Casp2, Casp3, Casp6, Casp7, and Casp9) are displayed in chapter **2.7.6** (cf. Figures 2.292-2.327).
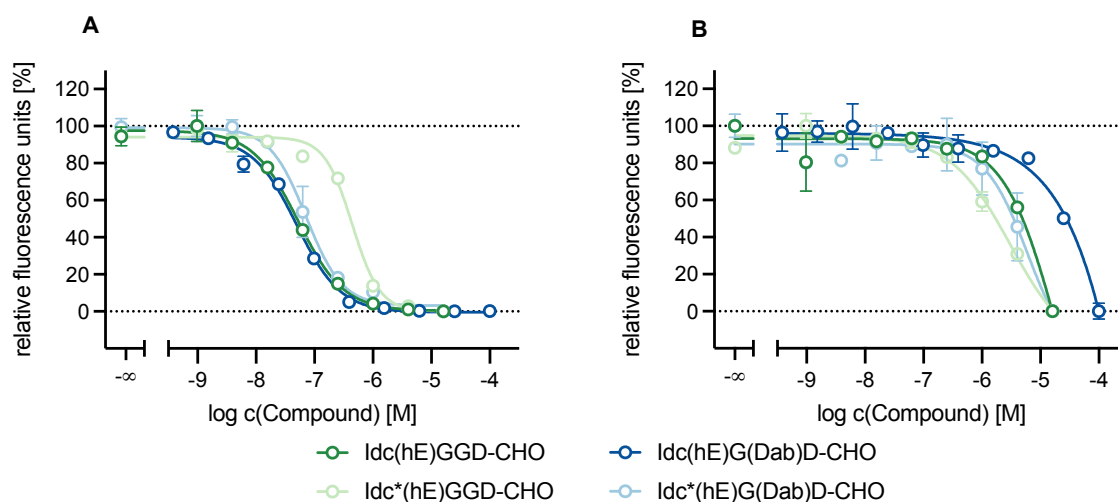
Figure 2.036. Concentration-response curves of Idc(hE)G(Dab)D-CHO (**2.114**), Idc(hE)GGD-CHO (**2.116**), Idc*(hE)G(Dab)D-CHO (**2.120**), and Idc*(hE)GGD-CHO (**2.122**), at Casp2 (**A**) and Casp3 (**B**) in the fluorometric enzyme assay. Data points represent mean values ± SEM from representative experiments, each performed in duplicate.

Table 2.14. Binding data (pK_i values) and selectivity ratios of peptides **2.110**-**2.126** at Casp2 and Casp3.

Sequence	Comp.	pK_i ± SEM				Selectivity ratios of K_i (Casp2: Casp3)
		Casp2	N	Casp3	N	
IdcGG(Dab)D-CHO	**2.110**	< 4[b]	2	< 4	2	-
Idc(AVA)(Dab)D-CHO	**2.111**	< 4[b]	2	< 4	2	-
IdcGG(S-Me-THIQ)D-CHO	**2.112**	< 4[b]	2	< 4	2	-
Idc(AVA)(S-Me-THIQ)D-CHO	**2.113**	< 4[b]	2	< 4	2	-
Idc(hE)G(Dab)D-CHO	**2.114**	7.51 ± 0.12[b]	3	4.54 ± 0.16	3	1:933
Idc(hE)G(S-Me-THIQ)D-CHO	**2.115**	7.77 ± 0.11[b]	2	5.26 ± 0.24	2	1:324
Idc(hE)GGD-CHO	**2.116**	7.29 ± 0.07[b]	4	5.46 ± 0.14	3	1:68
Idc(hE)VGD-CHO	**2.117**	7.39 ± 0.09[b]	4	4.87 ± 0.18	3	1:331
Idc(hE)(AVA)D-CHO	**2.118**	< 4[b]	3	< 4	3	-
Idc(hE)(pAbz)D-CHO	**2.119**	< 4[b]	3	< 4	3	-
Idc*(hE)G(Dab)D-CHO	**2.120**	6.99 ± 0.10[b]	3	4.89 ± 0.04	3	1:126
Idc*(hE)V(Dab)D-CHO	**2.121**	7.18 ± 0.11[b]	3	< 4	3	1:1514
Idc*(hE)GGD-CHO	**2.122**	6.59 ± 0.10[b]	3	5.57 ± 0.19	3	1:10
Idc*(hE)VGD-CHO	**2.123**	7.02 ± 0.10[b]	3	5.34 ± 0.17	3	1:48
Idc*(hE)(AVA)D-CHO	**2.124**	4.97 ± 0.01[b]	2	5.06 ± 0.01	2	1:1
Idc*(hE)(pAbz)D-CHO	**2.125**	5.66 ± 0.05[b]	3	< 4	3	> 1:46
Ind(hE)(BnT)(Dab)D-CHO	**2.126**	5.97[b]	1	4.55	1	1:26

Data shown are mean values ± SEM of N independent experiments, each performed in duplicate or triplicate. Data were analyzed by nonlinear regression and and were best fitted to sigmoidal concentration−response curves using 4PL regression using GraphPad Prism. [a]Data represent pK_i values determined with Casp2. [b]Data represent pK_i values determined with cpCasp2. Saturation binding curves of the enzymes can be seen in chapter **2.7.5** (cf. Figures 2.286, 2.287, and 2.288).

2.5.2.4 *In Silico* Determined Physicochemical and Pharmacokinetic Properties (ADME) of Peptides 2.107, 2.110, 2.111, 2.114, and 2.116-2.119

Table 2.15. *In silico* determined physicochemical and pharmacokinetic properties (ADME) of pentapeptides **2.107**, **2.110**, **2.111**, **2.114**, and **2.116-2.119**.

Properties	2.107	2.110	2.111	2.114	2.116	2.117	2.118	2.119
MW/g/mol	604.65	476.48	461.51	562.57	519.50	561.58	504.53	524.53
Rotatable bonds	22	17	17	21	19	20	19	16
HBA	10	8	7	10	9	9	8	8
HBD	8	7	6	8	7	7	6	6
Molar refractivity	156.1	120.7	122.5	141.7	129.4	143.8	131.2	138.3
TPSA/Å[a]	246.1	208.8	179.7	246.1	220.1	220.1	191.0	191.0
Lipophilicity, logP[b]	-1.06	-2.04	-0.64	-1.82	-0.93	-0.24	0.34	0.78
Solubility, logS[c]	-0.48	-0.98	0.26	0.57	-1.09	-2.13	-1.80	-2.78
Distribution, logD[d]	-7.31	-6.27	-4.19	-8.71	-9.15	-7.80	-6.76	-6.00
% human oral absorption[e]	24	37	47	24	33	33	43	43
BBB permeant	No	No	No	No	No	No	No	No
Bioavailability[f]	0.11	0.17	0.17	0.11	0.11	0.11	0.11	0.11
Drug-likeness[g]	No	No	No	No	No	No	No	No
CNS MPO score[h]	2.24	2.41	2.52	2.24	3.00	3.00	3.00	3.00

[a]TPSA: topological polar surface area: this parameter correlates with human intestinal absorption (empirical data suggest a value < 140).[130] [b]Consensus logP[129]: average of five predictions (iLOGP[131], XLOGP3[132], WLOGP[133], MLOGP[134,135] and SILICOS-IT[129]). [c]LogS values were calculated with ESOL[136]: insoluble < –10 < poorly < –6 < moderately < –4 < – soluble < –2 < very < 0 < highly. [d]LogD[137] were calculated with CDD Vault utilizing ChemAxon's method. [e]The percentage of human oral absorption was calculated using the TPSA by the formula, % human oral absorption = 109 – (0.345 x TPSA), > 89%: high, < 25%: poor[138]. [f]Abbot bioavailability score; 0.55: 55% of the neutral, zwitterionic, or cationic compounds that pass the Lipinski criteria have >10% bioavailability; 0.17: 17% of those that fail have > 10% bioavailability[139]. [g]Lipinski criteria[103] (molecular weight (MW) 500, H-bond donors (HBD) 5, H-bond acceptors (HBA) 10, logP 5); Ghose criteria[140] (160 ≤ MW ≤ 480, –0.4 ≤ logP ≤ 5.6, 40 ≤ molar refractivity ≤ 130, 20 ≤ atom number ≤ 70). [h]CNS MPO score[126,127]was calculated with CDD Vault (MPO desirability score for BBB crossing ≥ 4). The bioavailability radars generated with SwissADME web tool are shown in chapter **2.7.4** (cf. Figures 2.281-2.284).

An *in silico* study was performed to calculate various crucial physicochemical and pharmacokinetic parameters of peptides **2.107**, **2.110**, **2.111**, **2.114**, and **2.116-2.119**. The SwissADME web tool[129] and CDD Vault were employed, and the results are summarized in Table 2.15. The lead peptide **2.107** suffers from several violations of Lipinski's rule of five[103] and Ghosen's extension[140], while the peptides **2.110**, **2.111**,

2.114, and **2.116**-**2.119** demonstrate improved properties, e.g., reduced molecular weight and fewer H-bond donors/acceptors. In addition, the bridged peptides exhibit other favorable properties compared to the lead structure **2.107**, including a lower topological polar surface area (TPSA) (246.1 Å^2 (**2.107**) vs. 208.8 Å^2 (**2.110**), 179.7 Å^2 (**2.111**), 220.1 Å^2 (**2.116** and **2.117**), and 191.0 Å^2 (**2.118** and **2.119**); cf. Table 2.15) and a higher CNS MPO score[126,127] (2.24 (**2.107**) vs. 2.41 (**2.110**), 2.52 (**2.111**), and 3.00 (**2.116**-**2.119**); cf. Table 2.15). Moreover, the calculated human oral absorption (%) of the peptides was increased (e.g., 24 (**2.107**) to 33 (**2.116** and **2.117**)). Nevertheless, it must be pointed out that no Casp2 inhibitor within this series exhibits drug-likeness or the desired CNS MPO value of ≥ 4 for BBB crossing (cf. Table 2.15). The *in silico* data obtained indicate that the physicochemical and pharmacokinetic properties of the bridged peptides (**2.110**, **2.111**, **2.114**, and **2.116**-**2.119**) were enhanced. However, for **2.110**, **2.111**, **2.118**, and **2.119**, the improvement of physicochemical properties resulted in a decline in Casp2 activity. Nonetheless, the modifications of this series are an excellent starting point for the development of CNS-active Casp2 inhibitors (e.g., prodrugs).

2.5.3 Conclusion and Outlook

The introduction of glycine-glycine (GG) or 5-aminovaleric acid (AVA) at positions P3 and P4 demonstrated that the anionic hL-glutamic acid (hE) is crucial for inhibitory Casp2 affinity. The Casp2 inhibitor Idc(hE)VGD-CHO revealed that glycine can be introduced at amino acid position P2 (instead of (S)-6-Me-THIQ or Dab), without losing affinity and selectivity for Casp2 compared to the lead structures Idc(hE)V(S-Me-THIQ)D-CHO (**2.101**) and Idc(hE)V(Dab)D-CHO (**2.107**). The bridging of amino acid positions P2 (Dab or (S)-6-Me-THIQ) and P3 (valine) resulted in Idc(hE)GGD-CHO (**2.116**), a highly active and selective Casp2 inhibitor. The bridging of positions P2 and P3 with 5-aminovaleric acid (AVA) and *para*-aminobenzoic acid (pAbz) did not deliver the desired results regarding Casp2 activity. This can be explained by the different rigidity of the spacers and the absent peptide character of 5-aminovaleric acid and *para*-aminobenzoic acid. The oxidative stability of the Casp2 inhibitors was optimized by installing (S)-5-fluoro-3,3-dimethylindoline-2-carboxylic acid (Idc*) in place of (S)-indoline-2-carboxylic acid (Idc). Within this approach, the molecular weight of the Casp2 inhibitors was successfully lowered while affinity and selectivity for Casp2 were maintained. Likewise, the number of H-bond donors/acceptors was lowered. The altered physicochemical properties are apparent in the shift of the CNS MPO scores. The most promising results were delivered by Idc(hE)GGD-CHO (**2.116**). While maintaining affinity (Casp2 pK_i: 7.29) and selectivity (Casp3/cpCasp2 selectivity > 195-fold), molecular mass was reduced to 519.50 Da, and the CNS MPO score was improved from 2.24 (**2.107**) to 3.00 (**2.116**). However, the peptides do still not exhibit the desired properties for guaranteeing passive diffusion through the BBB and the distribution in the CNS. The calculated CNS MPO score of all Casp2 inhibitors still fails to reach the required value of ≥ 4 for BBB crossing (cf. Table 2.15). However, the Casp2 inhibitors served as excellent *in vitro* pharmacological tool, strengthening the case for targeting caspase-2 as a novel target for treating Alzheimer's disease. *In vitro* experiments revealed that Casp2 inhibitors could restore synaptic dysfunctions and prevent Δtau314 from accumulating in the dendritic spines. In addition, it was established that these beneficial effects were achieved by inhibition of the catalytic pathway of Casp2. The insights of this structure-activity relationship study pave the way toward peptidomimetic and small molecule Casp2 inhibitors with superior physicochemical and pharmacokinetic properties to ensure better bioavailability and

blood-brain barrier permeability. Furthermore, this study provides a reasonable basis for developing prodrugs processed by the fatty acid amide hydrolase (FAAH). All active and selective Casp2 inhibitors feature carboxylic acids at position P1 (aspartic acid) and P4 (hL-glutamic acid). These carboxylic acids are a prerequisite for high-affinity target engagement; however, the anionic functionality is a drawback for blood-brain barrier crossing because of charge repulsion at the barrier surface and the unfavorable electrostatic energetics of the cellular membrane potential.[141]
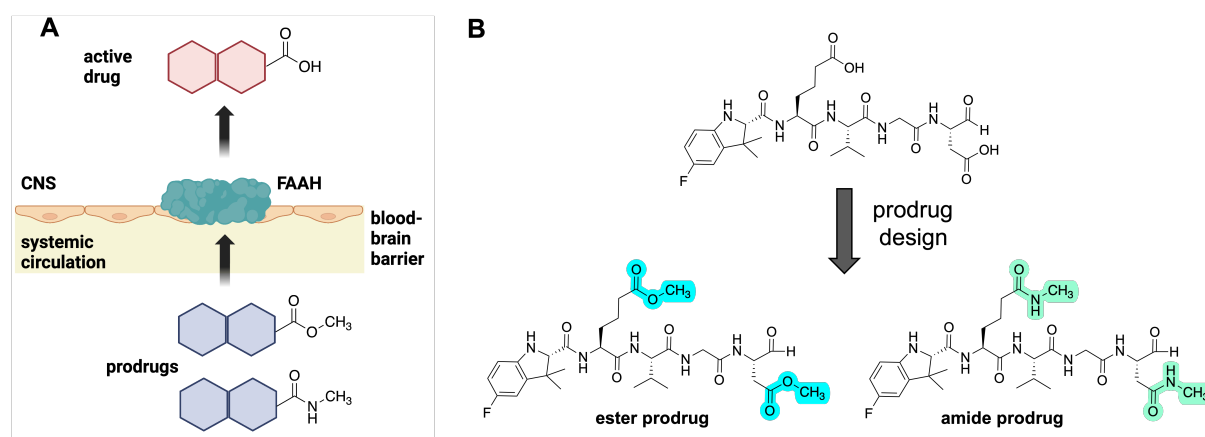
Figure 2.037. (**A**) Fatty acid amide hydrolase (FAAH) prodrug strategy (created with BioRender.com). Amide or ester prodrugs are metabolized to the active form in the CNS by the membrane-bound hydrolase FAAH. The prodrugs possess superior physicochemical properties, allowing the passive diffusion through the endothelia cells of the blood-brain barrier. FAAH combines both esterase and amidase activity. (**B**) Exemplary design of potential prodrugs (amides and esters) for the Casp2 inhibitor Idc*(hE)VGD-CHO (**2.123**). Figure (**A**) is adapted from Figure 1A of Ferrara and Scanlan (2020)[141].

A strategy to enhance blood-barrier crossing in order to achieve therapeutic exposure levels in the CNS is the development of prodrugs.[141–143] The carboxylic acids at positions P1 and P4 can be masked by the design of ester and amide prodrugs (cf. Figure 2.037B).[141,142] The prodrugs impart superior physicochemical properties, thus facilitating sufficient passive diffusion through the endothelial cells of the BBB from a peripherally administered systemic dose.[141,142] Once in the CNS, the prodrugs are processed by fatty acid amide hydrolase (FAAH) into the active form (cf. Figure 2.037A).[141–143] The fatty acid amide hydrolase (FAAH) demonstrates high expression levels in the CNS and belongs to a large class of hydrolytic enzymes, showing esterase and amidase activity.[141–145]

2.6 Experimental Part

2.6.1 Chemistry

2.6.1.1 General Experimental Conditions

Chemicals and solvents

Unless otherwise listed, chemicals and solvents were purchased from commercial suppliers and used as received. Canonical inhibitor AcVDVAD-CHO (**2.016**), AcLDESD-CHO, and AcDEVD-CHO were purchased from Bachem (Torrance/CA, USA). All the solvents were of analytical grade or distilled prior to use. Dimethylformamide (DMF), *N*-methyl-2-pyrrolidone (NMP), and L-homoglutamic acid (hE) were purchased from Iris Biotech (Marktredwitz, Germany). Sodium borohydride, oxalyl chloride, methanol, dichloromethane, diethyl ether, toluene, ethyl acetate, tetrahydrofuran, and hydrochloric acid 37% were obtained from Fisher Scientific/Acros Organics (Schwerte, Germany). If lower concentrations of hydrochloric acid were required, these were diluted accordingly. Isobutyl chloroformate, *tert*-butyl carbazate, *p*-toluenesulfonic acid, trans-4-(aminomethyl)cyclohexanecarboxylic acid, *N,N'*-diisopropylcarbodiimide (DIC), Oxyma and N-methylmorpholine were purchased from TCI (Eschborn, Germany). 1-Ethyl-3-(3-dimethylaminopropyl)carbodiimide (EDCI), 1-hydroxybenzotriazole hydrate (HOBt), 1-[bis(dimethylamino)methylene]-1*H*-1,2,3-triazolo[4,5-*b*]pyridinium 3-oxide hexafluorophosphate (HATU), *N,N*-diisopropylethylamine (DIPEA), and trifluoroacetic acid (TFA) were obtained from ABCR (Karlsruhe, Germany). 1,1'-Carbonyldiimidazole was purchased from Fluorochem (Derbyshire, United Kingdom). Aminomethylated polystyrene HL (100-200 mesh), acetic anhydride, and triethylamine were purchased from Merck (Darmstadt, Germany). Benzyl alcohol, dimethylsulfoxide, acetic acid, quinoline-2-carboxylic acid (quinaldic acid), Fmoc-5-Ava-OH (AVA), Fmoc-L-indoline-2-carboxylic acid (Idc), and acetonitrile for high-performance liquid chromatography (HPLC) were obtained from Sigma-Aldrich (Taufkirchen, Germany). Protected amino acids Fmoc-Tyr(*t*Bu)-OH, Fmoc-Arg(Pbf)-OH, Fmoc-Lys(Boc)-OH, Fmoc-Phe-OH, Fmoc-Pro-OH, Fmoc-Val-OH, Fmoc-Asp(O*t*Bu)-OH, Fmoc-Ala-OH, Fmoc-Orn(Boc)-OH, Fmoc-Dab(Boc)-OH, Fmoc-Dap(Boc)-OH, Fmoc-Lys(Ac)-OH, Fmoc-Thr(*t*Bu)-OH, Fmoc-Ile-OH, Fmoc-Glu(O*t*Bu)-OH, Fmoc-Gly-OH, Fmoc-Ser(*t*Bu)-OH, Fmoc-Trp(Boc)-OH, Fmoc-Gln-OH, Fmoc-Tle-OH, and Fmoc-Leu-OH were procured from Carbolution Chemicals (St.

Ingbert, Germany). Racemic 6-methyl-tetrahydroisoquinoline-1-carboxylic acid (6-Me-THIQ-COOH) and 6-bromo-tetrahydroisoquinoline-1-carboxylic acid (6-Br-THIQ-COOH) was purchased from a commercial supplier and was outsourced for chiral resolution by supercritical fluid chromatography (SFC). The enantiopure amino acids P1 and P2 (see chapter **2.7.3**, Figures 2.279 and 2.280) were subjected to N-Fmoc protection to obtain (*S*)-6 and (*R*)-6, respectively. The absolute configurations of (*S*)-6 and (*R*)-6 were determined by comparison with the reported specific rotation of the commercially available enantiopure *N*-Fmoc-tetrahydroisoquinoline-1-carboxylic acids. The synthesis of (*S*)-1-(*tert*-butoxycarbonyl)-5-fluoro-3,3-dimethylindoline-2-carboxylic acid was commissioned from Pharmaron. The absolute configuration was determined by comparison with the reported specific rotation of the commercially available enantiopure Fmoc-L-indoline-2-carboxylic acid. Deuterated solvents for nuclear magnetic resonance (NMR) spectroscopy were purchased from Deutero (Kastellaun, Germany). The orbital shaker (Multi Reax) was from Heidolph (Schwabach, Germany). The frits had a pore size of 35 μm and were procured from Roland Vetter Laborbedarf (Ammerbuch, Germany). The infrared lamp was from Medisana (Neuss, Germany), and the thermostat was from PEARL.GmbH (Buggingen, Germany). As syringes were used Injekt Luer Solo from Braun (Melsungen, Germany). For the preparation of stock solutions, buffers, and HPLC eluents millipore water was used.

Thin layer chromatography

Reactions were monitored by thin layer chromatography (TLC) on silica gel 60 F254 aluminium sheets (Merck), and compounds were detected with UV light at 254 nm.

NMR spectra

NMR spectra (^{1}H NMR, ^{13}C NMR, ^{19}F NMR, DEPT, ^{1}H COSY, HSQC, HMBC) were recorded on a Bruker Avance-300 (7.05 T, ^{1}H: 300 MHz, ^{13}C: 75.5 MHz, ^{19}F: 188) or Avance-400 (9.40 T, ^{1}H: 400 MHz, ^{13}C: 100.6 MHz, ^{19}F: 282) NMR spectrometer (Bruker, Karlsruhe, Germany). All chemical shifts are reported in the δ-scale as parts per million (ppm) relative to the solvent's residual peaks as the internal standard. Moreover, the multiplicity, coupling constant (*J*), and number of protons are stated.

Multiplicities are specified with the following abbreviations: s (singlet), d (doublet), t (triplet), q (quartet), p (pentet), m (multiplet), as well as combinations thereof.

High-resolution mass spectrometry

(HRMS) was performed on a Q-TOF 6540 ultrahigh definition (UHD) LC/MS system (Agilent Technologies) using an electrospray ionization (ESI) source or on an AccuTOF GCX GC/MS system (Jeol, Peabody, MA) using an electron ionization (EI) source.

Preparative HPLC

Preparative HPLC was performed with a system from Waters (Eschborn, Germany) consisting of a Waters 2545 binary gradient module, a Waters 2489 UV/vis-detector, a Waters Fraction Collector 3, and the column was a YMC Triart C18 (150 x 10 mm, 5 µm) (YMC, Dinslaken, Germany) at a flow rate of 20 mL/min or a HPLC from Knauer (Berlin, Germany) consisting of two K-1800 pumps, a K-2001 detector, and the column was a Phenomenex Gemini (250 x 21 mm, 5 µm) (Phenomenex, Aschaffenburg, Germany) at a flow rate of 15 mL/min. As a mobile phase, mixtures of MeCN and 0.1% aqueous (aq) TFA were used. The UV detection was carried out at 220 nm. For sample preparation, all compounds were dissolved in a mixture of water/acetonitrile (95/5 v/v) and filtered with PTFE filters (25 mm, 0.2 µm) (Phenomenex, Aschaffenburg, Germany). The purified peptides were lyophilized using a CHRIST Alpha 2-4 LD freeze dryer (Osterode am Harz, Germany) equipped with a RZ 6 rotary vane vacuum pump (Vacuubrand, Wertheim, Germany).

Analytical HPLC

Analytical purity and stability control were performed on a 1100 HPLC system from Agilent Technologies equipped with an Instant Pilot controller, a G1312A binary pump, a G1329A ALS autosampler, a G1379A vacuum degasser, a G1316A column compartment, and a G1315B diode array detector (DAD). The column was a Phenomenex Kinetex XB-C18 column (250 x 4.6 mm, 5 µm) (Phenomenex, Aschaffenburg, Germany) or a Phenomenex Gemini NX-C18 column (250 x 4.6 mm, 5 µm). The oven temperature during HPLC analysis was 30 °C. As a mobile phase,

mixtures of MeCN/aqueous TFA were used. Absorbance was detected at 220 nm. The injection volume was 20-80 µL at compound concentrations of 1 mM. The following linear gradient was applied: MeCN/TFA (0.05%) (v/v) 0 min: 10:90, 25 min: 95:5, 35 min: 95:5; flow rate: 1.0 mL/min, t_0 (Kinetex XB-C18) = 2.75 min, t_0 (Gemini NX-C18) = 3.00 min (t_0 = dead time). Retention (capacity) factors k were calculated from the retention times t_R according to $k = (t_R - t_0)/t_0$. The dead time was experimentally determined by injecting a sample of unretained thiourea (200 µM, 10 µL) and recording of the retention time (cf. Figure 2.038). The purities of the compounds were calculated by the percentage peak area of the chromatograms.
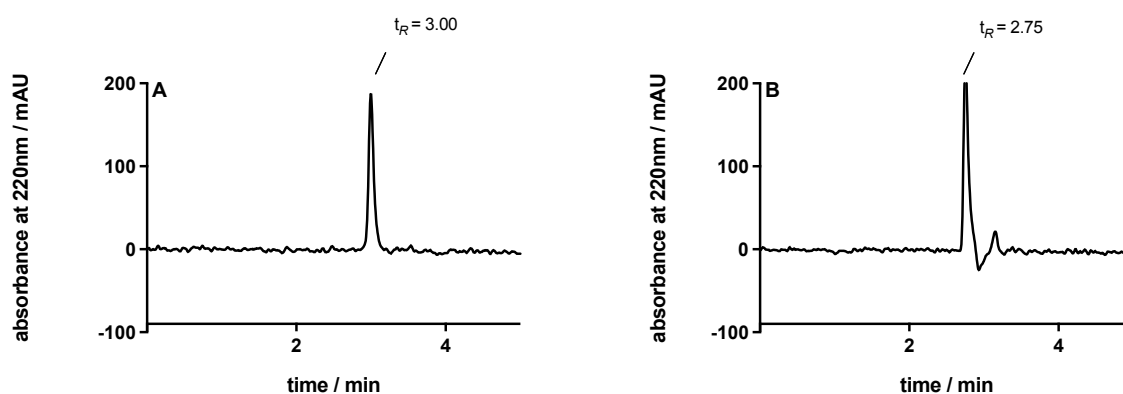
Figure 2.038. Measured retention time (t_R) of 10 µL of a 200 µM thiourea solution at a flow rate of 1.0 mL/min for (**A**) Phenomenex Gemini (250 x 4.6 mm, 5 µm) and (**B**) Phenomenex Kinetex XB-C18 column (250 x 4.6 mm, 5 µm).

2.6.1.2 Compound Characterization

The peptides were characterized using the following methods: HRMS, ^{1}H NMR spectroscopy and ^{13}C NMR spectroscopy (see chapter **2.7.1**, Figures 2.041-2.214). Additionally, for several compounds two-dimensional (2D) NMR spectra like HSQC were made. For purity control, HPLC (RP-HPLC) analysis was performed with a minimum purity standard of ≥ 95% (chromatograms are shown in chapter **2.7.2.1**, Figures 2.215-2.268).

2.6.1.3 Preparation and Analytical Data of Aspartic Acid Loaded Semicarbazide Amino-Merrifield Resin

Benzyl (1*r*,4*r*)-4-(aminomethyl)cyclohexane-1-carboxylate (2.001)[101]
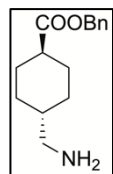
Trans-4-(aminomethyl)cyclohexanecarboxylic acid (30.0 g, 1 eq), benzyl alcohol (150 mL, 7.60 eq), and *p*-toluensulfonic acid (75.3 g, 2.30 eq) were dissolved in 210 mL toluene. The mixture was heated to 150 °C under Dean-Stark conditions. After 3 h of continuously stirring, the mixture was allowed to cool down to room temperature. The precipitated solid was filtrated and washed with diethyl ether (3 x 100 mL), yielding 76.3 g (95%) of a white solid. The product was used without any further purification. NMR data matches the literature reference.[101] HRMS (ESI-MS): *m/z* [M+H$^+$] calculated for C$_{15}$H$_{22}$NO$_2^+$: 248.1645, found 248.1650; C$_{15}$H$_{21}$NO$_2$ x *p*-toluensulfonic acid (419.54).

tert-Butyl 2-((((1*r*,4*r*)-4-((benzyloxy)carbonyl)cyclohexyl)methyl)carbamoyl)hydrazine-1-carboxylate (2.002)[101]
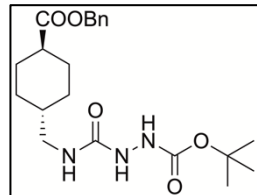
1,1'-Carbonyldiimidazole (14.49 g, 89.36 mmol, 1.2 eq) was dissolved in 200 mL DMF. The flask was flooded with argon. Afterward, a solution of *tert*-butyl carbazate (11.84 g, 89.36 mmol, 1.2 eq) dissolved in 200 mL of DMF was added dropwise over 40 min. After addition, the resultant solution was stirred for 10 min at rt. **2.001** (32.0 g, 76.27 mmol, 1 eq) dissolved in 200 mL DMF was added to the mixture over a period of 60 min. Triethylamine (44.61 mL, 320 mmol, 4.2 eq) was quickly dropped to the mixture, and stirring at rt was continued for 10 h. Subsequently, the mixture was acidified with 10% HCl, and the product was extracted with ethyl acetate. The combined organic layers were washed with saturated brine and dried over Na$_2$SO$_4$. The solvent was concentrated under reduced pressure, yielding 30.8 g (100%) of a white foam. The product was used without any further purification. NMR data matches the literature reference.[101] HRMS (ESI-MS): *m/z* [M+H$^+$] calculated for C$_{21}$H$_{32}$N$_3$O$_5^+$: 406.2336, found 406.2337; C$_{21}$H$_{31}$N$_3$O$_5$ (405.50).

(1*r*,4*r*)-4-((2-(*tert*-Butoxycarbonyl)hydrazine-1-carboxamido)methyl)cyclohexane-1-carboxylic acid (2.003)[101]
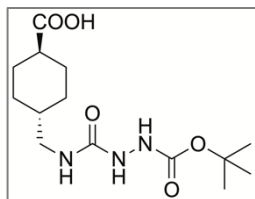
The cleavage of the benzyl protecting group was performed by palladium-on-carbon (Pd/C)-catalyzed hydrogenation. Therefore, Pd/C 10% (3.08 g) was added to a solution of **2.002** (30.8 g, 75.96 mmol, 1 eq) in 400 mL methanol. The mixture was hydrogenated at 5 bar for 15 h. After completion, the solution was filtrated over celite, and the solvent was concentrated under reduced pressure. The procedure afforded 20.2 g (84%) of the product as a white solid. HRMS (ESI-MS): *m/z* [M+H$^+$] calculated for C$_{14}$H$_{26}$N$_3$O$_5^+$: 316.1867, found 316.1863; C$_{14}$H$_{25}$N$_3$O$_5$ (315.37).

Semicarbazide amino-Merrifield resin (2.004)[102]
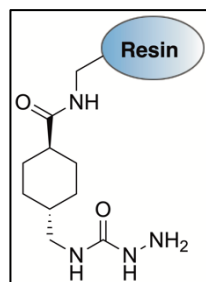
2.003 (4.10 g, 13.00 mmol, 1.0 eq), 1-Hydroxybenzotriazole (2.10 g, 15.54 mmol, 1.2 eq) and 1-ethyl-3-(3-dimethylaminopropyl)carbodiimide (2.98 g, 15.54 mmol, 1.2 eq) were dissolved in 180 mL DMF, then the amino-Merrifield resin (ca. 1.00 mmol/g, 8.20 g, 8.20 mmol, 0.6 eq) was added to the flask. The suspension was continuously stirred at rt for 15 h. Subsequently, the suspension was filtrated, the residual resin was washed with DMF, methanol, and with dichloromethane. The resin was dried under vacuum. Then the protecting groups of the semicarbazide were removed by resuspending the resin in a mixture of trifluoroacetic acid/dichloromethane (1/2 v/v). After continuously stirring for 2 h at rt, the suspension was filtered, and washed alternately with dichloromethane, methanol, and dichloromethane. The resin was dried under vacuum overnight to yield 10.80 g (approx. 0.76 mmol/g) of the semicarbazide loaded amino-Merrifield resin as a trifluoroacetic acid salt.

tert-Butyl (*S*)-3-((((9*H*-fluoren-9-yl)methoxy)carbonyl)amino)-4-hydroxybutanoate (2.005)[102]
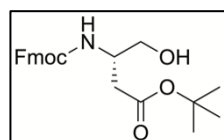
N-Fmoc-L-aspartic acid β-*tert*-butyl ester (10.0 g, 24.3 mmol, 1 eq) was dissolved in 100 mL tetrahydrofuran, after cooling to 0 °C using an ice bath, *N*-methylmorpholine (2.97 mL, 26.73 mmol, 1.1 eq) and isobutyl chloroformate (3.32 mL, 25.55 mmol, 1.05 eq) were added to the solution. After 45 min of stirring at 0 °C the mixture was cooled to -78 °C. Subsequently, sodium

borohydride (1.93 g, 51.03 mmol, 2.1 eq) and 20 mL methanol were added to the solution. After 2 h of continuous stirring at -78 °C, the reaction was quenched with 50 mL of saturated aqueous ammonium chloride. The product was extracted with ethyl acetate, washed with brine, dried over Na_2SO_4, and concentrated under reduced pressure. The residue was purified by column chromatography (EtOAc/PE 1/3 → EtOAc/PE 1/2), yielding 7.45 g (77%) of a white solid. NMR data matches the literature reference.[102] HRMS (ESI-MS): *m/z* [M+H$^+$] calculated for $C_{23}H_{28}NO_5^+$: 398.1962, found 398.1963; $C_{23}H_{27}NO_5$ (397.47).

tert-Butyl (*S*)-3-((((9*H*-fluoren-9-yl)methoxy)carbonyl)amino)-4-oxobutanoate (2.006)[102]
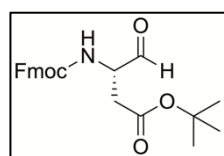
A solution of oxalyl chloride (1.93 mL, 18.74 mmol, 1.2 eq) in 100 mL dichloromethane was cooled to -78 °C. Dimethyl sulfoxide (2.93 mL, 22.49 mmol, 2.2 eq) was added to the solution. After 20 min of continuously stirring **2.005** (7.45 g, 18.74 mmol, 1 eq) in 30 mL dichloromethane was added dropwise to the mixture. Subsequently, the solution was stirred for 1 h at -78 °C, then *N*,*N*-diisopropylethylamine (9.79 mL, 56.23 mmol, 3 eq) was added. Stirring at -78 °C was continued for 1 h, then the mixture was allowed to warm up to -15 °C. 1M HCl was poured into the mixture and the product was extracted with dichloromethane. The combined organic layers were dried over Na_2SO_4 and evaporated. This provided 8.63 g of a crude yellow oil. Synthesis of the aspartic acid-loaded semicarbazide amino-Merrifield resin (**2.007**) was performed without further purification of the title compound. HRMS (ESI-MS): *m/z* [M+Na$^+$] calculated for $C_{23}H_{25}NNaO_5^+$: 418.1625, found 418.1624; $C_{23}H_{25}NO_5$ (395.46).

Aspartic acid loaded semicarbazide amino-Merrifield resin (2.007)[102]
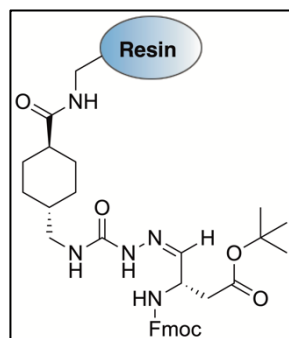
2.006 (8.63 g, 21.82 mmol, 2.7 eq) was dissolved in 100 mL tetrahydrofuran thereafter **2.004** (10.80 g, 8.20 mmol, 1 eq) and acetic acid (271 µL, 4.73 mmol, 0.6 eq) were added to the flask. The suspension was stirred for 12 h at rt. Then the resin was filtered off and sequentially washed with tetrahydrofuran, dichloromethane, and diethyl ether. The resin was dried under vacuum overnight to yield 13.12 g (ca. 0.63 mmol/g) of the aspartic acid-loaded semicarbazide amino-Merrifield resin.

2.6.1.4 Preparation and Analytical Data for Penta-, Tetra-, and Tripeptides 2.008-2.101 and 2.107-2.126

General Procedure for the synthesis of the peptides

The aspartic acid loaded semicarbazide amino-Merrifield resin (300 mg, 0.188 mmol, 1 eq) was weighed into a fritted 10 mL syringe. Subsequently, 5 mL of a mixture of piperidine 20% in DMF was drawn to remove the N-terminal Fmoc protecting group. The syringe was shaken on an orbital shaker at 35 °C for 15 min. The orbital shaker was covered with a box, which was insulated from the inside with aluminum foil. An infrared lamp was placed on an aperture on top. To keep the temperature constant at 35 °C the lamp was controlled by a thermostat. The liquid was then removed with the aid of a vacuum flask and the residual resin was washed with DMF (3 x 8 mL). The coupling of the amino acids to the N-terminus was performed by two different methods. The corresponding amino acid (5 eq) and HATU (357 mg, 0.94 mmol, 5 eq) (Method A) or Oxyma (134 mg, 0.94 mmol, 5 eq) (method B) were weighed in two separate Erlenmeyer flasks. Subsequently, both were dissolved in 3-4 mL of a mixture of DMF/NMP (8/2 v/v). Then *N,N*-diisopropylethylamine (164 µL, 0.94 mmol, 5 eq) (method A) or *N,N'*-diisopropylcarbodiimide (151 µL, 0.94 mmol, 5 eq) (method B) was added to the solution of HATU (procedure **A**) / Oxyma (procedure **B**). Subsequently, both solutions were drawn into the resin-loaded syringe and shaken at 35 °C for 45 min. The liquid was then removed with the aid of a vacuum flask and the residual resin was washed with DMF (3 x 8 mL).

The coupling and deprotection steps were repeated until the desired tri-, tetra-, or pentapeptide was built up. Then the N-terminal Fmoc protecting group was removed using piperidine in DMF (20%). Subsequently, the N-terminus of the peptide was acetylated by dissolving acetic anhydride (178 µL, 1.88 mmol, 10 eq) and *N,N*-diisopropylethylamine (328 µL, 1.88 mmol, 10 eq) in 6-8 mL DMF. The solution was drawn into the syringe and shaken for 30 min at room temperature. After completion, the liquid was removed, and the resin was washed with DMF (2 x 8 mL), methanol (2 x 8 mL), dichloromethane (2 x 8 mL), and finally with diethyl ether (2 x 8 mL). The peptide was cleaved off the resin, and the side chains were deprotected by drawing up 6 mL of trifluoroacetic acid 90% in water. The syringe was shaken for 1 h at room

temperature. The liquid was then poured into a round-bottomed flask. The step was repeated and then the cleavage cocktail was diluted with 50 mL water and freeze-dried. The crude product was purified by HPLC, yielding the corresponding peptide.

(S)-3-((S)-2-((S)-1-(Acetyl-L-tyrosyl-L-lysyl)pyrrolidine-2-carboxamido)-3-methylbutanamido)-4-oxobutanoic acid hydrotrifluoroacetate (2.008)

(Synthesized by Steffen Pockes)
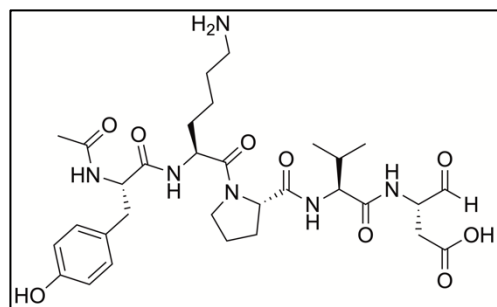
The title compound was synthesized according to general procedure **A** yielding a fluffy white solid (15.2 mg, 3%): RP-HPLC: 99%, (t_R = 6.83, k = 1.28). ^{1}H NMR (400 MHz, D_2O) δ 6.99 (d, J = 8.0 Hz, 2H), 6.70 (d, J = 8.5 Hz, 2H), 4.92 (dd, J = 4.6, 3.2 Hz, 1H), 4.42 (t, J = 6.5 Hz, 1H), 4.35 (t, J = 7.9 Hz, 1H), 4.26 – 4.20 (m, 1H), 4.20 – 4.09 (m, 1H), 3.92 (dd, J = 7.6, 4.7 Hz, 1H), 3.52 – 3.40 (m, 2H), 2.93 – 2.82 (m, 3H), 2.81 – 2.64 (m, 2H), 2.53 – 2.35 (m, 1H), 2.27 – 2.11 (m, 1H), 1.95 – 1.74 (m, 7H), 1.66 – 1.42 (m, 4H), 1.29 – 1.20 (m, 2H), 0.91 – 0.77 (m, 6H). ^{13}C NMR (101 MHz, D_2O) δ 173.96, 173.93, 172.96, 172.89, 170.73, 170.72, 154.45, 130.46, 127.86, 115.36, 89.68, 60.16, 59.81, 55.52, 51.54, 50.68, 47.92, 46.72, 39.22, 36.17, 34.54, 30.48, 30.23, 29.38, 27.45, 26.36, 24.55, 21.68, 21.56. HRMS (ESI-MS): m/z [M+H$^+$] calculated for $C_{31}H_{47}N_6O_9^+$: 647.3399, found 647.3413; $C_{31}H_{46}N_6O_9$ x $C_2HF_3O_2$ (760.77).

(S)-4-(2-Acetamidoacetamido)-5-({(S)-1-[(S)-2-{[(S)-1-carboxy-3-oxopropan-2-yl]carbamoyl}pyrrolidin-1-yl]-3-hydroxy-1-oxopropan-2-yl}amino)-5-oxopentanoic acid (2.009)
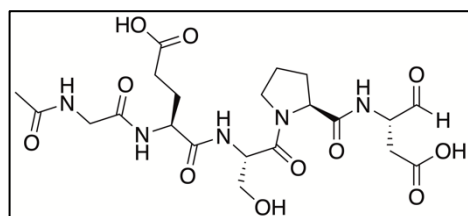
The title compound was synthesized according to general procedure **A** yielding a fluffy white solid (16.7 mg, 17%): RP-HPLC: > 99%, (t_R = 3.67, k = 0.22). ^{1}H NMR (400 MHz, D_2O) δ 4.95 – 4.85 (m, 1H), 4.66 – 4.60 (m, 1H), 4.42 – 4.04 (m, 3H), 3.80 (s, 2H), 3.77 – 3.54 (m, 4H), 2.71 – 2.38 (m, 2H), 2.35 (t, J = 7.3 Hz, 2H), 2.23 – 1.94 (m, 2H), 1.93 (s, 3H), 1.91 – 1.74 (m, 4H). ^{13}C NMR (101 MHz, D_2O) δ 177.05, 175.24, 174.94, 174.27, 173.77, 173.25 (d, J = 3.5 Hz), 171.70, 170.38, 89.67, 60.93, 60.74, 53.51, 52.77, 51.59, 48.09, 42.50,

33.96, 29.89, 29.42, 26.20, 24.46 (d, J = 27.4 Hz), 21.73. HRMS (ESI-MS): m/z [M+H$^+$] calculated for $C_{21}H_{32}N_5O_{11}^+$: 530.2093, found 530.2100; $C_{21}H_{31}N_5O_{11}$ (529.50).

(4S,7S,10S,13S,16S)-4-[(1H-Indol-3-yl)methyl]-7-(carboxymethyl)-16-formyl-10-(3-guanidinopropyl)-13-methyl-2,5,8,11,14-pentaoxo-3,6,9,12,15-pentaazaoctadecan-18-oic acid hydrotrifluoroacetate (2.010)
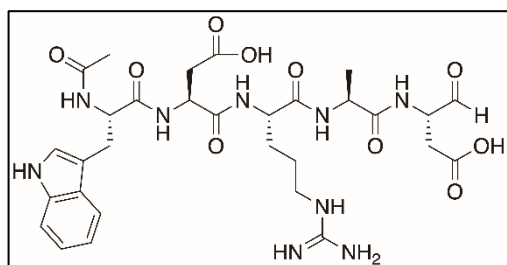
The title compound was synthesized according to general procedure **A** yielding a fluffy white solid (12.0 mg, 8%): RP-HPLC: 98%, (t_R = 7.48, k = 1.49). ^{1}H NMR (300 MHz, D$_2$O) δ 7.50 – 7.30 (m, 2H), 7.17 – 6.94 (m, 3H), 4.87 (dd, J = 4.6, 2.7 Hz, 1H), 4.42 (t, J = 6.9 Hz, 1H), 4.34 (t, J = 6.3 Hz, 1H), 4.17 – 3.91 (m, 3H), 3.09 (d, J = 7.0 Hz, 2H), 2.97 (t, J = 6.8 Hz, 2H), 2.65 – 2.28 (m, 4H), 1.83 (s, 3H), 1.71 – 1.46 (m, 2H), 1.45 – 1.30 (m, 2H), 1.25 – 1.16 (m, 3H). HRMS (ESI-MS): m/z [M+H$^+$] calculated for $C_{30}H_{42}N_9O_{10}^+$: 688.3049, found 688.3058; $C_{30}H_{41}N_9O_{10}$ x $C_2HF_3O_2$ (801.73).

(4S,7S,10S,13S,16S)-4-(3-Amino-3-oxopropyl)-7-(carboxymethyl)-16-formyl-13-(3-guanidinopropyl)-10-[(R)-1-hydroxyethyl]-2,5,8,11,14-pentaoxo-3,6,9,12,15-pentaazaoctadecan-18-oic acid hydrotrifluoroacetate (2.011)
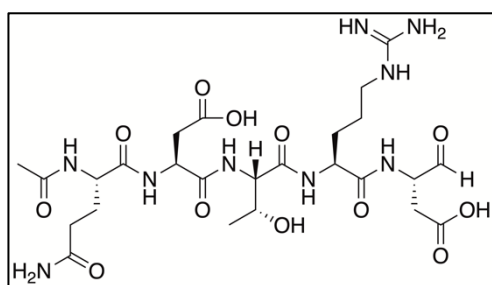
The title compound was synthesized according to general procedure **A** yielding a fluffy white solid (15.0 mg, 10%): RP-HPLC: > 99%, (t_R = 3.43, k = 0.14). ^{1}H NMR (300 MHz, D$_2$O) δ 4.88 (d, J = 2.2 Hz, 1H), 4.24 – 4.03 (m, 5H), 3.04 (t, J = 6.9 Hz, 2H), 2.90 – 2.27 (m, 5H), 2.22 (t, J = 7.5 Hz, 2H), 1.98 – 1.77 (m, 5H), 1.72 – 1.55 (m, 2H), 1.52 – 1.39 (m, 2H), 1.04 (d, J = 6.3 Hz, 3H). ^{13}C NMR (75 MHz, D$_2$O) δ 177.77, 175.19, 174.51, 174.30, 173.64, 173.50, 173.01, 172.68, 171.89, 171.62, 156.72, 89.68, 66.84, 59.33, 53.54, 53.46, 51.51, 50.22, 40.48, 35.21, 31.04, 28.08, 26.70, 25.84, 24.34, 21.64, 18.79. HRMS (ESI-MS): m/z [M+H$^+$] calculated for $C_{25}H_{42}N_9O_{12}^+$: 660.2947, found 660.2947; $C_{25}H_{41}N_9O_{12}$ x $C_2HF_3O_2$ (773.68).

(4S,7S,10S,13S,16S)-7-(Carboxymethyl)-16-formyl-10-(3-guanidinopropyl)-13-[(R)-1-hydroxyethyl]-4-methyl-2,5,8,11,14-pentaoxo-3,6,9,12,15-pentaazaoctadecan-18-oic acid hydrotrifluoroacetate (2.012)
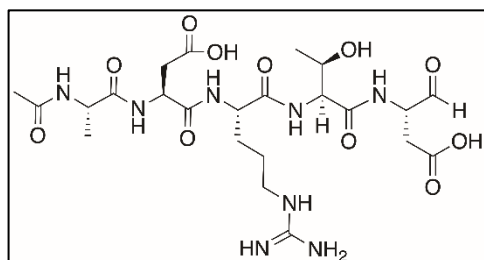
The title compound was synthesized according to general procedure **A** yielding a fluffy white solid (12.2 mg, 9%): RP-HPLC: > 99%, (t_R = 3.21, k = 0.07). ^{1}H NMR (300 MHz, D_2O) δ 4.93 – 4.87 (m, 1H), 4.56 – 4.49 (m, 1H), 4.28 – 4.20 (m, 1H), 4.17 – 3.99 (m, 4H), 3.06 (t, J = 6.8 Hz, 2H), 2.84 – 2.35 (m, 4H), 1.87 (s, 3H), 1.83 – 1.59 (m, 2H), 1.54 – 1.41 (m, 2H), 1.21 (d, J = 7.2 Hz, 3H), 1.09 – 1.00 (m, 3H). ^{13}C NMR (75 MHz, D_2O) δ 176.37, 175.47, 175.34, 174.61, 174.35, 173.52, 172.54, 171.41, 171.29, 156.72, 89.66, 67.06, 59.47, 53.45, 51.60, 50.23, 50.04, 40.47, 35.44, 34.23, 28.08, 24.30, 21.59, 18.80, 16.30. HRMS (ESI-MS): *m/z* [M+H$^+$] calculated for $C_{23}H_{39}N_8O_{11}^+$: 603.2733, found 603.2741; $C_{23}H_{38}N_8O_{11}$ x $C_2HF_3O_2$ (716.63).

(S)-3-[(S)-2-Acetamido-4-methylpentanamido]-4-{[(S)-1-((S)-2-{[(S)-1-carboxy-3-oxopropan-2-yl]carbamoyl}pyrrolidin-1-yl)-3-methyl-1-oxobutan-2-yl]amino}-4-oxobutanoic acid (2.013)
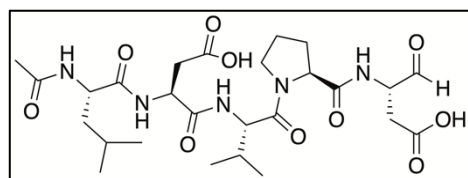
The title compound was synthesized according to general procedure **B** yielding a fluffy white solid (17.4 mg, 55%): RP-HPLC: > 99%, (t_R = 9.35, k = 2.12). ^{1}H NMR (300 MHz, D_2O) δ 4.99 – 4.84 (m, 1H), 4.57 (t, J = 6.8 Hz, 1H), 4.40 – 3.90 (m, 4H), 3.78 – 3.31 (m, 2H), 2.90 – 2.27 (m, 4H), 2.44 – 2.01 (m, 1H), 2.00 – 1.63 (m, 7H), 1.54 – 1.32 (m, 3H), 0.91 – 0.61 (m, 12H). ^{13}C NMR (75 MHz, D_2O) δ 175.33, 175.21, 174.74, 174.26, 174.01, 173.77, 171.71, 171.66, 171.60, 89.62, 60.77, 57.12, 52.56, 51.51, 51.39, 49.92, 48.25, 39.86, 35.00, 34.05, 33.86, 29.94, 29.66, 29.48, 24.69, 24.54, 24.32, 22.01, 21.59, 20.84, 18.42, 18.34, 17.36. *m/z* [M+H$^+$] calculated for $C_{26}H_{42}N_5O_{10}^+$: 584.2926, found 584.2934; $C_{26}H_{41}N_5O_{10}$ (583.64).

(*S*)-3-[(*S*)-2-Acetamido-3-phenylpropanamido]-4-{[(*S*)-1-((*S*)-2-{[(*S*)-1-carboxy-3-oxopropan-2-yl]carbamoyl}pyrrolidin-1-yl)-3-methyl-1-oxobutan-2-yl]amino}-4-oxobutanoic acid (2.014) *(Synthesized by Alexander Hubmann)*
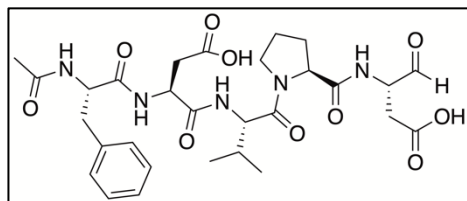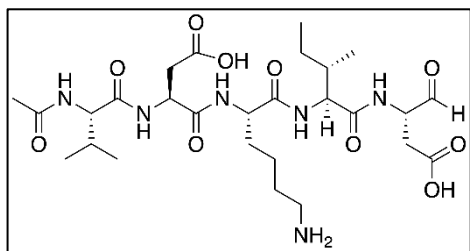

The title compound was synthesized according to general procedure **A** yielding a fluffy white solid (51.6 mg, 45%): RP-HPLC: > 99%, (t_R = 10.04, k = 2.35). ^{1}H NMR (300 MHz, D_2O) δ 7.31 – 6.93 (m, 5H), 4.91 (dd, J = 5.3, 4.4 Hz, 1H), 4.52 – 4.35 (m, 2H), 4.27 – 4.17 (m, 2H), 4.17 – 3.99 (m, 1H), 3.79 – 3.24 (m, 2H), 3.06 – 2.27 (m, 6H), 2.17 – 2.02 (m, 1H), 2.01 – 1.62 (m, 7H), 0.90 – 0.64 (m, 6H). ^{13}C NMR (75 MHz, D_2O) δ 175.32, 175.20, 174.00, 173.88, 173.73, 172.98, 171.79, 171.71, 171.65, 171.43, 136.18, 129.12, 128.78, 127.22, 89.61, 60.79, 57.20, 55.05, 51.51, 51.38, 49.86, 48.27, 36.97, 35.04, 34.06, 33.85, 29.89, 29.64, 29.47, 24.54, 21.60, 18.39, 18.29, 17.51. HRMS (ESI-MS): *m/z* [M+H$^+$] calculated for $C_{29}H_{40}N_5O_{10}^+$: 618.2770, found 618.2779; $C_{29}H_{39}N_5O_{10}$ (617.66).

(4*S*,7*S*,10*S*,13*S*,16*S*)-13-(4-Aminobutyl)-4-[(*S*)-*sec*-butyl]-16-formyl-7-[(*R*)-1-hydroxyethyl]-10-isopropyl-2,5,8,11,14-pentaoxo-3,6,9,12,15-pentaazaoctadecan-18-oic acid hydrotrifluoroacetate (2.015)
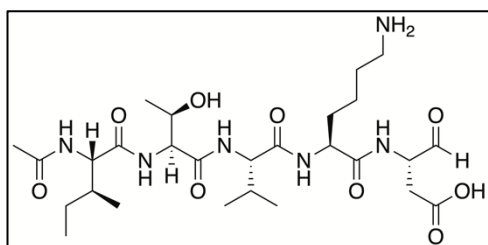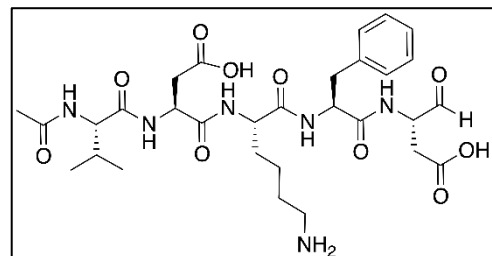

The title compound was synthesized according to general procedure **A** yielding a fluffy white solid (30.0 mg, 22%): RP-HPLC: > 99%, (t_R = 6.86, k = 1.29). ^{1}H NMR (400 MHz, D_2O) δ 4.94 (t, J = 4.8 Hz, 1H), 4.43 – 3.94 (m, 6H), 2.88 (t, J = 7.6 Hz, 2H), 2.69 – 2.32 (m, 2H), 1.94 (s, 4H), 1.80 – 1.51 (m, 5H), 1.43 – 1.23 (m, 3H), 1.16 – 1.03 (m, 4H), 0.90 – 0.72 (m, 12H). ^{13}C NMR (101 MHz, D_2O) δ 176.01, 175.64, 174.46, 174.24, 173.15, 172.91, 171.64, 171.57, 89.74, 67.14, 59.46, 58.98, 58.71, 53.59, 51.66, 39.20, 36.18, 34.62, 30.68, 30.12, 26.27, 24.64, 21.95, 21.66, 18.86, 18.43, 17.84, 14.88, 10.32. HRMS (ESI-MS): *m/z* [M+H$^+$] calculated for $C_{27}H_{49}N_6O_9^+$: 601.3556, found 601.2558; $C_{27}H_{48}N_6O_9$ x $C_2HF_3O_2$ (714.74).

(*S*)-3-((*S*)-2-Acetamido-3-methylbutanamido)-4-((*S*)-2-(((*S*)-1-(((*S*)-1-carboxy-3-oxopropan-2-yl)amino)-3-methyl-1-oxobutan-2-yl)carbamoyl)pyrrolidin-1-yl)-4-oxobutanoic acid (2.017)
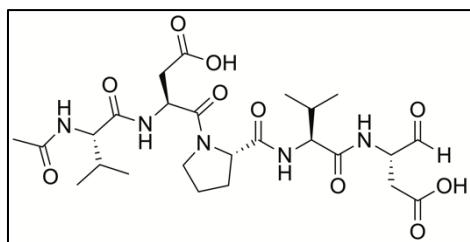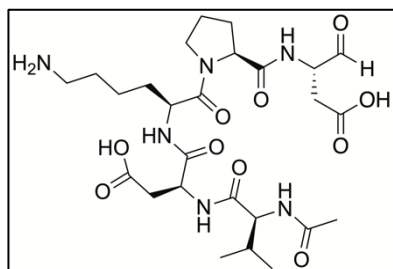

The title compound was synthesized according to general procedure **A** yielding a fluffy white solid (17.4 mg, 16%): RP-HPLC: 97%, (t_R = 7.27, k = 1.42). ^{1}H NMR (400 MHz, D$_2$O) δ 4.94 – 4.85 (m, 2H), 4.37 – 4.28 (m, 1H), 4.21 – 4.08 (m, 1H), 4.02 – 3.84 (m, 2H), 3.76 – 3.58 (m, 2H), 2.90 – 2.78 (m, 1H), 2.73 – 2.53 (m, 2H), 2.56 – 2.37 (m, 1H), 2.21 – 2.04 (m, 1H), 2.00 – 1.73 (m, 8H), 0.97 – 0.71 (m, 12H). ^{13}C NMR (101 MHz, D$_2$O) δ 175.27, 175.16, 174.37, 173.91, 173.44, 173.11, 173.03, 170.31, 170.24, 89.71, 60.60, 60.54, 59.87, 59.81, 59.56, 51.52, 51.47, 48.28, 48.06, 35.23, 33.94, 33.78, 29.98, 29.41, 24.55, 21.62, 18.33, 17.57. HRMS (ESI-MS): *m/z* [M+H$^+$] calculated for C$_{25}$H$_{40}$N$_5$O$_{10}^+$: 570.2770, found 570.2776; C$_{25}$H$_{39}$N$_5$O$_{10}$ (569.61).

(4*S*,7*S*,10*S*,13*S*,16*S*)-7-(Carboxymethyl)-16-formyl-4,10,13-triisopropyl-2,5,8,11,14-pentaoxo-3,6,9,12,15-pentaazaoctadecan-18-oic acid (2.018)
(Synthesized by Steffen Pockes)
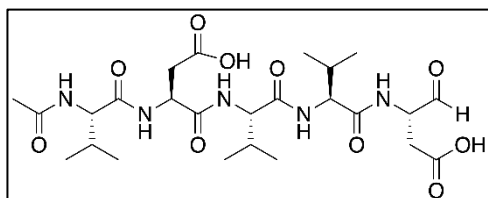
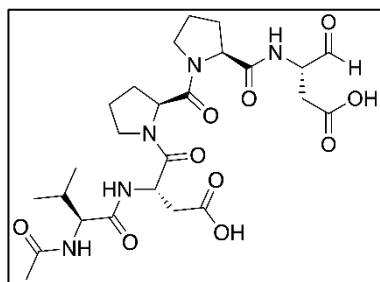The title compound was synthesized according to general procedure **A** yielding a fluffy white solid (32.5 mg, 18%): RP-HPLC: 99%, (t_R = 8.88, k = 1.96). ^{1}H NMR (400 MHz, CD$_3$OD) δ 4.78 – 4.67 (m, 1H), 4.61 – 4.51 (m, 1H), 4.35 – 4.24 (m, 1H), 4.23 – 4.07 (m, 3H), 2.97 – 2.83 (m, 1H), 2.83 – 2.59 (m, 2H), 2.57 – 2.42 (m, 1H), 2.20 – 2.02 (m, 3H), 2.00 (s, 3H), 1.06 – 0.85 (m, 18H). ^{13}C NMR (101 MHz, CD$_3$OD) δ 173.67, 172.72, 172.41, 172.26, 172.05, 171.82, 170.98, 97.00, 59.45, 59.29, 59.18, 50.56, 47.88, 34.92, 33.03, 30.35, 30.24, 30.19, 21.02, 18.31, 17.40, 17.26. HRMS (ESI-MS): *m/z* [M+H$^+$] calculated for C$_{25}$H$_{42}$N$_5$O$_{10}^+$: 572.2926, found 572.2933; C$_{25}$H$_{41}$N$_5$O$_{10}$ (571.63).

(4*S*,7*S*,10*S*,13*S*,16*S*)-10-(4-Aminobutyl)-7-(carboxymethyl)-16-formyl-4-isopropyl-13-methyl-2,5,8,11,14-pentaoxo-3,6,9,12,15-pentaazaoctadecan-18-oic acid hydrotrifluoroacetate (2.019)
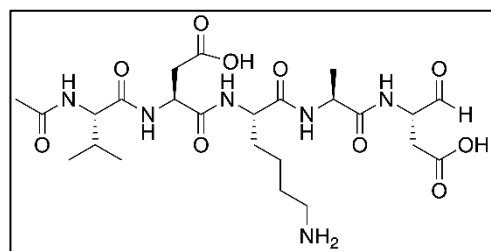
The title compound was synthesized according to general procedure **B** yielding a fluffy white solid (45.1 mg, 35%): RP-HPLC: > 99%, (t_R = 4.81, k = 0.60). ^{1}H NMR (300 MHz, D_2O) δ 4.89 (dd, J = 4.5, 3.1 Hz, 1H), 4.60 – 4.54 (m, 1H), 4.19 – 4.00 (m, 3H), 3.88 (dd, J = 7.1, 2.3 Hz, 1H), 2.91 – 2.78 (m, 3H), 2.75 – 2.32 (m, 3H), 1.97 – 1.82 (m, 4H), 1.77 – 1.45 (m, 4H), 1.34 – 1.17 (m, 5H), 0.82 – 0.75 (m, 6H). ^{13}C NMR (75 MHz, D_2O) δ 175.25, 175.16, 174.64, 174.09, 173.74, 173.23, 173.17, 172.31, 172.19, 89.70, 59.94, 53.65, 51.46, 50.04, 49.86, 39.15, 35.08, 34.01, 30.33, 29.84, 26.22, 21.94, 21.65, 18.27, 17.62, 16.61. HRMS (ESI-MS): *m/z* [M+H$^+$] calculated for $C_{24}H_{41}N_6O_{10}^+$: 573.2879, found 573.2886; $C_{24}H_{40}N_6O_{10}$ x $C_2HF_3O_2$ (686.64).

(4*S*,7*S*,10*S*,13*S*,16*S*)-7,10-Bis(4-aminobutyl)-16-formyl-4-(4-hydroxybenzyl)-13-isopropyl-2,5,8,11,14-pentaoxo-3,6,9,12,15-pentaazaoctadecan-18-oic acid dihydrotrifluoroacetate (2.020)
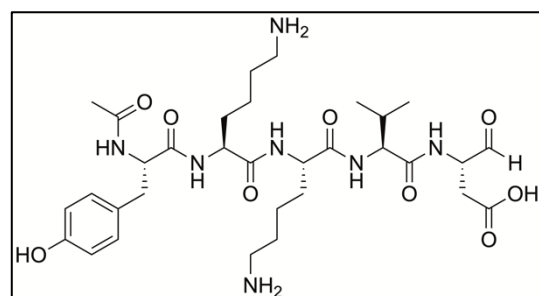
The title compound was synthesized according to general procedure **B** yielding a fluffy white solid (75.2 mg, 44%): RP-HPLC: 99%, (t_R = 5.42, k = 0.97). ^{1}H NMR (300 MHz, D_2O) δ 7.00 – 6.91 (m, 2H), 6.71 – 6.60 (m, 2H), 4.87 (dd, J = 6.8, 4.7 Hz, 1H), 4.31 (t, J = 7.6 Hz, 1H), 4.19 – 3.86 (m, 4H), 2.90 – 2.75 (m, 6H), 2.69 – 2.30 (m, 2H), 1.95 – 1.77 (m, 4H), 1.73 – 1.37 (m, 8H), 1.34 – 1.07 (m, 4H), 0.83 – 0.71 (m, 6H). ^{13}C NMR (75 MHz, D_2O) δ 175.33, 175.25, 174.07, 173.67, 173.49, 173.41, 173.35, 173.25, 173.19, 172.87, 172.74, 154.46, 130.47, 127.92, 115.44, 89.69, 59.61, 59.56, 55.51, 53.67, 53.61, 52.99, 51.59, 51.49, 39.18, 36.15, 34.25, 34.01, 30.62, 30.31, 26.35, 26.27, 22.06, 21.90, 21.60, 18.31, 17.70, 17.62. HRMS (ESI-MS): *m/z* [M+H$^+$] calculated for $C_{32}H_{52}N_7O_9^+$: 678.3821, found 678.3824; $C_{32}H_{51}N_7O_9$ x $C_4H_2F_6O_4$ (905.85).

(4S,7S,10S,13S,16S)-7,13-Bis(4-aminobutyl)-16-formyl-4-(4-hydroxybenzyl)-10-isopropyl-2,5,8,11,14-pentaoxo-3,6,9,12,15-pentaazaoctadecan-18-oic acid dihydrotrifluoroacetate (2.021)
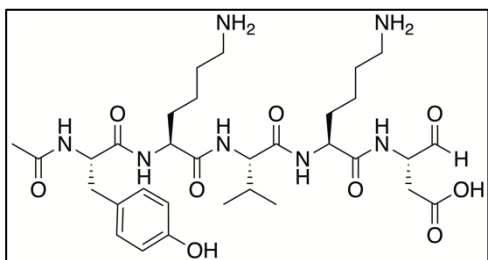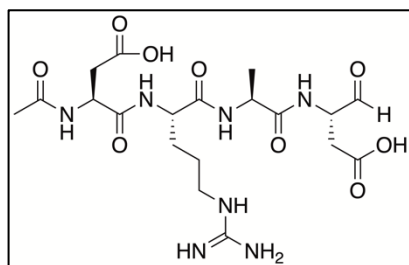

The title compound was synthesized according to general procedure **B** yielding a fluffy white solid (66.3 mg, 39%): RP-HPLC: 99%, (t_R = 5.48, k = 0.83). ^{1}H NMR (300 MHz, D_2O) δ 6.99 – 6.92 (m, 2H), 6.70 – 6.63 (m, 2H), 4.91 – 4.86 (m, 1H), 4.33 (t, J = 7.5 Hz, 1H), 4.18 – 4.03 (m, 3H), 3.90 – 3.81 (m, 1H), 2.86 – 2.73 (m, 6H), 2.68 – 2.31 (m, 2H), 1.94 – 1.77 (m, 4H), 1.69 – 1.39 (m, 8H), 1.33 – 1.10 (m, 4H), 0.79 (t, J = 6.1 Hz, 6H). ^{13}C NMR (75 MHz, D_2O) δ 175.26, 175.06, 174.04, 173.69, 173.18, 173.07, 163.21, 162.74, 154.44, 130.46, 127.90, 115.47, 89.64, 59.65, 55.48, 53.66, 53.05, 51.49, 39.17, 36.15, 34.23, 33.89, 30.51, 30.06, 26.30, 26.24, 21.94, 21.60, 18.40, 18.34, 18.00, 17.94. HRMS (ESI-MS): m/z [M+H$^+$] calculated for $C_{32}H_{52}N_7O_9^+$: 678.3821, found 678.3831; $C_{32}H_{51}N_7O_9$ x $C_4H_2F_6O_4$ (905.85).

(4S,7S,10S,13S,16S)-7-(4-Aminobutyl)-16-formyl-4,10,13-triisopropyl-2,5,8,11,14-pentaoxo-3,6,9,12,15-pentaazaoctadecan-18-oic acid hydrotrifluoroacetate (2.022)
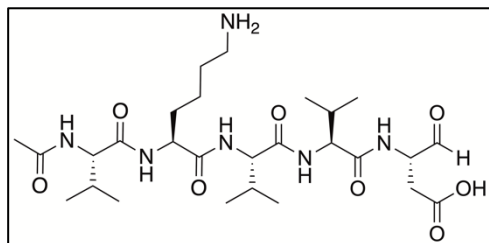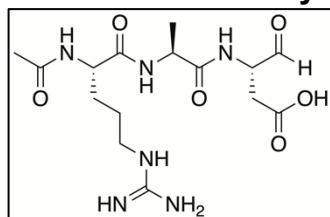

The title compound was synthesized according to general procedure **A** yielding a fluffy white solid (54.9 mg, 42%): RP-HPLC: > 99%, (t_R = 7.23, k = 1.41). ^{1}H NMR (300 MHz, D_2O) δ 4.87 (dd, J = 9.0, 4.7 Hz, 1H), 4.22 (t, J = 7.4 Hz, 1H), 4.18 – 4.02 (m, 1H), 3.98 – 3.84 (m, 3H), 2.82 (t, J = 7.6 Hz, 2H), 2.69 – 2.29 (m, 2H), 2.00 – 1.75 (m, 6H), 1.72 – 1.44 (m, 4H), 1.39 – 1.10 (m, 2H), 0.86 – 0.70 (m, 18H). ^{13}C NMR (75 MHz, D_2O) δ 175.62, 175.47, 174.40, 173.74, 173.45, 173.31, 173.16, 173.05, 172.76, 172.64, 89.68, 59.74, 59.67, 59.57, 53.22, 51.56, 39.19, 34.19, 30.40, 30.25, 30.15, 29.96, 26.23, 22.05, 21.57, 18.38, 18.02, 17.97, 17.80, 17.74. HRMS (ESI-MS): m/z [M+H$^+$] calculated for $C_{27}H_{49}N_6O_8^+$: 585.3606, found 585.3617; $C_{27}H_{48}N_6O_8$ x $C_2HF_3O_2$ (698.74).

(4*S*,7*S*,10*S*,13*S*,16*S*)-7,10-Bis(4-aminobutyl)-16-formyl-4,13-diisopropyl-2,5,8,11,14-pentaoxo-3,6,9,12,15-pentaazaoctadecan-18-oic acid dihydrotrifluoroacetate (2.023)
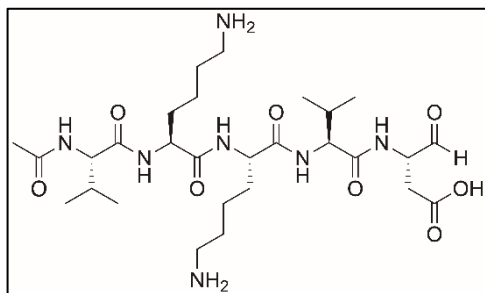
The title compound was synthesized according to general procedure **B** yielding a fluffy white solid (76.0 mg, 48%): RP-HPLC: > 99%, (t_R = 5.23, k = 0.90). ^{1}H NMR (300 MHz, D_2O) δ 4.88 (dd, J = 6.0, 4.7 Hz, 1H), 4.25 – 4.04 (m, 3H), 3.97 – 3.85 (m, 2H), 2.84 (t, J = 7.6 Hz, 4H), 2.71 – 2.32 (m, 2H), 1.98 – 1.78 (m, 5H), 1.72 – 1.45 (m, 8H), 1.41 – 1.14 (m, 4H), 0.84 – 0.72 (m, 12H). ^{13}C NMR (75 MHz, D_2O) δ 175.25, 175.15, 174.43, 173.83, 173.48, 173.36, 172.89, 172.76, 89.68, 59.79, 59.64, 59.59, 53.49, 53.43, 53.27, 51.58, 51.47, 39.18, 33.92, 30.45, 30.36, 30.27, 29.93, 26.25, 22.06, 22.02, 21.60, 18.36, 17.79, 17.70, 17.62. HRMS (ESI-MS): *m/z* [M+H$^+$] calculated for $C_{28}H_{52}N_7O_8^+$: 614.3872, found 614.3871; $C_{28}H_{51}N_7O_8$ x $C_4H_2F_6O_4$ (841.80).

(4*S*,7*S*,10*S*,13*S*,16*S*)-7,13-Bis(4-aminobutyl)-16-formyl-4,10-diisopropyl-2,5,8,11,14-pentaoxo-3,6,9,12,15-pentaazaoctadecan-18-oic acid dihydrotrifluoroacetate (2.024)
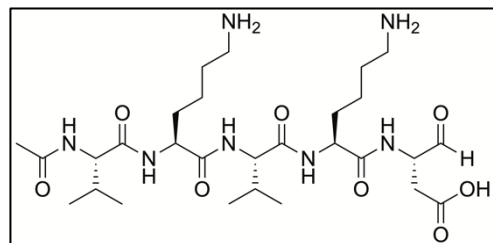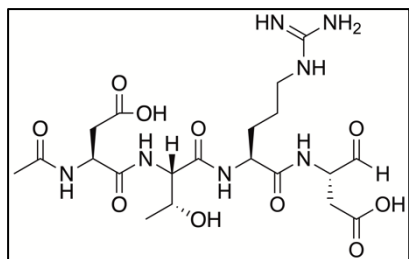

The title compound was synthesized according to general procedure **B** yielding a fluffy white solid (91.0 mg, 58%): RP-HPLC: > 99%, (t_R = 5.02, k = 0.67). ^{1}H NMR (400 MHz, D_2O) δ 4.95 – 4.91 (m, 1H), 4.34 – 4.07 (m, 3H), 4.02 – 3.86 (m, 2H), 2.88 (t, 4H), 2.74 – 2.36 (m, 2H), 2.00 – 1.84 (m, 5H), 1.78 – 1.50 (m, 8H), 1.40 – 1.19 (m, 4H), 0.87 – 0.77 (m, 12H). ^{13}C NMR (101 MHz, D_2O) δ 175.15, 174.47, 173.93, 173.88, 173.73, 173.70, 173.10, 173.04, 89.70, 59.87, 59.54, 53.71, 53.29, 51.53, 39.23, 39.19, 34.29, 30.31, 30.21, 29.92, 26.32, 26.20, 22.11, 22.02, 21.60, 18.40, 17.81. HRMS (ESI-MS): *m/z* [M+H$^+$] calculated for $C_{28}H_{52}N_7O_8^+$: 614.3872, found 614.3877; $C_{28}H_{51}N_7O_8$ x $C_4H_2F_6O_4$ (841.80).

(*S*)-3-((*S*)-2-((*S*)-1-(Acetyl-*L*-valyl-*L*-lysyl)pyrrolidine-2-carboxamido)-3-methylbutanamido)-4-oxobutanoic acid hydrotrifluoroacetate (2.025)
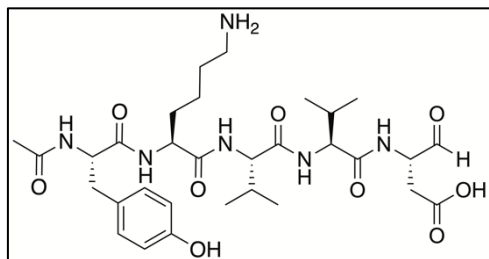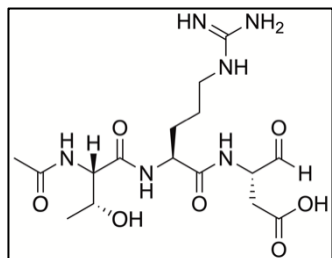

The title compound was synthesized according to general procedure **B** yielding a fluffy white solid (59.9 mg, 46%): RP-HPLC: > 99%, (t_R = 6.26, k = 1.28). ^{1}H NMR (300 MHz, D_2O) δ 4.88 (dd, J = 4.6, 1.4 Hz, 1H), 4.52 – 4.45 (m, 1H), 4.36 – 4.24 (m, 1H), 4.17 – 4.06 (m, 1H), 3.93 – 3.83 (m, 2H), 3.78 – 3.66 (m, 1H), 3.55 – 3.44 (m, 1H), 2.85 (t, J = 7.4 Hz, 2H), 2.71 – 2.32 (m, 2H), 2.27 – 2.07 (m, 1H), 1.98 – 1.49 (m, 12H), 1.44 – 1.21 (m, 2H), 0.88 – 0.72 (m, 12H). ^{13}C NMR (75 MHz, D_2O) δ 175.24, 175.18, 174.34, 173.98, 173.95, 173.73, 173.15, 173.04, 171.74, 89.68, 60.30, 60.27, 59.90, 59.85, 59.61, 51.53, 51.44, 51.28, 48.07, 39.21, 33.94, 33.85, 29.93, 29.42, 26.34, 24.68, 21.87, 21.58, 18.37, 17.77. HRMS (ESI-MS): *m/z* [M+H$^+$] calculated for $C_{27}H_{47}N_6O_8^+$: 583.3450, found 583.3454; $C_{27}H_{46}N_6O_8$ x $C_2HF_3O_2$ (696.72).

(4*S*,7*S*,10*S*,13*S*,16*S*)-7-(4-Aminobutyl)-16-formyl-4-(4-hydroxybenzyl)-10,13-diisopropyl-2,5,8,11,14-pentaoxo-3,6,9,12,15-pentaazaoctadecan-18-oic acid hydrotrifluoroacetate (2.026)
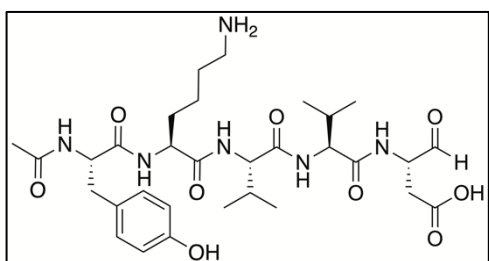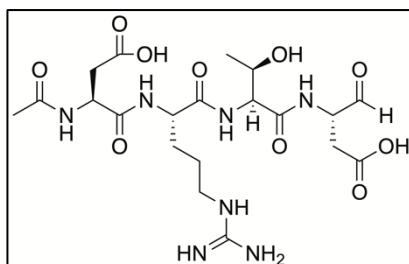

The title compound was synthesized according to general procedure **A** yielding a fluffy white solid (58.8 mg, 41%): RP-HPLC: 98%, (t_R = 7.33, k = 1.44). ^{1}H NMR (300 MHz, D_2O) δ 6.99 – 6.90 (m, 2H), 6.70 – 6.63 (m, 2H), 4.87 (dd, J = 9.1, 4.7 Hz, 1H), 4.34 (t, J = 9.0 Hz, 1H), 4.19 – 4.04 (m, 2H), 3.97 – 3.84 (m, 2H), 2.90 – 2.30 (m, 6H), 1.81 (s, 5H), 1.66 – 1.39 (m, 4H), 1.25 – 1.03 (m, 2H), 0.85 – 0.68 (m, 12H). ^{13}C NMR (75 MHz, D_2O) δ 175.33, 175.15, 173.99, 173.21, 173.08, 173.04, 172.75, 172.63, 154.44, 130.45, 127.89, 115.47, 89.66, 59.76, 59.53, 55.38, 52.95, 51.50, 39.17, 36.21, 33.98, 30.66, 30.28, 30.02, 26.27, 21.88, 21.59, 18.37, 17.74. HRMS (ESI-MS): *m/z* [M+H$^+$] calculated for $C_{31}H_{49}N_6O_9^+$: 649.3556, found 649.3566; $C_{31}H_{48}N_6O_9$ x $C_2HF_3O_2$ (762.78).

(4S,7S,10S,13S,16S)-10-(4-Aminobutyl)-7-(carboxymethyl)-16-formyl-4-(4-hydroxybenzyl)-13-isopropyl-2,5,8,11,14-pentaoxo-3,6,9,12,15-pentaazaoctadecan-18-oic acid hydrotrifluoroacetate (2.027)
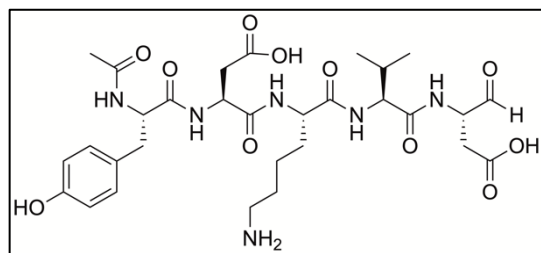
The title compound was synthesized according to general procedure **A** yielding a fluffy white solid (17.4 mg, 27%): RP-HPLC: > 99%, (t_R = 6.27, k = 1.09). ^{1}H NMR (400 MHz, D$_2$O) δ 7.03 – 6.98 (m, 2H), 6.75 – 6.68 (m, 2H), 4.91 (dd, J = 6.3, 4.7 Hz, 1H), 4.52 – 4.45 (m, 1H), 4.36 (t, J = 7.5 Hz, 1H), 4.25 – 4.06 (m, 2H), 3.96 (dd, J = 7.8, 1.6 Hz, 1H), 2.93 – 2.37 (m, 8H), 1.99 – 1.87 (m, 1H), 1.85 (s, 3H), 1.74 – 1.49 (m, 4H), 1.34 – 1.17 (m, 2H), 0.85 – 0.75 (m, 6H). ^{13}C NMR (101 MHz, D$_2$O) δ 175.21, 175.10, 174.21, 173.90, 173.41, 173.36, 173.27, 172.96, 172.85, 171.67, 171.60, 154.50, 130.48, 127.93, 115.50, 89.70, 59.73, 55.55, 53.63, 53.56, 51.58, 51.49, 49.91, 39.20, 36.00, 35.07, 33.91, 30.26, 30.11, 26.26, 22.00, 21.95, 21.67, 18.33, 18.29, 17.72, 17.67. HRMS (ESI-MS): m/z [M+H$^+$] calculated for C$_{30}$H$_{45}$N$_6$O$_{11}^+$: 665.3141, found 665.3155; C$_{30}$H$_{44}$N$_6$O$_{11}$ x C$_2$HF$_3$O$_2$ (778.70).

(4S,7S,10S,13S,16S)-13-(4-Aminobutyl)-7-(carboxymethyl)-16-formyl-4-(4-hydroxybenzyl)-10-isopropyl-2,5,8,11,14-pentaoxo-3,6,9,12,15-pentaazaoctadecan-18-oic acid hydrotrifluoroacetate (2.028)
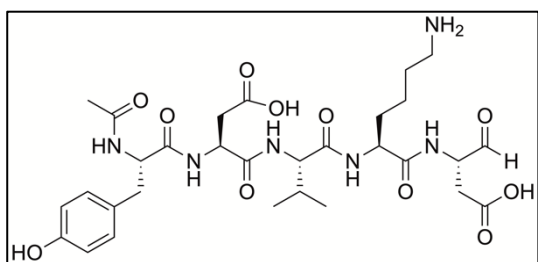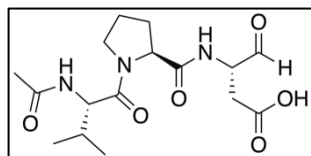

The title compound was synthesized according to general procedure **B** yielding a fluffy white solid (38.6 mg, 26%): RP-HPLC: > 99%, (t_R = 6.28, k = 1.09). ^{1}H NMR (400 MHz, D$_2$O) δ 7.04 – 6.99 (m, 2H), 6.75 – 6.70 (m, 2H), 4.92 (dd, J = 4.6, 1.5 Hz, 1H), 4.52 (t, J = 6.7 Hz, 1H), 4.38 (t, J = 7.6 Hz, 1H), 4.24 – 4.07 (m, 2H), 3.96 – 3.85 (m, 1H), 2.93 – 2.37 (m, 8H), 2.00 – 1.87 (m, 1H), 1.85 (s, 3H), 1.79 – 1.46 (m, 4H), 1.42 – 1.18 (m, 2H), 0.83 – 0.74 (m, 6H). ^{13}C NMR (101 MHz, D$_2$O) δ 175.29, 175.11, 174.18, 174.15, 173.78, 173.39, 173.36, 173.28, 173.20, 171.87, 171.78, 154.51, 130.49, 127.93, 115.53, 89.71, 59.87, 55.46, 53.56, 51.50, 49.91, 39.21, 36.07, 35.12, 34.20, 33.90, 29.89, 26.19, 22.00, 21.95, 21.63, 18.40, 17.81. HRMS (ESI-MS): m/z [M+H$^+$] calculated for C$_{30}$H$_{45}$N$_6$O$_{11}^+$: 615.3141, found 665.3146; C$_{30}$H$_{44}$N$_6$O$_{11}$ x C$_2$HF$_3$O$_2$ (778.74).

(*S*)-3-((*S*)-2-Acetamido-3-(4-hydroxyphenyl)propanamido)-4-((*S*)-2-(((*S*)-1-(((*S*)-1-carboxy-3-oxopropan-2-yl)amino)-3-methyl-1-oxobutan-2-yl)carbamoyl)pyrrolidin-1-yl)-4-oxobutanoic acid (2.029)
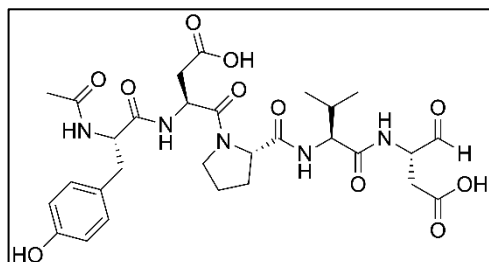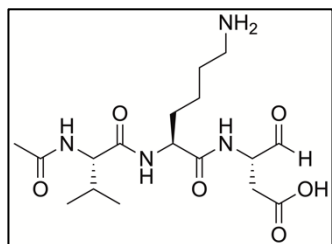

The title compound was synthesized according to general procedure **B** yielding a fluffy white solid (55.3 mg, 47%): RP-HPLC: 99%, (t_R = 7.69, k = 1.80). ^{1}H NMR (300 MHz, D$_2$O) δ 7.00 – 6.89 (m, 2H), 6.72 – 6.59 (m, 2H), 4.86 (dd, J = 4.6, 2.1 Hz, 1H), 4.73 (t, J = 7.0 Hz, 1H), 4.32 (t, J = 7.9 Hz, 1H), 4.20 – 4.00 (m, 2H), 3.86 (d, J = 7.7 Hz, 1H), 3.54 – 3.09 (m, 2H), 2.85 – 2.29 (m, 6H), 2.11 – 1.90 (m, 1H), 1.96 – 1.66 (m, 7H), 0.87 – 0.69 (m, 6H). ^{13}C NMR (75 MHz, D$_2$O) δ 175.24, 175.12, 174.00, 173.84, 173.06, 172.98, 172.53, 169.59, 169.49, 154.44, 130.49, 127.79, 115.37, 89.68, 60.50, 60.43, 59.83, 59.77, 55.20, 51.48, 51.43, 47.74, 47.61, 36.16, 35.45, 33.90, 29.87, 29.30, 24.36, 21.57, 17.73, 17.69. HRMS (ESI-MS): m/z [M+H$^+$] calculated for C$_{29}$H$_{40}$N$_5$O$_{11}^+$: 634.2719, found 634.2727; C$_{29}$H$_{39}$N$_5$O$_{11}$ (633.66).

(4*S*,7*S*,10*S*,13*S*,16*S*)-10-(4-Aminobutyl)-7-(carboxymethyl)-16-formyl-4,13-bis((*R*)-1-hydroxyethyl)-2,5,8,11,14-pentaoxo-3,6,9,12,15-pentaazaoctadecan-18-oic acid hydrotrifluoroacetate (2.030)
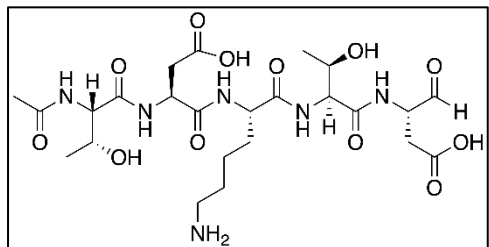
The title compound was synthesized according to general procedure **A** yielding a fluffy white solid (21.0 mg, 16%): RP-HPLC: > 99%, (t_R = 3.11, k = 0.04). ^{1}H NMR (300 MHz, D$_2$O) δ 4.93 – 4.88 (m, 1H), 4.60 – 4.52 (m, 1H), 4.25 – 3.98 (m, 6H), 2.90 – 2.59 (m, 5H), 2.48 – 2.35 (m, 1H), 1.95 (d, J = 4.1 Hz, 3H), 1.74 – 1.49 (m, 4H), 1.31 – 1.21 (m, 2H), 1.12 – 0.99 (m, 6H). HRMS (ESI-MS): m/z [M+H$^+$] calculated for C$_{24}$H$_{41}$N$_6$O$_{12}^+$: 605.2777, found 605.2783; C$_{24}$H$_{40}$N$_6$O$_{12}$ x C$_2$HF$_3$O$_2$ (718.64).

(4*S*,7*S*,10*S*,13*S*,16*S*)-10-(4-Aminobutyl)-13-((*S*)-*sec*-butyl)-7-(carboxymethyl)-16-formyl-4-isopropyl-2,5,8,11,14-pentaoxo-3,6,9,12,15-pentaazaoctadecan-18-oic acid hydrotrifluoroacetate (2.031)
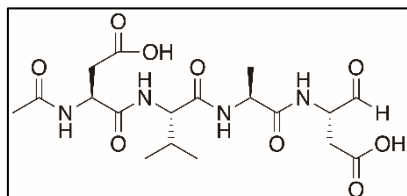

The title compound was synthesized according to general procedure **A** yielding a fluffy white solid (95.0 mg, 69%): RP-HPLC: 98%, (t_R = 7.06, k = 1.35). ^{1}H NMR (400 MHz, D_2O) δ 4.94 – 4.89 (m, 1H), 4.63 – 4.55 (m, 1H), 4.27 – 4.09 (m, 2H), 4.06 – 3.96 (m, 1H), 3.93 (d, *J* = 6.9 Hz, 1H), 2.94 – 2.38 (m, 6H), 2.01 – 1.86 (m, 4H), 1.81 – 1.66 (m, 2H), 1.66 – 1.61 (m, 1H), 1.60 – 1.51 (m, 2H), 1.42 – 0.99 (m, 4H), 0.91 – 0.65 (m, 12H). ^{13}C NMR (101 MHz, D_2O) δ 175.17, 175.08, 174.63, 173.90, 173.71, 173.53, 173.21, 172.96, 171.99, 89.69, 59.98, 58.52, 53.55, 51.51, 50.10, 39.20, 35.97, 35.12, 33.89, 30.33, 29.82, 26.23, 24.49, 21.95, 21.70, 18.31, 17.63, 14.71, 10.01. HRMS (ESI-MS): *m/z* [M+H$^+$] calculated for $C_{27}H_{47}N_6O_{10}^+$: 615.3348, found 615.3353; $C_{27}H_{46}N_6O_{10}$ x $C_2HF_3O_2$ (728.72).

(4*S*,7*S*,10*S*,13*S*,16*S*)-10-(4-Aminobutyl)-13-benzyl-7-(carboxymethyl)-16-formyl-4-isopropyl-2,5,8,11,14-pentaoxo-3,6,9,12,15-pentaazaoctadecan-18-oic acid hydrotrifluoroacetate (2.032)

The title compound was synthesized according to general procedure **A** yielding a fluffy white solid (90.5 mg, 60%): RP-HPLC: > 99%, (t_R = 7.72, k = 1.57). ^{1}H NMR (400 MHz, D_2O) δ 7.28 – 7.11 (m, 5H), 4.89 – 4.80 (m, 1H), 4.59 – 4.42 (m, 2H), 4.14 – 4.02 (m, 2H), 3.90 (dd, *J* = 7.0, 1.8 Hz, 1H), 3.11 – 2.37 (m, 8H), 1.99 – 1.86 (m, 4H), 1.62 – 1.40 (m, 4H), 1.20 – 1.02 (m, 2H), 0.81 (t, *J* = 1.1 Hz, 6H). ^{13}C NMR (101 MHz, D_2O) δ 175.02, 174.58, 174.02, 173.69, 173.28, 173.12, 172.56, 172.48, 172.21, 129.24, 128.80, 128.74, 127.13, 89.65, 59.96, 54.85, 53.80, 51.46, 49.99, 39.13, 36.80, 35.05, 33.85, 30.11, 29.83, 26.17, 21.81, 21.72, 21.67, 18.28, 17.63. HRMS (ESI-MS): *m/z* [M+H$^+$] calculated for $C_{30}H_{45}N_6O_{10}^+$: 649.3192, found 649.3197; $C_{30}H_{44}N_6O_{10}$ x $C_2HF_3O_2$ (762.70).

(S)-3-((S)-2-Acetamido-3-methylbutanamido)-4-(((S)-6-amino-1-((S)-2-(((S)-1-carboxy-3-oxopropan-2-yl)carbamoyl)pyrrolidin-1-yl)-1-oxohexan-2-yl)amino)-4-oxobutanoic acid hydrotrifluoroacetate (2.033)

The title compound was synthesized according to general procedure **A** yielding a fluffy white solid (25.4 mg, 19%): RP-HPLC: > 99%, (t_R = 4.91, k = 0.64). ^{1}H NMR (400 MHz, D$_2$O) δ 4.97 – 4.88 (m, 1H), 4.60 (dd, J = 8.0, 5.8 Hz, 1H), 4.53 – 4.45 (m, 1H), 4.37 – 4.24 (m, 1H), 4.24 – 4.06 (m, 1H), 3.94 (d, J = 7.0 Hz, 1H), 3.75 – 3.45 (m, 2H), 2.94 – 2.35 (m, 6H), 2.21 – 2.07 (m, 1H), 1.98 – 1.89 (m, 5H), 1.89 – 1.26 (m, 8H), 0.82 (dd, J = 6.8, 1.9 Hz, 6H). ^{13}C NMR (101 MHz, D$_2$O) δ 175.31, 175.23, 174.52, 173.91, 173.84, 173.65, 171.71, 171.63, 171.57, 89.69, 60.75, 60.70, 60.53, 59.82, 51.50, 51.45, 49.99, 47.93, 39.21, 35.18, 34.10, 29.87, 29.66, 29.48, 26.38, 24.67, 24.53, 21.75, 21.67, 18.30, 17.57. HRMS (ESI-MS): m/z [M+H$^+$] calculated for C$_{26}$H$_{43}$N$_6$O$_{10}$$^+$: 599.3035, found 599.3047; C$_{26}$H$_{42}$N$_6$O$_{10}$ x C$_2$HF$_3$O$_2$ (712.67).

(S)-3-((S)-2-Acetamido-3-methylbutanamido)-4-((S)-2-((S)-2-(((S)-1-carboxy-3-oxopropan-2-yl)carbamoyl)pyrrolidine-1-carbonyl)pyrrolidin-1-yl)-4-oxobutanoic acid (2.034)
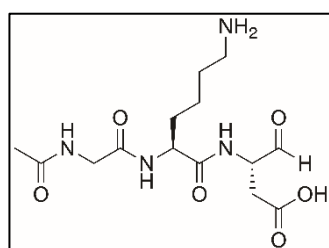

The title compound was synthesized according to general procedure **A** yielding a fluffy white solid (28.1 mg, 26%): RP-HPLC: > 99%, (t_R = 6.30, k = 1.10). ^{1}H NMR (400 MHz, D$_2$O) δ 4.96 – 4.91 (m, 1H), 4.91 – 4.84 (m, 1H), 4.61 – 4.53 (m, 1H), 4.34 – 3.98 (m, 2H), 3.94 (d, J = 7.3 Hz, 1H), 3.80 – 3.21 (m, 4H), 2.94 – 2.37 (m, 4H), 2.28 – 2.07 (m, 2H), 2.04 – 1.69 (m, 10H), 0.86 – 0.76 (m, 6H). ^{13}C NMR (101 MHz, D$_2$O) δ 175.33, 175.27, 174.33, 173.91, 173.79, 173.41, 172.19, 171.93, 169.55, 89.66, 60.65, 60.55, 59.56, 58.95, 51.48, 51.41, 48.38, 47.94, 47.74, 35.09, 34.06, 29.99, 29.30, 28.25, 24.61, 24.51, 21.62, 18.33, 17.53. HRMS (ESI-MS): m/z [M+H$^+$] calculated for C$_{25}$H$_{37}$N$_5$O$_{10}$$^+$: 568.2613, found 568.2624; C$_{25}$H$_{37}$N$_5$O$_{10}$ (567.60).

(*S*)-3-((*S*)-2-Acetamido-3-methylbutanamido)-4-((*S*)-2-(((*S*)-6-amino-1-(((*S*)-1-carboxy-3-oxopropan-2-yl)amino)-1-oxohexan-2-yl)carbamoyl)pyrrolidin-1-yl)-4-oxobutanoic acid hydrotrifluoroacetate (2.035)
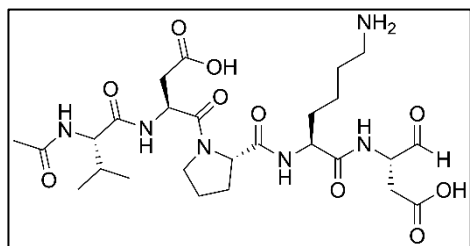
The title compound was synthesized according to general procedure **B** yielding a fluffy white solid (66.3 mg, 50%): RP-HPLC: 99%, (t_R = 5.43, k = 0.97). ^{1}H NMR (300 MHz, D$_2$O) δ 4.91 – 4.87 (m, 1H), 4.87 – 4.79 (m, 1H), 4.30 – 4.20 (m, 1H), 4.16 – 4.03 (m, 2H), 3.90 (d, J = 7.3 Hz, 1H), 3.78 – 3.47 (m, 2H), 2.91 – 2.32 (m, 6H), 2.21 – 2.05 (m, 1H), 1.97 – 1.73 (m, 7H), 1.73 – 1.46 (m, 4H), 1.39 – 1.19 (m, 2H), 0.84 – 0.71 (m, 6H). ^{13}C NMR (75 MHz, D$_2$O) δ 175.24, 175.11, 174.38, 174.21, 174.02, 173.96, 173.56, 173.49, 173.43, 170.43, 89.69, 60.72, 60.61, 59.58, 53.72, 53.68, 51.48, 51.44, 48.32, 48.27, 48.09, 39.20, 35.28, 34.13, 30.17, 29.94, 29.44, 26.14, 24.54, 22.08, 21.59, 18.31, 17.58. HRMS (ESI-MS): *m/z* [M+H$^+$] calculated for C$_{26}$H$_{43}$N$_6$O$_{10}^+$: 655.3661, found 655.3668; C$_{26}$H$_{42}$N$_6$O$_{10}$ x C$_2$HF$_3$O$_2$ (768.75).

(4*S*,7*S*,10*S*,13*S*,16*S*)-7-(Carboxymethyl)-16-formyl-4-(4-hydroxybenzyl)-10,13-diisopropyl-2,5,8,11,14-pentaoxo-3,6,9,12,15-pentaazaoctadecan-18-oic acid (2.036) *(Synthesized by Alexander Hubmann)*
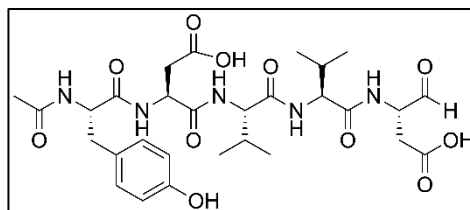
The title compound was synthesized according to general procedure **A** yielding a fluffy white solid (32.1 mg, 27%): RP-HPLC: 99%, (t_R = 8.88, k = 1.96). ^{1}H NMR (300 MHz, D$_2$O) δ 7.03 – 6.91 (m, 2H), 6.74 – 6.60 (m, 2H), 4.87 (dd, J = 6.8, 4.7 Hz, 1H), 4.48 (t, J = 6.7 Hz, 1H), 4.35 (t, J = 7.5 Hz, 1H), 4.18 – 4.03 (m, 1H), 3.97 – 3.86 (m, 2H), 2.96 – 2.28 (m, 6H), 1.96 – 1.76 (m, 5H), 0.83 – 0.67 (m, 12H). ^{13}C NMR (75 MHz, D$_2$O) δ 175.33, 175.16, 174.10, 174.05, 173.39, 173.34, 173.11, 172.88, 172.78, 171.66, 171.59, 154.48, 130.48, 127.95, 115.51, 89.69, 59.81, 59.69, 55.35, 51.51, 49.94, 36.10, 35.16, 33.94, 29.97, 21.62, 18.37, 17.88, 17.75. HRMS (ESI-MS): *m/z* [M+H$^+$] calculated for C$_{29}$H$_{42}$N$_5$O$_{11}^+$: 636.2875, found 636.2887; C$_{29}$H$_{41}$N$_5$O$_{11}$ (635.67).

(4S,7S,10S,13S)-4-(Carboxymethyl)-13-formyl-7-(3-guanidinopropyl)-10-methyl-2,5,8,11-tetraoxo-3,6,9,12-tetraazapentadecan-15-oic acid hydrotrifluoroacetate (2.037)
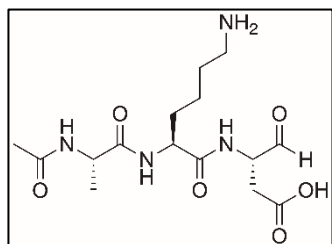

The title compound was synthesized according to general procedure **B** yielding a fluffy white solid (17.6 mg, 15%): RP-HPLC: > 99%, (t_R = 3.66, k = 0.22). ^{1}H NMR (400 MHz, D_2O) δ 4.93 (t, J = 3.8 Hz, 1H), 4.56 (d, J = 6.7 Hz, 1H), 4.28 – 4.07 (m, 3H), 3.10 (t, J = 6.9 Hz, 2H), 2.87 – 2.37 (m, 4H), 1.92 (s, 3H), 1.84 – 1.44 (m, 4H), 1.30 – 1.20 (m, 3H). ^{13}C NMR (101 MHz, D_2O) δ 175.30, 175.23, 174.66, 174.51, 174.25, 174.16, 173.03, 172.98, 172.90, 172.80, 156.79, 89.72, 53.35, 53.20, 51.49, 50.24, 49.89, 49.83, 40.51, 35.38, 34.12, 34.07, 28.08, 27.98, 24.31, 21.72, 16.81, 16.64. HRMS (ESI-MS): m/z [M+H$^+$] calculated for $C_{19}H_{32}N_7O_9^+$: 502.2257, found 502.2256; $C_{19}H_{31}N_7O_9$ x $C_2HF_3O_2$ (615.52).

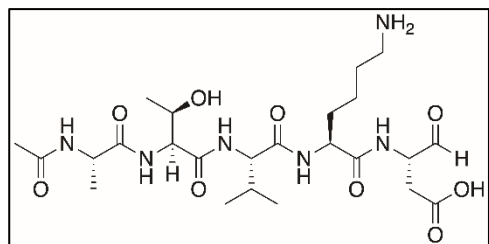## (S)-3-{(S)-2-[(S)-2-Acetamido-5-guanidinopentanamido]propanamido}-4-oxobutanoic acid hydrotrifluoroacetate (2.038)

The title compound was synthesized according to general procedure **B** yielding a fluffy white solid (9.6 mg, 10%): RP-HPLC: > 99%, (t_R = 3.74, k = 0.25). ^{1}H NMR (400 MHz, D_2O) δ 4.94 (dd, J = 4.5, 3.0 Hz, 1H), 4.28 – 4.05 (m, 3H), 3.10 (t, J = 6.8 Hz, 2H), 2.72 – 2.36 (m, 2H), 1.94 – 1.88 (m, 3H), 1.78 – 1.46 (m, 4H), 1.35 – 1.19 (m, 3H). ^{13}C NMR (101 MHz, D_2O) δ 175.34, 175.30, 174.66, 174.50, 174.42, 174.36, 173.56, 156.80, 89.72, 53.44, 53.33, 51.51, 49.77, 49.68, 40.57, 34.18, 28.22, 24.27, 21.65, 16.83, 16.67. HRMS (ESI-MS): m/z [M+H$^+$] calculated for $C_{15}H_{27}N_6O_6^+$: 387.1987, found 387.1985; $C_{15}H_{26}N_6O_6$ x $C_2HF_3O_2$ (500.43).

(4S,7S,10S,13S)-4-(Carboxymethyl)-13-formyl-10-(3-guanidinopropyl)-7-[(R)-1-hydroxyethyl]-2,5,8,11-tetraoxo-3,6,9,12-tetraazapentadecan-15-oic acid hydrotrifluoroacetate (2.039)

The title compound was synthesized according to general procedure **B** yielding a fluffy white solid (26.2 mg, 22%): RP-HPLC: > 99%, (t_R = 3.75, k = 0.25). ^{1}H NMR (400 MHz, D_2O) δ 4.92 (dd, J = 4.6, 2.3 Hz, 1H), 4.35 – 4.04 (m, 4H), 3.15 – 3.04 (m, 2H), 2.89 – 2.37 (m, 4H), 1.94 (s, 3H), 1.84 – 1.39 (m, 4H), 1.14 – 1.05 (m, 3H). ^{13}C NMR (101 MHz, D_2O) δ 175.24, 175.17, 174.40, 174.24, 173.21, 173.13, 173.05, 171.66, 171.57, 156.77, 89.71, 89.66, 66.89, 59.23, 59.13, 53.54, 53.48, 51.54, 51.51, 50.24, 40.50, 35.41, 34.21, 33.99, 28.33, 28.12, 24.35, 24.31, 21.76, 18.78. HRMS (ESI-MS): m/z [M+H^{+}] calculated for $C_{20}H_{34}N_7O_{10}^+$: 532.2362, found 532.2366; $C_{20}H_{33}N_7O_{10}$ x $C_2HF_3O_2$ (645.55).

(S)-3-{(S)-2-[(2S,3R)-2-Acetamido-3-hydroxybutanamido]-5-guanidinopentanamido}-4-oxobutanoic acid hydrotrifluoroacetate (2.040)
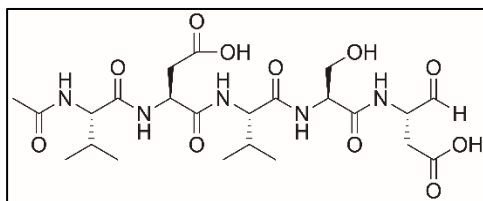

The title compound was synthesized according to general procedure **B** yielding a fluffy white solid (16.0 mg, 16%): RP-HPLC: > 99%, (t_R = 3.36, k = 0.22). ^{1}H NMR (400 MHz, D_2O) δ 4.98 – 4.90 (m, 1H), 4.32 – 4.21 (m, 1H), 4.19 – 4.00 (m, 2H), 3.17 – 3.02 (m, 2H), 2.73 – 2.34 (m, 2H), 2.05 – 1.88 (m, 3H), 1.83 – 1.43 (m, 4H), 1.32 – 1.04 (m, 3H). HRMS (ESI-MS): m/z [M+H^{+}] calculated for $C_{16}H_{29}N_6O_7^+$: 417.2092, found 417.2093; $C_{16}H_{28}N_6O_7$ x $C_2HF_3O_2$ (530.46).

(4S,7S,10S,13S)-4-(Carboxymethyl)-13-formyl-7-(3-guanidinopropyl)-10-[(R)-1-hydroxyethyl]-2,5,8,11-tetraoxo-3,6,9,12-tetraazapentadecan-15-oic acid hydrotrifluoroacetate (2.041)

The title compound was synthesized according to general procedure **B** yielding a fluffy white solid (17.4 mg, 14%): RP-HPLC: 97%, (t_R = 3.62, k = 0.21). ^{1}H NMR (300 MHz, D_2O) δ 4.90 (dd, J = 4.6, 1.6 Hz, 1H), 4.53 (t, J = 6.2 Hz, 1H), 4.36 – 3.93 (m, 4H), 3.06

(t, J = 6.9 Hz, 2H), 2.84 – 2.35 (m, 4H), 1.87 (s, 3H), 1.82 – 1.38 (m, 5H), 1.11 – 0.97 (m, 3H). HRMS (ESI-MS): m/z [M+H$^+$] calculated for $C_{20}H_{34}N_7O_{10}^+$: 532.2362, found 532.2364; $C_{20}H_{33}N_7O_{10}$ x $C_2HF_3O_2$ (645.55).

(S)-3-{(2S,3R)-2-[(S)-2-Acetamido-5-guanidinopentanamido]-3-hydroxybutanamido}-4-oxobutanoic acid hydrotrifluoroacetate (2.042)
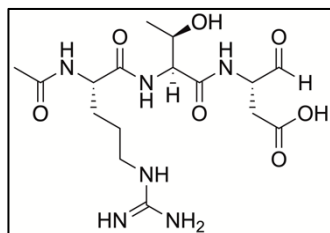
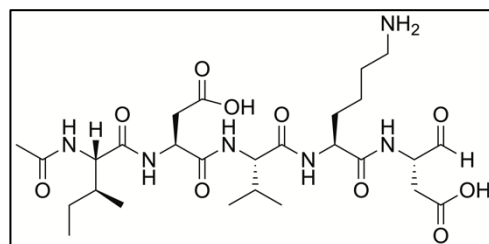

The title compound was synthesized according to general procedure **B** yielding a fluffy white solid (5.3 mg, 5%): RP-HPLC: > 99%, (t_R = 3.60, k = 0.20). ^{1}H NMR (400 MHz, D_2O) δ 4.97 – 4.91 (m, 1H), 4.30 – 4.01 (m, 4H), 3.11 (t, J = 6.8 Hz, 2H), 2.73 – 2.39 (m, 2H), 1.93 (s, 3H), 1.77 – 1.61 (m, 2H), 1.60 – 1.48 (m, 2H), 1.16 – 1.01 (m, 3H). HRMS (ESI-MS): m/z [M+H$^+$] calculated for $C_{16}H_{29}N_6O_7^+$: 417.2092, found 417.2096; $C_{16}H_{28}N_6O_7$ x $C_2HF_3O_2$ (530.46).

(S)-3-Acetamido-4-{[(S)-1-((S)-2-{[(S)-1-carboxy-3-oxopropan-2-yl]carbamoyl}pyrrolidin-1-yl)-3-methyl-1-oxobutan-2-yl]amino}-4-oxobutanoic acid (2.043)
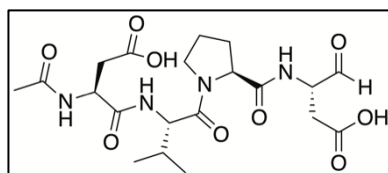
The title compound was synthesized according to general procedure **A** yielding a fluffy white solid (41.7 mg, 47%): RP-HPLC: 99%, (t_R = 6.17, k = 1.06). ^{1}H NMR (400 MHz, D_2O) δ 5.01 – 4.89 (m, 1H), 4.61 – 4.55 (m, 1H), 4.37 – 4.31 (m, 1H), 4.30 – 4.19 (m, 1H), 4.18 – 4.04 (m, 1H), 3.83 – 3.29 (m, 2H), 2.87 – 2.34 (m, 4H), 2.28 – 2.06 (m, 1H), 2.05 – 1.69 (m, 7H), 0.90 – 0.73 (m, 6H). ^{13}C NMR (101 MHz, D_2O) δ 175.36, 175.24, 174.18, 173.96, 173.79, 172.38, 171.84, 171.77, 171.69, 89.65, 60.83, 60.80, 57.08, 57.01, 51.55, 51.43, 50.12, 48.34, 35.39, 34.08, 33.92, 30.08, 30.03, 29.69, 29.52, 24.68, 24.56, 21.69, 18.42, 18.35, 17.30, 17.28. HRMS (ESI-MS): m/z [M+H$^+$] calculated for $C_{20}H_{31}N_4O_9^+$: 471.2086, found 471.2093; $C_{20}H_{30}N_4O_9$ (470.48).

(S)-3-[(S)-1-(Acetyl-L-valyl)pyrrolidine-2-carboxamido]-4-oxobutanoic acid (2.044)

The title compound was synthesized according to general procedure **A** yielding a fluffy white solid (26.2 mg, 39%): RP-HPLC: > 99%, (t_R = 6.66, k = 1.22). ^{1}H NMR (400 MHz, D$_2$O) δ 4.98 − 4.92 (m, 1H), 4.35 − 4.19 (m, 2H), 4.17 − 4.03 (m, 1H), 3.85 − 3.72 (m, 1H), 3.64 − 3.34 (m, 1H), 2.71 − 2.34 (m, 2H), 2.24 − 2.08 (m, 1H), 2.04 − 1.68 (m, 7H), 0.94 − 0.75 (m, 6H). ^{13}C NMR (101 MHz, D$_2$O) δ 175.37, 175.26, 174.21, 173.87, 172.51, 172.44, 172.36, 89.65, 60.86, 60.82, 57.30, 57.24, 51.56, 51.43, 48.31, 34.10, 33.92, 29.76, 29.69, 29.65, 29.48, 24.75, 24.61, 21.51, 18.35, 18.28, 17.36. HRMS (ESI-MS): m/z [M+H$^+$] calculated for C$_{16}$H$_{26}$N$_3$O$_5^+$: 356.1816, found 356.1821; C$_{16}$H$_{25}$N$_3$O$_5$ (355.39).

(4S,7S,10S,13S)-10-(4-Aminobutyl)-13-formyl-4-[(R)-1-hydroxyethyl]-7-isopropyl-2,5,8,11-tetraoxo-3,6,9,12-tetraazapentadecan-15-oic acid hydrotrifluoroacetate (2.045)
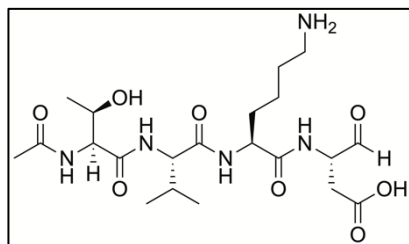
The title compound was synthesized according to general procedure **B** yielding a fluffy white solid (18.8 mg, 25%): RP-HPLC: > 99%, (t_R = 3.45, k = 0.15). ^{1}H NMR (300 MHz, D$_2$O) δ 4.89 (dd, J = 4.6, 2.0 Hz, 1H), 4.21 − 3.91 (m, 5H), 2.83 (t, J = 7.6 Hz, 2H), 2.72 − 2.33 (m, 2H), 2.00 − 1.81 (m, 4H), 1.73 − 1.47 (m, 4H), 1.38 − 1.17 (m, 2H), 1.05 (d, J = 6.4 Hz, 3H), 0.79 (t, J = 6.5 Hz, 6H). HRMS (ESI-MS): m/z [M+H$^+$] calculated for C$_{21}$H$_{38}$N$_5$O$_8^+$: 488.2715, found 488.2724; C$_{21}$H$_{37}$N$_5$O$_8$ x C$_2$HF$_3$O$_2$ (601.58).

(S)-3-{(S)-2-[(S)-2-Acetamido-3-methylbutanamido]-6-aminohexanamido}-4-oxobutanoic acid hydrotrifluoroacetate (2.046)

The title compound was synthesized according to general procedure **B** yielding a fluffy white solid (20.0 mg, 32%): RP-HPLC: > 99%, (t_R = 3.50, k = 0.17). ^{1}H NMR (300 MHz, D$_2$O) δ 4.88 (dd, J = 4.6, 2.3 Hz, 1H), 4.25 − 3.82 (m, 3H), 2.83 (t, J = 7.6 Hz, 2H), 2.70 − 2.30 (m, 2H), 1.96 − 1.80 (m, 4H), 1.75 − 1.46 (m, 4H), 1.39 − 1.15 (m, 2H), 0.80 (t, J = 5.5 Hz, 6H). ^{13}C NMR (75 MHz, D$_2$O) δ 206.60, 175.42, 174.44, 173.77, 173.27, 173.16, 89.66, 59.77, 53.50, 51.51, 39.17,

34.28, 30.51, 29.91, 26.19, 21.96, 21.56, 18.33, 17.75. HRMS (ESI-MS): *m/z* [M+H$^+$] calculated for $C_{17}H_{31}N_4O_6^+$: 387.2238, found 387.2243; $C_{17}H_{30}N_4O_6$ x $C_2HF_3O_2$ (500.47).

(4*S*,7*S*,10*S*,13*S*)-4-(Carboxymethyl)-13-formyl-7-isopropyl-10-methyl-2,5,8,11-tetraoxo-3,6,9,12-tetraazapentadecan-15-oic acid (2.047)

The title compound was synthesized according to general procedure **A** yielding a fluffy white solid (45.5 mg, 55%): RP-HPLC: > 99%, (t$_R$ = 5.36, *k* = 0.79). ^{1}H NMR (400 MHz, D$_2$O) δ 4.93 (dd, *J* = 4.5, 3.0 Hz, 1H), 4.61 (t, *J* = 6.8 Hz, 1H), 4.27 – 4.07 (m, 2H), 4.11 – 3.94 (m, 1H), 2.87 – 2.35 (m, 4H), 2.05 – 1.92 (m, 1H), 1.91 (s, 3H), 1.32 – 1.19 (m, 3H), 0.87 – 0.75 (m, 6H). ^{13}C NMR (101 MHz, D$_2$O) δ 175.27, 175.15, 174.97, 174.56, 174.40, 174.18, 174.08, 172.89, 172.80, 172.70, 89.69, 59.48, 59.30, 51.46, 50.13, 49.79, 35.32, 34.06, 33.89, 30.23, 30.13, 21.69, 18.42, 18.36, 17.43, 16.82, 16.70. HRMS (ESI-MS): *m/z* [M+H$^+$] calculated for $C_{18}H_{29}N_4O_9^+$: 445.1929, found 445.1933; $C_{18}H_{28}N_4O_9$ (444.44).

(*S*)-3-{(*S*)-2-[(*S*)-2-Acetamido-3-methylbutanamido]propanamido}-4-oxobutanoic acid (2.048)
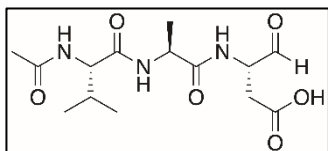
The title compound was synthesized according to general procedure **A** yielding a fluffy white solid (35.8 mg, 58%): RP-HPLC: > 99%, (t$_R$ = 5.37, *k* = 0.79). ^{1}H NMR (400 MHz, D$_2$O) δ 4.93 (dd, *J* = 4.6, 2.2 Hz, 1H), 4.30 – 4.05 (m, 2H), 4.00 – 3.93 (m, 1H), 2.71 – 2.37 (m, 2H), 2.02 – 1.88 (m, 4H), 1.33 – 1.21 (m, 3H), 0.83 (dd, *J* = 6.8, 3.0 Hz, 6H). ^{13}C NMR (101 MHz, D$_2$O) δ 175.28, 175.18, 174.59, 174.52, 174.42, 173.65, 173.49, 89.70, 89.67, 59.67, 59.52, 51.48, 51.45, 49.74, 49.65, 34.09, 33.95, 30.08, 30.02, 21.66, 18.38, 17.53, 16.85, 16.73. HRMS (ESI-MS): *m/z* [M+H$^+$] calculated for $C_{14}H_{24}N_3O_6^+$: 330.1660, found 330.1666; $C_{14}H_{23}N_3O_6$ (329.35).

(4*S*,7*S*,13*S*,16*S*)-13-(4-Aminobutyl)-4-[(*S*)-*sec*-butyl]-16-formyl-7-[(*R*)-1-hydroxyethyl]-2,5,8,11,14-pentaoxo-3,6,9,12,15-pentaazaoctadecan-18-oic acid hydrotrifluoroacetate (2.049)
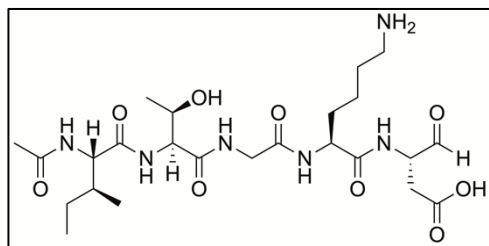
The title compound was synthesized according to general procedure **B** yielding a fluffy white solid (25.4 mg, 30%): RP-HPLC: 98%, (t_R = 5.81, k = 0.94). ^{1}H NMR (300 MHz, D_2O) δ 4.86 (d, J = 4.2 Hz, 1H), 4.44 – 3.99 (m, 5H), 3.90 – 3.72 (m, 2H), 2.83 (t, J = 7.4 Hz, 2H), 2.47 – 2.16 (m, 1H), 1.89 (s, 3H), 1.78 – 1.17 (m, 9H), 1.07 (d, J = 6.4 Hz, 4H), 0.80 – 0.68 (m, 6H). ^{13}C NMR (75 MHz, D_2O) δ 206.60, 174.62, 174.40, 173.18, 172.39, 172.30, 170.80, 170.34, 90.02, 67.08, 59.17, 58.73, 58.48, 53.58, 52.39, 42.57, 42.40, 39.19, 36.02, 30.84, 26.25, 24.58, 21.81, 21.66, 18.71, 14.86, 10.31. HRMS (ESI-MS): *m/z* [M+H$^+$] calculated for $C_{24}H_{43}N_6O_9^+$: 559.3086, found 559.3088; $C_{24}H_{42}N_6O_9$ x $C_2HF_3O_2$ (672.66).

(4*S*,10*S*,13*S*)-10-(4-Aminobutyl)-13-formyl-4-[(*R*)-1-hydroxyethyl]-2,5,8,11-tetraoxo-3,6,9,12-tetraazapentadecan-15-oic acid (2.050)
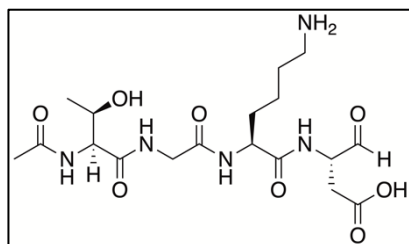
The title compound was synthesized according to general procedure **B** yielding a fluffy white solid (27.5 mg, 39%): RP-HPLC: > 99%, (t_R = 3.08, k = 0.12). ^{1}H NMR (300 MHz, D_2O) δ 4.92 – 4.85 (m, 1H), 4.31 – 4.02 (m, 4H), 3.89 – 3.72 (m, 2H), 2.83 (t, J = 7.5 Hz, 2H), 2.73 – 2.29 (m, 2H), 1.95 (s, 3H), 1.73 – 1.47 (m, 4H), 1.32 – 1.04 (m, 5H). HRMS (ESI-MS): *m/z* [M+H$^+$] calculated for $C_{18}H_{32}N_5O_8^+$: 446.2245, found 446.2251; $C_{18}H_{31}N_5O_8$ x $C_2HF_3O_2$ (559.50).

## (*S*)-3-{(*S*)-2-[2-Acetamidoacetamido]-6-aminohexanamido}-4-oxobutanoic acid hydrotrifluoroacetate (2.051)

The title compound was synthesized according to general procedure **B** yielding a fluffy white solid (35.1 mg, 41%): RP-HPLC: > 99%, (t_R = 2.58, k = -0.14). ^{1}H NMR (400 MHz, D_2O) δ 4.92 (t, J = 4.6 Hz, 1H), 4.35 – 4.01 (m, 2H), 3.89 – 3.71 (m, 2H), 2.91 – 2.81 (m, 2H), 2.74 – 2.56 (m, 1H), 2.54 – 2.30 (m, 1H), 1.93 (s, 3H), 1.88 – 1.47 (m, 4H), 1.44 – 1.17 (m, 2H). ^{13}C NMR (101 MHz,

D_2O) δ 175.51, 175.25, 175.23, 175.01, 174.92, 173.60, 171.68, 89.67, 53.61, 53.57, 52.33, 51.57, 51.52, 42.55, 42.46, 39.22, 34.22, 33.99, 29.97, 26.22, 26.13, 22.02, 21.69. HRMS (ESI-MS): *m/z* [M+H⁺] calculated for $C_{14}H_{25}N_4O_6^+$: 345.1769, found 345.1769; $C_{14}H_{24}N_4O_6$ x $C_2HF_3O_2$ (458.39).

(4*S*,7*S*,10*S*,13*S*,16*S*)-13-(4-Aminobutyl)-4-[(*S*)-*sec*-butyl]-16-formyl-7-[(*R*)-1-hydroxyethyl]-10-methyl-2,5,8,11,14-pentaoxo-3,6,9,12,15-pentaazaoctadecan-18-oic acid hydrotrifluoroacetate (2.052)
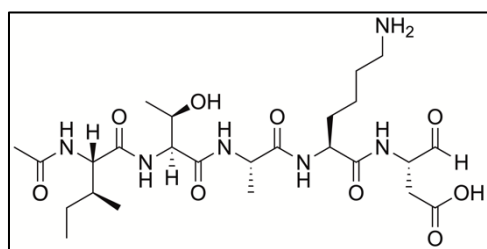
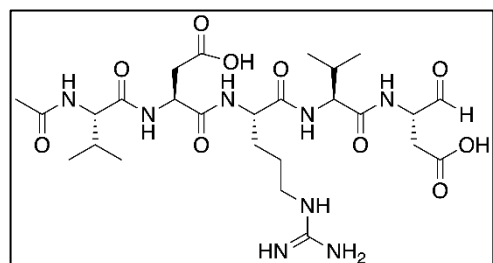

The title compound was synthesized according to general procedure **B** yielding a fluffy white solid (26.9 mg, 31%): RP-HPLC: 96%, (t_R = 5.98, *k* = 0.99). ¹H NMR (300 MHz, D_2O) δ 4.90 – 4.81 (m, 1H), 4.32 – 3.83 (m, 6H), 2.84 (t, *J* = 7.4 Hz, 2H), 2.73 – 1.98 (m, 2H), 1.88 (s, 3H), 1.75 – 1.45 (m, 5H), 1.37 – 1.21 (m, 5H), 1.05 (d, *J* = 6.4 Hz, 4H), 0.80 – 0.66 (m, 6H). ¹³C NMR (75 MHz, D_2O) δ 206.60, 178.81, 174.71, 174.51, 174.37, 174.31, 173.24, 173.13, 171.48, 171.29, 90.08, 67.26, 67.11, 58.83, 58.72, 53.84, 53.70, 52.48, 49.76, 49.57, 39.18, 36.08, 30.75, 30.49, 26.27, 24.62, 21.83, 21.64, 18.81, 16.56, 14.84, 10.27. HRMS (ESI-MS): *m/z* [M+H⁺] calculated for $C_{25}H_{45}N_6O_9^+$: 573.3243, found 573.3246; $C_{25}H_{44}N_6O_9$ x $C_2HF_3O_2$ (686.68).

(4*S*,7*S*,10*S*,13*S*)-10-(4-Aminobutyl)-13-formyl-4-[(*R*)-1-hydroxyethyl]-7-methyl-2,5,8,11-tetraoxo-3,6,9,12-tetraazapentadecan-15-oic acid hydrotrifluoroacetate (2.053)
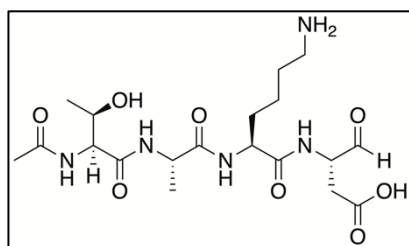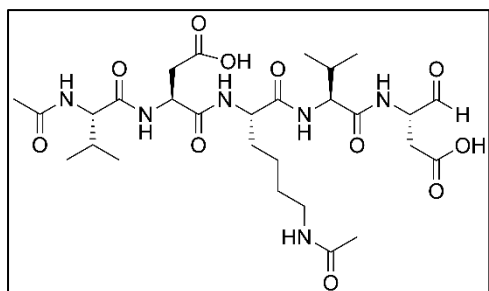

The title compound was synthesized according to general procedure **B** yielding a fluffy white solid (17.6 mg, 24%): RP-HPLC: > 99%, (t_R = 3.09, *k* = 0.11). ¹H NMR (300 MHz, D_2O) δ 4.88 (dd, *J* = 4.6, 1.9 Hz, 1H), 4.33 – 3.94 (m, 5H), 2.83 (t, *J* = 7.5 Hz, 2H), 2.73 – 2.25 (m, 2H), 2.01 – 1.88 (m, 3H), 1.75 – 1.45 (m, 4H), 1.36 – 1.03 (m, 8H). HRMS (ESI-MS): *m/z* [M+H⁺] calculated for $C_{19}H_{34}N_5O_8^+$: 460.2402, found 460.2408; $C_{19}H_{33}N_5O_8$ x $C_2HF_3O_2$ (573.52).

(*S*)-3-{(*S*)-2-[(*S*)-2-Acetamidopropanamido]-6-aminohexanamido}-4-oxobutanoic acid hydrotrifluoroacetate (2.054)

The title compound was synthesized according to general procedure **B** yielding a fluffy white solid (46.2 mg, 52%): RP-HPLC: > 99%, (t_R = 3.25, k = 0.19). ^{1}H NMR (400 MHz, D$_2$O) δ 4.92 (dd, J = 4.6, 2.5 Hz, 1H), 4.33 – 4.02 (m, 3H), 2.87 (t, J = 6.0 Hz, 2H), 2.73 – 2.58 (m, 1H), 2.51 – 2.33 (m, 1H), 1.89 (s, 3H), 1.86 – 1.48 (m, 4H), 1.43 – 1.18 (m, 5H). ^{13}C NMR (101 MHz, D$_2$O) δ 175.51, 175.44, 175.36, 175.25, 175.16, 174.22, 174.09, 173.52, 173.45, 89.65, 53.50, 52.27, 51.49, 49.79, 49.72, 39.23, 34.14, 33.95, 29.95, 26.20, 26.11, 22.01, 21.54, 16.45. HRMS (ESI-MS): *m/z* [M+H$^+$] calculated for C$_{15}$H$_{27}$N$_4$O$_6$$^+$: 359.1925, found 359.1929; C$_{15}$H$_{26}$N$_4$O$_6$ x C$_2$HF$_3$O$_2$ (472.42).

(4*S*,7*S*,10*S*,13*S*,16*S*)-13-(4-Aminobutyl)-16-formyl-7-[(*R*)-1-hydroxyethyl]-10-isopropyl-4-methyl-2,5,8,11,14-pentaoxo-3,6,9,12,15-pentaazaoctadecan-18-oic acid hydrotrifluoroacetate (2.055)

The title compound was synthesized according to general procedure **A** yielding a fluffy white solid (35.8 mg, 28%): RP-HPLC: > 99%, (t_R = 3.98, k = 0.33). ^{1}H NMR (400 MHz, D$_2$O) δ 4.93 (dd, J = 4.6, 2.3 Hz, 1H), 4.33 – 3.90 (m, 6H), 2.87 (t, J = 7.6 Hz, 2H), 2.75 – 2.35 (m, 2H), 2.01 – 1.86 (m, 4H), 1.79 – 1.46 (m, 4H), 1.33 – 1.18 (m, 5H), 1.08 (d, J = 6.4 Hz, 3H), 0.82 (t, J = 6.3 Hz, 6H). ^{13}C NMR (101 MHz, D$_2$O) δ 175.73, 175.27, 175.08, 174.28, 173.73, 173.23, 173.13, 173.02, 171.87, 171.81, 89.70, 67.11, 59.63, 59.49, 58.98, 53.63, 53.54, 51.51, 49.92, 49.89, 39.20, 34.19, 33.89, 30.63, 30.57, 30.17, 30.11, 26.24, 22.00, 21.96, 21.61, 18.86, 18.41, 18.36, 17.85, 17.81, 16.55. HRMS (ESI-MS): *m/z* [M+H$^+$] calculated for C$_{24}$H$_{43}$N$_6$O$_9$$^+$: 559.3086, found 559.3093; C$_{24}$H$_{42}$N$_6$O$_9$ x C$_2$HF$_3$O$_2$ (672.66).

(4S,7S,10S,13S,16S)-4-[(S)-sec-Butyl]-16-formyl-7-[(R)-1-hydroxyethyl]-13-(hydroxymethyl)-10-isopropyl-2,5,8,11,14-pentaoxo-3,6,9,12,15-pentaazaoctadecan-18-oic acid (2.056)
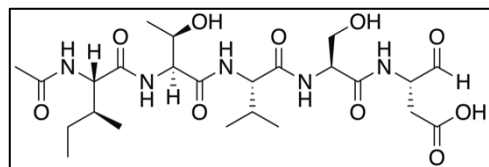
The title compound was synthesized according to general procedure **A** yielding a fluffy white solid (36.7 mg, 36%): RP-HPLC: 99%, (t_R = 8.30, k = 1.77). ^{1}H NMR (400 MHz, D_2O) δ 4.95 (d, J = 4.4 Hz, 1H), 4.41 – 4.23 (m, 2H), 4.22 – 3.98 (m, 4H), 3.81 – 3.62 (m, 2H), 2.73 – 2.35 (m, 2H), 2.07 – 1.85 (m, 4H), 1.81 – 1.67 (m, 2H), 1.47 – 1.27 (m, 1H), 1.19 – 0.99 (m, 4H), 0.88 – 0.69 (m, 12H). HRMS (ESI-MS): m/z [M+H$^+$] calculated for $C_{24}H_{42}N_5O_{10}^+$: 560.2926, found 560.2932; $C_{24}H_{41}N_5O_{10}$ (559.62).

(4S,7S,10S,13S,16S)-7-(Carboxymethyl)-16-formyl-13-(hydroxymethyl)-4,10-diisopropyl-2,5,8,11,14-pentaoxo-3,6,9,12,15-pentaazaoctadecan-18-oic acid (2.057)

The title compound was synthesized according to general procedure **A** yielding a fluffy white solid (45.2 mg, 43%): RP-HPLC: > 99%, (t_R = 7.17, k = 1.39). ^{1}H NMR (400 MHz, D_2O) δ 4.94 (d, J = 4.5 Hz, 1H), 4.65 – 4.64 (m, 1H), 4.39 – 4.28 (m, 1H), 4.19 – 3.89 (m, 3H), 3.87 – 3.64 (m, 2H), 3.07 – 2.38 (m, 4H), 2.11 – 1.87 (m, 5H), 0.90 – 0.76 (m, 12H). ^{13}C NMR (101 MHz, D_2O) δ 175.25, 175.17, 174.51, 174.18, 173.62, 173.36, 173.32, 172.35, 172.31, 171.18, 171.10, 89.65, 61.18, 61.09, 59.78, 59.66, 55.81, 55.62, 51.59, 50.08, 35.19, 34.09, 33.95, 29.94, 21.65, 18.45, 18.34, 17.61, 17.44. HRMS (ESI-MS): m/z [M+H$^+$] calculated for $C_{23}H_{38}N_5O_{11}^+$: 560.2562, found 560.2572; $C_{23}H_{37}N_5O_{11}$ (559.57).

(4S,7S,10S,13S,16S)-13-(4-Aminobutyl)-4-((S)-sec-butyl)-7-(carboxymethyl)-16-formyl-10-isopropyl-2,5,8,11,14-pentaoxo-3,6,9,12,15-pentaazaoctadecan-18-oic acid hydrotrifluoroacetate (2.058)

The title compound was synthesized according to general procedure **B** yielding a fluffy white solid (22 mg, 16%): RP-HPLC: 95%, (t_R = 7.05, k = 1.35). ^{1}H NMR (400 MHz, D_2O) δ 4.94 – 4.91 (m, 1H), 4.67 – 4.60 (m, 1H), 4.37 – 4.08 (m, 2H), 4.05

– 3.90 (m, 2H), 2.92 – 2.81 (m, 3H), 2.78 – 2.38 (m, 3H), 1.92 (s, 4H), 1.78 – 1.49 (m, 5H), 1.43 – 1.21 (m, 3H), 1.16 – 1.00 (m, 1H), 0.90 – 0.71 (m, 12H). ^{13}C NMR (101 MHz, D$_2$O) δ 175.30, 175.12, 174.53, 174.51, 174.17, 174.15, 173.80, 173.69, 173.29, 173.22, 173.15, 173.13, 172.16, 172.06, 89.70, 59.81, 58.75, 53.59, 51.50, 50.04, 39.22, 36.10, 35.17, 34.19, 33.90, 30.56, 30.44, 29.93, 26.20, 24.62, 22.01, 21.97, 21.65, 18.46, 18.41, 17.70, 14.75, 10.34. HRMS (ESI-MS): *m/z* [M+H$^+$] calculated for C$_{27}$H$_{47}$N$_6$O$_{10}$$^+$: 615.3348, found 615.3360; C$_{27}$H$_{46}$N$_6$O$_{10}$ x C$_2$HF$_3$O$_2$ (728.72).

(4*S*,7*S*,10*S*,13*S*,16*S*)-10-(4-Aminobutyl)-7-(carboxymethyl)-16-formyl-4,13-diisopropyl-2,5,8,11,14-pentaoxo-3,6,9,12,15-pentaazaoctadecan-18-oic acid hydrotrifluoroacetate (2.059) *(Synthesized by Steffen Pockes)*

The title compound was synthesized according to general procedure **A** yielding a fluffy white solid (45.1 mg, 20%): RP-HPLC: 99%, (t$_R$ = 6.53, *k* = 1.18). ^{1}H NMR (400 MHz, D$_2$O) δ 4.91 (dd, *J* = 6.0, 4.7 Hz, 1H), 4.62 – 4.58 (m, 1H), 4.26 – 4.08 (m, 2H), 3.99 – 3.89 (m, 2H), 2.92 – 2.79 (m, 3H), 2.76 – 2.63 (m, 2H), 2.51 – 2.35 (m, 1H), 2.00 – 1.86 (m, 5H), 1.77 – 1.49 (m, 4H), 1.39 – 1.16 (m, 2H), 0.80 (dt, *J* = 9.5, 5.4 Hz, 12H). ^{13}C NMR (101 MHz, D$_2$O) δ 175.23, 175.13, 174.62, 173.95, 173.72, 173.59, 173.44, 173.36, 173.30, 172.98, 172.87, 172.02, 171.96, 89.70, 59.95, 59.92, 59.76, 53.56, 53.50, 51.58, 51.50, 50.07, 39.19, 35.14, 34.08, 33.91, 30.38, 30.15, 30.10, 29.84, 26.24, 21.93, 21.68, 18.30, 17.61. HRMS (ESI-MS): *m/z* [M+H$^+$] calculated for C$_{26}$H$_{45}$N$_6$O$_{10}$$^+$: 601.3192, found 601.3201; C$_{26}$H$_{44}$N$_6$O$_{10}$ x C$_2$HF$_3$O$_2$ (714.69).
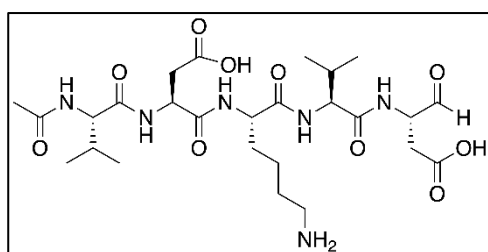
(4*S*,7*S*,10*S*,13*S*)-7-(4-Aminobutyl)-4-(carboxymethyl)-13-formyl-10-isopropyl-2,5,8,11-tetraoxo-3,6,9,12-tetraazapentadecan-15-oic acid hydrotrifluoroacetate (2.060)
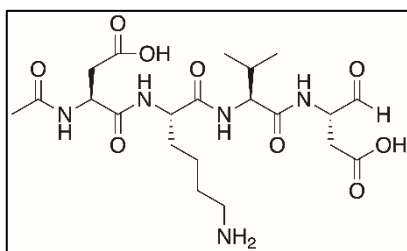
The title compound was synthesized according to general procedure **B** yielding a fluffy white solid (47.6 mg, 41%): RP-HPLC: > 99%, (t$_R$ = 3.67, *k* = 0.22). ^{1}H NMR (400 MHz, D$_2$O) δ 4.91 (dd, *J* = 6.4, 4.8 Hz, 1H), 4.55 (t, *J* = 6.8 Hz, 1H), 4.28 – 4.20 (m, 1H), 4.20 – 4.08 (m, 1H), 3.95 (d, *J* = 7.9 Hz, 1H), 2.87 (t, *J* = 7.6 Hz, 2H), 2.83 – 2.36 (m, 4H), 1.99 –

1.84 (m, 4H), 1.78 – 1.47 (m, 4H), 1.39 – 1.19 (m, 2H), 0.88 – 0.72 (m, 6H). ^{13}C NMR (101 MHz, D$_2$O) δ 175.25, 175.15, 174.22, 173.98, 173.66, 173.45, 173.38, 172.99, 172.88, 172.71, 172.68, 172.63, 172.57, 89.81, 89.69, 59.73, 53.50, 53.44, 51.58, 51.50, 50.21, 39.22, 35.41, 34.08, 33.92, 30.26, 30.15, 30.11, 26.21, 21.98, 21.93, 21.72, 18.39, 18.33, 18.29, 17.71, 17.65. HRMS (ESI-MS): *m/z* [M+H$^+$] calculated for C$_{21}$H$_{36}$N$_5$O$_9$$^+$: 502.2508, found 502.2514; C$_{21}$H$_{35}$N$_5$O$_9$ x C$_2$HF$_3$O$_2$ (615.56).

(4*S*,7*S*,10*S*,13*S*,16*S*)-13-(4-Aminobutyl)-7-(carboxymethyl)-16-formyl-4,10-diisopropyl-2,5,8,11,14-pentaoxo-3,6,9,12,15-pentaazaoctadecan-18-oic acid hydrotrifluoroacetate (2.061)
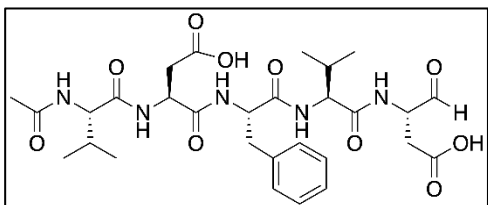

The title compound was synthesized according to general procedure **A** yielding a fluffy white solid (39.9 mg, 30%): RP-HPLC: 98%, (t$_R$ = 6.29, *k* = 1.10). ^{1}H NMR (400 MHz, D$_2$O) δ 4.94 – 4.90 (m, 1H), 4.65 – 4.61 (m, 1H), 4.31 – 4.02 (m, 2H), 4.00 – 3.89 (m, 2H), 2.91 – 2.79 (m, 3H), 2.74 – 2.56 (m, 2H), 2.51 – 2.34 (m, 1H), 2.02 – 1.88 (m, 5H), 1.77 – 1.49 (m, 4H), 1.39 – 1.22 (m, 2H), 0.87 – 0.76 (m, 12H). ^{13}C NMR (101 MHz, D$_2$O) δ 175.31, 175.13, 174.58, 174.19, 173.65, 173.29, 173.22, 173.14, 173.12, 172.20, 172.11, 89.70, 59.87, 59.65, 53.59, 51.50, 50.06, 39.22, 35.24, 30.45, 29.90, 26.20, 22.01, 21.65, 18.46, 18.40, 18.33, 17.70, 17.62. HRMS (ESI-MS): *m/z* [M+H$^+$] calculated for C$_{26}$H$_{45}$N$_6$O$_{10}$$^+$: 601.3192, found 601.3198; C$_{26}$H$_{44}$N$_6$O$_{10}$ x C$_2$HF$_3$O$_2$ (714.69).
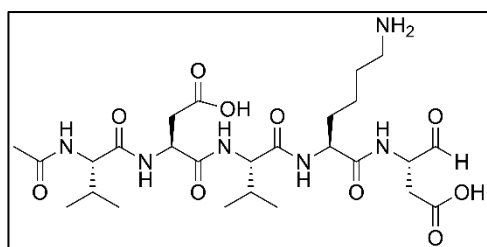
(4*S*,7*S*,10*S*,13*S*)-10-(4-Aminobutyl)-4-(carboxymethyl)-13-formyl-7-isopropyl-2,5,8,11-tetraoxo-3,6,9,12-tetraazapentadecan-15-oic acid hydrotrifluoroacetate (2.062)
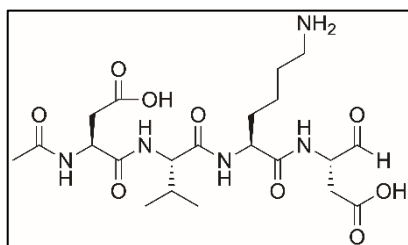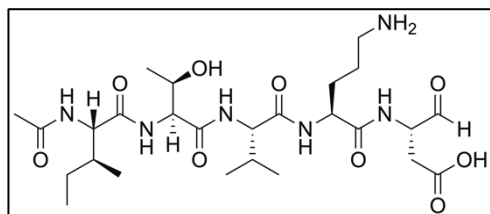

The title compound was synthesized according to general procedure **B** yielding a fluffy white solid (42.4 mg, 37%): RP-HPLC: > 99%, (t$_R$ = 3.77, *k* = 0.26). ^{1}H NMR (400 MHz, D$_2$O) δ 4.92 (dd, *J* = 4.6, 1.5 Hz, 1H), 4.59 (t, *J* = 6.4 Hz, 1H), 4.27 – 4.06 (m, 2H), 4.04 – 3.94 (m, 1H), 2.86 (t, *J* = 7.6 Hz, 2H), 2.85 – 2.35 (m, 4H), 2.02 – 1.85 (m, 4H), 1.77 – 1.48 (m, 4H), 1.40 – 1.18 (m, 2H), 0.86 – 0.75 (m, 6H). ^{13}C NMR (101 MHz, D$_2$O) δ 175.24, 175.07, 174.18, 174.06, 173.77, 173.38, 173.28, 173.18, 173.15, 172.71, 172.63,

89.69, 59.65, 59.51, 53.62, 53.56, 51.49, 50.15, 39.22, 35.33, 34.18, 33.88, 30.57, 30.45, 30.14, 30.07, 26.21, 26.18, 22.00, 21.95, 21.70, 18.43, 18.40, 17.62. HRMS (ESI-MS): *m/z* [M+H$^+$] calculated for $C_{21}H_{36}N_5O_9^+$: 502.2508, found 502.2513; $C_{21}H_{35}N_5O_9$ x $C_2HF_3O_2$ (615.56).

(4*S*,7*S*,10*S*,13*S*,16*S*)-10-(3-Aminopropyl)-7-(carboxymethyl)-16-formyl-4,13-diisopropyl-2,5,8,11,14-pentaoxo-3,6,9,12,15-pentaazaoctadecan-18-oic acid hydrotrifluoroacetate (2.063)
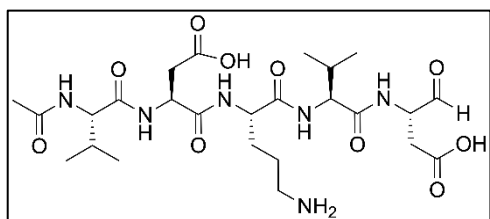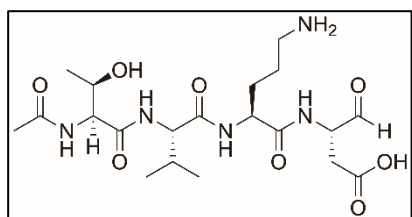

The title compound was synthesized according to general procedure **A** yielding a fluffy white solid (72.5 mg, 55%): RP-HPLC: > 99%, (t$_R$ = 5.91, *k* = 0.97). ^{1}H NMR (400 MHz, D$_2$O) δ 4.90 (dd, *J* = 4.7, 1.9 Hz, 1H), 4.62 – 4.55 (m, 1H), 4.30 – 4.06 (m, 2H), 4.00 – 3.86 (m, 2H), 2.95 – 2.36 (m, 6H), 1.98 – 1.84 (m, 5H), 1.79 – 1.48 (m, 4H), 0.84 – 0.74 (m, 12H). ^{13}C NMR (101 MHz, D$_2$O) δ 175.20, 175.13, 174.65, 173.85, 173.76, 173.41, 172.86, 172.69, 171.99, 89.70, 59.95, 59.78, 53.14, 53.05, 51.58, 51.45, 50.09, 38.86, 35.11, 34.09, 33.88, 30.08, 29.80, 27.90, 23.11, 21.66, 18.37, 18.28, 17.75, 17.57. HRMS (ESI-MS): *m/z* [M+H$^+$] calculated for $C_{25}H_{43}N_6O_{10}^+$: 587.3035, found 587.3042; $C_{25}H_{42}N_6O_{10}$ x $C_2HF_3O_2$ (700.67).

(4*S*,7*S*,10*S*,13*S*,16*S*)-10-(2-Aminoethyl)-7-(carboxymethyl)-16-formyl-4,13-diisopropyl-2,5,8,11,14-pentaoxo-3,6,9,12,15-pentaazaoctadecan-18-oic acid hydrotrifluoroacetate (2.064)
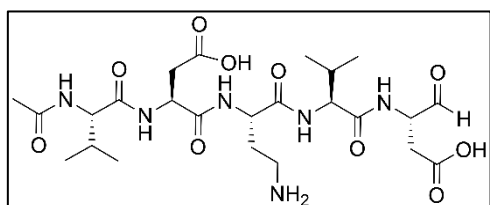
The title compound was synthesized according to general procedure **A** yielding a fluffy white solid (69.7mg, 54%): RP-HPLC: > 99%, (t$_R$ = 5.93, *k* = 0.98). ^{1}H NMR (400 MHz, D$_2$O) δ 4.91 (d, *J* = 4.9 Hz, 1H), 4.58 (t, *J* = 1.6 Hz, 1H), 4.40 – 4.09 (m, 2H), 3.99 – 3.88 (m, 2H), 2.96 – 2.37 (m, 6H), 2.12 – 2.01 (m, 1H), 2.00 – 1.87 (m, 6H), 0.86 – 0.75 (m, 12H). ^{13}C NMR (101 MHz, D$_2$O) δ 175.11, 174.70, 173.83, 173.39, 172.85, 172.27, 172.20, 171.96, 171.69, 89.70, 59.93, 51.60, 51.49, 51.13, 50.16, 36.18, 35.10, 33.92, 30.01, 29.79, 28.74, 21.67, 18.37, 18.30, 17.74, 17.54. HRMS (ESI-MS): *m/z* [M+H$^+$] calculated for $C_{24}H_{41}N_6O_{10}^+$: 573.2879, found 573.2886; $C_{24}H_{40}N_6O_{10}$ x $C_2HF_3O_2$ (686.64).

(4*S*,7*S*,10*S*,13*S*,16*S*)-10-(Aminomethyl)-7-(carboxymethyl)-16-formyl-4,13-diisopropyl-2,5,8,11,14-pentaoxo-3,6,9,12,15-pentaazaoctadecan-18-oic acid hydrotrifluoroacetate (2.065)
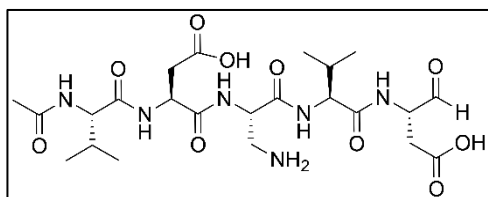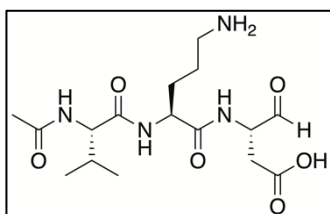

The title compound was synthesized according to general procedure **B** yielding a fluffy white solid (52.3 mg, 41%): RP-HPLC: 95%, (t_R = 6.12, k = 1.04). ^{1}H NMR (400 MHz, D$_2$O) δ 4.93 (d, *J* = 4.7 Hz, 1H), 4.65 – 4.55 (m, 2H), 4.23 – 4.10 (m, 1H), 4.04 – 3.90 (m, 2H), 3.44 – 3.14 (m, 2H), 2.94 – 2.59 (m, 4H), 2.02 – 1.90 (m, 5H), 0.87 – 0.76 (m, 12H). ^{13}C NMR (101 MHz, D$_2$O) δ 175.21, 174.90, 174.10, 173.95, 172.88, 172.83, 172.49, 169.50, 169.45, 89.76, 89.68, 60.06, 59.90, 51.64, 51.54, 50.70, 50.38, 39.81, 35.11, 34.12, 33.96, 29.71, 21.69, 18.37, 18.29, 17.73, 17.55. HRMS (ESI-MS): *m/z* [M+H$^+$] calculated for C$_{23}$H$_{39}$N$_6$O$_{10}^+$: 559.2722, found 559.2732; C$_{23}$H$_{38}$N$_6$O$_{10}$ x C$_2$HF$_3$O$_2$ (672.61).

(4*S*,7*S*,10*S*,13*S*,16*S*)-7-(Carboxymethyl)-16-formyl-10-(3-guanidinopropyl)-4,13-diisopropyl-2,5,8,11,14-pentaoxo-3,6,9,12,15-pentaazaoctadecan-18-oic acid hydrotrifluoroacetate (2.066) *(Synthesized by Steffen Pockes)*

The title compound was synthesized according to general procedure **A** yielding a fluffy white solid (4.0 mg, 2%): RP-HPLC: 96%, (t_R = 6.71, k = 1.90). ^{1}H NMR (400 MHz, CD$_3$OD) δ 4.68 – 4.60 (m, 1H), 4.58 – 4.51 (m, 1H), 4.42 – 4.34 (m, 1H), 4.33 – 4.24 (m, 1H), 4.17 – 4.09 (m, 1H), 4.09 – 4.02 (m, 1H), 3.22 – 3.12 (m, 2H), 2.95 – 2.87 (m, 1H), 2.84 – 2.76 (m, 1H), 2.73 – 2.62 (m, 1H), 2.53 – 2.44 (m, 1H), 2.23 – 2.02 (m, 2H), 2.01 (d, *J* = 1.3 Hz, 3H), 1.96 – 1.82 (m, 1H), 1.82 – 1.68 (m, 1H), 1.62 (p, *J* = 6.9 Hz, 2H), 1.01 – 0.89 (m, 12H). HRMS (ESI-MS): *m/z* [M+H$^+$] calculated for C$_{26}$H$_{45}$N$_8$O$_{10}^+$: 629.3253, found 629.3262; C$_{26}$H$_{44}$N$_8$O$_{10}$ x C$_2$HF$_3$O$_2$ (742.71).

(4*S*,7*S*,10*S*,13*S*,16*S*)-10-(4-Acetamidobutyl)-7-(carboxymethyl)-16-formyl-4,13-diisopropyl-2,5,8,11,14-pentaoxo-3,6,9,12,15-pentaazaoctadecan-18-oic acid (2.067)

The title compound was synthesized according to general procedure **B** yielding a fluffy white solid (72.9 mg, 60%): RP-HPLC: 99%, (t_R = 7.38, k = 1.46). ^{1}H NMR (400 MHz, D_2O) δ 4.93 – 4.87 (m, 1H), 4.60 (t, J = 2.0 Hz, 1H), 4.24 – 4.03 (m, 2H), 3.93 (dd, J = 11.8, 7.4 Hz, 2H), 3.02 (t, J = 6.9 Hz, 2H), 2.91 – 2.35 (m, 4H), 2.01 – 1.85 (m, 5H), 1.85 (s, 3H), 1.75 – 1.51 (m, 2H), 1.38 (p, J = 7.3 Hz, 2H), 1.32 – 1.09 (m, 2H), 0.85 – 0.73 (m, 12H). ^{13}C NMR (101 MHz, D_2O) δ 175.09, 174.56, 173.95, 173.91, 173.80, 173.59, 173.56, 173.36, 172.81, 172.03, 89.68, 59.90, 59.74, 53.83, 51.50, 50.02, 39.24, 35.10, 33.89, 30.53, 30.06, 29.91, 27.67, 22.40, 21.83, 21.67, 18.40, 18.31, 17.70, 17.65. HRMS (ESI-MS): *m/z* [M+H$^+$] calculated for $C_{28}H_{47}N_6O_{11}^+$: 643.3297, found 643.3312; $C_{28}H_{46}N_6O_{11}$ (642.71).

(4*S*,7*S*,10*S*,13*S*,16*S*)-13-(3-Aminopropyl)-7-(carboxymethyl)-16-formyl-4,10-diisopropyl-2,5,8,11,14-pentaoxo-3,6,9,12,15-pentaazaoctadecan-18-oic acid hydrotrifluoroacetate (2.068)
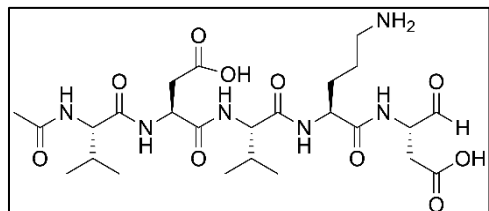
The title compound was synthesized according to general procedure **A** yielding a fluffy white solid (60.9 mg, 46%): RP-HPLC: > 99%, (t_R = 6.19, $k$ = 1.06). ^{1}H NMR (400 MHz, D_2O) δ 4.92 (dd, J = 4.6, 2.2 Hz, 1H), 4.67 – 4.59 (m, 1H), 4.30 – 4.19 (m, 1H), 4.16 – 4.09 (m, 1H), 4.00 – 3.90 (m, 2H), 3.02 – 2.80 (m, 3H), 2.76 – 2.53 (m, 2H), 2.47 – 2.37 (m, 1H), 2.03 – 1.87 (m, 5H), 1.81 – 1.50 (m, 4H), 0.86 – 0.77 (m, 12H). ^{13}C NMR (101 MHz, D_2O) δ 175.30, 175.07, 174.55, 174.19, 173.64, 173.37, 173.15, 172.78, 172.69, 172.21, 172.14, 89.70, 89.64, 59.85, 59.79, 59.69, 53.20, 51.52, 51.51, 51.50, 50.04, 38.89, 35.20, 34.23, 33.90, 29.91, 28.16, 28.05, 23.27, 23.20, 21.67, 18.46, 18.41, 18.33, 17.73, 17.63. HRMS (ESI-MS): *m/z* [M+H$^+$] calculated for $C_{25}H_{43}N_6O_{10}^+$: 587.3035, found 587.3043; $C_{25}H_{42}N_6O_{10}$ x $C_2HF_3O_2$ (700.67).

(4*S*,7*S*,10*S*,13*S*,16*S*)-13-(2-Aminoethyl)-7-(carboxymethyl)-16-formyl-4,10-diisopropyl-2,5,8,11,14-pentaoxo-3,6,9,12,15-pentaazaoctadecan-18-oic acid hydrotrifluoroacetate (2.069)
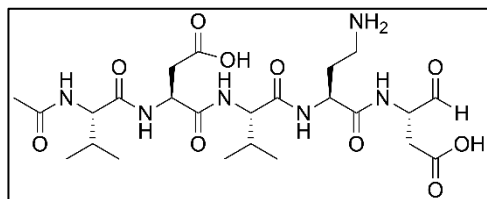
The title compound was synthesized according to general procedure **A** yielding a fluffy white solid (10.5 mg, 8%): RP-HPLC: 95%, (t_R = 6.20, k = 1.07). ^{1}H NMR (400 MHz, D$_2$O) δ 4.94 (t, *J* = 4.6 Hz, 1H), 4.65 – 4.62 (m, 1H), 4.40 – 4.30 (m, 1H), 4.19 – 4.10 (m, 1H), 4.01 – 3.92 (m, 2H), 3.00 – 2.80 (m, 3H), 2.76 – 2.55 (m, 2H), 2.49 – 2.39 (m, 1H), 2.12 – 1.89 (m, 7H), 0.87 – 0.78 (m, 12H). ^{13}C NMR (101 MHz, D$_2$O) δ 175.40, 175.10, 174.59, 174.40, 173.68, 173.39, 173.35, 172.77, 172.35, 172.30, 171.67, 89.68, 59.87, 59.82, 59.74, 51.59, 51.54, 51.26, 51.18, 50.07, 36.26, 36.22, 35.34, 34.36, 29.89, 29.03, 28.90, 21.65, 18.43, 18.39, 18.31, 17.74, 17.61. HRMS (ESI-MS): *m/z* [M+H$^+$] calculated for C$_{24}$H$_{41}$N$_6$O$_{10}$$^+$: 573.2879, found 573.2883; C$_{24}$H$_{40}$N$_6$O$_{10}$ x C$_2$HF$_3$O$_2$ (686.64).

(4*S*,7*S*,10*S*,13*S*)-10-(2-Aminoethyl)-4-(carboxymethyl)-13-formyl-7-isopropyl-2,5,8,11-tetraoxo-3,6,9,12-tetraazapentadecan-15-oic acid hydrotrifluoroacetate (2.070)
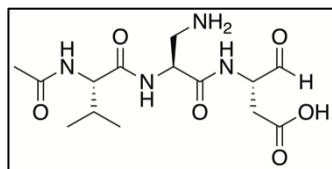

The title compound was synthesized according to general procedure **A** yielding a fluffy white solid (76.1 mg, 69%): RP-HPLC: 99%, (t_R = 3.68, k = 0.23). ^{1}H NMR (400 MHz, D$_2$O) δ 4.93 (t, *J* = 4.7 Hz, 1H), 4.59 (t, *J* = 6.4 Hz, 1H), 4.39 – 4.30 (m, 1H), 4.17 – 4.09 (m, 1H), 4.04 – 3.94 (m, 1H), 3.00 – 2.86 (m, 2H), 2.84 – 2.37 (m, 4H), 2.13 – 1.87 (m, 6H), 0.87 – 0.77 (m, 6H). ^{13}C NMR (101 MHz, D$_2$O) δ 175.26, 174.98, 174.21, 174.12, 173.41, 173.36, 172.81, 172.78, 171.77, 171.63, 89.66, 89.59, 59.69, 59.62, 51.55, 51.51, 51.24, 51.14, 50.13, 36.24, 35.34, 34.29, 33.87, 30.00, 29.04, 28.92, 21.69, 18.40, 18.38, 17.69, 17.65. HRMS (ESI-MS): *m/z* [M+H$^+$] calculated for C$_{19}$H$_{32}$N$_5$O$_9$$^+$: 474.2195, found 474.2200; C$_{19}$H$_{31}$N$_5$O$_9$ x C$_2$HF$_3$O$_2$ (587.51).
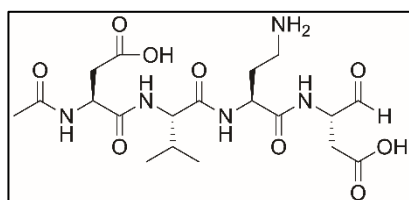
(4S,7S,10S,13S,16S)-13-(Aminomethyl)-7-(carboxymethyl)-16-formyl-4,10-diisopropyl-2,5,8,11,14-pentaoxo-3,6,9,12,15-pentaazaoctadecan-18-oic acid hydrotrifluoroacetate (2.071)
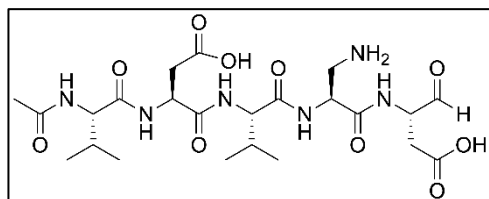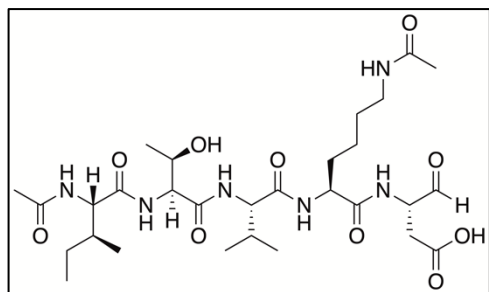

The title compound was synthesized according to general procedure **A** yielding a fluffy white solid (47.2 mg, 37%): RP-HPLC: > 99%, (t_R = 6.16, k = 1.05). ^{1}H NMR (400 MHz, D_2O) δ 4.94 (dd, J = 9.3, 4.6 Hz, 1H), 4.67 – 4.60 (m, 2H), 4.20 – 4.09 (m, 1H), 4.07 – 3.97 (m, 1H), 3.96 – 3.89 (m, 1H), 3.44 – 3.30 (m, 1H), 3.26 – 3.12 (m, 1H), 3.04 – 2.36 (m, 4H), 2.09 – 1.86 (m, 5H), 0.85 – 0.77 (m, 12H). ^{13}C NMR (101 MHz, D_2O) δ 175.36, 174.93, 174.62, 174.59, 174.46, 174.43, 173.73, 173.56, 172.56, 172.51, 169.83, 169.38, 169.37, 89.62, 89.57, 59.93, 59.70, 59.68, 51.66, 51.53, 50.85, 50.66, 50.09, 40.11, 39.97, 35.26, 34.34, 33.94, 29.89, 21.66, 18.46, 18.43, 18.31, 17.65, 17.56, 17.54. HRMS (ESI-MS): *m/z* [M+H$^+$] calculated for $C_{23}H_{39}N_6O_{10}^+$: 559.2722, found 559.2731; $C_{23}H_{38}N_6O_{10}$ x $C_2HF_3O_2$ (672.61).

(4S,7S,10S,13S,16S)-7-(Carboxymethyl)-16-formyl-13-(3-guanidinopropyl)-4,10-diisopropyl-2,5,8,11,14-pentaoxo-3,6,9,12,15-pentaazaoctadecan-18-oic acid hydrotrifluoroacetate (2.072)
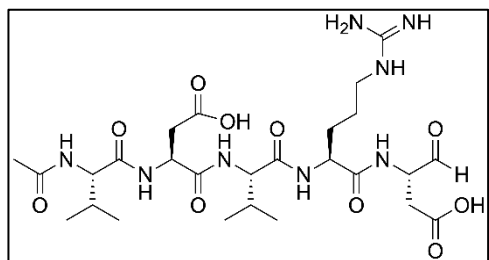
The title compound was synthesized according to general procedure **A** yielding a fluffy white solid (42.5 mg, 31%): RP-HPLC: > 99%, (t_R = 6.58, k = 1.39). ^{1}H NMR (300 MHz, D_2O) δ 4.89 (d, J = 4.6 Hz, 1H), 4.60 (t, J = 6.9 Hz, 1H), 4.31 – 4.02 (m, 2H), 3.98 – 3.84 (m, 2H), 3.06 (t, J = 6.5 Hz, 2H), 2.90 – 2.76 (m, 1H), 2.73 – 2.31 (m, 2H), 2.02 – 1.73 (m, 6H), 1.82 – 1.37 (m, 4H), 0.84 – 0.73 (m, 12H). ^{13}C NMR (75 MHz, D_2O) δ 175.09, 174.58, 174.54, 174.09, 174.04, 173.67, 173.28, 171.97, 156.73, 59.83, 59.70, 53.37, 52.24, 51.47, 50.03, 40.46, 40.41, 35.17, 29.88, 27.69, 24.39, 21.62, 18.34, 18.30, 17.70, 17.60. HRMS (ESI-MS): *m/z* [M+H$^+$] calculated for $C_{26}H_{45}N_8O_{10}^+$: 629.3253, found 629.3258; $C_{26}H_{44}N_8O_{10}$ x $C_2HF_3O_2$ (742.71).

(4*S*,7*S*,10*S*,13*S*,16*S*)-13-(4-Acetamidobutyl)-7-(carboxymethyl)-16-formyl-4,10-diisopropyl-2,5,8,11,14-pentaoxo-3,6,9,12,15-pentaazaoctadecan-18-oic acid (2.073)
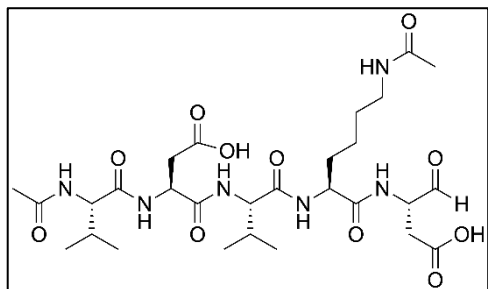
The title compound was synthesized according to general procedure **A** yielding a fluffy white solid (49.2 mg, 41%): RP-HPLC: > 99%, (t_R = 7.36, k = 1.68). ^{1}H NMR (300 MHz, D_2O) δ 4.88 (dd, J = 4.6, 0.9 Hz, 1H), 4.60 (t, 1H), 4.19 – 4.00 (m, 2H), 3.98 – 3.86 (m, 2H), 2.99 (t, J = 6.7 Hz, 2H), 2.90 – 2.31 (m, 4H), 2.01 – 1.84 (m, 5H), 1.81 (s, 3H), 1.68 – 1.49 (m, 2H), 1.41 – 1.10 (m, 4H), 0.83 – 0.72 (m, 12H). ^{13}C NMR (101 MHz, D_2O) δ 175.19, 175.10, 174.53, 174.51, 174.03, 173.99, 173.62, 173.53, 173.45, 173.11, 173.07, 172.20, 172.08, 89.68, 59.83, 59.80, 59.62, 53.83, 51.49, 50.05, 39.18, 35.13, 34.04, 33.84, 30.73, 30.61, 29.93, 27.71, 22.43, 22.37, 21.88, 21.65, 18.45, 18.42, 18.34, 17.62. HRMS (ESI-MS): *m/z* [M+H$^+$] calculated for $C_{28}H_{47}N_6O_{11}^+$: 643.3304, found 643.3297; $C_{28}H_{46}N_6O_{11}$ (642.71).

(4*S*,7*S*,10*S*,13*S*,16*S*)-10-Benzyl-7-(carboxymethyl)-16-formyl-4,13-diisopropyl-2,5,8,11,14-pentaoxo-3,6,9,12,15-pentaazaoctadecan-18-oic acid (2.074)

(Synthesized by Steffen Pockes)

The title compound was synthesized according to general procedure **A** yielding a fluffy white solid (36.4 mg, 18%): RP-HPLC: 97%, (t_R = 10.89, k = 2.63). ^{1}H NMR (400 MHz, CD_3OD) δ 7.32 – 7.09 (m, 5H), 4.66 – 4.61 (m, 1H), 4.61 – 4.50 (m, 2H), 4.36 – 4.23 (m, 1H), 4.17 – 4.10 (m, 1H), 4.10 – 4.02 (m, 1H), 3.18 (dd, J = 14.2, 4.8 Hz, 1H), 3.05 – 2.93 (m, 1H), 2.87 – 2.76 (m, 1H), 2.73 – 2.59 (m, 2H), 2.56 – 2.40 (m, 1H), 2.13 – 1.91 (m, 5H), 0.99 – 0.82 (m, 12H). ^{13}C NMR (101 MHz, CD_3OD) δ 173.68, 173.57, 172.62, 172.57, 172.43, 171.63, 171.32, 137.06, 128.89, 128.11, 126.32, 96.79, 59.45, 55.27, 50.55, 50.12, 47.89, 36.89, 34.90, 33.06, 30.42, 30.17, 21.09, 18.33, 17.38. HRMS (ESI-MS): *m/z* [M+H$^+$] calculated for $C_{29}H_{42}N_5O_{10}^+$: 620.2926, found 620.2931; $C_{29}H_{41}N_5O_{10}$ (619.67).

(4S,7S,10S,13S,16S)-13-(3-Aminopropyl)-4-[(S)-sec-butyl]-16-formyl-7-[(R)-1-hydroxyethyl]-10-isopropyl-2,5,8,11,14-pentaoxo-3,6,9,12,15-pentaazaoctadecan-18-oic acid hydrotrifluoroacetate (2.075)

The title compound was synthesized according to general procedure **A** yielding a fluffy white solid (42.2 mg, 48%): RP-HPLC: > 99%, (t_R = 7.07, k = 1.36). ^{1}H NMR (300 MHz, D_2O) δ 4.92 – 4.84 (m, 1H), 4.40 – 3.85 (m, 6H), 2.85 (t, J = 7.2 Hz, 2H), 2.68 – 2.28 (m, 2H), 2.00 – 1.79 (m, 4H), 1.77 – 1.23 (m, 6H), 1.13 – 0.95 (m, 3H), 0.86 – 0.64 (m, 12H). ^{13}C NMR (75 MHz, D_2O) δ 206.59, 175.94, 175.48, 174.45, 174.23, 172.96, 172.56, 171.65, 89.67, 67.12, 59.60, 58.92, 58.69, 53.15, 51.59, 38.85, 36.13, 34.56, 30.07, 28.16, 24.62, 23.20, 21.63, 18.83, 18.40, 17.86, 14.84, 10.29. HRMS (ESI-MS): m/z [M+H$^+$] calculated for $C_{26}H_{47}N_6O_9^+$: 587.3399, found 587.3410; $C_{26}H_{46}N_6O_9$ x $C_2HF_3O_2$ (700.71).

(4S,7S,10S,13S)-10-(3-Aminopropyl)-13-formyl-4-[(R)-1-hydroxyethyl]-7-isopropyl-2,5,8,11-tetraoxo-3,6,9,12-tetraazapentadecan-15-oic acid hydrotrifluoroacetate (2.076)

The title compound was synthesized according to general procedure **B** yielding a fluffy white solid (21.9 mg, 30%): RP-HPLC: > 99%, (t_R = 3.46, k = 0.15). ^{1}H NMR (300 MHz, D_2O) δ 4.88 (dd, J = 4.6, 3.1 Hz, 1H), 4.40 – 3.88 (m, 5H), 2.85 (t, J = 6.1 Hz, 2H), 2.69 – 2.32 (m, 2H), 1.98 – 1.81 (m, 4H), 1.75 – 1.47 (m, 4H), 1.05 (d, J = 6.4 Hz, 3H), 0.78 (t, J = 6.7 Hz, 6H). HRMS (ESI-MS): m/z [M+H$^+$] calculated for $C_{20}H_{36}N_5O_8^+$: 474.2558, found 474.2561; $C_{20}H_{35}N_5O_8$ x $C_2HF_3O_2$ (587.55).

(S)-3-{(S)-2-[(S)-2-Acetamido-3-methylbutanamido]-5-aminopentanamido}-4-oxobutanoic acid hydrotrifluoroacetate (2.077)

The title compound was synthesized according to general procedure **B** yielding a fluffy white solid (36.3 mg, 60%): RP-HPLC: > 99%, (t_R = 3.43, k = 0.14). ^{1}H NMR (300 MHz, D_2O) δ 4.92 – 4.82 (m, 1H), 4.27 – 4.18 (m, 1H), 4.15 – 4.03 (m, 1H), 3.92 – 3.79 (m, 1H), 2.85 (t, J = 7.0 Hz, 2H), 2.69 – 2.27 (m, 2H), 1.96 – 1.80 (m, 4H), 1.78 – 1.44 (m, 4H), 0.78 (t, J = 6.8 Hz, 6H). ^{13}C NMR (75 MHz, D_2O) δ 206.60,

175.17, 174.52, 173.82, 172.65, 89.66, 59.93, 53.05, 51.51, 38.85, 34.32, 29.89, 28.12, 23.22, 21.55, 18.37, 17.81. HRMS (ESI-MS): *m/z* [M+H$^+$] calculated for $C_{16}H_{29}N_4O_6^+$: 373.2082, found 373.2084; $C_{16}H_{28}N_4O_6$ x $C_2HF_3O_2$ (486.45).

(4*S*,7*S*,10*S*,13*S*,16*S*)-13-(2-Aminoethyl)-4-[(*S*)-*sec*-butyl]-16-formyl-7-[(*R*)-1-hydroxyethyl]-10-isopropyl-2,5,8,11,14-pentaoxo-3,6,9,12,15-pentaazaoctadecan-18-oic acid hydrotrifluoroacetate (2.078)
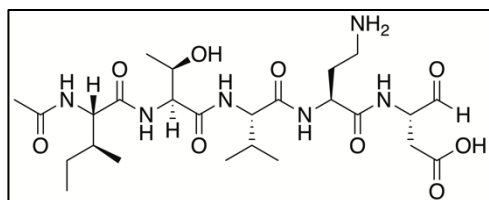
The title compound was synthesized according to general procedure **A** yielding a fluffy white solid (41.0 mg, 48 %): RP-HPLC: > 99%, (t$_R$ = 7.11, *k* = 1.37). ^{1}H NMR (300 MHz, D$_2$O) δ 4.89 (t, *J* = 4.9 Hz, 1H), 4.38 – 3.88 (m, 6H), 2.97 – 2.82 (m, 2H), 2.70 – 2.30 (m, 2H), 2.10 – 1.84 (m, 6H), 1.77 – 1.25 (m, 2H), 1.04 (d, *J* = 6.4 Hz, 3H), 0.84 – 0.68 (m, 12H). ^{13}C NMR (75 MHz, D$_2$O) δ 175.69, 175.26, 174.47, 174.26, 173.13, 172.10, 171.69, 171.55, 89.64, 67.13, 59.61, 58.84, 58.72, 51.57, 51.10, 36.18, 36.12, 34.52, 30.07, 29.04, 24.62, 21.63, 18.83, 18.37, 17.88, 14.84, 10.30. HRMS (ESI-MS): *m/z* [M+H$^+$] calculated for $C_{25}H_{45}N_6O_9^+$: 573.3243, found 573.3246; $C_{25}H_{44}N_6O_9$ x $C_2HF_3O_2$ (686.68).

(4*S*,7*S*,10*S*,13*S*)-10-(2-Aminoethyl)-13-formyl-4-[(*R*)-1-hydroxyethyl]-7-isopropyl-2,5,8,11-tetraoxo-3,6,9,12-tetraazapentadecan-15-oic acid hydrotrifluoroacetate (2.079)
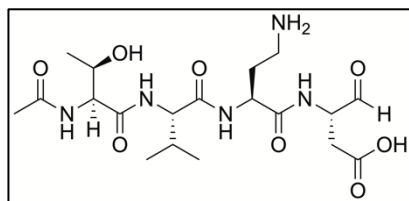
The title compound was synthesized according to general procedure **B** yielding a fluffy white solid (18.2 mg, 25%): RP-HPLC: > 99%, (t$_R$ = 3.44, *k* = 0.15). ^{1}H NMR (300 MHz, D$_2$O) δ 4.89 (t, *J* = 4.7 Hz, 1H), 4.40 – 3.90 (m, 5H), 2.99 – 2.80 (m, 2H), 2.70 – 2.30 (m, 2H), 2.06 – 1.84 (m, 6H), 1.05 (d, *J* = 6.4 Hz, 3H), 0.83 – 0.75 (m, 6H). HRMS (ESI-MS): *m/z* [M+H$^+$] calculated for $C_{19}H_{34}N_5O_8^+$: 460.2402, found 460.2412; $C_{19}H_{33}N_5O_8$ x $C_2HF_3O_2$ (573.52).

(*S*)-3-{(*S*)-2-[(*S*)-2-Acetamido-3-methylbutanamido]-4-aminobutanamido}-4-oxobutanoic acid hydrotrifluoroacetate (2.080)
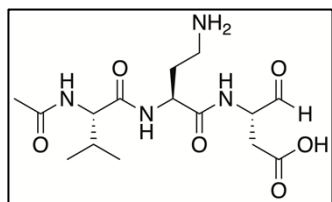
The title compound was synthesized according to general procedure **B** yielding a fluffy white solid (8.9 mg, 15%): RP-HPLC: 96%, (t_R = 3.53, k = 0.18). ^{1}H NMR (400 MHz, D$_2$O) δ 4.95 (d, J = 4.8 Hz, 1H), 4.44 – 4.29 (m, 1H), 4.18 – 4.10 (m, 1H), 3.92 (d, J = 7.3 Hz, 1H), 3.04 – 2.86 (m, 2H), 2.72 – 2.37 (m, 2H), 2.16 – 2.01 (m, 1H), 2.02 – 1.86 (m, 5H), 0.89 – 0.75 (m, 6H). ^{13}C NMR (101 MHz, D$_2$O) δ 175.06, 174.65, 174.20, 174.01, 172.20, 171.66, 89.68, 59.99, 51.54, 51.07, 36.27, 34.37, 29.86, 28.99, 21.57, 18.37, 17.84. HRMS (ESI-MS): *m/z* [M+H$^+$] calculated for C$_{15}$H$_{27}$N$_4$O$_6^+$: 359.1925, found 359.1930; C$_{15}$H$_{26}$N$_4$O$_6$ x C$_2$HF$_3$O$_2$ (472.42).

(4*S*,7*S*,10*S*,13*S*,16*S*)-13-(Aminomethyl)-4-[(*S*)-*sec*-butyl]-16-formyl-7-[(*R*)-1-hydroxyethyl]-10-isopropyl-2,5,8,11,14-pentaoxo-3,6,9,12,15-pentaazaoctadecan-18-oic acid hydrotrifluoroacetate (2.081)
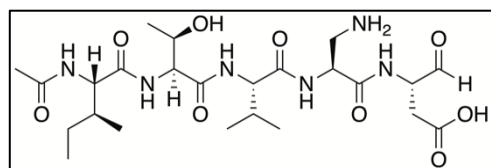
The title compound was synthesized according to general procedure **A** yielding a fluffy white solid (24.2 mg, 29%): RP-HPLC: > 99%, (t_R = 7.01, k = 1.34). ^{1}H NMR (300 MHz, D$_2$O) δ 4.91 (dd, J = 8.1, 4.6 Hz, 1H), 4.64 – 4.57 (m, 1H), 4.50 – 3.92 (m, 5H), 3.41 – 3.05 (m, 2H), 2.77 – 2.27 (m, 2H), 2.02 – 1.85 (m, 4H), 1.76 – 1.23 (m, 2H), 1.05 (d, J = 6.4 Hz, 3H), 0.86 – 0.68 (m, 12H). ^{13}C NMR (75 MHz, D$_2$O) δ 175.48, 174.95, 174.92, 174.52, 174.36, 173.56, 173.39, 171.91, 171.87, 169.73, 169.26, 89.56, 67.16, 67.01, 59.53, 58.81, 58.71, 58.12, 51.64, 51.52, 50.80, 50.57, 40.02, 36.08, 35.93, 34.40, 30.16, 29.89, 24.65, 24.52, 21.62, 21.51, 18.81, 18.37, 18.35, 17.73, 17.71, 17.69, 14.84, 14.68, 10.29, 10.12. HRMS (ESI-MS): *m/z* [M+H$^+$] calculated for C$_{24}$H$_{43}$N$_6$O$_9^+$: 559.3086, found 559.3093; C$_{24}$H$_{42}$N$_6$O$_9$ x C$_2$HF$_3$O$_2$ (672.66).

(4*S*,7*S*,10*S*,13*S*)-10-(Aminomethyl)-13-formyl-4-[(*R*)-1-hydroxyethyl]-7-isopropyl-2,5,8,11-tetraoxo-3,6,9,12-tetraazapentadecan-15-oic acid hydrotrifluoroacetate (2.082)
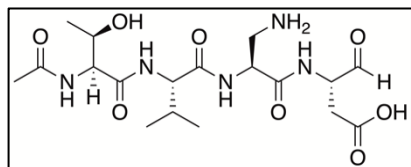
The title compound was synthesized according to general procedure **B** yielding a fluffy white solid (14.6 mg, 21%): RP-HPLC: > 99%, (t_R = 3.44, *k* = 0.15). ^{1}H NMR (300 MHz, D_2O) δ 4.91 (dd, *J* = 8.4, 4.6 Hz, 1H), 4.63 – 4.51 (m, 1H), 4.27 – 3.86 (m, 4H), 3.41 – 3.04 (m, 4H), 2.73 – 2.29 (m, 1H), 2.02 – 1.82 (m, 4H), 1.06 (d, *J* = 6.4 Hz, 3H), 0.89 – 0.74 (m, 6H). HRMS (ESI-MS): *m/z* [M+H$^+$] calculated for $C_{18}H_{32}N_5O_8^+$: 446.2245, found 446.2253; $C_{18}H_{31}N_5O_8$ x $C_2HF_3O_2$ (559.50).

(*S*)-3-{(*S*)-2-[(*S*)-2-Acetamido-3-methylbutanamido]-3-aminopropanamido}-4-oxobutanoic acid hydrotrifluoroacetate (2.083)

The title compound was synthesized according to general procedure **B** yielding a fluffy white solid (20.2 mg, 35%): RP-HPLC: > 99%, (t_R = 3.45, *k* = 0.15). ^{1}H NMR (300 MHz, D_2O) δ 4.94 – 4.86 (m, 1H), 4.64 – 4.54 (m, 1H), 4.20 – 3.82 (m, 2H), 3.40 – 3.06 (m, 2H), 2.73 – 2.32 (m, 2H), 2.02 – 1.84 (m, 4H), 0.87 – 0.75 (m, 6H). ^{13}C NMR (75 MHz, D_2O) δ 206.61, 175.36, 174.90, 174.79, 174.22, 169.41, 89.58, 59.88, 51.47, 50.45, 40.02, 34.31, 29.89, 21.58, 18.31, 17.66. HRMS (ESI-MS): *m/z* [M+H$^+$] calculated for $C_{14}H_{25}N_4O_6^+$: 345.1769, found 345.1776; $C_{14}H_{24}N_4O_6$ x $C_2HF_3O_2$ (458.39).

(4*S*,7*S*,10*S*,13*S*,16*S*)-13-(4-Acetamidobutyl)-4-[(*S*)-*sec*-butyl]-16-formyl-7-[(*R*)-1-hydroxyethyl]-10-isopropyl-2,5,8,11,14-pentaoxo-3,6,9,12,15-pentaazaoctadecan-18-oic acid (2.084)

The title compound was synthesized according to general procedure **A** yielding a fluffy white solid (26.0 mg, 39%): RP-HPLC: > 99%, (t_R = 8.20, *k* = 1.73). ^{1}H NMR (400 MHz, D_2O) δ 4.93 (d, *J* = 4.7 Hz, 1H), 4.32 – 4.24 (m, 1H), 4.22 – 3.95 (m, 5H), 3.08 – 3.00 (m, 2H), 2.73 – 2.36 (m, 3H), 2.04 – 1.90 (m, 4H), 1.86 (s, 3H), 1.78 – 1.52 (m, 2H), 1.45 – 1.32 (m, 2H), 1.30 – 1.17 (m, 2H), 1.07 (d, *J* = 6.5 Hz, 3H), 0.89 – 0.69 (m, 12H). ^{13}C NMR (75 MHz, DMSO-d$_6$) δ 206.43, 175.40, 175.40, 172.16, 171.93, 171.92, 171.88, 171.04, 169.47, 169.47,

102.87, 66.89, 58.57, 58.01, 57.50, 52.83, 38.75, 36.85, 33.48, 29.22, 24.84, 23.30, 23.05, 22.89, 20.05, 19.54, 18.28, 15.84, 11.44. HRMS (ESI-MS): *m/z* [M+H$^+$] calculated for $C_{29}H_{51}N_6O_{10}^+$: 643.3661, found 643.3670; $C_{29}H_{50}N_6O_{10}$ (642.75).

(4S,7S,10S,13S)-10-(4-Acetamidobutyl)-13-formyl-4-[(R)-1-hydroxyethyl]-7-isopropyl-2,5,8,11-tetraoxo-3,6,9,12-tetraazapentadecan-15-oic acid (2.085)
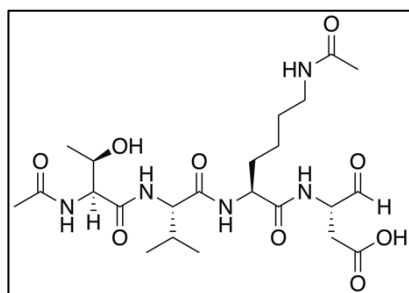
The title compound was synthesized according to general procedure **A** yielding a fluffy white solid (25.8 mg, 39%): RP-HPLC: > 99%, (t$_R$ = 5.74, *k* = 0.91). ^{1}H NMR (300 MHz, D$_2$O) δ 4.88 (d, *J* = 4.7 Hz, 1H), 4.20 – 3.87 (m, 5H), 2.99 (t, *J* = 2.0 Hz, 2H), 2.79 – 2.30 (m, 2H), 1.95 – 1.85 (m, 4H), 1.81 (s, 3H), 1.69 – 1.48 (m, 2H), 1.40 – 1.29 (m, 2H), 1.25 – 1.12 (m, 2H), 1.03 (d, *J* = 6.4 Hz, 3H), 0.78 (dd, *J* = 6.8, 4.6 Hz, 6H). ^{13}C NMR (75 MHz, D$_2$O) δ 175.20, 175.11, 174.52, 173.93, 173.41, 173.29, 173.01, 172.09, 89.66, 67.10, 59.55, 59.42, 56.09, 53.69, 51.48, 39.15, 34.07, 30.74, 30.11, 27.70, 22.36, 21.86, 21.69, 18.86, 18.39, 17.77. HRMS (ESI-MS): *m/z* [M+H$^+$] calculated for $C_{23}H_{40}N_4O_9^+$: 530.2821, found 530.2825; $C_{23}H_{39}N_4O_9$ (529.59).

(S)-3-{(S)-6-Acetamido-2-[(S)-2-acetamido-3-methylbutanamido]hexanamido}-4-oxobutanoic acid (2.086)
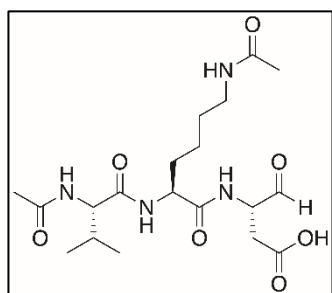
The title compound was synthesized according to general procedure **A** yielding a fluffy white solid (32.6 mg, 61%): RP-HPLC: > 99%, (t$_R$ = 5.50, *k* = 0.83). ^{1}H NMR (300 MHz, D$_2$O) δ 4.88 (d, *J* = 5.0 Hz, 1H), 4.24 – 4.01 (m, 2H), 3.95 – 3.86 (m, 1H), 3.00 (t, *J* = 6.7 Hz, 2H), 2.72 – 2.28 (m, 2H), 1.96 – 1.85 (m, 4H), 1.81 (s, 3H), 1.71 – 1.47 (m, 2H), 1.43 – 1.29 (m, 2H), 1.27 – 1.10 (m, 2H), 0.79 (dd, *J* = 6.8, 3.2 Hz, 6H). ^{13}C NMR (75 MHz, D$_2$O) δ 206.61, 175.14, 175.07, 174.43, 173.93, 173.66, 173.37, 89.66, 59.82, 53.60, 51.47, 39.14, 34.05, 30.67, 29.96, 27.70, 22.34, 21.84, 21.61, 18.39, 18.32, 17.68, 17.66. HRMS (ESI-MS): *m/z* [M+H$^+$] calculated for $C_{19}H_{31}N_4O_7^+$: 427.2198, found 427.2202; $C_{19}H_{30}N_4O_7$ (428.49).

(4*S*,7*S*,10*S*,13*S*,16*S*)-13-(2-Aminoethyl)-16-formyl-7-[(*R*)-1-hydroxyethyl]-10-isopropyl-4-methyl-2,5,8,11,14-pentaoxo-3,6,9,12,15-pentaazaoctadecan-18-oic acid hydrotrifluoroacetate (2.087)
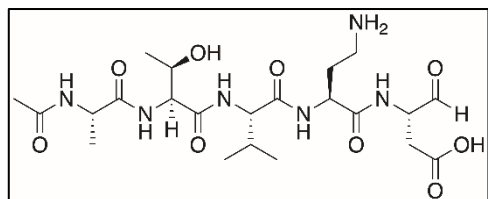
The title compound was synthesized according to general procedure **A** yielding a fluffy white solid (32.5 mg, 27%): RP-HPLC: > 99%, (t_R = 3.68, *k* = 0.23). ^{1}H NMR (400 MHz, D$_2$O) δ 4.97 – 4.91 (m, 1H), 4.44 – 4.30 (m, 1H), 4.30 – 4.04 (m, 4H), 4.11 – 3.94 (m, 1H), 3.03 – 2.86 (m, 2H), 2.75 – 2.36 (m, 2H), 2.22 – 1.84 (m, 6H), 1.32 – 1.23 (m, 3H), 1.09 (d, *J* = 6.4 Hz, 3H), 0.89 – 0.78 (m, 6H). ^{13}C NMR (101 MHz, D$_2$O) δ 175.80, 175.34, 175.02, 174.33, 173.29, 171.97, 171.76, 89.59, 67.13, 59.60, 58.90, 51.58, 51.23, 49.94, 36.18, 33.90, 30.09, 29.12, 21.61, 18.86, 18.34, 17.86, 16.54. HRMS (ESI-MS): *m/z* [M+H$^+$] calculated for C$_{22}$H$_{39}$N$_6$O$_9^+$: 531.2773, found 531.2782; C$_{22}$H$_{38}$N$_6$O$_9$ x C$_2$HF$_3$O$_2$ (644.60).

(4*S*,7*S*,10*S*,13*S*,16*S*)-7-(Carboxymethyl)-16-formyl-4,10-bis[(*R*)-1-hydroxyethyl]-13-methyl-2,5,8,11,14-pentaoxo-3,6,9,12,15-pentaazaoctadecan-18-oic acid (2.088)
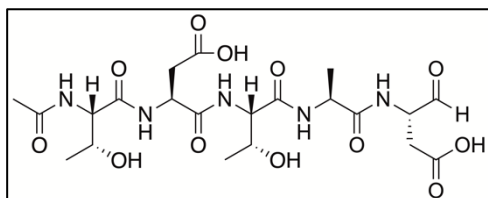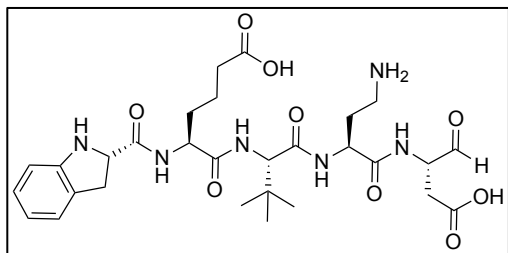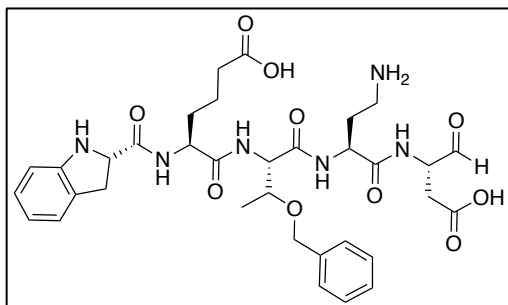

The title compound was synthesized according to general procedure **B** yielding a fluffy white solid (9.3 mg, 9%): RP-HPLC: > 99%, (t_R = 3.75, *k* = 0.25). ^{1}H NMR (400 MHz, D$_2$O) δ 4.92 (t, *J* = 4.7 Hz, 1H), 4.78 – 4.68 (m, 1H), 4.33 – 3.94 (m, 6H), 3.24 – 2.29 (m, 4H), 2.03 – 1.92 (m, 3H), 1.40 – 1.00 (m, 9H). ^{13}C NMR (101 MHz, D$_2$O) δ 175.24, 175.21, 174.78, 174.57, 174.50, 174.24, 172.68, 172.57, 172.16, 171.41, 171.31, 89.71, 67.00, 59.40, 59.25, 56.19, 51.51, 50.15, 49.91, 35.17, 34.08, 21.75, 18.82, 16.83, 16.65. HRMS (ESI-MS): *m/z* [M+H$^+$] calculated for C$_{21}$H$_{39}$N$_5$O$_{12}^+$: 548.2198, found 548.2198; C$_{21}$H$_{38}$N$_5$O$_{12}$ (547.52).

(*S*)-3-((*S*)-2-Acetamido-3-methylbutanamido)-4-(((*S*)-1-((*S*)-1-(((*S*)-1-carboxy-3-oxopropan-2-yl)carbamoyl)-6-methyl-3,4-dihydroisoquinolin-2(1*H*)-yl)-3-methyl-1-oxobutan-2-yl)amino)-4-oxobutanoic acid (2.093)
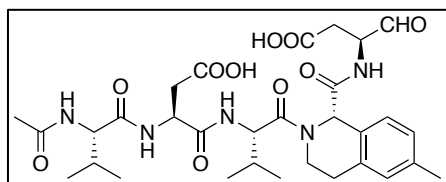
The title compound was synthesized according to general procedure **A** (using 2.7 eq of amino acid **2.090**) yielding a fluffy white solid (42.9 mg, 35%): RP-HPLC: 99%, (t_R = 12.07, *k* = 3.02). ^{1}H NMR (400 MHz, DMSO-d_6) δ 9.58 – 8.91 (m, 1H), 8.61 – 8.40 (m, 1H), 8.20 – 8.06 (m, 1H), 7.99 – 7.84 (m, 1H), 7.70 – 7.42 (m, 1H), 7.34 – 7.14 (m, 2H), 6.04 – 5.45 (m, 2H), 4.94 – 4.84 (m, 1H), 4.84 – 4.72 (m, 1H), 4.40 – 4.30 (m, 2H), 4.26 – 4.17 (m, 2H), 3.97 – 3.84 (m, 1H), 3.26 – 2.75 (m, 5H), 2.71 – 2.51 (m, 1H), 2.49 (d, *J* = 2.3 Hz, 3H), 2.32 – 2.20 (m, 1H), 2.20 – 2.11 (m, 1H), 2.09 (s, 3H), 1.17 – 0.99 (m, 12H). HRMS (ESI-MS): *m/z* [M+H^{+}] calculated for $C_{31}H_{44}N_5O_{10}^+$: 646.3083, found 646.3096; $C_{31}H_{43}N_5O_{10}$ (645.71).

(*S*)-3-((*S*)-2-Acetamido-3-methylbutanamido)-4-(((*S*)-1-((*R*)-1-(((*S*)-1-carboxy-3-oxopropan-2-yl)carbamoyl)-6-methyl-3,4-dihydroisoquinolin-2(1*H*)-yl)-3-methyl-1-oxobutan-2-yl)amino)-4-oxobutanoic acid (2.094)
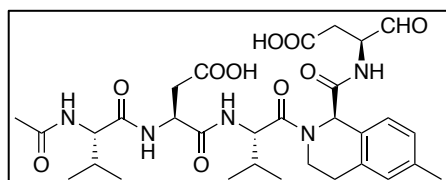
The title compound was synthesized according to general procedure **A** (using 150 mg resin and 2.0 eq of amino acid **2.089**) yielding a fluffy white solid (39.1 mg, 65%): RP-HPLC: > 99%, (t_R = 13.22, *k* = 3.41). ^{1}H NMR (400 MHz, DMSO-d_6) δ 9.44 – 8.57 (m, 1H), 8.46 – 8.07 (m, 1H), 8.01 – 7.83 (m, 1H), 7.79 – 7.62 (m, 1H), 7.44 – 7.21 (m, 1H), 7.07 – 6.91 (m, 2H), 6.00 – 5.16 (m, 2H), 4.68 – 4.44 (m, 2H), 4.29 – 4.09 (m, 1H), 4.10 – 3.93 (m, 2H), 3.69 – 3.61 (m, 2H), 3.05 – 2.51 (m, 5H), 2.49 – 2.28 (m, 1H), 2.25 (s, 3H), 2.05 – 1.89 (m, 1H), 1.85 (s, 3H), 0.91 – 0.71 (m, 12H). HRMS (ESI-MS): *m/z* [M+H^{+}] calculated for $C_{31}H_{44}N_5O_{10}^+$: 646.3083, found 646.3085; $C_{31}H_{43}N_5O_{10}$ (645.71).

(*S*)-3-((*S*)-2-Acetamido-3-methylbutanamido)-4-(((*S*)-1-((*S*)-6-bromo-1-(((*S*)-1-carboxy-3-oxopropan-2-yl)carbamoyl)-3,4-dihydroisoquinolin-2(1*H*)-yl)-3-methyl-1-oxobutan-2-yl)amino)-4-oxobutanoic acid (2.095)
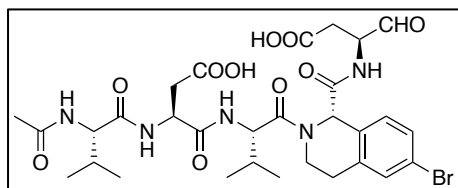
The title compound was synthesized according to general procedure **A** (using 2.7 eq of amino acid **2.092**) yielding a fluffy white solid (44.8 mg, 34%): RP-HPLC: > 99%, (t_R = 12.98, k = 3.33). ^{1}H NMR (400 MHz, DMSO-d_6) δ 9.51 – 8.76 (m, 1H), 8.58 – 8.18 (m, 1H), 7.99 – 7.81 (m, 1H), 7.77 – 7.59 (m, 1H), 7.53 – 7.23 (m, 3H), 6.16 – 5.16 (m, 2H), 4.69 – 4.58 (m, 1H), 4.58 – 4.41 (m, 1H), 4.42 – 4.21 (m, 2H), 4.15 – 4.05 (m, 1H), 4.05 – 3.91 (m, 1H), 3.89 – 3.66 (m, 1H), 3.05 – 2.50 (m, 5H), 2.48 – 2.22 (m, 1H), 2.14 – 1.84 (m, 2H), 1.85 (s, 3H), 1.07 – 0.53 (m, 12H). HRMS (ESI-MS): *m/z* [M+H$^+$] calculated for $C_{30}H_{41}BrN_5O_{10}^+$: 710.2031, found 710.2039; $C_{30}H_{40}BrN_5O_{10}$ (710.58).

(*S*)-3-((*S*)-2-Acetamido-3-methylbutanamido)-4-(((*S*)-1-((*R*)-6-bromo-1-(((*S*)-1-carboxy-3-oxopropan-2-yl)carbamoyl)-3,4-dihydroisoquinolin-2(1*H*)-yl)-3-methyl-1-oxobutan-2-yl)amino)-4-oxobutanoic acid (2.096)
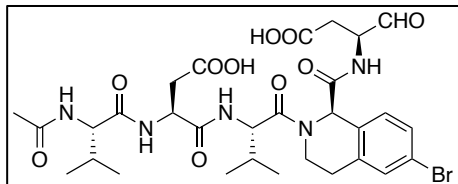
The title compound was synthesized according to general procedure **A** (using 150 mg resin and 2.0 eq of amino acid **2.092**) yielding a fluffy white solid (25.3 mg, 38%): RP-HPLC: > 99%, (t_R = 14.06, k = 3.69). ^{1}H NMR (400 MHz, DMSO-d_6) δ 9.43 – 8.63 (m, 1H), 8.39 – 8.12 (m, 1H), 7.94 – 7.67 (m, 2H), 7.59 – 7.25 (m, 3H), 6.08 – 5.16 (m, 2H), 4.67 – 4.53 (m, 2H), 4.50 – 4.22 (m, 1H), 4.20 – 4.12 (m, 1H), 4.11 – 3.94 (m, 2H), 3.85 – 3.75 (m, 1H), 3.09 – 2.51 (m, 5H), 2.46 – 2.21 (m, 1H), 2.04 – 1.89 (m, 2H), 1.86 (s, 3H), 0.97 – 0.62 (m, 12H). HRMS (ESI-MS): *m/z* [M+H$^+$] calculated for $C_{30}H_{41}BrN_5O_{10}^+$: 710.2031, found 710.2035; $C_{30}H_{40}BrN_5O_{10}$ (710.58).

(*S*)-4-(((*S*)-1-((*S*)-1-(((*S*)-1-Carboxy-3-oxopropan-2-yl)carbamoyl)-6-methyl-3,4-dihydroisoquinolin-2(1*H*)-yl)-3-methyl-1-oxobutan-2-yl)amino)-3-((*S*)-3-methyl-2-(quinoline-2-carboxamido)butanamido)-4-oxobutanoic acid hydrotrifluoroacetate (2.097)
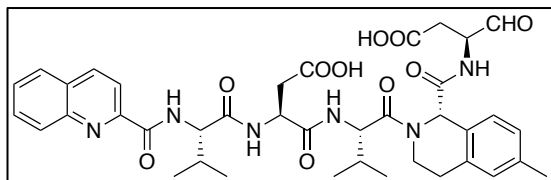
The title compound was synthesized according to general procedure **A** (using 150 mg resin and 2.0 eq of amino acid **2.090**) yielding a fluffy white solid (23.2 mg, 28%):

RP-HPLC: > 99%, (t_R = 17.05, k = 4.68). ^{1}H NMR (400 MHz, DMSO-d_6) δ 9.10 – 8.48 (m, 4H), 8.29 – 8.02 (m, 3H), 7.94 – 7.65 (m, 3H), 7.53 – 6.85 (m, 3H), 5.83 – 5.25 (m, 2H), 4.71 – 4.59 (m, 2H), 4.49 (t, J = 1.9 Hz, 1H), 4.31 – 4.15 (m, 1H), 4.06 – 3.92 (m, 2H), 3.78 – 3.59 (m, 1H), 3.05 – 2.51 (m, 5H), 2.46 – 2.28 (m, 1H), 2.24 (s, 3H), 2.18 – 1.92 (m, 2H), 1.03 – 0.55 (m, 12H). HRMS (ESI-MS): *m/z* [M+H$^+$] calculated for $C_{39}H_{47}N_6O_{10}^+$: 759.3348, found 759.3355; $C_{39}H_{46}N_6O_{10}$ x $C_2HF_3O_2$ (872.85).

(*S*)-4-(((*S*)-1-((*R*)-1-(((*S*)-1-Carboxy-3-oxopropan-2-yl)carbamoyl)-6-methyl-3,4-dihydroisoquinolin-2(1*H*)-yl)-3-methyl-1-oxobutan-2-yl)amino)-3-((*S*)-3-methyl-2-(quinoline-2-carboxamido)butanamido)-4-oxobutanoic acid hydrotrifluoroacetate (2.098)
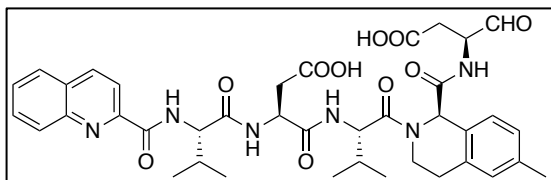
The title compound was synthesized according to general procedure **A** (using 150 mg resin and 2.0 eq of amino acid **2.089**) yielding a fluffy white solid (40.7 mg, 50%):

RP-HPLC: 99%, (t_R = 18.05, k = 5.02). ^{1}H NMR (400 MHz, DMSO-d_6) δ 9.43 – 8.46 (m, 4H), 8.26 – 8.03 (m, 3H), 8.00 – 7.81 (m, 2H), 7.73 (t, J = 1.2 Hz, 1H), 7.47 – 7.18 (m, 1H), 7.16 – 6.88 (m, 2H), 5.97 – 5.17 (m, 2H), 4.75 – 4.60 (m, 2H), 4.58 – 4.49 (m, 1H), 4.09 – 3.93 (m, 2H), 3.70 – 3.60 (m, 2H), 3.06 – 2.51 (m, 5H), 2.47 – 2.24 (m, 1H), 2.25 (s, 3H), 2.17 – 1.86 (m, 2H), 1.05 – 0.62 (m, 12H). HRMS (ESI-MS): *m/z* [M+H$^+$] calculated for $C_{39}H_{47}N_6O_{10}^+$: 759.3348, found 759.3362; $C_{39}H_{46}N_6O_{10}$ x $C_2HF_3O_2$ x $C_2HF_3O_2$ (872.85).

(*S*)-4-(((*S*)-1-((*S*)-6-Bromo-1-(((*S*)-1-carboxy-3-oxopropan-2-yl)carbamoyl)-3,4-dihydroisoquinolin-2(1*H*)-yl)-3-methyl-1-oxobutan-2-yl)amino)-3-((*S*)-3-methyl-2-(quinoline-2-carboxamido)butanamido)-4-oxobutanoic acid hydrotrifluoroacetate (2.099)
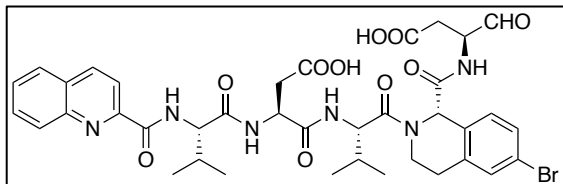
The title compound was synthesized according to general procedure **A** (using 150 mg resin and 2.0 eq of amino acid **2.092**) yielding a fluffy white solid (37.2 mg, 42%): RP-HPLC: > 99%, (t$_R$ = 17.75, k = 4.92). ^{1}H NMR (400 MHz, DMSO-d$_6$) δ 9.21 – 8.44 (m, 4H), 8.25 – 8.02 (m, 3H), 7.95 – 7.64 (m, 3H), 7.56 – 7.21 (m, 3H), 6.12 – 5.20 (m, 2H), 4.72 – 4.56 (m, 2H), 4.55 – 4.44 (m, 1H), 4.35 – 4.18 (m, 1H), 4.04 – 3.92 (m, 2H), 3.78 – 3.68 (m, 1H), 3.07 – 2.51 (m, 5H), 2.44 – 2.22 (m, 1H), 2.19 – 1.83 (m, 2H), 1.13 – 0.51 (m, 12H). HRMS (ESI-MS): *m/z* [M+H$^+$] calculated for C$_{38}$H$_{44}$BrN$_6$O$_{10}^+$: 823.2297, found 823.2299; C$_{38}$H$_{43}$BrN$_6$O$_{10}$ x C$_2$HF$_3$O$_2$ (937.72).

(*S*)-4-(((*S*)-1-((*R*)-6-Bromo-1-(((*S*)-1-carboxy-3-oxopropan-2-yl)carbamoyl)-3,4-dihydroisoquinolin-2(1*H*)-yl)-3-methyl-1-oxobutan-2-yl)amino)-3-((*S*)-3-methyl-2-(quinoline-2-carboxamido)butanamido)-4-oxobutanoic acid hydrotrifluoroacetate (2.100)
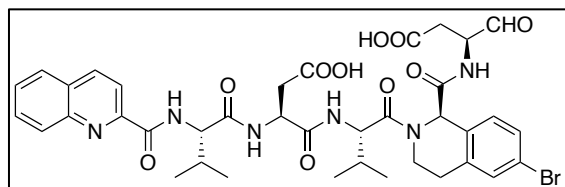
The title compound was synthesized according to general procedure **A** (using 150 mg resin and 2.0 eq of amino acid **2.091**) yielding a fluffy white solid (38.6 mg, 44%): RP-HPLC: > 99%, (t$_R$ = 18.74 k = 5.25). ^{1}H NMR (400 MHz, DMSO-d$_6$) δ 9.21 – 8.45 (m, 4H), 8.28 – 8.03 (m, 3H), 8.02 – 7.80 (m, 2H), 7.78 – 7.65 (m, 1H), 7.59 – 7.26 (m, 3H), 6.12 – 5.25 (m, 2H), 4.73 – 4.59 (m, 2H), 4.58 – 4.46 (m, 1H), 4.39 – 4.19 (m, 1H), 4.17 – 3.88 (m, 2H), 3.88 – 3.57 (m, 1H), 3.07 – 2.50 (m, 5H), 2.45 – 2.21 (m, 1H), 2.23 – 2.06 (m, 1H), 2.05 – 1.87 (m, 1H), 1.10 – 0.60 (m, 12H). HRMS (ESI-MS): *m/z* [M+H$^+$] calculated for C$_{38}$H$_{44}$BrN$_6$O$_{10}^+$: 823.2297, found 823.2297; C$_{38}$H$_{43}$BrN$_6$O$_{10}$ x C$_2$HF$_3$O$_2$ (937.72).

(*S*)-6-(((*S*)-1-((*S*)-1-(((*S*)-1-Carboxy-3-oxopropan-2-yl)carbamoyl)-6-methyl-3,4-dihydroisoquinolin-2(1*H*)-yl)-3-methyl-1-oxobutan-2-yl)amino)-5-((*S*)-indoline-2-carboxamido)-6-oxohexanoic acid hydrotrifluoroacetate (2.101) (*Synthesized by Gurpreet Singh*)
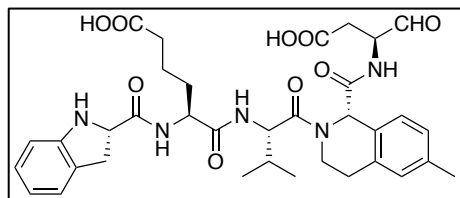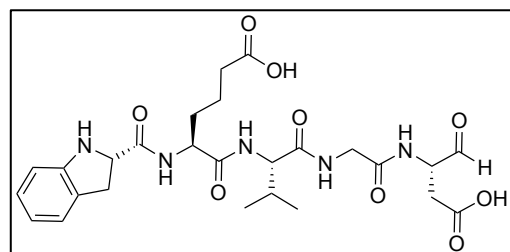

The title compound was synthesized according to general procedure **A** (using 150 mg resin) yielding a fluffy white solid (19.0 mg, 30%): RP-HPLC: 97%. ^{1}H NMR (400 MHz, DMSO-d6) δ12.1 – 11.7 (m, 0.6H), 9.06 – 8.76 (m, 1H), 7.61 – 6.75 (m, 7H), 6.06 – 4.20 (m, 4H), 4.15 – 2.54 (m, 13H), 2.93 – 1.67 (m, 4H), 3.11 – 2.57 (m, 4H), 1.43 – 0.28 (m, 7H). HRMS (ESI): *m/z* [M+H^{+}] calculated for $C_{35}H_{44}N_5O_9^+$: 678.3134, found 678.3133; $C_{35}H_{43}N_5O_9$ x $C_2HF_3O_2$ (791.78).

(3*S*,6*S*,9*S*,12*S*)-9-(2-Aminoethyl)-3-(3-carboxypropyl)-12-formyl-1-((*S*)-indolin-2-yl)-6-isopropyl-1,4,7,10-tetraoxo-2,5,8,11-tetraazatetradecan-14-oic acid dihydrotrifluoroacetate (2.107)
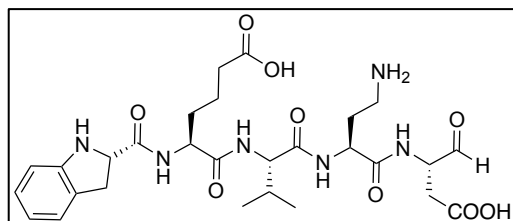
The title compound was synthesized according to general procedure **A** (using 600 mg resin) yielding a fluffy white solid (78.6 mg, 25%): RP-HPLC: 95%, (t$_R$ = 7.69, *k* = 1.56). ^{1}H NMR (300 MHz, D$_2$O) δ 7.27 – 7.10 (m, 4H), 4.92 – 4.86 (m, 1H), 4.75 – 4.68 (m, 1H), 4.31 – 4.19 (m, 2H), 4.13 – 4.05 (m, 1H), 3.96 – 3.87 (m, 1H), 3.64 – 3.48 (m, 1H), 3.20 – 3.08 (m, 1H), 2.94 – 2.72 (m, 2H), 2.70 – 2.32 (m, 2H), 2.27 (t, *J* = 7.2 Hz, 2H), 2.03 – 1.77 (m, 3H), 1.75 – 1.58 (m, 2H), 1.57 – 1.41 (m, 2H), 0.80 – 0.68 (m, 6H). HRMS (ESI-MS): *m/z* [M+H^{+}] calculated for $C_{28}H_{41}N_6O_9^+$: 605.2930, found 605.2930; $C_{28}H_{40}N_6O_9$ x $C_4H_2F_6O_4$ (832.71).

(3S,6S,9S,12S)-9-(2-Aminoethyl)-6-(tert-butyl)-3-(3-carboxypropyl)-12-formyl-1-((S)-indolin-2-yl)-1,4,7,10-tetraoxo-2,5,8,11-tetraazatetradecan-14-oic acid dihydrotrifluoroacetate (2.108)

The title compound was synthesized according to general procedure **A** (using 600 mg resin) yielding a fluffy white solid (90.0 mg, 28%): RP-HPLC: 96%, (t_R = 8.32, k = 1.77). ^{1}H NMR (300 MHz, D_2O) δ 7.26 – 7.08 (m, 4H), 4.92 – 4.87 (m, 1H), 4.75 – 4.68 (m, 1H), 4.36 – 4.21 (m, 2H), 4.14 – 4.04 (m, 1H), 4.04 – 3.98 (m, 1H), 3.64 – 3.47 (m, 1H), 3.20 – 3.05 (m, 2H), 2.95 – 2.71 (m, 2H), 2.68 – 2.31 (m, 2H), 2.26 (t, J = 7.2 Hz, 2H), 2.09 – 1.74 (m, 2H), 1.73 – 1.57 (m, 2H), 1.55 – 1.39 (m, 2H), 0.76 (s, 9H). HRMS (ESI-MS): m/z [M+H$^+$] calculated for $C_{29}H_{43}N_6O_9^+$: 619.3086, found 619.3088; $C_{29}H_{42}N_6O_9$ x $C_4H_2F_6O_4$ (846.73).

(3S,6S,9S,12S)-9-(2-Aminoethyl)-6-((S)-1-(benzyloxy)ethyl)-3-(3-carboxypropyl)-12-formyl-1-((S)-indolin-2-yl)-1,4,7,10-tetraoxo-2,5,8,11-tetraazatetradecan-14-oic acid dihydrotrifluoroacetate (2.109)

The title compound was synthesized according to general procedure **A** yielding a fluffy white solid (62.8 mg, 36%): RP-HPLC: 99%, (t_R = 10.17, k = 2.39). ^{1}H NMR (400 MHz, D_2O) δ 7.35 – 7.07 (m, 9H), 4.90 (d, J = 4.8 Hz, 1H), 4.85 – 4.77 (m, 1H), 4.47 (d, J = 11.5 Hz, 1H), 4.40 – 4.27 (m, 4H), 4.14 – 4.06 (m, 1H), 3.96 – 3.83 (m, 1H), 3.65 – 3.51 (m, 1H), 3.24 – 3.07 (m, 1H), 2.93 – 2.76 (m, 2H), 2.71 – 2.25 (m, 4H), 2.09 – 1.44 (m, 6H), 1.11 – 0.98 (m, 3H). HRMS (ESI-MS): m/z [M+H$^+$] calculated for $C_{34}H_{45}N_6O_{10}^+$: 697.3192, found 697.3195; $C_{34}H_{44}N_6O_{10}$ x $C_4H_2F_6O_4$ (924.80).

(9*S*,12*S*)-9-(2-Aminoethyl)-12-formyl-1-((*S*)-indolin-2-yl)-1,4,7,10-tetraoxo-2,5,8,11-tetraazatetradecan-14-oic acid dihydrotrifluoroacetate (2.110)
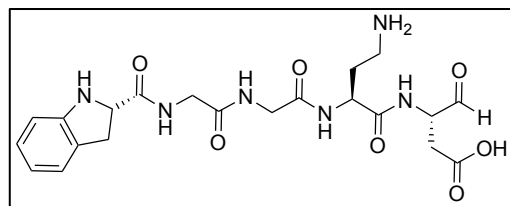
The title compound was synthesized according to general procedure **A** yielding a fluffy white solid (55.9 mg, 42%): RP-HPLC: 97%, (t_R = 5.79, k = 0.93). ^{1}H NMR (400 MHz, D_2O) δ 7.30 – 7.18 (m, 2H), 7.17 – 7.10 (m, 2H), 4.95 – 4.90 (m, 1H), 4.80 – 4.72 (m, 1H), 4.39 – 4.31 (m, 1H), 4.20 – 4.09 (m, 1H), 3.93 (s, 2H), 3.85 (s, 2H), 3.64 – 3.50 (m, 1H), 3.27 – 3.14 (m, 1H), 2.97 – 2.87 (m, 2H), 2.73 – 2.35 (m, 2H), 2.14 – 1.99 (m, 1H), 1.97 – 1.82 (m, 1H). HRMS (ESI-MS): *m/z* [M+H$^+$] calculated for $C_{21}H_{29}N_6O_7^+$: 477.2092, found 477.2096; $C_{21}H_{28}N_6O_7$ x $C_4H_2F_6O_4$ (704.54).

(*S*)-3-((*S*)-4-Amino-2-(5-((*S*)-indoline-2-carboxamido)pentanamido)butanamido)-4-oxobutanoic acid dihydrotrifluoroacetate (2.111)
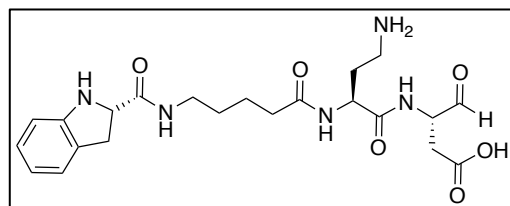
The title compound was synthesized according to general procedure **A** yielding a fluffy white solid (35.6 mg, 28%): RP-HPLC: 95%, (t_R = 6.41, k = 1.14). ^{1}H NMR (400 MHz, D_2O) δ 7.46 – 7.00 (m, 4H), 4.96 – 4.90 (m, 1H), 4.74 – 4.68 (m, 1H), 4.35 – 4.25 (m, 1H), 4.20 – 4.08 (m, 1H), 3.65 – 3.52 (m, 1H), 3.26 – 3.08 (m, 3H), 3.02 – 2.84 (m, 2H), 2.74 – 2.36 (m, 2H), 2.28 – 2.18 (m, 2H), 2.10 – 1.83 (m, 2H), 1.58 – 1.35 (m, 4H). HRMS (ESI-MS): *m/z* [M+H$^+$] calculated for $C_{22}H_{32}N_5O_6^+$: 462.2347, found 462.2348; $C_{22}H_{31}N_5O_6$ x $C_4H_2F_6O_4$ (689.57).

(*S*)-3-((*S*)-2-(((*S*)-Indoline-2-carbonyl)glycylglycyl)-6-methyl-1,2,3,4-tetrahydroisoquinoline-1-carboxamido)-4-oxobutanoic acid hydrotrifluoroacetate (2.112) *(Synthesized by Alexander Hubmann)*
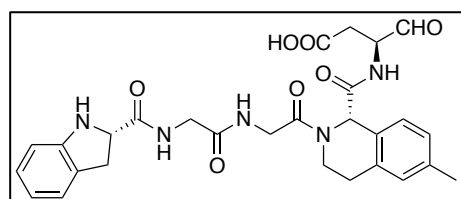
The title compound was synthesized according to general procedure **A** (using 150 mg resin) yielding a fluffy white solid (22 mg, 35%): RP-HPLC: 95%, (t_R = 12.82, k = 3.27). ^{1}H NMR (300 MHz, DMSO) δ 9.42 – 9.24 (m, 1H), 8.86 – 8.66 (m, 1H), 8.20 – 8.00 (m, 1H), 7.49 – 6.53 (m, 7H), 5.88 – 5.15 (m, 2H), 4.62 – 3.75 (m, 7H), 3.34 – 3.27 (m, 2H), 3.15 – 2.57 (m, 6H),

2.26 (s, 6H). HRMS (ESI-MS): *m/z* [M+H$^+$] calculated for C$_{28}$H$_{32}$N$_5$O$_7$$^+$: 550.2296, found 550.2292; C$_{28}$H$_{31}$N$_5$O$_7$ x C$_2$HF$_3$O$_2$ (663.61).

(*S*)-3-((*S*)-2-(5-((*S*)-Indoline-2-carboxamido)pentanoyl)-6-methyl-1,2,3,4-tetrahydroisoquinoline-1-carboxamido)-4-oxobutanoic acid hydrotrifluoroacetate (2.113) *(Synthesized by Alexander Hubmann)*

The title compound was synthesized according to general procedure **A** (using 150 mg resin) yielding a fluffy white solid (17 mg, 28%): RP-HPLC: 95%, (t$_R$ = 13.82, *k* = 3.61). ^{1}H NMR (300 MHz, DMSO) δ 9.30 (d, *J* = 10.6 Hz, 1H), 8.85 – 8.71 (m, 1H), 8.00 – 7.52 (m, 1H), 7.46 – 6.43 (m, 7H), 5.88 – 5.18 (m, 1H), 4.57 – 3.60 (m, 2H), 3.32 – 3.21 (m, 2H), 3.19 – 2.82 (m, 6H), 2.82 – 2.61 (m, 2H), 2.46 – 2.30 (m, 2H), 2.25 (s, 3H), 1.82 – 0.98 (m, 3H). HRMS (ESI-MS): *m/z* [M+H$^+$] calculated for C$_{29}$H$_{35}$N$_4$O$_6$$^+$: 535.2551, found 535.2548; C$_{29}$H$_{34}$N$_4$O$_6$ x C$_2$HF$_3$O$_2$ (648.64).
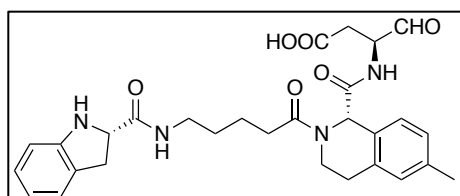
(3*S*,9*S*,12*S*)-9-(2-Aminoethyl)-3-(3-carboxypropyl)-12-formyl-1-((*S*)-indolin-2-yl)-1,4,7,10-tetraoxo-2,5,8,11-tetraazatetradecan-14-oic acid dihydrotrifluoroacetate (2.114)
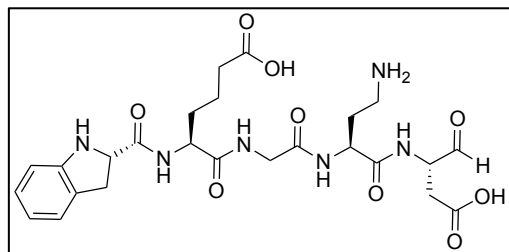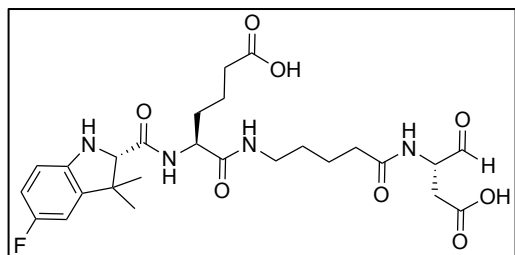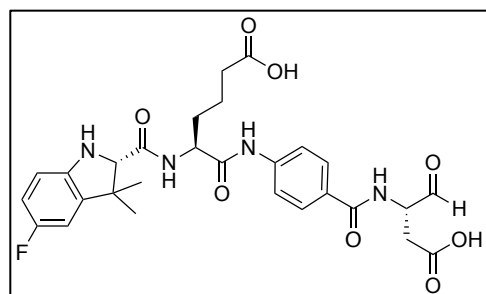

The title compound was synthesized according to general procedure **A** yielding a fluffy white solid (16.2 mg, 11%): RP-HPLC: > 99%, (t$_R$ = 6.67, *k* = 1.22). ^{1}H NMR (300 MHz, D$_2$O) δ 7.24 – 7.13 (m, 2H), 7.11 – 7.00 (m, 2H), 4.91 – 4.87 (m, 1H), 4.63 – 4.60 (m, 1H), 4.32 – 4.24 (m, 1H), 4.23 – 4.16 (m, 1H), 4.14 – 4.07 (m, 1H), 3.83 – 3.77 (m, 2H), 3.61 – 3.48 (m, 1H), 3.20 – 3.06 (m, 1H), 2.76 (t, *J* = 7.7 Hz, 2H), 2.68 – 2.33 (m, 2H), 2.27 (t, *J* = 7.2 Hz, 3H), 2.00 – 1.86 (m, 1H), 1.81 – 1.62 (m, 3H), 1.58 – 1.43 (m, 2H). HRMS (ESI-MS): *m/z* [M+H$^+$] calculated for C$_{25}$H$_{35}$N$_6$O$_9$$^+$: 563.2460, found 563.2464; C$_{25}$H$_{34}$N$_6$O$_9$ x C$_4$H$_2$F$_6$O$_4$ (790.63).

(S)-6-((2-((S)-1-(((S)-1-Carboxy-3-oxopropan-2-yl)carbamoyl)-6-methyl-3,4-dihydroisoquinolin-2(1H)-yl)-2-oxoethyl)amino)-5-((S)-indoline-2-carboxamido)-6-oxohexanoic acid hydrotrifluoroacetate (2.115) *(Synthesized by Alexander Hubmann)*
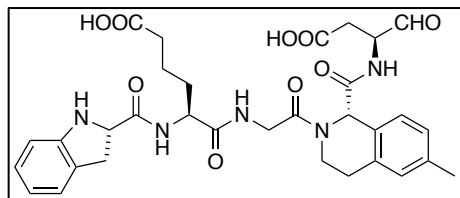
The title compound was synthesized according to general procedure **A** (using 150 mg resin) yielding a fluffy white solid (34 mg, 48%): RP-HPLC: > 99%, (t_R = 12.62, k = 3.21). ^{1}H NMR (300 MHz, DMSO-d$_6$) δ 9.46 – 9.20 (m, 1H), 9.12 – 8.75 (m, 1H), 8.40 – 8.18 (m, 1H), 8.00 – 7.84 (m, 1H), 7.47 – 7.24 (m, 1H), 7.20 – 6.90 (m, 5H), 6.84 – 6.51 (m, 2H), 5.99 – 5.21 (m, 2H), 4.50 – 4.21 (m, 2H), 3.39 – 3.23 (m, 1H), 3.10 – 2.65 (m, 4H), 2.38 – 1.98 (m, 7H), 1.86 – 1.16 (m, 6H). HRMS (ESI-MS): *m/z* [M+H$^+$] calculated for $C_{32}H_{38}N_5O_9^+$: 636.2591, found 636.2665; $C_{32}H_{37}N_5O_9$ x $C_2HF_3O_2$ (749.70).

(3S,12S)-3-(3-Carboxypropyl)-12-formyl-1-((S)-indolin-2-yl)-1,4,7,10-tetraoxo-2,5,8,11-tetraazatetradecan-14-oic acid dihydrotrifluoroacetate (2.116)
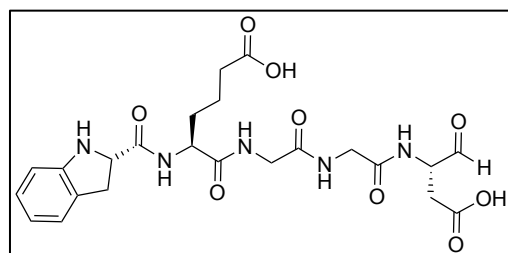
The title compound was synthesized according to general procedure **A** (using 600 mg resin) yielding a fluffy white solid (42.3 mg, 18%): RP-HPLC: 95%, (t_R = 8.17, k = 1.72). ^{1}H NMR (300 MHz, D$_2$O) δ 7.32 – 7.10 (m, 4H), 4.87 (d, *J* = 4.5 Hz, 1H), 4.84 – 4.74 (m, 1H), 4.28 – 4.17 (m, 1H), 4.11 – 4.02 (m, 1H), 3.92 – 3.45 (m, 5H), 3.28 – 3.14 (m, 1H), 2.63 – 2.32 (m, 2H), 2.28 (t, *J* = 7.2 Hz, 2H), 1.81 – 1.41 (m, 4H). HRMS (ESI-MS): *m/z* [M+H$^+$] calculated for $C_{23}H_{30}N_5O_9^+$: 520.2038, found 520.2045; $C_{23}H_{29}N_5O_9$ x $C_4H_2F_6O_4$ (633.53).

(3S,6S,12S)-3-(3-Carboxypropyl)-12-formyl-1-((S)-indolin-2-yl)-6-isopropyl-1,4,7,10-tetraoxo-2,5,8,11-tetraazatetradecan-14-oic acid hydrotrifluoroacetate (2.117)

The title compound was synthesized according to general procedure **A** (using 600 mg resin) yielding a fluffy white solid (39.3 mg, 16%): RP-HPLC: 95%, (t_R = 9.68, k = 2.23). ^{1}H NMR (300 MHz, D$_2$O) δ 7.35 – 7.18 (m, 4H), 4.89 (t, *J* = 4.6

Hz, 1H), 4.87 – 4.78 (m, 1H), 4.28 (t, J = 7.1 Hz, 1H), 4.17 – 4.06 (m, 1H), 3.99 – 3.73 (m, 3H), 3.70 – 3.57 (m, 1H), 3.31 – 3.13 (m, 1H), 2.69 – 2.33 (m, 2H), 2.29 (t, J = 7.1 Hz, 2H), 2.00 – 1.80 (m, 1H), 1.79 – 1.31 (m, 4H), 0.82 – 0.66 (m, 6H). HRMS (ESI-MS): m/z [M+H$^+$] calculated for $C_{26}H_{36}N_5O_9^+$: 562.2508, found 562.2518; $C_{26}H_{35}N_5O_9$ x $C_2HF_3O_2$ (675.62).

(*S*)-6-((5-(((*S*)-1-Carboxy-3-oxopropan-2-yl)amino)-5-oxopentyl)amino)-5-((*S*)-indoline-2-carboxamido)-6-oxohexanoic acid hydrotrifluoroacetate (2.118)
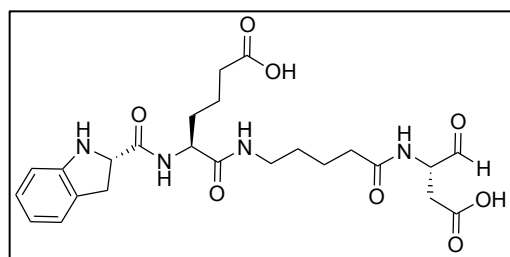
The title compound was synthesized according to general procedure **A** (using 600 mg resin) yielding a fluffy white solid (29.4 mg, 13%): RP-HPLC: > 99%, (t$_R$ = 8.74, k = 1.91). ^{1}H NMR (300 MHz, DMSO-d$_6$) δ 9.40 (d, J = 1.6 Hz, 1H), 8.90 – 8.23 (m, 1H), 8.11 – 7.89 (m, 1H), 7.82 – 7.34 (m, 1H), 7.24 – 6.57 (m, 3H), 6.24 – 5.24 (m, 1H), 4.84 – 4.47 (m, 1H), 4.42 – 4.27 (m, 2H), 3.52 – 2.61 (m, 6H), 2.38 – 1.29 (m, 12H). HRMS (ESI-MS): m/z [M+H$^+$] calculated for $C_{24}H_{33}N_4O_8^+$: 505.2293, found 505.2295; $C_{24}H_{32}N_4O_8$ x $C_2HF_3O_2$ (618.56).

(*S*)-6-((4-(((*S*)-1-Carboxy-3-oxopropan-2-yl)carbamoyl)phenyl)amino)-5-((*S*)-indoline-2-carboxamido)-6-oxohexanoic acid hydrotrifluoroacetate (2.119)
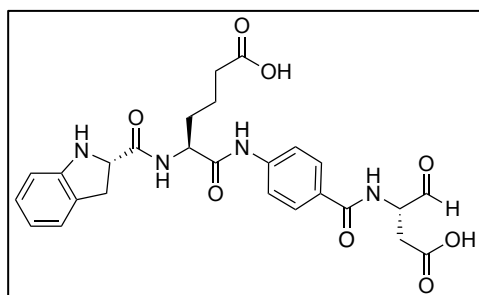
The title compound was synthesized according to general procedure **A** yielding a fluffy white solid (8.0 mg, 7%): RP-HPLC: 98%, (t$_R$ = 10.53, k = 2.51). ^{1}H NMR (300 MHz, DMSO-d$_6$) δ 10.39 (s, 1H), 9.51 (d, J = 1.3 Hz, 1H), 9.05 – 8.36 (m, 2H), 8.50 – 8.07 (m, 1H), 7.94 – 7.80 (m, 2H), 7.75 – 7.61 (m, 2H), 7.29 – 6.88 (m, 3H), 6.72 – 6.61 (m, 1H), 5.92 – 5.53 (m, 1H), 4.49 – 4.43 (m, 1H), 4.37 – 4.30 (m, 1H), 3.45 – 3.26 (m, 1H), 3.11 – 2.69 (m, 2H), 2.32 – 2.18 (m, 2H), 1.89 – 1.35 (m, 6H). HRMS (ESI-MS): m/z [M+H$^+$] calculated for $C_{26}H_{29}N_4O_8^+$: 525.1980, found 525.1984; $C_{26}H_{28}N_4O_8$ x $C_2HF_3O_2$ (638.55).

(3S,9S,12S)-9-(2-Aminoethyl)-3-(3-carboxypropyl)-1-((S)-5-fluoro-3,3-dimethylindolin-2-yl)-12-formyl-1,4,7,10-tetraoxo-2,5,8,11-tetraazatetradecan-14-oic acid dihydrotrifluoroacetate (2.120)
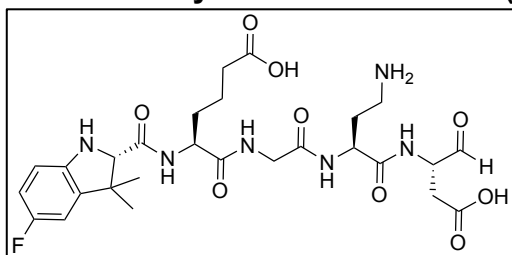
The title compound was synthesized according to general procedure **A** (using 600 mg resin) yielding a fluffy white solid (42.4 mg, 14%): RP-HPLC: 99%, (t_R = 9.28, k = 0.68). ^{1}H NMR (300 MHz, D_2O) δ 7.14 – 7.05 (m, 1H), 7.03 – 6.88 (m, 2H), 4.89 (d, J = 4.5 Hz, 1H), 4.39 – 4.25 (m, 3H), 4.18 – 4.05 (m, 1H), 3.81 (s, 2H), 2.94 – 2.78 (m, 2H), 2.69 – 2.33 (m, 2H), 2.28 (t, J = 7.1 Hz, 2H), 2.07 – 1.89 (m, 1H), 1.87 – 1.61 (m, 3H), 1.61 – 1.45 (m, 2H), 1.39 (s, 3H), 1.03 (s, 3H). HRMS (ESI-MS): m/z [M+H$^+$] calculated for $C_{27}H_{38}FN_6O_9^+$: 609.2679, found 609.2684; $C_{27}H_{37}FN_6O_9$ x $C_4H_2F_6O_4$ (836.67).

(3S,6S,9S,12S)-9-(2-Aminoethyl)-3-(3-carboxypropyl)-1-((S)-5-fluoro-3,3-dimethylindolin-2-yl)-12-formyl-6-isopropyl-1,4,7,10-tetraoxo-2,5,8,11-tetraazatetradecan-14-oic acid dihydrotrifluoroacetate (2.121)
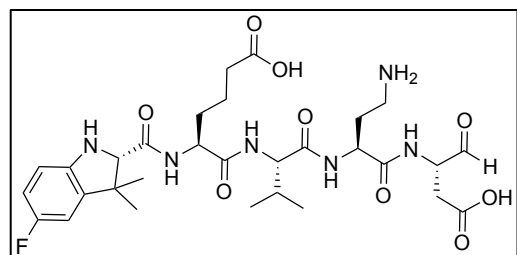
The title compound was synthesized according to general procedure **A** (using 600 mg resin) yielding a fluffy white solid (54.7 mg, 17%): RP-HPLC: 97%, (t_R = 9.95, k = 2.32). ^{1}H NMR (300 MHz, D_2O) δ 7.21 – 7.10 (m, 1H), 7.04 – 6.92 (m, 2H), 4.89 (t, J = 4.7 Hz, 1H), 4.43 – 4.24 (m, 3H), 4.14 – 4.04 (m, 1H), 3.98 – 3.89 (m, 1H), 2.97 – 2.81 (m, 2H), 2.70 – 2.32 (m, 2H), 2.27 (t, J = 7.2 Hz, 2H), 2.08 – 1.78 (m, 3H), 1.75 – 1.57 (m, 2H), 1.57 – 1.42 (m, 2H), 1.39 (s, 3H), 1.01 (s, 3H), 0.81 – 0.70 (m, 6H). HRMS (ESI-MS): m/z [M+H$^+$] calculated for $C_{30}H_{44}FN_6O_9^+$: 651.3148, found 651.3148; $C_{30}H_{43}FN_6O_9$ x $C_4H_2F_6O_4$ (878.75).

(3*S*,12*S*)-3-(3-Carboxypropyl)-1-((*S*)-5-fluoro-3,3-dimethylindolin-2-yl)-12-formyl-1,4,7,10-tetraoxo-2,5,8,11-tetraazatetradecan-14-oic acid hydrotrifluoroacetate (2.122)
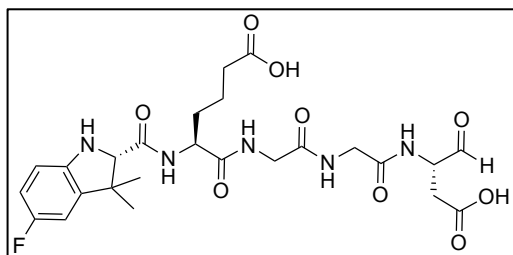
The title compound was synthesized according to general procedure **A** yielding a fluffy white solid (34.4 mg, 27%): RP-HPLC: 99%, (t_R = 11.28, k = 2.76). ^{1}H NMR (300 MHz, D$_2$O) δ 7.24 – 7.15 (m, 1H), 7.09 – 6.95 (m, 2H), 4.90 (d, J = 4.5 Hz, 1H), 4.48 – 4.42 (m, 1H), 4.33 (t, J = 6.7 Hz, 1H), 4.17 – 4.08 (m, 1H), 3.96 – 3.58 (m, 4H), 2.67 – 2.35 (m, 2H), 2.31 (t, J = 7.2 Hz, 2H), 1.83 – 1.66 (m, 2H), 1.67 – 1.50 (m, 2H), 1.46 – 1.40 (m, 3H), 1.05 (s, 3H). HRMS (ESI-MS): *m/z* [M+H$^+$] calculated for C$_{25}$H$_{33}$FN$_5$O$_9^+$: 566.2257, found 566.2259; C$_{25}$H$_{32}$FN$_5$O$_9$ x C$_2$HF$_3$O$_2$ (679.58).

(3*S*,6*S*,12*S*)-3-(3-Carboxypropyl)-1-((*S*)-5-fluoro-3,3-dimethylindolin-2-yl)-12-formyl-6-isopropyl-1,4,7,10-tetraoxo-2,5,8,11-tetraazatetradecan-14-oic acid hydrotrifluoroacetate (2.123)
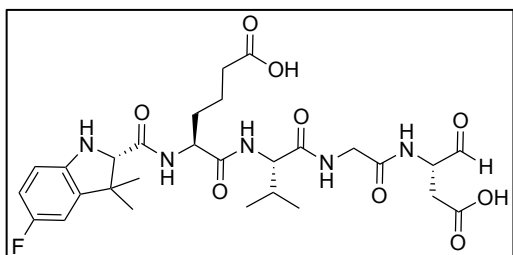
The title compound was synthesized according to general procedure **A** (using 150 mg resin) yielding a fluffy white solid (5.4 mg, 8%): RP-HPLC: 96%, (t_R = 12.51, k = 3.17). ^{1}H NMR (300 MHz, DMSO) δ 9.42 (d, J = 2.7 Hz, 1H), 8.48 – 7.92 (m, 2H), 7.86 – 7.74 (m, 1H), 6.96 – 6.85 (m, 1H), 6.84 – 6.72 (m, 1H), 6.62 – 6.53 (m, 1H), 5.51 – 5.43 (m, 1H), 4.57 – 4.41 (m, 1H), 4.16 – 4.03 (m, 2H), 3.88 (s, 2H), 3.73 – 3.67 (m, 1H), 2.17 (t, J = 7.3 Hz, 2H), 1.97 (s, 1H), 1.68 – 1.57 (m, 2H), 1.53 – 1.44 (m, 2H), 1.41 (s, 3H), 1.32 – 1.22 (m, 1H), 1.13 – 1.07 (m, 1H), 0.99 (s, 3H), 0.92 – 0.78 (m, 9H). HRMS (ESI-MS): *m/z* [M+H$^+$] calculated for C$_{28}$H$_{39}$FN$_5$O$_9^+$: 608.2726, found 608.2731; C$_{28}$H$_{38}$FN$_5$O$_9$ x C$_2$HF$_3$O$_2$ (721.66).

(S)-6-((5-(((S)-1-Carboxy-3-oxopropan-2-yl)amino)-5-oxopentyl)amino)-5-((S)-5-fluoro-3,3-dimethylindoline-2-carboxamido)-6-oxohexanoic acid hydrotrifluoroacetate (2.124)

The title compound was synthesized according to general procedure **A** yielding a fluffy white solid (5.3 mg, 4%): RP-HPLC: > 99%, (t_R = 12.02, k = 3.01). ^{1}H NMR (300 MHz, DMSO-d$_6$) δ 9.41 (s, 1H), 8.53 – 8.29 (m, 1H), 8.13 – 8.06 (m, 1H), 7.82 – 7.71 (m, 1H), 7.02 – 6.86 (m, 1H), 6.84 – 6.74 (m, 1H), 6.62 – 6.54 (m, 1H), 6.02 – 5.90 (m, 1H), 5.46 (d, J = 6.0 Hz, 1H), 4.38 – 4.27 (m, 1H), 4.12 – 4.04 (m, 1H), 3.87 (d, J = 3.6 Hz, 1H), 2.22 – 2.04 (m, 6H), 1.69 – 1.52 (m, 3H), 1.47 – 1.36 (m, 8H), 1.29 (s, 1H), 1.11 (s, 1H), 0.98 (s, 3H). HRMS (ESI-MS): m/z [M+H$^+$] calculated for $C_{26}H_{36}FN_4O_8^+$: 551.2512, found 551.2512; $C_{26}H_{35}FN_4O_8$ x $C_2HF_3O_2$ (664.61).

(S)-6-((4-(((S)-1-Carboxy-3-oxopropan-2-yl)carbamoyl)phenyl)amino)-5-((S)-5-fluoro-3,3-dimethylindoline-2-carboxamido)-6-oxohexanoic acid hydrotrifluoroacetate (2.125)

The title compound was synthesized according to general procedure **A** yielding a fluffy white solid (4.6 mg, 4%): RP-HPLC: 96%, (t_R = 13.64, k = 3.55). ^{1}H NMR (300 MHz, DMSO-d$_6$) δ 10.45 – 10.34 (m, 1H), 9.52 (s, 1H), 9.05 – 8.69 (m, 1H), 8.56 – 8.40 (m, 1H), 7.97 (d, J = 8.1 Hz, 1H), 7.90 – 7.81 (m, 2H), 7.74 – 7.62 (m, 2H), 6.98 – 6.89 (m, 1H), 6.86 – 6.75 (m, 1H), 6.69 – 6.59 (m, 1H), 5.95 – 5.53 (m, 1H), 4.62 – 4.51 (m, 1H), 4.40 – 4.24 (m, 1H), 3.95 (s, 1H), 2.23 (t, J = 7.2 Hz, 2H), 1.82 – 1.67 (m, 2H), 1.61 – 1.46 (m, 2H), 1.43 (s, 3H), 1.32 (s, 1H), 1.13 (s, 1H), 1.03 (s, 3H). HRMS (ESI-MS): m/z [M+H$^+$] calculated for $C_{28}H_{32}FN_4O_8^+$: 571.2203, found 571.2199; $C_{28}H_{31}FN_4O_8$ x $C_2HF_3O_2$ (684.60).

(3S,6S,9S,12S)-9-(2-Aminoethyl)-6-((S)-1-(benzyloxy)ethyl)-3-(3-carboxypropyl)-12-formyl-1-(1H-indol-2-yl)-1,4,7,10-tetraoxo-2,5,8,11-tetraazatetradecan-14-oic acid dihydrotrifluoroacetate (2.126)
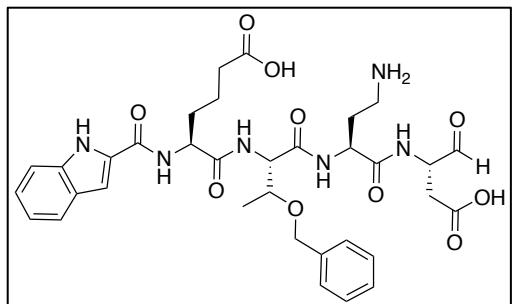
2.126 was obtained by isolating the degradation product of **2.109** by preparative HPLC yielding a fluffy white solid (3.2 mg). RP-HPLC: 96%, (t_R = 11.22, k = 2.74). HRMS (ESI-MS): m/z [M+H$^+$] calculated for $C_{34}H_{43}N_6O_{10}^+$: 695.3035, found 695.3035; $C_{34}H_{42}N_6O_{10}$ x $C_4H_2F_6O_4$ (922.79).

2.6.1.5 Preparation and Analytical Data for Fmoc Protected 6-Bromo-tetrahydroisoquinoline-1-carboxylic Acid and 6-Methyl-tetrahydroisoquinoline-1-carboxylic Acid

(R)-2-(((9H-Fluoren-9-yl)methoxy)carbonyl)-6-methyl-1,2,3,4 tetrahydroisoquinoline-1-carboxylic acid (2.089)
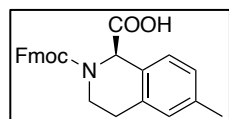
A mixture of enantiopure (R)-6-methyl-1,2,3,4-tetrahydroisoquinoline-1-carboxylic acid (P1) (100 mg, 0.523 mmol) was dissolved in 10% aqueous (aq.) Na_2CO_3 (5 mL). Fmoc-OSu (176 mg, 0.53 mmol) in THF (5 mL) was added dropwise to the mixture. After completion 10 mL water was added to the solution and stirring was continued overnight at room temperature. The reaction progress was monitored by TLC (R_f = 0.85, DCM/MeOH 90/10). The mixture was cooled to 0 °C and acidified to pH 3 by addition of aq. HCl (1N) and was extracted with ethyl acetate (50 mL x 3). The combined organic layers were dried over Na_2SO_4 and evaporated, yielding a white solid (210 mg, 97%). ^{1}H NMR (300 MHz, CDCl$_3$) δ 10.87 (s, 1H), 7.85 – 7.56 (m, 4H), 7.53 – 7.22 (m, 5H), 7.13 – 6.92 (m, 2H), 5.81 – 5.36 (m, 1H), 4.66 – 4.41 (m, 2H), 4.39 – 4.21 (m, 1H), 4.00 – 3.70 (m, 2H), 3.08 – 2.74 (m, 2H), 2.34 (s, 3H). ^{13}C NMR (75 MHz, CDCl$_3$) δ 176.21 (d, J = 8.6 Hz), 156.10 (d, J = 43.5 Hz), 144.03, 143.96, 143.86, 143.76, 141.97 – 141.11 (m), 138.07 (d, J = 2.3 Hz), 135.25, 135.01, 129.13 (d, J = 21.2 Hz), 128.26 (d, J = 17.1 Hz), 127.82 (d, J = 6.3 Hz), 127.21 (d, J = 3.9 Hz), 125.19 (d, J = 7.9 Hz), 124.97, 120.11, 68.17, 57.85 (d, J = 18.8 Hz), 47.25 (d, J = 2.2 Hz), 40.85 (d, J = 17.7

Hz), 28.39 (d, J = 25.0 Hz), 21.14. HRMS (ESI-MS): m/z [M+H$^+$] calculated for $C_{26}H_{24}NO_4^+$: 414.1700, found 414.1707; $C_{26}H_{23}NO_4$ (413.47).

(*S*)-2-(((9*H*-Fluoren-9-yl)methoxy)carbonyl)-6-methyl-1,2,3,4 tetrahydroisoquinoline-1-carboxylic acid (2.090)
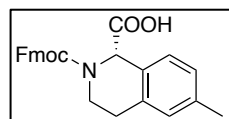
A mixture of enantiopure (*S*)-6-methyl-1,2,3,4-tetrahydroisoquinoline-1-carboxylic acid (P2) (200 mg, 1.046 mmol) was dissolved in 10% aqueous (aq.) Na$_2$CO$_3$ (10 mL). Fmoc-OSu (352 mg, 1.046 mmol) in THF (10 mL) was added dropwise to the mixture. After completion 15 mL water was added to the solution and stirring was continued overnight at room temperature. The reaction progress was monitored by TLC (R$_f$= 0.85, DCM/MeOH 90/10). The mixture was cooled to 0 °C and acidified to pH 3 by addition of aq. HCl (1N) and was extracted with ethyl acetate (50 mL x 3). The combined organic layers were dried over Na$_2$SO$_4$ and evaporated, yielding a white solid (430 mg, 99%). ^{1}H NMR (300 MHz, CDCl$_3$) δ 9.83 (s, 1H), 7.92 – 7.56 (m, 4H), 7.52 – 7.20 (m, 5H), 7.17 – 6.96 (m, 2H), 5.78 – 5.35 (m, 1H), 4.69 – 4.43 (m, 2H), 4.39 – 4.19 (m, 1H), 4.01 – 3.71 (m, 2H), 3.13 – 2.75 (m, 2H), 2.36 (s, 3H). ^{13}C NMR (75 MHz, CDCl$_3$) δ 176.25 (d, J = 12.5 Hz), 156.06 (d, J = 46.1 Hz), 144.05, 143.96, 143.88, 143.77, 141.42, 138.07, 135.26, 135.02, 129.14 (d, J = 21.7 Hz), 128.27 (d, J = 17.3 Hz), 127.82 (d, J = 6.2 Hz), 127.21 (d, J = 4.0 Hz), 125.20 (d, J = 8.1 Hz), 125.00, 120.11, 68.14, 57.85 (d, J = 20.6 Hz), 47.26, 40.84 (d, J = 19.9 Hz), 28.42 (d, J = 25.8 Hz), 21.22. HRMS (ESI-MS): m/z [M+H$^+$] calculated for $C_{26}H_{24}NO_4^+$: 414.1700, found 414.1710; $C_{26}H_{23}NO_4$ (413.47).

(*R*)-2-(((9*H*-Fluoren-9-yl)methoxy)carbonyl)-6-bromo-1,2,3,4-tetrahydroisoquinoline-1-carboxylic acid (2.091)
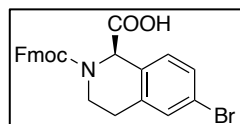
A mixture of enantiopure (*R*)-6-bromo-1,2,3,4-tetrahydroisoquinoline-1-carboxylic acid (P2) (268 mg, 1.046 mmol) was dissolved in 10% aqueous (aq.) Na$_2$CO$_3$ (10 mL). Fmoc-OSu (352 mg, 1.046 mmol) in THF (10 mL) was added dropwise to the mixture. After completion 15 mL water was added to the solution and stirring was continued overnight at room temperature. The reaction progress was monitored by TLC (R$_f$= 0.85, DCM/MeOH 90/10). The mixture was cooled to 0 °C and acidified to pH 3 by addition of aq. HCl (1N) and was extracted with ethyl acetate (50 mL x 3). The combined organic

layers were dried over Na_2SO_4 and evaporated, yielding a white solid (390 mg, 78%). ^{1}H NMR (300 MHz, $CDCl_3$) δ 10.42 (s, 1H), 7.92 – 7.10 (m, 11H), 5.69 – 5.39 (m, 1H), 4.62 – 4.34 (m, 2H), 4.30 – 4.15 (m, 1H), 4.07 – 3.79 (m, 2H), 3.09 – 2.62 (m, 2H). ^{13}C NMR (75 MHz, $CDCl_3$) δ 172.51 (d, J = 13.5 Hz), 154.75 (d, J = 41.9 Hz), 142.92, 142.67, 140.21, 136.36, 136.07, 130.21 (d, J = 23.7 Hz), 128.87 (d, J = 25.6 Hz), 126.72, 126.08, 124.52, 124.02 (d, J = 6.1 Hz), 120.63, 118.98, 66.87, 56.65 (d, J = 18.3 Hz), 46.14 (d, J = 12.0 Hz), 39.09 (d, J = 26.8 Hz), 29.33. HRMS (ESI-MS): m/z [M+H^{+}] calculated for $C_{25}H_{21}BrNO_4^+$: 478.0648, found 478.0657; $C_{25}H_{20}BrNO_4$ (478.34).

(S)-2-(((9H-Fluoren-9-yl)methoxy)carbonyl)-6-bromo-1,2,3,4-tetrahydroisoquinoline-1-carboxylic acid (2.092)
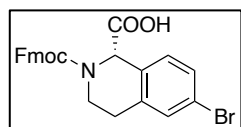
A mixture of enantiopure (S)-6-bromo-1,2,3,4-tetrahydroisoquinoline-1-carboxylic acid (P1) (134 mg, 0.523 mmol) was dissolved in 10% aqueous (aq.) Na_2CO_3 (5 mL). Fmoc-OSu (176 mg, 0.523 mmol) in THF (5 mL) was added dropwise to the mixture. After completion 10 mL water was added to the solution and stirring was continued overnight at room temperature. The reaction progress was monitored by TLC (R_f= 0.85, DCM/MeOH 90/10). The mixture was cooled to 0 °C and acidified to pH 3 by addition of aq. HCl (1N) and was extracted with ethyl acetate (50 mL x 3). The combined organic layers were dried over Na_2SO_4 and evaporated, yielding a white solid (240 mg, 96%). ^{1}H NMR (300 MHz, $CDCl_3$) δ 9.93 (s, 1H), 7.83 – 7.23 (m, 11H), 5.75 – 5.24 (m, 1H), 4.66 – 4.39 (m, 2H), 4.36 – 4.16 (m, 1H), 4.01 – 3.63 (m, 2H), 3.00 – 2.70 (m, 2H). ^{13}C NMR (75 MHz, $CDCl_3$) δ 175.11 (d, J = 13.4 Hz), 155.91 (d, J = 51.3 Hz), 143.91, 143.83, 143.71, 143.59, 141.38, 137.53, 137.25, 131.43 (d, J = 20.7 Hz), 130.08 (d, J = 13.4 Hz), 127.85 (d, J = 6.2 Hz), 127.21 (d, J = 5.5 Hz), 125.11 (d, J = 7.0 Hz), 124.90 (d, J = 6.5 Hz), 122.17, 120.14, 68.27, 57.47 (d, J = 17.3 Hz), 47.18, 40.25 (d, J = 24.8 Hz), 28.21 (d, J = 24.3 Hz). HRMS (ESI-MS): m/z [M+H^{+}] calculated for $C_{25}H_{21}BrNO_4^+$: 478.0648, found 478.0657; $C_{25}H_{20}BrNO_4$ (478.34).

2.6.1.6 Preparation and Analytical Data for Compound 2.098

((*S*)-2-((*S*)-1-(((9*H*-Fluoren-9-yl)methoxy)carbonyl)indoline-2-carboxamido)-6-(*tert*- butoxy)-6-oxohexanoyl)-L-valine (2.103) (*Synthesized by Gurpreet Singh*)
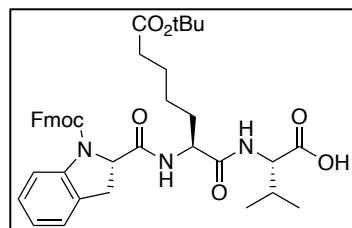
Step 1. Loading of Fmoc-Val-OH on resin: To 1g of 2-chlorotrityl chloride resin in a polyprep column 50 mL of CH_2Cl_2 was added. After 0.5 h the solvent was pushed out from the column under nitrogen flow. A solution of Fmoc-Val-OH (225 mg, 0.66 mmol) and 2,4,6-collidine (1.0 mL, 7.56 mmol) in 25 mL of CH_2Cl_2 was transferred to the resin. The mixture was rocked for 3 h at room temperature. The solvent was pushed out under nitrogen flow and the resin was washed with CH_2Cl_2 (3 x 50 mL). Then the resin was treated with a capping solution of CH_2Cl_2/MeOH/DIPEA (40 mL/4 mL/2 mL) for 1 h and the solvent was pushed out under nitrogen flow. The resin was washed with CH_2Cl_2 (3 x 50 mL) and DMF (3 x 50 mL).

Step 2. Fmoc deprotection: The resin from step 1 was treated with piperidine (30 mL, 20% in DMF) for 0.5 h. The solvent was pushed out under nitrogen flow and the resin was washed with DMF (3 x 50 mL).

Step 3. Coupling of Fmoc-hGlu-OH: A solution of Fmoc-hGlu-OH (308 mg, 0.70 mmol), HATU (266 mg, 0.70 mmol), and collidine (0.20 mL, 1.5 mmol) in CH_2Cl_2 (25 mL) was added. The reaction was rocked for 3 h at rt. The solvent was pushed out under nitrogen flow and Fmoc deprotection was carried out as described in Step 2. Fmoc-Idc-OH was coupled as described in Step 3 to complete the tripeptide sequence. The resin was sequentially washed with DMF, CH_2Cl_2, DMF, CH_2Cl_2 (3 x 50 mL). The peptide was cleaved from the resin by treating with 20% HFIP/CH_2Cl_2 solution for 2 h. The peptide solution was collected under nitrogen flow, evaporated, and subjected to purification by preparative HPLC. The product was obtained as an amorphous powder (210 mg, 0.307 mmol) after lyophilization of the pure fractions. MS (ESI) *m/z* [M+H$^+$] 684.4. ^{1}H NMR (400 MHz, CDCl$_3$) δ 7.62 (dd, *J* = 7.6, 3.9 Hz, 2H), 7.45 (t, *J* = 8.4 Hz, 2H), 7.25 (m, 2H), 7.21 – 7.08 (m, 4H), 6.93 (d, *J* = 7.4 Hz, 1H), 6.78 (m, 1H), 5.61 (m, 2H), 4.75 (dd, *J* = 11.1, 4.3 Hz, 1H), 4.65 – 4.01 (m, 4H), 3.54 – 3.13 (m, 1H), 3.02 (d, *J* = 16.1 Hz, 1H), 2.00 (m, 2H), 1.60 (m, 1H), 1.22 (s, 9H), 1.15 – 1.09 (m, 1H), 0.80 – 0.69 (m, 6H).

Benzyl(*S*)-3-cyano-3-((*S*)-6-methyl-1,2,3,4-tetrahydroisoquinoline-1-carboxamido)propanoate (2.105) (*Synthesized by Gurpreet Singh*)
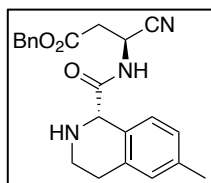
To a vigorously stirring phosphoric acid (5 mL, 85%), a solution of compound **2.104**[146] (402 mg, 1.32 mmol) in dichloromethane (2 mL) was added dropwise at rt. After 3 h stirring at rt, the reaction mixture was cooled to 0 °C in ice-bath and neutralized using sat. aq. NaHCO$_3$ solution. The resulting aqueous mixture was extracted with ethyl acetate (20 mL x 4) and collected over anhyd. Na$_2$SO$_4$. Filtration followed by concentration under reduced pressure gave the unprotected amine that was utilized for the next step without further purification. To a solution of **2.090** (275 mg, 0.66 mmol), HATU (250 mg, 0.66 mmol), and 2,4,6-collidine (0.26 mL, 1.98 mmol) in anhydrous acetonitrile (10 mL) at 0 °C was added a solution of the crude amine (in 5 mL acetonitrile) prepared above and the reaction mixture was stirred at room temperature for 4 h. The reaction was concentrated under reduced pressure, diluted with water (20 mL), and extracted with ethyl acetate (4 x 20 mL). The combined organic layer was sequentially washed with sat. aq. NaHCO$_3$ (20 mL), ice-cold 10% aq. KHSO$_4$ (20 mL), and brine (20 mL). The organic layer was collected over anhydrous sodium sulfate, filtered, and concentrated under reduced pressure to obtain the crude amide. The crude product was dissolved in acetonitrile (10 mL) and diethyl amine (5 mL) was added. The reaction mixture was stirred at rt for 3 h then concentrated under reduced pressure. The crude residue was triturated with hexane and the hexane layer was decanted. The residue was purified by silica gel flash chromatography (eluent 1% aq. NH$_3$ in 10% MeOH/DCM) to obtain amine **2.105** as light-yellow solid (110 mg, 44% yield). MS (ESI) *m/z* [M+H$^+$] 378.2. ^{1}H NMR (400 MHz, CDCl$_3$) δ 8.39 (d, *J* = 9.1 Hz, 1H), 7.37 (qd, *J* = 7.0, 3.8 Hz, 7H), 7.01 (dd, *J* = 8.0, 1.9 Hz, 1H), 6.91 (s, 1H), 5.21 (dt, *J* = 9.0, 5.3 Hz, 1H), 5.15 (s, 2H), 4.57 (s, 1H), 3.08 – 2.90 (m, 3H), 2.88 (d, *J* = 5.1 Hz, 1H), 2.80 (d, *J* = 5.7 Hz, 1H), 2.72 (ddd, *J* = 25.5, 13.9, 8.1 Hz, 3H), 2.31 (s, 3H).

(*S*)-6-(((*S*)-1-((*S*)-1-(((*S*)-2-Carboxy-1-cyanoethyl)carbamoyl)-6-methyl-3,4-dihydroisoquinolin-2(1*H*)-yl)-3-methyl-1-oxobutan-2-yl)amino)-5-((*S*)-indoline-2-carboxamido)-6-oxohexanoic acid (2.106) *(Synthesized by Gurpreet Singh)*
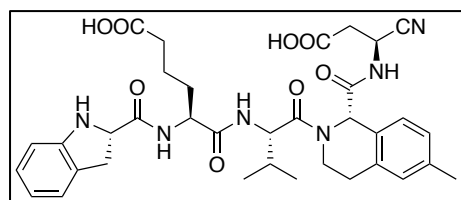
To a solution of tripeptide carboxylic acid **2.103** (267 mg, 0.39 mmol) in 5 mL of acetonitrile were added HATU (102 mg, 0.39), 2,4,6-collidine (1.56 mmol, 0.21 mL), and **2.105** (100 mg, 0.26 mmol). The reaction mixture was stirred at rt. for 6 h, and the solvent was evaporated. The crude residue was diluted with water (20 mL) and extracted with ethyl acetate (4 × 20 mL). The combined organic layer was sequentially washed with sat. aq. $NaHCO_3$ (20 mL), ice-cold 10% aq. $KHSO_4$ (20 mL), and brine (20 mL). The organic layer was collected over anhyd. Na_2SO_4, filtered, and concentrated under reduced pressure to obtain the crude peptide. The crude residue was dissolved in a minimum volume of dichloromethane (3 mL) and transferred to vigorously stirring phosphoric acid (85%, 3 mL). The completion of the reaction was monitored by UPLC-MS. The reaction mixture was diluted with water (5 mL) and extracted with ethyl acetate (4 × 10 mL). The organic layer was dried over anhyd. Na_2SO_4, filtered, and concentrated to obtain the crude carboxylic acid. The crude product was dissolved in acetonitrile (10 mL), and diethyl amine (3 mL) was added to it. The reaction mixture was stirred at rt. for 3 h and was concentrated under reduced pressure. The crude residue was triturated sequentially with hexane, diethyl ether, and the solvent decanted. The residue was dried under reduced pressure and dissolved in dimethylformamide (DMF, 3 mL). Palladium (10%, 10 mg) was added, and the reaction mixture was purged with hydrogen gas for 5 min and stirred under hydrogen (1 atm). The completion of the reaction was monitored by UPLC-MS. The reaction mixture was filtered over a thin layer of celite. The celite layer was washed with 2 mL of DMF. The solvent was evaporated, and the residue was purified by preparative HPLC. Lyophilization of the pure fractions provided the product 1 as a colorless amorphous powder (38 mg, 22% yield). RP-HPLC: 99%. ^{1}H NMR (400 MHz, CD_3OD) δ 9.02−8.72 (m, 0.5H), 8.43 (m, 0.7H), 8.13 (m, 1H), 7.64−7.29 (m, 1H), 7.25−6.43 (m, 7H), 5.58 (s, 0.6H), 5.40 (s, 0.4H), 4.63−4.15 (m, 3H), 4.07−3.83 (m, 1H), 3.81−3.61 (m, 1H), 3.60−3.3 (m, 1H), 3.13−2.45 (m, 5H), 2.38− 1.96 (m, 5H), 1.95−1.08 (m, 5H), 0.99−0.67 (m, 5H), 0.55 (d, *J* = 6.8 Hz 1H). HRMS (ESI) *m/z* [M+H$^+$] calculated for $C_{35}H_{43}N_6O_8^+$: 675.3137, found 675.3145.; $C_{35}H_{42}N_6O_8$ (674.76).

2.6.2 Biology

2.6.2.1 Fluorometric Enzyme Assay

384-well protocol:

Compound affinity for caspases were measured in fluorometric assays. Casp2, cpCasp2, and Casp3 were produced in house as described below. Human recombinant Casp1, 6, 7, and 9 were purchased from BioVision (Milpitas/CA, USA). AFC fluorogenic substrates and control peptides (AcYVAD-CHO, AcVDVAD-CHO, AcDEVD-CHO, AcVEID-CHO, and AcLEHD-CHO) were purchased from Bachem (Torrance/CA, USA). K_m values were determined experimentally to be the following: Casp1: 5.9 µM; Casp2: 37.1 µM; cpCasp2: 89.2 µM; Casp3: 7.6 µM; Casp6: 43.1 µM; Casp7: 13.8 µM; Casp9: 149.1 µM. Enzymes were diluted in buffer: 100 mM MES (pH 6.5) for Casp2 and cpCasp2 or 100 mM HEPES (pH 7.0) for all other caspases, plus 150 mM NaCl, 0.1% CHAPS, 1.5% sucrose, 10 mM DTT. Enzyme concentrations were 0.05 U/well for Casp1, 6, and 7; 0.5 U/well for Casp9, 20 nM/well for Casp2 and cpCasp2; and 2 nM/well for Casp3. Enzyme in buffer (19 µL) was added per well in a black 384-well Corning 4514 assay plate. Test compounds were serially diluted in dimethyl sulfoxide (DMSO) and plated in duplicate into a Corning 3656 transfer plate. Test compound was added to assay plates in 0.5 µL aliquots per well and mixed 10 times using a BiomekFX (Beckman Coulter). Compound and enzyme mixture was incubated at 37 °C for 5 min for reversible inhibitors. The BiomekFX was then used to add and mix 0.5 µL of the AFC substrate in DMSO from a Corning 3656 transfer plate (final assay concentrations: 5 µM AcYVAD-AFC for Casp1, 10 µM Z-VDVAD-AFC for Casp2 and cpCasp2, 5 µM AcDEVD-AFC for Casp3, 5 µM Z-VEID-AFC for Casp6, 5 µM AcDEVD-AFC for Casp7, and 34 µM AcLEHD-AFC for Casp9) to the assay plate for a total assay volume of 20 µL. Fluorescence from free AFC was read at 37 °C every 5 min over an hour using a CLARIOstar (BMG Labtech) plate reader (λ_{ex} = 400 nm, λ_{em} = 505 nm). The 40 minute time point was reported, consistent with reported literature.[92,98,99,147]

96-well protocol (Casp2/3):

Compound affinity for caspases were measured in fluorometric assays. Casp2, cpCasp2, and Casp3 were produced in house as described below. AFC fluorogenic substrates Z-VDVAD-AFC and AcDEVD-AFC and control peptides AcVDVAD-CHO and AcDEVD-CHO were purchased from Bachem (Torrance/CA, USA). Enzyme was diluted in buffer: 100 mM MES (pH 6.5) for Casp2 and cpCasp2 or 100 mM HEPES (pH 7.0) for Casp3, plus 150 mM NaCl, 0.1% CHAPS, 1.5% sucrose, and 10 mM DTT. Enzyme concentrations were 5 nM/well for Casp2 and cpCasp2; and 2 nM/well for Casp3. Enzyme in buffer (96.5 µL) was added per well in a black Corning 3356 96-well assay plate. Test compounds were serially diluted in dimethyl sulfoxide (DMSO) and plated in triplicate in a Corning 3357 transfer plate. Test compound was added to assay plates in 1 µL aliquots per well and mixed 10 times using a BiomekFX (Beckman Coulter). Compound and enzyme mixture was incubated at 37 °C for 5 min. The BiomekFX was then used to add and mix 2.5 µL of the AFC substrate in DMSO from a transfer plate (final assay concentrations: 25 µM Z-VDVAD-AFC for Casp2 and cpCasp2, 10 µM AcDEVD-AFC for Casp3) to the assay plate for a total assay volume of 100 µL in the assay plate. Fluorescence from free AFC was read at 37 °C every 5 min over an hour using a CLARIOstar (BMG Labtech) plate reader (λ_{ex} = 400 nm, λ_{em} = 505 nm). The 40 minute time point was reported, consistent with reported literature.[92,98,99,147]

Expression and purification of recombinant caspase-2 and tau

The pET23b vector encoding human caspase-2 was a gift from Prof. Dr. Michelle Arkin at University of California, San Francisco.[30] The htau0N4R-pET28a plasmid[51] was used as the initial template that encodes wild-type human microtubule-associated protein tau N4R isoform (containing four microtubule-binding domains but no amino-terminal inserts) ORF. Primers used to generate tau mutations were listed in Table 2.16. The DNA sequences of tau mutants were verified by classic Sanger sequencing analyses. Briefly, the Casp2 plasmid was transformed into *E. coli* Lemo21 DE3 cells with 2 mM rhamnose that were cultured at 1 L scale in shake flasks at 37 °C. When the culture reached an OD_{600} = 0.3, incubation temperature was reduced to 28 °C. When the OD_{600} reached 0.6-0.8, protein expression was induced with 0.1 mM IPTG

and allowed to shake at 250 RPM and 28 °C overnight. 16 hours post induction, cells were harvested through centrifugation (5000 RPM for 20 min at 4 °C), lysed by French press (2 passes at 1000 psi), and centrifuged again for 30 min at 20000 RPM at 4 °C. Supernatant was resuspended in buffer (100 mM Tris pH 8.0, 100 mM NaCl, 20 mM imidazole). Purification was performed on a Cytiva ÅKTA Pure system (Marlborough, MA) by nickel-affinity chromatography on a HisTrap FF crude column (Cytiva) followed by ion-exchange chromatography on a HiTrap Q FF column (Cytiva). Protein was diluted to 0.5 mg/mL, and stored at -80 °C in 100 mM MES (pH 6.5), 150 mM NaCl, 0.1% CHAPS, 1.5% sucrose, and 10 mM DTT. Typical yield for the expression, isolation, and purification was approximately 0.1 mg/L. Expression of recombinant Casp2 and tau proteins was induced using 150 µM isopropyl-β-D-thiogalactopyranoside (IPTG) (Promega, Madison, WI) in the BL21(DE3) *E. coli* strain (MilliporeSigma) at 16 °C for 14 h while shaking at 250 rpm. Cells were then harvested via centrifugation at 6,000 *g*, 4 °C for 15 min, followed by lysis via sonication. Proteins were initially purified using HisPur Ni-NTA resin (Thermo Fisher Scientific, Waltham, MA) followed by metal chelating chromatography (5 mL HiTrap Chelating HP columns (GE Healthcare Life Sciences, Piscataway, NJ)). Further purification was carried out using either anion exchange chromatography (5 mL HiTrap Q HP columns (GE Healthcare Life Sciences)) for Casp2 or cation exchange chromatography (5 mL HiTrap SP HP columns (GE Healthcare Life Sciences)) for tau. Proteins were stored in 1X phosphate-buffered saline (pH 7.4) at 10 mg/mL (concentration determined using a BCA assay (Thermo Fisher Scientific)), -80 °C until further use.

Expression and purification of circularly permutated caspase-2 (cpCasp2)

A circularly permuted caspase-2 (cpCasp2) based on modifications to Casp2 (UniProt P42575) suggested by Cserjan-Puschmann et al. (2020)[148] was expressed. The gene encoding 6H-Casp2$_{334-452}$-GS-Casp2$_{170-333}$ with a D$_{347}$ → A$_{347}$ mutation was inserted into a pET30a(+) vector (GenScript, Piscataway, NJ, USA) using NdeI and EcoRV restriction sites. The transformation into Lemo21 cells was performed as recommended by the vendor (New England Biolabs, Ipswich, MA, USA) and the plates were incubated overnight at 37 °C. A single colony was picked for primary culture using a sterile tip, added to sterile Luria Broth (LB) media containing antibiotics, and incubated overnight at 37 °C and 270 rpm. The primary culture was then diluted 1:100

into 1 L shake flasks containing sterile LB and the proper antibiotics. The liter cultures were incubated at 37 °C and 270 rpm and the OD was monitored until it reached between 0.6-0.8. Once the desired OD was reached, the cells were induced overnight with 0.1 mM IPTG at 28 °C and 270 rpm. After induction, the cells were harvested through centrifugation at 5,000 g for 20 min. Typical yield was about a 3.5 g cell pellet per liter. The pellets were stored at -20 °C until purification.

The pellets were resuspended in lysis buffer (Buffer A with 2.5 μM Leupeptin, 5 μM Pepstatin, 0.5 μM DNase, 1 mM PMSF, and 10 mM $MgCl_2$) and lysed through sonification. The lysate was clarified through centrifugation at 20,000 g for 30 min. The supernatant was filtered through a 0.45 μm filter before it was purified on a BioRad Biologic DuoFlow Chromatography System. For nickel affinity chromatography a 5 mL HisTrap FF column was equilibrated with 100% Buffer A (100 mM Tris, pH 8.0, 100 mM NaCl, 20 mM imidazole). A gradient of Buffer B (100 mM Tris, pH 8.0, 100 mM NaCl, 400 mM imidazole) was then applied from 0-50% to wash and elute the protein. cpCasp2 was eluted at about 20% Buffer B. Final purification was achieved on a Hi-Trap Q anion exchange column in 25 mM Tris, pH 8.0 utilizing a gradient of 0-1 M NaCl. cpCasp2 was eluted at about 150 mM NaCl. Final yield was 8-10 mg of cpCasp2 per liter. After adding 10% glycerol the protein was stored at -80 °C.

Expression and purification of recombinant caspase-3

The pET23b vector encoding human Casp3 was a gift from Prof. Dr. Michelle Arkin at University of California, San Francisco. Expression and purification of Casp3 was guided by previously described protocols.[149] Briefly, the plasmid was transformed into *E. coli* BL21 pLyss DE3 cells that were cultured at 1 L scale in shake flasks flasks at 37 °C. When the culture reached an OD_{600} = 0.3, incubation temperature was reduced to 30 C. When the OD_{600} reached 0.6-0.8, protein expression was induced with 0.2 mM IPTG. Three hours post induction, cells were harvested through centrifugation (5000 RPM for 30 min at 4 °C), lysed by sonication, and centrifuged again for 30 min at 20000 RPM at 4 °C. Supernatant was resuspended in buffer (100 mM Tris pH 8.0, 100 mM NaCl, 20 mM imidazole). Purification was performed on a Cytiva ÅKTA Pure system (Marlborough, MA) by nickel-affinity chromatography on a HisTrap FF crude column (Cytiva) followed by ion-exchange chromatography on a HiTrap Q FF column (Cytiva).

Protein was diluted to 0.5 mg/mL, and stored at -80 °C in100 mM HEPES (pH 7.0), 150 mM NaCl, 0.1% CHAPS, 1.5% sucrose, and 10 mM DTT. Typical yield for the expression, isolation, and purification was approximately 3 mg/L.

2.6.2.2 Analyzing Recombinant Tau Mutants in an *In vitro* Caspase-2-catalyzed Tau Cleavage Assay

Procedure

Purified recombinant Casp2 (final concentration: 1 nM) was incubated with purified recombinant tau (molar ratio = 1:1) at 37 °C water bath in 1X reaction buffer (25 mM 4-(2-hydroxyethyl)-1-piperazineethanesulfonic acid (HEPES), 0.1% (w/v) 3-[(3-cholamidopropyl)dimethylammonio]-1-propanesulfonate (CHAPS), 10 mM dithiothreitol (DTT), pH 7.5). Twenty µL of sample was transferred at designated time (i.e., 0, 5, 30, 60, 120, and 240 min after the reaction started) and the reaction was immediately stopped by adding Laemmli sample buffer (Bio-Rad, Hercules, CA) followed by boiling at 95 °C for 5 min.

Western blotting (WB)

The reaction samples were size-fractionated on 10% Criterion Tris-HCl Precast gels (Bio-Rad, Hercules, CA), and electrophoretically transferred onto 0.2 µm nitrocellulose membranes at a constant current of 0.4 A for 4 h at 4 °C. Membranes were first blocked using 5% (w/v) bovine serum albumin (BSA) blocking buffer (BSA dissolved in 1X phosphate-buffered saline, 0.1% (v/v) polyoxyethylene (20) sorbitan monolaurate (Tween 20), pH 7.4) at room temperature for 1 h, and then incubated with mouse monoclonal antibody tau-13 (directed against amino acids 15-25 of human tau; 1:30,000; BioLegend, San Diego, CA; Cat #835201; RRID: AB_2565341) at 4 °C overnight. Following 5 min washes with wash buffer (10 mM Tris-HCl, pH 7.4; 200 mM NaCl; 0.1% (v/v) Tween 20)) at room temperature five times, membranes were incubated at room temperature in goat-anti-mouse immunoglobulin G-conjugated horseradish peroxidase (HRP) (Thermo Fisher Scientific; diluted in wash buffer) for 1 h. Membranes were then washed again as described above. Western blots were developed using the West Pico electrochemiluminescence detection system (Thermo

Fisher Scientific). Densitometry-based quantification of the ~35 kDa cleavage product was performed using Optiquant (Packard Cyclone, Perkin-Elmer Life Sciences Inc., Boston, MA). The levels of proteins were determined from two independent experiments.

2.6.2.3 Analyzing Inhibitory Compounds in an *In vitro* Caspase-2-catalyzed Tau Cleavage Assay

In vitro caspase-2-catalyzed tau cleavage assay

Purified recombinant Casp2 (final concentration during pre-incubation: 67 µM) was pre-incubated with various concentrations of inhibitory compounds at 4 °C for 72 h. Pre-treated enzyme was then incubated with purified recombinant tau at a molar ratio of 1:1 in 37 °C water bath, 1x reaction buffer (25 mM 4-(2-hydroxyethyl)-1-piperazineethanesulfonic acid (HEPES), 0.1% (w/v) 3-[(3-cholamidopropyl)dimethylammonio]-1-propanesulfonate (CHAPS), 10 mM dithiothreitol (DTT), pH 7.5) for 7 h. The final volume of each reaction was 100 µL. At the end of the 7-h incubation, 0.1% (v/v) protease inhibitor cocktail (MilliporeSigma) was added to stop the reactions.

Immunoprecipitation (IP) / Western blotting (WB)

Immediately after the reaction was stopped, the 100 µL enzyme-product mixture was diluted in 400 µL IP buffer (50 mM Tris-HCl (pH 7.4) and 150 mM NaCl, containing 0.1 mM phenylmethylsulfonyl fluoride, 0.2 mM 1,10-phenanthroline monohydrate, and protease inhibitor cocktail (MilliporeSigma)), and then incubated with 10 µg of Δtau314-specific monoclonal antibody 4F3 and 50 µL of Protein G Sepharose 4 Fast Flow resin (GE Healthcare) at 4 °C for 14–16 h. Subsequent resin wash and protein elution were performed as described previously.[74] WB was performed according to a previously published protocol.[73]

Preparation of samples for mass spectrometry

Purified recombinant tau (1 mg) were incubated with purified recombinant caspase-2 at a molar ratio of 1:1 under the conditions described in the "*In vitro* caspase-2-catalyzed tau cleavage assay" section. The resulting material was diluted in an IP buffer (final volume: 1 mL) and incubated overnight at 4 °C with 4F3-bound Protein G-coupled magnetic beads. Following resin wash and protein elution, the immunocaptured proteins were size-fractionated, and the gel area containing proteins of interest was isolated using a protocol previously described.[150] The 4F3 antibody was covalently linked to Protein G magnetic beads as previously described.[73]

Mass spectrometry (MS)

In-gel trypsin digestion, liquid chromatography-MS/MS, mass spectral database search, and data interpretation were performed as previously described[150], except that Peaks Studio Xpro (Bioinformatics Solutions, Inc, Waterloo, Ontario, Canada) was used for interpretation of mass spectra (cf. Figure 2.039).
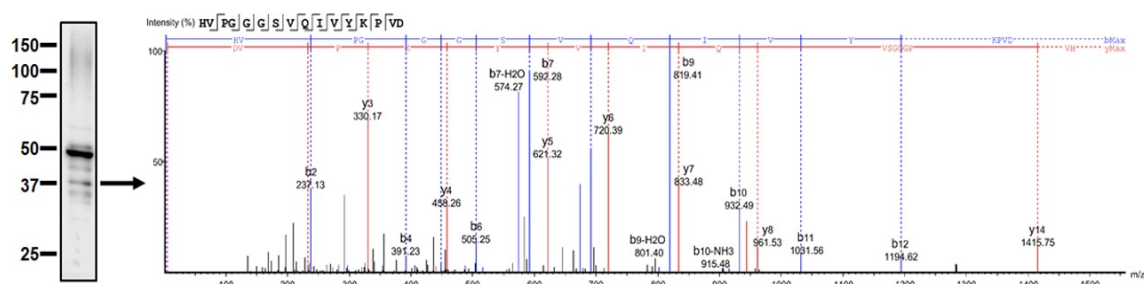
Figure 2.039. Mass spectrometry (MS) analysis confirmed the identity of a ~37-kDa tau cleavage product as Δtau314. A representative Western blot (WB) of Casp2-cleaved tau proteins immunoprecipitated by the Δtau314-specific 4F3 antibody was probed using biotin-conjugated pan-tau antibody tau-5 (tau-5-biotin). Liquid chromatography-MS/MS analysis identified the presence of Δtau314 in the ~37 kDa product as indicated by a representative MS spectrum of its trypsinized signature peptide at the C-terminus.

Expression and purification of recombinant caspase-2 and tau

The DNA sequences encoding human caspase-2 p19 and p12 subunits were cloned as two separate open reading frames in the pCOLADuet-1 vector (MilliporeSigma, Burlington, MA). The DNA sequence encoding human microtubule–associated protein tau 0N4R isoform was cloned in the pET28a vector (MilliporeSigma). Expression of recombinant human caspase-2 and tau was induced using 150 µM isopropyl-β-D-thiogalactopyranoside (IPTG) (Promega, Madison, WI) in the BL21(DE3) *E. coli* strain (MilliporeSigma) at room temperature for 16 h while shaking at 250 rpm. Cells were then harvested via centrifugation at 6,000 *g*, 4 °C for 15 min, followed by lysis via sonication. Proteins were purified using HisPur Ni-NTA resin (Thermo Fisher Scientific, Waltham, MA) followed by HiTrap Chelating HP columns (GE Healthcare Life Sciences, Piscataway, NJ). Proteins were stored in 1x phosphate-buffered saline (pH 7.4) at 10 mg/mL (determined using a BCA assay (Thermo Fisher Scientific)), -80 °C until further use.

2.6.2.4 Plasmids and PCR Mutagenesis

For cultured hippocampal neuron studies human tau and DsRed constructs were expressed in the pRK5 vector and driven by the cytomegalovirus promoter (Clontech Inc.). Human tau proteins were N-terminally fused to enhance GFP (eGFP). The wild-type, native human tau construct encoded human four-repeat tau lacking the transcriptional- variant N-terminal sequences (0N4R) and contained exons 1, 4, 5, 7, 9–13, 14, and intron 13 (RRID: Addgene_46904). The P301S mutant was created using site-directed mutagenesis (QuikChange SDM Kit, Agilent). PCR primers with lengths of 31 and 28 nucleotides were used for mutagenesis (sense: 5'-GCCGCCTCCCGaGACGTGTTTGATATTATCC-3'; antisense: 5'-TATCAAACACGTCtCGGGAGGCGGCAGT-3'; mutated nucleotide represented as lower case letter) (Integrated DNA Technologies). The nucleotide mutation as well as plasmid construct integrity were confirmed with Sanger Sequencing (UMN Genomics Center). Tau sequence numbering was based on the longest functional human isoform: 441-tau (2N4R tau; NCBI reference sequence: NP_005901.2).

2.6.2.5 Primary Hippocampal Neuron Cultures

Briefly, a 22 mm diameter glass coverslip (0.09 mm thickness) was silicone-sealant-fastened to the bottom of a 35 mm culture dish with a bored hole of 20 mm in diameter and sterilized as previously described. Coverslips were coated with poly-D-lysine. Hippocampi were dissected from neonatal Sprague-Dawley timed-pregnancy rats (Envigo) or appropriate transgenic mice and control littermates at post-natal day 0-1. Hippocampi were enzymatically digested in Earle's Balanced Salt Solution (EBSS) supplemented with 1% glucose and cysteine-activated papain. Digestion was blocked with dilute BSA (bovine serum albumin) and chicken ovomucoid, and cells were rinsed in fresh EBSS and plated in plating medium (minimal essential medium with Earle's salts, 10% fetal bovine serum, 5% horse serum, 2 mM glutamine, 10 mM sodium pyruvate, 0.6% glucose, 100 U/mL penicillin and 100 mg/mL streptomycin) at 1×10^6 cells/dish. After 18 h cell adherence was established. Cells were then grown in a neurobasal medium (a 1:5 mixture of NbActiv4 to NbActiv1; BrainBits LLC) and incubated at 37 °C in a 5% CO_2 biological incubator.

2.6.2.6 Low Efficiency Calcium-phosphate Transfection

At 5–7 days *in vitro* (DIV) cells were transfected. DNA plasmid transfection was performed using standard calcium phosphate precipitation and incubation as previously described.[73] Briefly, neurons were transfected with human tau constructs and DsRed (2:1 by plasmid DNA mass) for live imaging, and with human tau alone for electrophysiology and immunocytochemistry. Precipitated DNA was applied to cells in a solution of NbActiv4 neurobasal medium containing 100 µM AP5 ((2*R*)-amino-5-phosphovaleric acid) to prevent calcium-induced excitotoxicity. After 3–4 h of transfection time, cells were rinsed in a glial conditioned medium and grown in the neurobasal medium as described above until mature (21–28 DIV).

2.6.2.7 Electrophysiology

Miniature excitatory postsynaptic currents (mEPSCs) were recorded from cultured dissociated mouse hippocampal neurons at 17-21 DIV with a glass pipette (resistance

~ 5 MΩ) at holding potentials of –65 mV on an Axopatch 200B amplifier (output gain = 0.5; filtered at 1 kHz) as previously described by Miller et al (2014)[113]. Input and series resistances were assessed and found to have no significant difference before and after recording time (5–20 mins). Recording sweeps lasted 200 ms and were sampled for every 1 s (pClamp, v10, RRID:SCR_011323). Neurons were bathed in bubble-oxygenated artificial cerebrospinal fluid (ACSF) at 23 °C with 100 µM APV (NMDA receptor antagonist), 1 µM TTX (sodium channel blocker), and 100 µM picrotoxin (GABA$_A$ receptor antagonist). Passive oxygen perfusion was established with medical-grade 95% O_2–5% CO_2. ACSF contained (in mM) 119 NaCl, 2.5 KCl, 5.0 $CaCl_2$, 2.5 $MgCl_2$, 26.2 $NaHCO_3$, 1 NaH_2PO_4, and 11 D-glucose. The internal solution of the glass pipettes contained (in mM) 100 cesium gluconate, 0.2 EGTA, 0.5 $MgCl_2$, 2 ATP, 0.3 GTP, and 40 HEPES. The pH of the internal solution was normalized to 7.2 with cesium hydroxide and diluted to a trace osmotic deficit in comparison to ACSF (~300 mOsm). All analysis of recordings was performed using an automated detection software suit (Clampfit, 11.0.3, Molecular Devices, San Jose, CA, USA). Minimum analysis parameters were set at greater than 1 min stable recording time and events with amplitudes greater than 3 pA and smaller than 40 pA were included. A mEPSC event was identified by using a template which included a distinct fast-rising depolarization and slow-decaying repolarization. Combined individual events were used to form relative cumulative frequency curves; whereas the means of all events from individual recordings were treated as single samples for further statistical analysis. Example traces were exported from Clampfit and live-traced, simplified, and united in vector editing software (Adobe Illustrator CS5 and Affinity Designer).

2.6.3 Computational Chemistry

Molecular Modeling

Covalent docking studies were performed using the "Covalent Docking (CovDock)" module within the Schrödinger small-molecule drug discovery software suite (Schrödinger, LLC, New York, NY, Version 2021.3 unless otherwise noted. The crystal structures of Casp2 (PDBid: 1pyo) and Casp3 (PDBid: 3edq) were prepared using the module "Protein Preparation Wizard" in Maestro with the default protein parameters. Hydrogen atoms were added and water molecules that were beyond 5 Å from

heterocyclic groups were deleted. The covalently bound ligands AcLDESD-CHO:1pyo, AcLDESD-CHO:3edq where D-CHO represents "aspartic acid aldehyde" were included in the protein structures during their preparation for the covalent docking. In the experiments below, the protein structures prepared in this fashion are denoted by PP:PDBid, e.g., PP:1pyo. Hydrogen bonds were optimized, the partial charges were assigned, and the protein structure was energy-minimized using OPLS3e force field.[151] Following this preparation, the covalent bond connecting the ligand to the protein was broken and the now-separated aldehyde (reactive functional group) and cysteine (nucleophilic reaction group) were reconstituted by adjusting bond orders, adding hydrogens, and minimizing these groups in place. This free ligand (the "Workspace Ligand") was employed to create the covalent docking grid used in the covalent docking and scoring (*vide infra*). The individual target receptors were set up using the following reactive cysteine residues (A:155, 1pyo; A:163, 3edq). The "Reaction Type" SMARTS string {[H]C=O} was built as a customized nucleophilic addition to a double bond. The "Box Center" for the docking grid was set using the "Centroid of (the) Workspace Ligand". Docking was performed in the "Pose Prediction (Thorough)" mode. A "Minimization radius" of 3.0 Å was used, "Perform MM-GBSA scoring" was selected, and three (3) "Output poses per ligand reaction site" were selected (only the lowest energy pose is reported). Ligands for covalent docking experiments were drawn with ChemDraw, imported into Maestro as sdf, and refined into 3D structures using the "Ligand Preparation" module and its default parameters. These 3D structures, with the appropriate tautomers and charges, were directly used in "Covalent Docking" experiments and are designated as PL:ligand name, e.g., PL:AcLDESD-CHO. "Cdock Affinity" is reported in kcal/mol. Five starting points for cdock affinity prediction were created by the following protocol. These are structures **1-5** (state number) in Figure 2.040. (**1**) Standard input as described above; (**2**) Prime (module in the Schrödinger small-molecule drug discovery software suite) minimization of state **1**; (**3-5**) states selected from 433 states generated by searching of the conformational space of e.g., AcVDVAD-CHO with a 10 kcal/mol energy window (**3** = lowest energy state, **4** = middle energy state, and **5** = highest energy state).
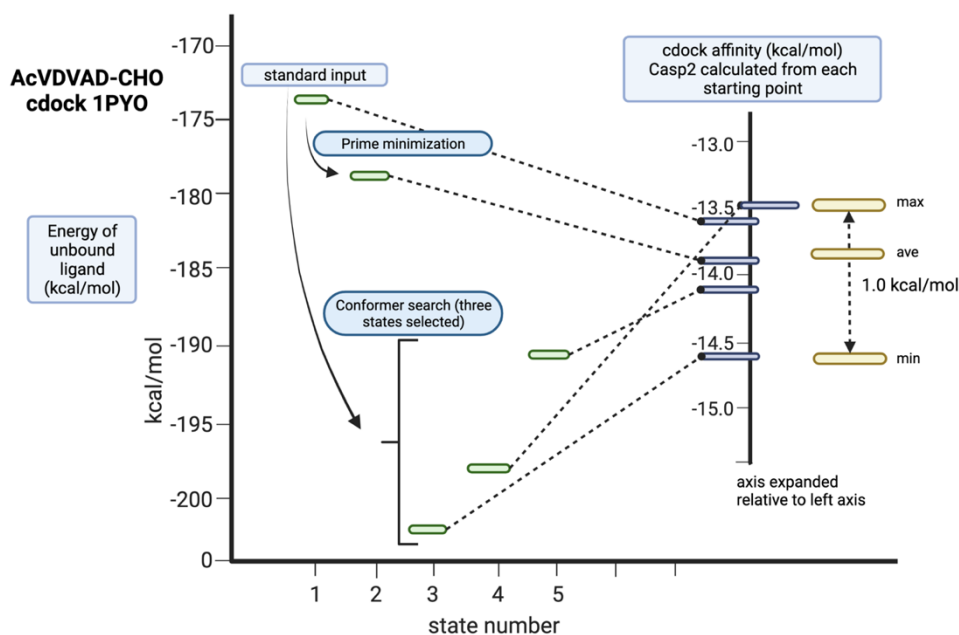
Figure 2.040. Cdock affinities (right axis (kcal/mol)) resulting from the docking of five different conformations of AcVDVAD-CHO (energies on left axis (kcal/mol)) with PDBid: 1pyo. Energies on the left axis calculated with Prime using the OPLS4 forcefield. Energies on the right axis calculated using Glide and the Covalent Docking module in Maestro (Schrödinger, 2021.3).

2.6.4 Crystallography

The preparation of Casp3 co-crystal structures with covalently bound inhibitors followed previously utilized protocols.[117,152] 500 mL of Casp3 at 0.5 mg/mL was incubated with 500 mM inhibitor for 30 min on ice prior to being concentrated to 4 mg/mL for crystallization. Crystals were grown by hanging-drop vapor diffusion in which 1 mL (protein) +1 mL (well solution) drops were suspended over either 15% PEG 6000, 5% glycerol (v:v), 100 mM sodium citrate pH 5.3, 10 mM DTT, and 30 mM NaN_3, or 16% PEG 6000, 5% glycerol, 100 mM sodium citrate pH 6.5, and 10 mM DTT. Plate-like crystals grew within 24-48 h and were cryoprotected with well solution supplemented with 10% PEG 6000 prior to flash freezing. Diffraction data were collected at IMCA-CAT beamline 17-ID at the Advanced Photon Source (APS), Argonne, Illinois, USA. The collection was completed at 100 K using radiation of wavelength 1.00 Ångstroms and a Dectris Eiger2 9M detector. Data were processed using *autoProc* and scaled using *aP_scale*.[153] All structures were solved using molecular replacement as implemented in *Phenix*.[154] The Casp3 structure with bound AcVDVAD-CHO, PDBid: 2h65, served as a search model. Iterative rounds of refinement and model building were conducted using *Phenix* and *Coot*.[155] Summary

data collection and refinement statistics for each of the structures are given in Table 2.08, 2.12, and 2.13.

2.6.5 Data Analysis

Statistical analyses were performed using GraphPad Prism version 8 (GraphPad Software, La Jolla, CA). GraphPad Prism version 9 was used to calculate the IC_{50} by fitting the dose-response data with four parameter variable slope nonlinear regression. These were transformed into pK_i values using the Cheng−Prusoff equation.[156] Since the compounds are covalent reversible inhibitors, they were characterized using pK_i values and not "k_{inact} / K_i", as would be necessary for covalent irreversible inhibitors. P < 0.05 was considered statistically significant. See legends of Tables 2.06, 2.07, 2.10, and 2.11 and Figures 2.013, 2.022, 2.023, and 2.024 for detailed statistical methods.

2.7 Supplementary Material

2.7.1 NMR Spectra of Peptides 2.008-2.015, 2.017-2.100, and 2.107-2.125
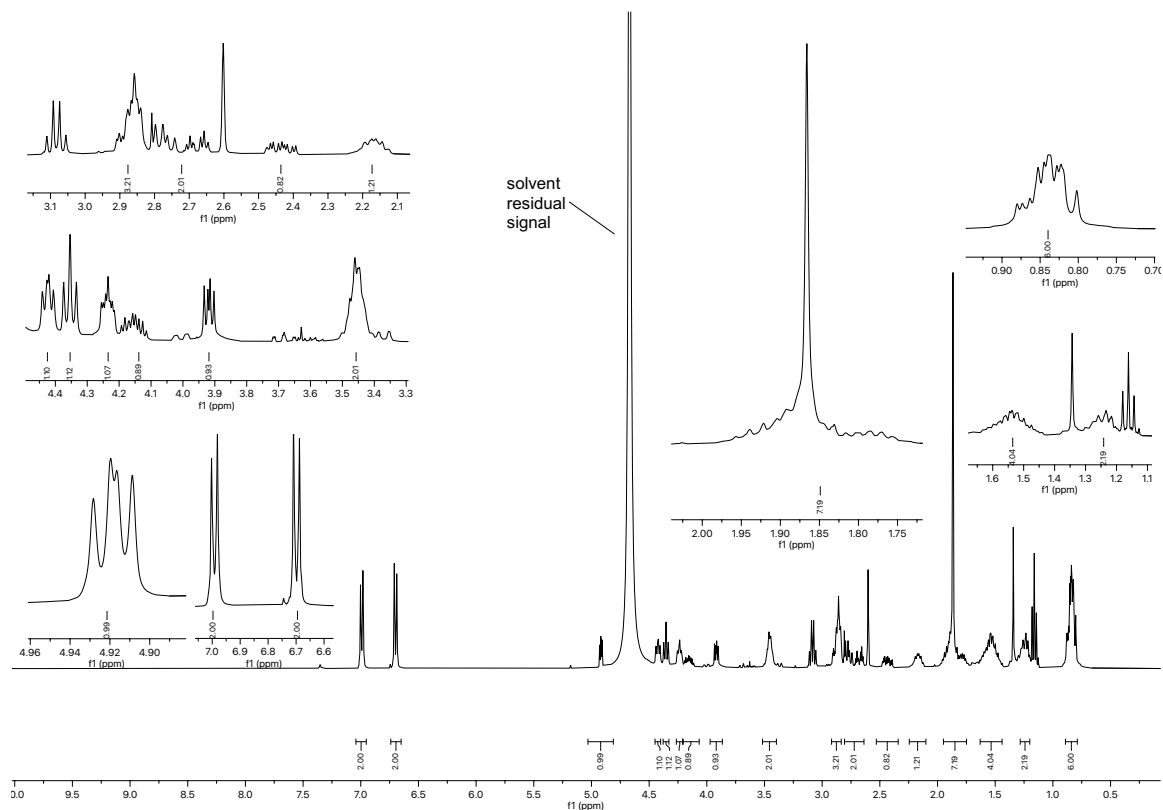
Figure 2.041. ^{1}H NMR spectrum (400 MHz, D$_2$O) of compound **2.008**.
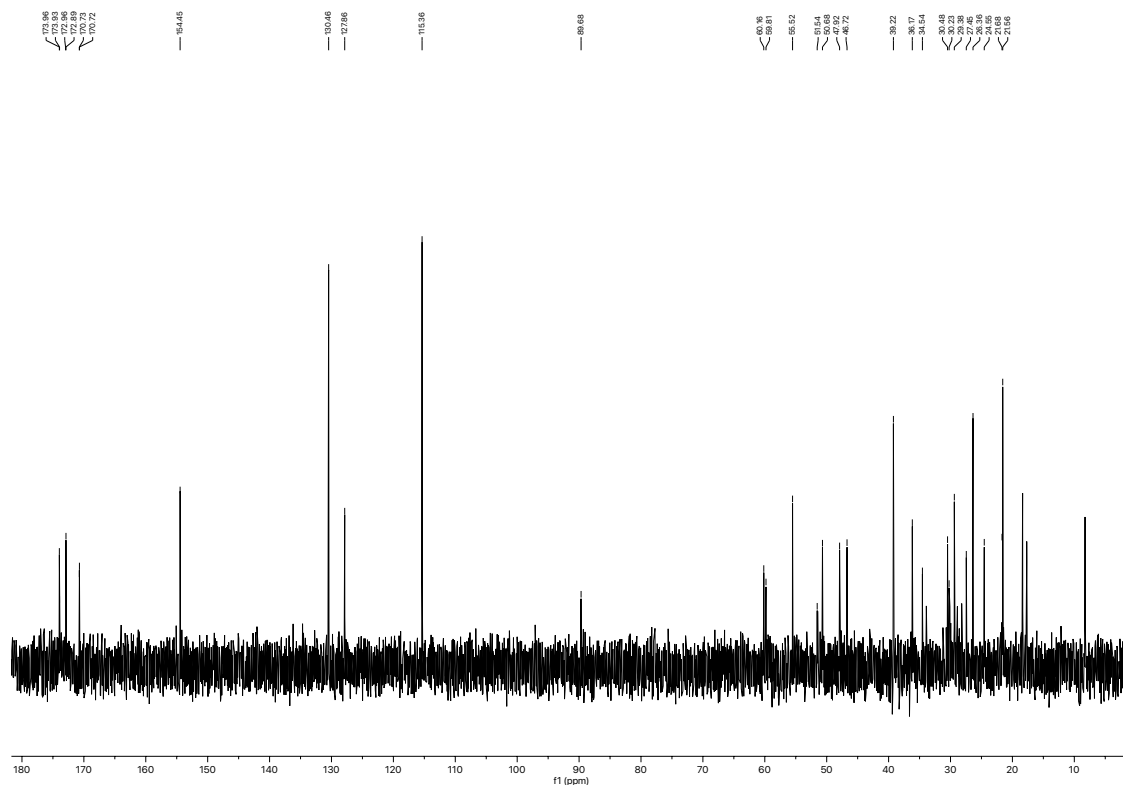
Figure 2.042. ^{13}C NMR spectrum (101 MHz, D$_2$O) of compound **2.008**.
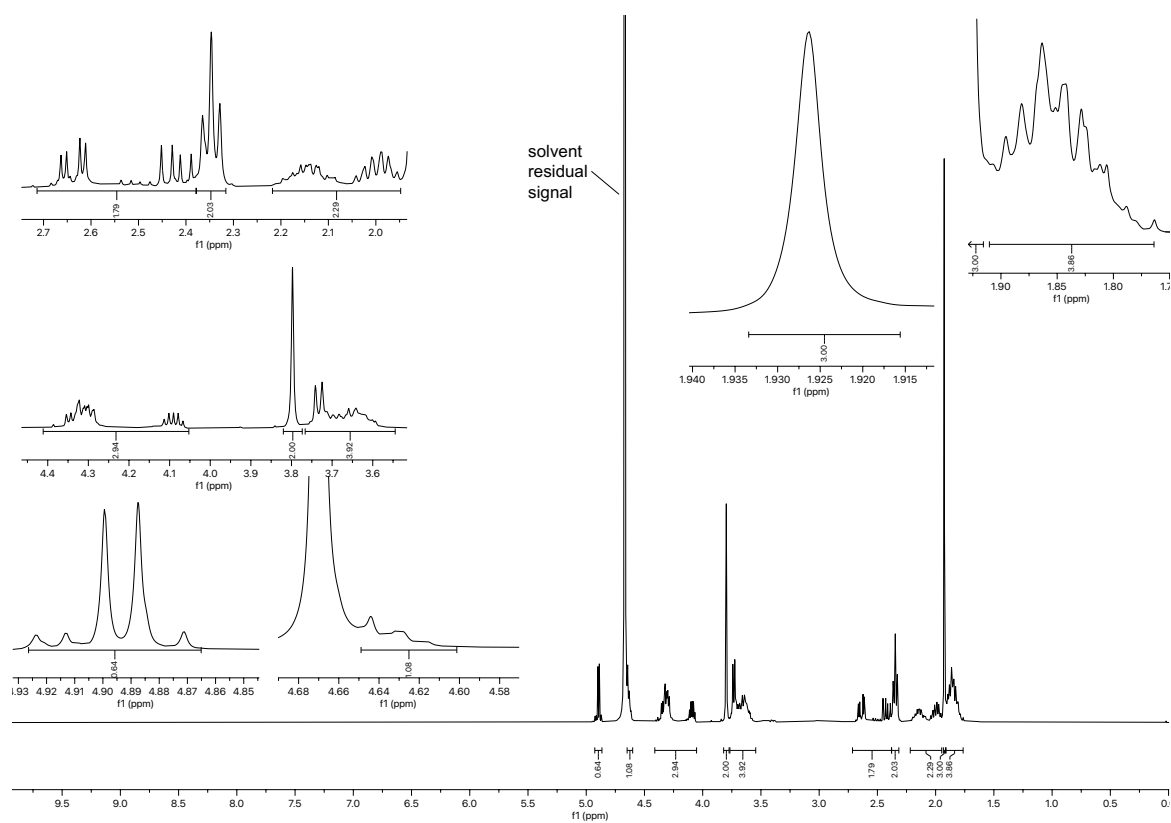
Figure 2.043. ^{1}H NMR spectrum (400 MHz, D$_2$O) of compound **2.009**.
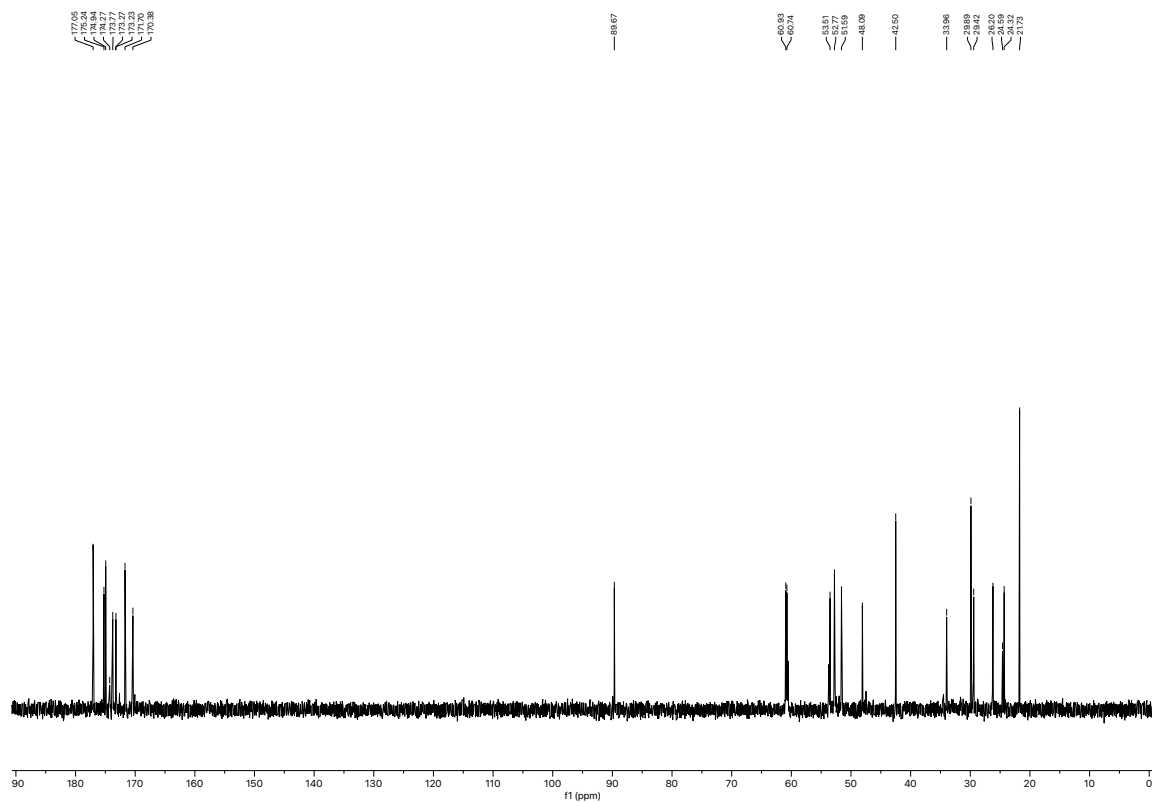
Figure 2.044. ^{13}C NMR spectrum (101 MHz, D$_2$O) of compound **2.009**.
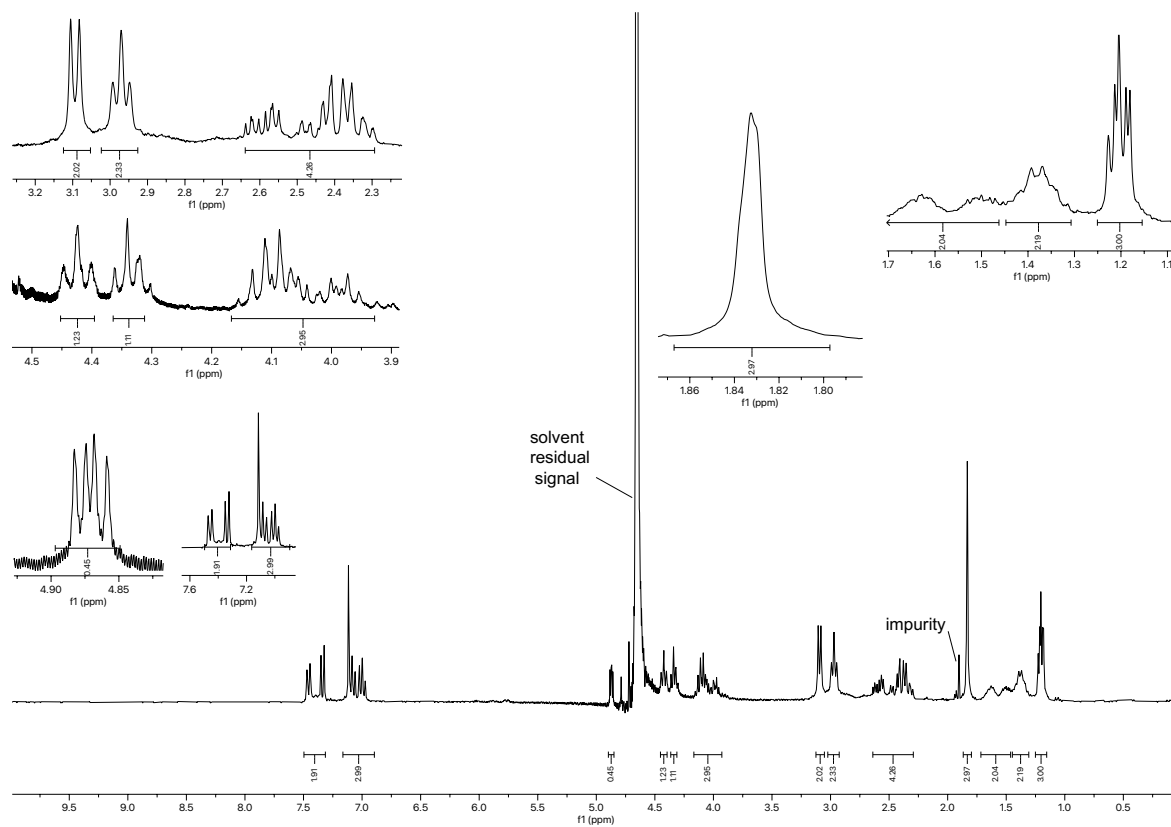
Figure 2.045. ^{1}H NMR spectrum (300 MHz, D$_2$O) of compound **2.010**.
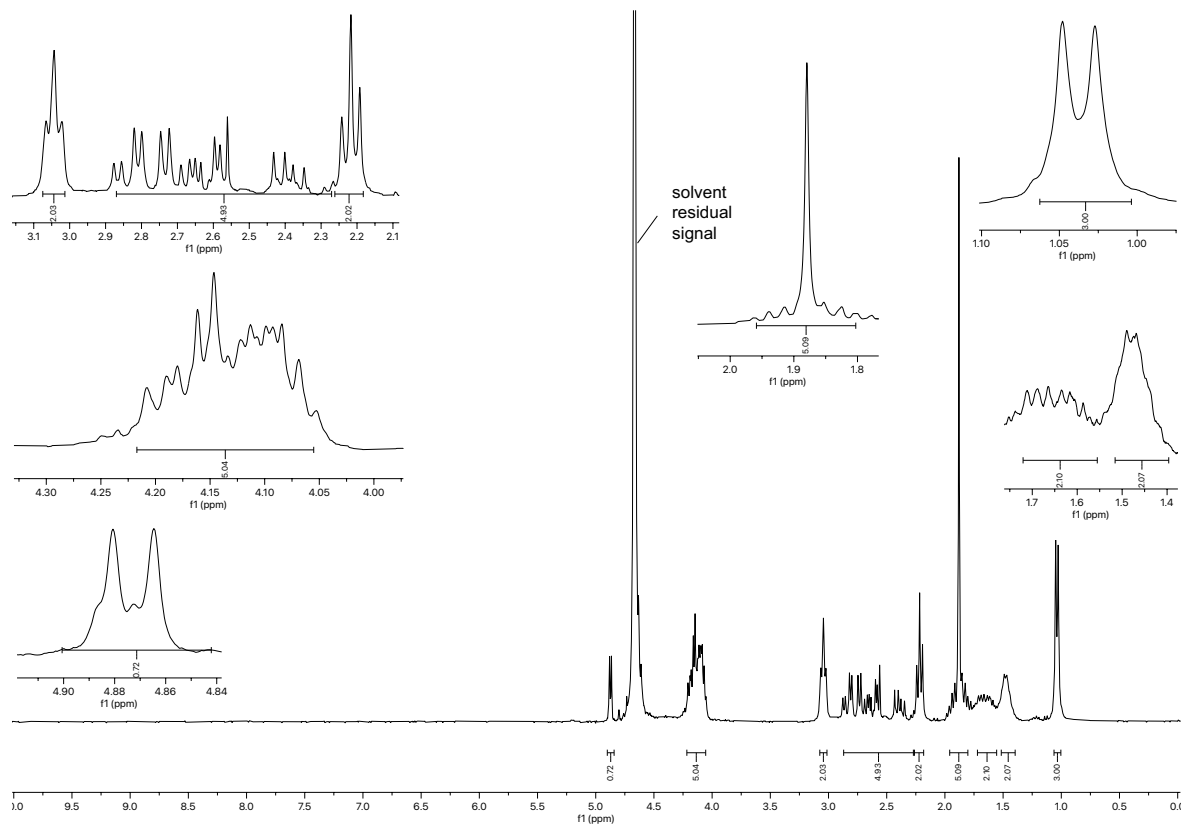
Figure 2.046. ^{1}H NMR spectrum (300 MHz, D$_2$O) of compound **2.011**.

185
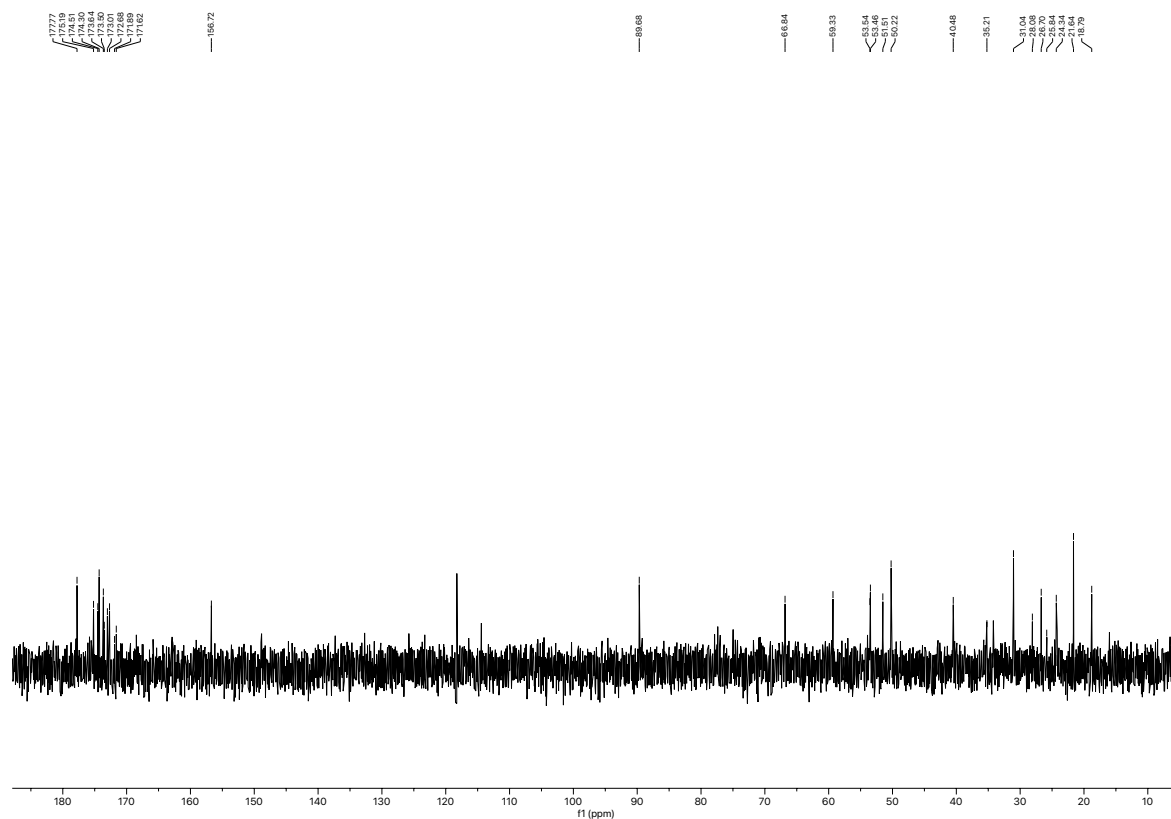
Figure 2.047. ^{13}C NMR spectrum (75 MHz, D$_2$O) of compound **2.011**.
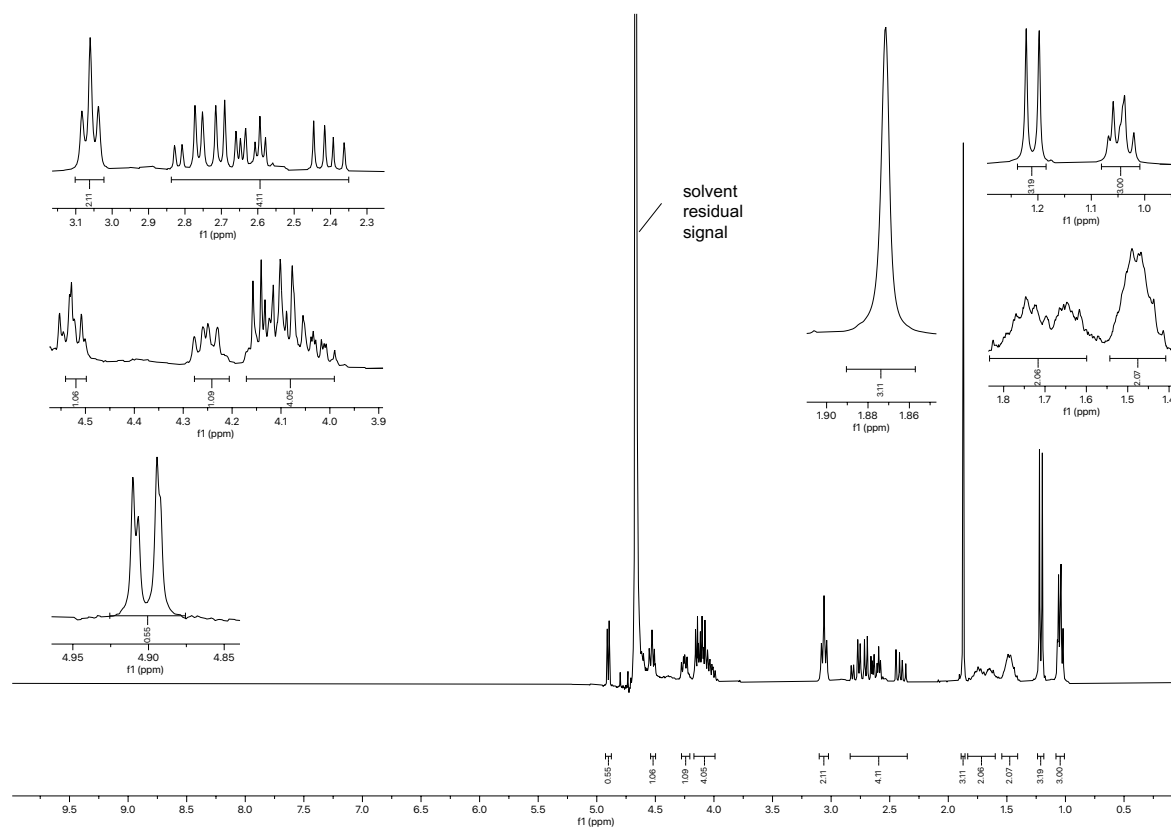
Figure 2.048. ^{1}H NMR spectrum (300 MHz, D$_2$O) of compound **2.012**.
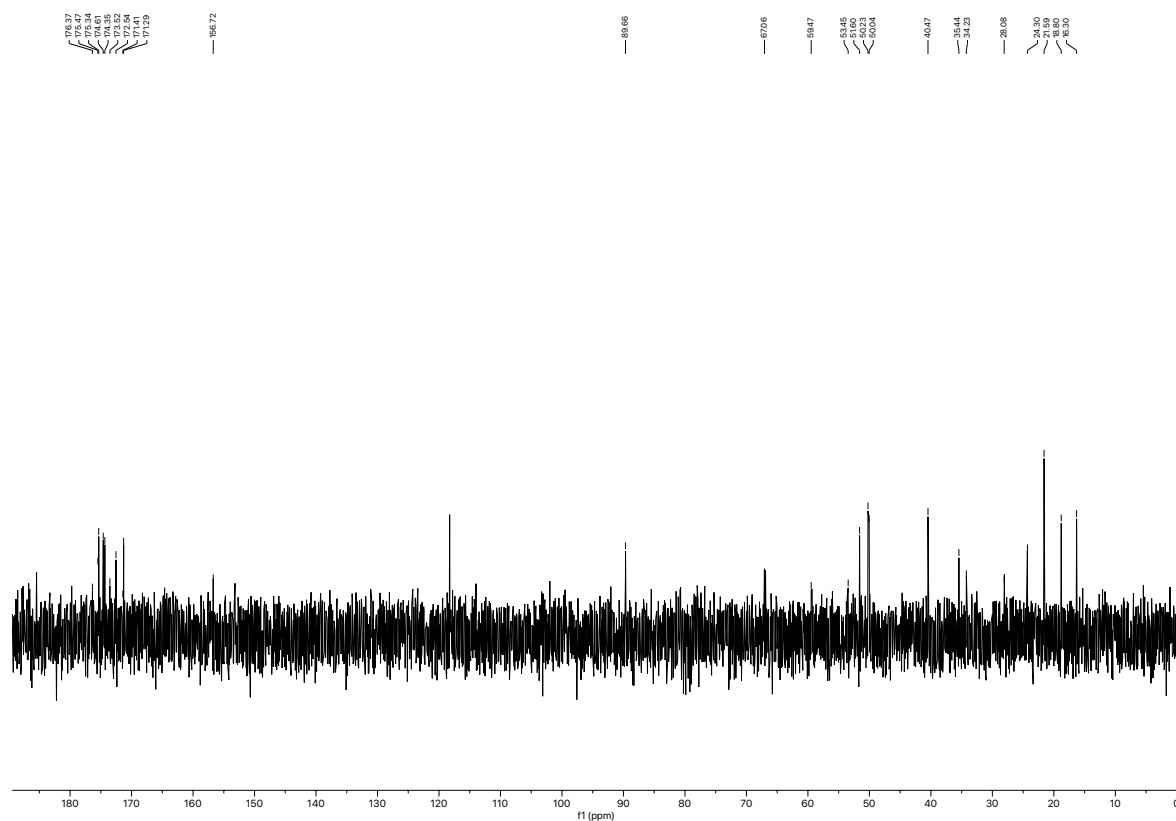
Figure 2.049. ^{13}C NMR spectrum (75 MHz, D$_2$O) of compound **2.012**.
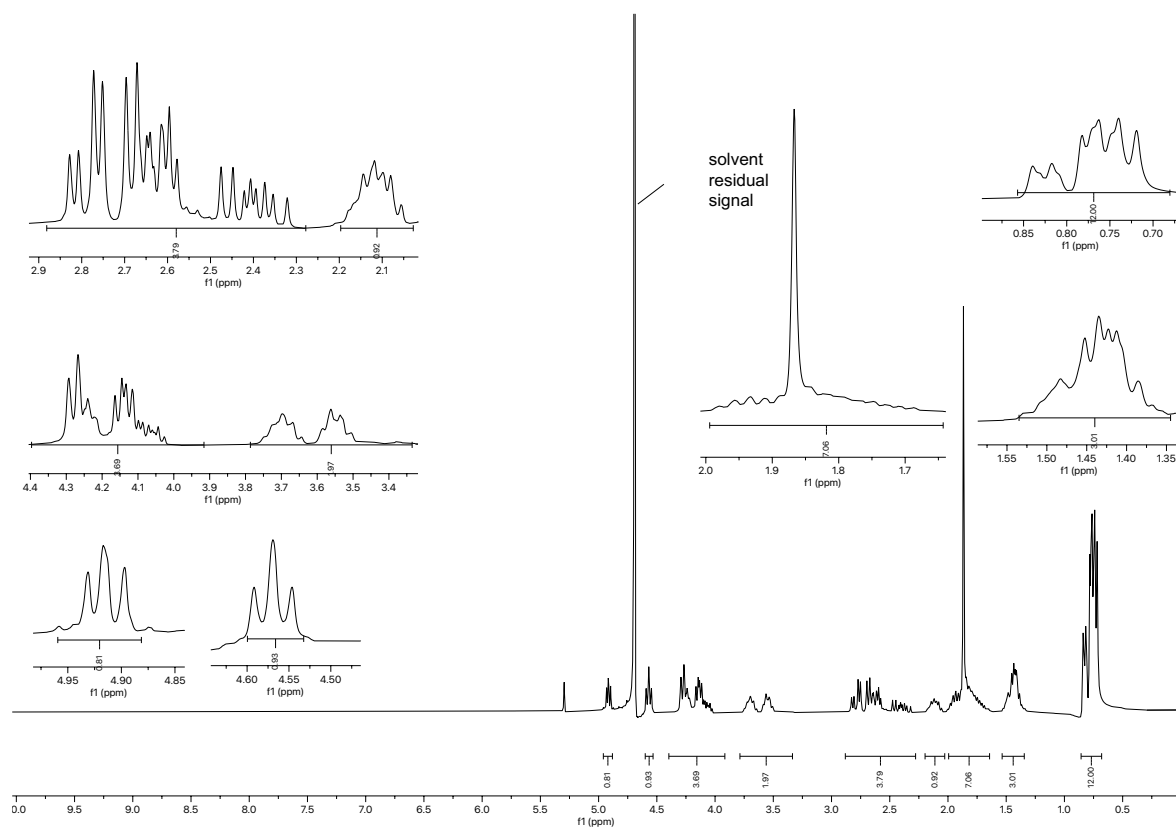
Figure 2.050. ^{1}H NMR spectrum (400 MHz, D$_2$O) of compound **2.013**.
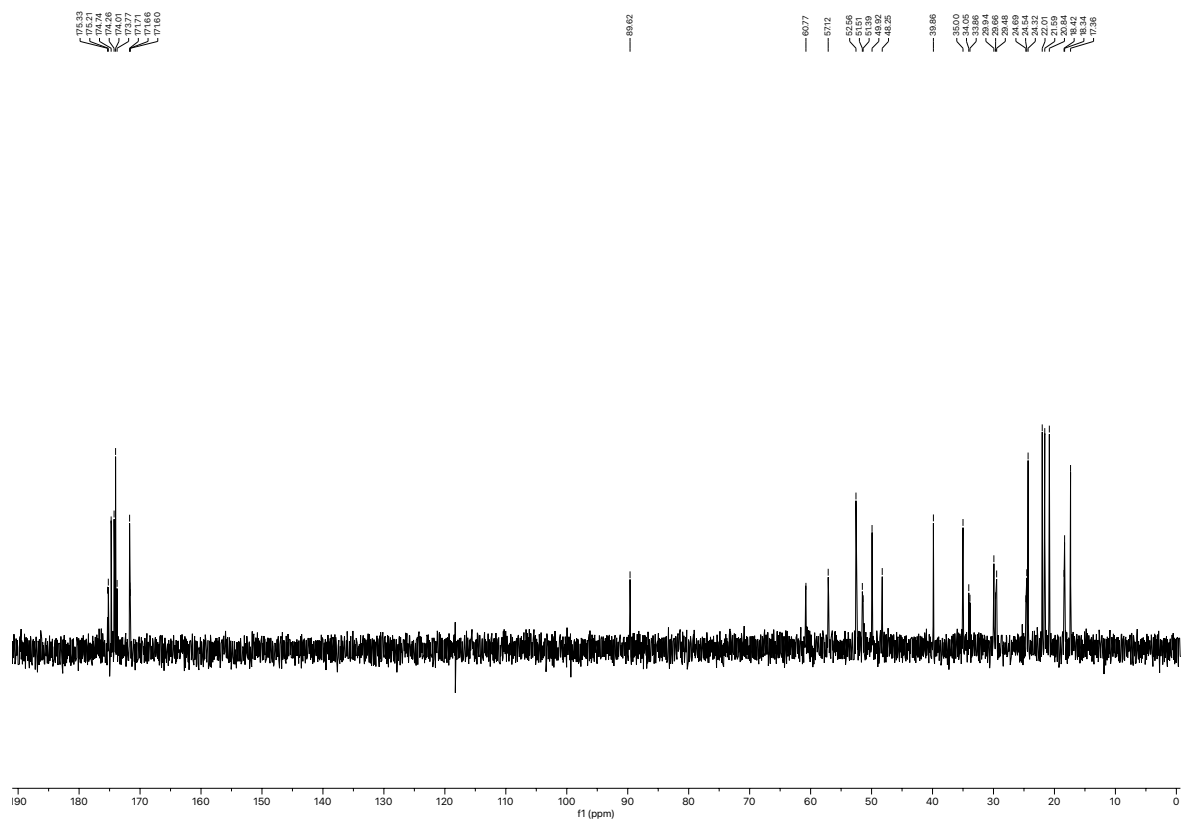
Figure 2.051. ^{13}C NMR spectrum (75 MHz, D$_2$O) of compound **2.013**.
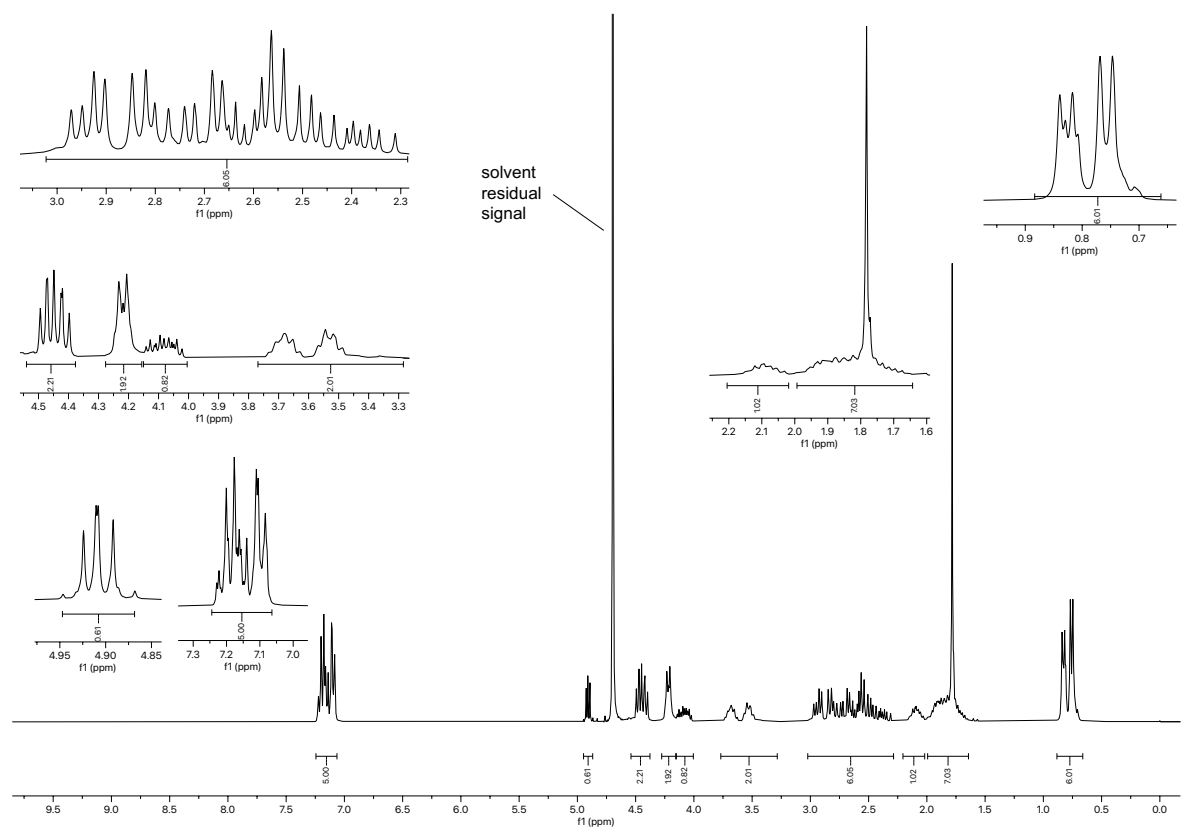
Figure 2.052. ^{1}H NMR spectrum (300 MHz, D$_2$O) of compound **2.014**.
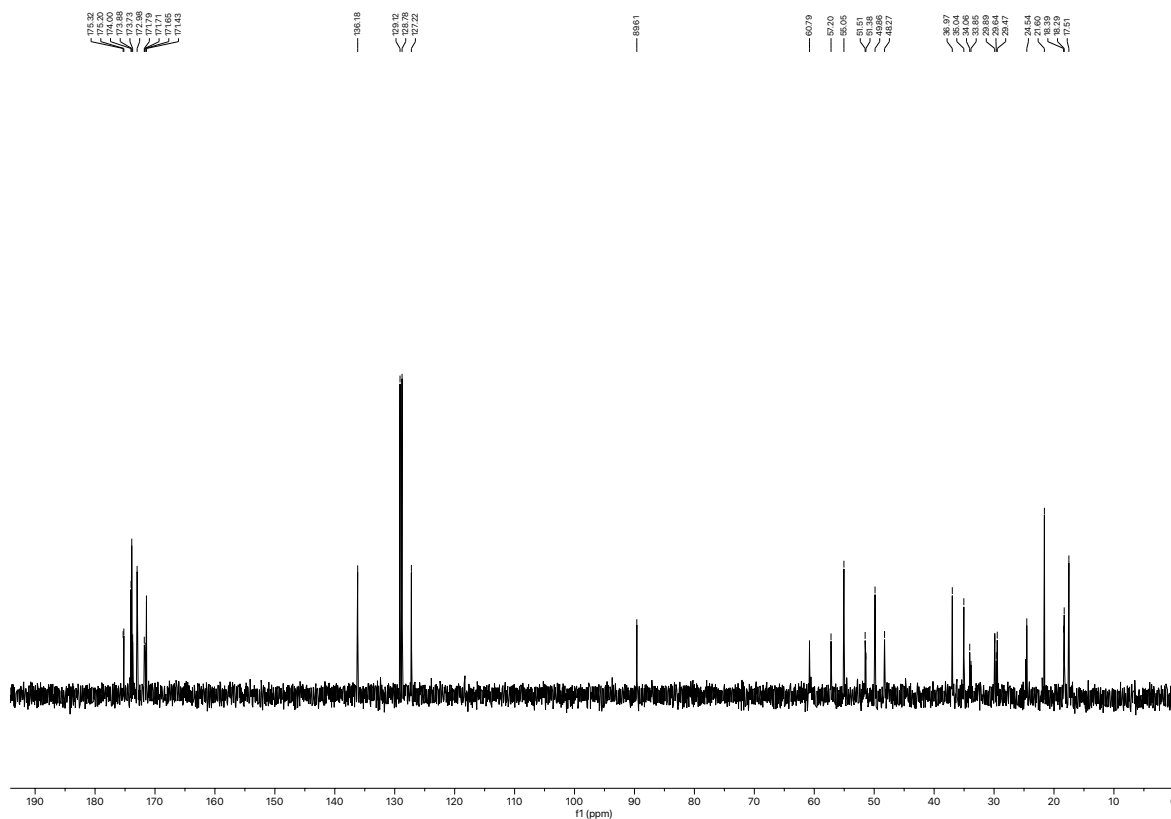
Figure 2.053. ^{13}C NMR spectrum (75 MHz, D$_2$O) of compound **2.014**.
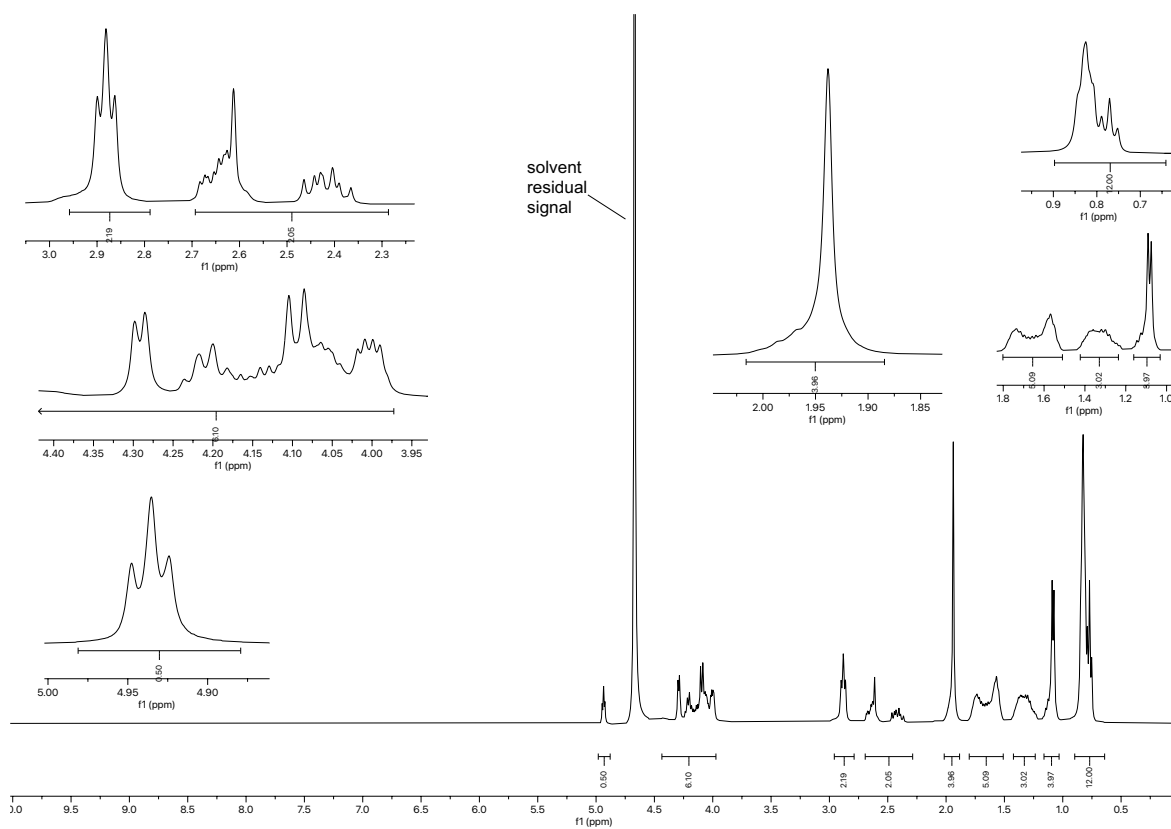
Figure 2.054. ^{1}H NMR spectrum (400 MHz, D$_2$O) of compound **2.015**.
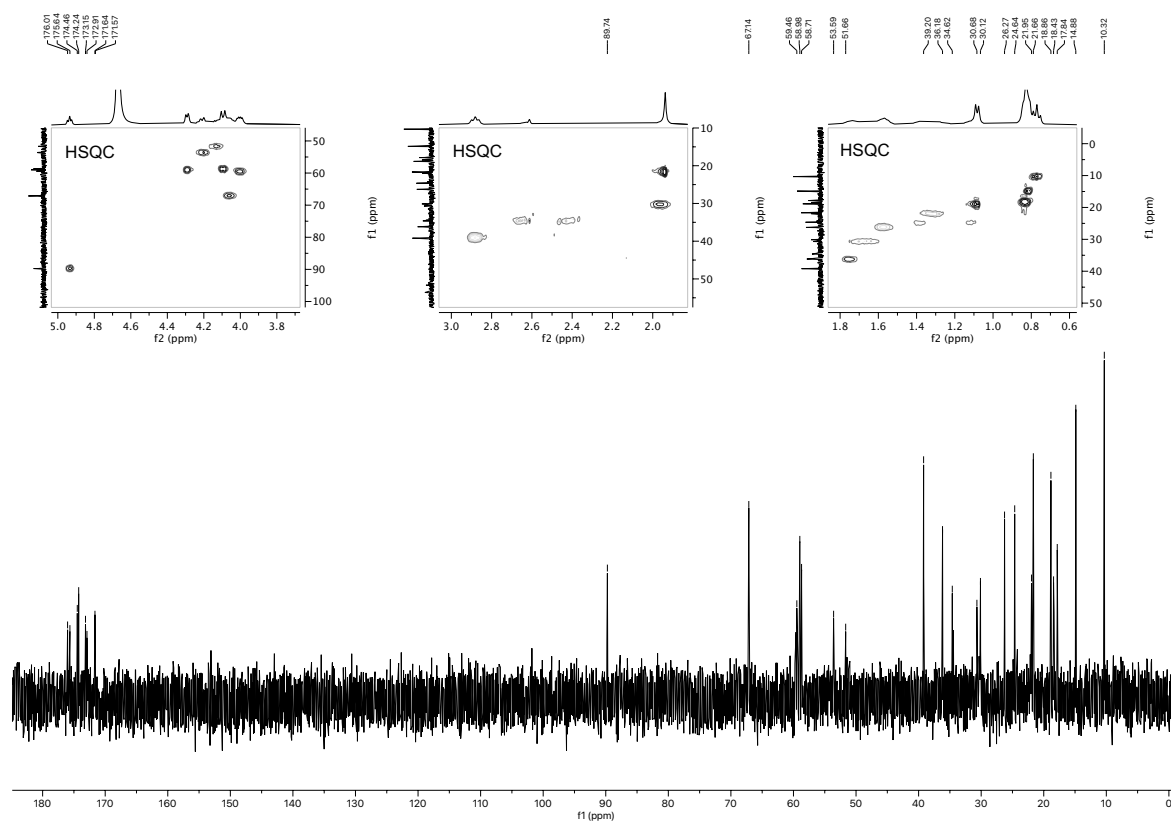
Figure 2.055. ^{13}C NMR spectrum (101 MHz, D$_2$O) of compound **2.015**.
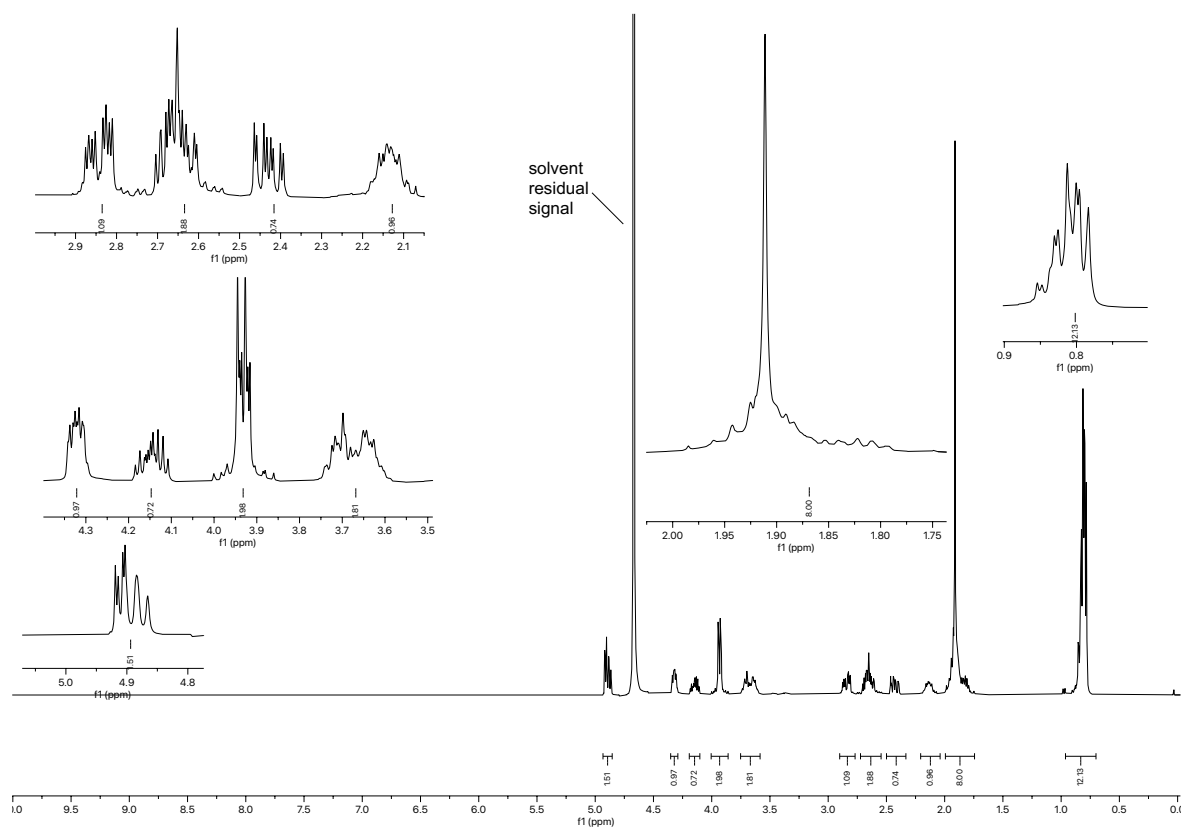
Figure 2.056. ^{1}H NMR spectrum (400 MHz, D$_2$O) of compound **2.017**.
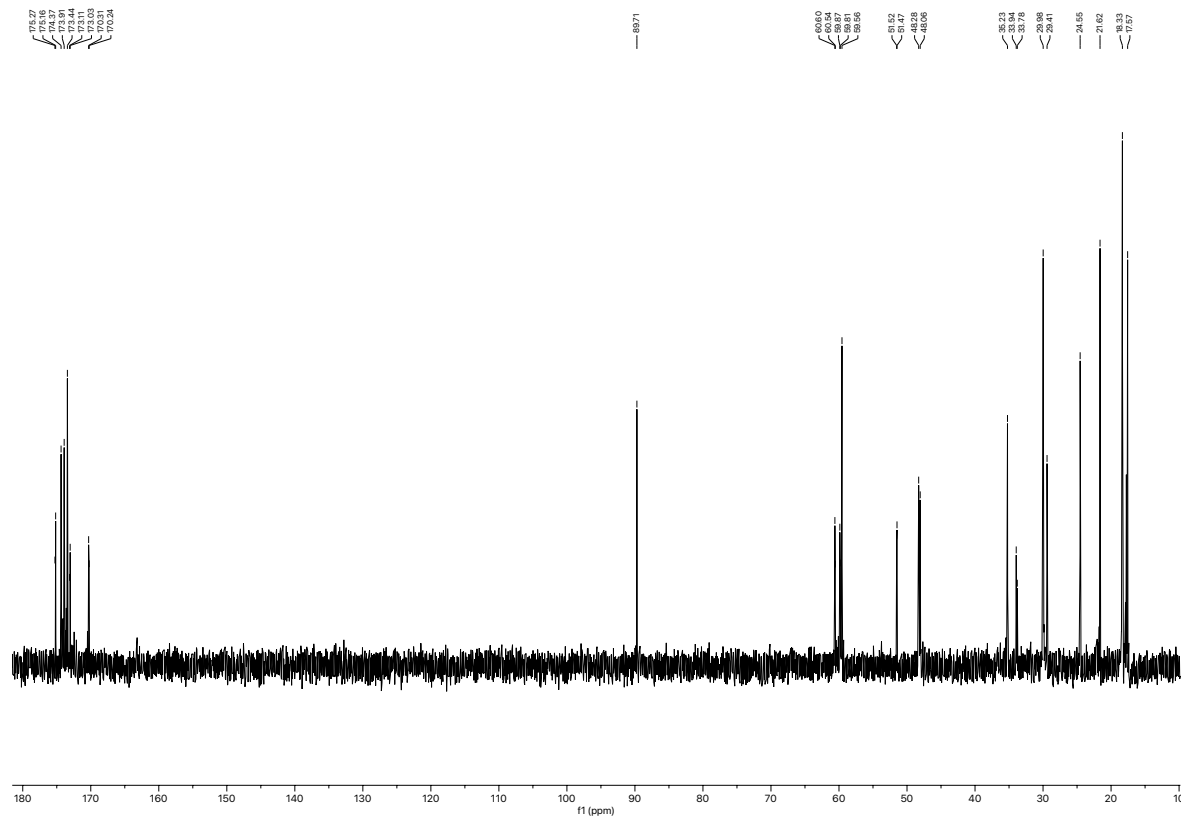
Figure 2.057. ^{13}C NMR spectrum (101 MHz, D$_2$O) of compound **2.017**.
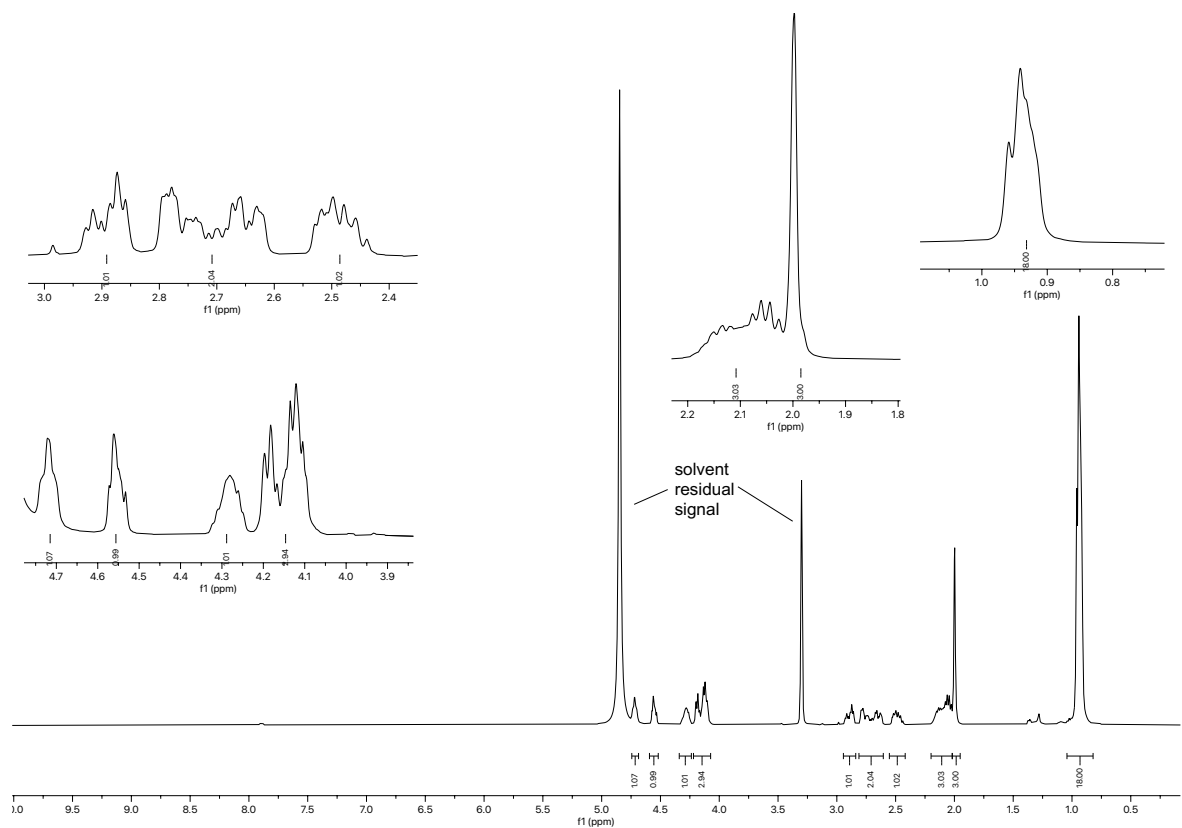
Figure 2.058. ^{1}H NMR spectrum (400 MHz, D$_2$O) of compound **2.018**.
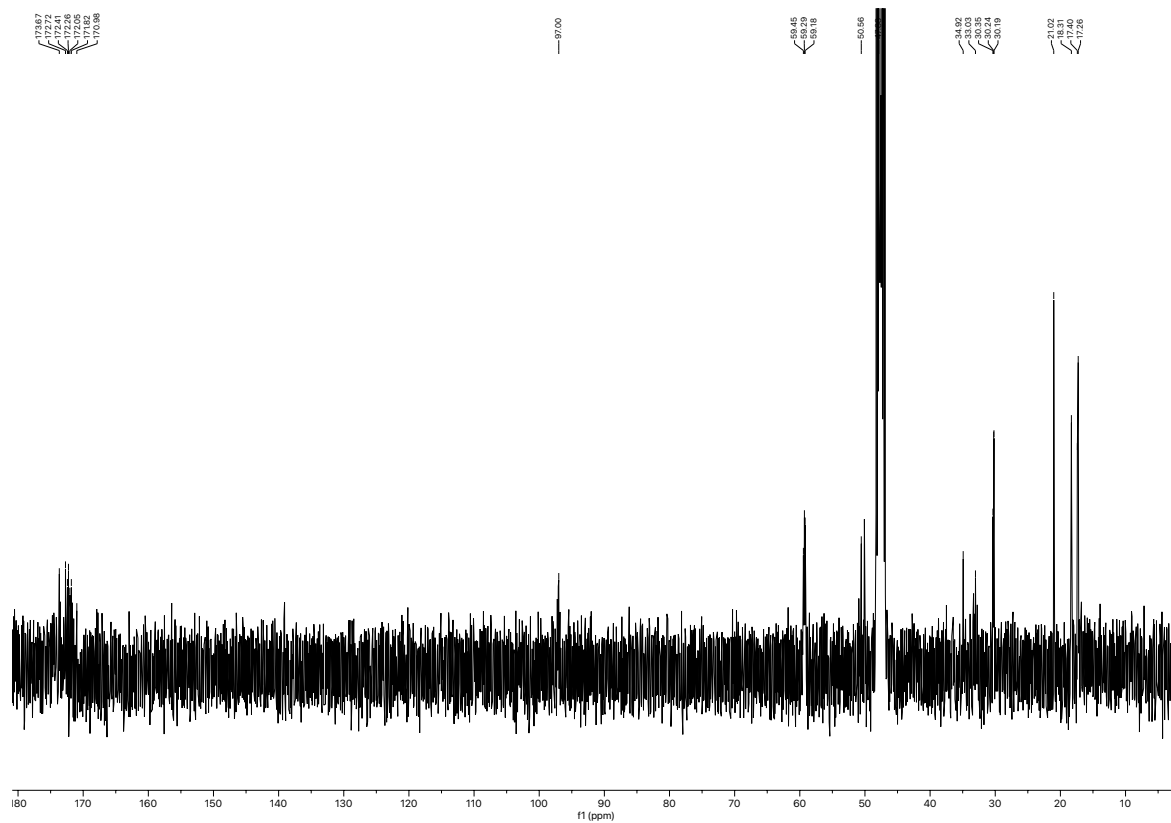
Figure 2.059. ^{1}H NMR spectrum (101 MHz, CD$_3$OD) of compound **2.018**.
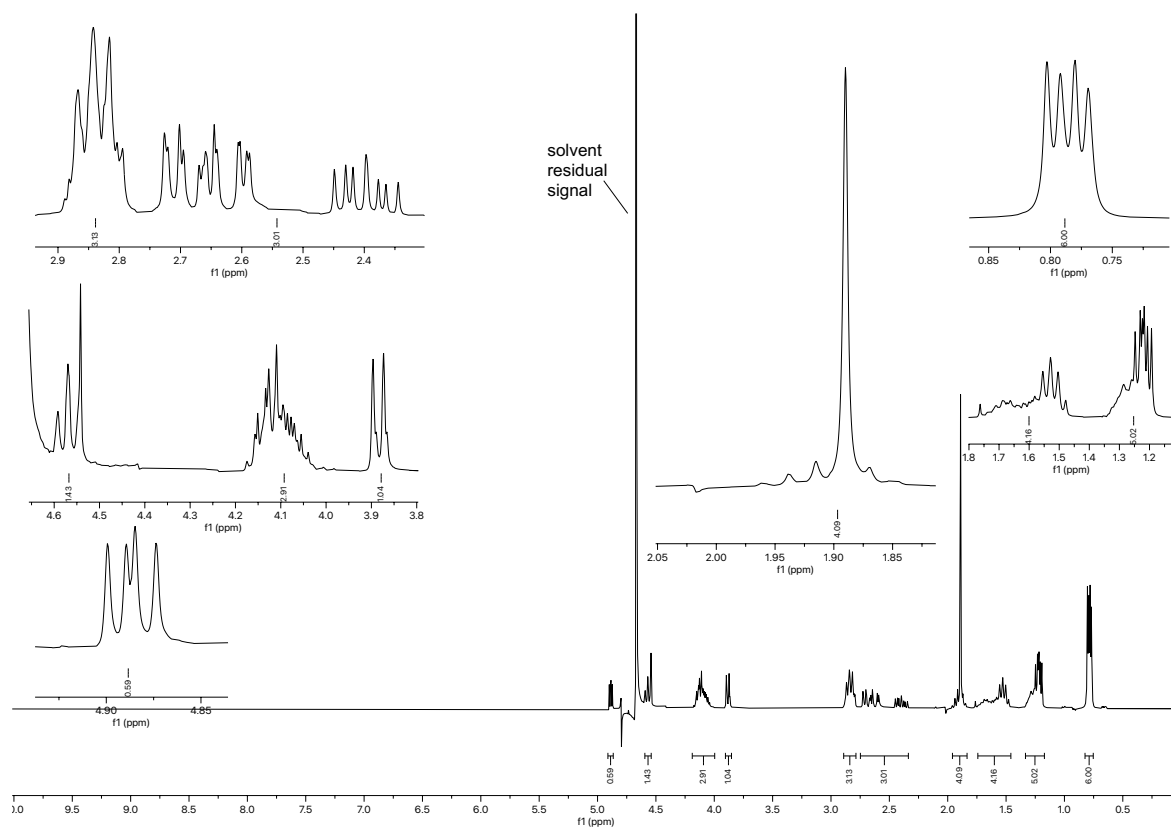
Figure 2.060. ^{1}H NMR spectrum (300 MHz, D$_2$O) of compound **2.019**.

192
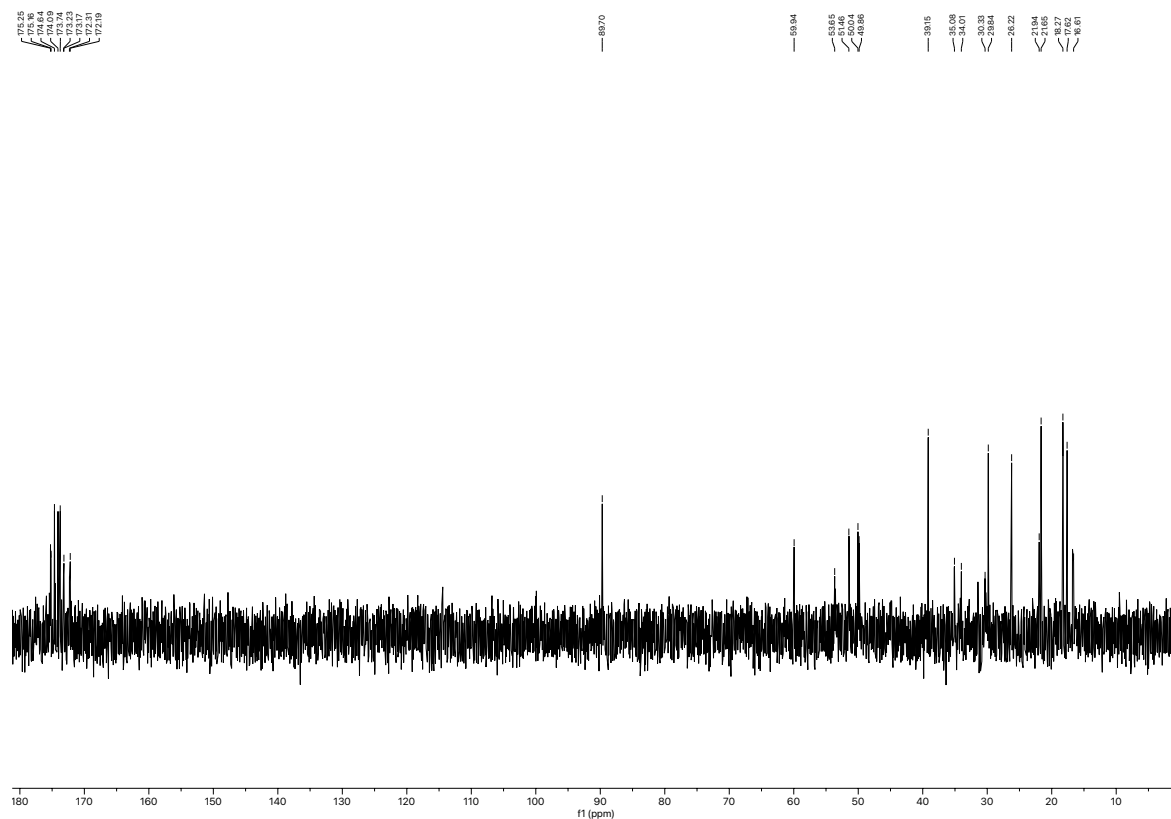
Figure 2.061. ^{13}C NMR spectrum (75 MHz, D_2O) of compound **2.019**.
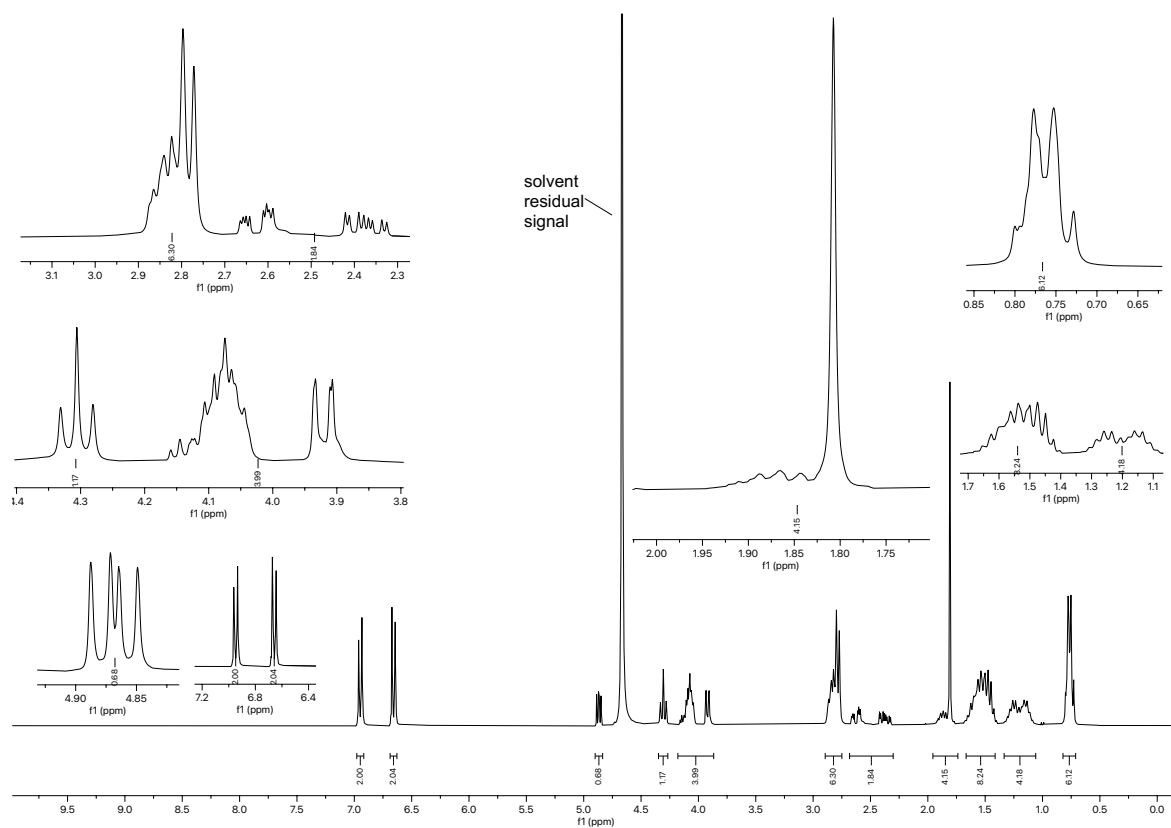
Figure 2.062. ^{1}H NMR spectrum (300 MHz, D_2O) of compound **2.020**.
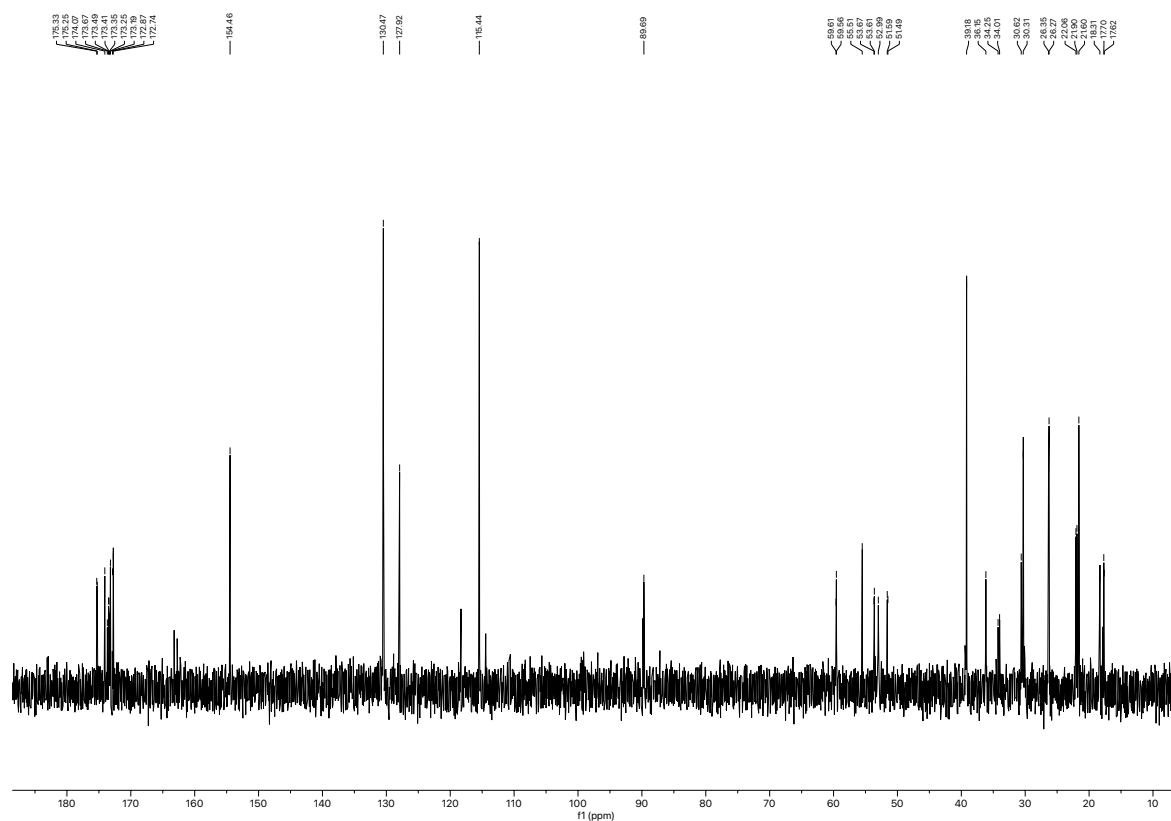
Figure 2.063. ^{13}H NMR spectrum (75 MHz, D$_2$O) of compound **2.020**.
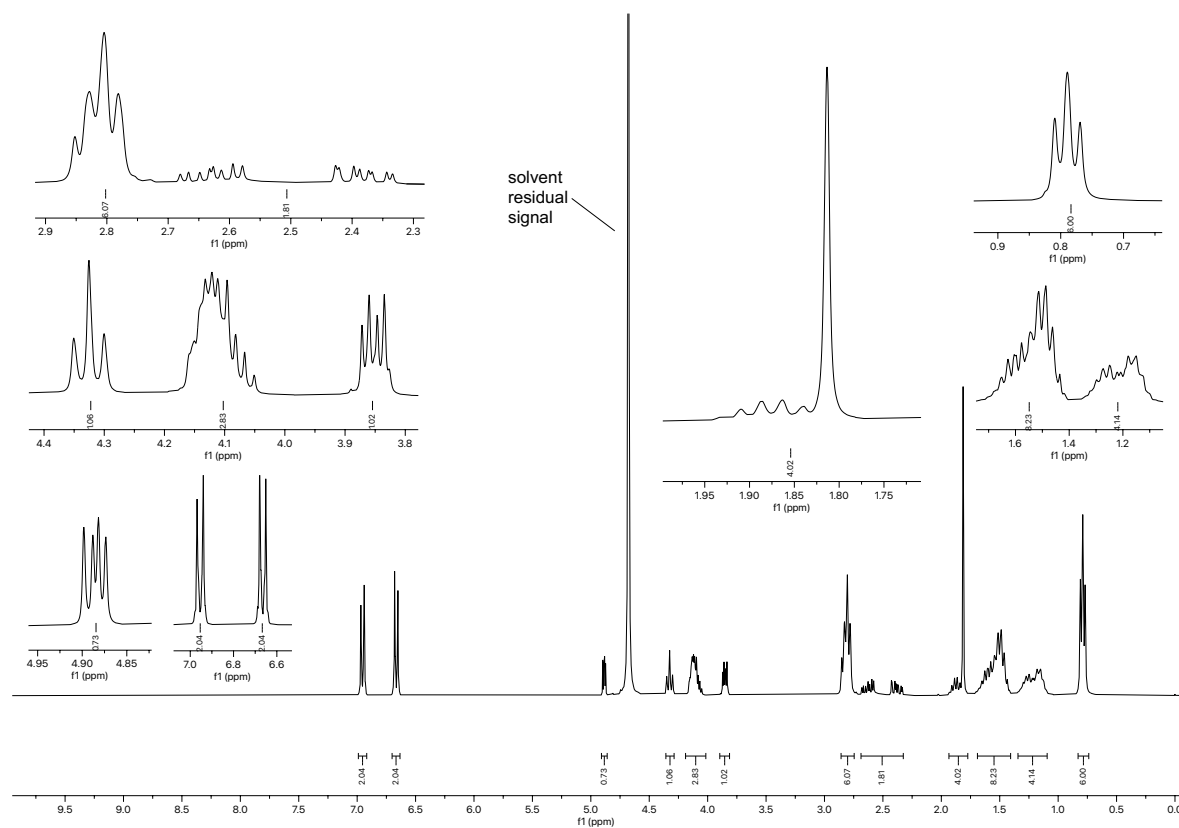
Figure 2.064. ^{1}H NMR spectrum (300 MHz, D$_2$O) of compound **2.021**.
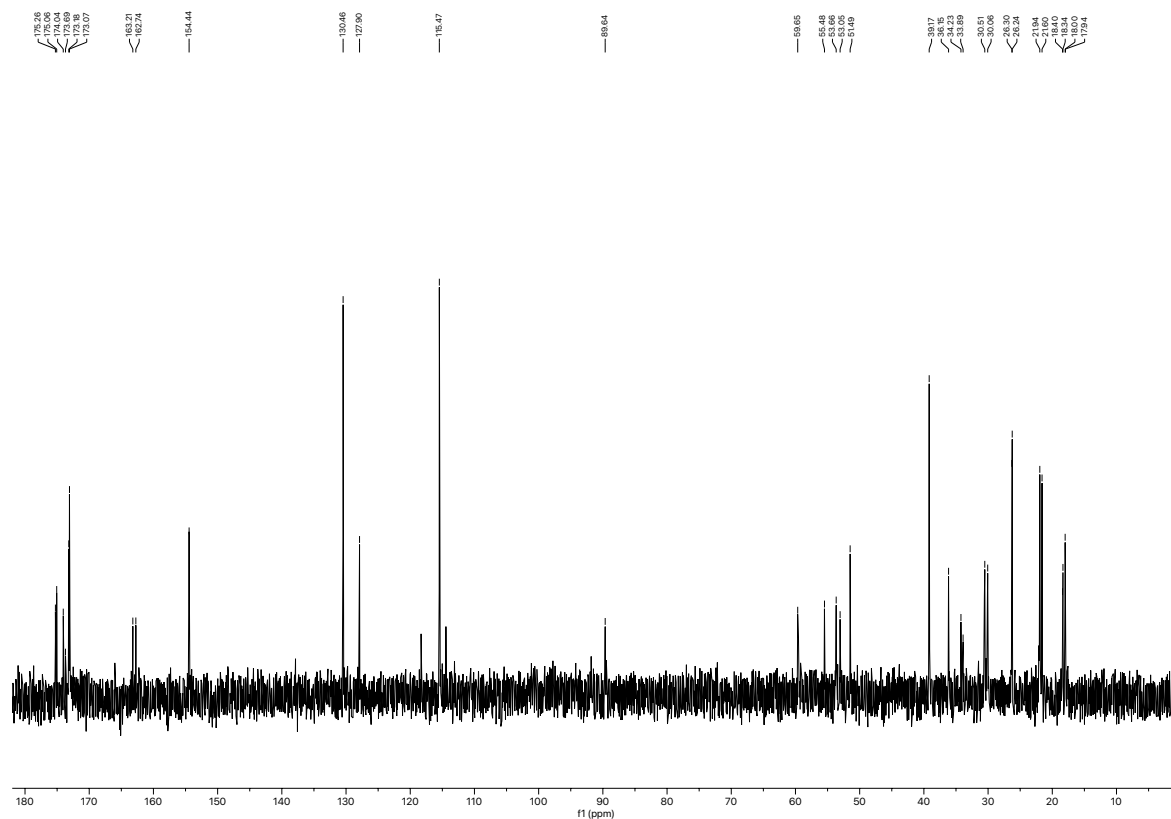
Figure 2.065. ^{13}C NMR spectrum (75 MHz, D$_2$O) of compound **2.021**.
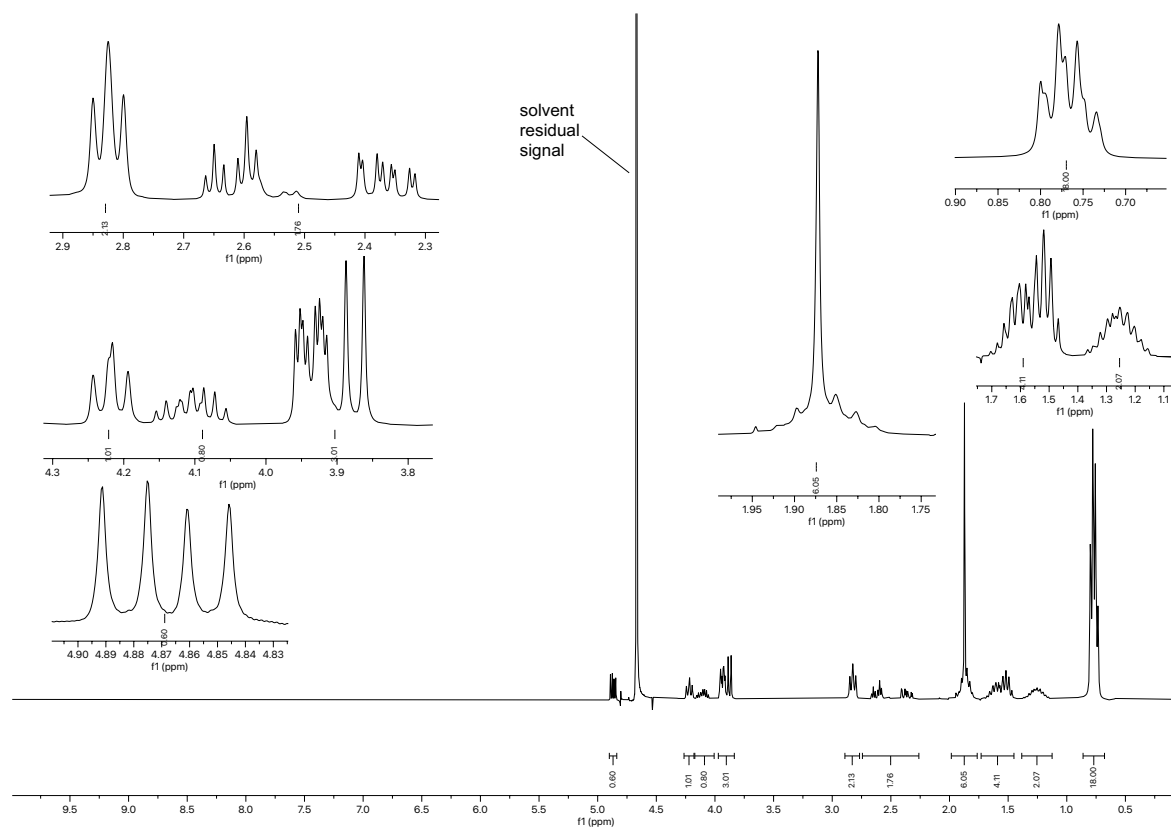
Figure 2.066. ^{1}H NMR spectrum (300 MHz, D$_2$O) of compound **2.022**.
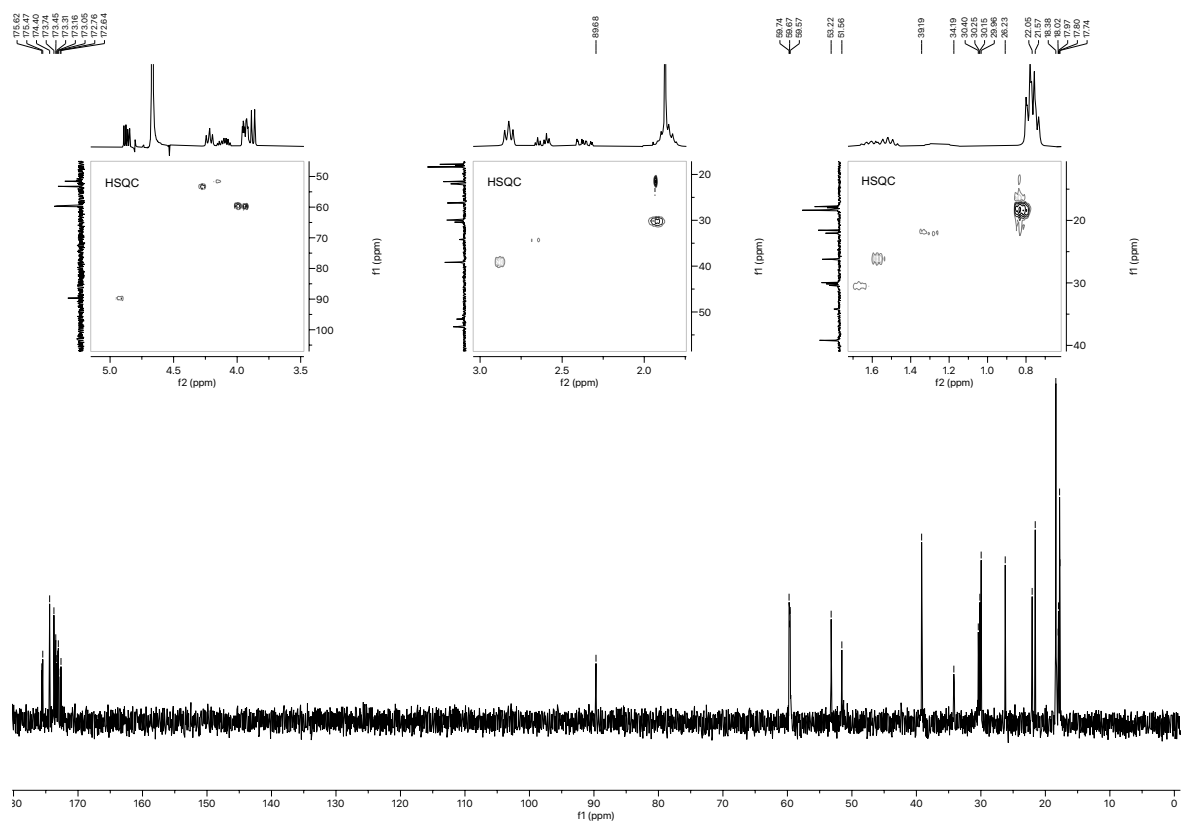
Figure 2.067. ^{13}C NMR spectrum (75 MHz, D$_2$O) of compound **2.022**.
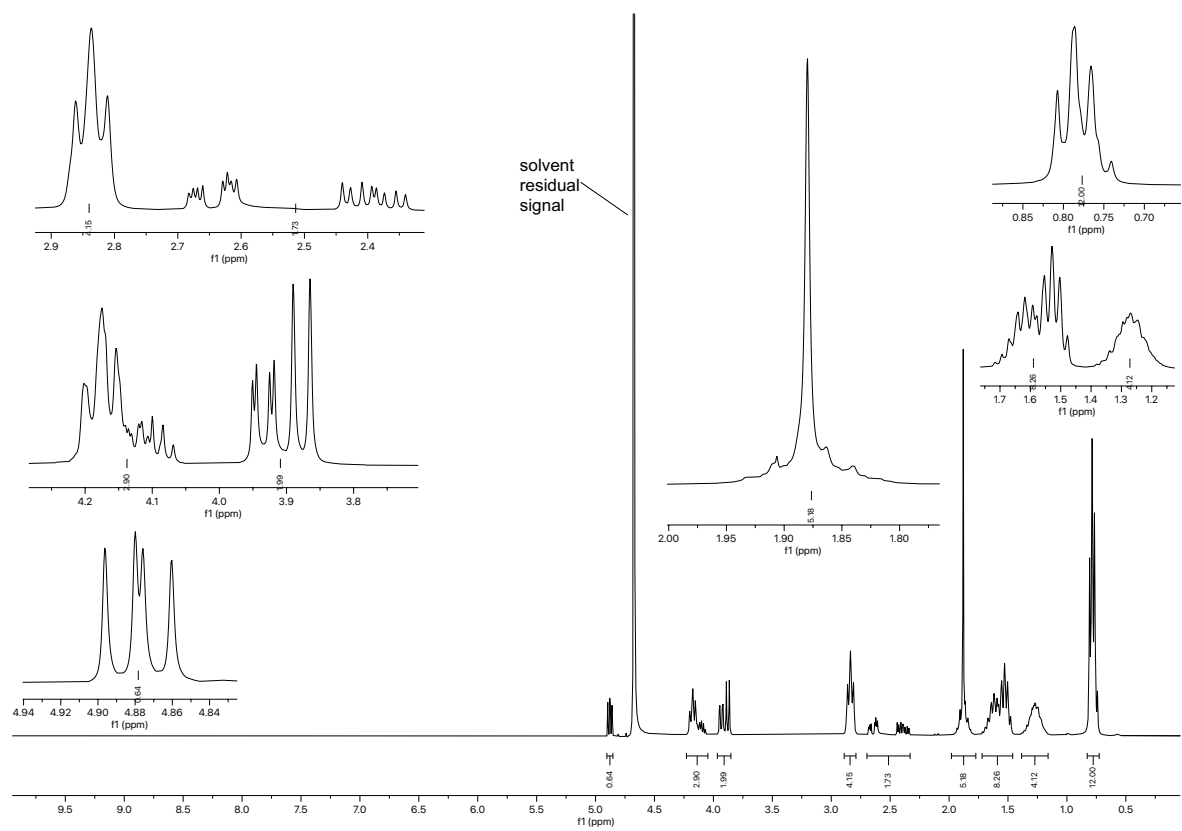
Figure 2.068. ^{1}H NMR spectrum (300 MHz, D$_2$O) of compound **2.023**.
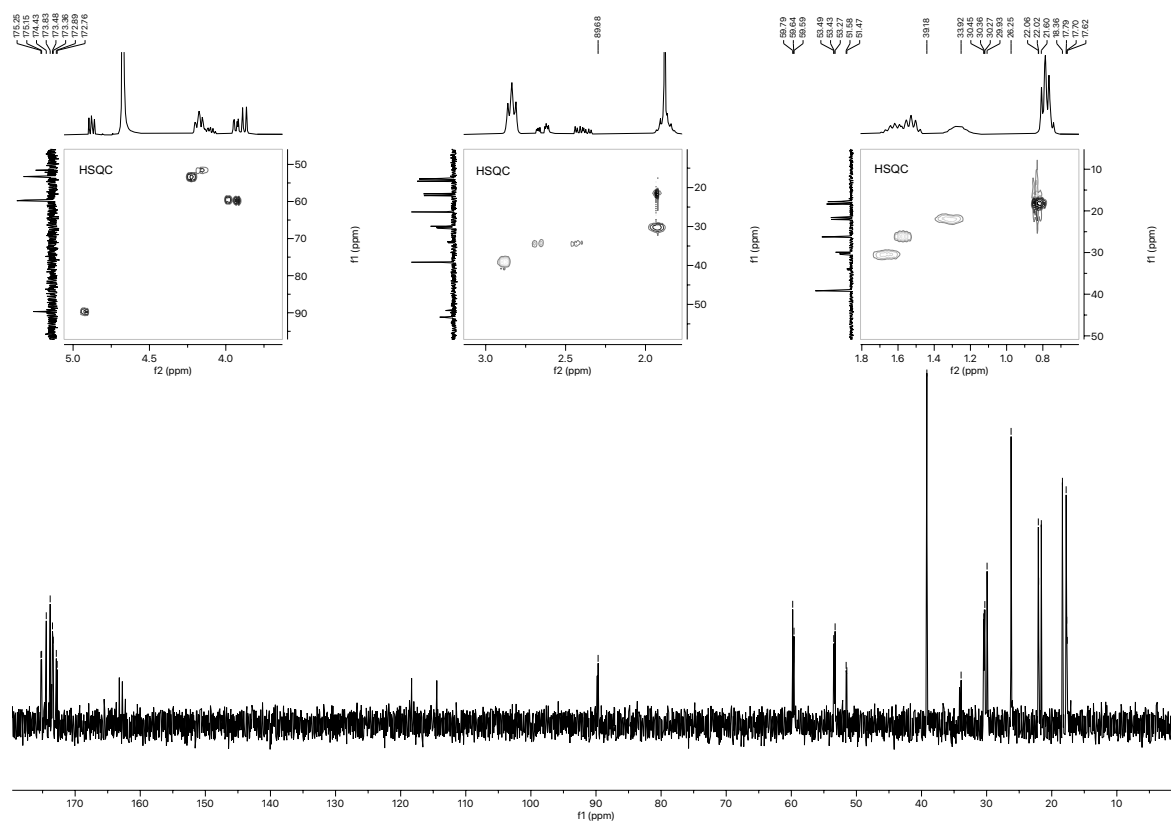
Figure 2.069. ^{13}C NMR spectrum (75 MHz, D_2O) of compound **2.023**.
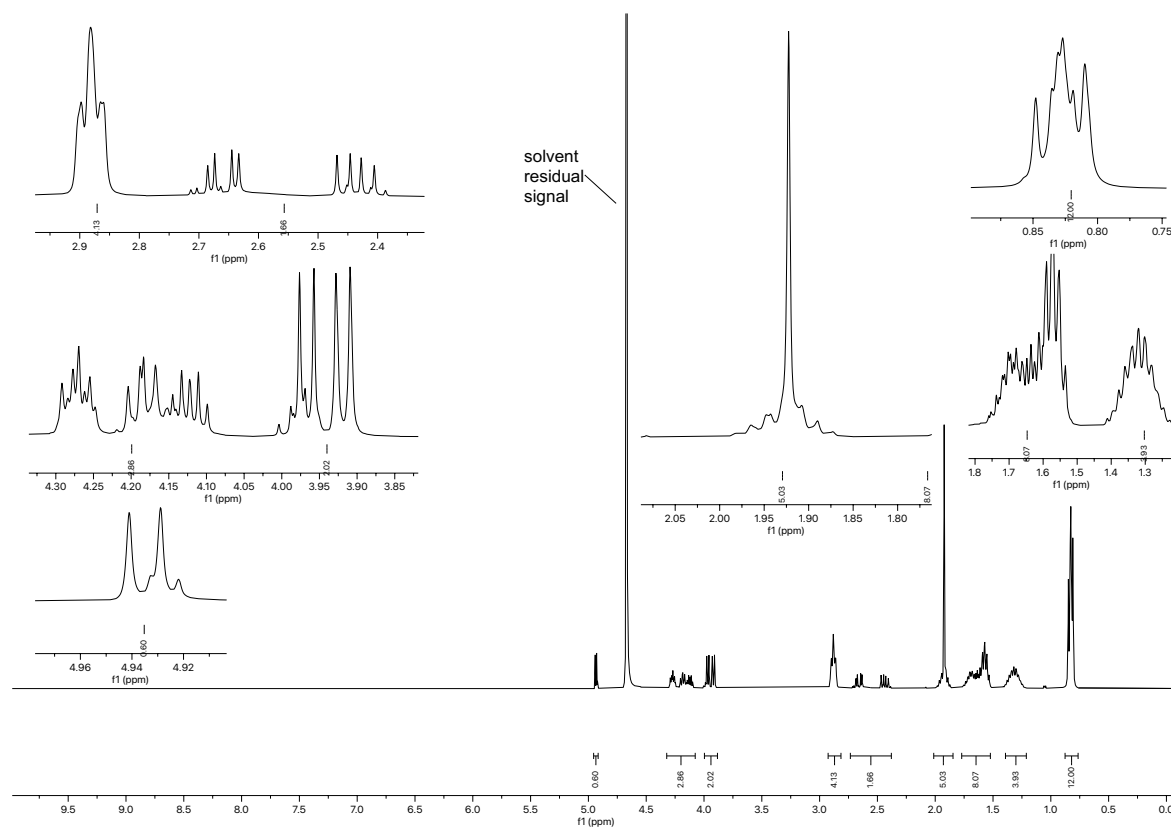
Figure 2.070. ^1H NMR spectrum (400 MHz, D_2O) of compound **2.024**.
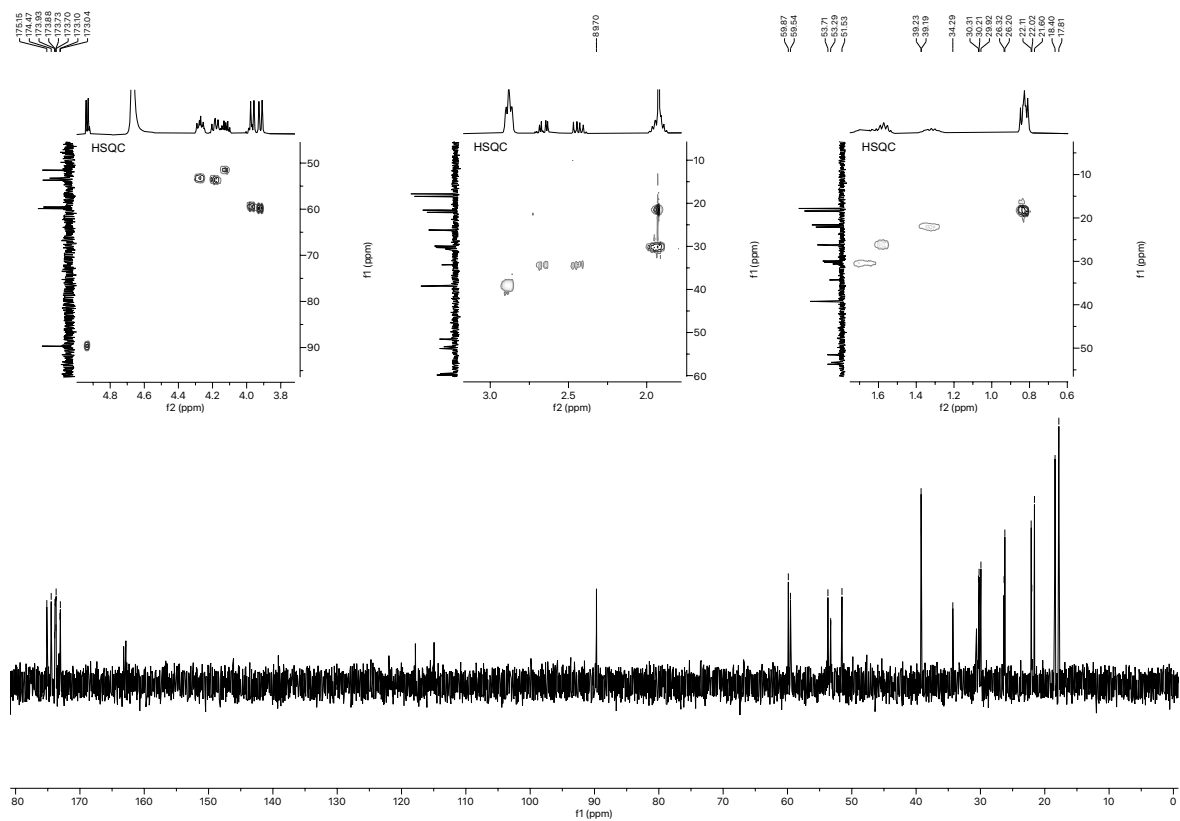
Figure 2.071. ^{13}C NMR spectrum (101 MHz, D_2O) of compound **2.024**.
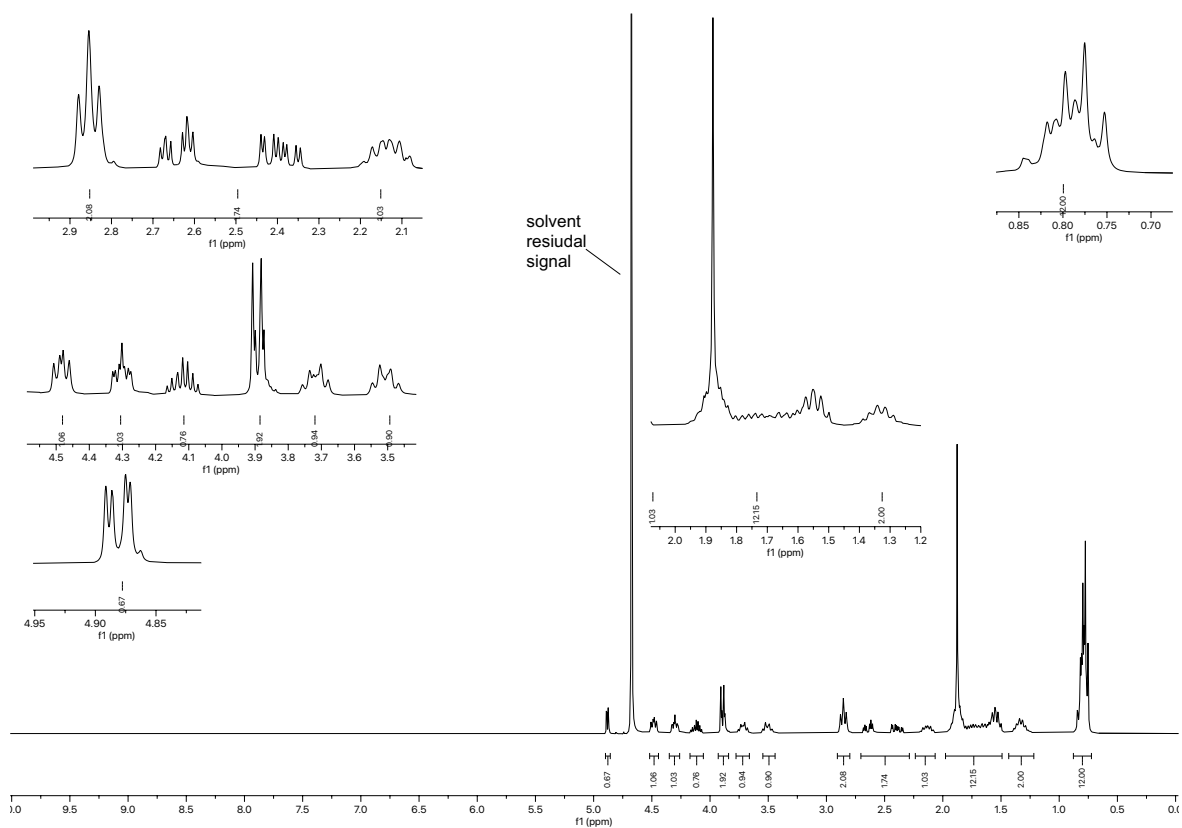
Figure 2.072. ^1H NMR spectrum (300 MHz, D_2O) of compound **2.025**.
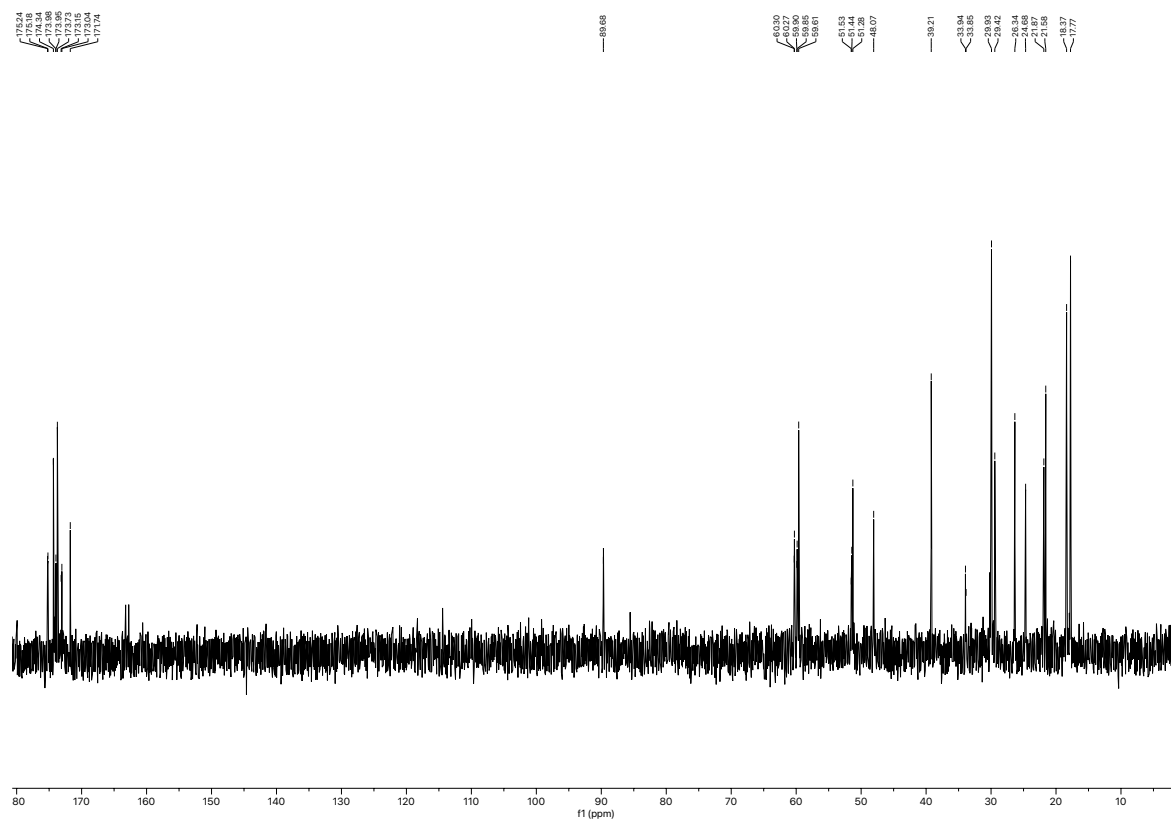
Figure 2.073. ^{13}C NMR spectrum (75 MHz, D$_2$O) of compound **2.025**.
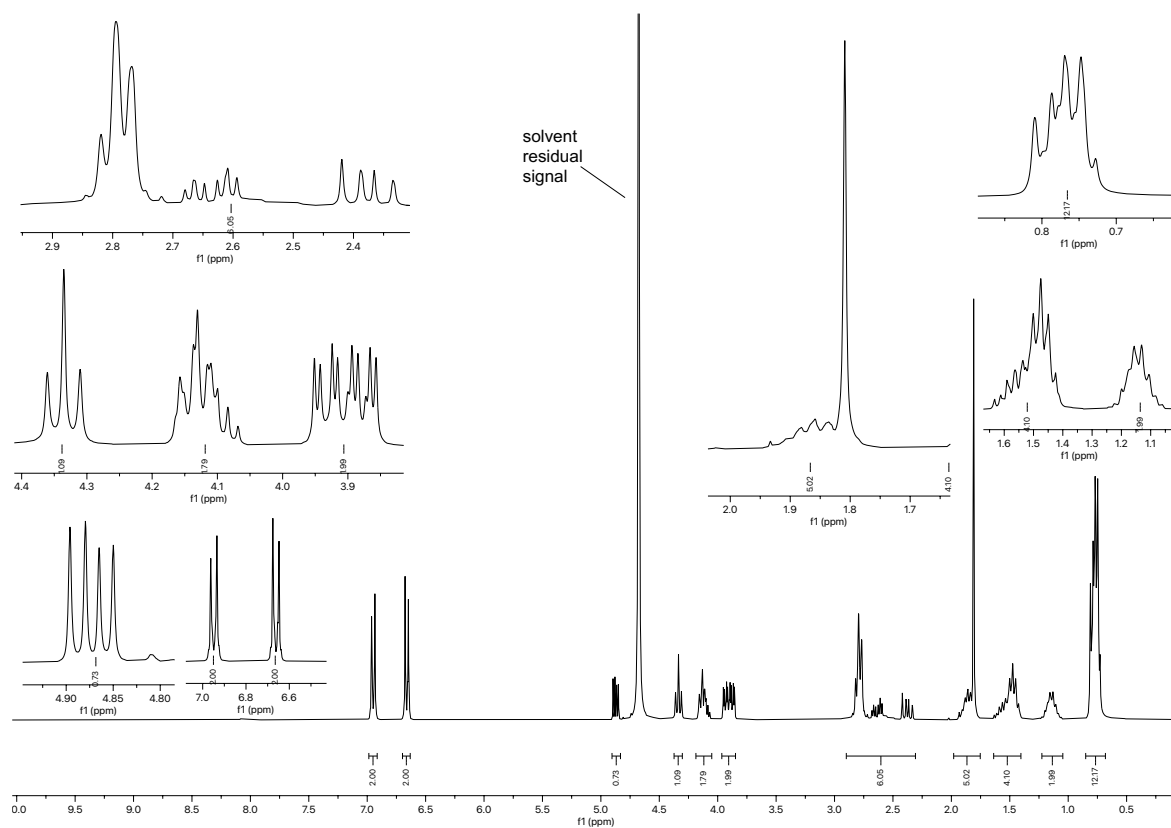
Figure 2.074. ^{1}H NMR spectrum (300 MHz, D$_2$O) of compound **2.026**.

199
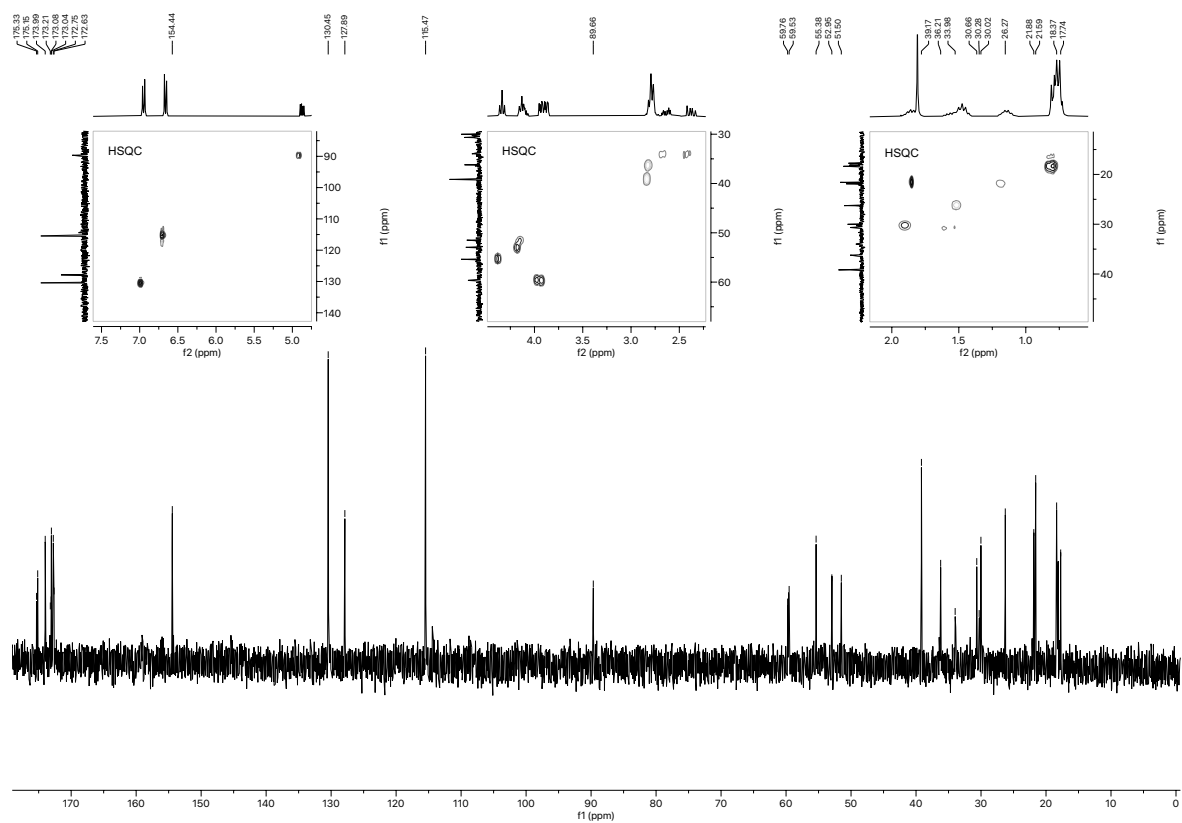
Figure 2.075. ^{13}C NMR spectrum (75 MHz, D_2O) of compound **2.026**.
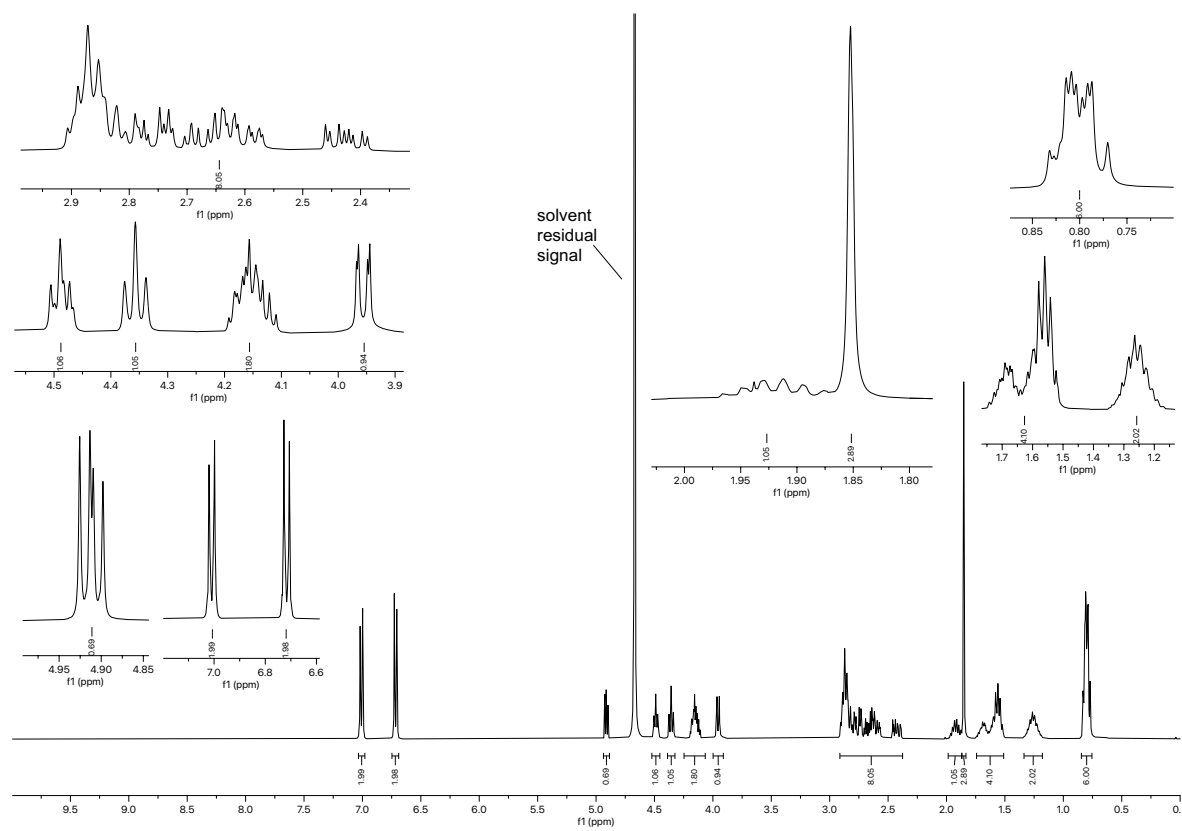
Figure 2.076. ^1H NMR spectrum (400 MHz, D_2O) of compound **2.027**.
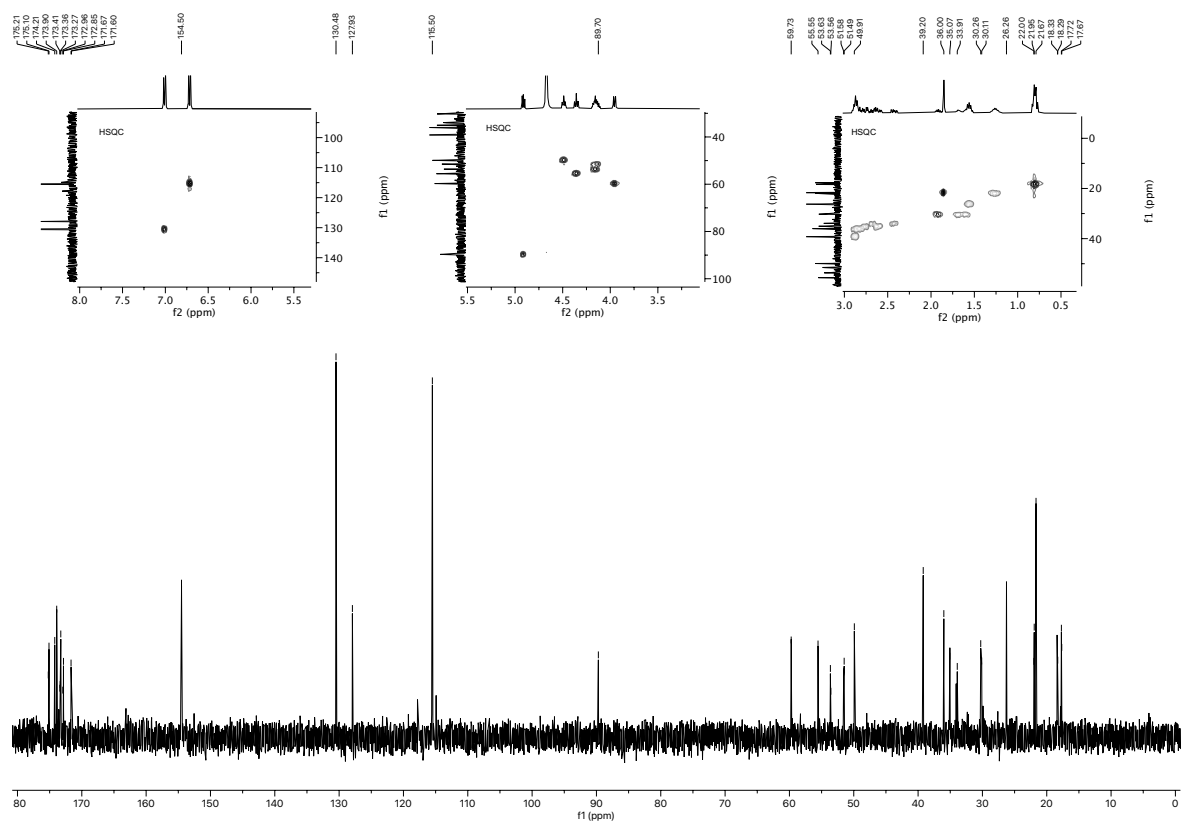
Figure 2.077. ^{13}C NMR spectrum (101 MHz, D_2O) of compound **2.027**.
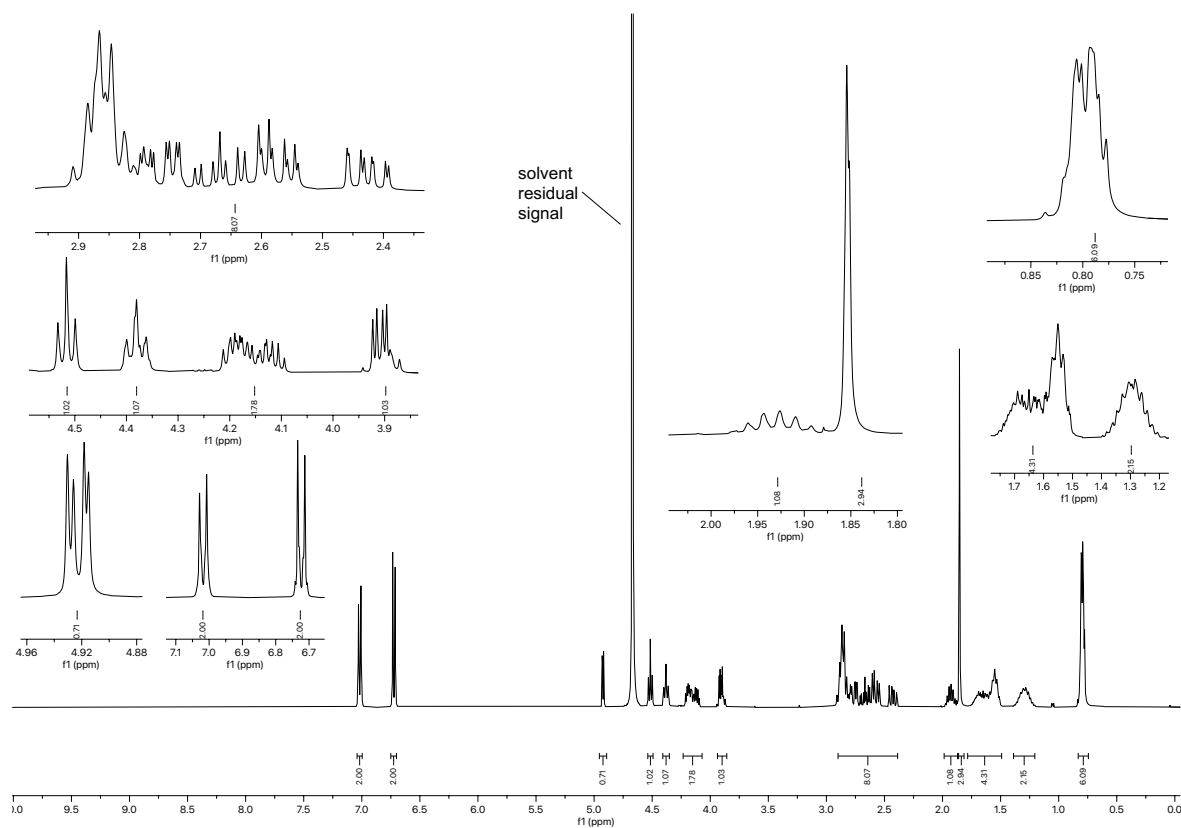
Figure 2.078. ^{1}H NMR spectrum (400 MHz, D_2O) of compound **2.028**.
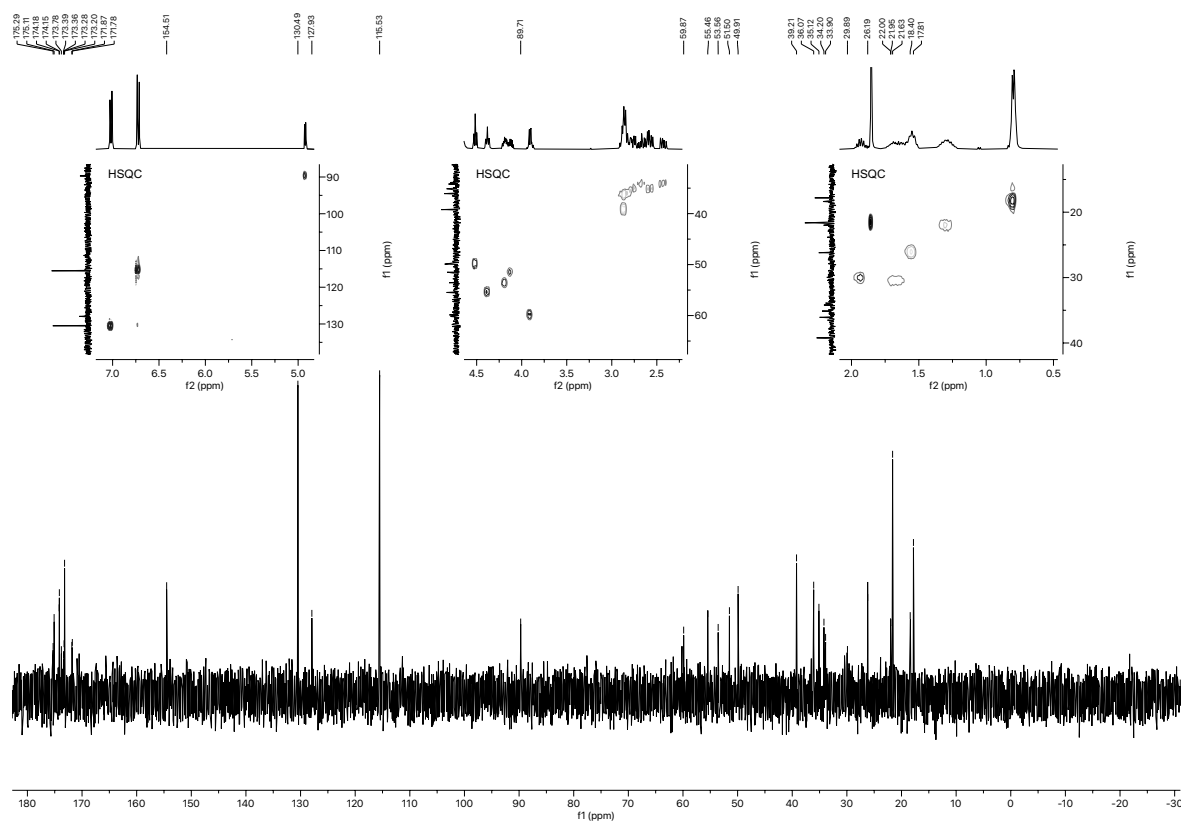
Figure 2.079. ^{13}C NMR spectrum (101 MHz, D$_2$O) of compound **2.028**.
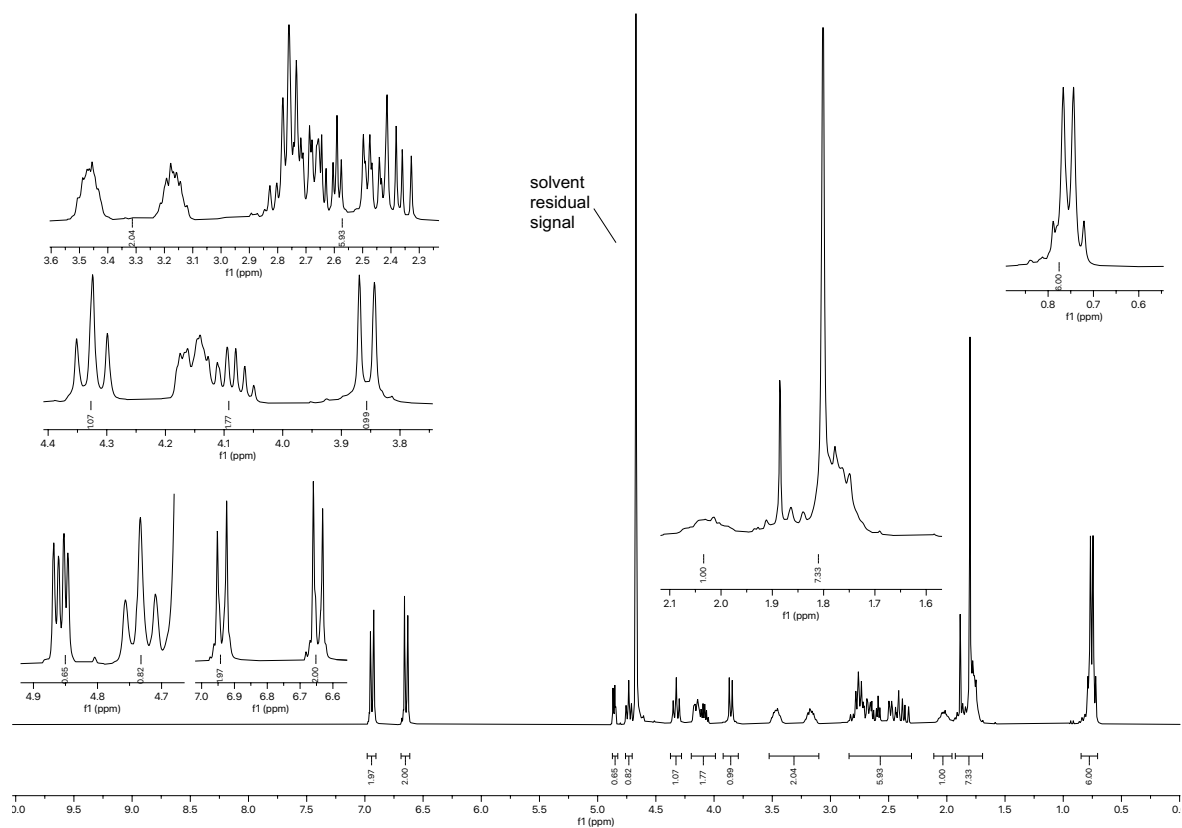
Figure 2.080. ^{1}H NMR spectrum (300 MHz, D$_2$O) of compound **2.029**.
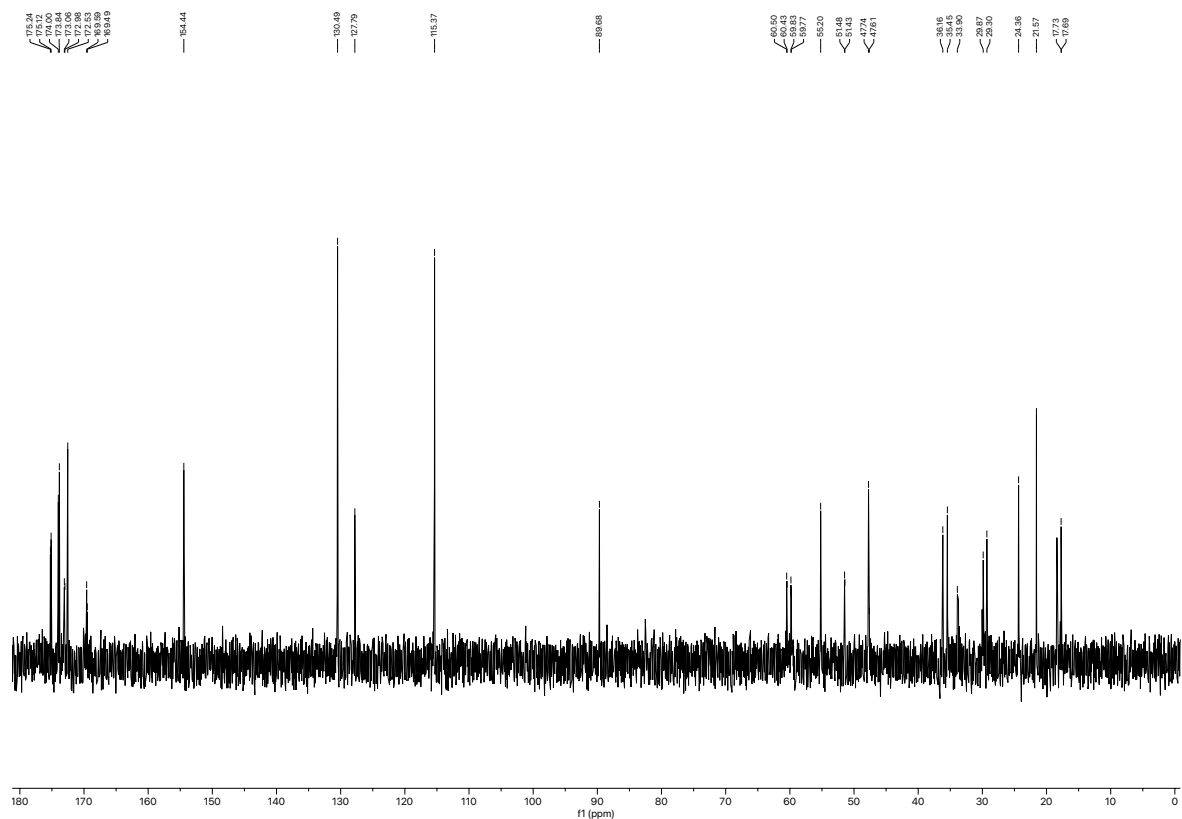
Figure 2.081. ^{13}C NMR spectrum (300 MHz, D$_2$O) of compound **2.029**.
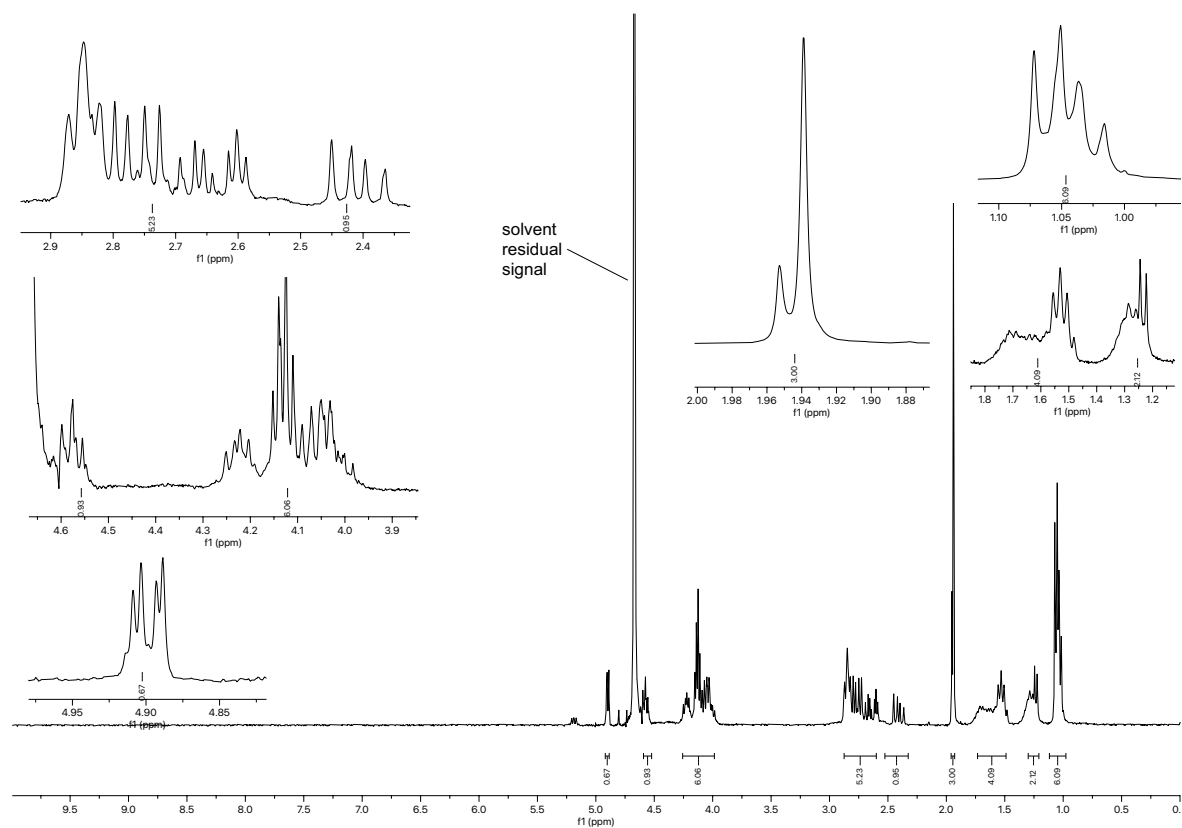
Figure 2.082. ^{1}H NMR spectrum (400 MHz, D$_2$O) of compound **2.030**.

203
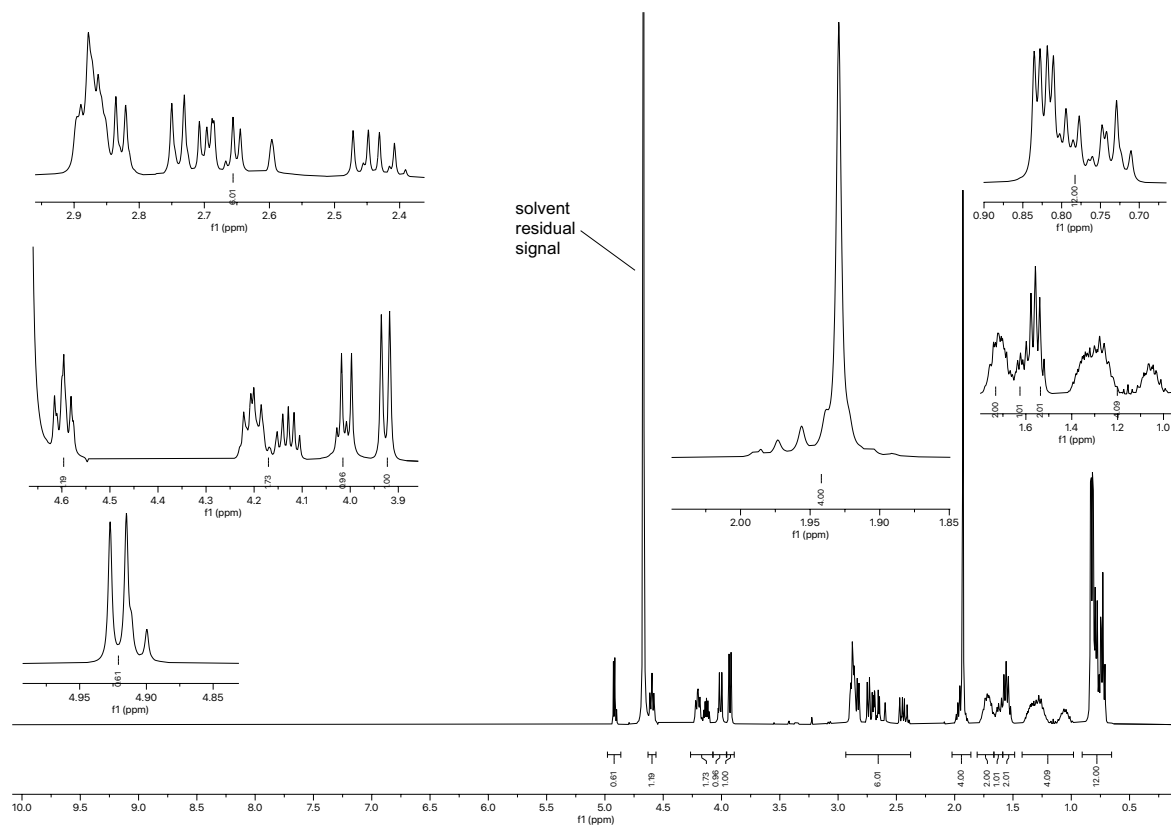
Figure 2.083. ^{1}H NMR spectrum (400 MHz, D$_2$O) of compound **2.031**.
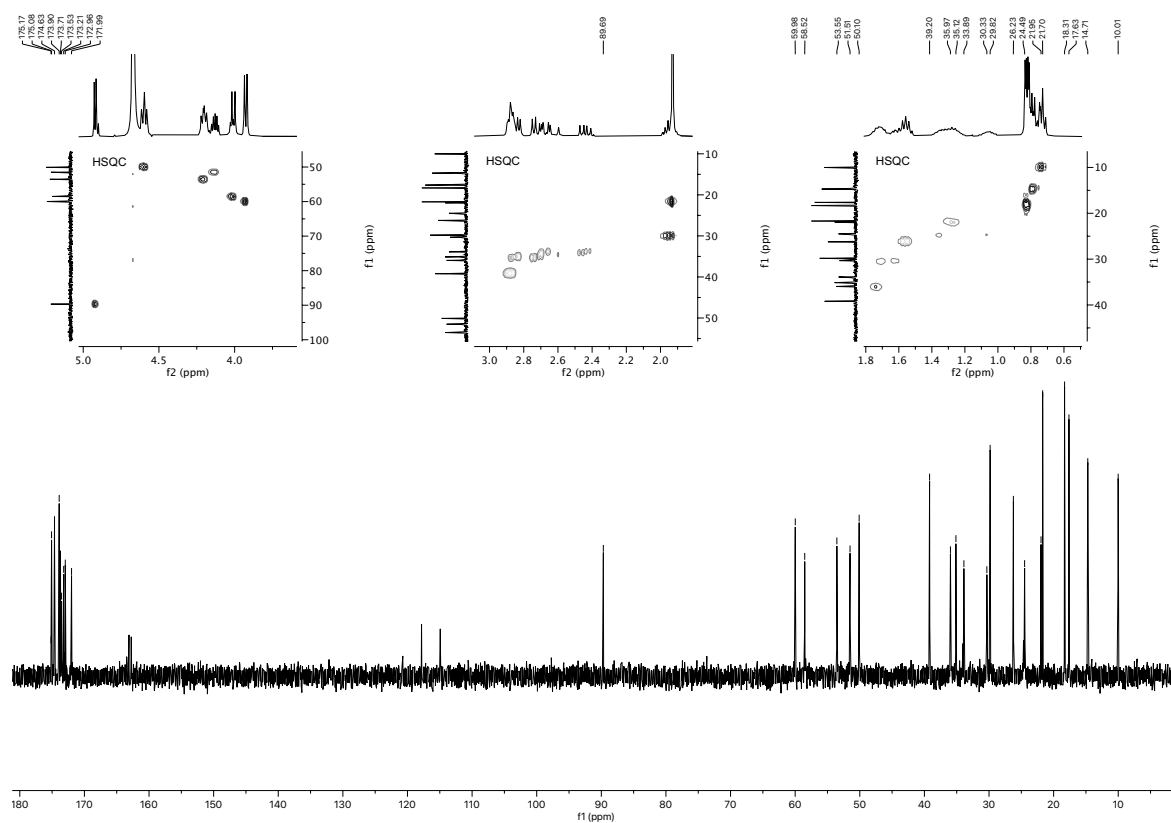
Figure 2.084. ^{13}C NMR spectrum (101 MHz, D$_2$O) of compound **2.031**.
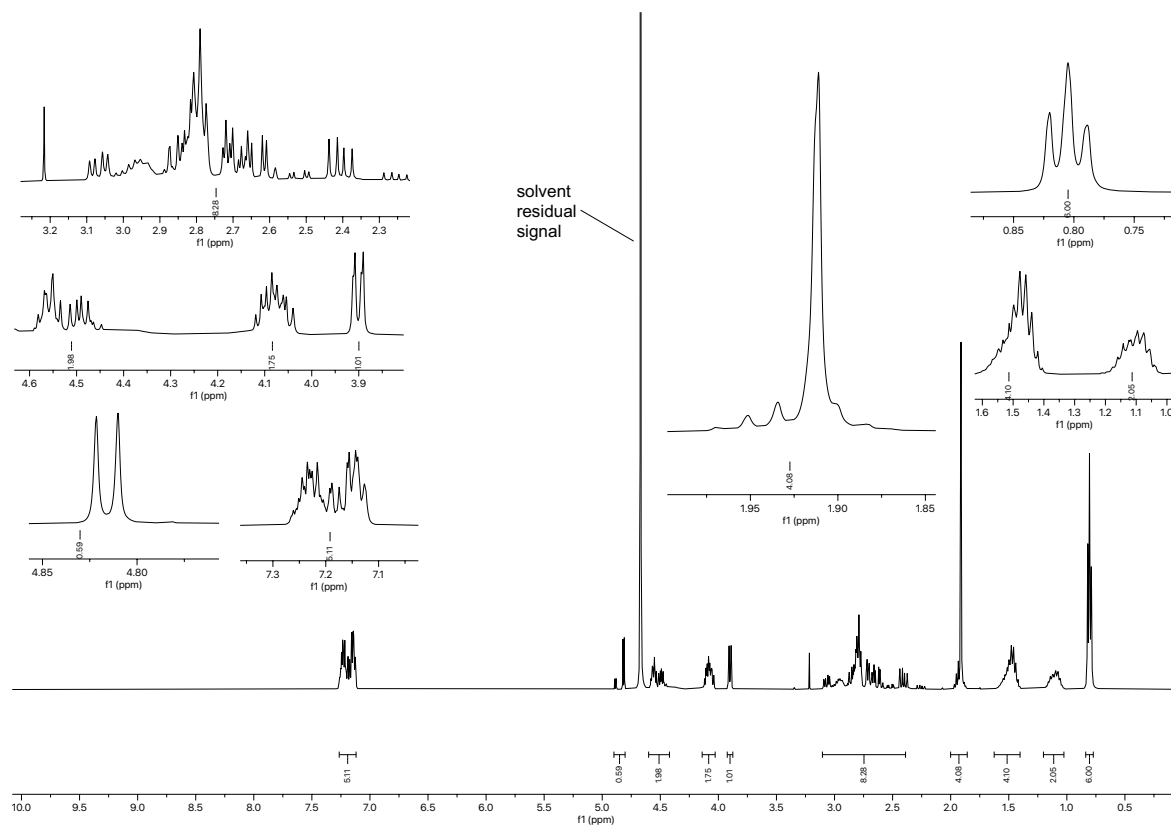
Figure 2.085. ^{1}H NMR spectrum (400 MHz, D$_2$O) of compound **2.032**.
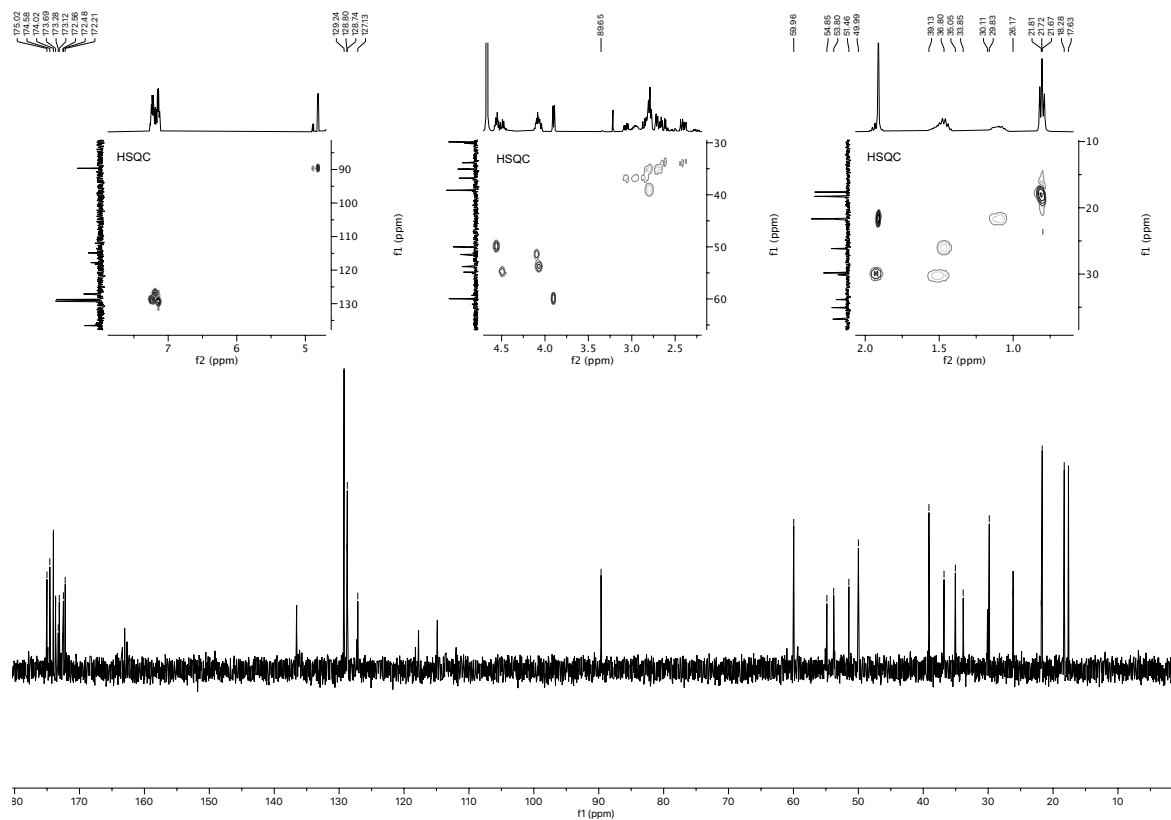
Figure 2.086. ^{13}C NMR spectrum (101 MHz, D$_2$O) of compound **2.032**.
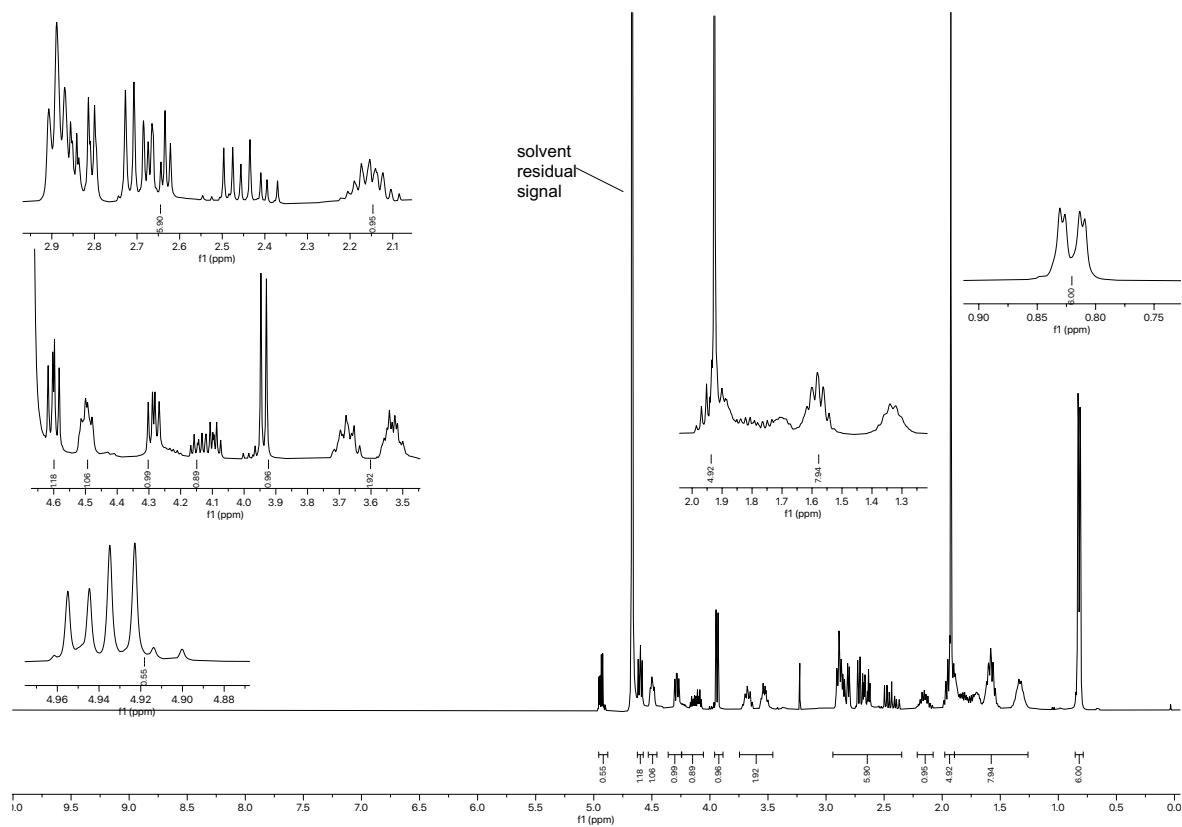
Figure 2.087. ^{1}H NMR spectrum (400 MHz, D$_2$O) of compound **2.033**.
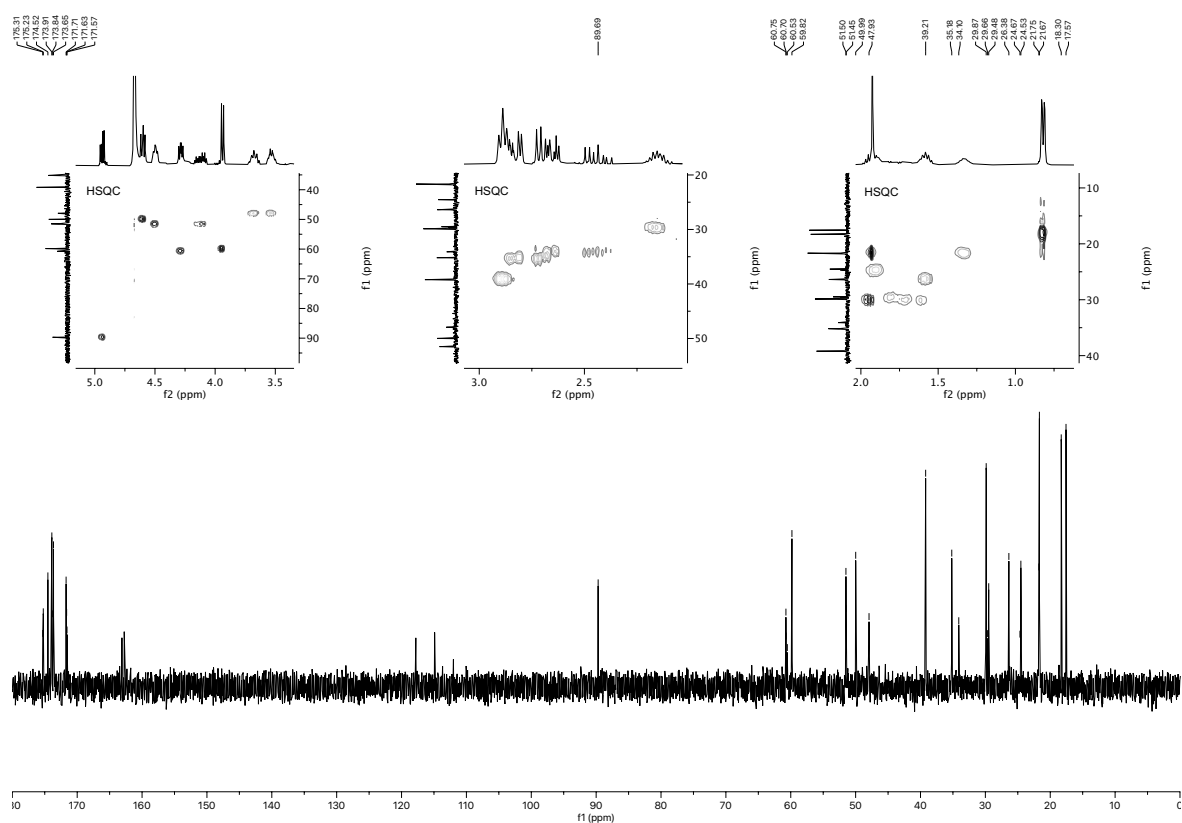
Figure 2.088. ^{13}C NMR spectrum (101 MHz, D$_2$O) of compound **2.033**.
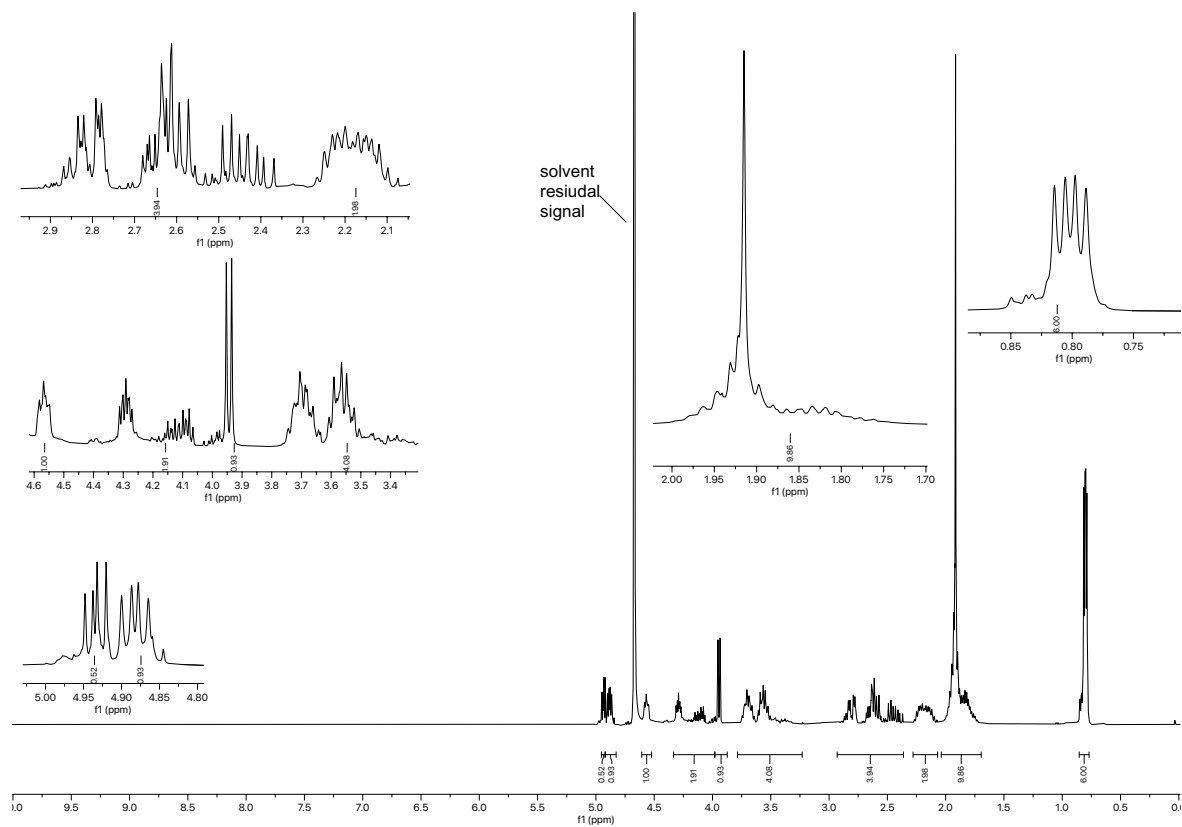
Figure 2.089. ^{1}H NMR spectrum (400 MHz, D$_2$O) of compound **2.034**.
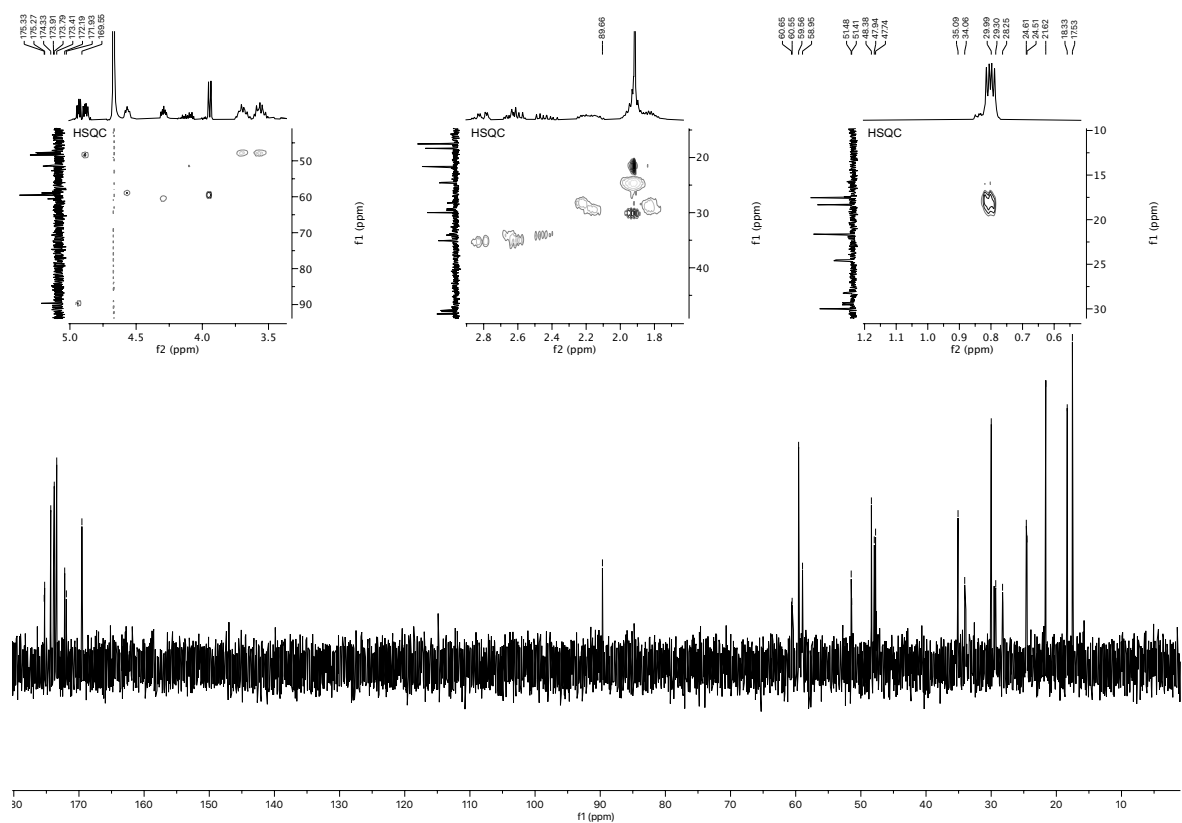
Figure 2.090. ^{13}C NMR spectrum (101 MHz, D$_2$O) of compound **2.034**.
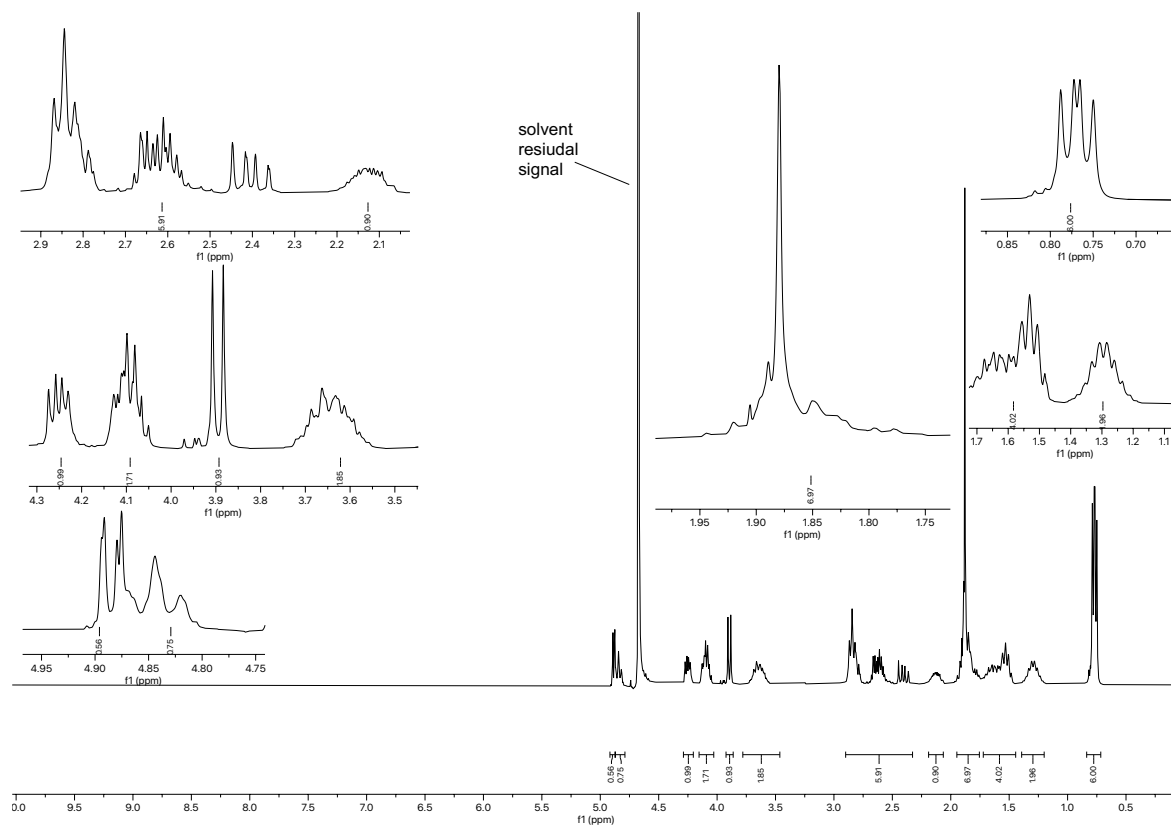
Figure 2.091. ^{1}H NMR spectrum (300 MHz, D$_2$O) of compound **2.035**.
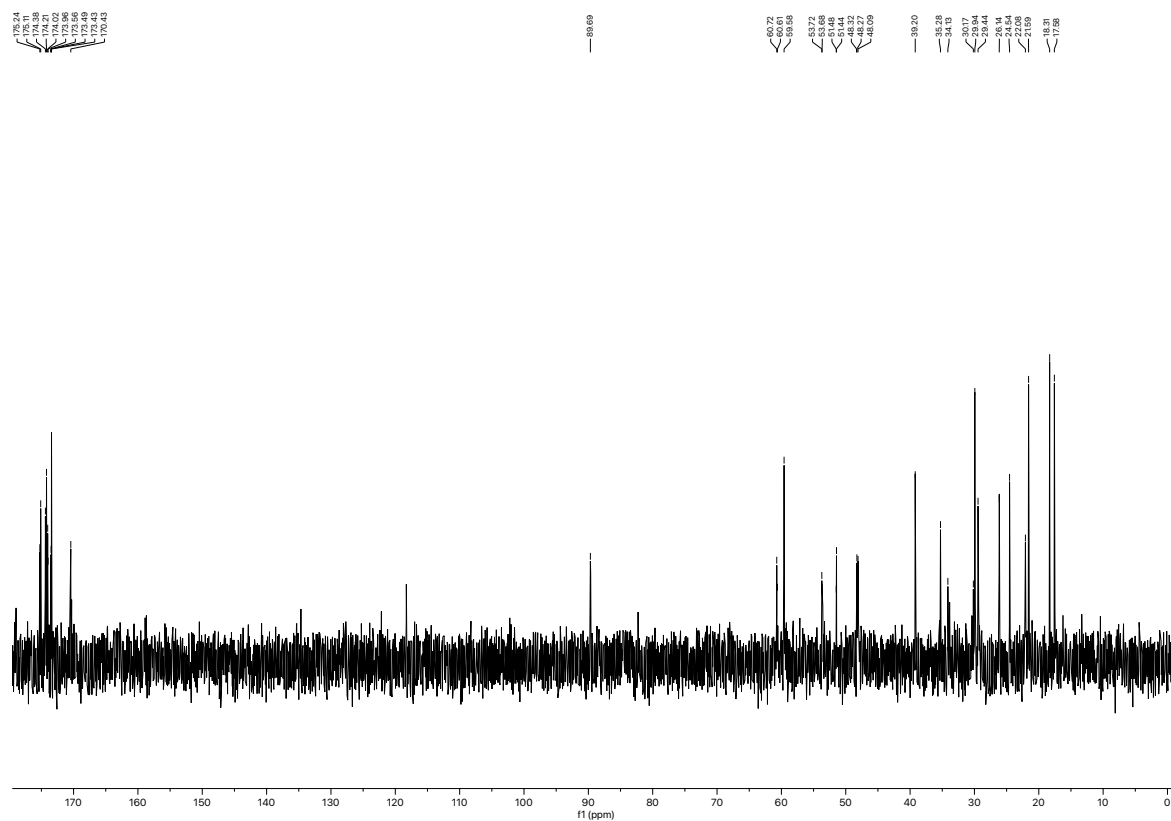
Figure 2.092. ^{13}C NMR spectrum (75 MHz, D$_2$O) of compound **2.035**.
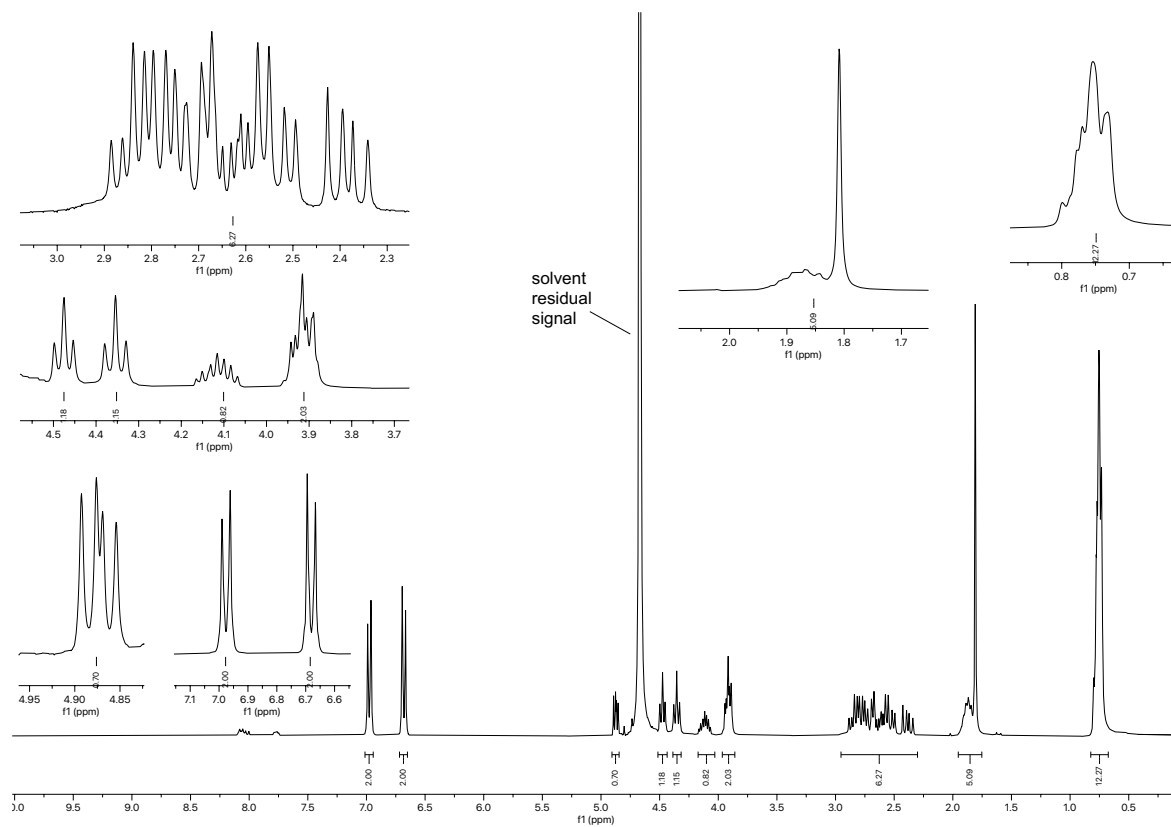
Figure 2.093. ^{1}H NMR spectrum (300 MHz, D$_2$O) of compound **2.036**.
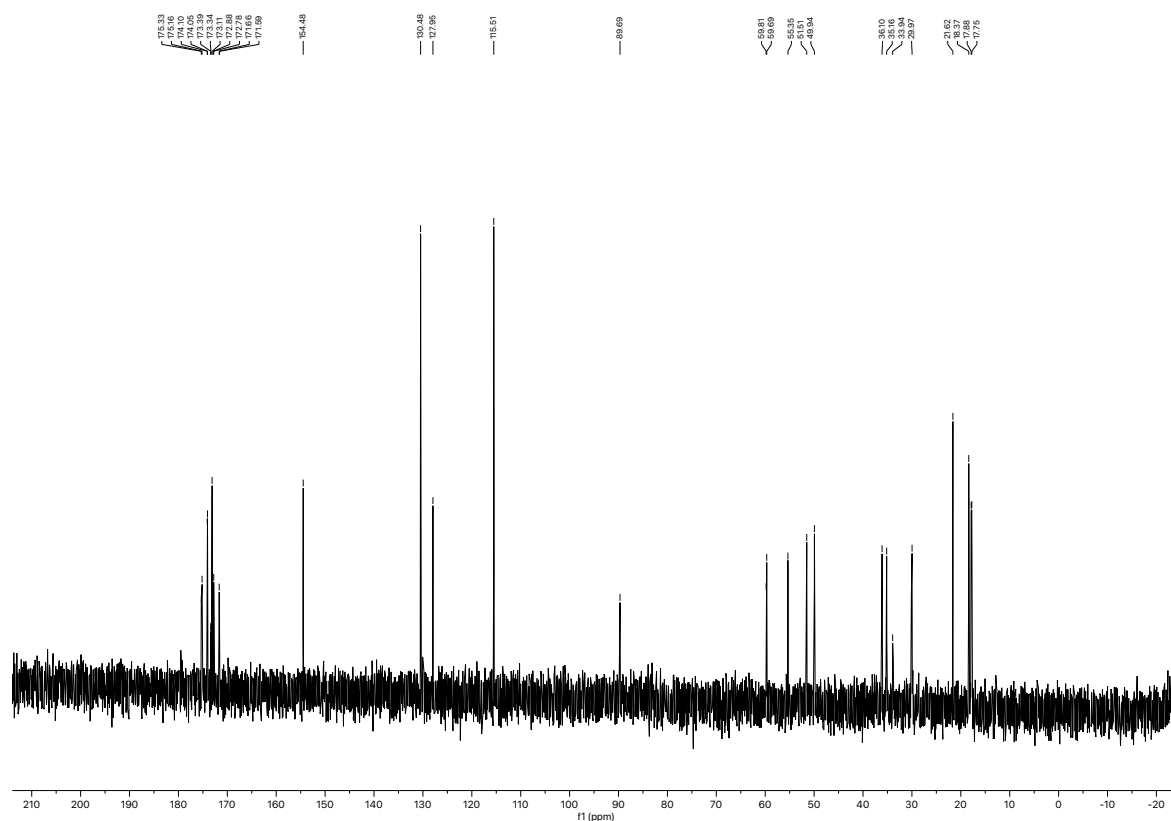
Figure 2.094. ^{1}H NMR spectrum (75 MHz, D$_2$O) of compound **2.036**.
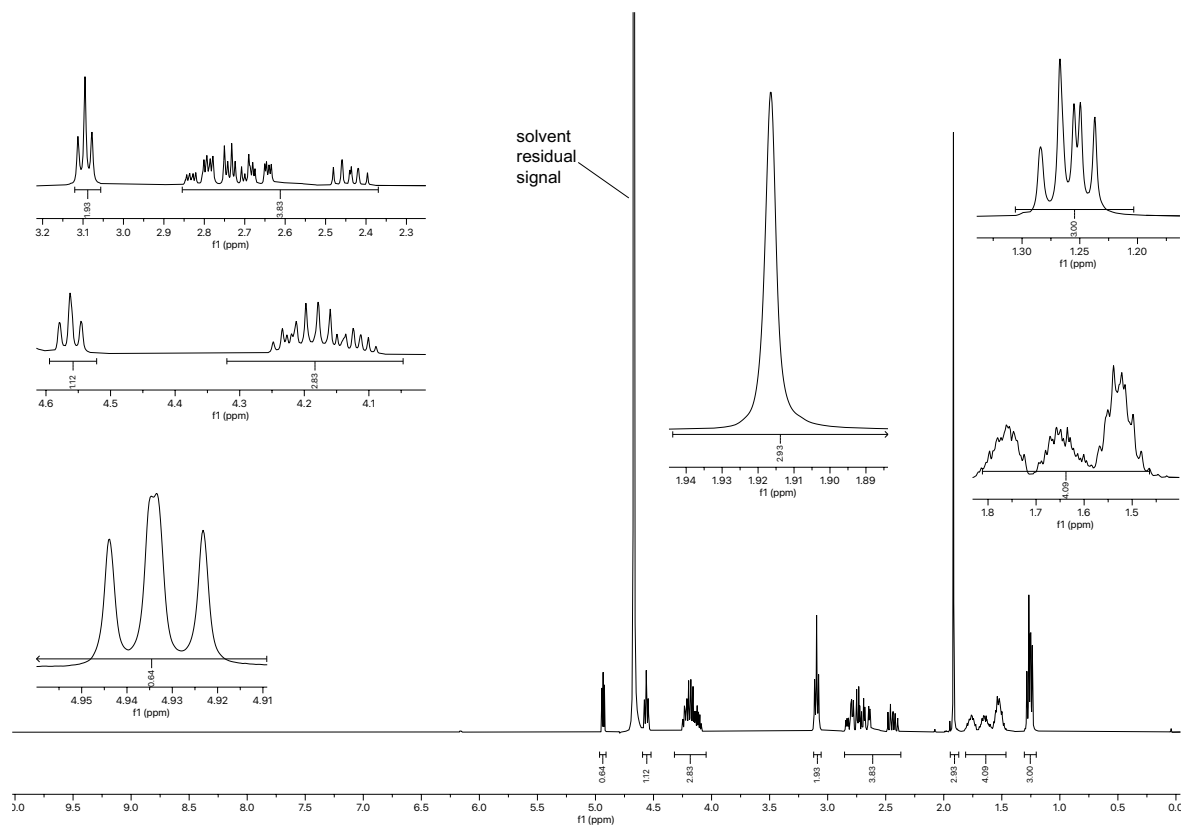
Figure 2.095. ¹H NMR spectrum (400 MHz, D₂O) of compound **2.037**.
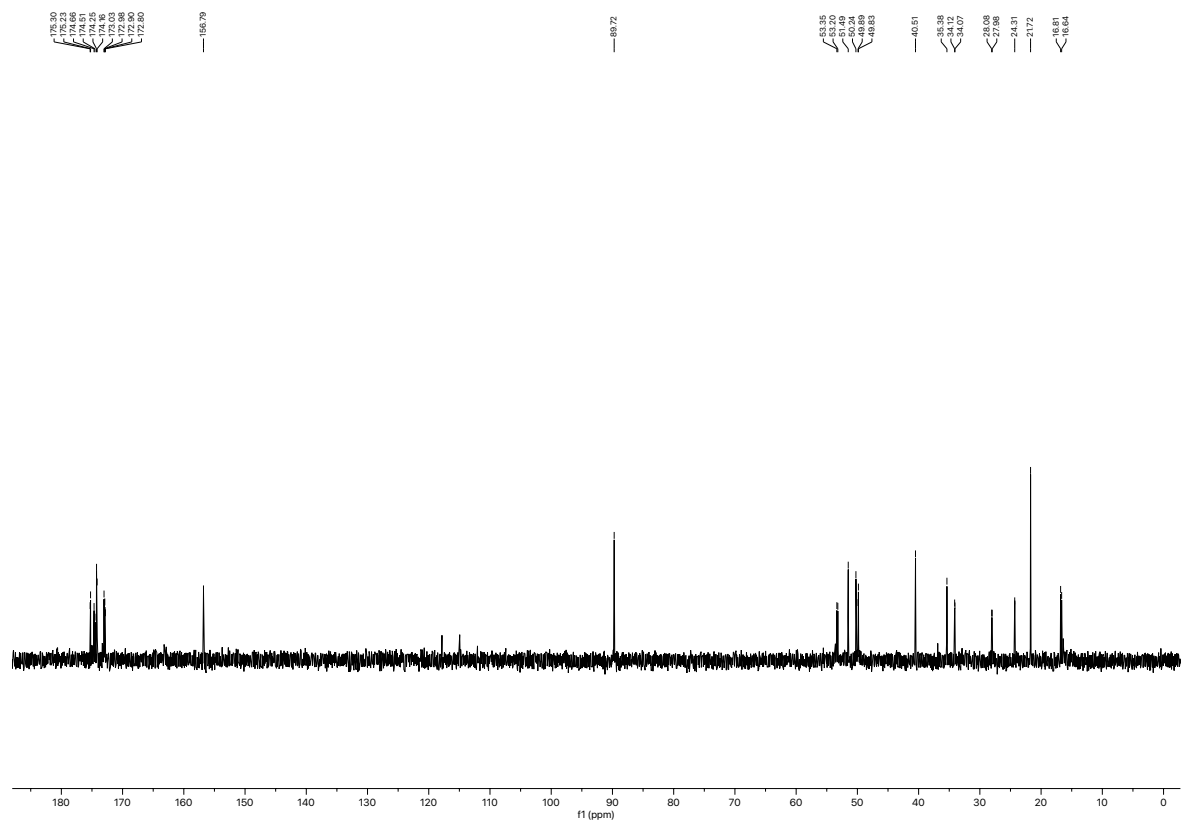
Figure 2.096. ¹³C NMR spectrum (101 MHz, D₂O) of compound **2.037**.
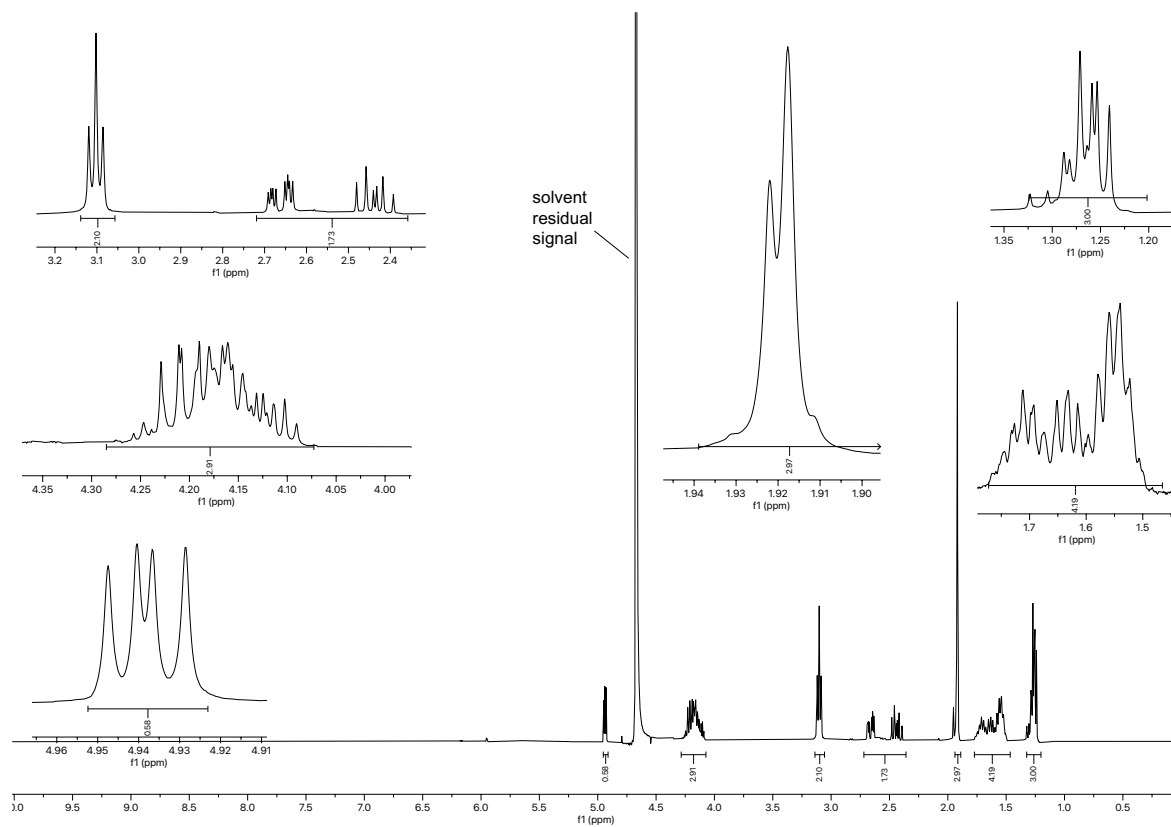
Figure 2.097. ^{1}H NMR spectrum (400 MHz, D_2O) of compound **2.038**.
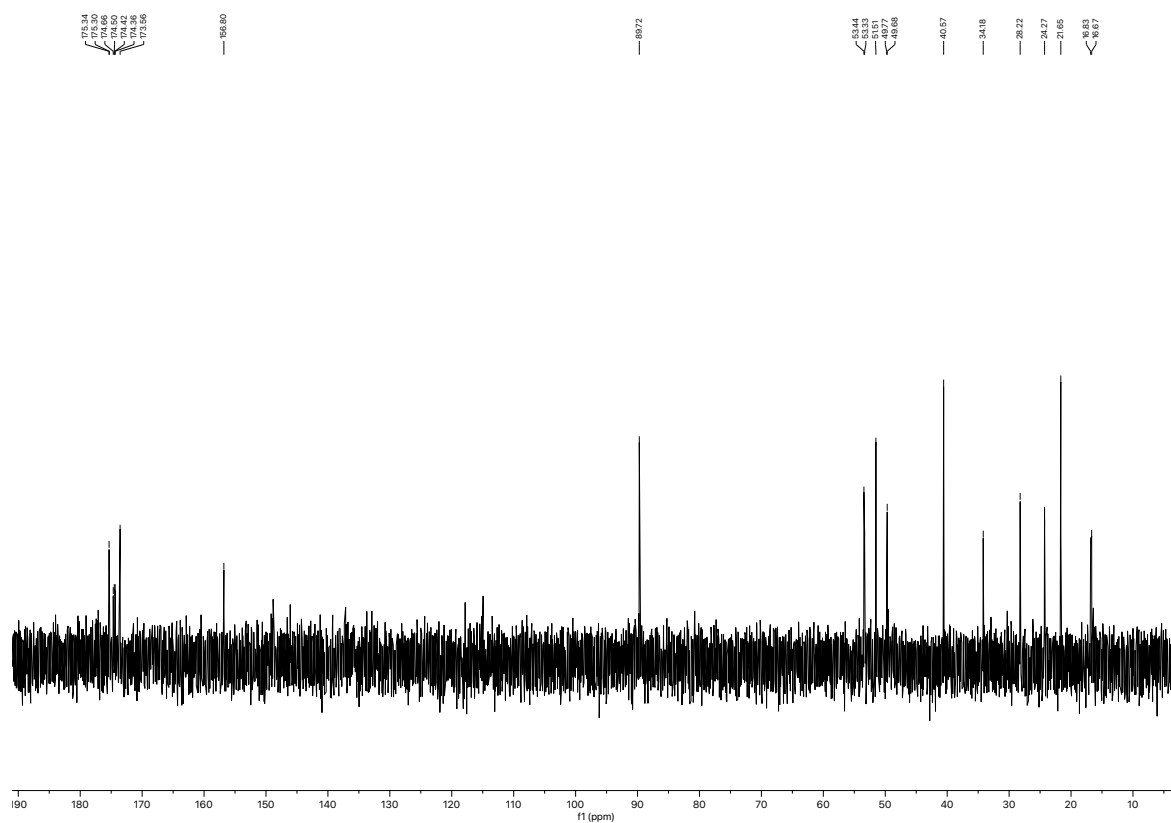
Figure 2.098. ^{13}C NMR spectrum (101 MHz, D_2O) of compound **2.038**.
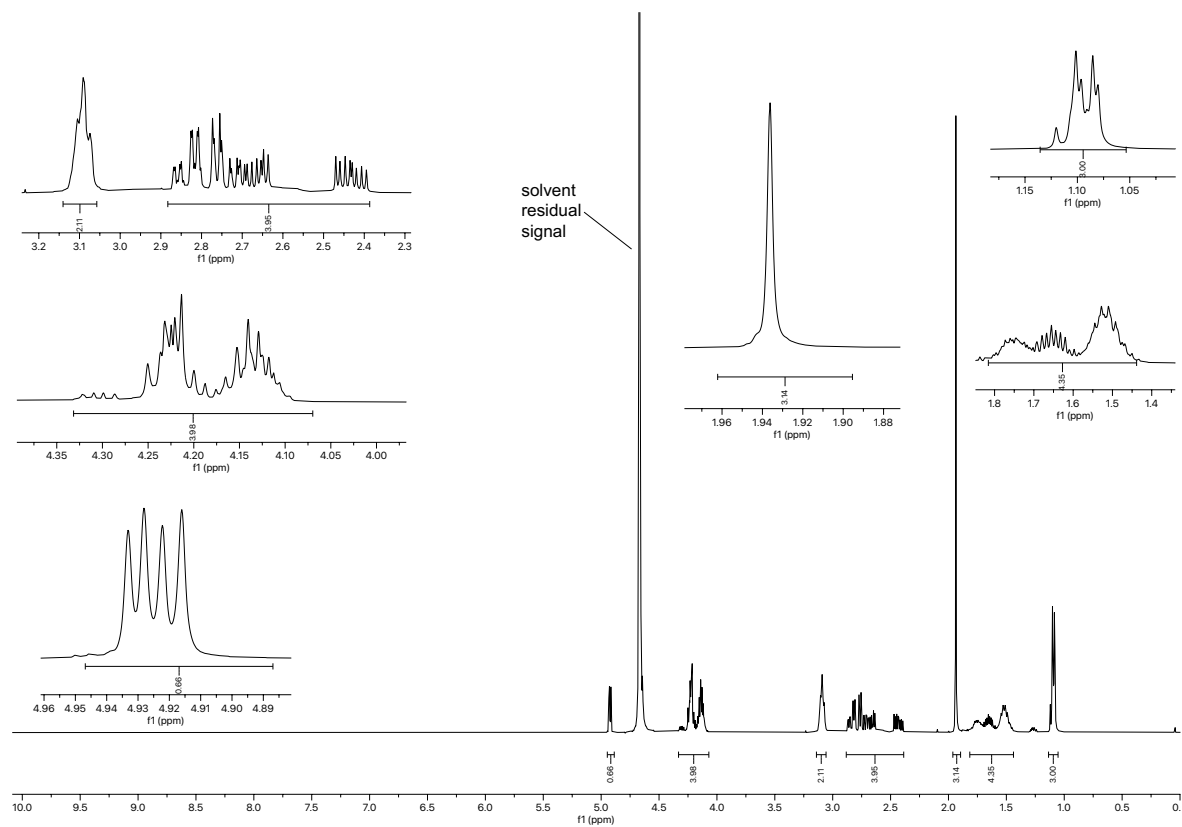
Figure 2.099. ^{1}H NMR spectrum (400 MHz, D$_2$O) of compound **2.039**.
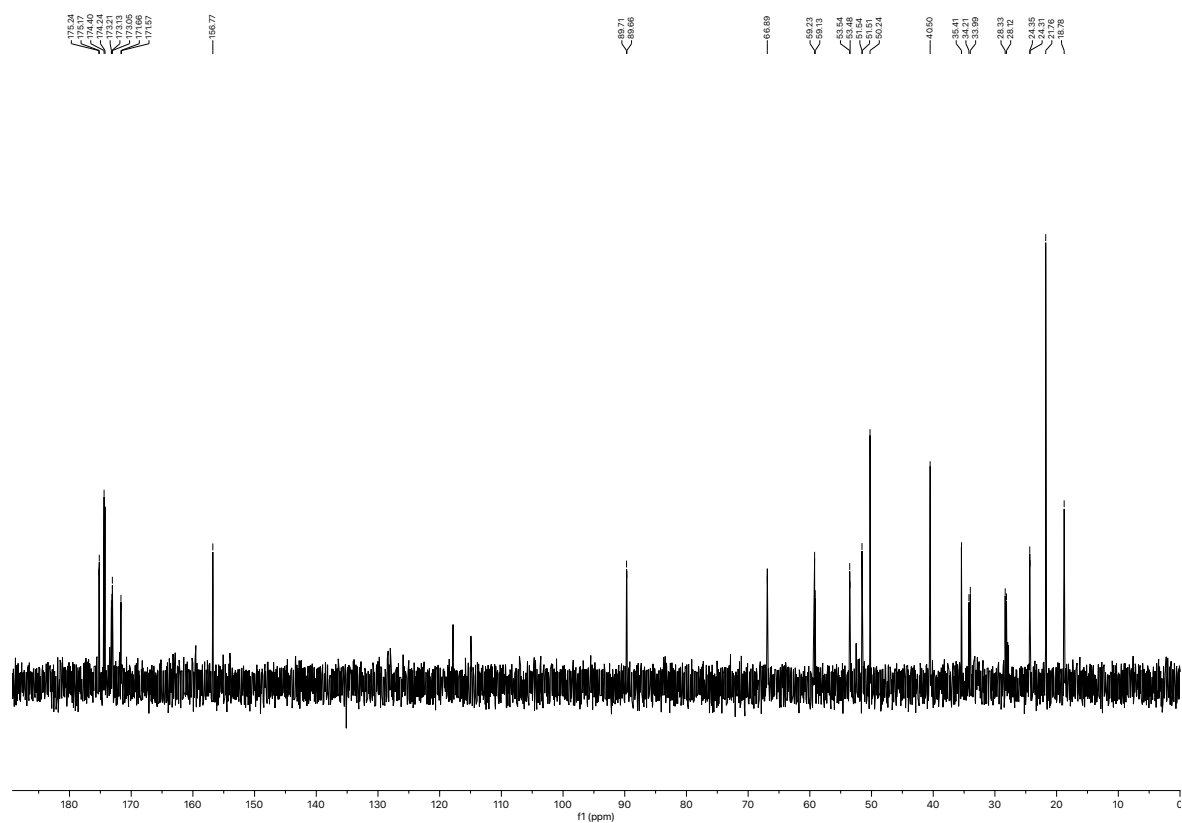
Figure 2.100. ^{13}C NMR spectrum (101 MHz, D$_2$O) of compound **2.039**.
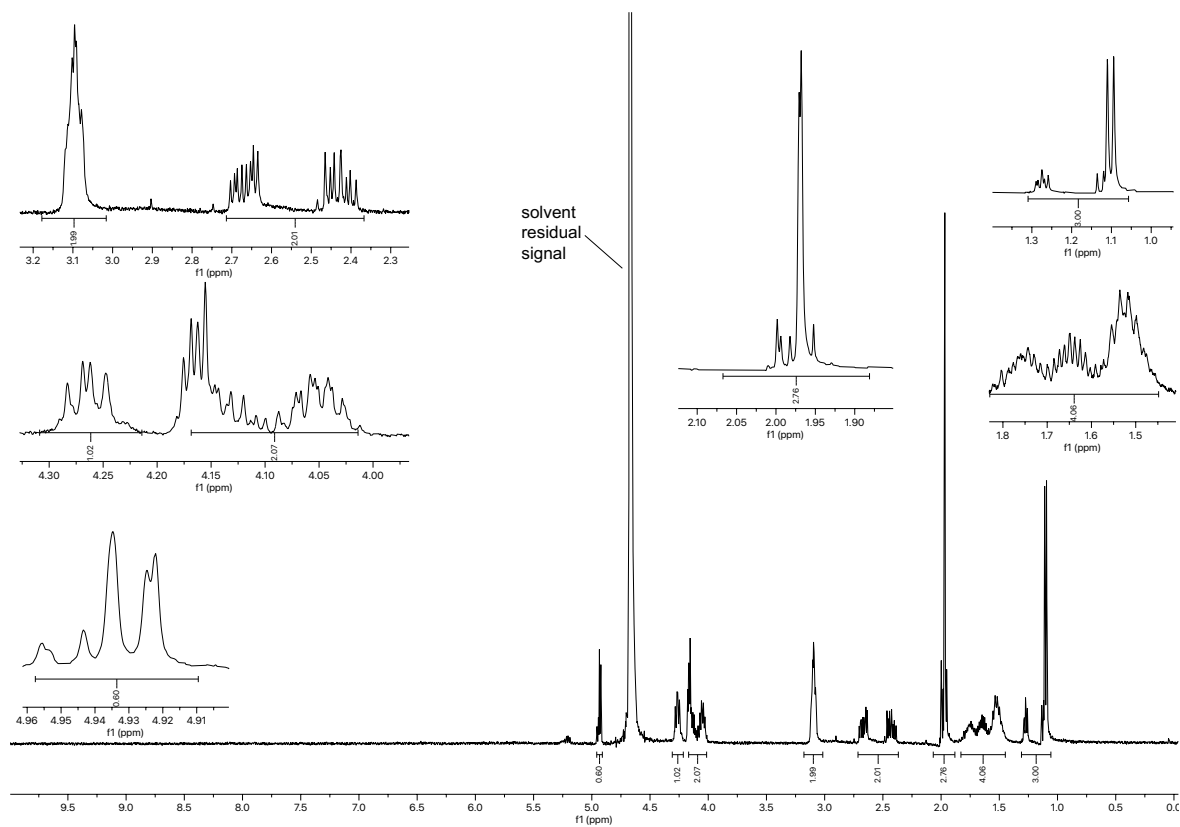
Figure 2.101. ^{1}H NMR spectrum (400 MHz, D$_2$O) of compound **2.040**.
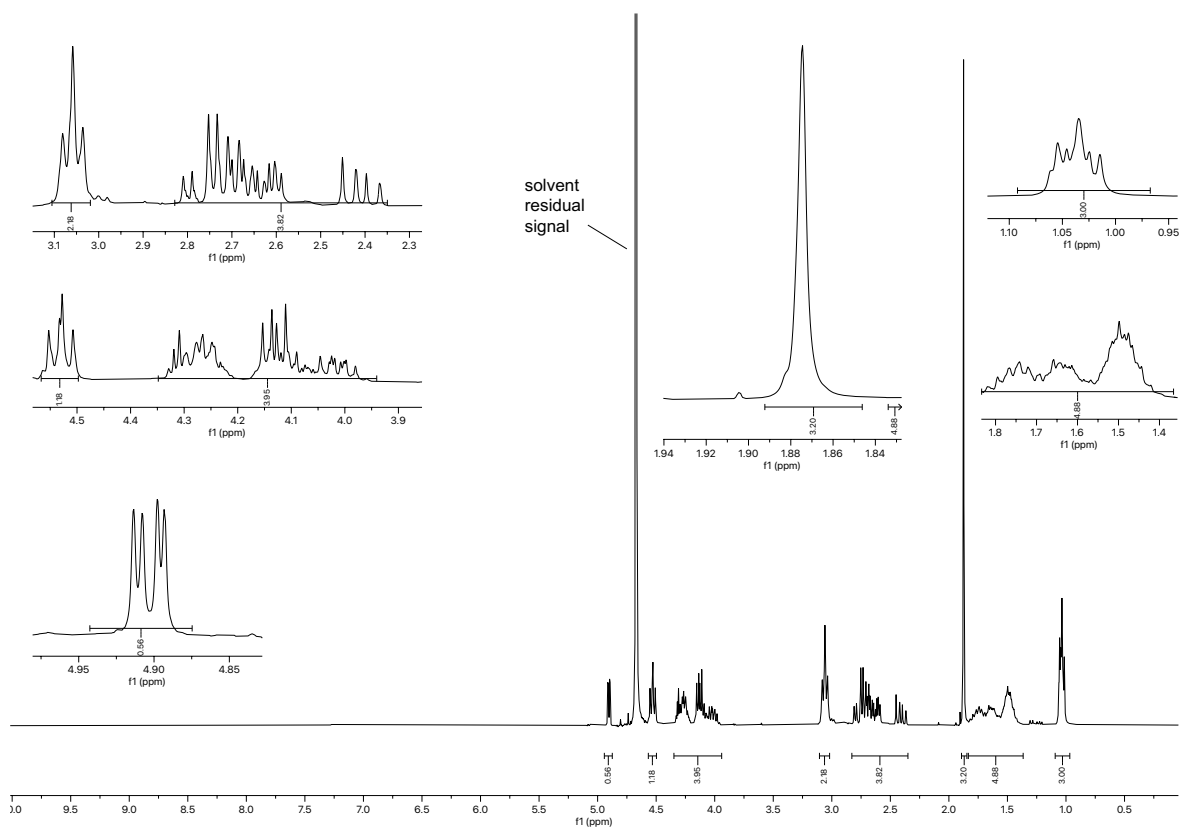
Figure 2.102. ^{1}H NMR spectrum (300 MHz, D$_2$O) of compound **2.041**.
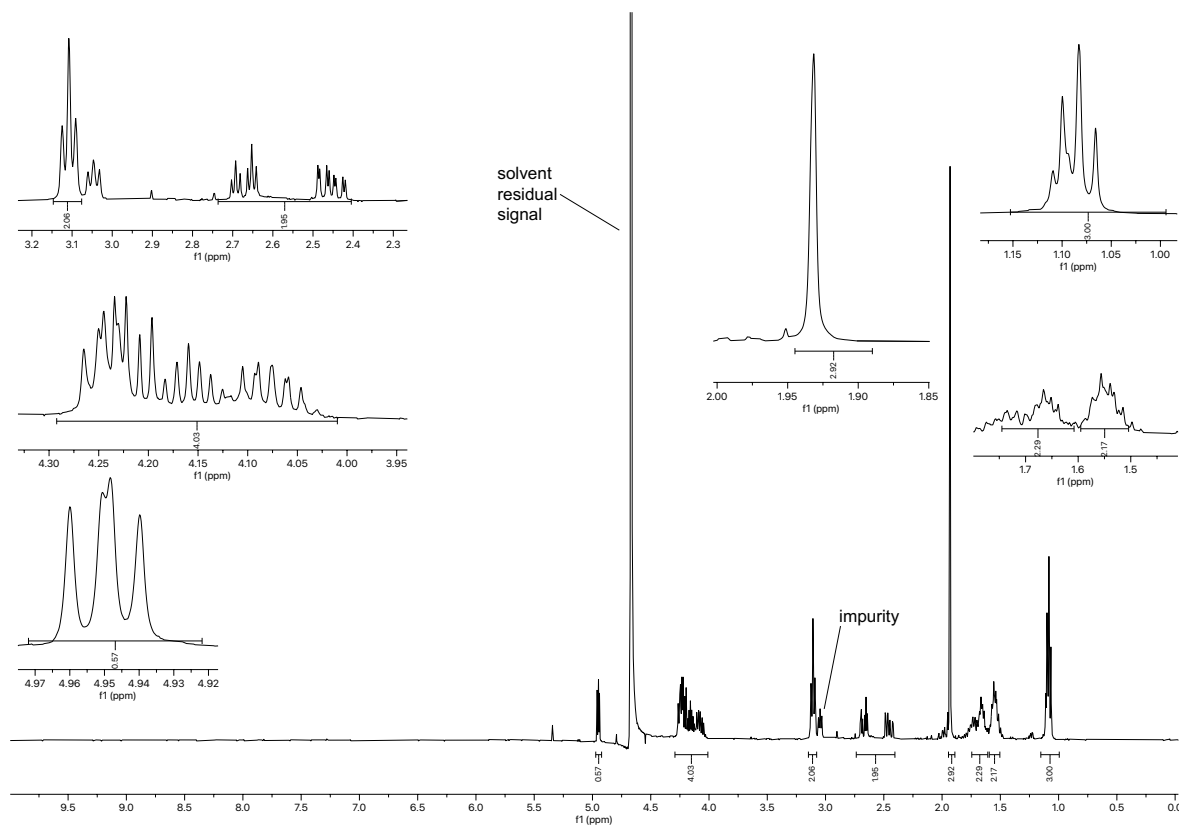
Figure 2.103. ^{1}H NMR spectrum (400 MHz, D_2O) of compound **2.042**.
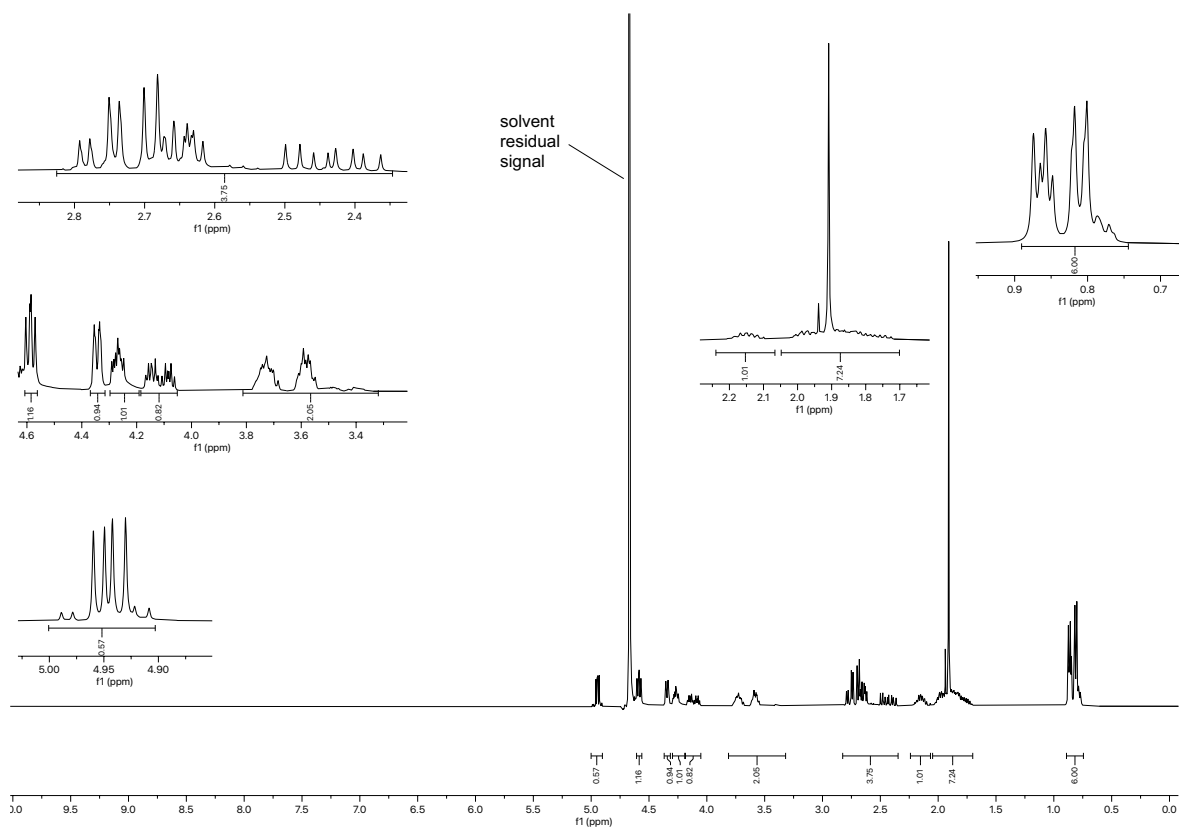
Figure 2.104. ^{1}H NMR spectrum (400 MHz, D_2O) of compound **2.043**.
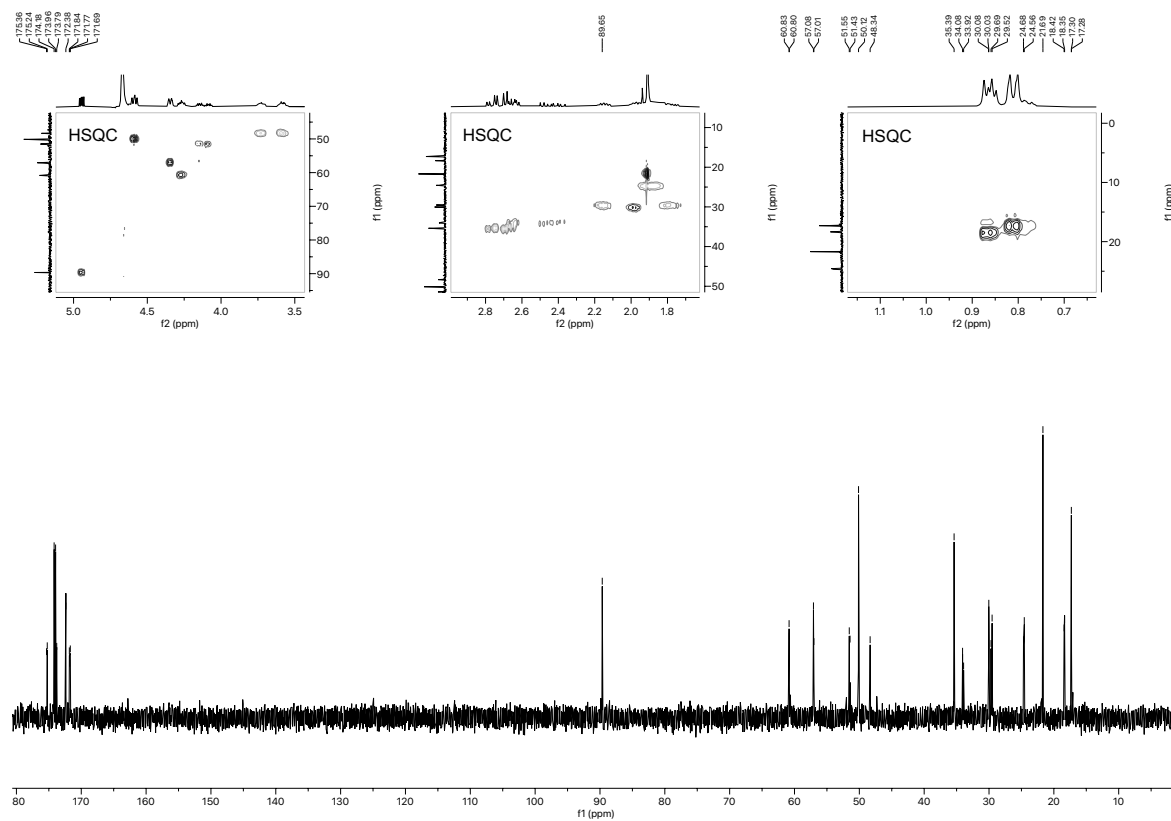
Figure 2.105. ^{13}C NMR spectrum (101 MHz, D$_2$O) of compound **2.043**.
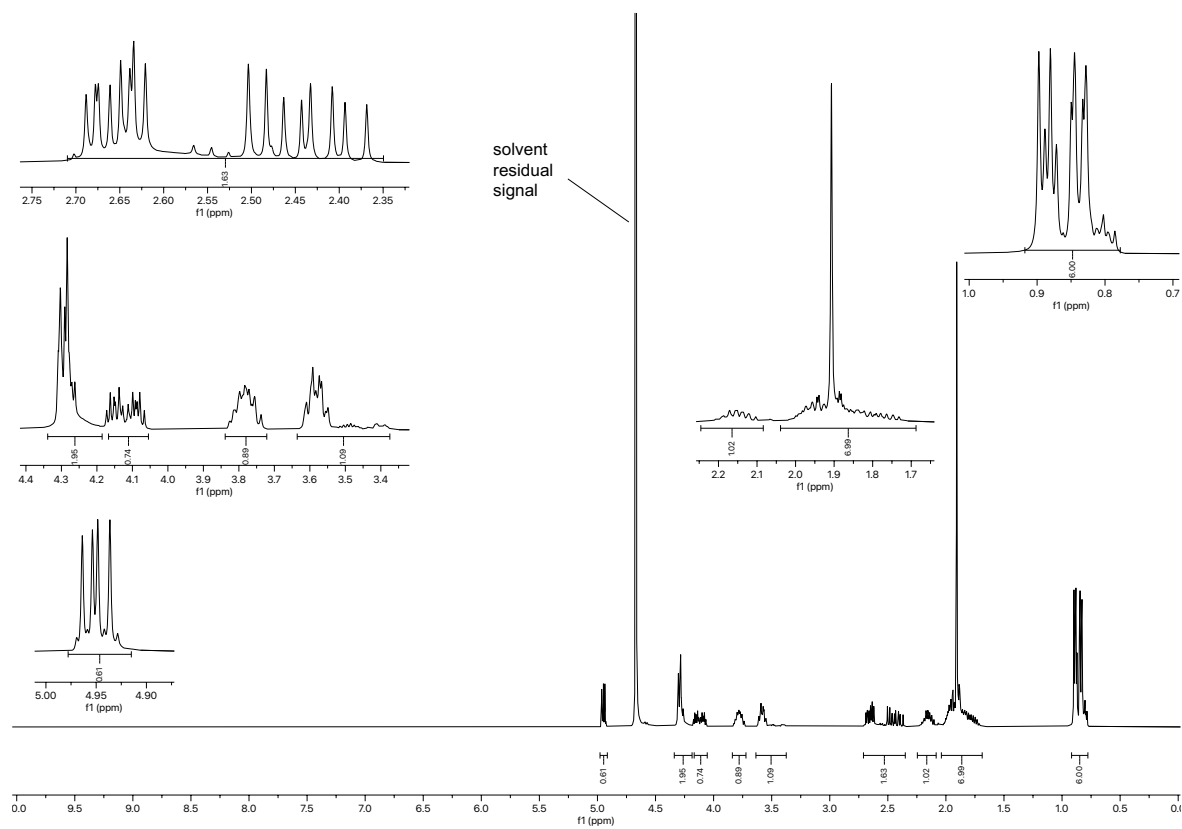
Figure 2.106. ^{1}H NMR spectrum (400 MHz, D$_2$O) of compound **2.044**.
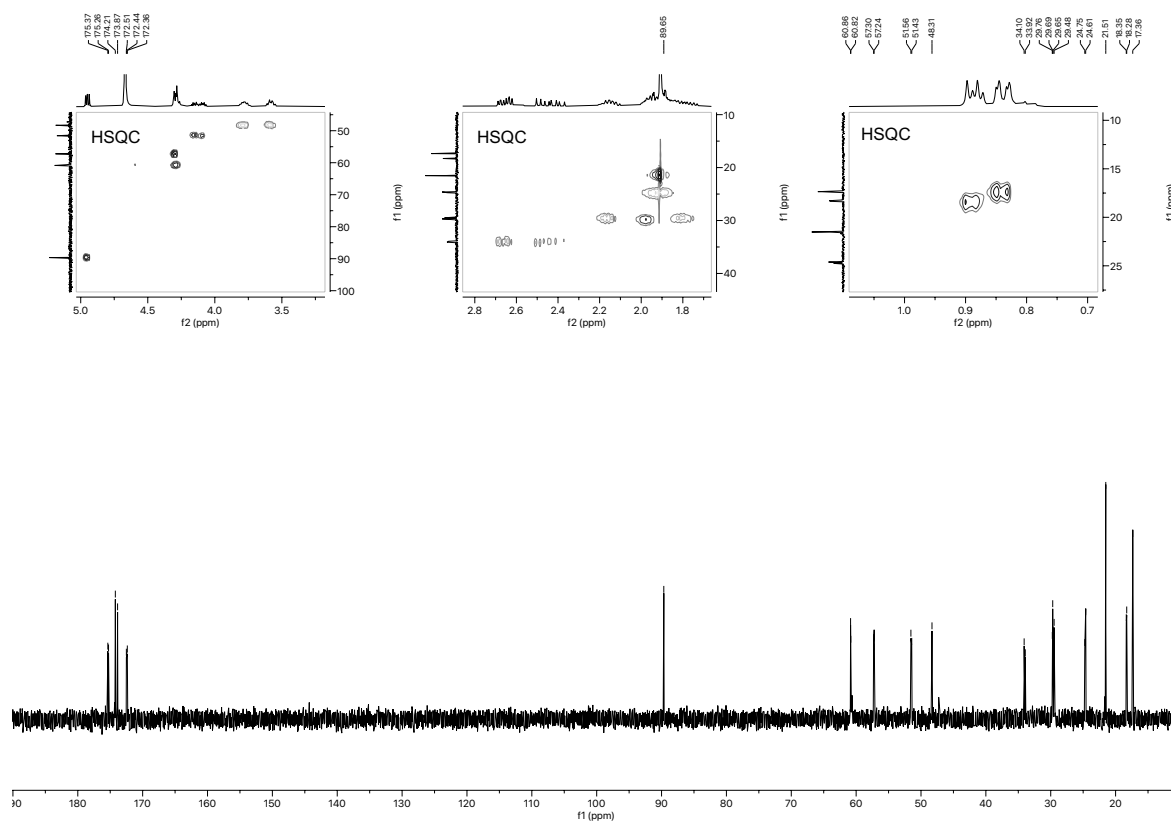
Figure 2.107. ^{13}C NMR spectrum (101 MHz, D$_2$O) of compound **2.044**.
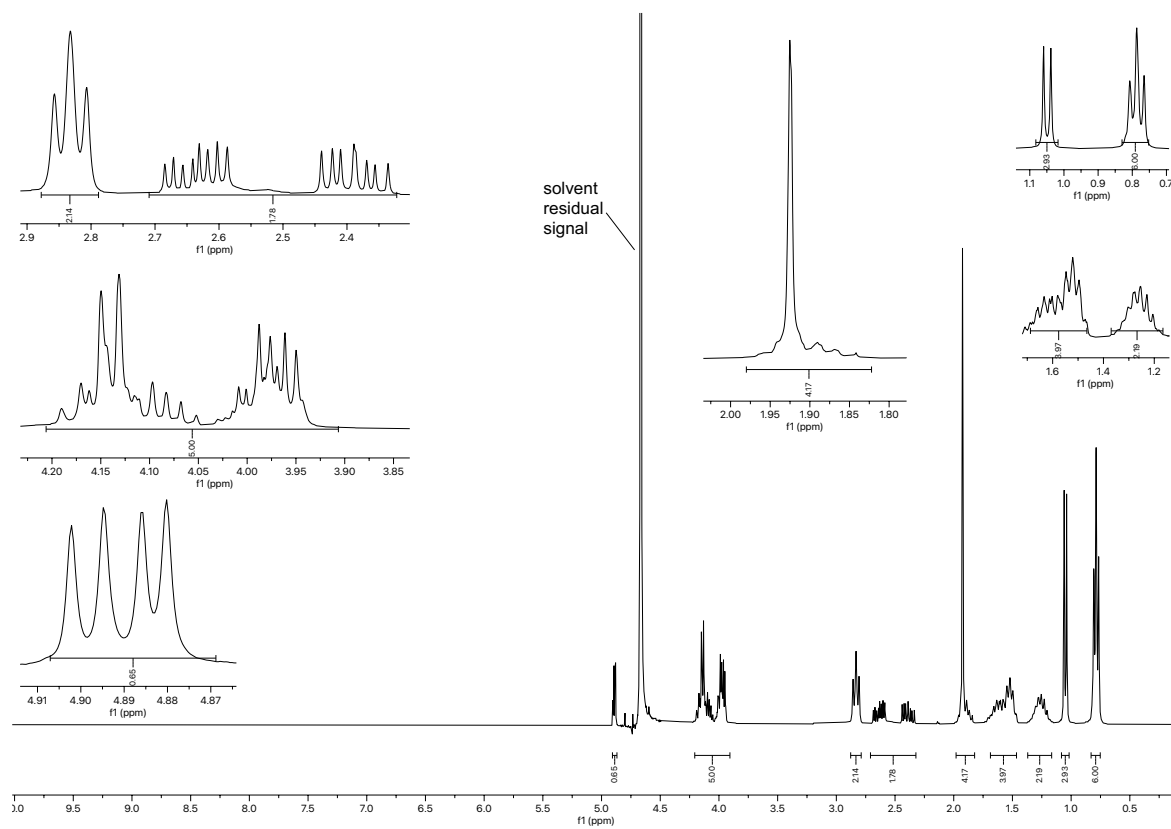
Figure 2.108. ^{1}H NMR spectrum (300 MHz, D$_2$O) of compound **2.045**.

216
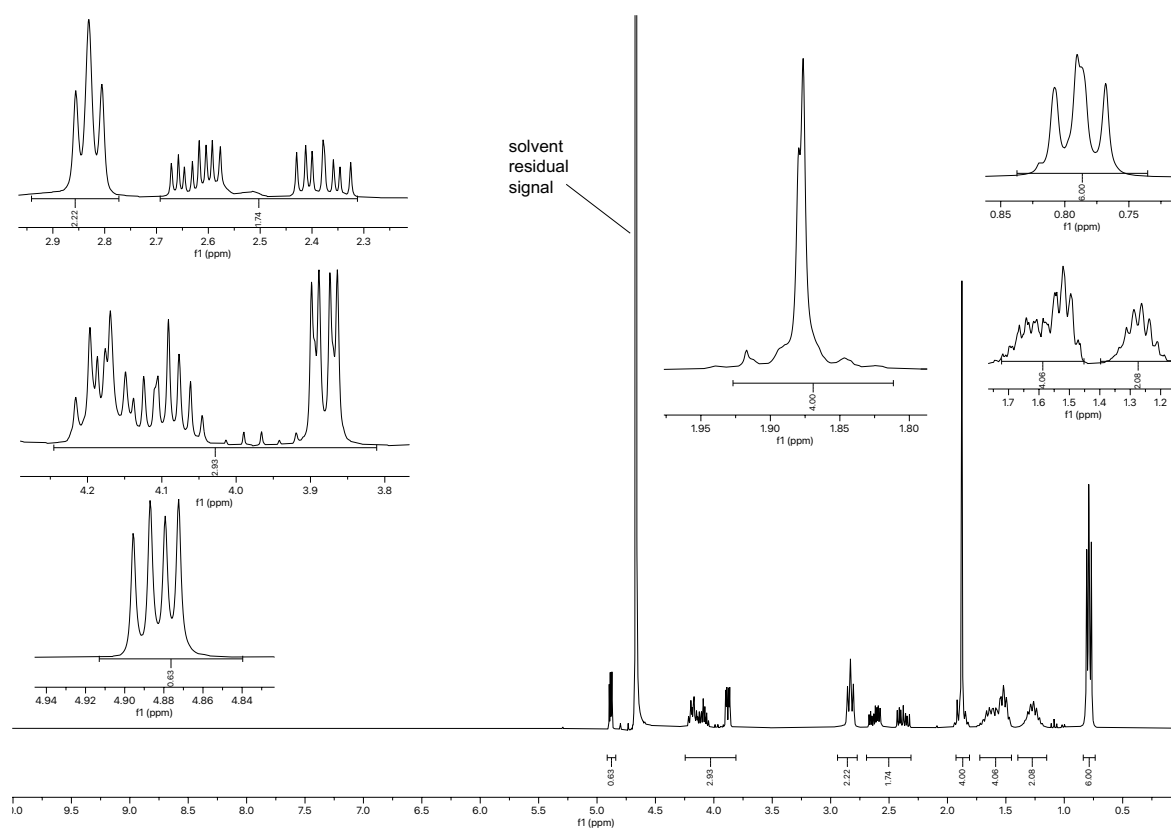
Figure 2.109. ^{1}H NMR spectrum (300 MHz, D$_2$O) of compound **2.046**.
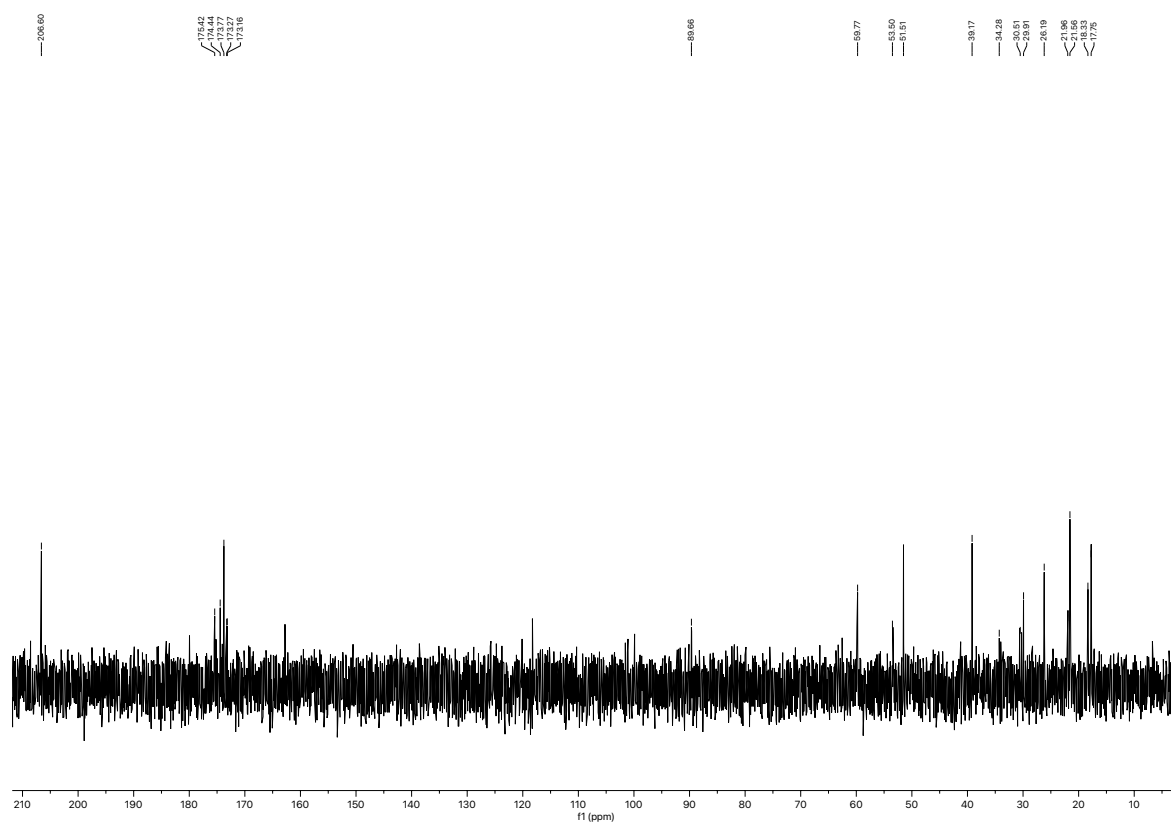
Figure 2.110. ^{13}C NMR spectrum (75 MHz, D$_2$O) of compound **2.046**.

217
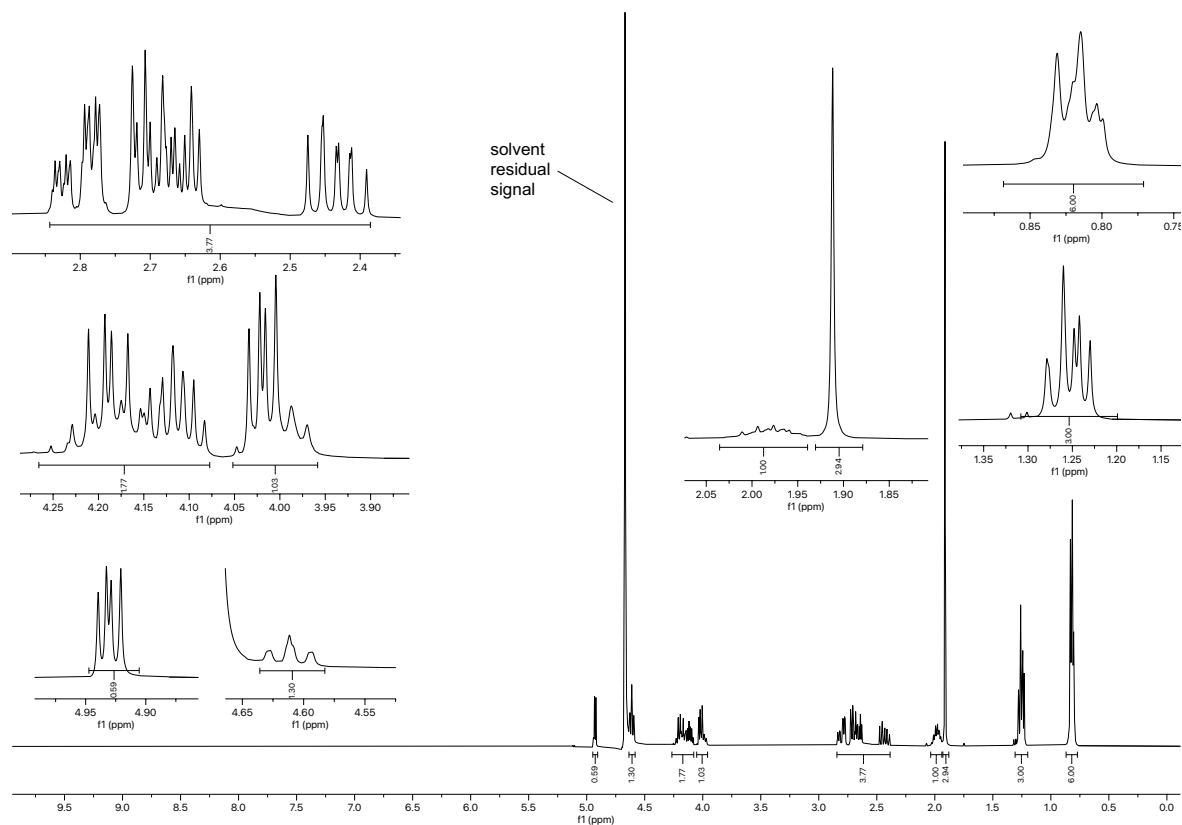
Figure 2.111. ^{1}H NMR spectrum (400 MHz, D$_2$O) of compound **2.047**.
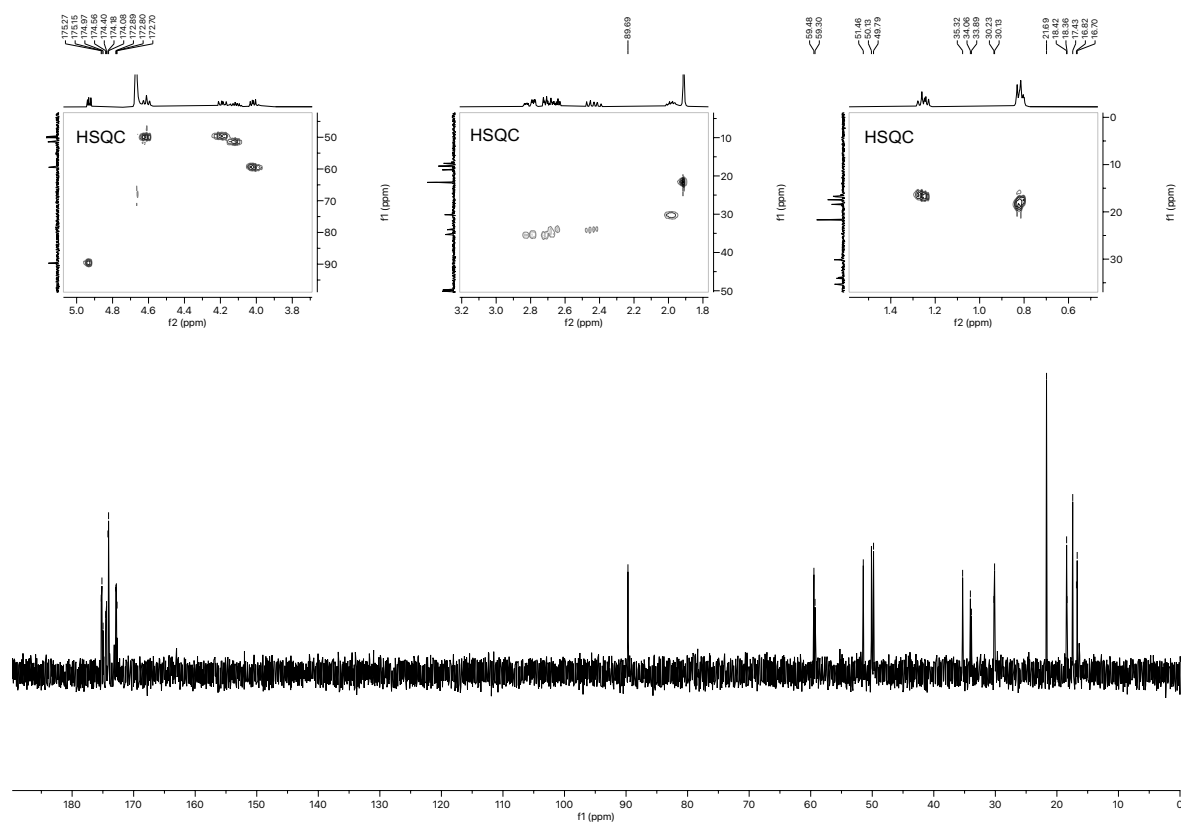
Figure 2.112. ^{13}C NMR spectrum (101 MHz, D$_2$O) of compound **2.047**.

218
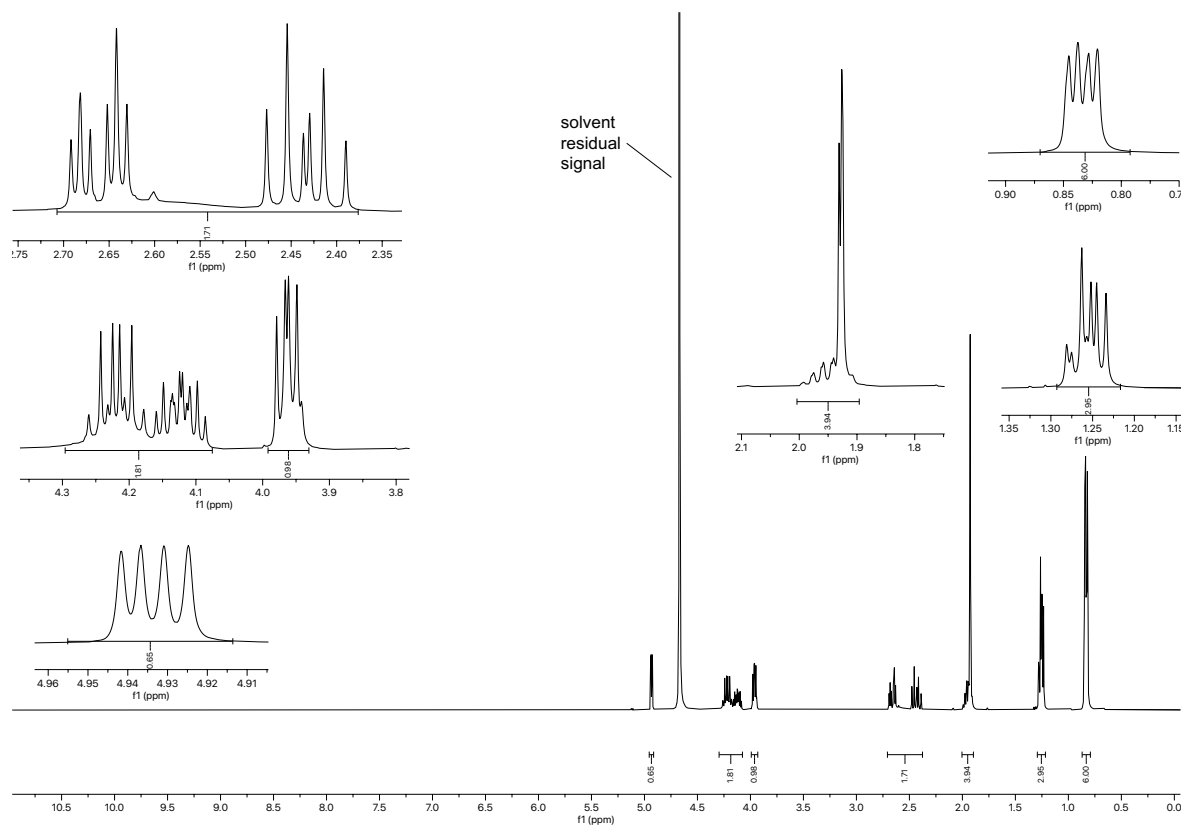
Figure 2.113. ^{1}H NMR spectrum (400 MHz, D$_2$O) of compound **2.048**.
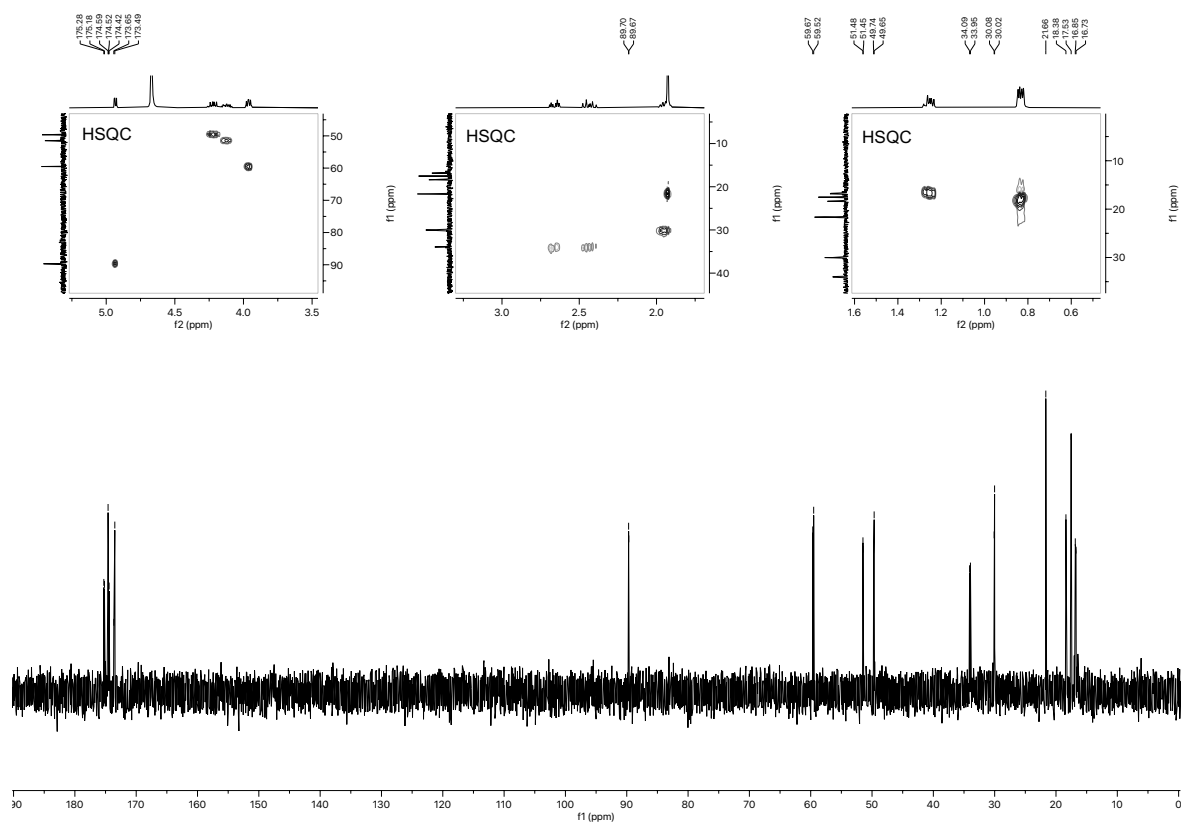
Figure 2.114. ^{13}C NMR spectrum (101 MHz, D$_2$O) of compound **2.048**.
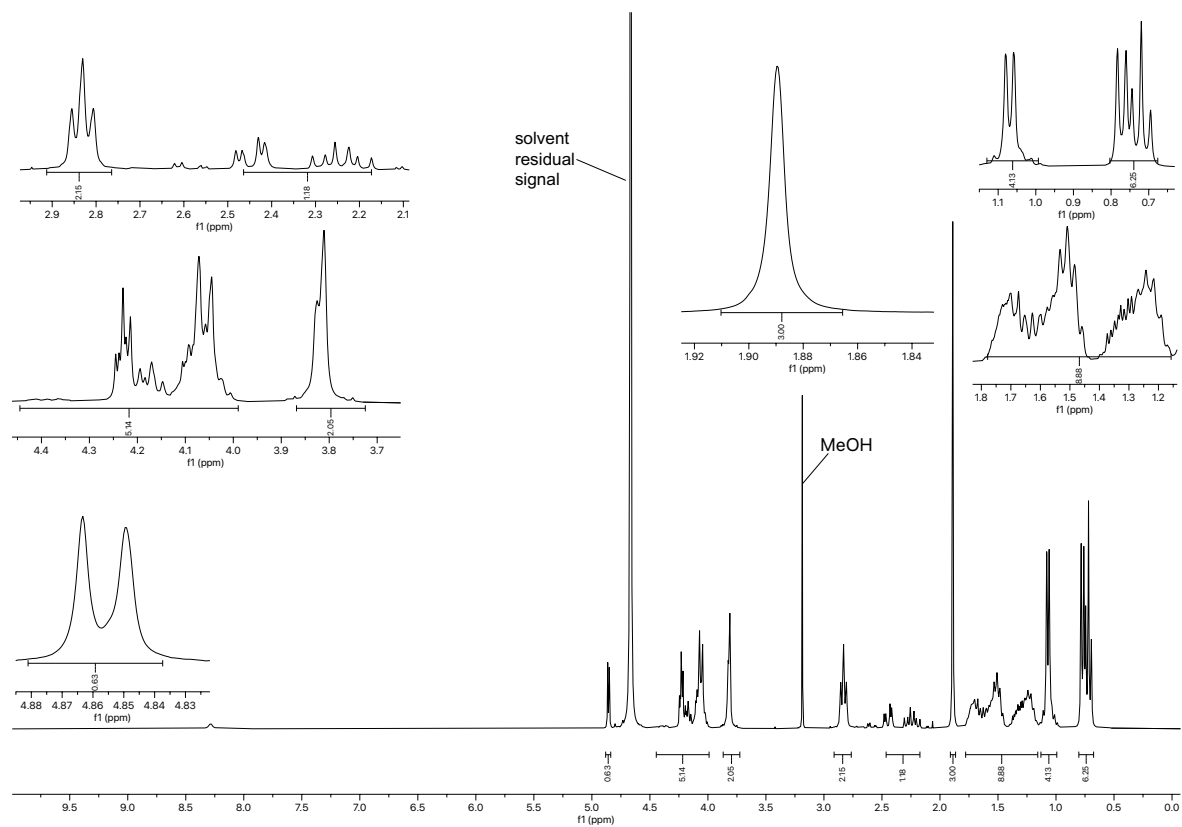
Figure 2.115. ^{1}H NMR spectrum (300 MHz, D$_2$O) of compound **2.049**.
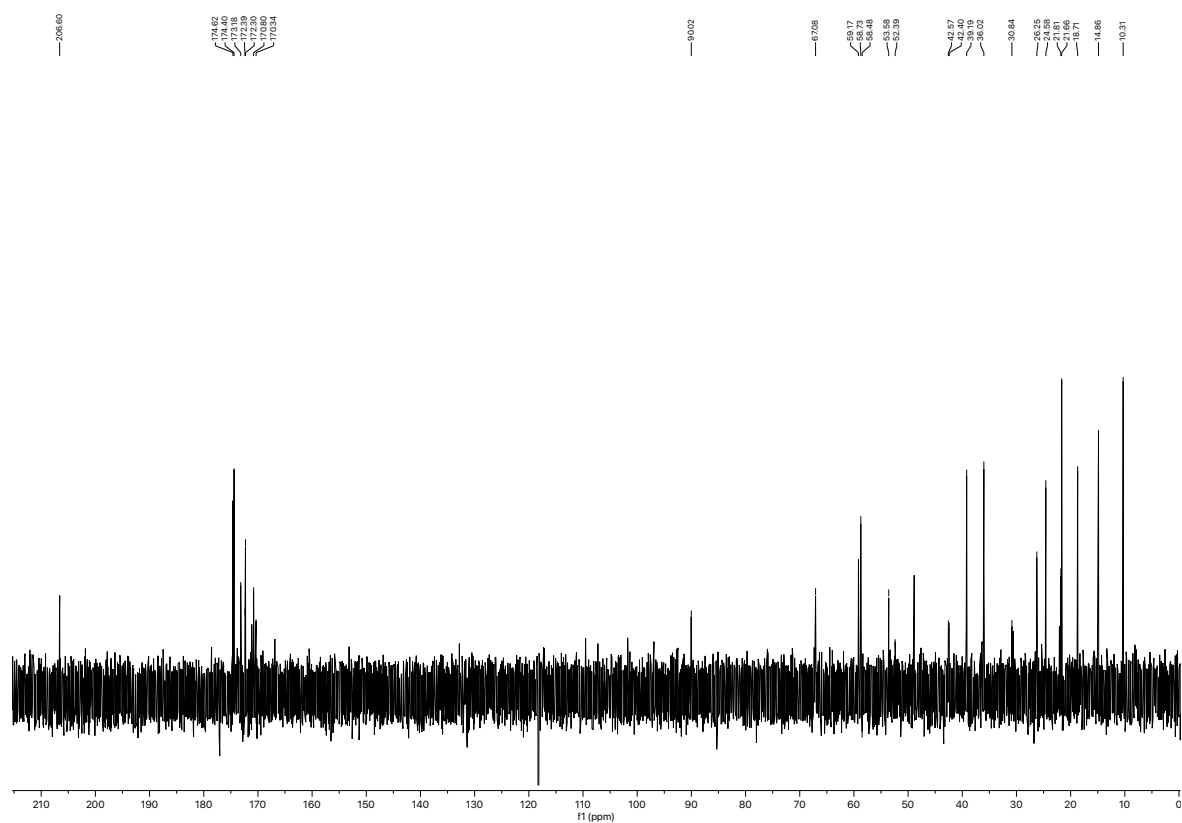
Figure 2.116. ^{13}C NMR spectrum (75 MHz, D$_2$O) of compound **2.049.**
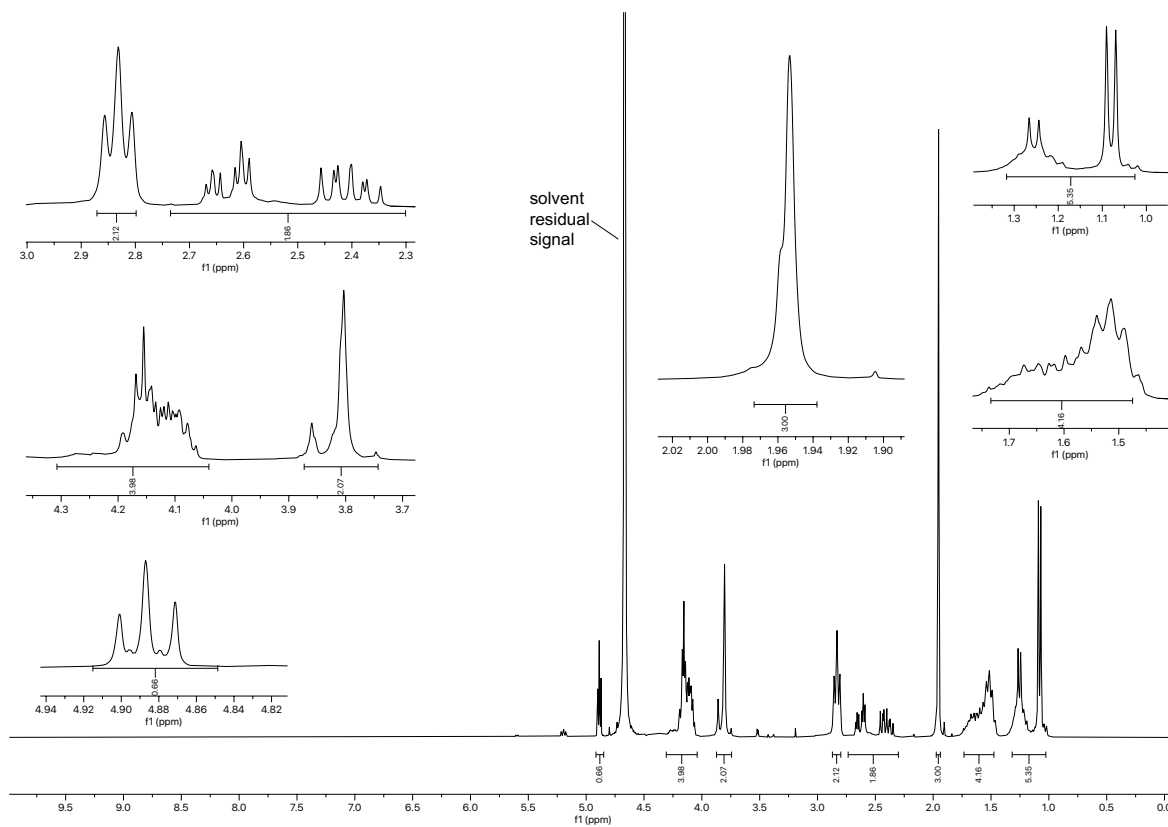
Figure 2.117. ^{1}H NMR spectrum (300 MHz, D_2O) of compound **2.050**.
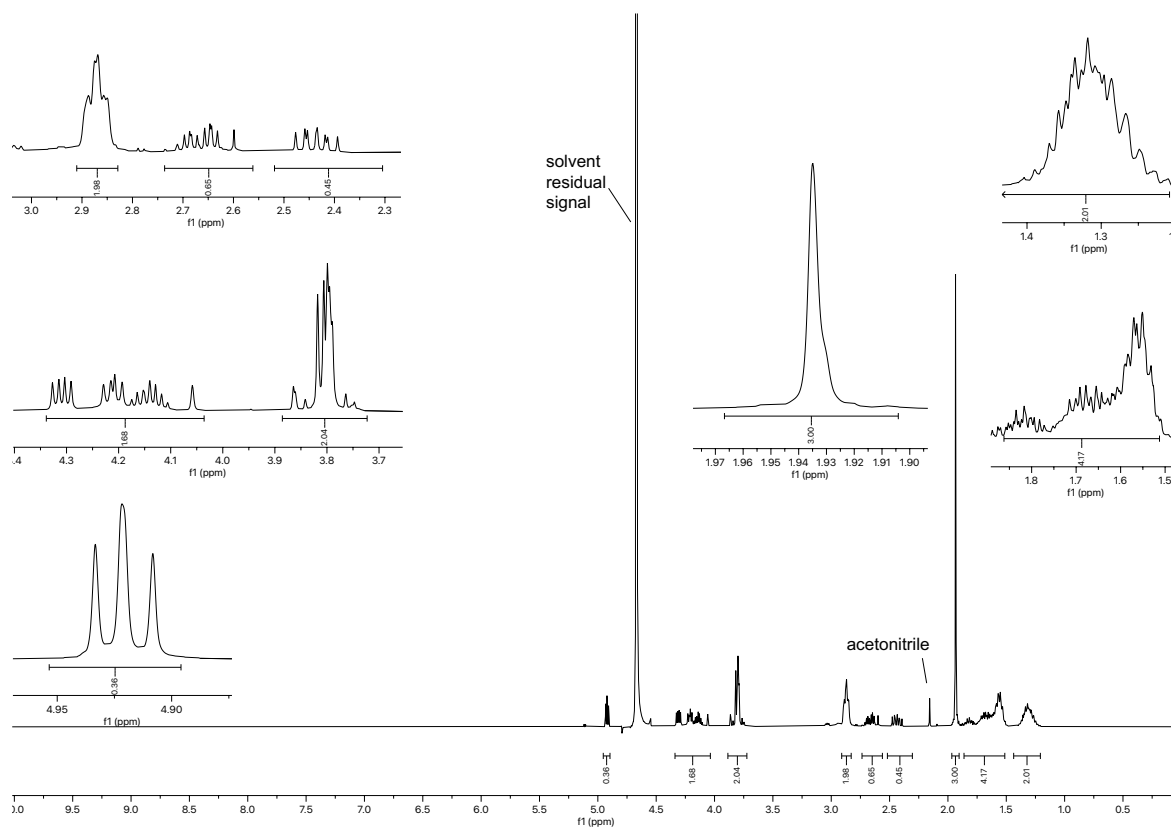
Figure 2.118. ^{1}H NMR spectrum (400 MHz, D_2O) of compound **2.051**.

221
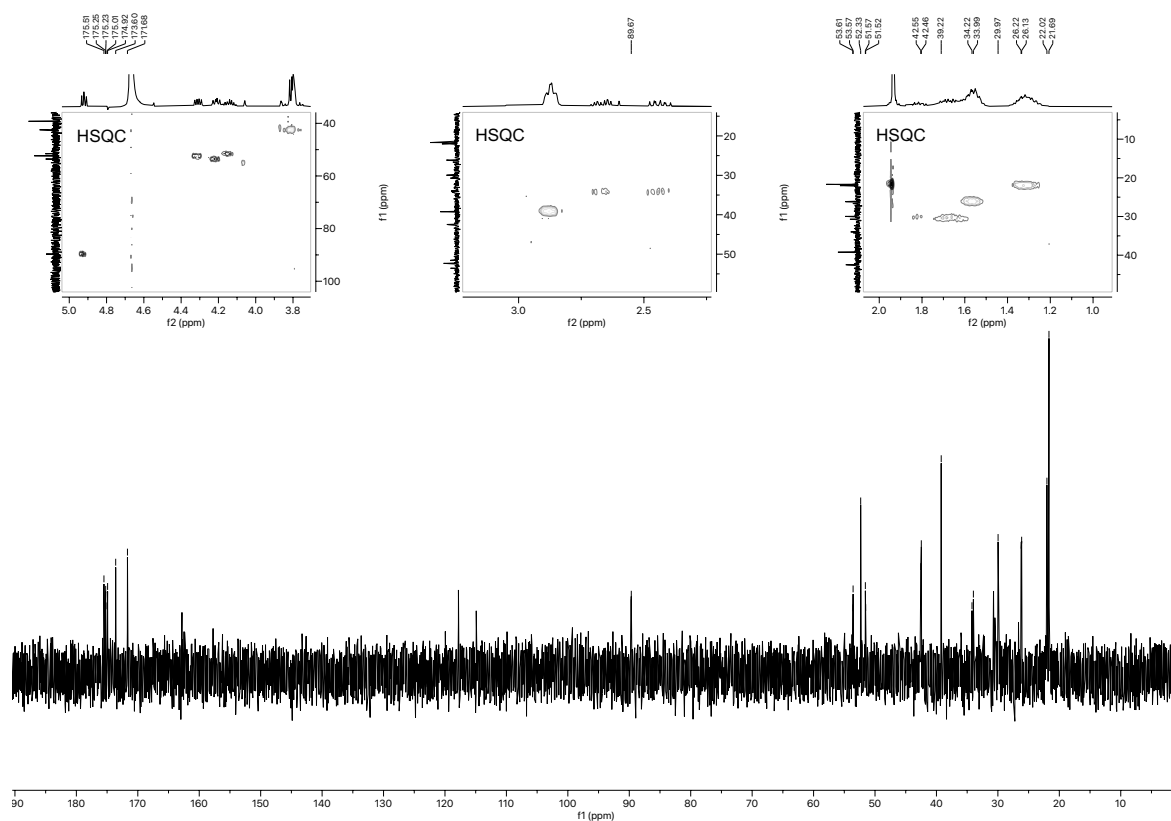
Figure 2.119. ^{13}C NMR spectrum (101 MHz, D$_2$O) of compound **2.051**.
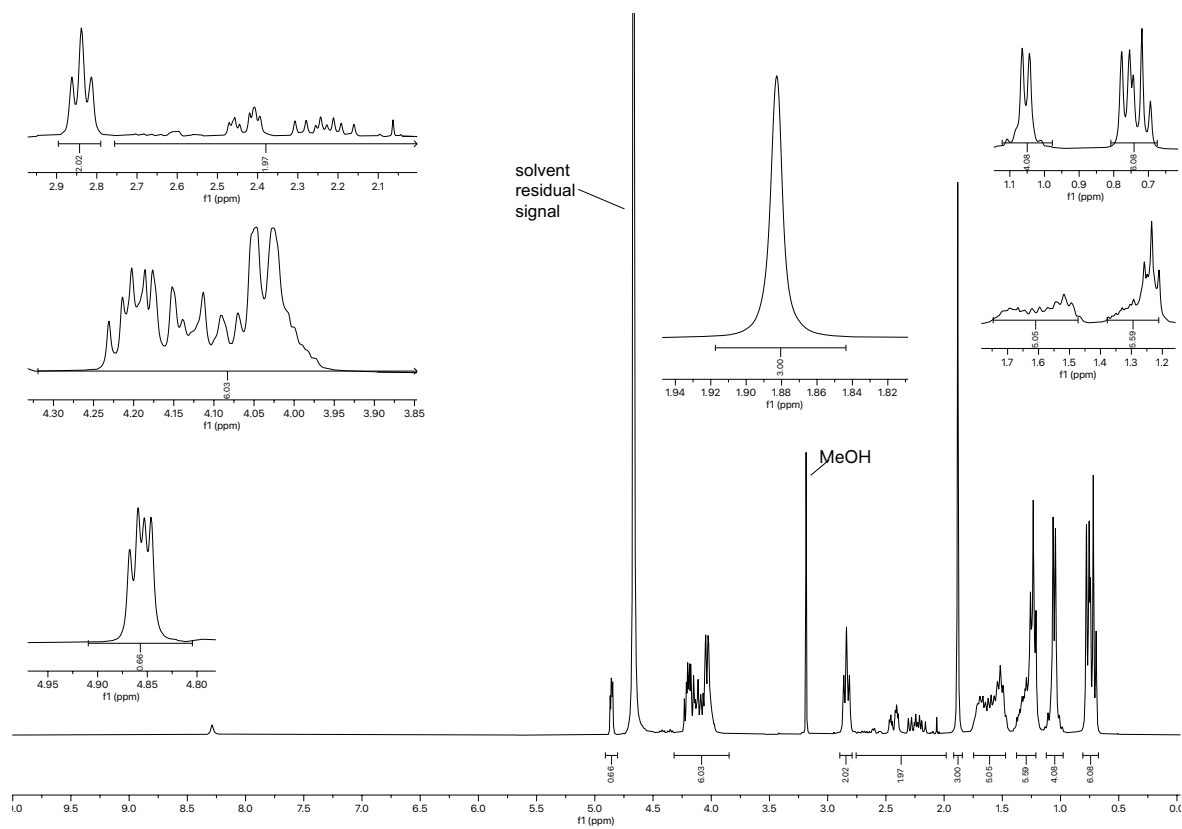
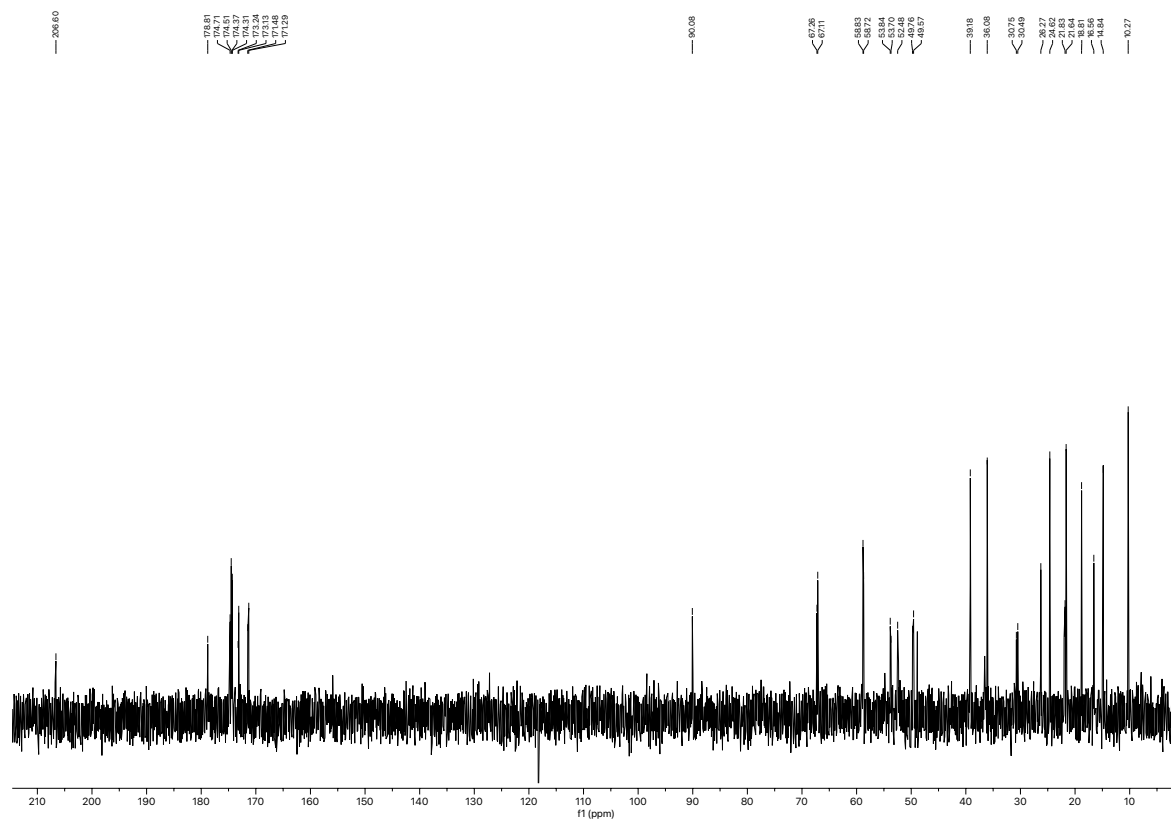**Figure 2.120.** ^{1}H NMR spectrum (300 MHz, D$_2$O) of compound **2.052**.

Figure 2.121. ^{13}C NMR spectrum (75 MHz, D_2O) of compound **2.052**.
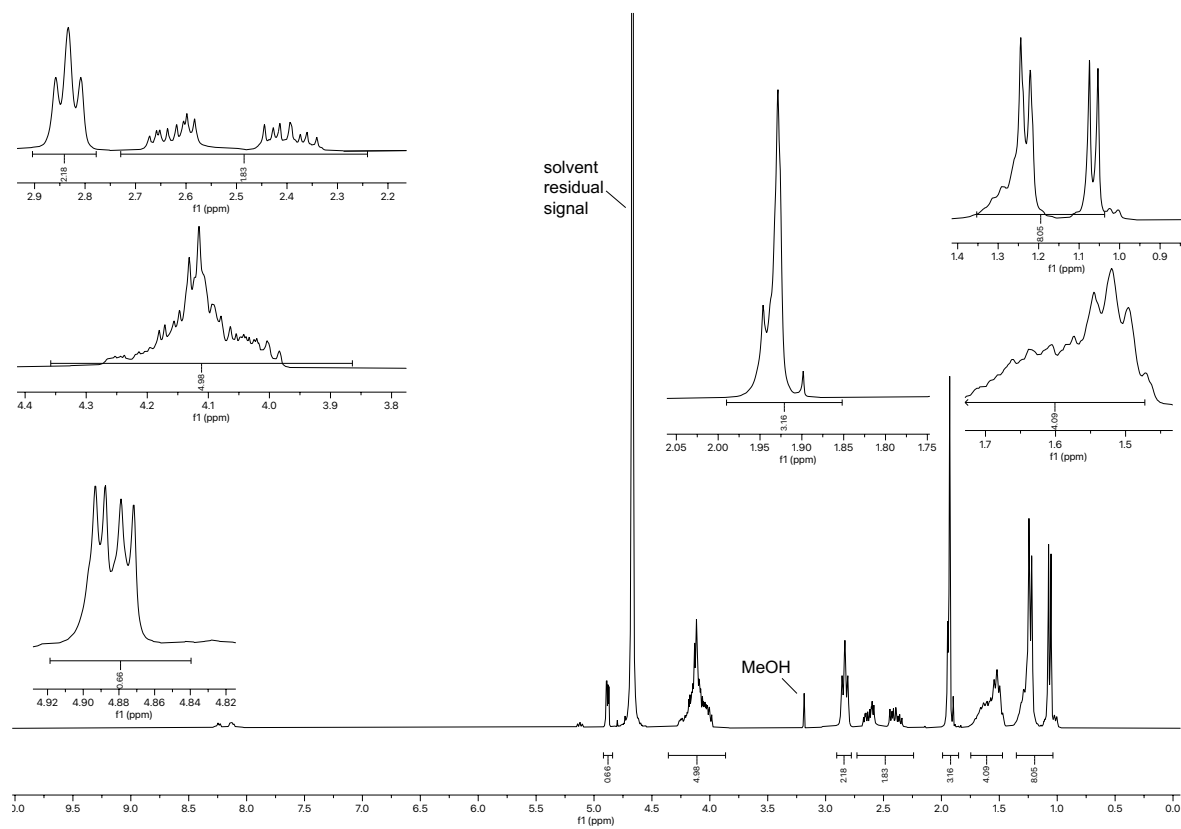
Figure 2.122. ^{1}H NMR spectrum (300 MHz, D_2O) of compound **2.053**.

223
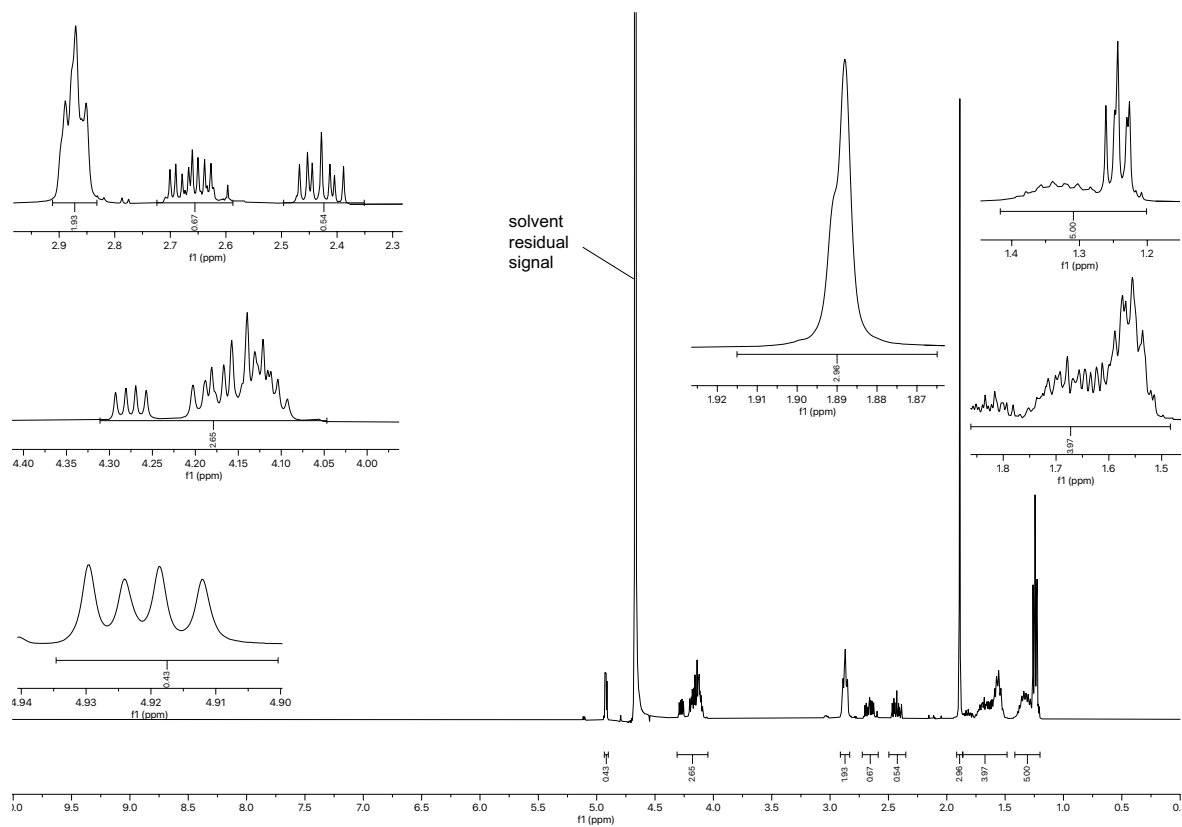
Figure 2.123. ^{1}H NMR spectrum (400 MHz, D$_2$O) of compound **2.054**.
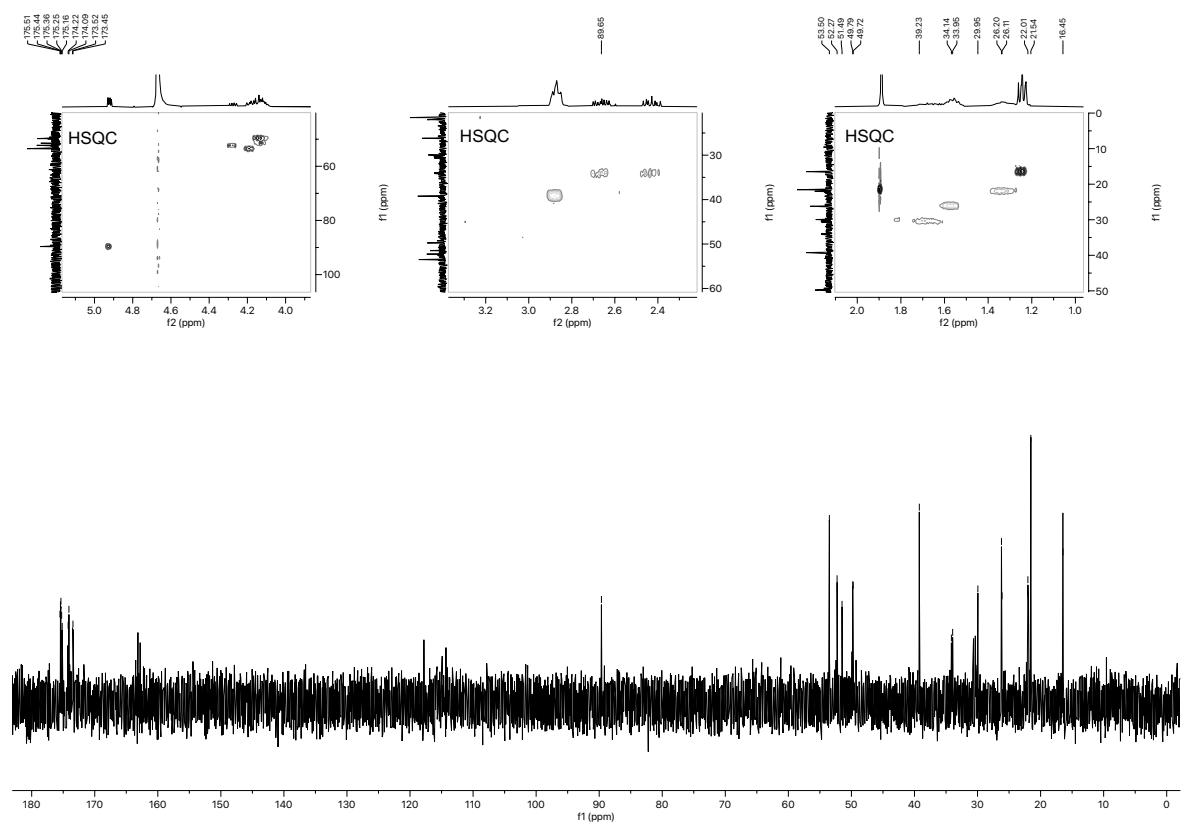
Figure 2.124. ^{13}C NMR spectrum (101 MHz, D$_2$O) of compound **2.054**.
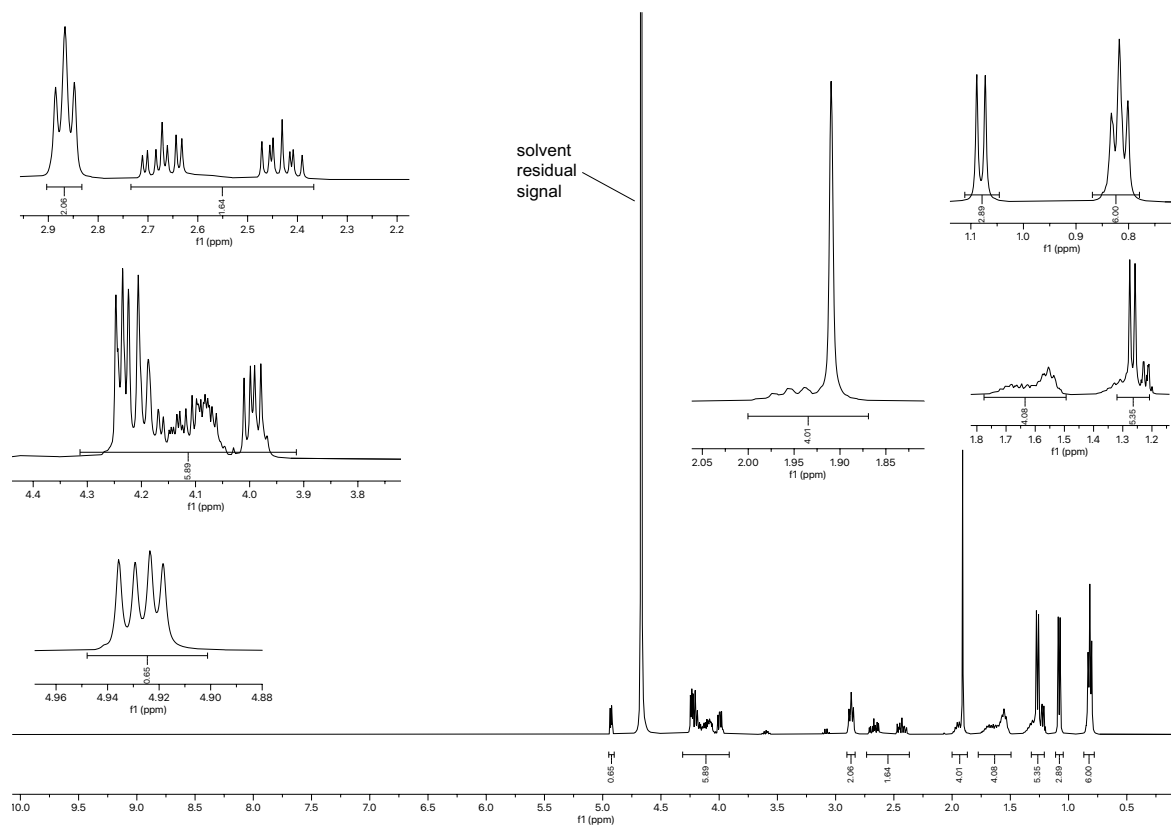
Figure 2.125. ^{1}H NMR spectrum (400 MHz, D$_2$O) of compound **2.055**.
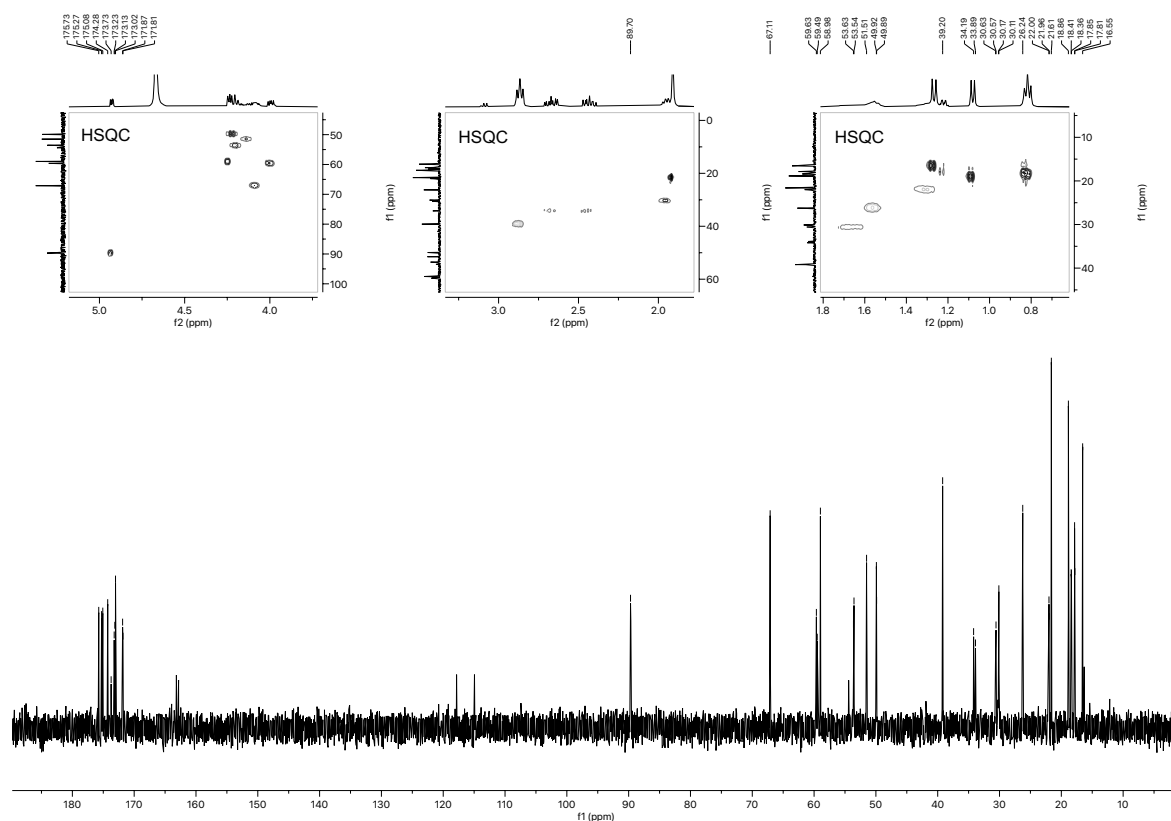
Figure 2.126. ^{13}C NMR spectrum (101 MHz, D$_2$O) of compound **2.055**.

225
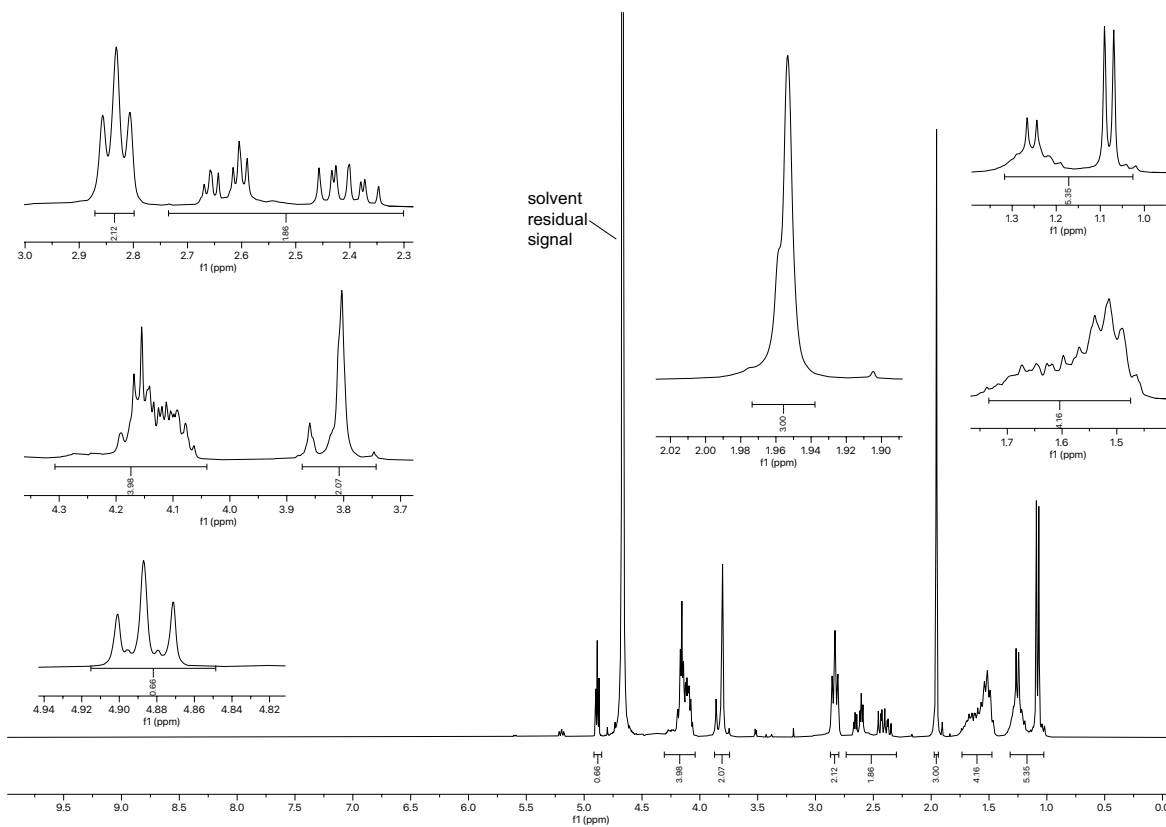
Figure 2.127. ^{1}H NMR spectrum (400 MHz, D_2O) of compound **2.056**.
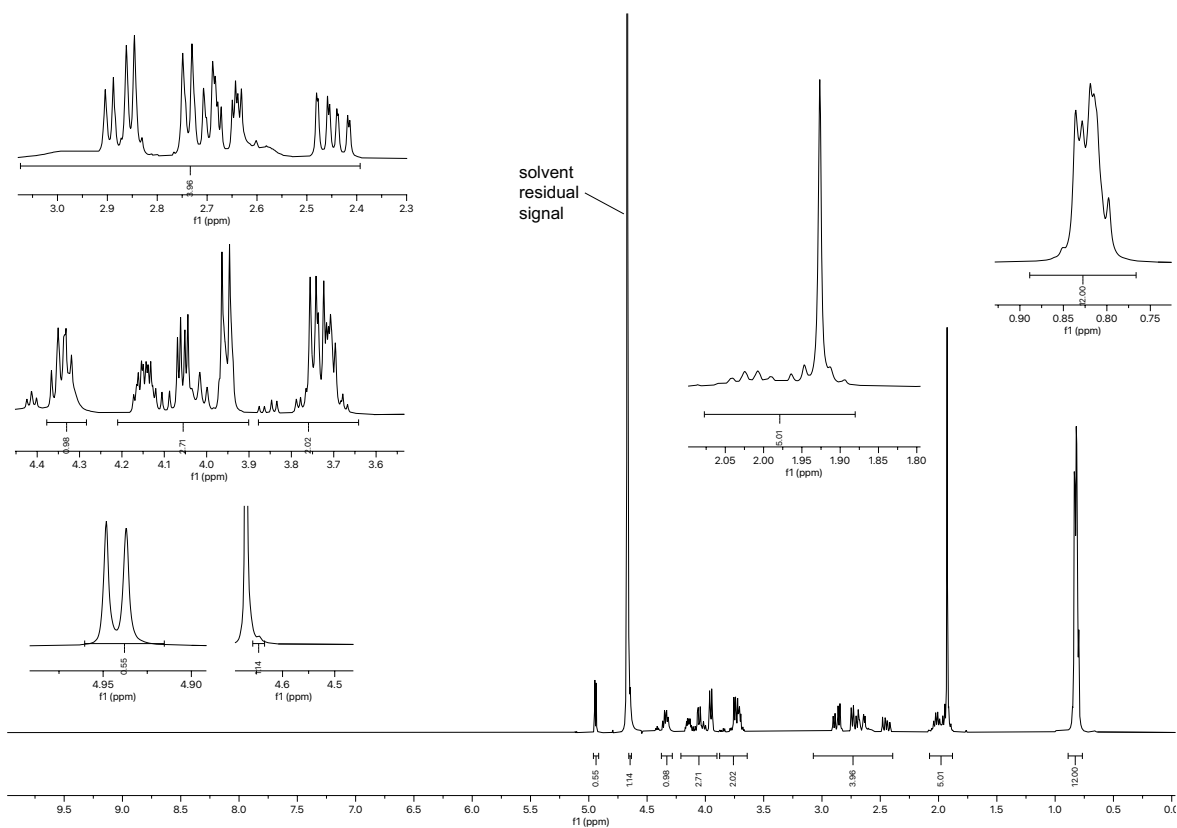
Figure 2.128. ^{1}H NMR spectrum (400 MHz, D_2O) of compound **2.057**.
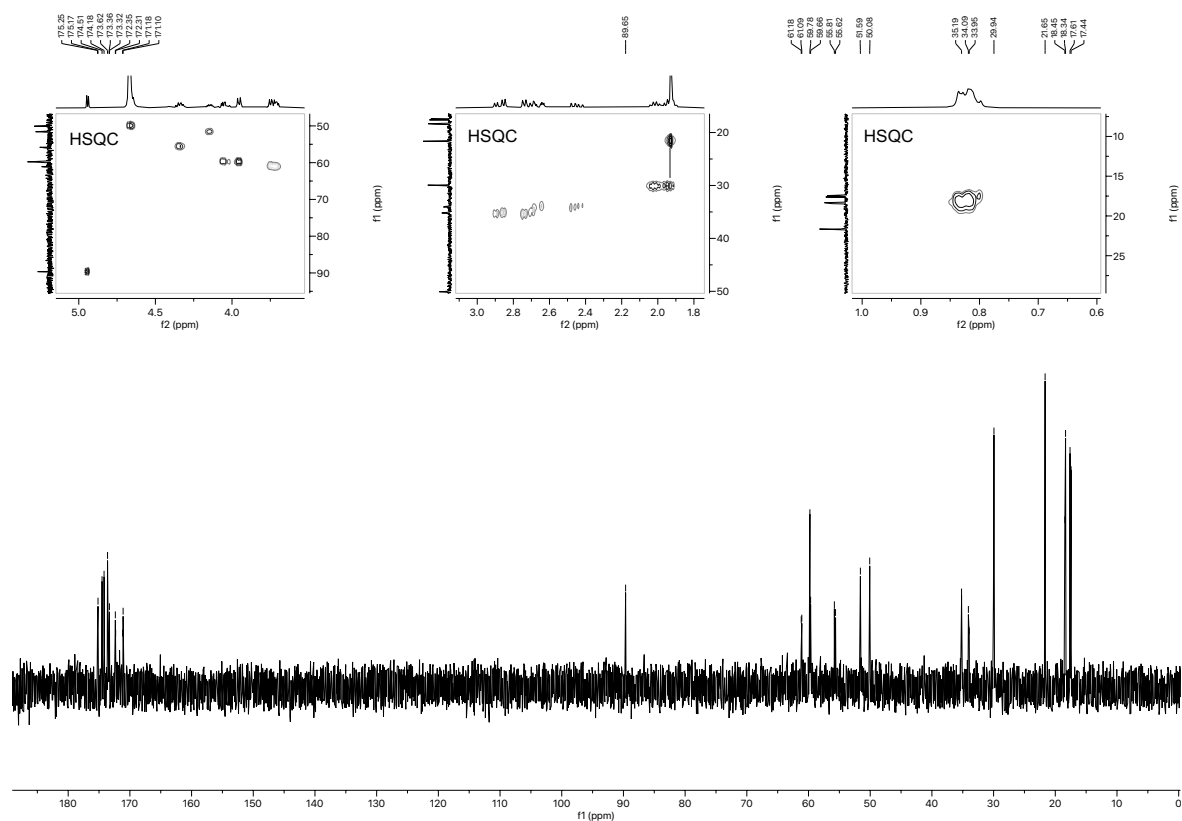
Figure 2.129. ^{13}C NMR spectrum (101 MHz, D_2O) of compound **2.057**.
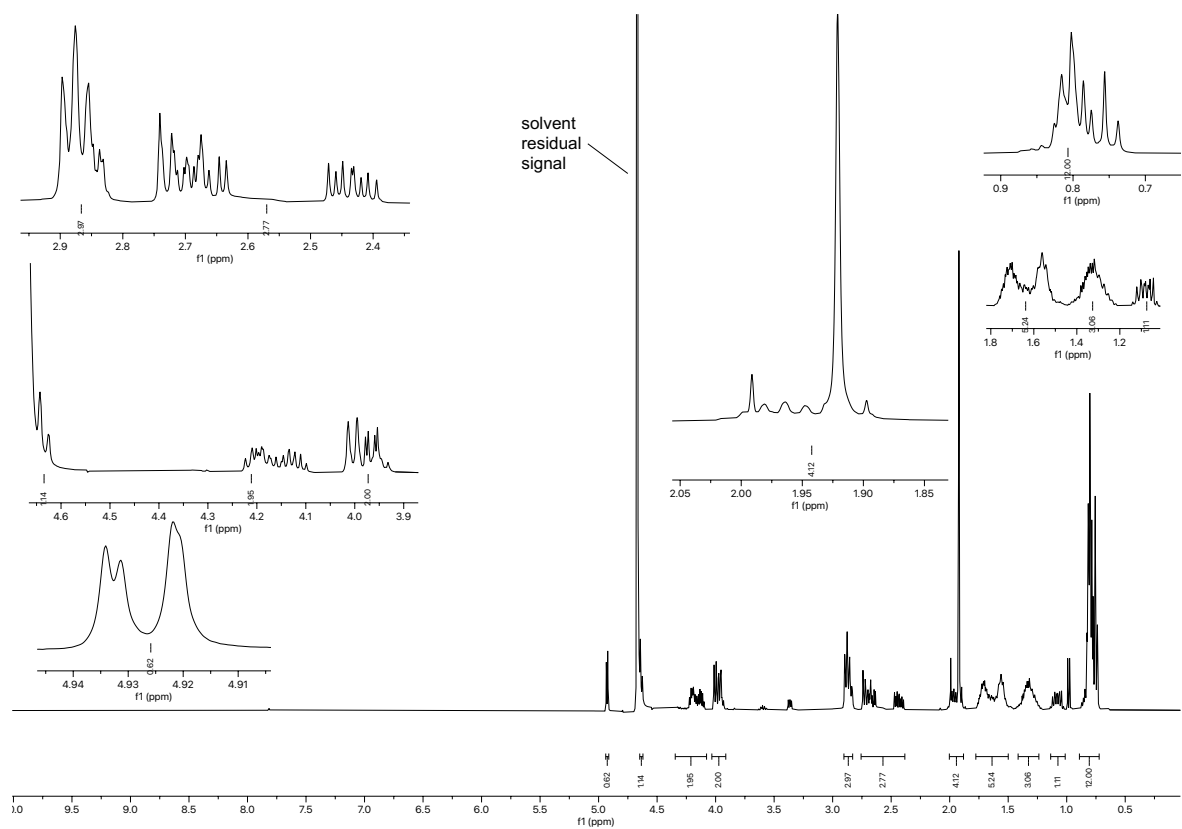
Figure 2.130. ^1H NMR spectrum (400 MHz, D_2O) of compound **2.058**.

227
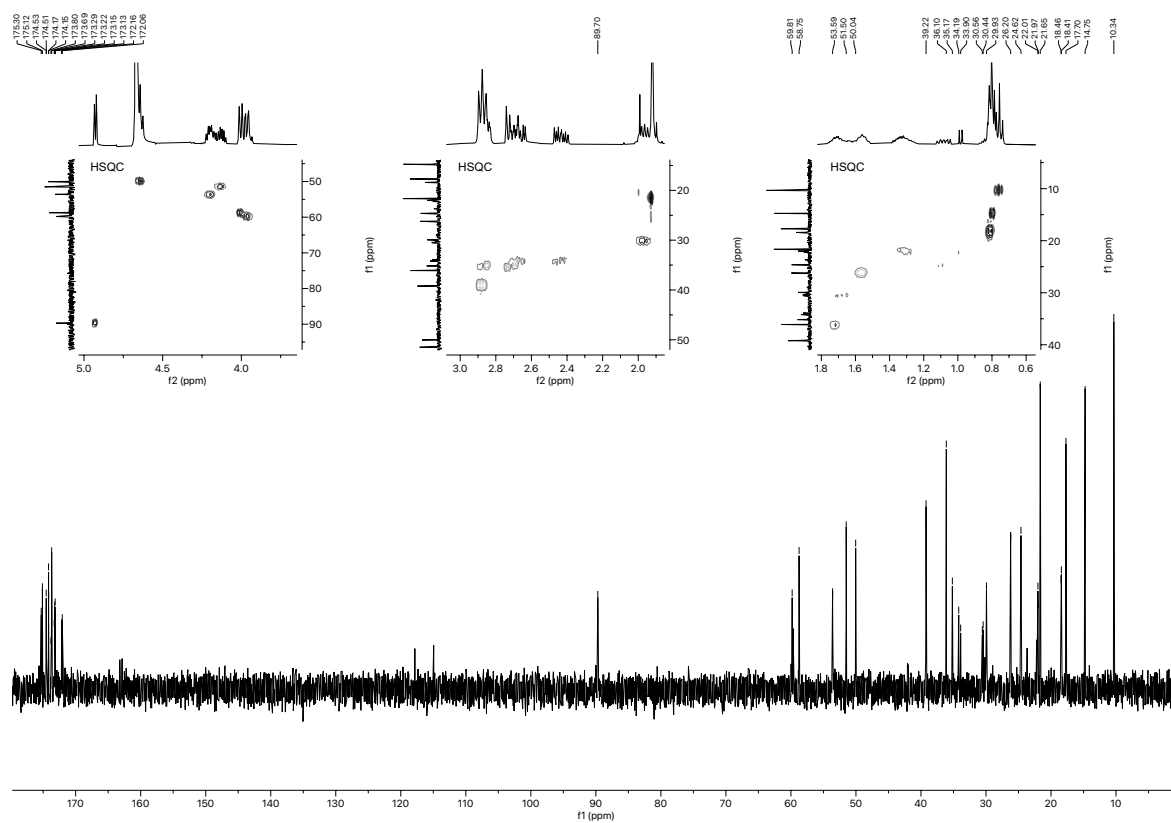
Figure 2.131. ^{1}H NMR spectrum (400 MHz, D$_2$O) of compound **2.058**.
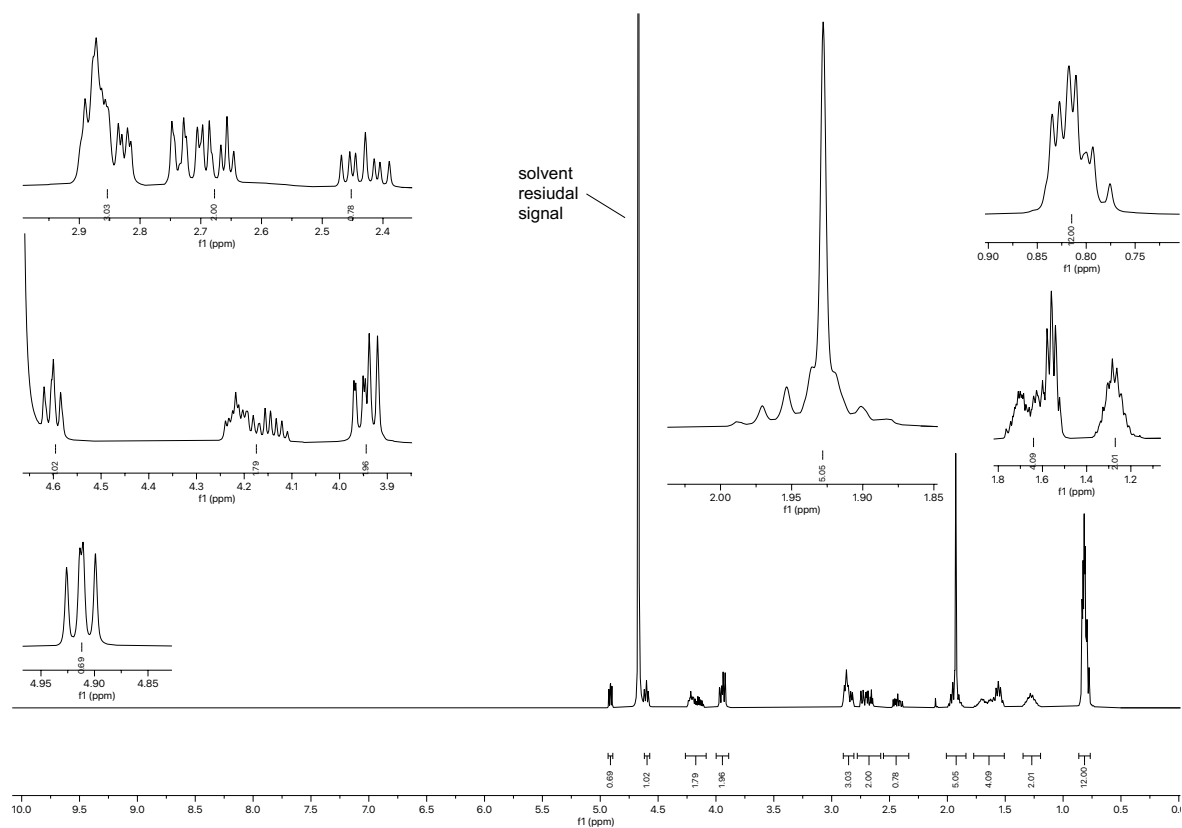
Figure 2.132. ^{1}H NMR spectrum (400 MHz, D$_2$O) of compound **2.059**.
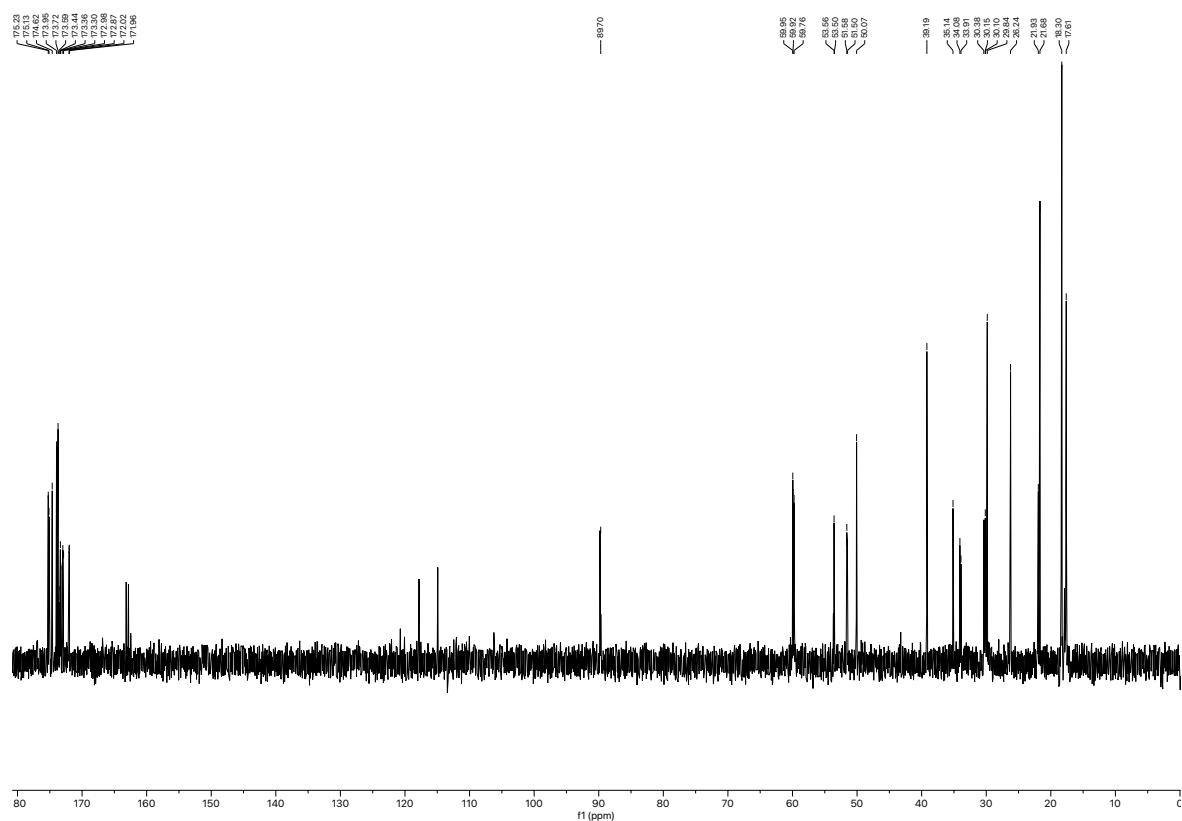
Figure 2.133. ^{13}C NMR spectrum (101 MHz, D$_2$O) of compound **2.059**.

solvent
residual
signal
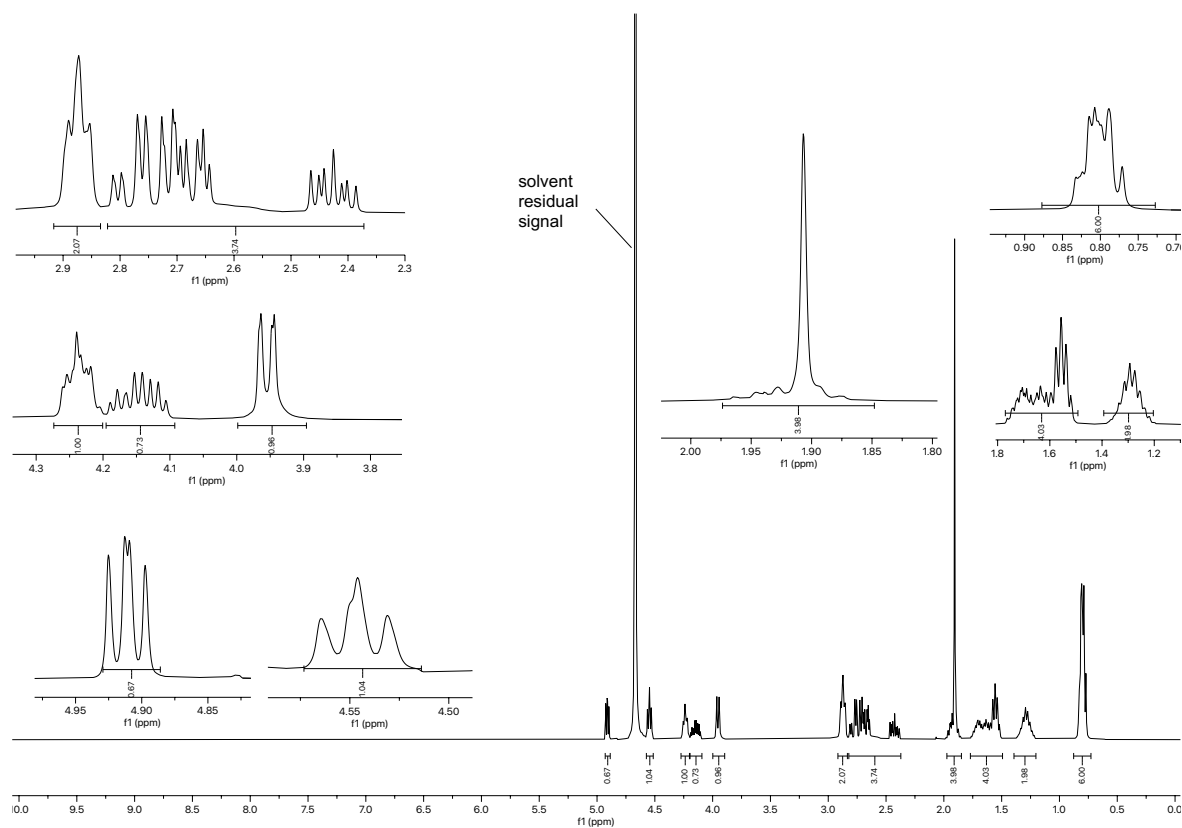
Figure 2.134. ^{1}H NMR spectrum (400 MHz, D$_2$O) of compound **2.060**.
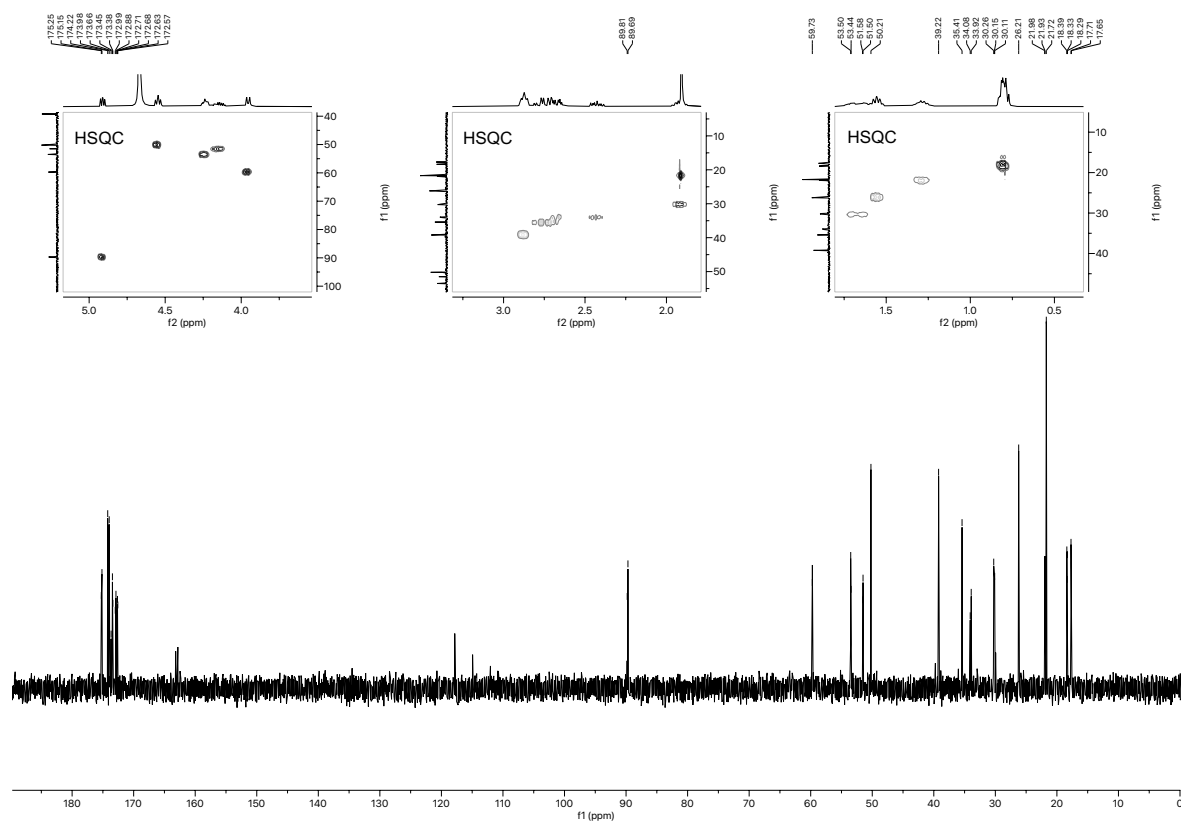
Figure 2.135. ^{13}C NMR spectrum (101 MHz, D$_2$O) of compound **2.060**.
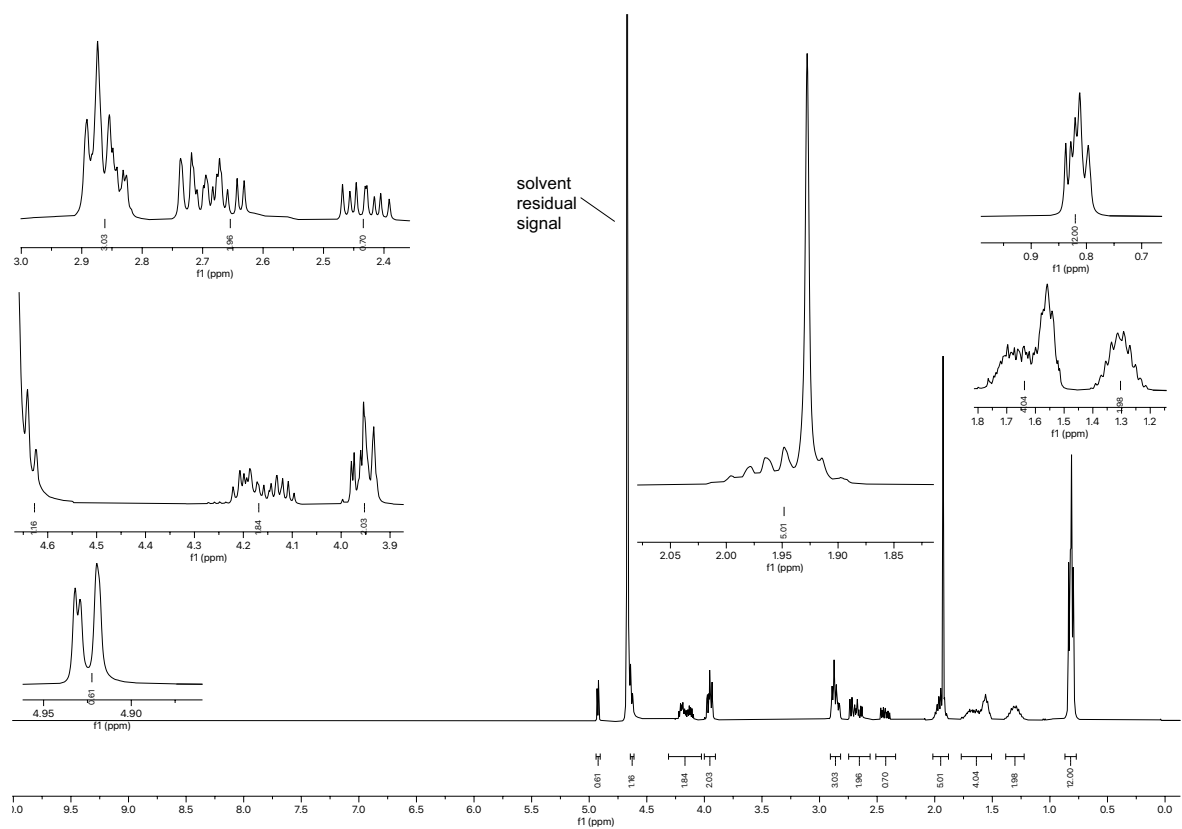
Figure 2.136. ^{1}H NMR spectrum (400 MHz, D$_2$O) of compound **2.061**.
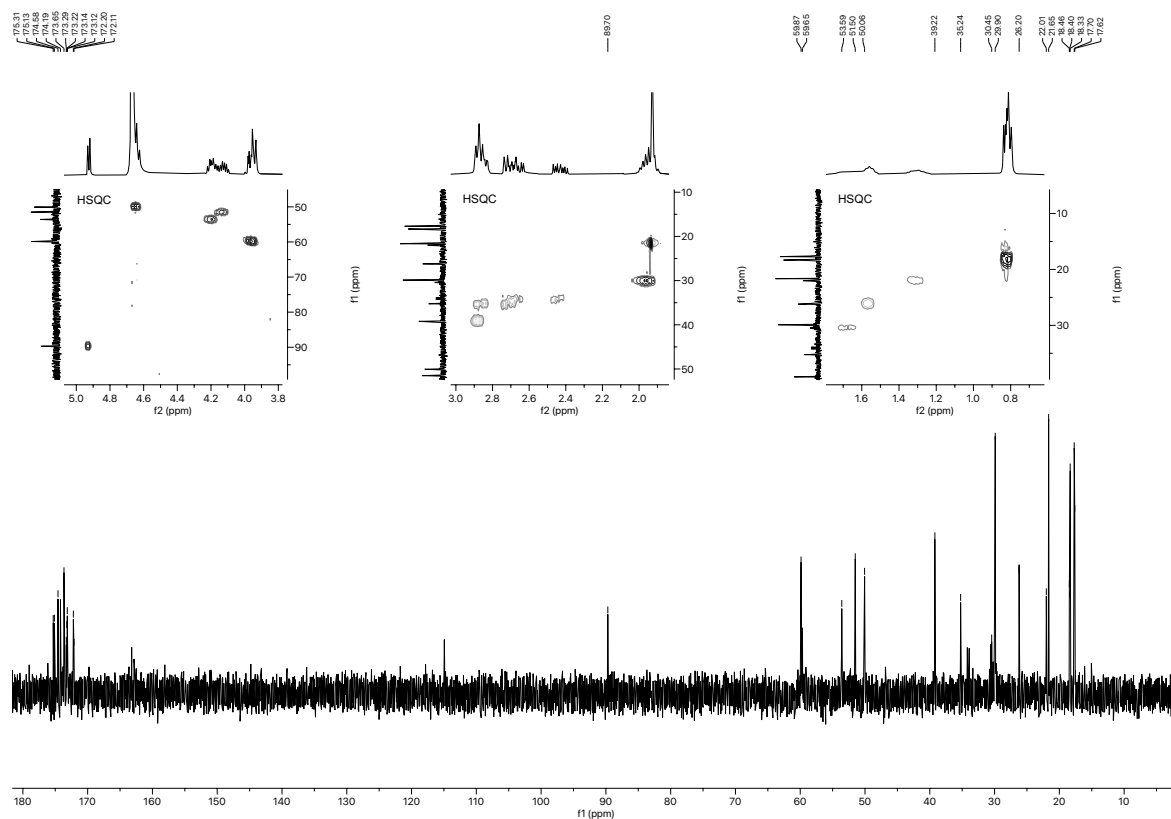
Figure 2.137. ^{13}C NMR spectrum (101 MHz, D$_2$O) of compound **2.061**.
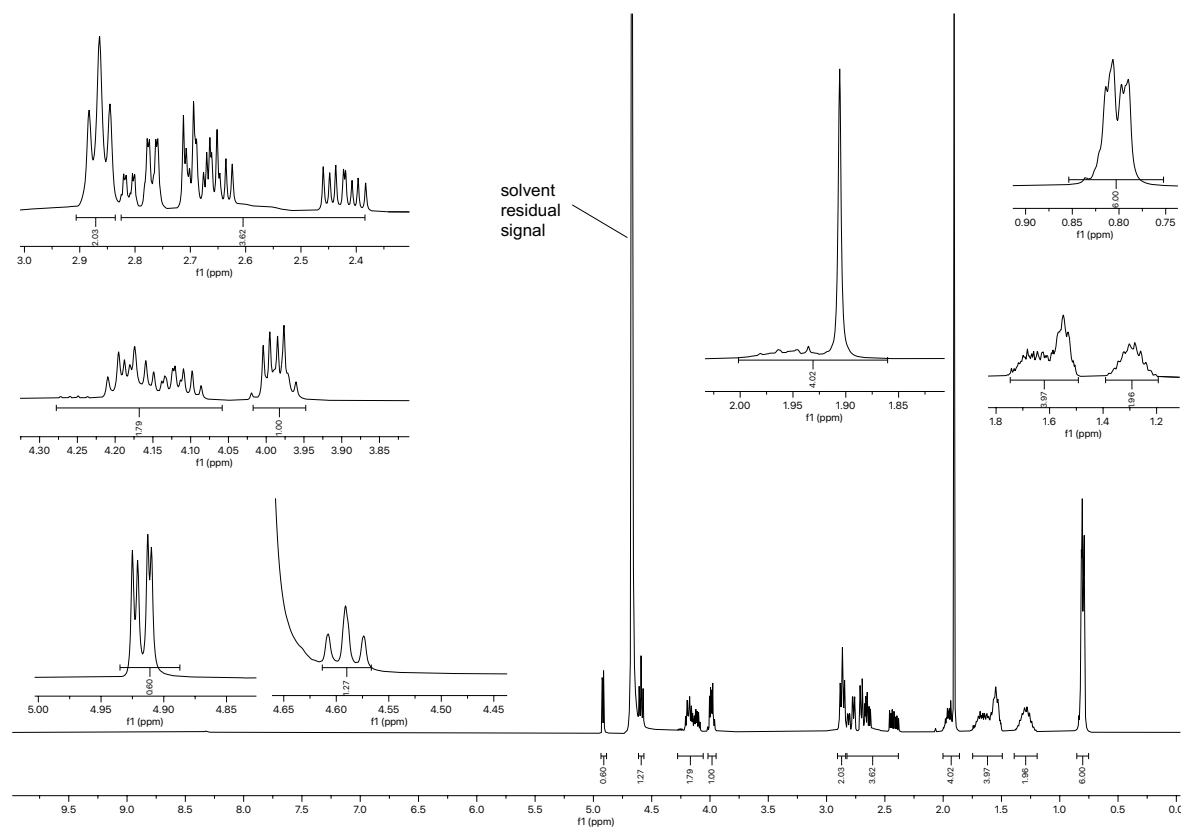
Figure 2.138. ^{1}H NMR spectrum (400 MHz, D$_2$O) of compound **2.062**.
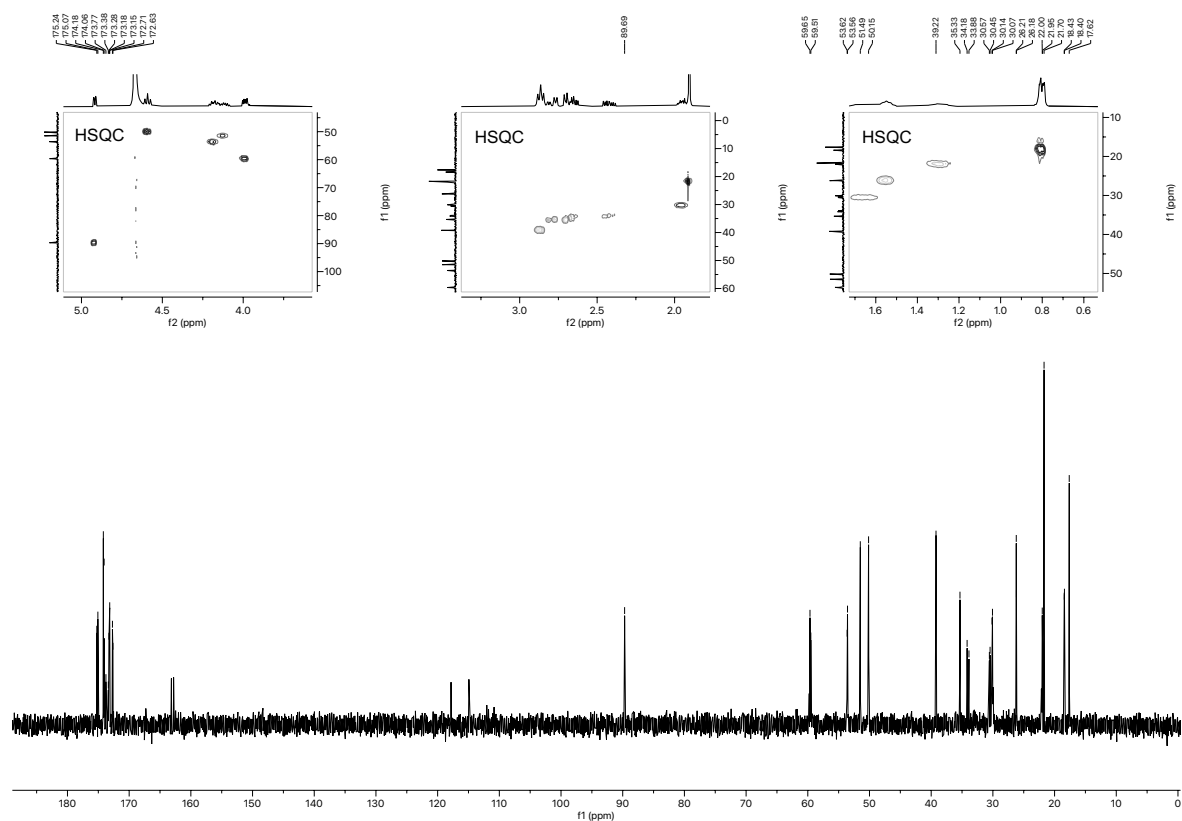
Figure 2.139. ^{13}C NMR spectrum (101 MHz, D_2O) of compound **2.062**.
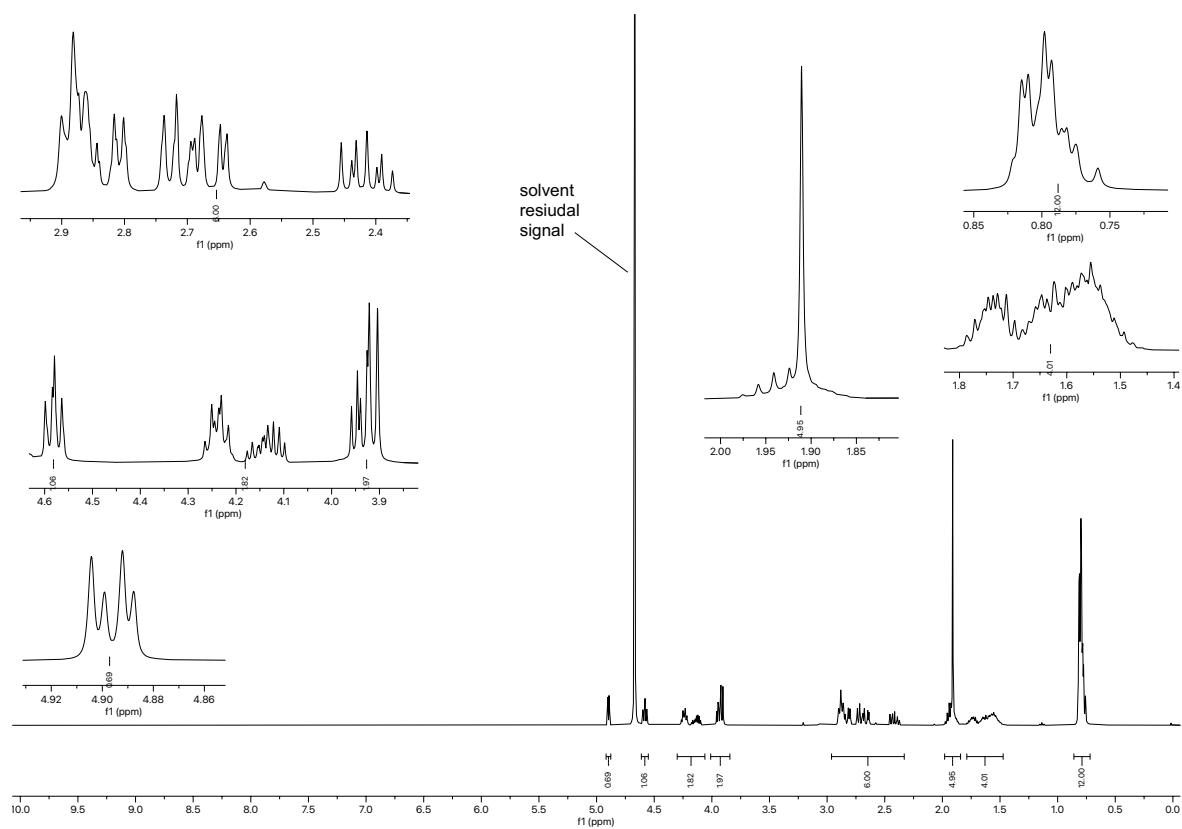
Figure 2.140. ^1H NMR spectrum (400 MHz, D_2O) of compound **2.063**.
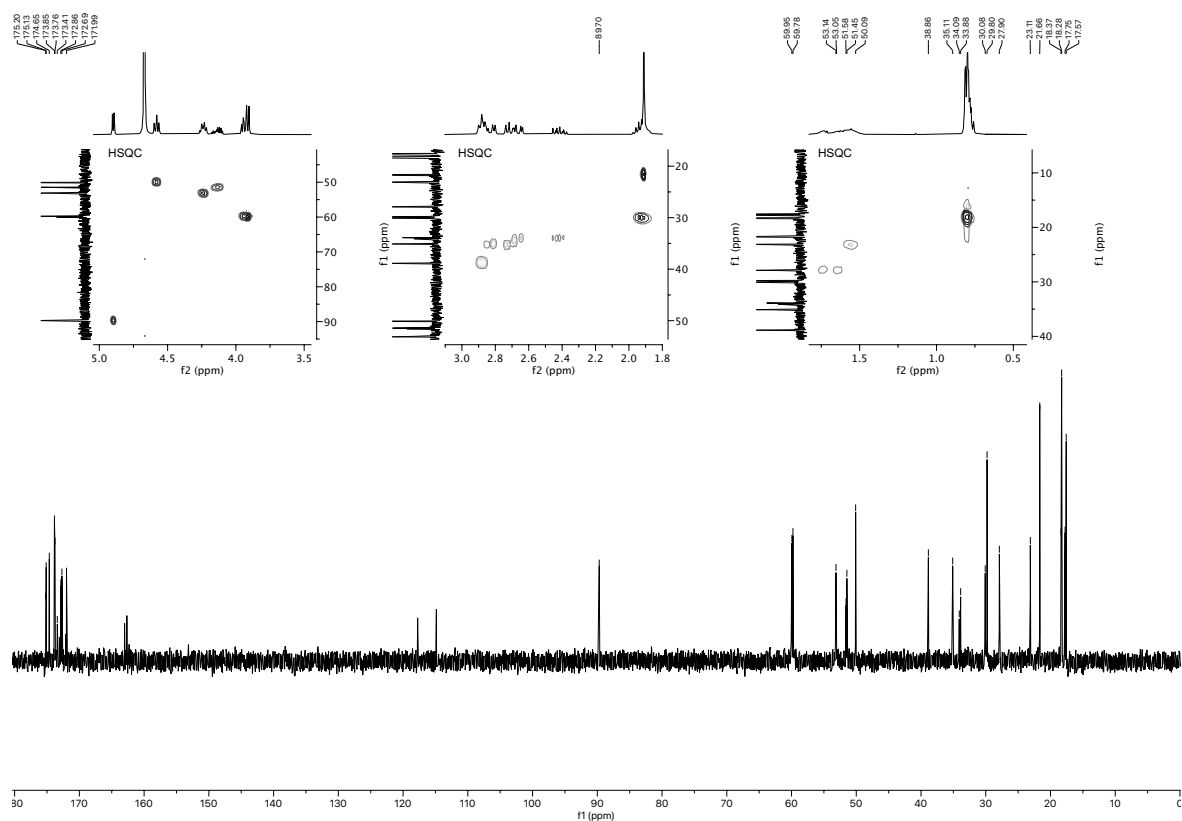
Figure 2.141. ^{13}C NMR spectrum (101 MHz, D$_2$O) of compound **2.063**.
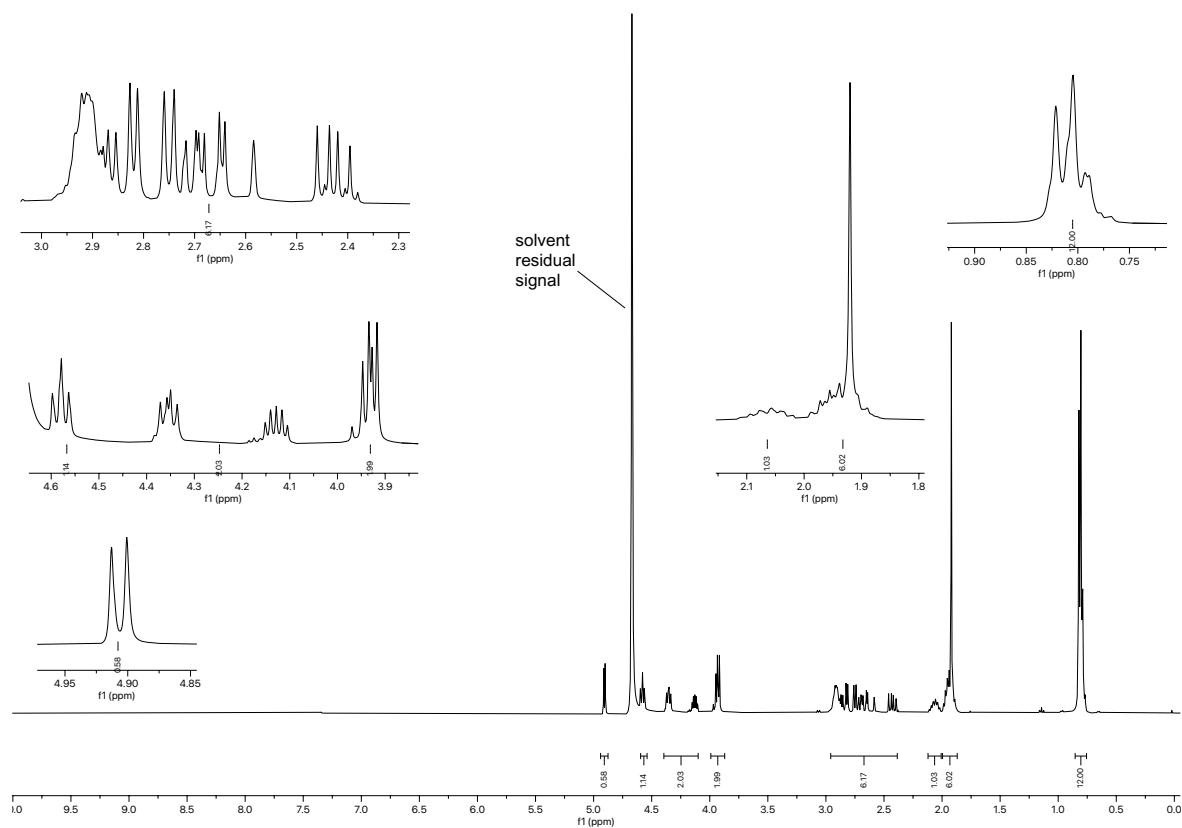
Figure 2.142. ^{1}H NMR spectrum (400 MHz, D$_2$O) of compound **2.064**.
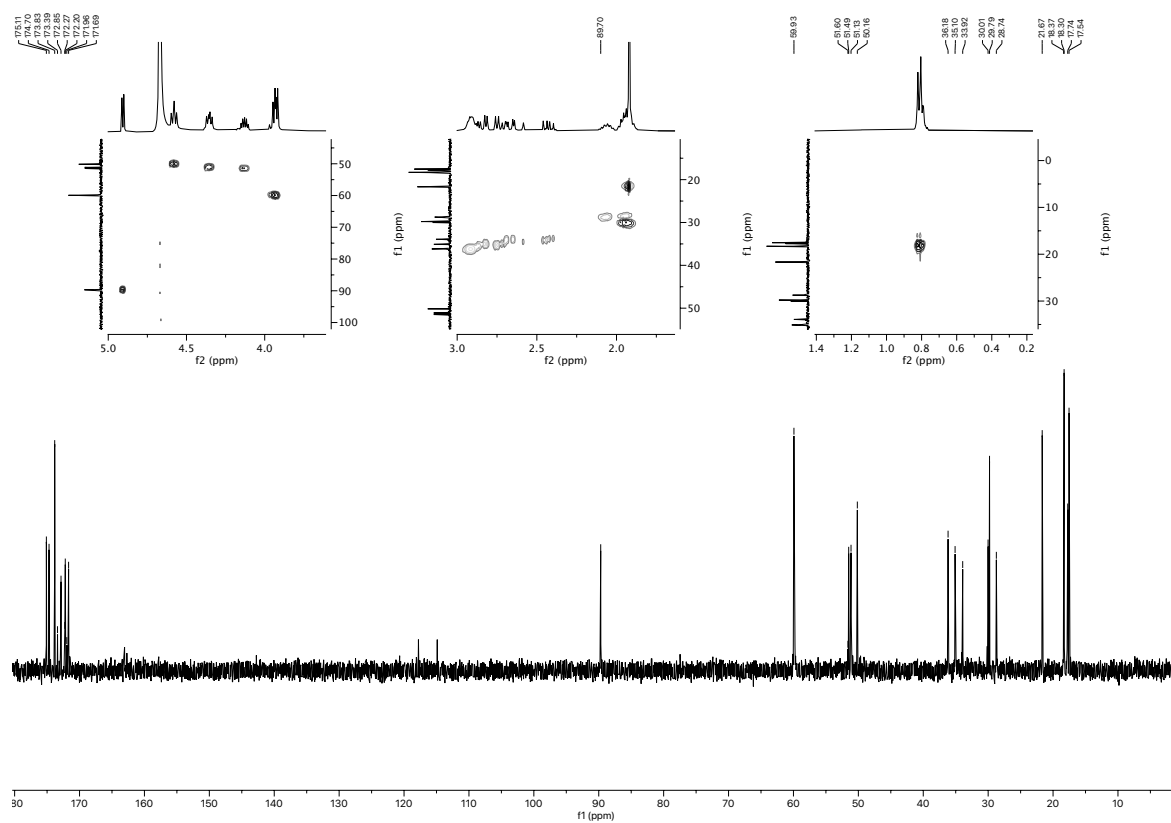
Figure 2.143. ^{13}C NMR spectrum (101 MHz, D$_2$O) of compound **2.064**.
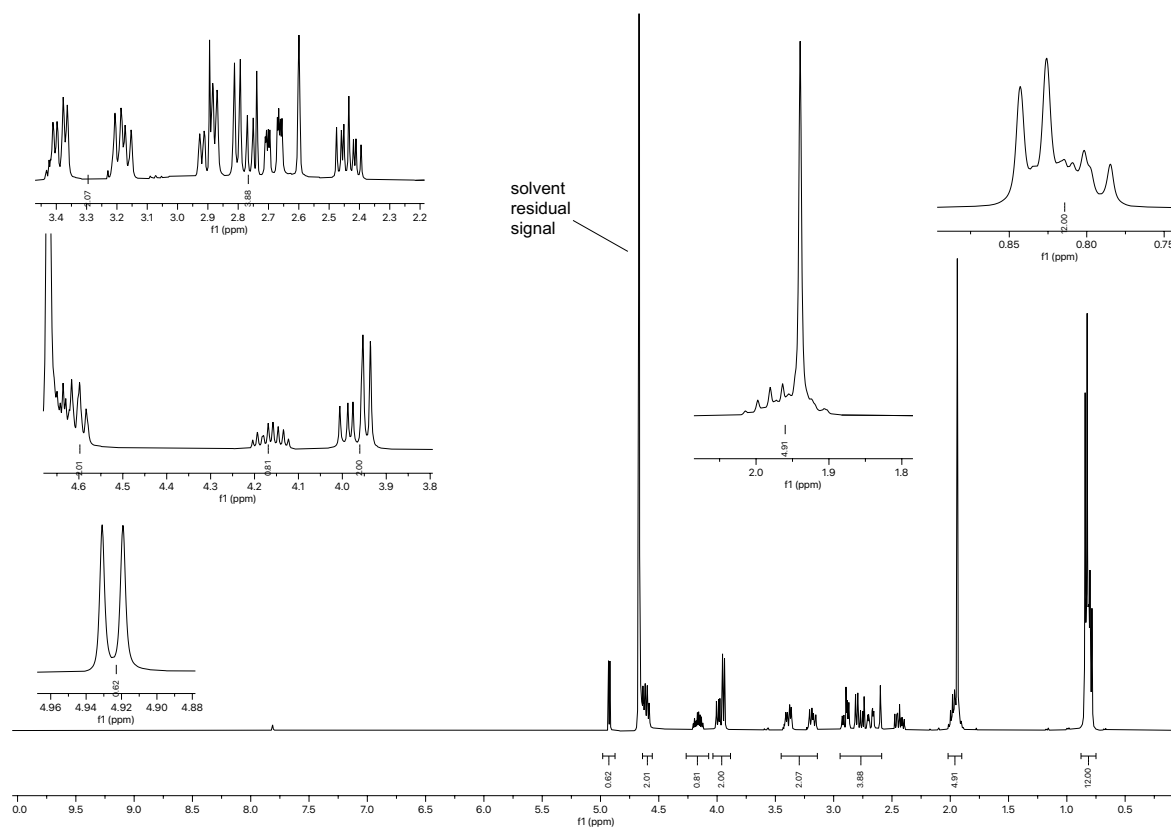
Figure 2.144. ^{1}H NMR spectrum (400 MHz, D$_2$O) of compound **2.065**.
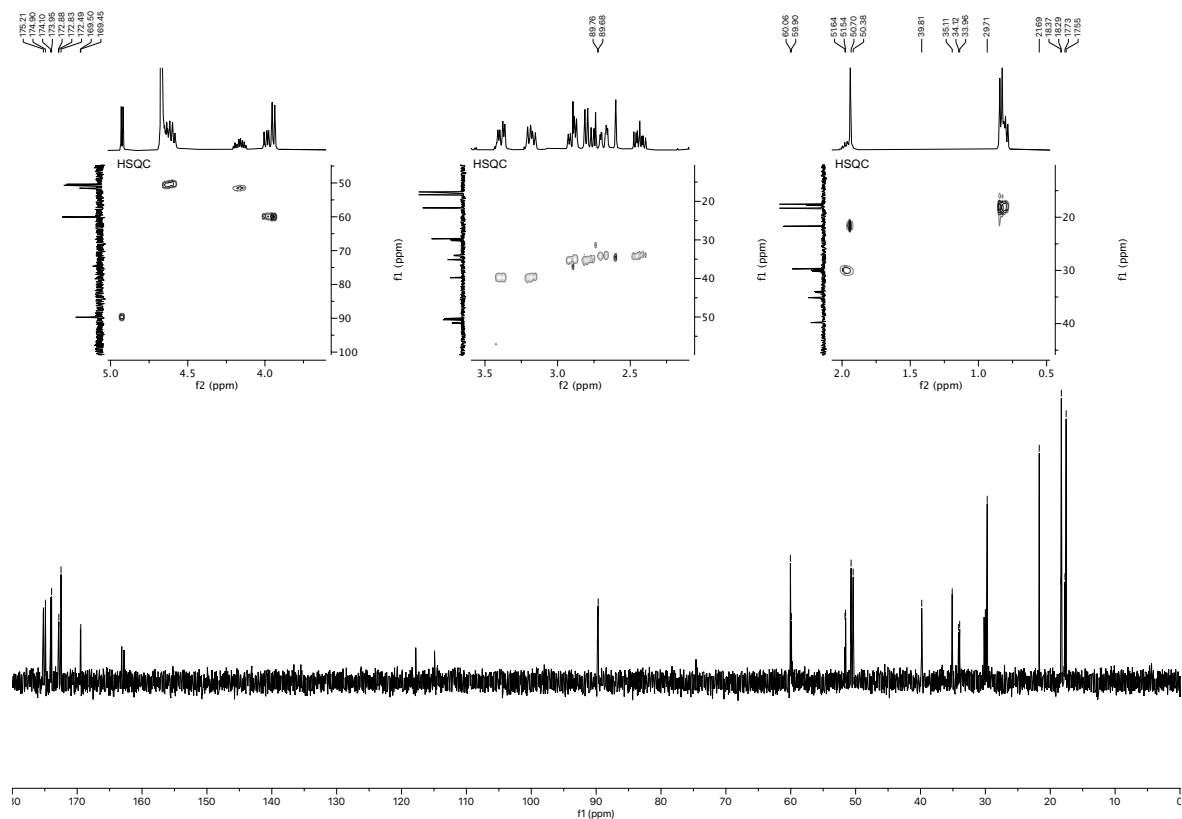
Figure 2.145. ^{1}H NMR spectrum (400 MHz, D$_2$O) of compound **2.065**.
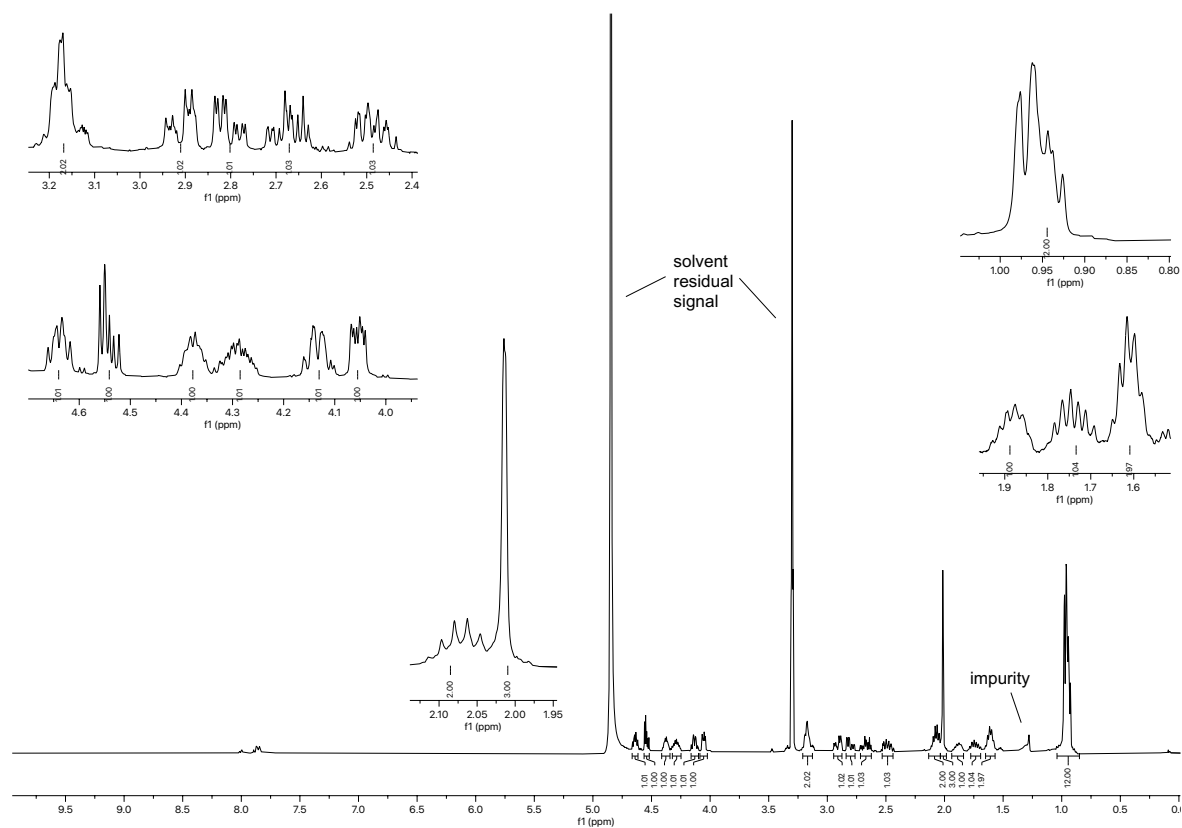
Figure 2.146. ^{1}H NMR spectrum (400 MHz, CD$_3$OD) of compound **2.066**.

235
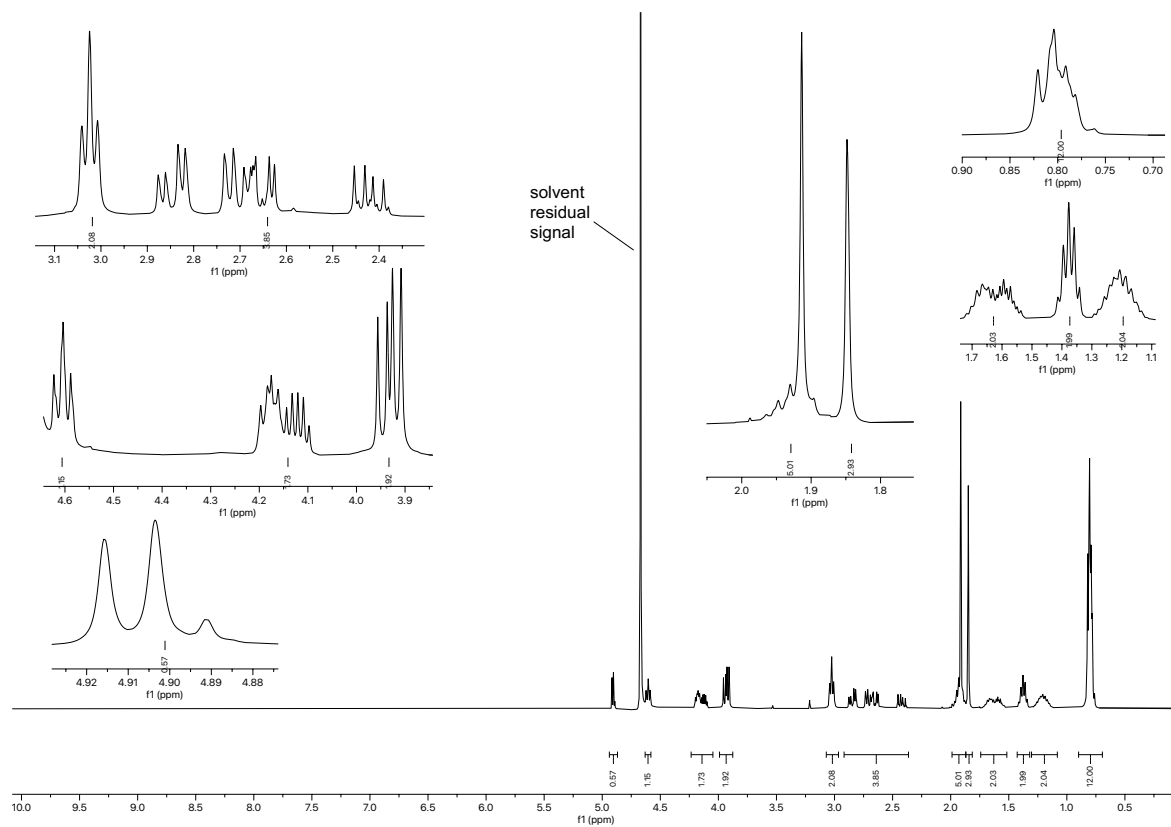
Figure 2.147. ^{1}H NMR spectrum (400 MHz, D$_2$O) of compound **2.067**.
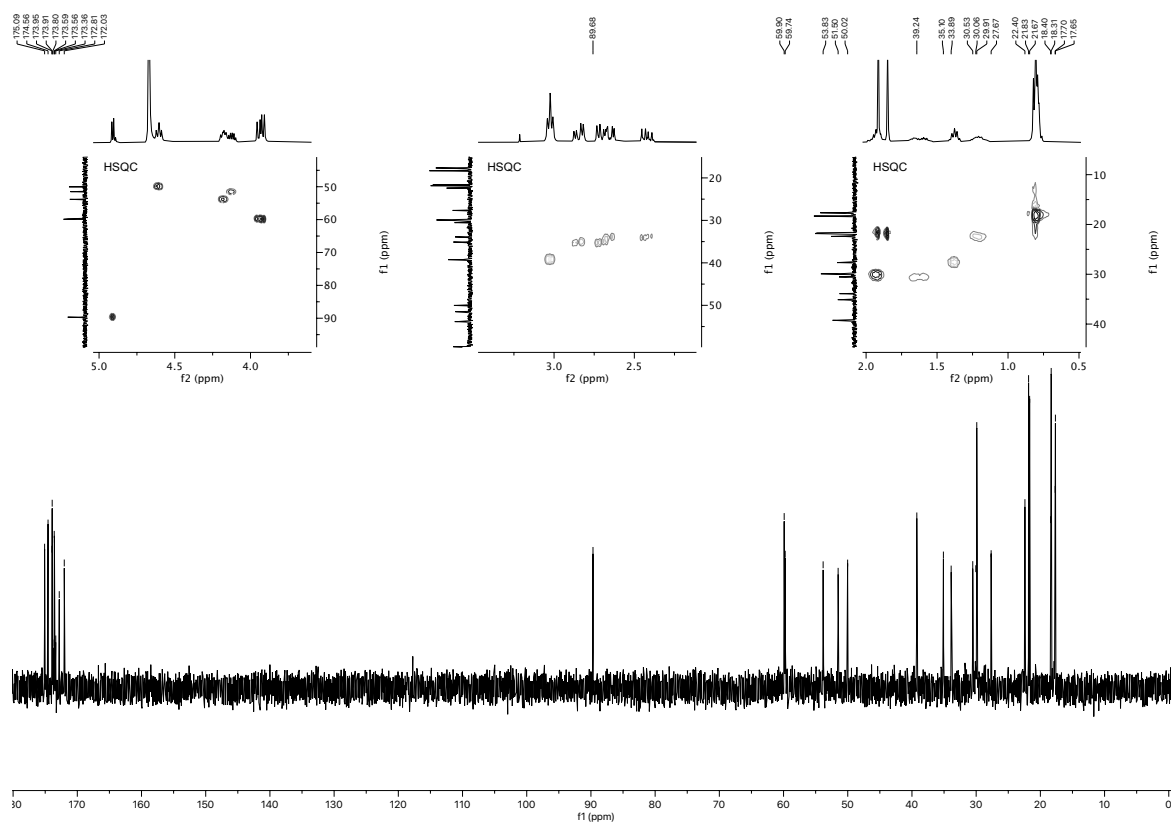
Figure 2.148. ^{13}C NMR spectrum (101 MHz, D$_2$O) of compound **2.067**.
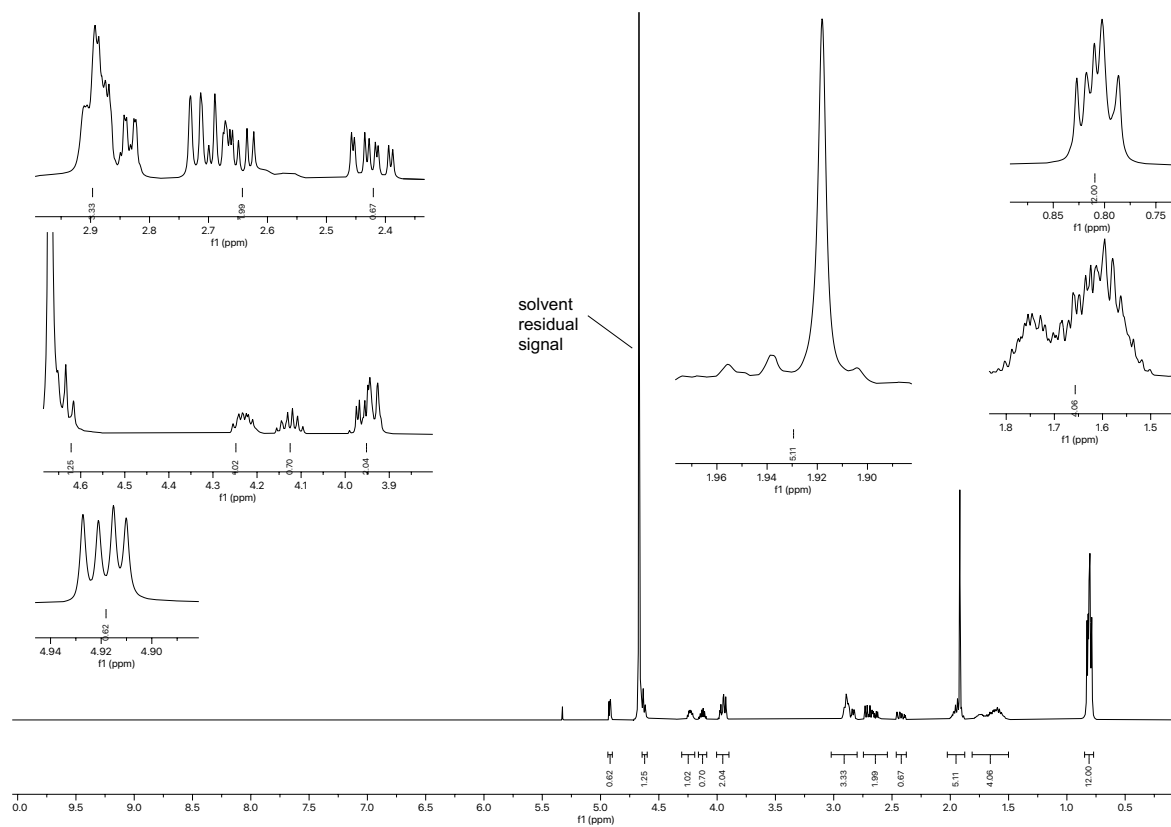
Figure 2.149. ^{1}H NMR spectrum (400 MHz, D$_2$O) of compound **2.068**.
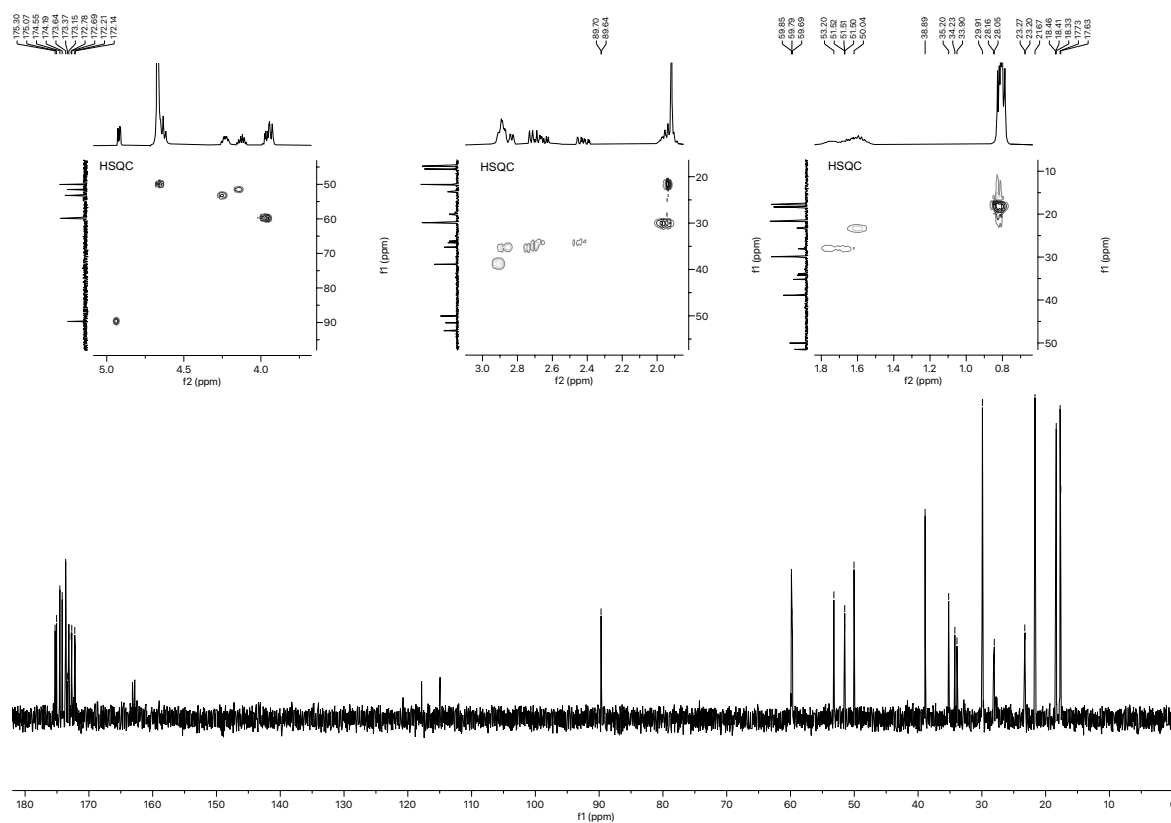
Figure 2.150. ^{13}C NMR spectrum (101 MHz, D$_2$O) of compound **2.068**.

237
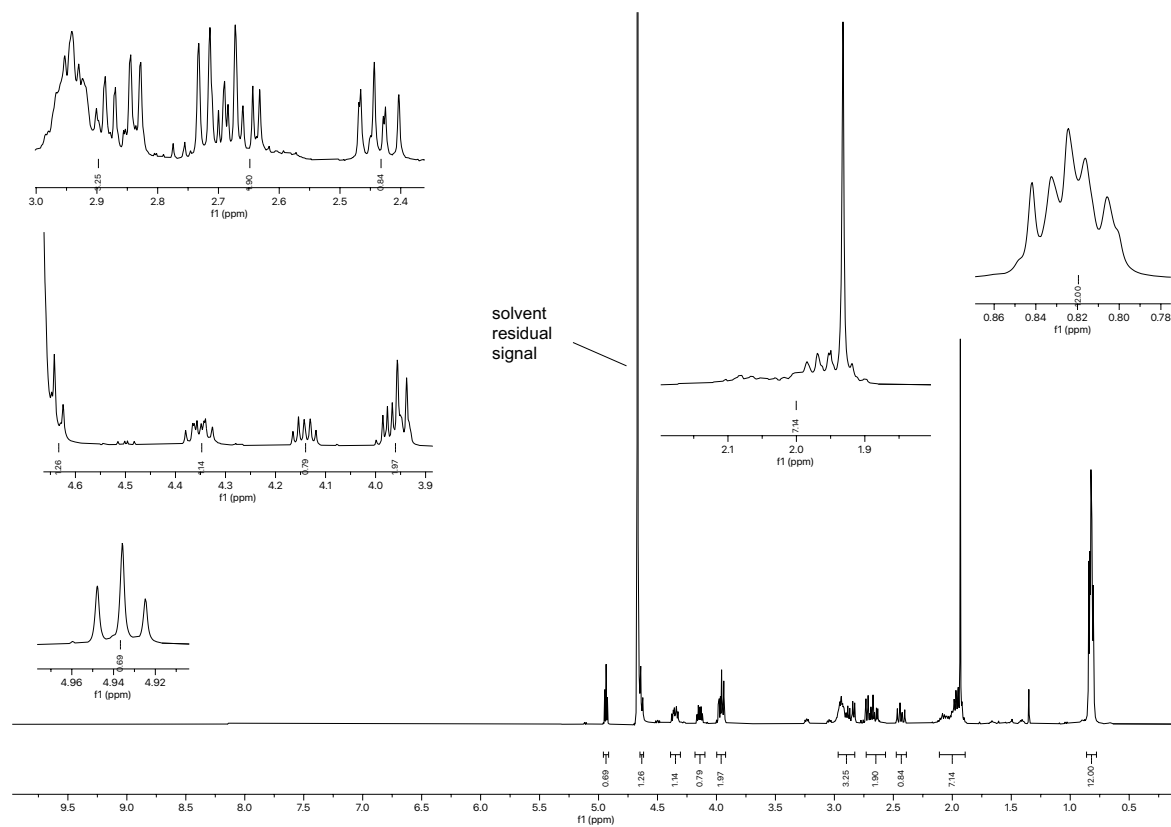
Figure 2.151. ^{1}H NMR spectrum (400 MHz, D$_2$O) of compound **2.069**.
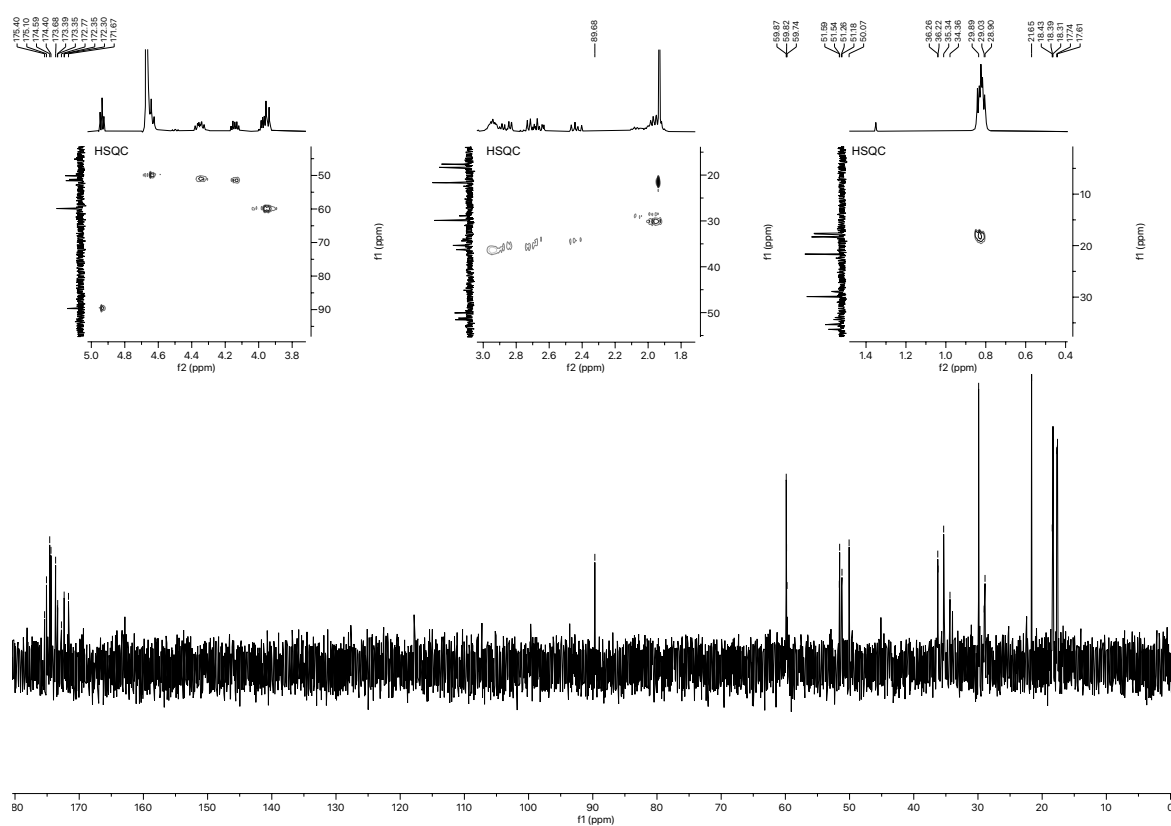
Figure 2.152. ^{13}C NMR spectrum (101 MHz, D$_2$O) of compound **2.069**.
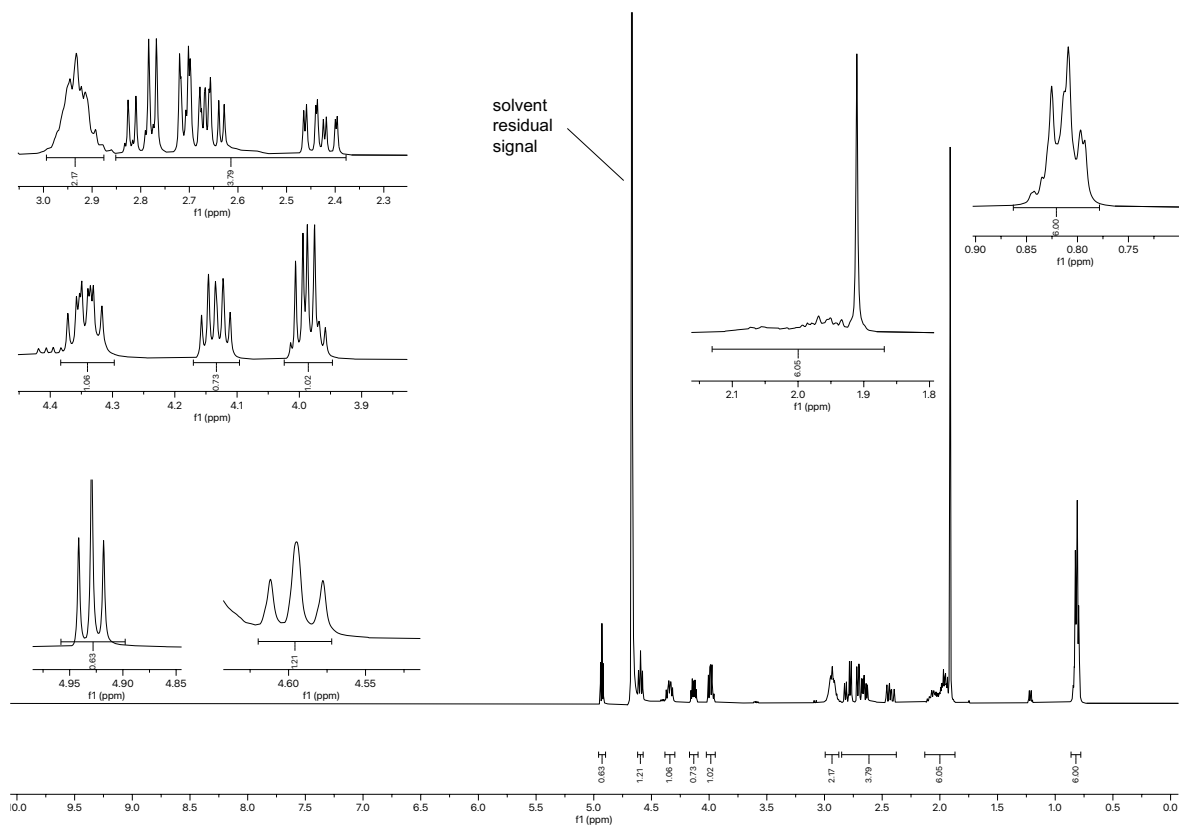
Figure 2.153. ^{1}H NMR spectrum (400 MHz, D$_2$O) of compound **2.070**.
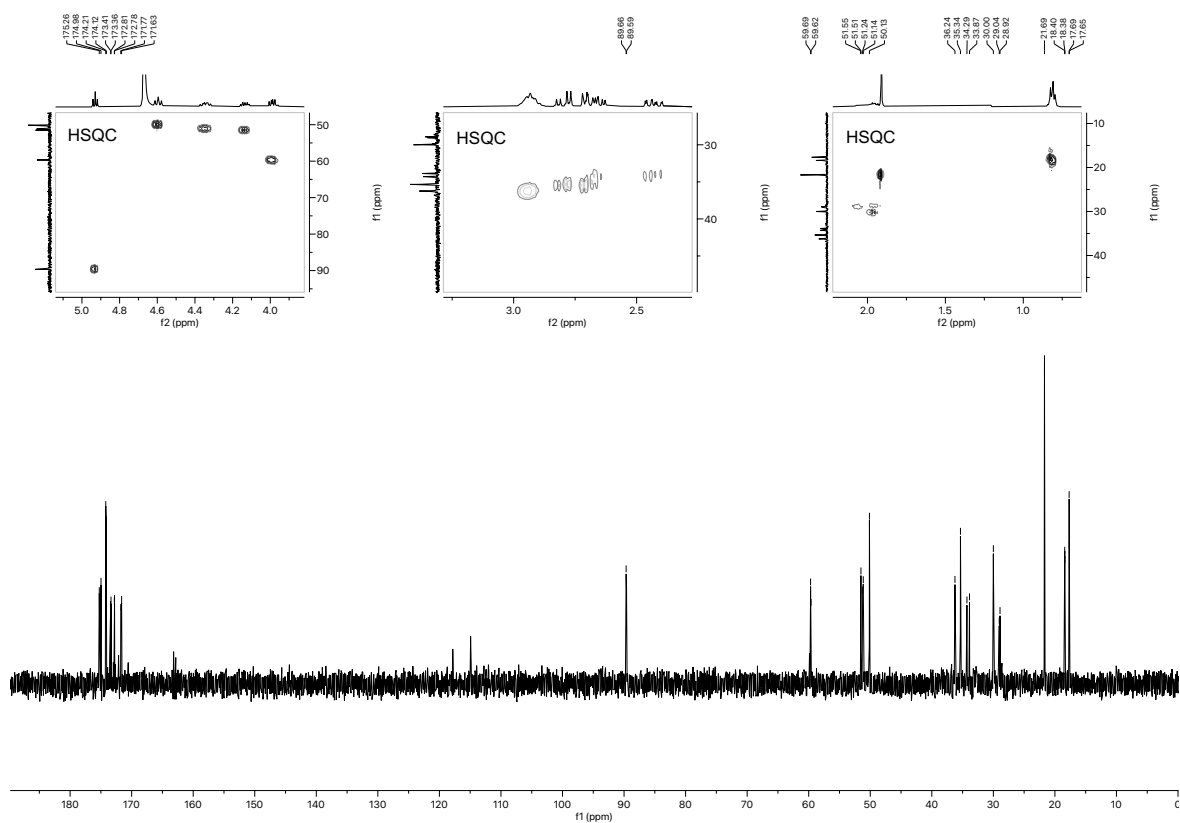
Figure 2.154. ^{13}C NMR spectrum (101 MHz, D$_2$O) of compound **2.070**.
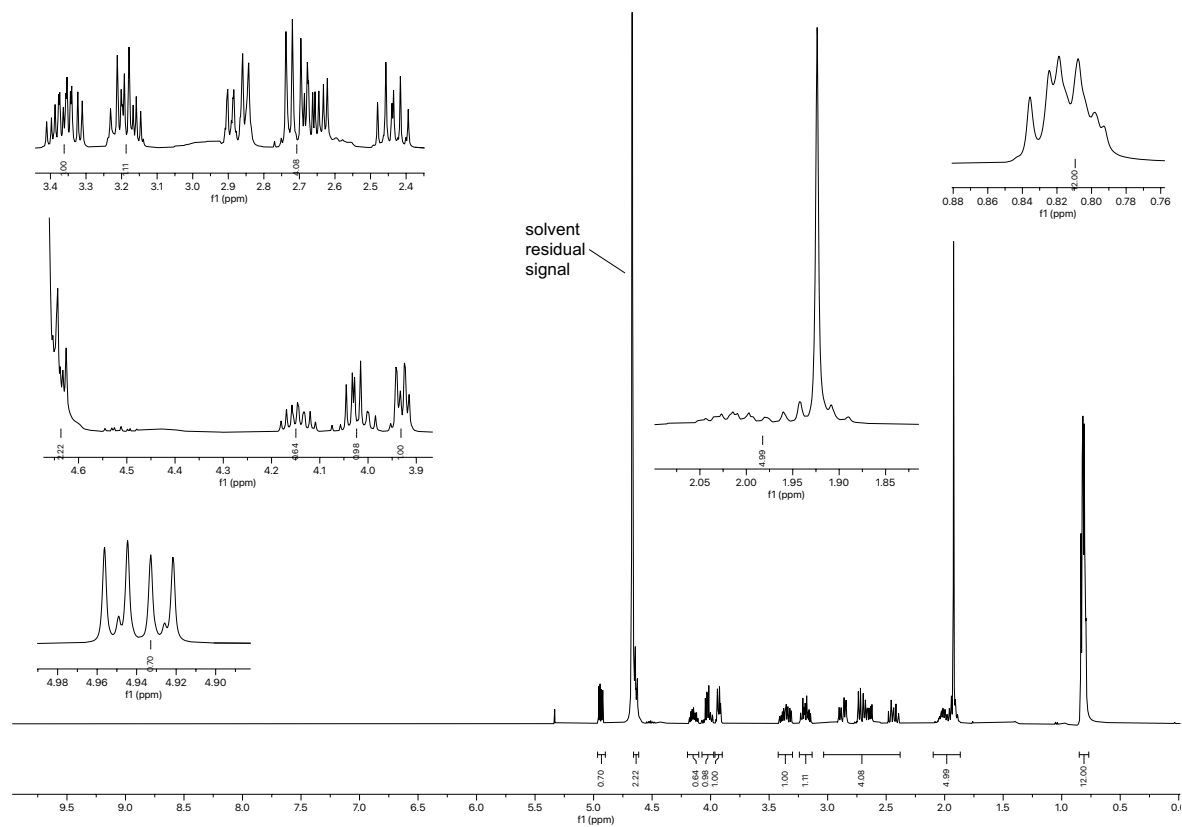
Figure 2.155. ^{1}H NMR spectrum (400 MHz, D$_2$O) of compound **2.071**.
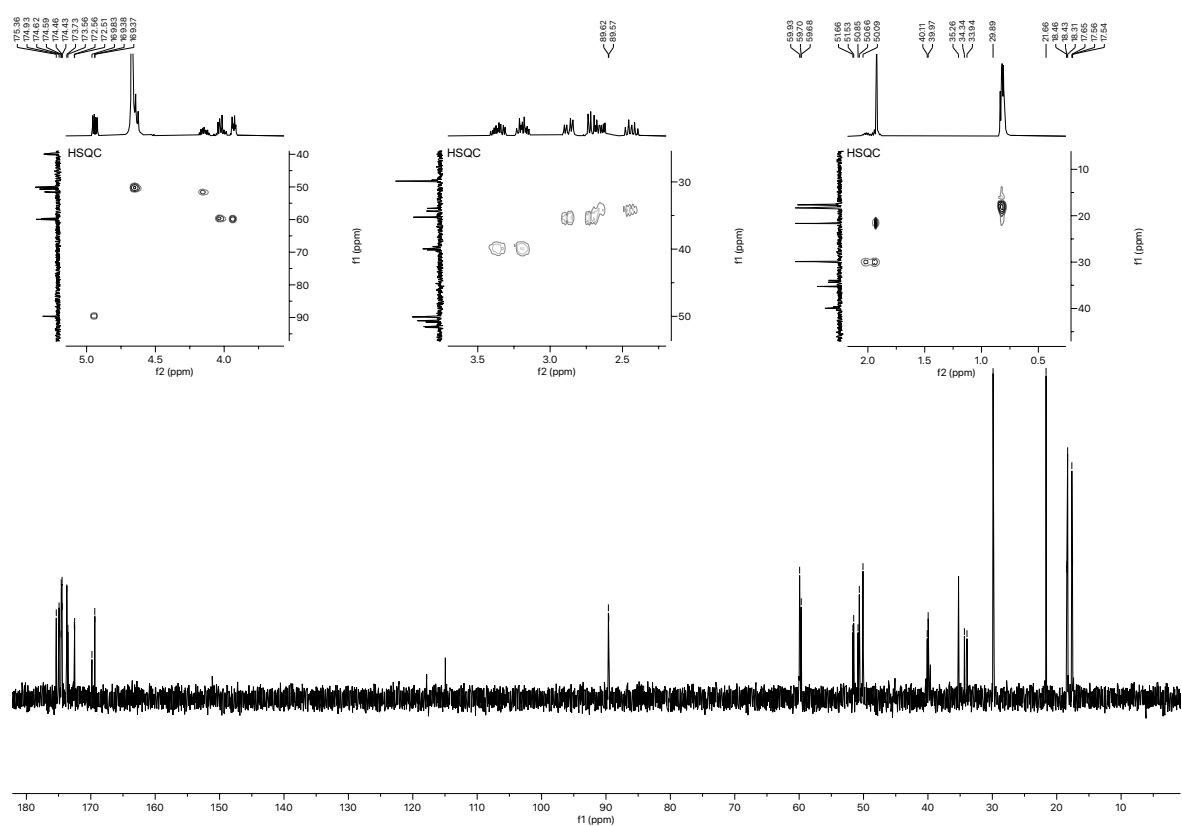
Figure 2.156. ^{13}C NMR spectrum (101 MHz, D$_2$O) of compound **2.071**.
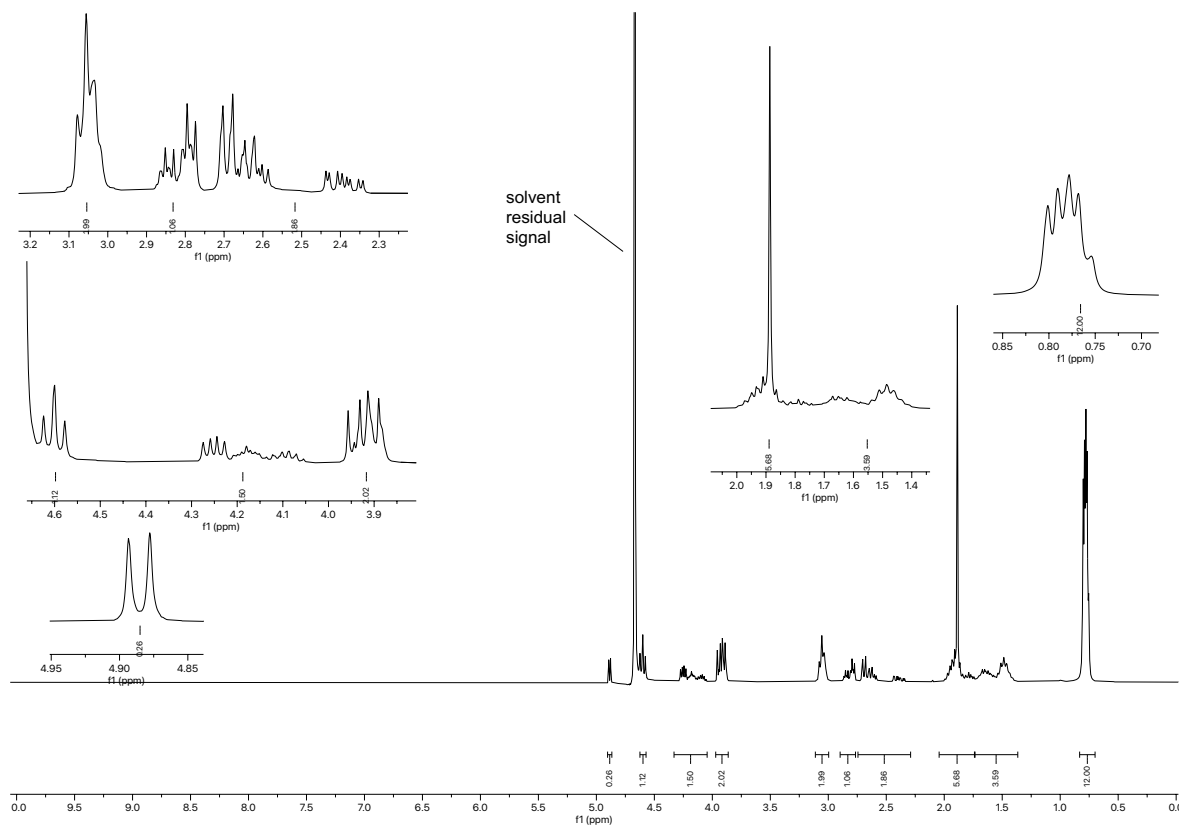
Figure 2.157. ^{1}H NMR spectrum (300 MHz, D$_2$O) of compound **2.072**.
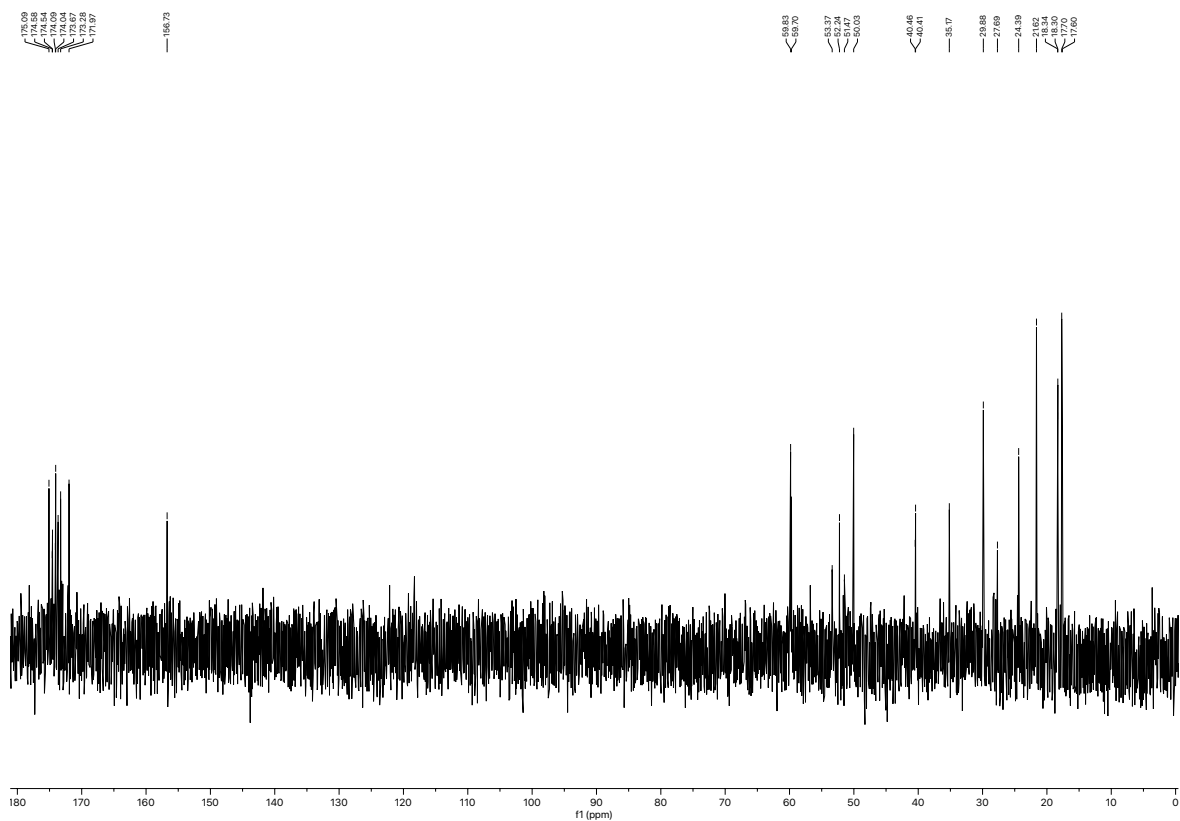
Figure 2.158. ^{13}C NMR spectrum (75 MHz, D$_2$O) of compound **2.072**.

241
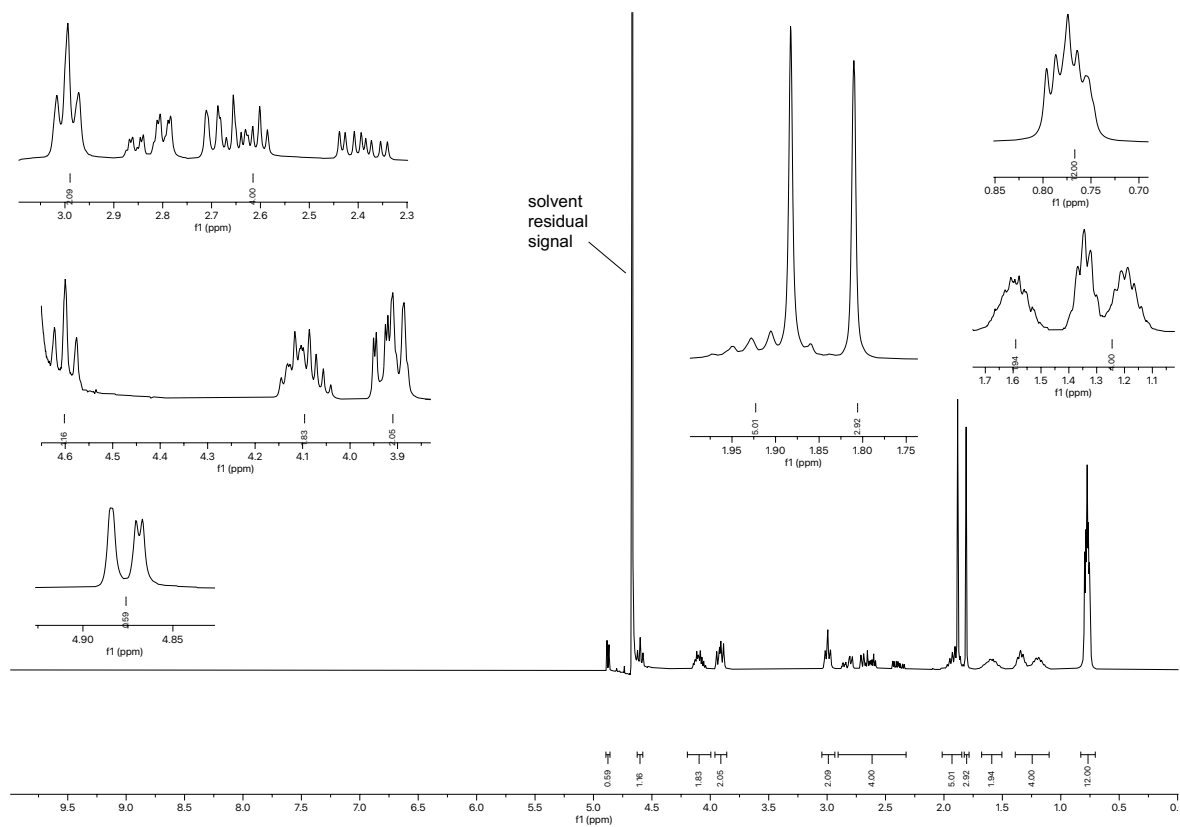
Figure 2.159. ^{1}H NMR spectrum (300 MHz, D$_2$O) of compound **2.073**.
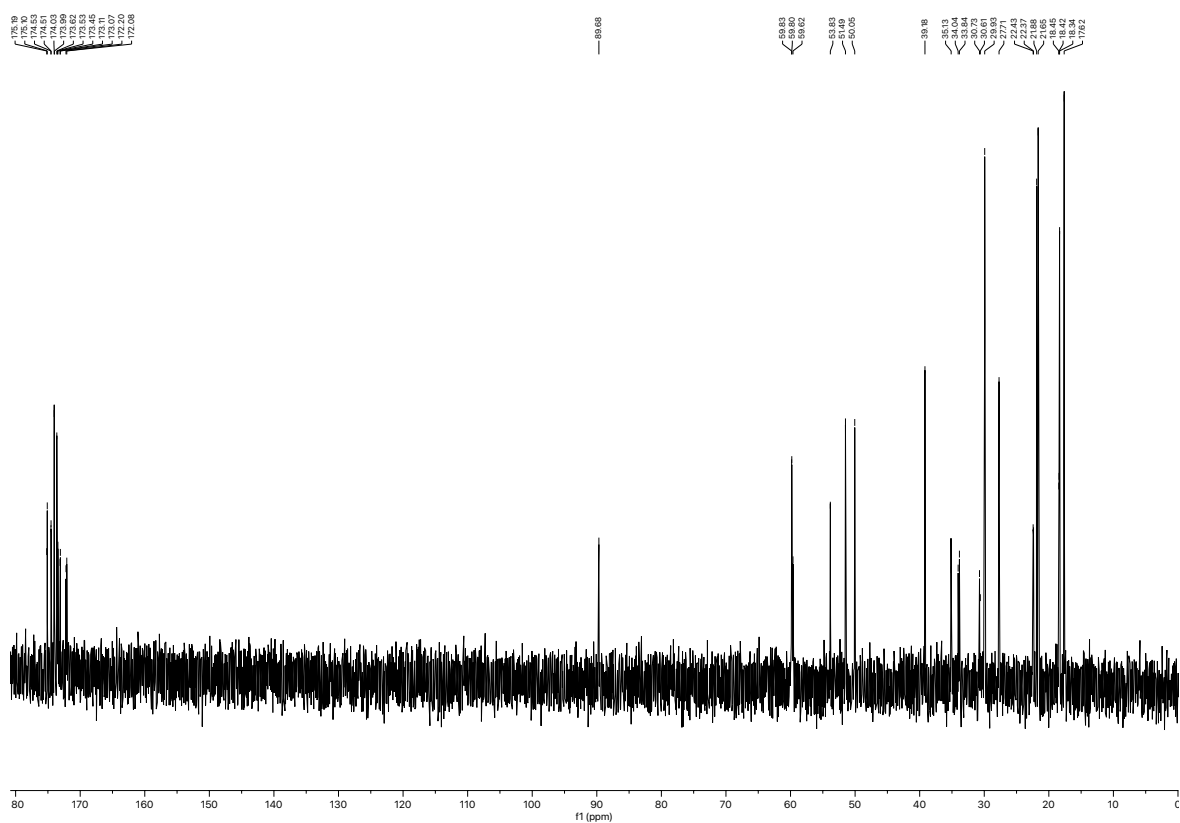
Figure 2.160. ^{13}C NMR spectrum (75 MHz, D$_2$O) of compound **2.073**.

242
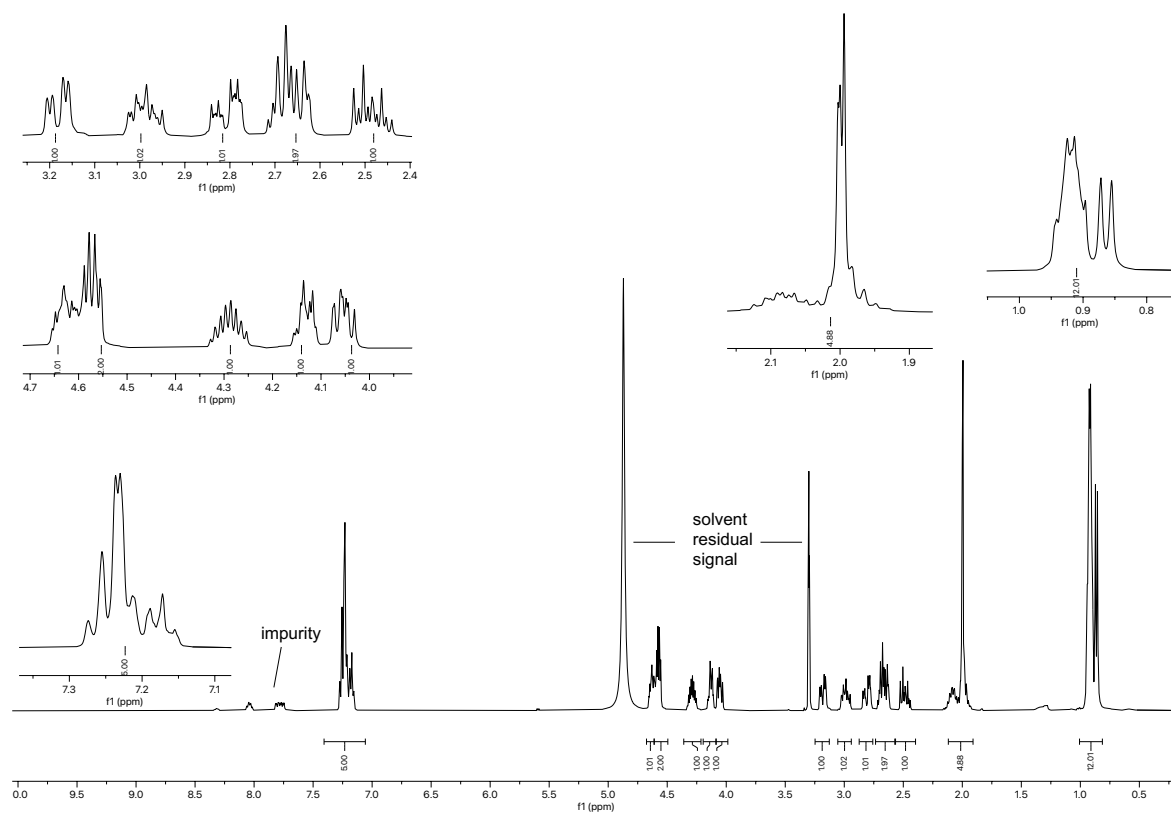
Figure 2.161. ^{1}H NMR spectrum (400 MHz, CD$_3$OD) of compound **2.074**.
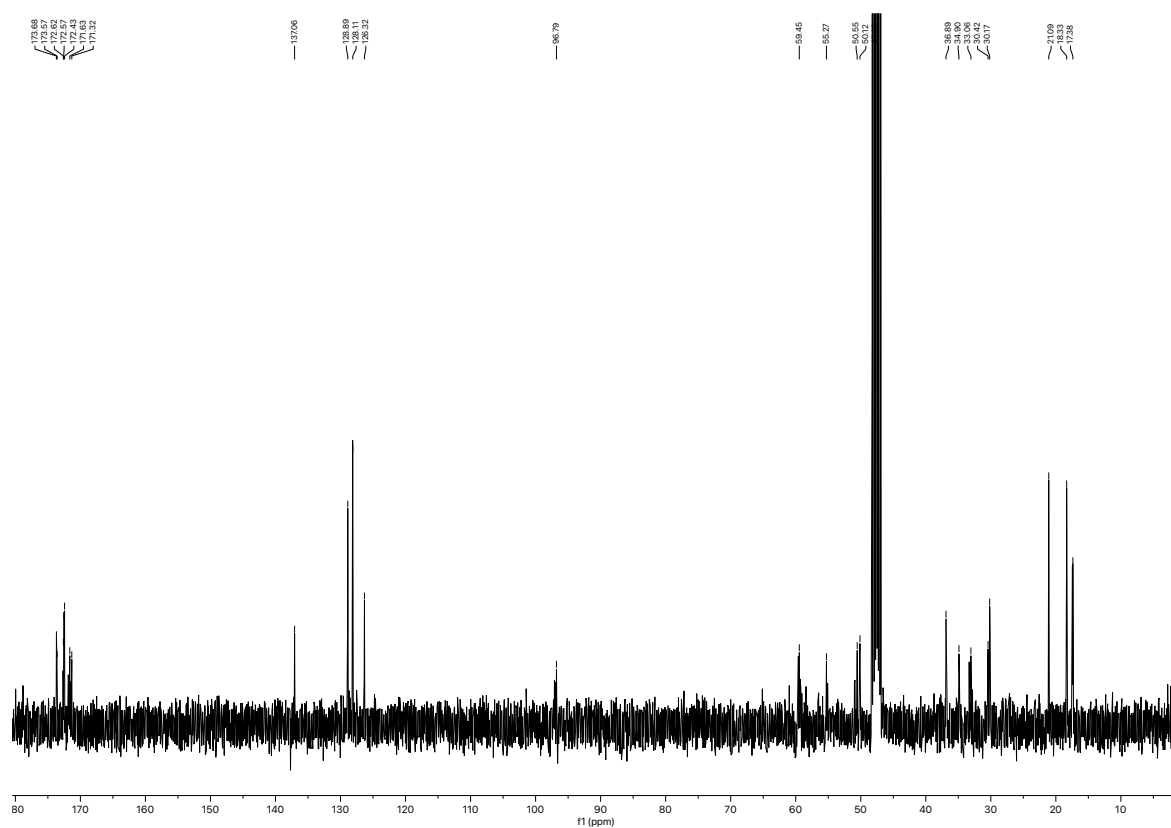
Figure 2.162. ^{1}H NMR spectrum (101 MHz, CD$_3$OD) of compound **2.074**.
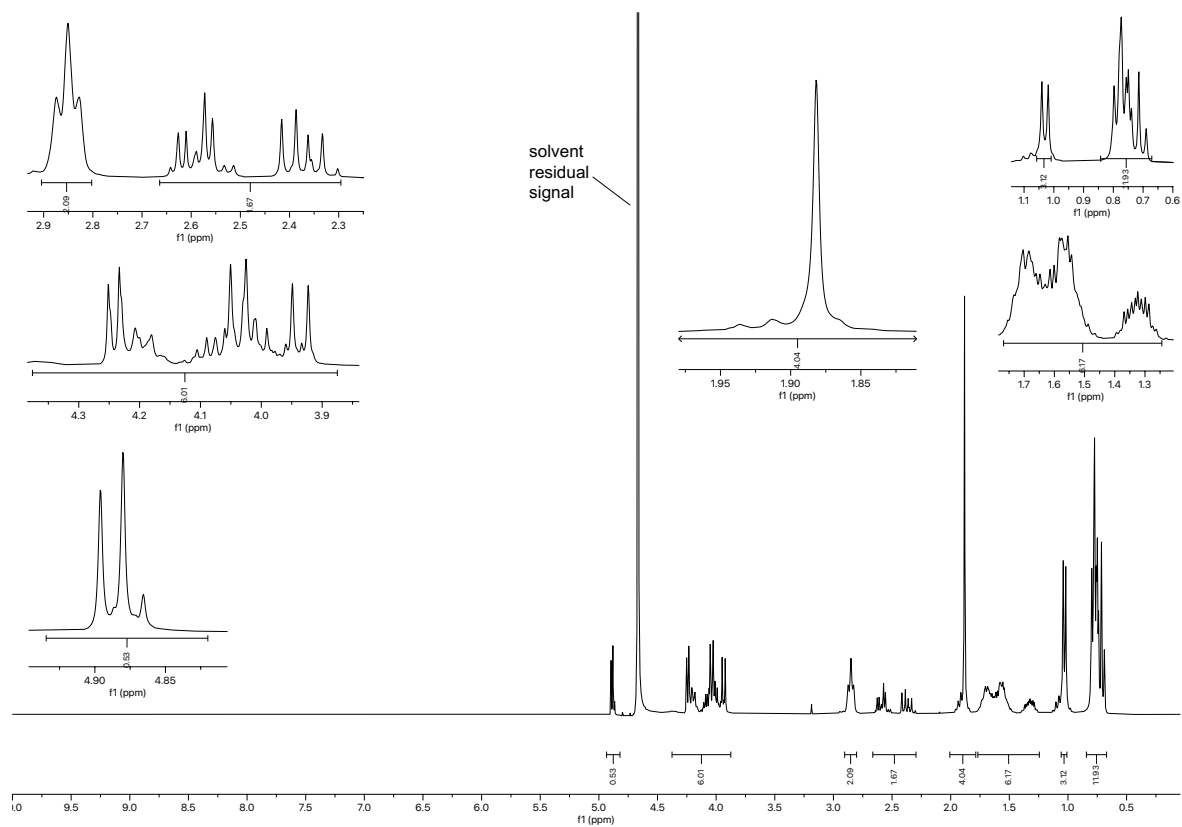
Figure 2.163. ^{1}H NMR spectrum (300 MHz, D$_2$O) of compound **2.075**.
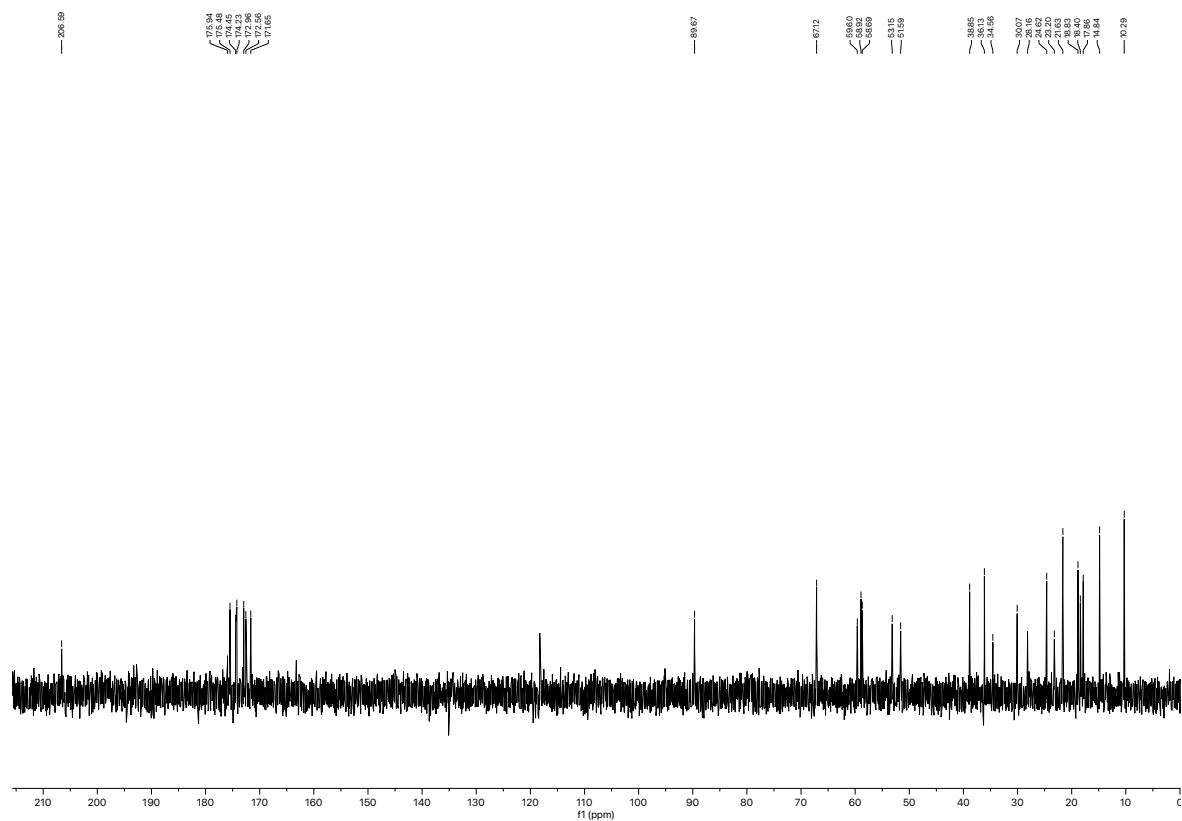
Figure 2.164. ^{13}C NMR spectrum (75 MHz, D$_2$O) of compound **2.075**.
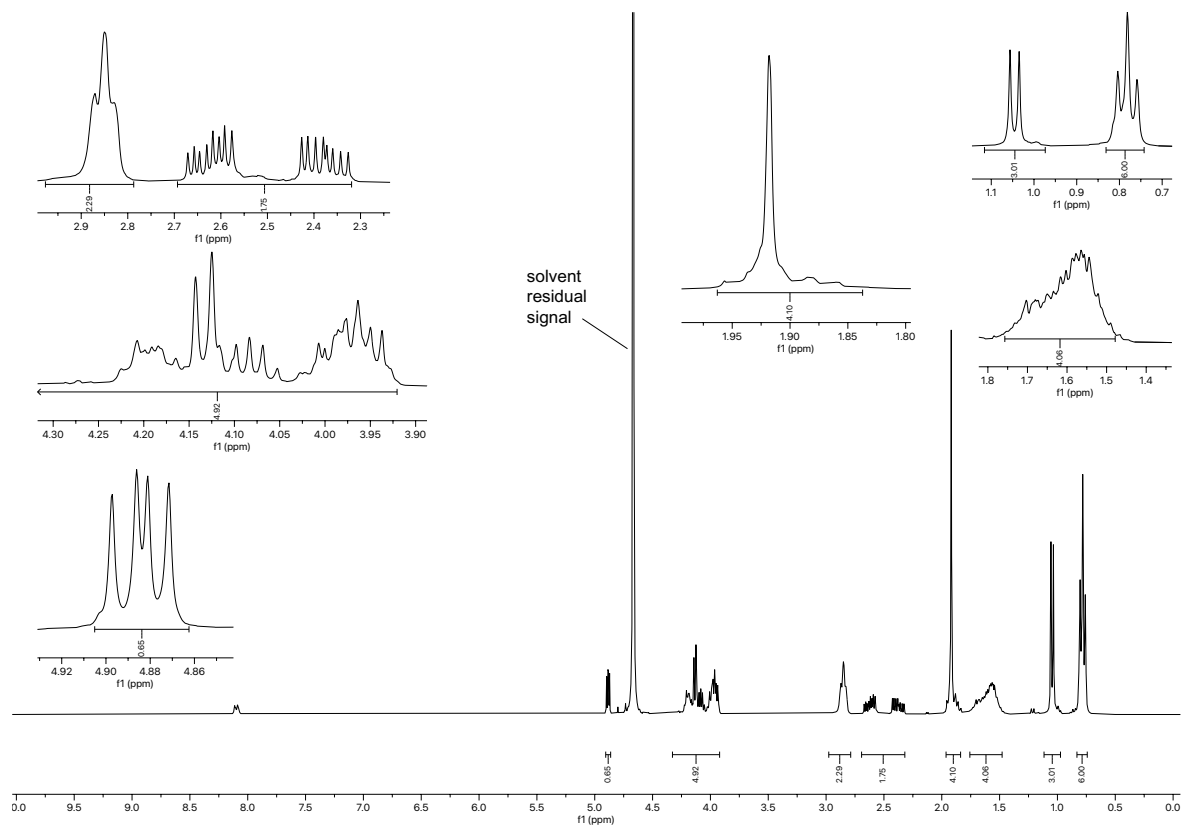
Figure 2.165. ^{1}H NMR spectrum (300 MHz, D$_2$O) of compound **2.076**.
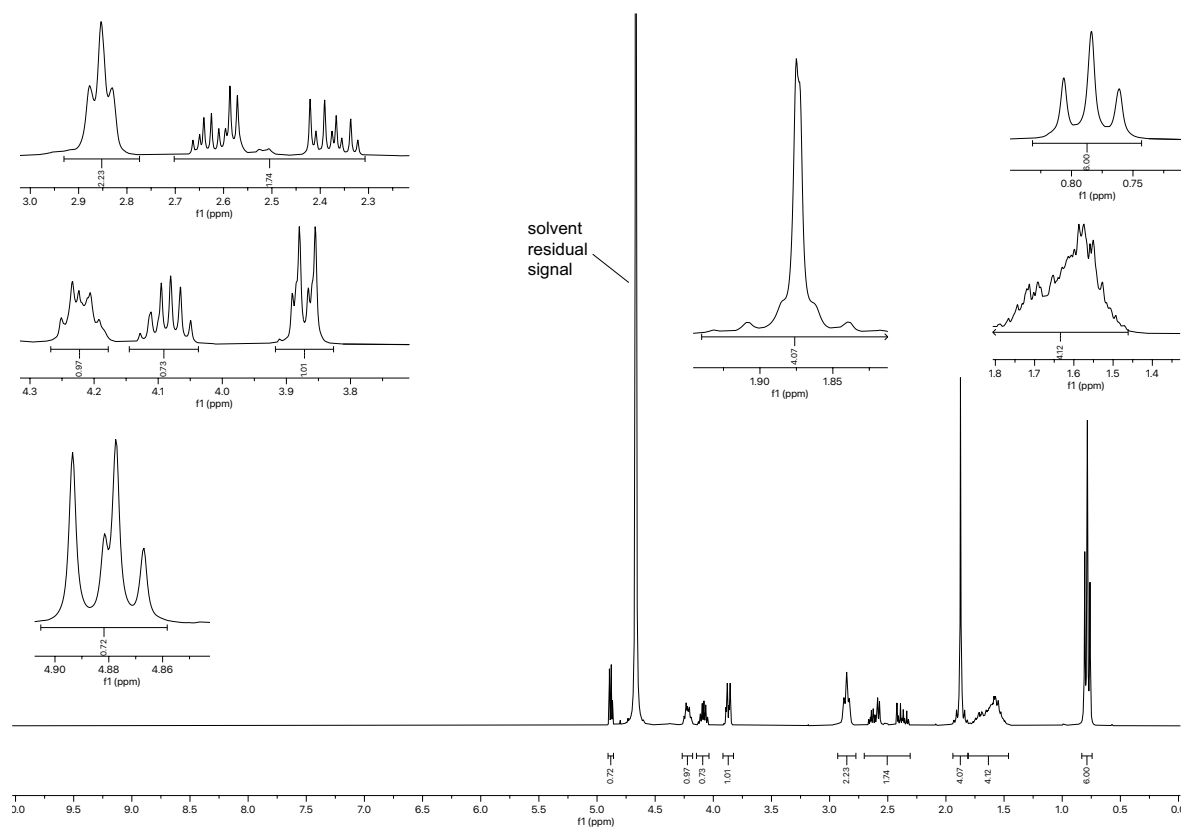
Figure 2.166. ^{1}H NMR spectrum (300 MHz, D$_2$O) of compound **2.077**.
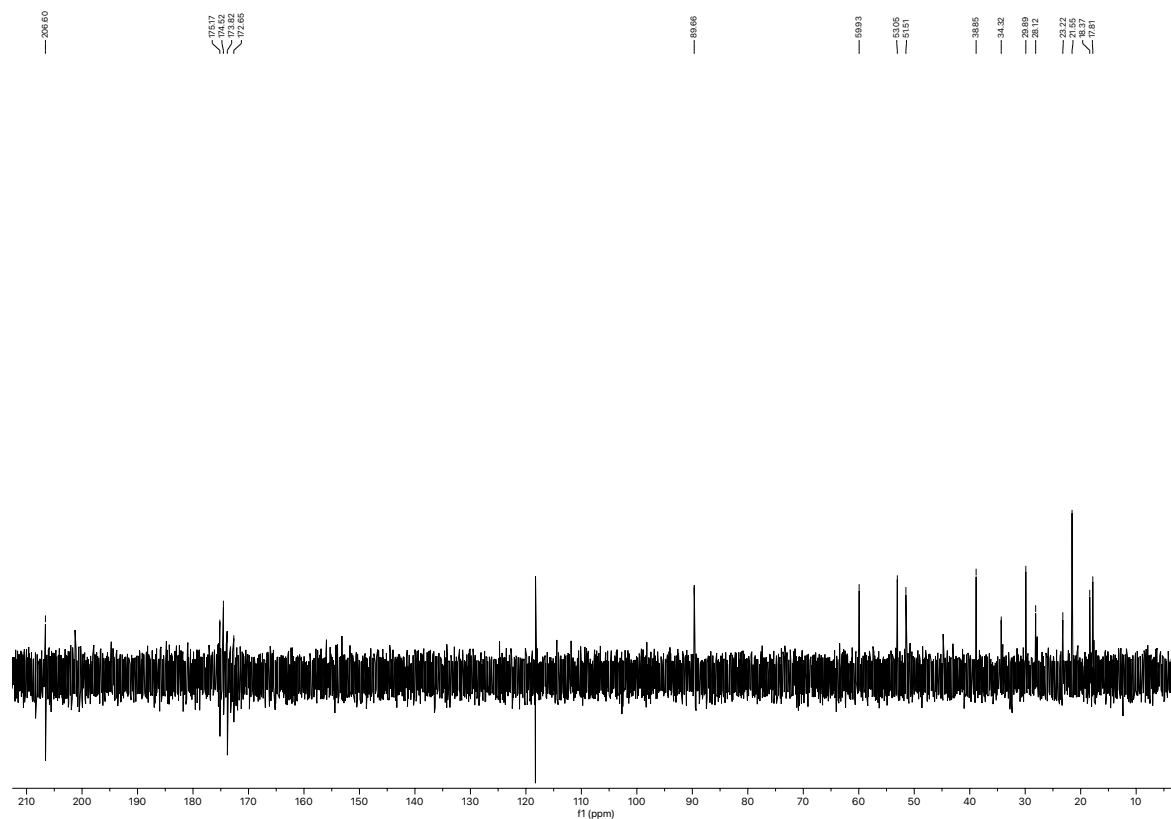
Figure 2.167. ^{13}CNMR spectrum (75 MHz, D$_2$O) of compound **2.077**.
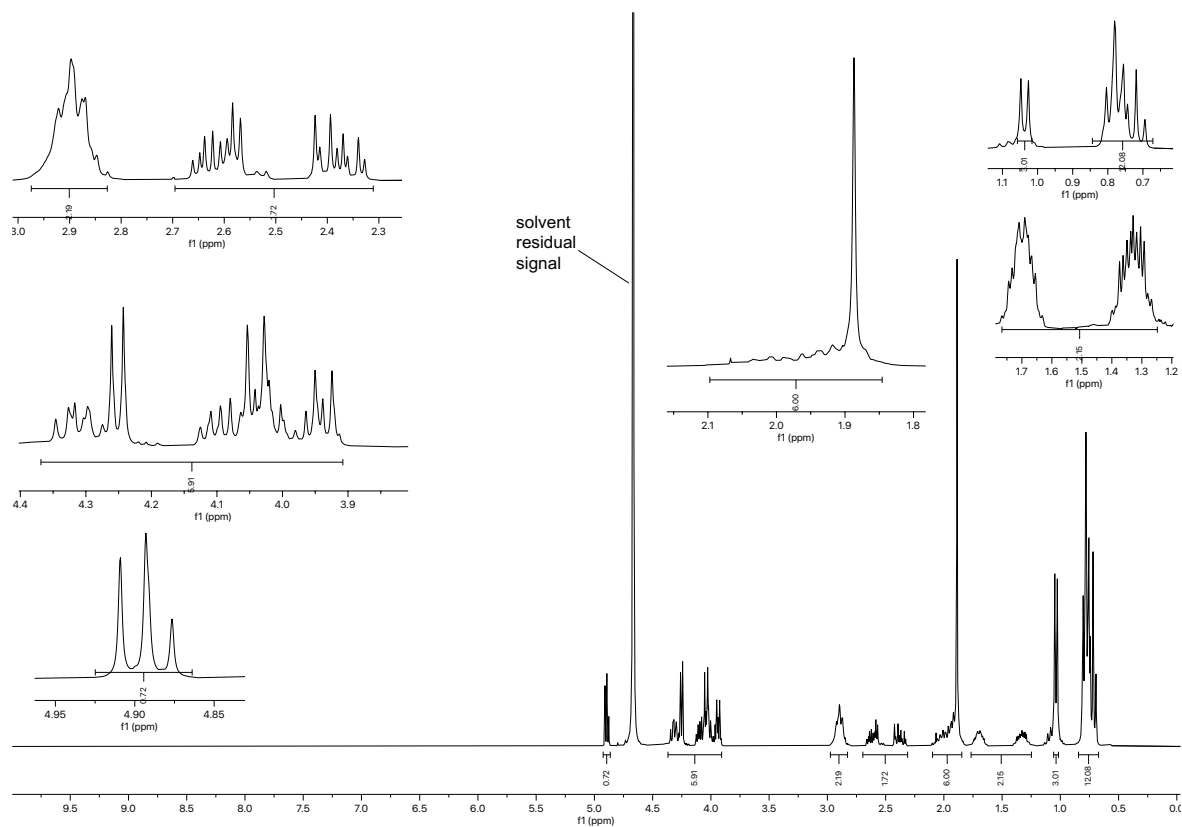
Figure 2.168. ^{1}H NMR spectrum (300 MHz, D$_2$O) of compound **2.078**.

246
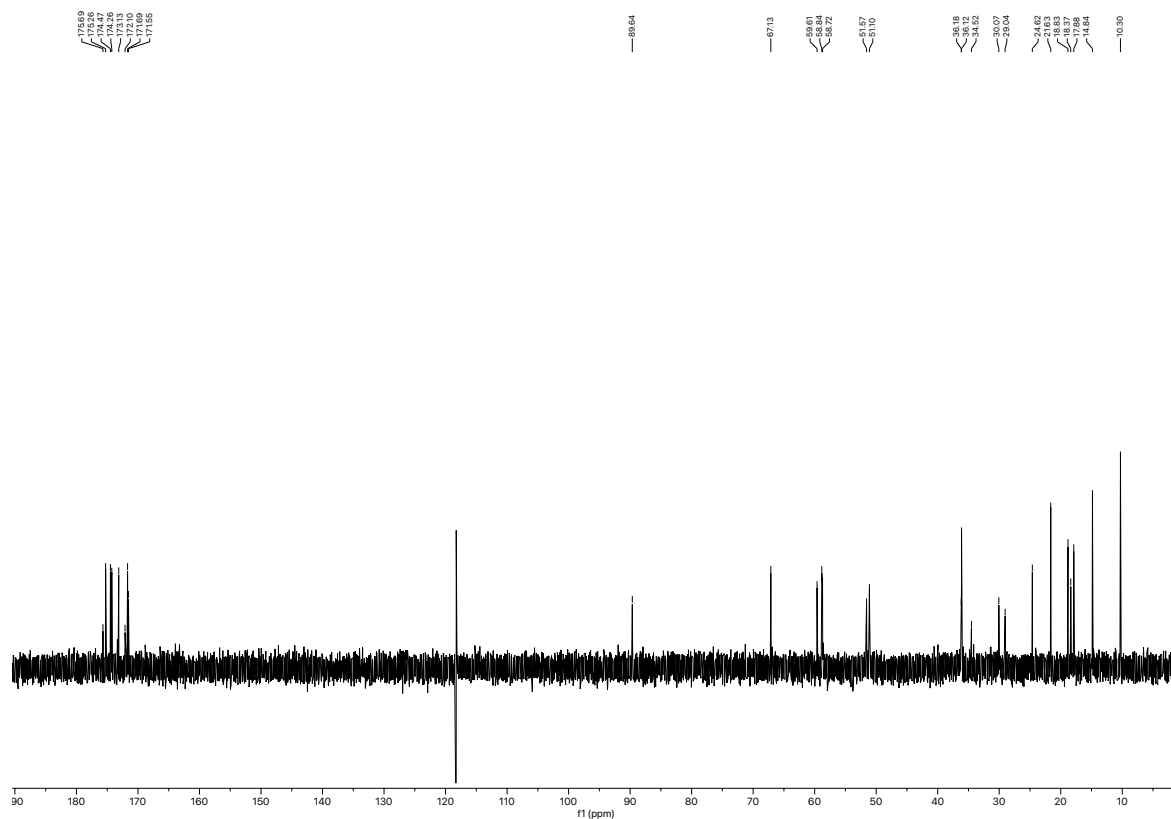
Figure 2.169. ^{13}C NMR spectrum (75 MHz, D$_2$O) of compound **2.078**.
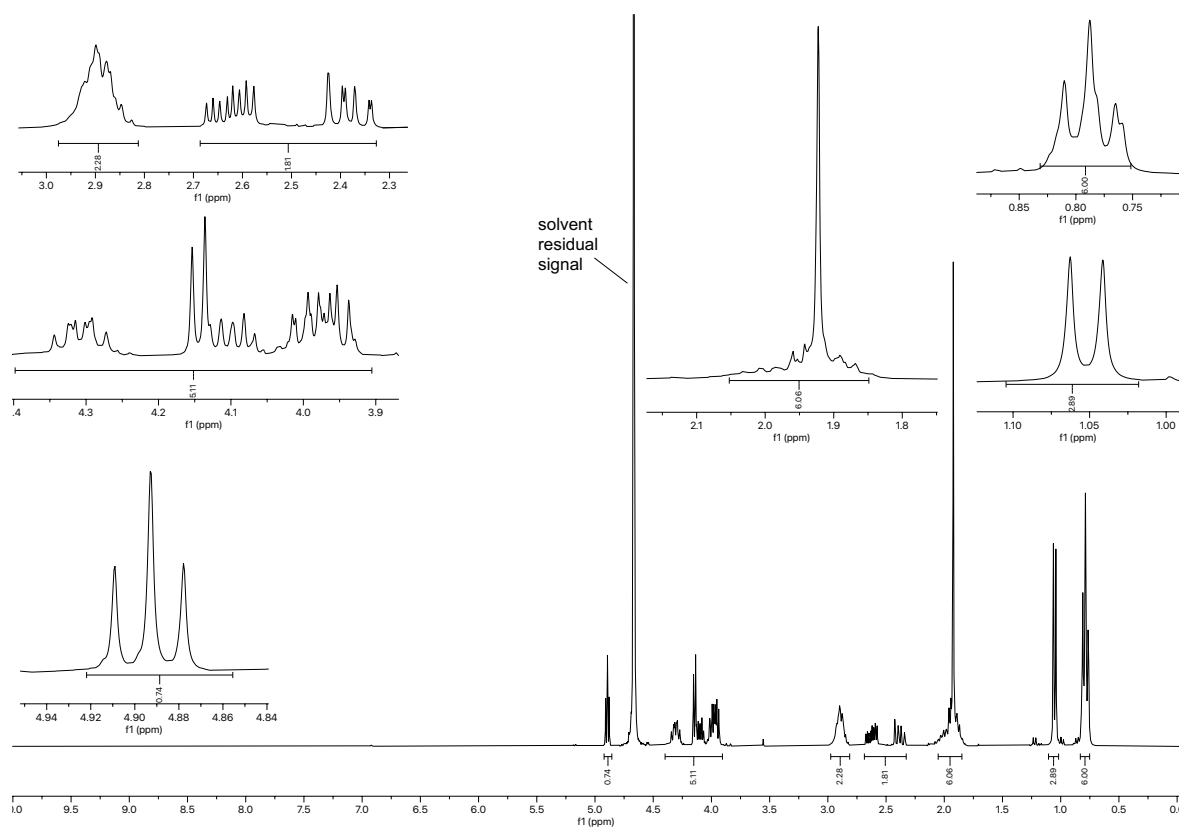
Figure 2.170. ^{1}H NMR spectrum (300 MHz, D$_2$O) of compound **2.079**.

247
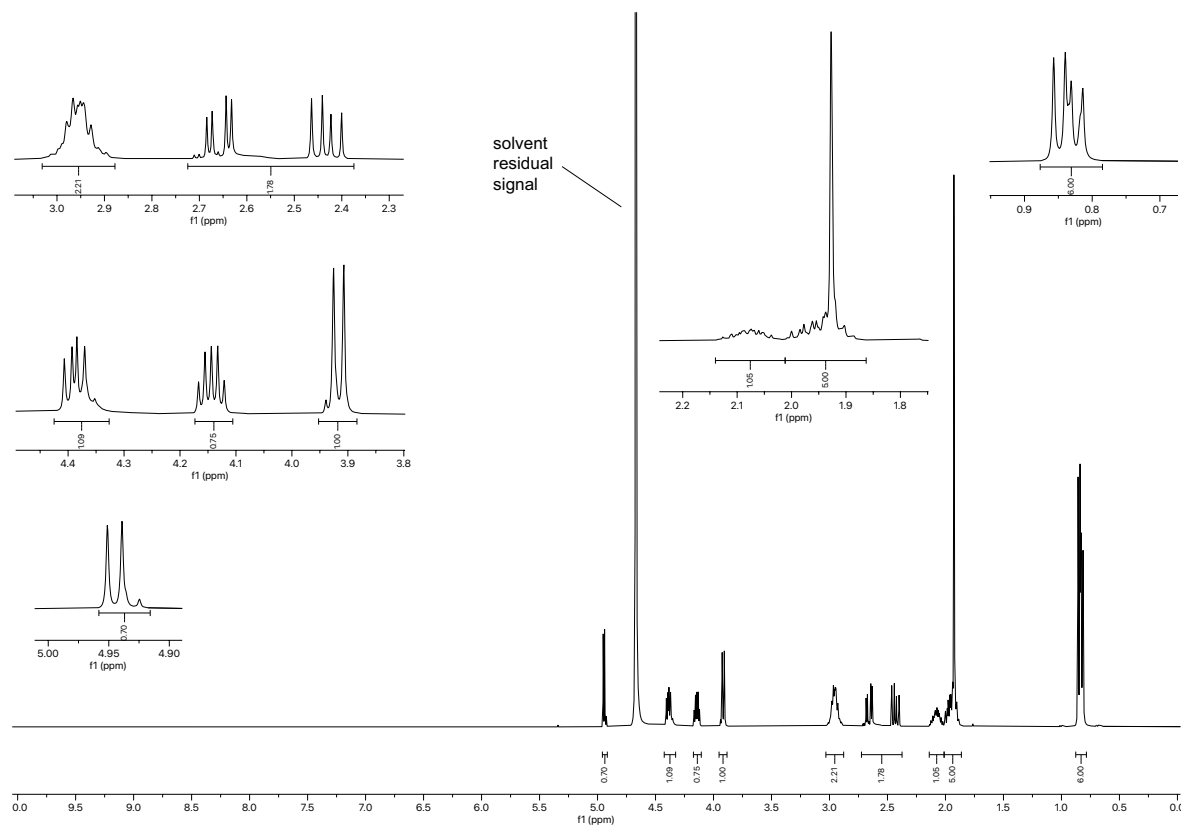
Figure 2.171. ^{1}H NMR spectrum (400 MHz, D$_2$O) of compound **2.080**.
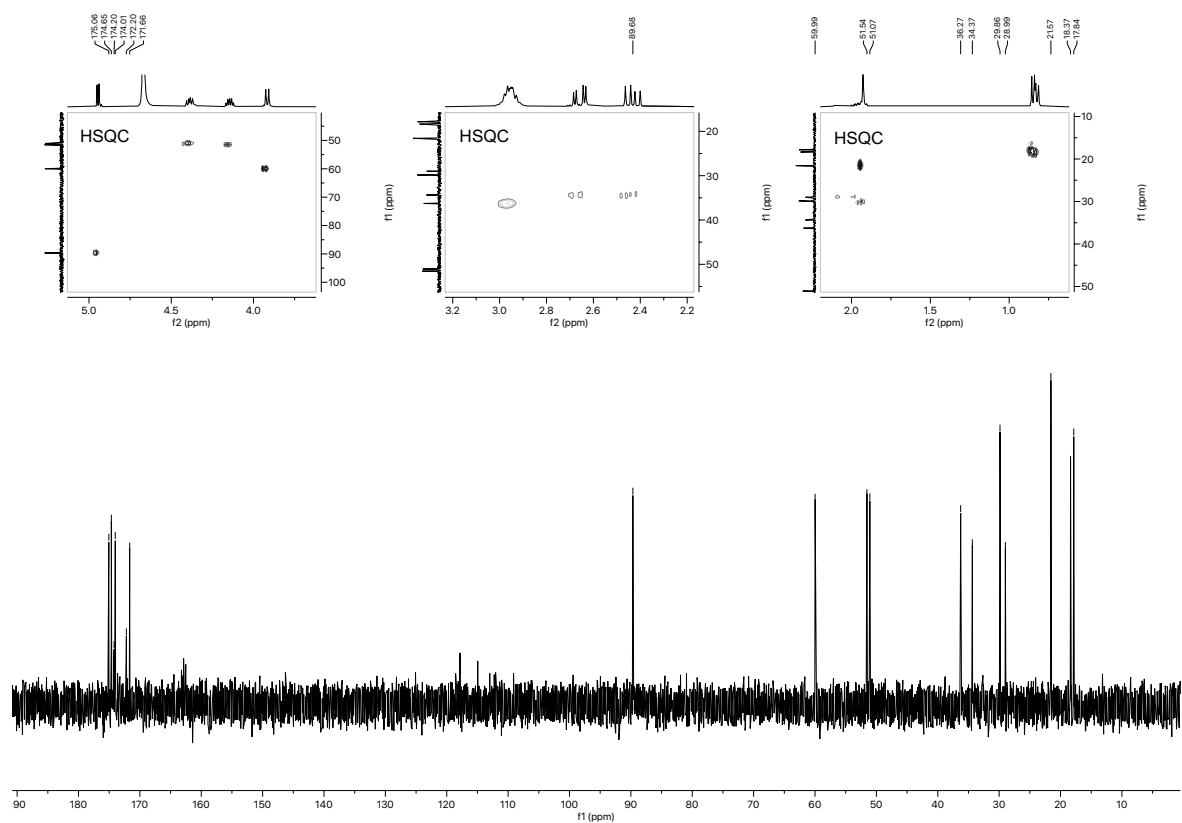
Figure 2.172. ^{13}CNMR spectrum (101 MHz, D$_2$O) of compound **2.080**.
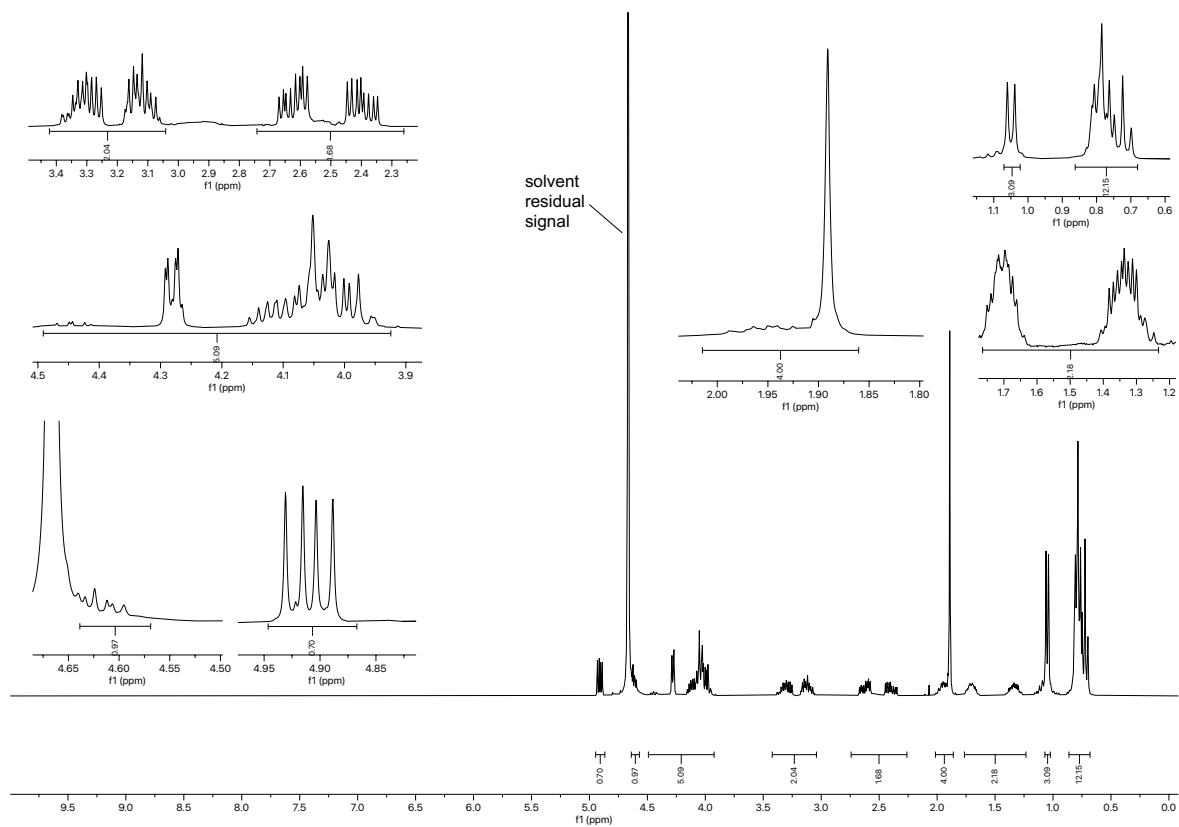
Figure 2.173. ^{1}H NMR spectrum (300 MHz, D$_2$O) of compound **2.081**.
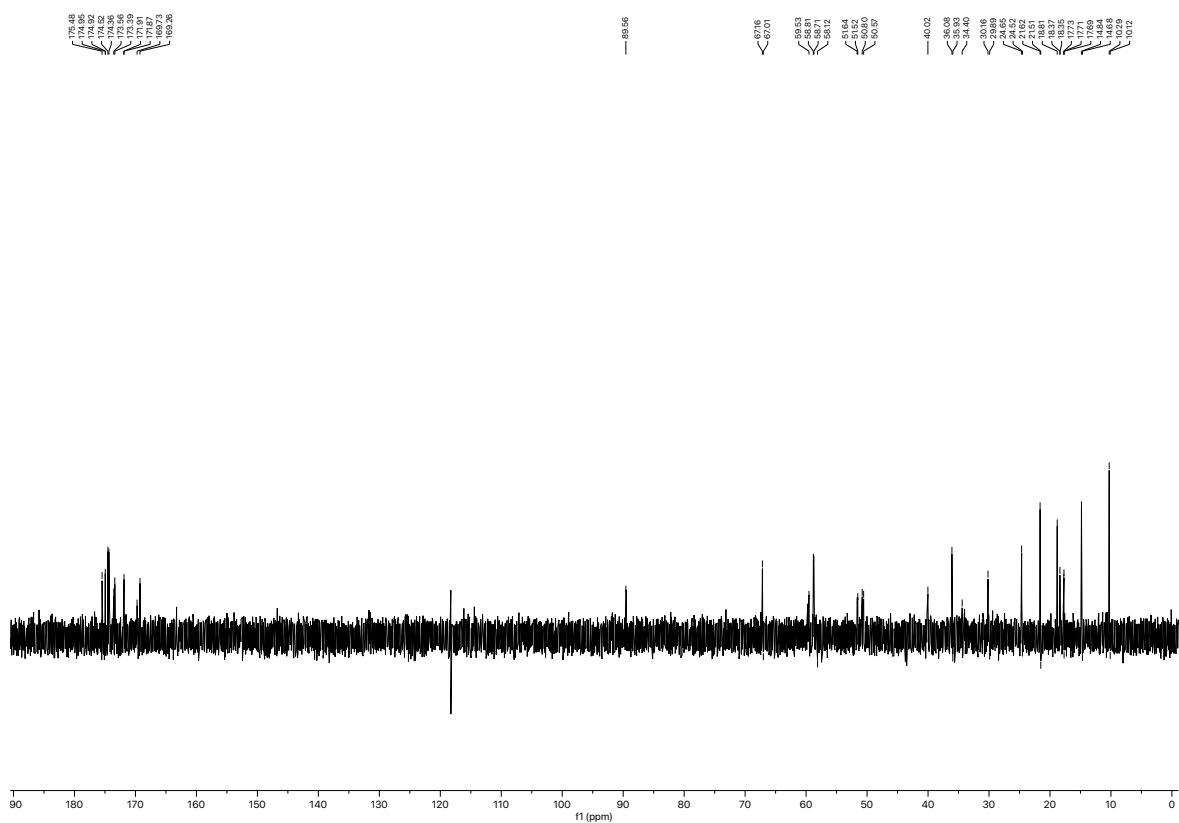
Figure 2.174. ^{13}C NMR spectrum (75 MHz, D$_2$O) of compound **2.081**.

249
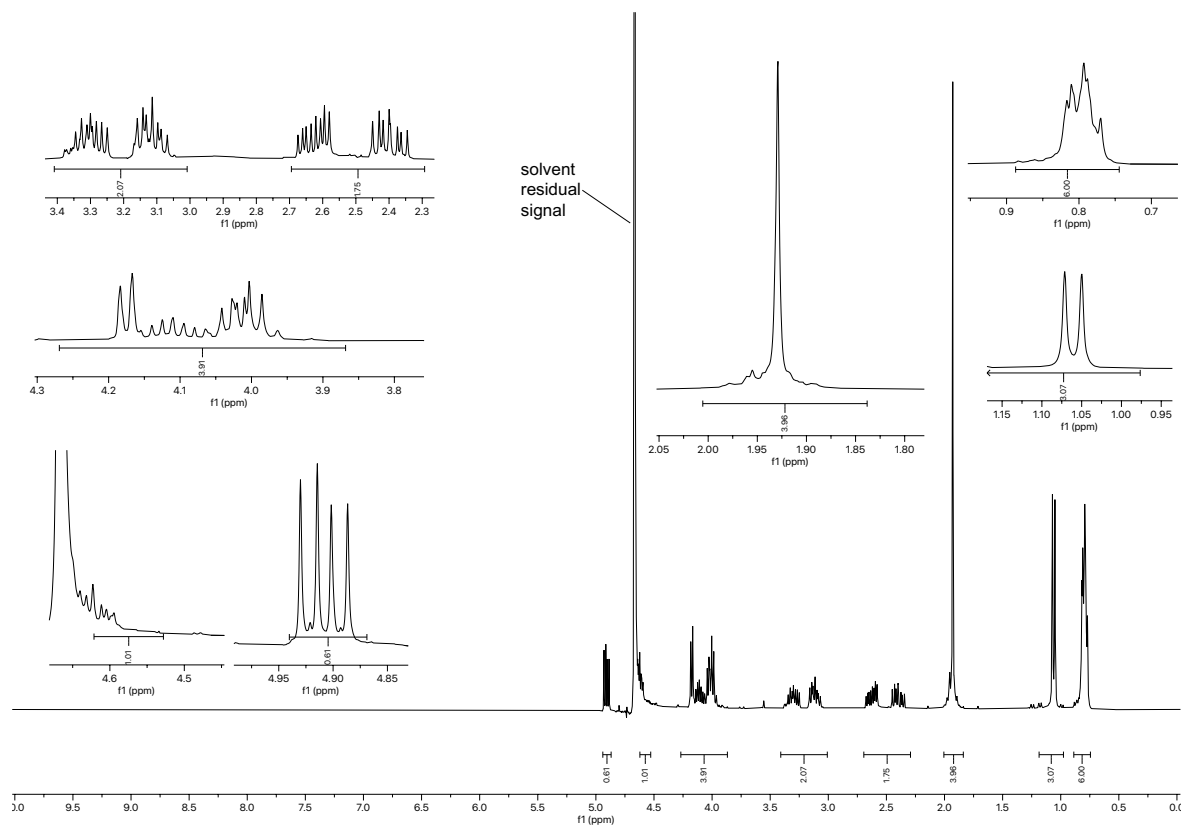
Figure 2.175. ^{1}H NMR spectrum (300 MHz, D$_2$O) of compound **2.082**.
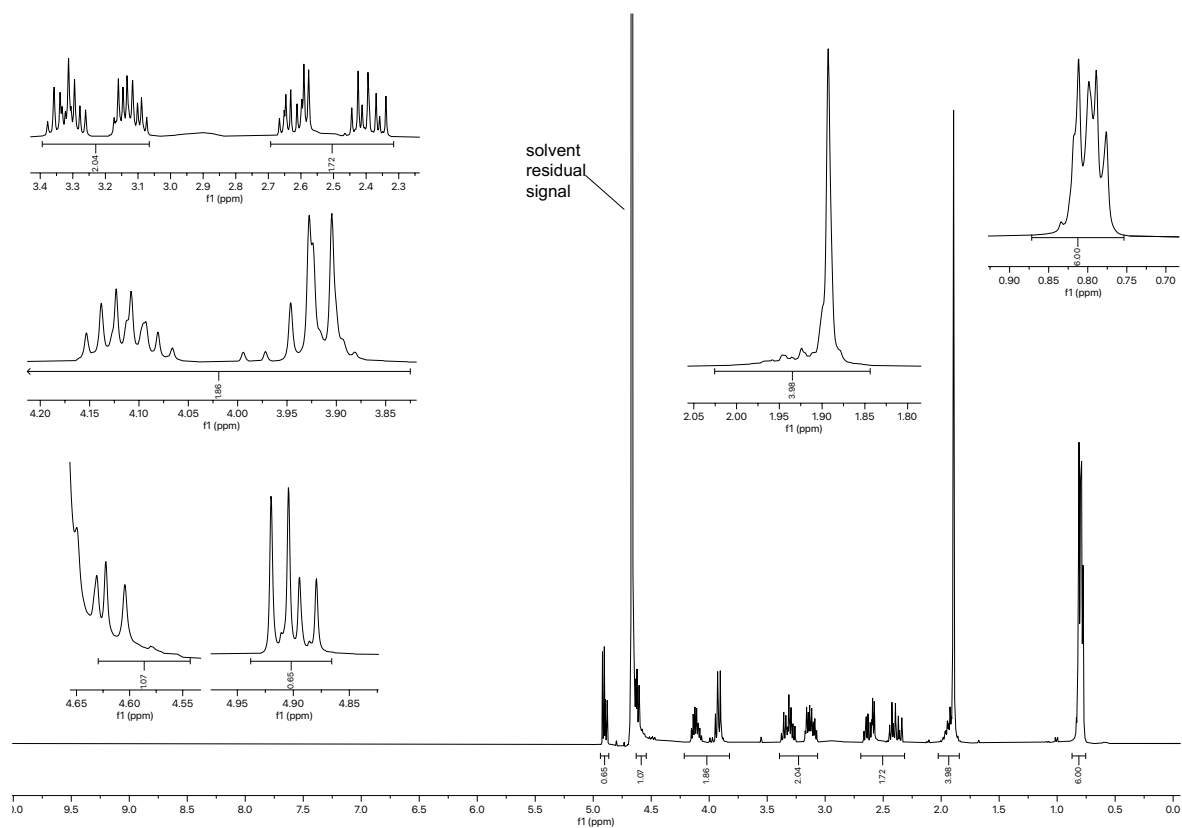
Figure 2.176. ^{1}H NMR spectrum (300 MHz, D$_2$O) of compound **2.083**.

250
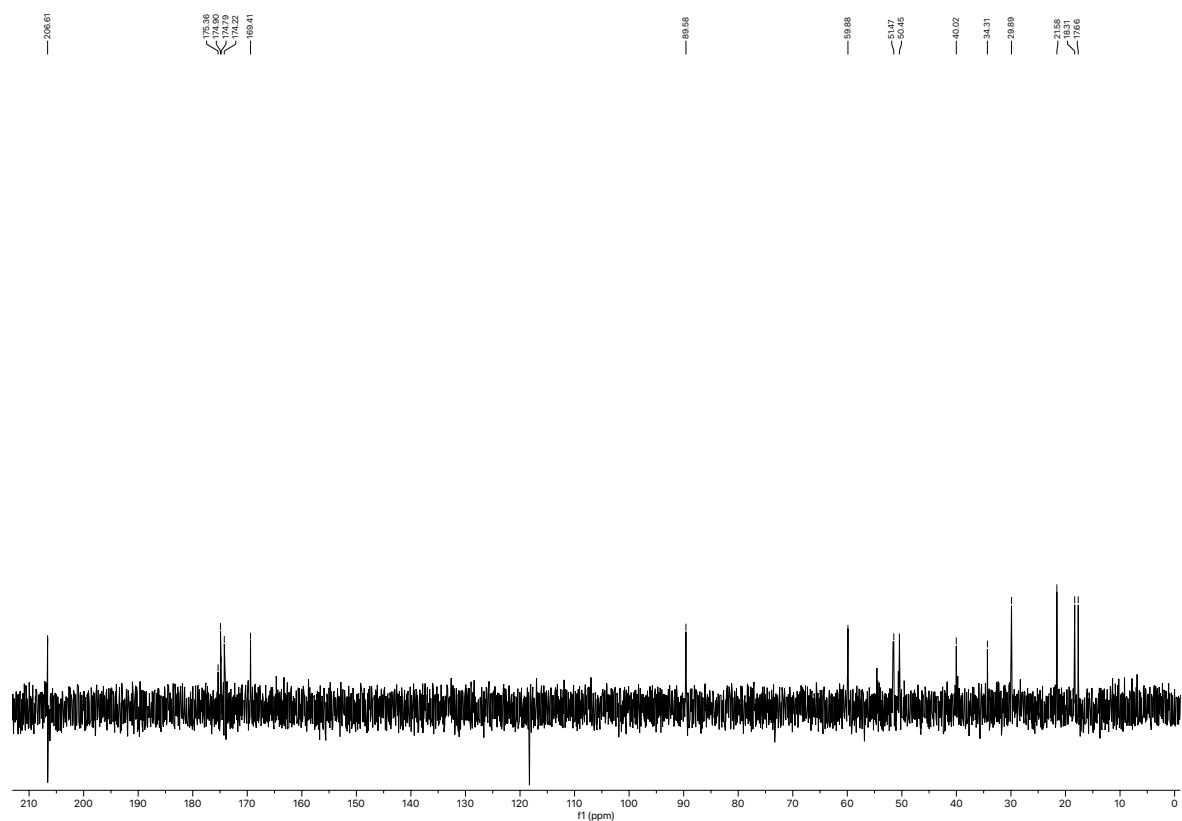
Figure 2.177. ^{13}C NMR spectrum (75 MHz, D$_2$O) of compound **2.083**.
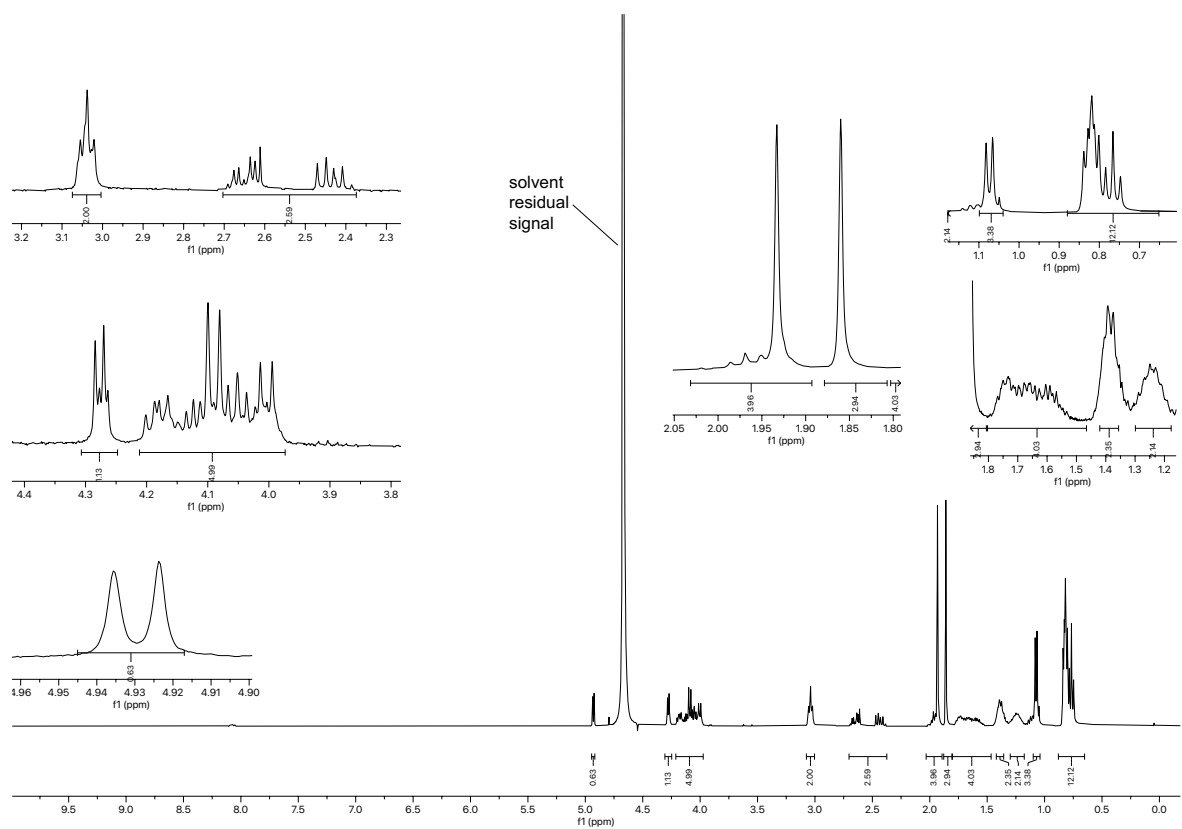
Figure 2.178. ^{1}H NMR spectrum (400 MHz, D$_2$O) of compound **2.084**.
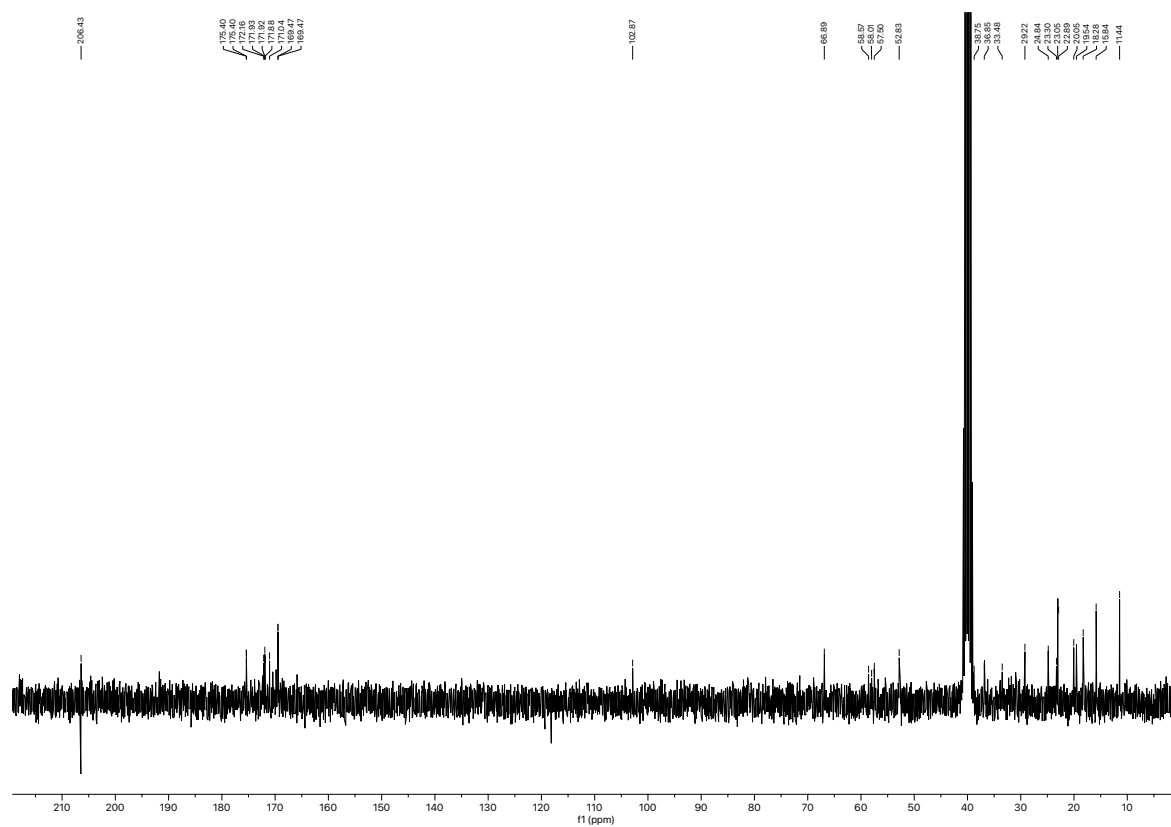
Figure 2.179. ^{13}C NMR spectrum (75 MHz, DMSO-d$_6$) of compound **2.084**.

solvent
residual
signal
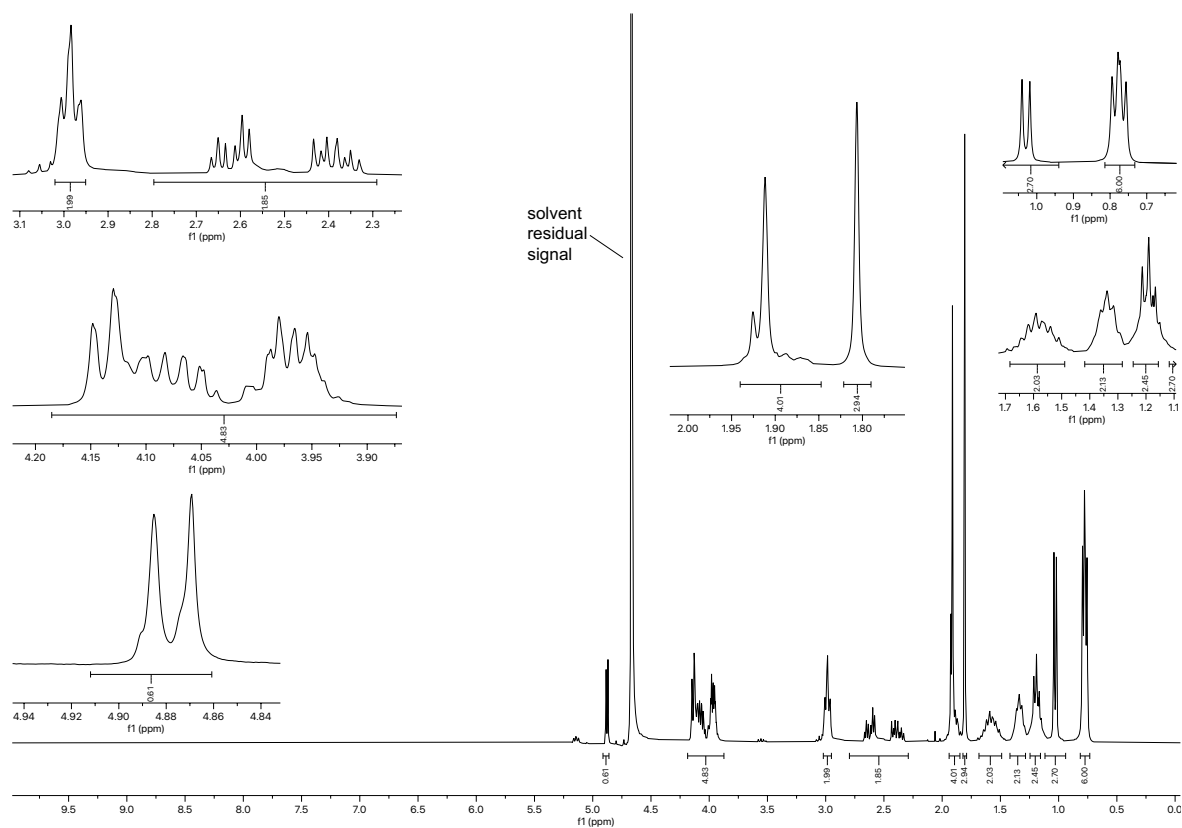
Figure 2.180. ^1H NMR spectrum (300 MHz, D$_2$O) of compound **2.085**.
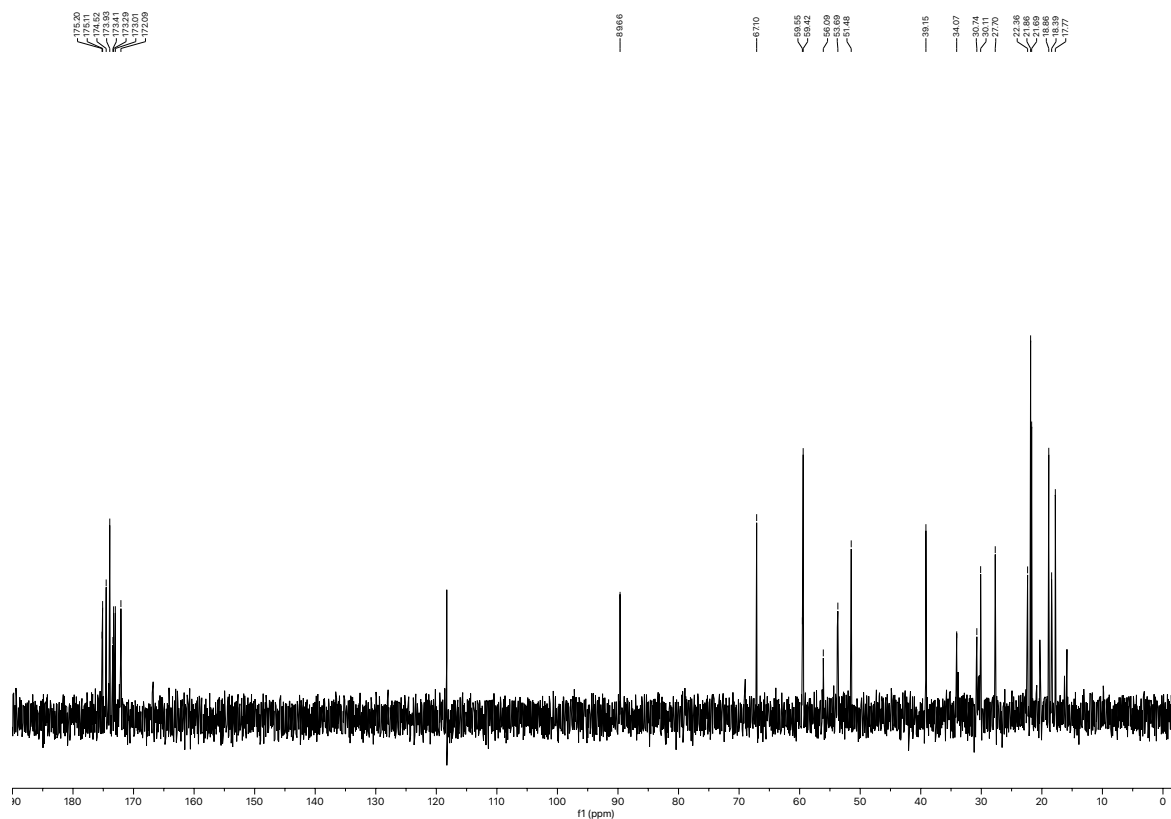
Figure 2.181. ^{13}CNMR spectrum (75 MHz, D$_2$O) of compound **2.085**.
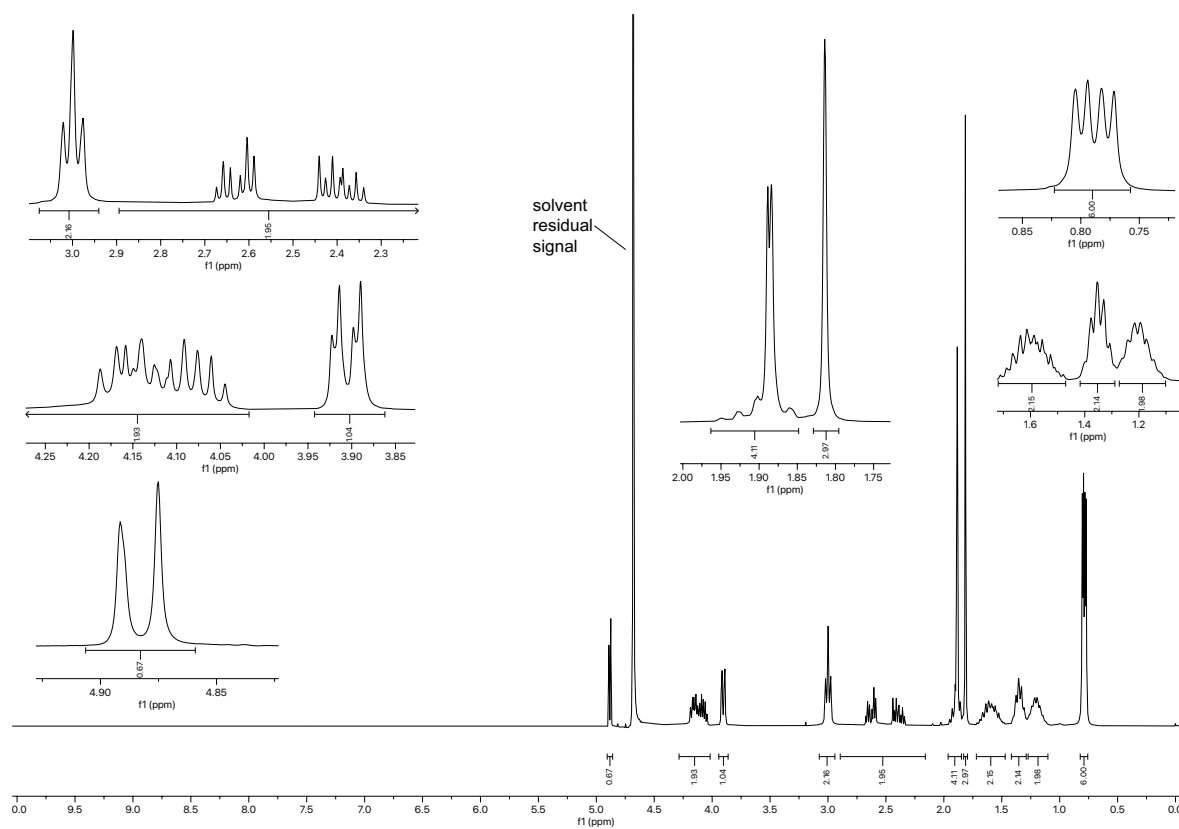
Figure 2.182. ^{1}H NMR spectrum (300 MHz, D$_2$O) of compound **2.086**.
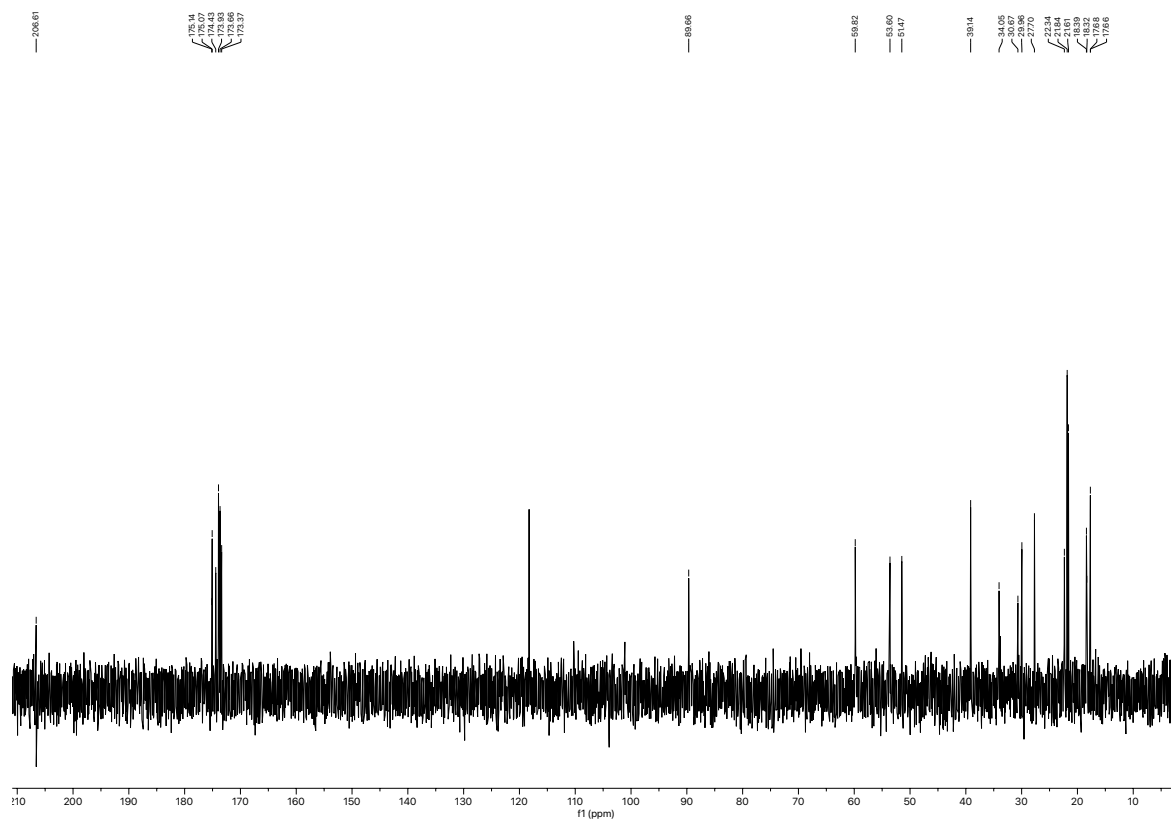
Figure 2.183. ^{13}C NMR spectrum (75 MHz, D_2O) of compound **2.086**.

solvent residual signal
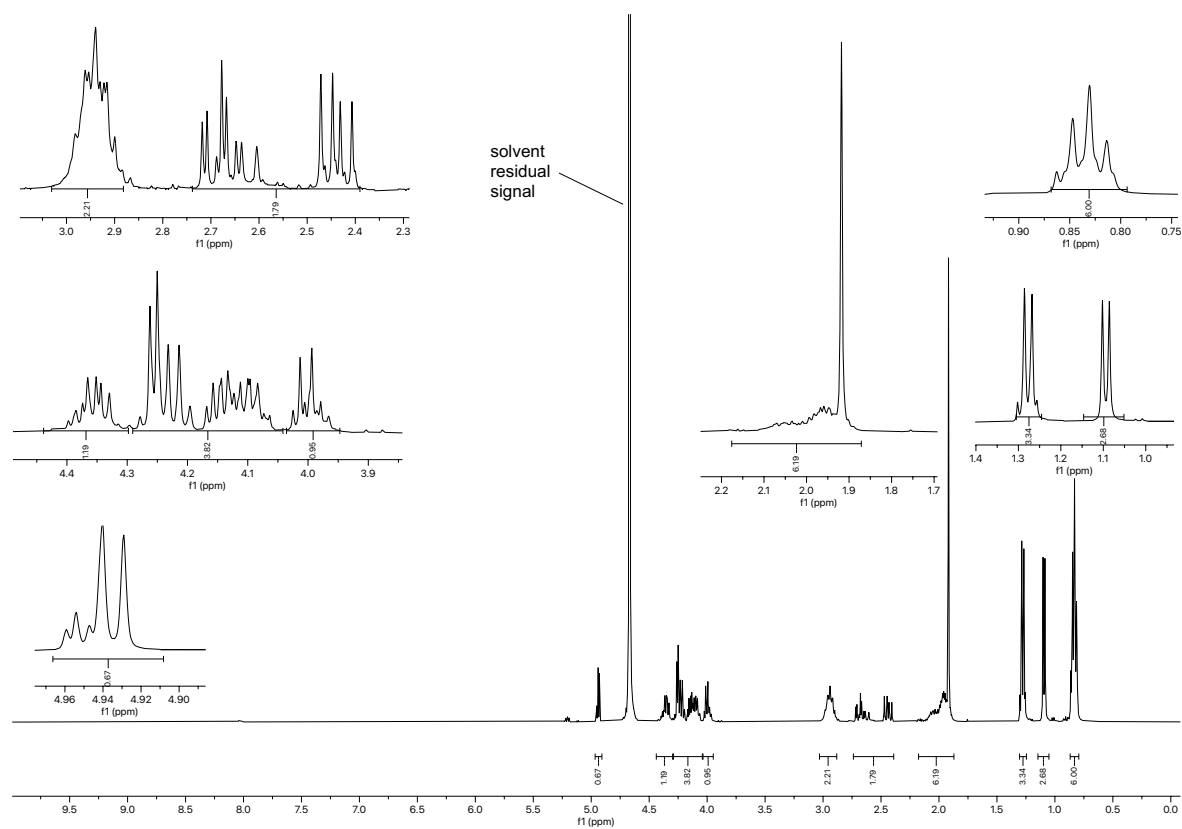
Figure 2.184. ^1H NMR spectrum (400 MHz, D_2O) of compound **2.087**.

254
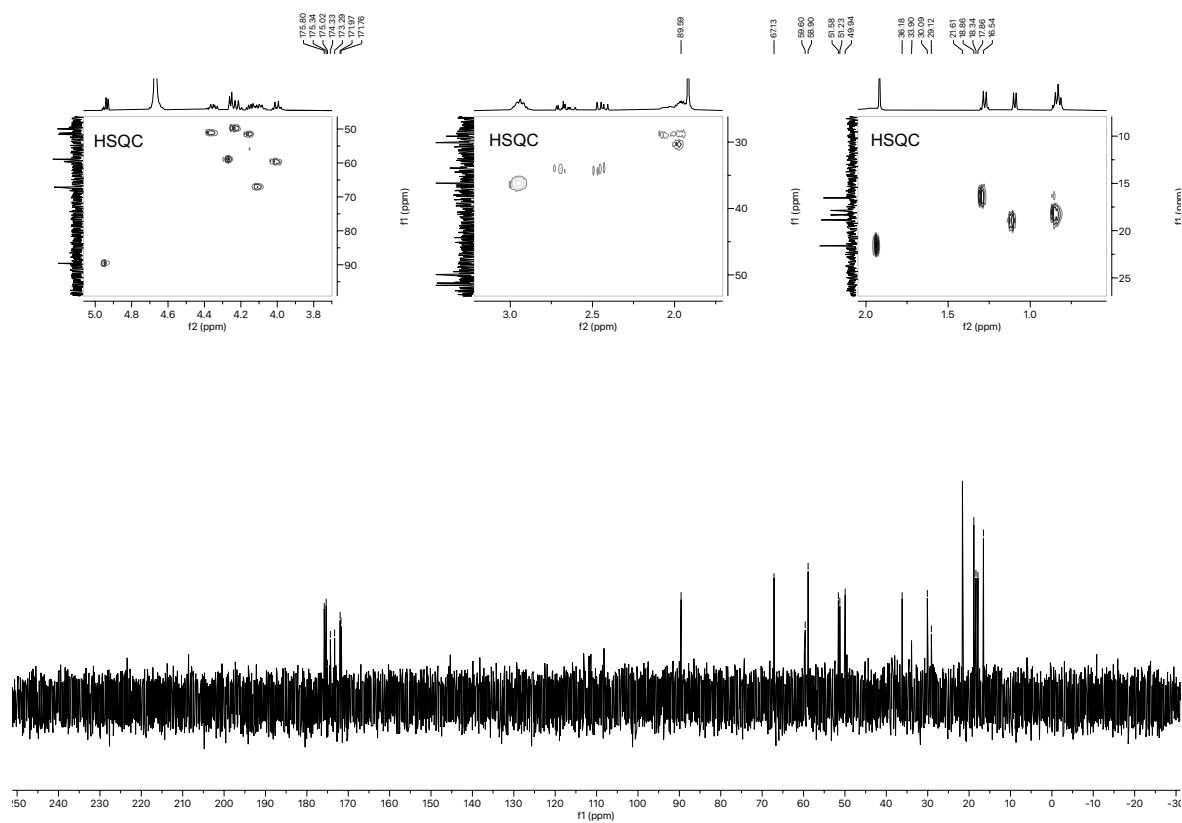
Figure 2.185. ^{13}CNMR spectrum (101 MHz, D$_2$O) of compound **2.087**.
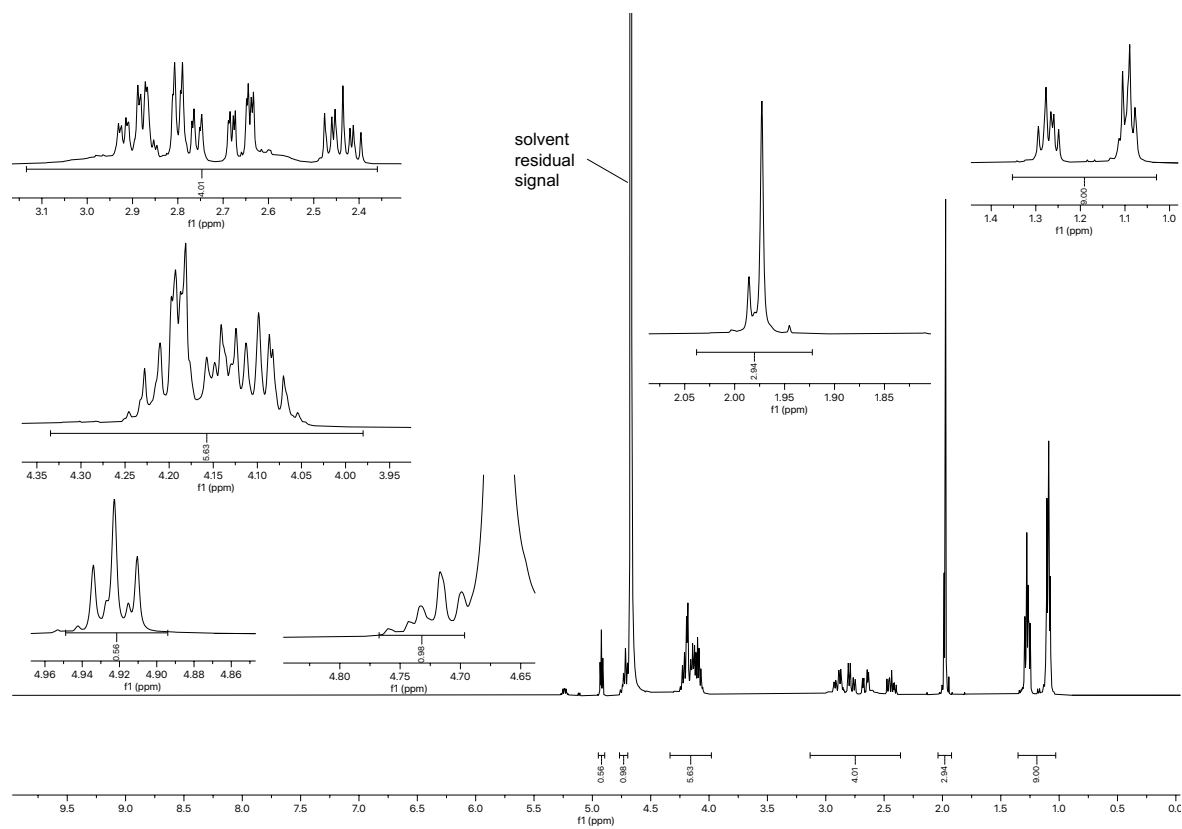
Figure 2.186. ^{1}H NMR spectrum (400 MHz, D$_2$O) of compound **2.088**.
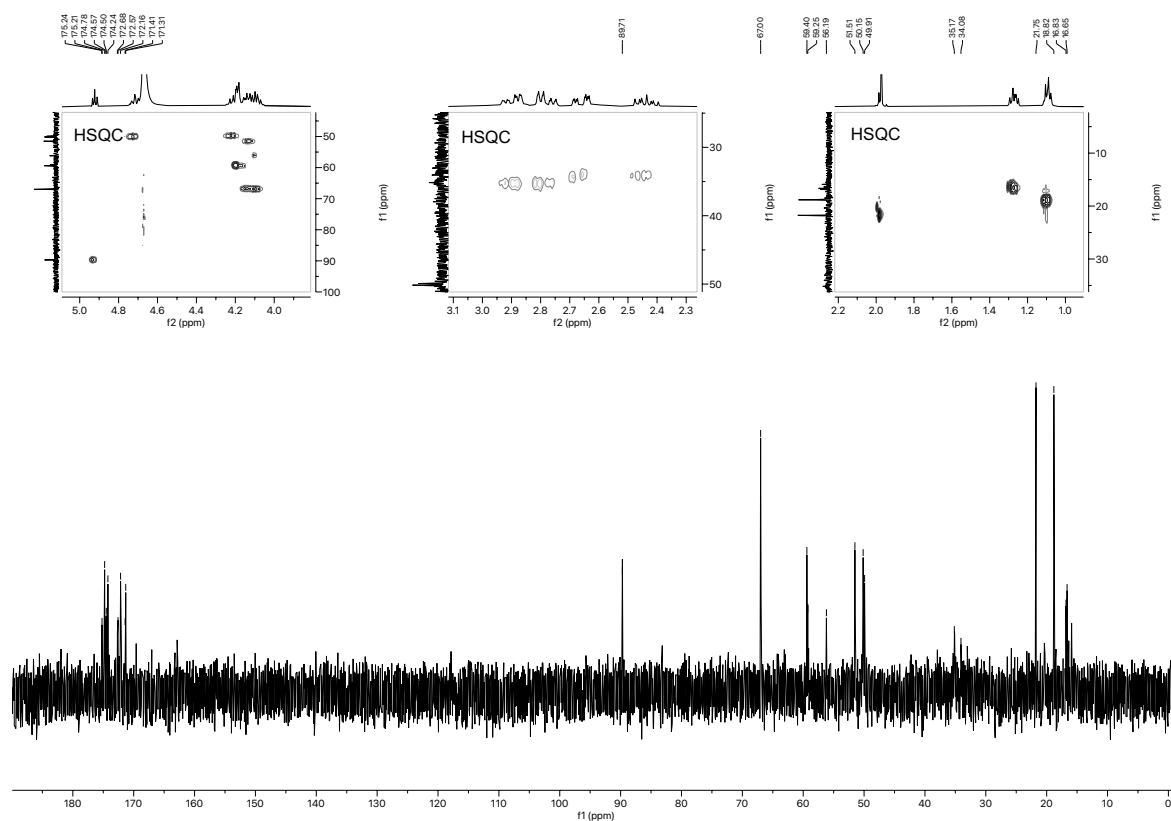
Figure 2.187. ^{13}C NMR spectrum (101 MHz, DMSO-d[6]) of compound **2.088**.
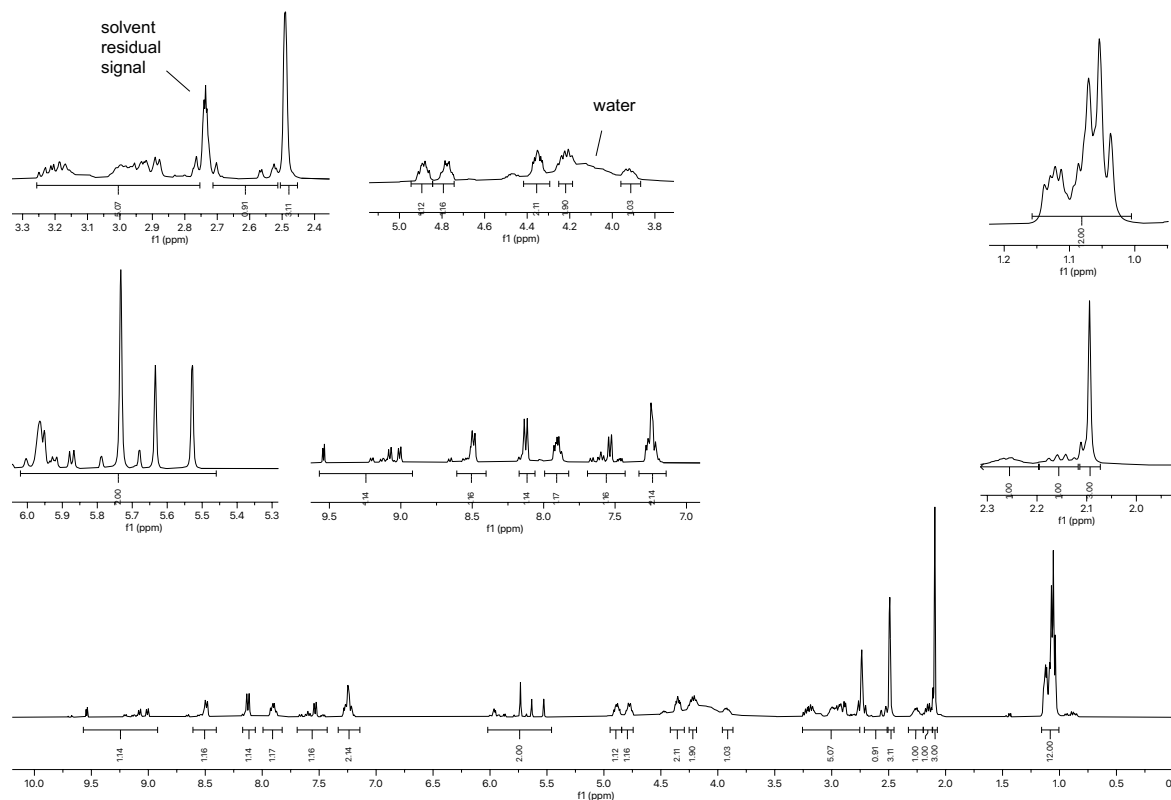
Figure 2.188. ^{1}H NMR spectrum (400 MHz, DMSO-d[6]) of compound **2.093**.
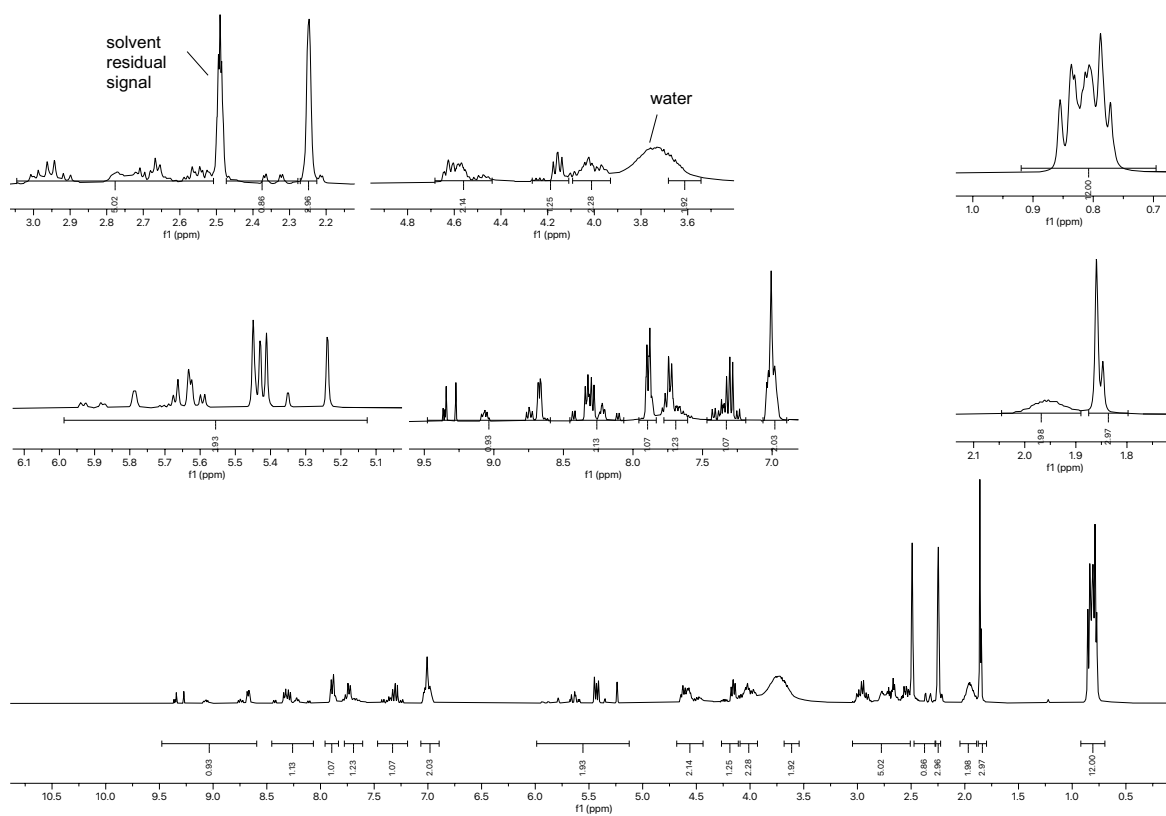
Figure 2.189. ^{1}H NMR spectrum (400 MHz, DMSO-d$_6$) of compound **2.094**.
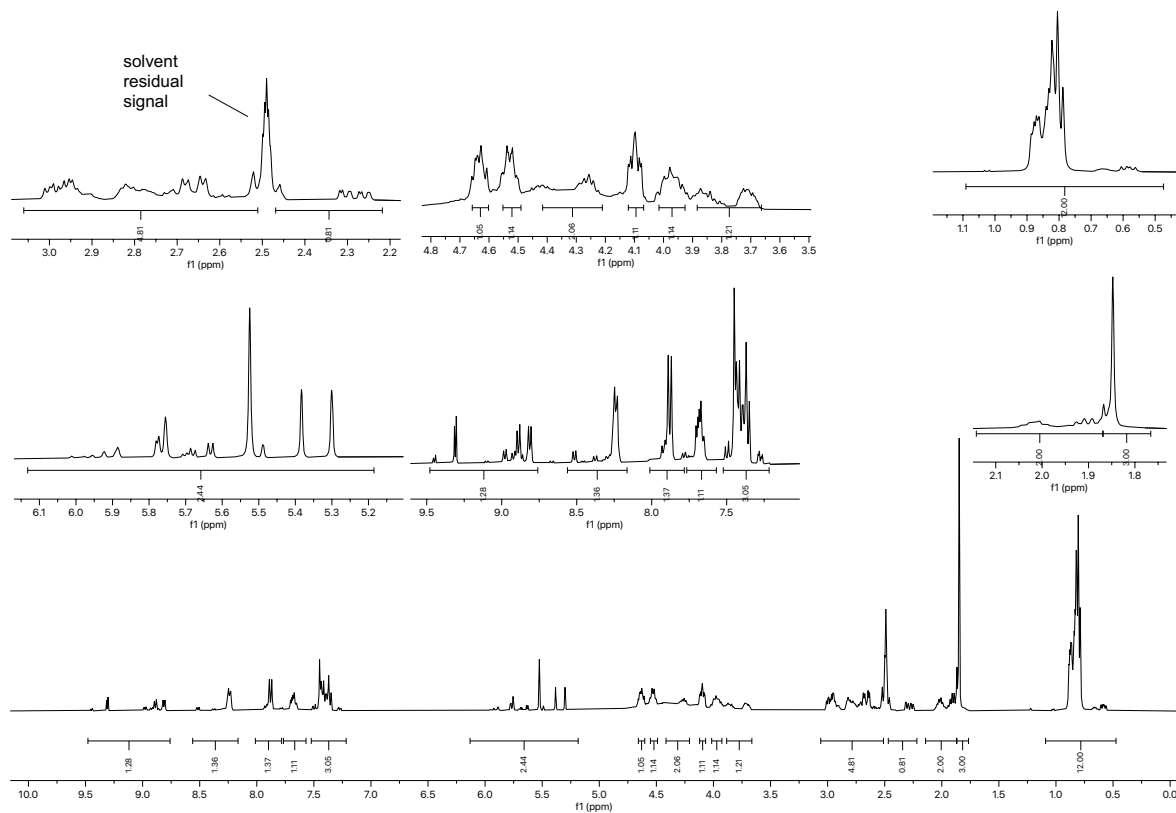
Figure 2.190. ^{1}H NMR spectrum (400 MHz, D$_2$O) of compound **2.095**.
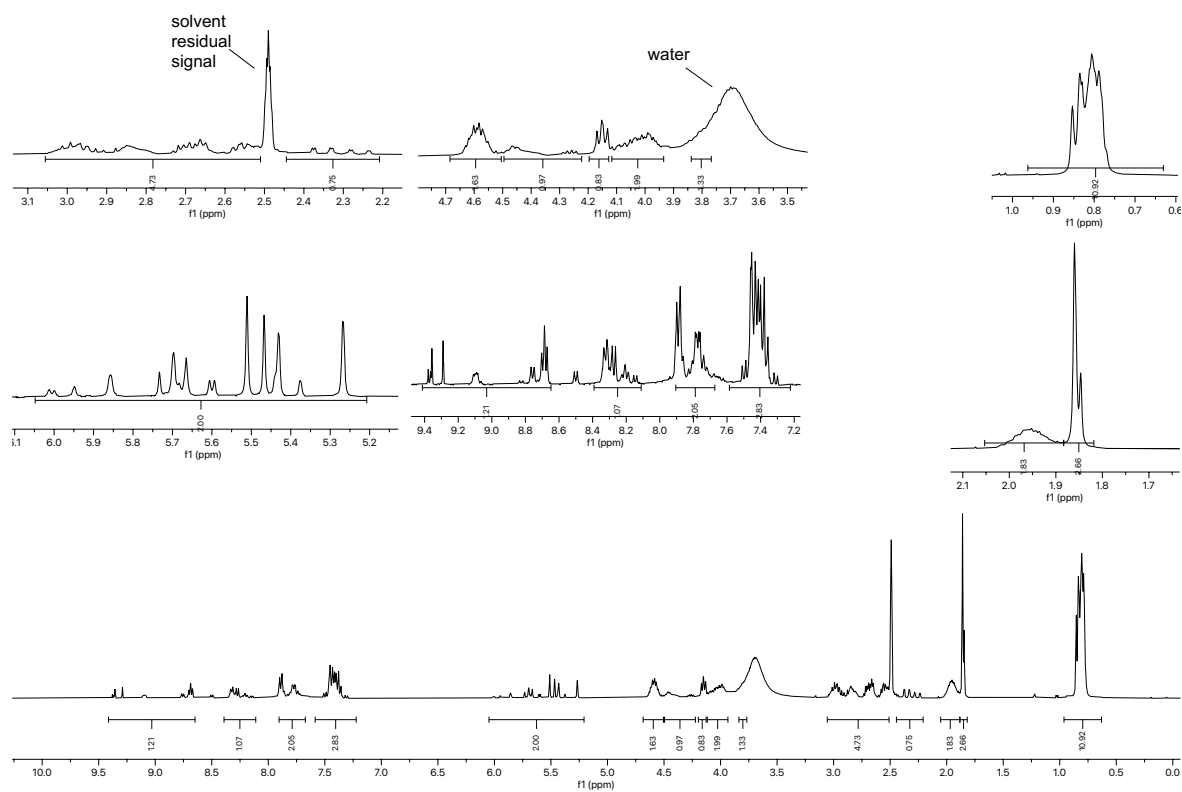
Figure 2.191. ^{1}H NMR spectrum (400 MHz, DMSO-d$_6$) of compound **2.096**.
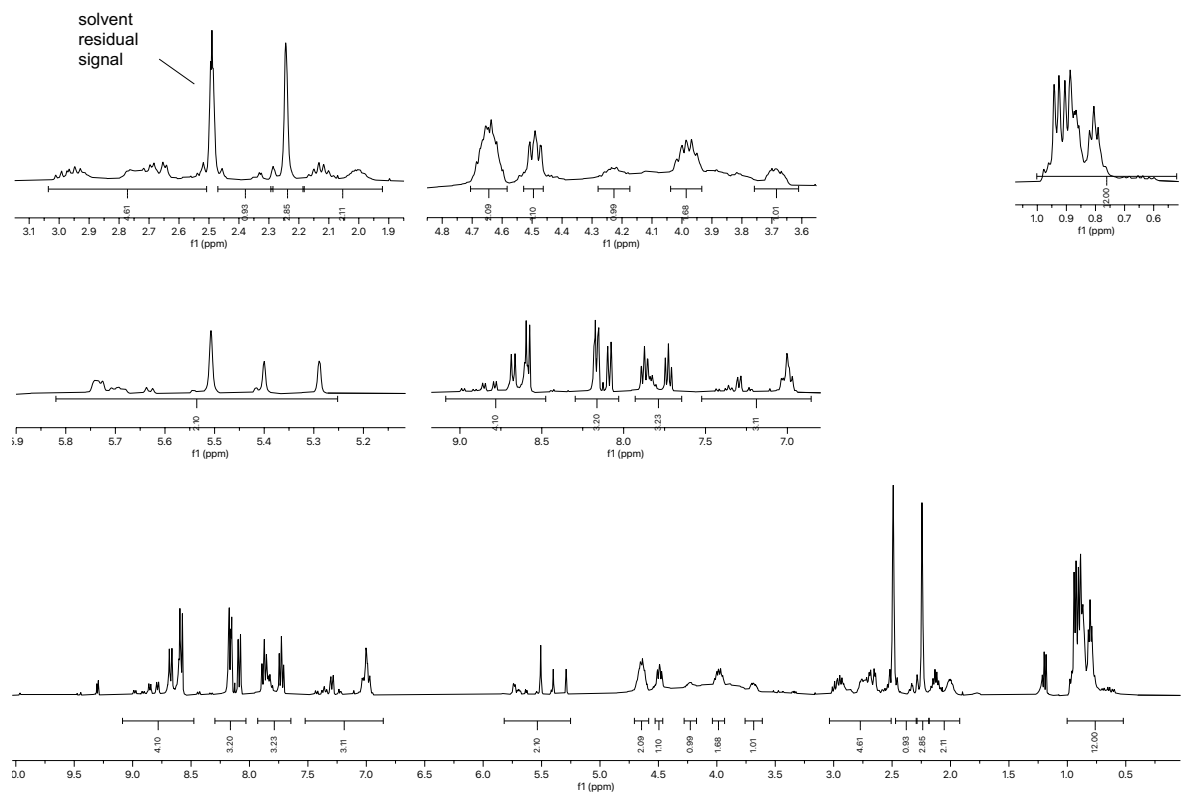
Figure 2.192. ^{1}H NMR spectrum (400 MHz, DMSO-d$_6$) of compound **2.097**.
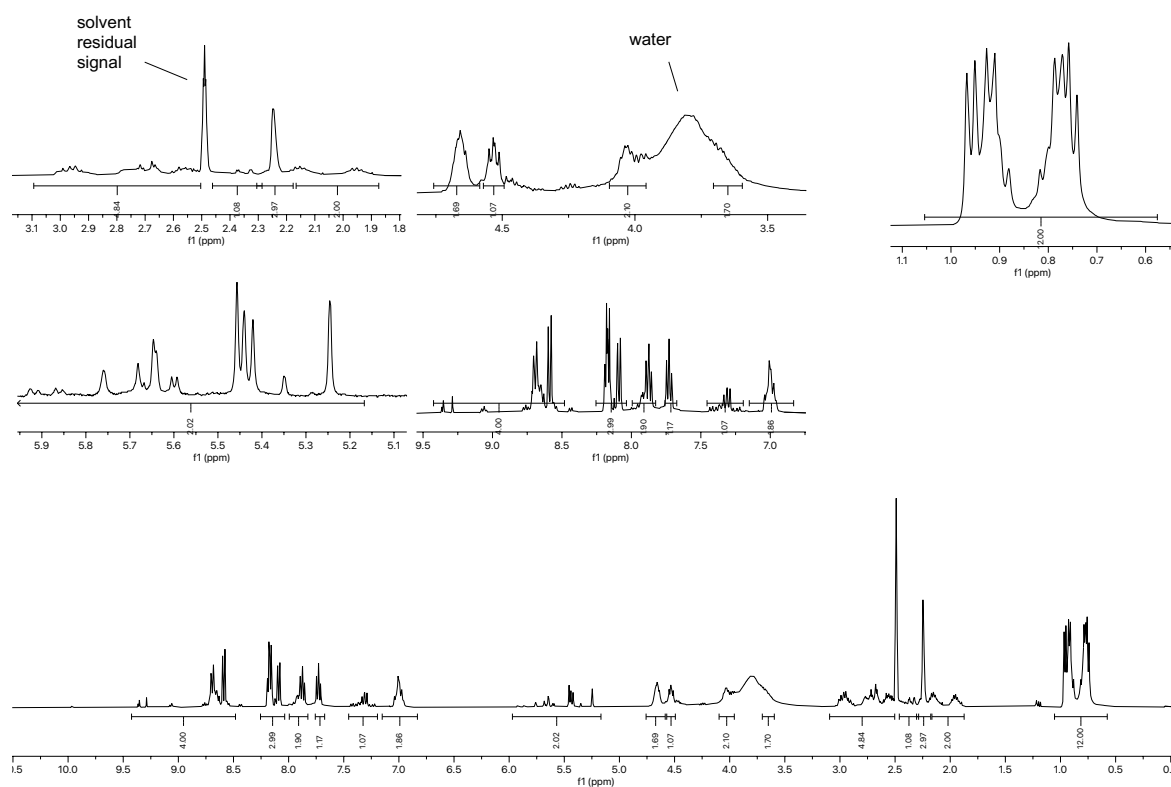
Figure 2.193. ^{1}H NMR spectrum (400 MHz, DMSO-d$_6$) of compound **2.098**.
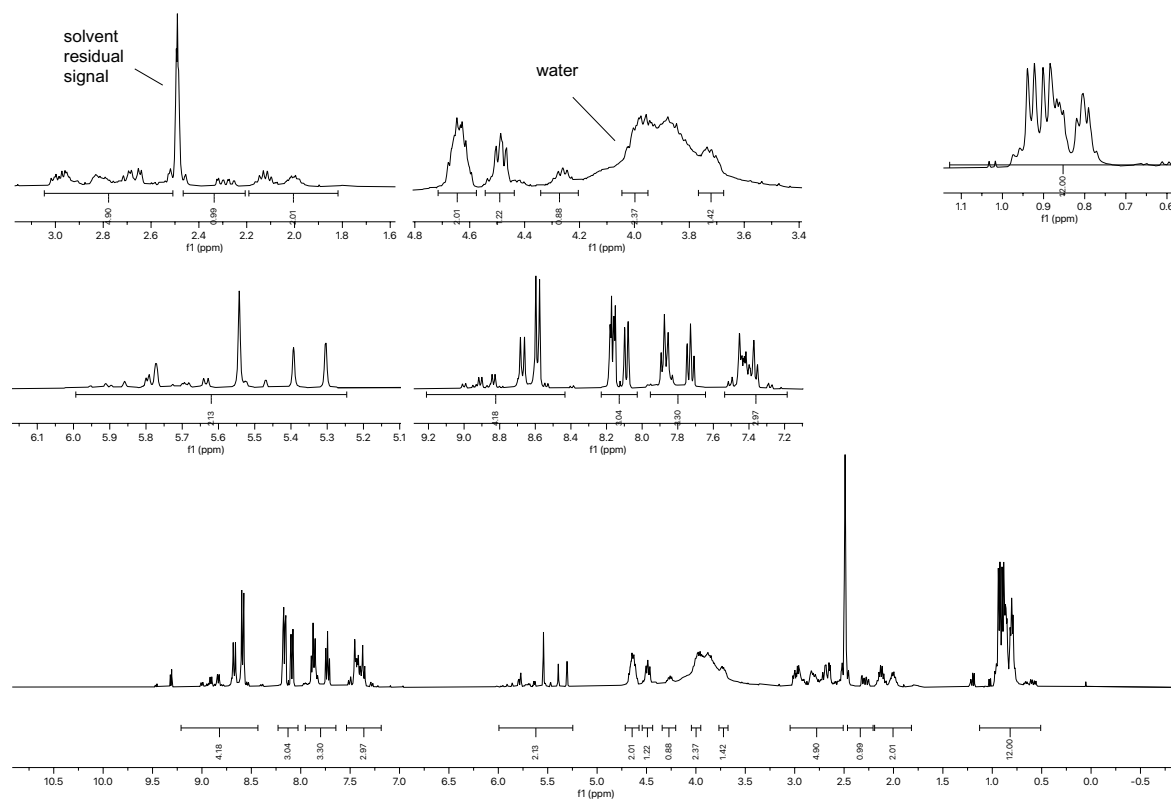
Figure 2.194. ^{1}H NMR spectrum (400 MHz, DMSO-d$_6$) of compound **2.099**.
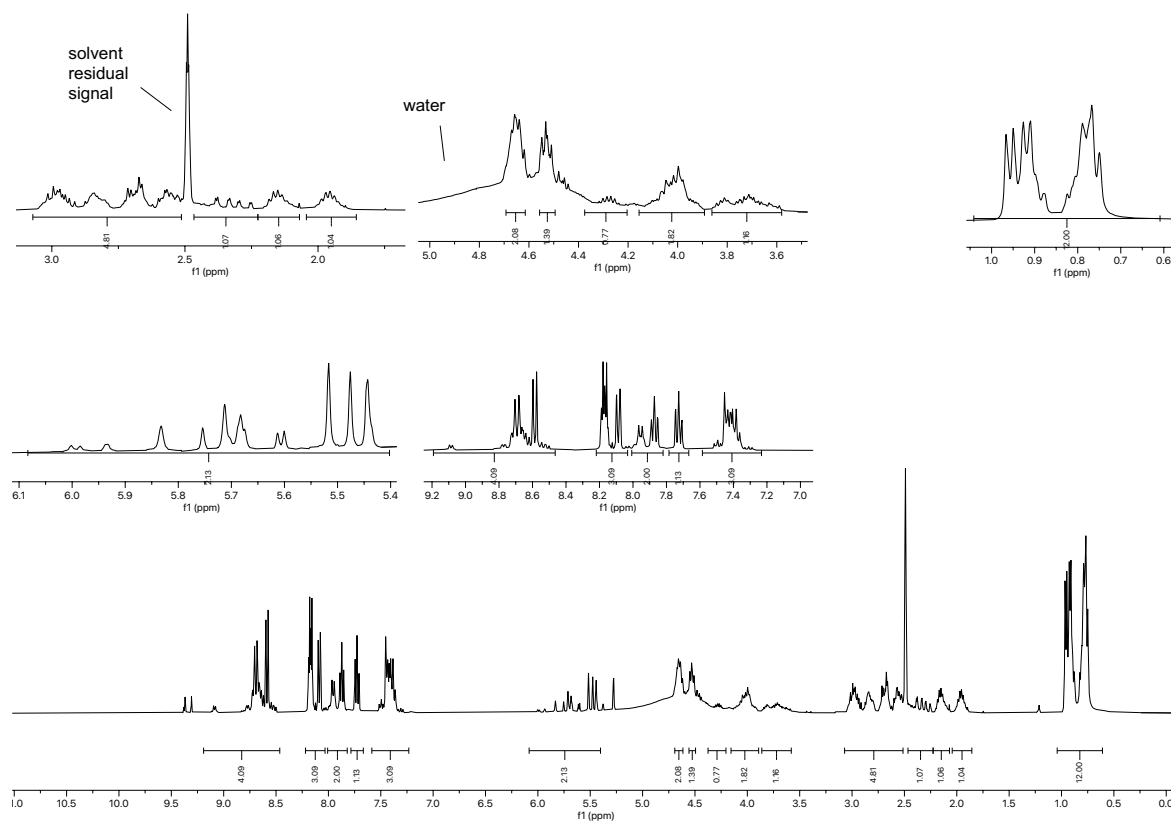
Figure 2.195. ^{1}H NMR spectrum (400 MHz, DMSO-d[6]) of compound **2.100**.
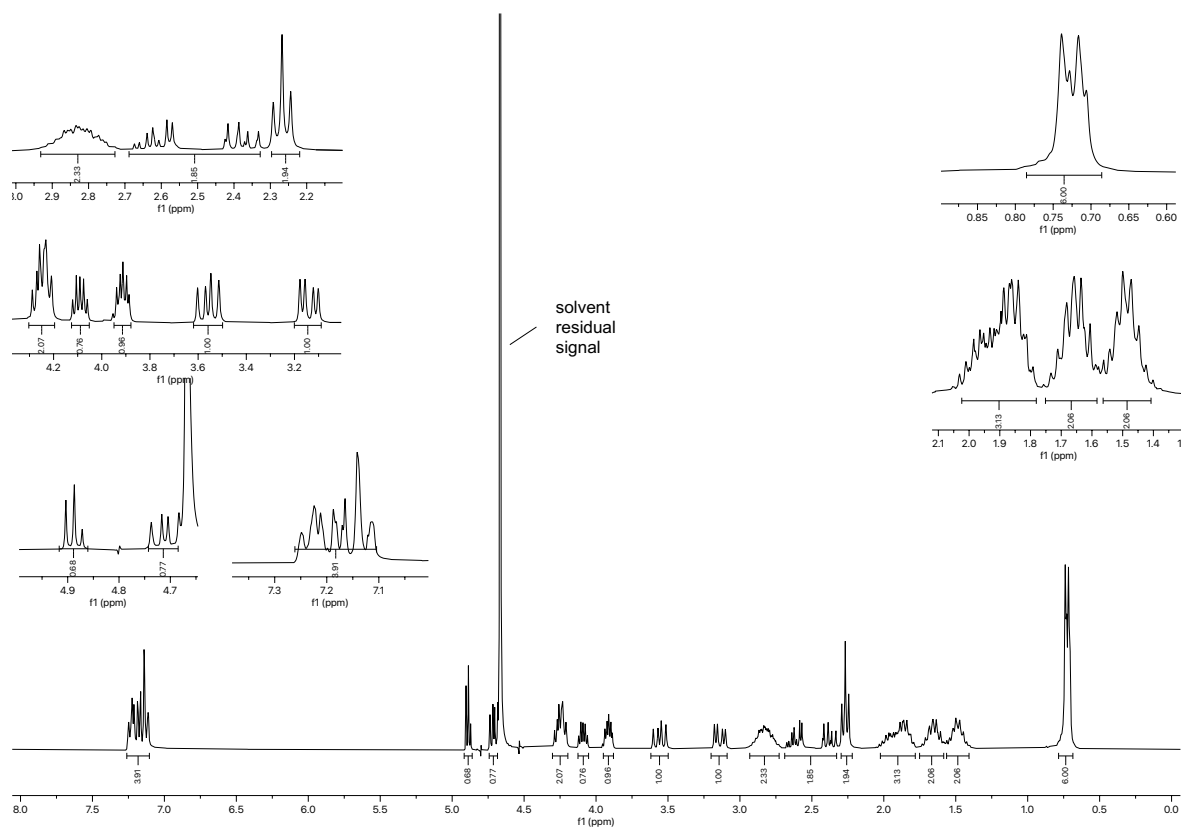
Figure 2.196. ^{1}HNMR spectrum (300 MHz, D[2]O) of compound **2.107**.
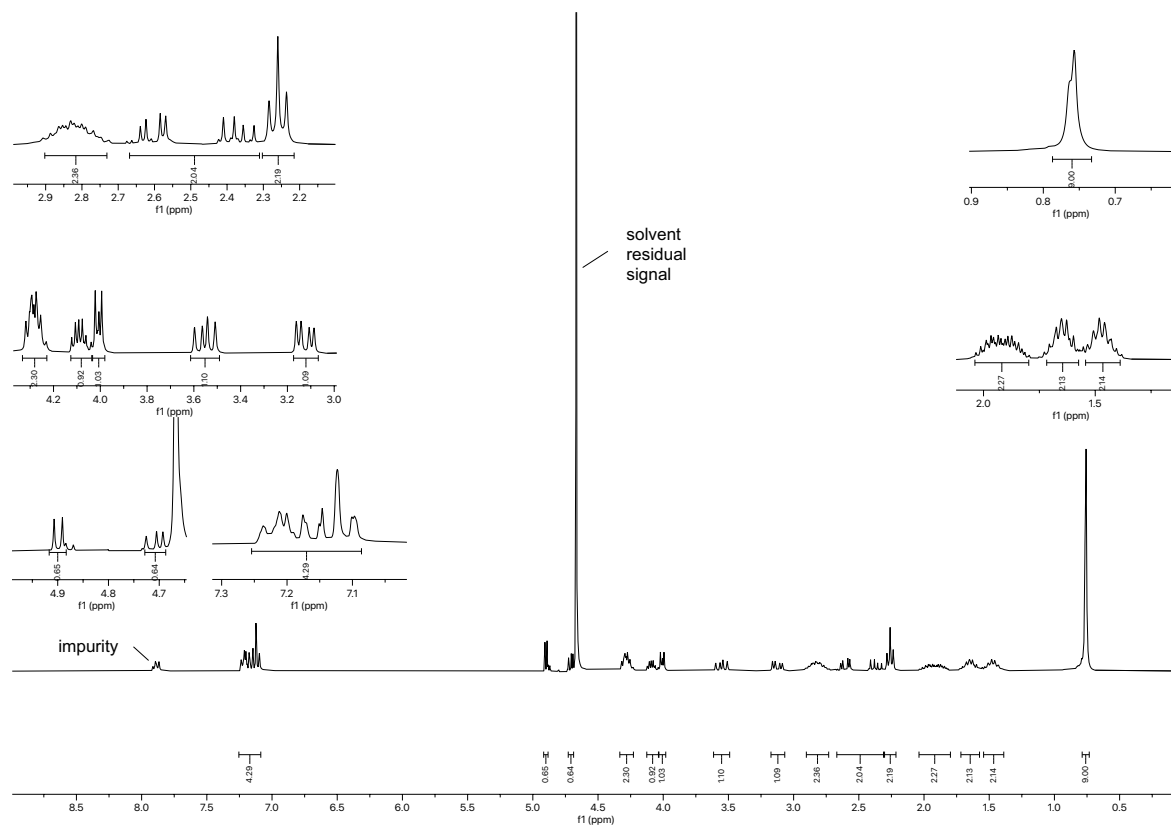
Figure 2.197. ^{1}H NMR spectrum (300 MHz, D$_2$O) of compound **2.108**.
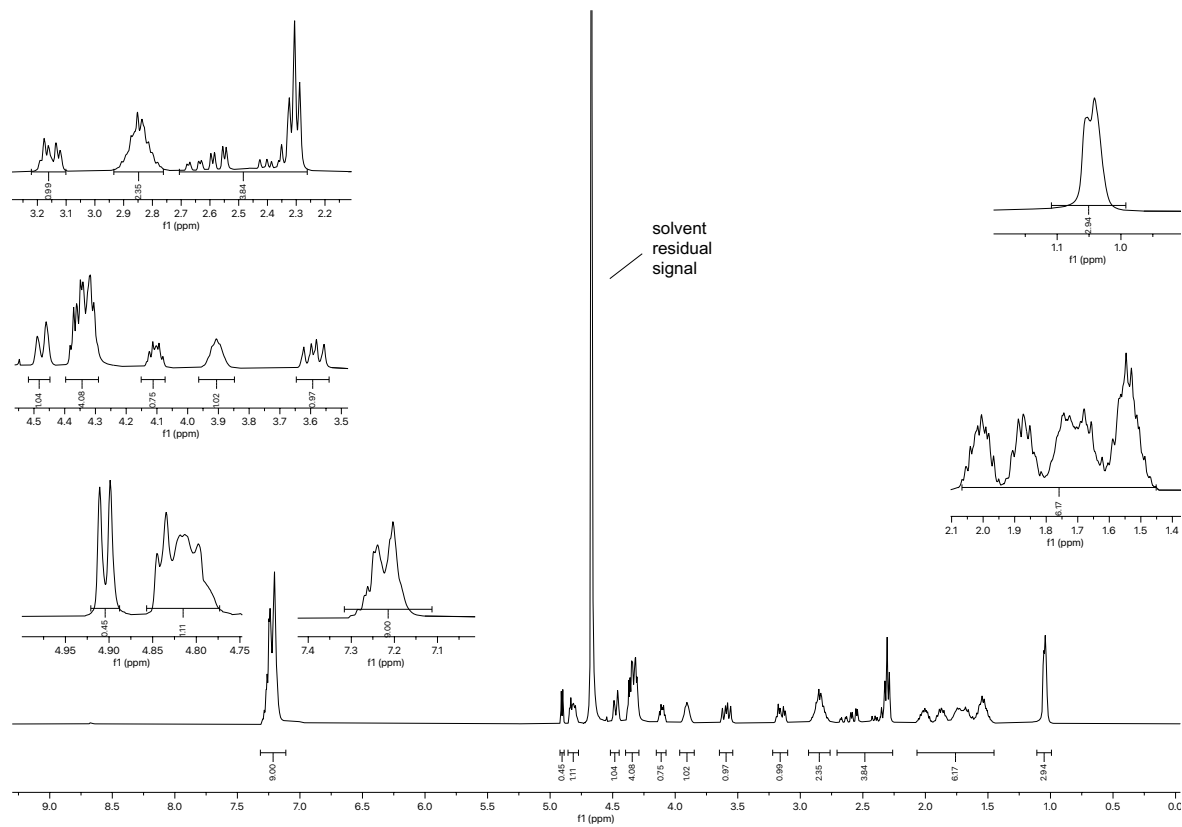
Figure 2.198. ^{1}H NMR spectrum (400 MHz, D$_2$O) of compound **2.109**.
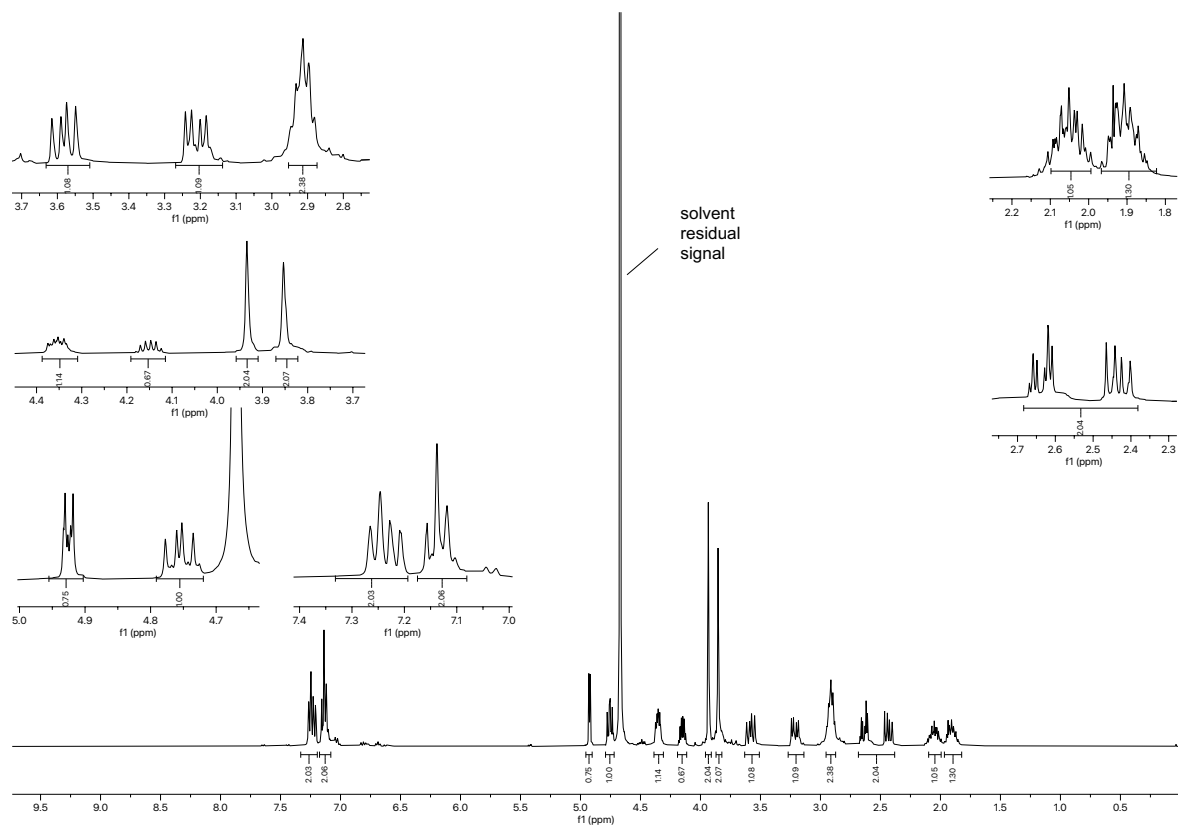
Figure 2.199. ^{1}H NMR spectrum (400 MHz, D_2O) of compound **2.110**.
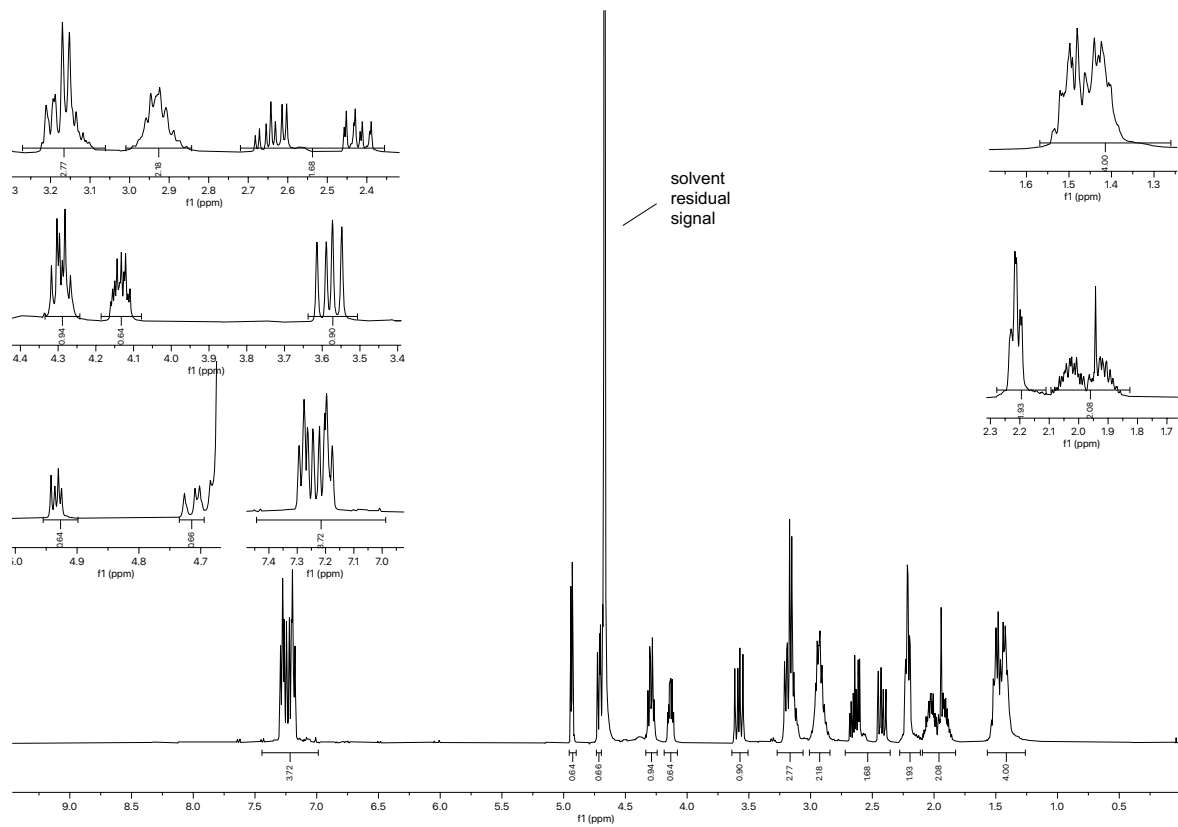
Figure 2.200. ^{1}H NMR spectrum (400 MHz, D_2O) of compound **2.111**.
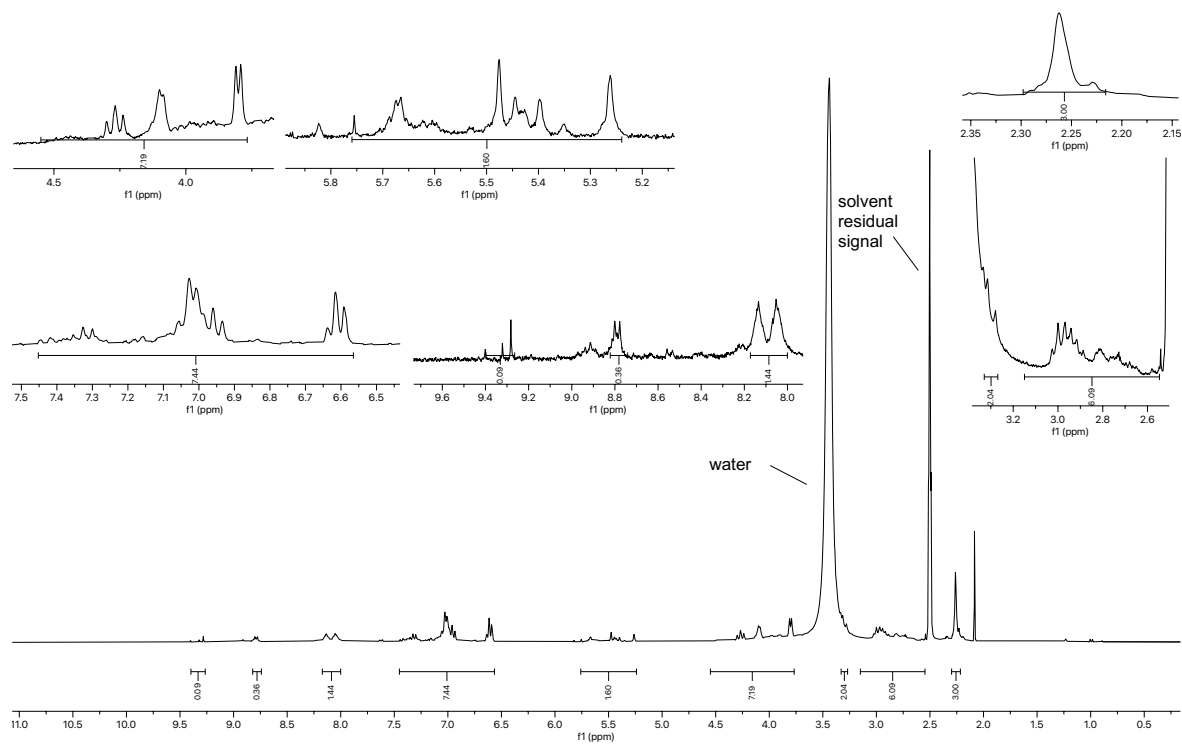
Figure 2.201. ^{1}H NMR spectrum (300 MHz, DMSO-d$_6$) of compound **2.112**.
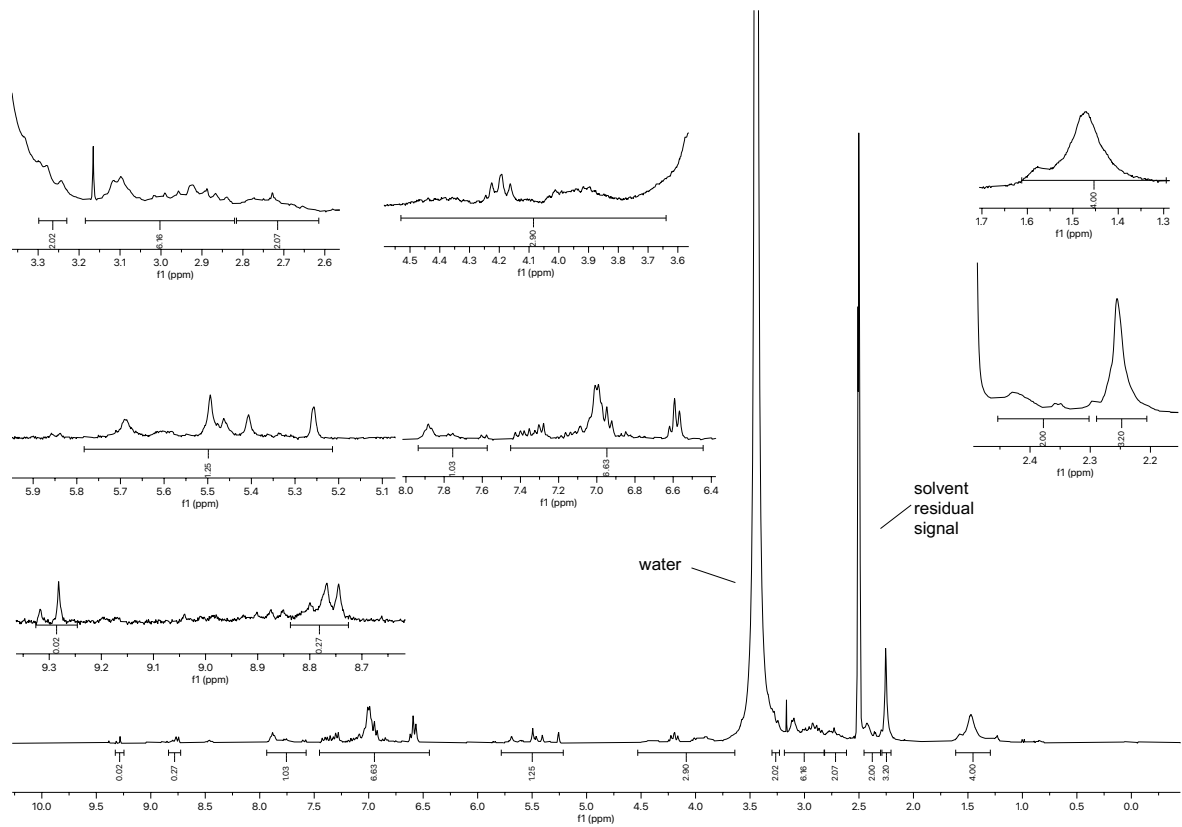
Figure 2.202. ^{1}H NMR spectrum (300 MHz, DMSO-d$_6$) of compound **2.113**.
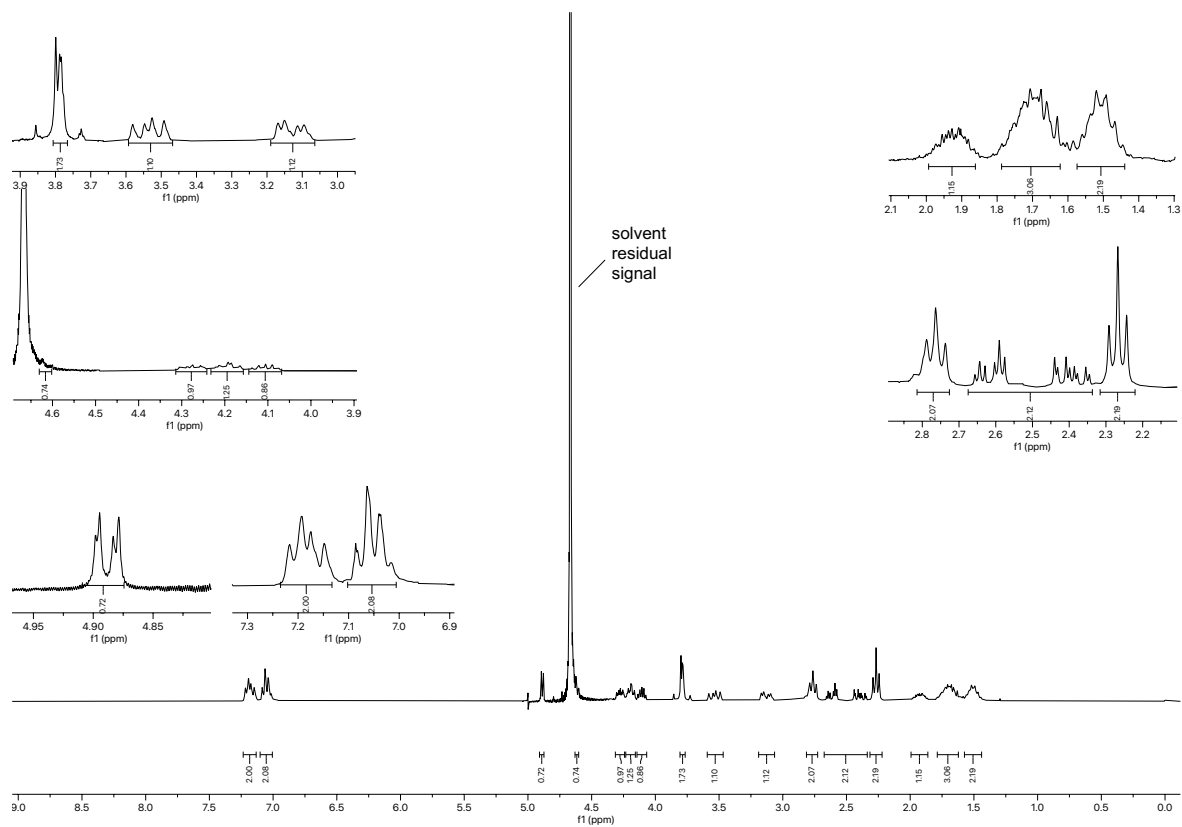
Figure 2.203. ^{1}H NMR spectrum (300 MHz, D$_2$O) of compound **2.114**.
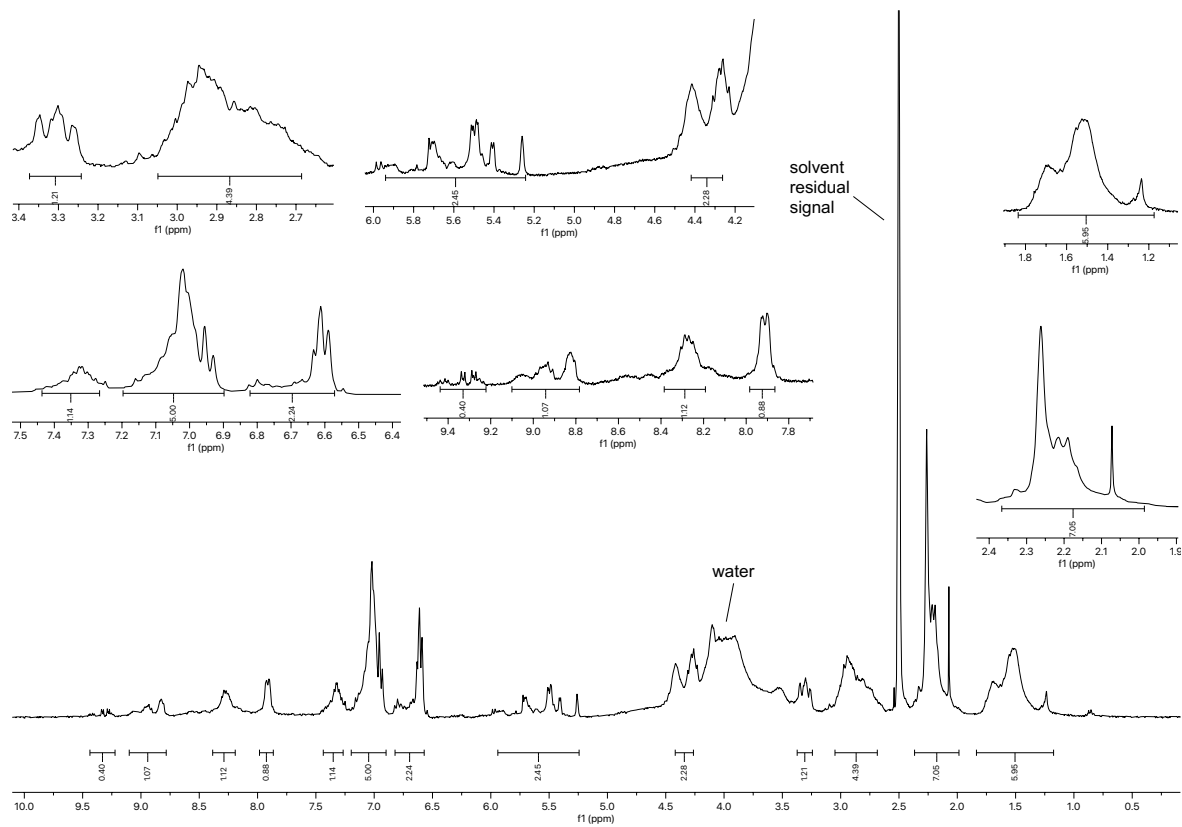
Figure 2.204. ^{1}H NMR spectrum (300 MHz, DMSO-d$_6$) of compound **2.115**.
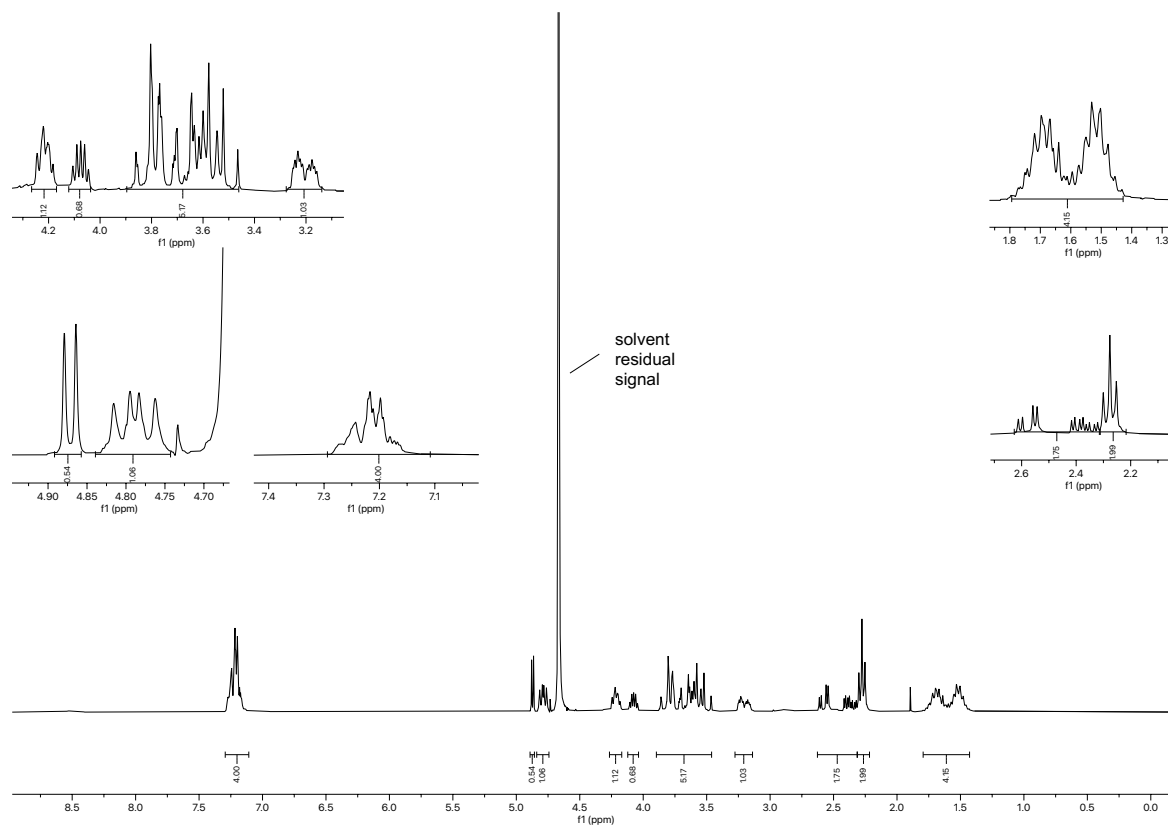
Figure 2.205. ^{1}H NMR spectrum (300 MHz, D$_2$O) of compound **2.116**.
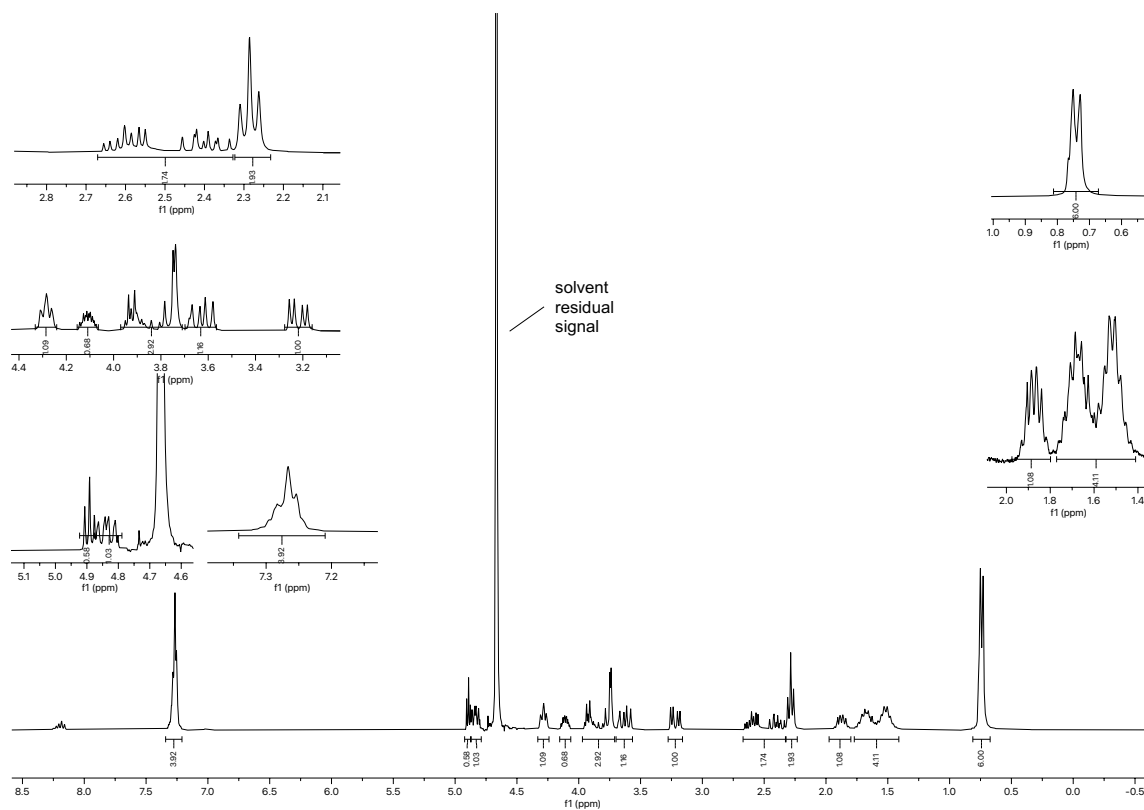
Figure 2.206. ^{1}H NMR spectrum (300 MHz, D$_2$O) of compound **2.117**.

265
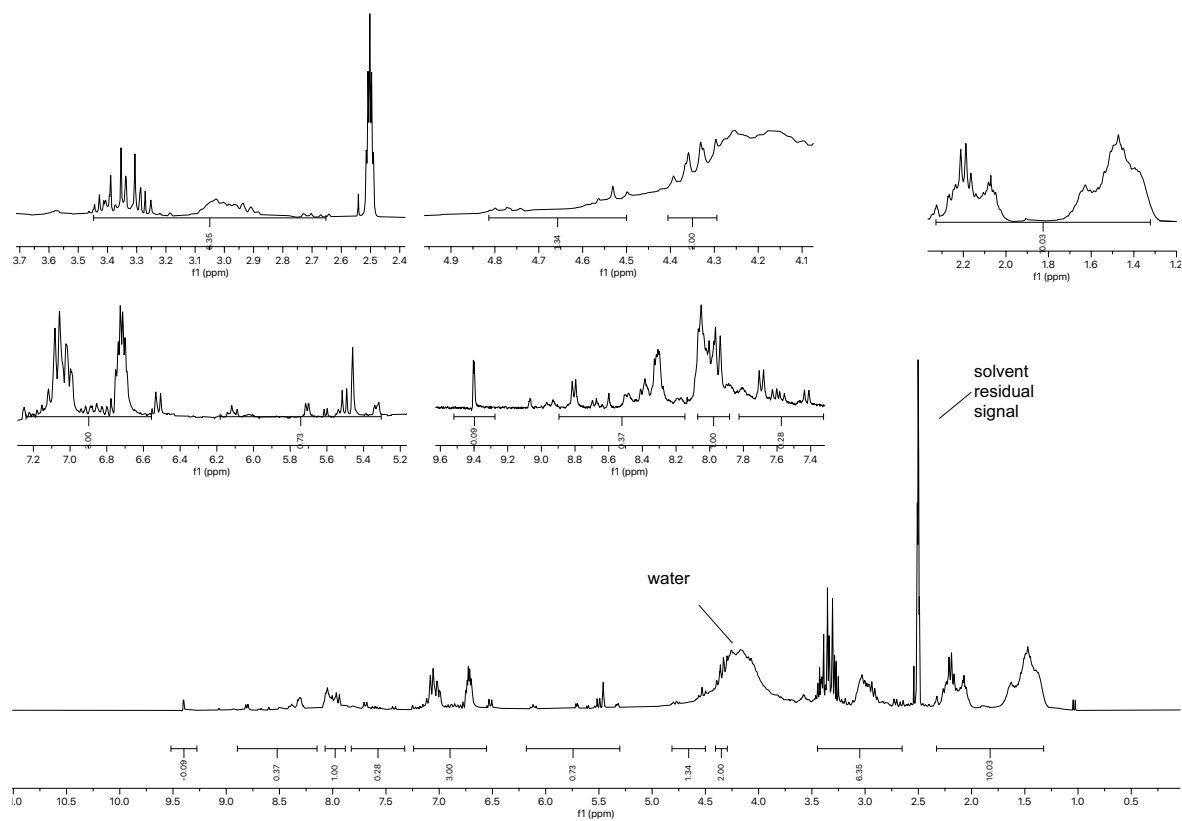
Figure 2.207. ^{1}H NMR spectrum (300 MHz, DMSO-d$_6$) of compound **2.118**.
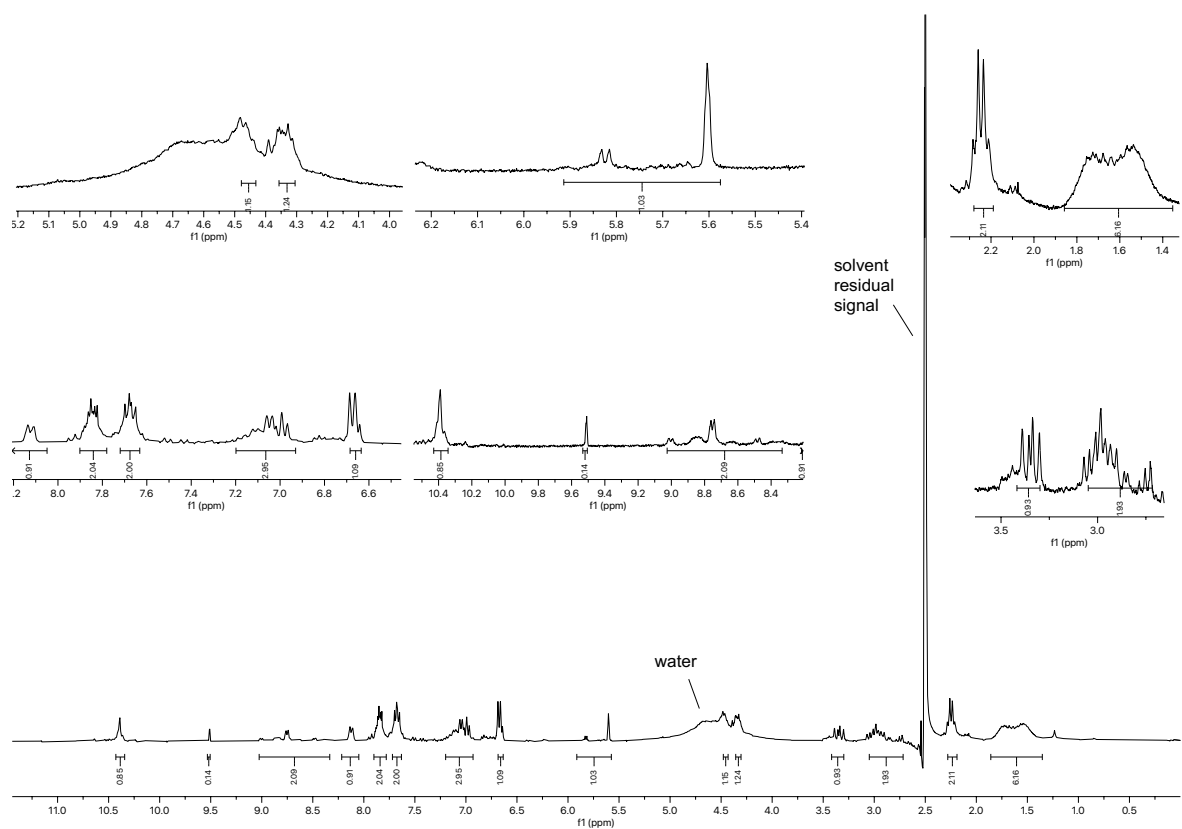
Figure 2.208. ^{1}H NMR spectrum (300 MHz, DMSO-d$_6$) of compound **2.119**.
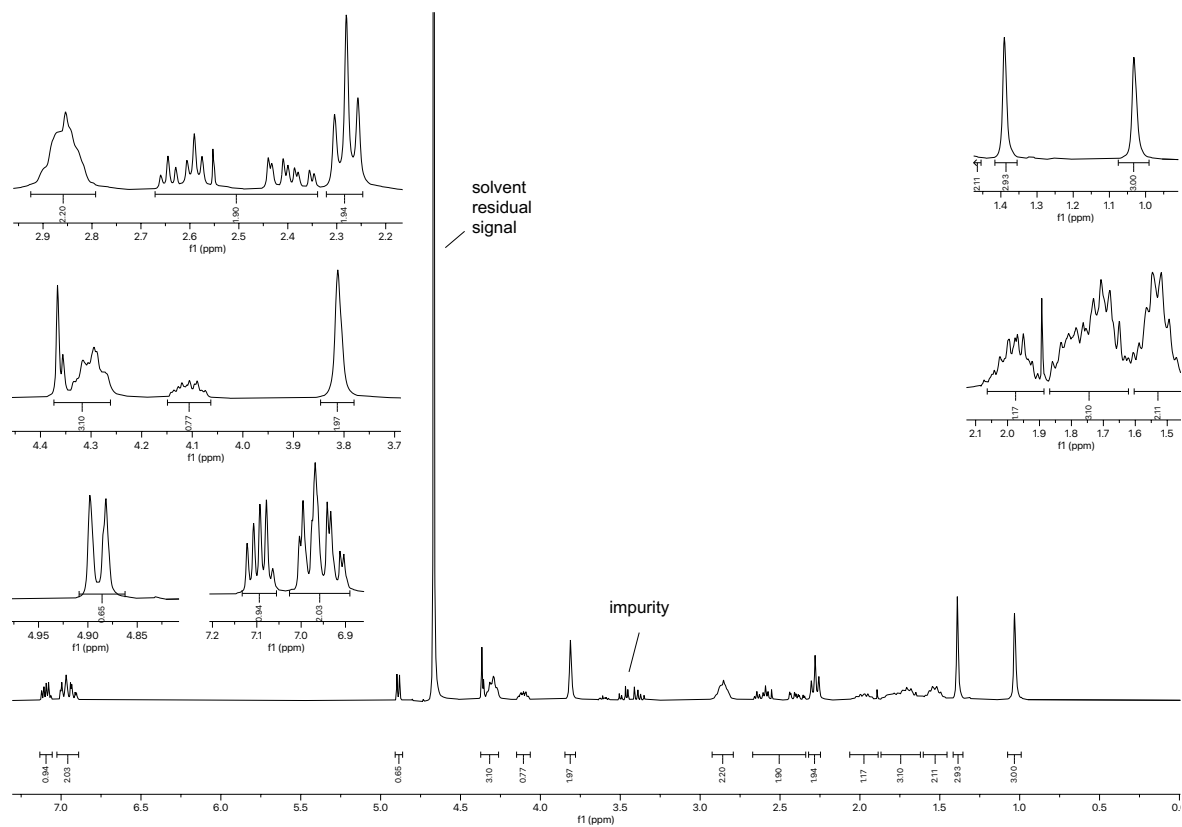
Figure 2.209. ^{1}H NMR spectrum (300 MHz, D_2O) of compound **2.120**.
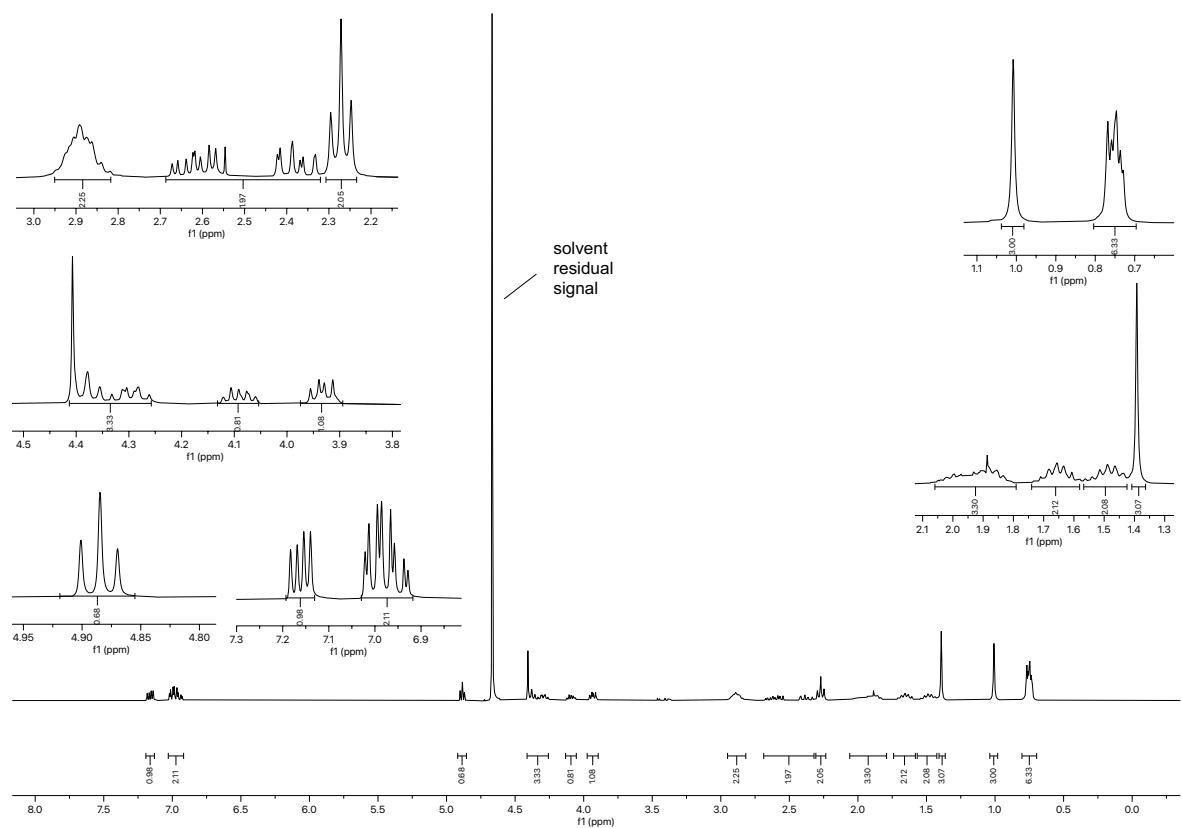
Figure 2.210. ^{1}H NMR spectrum (300 MHz, D_2O) of compound **2.121**.
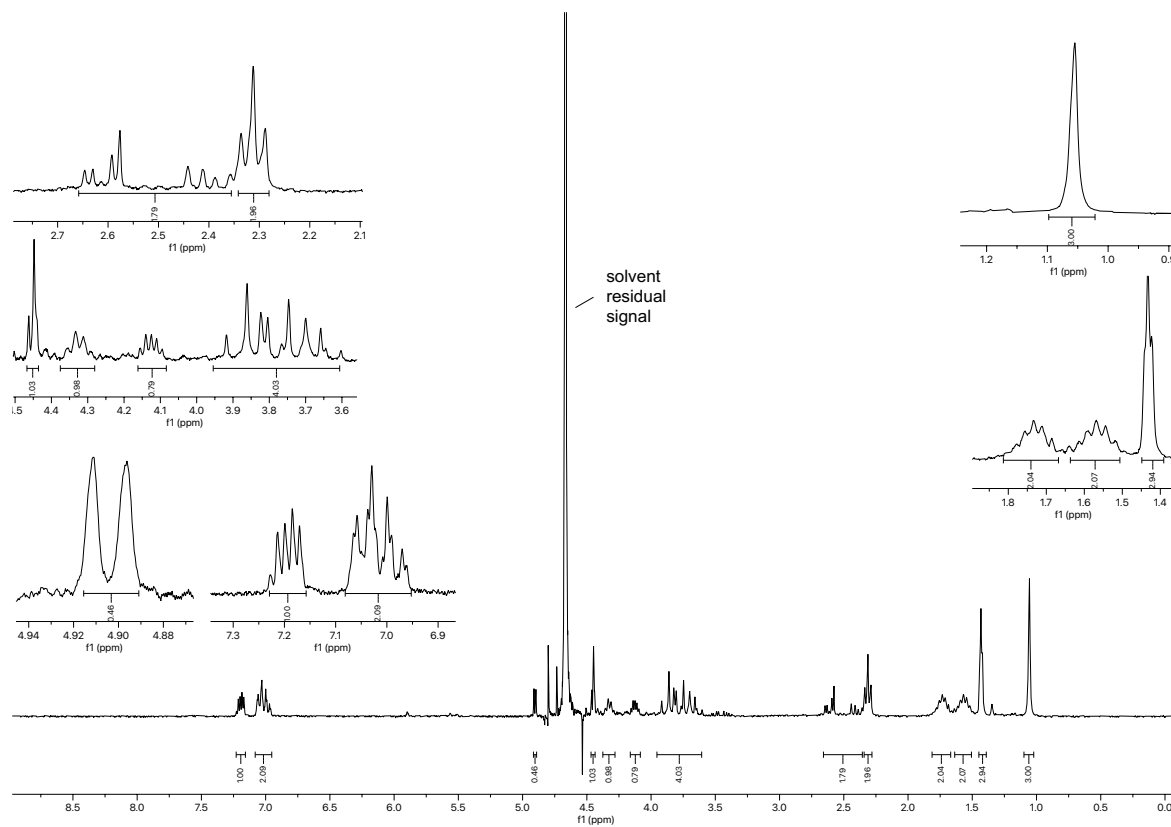
Figure 2.211. ^{1}H NMR spectrum (300 MHz, D$_2$O) of compound **2.122**.
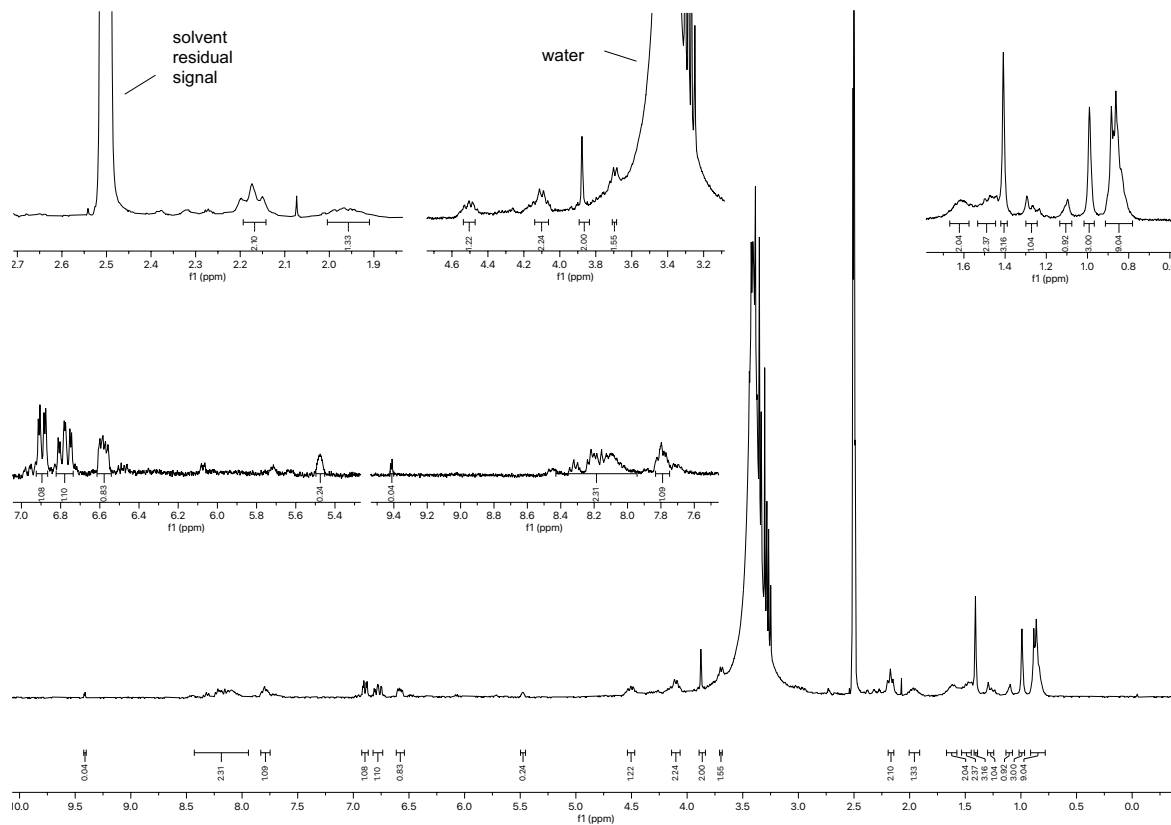
Figure 2.212. ^{1}H NMR spectrum (300 MHz, DMSO-d$_6$) of compound **2.123**.
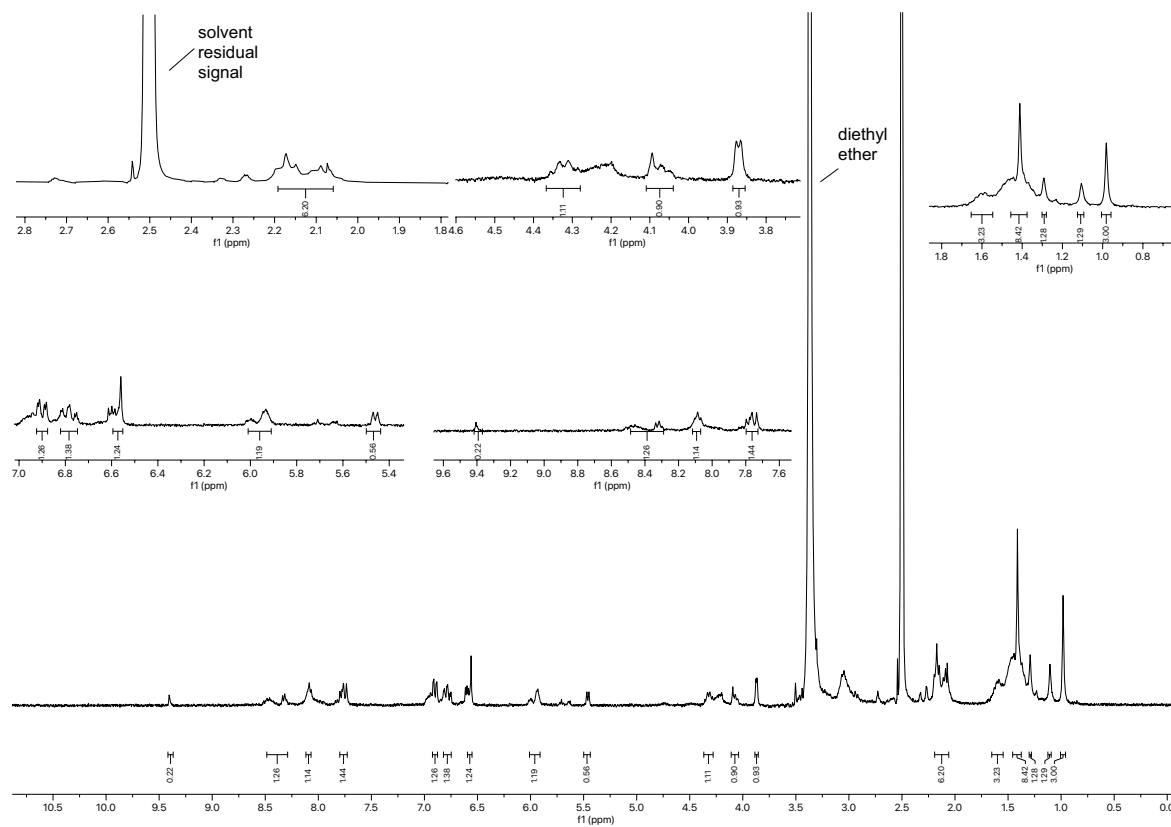
Figure 2.213. ^{1}H NMR spectrum (300 MHz, DMSO-d$_6$) of compound **2.124**.
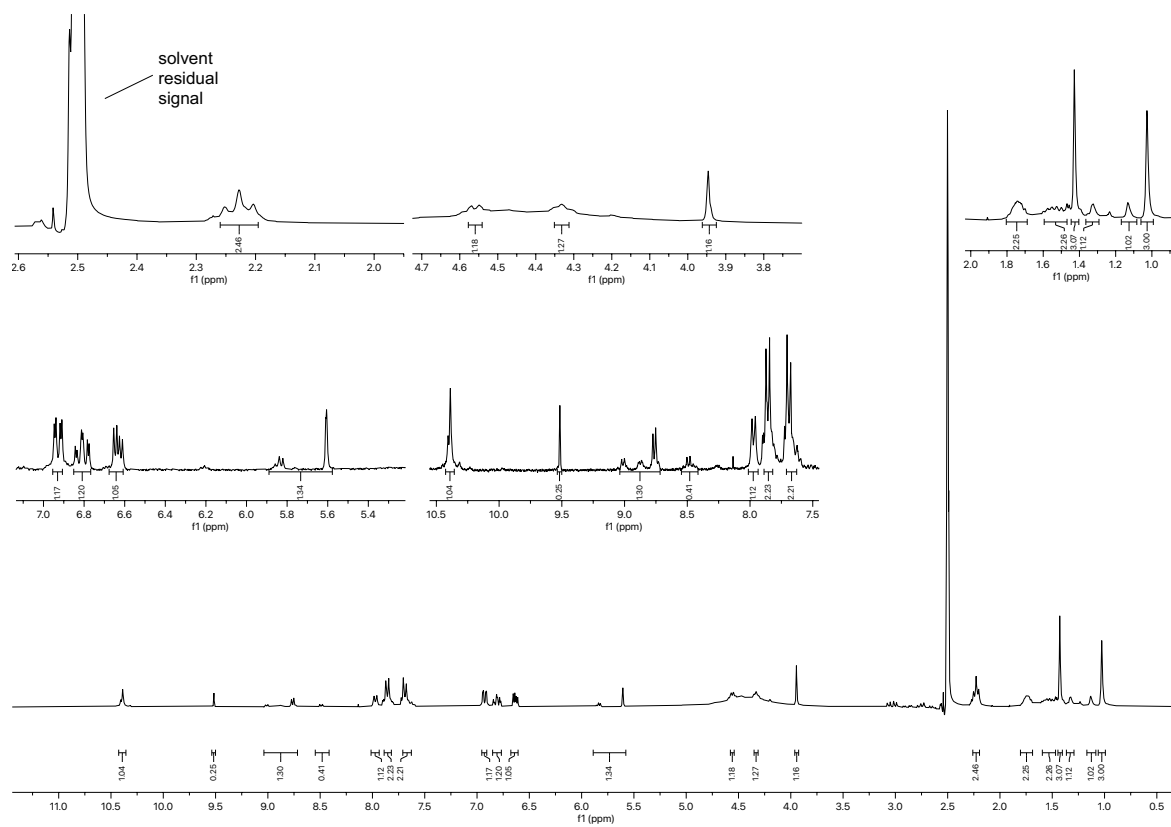
Figure 2.214. ^{1}H NMR spectrum (300 MHz, DMSO-d$_6$) of compound **2.125**.

2.7.2 RP-HPLC Chromatograms: Purity Control and Stability Control

2.7.2.1 Chemical Purity of Peptides 2.008-2.015, 2.017-2.100, and 2.107-2.126
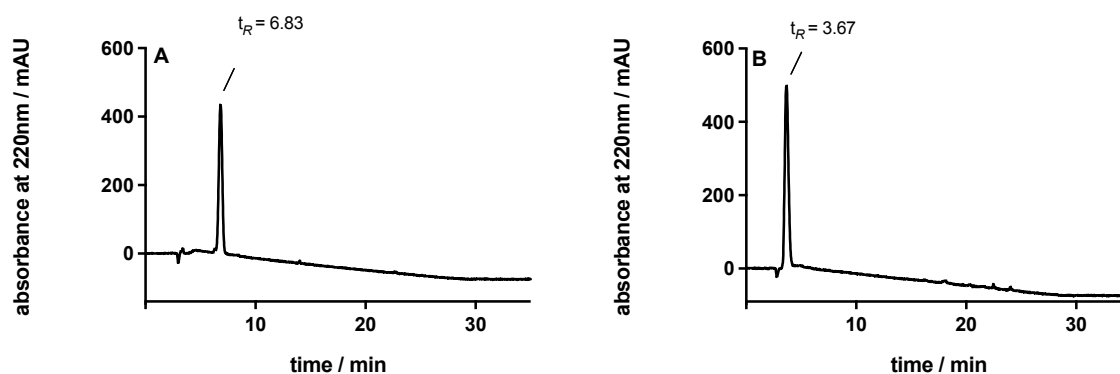
Figure 2.215 RP-HPLC analysis (purity control) of compound **2.008** (A) (99%, 220 nm) and compound **2.009** (B) (> 99%, 220 nm).
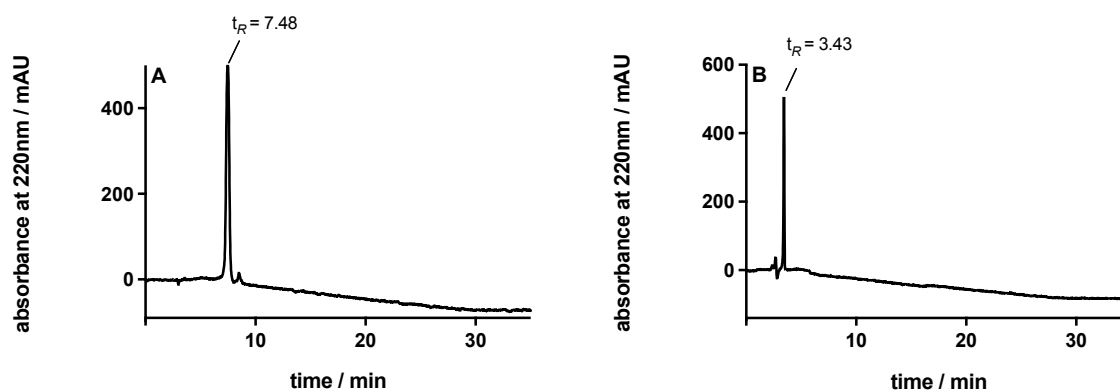
Figure 2.216. RP-HPLC analysis (purity control) of compound **2.010** (A) (98%, 220 nm) and compound **2.011** (B) (> 99%, 220 nm).
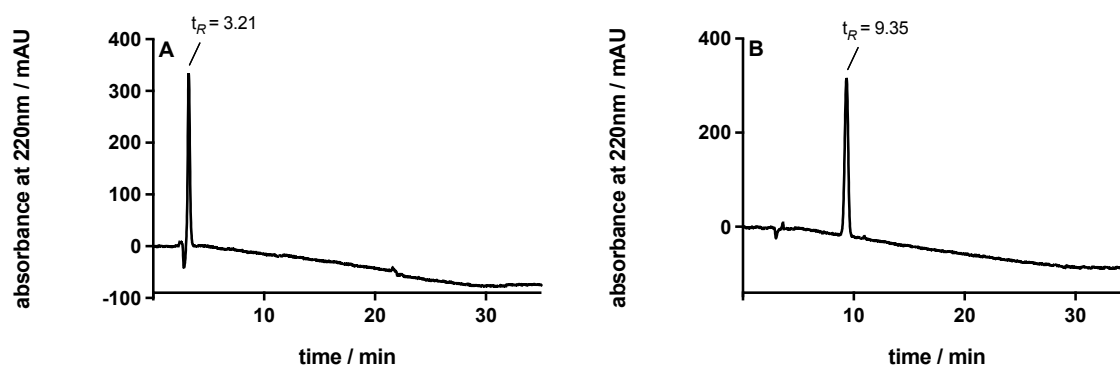
Figure 2.217. RP-HPLC analysis (purity control) of compound **2.012** (A) (> 99%, 220 nm) and compound **2.013** (B) (> 99%, 220 nm).
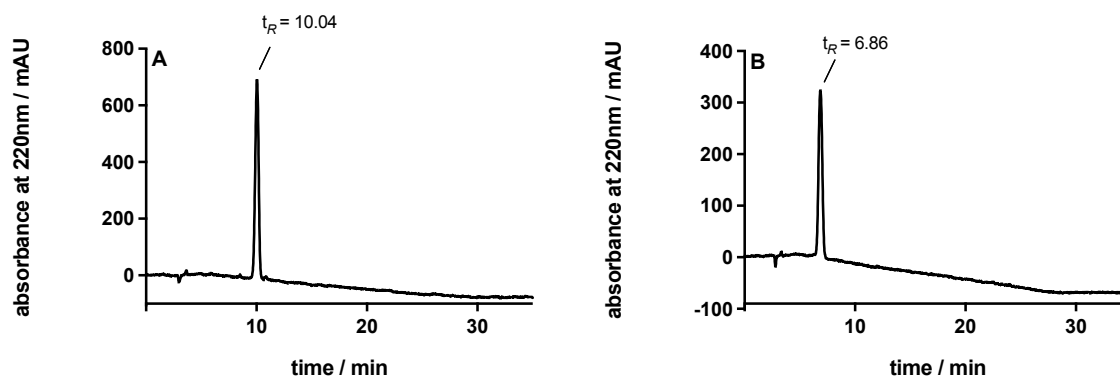
Figure 2.218. RP-HPLC analysis (purity control) of compound **2.014** (A) (> 99%, 220 nm) and compound **2.015** (B) (> 99%, 220 nm).
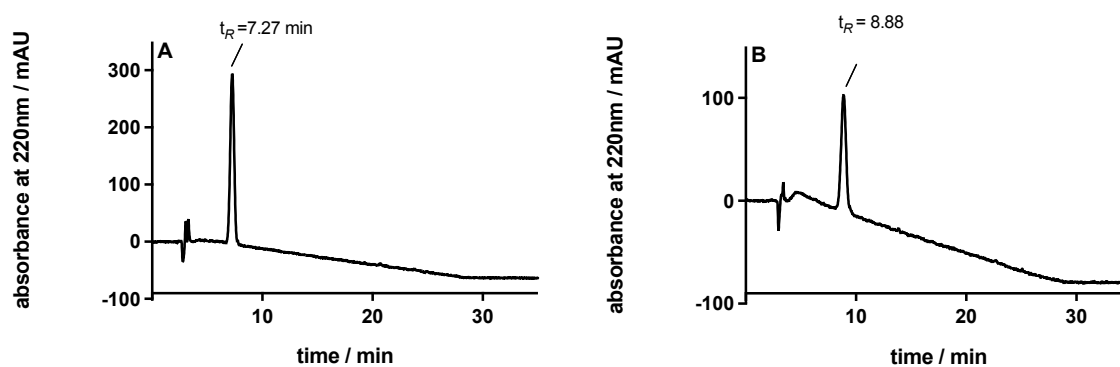
Figure 2.219. RP-HPLC analysis (purity control) of compound **2.017** (A) (97%, 220 nm) and compound **2.018** (B) (99%, 220 nm).
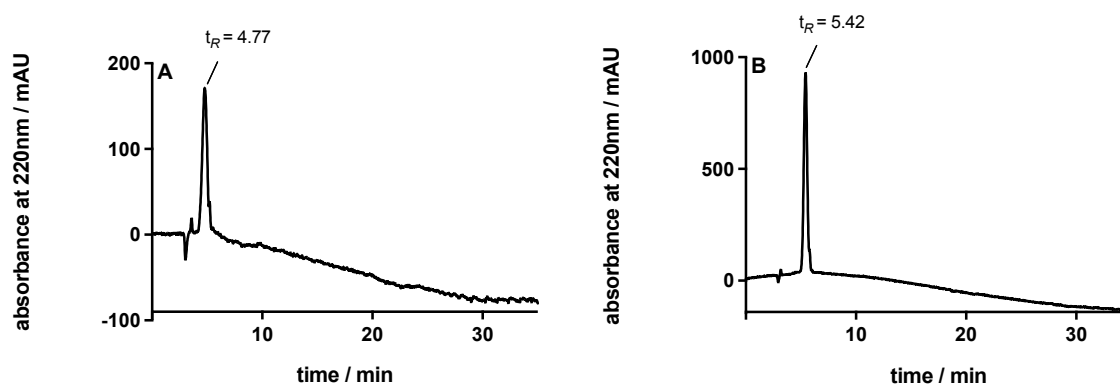
Figure 2.220. RP-HPLC analysis (purity control) of compound **2.019** (A) (> 99%, 220 nm) and compound **2.020** (B) (99%, 220 nm).
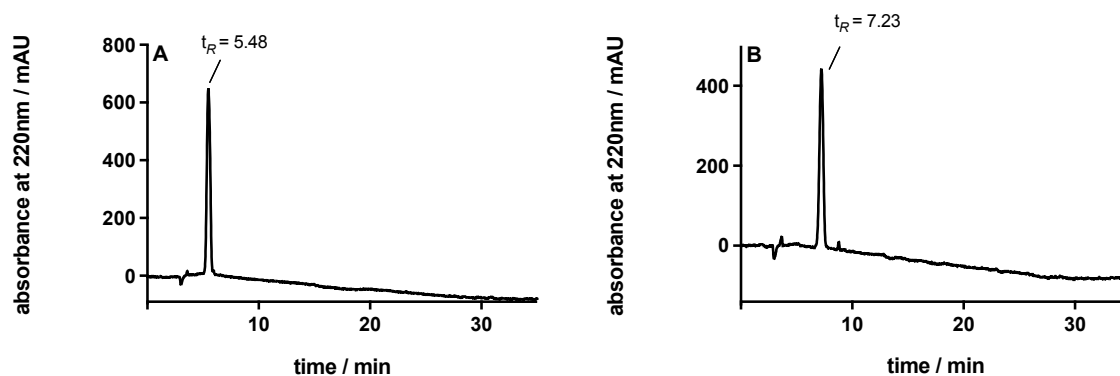
Figure 2.221. RP-HPLC analysis (purity control) of compound **2.021** (A) (99%, 220 nm) and compound **2.022** (B) (> 99%, 220 nm).
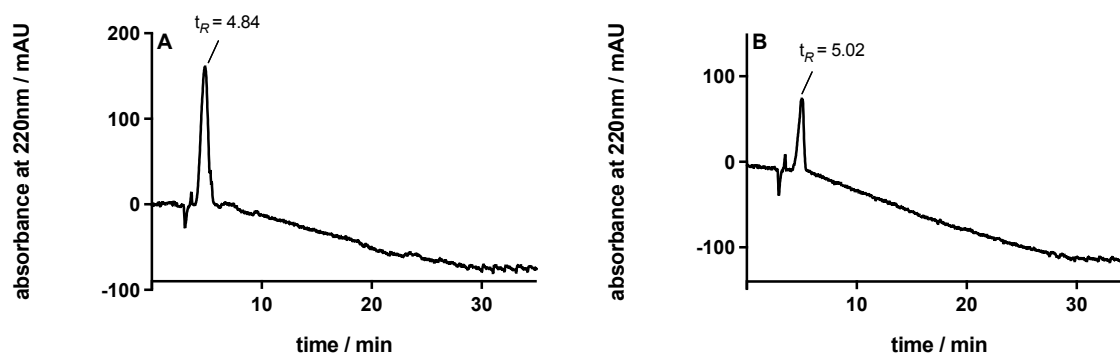
Figure 2.222. RP-HPLC analysis (purity control) of compound **2.023** (A) (> 99%, 220 nm) and compound **2.024** (B) (> 99%, 220 nm).
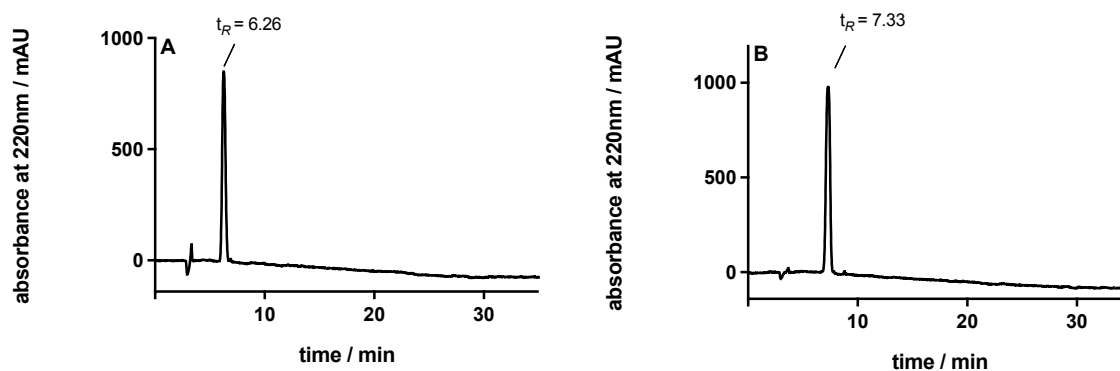
Figure 2.223. RP-HPLC analysis (purity control) of compound **2.025** (A) (> 99%, 220 nm) and compound **2.026** (B) (98%, 220 nm).
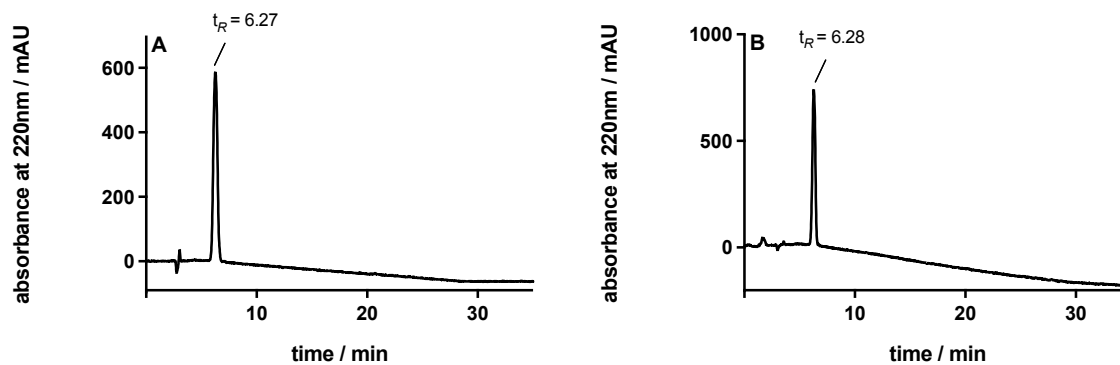
Figure 2.224. RP-HPLC analysis (purity control) of compound **2.027** (A) (> 99%, 220 nm) and compound **2.028** (B) (> 99%, 220 nm).
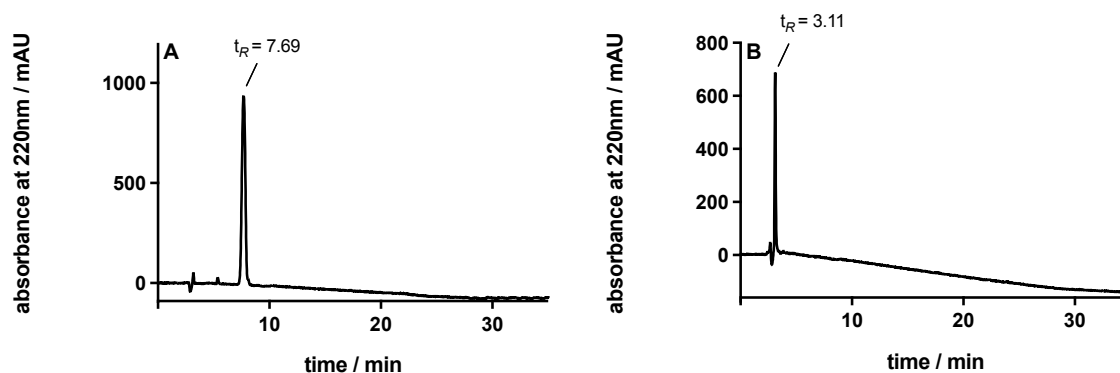
Figure 2.225. RP-HPLC analysis (purity control) of compound **2.029** (A) (99%, 220 nm) and compound **2.030** (B) (> 99%, 220 nm).
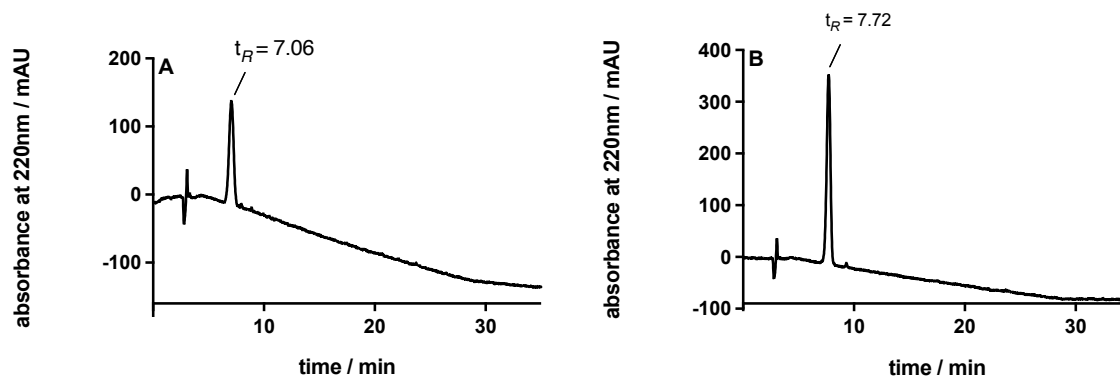
Figure 2.226. RP-HPLC analysis (purity control) of compound **2.031** (A) (98%, 220 nm) and compound **2.032** (B) (> 99%, 220 nm).

273
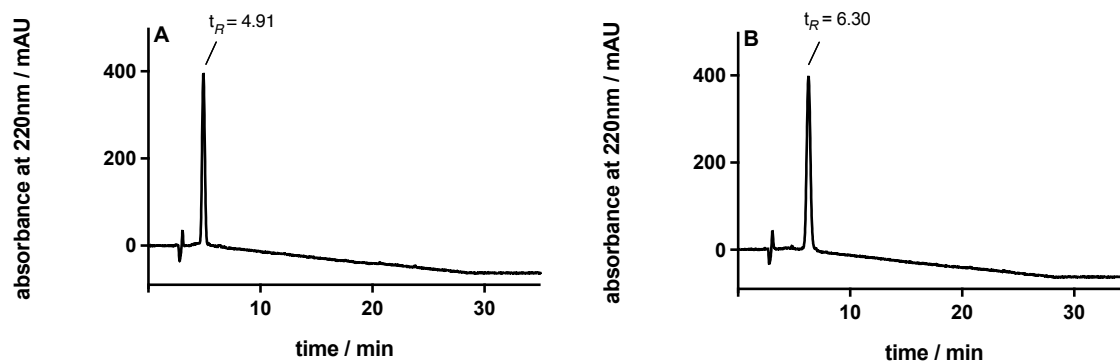
Figure 2.227. RP-HPLC analysis (purity control) of compound **2.033** (A) (> 99%, 220 nm) and compound **2.034** (B) (> 99%, 220 nm).
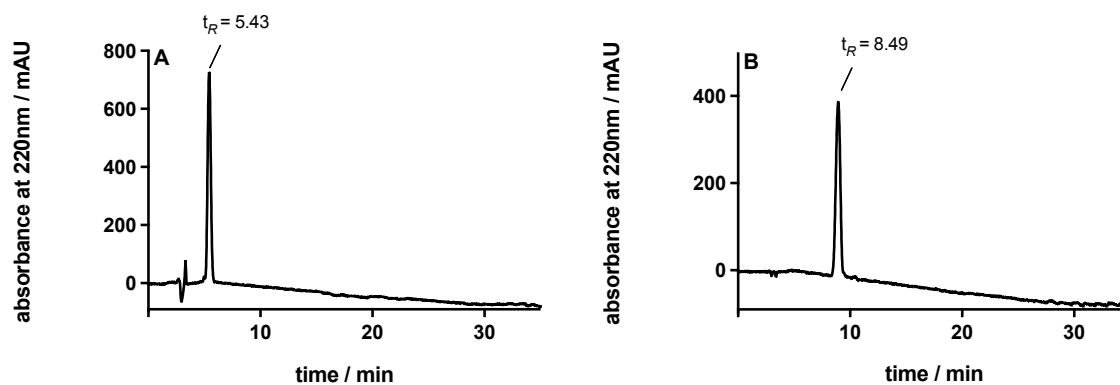
Figure 2.228. RP-HPLC analysis (purity control) of compound **2.035** (A) (99%, 220 nm) and compound **2.036** (B) (99%, 220 nm).
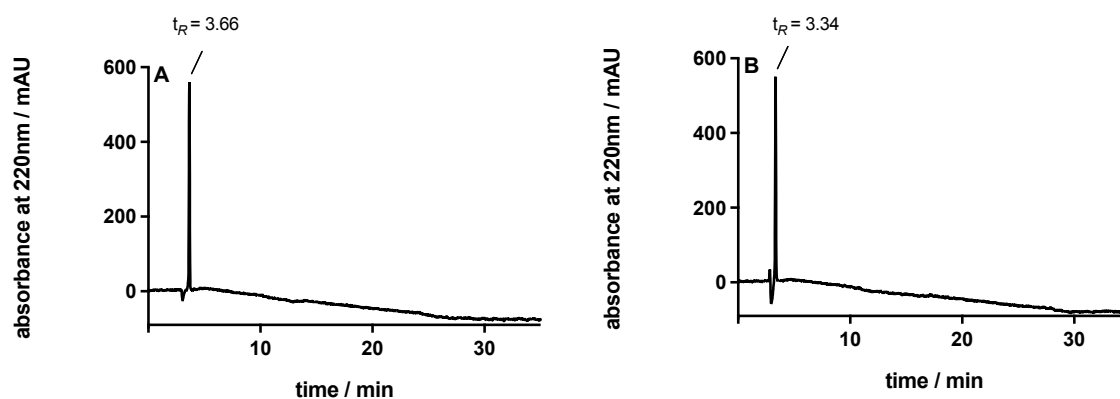
Figure 2.229. RP-HPLC analysis (purity control) of compound **2.037** (A) (> 99%, 220 nm) and compound **2.038** (B) (> 99%, 220 nm).
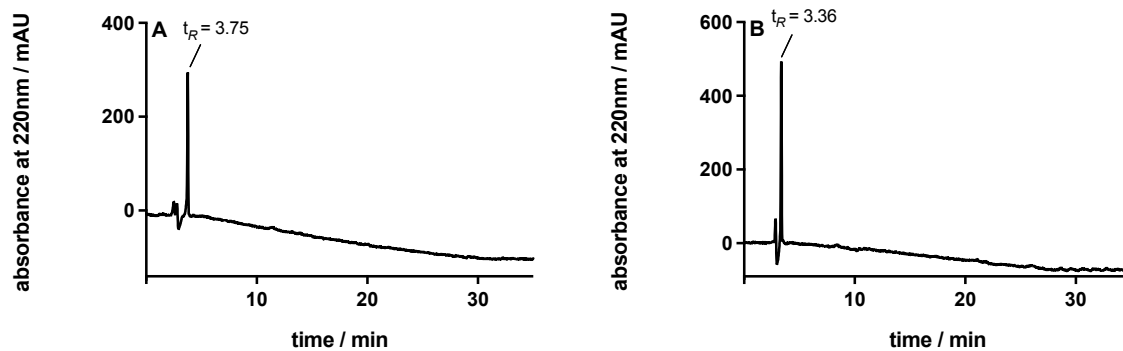
Figure 2.230. RP-HPLC analysis (purity control) of compound **2.039** (A) (> 99%, 220 nm) and compound **2.040** (B) (> 99%, 220 nm).
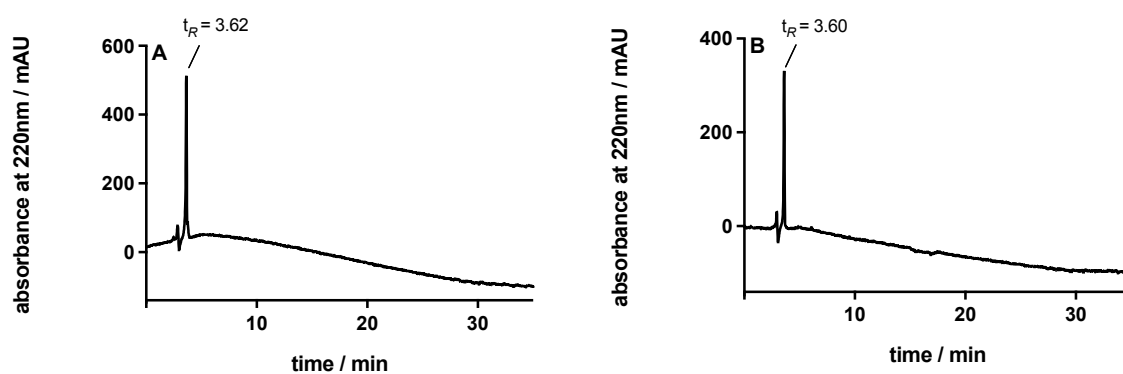
Figure 2.231. RP-HPLC analysis (purity control) of compound **2.041** (A) (97%, 220 nm) and compound **2.042** (B) (> 99%, 220 nm).
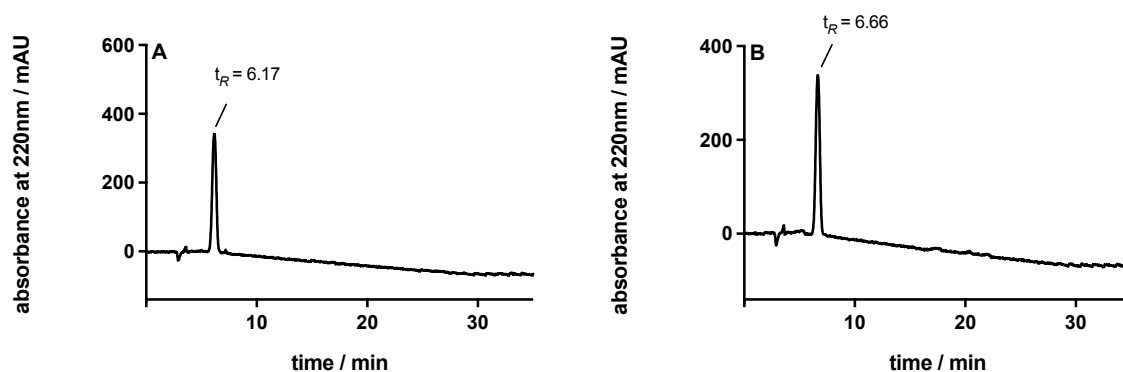
Figure 2.232. RP-HPLC analysis (purity control) of compound **2.043** (A) (99%, 220 nm) and compound **2.044** (B) (> 99%, 220 nm).
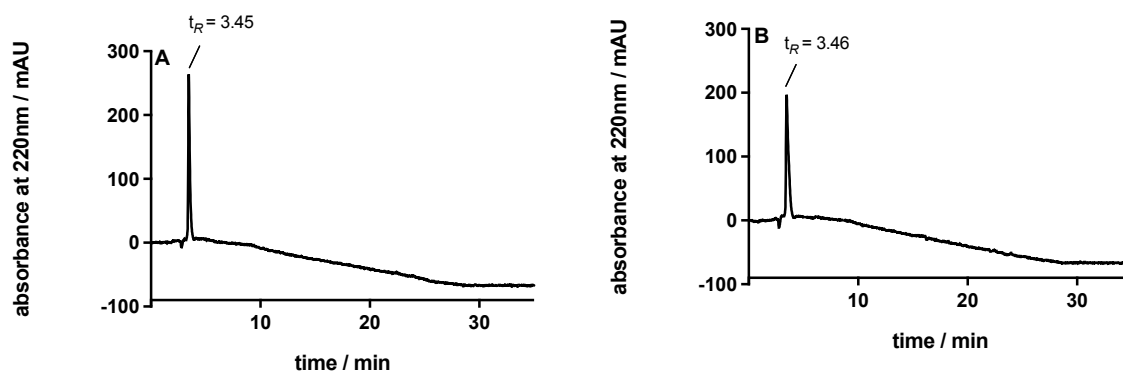
Figure 2.233. RP-HPLC analysis (purity control) of compound **2.045** (A) (> 99%, 220 nm) and compound **2.046** (B) (> 99%, 220 nm).
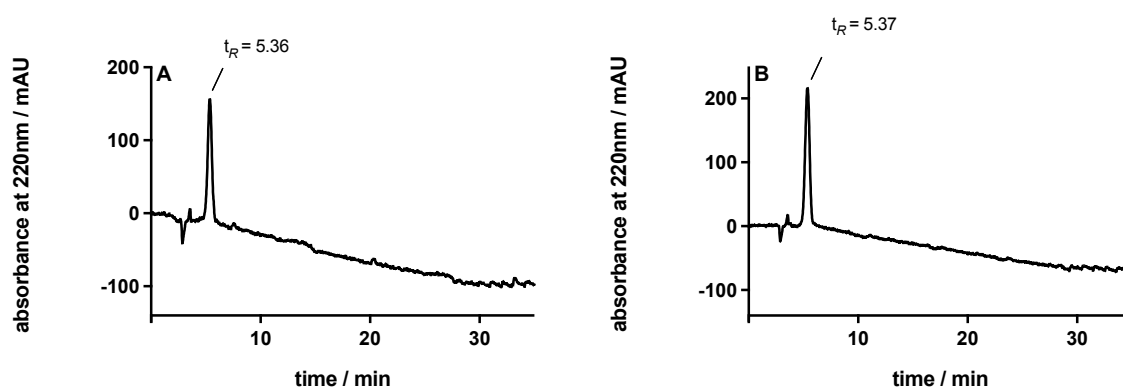
Figure 2.234. RP-HPLC analysis (purity control) of compound **2.047** (A) (> 99%, 220 nm) and compound **2.048** (B) (> 99%, 220 nm).
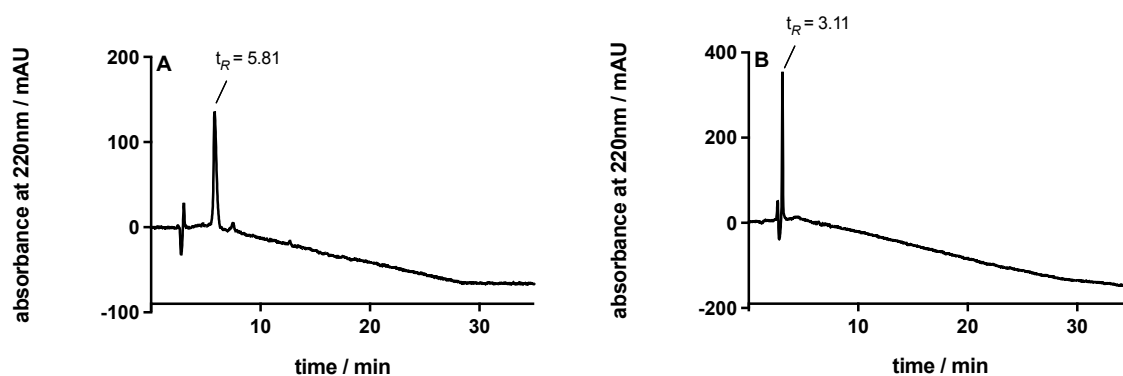
Figure 2.235. RP-HPLC analysis (purity control) of compound **2.049** (A) (98%, 220 nm) and compound **2.050** (B) (> 99%, 220 nm).
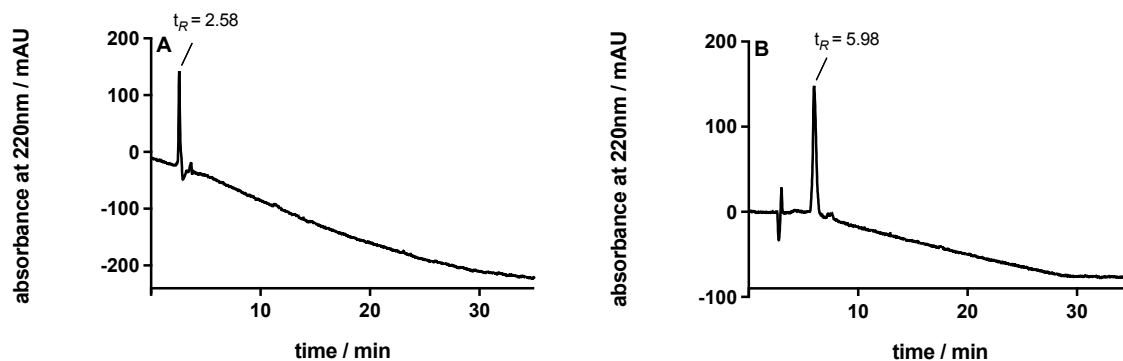
Figure 2.236. RP-HPLC analysis (purity control) of compound **2.051** (A) (> 99%, 220 nm) and compound **2.052** (B) (96%, 220 nm).
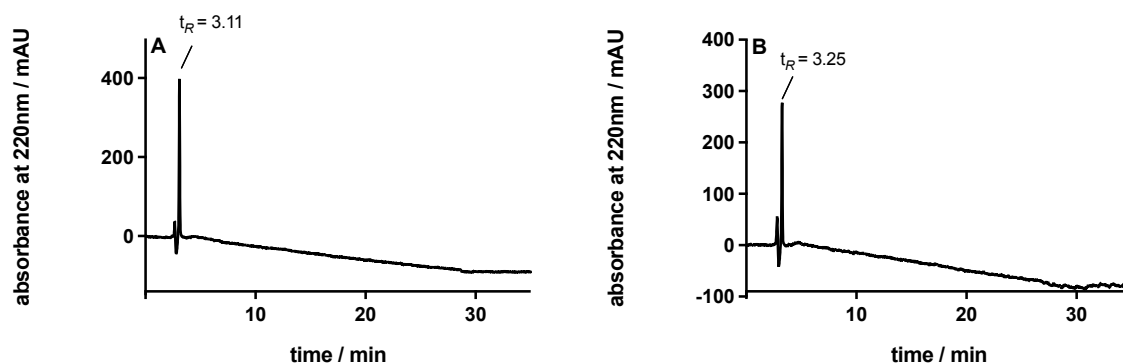
Figure 2.237. RP-HPLC analysis (purity control) of compound **2.053** (A) (> 99%, 220 nm) and compound **2.054** (B) (> 99%, 220 nm).
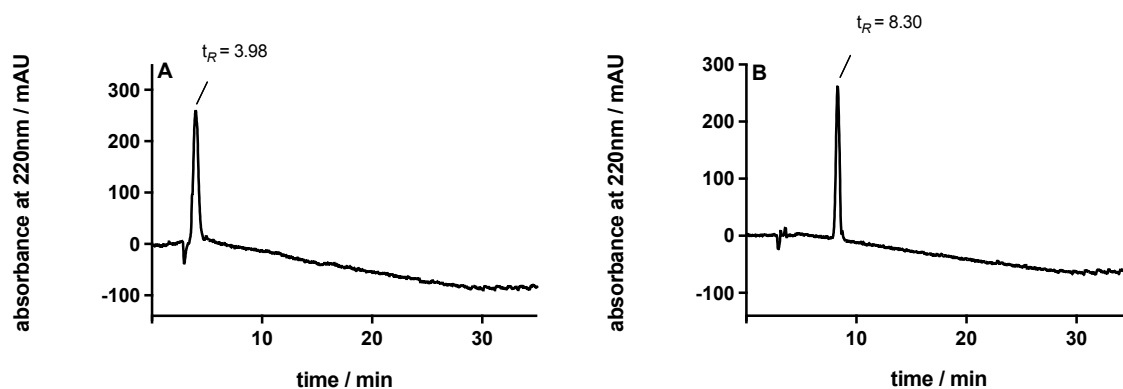
Figure 2.238. RP-HPLC analysis (purity control) of compound **2.055** (A) (> 99%, 220 nm) and compound **2.056** (B) (99%, 220 nm).
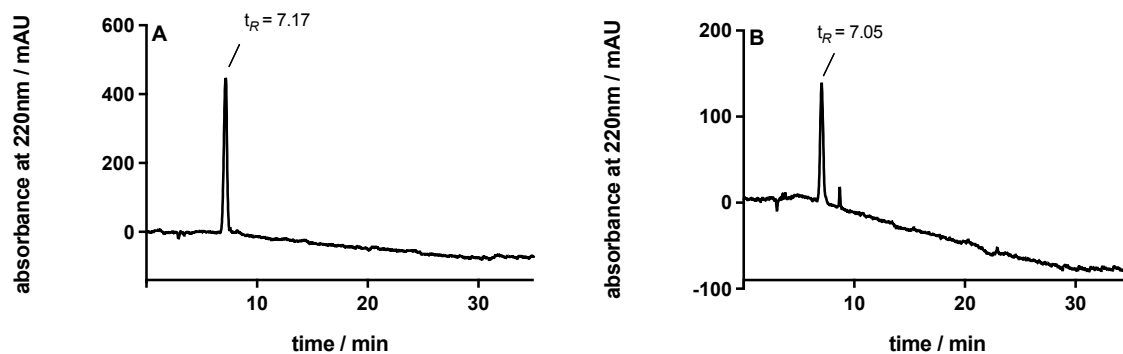
Figure 2.239. RP-HPLC analysis (purity control) of compound **2.057** (A) (> 99%, 220 nm) and compound **2.058** (B) (95%, 220 nm).
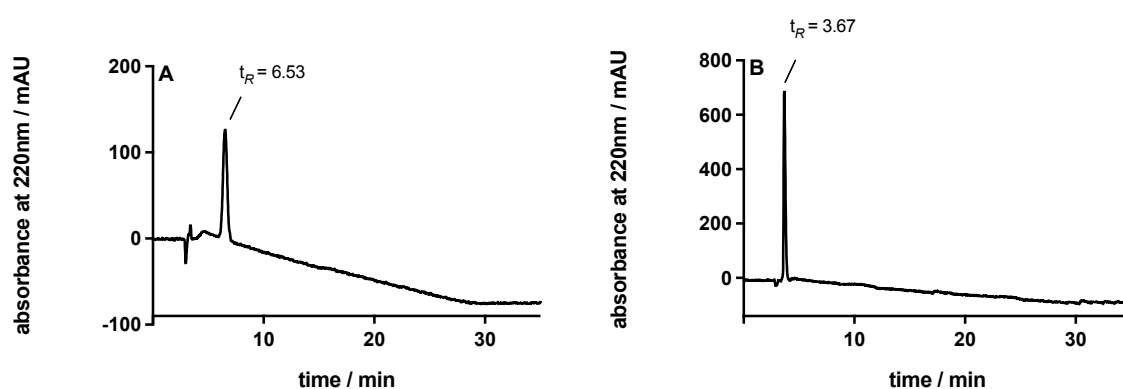
Figure 2.240. RP-HPLC analysis (purity control) of compound **2.059** (A) (99%, 220 nm) and compound **2.060** (B) (> 99%, 220 nm).
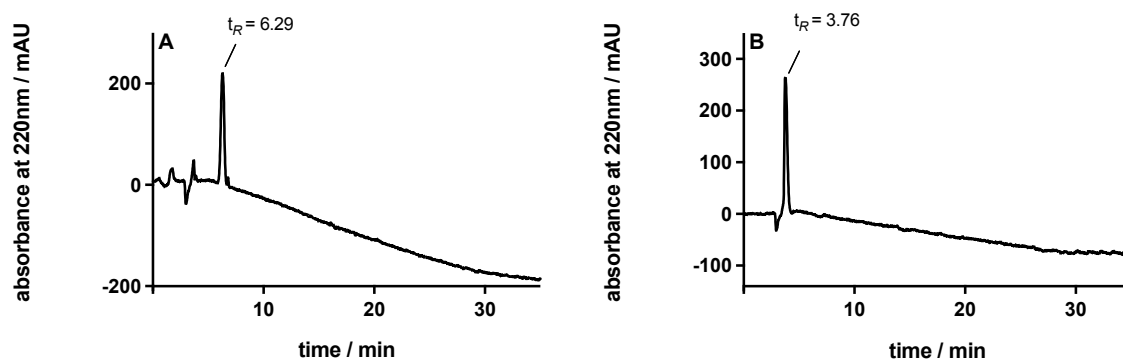
Figure 2.241. RP-HPLC analysis (purity control) of compound **2.061** (A) (98%, 220 nm) and compound **2.062** (B) (> 99%, 220 nm).
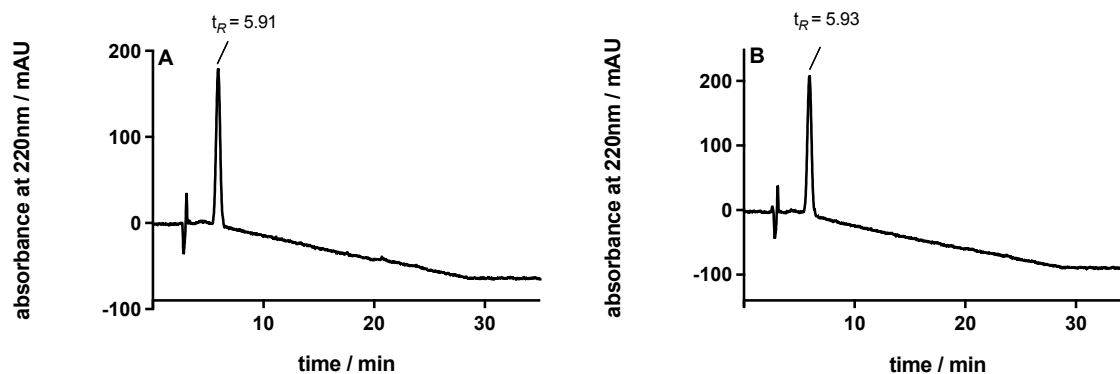
Figure 2.242. RP-HPLC analysis (purity control) of compound **2.063** (A) (> 99%, 220 nm) and compound **2.064** (B) (> 99%, 220 nm).
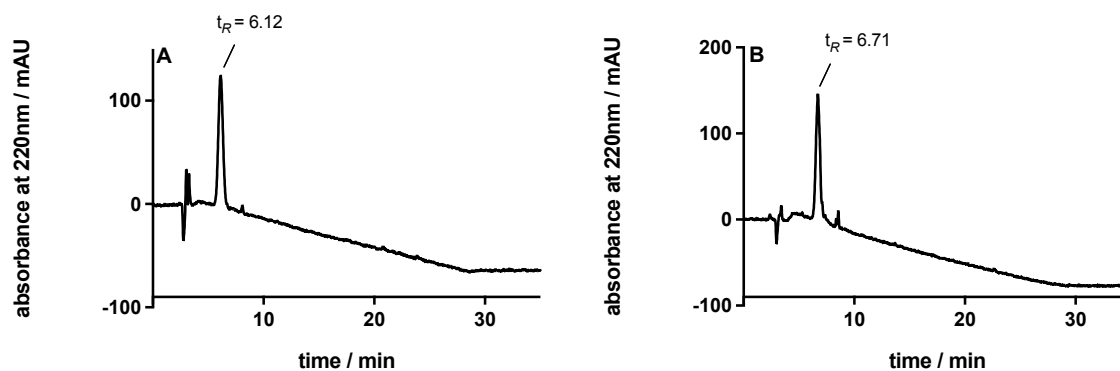
Figure 2.243. RP-HPLC analysis (purity control) of compound **2.065** (A) (95%, 220 nm) and compound **2.066** (B) (96%, 220 nm).
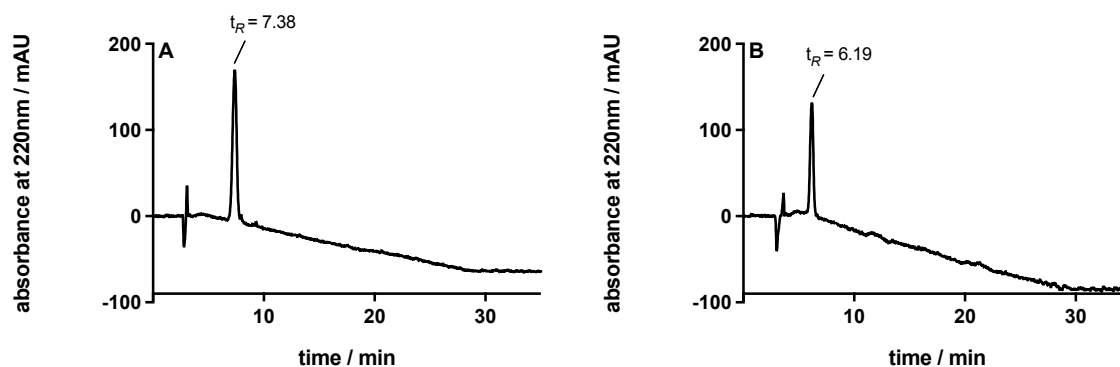
Figure 2.244. RP-HPLC analysis (purity control) of compound **2.067** (A) (99%, 220 nm) and compound **2.068** (B) (> 99%, 220 nm).
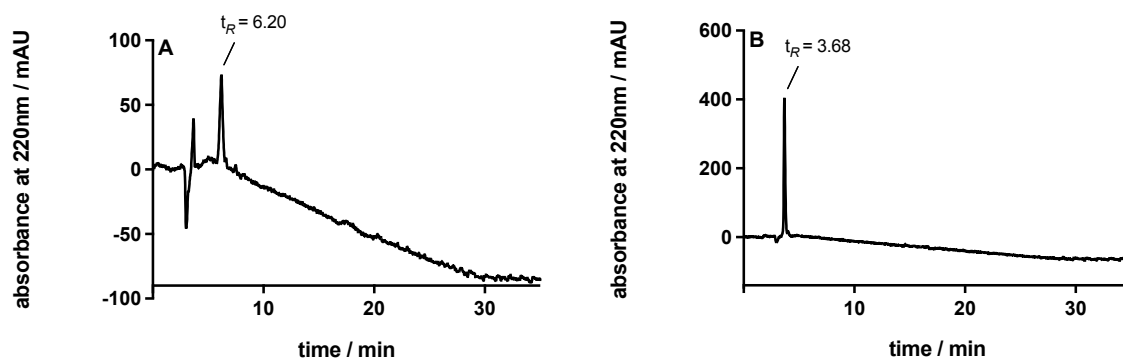
Figure 2.245. RP-HPLC analysis (purity control) of compound **2.069** (A) (95%, 220 nm) and compound **2.070** (B) (99%, 220 nm).
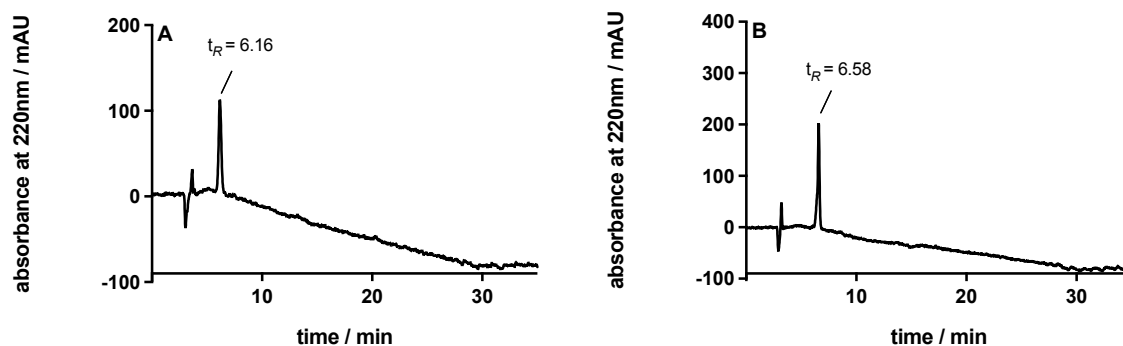
Figure 2.246. RP-HPLC analysis (purity control) of compound **2.071** (A) (> 99%, 220 nm) and compound **2.072** (B) (> 99%, 220 nm).
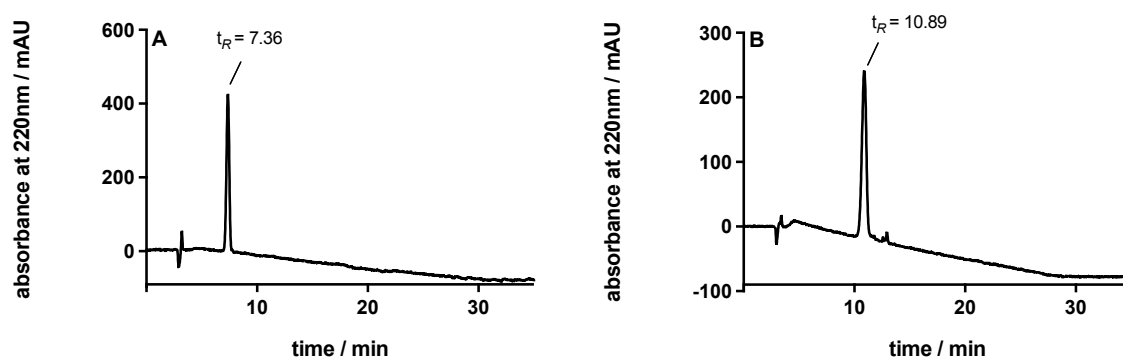
Figure 2.247. RP-HPLC analysis (purity control) of compound **2.073** (A) (> 99%, 220 nm) and compound **2.074** (B) (97%, 220 nm).
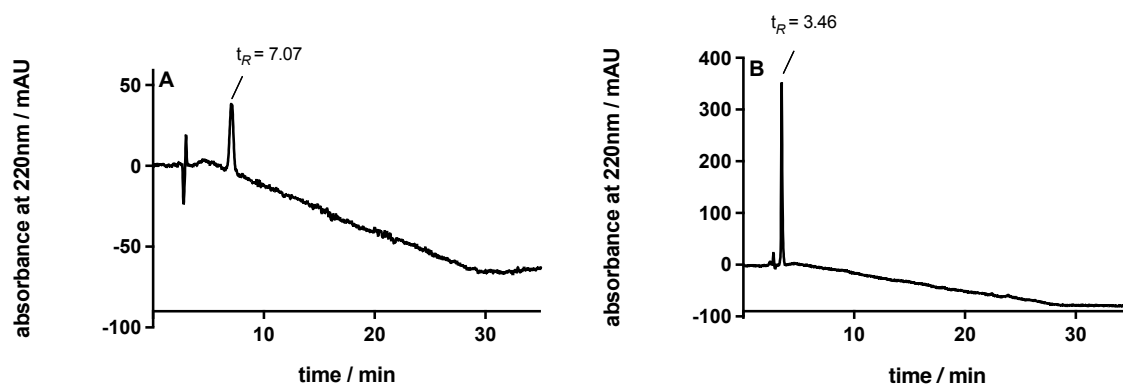
Figure 2.248. RP-HPLC analysis (purity control) of compound **2.075** (A) (> 99%, 220 nm) and compound **2.076** (B) (> 99%, 220 nm).
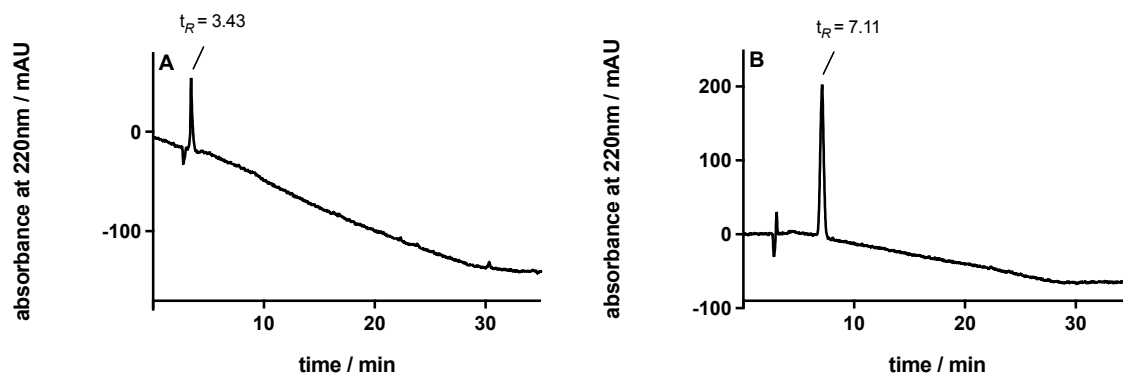
Figure 2.249. RP-HPLC analysis (purity control) of compound **2.077** (A) (> 99%, 220 nm) and compound **2.078** (B) (> 99%, 220 nm).
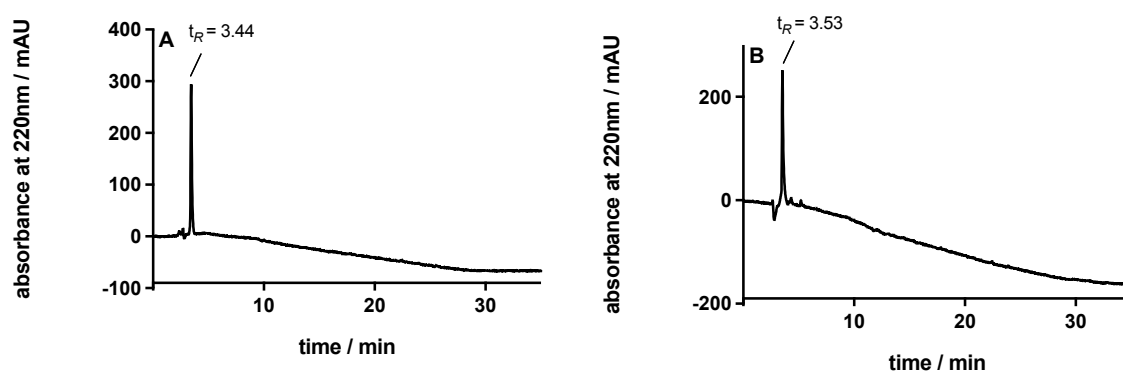
Figure 2.250. RP-HPLC analysis (purity control) of compound **2.079** (A) (> 99%, 220 nm) and compound **2.080** (B) (96%, 220 nm).
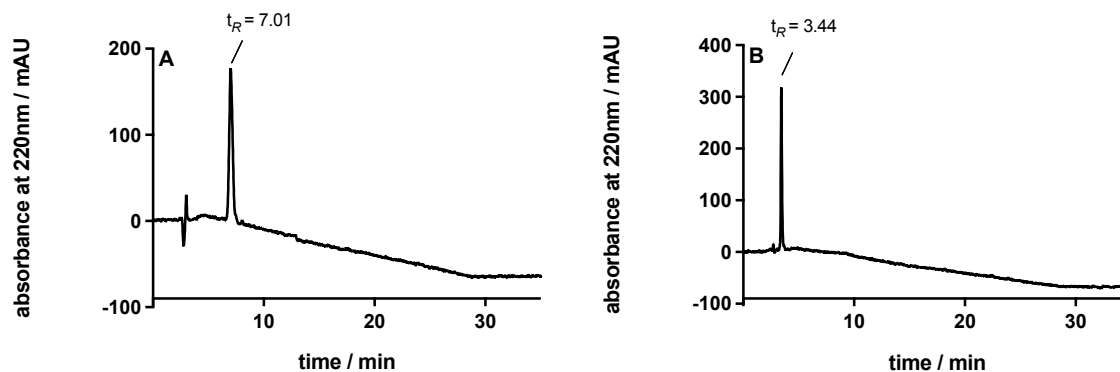
Figure 2.251. RP-HPLC analysis (purity control) of compound **2.081** (A) (> 99%, 220 nm) and compound **2.082** (B) (> 99%, 220 nm).
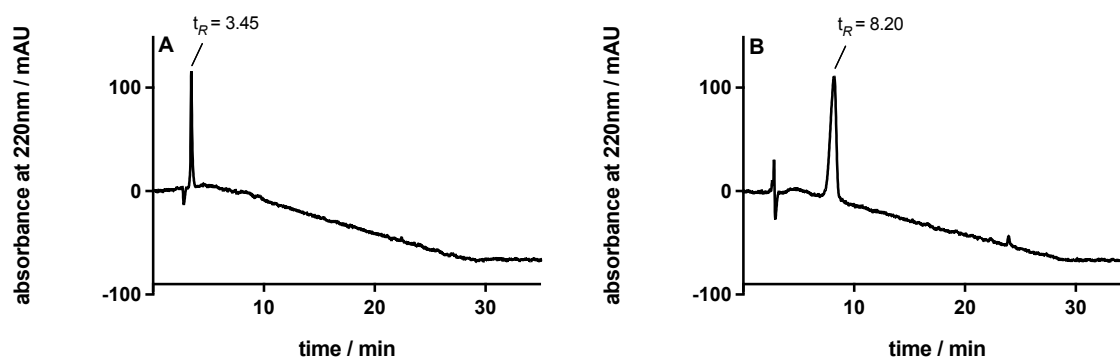
Figure 2.252. RP-HPLC analysis (purity control) of compound **2.083** (A) (> 99%, 220 nm) and compound **2.084** (B) (> 99%, 220 nm).
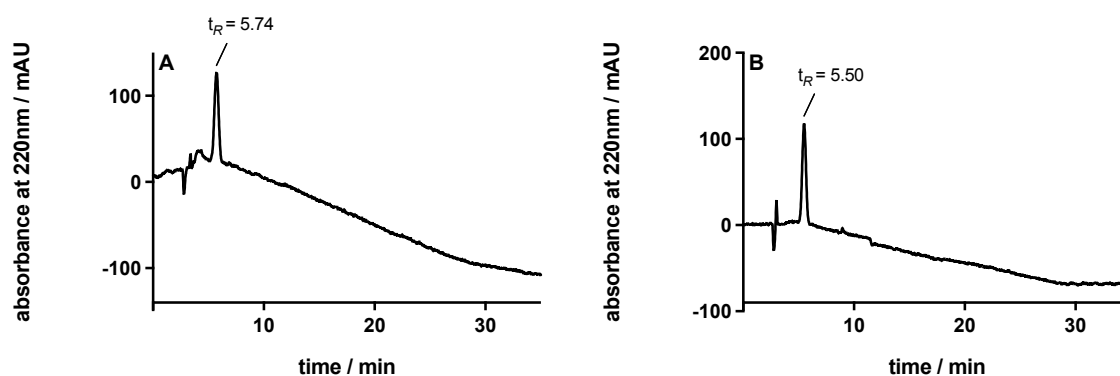
Figure 2.253. RP-HPLC analysis (purity control) of compound **2.085** (A) (> 99%, 220 nm) and compound **2.086** (B) (> 99%, 220 nm).
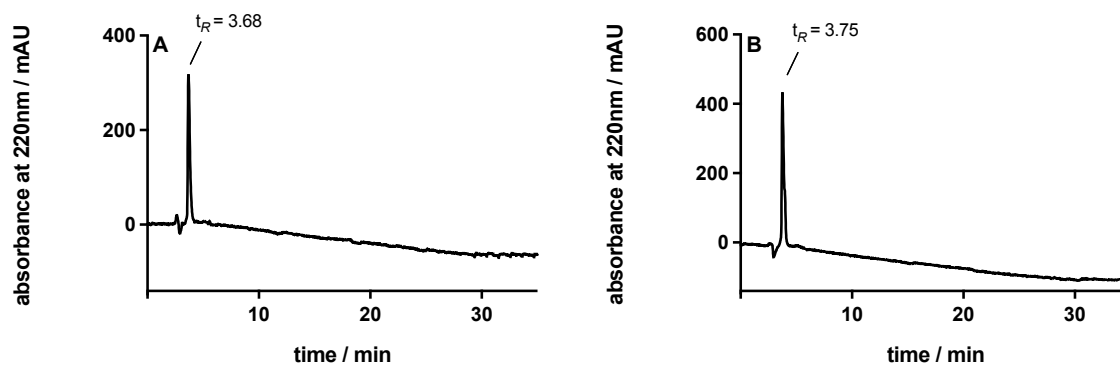
Figure 2.254. RP-HPLC analysis (purity control) of compound **2.087** (A) (> 99%, 220 nm) and compound **2.088** (B) (> 99%, 220 nm).
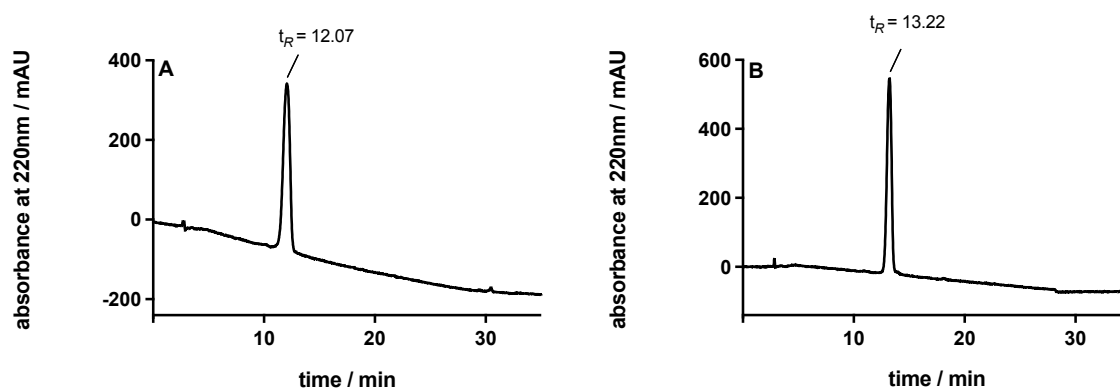
Figure 2.255. RP-HPLC analysis (purity control) of compound **2.093** (A) (99%, 220 nm) and compound **2.094** (B) (> 99%, 220 nm).
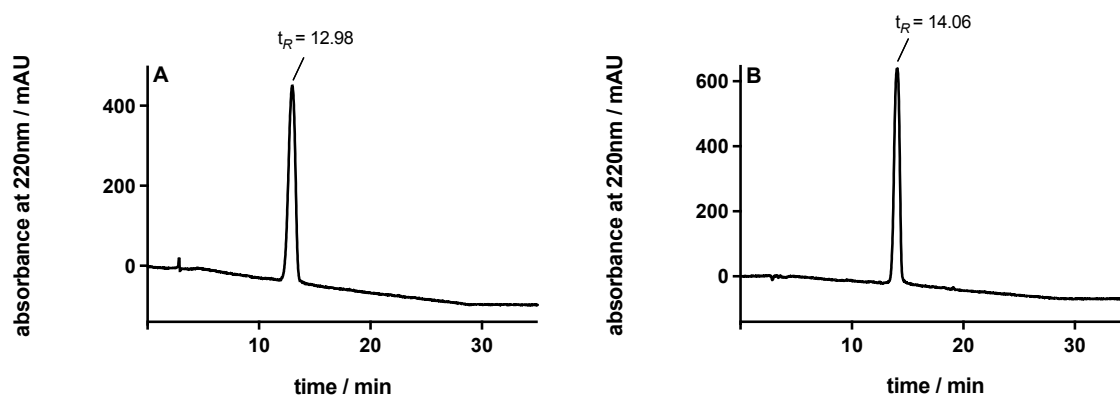
Figure 2.256. RP-HPLC analysis (purity control) of compound **2.095** (A) (> 99%, 220 nm) and compound **2.096** (B) (> 99%, 220 nm).
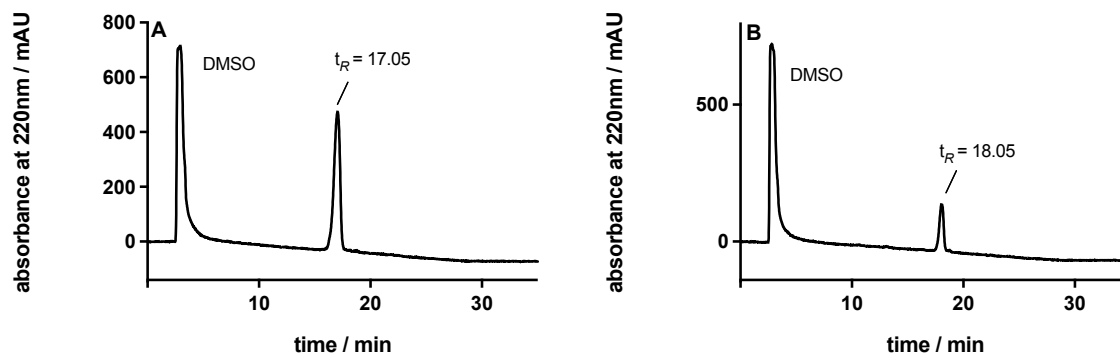
Figure 2.257. RP-HPLC analysis (purity control) of compound **2.097** (A) (> 99%, 220 nm) and compound **2.098** (B) (99%, 220 nm).
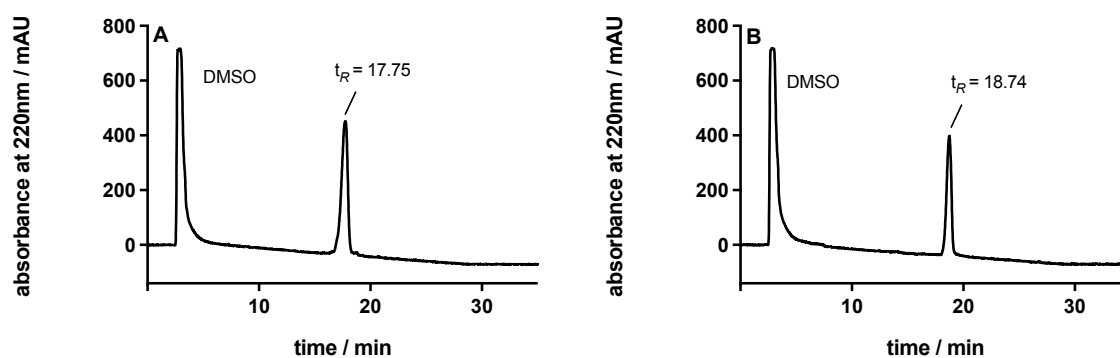
Figure 2.258. RP-HPLC analysis (purity control) of compound **2.099** (A) (> 99%, 220 nm) and compound **2.100** (B) (> 99%, 220 nm).
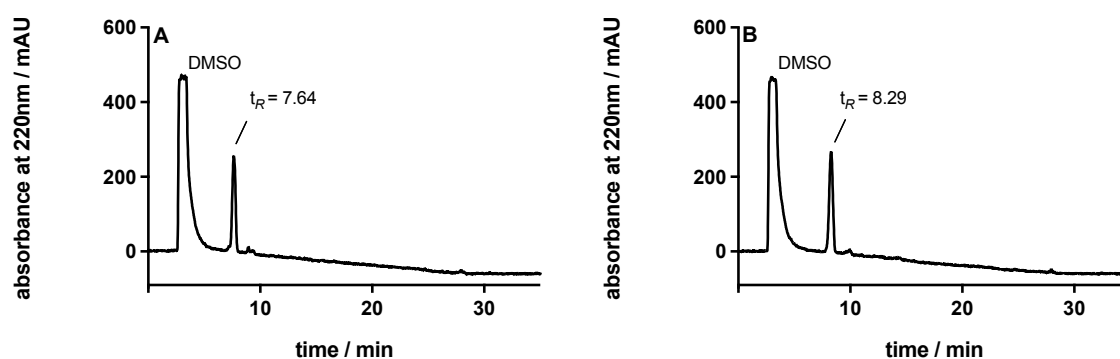
Figure 2.259. RP-HPLC analysis (purity control) of compound **2.107** (A) (95%, 220 nm) and compound **2.108** (B) (96%, 220 nm).
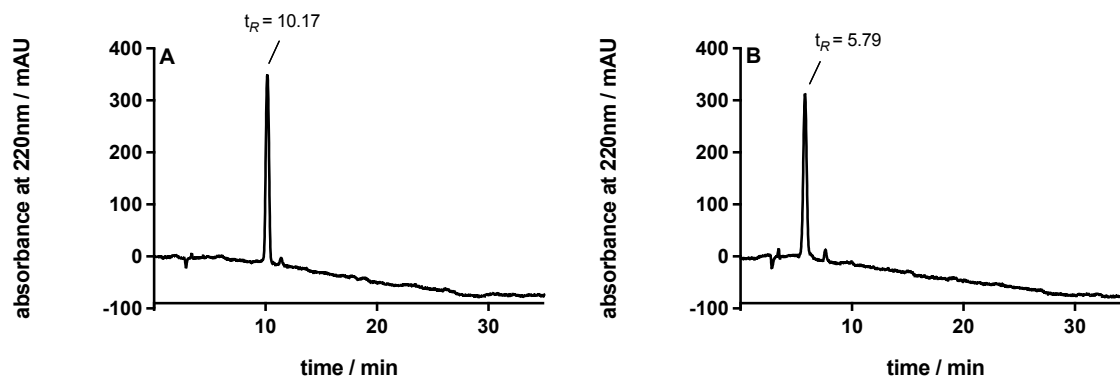
Figure 2.260. RP-HPLC analysis (purity control) of compound **2.109**(A) (99%, 220 nm) and compound **2.110** (B) (97%, 220 nm).
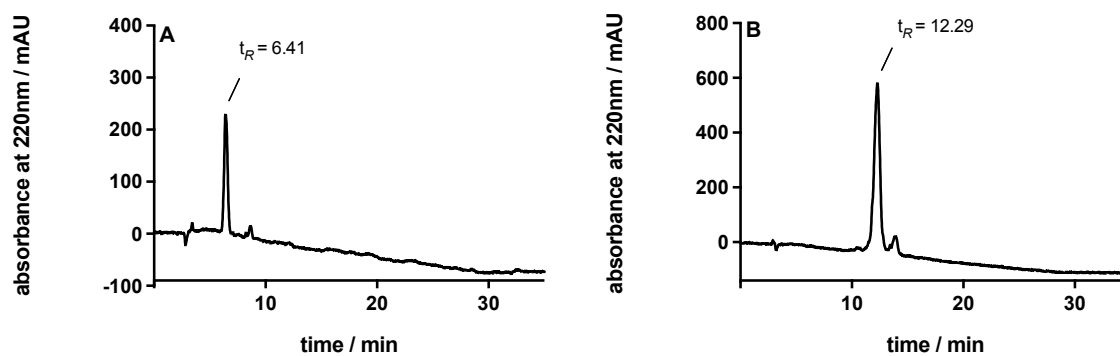
Figure 2.261. RP-HPLC analysis (purity control) of compound **2.111**(A) (95%, 220 nm) and compound **2.112** (B) (95%, 220 nm).
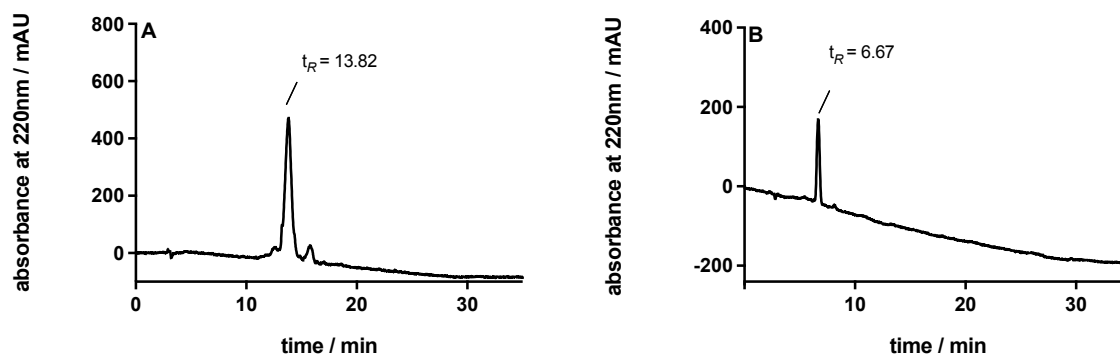
Figure 2.262. RP-HPLC analysis (purity control) of compound **2.113** (A) (95%, 220 nm) and compound **2.114** (B) (> 99%, 220 nm).
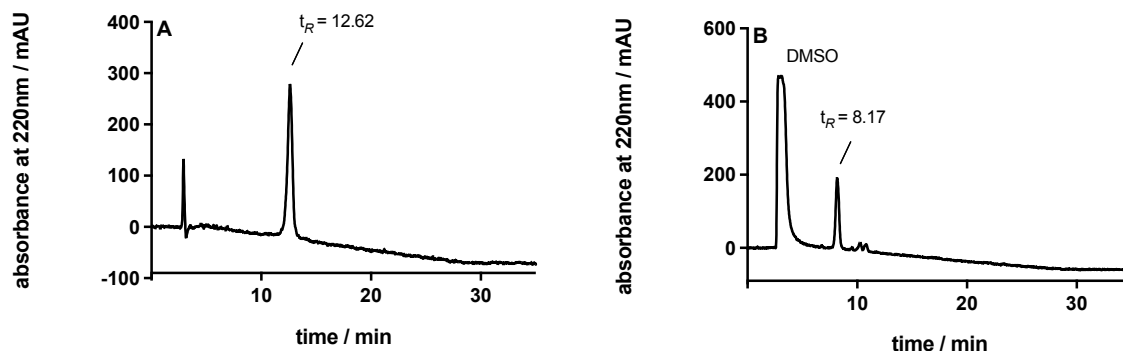
Figure 2.263. RP-HPLC analysis (purity control) of compound **2.115** (A) (> 99%, 220 nm) and compound **2.116** (B) (95%, 220 nm).
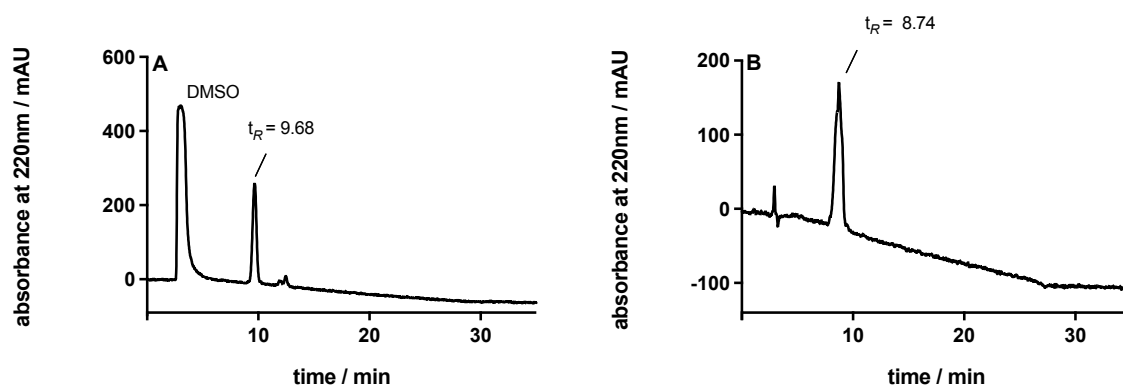
Figure 2.264. RP-HPLC analysis (purity control) of compound **2.117** (A) (95%, 220 nm) and compound **2.118** (B) (> 99%, 220 nm).
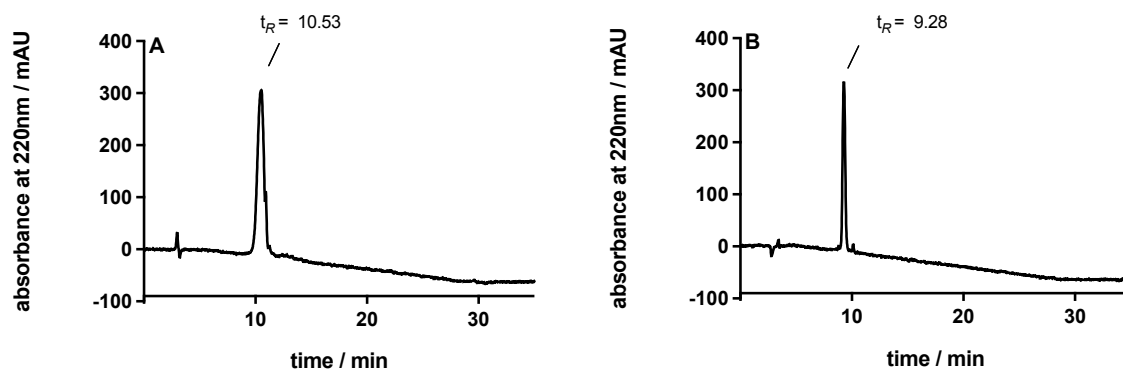
Figure 2.265. RP-HPLC analysis (purity control) of compound **2.119** (A) (98%, 220 nm) and compound **2.120** (B) (99%, 220 nm).
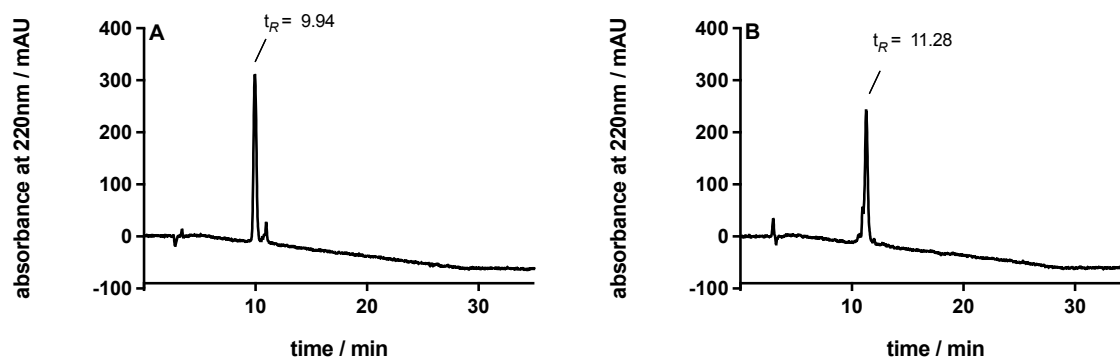
Figure 2.266. RP-HPLC analysis (purity control) of compound **2.121** (A) (97%, 220 nm) and compound **2.122** (B) (99%, 220 nm).
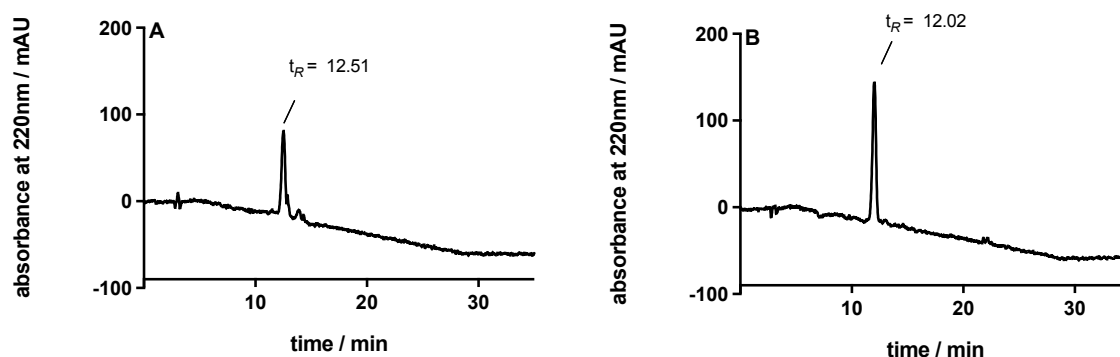
Figure 2.267. RP-HPLC analysis (purity control) of compound **2.123** (A) (95%, 220 nm) and compound **2.124** (B) (> 99%, 220 nm).
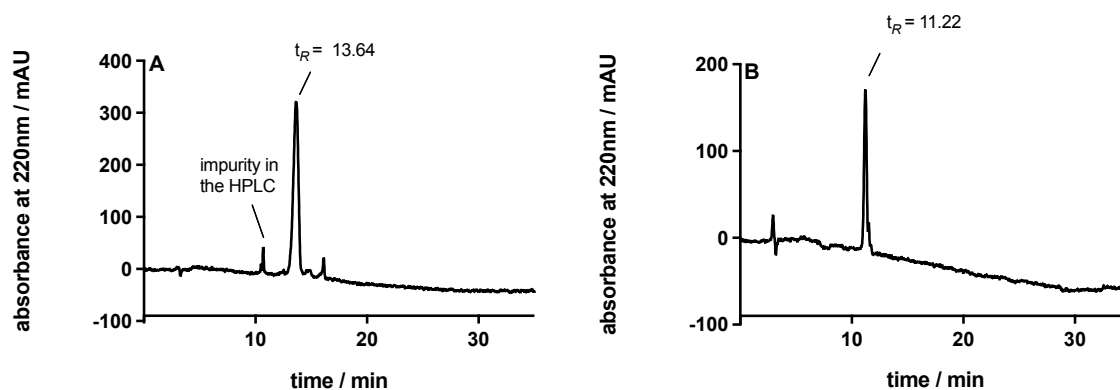
Figure 2.268. RP-HPLC analysis (purity control) of compound **2.125** (A) (96%, 220 nm) and compound **2.126** (B) (96%, 220 nm).

2.7.2.2 Chemical Stability of Peptides 2.013, 2.047, 2.048, 2.055, 2.057, and 2.088
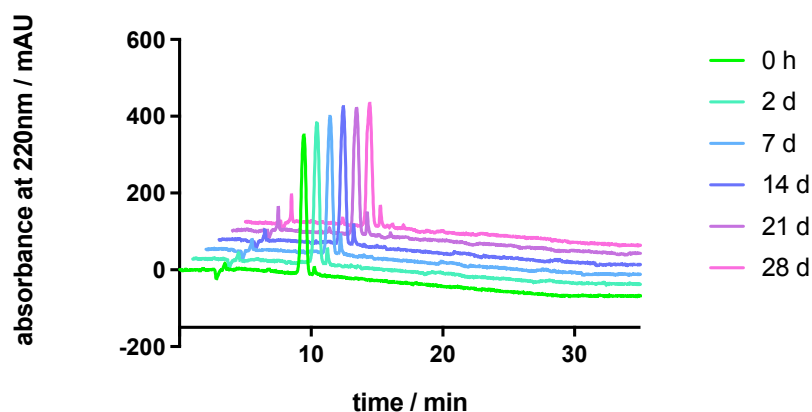
Figure 2.269 RP-HPLC analysis (stability control) of peptide **2.013** in water (1 mM) at rt for 28 days.
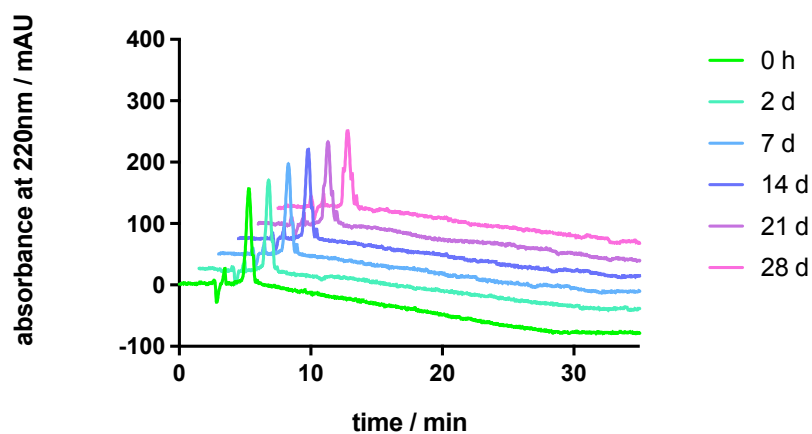
Figure 2.270. RP-HPLC analysis (stability control) of peptide **2.047** in water (1 mM) at rt for 28 days.
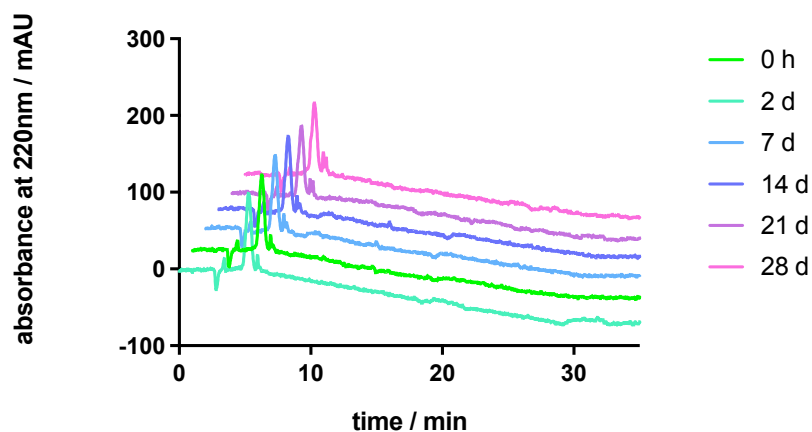
Figure 2.271. RP-HPLC analysis (stability control) of peptide **2.048** in water (1 mM) at rt for 28 days.
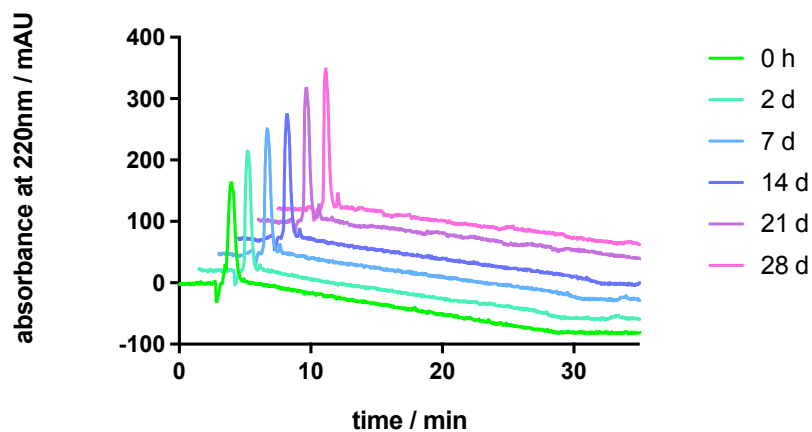
Figure 2.272. RP-HPLC analysis (stability control) of peptide **2.055** in water (1 mM) at rt for 28 days.
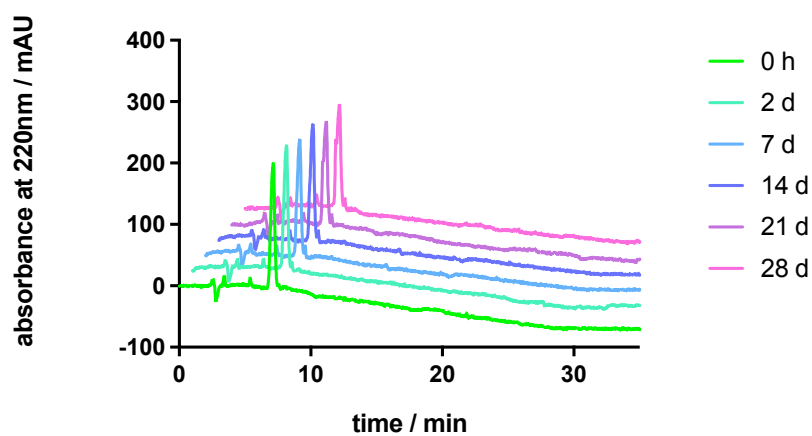
Figure 2.273. RP-HPLC analysis (stability control) of peptide **2.057** in water (1 mM) at rt for 28 days.
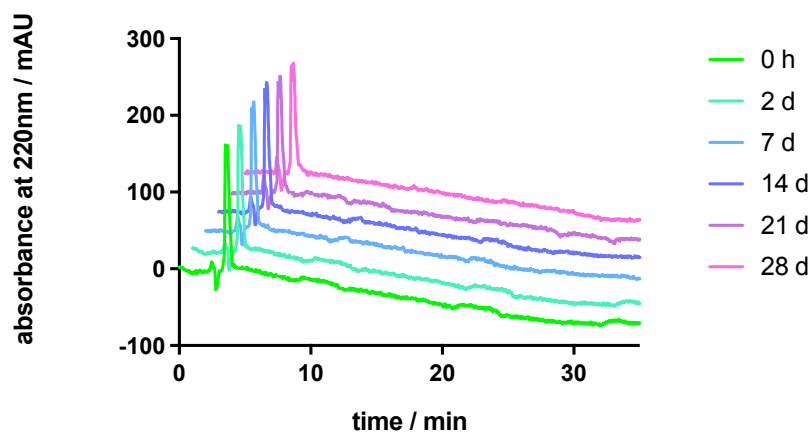
Figure 2.274. RP-HPLC analysis (stability control) of peptide **2.088** in water (1 mM) at rt for 28 days.

2.7.2.3 Chemical Stability of Indoline-containing Peptides 2.108 and 2.120
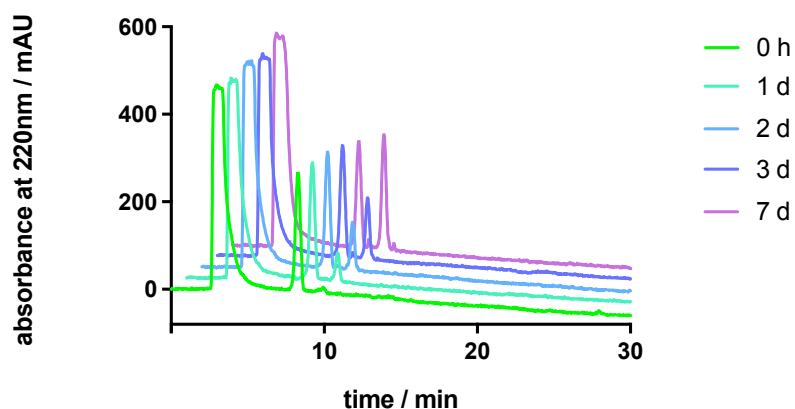
Figure 2.275. RP-HPLC analysis (stability control) of peptide **2.108** at rt in DMSO (5 mM) for 7 days.
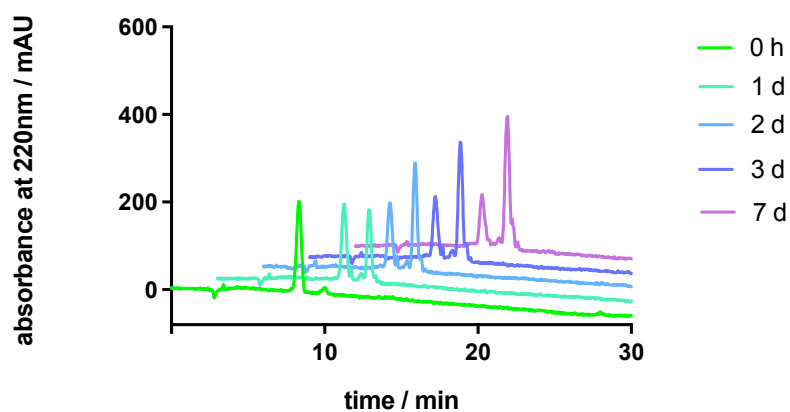
Figure 2.276. RP-HPLC analysis (stability control) of peptide **2.108** at rt in water (1 mM) for 7 days.
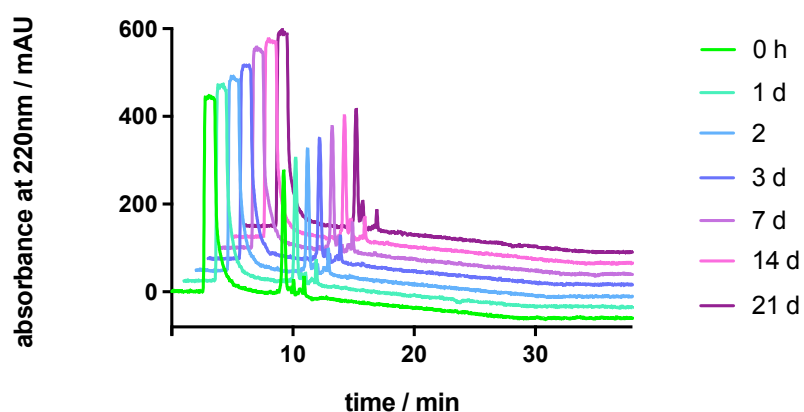
Figure 2.277. RP-HPLC analysis (stability control) of peptide **2.120** at rt in DMSO (5 mM) for 21 days.
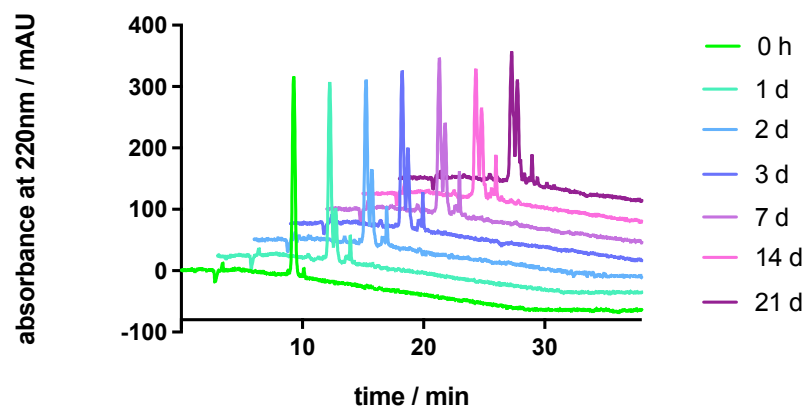
Figure 2.278. RP-HPLC analysis (stability control) of peptide **2.120** at rt in water (1 mM) for 21 days.

2.7.3 Chiral-SFC Chromatograms of 6-Methyl-tetrahydrosioquinoline-1-carboxylic Acid
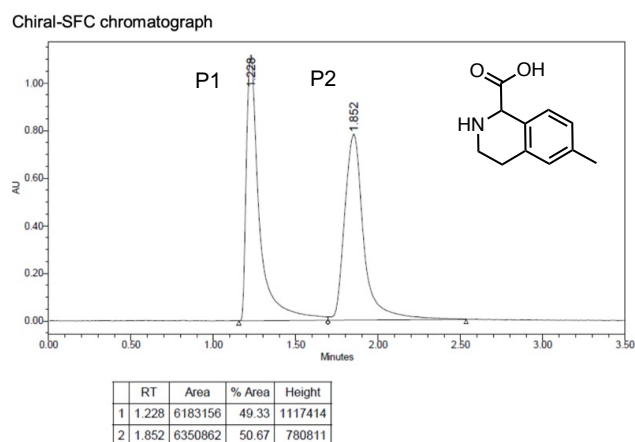
Preparative-SFC conditions:
Instrument: SFC-200 (Waters)
Column: CHIRALPAK 20x250mm, 10μm (Daicel)
Column temperature: 35 °C
Mobile phase: CO_2/MeOH (0.5% Methanol Ammonia) = 55/45
Flow rate: 120g/min
Back pressure: 100 bar
Detection wavelength: 214 nm
Cycle time: 4.9 min
Sample solution: 5000 mg dissolved in 200mL (MeOH+DCM)
Injection volume: 1.5 mL

	RT	Area	% Area	Height
1	1.228	6183156	49.33	1117414
2	1.852	6350862	50.67	780811

Figure 2.279. Chiral separation of (±)-6-methyl-tetrahydroisoquinoline-1-carboxylic acid.

	RT	Area	% Area	Height
1	1.228	3947717	100.00	696267
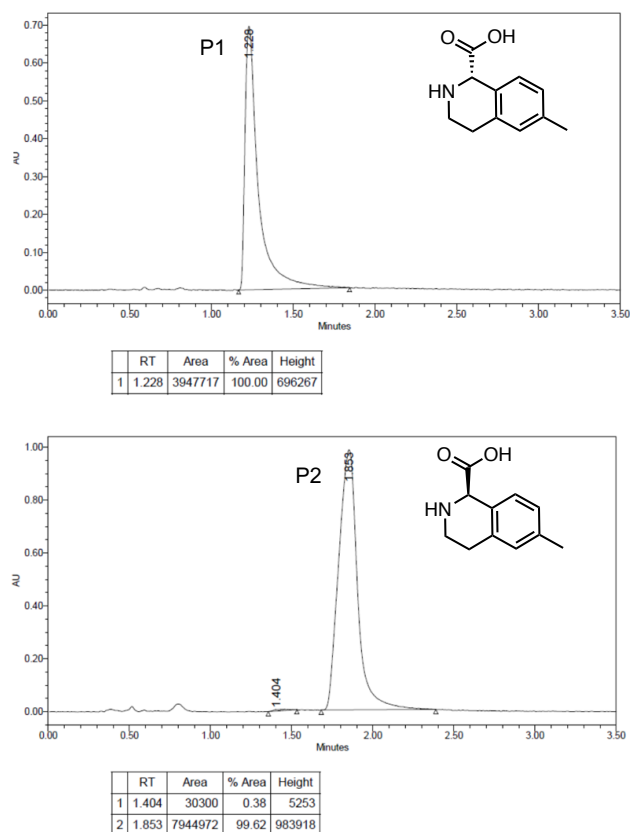
Analytical-SFC conditions:
Instrument: SFC Method Station (Thar, Waters)
Column: CHIRALPAK OZ 4.6x100mm, 5μm (Daicel)
Column temperature: 40 °C
Mobile phase: CO_2/MeOH (0.5% Methanol Ammonia) = 60/40
Flow rate: 4.0 mL/min
Back pressure: 120 bar
Detection wavelength: 214 nm
Injection volume: 1.0 μL

	RT	Area	% Area	Height
1	1.404	30300	0.38	5253
2	1.853	7944972	99.62	983918

Figure 2.280. Optical purity of (*S*)-6-methyl-tetrahydroisoquinoline-1-carboxylic acid and (*R*)-6-methyl-tetrahydroisoquinoline-1-carboxylic acid.

292

2.7.4 Bioavailability Radars Generated with SwissADME

Bioavailability radars of peptides **2.107**, **and 2.110-2.119** were generated by using SwissADME web tool.[129] Six parameters namely flexibility (FLEX, < 10 rotatable bonds), lipophilicity (LIPO, $-0.7 \leq$ logP (XLOGP[132]) $\leq$ 6), size (SIZE, $150 \leq$ MW $\leq$ 500), polarity (POLAR, $20 \leq$ TPSA $\leq$ 130;), solubility (INSOLU, logS (ESOL[136]) < -6) and saturation (INSATU, sp3 hybridized carbons / total carbon count $\geq$ 0.25) and their critical limits are depicted in the bioavailability radar. Ranges of optimal values are depicted as a pink area. The red radar of the compound must be fully encompassed by the pink area to consider it as drug-like and orally bioavailable. Any deviation signifies a suboptimal property for oral bioavailability.

Figure 2.281. Bioavailability Radar of **2.107** (A) and **2.110** (B).
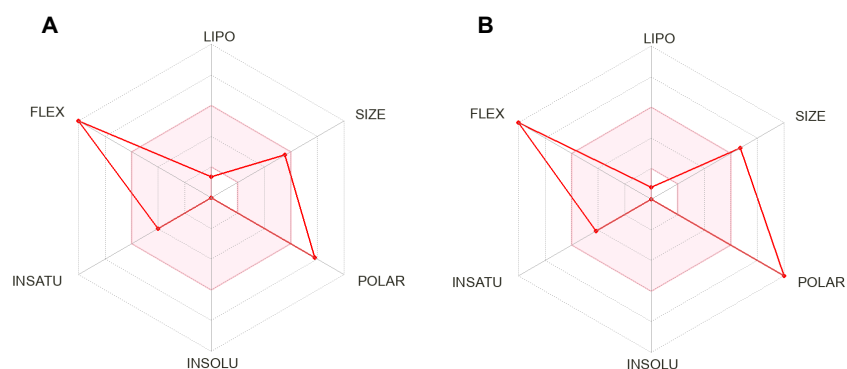
Figure 2.282. Bioavailability Radar of **2.111** (A) and **2.114** (B).

293
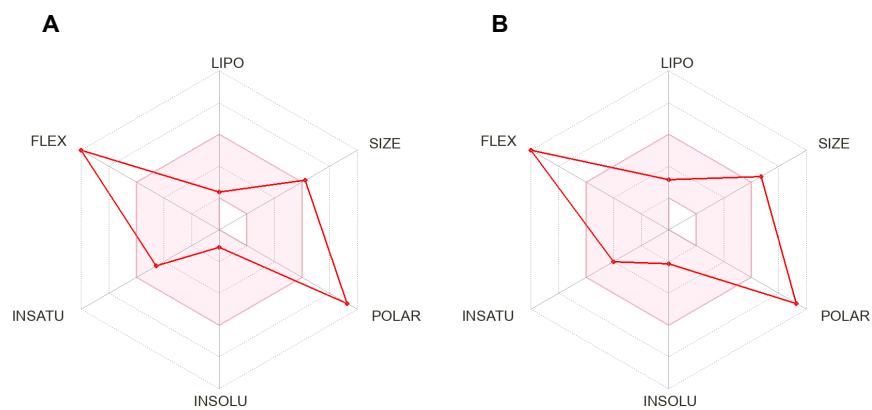
Figure 2.283. Bioavailability Radar of **2.116** (A) and **2.117** (B).
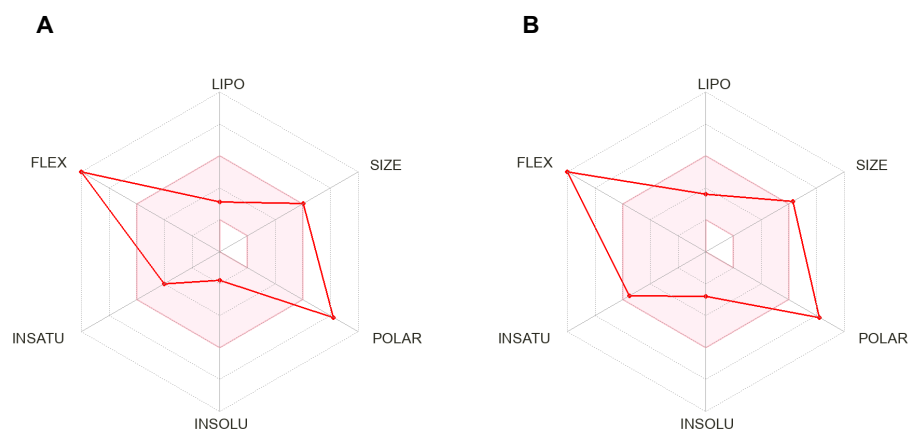
Figure 2.284. Bioavailability Radar of **2.118** (A) and **2.119** (B).

2.7.5 Saturation Binding Experiments in the Fluorometric Enzyme Assay
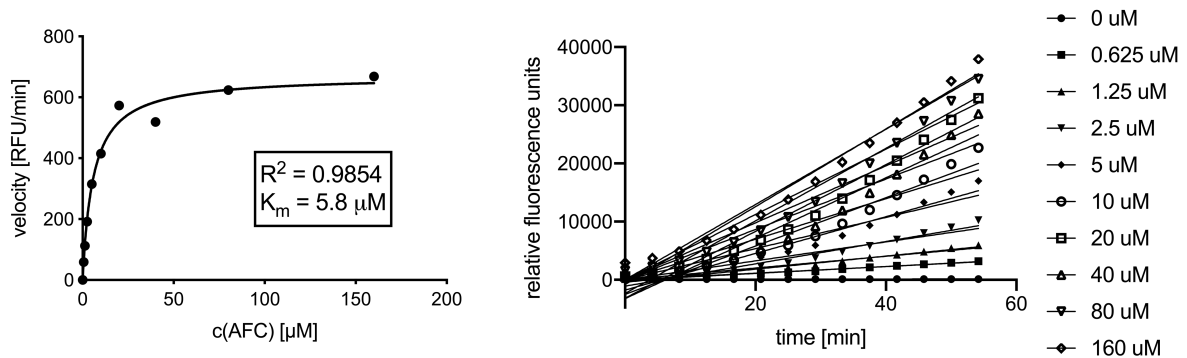
Figure 2.285. Saturation binding experiment (left) and representative fluorescence traces (right) of the fluorometric enzyme assay with AcYVAD-AFC and Casp1 (0.05 U/well).
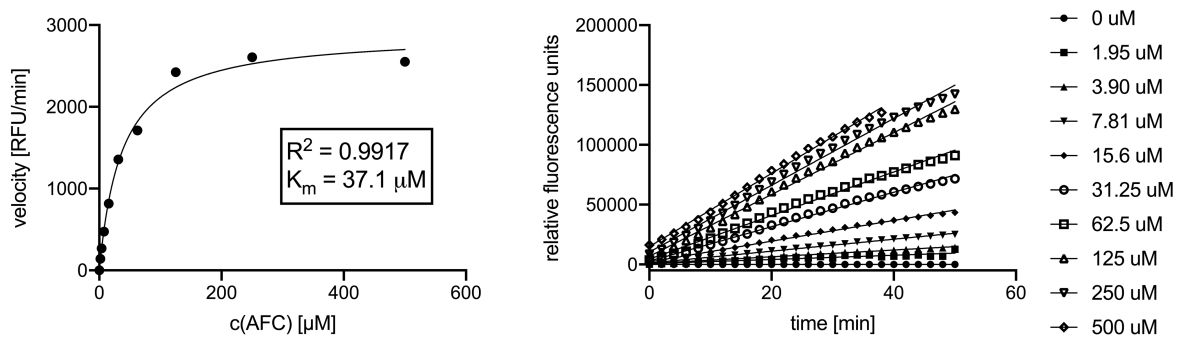
Figure 2.286. Saturation binding experiment (left) and representative fluorescence traces (right) of the fluorometric enzyme assay with Z-VDVAD-AFC and Casp2 (20 nM/well).
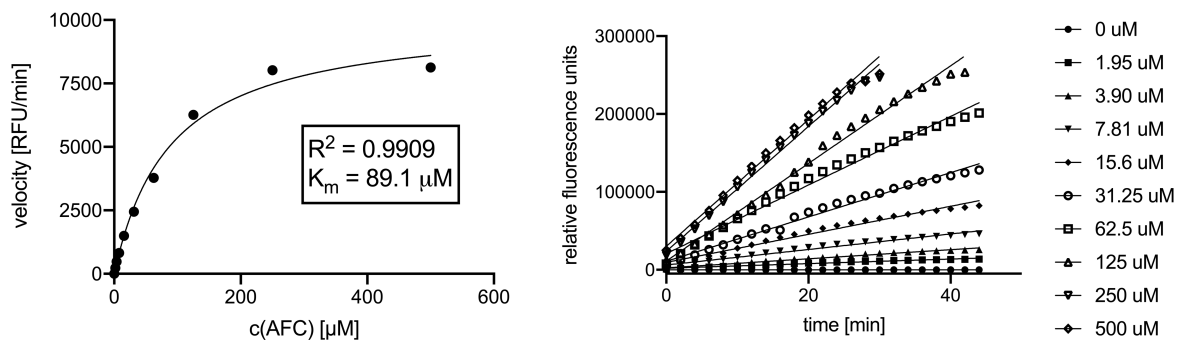
Figure 2.287. Saturation binding experiment (left) and representative fluorescence traces (right) of the fluorometric enzyme assay with Z-VDVAD-AFC and cpCasp2 (20 nM/well).
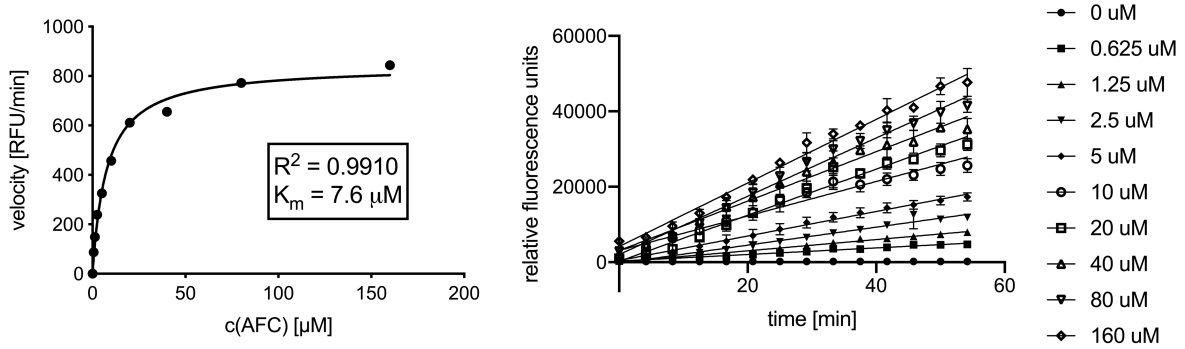
Figure 2.288. Saturation binding experiment (left) and representative fluorescence traces (right) of the fluorometric enzyme assay with AcDEVD-AFC and Casp3 (2 nM/well).
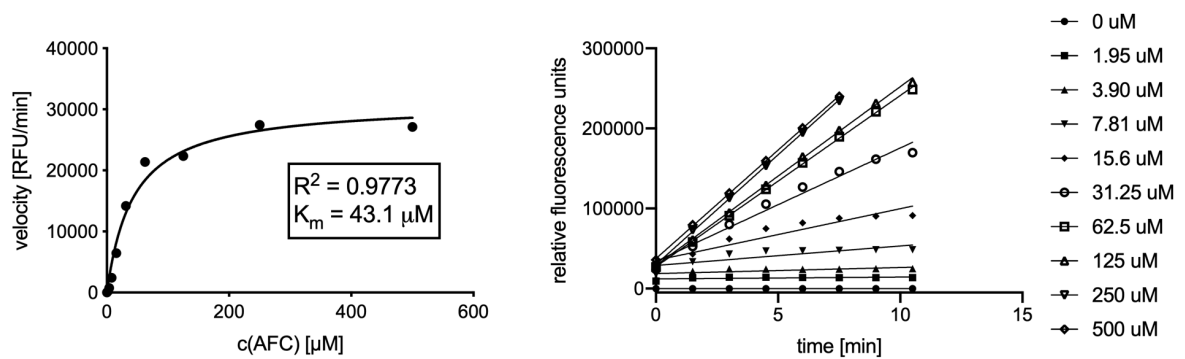
Figure 2.289. Saturation binding experiment (left) and representative fluorescence traces (right) of the fluorometric enzyme assay with Z-VEID-AFC and Casp6 (0.05 U/well).
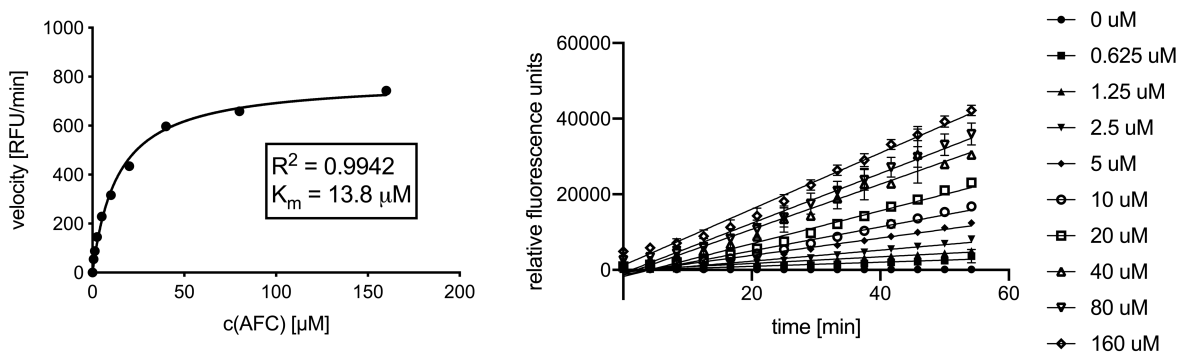
Figure 2.290. Saturation binding experiment (left) and representative fluorescence traces (right) of the fluorometric enzyme assay with AcDEVD-AFC and Casp7 (0.05 U/well).
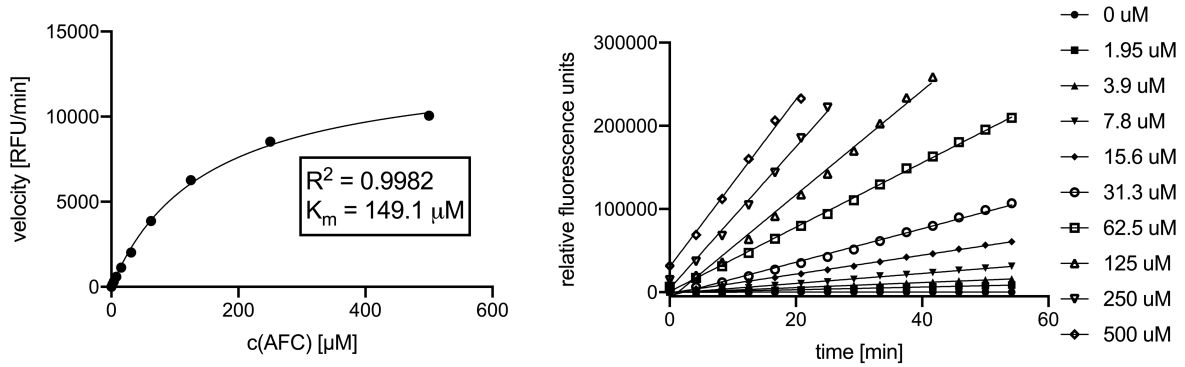
Figure 2.291. Saturation binding experiment (left) and representative fluorescence traces (right) of the fluorometric enzyme assay with AcLEHD-AFC and Casp9 (0.5 U/well).

2.7.6 Competition Binding Experiments of 2.008, 2.013, 2.014, 2.015, 2.059, 2.061, 2.064, 2.069, 2.093, 2.106 2.109, 2.114 in the Fluorometric Enzyme Assay
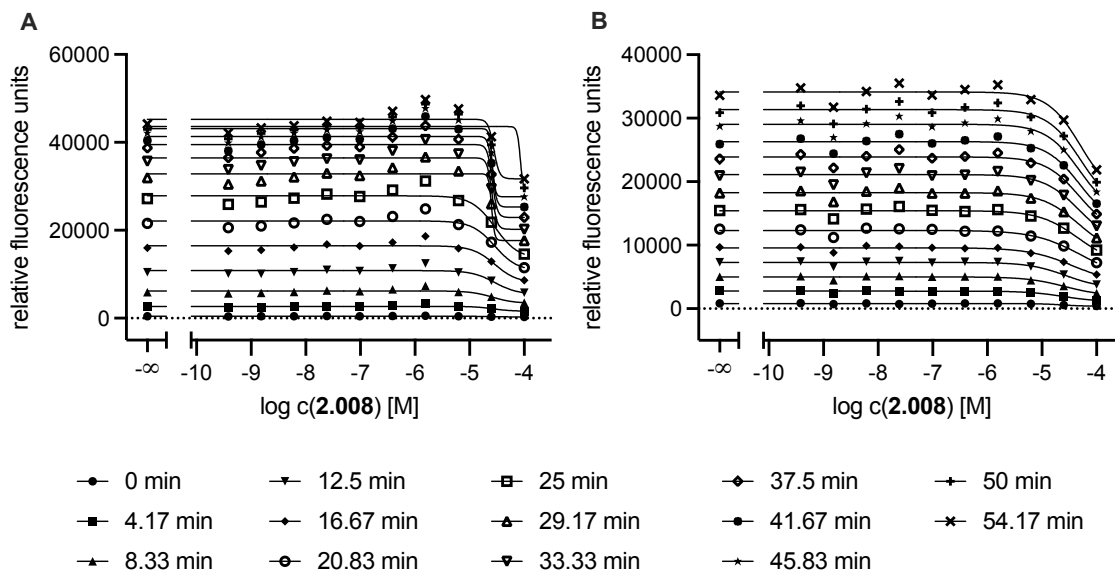
Figure 2.292. (**A**) Displacement curves from a representative competition binding experiment in the fluorometric enzyme assay of AcYVAD-AFC and AcYKPVD-CHO (**2.008**) with Casp1 (0.05 U/well) at different time points. (**B**) Displacement curves from a representative competition binding experiment in the fluorometric enzyme assay of Z-VDVAD-AFC and AcYKPVD-CHO (**2.008**) with Casp2 (20 nM/well) at different time points.
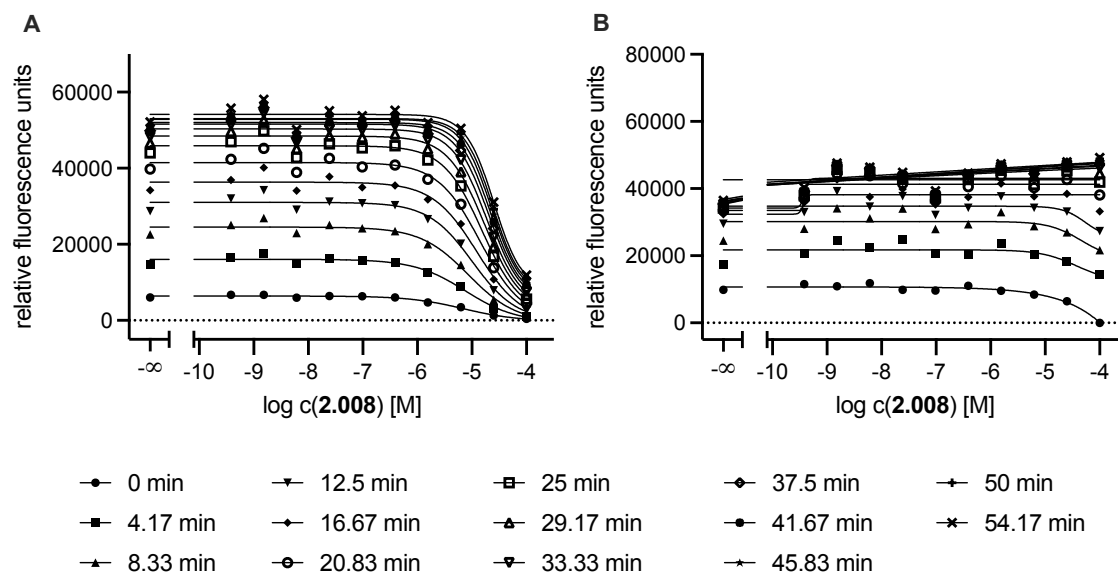
Figure 2.293. (**A**) Displacement curves from a representative competition binding experiment in the fluorometric enzyme assay of AcDEVD-AFC and AcYKPVD-CHO (**2.008**) with Casp3 (2 nM/well) at different time points. (**B**) Displacement curves from a representative competition binding experiment in the fluorometric enzyme assay of Z-VEID-AFC and AcYKPVD-CHO (**2.008**) with Casp6 (0.05 U/well) at different time points.
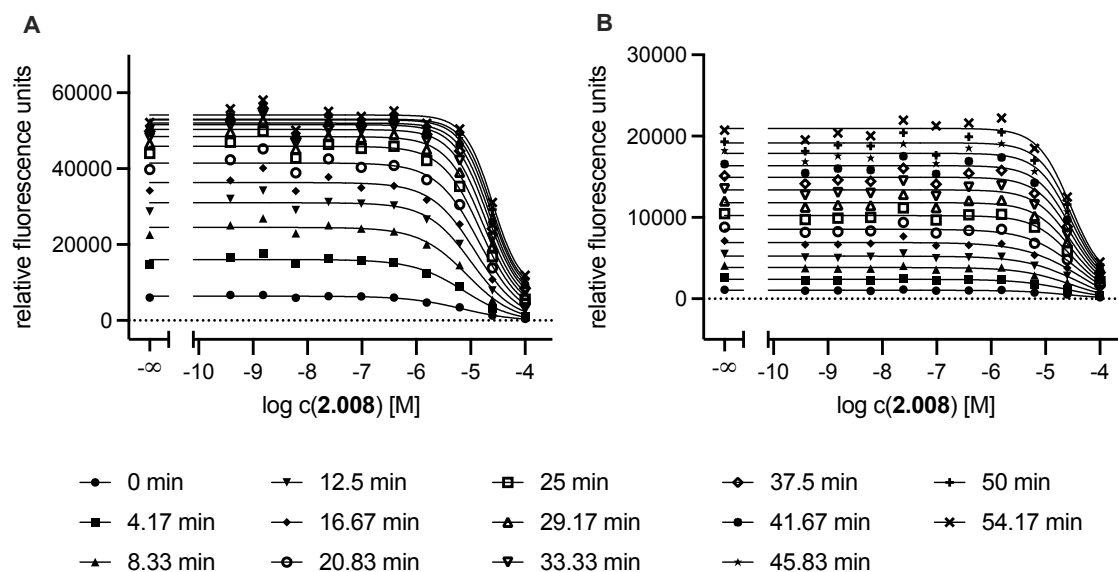
Figure 2.294. (**A**) Displacement curves from a representative competition binding experiment in the fluorometric enzyme assay of AcDEVD-AFC and AcYKPVD-CHO (**2.008**) with Casp7 (0.05 U/well) at different time points. (**B**) Displacement curves from a representative competition binding experiment in the fluorometric enzyme assay of AcLEHD-AFC and AcYKPVD-CHO (**2.008**) with Casp9 (0.5 U/well) at different time points.
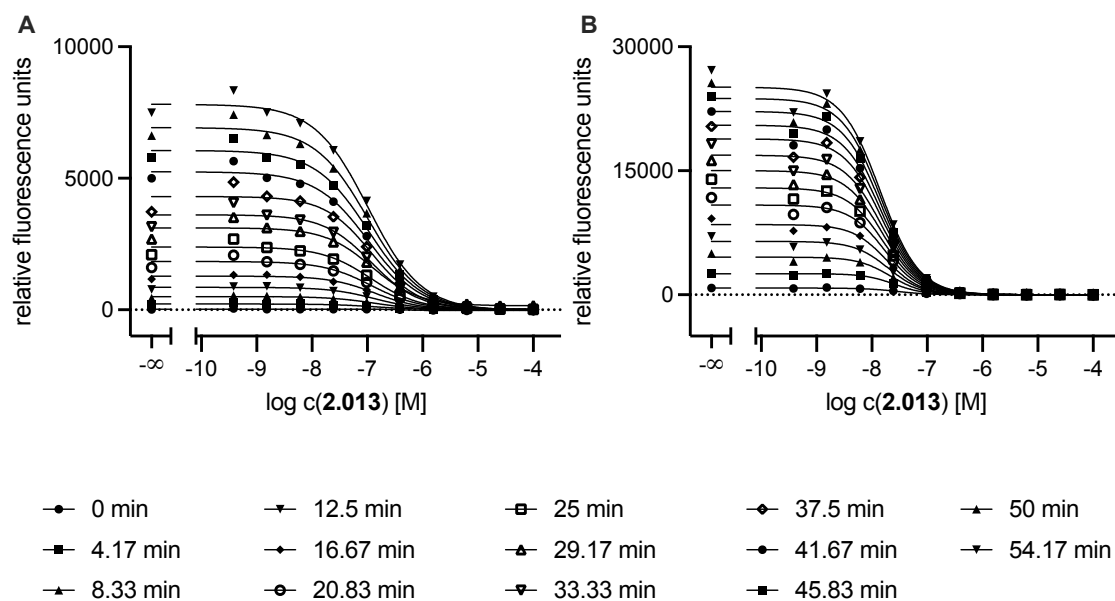
Figure 2.295. (**A**) Displacement curves from a representative competition binding experiment in the fluorometric enzyme assay of AcYVAD-AFC and AcLDVPD-CHO (**2.013**) with Casp1 (0.05 U/well) at different time points. (**B**) Displacement curves from a representative competition binding experiment in the fluorometric enzyme assay of Z-VDVAD-AFC and AcLDVPD-CHO (**2.013**) with Casp2 (20 nM/well) at different time points.
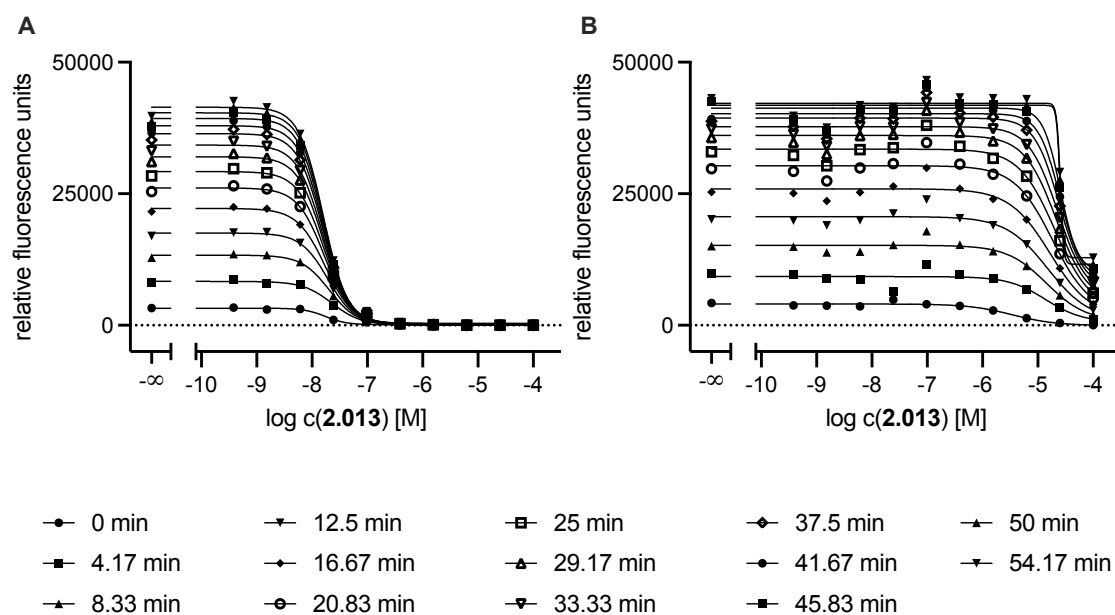
Figure 2.296. (**A**) Displacement curves from a representative competition binding experiment in the fluorometric enzyme assay of AcDEVD-AFC and AcLDVPD-CHO (**2.013**) with Casp3 (2 nM/well) at different time points. (**B**) Displacement curves from a representative competition binding experiment in the fluorometric enzyme assay of Z-VEID-AFC and AcLDVPD-CHO (**2.013**) with Casp6 (0.05 U/well) at different time points.
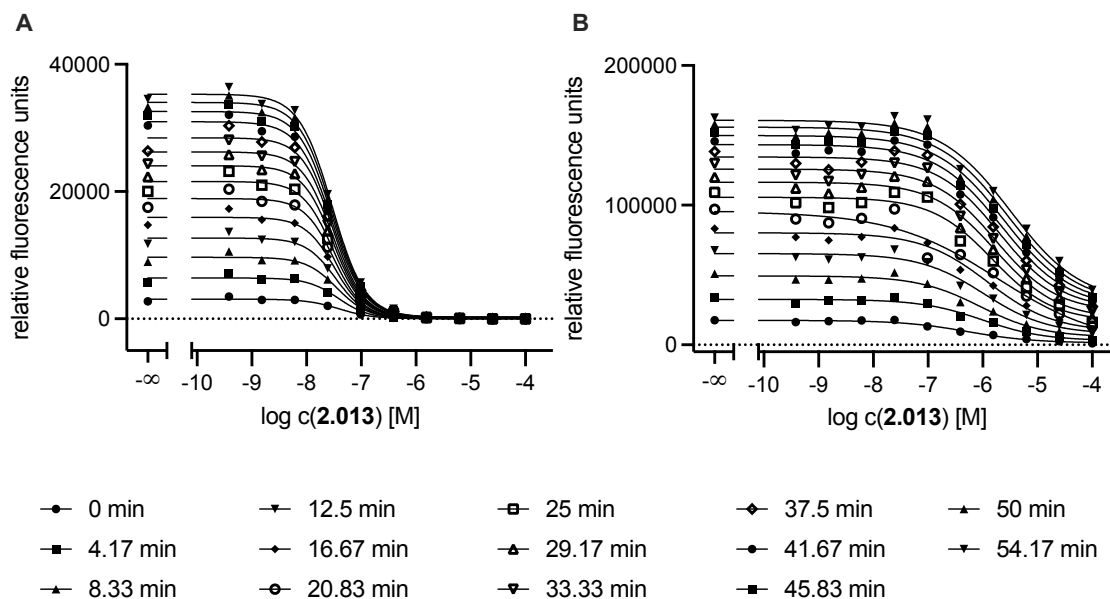
Figure 2.297. (**A**) Displacement curves from a representative competition binding experiment in the fluorometric enzyme assay of AcDEVD-AFC and AcLDVPD-CHO (**2.013**) with Casp7 (0.05 U/well) at different time points. (**B**) Displacement curves from a representative competition binding experiment in the fluorometric enzyme assay of AcLEHD-AFC and AcLDVPD-CHO (**2.013**) with Casp9 (0.5 U/well) at different time points.
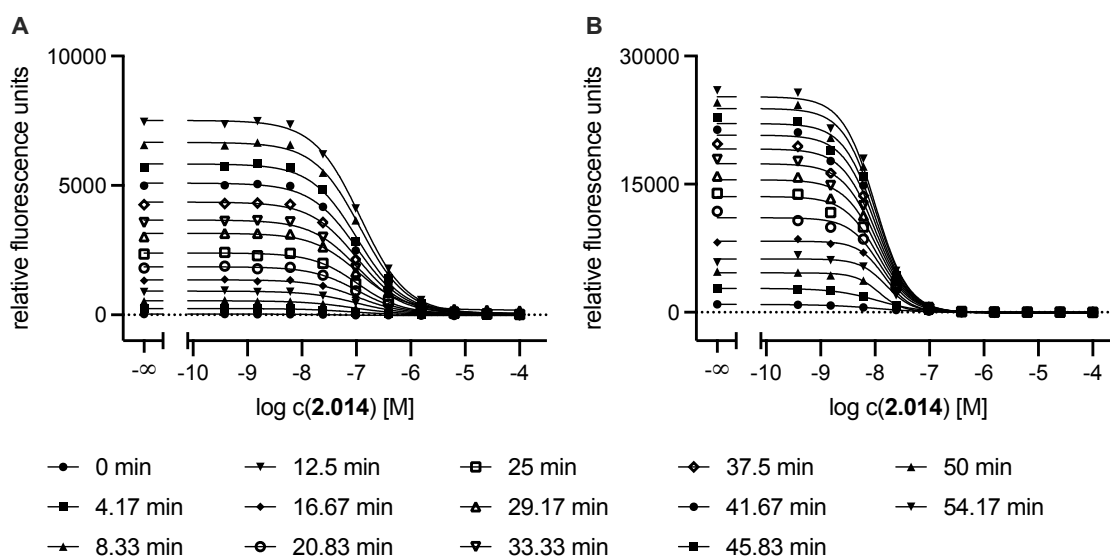
Figure 2.298. (**A**) Displacement curves from a representative competition binding experiment in the fluorometric enzyme assay of AcYVAD-AFC and AcFDVPD-CHO (**2.014**) with Casp1 (0.05 U/well) at different time points. (**B**) Displacement curves from a representative competition binding experiment in the fluorometric enzyme assay of Z-VDVAD-AFC and AcFDVPD-CHO (**2.014**) with Casp2 (20 nM/well) at different time points.
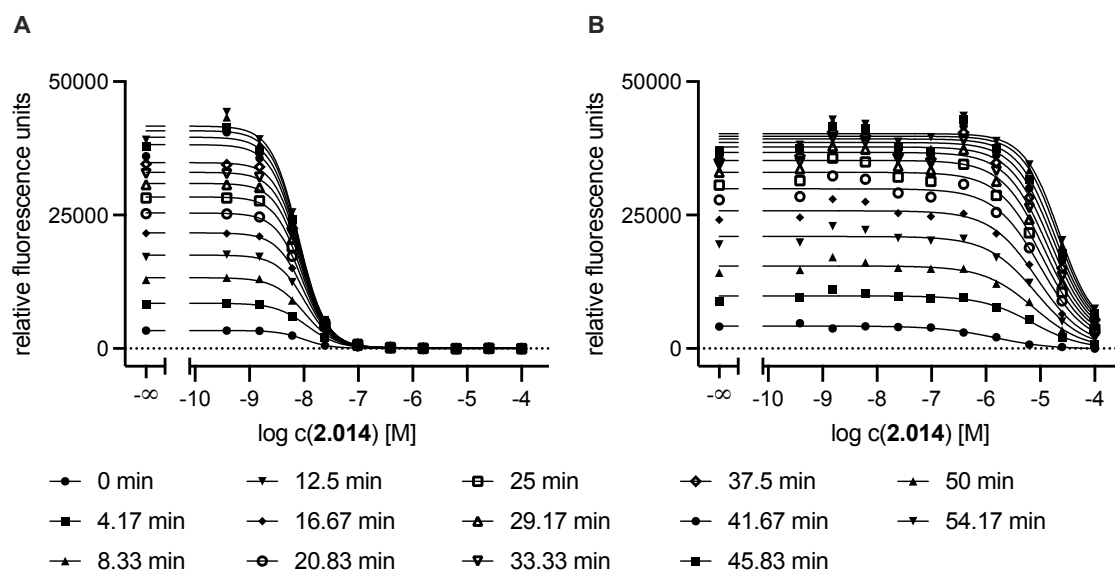
Figure 2.299. (**A**) Displacement curves from a representative competition binding experiment in the fluorometric enzyme assay of AcDEVD-AFC and AcFDVPD-CHO (**2.014**) with Casp3 (2 nM/well) at different time points. (**B**) Displacement curves from a representative competition binding experiment in the fluorometric enzyme assay of Z-VEID-AFC and AcFDVPD-CHO (**2.014**) with Casp6 (0.05 U/well) at different time points.
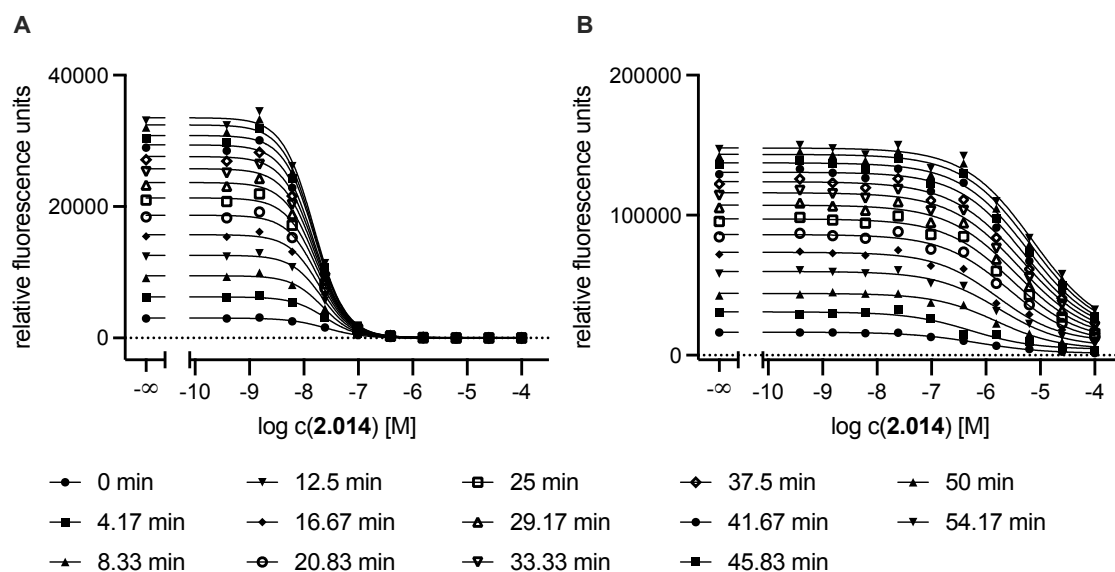
Figure 2.300. (**A**) Displacement curves from a representative competition binding experiment in the fluorometric enzyme assay of AcDEVD-AFC and AcFDVPD-CHO (**2.014**) with Casp7 (0.05 U/well) at different time points. (**B**) Displacement curves from a representative competition binding experiment in the fluorometric enzyme assay of AcLEHD-AFC and AcFDVPD-CHO (**2.014**) with Casp9 (0.5 U/well) at different time points.
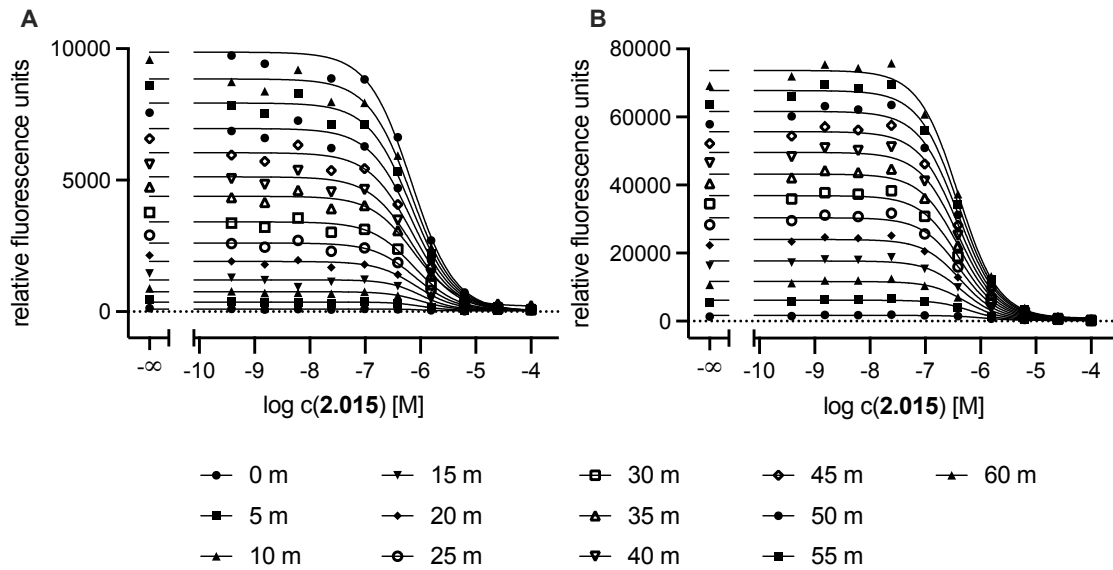
Figure 2.301. (**A**) Displacement curves from a representative competition binding experiment in the fluorometric enzyme assay of AcYVAD-AFC and AcITVKD-CHO (**2.015**) with Casp1 (0.05 U/well) at different time points. (**B**) Displacement curves from a representative competition binding experiment in the fluorometric enzyme assay of Z-VDVAD-AFC and AcITVKD-CHO (**2.015**) with Casp2 (20 nM/well) at different time points.
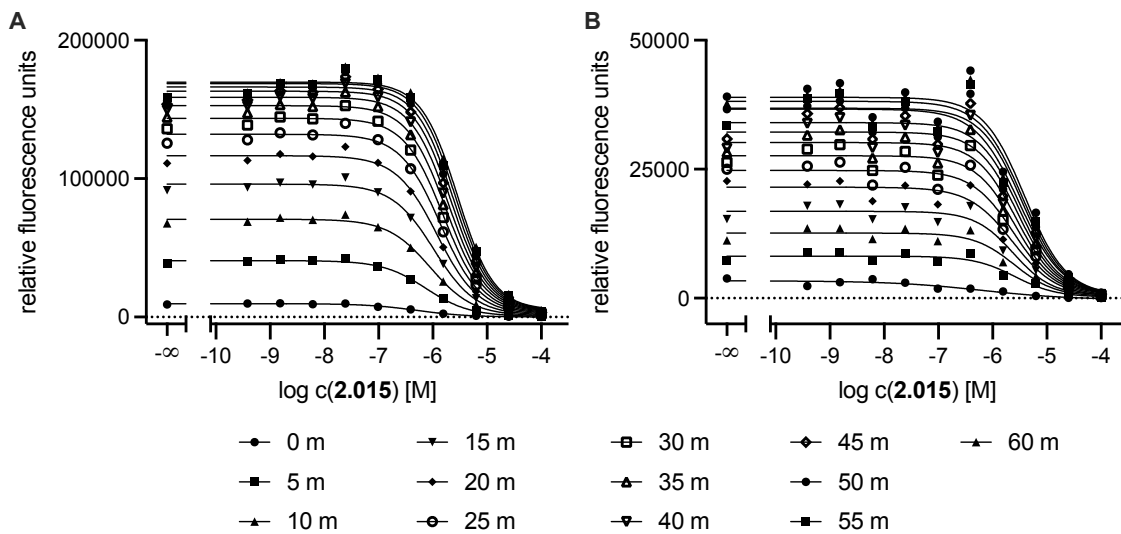
Figure 2.302. (**A**) Displacement curves from a representative competition binding experiment in the fluorometric enzyme assay of AcDEVD-AFC and AcITVKD-CHO (**2.015**) with Casp3 (2 nM/well) at different time points. (**B**) Displacement curves from a representative competition binding experiment in the fluorometric enzyme assay of Z-VEID-AFC and AcITVKD-CHO (**2.015**) with Casp6 (0.05 U/well) at different time points.
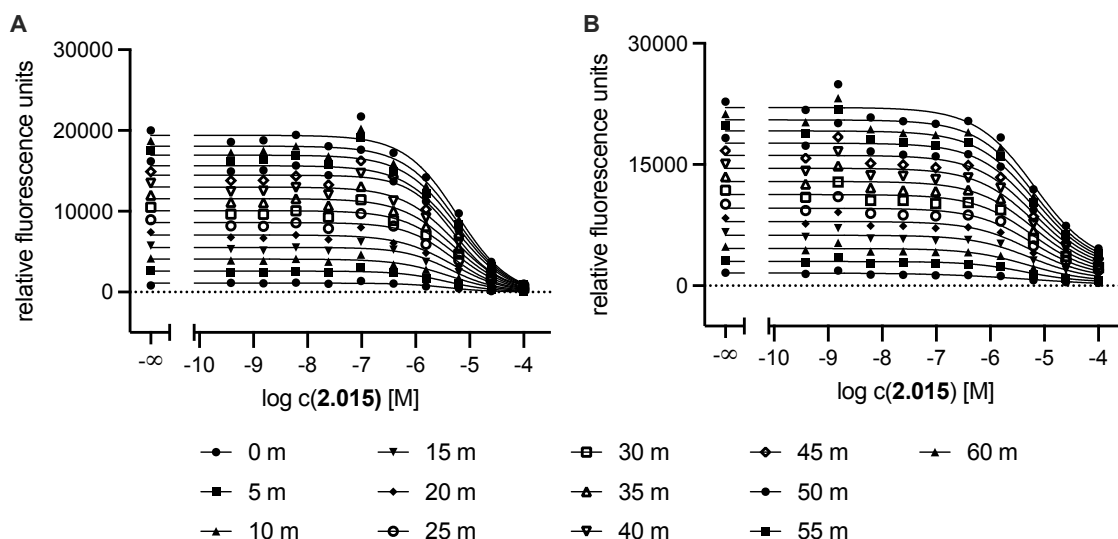
Figure 2.303. (**A**) Displacement curves from a representative competition binding experiment in the fluorometric enzyme assay of AcDEVD-AFC and AcITVKD-CHO (**2.015**) with Casp7 (0.05 U/well) at different time points. (**B**) Displacement curves from a representative competition binding experiment in the fluorometric enzyme assay of AcLEHD-AFC and AcITVKD-CHO (**2.015**) with Casp9 (0.5 U/well) at different time points.
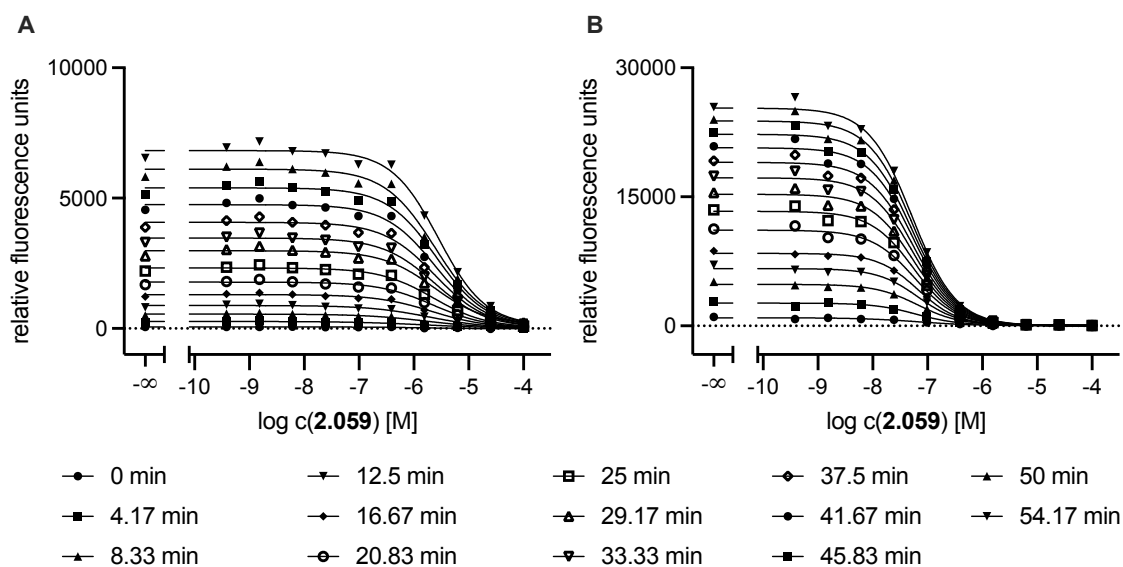
Figure 2.304. (**A**) Displacement curves from a representative competition binding experiment in the fluorometric enzyme assay of AcYVAD-AFC and AcVDKVD-CHO (**2.059**) with Casp1 (0.05 U/well) at different time points. (**B**) Displacement curves from a representative competition binding experiment in the fluorometric enzyme assay of Z-VDVAD-AFC and AcVDKVD-CHO (**2.059**) with Casp2 (20 nM/well) at different time points.
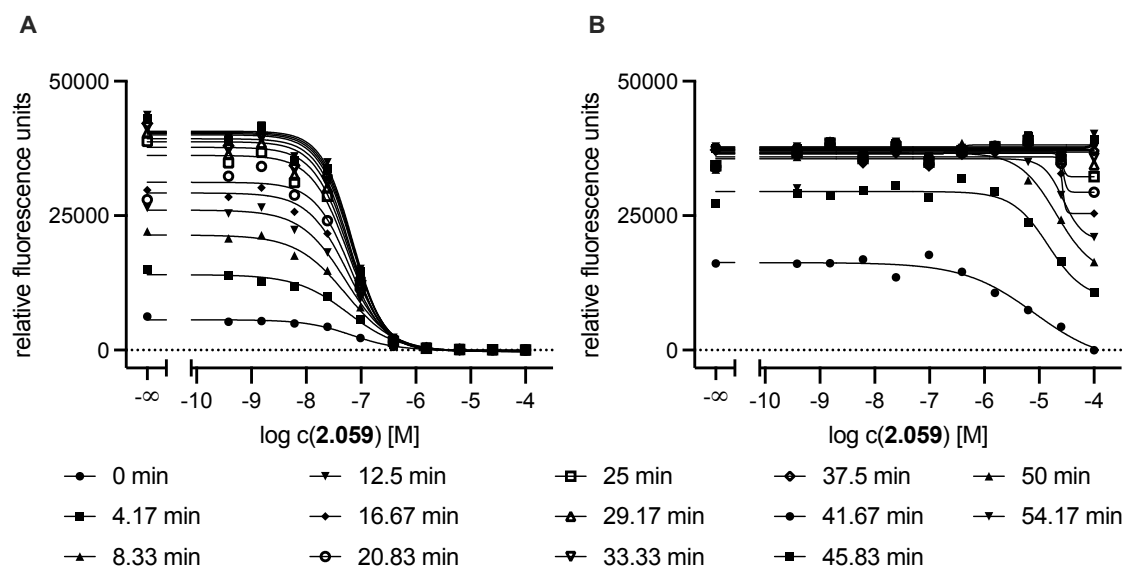
Figure 2.305. (**A**) Displacement curves from a representative competition binding experiment in the fluorometric enzyme assay of AcDEVD-AFC and AcVDKVD-CHO (**2.059**) with Casp3 (2 nM/well) at different time points. (**B**) Displacement curves from a representative competition binding experiment in the fluorometric enzyme assay of Z-VEID-AFC and AcVDKVD-CHO (**2.059**) with Casp6 (0.05 U/well) at different time points.
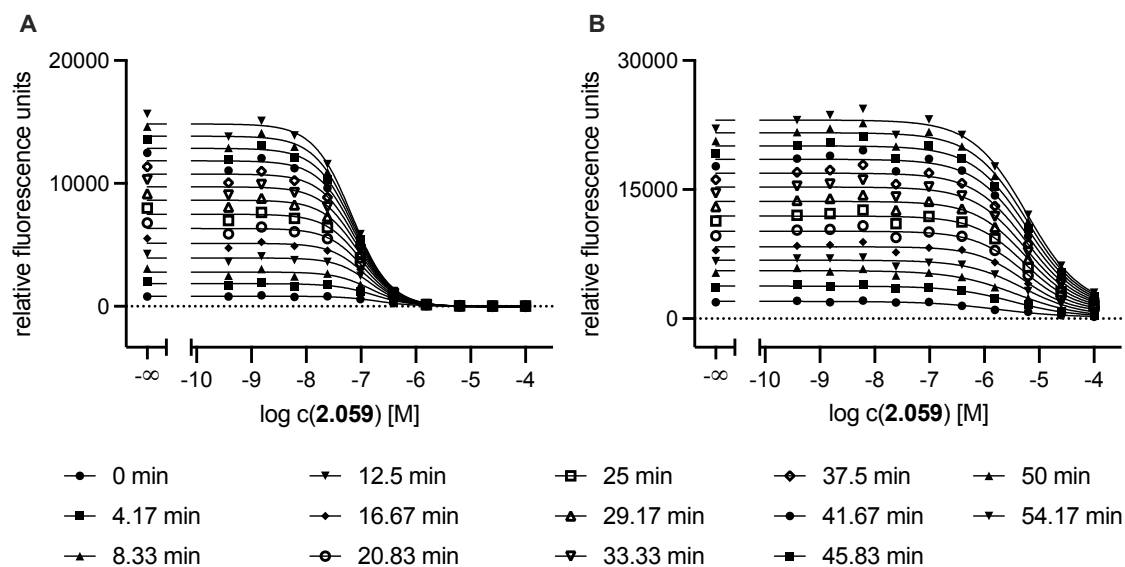
Figure 2.306. (**A**) Displacement curves from a representative competition binding experiment in the fluorometric enzyme assay of AcDEVD-AFC and AcVDKVD-CHO (**2.059**) with Casp7 (0.05 U/well) at different time points. (**B**) Displacement curves from a representative competition binding experiment in the fluorometric enzyme assay of AcLEHD-AFC and AcVDKVD-CHO (**2.059**) with Casp9 (0.5 U/well) at different time points.
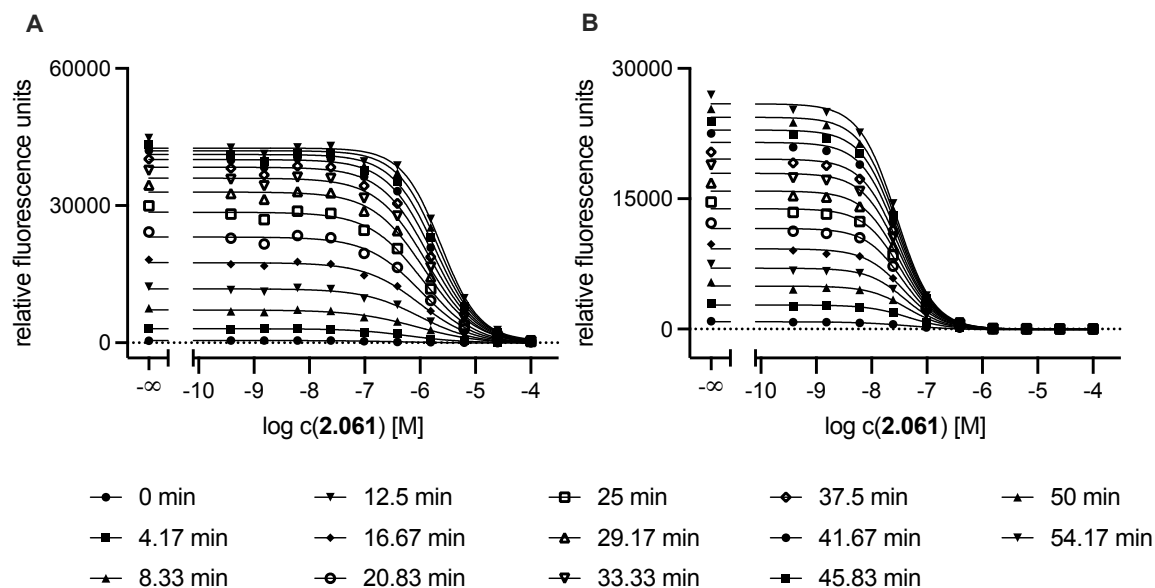
Figure 2.307. (**A**) Displacement curves from a representative competition binding experiment in the fluorometric enzyme assay of AcYVAD-AFC and AcVDVKD-CHO (**2.061**) with Casp1 (0.05 U/well) at different time points. (**B**) Displacement curves from a representative competition binding experiment in the fluorometric enzyme assay of Z-VDVAD-AFC and AcVDVKD-CHO (**2.061**) with Casp2 (20 nM/well) at different time points.
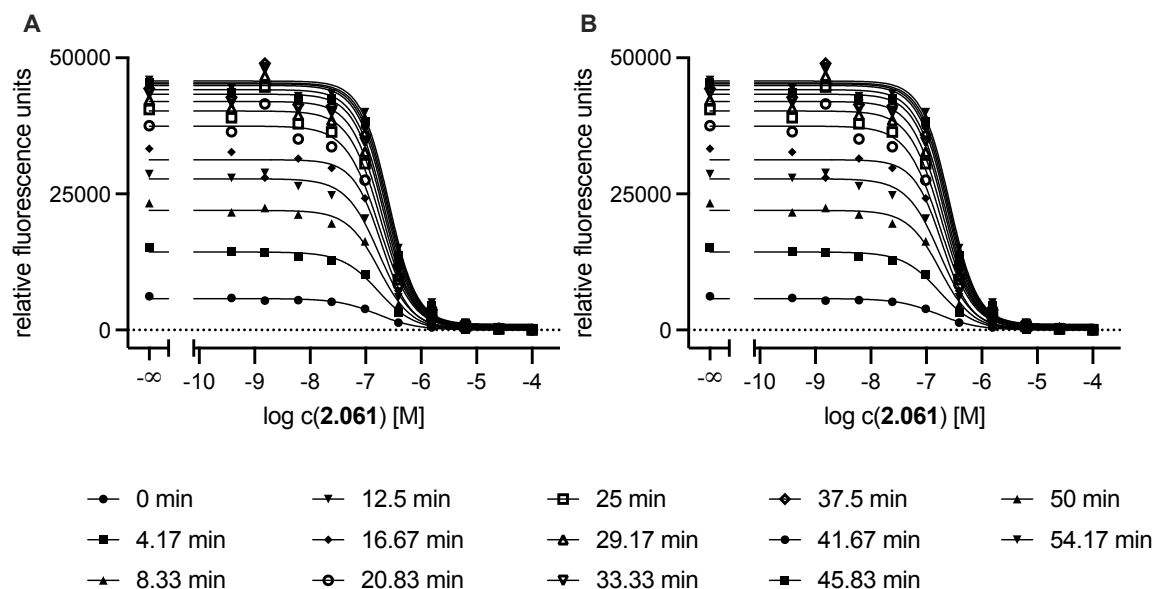
Figure 2.308. (**A**) Displacement curves from a representative competition binding experiment in the fluorometric enzyme assay of AcDEVD-AFC and AcVDVKD-CHO (**2.061**) with Casp3 (2 nM/well) at different time points. (**B**) Displacement curves from a representative competition binding experiment in the fluorometric enzyme assay of Z-VEID-AFC and AcVDVKD-CHO (**2.061**) with Casp6 (0.05 U/well) at different time points.
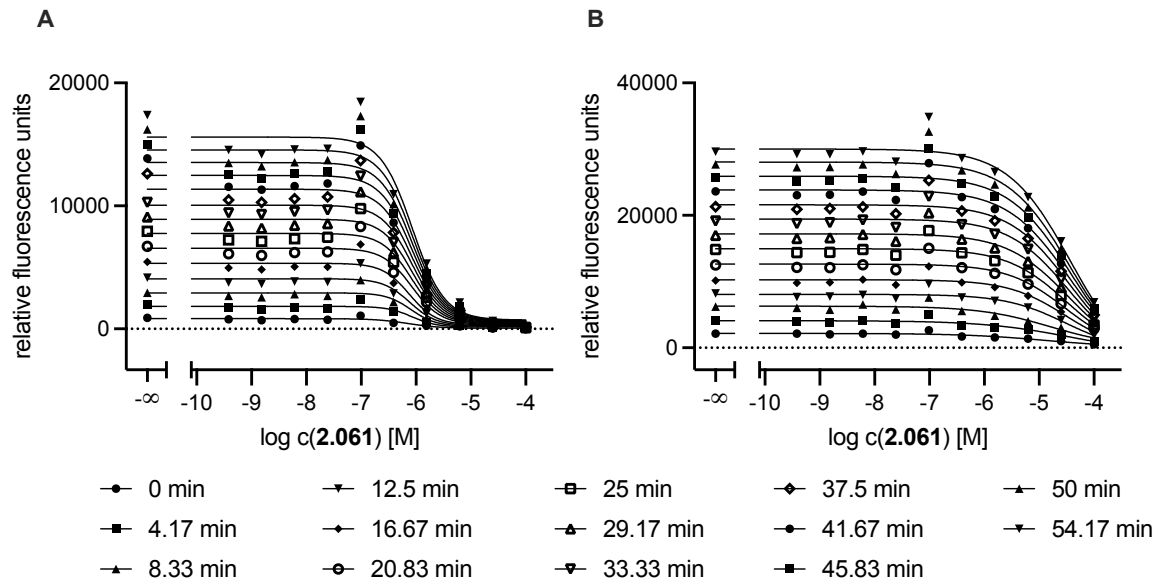
Figure 2.309. (**A**) Displacement curves from a representative competition binding experiment in the fluorometric enzyme assay of AcDEVD-AFC and AcVDVKD-CHO (**2.061**) with Casp7 (0.05 U/well) at different time points. (**B**) Displacement curves from a representative competition binding experiment in the fluorometric enzyme assay of AcLEHD-AFC and AcVDVKD-CHO (**2.061**) with Casp9 (0.5 U/well) at different time points.
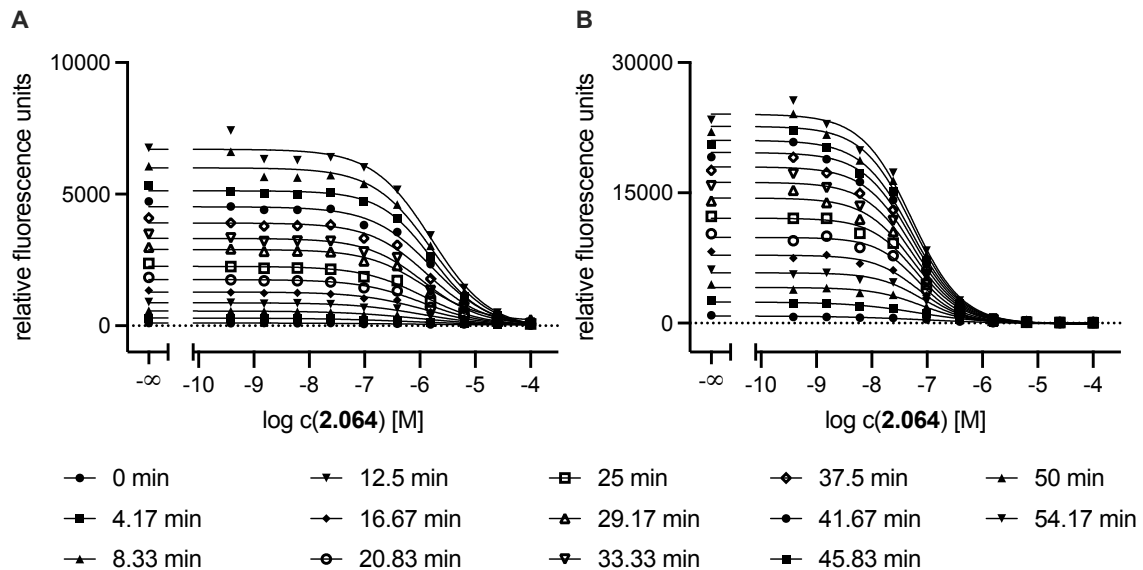
Figure 2.310. (**A**) Displacement curves from a representative competition binding experiment in the fluorometric enzyme assay of AcYVAD-AFC and AcVD(Dab)VD-CHO (**2.064**) with Casp1 (0.05 U/well) at different time points. (**B**) Displacement curves from a representative competition binding experiment in the fluorometric enzyme assay of Z-VDVAD-AFC and AcVD(Dab)VD-CHO (**2.064**) with Casp2 (20 nM/well) at different time points.
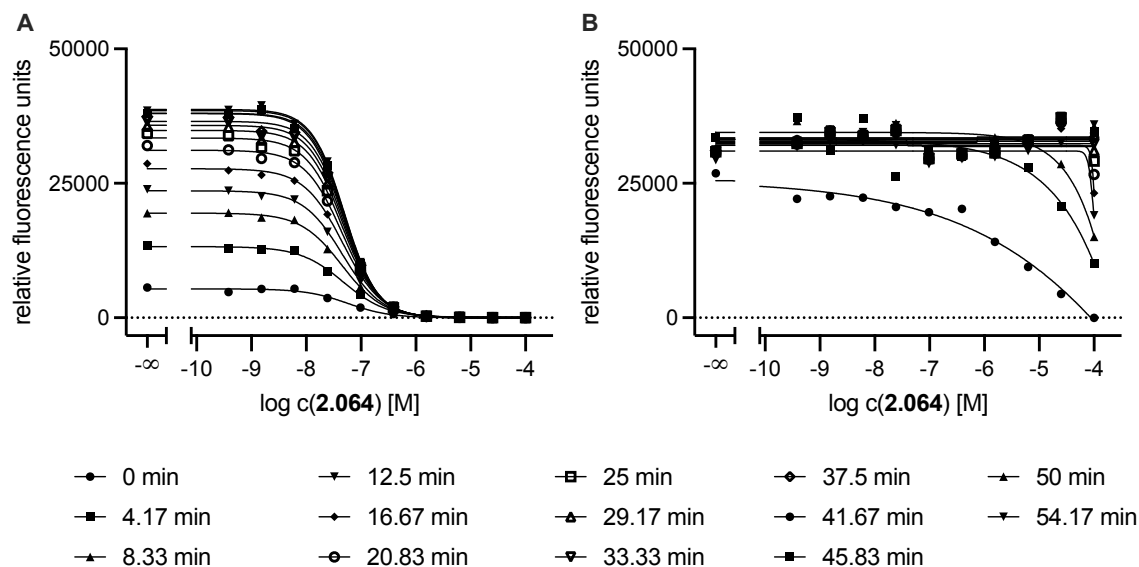
Figure 2.311. (**A**) Displacement curves from a representative competition binding experiment in the fluorometric enzyme assay of AcDEVD-AFC and AcVD(Dab)VD-CHO (**2.064**) with Casp3 (2 nM/well) at different time points. (**B**) Displacement curves from a representative competition binding experiment in the fluorometric enzyme assay of Z-VEID-AFC and AcVD(Dab)VD-CHO (**2.064**) with Casp6 (0.05 U/well) at different time points.
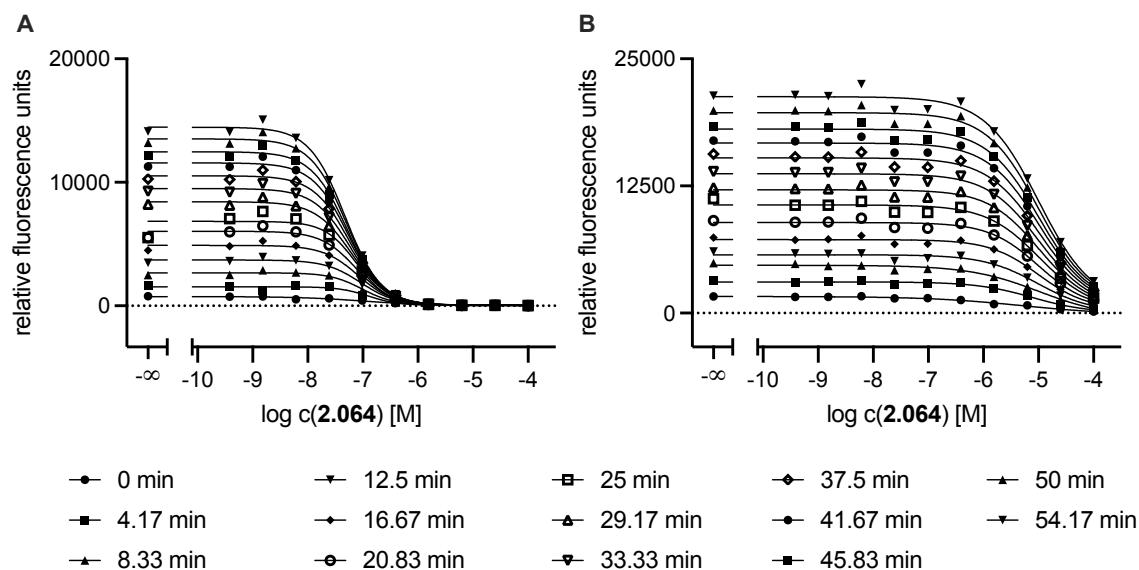
Figure 2.312. (**A**) Displacement curves from a representative competition binding experiment in the fluorometric enzyme assay of AcDEVD-AFC and AcVD(Dab)VD-CHO (**2.064**) with Casp7 (0.05 U/well) at different time points. (**B**) Displacement curves from a representative competition binding experiment in the fluorometric enzyme assay of AcLEHD-AFC and AcVD(Dab)VD-CHO (**2.064**) with Casp9 (0.5 U/well) at different time points.
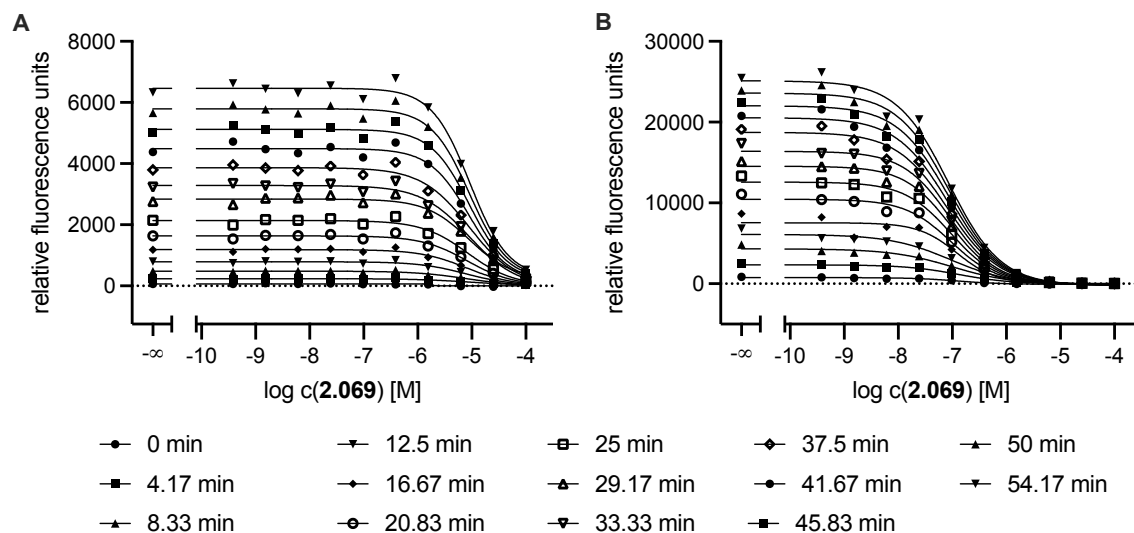
Figure 2.313. (**A**) Displacement curves from a representative competition binding experiment in the fluorometric enzyme assay of AcYVAD-AFC and AcVDV(Dab)D-CHO (**2.069**) with Casp1 (0.05 U/well) at different time points. (**B**) Displacement curves from a representative competition binding experiment in the fluorometric enzyme assay of Z-VDVAD-AFC and AcVDV(Dab)D-CHO (**2.069**) with Casp2 (20 nM/well) at different time points.
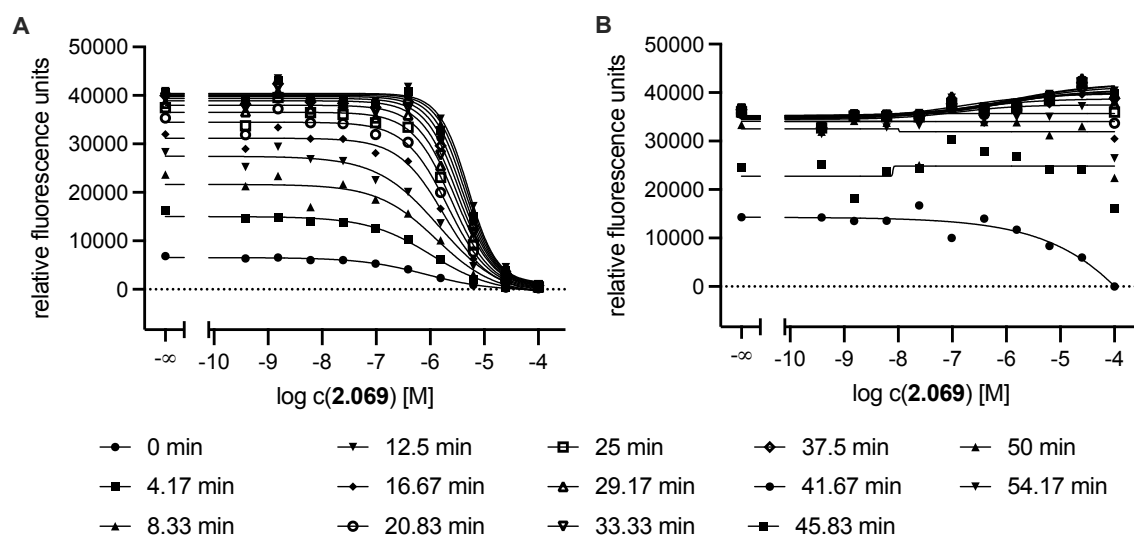
Figure 2.314. (**A**) Displacement curves from a representative competition binding experiment in the fluorometric enzyme assay of AcDEVD-AFC and AcVDV(Dab)D-CHO (**2.069**) with Casp3 (2 nM/well) at different time points. (**B**) Displacement curves from a representative competition binding experiment in the fluorometric enzyme assay of Z-VEID-AFC and AcVDV(Dab)D-CHO (**2.069**) with Casp6 (0.05 U/well) at different time points.
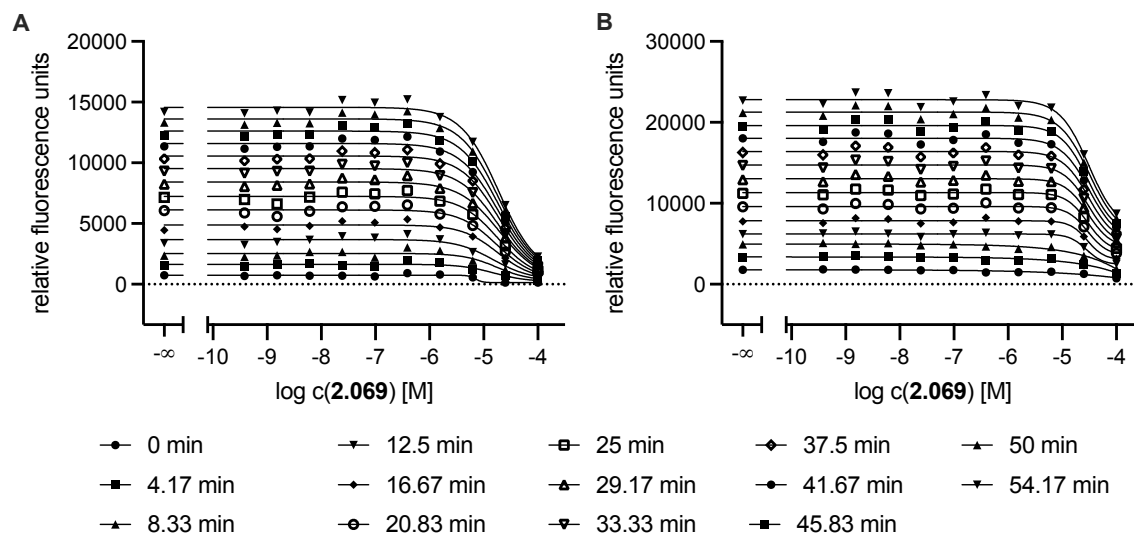
Figure 2.315. (**A**) Displacement curves from a representative competition binding experiment in the fluorometric enzyme assay of AcDEVD-AFC and AcVDV(Dab)D-CHO (**2.069**) with Casp7 (0.05 U/well) at different time points. (**B**) Displacement curves from a representative competition binding experiment in the fluorometric enzyme assay of AcLEHD-AFC and AcVDV(Dab)D-CHO (**2.069**) with Casp9 (0.5 U/well) at different time points.
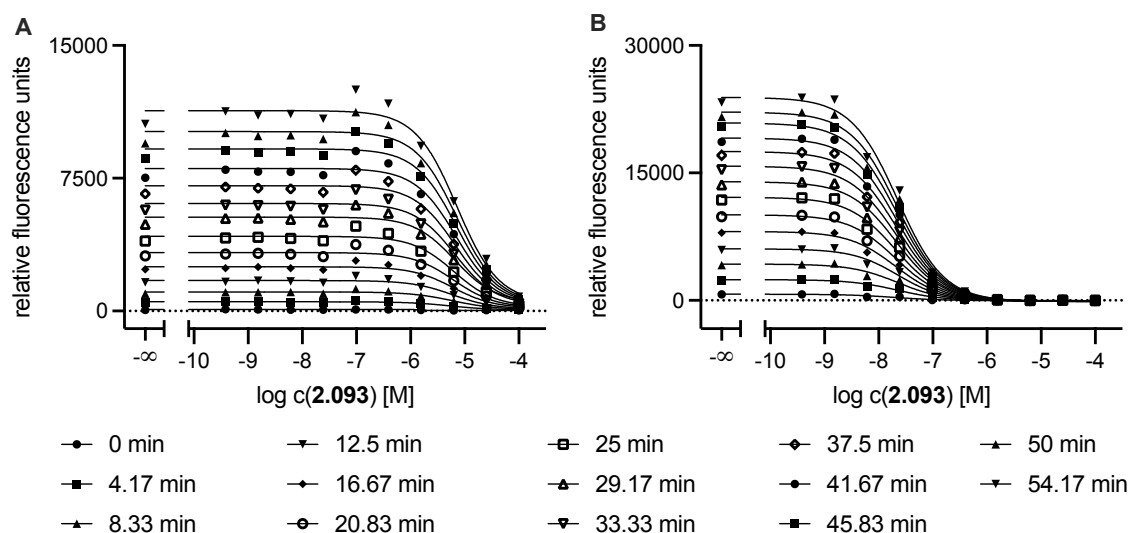
Figure 2.316. (**A**) Displacement curves from a representative competition binding experiment in the fluorometric enzyme assay of AcYVAD-AFC and AcVDV(*S*-Me-THIQ)D-CHO (**2.093**) with Casp1 (0.05 U/well) at different time points. (**B**) Displacement curves from a representative competition binding experiment in the fluorometric enzyme assay of Z-VDVAD-AFC and AcVDV(*S*-Me-THIQ)D-CHO (**2.093**) with Casp2 (20 nM/well) at different time points.
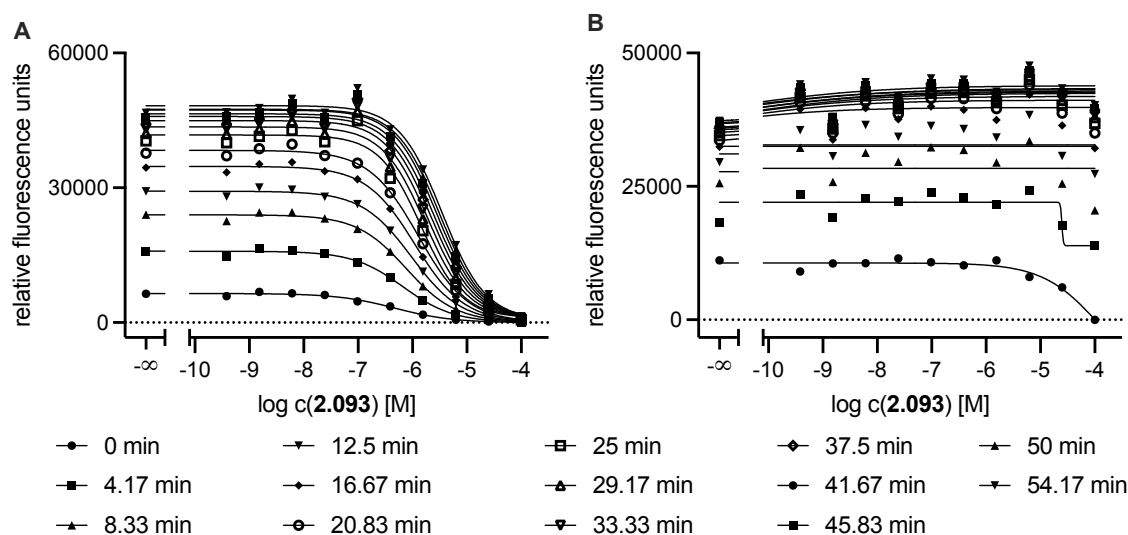
Figure 2.317. (**A**) Displacement curves from a representative competition binding experiment in the fluorometric enzyme assay of AcDEVD-AFC and AcVDV(*S*-Me-THIQ)D-CHO (**2.093**) with Casp3 (2 nM/well) at different time points. (**B**) Displacement curves from a representative competition binding experiment in the fluorometric enzyme assay of Z-VEID-AFC and AcVDV(*S*-Me-THIQ)D-CHO (**2.093**) with Casp6 (0.05 U/well) at different time points.
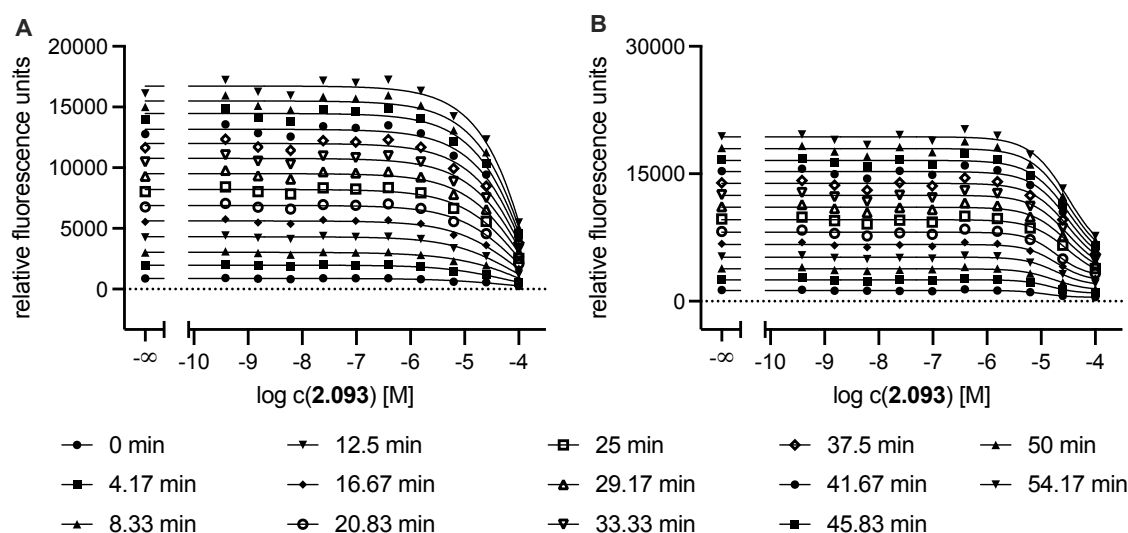
Figure 2.318. (**A**) Displacement curves from a representative competition binding experiment in the fluorometric enzyme assay of AcDEVD-AFC and AcVDV(*S*-Me-THIQ)D-CHO (**2.093**) with Casp7 (0.05 U/well) at different time points. (**B**) Displacement curves from a representative competition binding experiment in the fluorometric enzyme assay of AcLEHD-AFC and AcVDV(*S*-Me-THIQ)D-CHO (**2.093**) with Casp9 (0.5 U/well) at different time points.
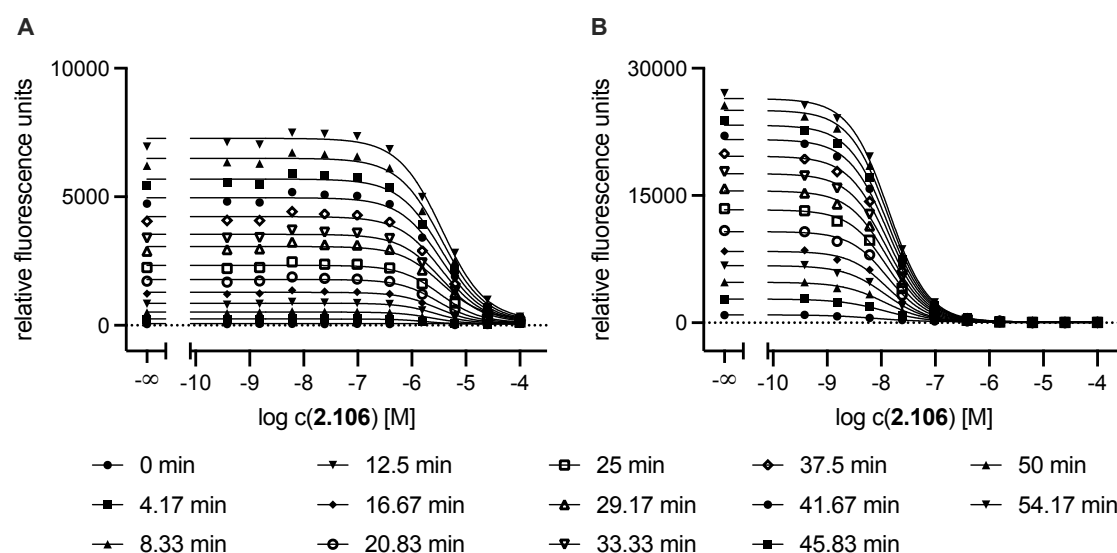
Figure 2.319. (**A**) Displacement curves from a representative competition binding experiment in the fluorometric enzyme assay of AcYVAD-AFC and Idc(hE)V(*S*-Me-THIQ)D-CN (**2.106**) with Casp1 (0.05 U/well) at different time points. (**B**) Displacement curves from a representative competition binding experiment in the fluorometric enzyme assay of Z-VDVAD-AFC and Idc(hE)V(*S*-Me-THIQ)D-CN (**2.106**) with Casp2 (20 nM/well) at different time points.
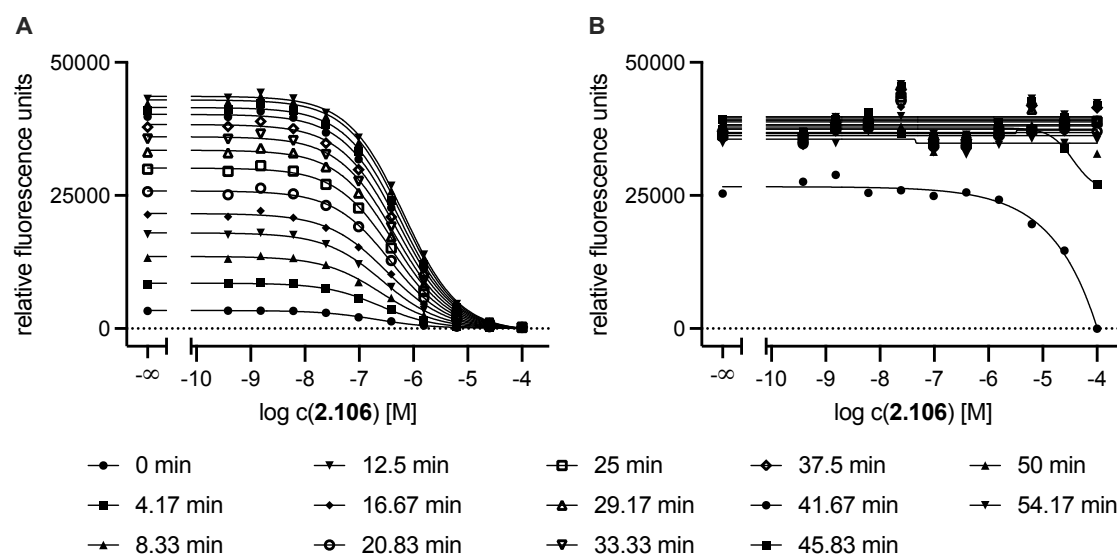
Figure 2.320. (**A**) Displacement curves from a representative competition binding experiment in the fluorometric enzyme assay of AcDEVD-AFC and Idc(hE)V(*S*-Me-THIQ)D-CN (**2.106**) with Casp3 (2 nM/well) at different time points. (**B**) Displacement curves from a representative competition binding experiment in the fluorometric enzyme assay of Z-VEID-AFC and Idc(hE)V(*S*-Me-THIQ)D-CN (**2.106**) with Casp6 (0.05 U/well) at different time points.
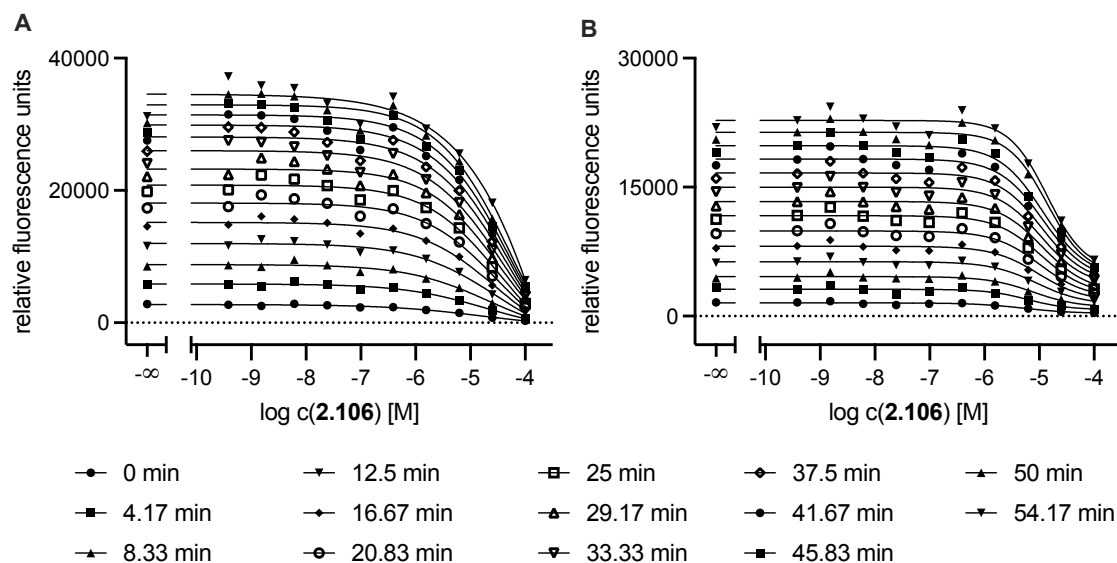
Figure 2.321. (**A**) Displacement curves from a representative competition binding experiment in the fluorometric enzyme assay of AcDEVD-AFC and Idc(hE)V(*S*-Me-THIQ)D-CN (**2.106**) with Casp7 (0.05 U/well) at different time points. (**B**) Displacement curves from a representative competition binding experiment in the fluorometric enzyme assay of AcLEHD-AFC and Idc(hE)V(*S*-Me-THIQ)D-CN (**2.106**) with Casp9 (0.5 U/well) at different time points.
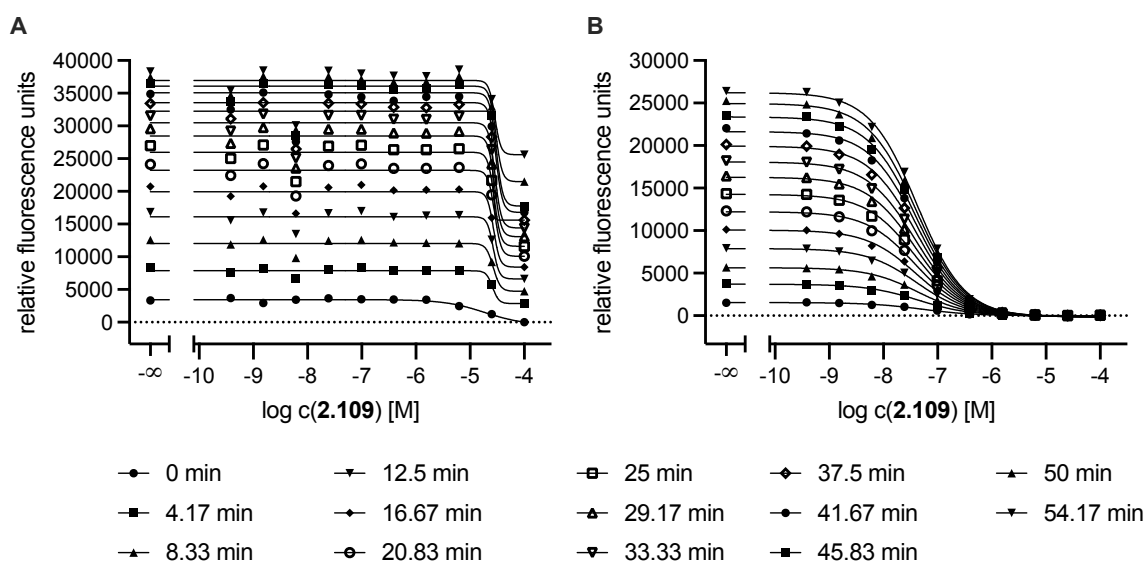
Figure 2.322. (A) Displacement curves from a representative competition binding experiment in the fluorometric enzyme assay of AcYVAD-AFC and Idc(hE)(BnT)(Dab)D-CHO (**2.109**) with Casp1 (0.05 U/well) at different time points. (**B**) Displacement curves from a representative competition binding experiment in the fluorometric enzyme assay of Z-VDVAD-AFC and Idc(hE)(BnT)(Dab)D-CHO (**2.109**) with cpCasp2 (20 nM/well) at different time points.
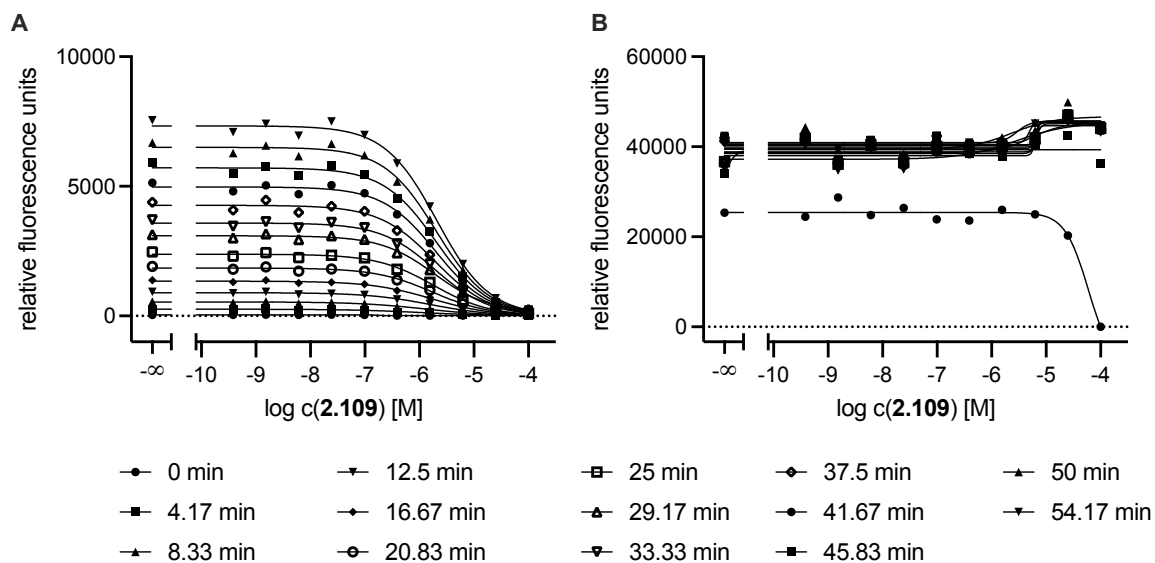
Figure 2.323. (**A**) Displacement curves from a representative competition binding experiment in the fluorometric enzyme assay of AcDEVD-AFC and Idc(hE)(BnT)(Dab)D-CHO (**2.109**) with Casp3 (2 nM/well) at different time points. (**B**) Displacement curves from a representative competition binding experiment in the fluorometric enzyme assay of Z-VEID-AFC and Idc(hE)(BnT)(Dab)D-CHO (**2.109**) with Casp6 (0.05 U/well) at different time points.
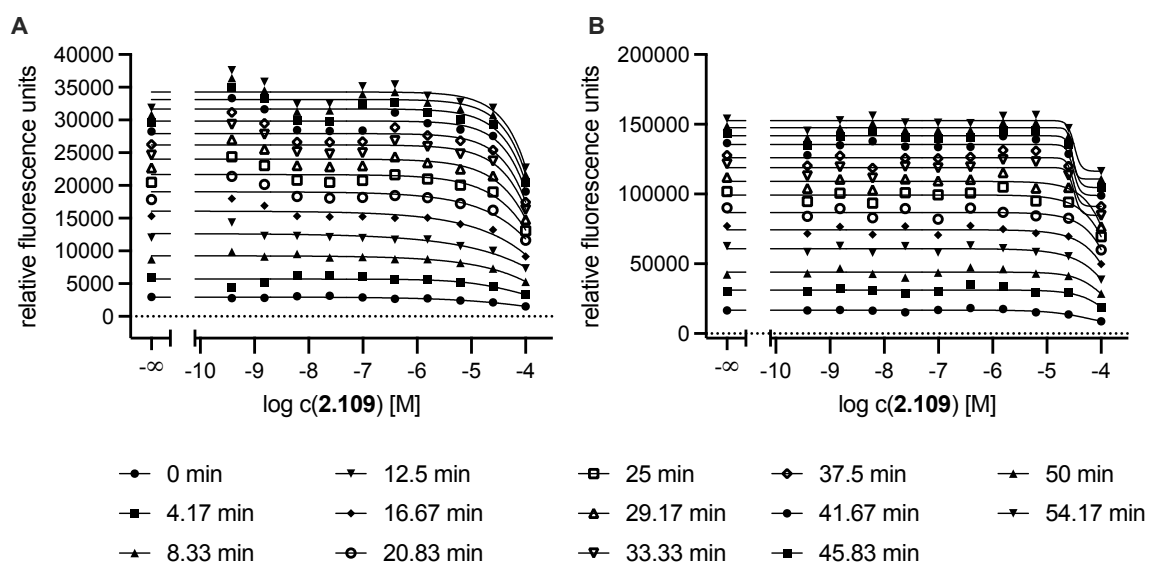
Figure 2.324. (**A**) Displacement curves from a representative competition binding experiment in the fluorometric enzyme assay of AcDEVD-AFC and Idc(hE)(BnT)(Dab)D-CHO (**2.109**) with Casp7 (0.05 U/well) at different time points. (**B**) Displacement curves from a representative competition binding experiment in the fluorometric enzyme assay of AcLEHD-AFC and Idc(hE)(BnT)(Dab)D-CHO (**2.109**) with Casp9 (0.5 U/well) at different time points.
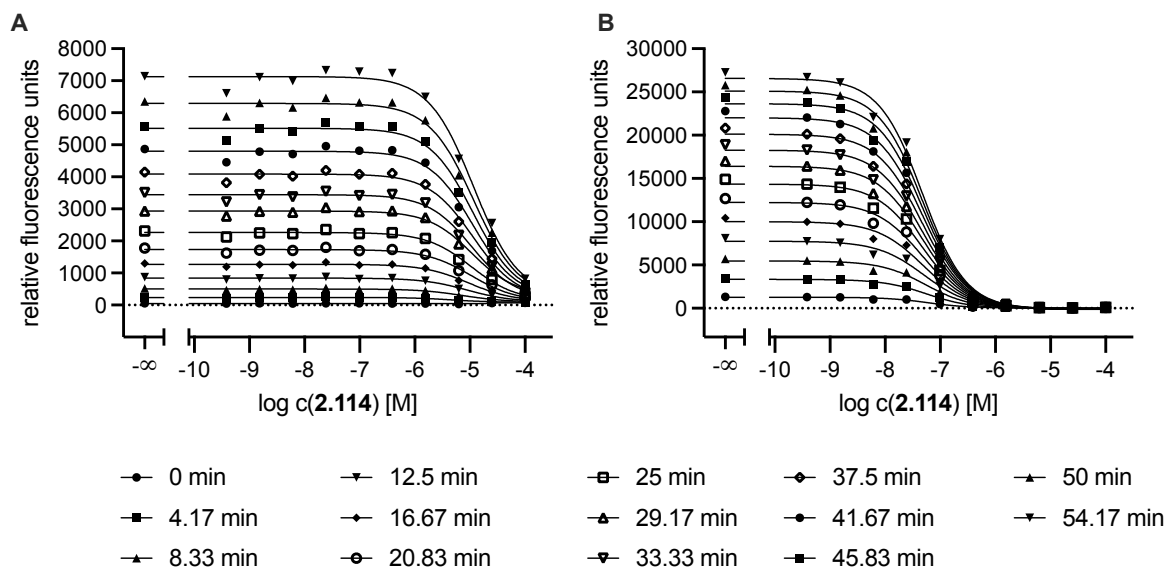
Figure 2.325. (**A**) Displacement curves from a representative competition binding experiment in the fluorometric enzyme assay of AcYVAD-AFC and Idc(hE)G(Dab)D-CHO (**2.114**) with Casp1 (0.05 U/well) at different time points. (**B**) Displacement curves from a representative competition binding experiment in the fluorometric enzyme assay of Z-VDVAD-AFC Idc(hE)G(Dab)D-CHO (**2.114**) with cpCasp2 (20 nM/well) at different time points.
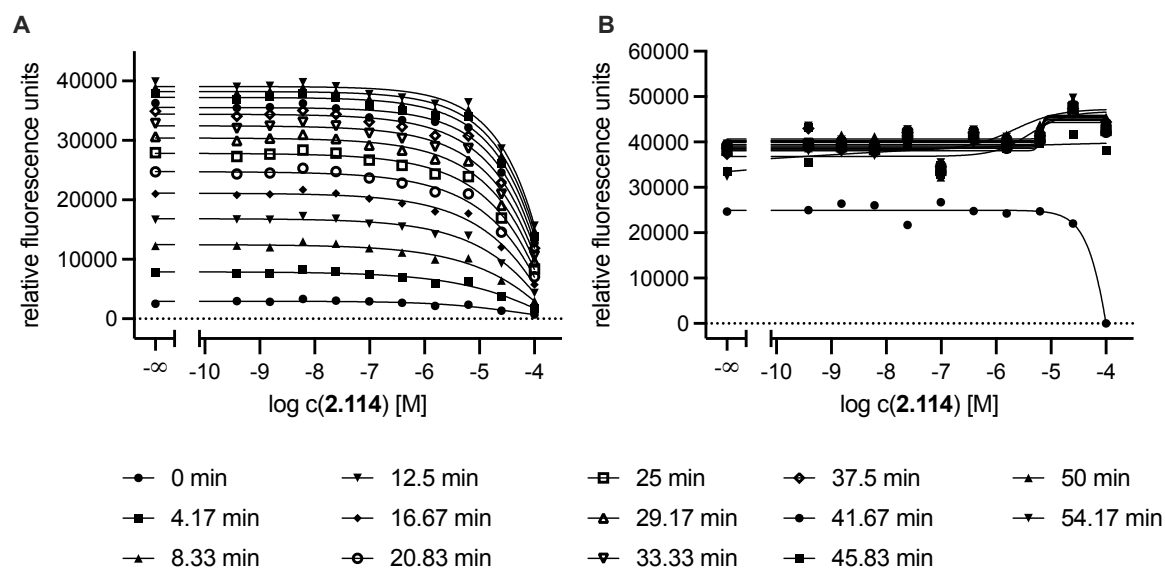
Figure 2.326. (**A**) Displacement curves from a representative competition binding experiment in the fluorometric enzyme assay of AcDEVD-AFC and Idc(hE)G(Dab)D-CHO (**2.114**) with Casp3 (2 nM/well) at different time points. (**B**) Displacement curves from a representative competition binding experiment in the fluorometric enzyme assay of Z-VEID-AFC and Idc(hE)G(Dab)D-CHO (**2.114**) with Casp6 (0.05 U/well) at different time points.
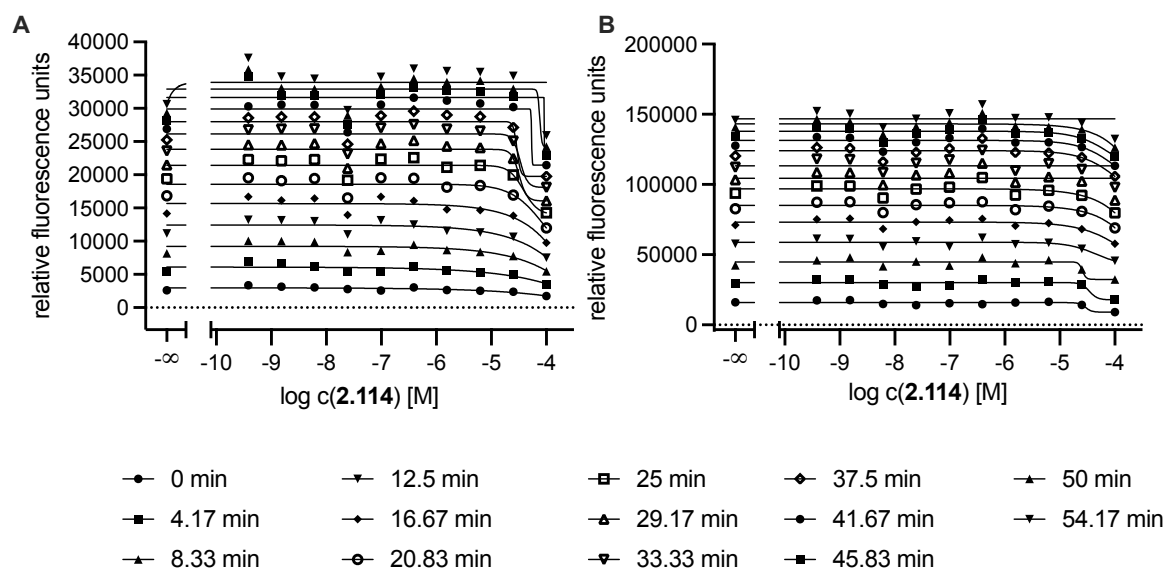
Figure 2.327. (**A**) Displacement curves from a representative competition binding experiment in the fluorometric enzyme assay of AcDEVD-AFC and Idc(hE)G(Dab)D-CHO (**2.114**) with Casp7 (0.05 U/well) at different time points. (**B**) Displacement curves from a representative competition binding experiment in the fluorometric enzyme assay of AcLEHD-AFC and Idc(hE)G(Dab)D-CHO (**2.114**) with Casp9 (0.5 U/well) at different time points.

2.7.7 Mutagenesis of Tau Protein

Table 2.16. Primers used for site-directed mutagenesis.

Human tau mutation	Forward primer	Reverse primer
K311D	5'-CAGTGTGCAAATAGTCTACGATCCAGTTGACCTGAGCAAG-3'	5'-CTTGCTCAGGTCAACTGGATCACTATTTGCACACTG-3'
P312V	5'-GTGTGCAAATAGTCTACAAAGTGGTTGACCTGAGCAAGGTGACC-3'	5'-GGTCACCTTGCTCAGGTCAACTTGTAGACTATTTGCACAC-3'
K311D P312V	5'-GTGTGCAAATAGTCTACGATGTGGTTGACCTGAGCAAGGTGACC-3'	5'-GGTCACCTTGCTCAGGTCAACTCGTAGACTATTTGCACAC-3'
Y310V K311D P312V	5'-GGCAGTGTGCAAATAGTCGTGGATGTGGTTGACCTGAGCAAG-3'	5'-CTTGCTCAGGTCAACCACATCACTATTTGCACACTGCC-3'
Y310V K311D P312V V313A	5'-CAAATAGTCGTGGATGTGGCGGACCTGAGCAAGGTGAC-3'	5'-GTCACCTTGCTCAGGTCCGCCCACGACTATTTG-3'

315

Chapter 3

Design and Biological Evaluation of Histamine H$_2$-Receptor Ligands

3 Design and Biological Evaluation of Histamine H$_2$-Receptor Ligands

3.1 Introduction GPCRs and Histamine

3.1.1 G-Protein Coupled Receptors

3.1.1.1 GPCRs: Overview and Classification

GPCRs (G-protein-coupled receptors) are a superfamily of biological receptors and represent the largest and most precisely investigated class of cell surface receptors. GPCRs mediate cellular response after a variety of extracellular stimuli via GTP-binding proteins. However, for a large number of GPCRs, G-protein-independent signaling pathways have been discovered.[157,158] GPCRs are responsible for regulating various (patho)physiological processes in the organism. Accordingly, targeting GPCRs is an established therapeutic approach for the treatment of numerous diseases (e.g., cardiovascular, gastrointestinal, metabolic, and CNS diseases).[159–161] About 800 different GPCRs have been discovered in humans.[158] They are subdivided into the class of chemosensory GPCRs (~ 450 reported GPCRs), which respond to external signals like odors, tastes, photons, and pheromones, and the class of endoGPCRs (~ 350 reported GPCRs), that respond to endogenous ligands, e.g., peptides, lipids, prostanoids, neurotransmitters, nucleosides, and nucleotides.[158,162,163] There are about 80-100 endoGPCRs with no identified endogenous ligand (so-called orphan receptors, e.g., GPR3).[164,165] Based on structural and phylogenetic differences, vertebrate GPCRs can be classified into the following groups (GRAFS system): Glutamate receptor family, Rhodopsin receptor family, Adhesion receptor family, Frizzled family, and Secretin receptor family.[158] The International Union of Basic and Clinical Pharmacology (IUPHAR) suggests an alternative classification (six different classes) for vertebrate and invertebrate GPCRs in their nomenclature guidelines: class A (rhodopsin-like), class B (secretin-like), class C (metabotropic glutamate-like), class D (pheromone receptors in yeasts), class E (cAMP receptors in nematodes), and class F (Frizzled (FZD$_{1-10}$) and Smoothened (SMO) GPCRs).[168] The main difference between the GRAFS classification and the A-F classification is the subdivision of class B into the Secretin family and the Adhesion family in the GRAFS system.[166–168] The human GPCR superfamily contains receptors of class A, B, C, and F.[169] The Class F GPCRs, including ten Frizzleds (FZD$_{1-10}$) and one Smoothened (SMO), remain one of the most enigmatic GPCR families in the human genome.[169,170] While the receptor activation in Class A, B, and C GPCRs is examined quite well, the activation of class

F receptors still needs to be elucidated.[169,170] The rhodopsin receptor family (class A) represents the largest class of GPCRs with about 680 GPCRs (endo- and csGPCRs) and is subdivided into α, β, γ, and δ.[168] Class A GPCRs can also be subdivided into olfactory (mainly orphan receptors) and non-olfactory (predominantly non-orphan receptors) receptors.[168] The secretin-like receptors (class B) contain about 15 members, and glutamate-like receptors (class C) about 22 members.[168] GPCRs possess a similar receptor design, with seven transmembrane-spanning α-helices (TM1-TM7), all consisting of 25 to 35 amino acids.[171,172] The membrane-spanning α-helices are jointed with three extracellular and three intracellular loops (IL1-3; EL1-3).[171,172] The N-terminus of GPCRs is located at the extracellular site and the C-terminus at the intracellular site of the plasma membrane.[171] Class B and C GPCRs are distinguished by more extended C- and N-termini. The ligand binding takes place at the extracellular site of the GPCR or in the lipid layer in binding pockets formed by the transmembrane helices. GPCRs interact with intracellular heterotrimeric G proteins at the C-terminus and at IL2 and IL3.[157,158,173–176]

3.1.1.2 G-Protein Signaling of GPCRs

G-proteins (guanine nucleotide-binding proteins) are composed of an α-subunit, a β-subunit, and a γ-subunit. The binding of agonists to extracellular or transmembrane binding areas of the GPCR causes conformational changes in the intracellular domains of the GPCR, inducing the binding of inactive heterotrimeric G proteins to the C-terminus or to intracellular loops of the GPCR (cf. Figure 3.001). Subsequently, GDP is dissociated from the α-subunit of the inactive G protein, resulting in the formation of a ternary complex consisting of the agonist, receptor, and nucleotide-free G protein.[177,178] In the following, GTP binds to the Gα-subunit, leading to a conformational change that triggers the separation of the G protein from the ternary complex and the dissociation of the Gα-GTP-subunit from the G$\beta\gamma$ heterodimer (cf. Figure 3.001). Then the cellular transduction of the GPCR is initiated by the interaction of the Gα-GTP-subunit and the G$\beta\gamma$-subunit with a multitude of signal-effector proteins (cf. Figure 3.001). The Gα-GTP-subunit regulates effector proteins such as adenylate cyclase, phospholipase C-β, and Rho guanine nucleotide exchange factor. The G$\beta\gamma$ heterodimer activates effector proteins like ion channels. The specific type of cellular signal transduction depends on the isoform of the Gα-subunit (e.g., G$_i\alpha$ and G$_s\alpha$)

involved.[163,179,180] Simultaneously, the conformational change decreases the affinity of the agonist for the GPCR, allowing the ligand to dissociate (cf. Figure 3.001). The biological effects induced by Gα-GTP are regulated by the intrinsic GTPase activity of Gα. GTP bound to Gα is hydrolyzed to GDP and phosphate, leading to the re-association of the Gα-subunit and Gβγ-subunit, allowing the next G-protein cycle (cf. Figure 3.001).[181–183] GTPase activity of the Gα-GTP subunit is additionally controlled by a family of proteins known as regulators of G-protein signal transduction (RGS).[181,182,184–186]
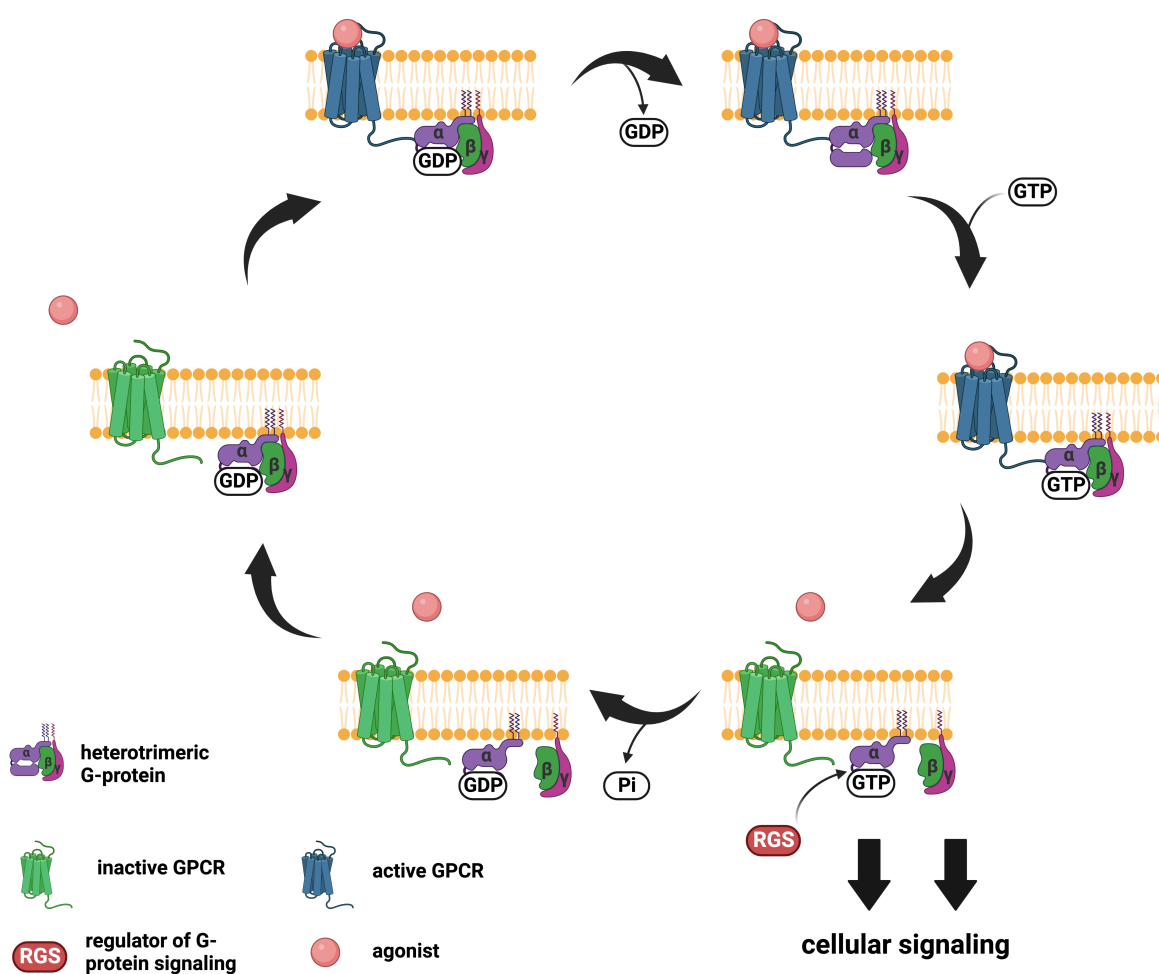
Figure 3.001. The G-protein cycle. Figure adapted from Figure 1.1 of Igel (2008)[181]. Figure created with BioRender.com.

There are four different groups of heterotrimeric G-proteins, each triggering individual signal transduction (cf. Figure 3.002). G-proteins of the G$_s$α family stimulate the activation of membrane-bound adenylate cyclases (AC), resulting in the formation of the second messenger cyclic adenosine monophosphate (cAMP), which in turn

activates protein kinase A (PKA). Protein kinase A can activate a variety of downstream effectors (e.g., metabolic enzymes, small G-proteins, and the transcription factor cAMP-response element-binding protein (CREB)) via phosphorylation (cf. Figure 3.002).[187–189]
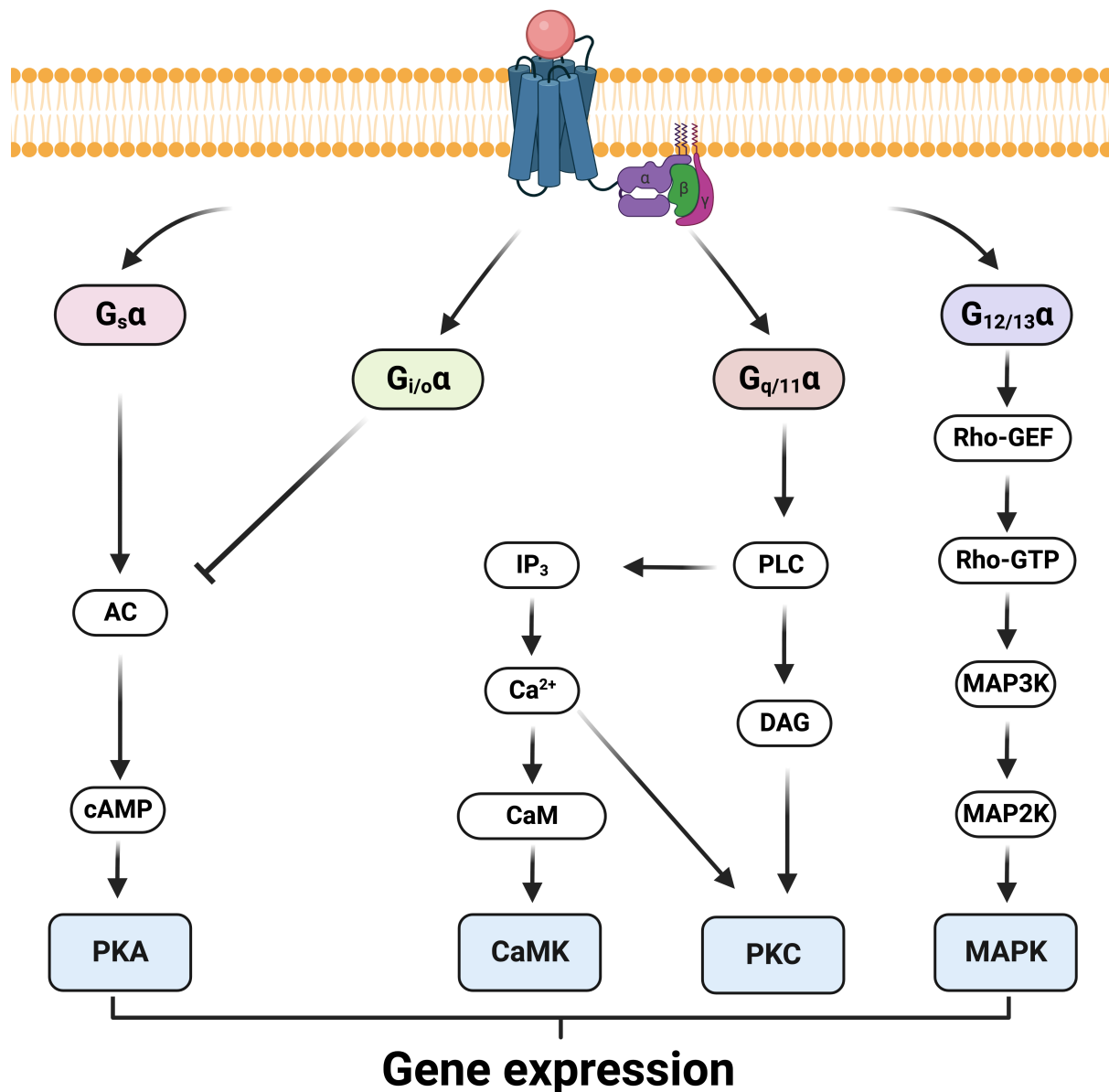
Figure 3.002. Signal transduction pathways of distinct G-proteins. AC: Adenylyl cyclase; cAMP: Cyclic adenosine monophosphate; PKA: Protein kinase A; PLC: Phospholipase C; IP$_3$: Inositol trisphosphate; CaM: Calmodulin; CaMK: Ca^{2+}/calmodulin-dependent protein kinase; DAG: Diglyceride; PKC: Protein kinase C; Rho-GEF: Rho guanine nucleotide exchange factors; Rho-GTP: Rho-family GTPases; MAP3K: Mitogen-activated Protein (MAP) kinase kinase kinase; MAP2K: Mitogen-activated protein (MAP) kinase kinase; MAPK: Mitogen-activated protein (MAP) kinase. Figure adapted from Figure 1.2 of Pockes (2015)[173]. Figure created with BioRender.com.

G-proteins of the $G_{i}\alpha$ family induce the inhibition of membrane-bound adenylate cyclases (AC), resulting in the reduced production of cAMP and thereby impairing the cAMP-mediated effects (cf. Figure 3.002).[187,190,191] G-proteins of the $G_{q}\alpha$ family activate the phospholipase Cβ (PLCβ). Phospholipase Cβ catalyzes the formation of the second messenger's diacylglycerol (DAG) and inositol trisphosphate (IP_3) from phosphatidylinositol 4,5-bisphosphate.[192] Inositol trisphosphate binds to the inositol trisphosphate receptor, causing an increased cytosolic calcium concentration by releasing Ca^{2+} from the endoplasmic reticulum (ER).[187,193] Subsequently, calcium activates a variety of signaling proteins like Ca^{2+}/calmodulin dependent protein kinases (CaMK), protein kinase C (PKC), and several transcription factors.[187,194] Diacylglycerol enables protein kinase C (PKC), protein kinase D (PKD), the DAG kinases, and the MRCK proteins (cf. Figure 3.002).[187,195,196] $G_{12}\alpha$ and $G_{13}\alpha$ comprise the fourth family of G-proteins, which predominantly mediate their signal transduction cascade through the small GTPase Rho (cf. Figure 3.002).[187,197] A variety of distinct G-protein isoforms have been identified in mammals. For instance, 16 different isoforms have been discovered for the Gα-subunit, 5 different for the Gβ, and 12 for the Gγ-subunit. Receptor specificity of the G-protein is predominantly determined by the Gα-subunit.[187,198,199]

3.1.1.3 Arrestin

The arrestin family includes four isoforms (arrestin 1-4) which display high sequence homology. Arrestin 2 and 3 (also referred to as β-arrestin 1 and 2) are ubiquitously expressed cytosolic adaptor proteins of mammals, while arrestin 1 and 4 are exclusively located in the retina.[200] It was demonstrated that β-arrestin 1 and 2 co-act with a multitude of GPCRs and play a crucial role in receptor desensitization and trafficking.[201–203] Besides mediating the G-protein signal transduction, the binding of a ligand to the GPCR results in the activation of second messenger-dependent kinases and G protein-coupled receptor kinases (GRKs) (cf. Figure 3.003). These kinases phosphorylate the GPCR at serine or threonine residues at its third intracellular loop and/or its C-terminus,[204] which strengthens β-arrestin binding to the receptor (cf. Figure 3.003). β-Arrestin regulates the GPCR signaling by physically obstructing the G-protein binding site of the GPCR and by initiating the internalization of the receptor via clathrin-coated pits.[205–211] After endocytosis, the receptor can be recycled to the plasma membrane or degraded (cf. Figure 3.003).[212] β-Arrestin is not only known as a negative

regulator by the inhibition of the G-protein binding site and the endocytosis of the receptor for the G-protein mediated signaling pathway. Nowadays, β-arrestin is also known to mediate a variety of G-protein-independent signaling pathways on its own (cf. Figure 3.003).[213] The functions of arrestins are not only limited to receptor-bound arrestin but also to non-receptor-bound arrestin.[214] β-Arrestin recruits signaling molecules to the GPCRs and thereby connects the receptors to a multitude of pathways (e.g., MAPK cascades). Furthermore, β-arrestin regulates the activity of the transcription factors p53 and NF-κB by binding to IκBα and MDM2, respectively.[215–219] Moreover, β-arrestin 1 assembles in the nucleus and initiates the transcription of several genes by recruiting cofactors such as p300 and increasing histone acetylation.[220]
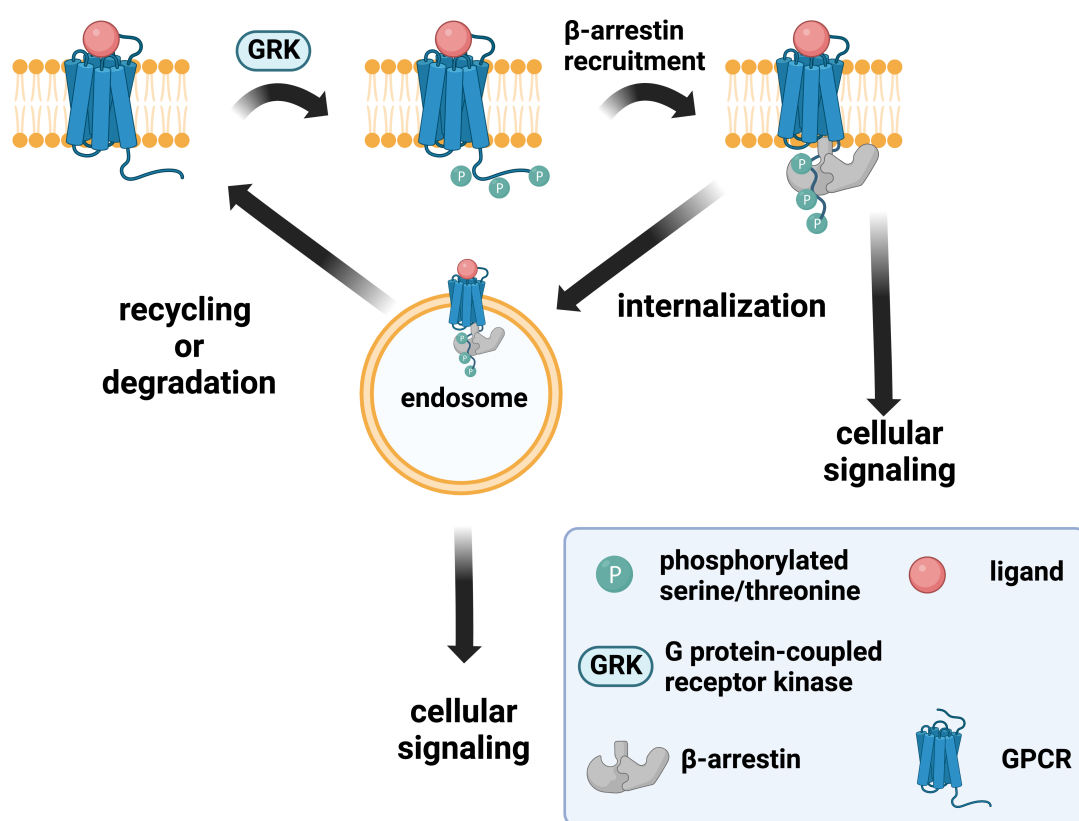
Figure 3.003. Scheme for the desensitization, internalization, and recycling of GPCRs promoted by β-arrestin. The binding of a ligand to the GPCR induces phosphorylation of the receptor by GRKs, leading to β-arrestin recruitment. β-arrestin initiates the endocytosis of agonist-occupied receptors by the formation of clathrin-coated pits. Subsequently, the clathrin-coated vesicles turn into endosomes. The GPCRs can be recycled for re-sensitization or degraded. β-arrestin also mediates cellular signaling. Figure adapted from Figure 1 of Ma and Pei (2006)[219] and Figure 3 of Luttrell (2008)[190]. Figure created with BioRender.com.

3.1.1.4 Receptor Binding Model of GPCRs, Classification of Ligands, and the Concept of Biased Signaling

In the classic ternary complex model, also referred to as two-state model (active state vs. inactive state), the cellular signaling of GPCRs depends on the conformation of the receptor. The active state of the GPCR interacts with the G-protein and induces signal transduction, while the inactive state is not able to mediate cellular signaling (cf. Figure 3.004B).[221] GPCRs are also capable of eliciting cellular signaling by a ligand-independent interaction of the receptor with the G-protein, also referred to as constitutive activity (cf. Figure 3.004B). This basal activity of the receptors resulted in the identification of inverse agonists.[221] GPCRs in the inactive state can also associate with G-proteins but are not able to exert cellular effects (cf. Figure 3.004B).
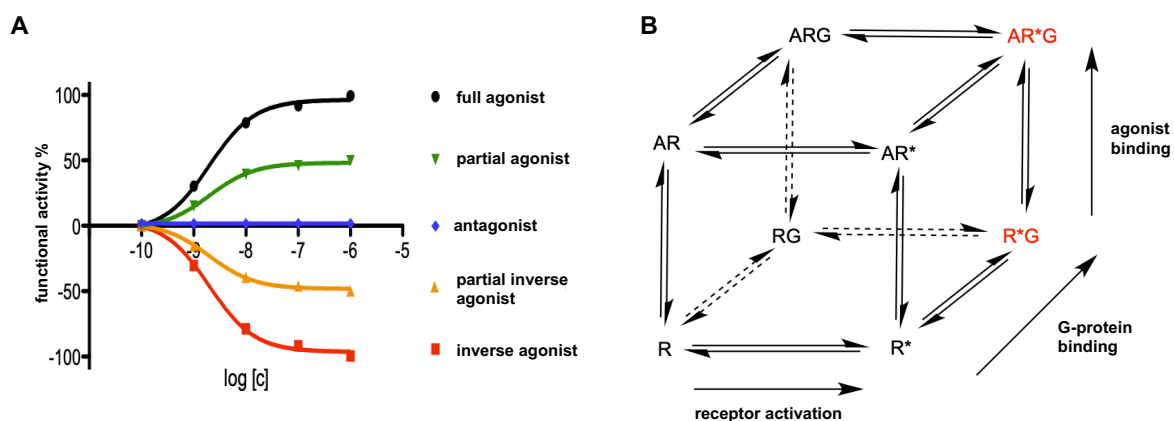
Figure 3.004. A) Ligand classification with respect to their functional activity. **B**) Extended ternary complex model[222] describing the interaction between GPCR, agonist, and G-protein. R: inactive state of the receptor; R*: active state of the receptor; G: G-protein; A: agonist. Figure (**A**) adapted from Figure 1.4 of Pockes (2015)[173] and Figure (**B**) from Figure 1.3 of Igel (2008)[181].

Agonists demonstrate an enhanced binding affinity to active receptors, thus shifting the equilibrium from the inactive state toward the active state (cf. Figure 3.004A). In contrast, inverse agonists reduce the signal transduction of the receptor beneath the level of basal activity (cf. Figure 3.004A). Partial (inverse) agonists can only partially shift the balance between the active state and inactive state in comparison to a full agonist (cf. Figure 3.004A). Neutral antagonists can preserve the unimpaired equilibrium between active and inactive receptors (cf. Figure 3.004A).[223,224]

However, GPCR signal transduction is more complex and cannot be described by a single-state active model. For instance, cellular signaling of GPCRs can be mediated by G-proteins or by GRK phosphorylation of the receptor and a following β-arrestin recruitment.[213,221] The observation that ligands binding at the same GPCR can stabilize multiple active state conformations is commonly referred to as biased agonism.[221] The cellular signaling pathways can be equally activated by agonists. However, it is also possible to preferentially enable one of the signaling pathways or, in some cases, to activate one signal pathway exclusively (cf. Figure 3.005).[213]
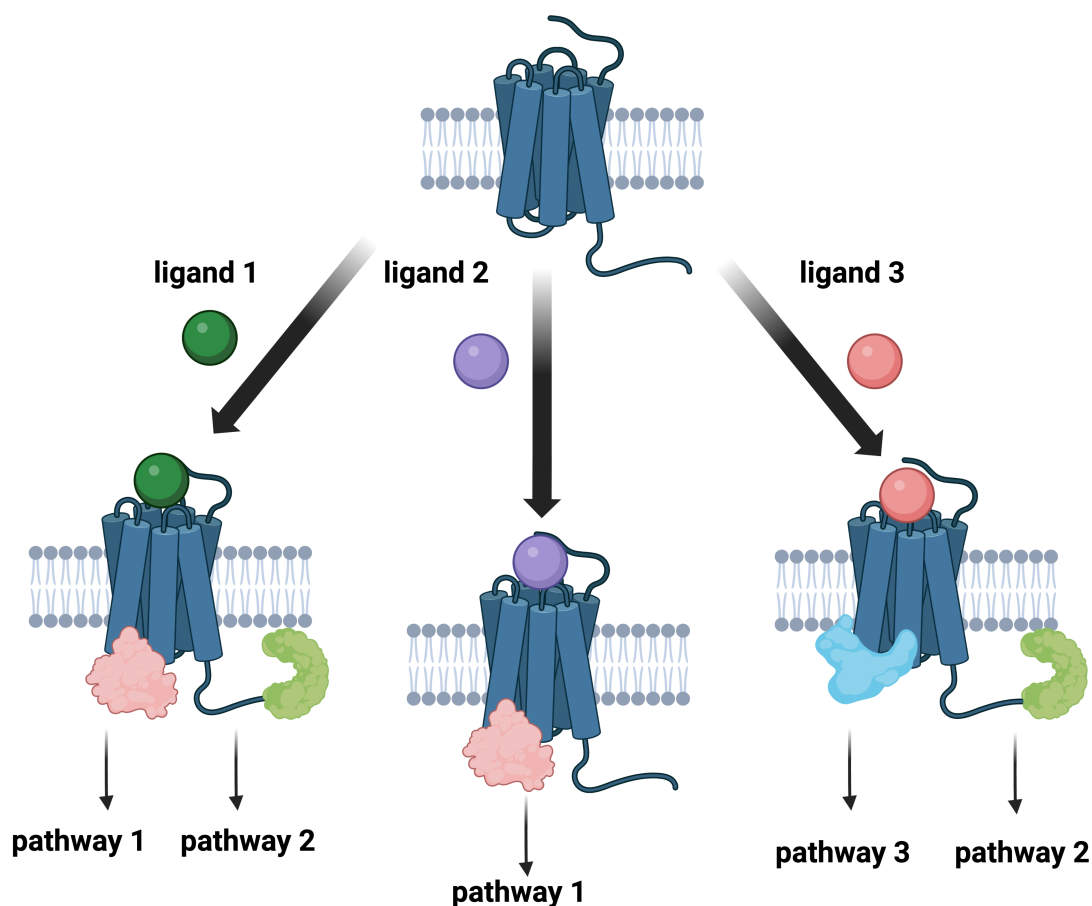
Figure 3.005. Schematic illustration of biased agonism. Different ligands (L1–L3) can stabilize various receptor conformations. Each receptor-effector complex is able to promote distinct cellular signaling pathways. Figure adapted from Figure 1 of Shonberg et al. (2014)[221]. Figure created with BioRender.com.

3.1.2 Histamine: Hormone and Neurotransmitter

The chemists Windaus and Vogt successfully synthesized the biogenic amine histamine for the first time in 1907.[225] Shortly afterward, Henry Dale and George Barger were able to isolate histamine from ergot (Secale cornutum).[226] At the same time, the first essential functions of histamine in the organism were investigated by Patrick Laidlaw and Henry Dale.[227] These findings successfully provided the basis for decades of histamine receptor research.

Histamine possesses a primary aliphatic amine (N^α) with a pK_a value of 9.4 (cf. Figure 3.006). In addition, it contains another basic functionality (p$K_a \sim 5.8$) with the imidazole heterocycle (N^τ). Under physiological conditions, histamine is predominantly present as a monocation (N^α).[228,229]

The pyridoxal phosphate (PLP) dependent biosynthesis of histamine in the organism occurs by the enzyme L-histidine decarboxylase (HDC) starting from the amino acid L-histidine (cf. Figure 3.006).[230,231] In addition to L-histidine decarboxylase (HDC), a minor part of histamine is also generated by nonspecific aromatic L-amino acid decarboxylase (AADC).[231]
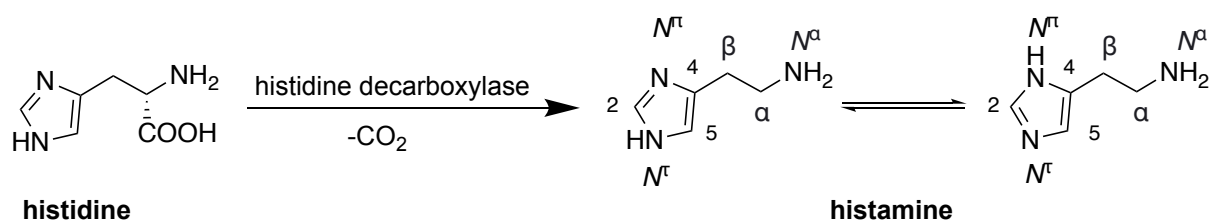
Figure 3.006. Biosynthesis and tautomerism (N$^\tau$-N$^\pi$) of histamine.

The metabolization of released histamine in the organism proceeds very fast. Essentially, two distinct metabolic pathways are involved in the degradation. The first pathway is characterized by a two-step enzyme-catalyzed (diamine oxidase (DAO) and xanthine oxidase (XO)) oxidation of the primary amine, followed by the ribosylation of imidazole-4-acetic acid (cf. Figure 3.007). The second metabolic pathway, and at the same time the most important one in the human organism, initiates with the methylation of the N$^\tau$-nitrogen of the imidazole heterocycle catalyzed by histamine *N*-methyltransferase (HNMT) (cofactor *S*-adenosyl-methionine). Thereafter, N$^\tau$-

methylhistamine is catalytically oxidized to the corresponding carboxylic acid via two stages (cf. Figure 3.007).[232]
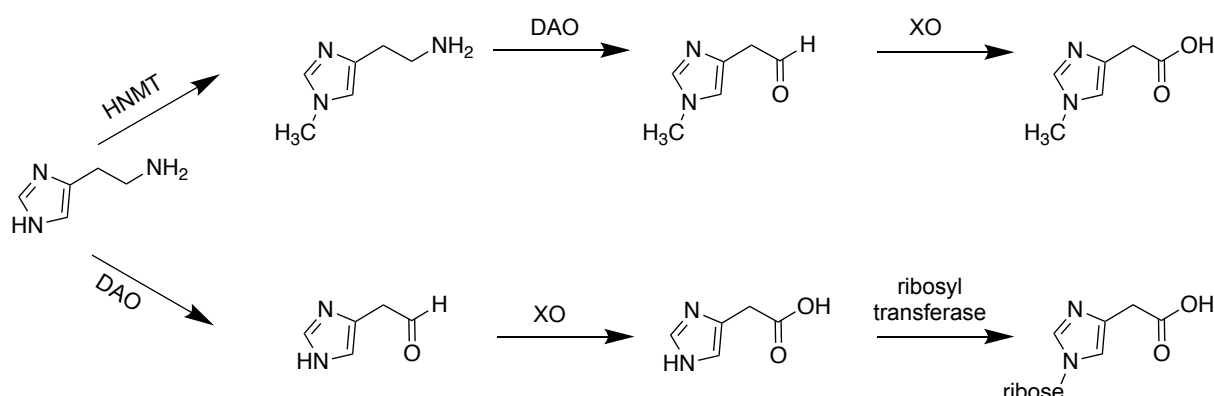
Figure 3.007. Biotransformation of histamine. HNMT: histamine *N*-methyltransferase; DAO: diamineoxidase; XO: xanthineoxidase.

Histamine is present in nearly all tissues (e.g., lung, skin, gastrointestinal tract, and the brain) of the organism and serves as a neurotransmitter and hormone.[233,234] It can be found in mast cells[235], basophils[236], platelets[236], enterochromaffin-like (ECL) cells of the stomach[237], endothelial cells[238], and neurons[239]. Histamine released from ECL cells is responsible for the regulation of gastric acid secretion from parietal cells.[240] Furthermore, it is responsible for smooth muscle contraction, vasodilatation, and the increase of vascular permeability during allergic reactions.[241] In the central nervous system (CNS), histamine acts as a neurotransmitter that regulates the sleep/waking cycle, learning and memory, anxiety, locomotion, and neuroendocrine secretion.[242,243] The various effects of histamine are mediated via the four G-protein coupled histamine receptors (H$_1$R, H$_2$R, H$_3$R, and H$_4$R).[244,245]

3.1.3 Histamine Receptors and their Ligands

The four histamine receptors (H$_1$R, H$_2$R, H$_3$R, and H$_4$R) are part of the class A rhodopsin-like GPCRs.[244,245] Via the different signaling pathways, histamine receptors can exhibit a variety of different biological effects. In 1966 Ash and Schild introduced the term histamine H$_1$ receptor (H$_1$R) while investigating the biological effects of histamine. However, they postulated the existence of an additional histamine receptor (non-H$_1$ receptor, H$_2$R), since there were several biological effects of histamine that failed to be antagonized with classical antihistamines.[246] A few years later, the histamine H$_2$ receptor (H$_2$R) was discovered and characterized by Black et al.

(1972).[247] The H$_1$R (e.g., cetirizine for allergic reactions) and the H$_2$R (e.g., cimetidine to inhibit stomach acid production) became targets for blockbuster drugs for decades. Subsequently, the H$_3$R was revealed by Arrang et al. (1983).[248] The H$_3$R is expressed in the brain and is considered a regulatory factor in the central nervous system. Finally, the H$_4$R was uncovered by several research groups at the same time due to its high homology to the H$_3$R (Oda et al. (2000), Nakamura et al. (2000), Liu et al. (2001), Morse et al. (2001), Nguyen et al. (2001), and Zhu et al. (2001)).[245,249–254]

3.1.3.1 The Histamine H$_1$ Receptor

The human histamine H$_1$ receptor (H$_1$R) consists of a sequence of 487 amino acids and favorably couples to a pertussis toxin-insensitive G$_{q/11}$-protein.[255]. This results in the activation of phospholipase C (PLC) and consecutively in the release of the second messenger's inositol trisphosphate (IP$_3$) and diacylglycerol (DAG), which mediate the activation of protein kinase C (PKC) and the release of Ca^{2+} (cf. Figure 3.002).[255,256] Debacker et al. (1993)[257] accomplished the first cloning of the H$_1$R in 1993.

The receptor is expressed in the brain, smooth muscles from airways, blood vessels, the cardiovascular system, endothelial cells, lymphocytes, and the gastrointestinal tract.[255] The circadian rhythm, cognitive processes, thermoregulation, and pain are regulated by the activation of H$_1$R in the central nervous system.[181,258–263] Smooth muscle cell contraction is regulated by the H$_1$R-mediated release of calcium from intracellular stores.[181,264,265] The dilatation of vascular smooth muscles is triggered by the H$_1$R activation and the resulting release of nitric oxide from endothelial cells (causing the decrease in blood pressure).[181,266,267] Furthermore, vascular permeability is regulated by the H$_1$R-mediated contraction of endothelial cells.[181,268–270] These biological effects of the histamine H$_1$ receptor (H$_1$R) are the cause for typical allergic reactions like urticaria, bronchoconstriction, and a decrease in blood pressure. Typical indications of drugs targeting the H$_1$R are allergic reactions (e.g., cetirizine), sedation (e.g., diphenhydramine), and nausea (e.g., dimenhydrinate) (cf. Figure 3.008). The drugs can be used in topical administration (e.g., Fenistil$^©$ Gel) and systemic administration (e.g., Fenistil$^©$ Dragée). All approved drugs (except betahistine for the treatment of Ménière's disease[271] (cf. Figure 3.008)) targeting the H$_1$R are antagonists. H$_1$R agonists are mainly used as pharmacological tools (e.g., suprahistaprodifen[272]) (cf. Figure 3.008).

agonists

betahistine

suprahistaprodifen

antagonists

cetirizine

diphenhydramine
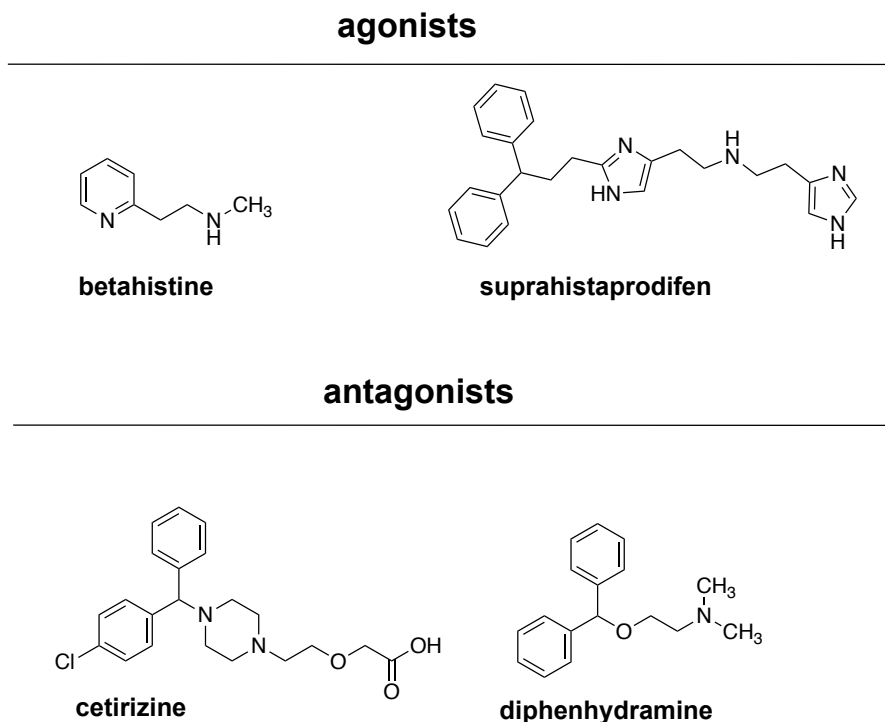
Figure 3.008. Structures of selected H$_1$R ligands.

3.1.3.2 The Histamine H$_2$ Receptor

In 1966, Ash and Schild already assumed the presence of another histamine receptor.[246] Finally, Black et al. (1972) discovered the H$_2$R by using burimamide (first know H$_2$R antagonist) to suppress the histamine-induced gastric acid secretion and the positive inotropic effects on the heart.[247] The human histamine H$_2$ receptor (H$_2$R) consists of a sequence of 359 amino acids and couples to the G$_{\alpha s}$-protein, resulting in the activation of adenylyl cyclase (AC).[244] That mediates the increased transformation of adenosine triphosphate (ATP) in cyclic adenosine monophosphate (cAMP), which in turn enables protein kinase A (PKA). PKA realizes enhanced gene expression in the nucleus through the phosphorylation of proteins (e.g., CREB: cAMP element-binding protein) (cf. Figure 3.002).[273] Gantz and colleagues accomplished the first cloning of the H$_2$R (dogs and humans) in 1991.[274]

The H$_2$R is mainly expressed in neurons[275], heart[276], gastric parietal cells[241], uterine[277], airway[278], immune cells[241], lungs[278], and blood vessels[279]. Histamine-induced activation of cardiac H$_2$R leads to a positive chronotropic and inotropic response of the heart.[181,247,280,281] Activation of H$_2$R in the parietal cells of the stomach enhances gastric acid secretion.[247] Furthermore, smooth muscle relaxation in the airway, uterine, and

blood vessels is regulated by H_2R.[181,247,277,278,282] Stimulation of H_2R in the central nervous system (CNS) mediates and/or potentiates excitatory effects by inhibiting the long-lasting afterhyperpolarization after Ca^{2+} influx and blocking the accommodation of action potential after firing.[181,275] H_2R knockout mice are marked by selective cognitive deficits, an impairment in hippocampal potentiation[283], as well as misperceptions in relation to pain.[284–286] The blood-brain barrier crossing of available H_2R ligands is shallow. Hence, there are still numerous ambiguities as to the function of histamine H_2 receptors in the brain.[233] Nevertheless, due to the prominent expression and the variety of functions, the H_2R may be a target to tackle neurodegenerative diseases.
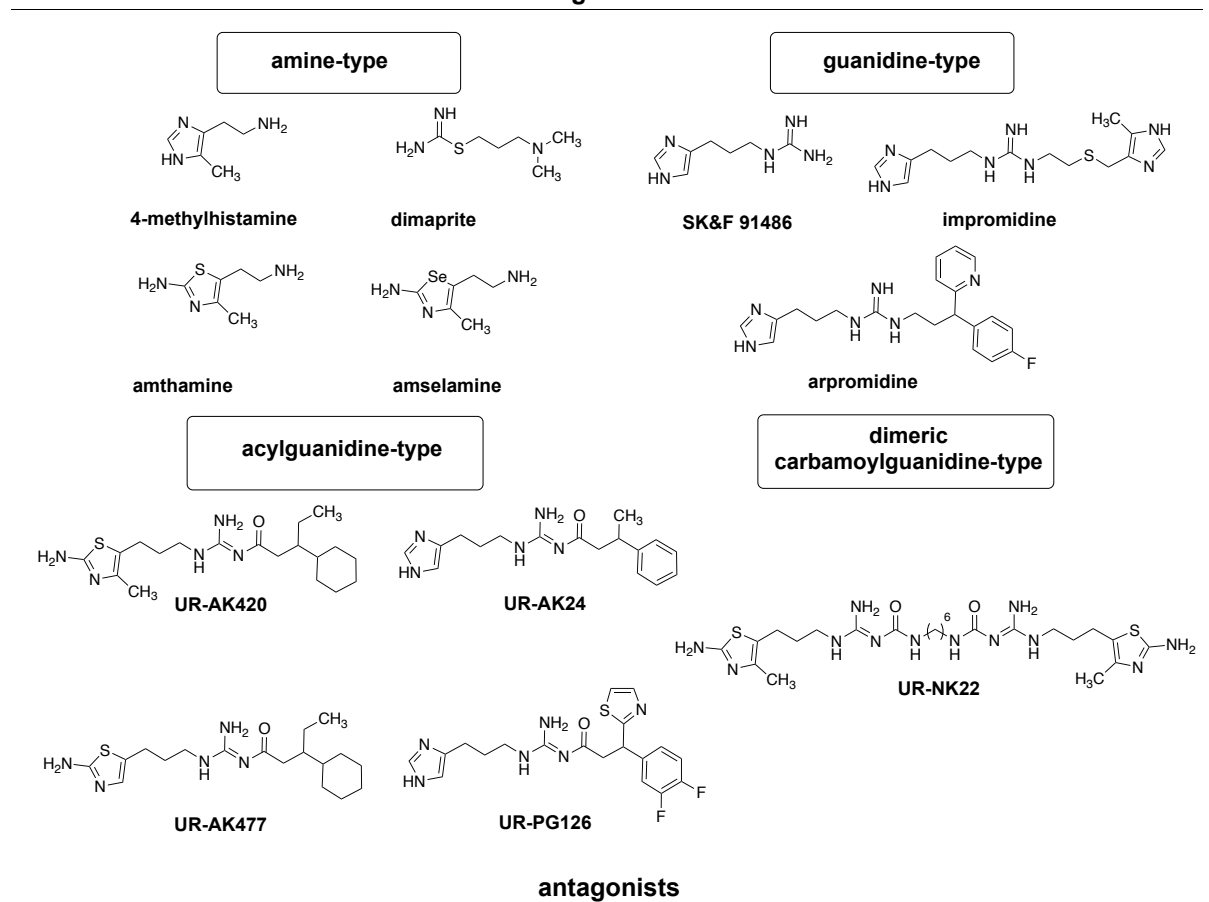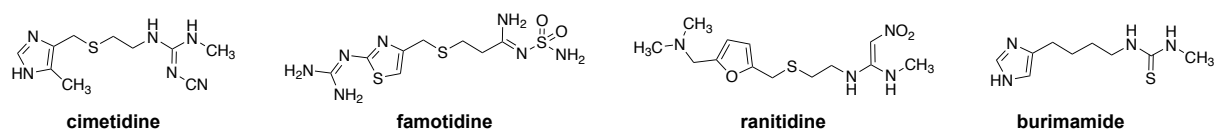
Figure 3.009. Structures of selected H_2R ligands.

H_2R agonists can be subdivided into two groups. Agonists of the amine-type are structurally very similar to the endogenous ligand histamine. The first H_2 agonist demonstrating selectivity for the histamine H_2 receptor within the histamine family was

4-methylhistamine (cf. Figure 3.009).[287,288] Additional representatives of the amine-type H$_2$ ligands are dimaprite[289,290], amthamine[291], and amselamine[292]. (cf. Figure 3.009) They are all characterized by similar activity for the H$_2$R, but with a more favorable selectivity profile within the histamine receptor family compared to the endogenous ligand. Further development of the isothiourea partial structure of dimaprit to a heterocycle resulted in amthamine, the first H$_2$R agonist with a 2-amino-4-methylthiazol partial structure serving as a bioisosteric replacement of the imidazole ring.[291] Another successful approach of bioisosteric replacement was the exchange of the sulfur atom by selenium resulting in amselamine.[292] The guanidine-type H$_2$ agonists (e.g., SK&F 91486) are characterized by the replacement of the aliphatic amine with guanidine. The prototype of this substance class is the weak partial agonist SK&F 91486 designed by Smith, Kline & French (cf. Figure 3.009).[293] The ongoing refinements of SK&F 91486 progressed to impromidine and arpromidine (cf. Figure 3.009).[294,295] Both demonstrate outstanding activity and selectivity compared to the endogenous ligand. Until today, impromidine is the only H$_2$R agonist investigated in clinical trials for the treatment of catecholamine-refractory myocardial insufficiency. Impromidine was evaluated as an effective drug, but the unfavorable side effect profile (e.g., massive gastric acid production and arrhythmias) prevented the compound approval as a potential treatment.[296] An unfavorable feature of guanidine-type H$_2$ agonists is the high basicity (pK_a ~ 13) of the compounds, which leads to low bioavailability and poor blood-brain barrier crossing.[103,297,298] To enhance the physicochemical properties of the H$_2$ ligands, acylguanidines (e.g., UR-AK24)[298] and subsequently (dimeric) carbamoylguanidines (e.g., UR-NK22)[299] were successfully designed (cf. Figure 3.009). The introduction of an electron-withdrawing group in proximity to the guanidine resulted in H$_2$ agonists with lower basicity (pK_a ~ 8)[298,300] and thus higher bioavailability while retaining the activity for H$_2$R. The acylguanidines UR-AK24[298] and UR-PG126[298] demonstrate high bioavailability and are capable of penetrating the blood-brain barrier after administration to mice. The imidazole heterocycle of the guanidines and N^G-acylated analogs was bioisosterically replaced by 2-amino-4-methylthiazole or 2-aminothiazole rings without losing the H$_2$R agonistic activity but gaining selectivity for H$_2$R over H$_3$R (e.g., UR-AK420 and UR-AK477) (cf. Figure 3.009).[291,301–303] Carbamoylguanidines were developed because acylguanidines turned out to undergo hydrolytic cleavage in an aqueous solution.[299,304] At the beginning of the 1970s, antagonists of the H$_2$R (e.g., cimetidine, ranitidine, and

famotidine (cf. Figure 3.009)) were designed and turned out to be blockbuster drugs for the treatment of gastric and duodenal ulcers.[305,306] Nowadays, these drugs have been displaced nearly completely by proton pump inhibitors (e.g., omeprazole).[307] Nevertheless, H$_2$R antagonists still have particular relevance as pharmacological tools.

3.1.3.3 The Histamine H$_3$ Receptor

The starting point for the H$_3$R discovery was the identification of histamine as a CNS active neurotransmitter. Moreover, histamine was shown to be able to inhibit its own release from rat cortex neurons.[239,308,309] This finding paved the way for Arrang et al. (1983)[248] to postulate the existence of the histamine H$_3$ receptor (H$_3$R), as the H$_2$R antagonist burimamide (cf. Figure 3.009) suppressed the histamine release at nanomolar concentrations, which is substantially below the concentration required to block the H$_2$R. The subsequent design of the selective H$_3$R agonist (R)-α-methylhistamine and the selective H$_3$R inverse agonist thioperamide in 1987 confirmed the assumption.[310] The first cloning of human H$_3$R was accomplished by Lovenberg et al. (1999).[311] The H$_3$R demonstrates low sequence homology with the H$_1$R and the H$_2$R, which is comparable to other aminergic GPCRs.[311] However, referring to the H$_4$R, there is a high level of homology (about 40% overall sequence identity and 58% sequence identity within the transmembrane), which also enabled the discovery of the histamine H$_4$ receptor.[249,250,312] The human histamine H$_3$ receptor (H$_3$R) consists of a sequence of 445 amino acids and couples to the pertussis toxin-sensitive G$_{i/o}$ protein, resulting in the inhibition of the adenylyl cyclase (AC), activation of mitogen-activated protein kinase (MAPK), activation of phospholipase A$_2$ (PLA$_2$), lowering of the intracellular Ca^{2+} levels, and the inhibition of the Na$^+$/H$^+$ exchanger (cf. Figure 3.002). Furthermore, a constitutive activity is reported for the H$_3$R.[313–316]

The H$_3$R mainly occurs in the central nervous system (e.g., hippocampus, cerebral cortex, basal ganglia) and the peripheral nervous system (e.g., GI tract, cardiovascular system, and lungs).[317,318] H$_3$R autoreceptors in the central nervous system control the synthesis and release of histamine from histaminergic neurons.[181,319,320] Presynaptic H$_3$R heteroreceptors are also responsible for the release of neurotransmitters like dopamine[321], serotonin[322], noradrenaline[323], acetylcholine[324], and γ-aminobutyric acid[325].[181] The histamine H$_3$ receptor regulates sleep-wake rhythms, cognitive processes, thermoregulation, obesity, and pain.[326–328] The high homology between the

H$_3$ and H$_4$ receptors makes the design of H$_3$R ligands quite challenging.[249,250,312] Histamine-related H$_3$R agonists are N$^\alpha$-methylhistamine and (*R*)-α-methylhistamine (cf. Figure 3.010). Agonists with more significant structural differences are imetit and the very selective methimepip (cf. Figure 3.010). Until now, H$_3$R agonists are only used as pharmacological tools, even though they may be helpful for the treatment of insomnia[329], pain[330], inflammation[331,332], and migraine[333]. H$_3$R antagonist/inverse agonists are divided into two groups, the imidazole (e.g., thioperamide[310] and clobenpropit[334]) and non-imidazole group (e.g., pitolisant[335], JNJ-5207852[336], and JNJ-10181457[336]) (cf. Figure 3.010). The inverse agonist pitolisant (cf. Figure 3.010) is the only drug targeting the H$_3$R that was approved for the treatment of narcolepsy (2016)[337] and obstructive sleep apnea (2021)[338]. Prader-Willi syndrome might also be treated with pitolisant, as initial results of studies are encouraging.[339] H$_3$R antagonists/inverse agonists are also potential drug candidates for the treatment of Alzheimer's disease[340], schizophrenia[316], attention deficit hyperactivity disorder (ADHD), and epilepsy.[341–343]

agonists
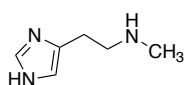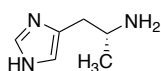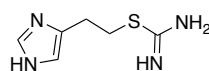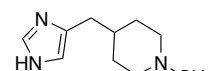
antagonists/inverse agonists
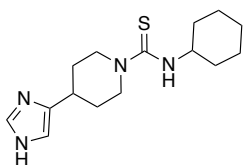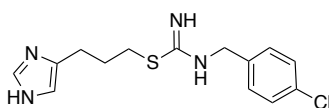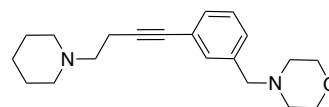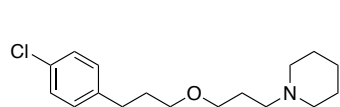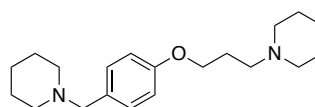
Figure 3.010. Structures of selected H$_3$R ligands.

3.1.3.4 The Histamine H$_4$ Receptor

Raible et al. (1994) postulated the existence of the histamine H$_4$ receptor, as they perceived that H$_1$R and H$_2$R antagonists were not able to prevent the histamine-triggered calcium mobilization in human eosinophils. The H$_3$R inverse agonist thioperamide (cf. Figure 3.010) was capable of inhibiting calcium mobilization. However, the H$_3$R agonist (R)-α-methylhistamine (cf. Figure 3.010) was only able to activate calcium mobilization to a lesser extent than histamine. These findings suggested the presence of a fourth histamine receptor in human eosinophils.[344,345] Finally, in 2000 and 2001, a few research groups were able to verify the existence of the histamine H$_4$ receptor and clone it successfully.[249–254,312] The human histamine H$_4$ receptor (H$_4$R) consists of a sequence of 390 amino acids and couples to the pertussis toxin-sensitive G$_{i/o}$-protein, resulting in the inhibition of adenylyl cyclase (AC) and the activation of the MAPK pathway.[181,249,252] Likewise, phospholipase C$_\beta$ (PLC$_\beta$) activation and, thus, Ca^{2+} mobilization was observed as a consequence of H$_4$R stimulation (cf. Figure 3.002). These effects are likely related to the G$_{\beta\gamma}$-subunit of the G$_{i/o}$-protein.[181,346,347] The G protein-independent β-arrestin signaling pathway was also determined for the histamine H$_4$ receptor.[348,349] In addition, high constitutive activity is reported for the H$_4$R, just as for the H$_3$R.[350,351] The H$_4$R occurs in a variety of cells of the immune system, like mast cells, basophils, T-lymphocytes, eosinophils, and dendritic cells.[181,249,251,252,254,346,352] Furthermore, the H$_4$R is also expressed in cells of the enteric nervous system (ENS) and central nervous system (CNS).[346,353] The exact physiological role of the H$_4$R has not yet been definitively revealed. However, participation in immunological and inflammatory processes seems evident.[354] Therefore, targeting the H$_4$R appears to be a promising approach for the treatment of autoimmune diseases[355,356] (e.g., rheumatoid arthritis and multiple sclerosis), asthma[357], and atopic dermatitits[358].

The first selective H$_4$R agonist was the chiral tetrahydrofuran analog OUP-16 (deriving from the H$_3$R agonist imifuramine) (cf. Figure 3.011).[359] Other known H$_4$R agonists include 4-methylhistamine (reported initially as a selective H$_2$ agonist), clozapine[249], and VUF-8430 (deriving from the H$_2$R agonist dimaprit) (cf. Figure 3.011).[360] Another class of highly selective H$_4$R agonists are cyanoguanidines (e.g., UR-PI376).

agonists
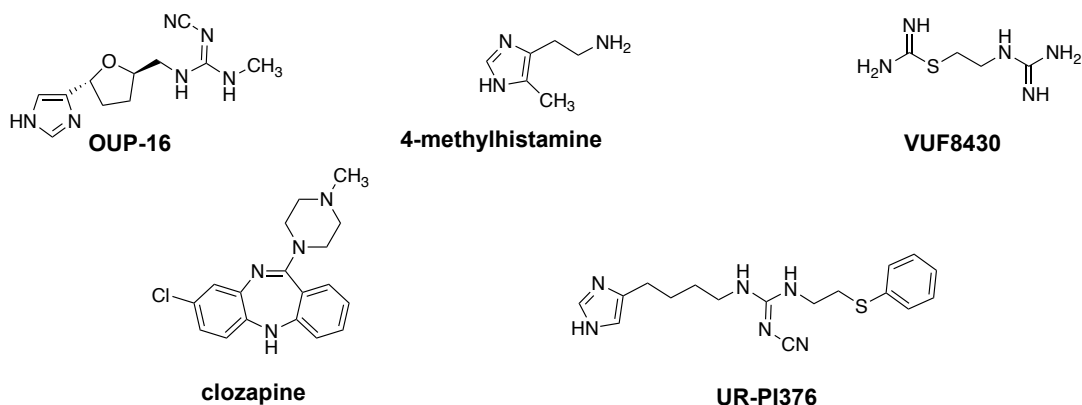
antagonist
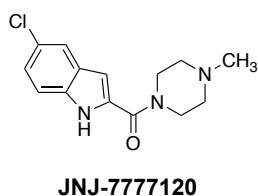
Figure 3.011. Structures of selected H$_4$R ligands.

By introducing a non-basic cyanoguanidine group in place of the acylguanidine moiety the activity for H$_2$R and H$_3$R drops drastically.[181,361,362] Thioperamide, as mentioned earlier, is an inverse agonist for the H$_3$R and H$_4$R. JNJ-7777120 (cf. Figure 3.011) is a highly selective H$_4$R antagonist, representing an essential pharmacological tool to elucidate the biological role of H$_4$R in several animal models.[181,354,363–366] Further H$_4$R antagonists are of the 2-aminopyrimidine,[367,368] quinazoline, and quinoxaline types.[369,370]

3.2 Scope and Objectives

The goal of this work was the development and biological evaluation of selective and potent histamine H_2 receptor agonists, which are supposed to serve as pharmacological tools to understand the function of H_2R in the central nervous system (CNS). The H_2 receptor, just as the H_3R, is involved in the transmission of histamine and other neurotransmitters (e.g., acetylcholine) in the CNS. In previous studies, dual-acting acetylcholinesterase inhibitors and H_3R antagonists were shown to be beneficial for learning and memory processes in the CNS by inhibiting H_3-autoreceptors.[371–373] The inhibition of H_3-autoreceptor results in an increased release of histamine and a subsequent stimulation of postsynaptic H_2Rs (cf. Figure 3.012). Therefore, targeting the H_2R could be a potential treatment of neurodegenerative diseases such as Alzheimer's. In this context, it is essential to overcome the drawbacks of previous H_2 agonists, especially the poor bioavailability and blood-brain barrier crossing of guanidine-type H_2 agonists (e.g., arpromidine and impromidine) as well as the stability problems of acylguanidine-type H_2 agonists (e.g., UR-AK24[298]). As recently reported, H_2 agonists of the carbamoylguanidine-typ (e.g., UR-NK22[299]) can overcome these disadvantages.
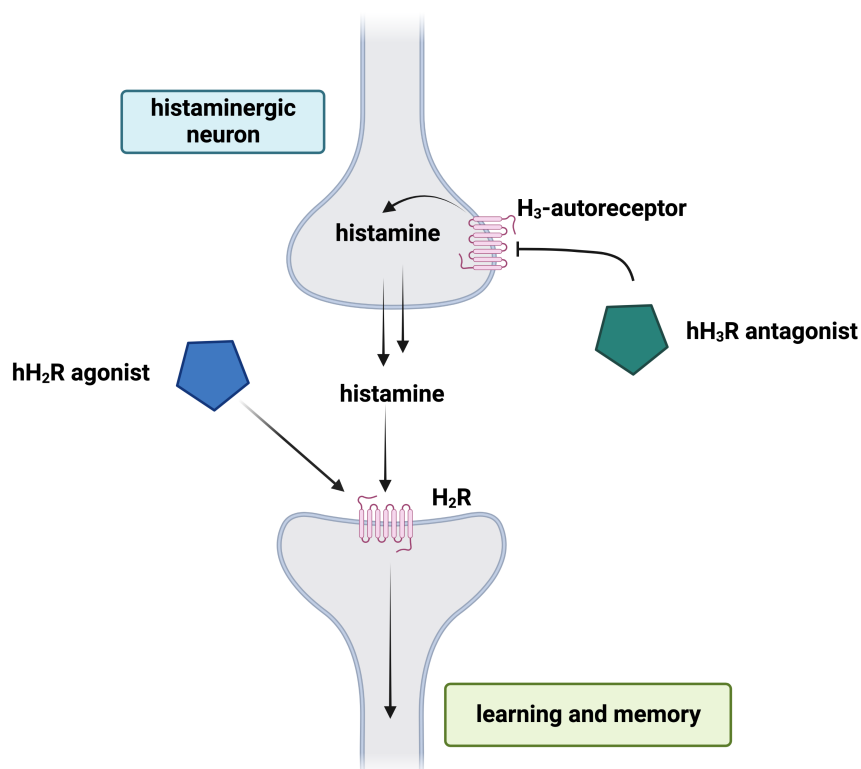
Figure 3.012. Synaptic gap: Mode of action of H_2R agonists (direct stimulation) and H_3R antagonists (indirect stimulation). Activation of postsynaptic H_2 receptors mediates learning and memory processes. Figure adapted from Figure 1 of Khan et al. (2016).[371]

The dimeric carbamoylguanidines designed by Kagermeier et al. (2015)[299] demonstrated retained activity for the H$_2$R, reduced basicity, and improved stability against hydrolytic cleavage. However, with respect to Lipinski's rule of five[103] dimeric H$_2$ agonists are inappropriate as pharmacological tools to elucidate the role of the H$_2$R in the CNS. Thus, a series of monomeric carbamoylguanidine H$_2$R agonists with variations in the side chain were synthesized to find a centrally active H$_2$R agonist. As recently reported, the bioisosteric replacement of the imidazole heterocycle by a 2-amino-4-methylthiazole group resulted in H$_2$R agonists with improved selectivity over the H$_3$R.[291,301–303] In the course of this work, further bioisosteric replacements of this structural feature were made to get a more profound understanding of the structure-activity relationship (SAR) and to design H$_2$R agonists with an improved selectivity profile, not only within the histamine receptor family but also over other GPCRs (e.g., D$_2$R and D$_3$R). The new compounds were tested for H$_2$R agonistic potency on the isolated guinea pig right atrium and their binding affinities for the four histamine receptors in a radioligand competition binding assay. Selected compounds were also investigated for agonism in the β-arrestin2 recruitment assay on HEK293T-β-Arr2-hH$_2$R cells and for hH$_2$R agonism in the [^{35}S]GTPγS binding assay. Furthermore, they were investigated for the binding affinities and the β-arrestin2 recruitment at the hD$_{2long}$R and hD$_3$R. An off-target screening provided insights into the selectivity over other GPCRs. The pK_a value of selected compounds was determined as the acid-base dissociation constant represents a key physicochemical parameter influencing bioavailability and blood-barrier crossing of the H$_2$R ligands.[297]

3.3 Pharmacological Characterization of a New Series of Carbamoylguanidines Reveals Potent Agonism at the H₂R and D₃R
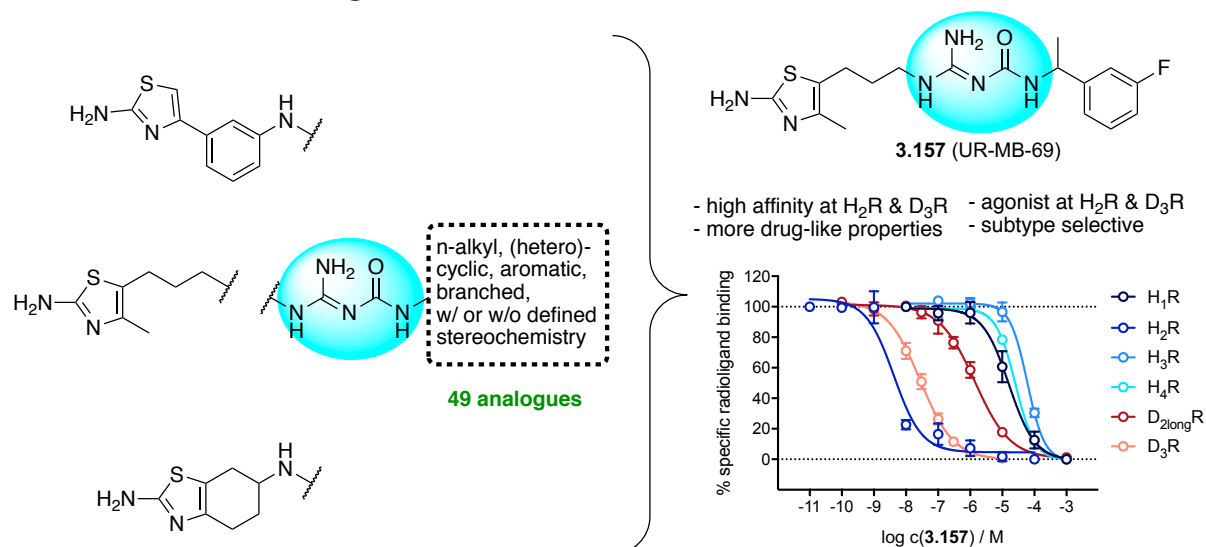
Even today, the role of the histamine H_2 receptor (H_2R) in the central nervous system (CNS) is widely unknown. In previous research, many dimeric, high-affinity and subtype-selective carbamoylguanidine-type ligands such as UR-NK22 (**3.005**, pK_i = 8.07) were reported as H_2R agonists. However, their applicability to the study of the H_2R in the CNS is compromised by their molecular and pharmacokinetic properties, such as high molecular weight and, consequently, a limited bioavailability. To address the need for more drug-like H_2R agonists with high affinity, a series of monomeric (thio)carbamoylguanidine-type ligands containing various spacers and side-chain moieties was synthesized. This structural simplification resulted in potent (partial) agonists (guinea pig right atrium, [^{35}S]GTPγS and β-arrestin2 recruitment assays) with hH_2R affinities in the one-digit nanomolar range (pK_i (**3.139**, UR-KAT523): 8.35; pK_i (**3.157**, UR-MB-69)): 8.69). Most of the compounds presented here exhibited an excellent selectivity profile towards the hH_2R, e.g., **3.157** being at least 3800-fold selective within the histamine receptor family. The structural similarities of the monomeric ligands to pramipexole (**3.006**), a dopamine receptor agonist, suggested an investigation of the binding behavior at those receptors. The target compounds were (partial) agonists with moderate affinity at the $hD_{2long}R$ and agonists with high affinity at the hD_3R receptor (e.g., pK_i (**3.139**, UR-KAT523): 7.80; pK_i (**3.157**, UR-MB-69)): 8.06). In summary, a series of novel, more drug-like H_2R and D_3R agonists was developed for the application in recombinant systems in which either the H_2R or the D_3R is solely expressed. Furthermore, the new ligands are promising lead compounds in the development of selective H_2R agonists for future *in vivo* studies or experiments utilizing primary tissue to unravel the role and function of the H_2R in the CNS.

338

This chapter has been published in:

Author contributions:

S.B., **M.B.**, **K.T.**, **C.H.**, and **S.P.** performed the synthesis and the analytical characterization of chemical compounds. **S.B.** synthesized H$_2$R ligands **3.163**, **3.166**-**3.171**, **3.179**-**3.186** and the corresponding precursor compounds therefore. **M.B.** synthesized H$_2$R ligands **3.147**-**3.160**, **3.213**, and **3.216** and the corresponding precursor compounds therefore. **K.T.** synthesized H$_2$R ligands **3.139** and **3.172** and the corresponding precursor compounds therefore. **C.H.** synthesized H$_2$R ligands **3.138**, **3.140**-**3.143**, and **3.161** and the corresponding precursor compounds therefore. **S.P.** synthesized H$_2$R ligands **3.144**-**1.146**, **3.162**, **3.164, 3.165**, and **3.173**-**3.178** and the corresponding precursor compounds therefore. **M.B.** performed the determination of pK_a values. **C.H.** performed the investigation of the chemical stability. **S.P.** performed the determination of the enantiomeric purities. **S.B.**, **M.B.**, **K.T.**, **C.H.**, and **S.P.** performed the radioligand competition binding experiments (hH$_{1-4R}$). **L.F.** performed the radioligand competition binding experiments (hD$_{2long}$/$_3$R). **S.B.** performed the [^{35}S]GTPγS binding experiments. **S.B.** and **K.T**. performed the β-arrestin2 recruitment assays at the hH$_2$R. **L.F.** and **K.T.** performed the β-arrestin2 recruitment assays at the hD$_2$longR and hD$_3$R. **M.B.** and **S.P.** performed the guinea pig right atrium experiments. **A.B.** initiated the project. **A.B.**, **G.B.**, and **S.P.** supervised the research. **S.B.**, **M.B.**, **K.T.**, and **S.P.** wrote the manuscript. **S.B.**, **M.B.**, and **K.T.** contributed equally.

3.3.1 Introduction

G protein coupled receptors (GPCRs) constitute one of the most important bioactive complexes in humans and are composed of seven transmembrane domains with three extracellular and three intracellular loops.[172,175] Their versatile role in cell signal transduction makes these proteins valuable pharmacological targets to be exploited by the pharmaceutical industry and in academic research.[172,175] A well-studied GPCR subclass is the histamine receptor family (H$_1$R, H$_2$R, H$_3$R, and H$_4$R), which belongs to the rhodopsin-like family (class A).[244,245,374,375] Among these, the histamine H$_2$ receptor (H$_2$R)[247] has been the subject of many research investigations due to its occurrence in a variety of tissues and cells (e.g., leukocytes, heart, airways, uterus, vascular smooth muscles) and in the brain.[244,376,377] Therefore, numerous H$_2$R agonists and antagonists have been identified. However, only antagonists have found use in the clinic (e.g., for the treatment of gastroesophageal reflux disease and gastroduodenal ulcer).[244,374] H$_2$R agonists, on the other hand, have been employed as pharmacological tools *in vitro* or *in vivo* to provide further insight into the pharmacological properties of the H$_2$R, especially to elucidate its role in the central nervous system (CNS). Within the last decades numerous agonists for the H$_2$R were developed (cf. Figure 3.013). However, most of these ligands cannot be used to study the role of CNS-located H$_2$Rs in detail due to their respective individual drawbacks. The low potency of the endogenous H$_2$R ligand histamine (**3.001**; cf. Figure 3.013) could be improved by compounds of the guanidine-type (e.g., arpromidine (**3.002**); cf. Figure 3.013) with significantly higher potency. However, protonation of the strongly basic guanidine group under physiological conditions leads to insufficient oral bioavailability and lack of CNS penetration.[298] During further studies, acylated guanidines with reduced basicity and similar potency were developed.[298] Subsequent bioisosteric replacement of the imidazole ring by an amino(methyl)thiazole moiety, derived from amthamine (**3.003**; cf. Figure 3.013), finally led to the desired selectivity towards the H$_2$R (**3.004**; cf. Figure 3.013).[302] The potency of such ligands was further increased by connecting two acylguanidine pharmacophores via an alkyl spacer, resulting in dimeric ligands.[302,378] Recently, dimeric carbamoylguanidine analogues (e.g., UR-NK22 (**3.005**); cf. Figure 3.013) with enhanced stability properties with respect to hydrolytic cleavage, have been reported.[299] However, empirical studies suggest high (oral) bioavailability only for ligands which follow the "rule of five".[103,140,379] Despite their high potency and stability, dimeric ligands fail to meet most of those criteria. Moreover,

studies with radioactively or fluorescently labeled dimeric carbamoylguanidines indicated a high unspecific binding and receptor independent uptake in cells.[299]
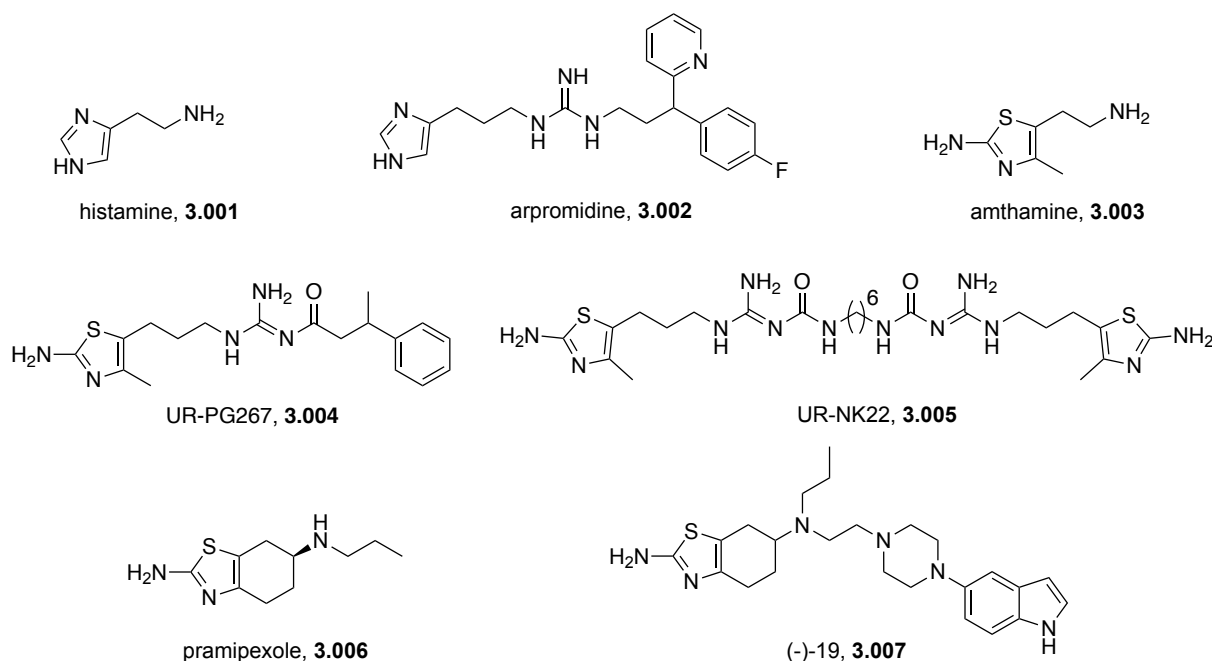
Figure 3.013. Structures of histamine (**3.001**), representative monomeric and dimeric H$_2$R agonists (**3.002**-**3.005**), and the D$_{2/3}$R agonists pramipexole (**3.006**) and (-)-19 (**3.007**).

The aim of this study was the development of a series of aminothiazole-containing carbamoylguanidine-type ligands with improved and enhanced drug-like properties while possessing the high H$_2$R subtype selectivity and potency of the dimeric ligands. Therefore, the complexity and size of the compounds was reduced to ligands consisting of a single pharmacophore and a non-polar side chain. There are significant structural similarities between these H$_2$R ligands and dopamine D$_{2/3}$ receptor (D$_{2/3}$R) agonists (e.g., pramipexole (**3.006**)[380,381], (-)-19 (**3.007**)[382]; cf. Figure 3.013). Since dopamine receptors play an important role in the brain, the binding behavior of the H$_2$R ligands at these receptors was investigated to avoid experimental bias. In this study, the synthesis, as well as the chemical and pharmacological characterization (competition binding-, [^{35}S]GTPγS-, β-arrestin2 recruitment- and guinea pig (gp) right atrium assays) of novel, monomeric carbamoylguanidine type H$_2$R ligands and the first investigations (competition binding- and β-arrestin2 recruitment assays) of such ligands at the dopamine D$_{2long}$ and D$_3$ receptors are reported.

3.3.2 Results and Discussion

3.3.2.1 Chemistry

The preparation of the monomeric N^G-carbamoylated guanidines **3.138**-**3.172** and **3.179**-**3.186** was performed by guanidinylation of the amine building blocks **3.009a/b** or **3.011**-**3.012** in analogy with the isocyanate-based procedure developed for the dimeric N^G-carbamoylated guanidines (cf. Scheme 3.01).[299] The (thio)carbamoylguanidines **3.173**-**3.178** were prepared using the guanidine building block **3.010** and a slightly modified procedure (cf. Scheme 3.01), due to the less reactive isothiocyanates, in comparison to isocyanates.[383] The required building blocks mono-Boc-protected *S*-methylisothiourea **3.008**, the amines **3.009a/b** and **3.011**-**3.012**, and the guanidine **3.010** were synthesized as previously published or as described in chapter **3.5.1.3** (cf. Schemes 3.01, 3.04, and 3.05).[302] The Boc-protected isothioureas **3.048**-**3.082** play a central role as guanidinylating reagents in the synthesis of the target compounds. They were synthesized by treatment of **3.008** with the respective isocyanates in the presence of triethylamine (NEt₃) or Hünig's base (DIPEA). The isocyanates were either commercially available (**3.034**-**3.039**) or prepared by two different strategies starting from the corresponding amines **3.013**-**3.033** using triphosgene/phosgene or from the branched carboxylic acids **3.040**-**3.047** applying the Curtius rearrangement. The respective amines **3.013**-**3.016**, **3.018**, **3.020**-**3.023**, **3.028**, and **3.031**-**3.033** were commercially available while **3.017**, **3.019**, **3.024**-**3.027**, and **3.029**-**3.030** were synthesized from commercially available ketones (see chapter **3.5.1.4**, cf. Scheme 3.06). The respective carboxylic acids were synthesized as previously described.[302] Because of their instability the intermediate isocyanates were not isolated, but immediately reacted with **3.008** in a one-pot reaction. The protected N^G-carbamoylated guanidines **3.089**-**3.123** and **3.130**-**3.137** were prepared by treating the amine building blocks **3.009a/b** or **3.011**-**3.012** with the respective Boc-protected isothioureas (**3.048**-**3.082**) in the presence of HgCl₂ and NEt₃. The synthesis of the Boc-protected (thio)carbamoylguanidines **3.124**-**3.129** started with the conversion of amines **3.014**-**3.016** and **3.031**-**3.033** with thiophosgene to the corresponding isothiocyanates **3.083**-**3.088**. In the next step, these isothiocyanates were converted with the guanidine building block **3.010** under reflux (dichloromethane (DCM)) to give the respective Boc-protected N^G-(thio)carbamoylated intermediates **3.124**-**3.129**. Finally, the resulting precursors **3.089**-**3.137** were treated with trifluoroacetic acid (TFA) to obtain the title compounds **3.138**-**3.186** with high purity

(cf. Figures 3.144-3.168A) after purification with preparative HPLC or recrystallization with HCl/1,4-dioxane/diethyl ether. The chemical stability of the representative carbamoylguanidines **3.141**, **3.142**, and **3.161** and related acylguanidines are demonstrated in chapter **3.5.1.16** (cf. Figures 3.029-3.034).
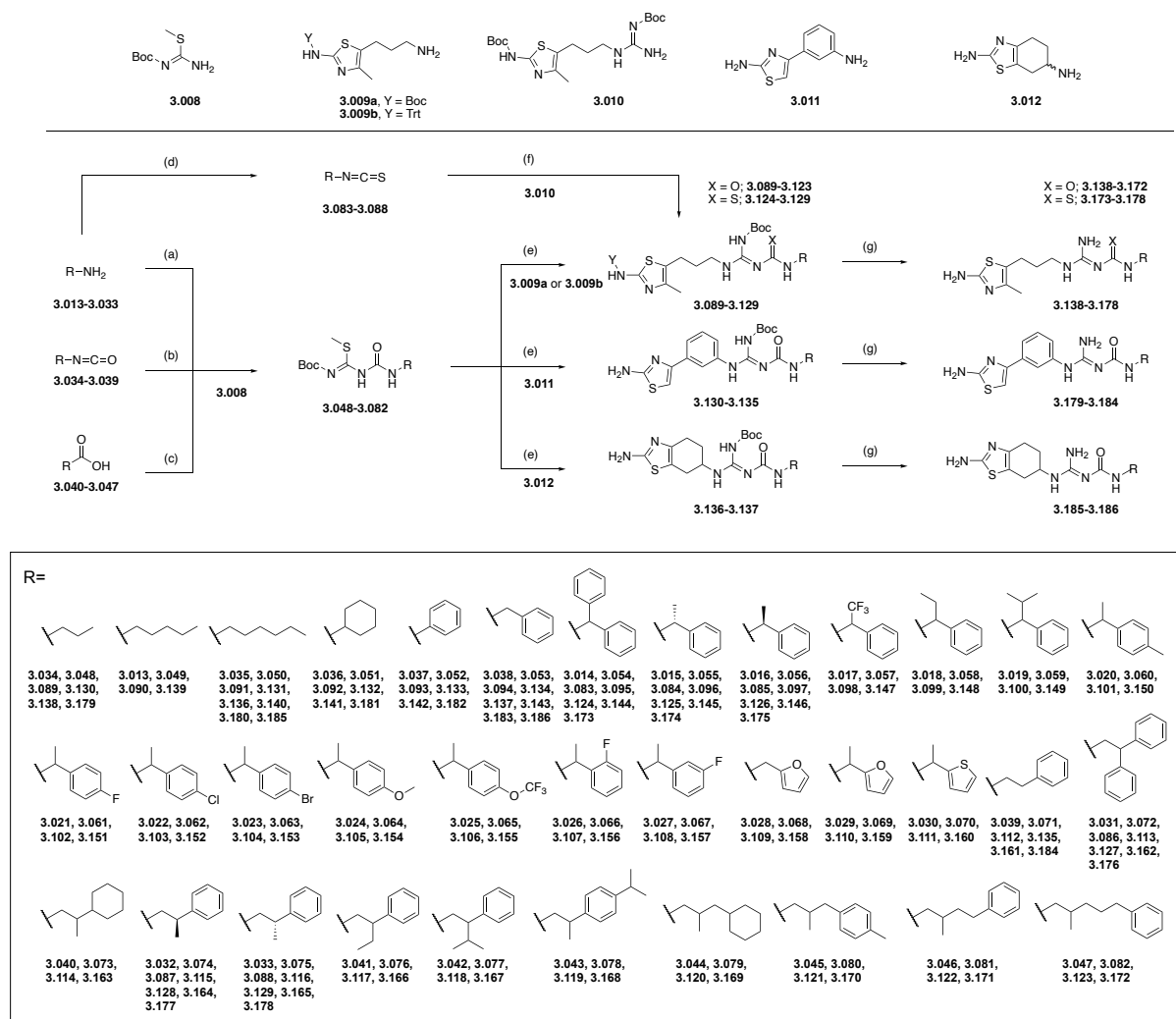
Scheme 3.01. Synthesis of the monomeric (thio)carbamoylguanidine-type ligands **3.138**-**3.186**. Reagents and conditions: (a) 15% phosgene in toluene or triphosgene, DIPEA, DCM, (Ar-atmosphere), 5-30 min, 0 °C → **3.008**, 2-3 h, room temperature (rt); (b) **3.008**, NEt₃, DCM, overnight, rt; (c) oxalyl chloride, DMF (cat.), DCM, Ar-atmosphere, 0 °C-rt, 25 min → NaN₃, acetone/H₂O, 30 min, 0 °C → DCM, reflux, 30 min → **3.008**, NEt₃, DCM, rt, overnight; (d) thiophosgene, NaHCO₃, DCM/H₂O, rt, 30 min; (e) HgCl₂, NEt₃, DCM, (Ar-atmosphere), rt, overnight; (f) DCM, reflux, 3-4 days; (g) TFA, DCM, rt or reflux, overnight.

3.3.2.2 Determination of pK_a Values and *In Silico* ADME

In vivo behavior, including bioavailability and CNS permeability, of a compound is influenced by its physicochemical properties.[103,297] In addition, information about the substance-specific acid-base properties are of great importance. Empirical studies by others have revealed a marked cut off for CNS distribution of bases, since no known CNS-penetrable compound has a pK_a over 10.5.[297] As already explained in the introduction, acylguanidines represent a class of compounds with improved physicochemical properties (pK_a ~ 8) compared to the strongly basic guanidine-type ligands (pK_a ~ 12-13).[298] It is widely assumed, that the more chemically stable carbamoylguanidines have a similar basicity to their acylguanidine counterparts, but there is no experimental data available to support that assumption. Therefore, the pK_a values of **3.145** (UR-Po563) containing both a carbamoylguanidine and an aminothiazole motif, as well as **3.213** and **3.216** (for synthesis, see chapter **3.5.1.10**; cf. Scheme 3.07) incorporating solely the carbamoylguanidine motif and the aminothiazoles **3.217** and **3.218** were determined (cf. Table 3.01a).

The pK_a values were determined by titration of the free base (**3.145**) with 1 M HCl or the titration of the HCl salts (**3.213** and **3.216**-**3.218**) with NaOH (0.01 or 0.1 M) in aqueous solution or ethanol (EtOH). These titrations were performed in the presence of a freshly calibrated glass electrode and the pK_a values were determined from the half-equivalence point (cf. Figures 3.037-3.039 and 3.189-3.191). Compounds **3.213** and **3.216**-**3.218** were used as HCl salts due to their superior solubility in water and EtOH compared to the corresponding TFA salts. Apart from the commercially available HCl salts of **3.217** and **3.218**, TFA salts of compounds **3.213** and **3.216** were prepared as hydrochlorides using 5-6 N HCl in 2-propanol and diethyl ether, as described in chapter **3.5.1.10**. The pK_a values were in good agreement with both the published data and calculated values (cf. Table 3.01a). These results confirm that the carbamoyl guanidine motif possesses a similar pK_a compared to the acylguanidine motif.

Table 3.01a. Comparison of the determined pK_a values with reference data.
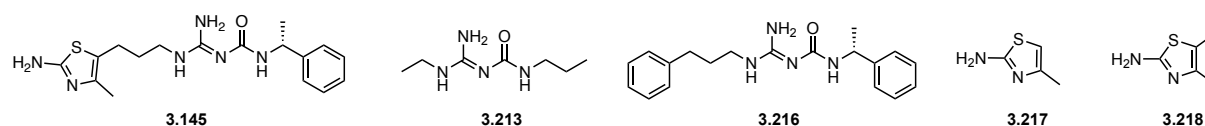
Comp.	pK_a[a]	reference/ predicted pK_a
3.145	4.68 ± 0.02 (pK_{a1}) 7.47 ± 0.04 (pK_{a2})	-
3.213	8.31 ± 0.02	-
3.216	7.96 ± 0.01	-
3.217	5.77 ± 0.02	5.95[b]; 4.64[c]; 5.36 ± 0.10*
3.218	6.28 ± 0.04	6.29[d]; 5.97 ± 0.10*

[a]pK_a values were determined by manual titration of the free base (**3.145**) with 1 M HCl or HCl salts (**3.213**, **3.216-3.217**, or **3.218**) with 0.01 or 0.1 M NaOH at rt. Data shown are means ± SEM of 3 independent experiments. [b]The exact titration conditions were not reported in the literature. The authors only stated that an aqueous solution was titrated.[384,385] [c]pK_a value was determined by titration of an aqueous solution of the free base with 0.5 M HCl at rt using a pH meter.[386] [d]pK_a value was determined by a spectrometric method in aqueous solution containing 4% EtOH at 26 °C.[385,387] *predicted pK_a values from SciFinder (conditions: most basic, T = 25 °C).

In addition to the determination of pK_a values an *in silico* study predicting several crucial physicochemical and pharmacokinetic parameters of representative monomeric (**3.139**, **3.157**, and **3.163**) and dimeric carbamoylguanidines (UR-NK22 (**3.005**)[299], UR-NK41 (**3.219**)[299], and UR-NK53 (**3.220**)[299] was conducted. Moreover, compounds which are reported to be orally bioavailable and CNS penetrable such as the anti-Parkinson agent pramipexole (**3.006**) and the acylguanidines UR-AK24 (**3.221**)[298] and UR-PG126 (**3.222**[298] were included for comparison. To obtain the data, the SwissADME web tool[129] was employed and the results are summarized in Table 3.01b. As expected, the monomeric ligands (**3.139**, **3.157**, and **3.163**) match Lipinski's rule of five[103] and Ghosen's extension[140], while the dimeric ligands suffer from several violations, e.g., due to their molecular size. In addition, the monomeric ligands possess more favorable properties including lower topological polar surface area (TPSA) (monomeric: 146.66 Å^2 vs. dimeric: 293.32 Å^2, Table 3.01b) and higher bioavailability (Abbot bioavailability score[139]; monomeric: 0.55 vs. dimeric: 0.17, Table 3.01b) if compared with their dimeric counterparts. Surprisingly, all compounds, including **3.006** and **3.221**-**3.222**, were predicted not to cross the blood-brain barrier (BBB), although experimental evidence suggests the contrary.[298] These predicted results might indicate

a potential limit of this *in silico* model since ionic transport, which is postulated for pramipexole (**3.006**)[388], can probably not be calculated.

Table 3.01b. *In silico* determined physicochemical and pharmacokinetic properties (ADME).
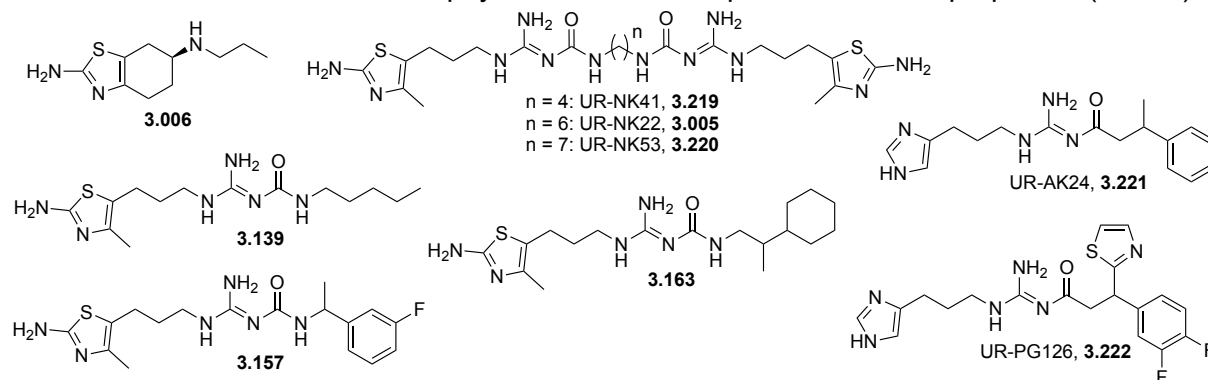
Properties	3.005	3.006	3.139	3.157	3.163	3.219	3.220	3.221	3.222
MW / g/mol	594.8	211.3	326.5	378.5	380.6	566.8	608.8	313.4	418.6
Rotatable bonds	21	3	11	9	10	19	22	9	10
HBA	6	2	3	4	3	6	6	3	6
HBD	8	2	4	4	4	8	8	3	3
Molar refractivity	163.3	61.2	92.3	102.3	109.4	153.6	168.1	91.1	106.4
TPSA / Å^{2a}	293.3	79.2	146.7	146.7	146.7	293.3	293.3	96.2	137.3
Lipophilicity, logP^b	2.28	1.88	2.10	2.54	3.03	1.70	2.55	2.09	3.08
Solubility, logS^c	-4.15	-2.39	-2.96	-3.69	-4.43	-3.66	-4.50	-2.99	-3.87
% human oral absorption^d	8	82	58	58	58	8	8	76	62
BBB permeant	No	No	No	No	No	No	No	No	No
Bioavailability^e	0.17	0.55	0.55	0.55	0.55	0.17	0.17	0.55	0.55
Drug-likeness^f	No	Yes	Yes	Yes	Yes	No	No	Yes	Yes

^{a}TPSA: topological polar surface area: this parameter correlates with human intestinal absorption (empirical data suggest a value < 140).[130] ^{b}Consensus logP[129]: average of five predictions (iLOGP[131], XLOGP3[132], WLOGP[133], MLOGP[134,135] and SILICOS-IT[129]). ^{c}LogS values were calculated with ESOL[136]: insoluble < -10 < poorly < -6 < moderately < -4 < soluble < -2 < very < 0 < highly. ^{d}The percentage of human oral absorption was calculated using the TPSA by the formula, % human oral absorption = 109 – (0.345 x TPSA), > 89%: high, < 25%: poor.[138] ^{e}Abbot bioavailability score; 0.55: 55% of the neutral, zwitterionic, or cationic compounds that pass the Lipinski criteria have >10% bioavailability; 0.17: 17% of those that fail have > 10% bioavailability.[139] ^{f}Lipinski criteria[103] (molecular weight (MW) ≤ 500, H-bond donors (HBD) ≤ 5, H-bond acceptors (HBA) ≤ 10, logP ≤ 5); Ghose criteria[140] (160 ≤ MW ≤ 480, -0.4 ≤ logP ≤ 5.6, 40 ≤ molar refractivity ≤ 130, 20 ≤ atom number ≤ 70). The bioavailability radars generated with SwissADME web tool are shown in chapter **3.6.16** (cf. Figure 3.211).

Since the compounds **3.139**, **3.157**, and **3.163**, containing both an aminothiazole and a carbamoylguanidine partial structure, possess appropriate pK_a values as well as good physicochemical and pharmacokinetic properties, it can be concluded that the optimization and simplification strategy was in many cases very successful. The obtained *in silico* data indicate that the compounds **3.139**, **3.157**, and **3.163** are more

drug-like than their dimeric counterparts and should be promising lead structures for the elucidation of the role of the H$_2$R in the CNS.

3.3.2.3 Binding Affinities at the Human Histamine Receptor Family

The (thio)carbamoylated guanidines **3.138**-**3.186** were investigated in radioligand competition binding experiments to elucidate their structure-affinity relationships at the hH$_2$R and their selectivity over the hH$_1$R, hH$_3$R, and hH$_4$R subtypes. The results are presented in Table 3.02 as binding constants (pK_i values), determined on membrane preparations of Sf9 insect cells expressing the hH$_{1-4}$R, respectively. Radioligand displacement curves of representative compounds are shown in Figure 3.014 and additional curves are shown in chapter **3.6.7** (cf. Figures 3.196-3.198). In case of the aminothiazolylpropyl carbamoylguanidines, a large number of variations of the residue R were well tolerated, leading to high affinity hH$_2$R ligands with pK_i values over 7 (compounds: **3.138**-**3.172**). However, there were some exceptions: e.g., a cyclohexyl (**3.141**) or a phenyl (**3.142**) residue resulted in low to moderate hH$_2$R affinity with pK_i values of 5.50 and 6.77 (cf. Table 3.02). This leads to the assumption that bulky substituents are not well tolerated in very close proximity to the carbamoylguanidine function. The hH$_2$R affinity of aminomethylthiazolylpropyl carbamoylated guanidines with a terminal n-alkyl residue was dependent on the chain length (**3.138**-**3.140**). While the n-propyl containing ligand **3.138** showed a moderate affinity with a pK_i value of 6.98, the ligands containing a n-hexyl or n-pentyl residue showed higher affinities with pK_i values of 7.54 (**3.140**) and 8.35 (**3.139**, UR-KAT523) (cf. Table 3.02). Interestingly, most of the ligands investigated containing a benzyl residue with or without further substituents (**3.143**-**3.157**) showed high hH$_2$R affinities with pK_i values over 7. Only the trifluoromethyl containing ligands **3.147** and **3.155** showed moderate affinities with pK_i values of 6.64 and 6.90 (cf. Table 3.02). Branched residues were also well-tolerated as were the introduction of a phenyl, methyl, ethyl or isopropyl substituents (ligands **3.144**-**3.149**: pK_i: 7.2-7.8) which resulted in no change or even an increase of affinity compared to the unbranched analogue (pK_i (**3.143**): 7.16) (cf. Table 3.02). Furthermore, substituents in ortho-, meta-, and para-position of the phenyl ring of the branched 1-phenyleth-1-yl containing ligands were also well tolerated. Methyl, fluoro-, chloro-, bromo-, and methoxy- substituents in the para or a fluoro-substituent in the ortho position led to high affinity hH$_2$R ligands with pK_i values of 7.3-7.5 (ligands **3.150**-**3.154** and **3.156**) (cf. Table 3.02). Noteworthily, a fluoro-substituent in the meta position

of the phenyl ring of the 1-phenyleth-1-yl residue (**3.157**, (UR-MB-69)) resulted in an increased affinity (pK_i: 8.69) compared to the para or ortho fluoro-substituted ligands (pK_i (**3.151**): 7.50 and pK_i (**3.156**): 7.54) (cf. Table 3.02). Heteroarene (e.g., fur-2-yl-methyl, 1-(fur-2-yl)-eth-1-yl or 1-(thiophen-2-yl)-eth-1-yl) containing ligands (**3.158**-**3.160**) showed high hH₂R affinities with pK_i values of 7.2-8.0 (cf. Table 3.02). A 2-phenyl-eth-1-yl scaffold as a residue resulted in aminothiazolylpropyl carbamoyl guanidines (**3.161**, **3.162**, and **3.164**-**3.168**) with pK_i values of around 7. The introduction of an aliphatic 2-cyclohexyl-eth-1-yl residue (**3.163**) resulted in a slightly higher affinity with a pK_i value of 7.40 compared to the aromatic counterpart (pK_i (**3.164**): 7.16) (cf. Table 3.02). Aminothiazolylpropyl carbamoylated guanidines with residues containing longer linkers, as represented in **3.169**-**3.172**, showed high affinities with pK_i values of 7.1-7.2 (cf. Table 3.02), but did not bring a significant improvement in ligand affinity at the hH₂R. All attempted modifications of the aminothiazolylpropyl carbamoylguanidine pharmacophore (**3.173**-**3.186**), for example, by rigidization of the aminothiazolylpropyl moiety or the bioisosteric replacement of the carbamoylguanidine by a thiocarbamoylguanidine, resulted in low to moderate hH₂R affinity ligands with pK_i values of 3.4-6.9 (cf. Table 3.02). All investigated ligands showed a low affinity at the other hHR subtypes (hH$_{1,3,4}$Rs) with pK_i values of 4.1-5.9 (cf. Table 3.02). The high affinity at the hH₂R combined with the low affinity at the other subtypes led to an excellent subtype selectivity (3 to 4 orders of magnitude) for the ligands **3.139** and **3.157**-**3.159**. The ligands **3.139**, **3.157**, and **3.158** showed similar or even higher hH₂R affinities (pK_i values of 8.35, 8.69, and 7.98) than the already described dimeric aminothiazole containing carbamoylguanidine UR-NK22 (**3.005**)[299] (pK_i: 8.07[299]) (cf. Table 3.02). In addition, the subtype selectivity of these small molecules (molecular weight: < 400 g/mol) is improved compared to the bulky dimeric ligands like **3.005** and analogues (molecular weight: > 550 g/mol). A summary of the structure-affinity relationships based on the H₂R affinity of the synthesized carbamoylguanidines is presented in Figure 3.015. The influence of the stereochemistry on hH₂R affinity and subtype selectivity was investigated based on the enantiomeric pairs **3.145** and **3.146**, **3.164** and **3.165**, **3.174** and **3.175**, as well as **3.177** and **3.178**. The enantiomeric pairs showed only slight differences in hH₂R affinity and subtype selectivity. For example, the ligands **3.145** (pK_i: 7.75) and **3.174** (pK_i: 6.94) with (*R*)-configuration tended to show slightly higher hH₂R affinities when compared to their counterparts **3.146** (pK_i: 7.29) and **3.175** (pK_i: 6.47) with

(*S*)-configuration (cf. Table 3.02). The enantiomeric purity of **3.145**, **3.146**, **3.164**, **3.165**, **3.174**, **3.175**, **3.177**, and **3.178** was determined as described in chapter **3.5.1.17** (cf. Figures 3.035 and 3.036).
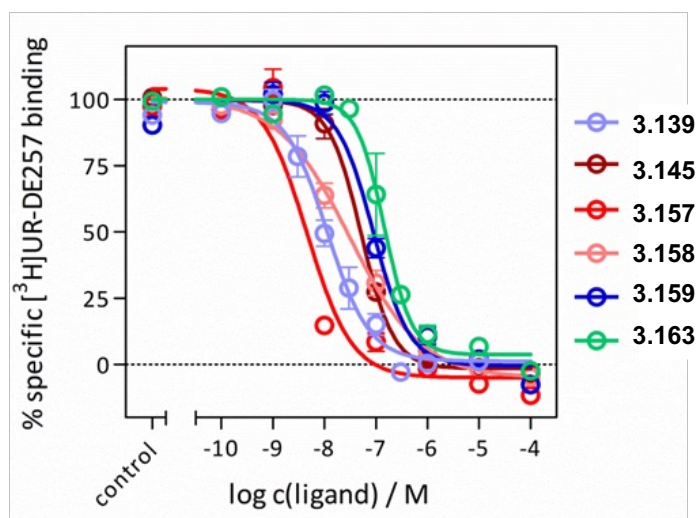
Figure 3.014. Displacement of the radioligand [³H]UR-DE257[38] (c = 20 nM, K_d = 12.2 nM) by increasing concentrations of the respective ligand determined on membrane preparations of Sf9 insect cells expressing the hH₂R-G$_{sαS}$ fusion protein. Data represent mean values ± SEM of 2-3 independent experiments, each performed in triplicate.
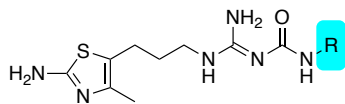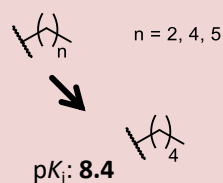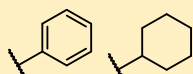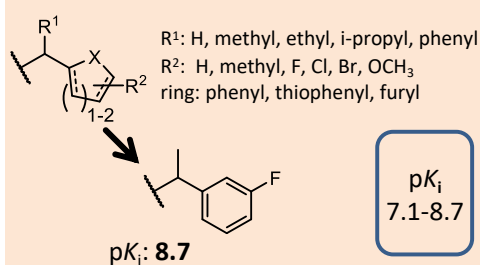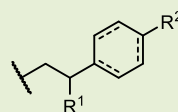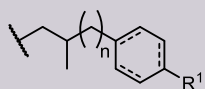
Figure 3.015. H₂R affinity of agonistic carbamoylguanidines: summary of structure-affinity relationships.

Table 3.02. Affinities of the monomeric (thio)carbamoylated guanidines **3.138-3.186** at the hH$_{1-4}$R, obtained from competition binding studies on membrane preparations of Sf9 insect cells expressing the respective histamine receptor subtype.

3.138-3.172

3.173-3.178

3.179-3.184

3.185-3.186

Comp.	R	pK$_i$								Selectivity ratios of K$_i$ H₁R / H₂R / H₃R / H₄R)
		hH₁R[a]	N	hH₂R[b]	N	hH₃R[c]	N	hH₄R[e]	N	
3.001	-	5.62 ± 0.03[389]	3	6.58 ± 0.04[389]	48	7.59 ± 0.01[389]	42	7.60 ± 0.01[389]	45	9 / 1 / 0.1 / 0.1
3.005	-	6.06 ± 0.05[299]	2	8.07 ± 0.05[299]	3	5.94 ± 0.16[299]	3	5.69 ± 0.07[299]	4	102 / 1 / 135 / 240
3.006	-	n.d.	-	4.86 ± 0.07	5	n.d.	-	n.d.	-	-
3.138		4.54 ± 0.02	3	6.98 ± 0.11	3	4.35 ± 0.01	3	4.06 ± 0.06	2	275 / 1 / 427 / 832
3.139		4.97 ± 0.10	3	8.35 ± 0.08	3	4.98 ± 0.17	3	5.37 ± 0.09	3	2399 / 1 / 2344 / 955
3.140		5.11 ± 0.03	3	7.54 ± 0.07	4	5.25 ± 0.02	3	5.09 ± 0.02	2	269 / 1 / 195 / 282
3.141		4.61 ± 0.09	3	6.77 ± 0.27	3	n.d.	-	4.50 ± 0.06	2	145 / 1 / - / 186
3.142		n.d.	-	5.50 ± 0.08	3	n.d.	-	4.65 ± 0.05	2	- / 1 / - /7
3.143		5.21 ± 0.02	3	7.16 ± 0.05	3	4.71 ± 0.05	3	4.72 ± 0.09	2	89 / 1 /282 / 275
3.144		4.80 ± 0.02	3	7.36 ± 0.01	3	5.04 ± 0.08	3	5.20 ± 0.04	3	363 / 1 / 209 / 145
3.145		5.06 ± 0.05	3	7.75 ± 0.05	3	4.36 ± 0.04	3	4.87 ± 0.01	3	490 / 1 / 2455 / 759
3.146		4.67 ± 0.06	3	7.29 ± 0.04	3	4.48 ± 0.02	3	4.75 ± 0.01	3	417 / 1 / 646 / 347
3.147		4.27 ± 0.02	3	6.64 ± 0.02	3	4.50 ± 0.02	3	4.76 ± 0.08	3	234 / 1 /138 /76

Table 3.02 (continued)

3.138-3.172

3.173-3.178

3.179-3.184

3.185-3.186

Comp.	R	pK_i								Selectivity ratios of K_i $H_1R / H_2R / H_3R / H_4R)$
		hH_1R^a	N	hH_2R^b	N	hH_3R^c	N	hH_4R^e	N	
3.148		4.90 ± 0.04	3	7.20 ± 0.04	3	4.66 ± 0.02	3	4.95 ± 0.03	3	200 / 1 / 347 /178
3.149		4.61 ± 0.14	3	7.45 ± 0.02	3	4.72 ± 0.05	3	5.10 ± 0.10	3	692 / 1 / 537 / 224
3.150		5.29 ± 0.04	3	7.51 ± 0.04	3	4.58 ± 0.03	3	4.95 ± 0.01	3	166 / 1 / 851 / 363
3.151		4.99 ± 0.03	3	7.50 ± 0.06	3	4.59 ± 0.04	3	4.86 ± 0.04	3	324 / 1 / 813 / 437
3.152		5.35 ± 0.04	3	7.33 ± 0.03	3	4.75 ± 0.02	3	5.07 ± 0.01	3	95 / 1 / 380 / 182
3.153		5.54 ± 0.01	3	7.52 ± 0.06	3	4.89 ± 0.01	3	5.09 ± 0.03	3	95 / 1 / 427 / 269
3.154		5.23 ± 0.06	3	7.43 ± 0.03	3	4.48 ± 0.04	3	4.70 ± 0.03	3	158 / 1 / 891 / 537
3.155		4.66 ± 0.13	3	6.90 ± 0.07	3	4.84 ± 0.07	3	5.09 ± 0.07	3	174 / 1 / 115 / 65
3.156		4.77 ± 0.10	3	7.54 ± 0.02	3	4.51 ± 0.06	3	4.89 ± 0.03	3	589 / 1 / 1072 / 447
3.157		5.11 ± 0.10	3	8.69 ± 0.10	3	4.41 ± 0.06	3	4.88 ± 0.01	3	3802 / 1 / 19055 / 6457
3.158		4.62 ± 0.09	3	7.98 ± 0.01	3	4.13 ± 0.01	3	4.12 ± 0.06	3	2291 / 1 / 7079 / 7244
3.159		4.34 ± 0.11	3	7.50 ± 0.08	3	4.36 ± 0.07	3	4.34 ± 0.05	3	1445 /1 / 1380 / 1445
3.160		4.59 ± 0.02	3	7.20 ± 0.03	3	4.23 ± 0.01	3	4.52 ± 0.03	3	407 / 1 / 933 / 479
3.161		n.d.	-	6.80 ± 0.20	4	n.d.	-	4.83 ± 0.06	2	- / 1 / - / 93
3.162		5.28 ± 0.01	3	7.06 ± 0.04	3	5.00 ± 0.01	3	5.31 ± 0.03	3	60 / 1 / 115 / 56
3.163		5.63 ± 0.06	3	7.40 ± 0.01	2	5.00 ± 0.08	3	5.72 ± 0.05^f	3	59 / 1 /251 / 48

351

Table 3.02 (continued)

3.138-3.172

3.173-3.178

3.179-3.184

3.185-3.186

Comp.	R	pK_i								Selectivity ratios of K_i H₁R / H₂R / H₃R / H₄R)
		hH₁R[a]	N	hH₂R[b]	N	hH₃R[c]	N	hH₄R[e]	N	
3.164		5.06 ± 0.06	3	7.00 ± 0.05	3	4.77 ± 0.05	3	4.92 ± 0.02	3	87 / 1 / 170 / 120
3.165		5.02 ± 0.05	3	6.99 ± 0.06	3	4.57 ± 0.06	3	4.87 ± 0.01	3	93 / 1 / 263 / 132
3.166		5.10 ± 0.08	3	7.11 ± 0.03	3	4.78 ± 0.03[d]	3	5.17 ± 0.02[f]	3	102 / 1 / 214 / 87
3.167		5.23 ± 0.03	3	6.99 ± 0.05	3	4.93 ± 0.03[d]	3	5.23 ± 0.03[f]	3	58 / 1 / 115 / 58
3.168		5.31 ± 0.02	3	6.83 ± 0.08	3	5.10 ± 0.02[d]	3	5.58 ± 0.01	3	33 / 1 / 54 / 18
3.169		5.42 ± 0.07	3	7.15 ± 0.02	4	5.13 ± 0.01[d]	3	5.43 ± 0.01[f]	3	54 / 1 / 105 / 52
3.170		5.78 ± 0.13	3	7.14 ± 0.08	2	5.49 ± 0.01	3	5.44 ± 0.02[f]	3	23 / 1 / 45 / 50
3.171		5.87 ± 0.09	3	7.20 ± 0.04	3	5.04 ± 0.04[d]	3	5.49 ± 0.08[f]	3	21 / 1 / 145 / 51
3.172		5.15 ± 0.07	3	7.22 ± 0.05	3	5.64 ± 0.08	3	6.11 ± 0.13	3	117 / 1 / 38 / 13
3.173		4.33 ± 0.01	3	6.22 ± 0.10	3	4.36 ± 0.06	3	4.63 ± 0.02	3	78 / 1 / 72 / 39
3.174		3.96 ± 0.07	3	6.94 ± 0.08	3	4.19 ± 0.03	3	4.57 ± 0.01	3	955 / 1 / 562 / 234
3.175		4.11 ± 0.06	3	6.47 ± 0.05	3	4.09 ± 0.07	3	4.26 ± 0.02	3	229 / 1 / 240 / 162
3.176		4.35 ± 0.01	3	5.84 ± 0.02	3	4.33 ± 0.06	3	4.67 ± 0.02	3	31 / 1 / 32 / 15
3.177		4.20 ± 0.03	3	5.94 ± 0.06	3	4.16 ± 0.03	3	4.35 ± 0.01	3	55 / 1 / 60 / 39

Table 3.02 (continued)
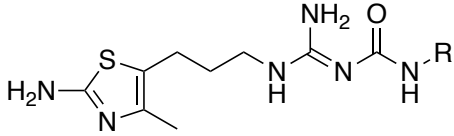
3.138-3.172

3.173-3.178

3.179-3.184

3.185-3.186

Comp.	R	pK_i								Selectivity ratios of K_i
		hH_1R^a	N	hH_2R^b	N	hH_3R^c	N	hH_4R^e	N	H_1R / H_2R / H_3R / H_4R)
3.178		4.28 ± 0.01	3	6.37 ± 0.06	3	4.08 ± 0.10	3	4.49 ± 0.02	3	123 / 1 /195 / 76
3.179		n.d.	-	5.28 ± 0.06	4	n.d.	-	<4.0	2	- / 1 / - / >19
3.180		n.d.	-	6.16 ± 0.07	4	4.96 ± 0.07	3	5.02 ± 0.06	2	- / 1 / 16 / 14
3.181		n.d.	-	5.35 ± 0.02	3	n.d.	-	4.87 ± 0.03	2	- / 1 / - / 3
3.182		n.d.	-	3.43 ± 0.07	3	n.d.	-	4.19 ± 0.10	2	- / 1 / - / 0.2
3.183		n.d.	-	5.70 ± 0.10	3	n.d.	-	4.46 ± 0.01	2	- / 1 / - / 17
3.184		n.d.	-	5.40 ± 0.05	3	n.d.	-	4.52 ± 0.13	2	- / 1 / - / 8
3.185		5.71 ± 0.02	3	5.95 ± 0.06	4	5.82 ± 0.03	3	4.78 ± 0.05	2	2 / 1 / 1 / 15
3.186		5.92 ± 0.02	3	6.29 ± 0.08	3	5.48 ± 0.06	3	4.52 ± 0.01	2	2 / 1 / 6 / 59

Competition binding assay on membrane preparations of Sf9 insect cells: [a]co-expression of the hH₁R and RGS4 proteins (radioligand: [³H]mepyramine, c = 5 nM, K_d = 4.5 nM), [b]expression of the hH₂R-G$_{saS}$ fusion protein (radioligand: [³H]UR-DE257[390], c = 20 nM, K_d = 12.2 nM), [c]co-expression of the hH₃R, G$_{αi2}$, and G$_{β1γ2}$ proteins (radioligand: [³H]UR-PI294[391] c = 2 nM, K_d = 1.1 nM or [d][³H]histamine c = 15 nM, K_d = 12.1 nM), or [e]co-expression of the hH₄R, G$_{αi2}$, and G$_{β1γ2}$ proteins (radioligand: [³H]histamine c = 10 nM, K_d = 15.9 nM or [f][³H]UR-PI294[391] c = 5 nM, K_d = 5.1 nM). Data were analyzed by nonlinear regression and were best-fitted to four-parameter sigmoidal concentration-response curves. Data shown are means ± SEM of N independent experiments, each performed in triplicate. n.d.: not determined.
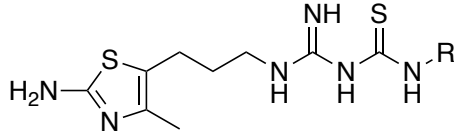
3.3.2.4 Functional Characterization of Selected (Thio)Carbamoylguanidines at the Guinea Pig/Human H₂Rs

The aminothiazoles **3.138**-**3.186** were investigated for gp/hH₂R agonism in the guinea pig right atrium assay[389,392] (gpH₂R) (cf. Table 3.03 and Figure 3.192), the [³⁵S]GTPγS binding assay[299,389,393,394] (hH₂R) and/or the β-arrestin2 recruitment assay[187,394,395] (hH₂R) (cf. Table 3.04). The aminothiazolylpropyl containing N^G-carbamoylated guanidines **3.139**, **3.140**, **3.144**-**3.154**, **3.156**-**3.160**, **3.164**, and **3.165** showed high agonistic activities at the gpH₂R with pEC₅₀ values of 7.3-8.2 and were primarily strong partial or even full agonists (e.g., **3.146**, **3.149**, and **3.159**) (cf. Table 3.03). Only the carbamoylguanidines **3.155** and **3.162** were moderately active partial agonists with pEC₅₀ values of 6.14 and 6.76 (cf. Table 3.03). The N^G-thiocarbamoylated guanidines **3.173**-**3.178** were partial agonists at the gpH₂R with pEC₅₀ values of 6.3-7.2 (cf. Table 3.03). The bulky ligand **3.176** was inactive at the gpH₂R within the concentration range of the assay. The highest potencies at the gpH₂R were shown by the n-pentyl residue-containing ligand **3.139** (pEC₅₀: 8.24) and the 2-phenyl-eth-2-yl residue-containing ligand **3.145** with (R)-configuration (pEC₅₀ value of 8.12): appearing as strong partial agonist or full agonist (α: 0.78 and 0.95, respectively) (cf. Table 3.03). The high affinity hH₂R ligand **3.157** (pK_i: 8.69) was a strong partial agonist (α: 0.85) at the gpH₂R with a pEC₅₀ value of 7.58 (cf. Table 3.03). The enantiomeric pairs **3.145** and **3.146**, **3.164** and **3.165**, **3.174** and **3.175**, as well as **3.177** and **3.178** showed only slight differences in agonistic potency and efficacy with eudismic ratios (EC₅₀ value of the eutomer divided by EC₅₀ value of the distomer) ranging from 2.0-3.3. The ligands **3.145** (pEC₅₀: 8.12) and **3.174** (pEC₅₀: 7.05) with (R)-configuration tended to possess higher gpH₂R potencies when compared to their counterparts **3.146** (pEC₅₀: 7.63) and **3.175** (pEC₅₀: 6.65) with (S)-configuration (cf. Table 3.03). On the other hand, the ligands **3.165** (pEC₅₀: 7.89) and **3.178** (pEC₅₀: 6.83) with (S)-configuration tended to possess higher gpH₂R potencies compared to their counterparts **3.164** (pEC₅₀: 7.59) and **3.177** (pEC₅₀: 6.31) with (R)-configuration (cf. Table 3.03). Noteworthy, due to the side chain elongation in **3.164** and **3.177** (one methylene group), the orientation of the methyl group in the binding pocket should be identical for all the four eutomers described.
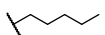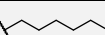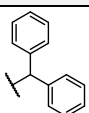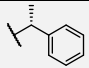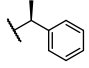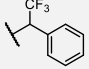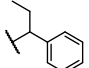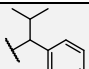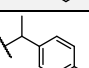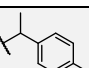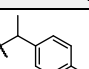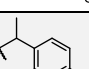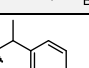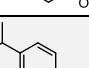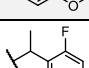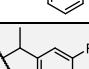
Table 3.03. gpH$_2$R agonism and the calculated pEC$_{50}$ values of the monomeric (thio)carbamoylated guanidines determined by organ bath studies (spontaneously beating guinea pig right atrium).

3.139-3.140, 3.144-3.160, 3.162, 3.164-3.165

3.173-3.178

Comp.	R	gpH$_2$R (atrium)[c]		
		pEC$_{50}$	α	N
3.001	-	6.16 ± 0.01^{389}	1.00^{389}	225
3.139		8.24 ± 0.03	0.78 ± 0.03	3
3.140		7.80 ± 0.07	0.95 ± 0.06	3
3.144		7.40 ± 0.13	0.90 ± 0.06	3
3.145		8.12 ± 0.07	0.95 ± 0.07	4
3.146		7.63 ± 0.13	1.08 ± 0.07	3
3.147		7.32 ± 0.14	0.85 ± 0.06	3
3.148		7.97 ± 0.09	0.93 ± 0.04	3
3.149		7.46 ± 0.13	1.04 ± 0.04	3
3.150		7.65 ± 0.07	0.85 ± 0.05	3
3.151		7.63 ± 0.05	0.92 ± 0.01	3
3.152		7.61 ± 0.06	0.93 ± 0.04	3
3.153		7.26 ± 0.05	0.87 ± 0.04	3
3.154		7.42 ± 0.07	0.91 ± 0.04	3
3.155		6.14 ± 0.10	0.61 ± 0.05	3
3.156		7.91 ± 0.01	0.93 ± 0.03	3
3.157		7.58 ± 0.14	0.85 ± 0.05	4

Table 3.03 (continued)

**3.139-3.140, 3.144-3.160,
3.162, 3.164-3.165**

3.173-3.178

Comp.	R	gpH$_2$R (atrium)^c		
		pEC$_{50}$	α	N
3.158		7.93 ± 0.07	0.58 ± 0.05	3
3.159		8.01 ± 0.18	1.00 ± 0.04	3
3.160		8.00 ± 0.05	0.88 ± 0.04	3
3.162		6.76 ± 0.11	0.76 ± 0.05	3
3.164		7.59 ± 0.05	0.99 ± 0.07	3
3.165		7.89 ± 0.10	0.98 ± 0.06	3
3.173		7.18 ± 0.10	0.67 ± 0.05	4
3.174		7.05 ±0.16	0.87 ± 0.02	3
3.175		6.65 ± 0.14	0.65 ± 0.04	3
3.176		inactive	-	3
3.177		6.31 ± 0.05	0.44 ± 0.03	3
3.178		6.83 ± 0.06	0.66 ± 0.04	3

Data were analyzed by nonlinear regression and were best fitted to sigmoidal concentration response curves. ^{a}pEC$_{50}$ = -log EC$_{50}$. ^{b}pEC$_{50}$ was calculated from the mean-corrected shift ΔpEC$_{50}$ of the agonist curve relative to the histamine reference (pEC$_{50}$ = 6.16, N = 225)[389] curve by equation pEC$_{50}$ = 6.16 + ΔpEC$_{50}$. ^{c}The intrinsic activity (α) of histamine was set to 1.00, and α values of investigated compounds were referred to this value. Data represent mean values ± SEM of N independent experiments.

The N^G-carbamoylated guanidines **3.138**, **3.140**-**3.143**, **3.161**, **3.163**, **3.166**-**3.171**, and **3.185**-**3.186** were investigated for hH$_2$R agonism in the [^{35}S]GTPγS binding assay on membrane preparations of Sf9 insect cells expressing the hH$_2$R-G$_{s\alpha S}$ fusion protein (cf. Table 3.04). Compounds **3.179**-**3.184** were tested in the antagonistic mode versus

histamine to determine their pK_b values. The ligands **3.138**-**3.143**, **3.145**-**3.146**, **3.157**, **3.159**, **3.161**, **3.163**, **3.166**-**3.172**, **3.174**, and **3.186** were also investigated for agonism in the β-arrestin2 recruitment assay on HEK293T-β-Arr2-hH₂R cells, stably expressing the hH₂R-ElucC and βArr2-ElucN fusion constructs.[187] Functional testing in the gpH₂R right atrium and β-arrestin2 recruitment assays ensured a comprehensive characterization, at least for the most interesting compounds. The monomeric N^G-carbamoylated amino(methyl)thiazolylpropylguanidines **3.138**, **3.140**-**3.143**, **3.161**, **3.163**, and **3.166**-**3.171** were partial to full agonists in the [³⁵S]GTPγS binding assay and showed moderate to high hH₂R potencies with pEC_{50} values of 6.3-7.8 (cf. Table 3.04). The benzyl residue containing ligand **3.143** showed a high potency with a pEC_{50} value of 7.54 combined with strong partial agonism. Ligands containing a n-hexyl residue (**3.140**), a branched 2-phenyl-eth-1-yl residue (**3.166**-**3.168**, **3.170**, and **3.171**), or a branched 2-cyclohexyl-eth-1-yl residue (**3.163** and **3.169**) were highly potent partial agonists with pEC_{50} value of 7.2-7.8 (cf. Table 3.04). Interestingly, the aminothiazolylphenyl containing ligands **3.179**-**3.184** appeared as weak antagonists at the hH₂R with pK_b values (4.8-6.1, Table 3.04) which were in good agreement with the pK_i values obtained (3.4-6.2, Table 3.02). Introduction of the less flexible 2-amino-4,5,6,7-tetrahydrobenzothiazol-6-yl moiety (**3.185** and **3.186**) resulted in partial agonism (**3.186**, α: 0.57, pEC_{50}: 6.67) or weak partial agonism (**3.185**, α: 0.16, pEC_{50}: 5.57) (cf. Table 3.04). The structurally related dopamine receptor agonist pramipexole (**3.006**) was also a partial agonist at the hH₂R (α: 0.66, pEC_{50}: 5.07) (cf. Table 3.04). Ligand characterization in the β-arrestin2 recruitment assay showed that compounds **3.138**-**3.143**, **3.145**-**3.146**, **3.157**, **3.159**, **3.161**, **3.163**, **3.166**-**3.172**, **3.174**, and **3.186** were partial agonists with pEC_{50} values of 5.4-7.3 (cf. Figure 3.193, chapter **3.6.6**). The data obtained were comparable with the [³⁵S]GTPγS assay data but generally lower potencies and efficacies in the β-arrestin2 recruitment assay were observed. The enantiopure ligand **3.145** and the 1-(3-fluoro-phenyl)eth-1-yl residue containing ligand **3.156** showed the highest agonistic potencies resulting in pEC_{50} values in the two-digit nanomolar range (7.34 and 7.19) (cf. Table 3.04). Overall, the (partial) agonists investigated in both [³⁵S]GTPγS and β-arrestin2 recruitment assay showed varying degrees of bias for G protein activation (cf. Figure 3.209, chapter **3.6.14**). This is in agreement with the findings for acylguanidines and dimeric carbamoylguanidines.[187]

Table 3.04. hH$_2$R agonism or antagonism and the calculated pEC$_{50}$ or pK_b values of the monomeric (thio)carbamoylated guanidines determined by a [^{35}S]GTPγS binding assay and/or β-arrestin2 recruitment assay.

3.138-3.143, 3.145-3.146, 3.157, 3.159, 3.161, 3.163, 3.166-3.172

3.174

3.179-3.184

3.185-3.186
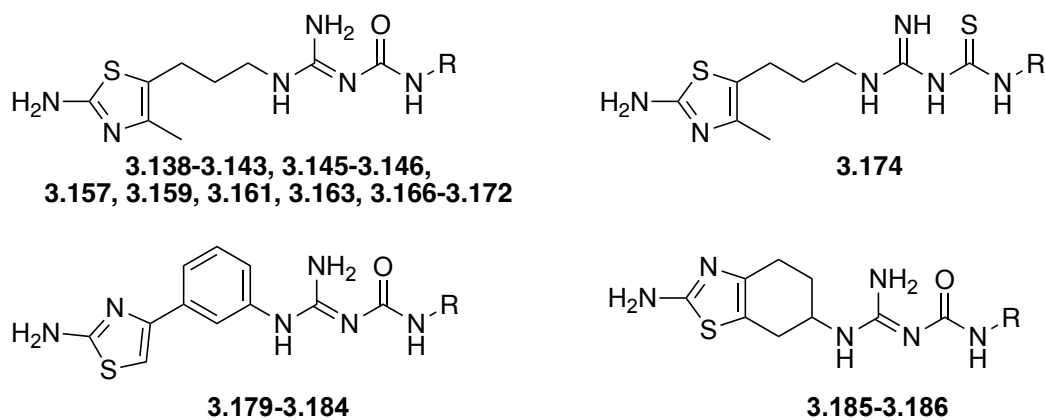
Comp.	R	hH$_2$R ([^{35}S]GTPγS)[a]			hH$_2$R (β-arrestin2 recruitment)[b]		
		pEC$_{50}$ (pK_b)	N	α	pEC$_{50}$	N	α
3.001	-	6.01 ± 0.07[389]	7	1.00[389]	5.42 ± 0.02[187]	3	1.00[187]
3.006	-	5.07 ± 0.06	5	0.66 ± 0.08	4.40 ± 0.10	3	0.35 ± 0.03
3.138		6.75 ± 0.06	3	0.79 ± 0.09*	6.77 ± 0.04	3	0.32 ± 0.01
3.139		n.d.	-	n.d.	6.75 ± 0.12	3	0.15 ± 0.02
3.140		7.41 ± 0.07	3	0.60 ± 0.09*	7.07 ± 0.02	3	0.28 ± 0.03
3.141		6.83 ± 0.20	3	0.96 ± 0.07	6.41 ± 0.03	3	0.43 ± 0.06
3.142		6.28 ± 0.24	2	0.59 ± 0.02*	5.47 ± 0.06	3	0.25 ± 0.02
3.143		7.54 ± 0.12	4	0.91 ± 0.07*	7.00 ± 0.08	3	0.33 ± 0.03
3.145		n.d.	-	n.d.	7.34 ± 0.11	4	0.34 ± 0.03
3.146		n.d.	-	n.d.	6.48 ± 0.06	4	0.46 ± 0.02
3.157		n.d.	-	n.d.	7.19 ± 0.11	4	0.30 ± 0.01
3.159		n.d.	-	n.d.	6.63 ± 0.06	3	0.25 ± 0.01

Table 3.04 (continued)
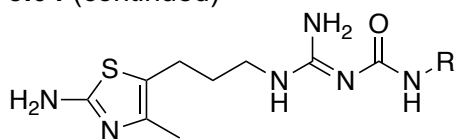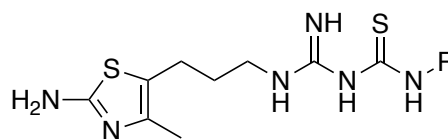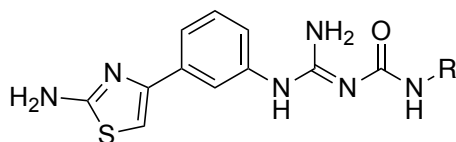
**3.138-3.143, 3.145-3.146,
3.157, 3.159, 3.161, 3.163, 3.166-3.172**

3.174

3.179-3.184
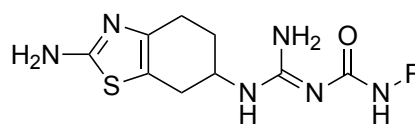
3.185-3.186

Comp.	R	hH$_2$R ([^{35}S]GTPγS)[a]			hH$_2$R (β-arrestin2 recruitment)[b]		
		pEC$_{50}$ (pK_b)	N	α	pEC$_{50}$	N	α
3.161		7.35 ± 0.16	3	0.72 ± 0.06*	6.78 ± 0.03	3	0.29 ± 0.02
3.163		7.66 ± 0.08	3	0.65 ± 0.03*	6.65 ± 0.09	3	0.40 ± 0.06*
3.166		7.54 ± 0.14	3	0.60 ± 0.04	6.57 ± 0.08	3	0.16 ± 0.02*
3.167		7.51 ± 0.06	3	0.52 ± 0.03*	6.80 ± 0.10	3	0.11 ± 0.01*
3.168		7.46 ±0.03	3	0.59 ± 0.02*	6.55 ± 0.02	3	0.25 ± 0.03*
3.169		7.76 ± 0.04	3	0.60 ±0.07	6.52 ± 0.07	3	0.22 ± 0.01*
3.170		7.22 ± 0.1	5	0.68 ± 0.07*	6.88 ± 0.10	3	0.10 ± 0.01*
3.171		7.53 ± 0.06	3	0.69 ± 0.02*	6.45 ± 0.06	3	0.20 ± 0.02*
3.172		n.d.	-	n.d.	5.60 ± 0.11	4	0.14 ± 0.02
3.174		n.d.	-	n.d.	6.43 ± 0.06	3	0.11 ± 0.01
3.179		(4.91 ± 0.09)	3	n.d.	n.d.	-	n.d.
3.180		(6.14 ± 0.03)	3	n.d.	n.d.	-	n.d.

Table 3.04 (continued)

**3.138-3.143, 3.145-3.146,
3.157, 3.159, 3.161, 3.163, 3.166-3.172**

3.174

3.179-3.184

3.185-3.186
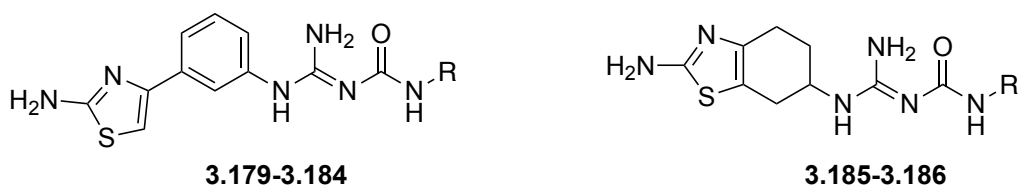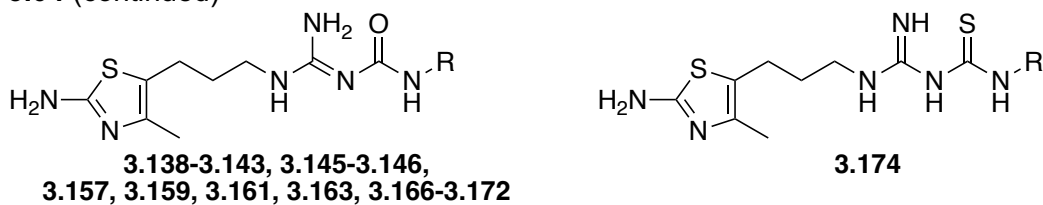
Comp.	R	hH$_2$R ([^{35}S]GTPγS)^a			hH$_2$R (β-arrestin2 recruitment)^b		
		pEC$_{50}$ (pK_b)	N	α	pEC$_{50}$	N	α
3.181		(5.40 ± 0.02)	3	n.d.	n.d.	-	n.d.
3.182		(4.76 ± 0.11)	3	n.d.	n.d.	-	n.d.
3.183		(5.44 ± 0.02)	3	n.d.	n.d.	-	n.d.
3.184		(5.52 ± 0.05)	3	n.d.	n.d.	-	n.d.
3.185		6.83 ± 0.06	3	0.16 ± 0.07*	n.d.	-	n.d.
3.186		6.67 ± 0.31	3	0.53 ± 0.05*	5.36 ± 0.05	3	0.31 ± 0.03

^{a}[^{35}S]GTPγS assay performed with membrane preparations of Sf9 insect cells expressing the hH$_2$R-G$_{sαS}$ fusion protein.[299,389,393,394] ^{b}β-arrestin2 recruitment determined using HEK293T-β-Arr2-hH$_2$R cells, stably expressing the hH$_2$R-ElucC and βArr2-ElucN fusion constructs.[187,394,395] The intrinsic activity (α) of histamine was set to 1.00, and the α values of investigated compounds were referred to this value. The pK_b values of **3.179**-**3.184** were determined in the antagonist mode versus histamine (c = 1 µM). Data represent mean values ± SEM of N independent experiments, each performed in triplicate ([^{35}S]GTPγS assay) or duplicate/triplicate (β-arrestin2 recruitment assay). n.d.: not determined. *At concentrations ≥ 30 µM a varying degree of depression of the maximum effect was observed. This effect has already been reported for several GPCRs in the literature.[396–402]

3.3.2.5 Binding Affinities at the Human D$_{2long}$R and D$_3$R

Aminothiazole containing ligands such as pramipexole (**3.006**) and its derivatives (e.g., **3.007**) are described as high affinity dopamine receptor ligands (preferring the D$_2$-like family).[403] Because of the structural similarity between pramipexole (**3.006**) and the N^G-(thio)carbamoylated guanidines that were prepared, selected ligands **3.139**, **3.140**, **3.143**, **3.145**, **3.146**, **3.157**, **3.159**, **3.163**, **3.166**, **3.169-3.172**, **3.174**, **3.180**, **3.185**, and **3.186** were investigated in competition binding experiments on homogenates of HEK293T-CRE-Luc-hD$_{2long}$R and HEK293T-CRE-Luc-hD$_3$R cells using [^{3}H]N-methylspiperone as radioligand.[404] The results are summarized in Table 3.05 and radioligand displacement curves (hD$_3$R) of representative compounds are shown in Figure 3.016. For the standard agonist pramipexole biphasic displacement curves were reported at the hD$_{2long}$R with pK_i values for high (p$K_{i/high}$ value) and low affinity binding (p$K_{i/low}$ value) sites.[404] The N^G-(thio)carbamoylated guanidines **3.139**, **3.140**, **3.143**, **3.145**, **3.146**, **3.157**, **3.159**, **3.163**, **3.166**, **3.169-3.172**, **3.174**, **3.180**, **3.185**, and **3.186** showed monophasic displacement curves. The amino(methyl)thiazolylpropyl (**3.139**, **3.140**, **3.143**, **3.145**, **3.146**, **3.157**, **3.159**, **3.163**, **3.166**, **3.169-3.172**, and **3.174**), aminothiazolylphenyl (**3.180**), and 2-amino-4,5,6,7-tetrahydrobenzothiazol-6-yl (**3.185** and **3.186**) containing ligand(s) showed a weak to moderate affinity for the hD$_{2long}$R (pK_i: 5.6-6.6) (cf. Table 3.05 and Figure 3.199 (chapter **3.6.8**)). This is in contrast to the behavior at the D$_3$R. Apart from the weak H$_2$R agonists **3.180**, **3.185**, and **3.186**, the potent H$_2$R ligands showed consistently high affinities at the D$_3$R. The two potent H$_2$R agonists **3.145** and **3.157** showed the highest affinity at the D$_3$R (pK_i: 8.21 and 8.06, respectively) (cf. Table 3.05). To obtain further information about the functional behavior of the ligands **3.139**, **3.140**, **3.143**, **3.145**, **3.146**, **3.157**, **3.159**, **3.163**, **3.166**, **3.169-3.172**, and **3.174**, the recently described β-arrestin2 recruitment assay at the hD$_{2long}$R and hD$_3$R was performed (cf. Figures 3.194 and 3.195, chapter **3.6.6**).[404] The potencies in both assays are in very good agreement with the respective binding affinities, showing again high potencies at the D$_3$R (e.g., pEC$_{50}$ (**3.145**): 7.81, Table 3.06). While the ligands appeared predominantly as moderate to strong partial agonists at the D$_{2long}$R, several full agonists at the D$_3$R were found (cf. Table 3.06).
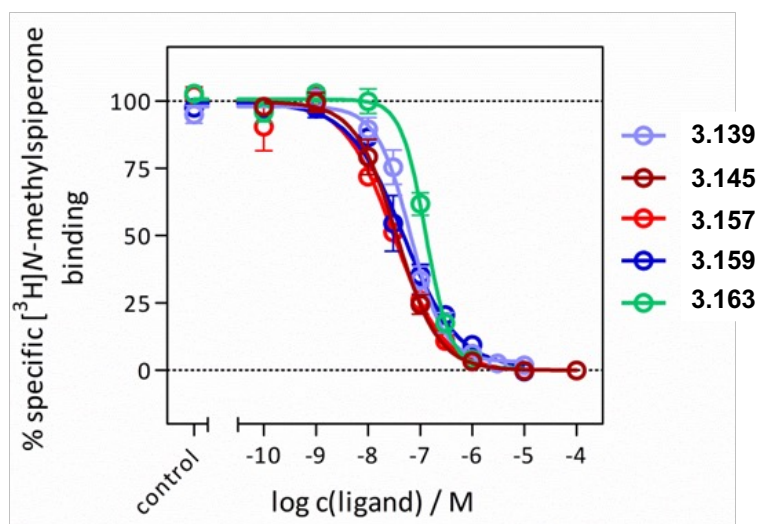
Figure 3.016. Displacement of the radioligand [³H]*N*-methylspiperone (c = 0.05 nM, K_d = 0.0258 nM) by increasing concentrations of the respective ligand at homogenates of HEK293T-CRE-Luc-hD₃R cells.[404] Data represent mean values ± SEM of 3 independent experiments, each performed in triplicate.

Table 3.05. Affinities of the monomeric (thio)carbamoylated guanidines to the dopamine receptors hD$_{2long}$R and hD₃R, obtained from competition binding studies.

3.139-3.140, 3.143, 3.145-3.146, 3.157, 3.159, 3.163, 3.166, 3.169-3.172

3.174

3.180

3.185-3.186

Comp.	R	pK_i				Selectivity ratios of K_i
		hD$_{2long}$R[a]	N	hD₃R[b]	N	(D$_{2long}$R / D₃R / H_2R)
haloperidol		9.58 ± 0.13[404]	3	8.95 ± 0.03[404]	3	-
3.006		(p$K_{i/high}$: 7.59 ± 0.12 / p$K_{i/low}$: 6.00 ± 0.03)[404]	3	9.18 ± 0.06[404]	3	0.002* / 0.00005 / 1
3.139		6.35 ± 0.01	3	7.80 ± 0.09	3	100 / 4 / 1
3.140		6.25 ± 0.06	3	7.85 ± 0.08	3	19 / 0.5 / 1

Table 3.05 (continued)

**3.139-3.140, 3.143, 3.145-3.146,
3.157, 3.159, 3.163, 3.166, 3.169-3.172**

3.174

3.180

3.185-3.186
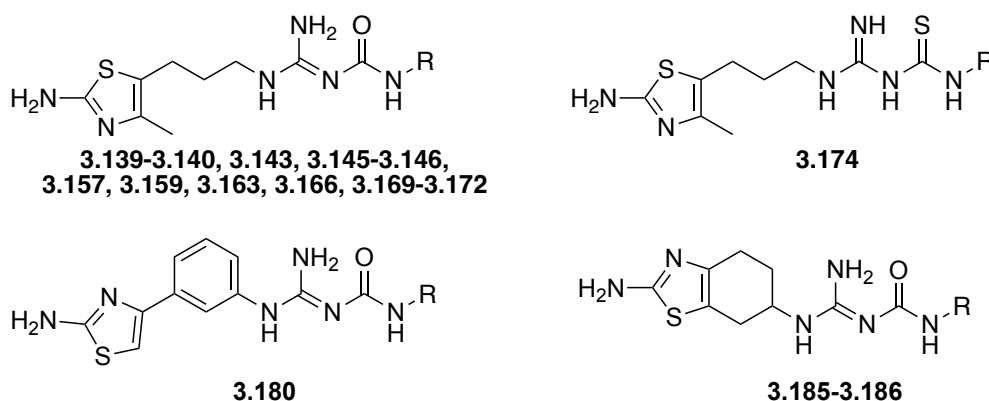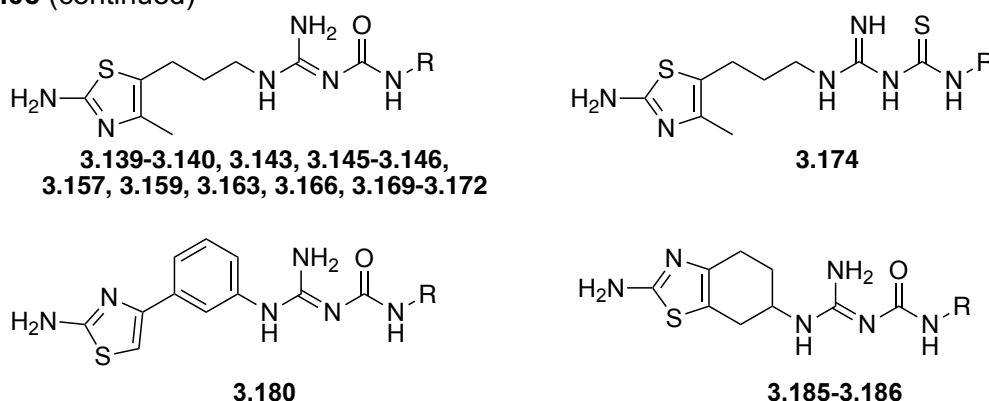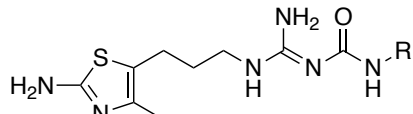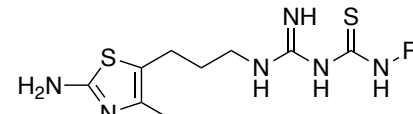
Comp.	R	pK$_i$				Selectivity ratios of K$_i$ (D$_{2long}$R / D$_3$R / H$_2$R)
		hD$_{2long}$R[a]	N	hD$_3$R[b]	N	
3.143		6.22 ± 0.08	3	7.34 ± 0.02	3	9 / 0.7 / 1
3.145		6.81 ± 0.13	3	8.21 ± 0.10	3	9 / 0.3 / 1
3.146		6.10 ± 0.07	3	7.61 ± 0.12	3	15 / 0.5 / 1
3.157		6.50 ± 0.06	3	8.06 ± 0.10	3	155 / 4 / 1
3.159		5.77 ± 0.12	3	7.76 ± 0.17	3	54 / 0.5 / 1
3.163		6.58 ± 0.03	3	7.36 ± 0.04	3	7 / 1 / 1
3.166		6.28 ± 0.08	3	7.19 ± 0.06	3	7 /0.8 / 1
3.169		6.32 ± 0.08	3	6.88 ± 0.04	3	7 /2 / 1
3.170		6.30 ± 0.10	3	7.07 ± 0.06	3	7 / 1 / 1
3.171		6.45 ± 0.07	3	7.34 ± 0.04	3	6 / 0.7 / 1
3.172		6.23 ± 0.06	3	7.25 ± 0.06	3	10 / 0.9 / 1
3.174		5.93 ± 0.08	3	7.22 ± 0.06	3	10 / 0.5 / 1
3.180		5.60 ± 0.20	3	5.89 ± 0.05	3	4 / 2 / 1
3.185		5.90 ± 0.10	3	5.90 ± 0.20	3	1 / 1 / 1
3.186		6.26 ± 0.10	3	5.30 ± 0.10	3	1 / 10 / 1

Determined by displacing [^{3}H]N-methylspiperone ([a]hD$_{2long}$R: K_d = 0.0149 nM, c = 0.05 nM or [b]hD$_3$R: K_d = 0.0258 nM, c = 0.05 nM) by increasing concentrations of the respective ligand at homogenates of [a]HEK293T-CRE-Luc-hD$_{2long}$R or [b]HEK293T-CRE-Luc-hD$_3$R cells.[404] Data were analyzed by nonlinear regression and were best fitted to four-parameter sigmoidal concentration-response curves. Data shown are means ± SEM of N independent experiments, each performed in triplicate. *Calculated using pK$_{i/high}$ value.
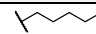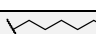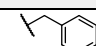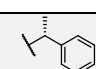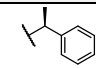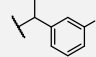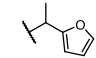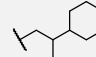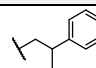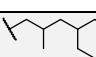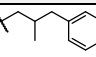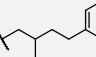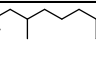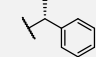
Table 3.06. $hD_{2long,3}R$ agonism and the calculated pEC_{50} values of the monomeric (thio)carbamoylated guanidines determined by a β-arrestin2 recruitment assay.

3.139-3.140, 3.143, 3.145-3.146, 3.157, 3.159, 3.163, 3.166, 3.169-3.172

3.174

Comp.	R	$hD_{2long}R$ (β-arrestin2 recruitment)[a]			hD_3R (β-arrestin2 recruitment)[b]		
		pEC_{50}	N	α	pEC_{50}	N	α
quinpirole	-	7.55 ± 0.07[404]	5	1.00[404]	8.75 ± 0.07[404]	6	1.00[404]
3.139		5.98 ± 0.02	4	0.41 ± 0.05	7.80 ± 0.05	3	0.96 ± 0.05
3.140		5.76 ± 0.06	3	0.44 ± 0.05	7.63 ± 0.12	4	0.95 ± 0.05
3.143		5.78 ± 0.05	3	0.49 ± 0.03	7.47 ± 0.08	3	0.93 ± 0.03
3.145		6.47 ± 0.10	4	0.60 ± 0.05	7.81 ± 0.03	4	0.86 ± 0.05
3.146		5.57 ± 0.28	3	0.36 ± 0.04	6.64 ± 0.07	3	1.05 ± 0.09
3.157		6.23 ± 0.10	3	0.73 ± 0.05	7.14 ± 0.16	3	0.98 ± 0.05
3.159		5.97 ± 0.09	3	0.82 ± 0.03	6.99 ± 0.09	3	1.03 ± 0.10
3.163		5.49 ± 0.15	4	0.39 ± 0.06	6.58 ± 0.05	3	1.09 ± 0.09
3.166		5.95 ± 0.04	3	0.58 ± 0.02	7.39 ± 0.08	3	0.93 ± 0.04
3.169		5.77 ± 0.04	3	0.57 ± 0.02	6.52 ± 0.02	3	0.86 ± 0.01
3.170		5.96 ± 0.05	5	0.92 ± 0.10	6.55 ± 0.13	3	1.01 ± 0.07
3.171		5.27 ± 0.07	3	0.70 ± 0.08	6.05 ± 0.11	3	0.95 ± 0.11
3.172		5.53 ± 0.02	3	0.70 ± 0.11	6.38 ± 0.10	3	0.67 ± 0.06
3.174		5.82 ± 0.06	3	0.66 ± 0.08	6.78 ± 0.09	3	0.84 ± 0.04

β-arrestin2 recruitment determined using [a]HEK293T ElucN-βarr2 $hD_{2long}R$-ElucC cells or [b]HEK293T ElucN-βarr2 hD_3R-ElucC cells, stably expressing the $hD_{2long}R$-ElucC or hD_3R-ElucC and βarr2-ElucN fusion constructs.[404] The intrinsic activity (α) of quinpirole was set to 1.00, and α values of investigated compounds were referred to this value. Data represent mean values ± SEM of 3-4 independent experiments, each performed in duplicate or triplicate.

3.3.3 Conclusion

In this study, 49 monomeric, 2-aminothiazolyl ring-containing (thio)carbamoylguanidine-type H$_2$R ligands were synthesized and characterized. These ligands featured either flexible or rigid spacers and were functionalized with side chains (n-alkyl, cyclic, aromatic, branched, with and without defined stereochemistry etc.) linked to the carbamoyl guanidine core. The structural simplification of previously reported dimeric ligands into monomeric ligands resulted in potent agonists (guinea pig right atrium and β-arrestin2 recruitment assays) with H$_2$R affinities in the one-digit nanomolar range (pK_i (**3.139**, UR-KAT523): 8.35; pK_i (**3.157**, UR-MB-69)): 8.69). Most of the compounds exhibited an excellent selectivity profile towards the H$_2$R, for example **3.157** being at least 3800-fold selective within the histamine receptor family. These properties turn them into the highest affinity and subtype-selective carbamoylguanidine-type H$_2$R agonists known to date. On the other hand, it was recognized that the 2-aminothiazole residue, which is responsible for the subtype-selectivity of monomeric and/or dimeric H$_2$R ligands, is also a known bioisostere of the catechol moiety present in some dopamine receptor ligands. Therefore, the dopamine receptor affinity in radioligand competition binding studies at the D$_{2long}$ and D$_3$ receptors with selected H$_2$R agonists was investigated. The experiments revealed a considerable affinity for the respective dopamine receptor subtypes, especially for the D$_3$ receptor. Furthermore, functional studies (β-arrestin2 recruitment assays) with these ligands showed that they act as partial and full agonists at the dopamine receptors which were investigated. These findings limit the application of our ligands to recombinant systems in which either the H$_2$R or the D$_3$R is expressed. In summary, the aim of this work was the development of a series of H$_2$R agonists with enhanced drug-like properties while maintaining the high H$_2$R subtype selectivity and potency of the dimeric ligands. The 2-aminothiazolyl ring containing (thio)carbamoylguanidine-type H$_2$R ligands represent a class of high affinity molecular tools for the application in recombinant systems in which the H$_2$R is solely expressed. Furthermore, our ligands establish a solid base of small molecule ligands with an improved selectivity profile over previously reported ligands, enabling *in vivo* studies and experiments utilizing primary tissue. Consequently, the goal of future work will be the optimization of our reported compounds towards exclusive selectivity for the H$_2$R.

3.4 Abolishing Dopamine D_{2long}/D_3 Receptor Affinity of Subtype-Selective Carbamoylguanidine-Type Histamine H₂R Agonists

UR-MB-69 (3.157) high H₂R and D₃R affinity

UR-MB-165 (3.264) high H₂R and low D₃R affinity

41 analogues

SAR — imidazol, triazole, thiadiazole, oxazole, etc.

SAR — bicycle, aromatic ring

SAR — n-alkyl, aliphatic, aromatic cycles, dimeric

comp.	pK_i					
	H₁R	H₂R	H₃R	H₄R	D₂longR	D₃R
UR-MB-69	5.11	8.69	4.41	4.88	6.50	8.06
UR-MB-165	4.98	8.09	< 5	< 5	< 5	6.18
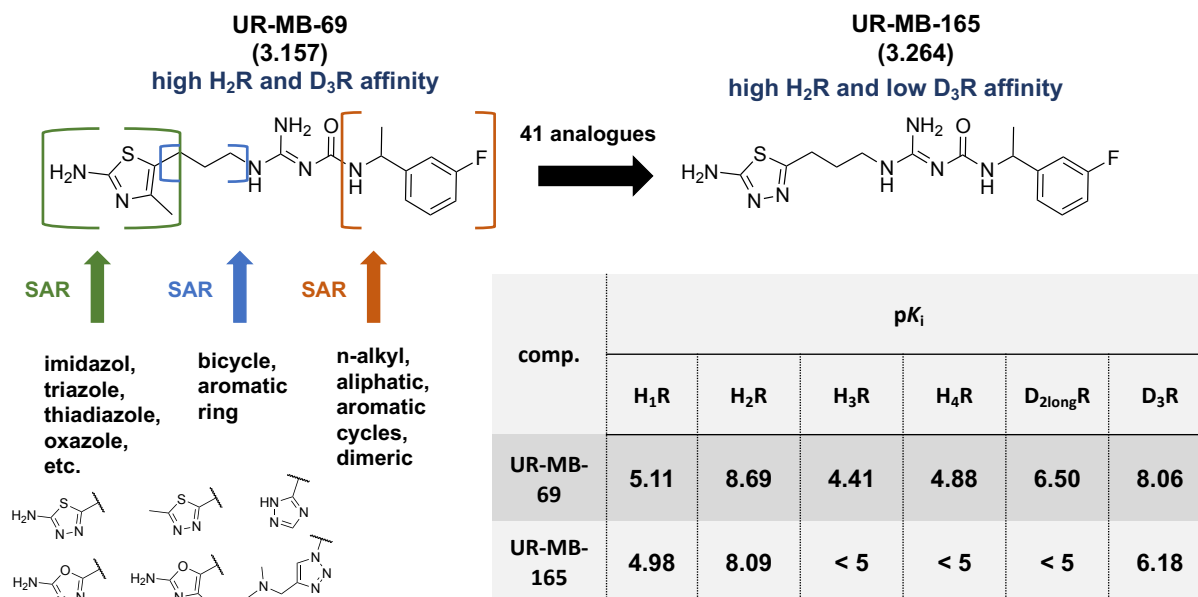
3-(2-Amino-4-methylthiazol-5-yl)propyl substituted carbamoylguanidines are potent, subtype-selective histamine H₂ receptor (H₂R) agonists. Nevertheless, their applicability as pharmacological tools to elucidate the largely unknown H₂R functions in the central nervous system (CNS) is compromised by their concomitantly high affinity towards dopamine D₂-like receptors (especially to the D₃R). To improve the selectivity, a series of novel carbamoylguanidine-type ligands containing various heterocycles, spacers, and side residues was rationally designed, synthesized, and tested in binding and/or functional assays at H₁₋₄ and D₂long/₃ receptors. This study revealed a couple of selective candidates (among others **3.239** (UR-KAT505), **3.255** (UR-KAT533), and **3.264** (UR-MB-165)). The most promising ones were screened at several off-target receptors, showing good selectivities. These results provide a solid base for the exploration of the H₂R functions in the brain in further studies.

Results of this chapter have been published in:

Author contributions:

K.T. and **M.B**. performed the synthesis and analytical characterization of chemical compounds. **M.B.** synthesized H$_2$R ligands **3.145** (di-HCl salt for chapter **3.4.2.8**) and **3.260**-**3.264** and the corresponding precursor compounds therefore. **K.T.** synthesized H$_2$R ligands **3.238**-**3.259** and **3.265**-**3.278** and the corresponding precursor compounds therefore. **M.B.** determined the pK_a value for the 2-aminothiadiazole. **K.T.** and **M.B.** performed radioligand competition binding experiments at H$_{1-4}$Rs and analyzed the data. **L.F.** performed radioligand competition binding experiments at D$_{1-5}$Rs and analyzed the data. **D.M.** generated the HEK293T-CRE-Luc-hD$_5$R cell line and prepared the corresponding homogenates. **K.T.** performed radioligand competition binding experiments at M$_{1-5}$R and analyzed the data. **H.H.** and **P.G.** performed the radioligand binding studies at the human adrenoceptors α$_{1A}$, α$_{2A}$, β$_1$, and β$_2$ as well as to the human serotonin receptor 5-HT$_{1A}$ and the human opioid receptor μOR and analyzed the data. **K.T.** performed the functional studies at H$_2$R and analyzed the data, with exception of guinea right atrium experiments, which were performed and analyzed by **M.B.**, **L.F.**, and **K.T.** performed and analyzed functional studies at D$_{2long/3}$Rs. **A.B.** and **A.S.** initiated and planned the project. **S.P.** and **A.S.** supervised the research. **K.T.**, **S.P.**, and **A.S.** wrote the manuscript. [#]**M.B.** and **L.F.** contributed equally

Gergs, U.; Büxel, M. L.; **<u>Bresinsky, M.</u>**; Kirchhefer, U.; Fehse, C.; Höring, C.; Hofmann, B.; Marušáková, M.; Čináková, A.; Schwarz, R.; Pockes, S.; Neumann, J. Cardiac Effects of Novel Histamine H$_2$ Receptor Agonists. *J Pharmacol Exp Ther* **2021**, *379* (3), 223–234.

Author contributions:

U.G. and **J.N.** participated in research design. **M.Bü.**, **M.B.** (synthesis of compound **3.145** (UR-Po563), **3.261** (UR-MB-158), and **3.262** (UR-MB-159)), **K.U**, **F.C**, **H.C**, **H.B**, **M.M**, **A.Č.**, **R.S**, and **S.P.** conducted experiments. **M.B.**, **C.H.**, and **S.P.** contributed new reagents or analytic tools. **M.Bü.**, **M.B.**, **C.F.**, **C.H.**, **M.M.**, **A.Č.**, **R.S.**, and **S.P.** performed data analysis. **U.G.**, **S.P.**, and **J.N.** wrote or contributed to the writing of the manuscript.

3.4.1 Introduction

The histamine H$_2$ receptor (H$_2$R) has been the subject of many research studies due to its versatile physiological properties.[244,374] The H$_2$R belongs to the class A G protein-coupled receptors (GPCRs) and is expressed throughout the whole human body, most notably in the stomach, heart, and central nervous system (CNS).[244,374,376,377] Activation of the H$_2$R by its endogenous ligand histamine (**3.001**, Figure 3.017A) leads to adenylyl cyclase activation by coupling to the Gs protein.[374] The central role of the H$_2$R in the stimulation of gastric acid secretion[247,374] is the basis for the therapeutic use of H$_2$R antagonists to treat gastroesophageal reflux disease and gastroduodenal ulcers.[244,405] The function of the H$_2$R in the CNS is largely unknown but includes, e.g., modulation of cognitive processes and circadian rhythm.[406] Furthermore, positive effects of the H$_2$-antagonist famotidine (**3.223**, Figure 3.017A) in schizophrenia and an improvement in L-DOPA-induced dyskinesia are reported in the literature.[406–414] In addition, studies are reporting that stimulation of postsynaptic H$_2$R has positive effects on learning and memory.[371] So far, these effects have only been shown with dual-acting acetylcholinesterase inhibitors and H$_3$R antagonists, as these molecules initiate this process through the inhibition of presynaptic H$_3$-autoreceptors.[371–373] Therefore, the use of CNS-penetrating H$_2$R agonists is of great interest.

Starting from the H$_2$R agonists of the arpromidine (**3.002**; cf. Figure 3.017A) series, several highly potent (up to 3000 times the potency of histamine) monomeric and dimeric H$_2$R agonists with acylguanidine or carbamoylguanidine partial structure were developed (**3.005**, **3.139**, and **3.224**; cf. Figure 3.017A).[298,299,302,304,415,416] In contrast to acylguanidines, the carbamoylguanidines are chemically stable and possess an excellent selectivity over the other three histamine receptors (H$_{1,3,4}$) if a 2-aminothiazole ring is used for bioisosteric replacement of the imidazole ring (**3.005** and **3.139**; cf. Figure 3.017A).[299,304,378] Based on the existing knowledge about the physicochemical and/or pharmacokinetic properties of acyl- and carbamoylguanidines, it can be assumed that carbamoylguanidines are also able to overcome the blood-brain barrier.[298,302,304,417] This advantage over previously reported H$_2$R agonists (cf. guanidines, e.g., **3.002**; cf. Figure 3.017A) should enable access to the H$_2$R in the CNS.[298,302] On the other hand, direct injection of the ligand into the brain is also possible as means of application in case of insufficient bioavailability and/or BBB penetration.[418] However, the 2-aminothiazole structural motif is also part of the

dopamine receptor agonist pramipexole (**3.006**; cf. Figure 3.017A), which is employed as a drug for the treatment of Parkinson's disease.[380,419] Due to these similarities, it can be assumed that H$_2$R agonists containing the 2-aminothiazole motif might also bind to dopamine receptors. This assumption was approved in previous studies (see chapter **3.3**) with radioligand binding experiments. It was revealed that such H$_2$R agonists exhibit a considerable affinity to dopamine receptors of the D$_2$-like family, particularly to the D$_3$ receptor.[304,416]

In order to enable the use of carbamoylguanidines as pharmacological tools to elucidate the H$_2$R functions in the CNS, improved molecules that bind solely to the H$_2$ receptor are needed. Thus, this study reports the synthesis and pharmacological characterization of this novel, subtype-selective H$_2$R ligands. The selectivity was achieved by the variation of the carbamoylguanidine-based scaffold with different heterocycles, spacers, and side residues (cf. Figure 3.017B). The synthesized compounds were investigated for their functional activity at the H$_2$R and/or D$_{2long/3}$R in minimal G (mini-G) protein- and/or β-arrestin2-recruitment assays as well as on the isolated spontaneously beating guinea pig (gp) right atrium in a more complex, but well-established standard model for the characterization of H$_2$R ligands.[244,420] The selectivity for the human (h) H$_2$R over hH$_{1/3/4}$R and hD$_{2long/3}$R was evaluated in radioligand competition binding experiments. Finally, an affinity screening of the best compounds at common off-target GPCRs (cf. Table 3.12 and Figure 3.019) was performed and the GI absorption and BBB penetration of these ligands was estimated by the SwissADME online tool (cf. Table 3.15 and Figure 3.027).
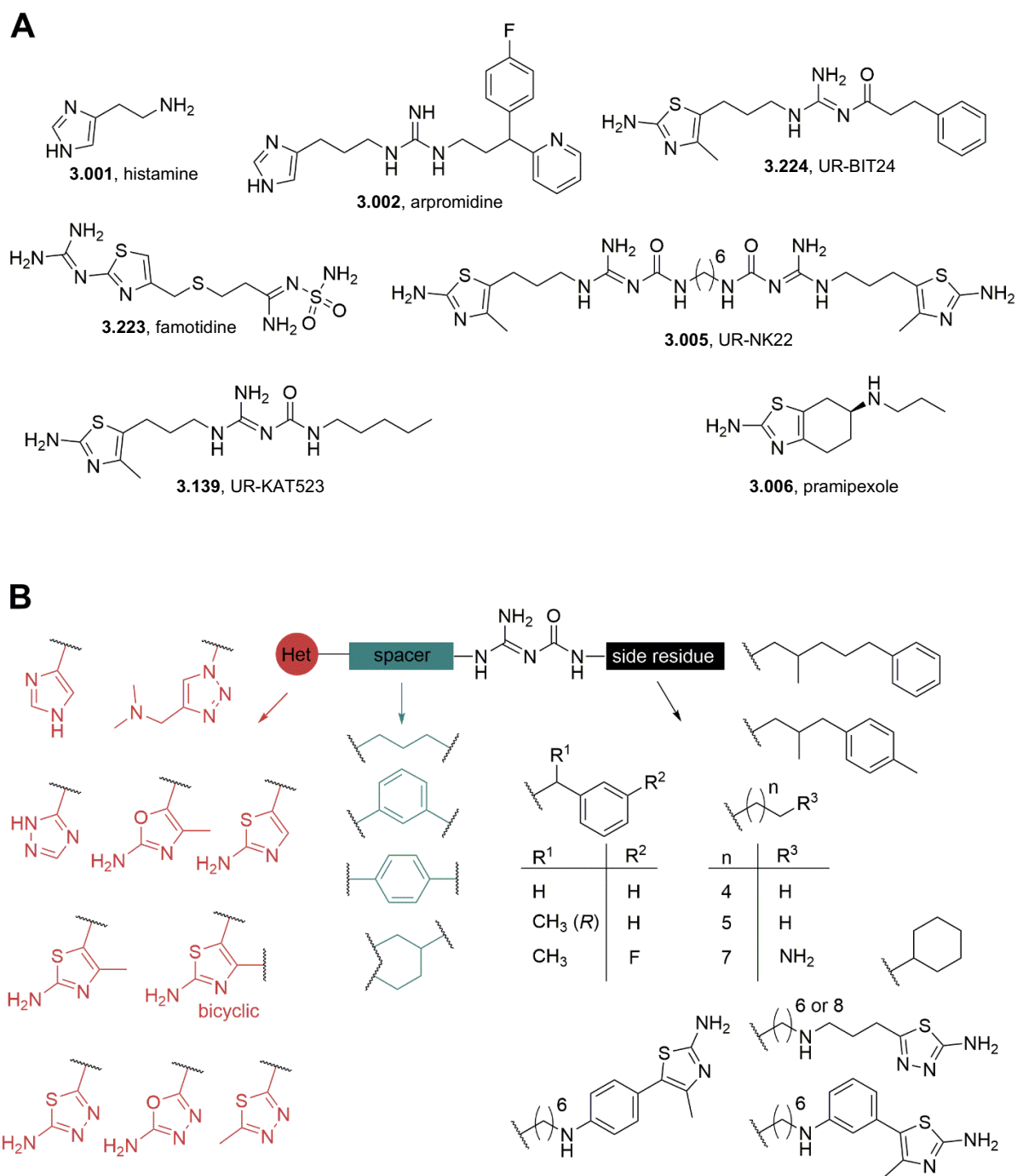
Figure 3.017. A: Structures of histamine (**3.001**), arpromidine **(3.002)**, famotidine **(3.223)**, and related prototypical acylguanidine-type **(3.224)** and carbamoylguanidine-type (**3.005** and **3.139**) H₂R agonists, as well as the D₂-like receptor agonist pramipexole (**3.006**). **B**: Structural modifications of N^G-carbamoylated guanidines resulting in the title compounds. Het: heterocycle.

3.4.2 Results and Discussion
3.4.2.1 Chemistry

The amines **3.225-3.234**[298,302,421–423] (cf. Figure 3.018) and the guanidinylating reagents **3.049-3.051**, **3.053**, **3.055**, **3.067**, **3.073**, **3.080**, **3.082**, and **3.235-3.237**[299,304,416,417] (cf. Schemes 3.02 and 3.03) were synthesized as reported in chapter **3.5.1.5**, chapter **3.5.1.11**, and chapter **3.5.1.12** or in the literature. Several different side residues for the guanidinylating reagents **3.049**-**3.051**, **3.053**, **3.055**, **3.067**, **3.073**, **3.080**, **3.082**, and **3.235**-**3.237** were selected, which performed well in recent studies about 2-aminothiazoles.[298,299,302,304,415–417] The monomeric (cf. Scheme 3.02) or dimeric (cf. Scheme 3.03) carbamoylguanidine-type ligands were prepared by reacting the amines **3.225**-**3.234** with the guanidinylating reagents **3.049**-**3.051**, **3.053**, **3.055**, **3.067**, **3.073**, **3.080**, **3.082**, and **3.235**-**3.237** in the presence of HgCl$_2$ and triethylamine (NEt$_3$).[424] Finally, the protected carbamoylguanidine-type intermediates were treated with TFA giving compounds **3.238-3.244**, **3.246-3.265**, and **3.267-3.278** (cf. Schemes 3.02 and 3.03), which were purified by preparative HPLC (acetonitrile (MeCN)/0.1% TFA in H$_2$O) or column chromatography (CH$_2$Cl$_2$/7 N NH$_3$ in MeOH) and subsequent recrystallization into the corresponding HCl salts (see chapter **3.6.2** for purity control; cf. Figures 3.168B-3.188). **3.245** and **3.266** were synthesized using a modified synthetic procedure (for details, see chapter **3.5.1.13** and **3.5.1.15**; cf. Scheme 3.15). The pK_a value of 2-amino-5-methyl-1,3,4-thiadiazole (**3.322**) was determined by acid-base titration (cf. Figure 3.039) to evaluate the acid-base dissociation constant of building block **3.228**. For details of the procedure and the titration curves, see chapter **3.5.1.18**.
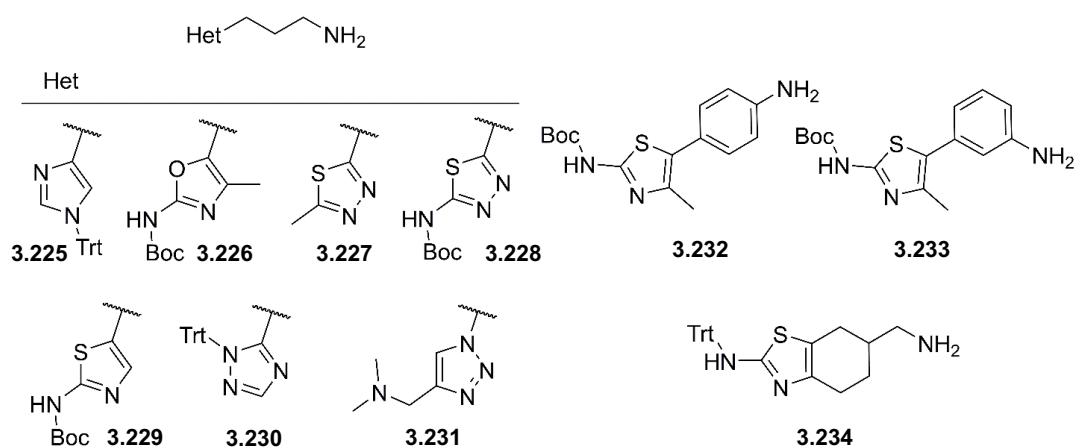
Figure 3.018. Structures of amines **3.225-3.234** used for the synthesis of monomeric (**3.238-3.244**, **3.246-3.265**, and **3.267-3.274**) and dimeric (**3.275-3.278**) carbamoylguanidines. Het: heterocycle. For more details regarding **3.225-3.234**, see chapter **3.5.1.12**.

3.225-**3.234** $\xrightarrow{\text{a}}$ $\xrightarrow{\text{b}}$

3.049-**3.051**, **3.053**, **3.055**, **3.067**, **3.073**, **3.080**, **3.082**, and **3.235**

Het

3.225 (BB1) **3.226 (BB2)** **3.227 (BB3)** **3.228 (BB4)**

*BB5 **3.229 (BB6)** **3.230 (BB7)** **3.231 (BB8)**

para: **3.232 (BB9)**
meta: **3.233 (BB10)**

3.234 (BB11)

R$_1$:

- : **3.049**
BB3: **3.238** (34%)
BB4: **3.239** (19%)
BB6: **3.240** (26%)
BB9: **3.241** (45%)
BB10: **3.242** (48%)
BB11: **3.243** (22%)

- : **3.050**
BB4: **3.224** (18%)
BB5: **3.245** (6%)*

-, R$_2$ = Boc: **3.235**
BB3, R$_2$ = H: **3.246** (37%)
BB4, R$_2$ = H: **3.247** (26%)

- : **3.051**
BB9: **3.248** (53%)

- : **3.073**
BB2: **3.249** (24%)
BB3: **3.250** (19%)
BB4: **3.251** (17%)
BB9: **3.252** (64%)

- : **3.053**
BB2: **3.253** (27%)
BB3: **3.254** (20%)
BB4: **3.255** (23%)
BB6: **3.256** (30%)
BB9: **3.257** (48%)
BB10: **3.258** (44%)
BB11: **3.259** (38%)

- : **3.055**
BB1: **3.260** (37%)
BB4: **3.261** (8%)
BB7: **3.262** (47%)
BB8: **3.263** (5%)

- : **3.067**
BB4: **3.264** (32%)

- : **3.080**
BB4: **3.265** (18%)
BB5: **3.266** (61%)*
BB6: **3.267** (23%)
BB9: **3.268** (55%)
BB10: **3.269** (34%)
BB11: **3.270** (16%)

- : **3.082**
BB4: **3.271** (12%)
BB9: **3.272** (41%)
BB10: **3.273** (38%)
BB11: **3.274** (14%)

Scheme 3.02. Synthesis of monomeric carbamoylguanidines **3.238**-**3.274**. Reagents and conditions: a) NEt$_3$, HgCl$_2$, CH$_2$Cl$_2$, rt, 4-48 h; (b) TFA, CH$_2$Cl$_2$, rt, 7-18 h, 4-64% over two steps (see chapter **3.5.1.14**). Isolated yields over two steps are given in brackets. *Modified synthetic procedure (see chapter **3.5.1.15**; cf. Scheme 3.15). BB: building block. Het: heterocycle. Amines **3.225**-**3.234**: all compounds were used as free bases; guanidinylating reagents **3.049**-**3.051**, **3.053**, **3.055**, **3.067**, **3.073**, **3.080**, and **3.082**: all compounds were used as mono-Boc protected (or di-Boc protected if applicable) intermediates. The target compounds **3.238**-**3.260**, **3.263**, and **3.265**-**3.274** were obtained as TFA and **3.261**-**3.262** and **3.264** as HCl salts.
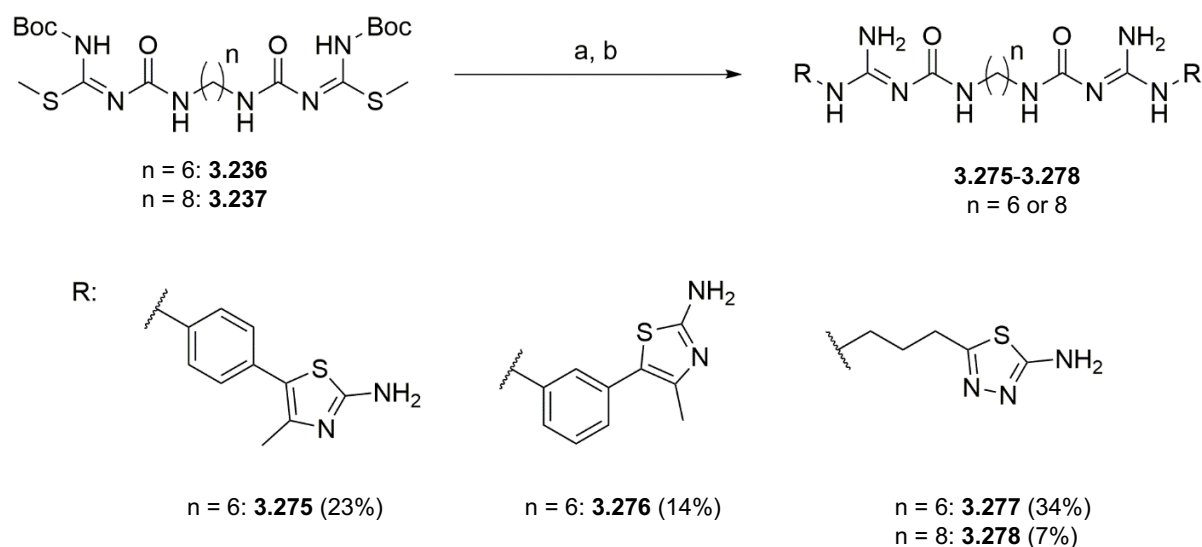
Scheme 3.03. Synthesis of the dimeric N^G-carbamoylated guanidines **3.275**-**3.278**. Reagents and conditions: a) **3.228**, **3.232**, or **3.233**, NEt₃, HgCl₂, CH₂Cl₂, rt, 8 h; (b) TFA, CH₂Cl₂, rt, 6-16 h, 7-23% over two steps. Isolated yields over two steps are given in brackets. For more details regarding **3.228**, **3.232**, **3.233**, and **3.236**-**3.237** see chapter **3.5.1.11** and **3.5.1.12**. Amines **3.228**, **3.232**, and **3.233**: all compounds were used as free bases; guanidinylating reagents **3.236**-**3.237**: all compounds were used as di-Boc protected intermediates. The target compounds **3.275**-**3.278** were obtained as TFA salts.

3.4.2.2 H₂R Affinity and Receptor Subtype Selectivity

The pK_i values of all target compounds were determined in competition binding studies on membrane preparations of Sf9 cells expressing the hH₂R-G$_{sαS}$ fusion protein using the radioligand [³H]UR-DE257[390] (cf. Table 3.07). First of all, the influence of the linker on the binding affinity was investigated. The conformationally restricted compounds (e.g., **3.241** (para, pK_i = 6.34), **3.242** (meta, pK_i = 6.72), and **3.243** (bicyclic, pK_i = 6.81); cf. Table 3.07) bind well to the hH₂R albeit with lower affinities compared to their flexible (propyl linker) counterparts (e.g., **3.139**[304] (pK_i = 8.32[304]); cf. Table 3.07).

Subsequently, the impact of the heterocycle was determined. The replacement of the sulfur atom in the 2-amino-4-methylthiazole by an oxygen atom resulted in decreased hH₂R affinity (e.g., oxazole: **3.253** (pK_i = 6.41; Table 3.07) vs. thiazole **3.143** (UR-CH22)[304,416] (pK_i = 7.16[304,416]; cf. Table 3.02). The omission of the methyl group in position 4 of the heterocyclic ring did not cause a significant change in hH₂R affinity (**3.240** (UR-KAT583), **3.256**, and **3.267** vs. **3.139**[304] (cf. Table 3.07), **3.143** (UR-CH22)[304,416], and **3.170** (UR-SB257)[304,416] (cf. Table 3.02). However, the replacement

of the amino(methyl)thiazole by a 2-amino-1,3,4-thiadiazole was favorable: the K_i-values of compounds **3.239** (pK_i = 8.52), **3.244** (pK_i = 8.29), **3.255** (pK_i = 8.30), **3.264** (pK_i = 8.09), and **3.265** (pK_i = 8.19) were in the single-digit nanomolar range (cf. Table 3.07). Also, in the case of the diazoles, the substitution of the sulfur atom by an oxygen atom resulted in decreased hH$_2$R affinity (e.g., oxadiazole: **3.266** (pK_i = 6.17) vs. thiadiazole **3.265** (pK_i = 8.19); cf. Table 3.07). The replacement of the free amine group in the 2-amino-1,3,4-thiadiazole by a methyl group (**3.238**, **3.246**, **3.250**, and **3.254**) resulted in a dramatic decrease of hH$_2$R affinity (cf. Table 3.07), indicating that the heteroaromatic amine group is essential for high affinity. Finally, using the reported 1H-1,2,4-triazole[421] or a more explorative 4-(dimethylamino)methyl-1,2,3-triazole instead of the 2-amino-4-methylthiazole resulted in decreased hH$_2$R affinities (1,2,4-triazole **3.262** (pK_i = 7.27; cf. Table 3.07) and 1,2,3-triazole **3.263** (pK_i = 5.35; cf. Table 3.07) vs. thiazole UR-Po563[304] (pK_i = 7.75[304]; cf. Table 3.02). It is literature known that dimeric ligands possess a significantly increased H$_2$R affinity (human or guinea pig).[299,378] Therefore, several dimeric compounds, e.g., the 2-amino-1,3,4-thiadiazole heterocycle containing ligands **3.277** (hexyl-spacer, pK_i = 8.28; cf. Table 3.07) and **3.278** (octyl-spacer, pK_i = 8.32; cf. Table 3.07) were synthesized. However, no additional increase in affinity was achieved compared to the monomeric compounds **3.239** (pentyl, pK_i = 8.52; cf. Table 3.07) and **3.244** (hexyl, pK_i = 8.29; cf. Table 3.07). The pK_i values of all synthesized compounds were also determined at the hH$_1$, hH$_3$, and hH$_4$ receptors on membranes of Sf9 cells expressing the respective histamine receptor using the radioligands [^{3}H]mepyramine (hH$_1$R), [^{5}H]N^α-methylhistamine or [^{3}H]UR-PI294[391] (hH$_3$R) and [^{3}H]**3.001** (hH$_4$R; cf. Table 3.07). The imidazole-containing ligand **3.260** was synthesized as a control compound to showcase that the subtype selectivity is largely influenced by the heterocycle. Unsurprisingly, despite a high affinity at the H$_2$R, it bound similarly or even better to the H$_3$R and H$_4$R. In contrast, neither of the 2-amino-1,3,4-thiadiazoles (**3.239**, **3.244**, **3.251**, **3.255**, **3.261**, **3.264**, **3.265**, **3.271**, **3.277**, and **3.278**) displayed remarkable affinity to the hH$_1$, hH$_3$, or hH$_4$ receptors leading to at least 100-fold selectivity for the hH$_2$R (cf. Table 3.07). The only exception among the thiadiazoles was observed for compound **3.247**, which contains the 8-aminooctyl side chain. Within the synthesized series, compound **3.239** (UR-KAT505) showed the highest affinity (pK_i = 8.52; cf. Table 3.07) and subtype selectivity (ratio of K_i H$_1$R/H$_3$R/H$_4$R of 2138 : > 3311 : > 3311, Table 3.07).
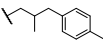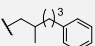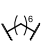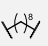
Table 3.07. Binding data of the compounds **3.238**-**3.278** on human histamine receptor subtypes.[a]

Comp.	structure		hH$_1$R[b]	N	hH$_2$R[c]	N	hH$_3$R[d,e]	N	hH$_4$R[f]	N	H$_1$	H$_3$	H$_4$
	BB	R			pK$_i$						H$_2$R selectivity K$_i$(H$_x$R)/K$_i$(H$_2$R)		
3.001	-	-	5.62 ± 0.03[389]	4	6.58 ± 0.04[389]	48	7.59 ± 0.01[389]	42	7.60 ± 0.01[389]	45	9	0.1	0.1
3.005[299]	-	-	6.06 ± 0.05[299]	-	8.07 ± 0.05[299]	-	5.94 ± 0.16[299]	-	5.69 ± 0.07[299]	-	102	135	240
3.006	-	-	n.d.	-	4.86 ± 0.07[304]	-	n.d.	-	n.d.	-	-	-	-
3.139[304]	-		4.97 ± 0.10[304]	3	8.35 ± 0.08[304]	3	4.98 ± 0.17[304]	3	5.37 ± 0.09[304]	3	2399	2344	955
3.238	3		< 5	3	5.66 ± 0.15	3	< 5[e]	3	< 5	3	> 5	> 5	> 5
3.239	4		5.19 ± 0.05	3	8.52 ± 0.16	3	< 5[e]	3	< 5	3	2138	>3311	>3311
3.240	6		5.02 ± 0.03	3	7.64 ± 0.07	3	< 5[e]	3	< 5	3	417	> 437	> 437
3.241	9		5.43 ± 0.09	3	6.34 ± 0.06	3	4.94 ± 0.06[d,e]	3	5.11 ± 0.04	3	8	25	17
3.242	10		5.18 ± 0.09	3	6.72 ± 0.03	3	5.02 ± 0.07[e]	3	5.13 ± 0.05	3	35	50	39
3.243	11		5.28 ± 0.10	3	6.81 ± 0.07	3	5.18 ± 0.15[d,e]	3	5.23 ± 0.04	3	34	43	38
3.244	4		5.30 ± 0.09	3	8.29 ± 0.20	3	< 5[e]	3	< 5	3	977	> 1950	> 1950
3.245	5		5.05 ± 0.06	3	6.41 ± 0.01	3	< 5[e]	3	< 5	3	23	> 26	> 26
3.246	3		6.51 ± 0.19	3	5.74 ± 0.14	3	4.93 ± 0.18[e]	3	< 5	3	0.2	7	> 5
3.247	4		6.28 ± 0.09	3	7.48 ± 0.14	3	< 5[e]	3	< 5	3	16	> 302	> 302
3.248	9		5.26 ± 0.17	3	6.26 ± 0.14	3	4.91 ± 0.09[d,e]	3	5.16 ± 0.07	3	10	22	13

Table 3.07 (continued)

Comp.	structure		hH₁R[b]	N	hH₂R[c]	N	hH₃R[d,e]	N	hH₄R[f]	N	H₁	H₃	H₄
	BB	R											
3.249	2		5.22 ± 0.04	3	6.61 ± 0.08	3	5.08 ± 0.11[e]	3	5.12 ± 0.07	3	25	34	31
3.250	3		5.15 ± 0.01	3	5.98 ± 0.12	3	4.94 ± 0.06	3	< 5	3	7	11	> 10
3.251	4		5.13 ± 0.06	3	7.71 ± 0.14	4	5.56 ± 0.10[e]	3	4.90 ± 0.12	3	380	141	646
3.252	9		5.54 ± 0.13	3	6.51 ± 0.10	3	5.25 ± 0.05[e]	3	5.11 ± 0.04	3	9	18	25
3.253	2		5.05 ± 0.06	3	6.41 ± 0.11	3	< 5[e]	3	< 5	3	23	> 26	> 26
3.254	3		4.97 ± 0.08	3	5.25 ± 0.15	3	< 5[e]	3	< 5	3	2	> 2	> 2
3.255	4		5.27 ± 0.12	3	8.30 ± 0.07	3	< 5[e]	3	< 5	3	1072	> 1995	> 1995
3.256	6		5.25 ± 0.01	3	7.57 ± 0.07	3	< 5[e]	3	< 5	3	209	> 372	> 372
3.257	9		5.89 ± 0.03	3	6.67 ± 0.05	3	5.07 ± 0.10[d,e]	3	4.92 ± 0.14	3	6	40	56
3.258	10		5.14 ± 0.14	3	6.52 ± 0.13	3	< 5[e]	3	< 5	3	24	> 33	> 33
3.259	11		5.41 ± 0.12	3	6.52 ± 0.02	3	4.95 ± 0.06[d]	3	5.23 ± 0.02	3	13	37	19
3.260	1		5.40 ± 0.04	3	8.21 ± 0.09	3	8.77 ± 0.02[d,e]	3	8.07 ± 0.06	3	646	0.3	1
3.261[†]	4		< 5	3	7.89 ± 0.06	3	< 5[e]	3	< 5	3	> 776	> 776	> 776
3.262[†]	7		5.10 ± 0.05	3	7.27 ± 0.07	3	< 5[e]	3	< 5	3	148	> 186	> 186
3.263	8		< 5	3	5.35 ± 0.02	3	4.99 ± 0.02[e]	3	< 5	3	> 2	2	> 2
3.264[†]	4		4.98 ± 0.02	3	8.09 ± 0.03	3	< 5[e]	3	< 5	3	1288	> 1230	> 1230
3.265	4		5.87 ± 0.12	3	8.19 ± 0.11	3	5.63 ± 0.11[e]	3	5.16 ± 0.11	3	209	363	1072

Header for the table: **pK$_i$** spanning hH₁R–hH₄R columns; **H₂R selectivity K_i(H$_x$R)/K_i(H₂R)** spanning H₁, H₃, H₄ columns.

Table 3.07 (continued)

Comp.	structure		pK$_i$								H₂R selectivity K_i(H$_x$R)/K_i(H₂R)		
	BB	R	hH₁R^b	N	hH₂R^c	N	hH₃R^{d,e}	N	hH₄R^f	N	H₁	H₃	H₄
3.266	5		5.57 ± 0.09	3	6.17 ± 0.08	3	5.04 ± 0.03^e	3	< 5	3	4	13	> 15
3.267	6		5.60 ± 0.05	3	7.19 ± 0.14	3	5.32 ± 0.11^e	3	5.35 ± 0.11	3	39	74	69
3.268	9		5.74 ± 0.14	4	6.48 ± 0.04	3	5.08 ± 0.07^{d,e}	3	5.20 ± 0.03	3	5	25	19
3.269	10		5.28 ± 0.18	3	6.63 ± 0.06	3	4.89 ± 0.13^e	3	5.13 ± 0.06	3	22	45	32
3.270	11		6.74 ± 0.12	3	6.97 ± 0.03	3	5.71 ± 0.10^d	3	5.47 ± 0.10	3	2	18	32
3.271	4		5.29 ± 0.08	3	7.82 ± 0.11	3	5.40 ± 0.13^e	3	5.31 ± 0.16	3	339	263	324
3.272	9		5.12 ± 0.11	3	6.50 ± 0.05	3	5.10 ± 0.11^{d,e}	3	5.22 ± 0.03	3	24	25	19
3.273	10		4.88 ± 0.15	3	6.63 ± 0.07	3	4.97 ± 0.10^e	3	5.15 ± 0.03	3	56	46	30
3.274	11		5.41 ± 0.08	3	6.96 ± 0.19	3	5.76 ± 0.13^{d,e}	3	5.39 ± 0.11	3	35	16	37
3.275	9		5.67 ± 0.14	3	6.46 ± 0.18	3	5.71 ± 0.09^e	3	5.67 ± 0.10	3	6	6	6
3.276	10	dimeric	5.84 ± 0.03	3	6.42 ± 0.02	3	6.15 ± 0.04^e	3	5.63 ± 0.04	3	4	2	6
3.277	4		5.45 ± 0.08	3	8.28 ± 0.13	3	5.00 ± 0.06^e	3	< 5	3	676	1905	> 1905
3.278	4	dimeric	5.74 ± 0.08	3	8.32 ± 0.11	3	5.16 ± 0.06^e	3	5.05 ± 0.07	3	380	1445	1862

[a]Radioligand competition binding assay using membrane preparations of Sf9 cells expressing the hH₂R-G$_{sαS}$, the hH₃R + G$_{αi2}$ + G$_{β1γ2}$ or the hH₄R + G$_{αi2}$ + G$_{β1γ2}$. All compounds were tested as TFA salts unless otherwise noted. †Tested as HCl salt instead of TFA salt. Data represent mean values ± SEM of N independent experiments, each performed in triplicate. The displacement curves of compounds **3.239**-**3.240**, **3.244**, **3.251**, **3.255**, **3.261**-**3.262**, **3.264**-**3.265**, **3.267**, **3.271**, and **3.277** are presented in Figures 3.205 and 3.206 in chapter **3.6.11**. [b]Displacement of 5 nM [³H]mepyramine (Kd = 4.5 nM). [c]Displacement of 20 nM [³H]UR-DE257[390] (K$_d$ = 12.2 nM). [d]Displacement of 8.6 nM [³H]Nα-methylhistamine (K$_d$ = 3 nM). [e]Displacement of 2 nM [³H]UR-PI294[391] (K$_d$ = 3 nM). [f]Displacement of 15 nM [³H]**3.001** (K$_d$ = 16 nM). n.d.: not determined.

3.4.2.3 D$_{2long}$R and D$_3$R Affinities of N^G-Carbamoylated Guanidines

N^G-carbamoylated guanidines with a pK_i value > 7.0 at the hH$_2$R were investigated for their affinities to the hD$_{2long}$- and hD$_3$ receptors in radioligand binding assays on homogenates of HEK293T-CRE-Luc cells co-expressing the respective receptor (cf. Table 3.08). Ligands with pK_i values < 7 were not tested, as they are not suitable as pharmacological tools to study H$_2$R function in the brain due to their low affinity. Compounds containing the 2-aminothiazole heterocycle without a methyl group in position 4 (**3.240**, **3.256**, and **3.267**) still showed high to moderate affinities to the hD$_{2long/3}$ receptors, especially to the hD$_3$R (cf. Table 3.08). The determined hD$_{2long/3}$ receptor affinities were comparable to affinities published for 2-amino(4-methyl)thiazoles.[304] Fortunately, compounds containing the 2-amino-1,3,4-thiadiazole or the 1H-1,2,4-triazole heterocycle displayed only low affinity to the hD$_{2long}$- and hD$_3$ receptors. Some of them (**3.239**, **3.244**, **3.255**, **3.261**-**3.262**, and **3.265**) even demonstrated more than 100-fold selectivity for the hH$_2$R over the hD$_{2long}$ and hD$_3$ receptors (cf. Table 3.08). This trend indicates that the nitrogen in the 4 position might be responsible for the lower affinity to the hD$_3$R. In addition to the effect of the heterocycle, the side residue played an essential role regarding the dopamine hD$_{2long/3}$ receptor affinities. For example, thiadiazoles **3.251** (2-cyclohexylpropyl side residue) and **3.271** (2-methyl-5-phenylpentyl side residue) still had a moderate affinity for the hD$_{2long/3}$ receptors, which might indicate an additional (hydrophobic) interaction in the binding pocket of D$_{2long/3}$ receptors (not further investigated). Finally, the dimeric ligand **3.277** also possessed a high hD$_{2long}$- and hD$_3$ receptor affinity compared to the corresponding monomeric ligands **3.239** and **3.244** (cf. Table 3.08). Therefore, **3.278**, also a dimeric ligand, was not investigated further. **3.247** and **3.260** were, despite their high H$_2$R affinity, also excluded from additional experiments due to their low subtype selectivity (cf. Table 3.07).

In summary, although many ligands (**3.239**, **3.244**, **3.255**, **3.261**-**3.262**, and **3.265**) showed a decent selectivity for the hH$_2$R over the hD$_{2long}$- and hD$_3$ receptors (ratios of K_i > 100), **3.239** and **3.255** turned out to be the most promising candidates due to their excellent selectivity profiles.

Table 3.08. Binding data of the selected N^G-carbamoylated guanidines on human dopamine D$_{2long}$ and D$_3$ receptors.[a]

Comp.	structure		pK$_i$				H₂R selectivity K_i(hD$_x$R)/K_i(hH₂R)	
	BB	**R**	**hD$_{2long}$R**[b]	**N**	**hD$_3$R**[c]	**N**	**hD$_{2long}$R**	**hD$_3$R**
pramipexole (**3.006**)	-	-	hi 7.59 ± 0.12[404] low 6.00 ± 0.03[404]	3	9.18 ± 0.06[404]	3	0.002*	0.00005
3.005[299]	-	-	7.09 ± 0.07	3	8.70 ± 0.04	3	10	0.2
3.139[304]	-		6.35 ± 0.01[304]	3	7.80 ± 0.09[304]	3	100	4
3.239	4		5.02 ± 0.15	3	6.10 ± 0.05	4	3162	263
3.240	6		5.46 ± 0.07	3	7.50 ± 0.02	3	151	1
3.244	4		< 5	3	6.23 ± 0.02	3	> 1950	115
3.251	4		5.79 ± 0.01	3	6.63 ± 0.08	3	83	12
3.255	4		5.20 ± 0.04	3	5.58 ± 0.17	3	1259	525
3.256	6		5.34 ± 0.07	3	7.13 ± 0.04	3	170	3
3.261[†]	4		< 5	3	5.49 ± 0.10	3	> 776	251
3.262[†]	7		< 5	3	< 5	3	> 186	> 186
3.264[†]	4		< 5	3	6.18 ± 0.10	3	> 1230	81
3.265	4		5.97 ± 0.07	3	5.69 ± 0.11	4	166	316
3.267	6		6.31 ± 0.07	3	6.64 ± 0.01	3	8	4
3.271	4		6.35 ± 0.06	3	6.49 ± 0.02	3	30	21
3.277	4	dimeric	6.02 ± 0.10	3	7.22 ± 0.07	3	182	12
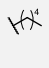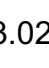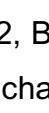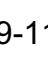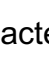
[a]Data represent mean values ± SEM from N independent experiments, each performed in triplicate. Radioligand competition binding assay with [³H]*N*-methylspiperone ([b]hD$_{2long}$R: K$_d$ = 0.0149 nM, c = 0.05 nM or [c]hD3R: K$_d$ = 0.0258 nM, c = 0.05 nM) using homogenates of [b]HEK293T-CRE-Luc-hD$_{2long}$R or [c]HEK293T-CRE-Luc-hD$_3$R cells.[404] All compounds were tested as TFA salts unless otherwise noted. †Tested as HCl salt instead of TFA salt. The displacement curves are presented in Figures 3.207 and 3.208 in chapter **3.6.12**. *Calculated using pK$_i$ high value.

3.4.2.4 Functional Studies at the Human H_2R
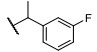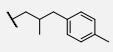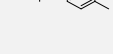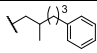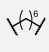
To get further insights into the general structure-activity relationship of the N^G-carbamoylated guanidines, all target compounds **3.238**-**3.278** were investigated for hH_2R agonism and antagonism in the β-arrestin2- and mini-G protein-recruitment assays using genetically engineered HEK293T cells, respectively. Only the functional data of the most interesting molecules (**3.239**-**3.240**, **3.244**, **3.251**, **3.255**-**3.256**, **3.261**-**3.262**, **3.264**-**3.265**, **3.267**, **3.271**, and **3.277**) are shown in Table 3.09 (for functional data of the remaining and reference compounds see Table 3.17 in chapter **3.6.13**). The responses in both assays were normalized to the maximum effect induced by 100 μM histamine (**3.001**, E_{max} = 1.00) and buffer control (E_{max} = 0). Thus, **3.001** is defined as a full, unbiased agonist in either readout. **3.001** exhibits a significantly lower potency in the β-arrestin2 recruitment assay compared to the mini-G protein recruitment assay (pEC_{50} (β-arrestin2) = 5.42[187]; pEC_{50} (mGs (minimal $G_{αs}$ protein)) = 6.94[425]; cf. Table 3.09). Similarly, the potencies of the investigated N^G-carbamoylated guanidines were also lower in the β-arrestin2 recruitment assay (cf. Table 3.09). A possible explanation for this trend could be the use of the mGs protein, since it is known that mG proteins stabilize active states of GPCRs, which favors the binding of agonists.[425–428] The compounds shown in Table 3.09 proved to be strong partial agonists or full agonists (E_{max} = 0.83 to 0.95, cf. Table 3.09) in the mini-G protein recruitment assay with pEC_{50} values > 7.0. The determined pEC_{50} values agree in most cases very well with the pK_i values from the radioligand binding assay. Compound **3.255**, containing the benzyl side residue, showed the highest hH_2R potency with a pEC_{50} of 8.48, but also **3.239** (pentyl side residue, pEC_{50} = 8.22) showed an excellent potency in the single-digit nanomolar range (cf. Table 3.09). The incorporation of a ring system (cf. Scheme 3.02, BB9-11) in the spacer resulted in either antagonists or partial agonists depending on the side residue (cf. Table 3.17). Surprisingly, some of the tested compounds revealed a completely different functional profile in the β-arrestin2 recruitment assay (cf. Table 3.09 and Table 3.17). Almost all tested 2-aminothiazoles **3.139** (UR-KAT523)[304], **3.140** (UR-CH20)[304,416], **3.143** (UR-CH22)[304,416], **3.145** (UR-Po563)[304], **3.157** (UR-MB-69)[304], **3.170** (UR-SB257)[304,416], **3.172** (UR-KAT527)[304], **3.240**, **3.256**, and **3.267** and the thiadiazoles **3.265** and **3.271**, containing a propyl spacer, as well as triazole **3.262** exhibited a certain degree of efficacy bias towards G protein activation (cf. Figure 3.210, for details see chapter **3.6.15**). The compounds acted as strong partial agonists or full agonists (E_{max} = 0.73

to 0.94; cf. Table 3.09 and Table 3.17) in the mini-G protein recruitment assay but were only partial agonists in the β-arrestin2 recruitment assay (E$_{max}$ = 0.10 to 0.73; cf. Table 3.09 and Table 3.17). By contrast, since most of the thiadiazoles (including the most promising candidates **3.239** (UR-KAT505) and **3.255** (UR-KAT533)) exhibited no significant bias, they behave in a similar way as the endogenous ligand histamine. This advantage should enable an authentic examination of the function of the H$_2$R in the CNS with these ligands. Finally, the dimeric ligands (e.g., thiazole: **3.005**[299], thiadiazole: **3.277**) exhibited similar characteristics as their monomeric counterparts and all compounds containing a rigidized spacer (cf. Scheme 3.02, BB9-11) acted as antagonists in the β-arrestin2 recruitment assay (cf. Table 3.17 in chapter **3.6.13**).

Table 3.09. Potencies and efficacies of the selected N^G-carbamoylated guanidines in the β-arrestin2 and mini-G protein recruitment assays at the hH$_2$R.[a]

Comp.	structure		β-arrestin2 recruitment[b]			mGs recruitment[c]		
	BB	**R**	**pEC$_{50}$**	**E$_{max}$[d]**	**N**	**pEC$_{50}$**	**E$_{max}$[d]**	**N**
3.001	-	-	5.42 ± 0.02[187]	1.00[187]	3	6.94 ± 0.06[425]	1.00[425]	9
3.005[299]	-	-	6.80 ± 0.14	0.30 ± 0.04	6	7.62 ± 0.02	0.89 ± 0.01	3
3.006	-	-	4.40 ± 0.10[304]	0.35 ± 0.03[304]	3	6.78 ± 0.01	0.95 ± 0.01	
3.139[304]	-		6.75 ± 0.12[304]	0.15 ± 0.02[304]	4	8.34 ± 0.05	0.88 ± 0.01	3
3.239*	4		6.63 ± 0.08	0.94 ± 0.06	6	8.24 ± 0.22	0.93 ± 0.01	3
3.240	6		7.25 ± 0.04	0.64 ± 0.04	4	8.22 ± 0.04	0.89 ± 0.01	3
3.244	4		5.97 ± 0.04	1.16 ± 0.05	5	8.22 ± 0.06	0.95 ± 0.02	3
3.251*	4		6.87 ± 0.09	0.90 ± 0.04	6	7.97 ± 0.03	0.88 ± 0.03	3
3.255	4		6.86 ± 0.13	0.94 ± 0.06	5	8.48 ± 0.07	0.92 ± 0.01	4
3.256	6		7.31 ± 0.05	0.73 ± 0.03	4	8.31 ± 0.14	0.94 ± 0.03	4
3.261[†]	4		6.55 ± 0.09	0.87 ± 0.02	5	7.70 ± 0.04	0.91 ± 0.02	3
3.262[†]	7		6.49 ± 0.10	0.37 ± 0.02	4	7.59 ± 0.04	0.90 ± 0.02	3

Table 3.09 (continued)

Comp.	structure		β-arrestin2 recruitment[b]			mGs recruitment[c]		
	BB	**R**	**pEC₅₀**	**Eₘₐₓ[d]**	**N**	**pEC₅₀**	**Eₘₐₓ[d]**	**N**
3.264[†]	4		7.12 ± 0.05	1.04 ± 0.03	6	8.09 ± 0.04	0.95 ± 0.01	3
3.265*	4		6.89 ± 0.17	0.53 ± 0.04	5	7.21 ± 0.09	0.91 ± 0.01	4
3.267	6		6.63 ± 0.08	0.16 ± 0.01	4	7.11 ± 0.04	0.83 ± 0.01	4
3.271	4		6.54 ± 0.17	0.38 ± 0.04	5	7.62 ± 0.09	0.84 ± 0.02	4
3.277*	4	dimeric	6.39 ± 0.07	0.82 ± 0.06	4	7.70 ± 0.12	0.94 ± 0.01	3

[a]Data represent mean values ± SEM from N independent experiments, each performed in triplicate. All compounds were tested as TFA salts unless otherwise noted. [†]Tested as HCl salt instead of TFA salt. [b]β-arrestin2 recruitment assay was performed using HEK293T-ARRB2-H₂R cells.[187,395] [c]Mini-G protein recruitment assay was performed using HEK293T NlucN-mGs/hH₂R-NlucC cells.[425] [d]The response in both assays was normalized to the maximal effect induced by 100 µM **3.001** (Eₘₐₓ = 1.00) and buffer control (Eₘₐₓ = 0.00). The concentration-response curves are presented in Figure 3.200 (see chapter **3.6.9**) and Figure 3.202 (see chapter **3.6.10**). *Selected compounds were investigated for functional activity in the [³⁵S]GTPγS binding assay at the hH₂R-G$_{sαS}$ fusion protein[299,389,393]: **3.239**: pEC₅₀ = 7.59 ± 0.11, Eₘₐₓ = 0.84 ± 0.04 (N = 3); **3.251**: pEC₅₀ = 7.88 ± 0.09, Eₘₐₓ = 0.78 ± 0.07 (N = 3); **3.265**: pEC₅₀ = 7.89 ± 0.11, Eₘₐₓ = 0.88 ± 0.06 (N = 4); **3.277**: pEC₅₀ = 7.46 ± 0.09, Eₘₐₓ = 0.71 ± 0.06 (N = 3). The obtained results were in good agreement with the results from the mini-G protein recruitment assay.

3.4.2.5 Functional Studies at the Guinea Pig H₂R

Furthermore, a selection of compounds (with a pK_i > 7.0 at the hH₂R and a selectivity over the hD$_{2long/3}$ receptors) was investigated on the isolated spontaneously beating guinea pig right atrium as a more complex, well-established standard model for the characterization of H₂R ligands (cf. Table 3.10).[244,420] All compounds turned out to be full agonists in this assay (Eₘₐₓ = 0.98 to 1.15; cf. Table 3.10). The obtained data are generally comparable with the results from the gpH₂R mini-G protein recruitment assay in terms of potency and efficacy (cf. Table 3.10). Noteworthily, **3.261**, **3.264**, and **3.265** showed the highest discrepancies regarding the potency in both assays. While **3.261** and **3.264** showed higher potencies by about one logarithmic unit on the guinea pig right atrium, **3.265** behaved precisely the opposite (cf. Table 3.10). The thiadiazole **3.264** (pEC₅₀ = 9.04) showed the highest potency on the guinea pig right atrium whereas, **3.255** was the most potent compound in the mini-G protein recruitment assay (pEC₅₀ = 8.66). In general, a comparison of the mini-G protein recruitment assay data at the guinea pig and human H₂Rs showed that the potencies at the gpH₂R were

slightly better for all substances tested, while the efficacies were pretty much the same. A similar observation was already published for the [^{35}S]GTPγS assay and the steady state GTPase assay.[302,378,393,429]

Table 3.10. Potencies and efficacies of the tested N^G-carbamoylated guanidines determined in the mini-G protein recruitment assay at the gpH₂R or by organ bath studies at the spontaneously beating guinea pig right atrium.[a]

Comp.	structure		mGs recruitment[b]			atrium[d]		
	BB	**R**	pEC₅₀	E_max[c]	N	pEC₅₀[e]	E_max[f]	N
3.001	-	-	6.60 ± 0.07[417]	1.00[417]	3	6.16 ± 0.01[389]	1.00[389]	225
3.139[304]	-		n.d.	n.d.	-	8.24 ± 0.03[304]	0.78 ± 0.03[304]	3
3.239	4		8.36 ± 0.07	0.94 ± 0.01	3	8.25 ± 0.11	1.09 ± 0.02	3
3.244	4		8.64 ± 0.05	0.96 ± 0.01	3	8.32 ± 0.06	1.06 ± 0.05	3
3.255	4		8.66 ± 0.04	0.94 ± 0.01	3	8.88 ± 0.03	1.05 ± 0.01	3
3.261[†]	4		7.60 ± 0.03	0.90 ± 0.02	3	8.54 ± 0.09	0.98 ± 0.04	3
3.262[†]	7		7.79 ± 0.02	0.86 ± 0.03	3	7.42 ± 0.10	1.15 ± 0.11	3
3.264[†]	4		8.16 ± 0.03	0.93 ± 0.02	3	9.04 ± 0.10	1.10 ± 0.05	3
3.265	4		7.83 ± 0.09	0.92 ± 0.01	3	7.02 ± 0.08	1.02 ± 0.10	3

[a]Data represent mean values ± SEM from N independent experiments, each performed in triplicate. All compounds were tested as TFA salts unless otherwise noted. [†]Tested as HCl salt instead of TFA salt. [b]Mini-G protein recruitment assay was performed using HEK293T NlucN-mGs/gpH₂R-NlucC cells.[417] [c]The response was normalized to the maximal effect induced by 100 µM **3.001** (E_max = 1.00) and buffer control (E_max = 0.00). The concentration-response curves are presented in Figure 3.201 (see chapter **3.6.9**). [d]Organ bath studies using the isolated, spontaneously beating guinea pig right atrium.[389] [e]pEC₅₀ was calculated from the mean corrected shift ΔEC₅₀ of the agonist curve relative to the histamine reference curve by equation: pEC₅₀ = 6.16 + ΔpEC₅₀. [f]E_max: maximal response relative to the maximal increase in heart rate induced by 30 µM **3.001** (E_max = 1.00). n.d.: not determined.

3.4.2.6 Functional Studies at the Human D$_{2long/3}$ Receptors

Although the relevant N^G-carbamoylated guanidines (**3.239**-**3.240**, **3.244**, **3.255**, **3.261**-**3.262**, and **3.264**-**3.265**) bind to the hD$_{2long/3}$ receptors only with low affinity (pK_i < 6.5 (only **3.240** has a pK_i > 6.5 at the D$_3$R), see Table 3.08), the ligands were characterized in the β-arrestin2 assay.[404] In addition, the data of **3.005**[299], **3.251**, **3.256**, **3.267**, **3.271**, and **3.277** were collected for a broader comparison of the compounds. The measured potencies and efficacies are presented in Table 3.11. All tested compounds showed agonistic activities in the β-arrestin2 recruitment assay at the hD$_3$R. In the β-arrestin2 recruitment assay at the hD$_{2long}$R, **3.255** and **3.262** were inactive (up to a tested concentration of 10 μM; cf. Table 3.11). The remaining compounds (**3.005**[299], **3.239**-**3.240**, **3.244**, **3.251**, **3.256**, **3.261**, **3.264**, **3.267**, and **3.277**) acted as agonists with the exception of **3.265** and **3.271**, which were antagonists. Some compounds (**3.239**, **3.244**, **3.251**, **3.261**, and **3.264** at the hD$_{2long}$R and **3.262** and **3.265** at the hD$_3$R) showed only very weak partial agonism at the highest tested concentration of 10 μM, which could not be fitted. In general, thiadiazoles showed lower potencies and efficacies at the hD$_{2long/3}$ receptors than their thiazole counterparts (cf. Table 3.11).

Table 3.11. Potencies and efficacies of selected N^G-carbamoylated guanidines determined in the β-arrestin2 recruitment assay at the hD$_{2long}$R or hD$_3$R.^{a}

Comp.	structure		hD$_{2long}$R^b			hD$_3$R^c		
	BB	**R**	**pEC$_{50}$/(pK_b)^d**	**E$_{max}$^{e}**	**N**	**pEC$_{50}$**	**E$_{max}$^{e}**	**N**
quinpirole	-	-	7.55 ± 0.07[404]	1.00[404]	5	8.75 ± 0.07[404]	1.00[404]	6
pramipexole (**3.006**)	-	-	8.19 ± 0.05[404]	0.86 ± 0.04[404]	4	9.09 ± 0.06[404]	0.99 ± 0.04[404]	4
3.005[299]	-	-	6.67 ± 0.09	0.88 ± 0.07	4	7.70 ± 0.08	1.01 ± 0.06	6
3.139[304]	-		5.98 ± 0.02[304]	0.41 ± 0.05[304]	4	7.80 ± 0.05[304]	0.96 ± 0.05[304]	3
3.239	4		< 5	0.11 ± 0.01*	3	5.55 ± 0.18	0.74 ± 0.08	3
3.240	6		5.85 ± 0.07	0.56 ± 0.05	4	7.40 ± 0.01	0.87 ± 0.01	3

Table 3.11 (continued)

Comp.	structure		hD$_{2long}$R[b]			hD$_3$R[c]		
	BB	R	pEC$_{50}$/(pK_b)[d]	E$_{max}$[e]	N	pEC$_{50}$	E$_{max}$[e]	N
3.244	4		< 5	0.15 ± 0.01*	3	6.09 ± 0.09	0.73 ± 0.07	4
3.251	4		< 5	0.17 ± 0.05*	3	5.87 ± 0.10	0.26 ± 0.05	3
3.255	4		< 5	n.a.	5	5.92 ± 0.14	0.43 ± 0.02	4
3.256	6		5.47 ± 0.08	0.23 ± 0.04	3	7.17 ± 0.03	0.87 ± 0.04	3
3.261[†]	4		< 5	0.06 ± 0.01*	3	5.97 ± 0.16	0.71 ± 0.04	3
3.262[†]	7		< 5	n.a.	3	< 5	0.18 ± 0.05*	3
3.264[†]	4		< 5	0.07 ± 0.01*	3	5.72 ± 0.07	0.73 ± 0.11	3
3.265	4		(5.69 ± 0.01)	n.a.**	3	< 5	0.12 ± 0.01*	3
3.267	6		5.35 ± 0.06	0.31 ± 0.04	3	5.98 ± 0.02	0.71 ± 0.02	4
3.271	4		(5.42 ± 0.01)	n.a.**	4	6.33 ± 0.07	0.56 ± 0.05	3
3.277	4	dimeric	5.95 ± 0.05	0.32 ± 0.05	3	6.53 ± 0.12	0.80 ± 0.03	3

[a]Data represent mean values ± SEM from N independent experiments, each performed in triplicate. β-arrestin2 recruitment assay was performed using HEK293T ElucN-βarr2 hD$_{2long}$R-ElucC[b] or HEK293T ElucN-βarr2 hD$_3$R-ElucC[c] cells. All compounds were tested as TFA salts unless otherwise noted. [†]Tested as HCl salt instead of TFA salt.[404] [d]pK_b = -logK_b. K_b values were calculated according to the Cheng-Prusoff equation.[156] The IC$_{50}$ values of antagonists were determined in the antagonist mode versus quinpirole (50 nM, D$_{2long}$R). [e]The response in both assays was normalized to the maximal effect induced by 10 µM (E$_{max}$ = 1.00) and buffer control (E$_{max}$ = 0.00). *E$_{max}$ at c = 10 µM. **Silent antagonist. n.a. = not active. The concentration-response curves are presented in Figure 3.203 and Figure 3.204 (see chapter **3.6.10**).

3.4.2.7 Off-target Studies

In order to be able to differentiate between on-target and off-target effects, the ligands should selectively bind to the H$_2$R. Therefore, selected compounds **3.139**, **3.239**, **3.255**, and **3.262** were additionally investigated in radioligand competition binding studies for their ability to bind to other peripheral and central aminergic GPCRs (off-target studies). Some of these receptors are frequently found anti-target receptors (e.g., α_{1A} adrenergic, M$_{1-5}$ muscarinic). The results are summarized in Table 3.12 and indicate that the most promising thiadiazoles **3.239** and **3.255** have a more than 100-fold higher affinity at the H$_2$R compared to the other tested GPCRs (cf. selectivity profiles B and C in Figure 3.019). The thiazole **3.139**, tested as a control, also showed a moderate affinity to D$_1$ and D$_{4.4}$ receptors (D$_1$R: pK_i = 6.59; D$_{4.4}$R: pK_i = 6.96; cf. Table 3.12) in addition to the already published high affinity for the D$_3$R (pK_i = 7.80; cf. Table 3.08). Although triazole **3.262** showed low affinities (pK_i ≤ 6.07) at the 14 additionally tested aminergic GPCRs, it did not achieve a sufficient selectivity (factor < 100, cf. selectivity profile D in Figure 3.019) due to the double-digit nanomolar affinity for the H$_2$R (pK_i = 7.27; cf. Table 3.07).
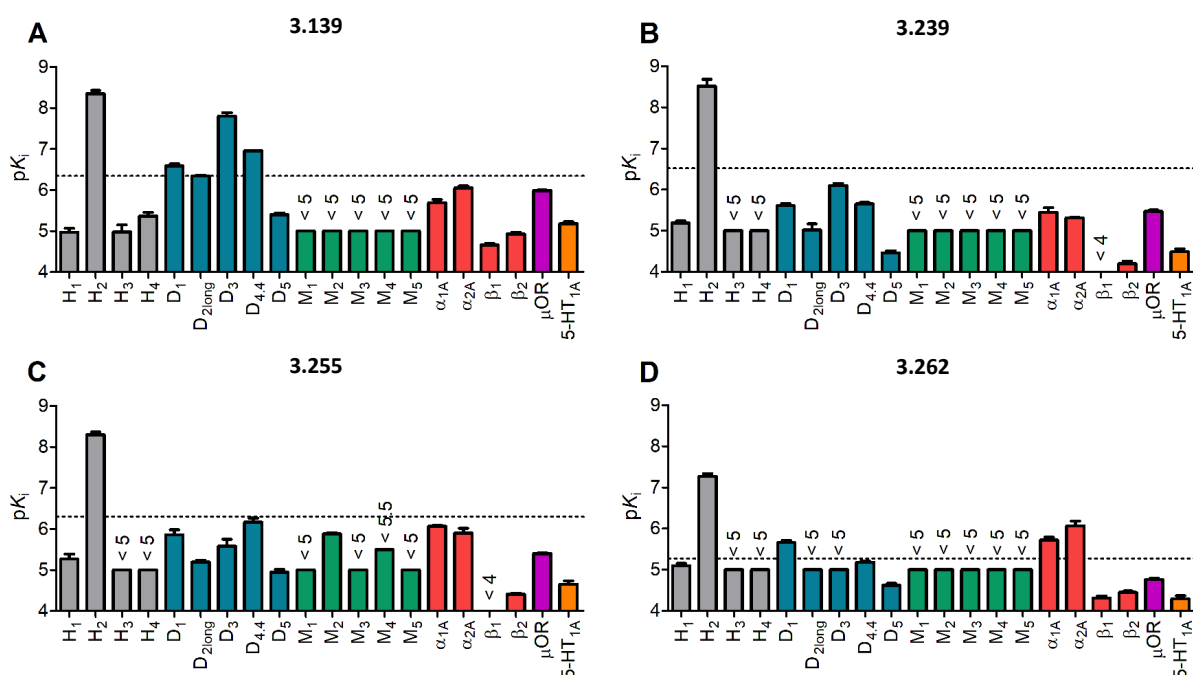
Figure 3.019. Selectivity over representative aminergic GPCRs, including histaminergic (grey), dopaminergic (blue), muscarinic (green), adrenergic (red), opioid (magenta), and serotonergic (orange) receptors, were determined by radioligand competition binding experiments and compared to the affinity at the H$_2$R of (A) **3.139**, (B) **3.239**, (C) **3.255**, and (D) **3.262**. The dashed line indicates an at least 100-fold selectivity for the H$_2$R of the respective compound. Bars represent the mean ± SEM of 3-4 individual experiments, each performed in triplicate.

Table 3.12. Receptor selectivity studies of **3.139**, **3.239**, **3.255**, and **3.262** determined by competition binding.

Receptor	pK_i							
	3.139	N	**3.239**	N	**3.255**	N	**3.262**	N
Dopamine D$_1$[a]	6.59 ± 0.05	3	5.61 ± 0.05	3	5.86 ± 0.12	3	5.66 ± 0.05	3
Dopamine D$_{4.4}$[b]	6.96 ± 0.01	3	5.65 ± 0.04	3	6.17 ± 0.10	3	5.18 ± 0.03	3
Dopamine D$_5$[c]	5.40 ± 0.04	3	4.46 ± 0.05	3	4.95 ± 0.07	3	4.62 ± 0.05	3
Muscarinic acetylcholine M$_1$[d]	<5	3	<5	3	<5	3	<5	3
Muscarinic acetylcholine M$_2$[e]	<5	3	<5	3	5.88 ± 0.03	3	<5	3
Muscarinic acetylcholine M$_3$[f]	<5	3	<5	3	<5	3	<5	3
Muscarinic acetylcholine M$_4$[g]	<5	3	<5	3	<5.5	3	<5	3
Muscarinic acetylcholine M$_5$[h]	<5	3	<5	3	<5	3	<5	3
α$_{1A}$ adrenergic[i]	5.69 ± 0.08	3	5.45 ± 0.11	3	6.07 ± 0.02	3	5.72 ± 0.07	3
α$_{2A}$ adrenergic[j]	6.05 ± 0.05	3	5.31 ± 0.02	3	5.90 ± 0.12	3	6.07 ± 0.11	3
β$_1$ adrenergic[k]	4.66 ± 0.04	3	<4	3	<4	3	4.31 ± 0.05	3
β$_2$ adrenergic[l]	4.93 ± 0.04	3	4.20 ± 0.06	3	4.40 ± 0.02	3	4.45 ± 0.03	3
μ-opioid[m]	5.99 ± 0.01	3	5.47 ± 0.03	3	5.40 ± 0.02	3	4.76 ± 0.03	3
Serotonin 5-HT$_{1A}$[n]	5.18 ± 0.05	3	4.49 ± 0.07	3	4.56 ± 0.05	4	4.29 ± 0.08	3

Determined by competition binding [a,c]with [^{3}H]SCH23390 (K_d/applied conc: D$_1$, 0.23/0.4 nM; D$_5$, 0.24/0.4 nM) using homogenates from HEK293T-CRE-Luc-hD$_x$R cells (x = 1 or 5),[404] [b]with [^{3}H]N-methylspiperone (K_d/applied conc: D$_{4.4}$, 0.078/0.1 nM) using homogenates from HEK293T ElucN-βarr2 hD$_{4.4}$R-ELuc cells,[404] [d-h]with [^{3}H]N-methylscopolamine (K_d/applied conc: M$_1$, 0.17/0.2 nM; M$_2$, 0.10/0.2 nM; M$_3$, 0.12/0.2 nM; M$_4$, 0.052/0.1 nM, M$_5$, 0.20/0.3 nM) using whole CHO-hM$_x$R cells (x = 1-5).[430], with [i][^{3}H]prazosin (K_d/applied conc: α$_{1A}$, 0.25/0.1 nM), [j][^{3}H]RX821002 (α$_{2A}$, 0.60/0.1 nM), [k-l][^{3}H]CGP12177 (β$_1$, 0.075/0.2 nM; β$_2$, 0.070/0.2 nM), [m][^{3}H]diprenorphine (5-HT$_{1A}$, 0.090/0.3 nM), [n][^{3}H]WAY600135 (0.080/0.2 nM) using membranes from HEK293T cells transiently transfected with cDNA of human adrenoceptors [i]α$_{1A}$, [j]α$_{2A}$, [k]β$_1$, [l]β$_2$, human receptor [m]5-HT$_{1A}$ or human receptor [n]μOR.[431,432]

3.4.2.8 Cardiac (Side) Effects of Histamine H₂ Receptor Ligands 3.145, 3.261, and 3.262

As already mentioned, stimulation of postsynaptic H_2Rs in the CNS might be a promising approach for the treatment of Alzheimer's disease. In previous studies, dual-acting acetylcholinesterase inhibitors and H_3R antagonists showed to be beneficial for learning and memory processes in the CNS by inhibiting H_3-autoreceptors (cf. Figure 3.012).[371–373] The inhibition of the H_3-autoreceptor results in an increased release of histamine and subsequent stimulation of postsynaptic H_2Rs. Accordingly, the use of CNS-penetrating H_2R agonists might be of great interest. Nonetheless, peripheral effects of this novel H_2R ligands, for instance, on the heart, must be examined to justify its possible use as a drug. Histaminergic effects in the heart were first described by Dale and Laidlaw (1910)[227] and Ackermann and Kutscher (1910)[433]. The expression level of the H_1R in the heart is more elevated than that of the H_2R;[434,435] nevertheless, the H_2 receptors are responsible for the positive inotropic and positive chronotropic effects in the human atrium.[436,437] The effects of H_2 agonists on the heart can be diminished by the administration of H_2 antagonists (e.g., cimetidine and famotidine).[374,438] Eventual cardiac (side) effects were investigated in the heart of mice that overexpress the human H_2 receptor (H_2-TG mice, for further information see chapter **3.5.2.7**)[439] and littermate wild type (WT) control mice.[440] The human H_2R is only overexpressed in the cardiomyocytes of the transgenic mice.[439] Histamine mediates its contractile effects solely in living H_2-TG mice, isolated perfused hearts from H_2-TG mice, isolated cells from H_2-TG mice, and isolated atrial preparations from H_2-TG mice, but not in cells or preparations from WT mice.[439,441–443] Hence, the H_2-TG mouse model is ideally suited to investigate the effects of H_2R agonists on the human heart. Moreover, muscle preparations from patients undergoing cardiac surgery were used for the examination of the H_2R agonist's effects on the heart.

At cumulative dosing, histamine successively increased the force of contraction in isolated electrically (1 Hz) driven left atrial preparations (for further information see chapter **3.5.2.8**) from H_2-TG mice (pEC$_{50}$ value of 6.73)[439] (original recording in Figure 3.021A and 3.021B) but failed to affect the force of contraction in preparations from WT mice (cf. Figure 3.021B). Moreover, histamine concentration dependently increased the velocity of contraction (maximum rate of tension development: cf. Figure 3.021C) and decreased the velocity of relaxation (minimum rate of tension

development: cf. Figure 3.021D). In spontaneously contracting right atrial preparations (for further information see chapter **3.5.2.8**) from H_2-TG mice histamine was capable to increase the beating rate in a time- and concentration-dependent fashion (cf. Figure 3.021E), whereas in preparations from WT mice no effect was determined (cf. Figure 3.021E). These findings are in line with previous reports.[439,441–443] The H_2R histaminergic effects (an increase of contraction force and beating rate) on preparations of H_2-TG mice were successfully antagonized by H_2R antagonists (e.g., cimetidine[439] or famotidine[442]) applied 30 minutes before application of histamine as already reported in previous studies.

Comparable to histamine (cf. Figure 3.021), UR-Po563 (**3.145**) augmented the force of contraction in a time- and concentration-dependent manner in atrial preparations only from H_2-TG, not from WT mice (cf. Figures 3.022A and 3.022B). The respective pEC_{50} value (force of contraction) of UR-Po563 is 8.27. Moreover, UR-Po563 concentration-dependently increased the velocity of contraction (maximum rate of tension development (dF/dt): cf. Figure 3.022D) and decreased the velocity of relaxation (minimum rate of tension development (dF/dt): cf. Figure 3.022E). UR-Po563 also increased the beating rate in right atrial preparations from H_2-TG but not from WT mice (cf. Figure 3.022C). The respective pEC_{50} value (beating rate) of UR-Po563 is 9.01. All effects of UR-Po563 in preparations of H_2-TG were antagonized by famotidine (cf. Figure 3.022). The same effects were found for UR-MB-158 (**3.261**) and UR-MB-159 (**3.262**). The H_2R agonists increased to a greater extent than histamine the force of contraction (UR-MB-158 (pEC_{50}: 9.38) and UR-MB-159 (pEC_{50}: 8.28)) in atrial preparations only from H_2-TG, while no effect was detected in preparations from WT mice (cf. Figures 3.023 and 3.024). Both compounds influenced concentration-dependently the velocity of contraction (maximum rate of tension development (Figure 3.023D and Figure 3.024D)) and the velocity of relaxation (minimum rate of tension development (cf. Figures 3.023E and 3.024E)). The spontaneous beating of right atrium preparations of H_2T-mice was raised by cumulative dosing of the compounds, revealing a pEC_{50} of 9.24 (UR-MB-158) and 7.91 (UR-MB-159). No concentration-dependently increase of effects were detected at preparations from WT mice (cf. Figures 3.023 and 3.024). All effects were successfully antagonized with famotidine (cf. Figures 3.023 and 3.024).

Table 3.13. Effect of UR-Po563 (1 μM) on force of contraction and beating rate in isolated perfused Langendorff hearts from H$_2$-TG and WT (n=3–4, each). Hearts were perfused initially with buffer for about 30 minutes for stabilization and allowed to beat spontaneously. Then with a syringe, driven by an electric pump, UR-Po563 solution was added to the perfusion buffer. Force was measured with a hook applied to the apex cordis and fed into a computer. After 5 minutes of drug perfusion the whole heart was rapidly frozen with Wollenberger clamps precooled in liquid nitrogen.

	WT		H$_2$-TG	
	Basal	UR-Po563	Basal	UR-Po563
Force (mM)	7.89 ± 1.28	8.95 ± 1.95	11.49 ± 2.07	20.46 ± 2.81*
Beating rate (bpm)	308 ± 8.60	321 ± 13.2	351 ± 37.3	391 ± 16.2
dF/dt max (mN/s)	204.6 ± 43.8	220.6 ± 36.1	296 ± 42.5	718 ± 90.9*
dF/dt min (mN/s)	-151 ± 53.2	-172 ± 56.5	-230 ± 39.3	-566 ± 52.7*

bpm, beats per minute.
*$P < 0.05$ versus basal.

Of further interest was investigating the ventricular effects of the H$_2$R ligands; for this purpose, spontaneously beating Langendorff preparations (isolated retrogradely perfused hearts, for further information see chapter **3.5.2.9**) were used. The left ventricular force was determined by the recording of the contraction from the apex cordis. UR-Po563 at a concentration of 1 μM increased the force of contraction in hearts from H$_2$-TG but not WT mice (results are summarized in Table 3.13). The results obtained were consistent with previous reports on histamine in Langendorff-perfused hearts.[439,442–444]
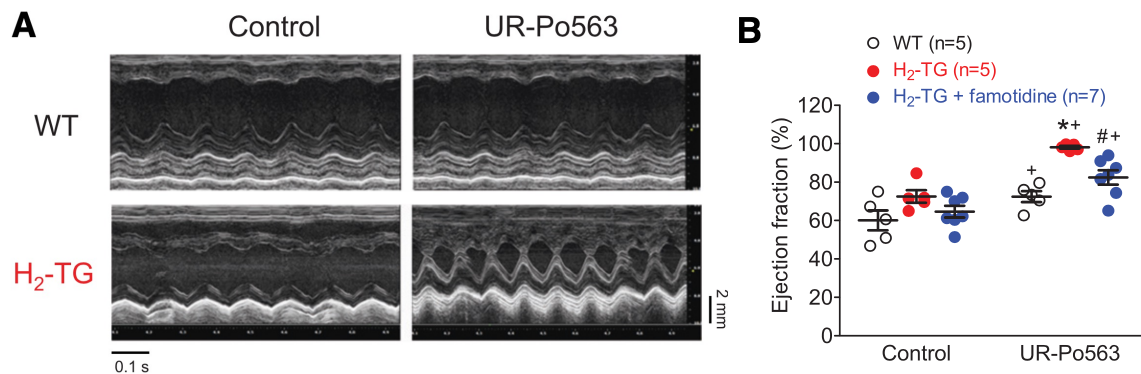
Figure 3.020. Echocardiography. (**A**) M-mode pictures of H$_2$-TG or WT injected into the peritoneum with 100 μL of a 1 mM solution of UR- Po563. The left ventricle is visible. UR-Po563 led to an increase in systolic wall motion in H$_2$-TG but not in WT. Pictures were taken before (control 5 baseline values) and 5 minutes after injection of UR-Po563 solution. Vertical bar indicates the size marker in millimeters, and horizontal bar indicates the time marker in seconds. Data are summarized in (**B**) as well as in Table 3.14. Figure was taken from Gergs et al. (2021).[440]

H$_2$R ligands (e.g., compound **3.145** (UR-Po563)) were also investigated *in vivo* for their cardiovascular performance by echocardiography measurements (for further information see chapter **3.5.2.11**) in H$_2$-TG and WT mice after intraperitoneal injection under anesthesia (original M-mode recordings: Figure 3.020A). Intraperitoneally injected UR-Po563 increased left ventricular ejection fraction (74.31 % (basal) vs. 98.21 % (UR-Po563)) and beating rate (499.0 bpm (basal) vs. 626.8 bpm (UR-Po563)) in H$_2$-TG mice (cf. Table 3.14 and Figure 3.020B). It must be noted that the effects of UR-Po563 were antagonized by famotidine (cf. Table 3.14 and Figure 3.020B). Furthermore, using echocardiography, alterations of the left ventricular systolic and diastolic diameters of H$_2$-TG mice (but not in WT mice) were detected after UR-Po563 administration compared to the basal conditions (cf. Figure 3.020A). These results are in agreement with previously published ones with histamine.[439] Further results are summarized in Table 3.14. Finally, the effects of UR-Po563 in the human heart were investigated by using electrically driven (1 Hz) isolated right atrial strips obtained from routine bypass surgeries (fur further information see chapter **3.5.2.10**). In this model, UR-Po563 once again demonstrated a concentration-dependently increase of the contraction force (cf. Figure 3.025). Furthermore, it increased the velocity of contraction and decreased the velocity of relaxation (cf. Figure 3.025).

Table 3.14. Effects of UR-Po563, UR-MB-158, and UR-MB-159 in echocardiography. Mice were studied under isoflurane narcosis. Drugs were applied via injection into the peritoneum. Transthoracic ultrasound was performed in supine mice. B-mode and M-mode pictures were taken before and 5 minutes after injection of UR-Po563 into H$_2$-TG and WT.

	Heart rate (bpm)		Ejection fraction (%)	
	Basal	Stimulated	Basal	Stimulated
UR-Po563 (3.145)				
WT (n = 5)	436.8 ± 23.2	511.9 ± 113.6	60.14 ± 11.58	72.44 ± 6.40
H$_2$-TG (n = 5)	499.0 ± 83.3	626.8 ± 64.5*	74.31 ± 7.84	98.21 ± 9.97*
H$_2$-TG (n = 5) + famotidine	469.8 ± 99.8	517.4 ± 131.2	64.61 ± 8.19	82.47 ± 9.97*
UR-MB-158 (3.261)				
WT (n = 1)	447.5	596.5	55.83	83.2
H$_2$-TG (n = 2)	526.3	656.2	62.34	98.15
UR-MB-159 (3.262)				
WT (n = 1)	417.8	513.0	51.62	82.42
H$_2$-TG (n = 2)	380.9	686.3	54.04	94.21

*P < 0.05 versus basal (5 predrug values)

In summary, it can be stated, that UR-Po563, UR-MB-158, and UR-MB-159 act as full functional agonists (even more potent than histamine) on human cardiac H$_2$ receptors. The tested compounds are capable to stimulate human cardiac H$_2$ receptors (e.g., increase of contraction force and beating rate) of right and left atrial preparations of H$_2$-TG but not WT mice. Moreover, *in vitro* and *in vivo* models of H$_2$-TG mice demonstrated that the novel H$_2$R ligands can stimulate the H$_2$ receptors in ventricles (e.g., increase of beating rate, ejection fraction, and contraction force). Finally, investigations on isolated right atrial strips of the human revealed that UR-Po563 is able to increase the force of contraction in the human heart. Baumann et al. suggested that H$_2$R agonists might be a potential treatment for patients suffering from acute heart failure.[296,434,445] Hence, impromidine was investigated in clinical trials; apart from demonstrating beneficial effects in intensive care unit patients, the clinical trials revealed severe side effects of the probes, like increased gastric acid secretion.[296,446] The outcomes from this study can justify the clinical application of H$_2$R ligands. Even though initial trials on H$_2$R ligands failed due to the side effects, they could be clinically valuable for particular patients in intensive care. Therefore, the investigated compounds might have a twofold clinical utility. If stimulation of H$_2$ receptors is a valid concept to increase the force of contraction in patients, compounds UR-Po563, UR-MB-158, and UR-MB-159 are more potent than histamine and older H$_2$R agonists in functional studies on human H$_2$ receptors. Thus, they may be tested for patients with end-stage heart failure to sustain contractility under clinical conditions. Alternatively, previous studies demonstrated that stimulation of postsynaptic H$_2$ receptors could be beneficial for the treatment of patients with Alzheimer's disease. If used for the treatment of Alzheimer's disease, the cardiac side effects might be blocked by treating the patients concomitantly with a H$_2$R antagonist that does not pass through the blood-brain barrier.
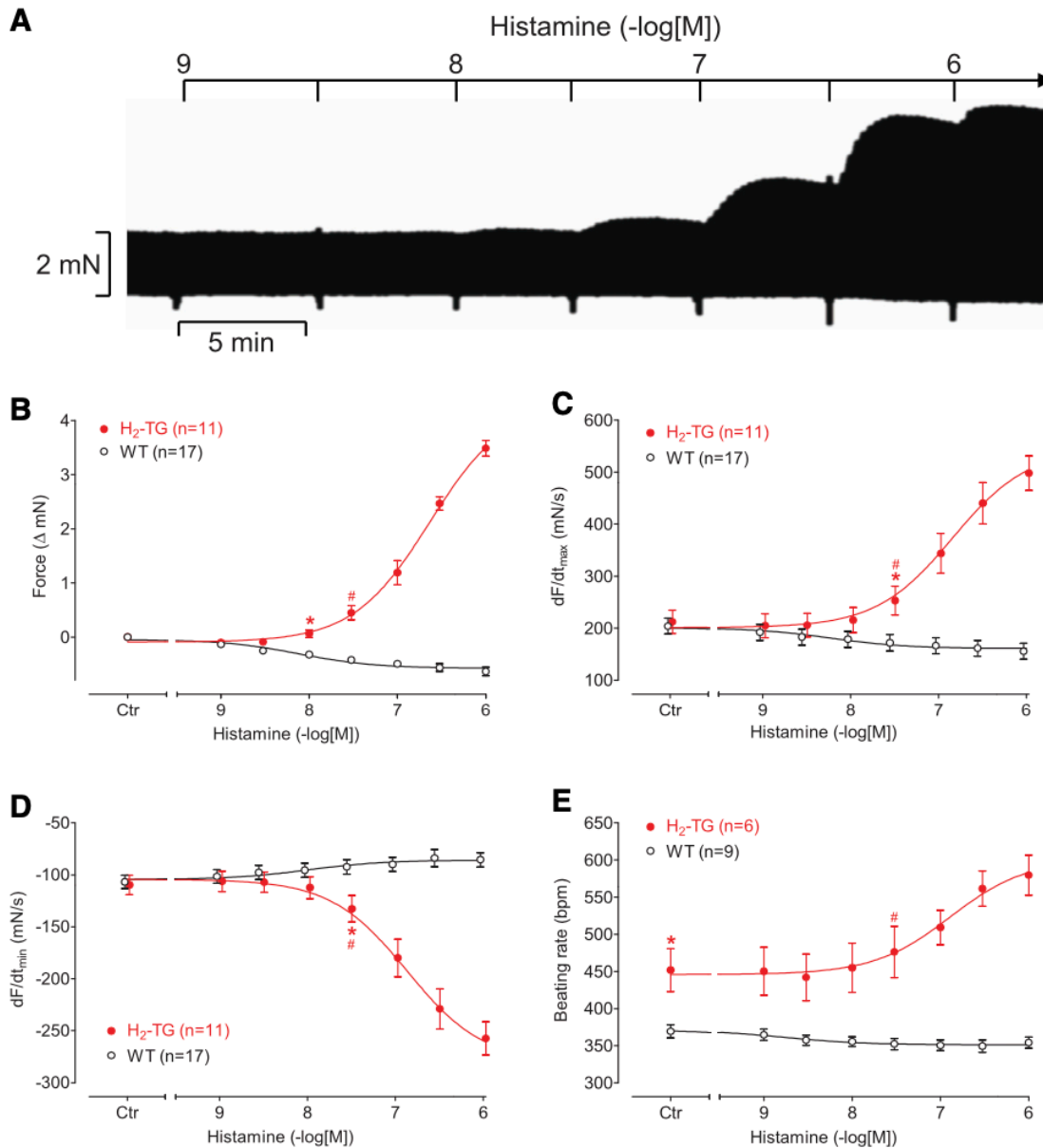
Figure 3.021. Histamine increases contractility in H$_2$-TG but not WT. (**A**) Original recordings of the effect of cumulatively applied histamine on force of contraction in isolated electrically driven (1 Hz) left atrial preparations. Horizontal bar indicates time in minutes; vertical bar indicates developed force in milli-Newtons. (**B**) Effects of histamine in H$_2$-TG and WT left atrium on developed force. (**C**) Effects of histamine in H$_2$-TG and WT left atrium on time to maximum rate of tension development dF/dt in mN/s. (**D**) Effects of histamine in H$_2$-TG and and WT on time to minimum rate of tension development dF/dt in mN/s. (**E**) Effects of histamine in H$_2$-TG and WT in spontaneously beating right atrium on beating rate in beats per minute (bpm). *First $P < 0.05$ versus WT; #first $P < 0.05$ versus Ctr. Abscissae: negative logarithmic concentrations of histamine in moles. Figure was taken from Gergs et al. (2021).[440]
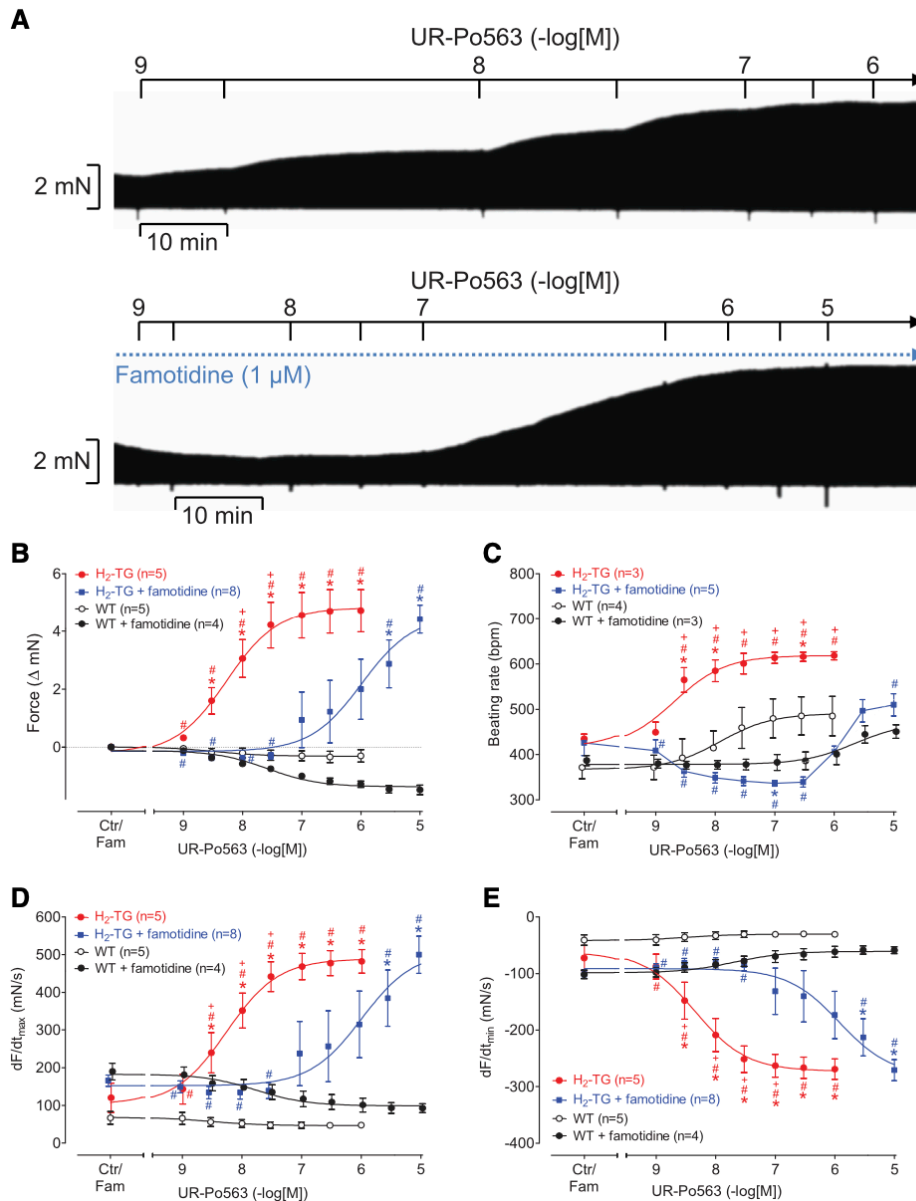
Figure 3.022. Contractile effects of UR-Po563. (**A**) Original recordings of the effect of cumulatively applied UR-Po563 on force of contraction in isolated electrically driven (1 Hz) left atrial preparations. Horizontal bar indicates time in minutes; vertical bar indicates developed force in milli-Newtons. (**B**) Effects of UR-Po563 in H_2-TG and WT left atrium on developed force versus H_2-TG and WT in presence of famotidine. (**C**) Effects of UR-Po563 in H_2-TG and WT in spontaneously beating right atrium on beating rate in beats per minute (bpm) versus H_2-TG and WT in presence of famotidine. (**D**) Effects of UR-Po563 in H_2-TG and WT left atrium on time to maximum rate of tension development dF/dt in mN/s versus H_2-TG and WT in presence of famotidine. (**E**) Effects of UR-Po563 in H_2-TG and WT left atrium on time to minimum rate of tension development dF/dt in mN/s versus H_2-TG and WT in presence of famotidine. Abscissae: negative logarithmic concentrations of UR-Po563 in moles. [#]Significant effects of UR-Po563 compared with predrug values (Ctr./Fam); [*]significant effects of UR-Po563 in H_2-TG compared with WT; [+]significant effects of Po563 in H_2-TG compared with H_2-TG in presence of famotidine. Figure was taken from Gergs et al. (2021).[440]
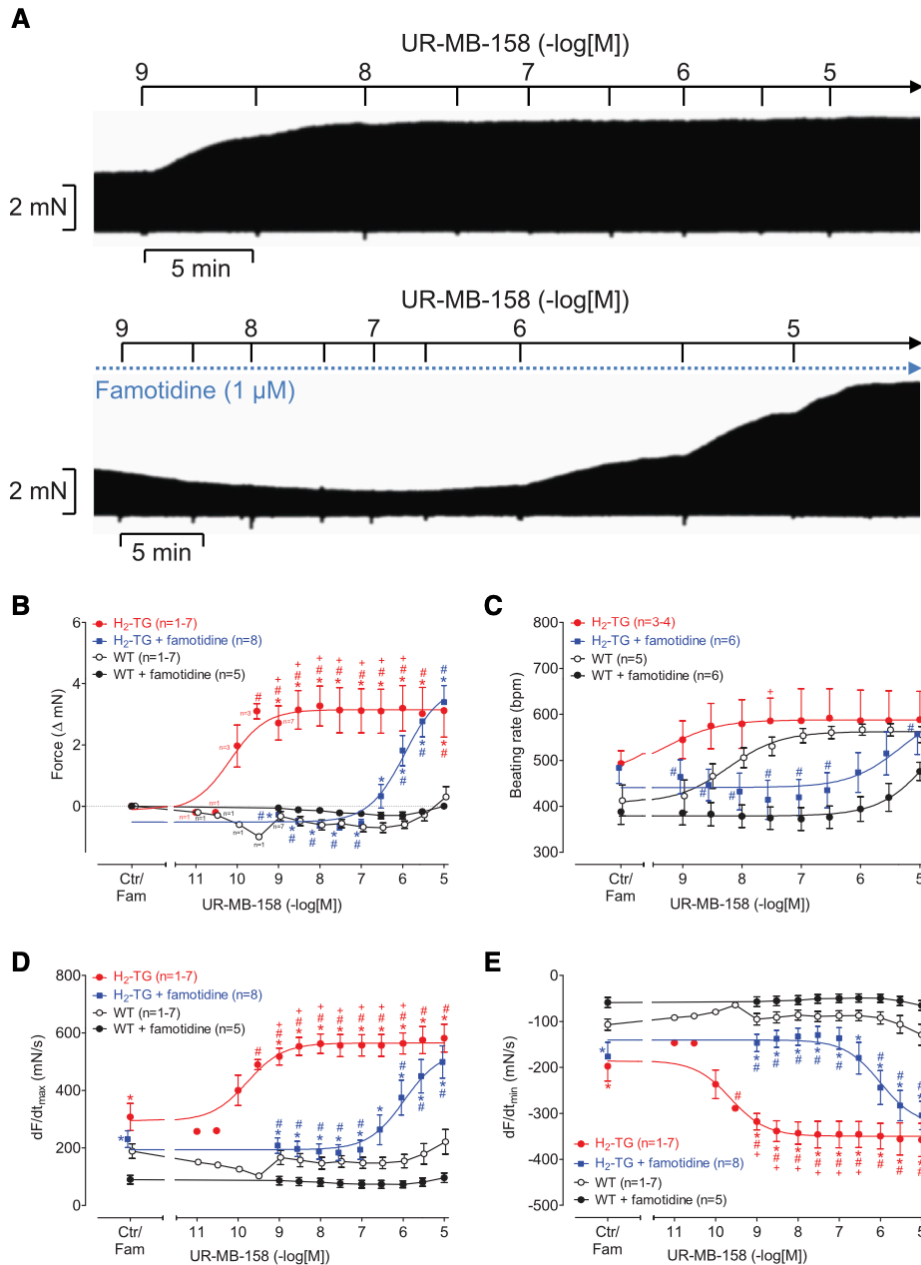
Figure 3.023. Contractile effects of UR-MB-158. (**A**) Original recordings of the effect of cumulatively applied UR-MB-158 on force of contraction in isolated electrically driven (1 Hz) left atrial preparations. Horizontal bar indicates time in minutes; vertical bar indicates developed force in milli-Newtons. (**B**) Effects of UR-MB-158 in H$_2$-TG and WT left atrium on developed force versus H$_2$-TG and WT in presence of famotidine. (**C**) Effects of UR-MB-158 in H$_2$-TG and WT in spontaneously beating right atrium on beating rate in beats per minute (bpm) versus H$_2$-TG and WT in presence of famotidine. (**D**) Effects of UR-MB-158 in H$_2$-TG and WT left atrium on time to maximum rate of tension development dF/dt in mN/s versus H$_2$-TG and WT in presence of famotidine. (**E**) Effects of UR-MB-158 in H$_2$-TG and WT left atrium on time to minimum rate of tension development dF/dt in mN/s versus H$_2$-TG and WT in presence of famotidine. Abscissae: negative logarithmic concentrations of UR-MB-158 in moles. [#]Significant effects of UR-MB-158 compared with predrug values (Ctr.); [*]significant effects of UR-MB-158 in H$_2$-TG compared with WT; [+]significant effects of UR-MB-158 in H$_2$-TG compared with H$_2$-TG in presence of famotidine. Figure was taken from Gergs et al. (2021).[440]
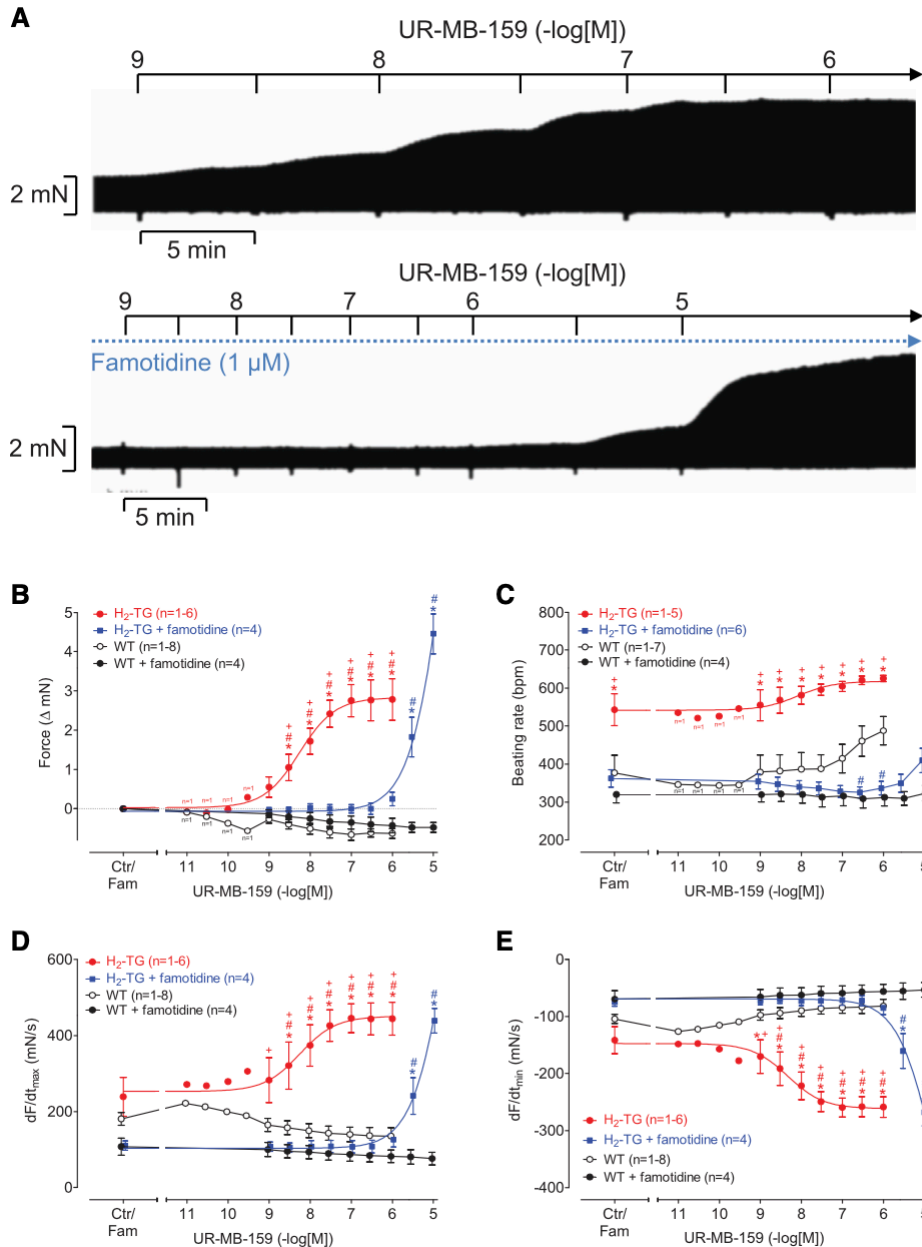
Figure 3.024. Contractile effects of UR-MB-159. (**A**) Original recordings of the effect of cumulatively applied UR-MB-159 on force of contraction in isolated electrically driven (1 Hz) left atrial preparations. Horizontal bar indicates time in minutes; vertical bar indicates developed force in milli-Newtons. (**B**) Effects of UR-MB-159 in H$_2$-TG (n=6) and WT (n=8) left atrium on developed force (ordinate in milli-Newtons) versus H$_2$-TG (n =4) and WT (n =4) in presence of famotidine. (**C**) Effects of UR-MB-159 in H$_2$-TG (n=5) and WT (n=7) in spontaneously beating right atrium on beating rate (ordinate) in beats per minute (bpm) versus H$_2$-TG and WT in presence of famotidine. (**D**) Effects of UR-MB-159 in H$_2$-TG and WT left atrium on time to maximum rate of tension development dF/dt in mN/s versus H$_2$-TG and WT in presence of famotidine. (**E**) Effects of UR-MB-159 in H$_2$-TG and WT left atrium on time to minimum rate of tension development dF/dt in mN/s versus H$_2$-TG and WT in presence of famotidine. Abscissae: negative logarithmic concentrations of UR-MB-159 in moles. #Significant effects of UR-MB-159 compared with predrug values (Ctr.); *significant effects of UR-MB-159 in H$_2$-TG compared with WT; +significant effects of UR-MB-159 in H$_2$-TG compared with H$_2$-TG in presence of famotidine. Figure was taken from Gergs et al. (2021).[440]
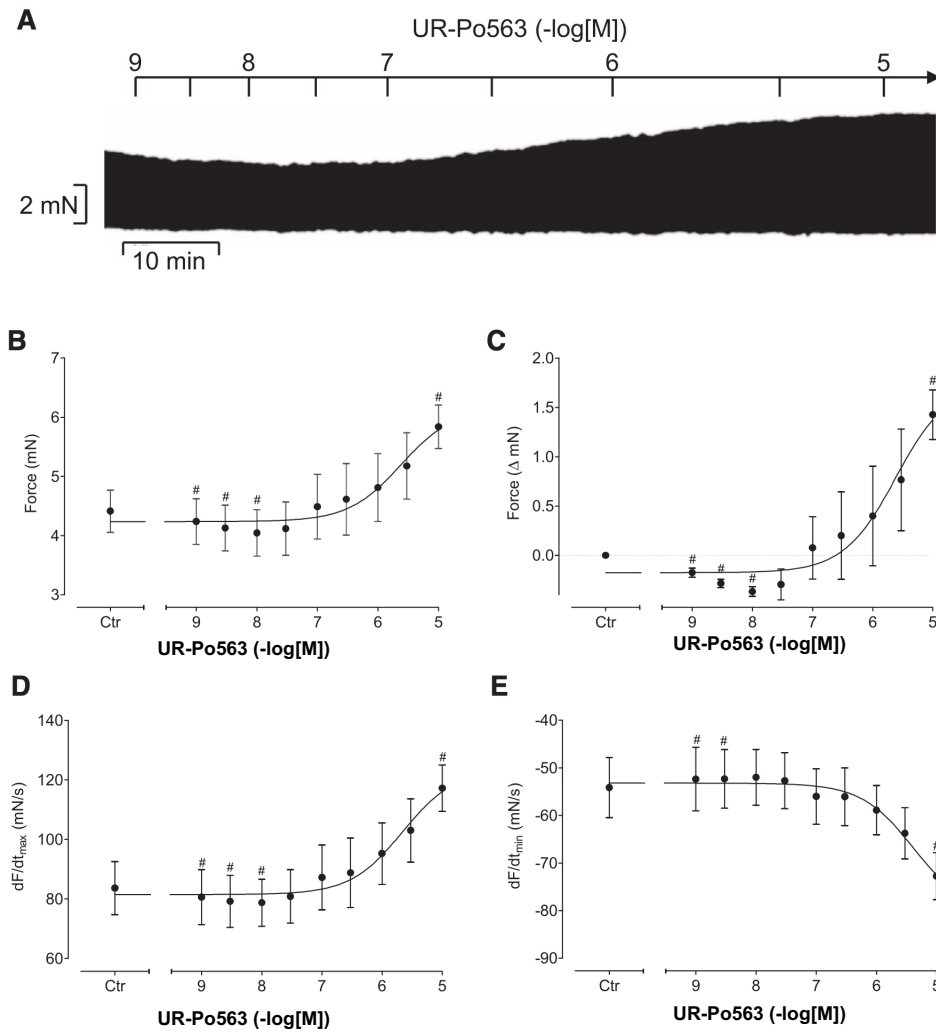
Figure 3.025. Human atrial preparations. (**A**) Original recording of the effect of cumulatively applied UR-Po563 on force of contraction in an isolated electrically driven (1 Hz) human right atrial preparation. Horizontal bar indicates time in minutes; vertical bar indicates developed force in milli-Newtons. (**B**) Effects of UR-Po563 in human right atrial preparations (n=5) on developed force (ordinate in milli-Newtons). (**C**) Effects of UR- Po563 in human right atrial preparations (n=5) on developed force presented as delta milli-Newtons. (**D**) Effects of UR-Po563 in human right atrial preparations (n=5) on the maximum rate of tension development dF/dt in mN/s (ordinate). (**E**) Effects of UR-Po563 in human right atrial preparations (n=5) on the minimum rate of tension development dF/dt in mN/s (ordinate). #$P < 0.05$ versus Ctr. Abscissae: negative logarithmic concentrations of UR-Po563 in moles. Figure was taken from Gergs et al. (2021).[440]

3.4.2.9 Computational Prediction of the Membrane Permeability

The BOILED-egg model[447] (integrated in the SwissADME web tool[129] was used to predict the gastrointestinal (GI) absorption and BBB permeation of compounds **3.139**, **3.157**, **3.239**, **3.255**, **3.262**, and **3.264**. As control, pramipexole (**3.006**), the acylguanidines UR-AK24 (**3.221**)[298,304] and UR-PG126 (**3.222**)[298,304] (cf. Figure 3.026) were used. These molecules were experimentally proven to be GI-absorbable as well as BBB-permeable and share structural similarities with our novel ligands. The outcome of the BOILED-egg model[447] is based on two parameters: log P (according to Wildman and Crippen (WLOGP)[133] and topological polar surface area (tPSA)[448], indicating the lipophilicity and polarity of the respective compound (cf. Table 3.15).

UR-AK24
3.221
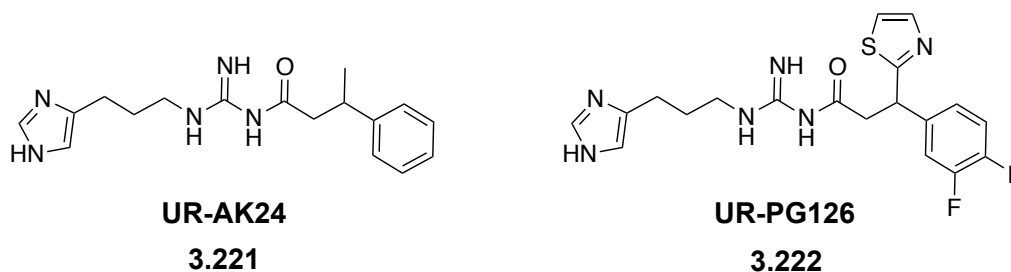
UR-PG126
3.222

Figure 3.026. Chemical structures of the published GI-absorbable and BBB-penetrant acylguanidines UR-AK24 (**3.221**) and UR-PG126 (**3.222**).[298,304]

Table 3.15. Overview of predicted GI absorptions and BBB penetrations of selected compounds based on calculated WLOGP and tPSA values.

	3.006	3.139	3.157	3.221	3.222	3.239	3.255	3.262	3.264
Log P (WLOGP)‡	1.59	1.78	2.79	1.97	3.57	0.86	0.72	0.79	1.88
tPSA/Å	79.2	146.7	144.2	96.2	137.3	159.6	159.6	121.1	157.1
GI absorption*	High	Low	Low	High	Low	Low	Low	High	Low
BBB permeant**	No	No	No	No	No	No	No	No	No

WLOGP was calculated using the atomistic method based on the fragmental system of Wildman and Crippen.[133] Calculated as a sum of fragment-based contributions according to Ertl et al.[448] *According to the white of the BOILED-egg model.[447] **According to the yolk of the BOILED-egg model.[447]

Surprisingly, none of the tested compounds (including the experimentally proven GI-absorbable and BBB-penetrable ones) was predicted to be BBB-penetrable by the BOILED-egg model[447] (cf. Table 3.15 and Figure 3.027). Moreover, good GI absorption was only assumed for **3.262**, the acylguanidine UR-AK24 (**3.221**)[298,304], and pramipexole (**3.006**), while no GI absorption was assumed for the other ligands (cf. Figure 3.027).
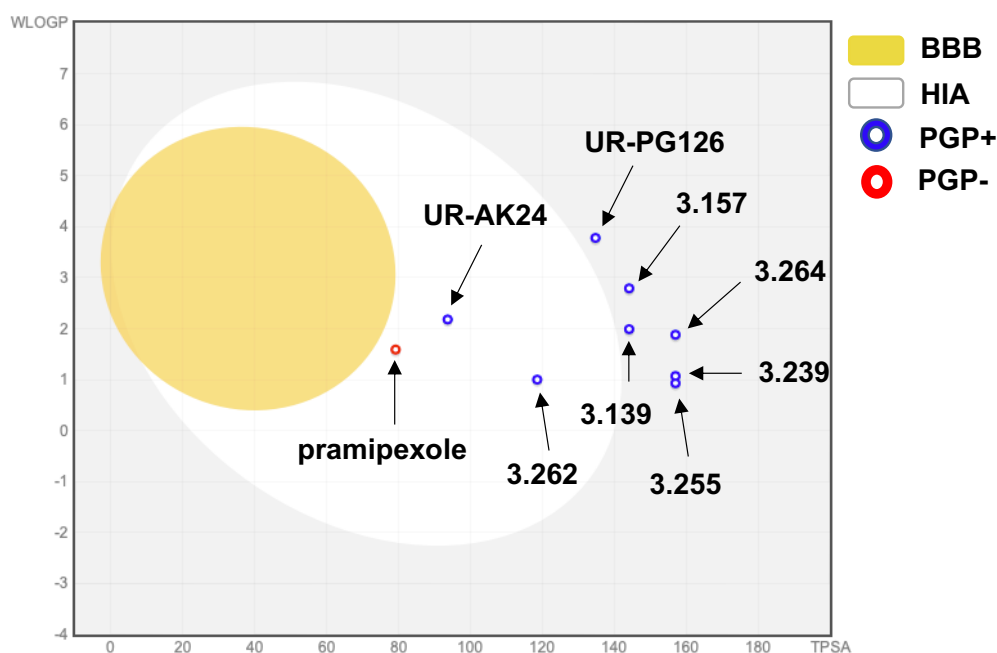
Figure 3.027. Boiled-egg model of 9 screened compounds (pramipexole (**3.006**), **3.139**, **3.157**, UR-AK24 (**3.221**)[298,304], UR-PG126 (**3.222**)[298,304], **3.239**, **3.255**, **3.262**, and **3.264**) obtained by SwissADME software. HIA: human passive intestinal absorption. BBB: blood-brain barrier penetration. PGP+: actively effluxes by P-glycoprotein (Pgp). PGP-: no substrate of P-glycoprotein (Pgp).

Since the GI absorption and the BBB penetration of pramipexole, UR-AK24 (**3.221**), and UR-PG126 (**3.222**) were proven, the Boiled-egg models[447] predictions seem to be inaccurate for this particular class of compounds. However, the model takes only passive transport through GI and BBB into account.[447] Since pramipexole is postulated to penetrate the BBB via active transport[388], the other control compounds, as well as our new ones, might be able to enter the brain via a similar pathway. To elucidate this phenomenon, the *in vivo* pharmacokinetics of the ligands will be examined throughout future research. Specifically, an *in vitro* Coco-2 permeability assay[449–452] and/or *in vivo* studies in laboratory animals could be performed. The obtained data will help to find the appropriate means of application and enable to study the H$_2$ receptors expressed in the CNS.

3.4.3 Conclusion

In summary, the study aimed the development of novel, subtype-selective H$_2$R ligands, which also have a selectivity over dopamine D$_{2long/3}$ receptors. To achieve this, a series of 40 compounds containing a carbamoylguanidine as a key motif, as well as varying heterocycles, spacers, and side residues, was synthesized and characterized. It was observed that the replacement of the thiazole by a thiadiazole ring in N^G-carbamoylated thiazolylpropylguanidines resulted in potent H$_2$R agonists with affinities in the low one-digit nanomolar range. Furthermore, ligands containing this modification possess a significantly increased selectivity for the hH$_2$R over dopamine hD$_{2long/3}$ receptors. Within the synthesized thiadiazole-containing ligand series, compounds **3.239** (UR-KAT505), **3.255** (UR-KAT533), and **3.264** (UR-MB-165) turned out to be the most promising candidates reaching up to 1000-fold selectivity over the other three receptor subtypes (hH$_{1,3,4}$R). **3.239** showed the highest selectivity for hH$_2$R over hD$_{2long}$R (> 2000-fold) and 260-fold selectivity for hH$_2$R over hD$_3$R. **3.255**, on the other hand, showed excellent selectivity for the hH$_2$R over hD$_{2long}$R (>1000-fold) and the highest selectivity for the hH$_2$R over hD$_3$R (> 520-fold). **3.264** demonstrated >1000-fold selectivity for the hH$_2$R over hD$_{2long}$R and 80-fold selectivity for the hH$_2$R over hD$_3$R. Moreover, **3.239** and **3.255** were shown to be selective H$_2$R agonists (> 100-fold) relative to 14 additional peripheral and central GPCRs (including dopaminergic, muscarinic, adrenergic, serotonergic, and opioid receptors). These key characteristics render **3.239** and **3.255** the most affine and selective monomeric carbamoylguanidine-type agonists known so far. The developed H$_2$R ligands might serve as pharmacological tools for further investigations on the physiological and pathophysiological role of the H$_2$R to elucidate the largely unknown function of H$_2$ receptors in the CNS.

3.5 Experimental Part
3.5.1 Chemistry
3.5.1.1 General Experimental Conditions

Chemicals and solvents

Unless otherwise stated, chemicals and solvents were procured from commercial suppliers and used as received. All the solvents were of analytical grade or distilled prior to use. Anhydrous solvents were stored over molecular sieves under protective gas. Deuterated solvents for nuclear magnetic resonance (NMR) spectroscopy were purchased from Deutero (Kastellaun, Germany). For the preparation of buffers and HPLC eluents, Millipore-grade water was used.

Thin layer chromatography

Reactions were monitored by thin layer chromatography (TLC) on silica gel 60 F254 aluminum sheets (Merck), and compounds were detected with UV light at 254 nm and ninhydrin solution (0.8 g ninhydrin, 200 mL *n*-butanol, 6 mL acetic acid).

Melting points

Melting points were determined with a B-540 apparatus (BÜCHI, Essen, Germany).

NMR spectra

NMR spectra (^{1}H NMR and ^{13}C NMR, ^{19}F NMR, DEPT, 2D NMR) were recorded on a Bruker Avance-300 (7.05 T, ^{1}H: 300 MHz, ^{13}C: 75.5 MHz, ^{19}F: 188), Avance-400 (9.40 T, ^{1}H: 400 MHz, ^{13}C: 100.6 MHz, ^{19}F: 282), or Avance-600 (14.1 T; ^{1}H: 600 MHz, ^{13}C: 150.9 MHz; cryogenic probe) NMR spectrometer (Bruker, Karlsruhe, Germany). Multiplicities are specified with the following abbreviations: s (singlet), d (doublet), t (triplet), q (quartet), p (pentet), m (multiplet), br (broad), as well as combinations thereof.

High-resolution mass spectrometry

High-resolution mass spectrometry (HRMS) was performed on an AccuTOF GCX GC/MS system (Jeol, Peabody, MA, USA) using an EI source or a Q-TOF 6540 UHD LC or GC/MS system (Agilent Technologies, Santa Clara, USA) using an ESI (in case of LC coupling) or an APCI (in case of GC coupling) source.

Polarimetry

Optical rotations at 589 nm (Na D line) were measured on a polarimeter P8000-T equipped with an electronic Peltier thermostat PT31 (A. KRÜSS Optronic, Hamburg, Germany) using a thermostated (20 °C) microcuvette (layer thickness of 1 dm, volume of 0.9 mL) and methanol (MeOH) as solvent.

Column chromatography

For column chromatography, silica gel 60 (0.04-0.063 mm, Merck, Darmstadt, Germany) was used.

Flash chromatography

Flash chromatography was performed on an Intelli Flash-310 workstation from Varian Deutschland GmbH (Darmstadt, Germany) with SuperFlash (SF) columns (Si50, 4-40 g) from Agilent Technologies (Santa Clara, CA, USA).

Preparative HPLC

Preparative HPLC was performed with a system from Knauer (Berlin, Germany) consisting of two K-1800 pumps and a K-2001 detector or with a Prep 150 LC system from Waters (Eschborn, Germany) consisting of a 2545 binary gradient module, a 2489 UV/visible detector and a fraction collector III. The following columns were used: Nucleodur 100-5 C18 (5 µm, 250 x 21 mm, Macherey-Nagel, Düren, Germany), a Kinetex XB-C18 100A (5 µm, 250 x 21.2 mm, Phenomenex, Aschaffenburg, Germany), an Interchim PuriFlash PF15 C18 HQ (15 µm, 120 g, Interchim, Montluçon, France) and a Gemini-NX C18 (5 µm, 250 mm x 21 mm; Phenomenex). Solvent flow rates of either 15-20 mL/min (Nucleodur, Kinetex, and Gemini columns) or 30 mL/min (Interchim column) at rt were employed. A detection wavelength of 220 nm and mixtures of acetonitrile (MeCN) and 0.05-0.1% aqueous TFA were used as mobile phases. MeCN was removed from the eluates under reduced pressure prior to freeze-drying (Christ Alpha 2-4 LD freeze dryer (Martin Christ, Osterode am Harz, Germany) or ScanVac CoolSafe 4-15L freeze dryer from Labogene (LMS, Brigachtal, Germany), both equipped with a RZ 6 rotary vane vacuum pump (Vacuubrand, Wertheim, Germany)).

Analytical HPLC

Analytical HPLC analysis was performed on a system from Merck Hitachi, composed of a D-6000 interface, a L-6200A pump, an AS2000A autosampler, and a L-4000 UV-VIS detector or with a 1100 HPLC system from Agilent technologies, equipped with an Instant Pilot controller, a G1312A binary pump, a G1329A ALS autosampler, a G1379A vacuum degasser, a G1316A column compartment, and a G1315B DAD detector. A Kinetex XB-C18 100A (5 µm, 250 x 4.6 mm (Phenomenex)) served as the column: t_0 = 2.90 min (Merck Hitachi, flow: 0.8 mL/min), t_0 = 3.16 min (Merck Hitachi, flow: 0.8 mL/min, different Kinetex XB-C18 100A column), t_0 = 2.85 min (Merck Hitachi, flow: 1.0 mL/min, different Kinetex XB-C18 100A column), t_0 = 3.21 min (Agilent, flow: 0.8 mL/min) or t_0 = 2.67 min (Agilent, flow: 1.0 mL/min). As the mobile phase, mixtures of MeCN (with (A) or without (B) 0.05% TFA) and 0.05% aqueous TFA (C) were used. The following linear gradients were applied. Compounds **3.179**-**3.180** and **3.182**-**3.186** (Merck Hitachi, t_0 = 2.90 min): 0-30 min: A/C 5:95-80:20; 30-32 min: 80:20-95:5; 32-42 min: 95:5; flow rate: 0.8 mL/min. Compounds **3.138**, **3.140**-**143**, **3.161**, **3.163**, **3.166**-**3.171**, and **3.181** (Merck Hitachi, t_0 = 2.90 min): 0-30 min: A/C 10:90-80:20; 30-32 min: 80:20-95:5; 32-42 min: 95:5; flow rate: 0.8 mL/min. Compounds **3.144**-**146**, **3.162**, **3.164**-**3.165**, and **3.173**-**3.178** (Merck Hitachi, t_0 = 3.16 min): 0-25 min: B/C 20:80-80:20; 25-26 min: 80:20-95:5; 26-35 min: 95:5; flow rate: 0.8 mL/min. Compounds **3.149** (Merck Hitachi, t_0 = 2.85 min): 0-25 min: B/C 5:95-95:5; 25-35 min: 95:5; flow rate: 1.0 mL/min. Compounds **3.139**, **3.172**, **3.238**-**3.259**, and **3.265**-**3.278** (Agilent, t_0 = 3.21 min): 0-30 min: B/C 10:90-90:10; 30-33 min: 90:10-95:5; 33-40 min: 95:5; flow rate: 0.8 mL/min. Compounds **3.147**-**3.148**, **3.150**-**3.160**, and **3.260**-**3.264** (Agilent, t_0 = 2.67 min): 0-25 min: B/C 10:90-95:5; 25-35 min: 95:5; flow rate: 1.0 mL/min. For analytical HPLC runs on the 1100 HPLC system from Agilent Technologies the oven temperature was set to 30 °C. At the HPLC system from Merck Hitachi room temperature was used. The injection volume was 5-100 µL, and detection was performed at 220 nm. Compound concentrations were between 0.1-1 mM. Compounds purities were calculated as the percentage peak area of the analyzed compound by UV detection at 220 nm.

3.5.1.2 Compound Characterization

Compounds **3.139**-**3.186** and **3.238**-**3.278** were characterized using the following methods: HRMS, ^{1}H NMR spectroscopy, ^{13}C NMR spectroscopy, and 2D NMR (COSY, HSQC, HMBC) spectroscopy (see chapter **3.6.1**, Figures 3.040-3.143). The purities of the target compounds **3.139**-**3.186** and **3.238**-**3.278** used for pharmacological investigation were ≥ 95% (chromatograms are shown in chapter **3.6.12**, Figures 3.144-3.188). For biological testing, the target compounds (TFA or HCl salts) were dissolved in DMSO, DMSO/H_2O 1:1 (v/v), or DMSO/20 mM aq HCl 1:1 (v/v) to get a final concentration of 10 mM.

3.5.1.3 Synthesis and Analytical Data of the Building Blocks 3.009b, 3.011 and 3.012
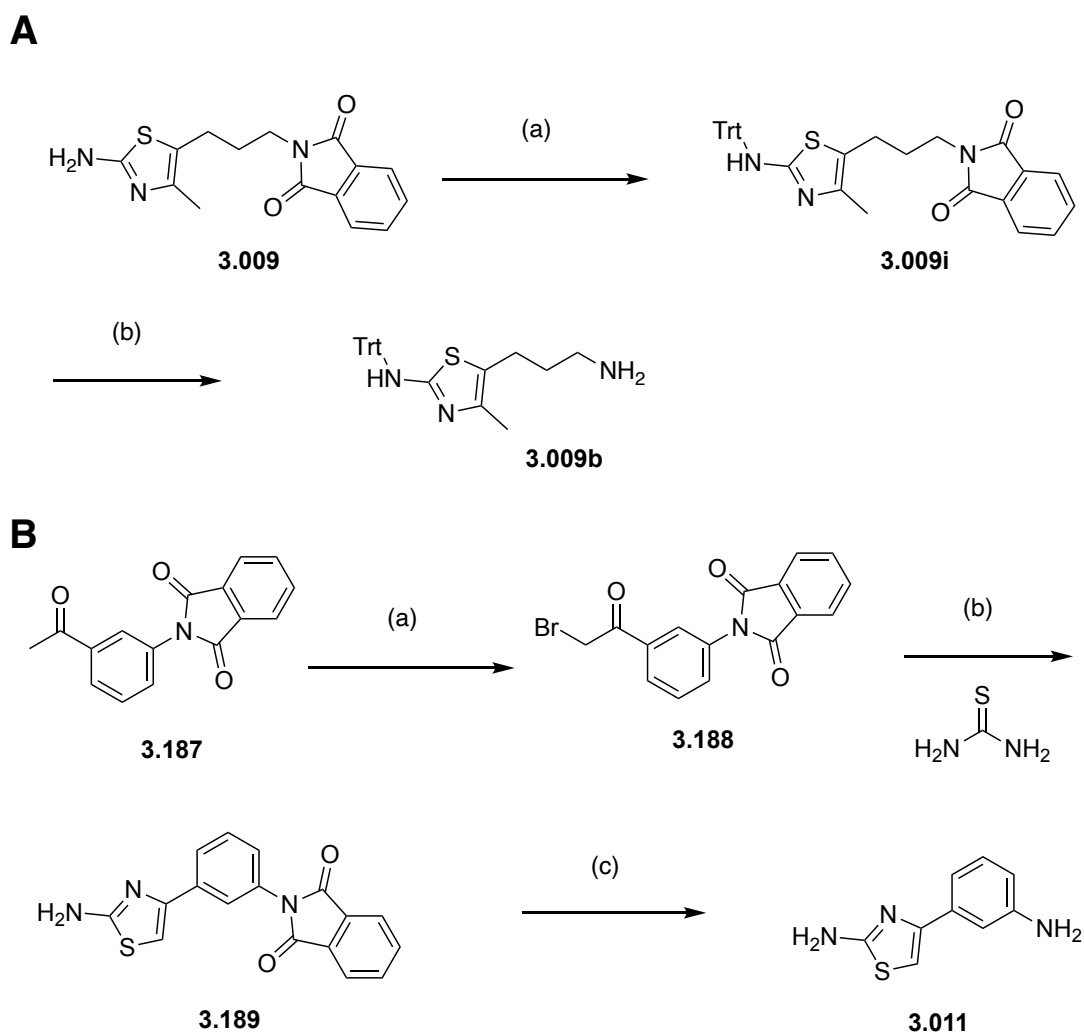
Scheme 3.04. Synthesis of the building blocks **3.009b** and **3.011**. Reagents and conditions: **A**: (a) trityl chloride, NEt$_3$, MeCN, 16 h, rt; (b) hydrazine monohydrate, *n*-butanol, 16 h, rt. **B**: (a) Br$_2$, HBr in acetic acid (HOAc), CHCl$_3$, 1 h, rt; (b) thiourea, MeCN/EtOH, 3 h, reflux; (c) HCl/HOAc (1/1), overnight, reflux.

2-(3-(4-Methyl-2-(tritylamino)thiazol-5-yl)propyl)isoindoline-1,3-dione (3.009i)

(Synthesized by Katharina Tropmann)

3.009 (2 g, 6.64 mmol), which was prepared as previously described,[302,415] was dissolved in MeCN (120 mL), and trityl chloride (2.22 g, 7.97 mol) and NEt$_3$ (1.66 mL, 11.95 mmol) were added. The mixture was stirred for 16 h at rt. The solvent was removed under reduced pressure and the crude product was purified by flash chromatography on silica gel (EtOAc/PE 0/100 - 2/3 in 20 min, R$_f$ = 0.62 in EtOAc/PE 1/1) to obtain **3.009i** as a yellow foam (1.73 mg, 48%). ^{1}H NMR (300 MHz, CDCl$_3$) δ (ppm) 7.86 – 7.79 (m, 2H), 7.74 – 7.67 (m, 2H), 7.36 – 7.22 (m, 15H), 3.58 (t, *J* = 7.3 Hz, 2H), 2.50 – 2.41 (m, 2H), 2.07 (s, 3H), 1.77 – 1.66 (m, 2H). ^{13}C NMR (75 MHz, CDCl$_3$) δ (ppm) 168.27, 165.03, 143.75, 133.97, 132.08, 129.23, 128.12, 127.38, 123.24, 119.96, 71.79, 37.48, 30.30, 23.77, 14.41. HRMS (ESI-MS): *m/z* [M+H$^+$] calculated for C$_{34}$H$_{30}$N$_3$O$_2$S$^+$: 544.2053, found 544.2082; C$_{34}$H$_{29}$N$_3$O$_2$S (543.69).

5-(3-Aminopropyl)-4-methyl-*N*-tritylthiazol-2-amine (3.009b) *(Synthesized by Katharina Tropmann)*

A solution of **3.009i** (1.73 g, 3.18 mmol) in *n*-butanol and hydrazine monohydrate (772 μL, 15.91 mmol) was stirred at rt for 16 h. After cooling to 0 °C by using an ice-bath, the reaction mixture was filtered and evaporated to dryness to afford the crude product as a yellow oil. The crude product was purified by flash chromatography (DCM/MeOH 100/0 - 90/10 in 20 min, R$_f$ = 0.31 in DCM/MeOH 9/1), yielding **3.009b** as a yellow solid (900 mg, 68%). ^{1}H NMR (300 MHz, CD$_3$OD) δ (ppm) 7.36 – 7.16 (m, 15H), 2.69 (t, *J* = 7.6 Hz, 2H), 2.50 – 2.36 (m, 2H), 2.00 (s, 3H), 1.67 – 1.55 (m, 2H). ^{13}C NMR (75 MHz, CD$_3$OD) δ (ppm) 14.26, 23.87, 31.97, 40.47, 73.03, 120.82, 128.38, 129.04, 130.34, 142.44, 145.22, 161.18. HRMS (ESI-MS): *m/z* [M+H$^+$] calculated for C$_{26}$H$_{28}$N$_3$S$^+$: 414.1998, found 414.1995; C$_{26}$H$_{27}$N$_3$S (413.58).

2-Amino-4-(3-phthalimidophenyl)thiazole (3.189) *(Synthesized by Sabrina Biselli)*

The title compound was prepared in analogy to the previously described procedure described.[453] To a solution of **3.187** (2.00 g, 7.54 mmol) in CHCl$_3$ (20 mL) HBr solution in acetic acid (45 % w/v, 1 mL) was added under stirring. Bromine (1.20 g, 7.54 mmol) in CHCl$_3$ (10 mL) was added dropwise. The reaction mixture was stirred for 1 h at rt. Removal of the solvent in vacuo afforded **3.188** as a white solid, which was applied to

the next step without further purification. Crude **3.188** was dissolved in MeCN (30 mL) at 50°C and poured into a warm solution of thiourea (574 mg, 7.54 mmol) in ethanol (EtOH, 30 mL). The reaction mixture was stirred under reflux for 3 h. Removal of the solvent in vacuo afforded a beige solid, which was recrystallized in EtOAc (100 mL) and filtered through a Buchner funnel. **3.189** was afforded as a white solid (2.35 g, 78%, R_f = 0.70 in DCM/1.75 N NH$_3$ in MeOH 9/1), mp: 269-279°C. ^{1}H-NMR (400 MHz, DMSO-d$_6$, hydrobromide): δ (ppm) 8.94 (br s, 3H), 8.01 – 7.98 (m, 2H), 7.96 – 7.93 (m, 2H), 7.85 – 7.81 (m, 2H), 7.66 (t, *J* = 7.9 Hz, 1H), 7.54 – 7.51 (m, 1H), 7.26 (s, 1H). ^{13}C-NMR (100 MHz, DMSO-d$_6$, hydrobromide): δ (ppm) 170.60, 167.30, 139.70, 135.40, 133.00, 131.90, 130.60, 130.10, 128.70, 125.90, 125.30, 124.00, 104.30. HRMS (ESI-MS): *m/z* [M+H$^+$] calculated for C$_{17}$H$_{12}$N$_3$O$_2$S$^+$: 322.0645, found 322.0650; C$_{17}$H$_{11}$N$_3$O$_2$S x HBr (402.26).

2-Amino-4-(3-aminophenyl)thiazole (3.011)[454] *(Synthesized by Sabrina Biselli)*
3.189 (1.69 g, 4.20 mmol) was suspended in a mixture of concentrated hydrochloric acid (30 mL) and acetic acid (30 mL) and the reaction mixture was stirred under reflux overnight. The solvent was removed under reduced pressure and the residue was suspended in an aqueous NaOH solution (0.03 M, 30 mL). The resulting precipitate (by-product: phthalic acid) was filtered through a Buchner funnel and washed with H$_2$O (20 mL). Aqueous layers were combined and part of the solvent was removed under reduced pressure. Aqueous NH$_3$ solution (25%, 5 mL) was added and the resulting precipitate was filtered off. The solid was washed with H$_2$O (40 mL) and the residual solvent was removed under reduced pressure. **3.011** was afforded as a yellow solid (560 mg, 60%, R_f = 0.6 in DCM/1.75 N NH$_3$ in MeOH 9/1), mp: 177-178 °C. ^{1}H NMR (300 MHz, DMSO-d$_6$): δ (ppm) 7.03 – 6.91 (m, 5H), 6.77 (s, 1H), 6.43 – 6.47 (m, 1H), 5.05 (br s, 2H). ^{13}C NMR (100 MHz, DMSO-d$_6$): δ (ppm) 168.30, 151.20, 149.10, 136.00, 129.30, 114.00, 113.50, 111.90, 101.10. HRMS (ESI-MS): *m/z* [M+H$^+$] calculated for C$_9$H$_{10}$N$_3$S$^+$: 192.0590, found 192.0590; C$_9$H$_9$N$_3$S (191.25).
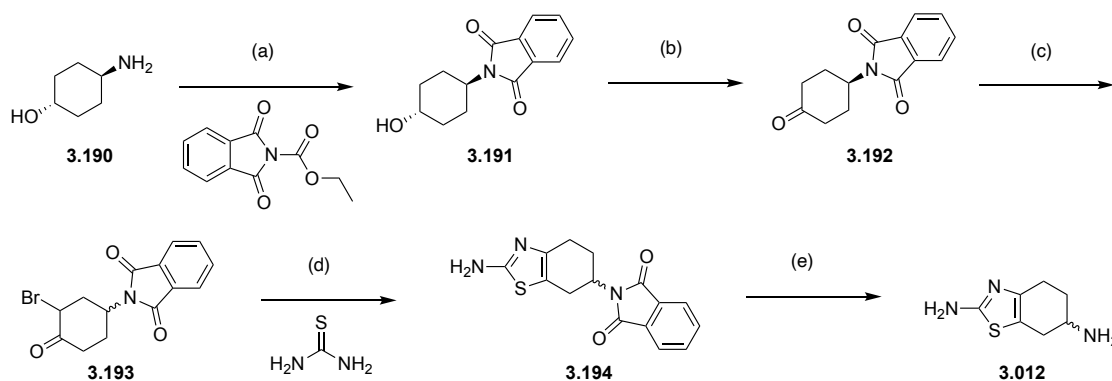
Scheme 3.05. Synthesis of the building block **3.012**. Reagents and conditions: (a) *N*-(ethoxycarbonyl)phthalimide, K$_2$CO$_3$, H$_2$O, 30 min, rt; (b) PCC, DCM, 3.5 h, rt; (c) Br$_2$, dioxane/DCM, 1.5 h, rt. (d) thiourea, DMF, 2 h, 100°C; (e) HCl/HOAc (1/1), overnight, reflux.

2-((1*R*, 4*R*)-4-Hydroxycyclohexyl)isoindoline-1,3-dione (3.191)[455] *(Synthesized by Sabrina Biselli)*

K$_2$CO$_3$ (10.50 g, 75.97 mmol) was added to a solution of **3.190** (5.00 g, 43.41 mmol) in H$_2$O (50 mL). *N*-(ethoxycarbonyl)phthalimide (10.24 g, 49.92 mmol) was added under stirring and the reaction mixture was stirred for 30 min at room temperature. The resulting precipitate was filtered off and washed with H$_2$O (50 mL). Removal of the residual solvent in vacuo afforded the product as a beige solid (10.43 g, 98%, R$_f$ = 0.2 in EtOAc/PE 1/3), mp: 183-185 °C (Lit.[455] mp: 177-178 °C). ^{1}H NMR (400 MHz, DMSO-d$_6$): δ (ppm) 7.85 – 7.80 (m, 4H), 4.64 (d, *J* = 4.3 Hz, 1H), 3.99 – 3.91 (m, 1H), 3.49 – 3.41 (m, 1H), 2.19 – 2.08 (m, 2H), 1.93 – 1.90 (m, 2H), 1.69 – 1.66 (m, 2H), 1.32 – 1.21 (m, 2H). ^{13}C NMR (100 MHz, DMSO-d$_6$): δ (ppm) 168.30, 134.80, 131.90, 123.40, 68.50, 49.90, 35.10, 27.80. HRMS (ESI-MS): *m/z* [M+H$^+$] calculated for C$_{14}$H$_{16}$NO$_3$$^+$: 246.1125, found 246.1126; C$_{14}$H$_{15}$NO$_3$ (245.28).

2-(4-Oxocyclohexyl)isoindoline-1,3-dione (3.192)[455] *(Synthesized by Sabrina Biselli)*

3.191 (2.60 g, 10.61 mmol) was dissolved in anhydrous DCM (70 mL). Under Ar-atmosphere two spoons of Celite were added followed by pyridinium chlorochromate (PCC, 5.58 g, 25.88 mmol). The reaction mixture was stirred for 3.5 h at room temperature. 2-Propanol (2 mL) was added and after stirring for additional 30 min the solvent was removed under reduced pressure. The residue was purified by automated flash chromatography with EtOAc. Removal of the solvent afforded the product as light beige solid (1.82 g, 71%, R$_f$ = 0.4 in EtOAc/PE 1/1), mp: 144-145 °C. ^{1}H NMR (300 MHz, CDCl$_3$): δ (ppm) 7.87 – 7.80 (m, 2H), 7.75 – 7.69 (m, 2H), 4.68 – 4.57 (m, 1H),

2.79 – 2.65 (m, 2H), 2.54 – 2.48 (m, 4H), 2.10 – 2.02 (m, 2H). ^{13}C NMR (75 MHz, CDCl$_3$): δ (ppm) 209.00, 168.10, 134.10, 131.80, 123.30, 48.30, 39.90, 28.60. HRMS (ESI-MS): *m/z* [M+H$^+$] calculated for C$_{14}$H$_{14}$NO$_3^+$: 244.0968, found 244.0973; C$_{14}$H$_{13}$NO$_3$ (243.26).

2-(2-Amino-4,5,6,7-tetrahydrobenzo[*d*]thiazol-6-yl)isoindoline-1,3-dione

(3.194)[456,457] *(Synthesized by Sabrina Biselli)*

3.192 (1.93 g, 7.93 mmol) was dissolved in a mixture of dioxane (22 mL) and DCM (14 mL). Bromine (1.40 g, 8.73 mmol) dissolved in DCM (24 mL) was added dropwise and the reaction mixture was stirred for 1.5 h at room temperature. The solvent was removed under reduced pressure and the residue (crude **3.193**) was dissolved in DMF (60 mL). After the addition of thiourea (0.60 g, 7.93 mmol) the reaction mixture was stirred for 2 h at 100 °C. The solvent was removed under reduced pressure and the residue was suspended in EtOAc (50 mL). The precipitate was filtered off and the residual solvent was removed in vacuo to afford the product as a beige solid (2.77 g, 92%, R$_f$ = 0.90 in DCM/1.75 N NH$_3$ in MeOH 9/1, mp: > 300 °C decomposition (Lit.[6] mp: 244-246 °C decomposition). ^{1}H NMR (400 MHz, DMSO-d$_6$): δ (ppm) 7.90 – 7.84 (m, 4H), 4.49 – 4.41 (m, 1H), 3.36 – 3.11 (m, 1H), 2.93 – 2.88 (m, 1H), 2.77 – 2.60 (m, 3H), 2.05 – 1.99 (m, 1H). HRMS (ESI-MS): *m/z* [M+H$^+$] calculated for C$_{15}$H$_{14}$N$_3$O$_2$S$^+$: 300.0801, found 300.0817; C$_{15}$H$_{13}$N$_3$O$_2$S (299.35).

4,5,6,7-Tetrahydrobenzo[*d*]thiazole-2,6-diamine (3.012)[456] *(Synthesized by Sabrina Biselli)*

3.194 (200 mg, 0.53 mmol) was suspended in a mixture of hydrochloric acid (37%, w/v, 5 mL) and acetic acid (5 mL). The reaction mixture was stirred overnight at 100 °C. The solvent was removed under reduced pressure and the residue was dissolved in H$_2$O (5 mL). The pH value was adjusted to 6 by the addition of NaOH solution (1 M, 2 mL). The aqueous layer was washed three times with DCM in order to remove by-products. Then additional NaOH solution (5 mL) was added until a pH value of 9 was reached. The aqueous layer was extracted with DCM (10 mL) and six times with EtOAc (10 mL). In order to extract the remaining product from the aqueous layer, NaCl was dissolved in the mixture and the layer was again extracted three times with EtOAc (10 mL). Water was partly removed under reduced pressure and the aqueous layer was again extracted five times with EtOAc (100 mL). All organic layers were combined

and dried over Na$_2$SO$_4$. Removal of the solvent in vacuo afforded the product as a yellow hygroscopic solid (65 mg, 73%, R$_f$ = 0.13 in DCM/1.75 N NH$_3$ in MeOH 9/1). ^{1}H NMR (300 MHz, DMSO-d$_6$): δ (ppm) 6.60 (br s, 2H), 3.03 – 2.94 (m, 1H), 2.67 – 2.60 (m, 1H), 2.41 – 2.31 (m, 2H), 2.21 – 2.13 (m, 1H), 1.82 – 1.78 (m, 1H), 1.53 – 1.40 (m, 1H). HRMS (ESI-MS): *m/z* [M+H$^+$] calculated for C$_7$H$_{12}$N$_3$S$^+$: 170.0746, found 170.0747; C$_7$H$_{11}$N$_3$S (169.25).

3.5.1.4 Synthesis and Analytical Data of the Amines 3.017, 3.019, 3.024-3.027, and 3.029-3.030 via Oximes 3.203-3.210

No.	R^1	R^2	R
3.195, 3.203	CF$_3$	phenyl	
3.196, 3.204	i-propyl	phenyl	
3.197, 3.205	CH$_3$	4-methoxyphenyl	
3.198, 3.206	CH$_3$	4-trifluoromethoxyphenyl	
3.199, 3.207	CH$_3$	2-fluorophenyl	
3.200, 3.208	CH$_3$	3-fluorophenyl	
3.201, 3.309	CH$_3$	furan-2-yl	
3.202, 3.210	CH$_3$	thiophen-2-yl	

Scheme 3.06. Synthesis of the amines **3.017**, **3.019**, **3.024**-**3.027**, and **3.029**-**3.030**. Reagents and conditions: (a) hydroxylamine hydrochloride, Na$_2$CO$_3$, EtOH, overnight, 70 °C; (b) Zn, CuSO$_4$, EtOH → 3 N HCl, 3 h, rt.

General procedure for the synthesis of the oximes 3.203-3.210[458]

To a mixture of the pertinent ketone (**3.195**-**3.202**, 1 eq), hydroxylammonium chloride (2 eq), and Na$_2$CO$_3$ (5 eq), ethanol (EtOH, 100 mL) was added. The resulting suspension was stirred at 70 °C overnight, cooled to rt, and evaporated under reduced pressure. Extraction of the residue with dichloromethane (DCM) gave the pure oxime after evaporation of the organic solvent.

2,2,2-Trifluoro-1-phenylethan-1-one oxime (3.203)

The title compound was synthesized from 2,2,2-trifluoroacetophenone (**3.195**, 2.02 mL, 14.36 mmol), hydroxylammonium chloride (2.00 g, 28.71 mmol), and Na$_2$CO$_3$ (7.61 g, 71.79 mmol) in EtOH according to the general procedure (R$_f$ = 0.50 in EtOAc/PE 1/9) yielding a mixture of the E- and Z-isomers as colorless solid (2.45 g, 90%). ^{1}H NMR (400 MHz, CDCl$_3$) δ (ppm) 8.92 (s, 1H), 7.34 – 7.15 (m, 5H). ^{13}C NMR (101 MHz, CDCl$_3$) δ (ppm) 148.54 – 147.65 (m), 130.84, 130.58, 128.73 (d, *J* = 2.3 Hz), 128.47, 119.57 (ddd, *J* = 229.8, 222.1, 52.9 Hz). HRMS (EI-MS): *m/z* [M$^{•+}$] calculated for C$_8$H$_6$F$_3$NO$^{•+}$: 189.03960, found 189.03954 and 189.03964; C$_8$H$_6$F$_3$NO (189.14).

2-Methyl-1-phenylpropan-1-one oxime (3.204)

The title compound was synthesized from isobutyrophenone (**3.196**, 2.23 mL, 14.84 mmol), hydroxylammonium chloride (2.06 g, 29.69 mmol), and Na$_2$CO$_3$ (7.86 g, 74.16 mmol) in EtOH according to the general procedure (R$_f$ = 0.85 in EtOAc/PE 1/2) yielding a mixture of the E- and Z-isomers as a colorless oil (2.05 g, 85%). ^{1}H NMR (300 MHz, CDCl$_3$, isomer 1) δ (ppm) 9.73 (s, 1H), δ 7.50 – 7.28 (m, 5H), 2.95 – 2.79 (m, 1H), 1.16 (d, *J* = 6.8 Hz, 6H) and ^{1}H NMR (300 MHz, CDCl$_3$, isomer 2) δ (ppm) 9.73 (s, 1H), δ 7.50 – 7.28 (m, 5H), 3.76 – 3.48 (m, 1H), 1.24 (d, *J* = 7.1 Hz, 6H). ^{13}C NMR (75 MHz, CDCl$_3$, both isomers) δ (ppm) 164.88, 163.26, 135.81, 133.77, 128.55, 128.50, 128.21, 128.18, 127.77, 127.59, 34.57, 27.73, 20.17, 19.44. HRMS (EI-MS): *m/z* [M$^{•+}$] calculated for C$_{10}$H$_{13}$NO$^{•+}$: 163.09917, found 163.09885 and 163.09868; C$_{10}$H$_{13}$NO (163.22).

1-(4-Methoxyphenyl)ethan-1-one oxime (3.205)

The title compound was synthesized from 4-methoxyacetophenone (**3.197**, 3.00 g, 19.98 mmol), hydroxylammonium chloride (2.78 g, 39.96 mmol), and Na$_2$CO$_3$ (10.60 g, 99.88 mmol) in EtOH according to the general procedure (R$_f$ = 0.71 in EtOAc/PE 1/2) yielding a mixture of the E- and Z-isomers as a colorless solid (3.00 g, 92%). ^{1}H NMR (300 MHz, CDCl$_3$) δ (ppm) 9.65 (s, 1H), 7.62 – 7.55 (m, 2H), 6.97 – 6.86 (m, 2H), 3.83 (s, 3H), 2.29 (s, 3H). ^{13}C NMR (75 MHz, CDCl$_3$) δ (ppm) 160.49, 155.51, 129.04, 127.41, 113.91, 55.35, 12.30. HRMS (ESI-MS): *m/z* [M+H$^+$] calculated for C$_9$H$_{12}$NO$_2^+$: 166.0863, found 166.0863 and 166.0862; C$_9$H$_{11}$NO$_2$ (165.19).

1-(4-Trifluoromethoxyphenyl)ethan-1-one oxime (3.206)

The title compound was synthesized from 4-trifluoromethoxyacetophenone (**3.198**, 1.96 g, 12.25 mmol), hydroxylammonium chloride (1.70 g, 24.49 mmol), and Na$_2$CO$_3$ (6.49 g, 61.23 mmol) in EtOH according to the general procedure (R$_f$ = 0.85 in EtOAc/PE 1/2) yielding a mixture of the E- and Z-isomers as a colorless solid (2.36 g, 88%). ^{1}H NMR (300 MHz, CD$_3$OD) δ (ppm) 7.73 – 7.67 (m, 2H), 7.24 – 7.19 (m, 2H), 2.20 (s, 2H). ^{13}C NMR (75 MHz, CD$_3$OD) δ (ppm) 153.13, 149.29, 136.13, 127.24, 120.47 (d, *J* = 255.8 Hz), 120.32, 10.47. HRMS (EI-MS): *m/z* [M$^{•+}$] calculated for C$_9$H$_8$F$_3$NO$_2$$^{•+}$: 219.05016, found 219.05030; C$_9$H$_8$F$_3$NO$_2$ (219.16).

1-(2-Fluorophenyl)ethan-1-one oxime (3.207)

The title compound was synthesized from 2-fluoroacetophenone (**3.199**, 2.22 mL, 18.09 mmol), hydroxylammonium chloride (2.52 g, 33.02 mmol), and Na$_2$CO$_3$ (9.60 g, 82.55 mmol) in EtOH according to the general procedure (R$_f$ = 0.28 in DCM) yielding a mixture of the E- and Z-isomers as a colorless solid (2.49 g, 90%). ^{1}H NMR (300 MHz, CD$_3$OD) δ (ppm) 7.44 – 7.31 (m, 2H), 7.17 – 7.05 (m, 2H), 2.18 (d, *J* = 2.4 Hz, 3H). ^{13}C NMR (75 MHz, CD$_3$OD, both isomers) δ (ppm) 161.84 (d, *J* = 247.8 Hz), 154.11, 131.67 (d, *J* = 8.4 Hz), 130.76 (d, *J* = 3.5 Hz), 127.09 (d, *J* = 13.0 Hz), 125.27 (d, *J* = 3.6 Hz), 116.88 (d, *J* = 22.1 Hz), 15.02 (d, *J* = 4.6 Hz). HRMS (EI-MS): *m/z* [M$^{•+}$] calculated for C$_8$H$_8$FNO$^{•+}$: 153.05844, found 153.05827; C$_8$H$_8$FNO (153.16).

1-(3-Fluorophenyl)ethan-1-one oxime (3.208)

The title compound was synthesized from 3-fluoroacetophenone (**3.200**, 2.22 mL, 18.09 mmol), hydroxylammonium chloride (2.52 g, 33.02 mmol), and Na$_2$CO$_3$ (9.60 g, 82.55 mmol) in EtOH according to the general procedure (R$_f$ = 0.28 in DCM) yielding a mixture of the E- and Z-isomers as a colorless solid (2.32 g, 84%). ^{1}H NMR (300 MHz, CD$_3$OD) δ (ppm) 7.42 – 7.28 (m, 3H), 7.07 – 6.99 (m, 1H), 2.17 (s, 3H). ^{13}C NMR (75 MHz, CD$_3$OD) δ (ppm) 164.15 (d, *J* = 243.8 Hz), 154.58 (d, *J* = 2.8 Hz), 140.92 (d, *J* = 7.7 Hz), 131.04 (d, *J* = 8.4 Hz), 122.80 (d, *J* = 2.9 Hz), 116.34 (d, *J* = 21.5 Hz), 113.44 (d, *J* = 23.1 Hz), 11.80. HRMS (EI-MS): *m/z* [M$^{•+}$] calculated for C$_8$H$_8$FNO$^{•+}$: 153.05844, found 153.05829 and 153.05869; C$_8$H$_8$FNO (153.16).

1-(Furan-2-yl)ethan-1-one oxime (3.209)

The title compound was synthesized from 2-acetylfuran (**3.201**, 2.67 mL, 27.25 mmol), hydroxylammonium chloride (3.79 g, 54.50 mmol), and Na$_2$CO$_3$ (14.44 g, 136.25 mmol) in EtOH according to the general procedure (R$_f$ = 0.18 in DCM) yielding a mixture of the E- and Z-isomers as a colorless solid (3.16 g, 93%). ^{1}H NMR (400 MHz, CDCl$_3$, isomer 1) δ (ppm) 9.41 (s, 1H), δ 7.26 (dd, J = 1.8, 0.7 Hz, 1H), 6.44 (dd, J = 3.5, 0.7 Hz, 1H), 6.23 (dd, J = 3.4, 1.8 Hz, 1H), 2.03 (s, 3H) and ^{1}H NMR (400 MHz, CDCl$_3$, isomer 2) δ (ppm) 9.41 (s, 1H), δ 7.30 – 7.27 (m, 2H), 6.34 (dd, J = 3.5, 1.8 Hz, 1H), 2.10 (s, 3H). ^{13}C NMR (101 MHz, CDCl$_3$, both isomers) δ (ppm) 150.25, 147.64, 146.05, 144.42, 143.73, 142.76, 118.13, 112.23, 111.36, 110.12, 17.39, 11.32. HRMS (EI-MS): m/z [M$^{•+}$] calculated for C$_6$H$_7$NO$_2$$^{•+}$: 125.04713, found 125.04689 and 125.04687; C$_6$H$_7$NO$_2$ (125.13).

1-(Thiophen-2-yl)ethan-1-one oxime (3.210)

The title compound was synthesized from 2-acetylthiophene (**3.202**, 2.57 mL, 23.78 mmol), hydroxylammonium chloride (3.31 g, 47.56 mmol), and Na$_2$CO$_3$ (12.60 g, 118.90 mmol) in EtOH according to the general procedure (R$_f$ = 0.10 in DCM) yielding a mixture of the E- and Z-isomers as a colorless solid (3.12 g, 93%). ^{1}H NMR (400 MHz, CDCl$_3$, isomer 1) δ (ppm) 8.97 (s, 1H), δ 7.31 – 7.24 (m, 1H), 7.04 (dd, J = 5.1, 3.7 Hz, 0H), 2.33 (s, 1H) and ^{1}H NMR (400 MHz, CDCl$_3$, isomer 2) δ (ppm) 8.97 (s, 1H), δ 7.62 – 7.53 (m, 2H), 7.13 (dd, J = 5.1, 3.9 Hz, 1H), 2.41 (s, 3H). ^{13}C NMR (101 MHz, CDCl$_3$, both isomers) δ (ppm) 151.89, 147.16, 140.22, 132.19, 131.40, 130.21, 127.27, 126.92, 126.64, 125.80, 19.74, 12.54. HRMS (EI-MS): m/z [M$^{•+}$] calculated for C$_6$H$_7$NOS$^{•+}$: 141.02429, found 141.02449 and 141.02449; C$_6$H$_7$NOS (141.19).

General procedure for the synthesis of the amines 3.017, 3.019, 3.024-3.027, and 3.029-3.030.

The general procedure was carried out in analogy to Winthrop et al. (1959)[459] with minor modifications, using HCl instead of acetic acid and CuSO$_4$. Zinc powder (18 eq) and CuSO$_4$ (cat.) were added to a solution of the respective oxime (**3.203**-**3.210**, 1 eq) in EtOH (50 mL). After the dropwise addition of 3 N HCl (100 mL), the reaction mixture was stirred for 3 h at rt. Subsequently, the reaction mixture was filtered, neutralized with NH$_3$ (25% in H$_2$O), and extracted with DCM (3 x 30 mL). The combined organic

layers were dried over Na$_2$SO$_4$ and evaporated. The crude product was purified by column chromatography (DCM/MeOH/7 N NH$_3$ in MeOH 100/0/0 - 50/49/1 or EtOAc/PE 1/2 in the case of **3.017**) or recrystallized with 2 N HCl in diethyl ether after dissolving in dioxane, in the case of **3.019** and **3.025**.

2,2,2-Trifluoro-1-phenylethan-1-amine (3.017)

The amine **3.017** was prepared from **3.203** (2.30 g, 12.16 mmol), zinc powder (14.31 g, 218.89 mmol), and CuSO$_4$ (0.10 g, cat.) in EtOH according to the general procedure (R$_f$ = 0.52 in EtOAc/PE 1/2) yielding **3.017** as a yellow oil (2.01 g, 94%). ^{1}H NMR (300 MHz, DMSO-d$_6$) δ (ppm) 7.56 – 7.36 (m, 5H), 6.99 (s, 2H), 4.75 (q, *J* = 8.2 Hz, 1H). ^{13}C NMR (75 MHz, DMSO-d$_6$) δ (ppm) 134.89, 128.85, 128.44, 128.27, 125.65 (d, *J* = 282.0 Hz), 56.14 (q, *J* = 29.5 Hz). HRMS (EI-MS): *m/z* [M$^{•+}$] calculated for C$_8$H$_8$F$_3$N$^{•+}$: 175.06022, found 175.06034; C$_8$H$_8$F$_3$N (175.15).

2-Methyl-1-phenylpropan-1-amine hydrochloride (3.019)

The amine **3.019** was prepared from **3.204** (2.05 g, 12.56 mmol), zinc powder (14.78 g, 226.08 mmol), and CuSO$_4$ (0.10 g, cat.) in EtOH according to the general procedure (R$_f$ = 0.44 in DCM/MeOH/7 N NH$_3$ in MeOH 84/15/1) yielding **3.019**-HCl as a colorless solid (0.50 g, 21%). ^{1}H NMR (300 MHz, CD$_3$OD, hydrochloride) δ (ppm) 7.48 – 7.35 (m, 5H), 3.91 (d, *J* = 9.2 Hz, 1H), 2.29 – 2.10 (m, 1H), 1.12 (d, *J* = 6.6 Hz, 3H), 0.77 (d, *J* = 6.7 Hz, 3H). ^{13}C NMR (75 MHz, CD$_3$OD, hydrochloride) δ (ppm) 136.71, 128.80, 128.76, 127.21, 61.70, 32.49, 18.30, 18.06. HRMS (ESI-MS): *m/z* [M+H$^+$] calculated for C$_{10}$H$_{16}$N$^+$: 150.1278, found 150.1277; C$_{10}$H$_{15}$N x HCl (185.70).

1-(4-Methoxyphenyl)ethan-1-amine (3.024)

The amine **3.024** was prepared from **3.205** (3.00 g, 18.16 mmol), zinc powder (21.37 g, 326.88 mmol), and CuSO$_4$ (0.10 g, cat.) in EtOH according to the general procedure (R$_f$ = 0.53 in DCM/MeOH/7 N NH$_3$ in MeOH 84/15/1) yielding **3.024** as a colorless oil (2.29 g, 83%). ^{1}H NMR (300 MHz, CDCl$_3$) δ (ppm) 7.28 – 7.20 (m, 2H), 6.88 – 6.81 (m, 2H), 4.04 (q, *J* = 6.6 Hz, 1H), 3.76 (s, 3H), 1.60 (s, 2H), 1.33 (d, *J* = 6.6 Hz, 2H). ^{13}C NMR (75 MHz, CDCl$_3$) δ (ppm) 158.42, 139.91, 126.74, 113.79, 55.24, 50.67, 25.76. HRMS (EI-MS): *m/z* [M$^{•+}$] calculated for C$_{10}$H$_{13}$N$^{•+}$: 151.09917, found 150.09952; C$_{10}$H$_{13}$N (151.21).

1-(4-Trifluoromethoxyphenyl)ethan-1-amine hydrochloride (3.025)

The amine **3.025** was prepared from **3.206** (2.36 g, 10.77 mmol), zinc powder (12.67 g, 193.83 mmol), and CuSO$_4$ (0.10 g, cat.) in EtOH according to the general procedure (R$_f$ = 0.64 in DCM/MeOH/7 N NH$_3$ in MeOH 84/15/1) yielding **3.025**-HCl as a colorless solid (0.61 g, 23%). ^{1}H NMR (300 MHz, CD$_3$OD, hydrochloride) δ (ppm) 7.62 – 7.55 (m, 2H), 7.39 – 7.33 (m, 2H), 4.49 (q, *J* = 6.9 Hz, 1H), 1.62 (d, *J* = 6.9 Hz, 2H). ^{13}C NMR (75 MHz, CD$_3$OD, hydrochloride) δ (ppm) 149.25, 138.22, 128.33, 121.27, 120.16 (d, *J* = 298.4 Hz), 50.19, 19.65. HRMS (ESI-MS): *m/z* [M+H$^+$] calculated for C$_9$H$_{11}$F$_3$NO$^+$: 206.0787, found 206.0790; C$_9$H$_{10}$F$_3$NO x HCl (241.64).

1-(2-Fluorophenyl)ethan-1-amine (3.026)

The amine **3.026** was prepared from **3.207** (2.49 g, 12.57 mmol), zinc powder (14.79 g, 226.28 mmol), and CuSO$_4$ (0.10 g, cat.) in EtOH according to the general procedure (R$_f$ = 0.61 in DCM/MeOH/7 N NH$_3$ in MeOH 84/15/1) yielding **3.026** as a yellow oil (1.50 g, 86%). ^{1}H NMR (400 MHz, DMSO-d$_6$) δ (ppm) 8.94 (s, 2H), 7.77 (t, *J* = 6.9 Hz, 1H), 7.39 – 7.31 (m, 1H), 7.24 – 7.14 (m, 2H), 4.64 – 4.42 (m, 1H), 1.50 (d, *J* = 6.8 Hz, 3H). ^{13}C NMR (101 MHz, DMSO-d$_6$) δ (ppm) 159.33 (d, *J* = 246.2 Hz), 130.64 (d, *J* = 8.3 Hz), 128.36 (d, *J* = 3.0 Hz), 126.46 (d, *J* = 13.4 Hz), 125.07 (d, *J* = 3.3 Hz), 115.77 (d, *J* = 21.5 Hz), 43.73 (d, *J* = 4.3 Hz), 20.25. HRMS (ESI-MS): *m/z* [M+H$^+$] calculated for C$_8$H$_{11}$FN$^+$: 140.0870, found 140.0868; C$_8$H$_{10}$FN (139.17).

1-(3-Fluorophenyl)ethan-1-amine (3.027)

The amine **3.027** was prepared from **3.208** (2.28 g, 11.51 mmol), zinc powder (13.55 g, 207.19 mmol), and CuSO$_4$ (0.10 g, cat.) in EtOH according to the general procedure (R$_f$ = 0.41 in DCM/MeOH/7 N NH$_3$ in MeOH 84/15/1) yielding **3.027** as a yellow oil (1.60 g, 100%). ^{1}H NMR (400 MHz, CDCl$_3$) δ (ppm) 7.42 – 7.22 (m, 3H), 7.05 (td, *J* = 8.4, 2.5 Hz, 1H), 5.95 (s, 2H), 4.31 (q, *J* = 6.7 Hz, 1H), 1.59 (d, *J* = 6.6 Hz, 3H). ^{13}C NMR (101 MHz, CDCl$_3$) δ (ppm) 163.01 (d, *J* = 246.5 Hz), 145.17 (d, *J* = 6.8 Hz), 130.46 (d, *J* = 8.2 Hz), 122.14 (d, *J* = 3.0 Hz), 114.89 (d, *J* = 21.1 Hz), 113.46 (d, *J* = 22.0 Hz), 51.12, 22.99. HRMS (ESI-MS): *m/z* [M+H$^+$] calculated for C$_8$H$_{11}$FN$^+$: 140.0870, found 140.0870; C$_8$H$_{10}$FN (139.17).

1-(Furan-2-yl)ethan-1-amine (3.029)

The amine **3.029** was prepared from **3.209** (3.16 g, 25.25 mmol), zinc powder (29.72 g, 454.57 mmol), and $CuSO_4$ (0.10 g, cat.) in EtOH according to the general procedure (R_f = 0.61 in DCM/MeOH/7 N NH_3 in MeOH 84/15/1) yielding **3.029** as a red oil (0.65 g, 23%). ^1H NMR (300 MHz, CD_3OD) δ (ppm) 7.59 (dd, J = 1.9, 0.8 Hz, 1H), 6.54 – 6.45 (m, 2H), 4.57 (q, J = 6.9, 0.7 Hz, 1H), 1.65 (d, J = 6.9 Hz, 3H). ^{13}C NMR (75 MHz, CD_3OD) δ (ppm) 152.05, 144.83, 111.80, 109.56, 45.63, 17.69. HRMS (ESI-MS): *m/z* [M+H⁺] calculated for $C_6H_{10}NO^+$: 112.0757, found 112.0755; C_6H_9NO (111.14).

1-(Thiophen-2-yl)ethan-1-amine (3.030)

The amine **3.030** was prepared from **3.210** (3.12 g, 22.10 mmol), zinc powder (26.00 g, 397.76 mmol), and $CuSO_4$ (0.10 g, cat.) in EtOH according to the general procedure (R_f = 0.59 in DCM/MeOH/7 N NH_3 in MeOH 84/15/1) yielding **3.030** as a red oil (0.40 g, 14%). ^1H NMR (400 MHz, DMSO-d_6) δ (ppm) 8.77 (s, 2H), 7.51 (dd, J = 5.1, 1.2 Hz, 1H), 7.29 (d, J = 3.4 Hz, 1H), 7.01 (dd, J = 5.1, 3.5 Hz, 1H), 4.64 (d, J = 7.1 Hz, 1H), 1.58 (d, J = 6.8 Hz, 3H). ^{13}C NMR (101 MHz, DMSO-d_6) δ (ppm) 141.76, 127.26, 126.95, 126.34, 45.48, 21.09. HRMS (ESI-MS): *m/z* [M+H⁺] calculated for $C_6H_{10}NS^+$: 128.0528, found 128.0527; C_6H_9NS (127.21).

3.5.1.5 Synthesis and Analytical Data of the Boc-protected Isothioureas 3.048-3.082

Method A: A solution of 15% phosgene in toluene or triphosgene (1 eq) was diluted in DCM and cooled to 0 °C. Subsequently, a mixture of the respective amine (**3.013-3.033**, 1 eq) and diisopropylethylamine (DIPEA, 3 eq) in DCM was added dropwise. After the solution was stirred for 5 minutes, a solution of **3.008** (2 eq) in DCM was added via a dropping funnel. The reaction was allowed to stir at rt for 2-3 h and washed with H_2O and brine. The organic layer was dried over Na_2SO_4, the solvent was removed under reduced pressure, and the crude product was purified by column chromatography (DCM).

Method B: The respective isocyanate (**3.034-3.039**, 1 eq) and NEt_3 (2.25 eq) were added to a solution of **3.008** (1.5 eq) in DCM (20 mL). The reaction mixture was stirred overnight at rt. The organic layer was washed three times with H_2O (30 mL) and subsequently with brine (30 mL). The organic layer was dried over Na_2SO_4 and the

solvent was removed under reduced pressure. The crude product was purified by flash chromatography (ethyl acetate (EtOAc)/petroleum ether (PE) 0/100 - 15/85).

Method C: The respective carbonic acid (**3.040-3.047**, 1 eq) was dissolved in DCM (2.5-4.5 mL) and cooled with an ice bath. Dimethylformamide (DMF, 25-45 µL) and oxalyl chloride (1.5 eq) were added under argon atmosphere. The reaction mixture was stirred for 10 min under cooling. The ice bath was removed and stirring was continued for another 15 min at rt. The solvent was carefully removed under reduced pressure (water bath temperature below 30 °C). The residue was dissolved in anhydrous acetone (2.5-4.5 mL) and added dropwise under cooling to an ice-cold solution of sodium azide (2.4 eq) in H$_2$O (1-3 mL). The reaction mixture was stirred for 30 min under cooling. Brine (5-10 mL) was added and the acyl azide was extracted three times with DCM (10 mL). The organic layers were combined and dried over Na$_2$SO$_4$. A molecular sieve was added and the solvent was partially removed under reduced pressure. The resulting yellow solution was stirred for 30 min under reflux conditions to afford the isocyanate. The solution was cooled to rt followed by the addition of **3.008** (1 eq) and NEt$_3$ (5 eq). The reaction mixture was stirred overnight at rt. The molecular sieve was filtered off and the organic layer was washed three times with H$_2$O (10 mL) and three times with brine (10 mL). The organic layers were combined, dried over Na$_2$SO$_4$, and the solvent was removed under reduced pressure. The crude product was purified by either automated flash chromatography or column chromatography (EtOAc/PE).

N'-*tert*-Butoxycarbonyl-*S*-methyl-*N*-propylcarbamoylisothiourea (3.048)

The title compound was prepared from propylisocyanate (**3.034**, 149 mg, 1.75 mmol), **3.008** (500 mg, 2.63 mmol) and NEt$_3$ (0.55 mL, 3.94 mmol) according to the general procedure (method B) (EtOAc/PE 0/100-15/85 in 30 min, R$_f$ = 0.72 in EtOAc/PE 1/3) yielding a white solid (0.31 g, 64%), mp 56 – 60 °C. ^{1}H NMR (400 MHz, CDCl$_3$): δ (ppm) 12.34 (br s, 1H), 3.18 (q, *J* = 6.9 Hz, 2H), 2.31 (s, 3H), 1.56 (m, 2H), 1.47 (s, 9H), 0.94 (t, *J* = 7.4 Hz, 3H). ^{13}C NMR (100 MHz, CDCl$_3$): δ (ppm) 167.50, 161.90, 151.10, 82.60, 41.90, 28.00, 22.90, 14.30, 11.40. HRMS (ESI-MS): *m/z* [M+H$^+$] calculated for C$_{11}$H$_{22}$N$_3$O$_3$S$^+$: 276.1376, found 276.1379; C$_{11}$H$_{21}$N$_3$O$_3$S (275.37).

N'-tert-Butoxycarbonyl-S-methyl-N-pentylcarbamoylisothiourea (3.049)

(Synthesized by Katharina Tropmann)

The reaction was carried out with triphosgene (340 mg, 1.15 mmol), pentan-1-amine (**3.014**, 132 µL, 1.15 mmol), DIPEA (0.60 mL, 3.45 mmol), **3.008** (0.44 g, 2.30 mmol) and a total of 60 mL DCM according to the general procedure (method A) (R_f = 0.64 in EtOAc/PE 1/5) yielding a colorless foamlike solid (0.30 g, 84%). ^{1}H NMR (300 MHz, CDCl$_3$): δ (ppm) 12.27 (br s, 1H), 5.51 (s, 1H), 3.15 (q, J = 6.72 Hz, 2H), 2.23 (s, 3H), 1.58 – 1.42 (m, 2H), 1.41 (s, 9H), 1.34 – 1.19 (m, 4H), 0.91 – 0.75 (m, 3H). ^{13}C NMR (75 MHz, CDCl$_3$): δ (ppm) 167.31, 162.05, 151.27, 82.64, 40.28, 29.53, 29.22, 28.16, 22.52, 14.39, 14.13. HRMS (ESI-MS): *m/z* [M+H$^+$] calculated for C$_{13}$H$_{26}$N$_3$O$_3$S$^+$: 304.1689, found 304.1713; C$_{13}$H$_{25}$N$_3$O$_3$S (303.42).

N'-tert-Butoxycarbonyl-S-methyl-N-hexylcarbamoylisothiourea (3.050)

(Synthesized by Sabrina Biselli and Claudia Honisch)

The title compound was prepared from hexylisocyanate (**3.035**, 223 mg, 1.75 mmol), **3.008** (500 mg, 2.63 mmol) and NEt$_3$ (0.55 mL, 3.94 mmol) according to the general procedure (method B) (EtOAc/PE 0/100-15/85 in 30 min, R_f = 0.67 in EtOAc/PE 1/3) yielding a white solid (0.45 g, 81%), mp 56 – 59 °C. ^{1}H NMR (400 MHz, CDCl$_3$): δ (ppm) 12.35 (br s, 1H), 3.24 – 3.19 (m, 2H), 2.31 (s, 3H), 1.59 – 1.49 (m, 2H), 1.47 (s, 9H), 1.37 – 1.26 (m, 6H), 0.90 – 0.85 (m, 3H). ^{13}C NMR (100 MHz, CDCl$_3$): δ (ppm) 167.70, 161.80, 151.10, 82.60, 40.20, 31.50, 29.70, 28.00, 26.60, 22.60, 14.30, 14.00. HRMS (ESI-MS): *m/z* [M+H$^+$] calculated for C$_{14}$H$_{28}$N$_3$O$_3$S$^+$: 318.1846, found 318.1851; C$_{14}$H$_{27}$N$_3$O$_3$S (317.45).

N'-tert-Butoxycarbonyl-S-methyl-N-cyclohexylcarbamoylisothiourea (3.051)

(Synthesized by Sabrina Biselli and Claudia Honisch)

The title compound was prepared from cyclohexylisocyanate (**3.036**, 219 mg, 1.75 mmol), **3.008** (500 mg, 2.63 mmol) and NEt$_3$ (0.55 mL, 3.94 mmol) according to the general procedure (method B) (EtOAc/PE 0/100-15/85 in 35 min, R_f = 0.63 in EtOAc/PE 1/3) yielding a white solid (0.47 g, 85%), mp 150 – 152 °C. ^{1}H NMR (400 MHz, CDCl$_3$): δ (ppm) 12.43 (br s, 1H), 3.63 – 3.53 (m, 1H), 2.34 (s, 3H), 1.97 – 1.93 (m, 2H), 1.76 – 1.71 (m, 2H), 1.66 – 1.59 (m, 1H), 1.47 (s, 9H), 1.42 – 1.31 (m, 2H), 1.26 – 1.12 (m, 3H). ^{13}C NMR (100 MHz, CDCl$_3$): δ (ppm) 167.60, 160.90, 151.00,

82.70, 49.10, 33.10, 28.00, 25.50, 24.90, 14.40. HRMS (ESI-MS): *m/z* [M+H$^+$] calculated for C$_{14}$H$_{26}$N$_3$O$_3$S$^+$: 316.1689, found 316.1700; C$_{14}$H$_{25}$N$_3$O$_3$S (315.43).

N'-*tert*-Butoxycarbonyl-*S*-methyl-*N*-phenylcarbamoylisothiourea (3.052)

(Synthesized by Sabrina Biselli and Claudia Honisch)

The title compound was prepared from phenylisocyanate (**3.037**, 210 mg, 1.75 mmol), **3.008** (500 mg, 2.63 mmol) and NEt$_3$ (0.55 mL, 3.94 mmol) according to the general procedure (method B) (EtOAc/PE 0/100-10/90 in 25 min, R$_f$ = 0.66 in EtOAc/PE 1/3) yielding a white solid (0.31 g, 57%), mp 126 – 130 °C. ^{1}H NMR (400 MHz, CDCl$_3$): δ (ppm) 12.22 (br s, 1H), 7.51 – 7.49 (m, 2H), 7.42 (br s, 1H), 7.35 – 7.31 (m, 2H), 7.12 – 7.08 (m, 1H), 2.40 (s, 3H), 1.50 (s, 9H). ^{13}C NMR (100 MHz, CDCl$_3$): δ (ppm) 169.20, 159.30, 151.00, 137.90, 129.10, 124.00, 119.40, 83.10, 28.00, 14.60. HRMS (ESI-MS): *m/z* [M+H$^+$] calculated for C$_{14}$H$_{20}$N$_3$O$_3$S$^+$: 310.1220, found 310.1228; C$_{14}$H$_{19}$N$_3$O$_3$S (309.38).

N'-*tert*-Butoxycarbonyl-*S*-methyl-*N*-benzylcarbamoylisothiourea (3.053)

(Synthesized by Sabrina Biselli and Claudia Honisch)

The title compound was prepared from benzylisocyanate (**3.038**, 234 mg, 1.75 mmol), **3.008** (500 mg, 2.63 mmol) and NEt$_3$ (0.55 mL, 3.94 mmol) according to the general procedure (method B) (EtOAc/PE 0/100-15/85 in 35 min, R$_f$ = 0.77 in EtOAc/PE 1/3) yielding a white solid (0.45 g, 80%), mp 104 – 107 °C. ^{1}H NMR (400MHz, CDCl$_3$): δ (ppm) 12.38 (br s, 1H), 7.37 – 7.27 (m, 5H), 6.09 (br s, 1H), 4.43 (d, *J* = 6.1 Hz, 2H), 2.34 (s, 3H), 1.49 (s, 9H). ^{13}C NMR (100 MHz, CDCl$_3$): δ (ppm) 168.50, 155.30, 151.00, 138.20, 128.80, 127.64, 127.56, 83.00, 44.20, 28.00, 14.50. HRMS (ESI-MS): *m/z* [M+H$^+$] calculated for C$_{15}$H$_{22}$N$_3$O$_3$S$^+$: 324.1376, found 324.1384; C$_{15}$H$_{21}$N$_3$O$_3$S (323.41).

N'-*tert*-Butoxycarbonyl-*S*-methyl-*N*-diphenylmethylcarbamoylisothiourea (3.054) *(Synthesized by Steffen Pockes)*

The reaction was carried out with 15% phosgene in toluene (1.35 mL, 1.89 mmol), diphenylmethanamine (**3.014**, 0.35 g, 1.89 mmol), DIPEA (1.02 mL, 5.67 mmol), **3.008** (0.72 g, 3.78 mmol) and a total of 60 mL DCM according to the general procedure (method A) (R$_f$ = 0.55 in DCM) yielding a colorless foamlike solid (0.25 g, 33%). ^{1}H NMR (300 MHz, CDCl$_3$) δ (ppm) 12.32 (br s, 1H), 7.38 – 7.25 (m, 10H), 6.18 (br s, 1H),

6.05 (d, J = 7.6 Hz, 1H), 2.33 (s, 3H), 1.46 (s, 9H). ^{13}C NMR (75 MHz, CDCl$_3$) δ (ppm) 168.65, 160.96, 151.07, 141.43, 128.79, 127.61, 127.40, 82.78, 58.23, 28.03, 14.49. HRMS (ESI-MS): *m/z* [M+H$^+$] calculated for C$_{21}$H$_{26}$N$_3$O$_3$S$^+$: 400.1689, found 400.1695; C$_{21}$H$_{25}$N$_3$O$_3$S (399.51).

(*R*)-*N'*-*tert*-Butoxycarbonyl-*S*-methyl-*N*-(1-phenylethyl)carbamoylisothiourea (3.055)

The reaction was carried out with 15% phosgene in toluene (5.89 mL, 8.25 mmol), (*R*)-1-phenylethan-1-amine (**3.015**, 1.00 g, 8.25 mmol), DIPEA (4.46 mL, 24.75 mmol), **3.008** (3.14 g, 16.50 mmol) and a total of 150 mL DCM according to the general procedure (method A) (R$_f$ = 0.50 in DCM) yielding a colorless foamlike solid (1.60 g, 57%). ^{1}H NMR (300 MHz, CDCl$_3$) δ (ppm) 12.29 (br s, 1H), 7.41 – 7.26 (m, 5H), 5.81 (br s, 1H), 4.93 (p, J = 7.1 Hz, 1H), 2.32 (s, 3H), 1.52 (d, J = 6.9 Hz, 3H), 1.46 (s, 9H). ^{13}C NMR (75 MHz, CDCl$_3$) δ (ppm) 167.92, 161.02, 151.13, 143.44, 128.75, 127.39, 125.98, 82.67, 49.79, 28.04, 22.31, 14.38. HRMS (ESI-MS): *m/z* [M+H$^+$] calculated for C$_{16}$H$_{24}$N$_3$O$_3$S$^+$: 338.1533, found 338.1542; C$_{16}$H$_{23}$N$_3$O$_3$S (337.44).

(*S*)-*N'*-*tert*-Butoxycarbonyl-*S*-methyl-*N*-(1-phenylethyl)carbamoylisothiourea (3.056) *(Synthesized by Steffen Pockes)*

The reaction was carried out with 15% phosgene in toluene (1.22 mL, 1.71 mmol), (*S*)-1-phenylethan-1-amine (**3.016**, 0.21 g, 1.71 mmol), DIPEA (0.89 mL, 5.12 mmol), **3.008** (0.65 g, 3.42 mmol) and a total of 40 mL DCM according to the general procedure (method A) (R$_f$ = 0.50 in DCM) yielding a colorless foamlike solid (0.44 g, 76%). ^{1}H NMR (300 MHz, CDCl$_3$) δ (ppm) 12.30 (br s, 1H), 7.41 – 7.27 (m, 5H), 5.81 (br s, 1H), 4.93 (p, J = 7.1 Hz, 1H), 2.32 (s, 3H), 1.53 (d, J = 7.0 Hz, 3H), 1.46 (s, 9H). ^{13}C NMR (75 MHz, CDCl$_3$) δ (ppm) 167.95, 161.09, 151.11, 143.43, 128.75, 127.39, 125.98, 82.70, 49.80, 28.03, 22.32, 14.39. HRMS (ESI-MS): *m/z* [M+H$^+$] calculated for C$_{16}$H$_{24}$N$_3$O$_3$S$^+$: 338.1533, found 338.1542; C$_{16}$H$_{23}$N$_3$O$_3$S (337.44).

N'-*tert*-Butoxycarbonyl-*S*-methyl-*N*-(2,2,2-trifluoro-1-phenylethyl)carbamoylisothiourea (3.057)

The reaction was carried out with 15% phosgene in toluene (2.44 mL, 3.42 mmol), **3.017** (0.60 g, 3.42 mmol), DIPEA (1.74 mL, 10.26 mmol), **3.008** (1.30 g, 6.84 mmol) and a total of 100 mL DCM according to the general procedure (method A) (R$_f$ = 0.84

in DCM) yielding a colorless solid (1.01 g, 75%), mp 124 - 128 °C. ^{1}H NMR (300 MHz, CDCl$_3$) δ (ppm) 12.08 (s, 1H), 7.46 – 7.31 (m, 5H), 6.20 (d, J = 9.7 Hz, 1H), 5.59 – 5.41 (m, 1H), 2.33 (s, 3H), 1.47 (s, 9H). ^{13}C NMR (75 MHz, CDCl$_3$) δ (ppm) 170.19, 161.00, 150.90, 132.99, 129.38, 129.08, 127.95, 124.66 (d, J = 281.8 Hz), 83.17, 55.61 (q, J = 31.3 Hz), 28.05, 14.54. HRMS (ESI-MS): m/z [M+H$^+$] calculated for C$_{16}$H$_{21}$F$_3$N$_3$O$_3$S$^+$: 392.1250, found 392.1254; C$_{16}$H$_{20}$F$_3$N$_3$O$_3$S (391.41).

N'-tert-Butoxycarbonyl-S-methyl-N-(1-phenylpropyl)carbamoylisothiourea (3.058)

The reaction was carried out with 15% phosgene in toluene (1.22 mL, 1.71 mmol), 1-phenylpropylamine (**3.018**, 0.23 g, 1.71 mmol), DIPEA (0.89 mL, 5.12 mmol), **3.008** (0.65 g, 3.42 mmol) and a total of 60 mL DCM according to the general procedure (method A) (R$_f$ = 0.75 in DCM) yielding a colorless foamlike solid (0.37 g, 62%). ^{1}H NMR (300 MHz, CDCl$_3$) δ (ppm) 12.29 (s, 1H), 7.38 – 7.24 (m, 5H), 5.79 (d, J = 8.2 Hz, 1H), 4.67 (q, J = 7.5 Hz, 1H), 2.31 (s, 3H), 1.98 – 1.71 (m, 2H), 1.45 (s, 9H), 0.92 (t, J = 7.4 Hz, 3H). ^{13}C NMR (75 MHz, CDCl$_3$) δ (ppm) 167.91, 161.45, 151.25, 142.42, 128.80, 127.48, 126.58, 82.69, 56.12, 29.62, 28.13, 14.46, 10.97. HRMS (ESI-MS): m/z [M+H$^+$] calculated for C$_{17}$H$_{26}$N$_3$O$_3$S$^+$: 352.1689, found 352.1693; C$_{17}$H$_{25}$N$_3$O$_3$S (351.47).

N'-tert-Butoxycarbonyl-S-methyl-N-(1-phenylisobutyl)carbamoylisothiourea (3.059)

The reaction was carried out with 15% phosgene in toluene (1.54 mL, 2.15 mmol), **3.019**-HCl (0.40 g, 2.15 mmol), DIPEA (1.12 mL, 6.45 mmol), **3.008** (0.82 g, 4.30 mmol) and a total of 60 mL DCM according to the general procedure (method A) (R$_f$ = 0.90 in DCM) yielding a colorless oil (0.61 g, 77%). ^{1}H NMR (300 MHz, CDCl$_3$) δ (ppm) 12.29 (s, 1H), 7.38 – 7.22 (m, 5H), 5.86 (d, J = 9.0 Hz, 1H), 4.54 (t, 1H), 2.32 (s, 3H), 2.11 – 1.98 (m, 1H), 1.44 (s, 9H), 0.99 (d, J = 6.7 Hz, 3H), 0.85 (d, J = 6.7 Hz, 3H). ^{13}C NMR (75 MHz, CDCl$_3$) δ (ppm) 167.75, 161.49, 151.12, 141.64, 128.49, 127.20, 126.86, 82.55, 60.25, 33.58, 28.03, 19 .85, 18.87, 14.37. HRMS (ESI-MS): m/z [M+H$^+$] calculated for C$_{18}$H$_{28}$N$_3$O$_3$S$^+$: 366.1846, found 366.1853; C$_{18}$H$_{27}$N$_3$O$_3$S (365.49).

N'-*tert*-Butoxycarbonyl-*S*-methyl-*N*-(1-(*p*-tolyl)ethyl)carbamoylisothiourea (3.060)

The reaction was carried out with 15% phosgene in toluene (1.22 mL, 1.71 mmol), 1-(-4-methylphenyl)ethylamine (**3.020**, 0.23 g, 1.71 mmol), DIPEA (0.89 mL, 5.12 mmol), **3.008** (0.65 g, 3.42 mmol) and a total of 60 mL DCM according to the general procedure (method A) (R$_f$ = 0.69 in DCM) yielding a colorless solid (0.43 g, 72%), mp 108 - 109.5 °C. ^{1}H NMR (300 MHz, CDCl$_3$) δ (ppm) 12.30 (s, 1H), 7.24 (d, *J* = 8.1 Hz, 2H), 7.16 (d, *J* = 8.0 Hz, 2H), 5.77 (s, 1H), 4.89 (p, *J* = 7.0 Hz, 1H), 2.33 (s, 3H), 2.30 (s, 3H), 1.50 (d, *J* = 6.9 Hz, 3H), 1.46 (s, 9H). ^{13}C NMR (75 MHz, CDCl$_3$) δ (ppm) 167.89, 161.12, 151.25, 140.58, 137.16, 129.51, 126.02, 82.73, 49.66, 28.16, 22.41, 21.22, 14.48. HRMS (ESI-MS): *m/z* [M+H$^+$] calculated for C$_{17}$H$_{26}$N$_3$O$_3$S$^+$: 352.1689, found 352.1692; C$_{17}$H$_{25}$N$_3$O$_3$S (351.47).

N'-*tert*-Butoxycarbonyl-*S*-methyl-*N*-(1-(4-fluorophenyl)ethyl)carbamoylisothiourea (3.061)

The reaction was carried out with 15% phosgene in toluene (1.22 mL, 1.71 mmol), 1-(-4-fluorophenyl)ethylamine (**3.021**, 0.24 g, 1.71 mmol), DIPEA (0.89 mL, 5.12 mmol), **3.008** (0.65 g, 3.42 mmol) and a total of 60 mL DCM according to the general procedure (method A) (R$_f$ = 0.72 in DCM) yielding a colorless foamlike solid (0.35 g, 58%). ^{1}H NMR (300 MHz, CDCl$_3$) δ (ppm) 12.24 (s, 1H), 7.33 – 7.28 (m, 2H), 7.07 – 7.00 (m, 2H), 5.76 (d, *J* = 7.7 Hz, 1H), 4.90 (p, *J* = 7.1 Hz, 1H), 2.31 (s, 3H), 1.50 (d, *J* = 2.9 Hz, 3H), 1.46 (s, 9H). ^{13}C NMR (75 MHz, CDCl$_3$) δ (ppm) 168.12, 161.98 (d, *J* = 245.4 Hz), 161.06, 151.10, 139.28, 127.56 (d, *J* = 8.0 Hz), 115.52 (d, *J* = 21.4 Hz), 82.71, 49.15, 28.02, 22.40, 14.36. HRMS (ESI-MS): *m/z* [M+H$^+$] calculated for C$_{16}$H$_{23}$FN$_3$O$_3$S$^+$: 356.1439, found 356.1441; C$_{16}$H$_{22}$FN$_3$O$_3$S (355.43).

N'-*tert*-Butoxycarbonyl-*S*-methyl-*N*-(1-(4-chlorophenyl)ethyl)carbamoylisothiourea (3.062)

The reaction was carried out with 15% phosgene in toluene (1.22 mL, 1.71 mmol), 1-(-4-chlorophenyl)ethylamine (**3.022**, 0.27 g, 1.71 mmol), DIPEA (0.89 mL, 5.12 mmol), **3.008** (0.65 g, 3.42 mmol) and a total of 60 mL DCM according to the general procedure (method A) (R$_f$ = 0.72 in DCM) yielding a colorless oil (0.22 g, 35%). ^{1}H NMR (300 MHz, CDCl$_3$) δ (ppm) 12.22 (s, 1H), 7.39 – 7.18 (m, 4H), 5.75 (d, *J* = 7.6 Hz, 1H), 4.89 (p, *J* = 7.1 Hz, 1H), 2.31 (s, 3H), 1.49 (d, *J* = 6.9 Hz, 3H), 1.46 (s, 9H).

^{13}C NMR (75 MHz, CDCl$_3$) δ (ppm) 168.35, 161.21, 151.21, 142.26, 133.15, 128.97, 127.44, 82.85, 49.38, 28.14, 22.47, 14.49. HRMS (ESI-MS): *m/z* [M+H$^+$] calculated for C$_{16}$H$_{23}$ClN$_3$O$_3$S$^+$: 372.1143, found 372.1142; C$_{16}$H$_{22}$ClN$_3$O$_3$S (371.88).

N'-*tert*-Butoxycarbonyl-*S*-methyl-*N*-(1-(4-bromophenyl)ethyl)carbamoylisothiourea (3.063)

The reaction was carried out with 15% phosgene in toluene (1.22 mL, 1.71 mmol), 1-(-4-bromophenyl)ethylamine (**3.023**, 0.34 g, 1.71 mmol), DIPEA (0.89 mL, 5.12 mmol), **3.008** (0.65 g, 3.42 mmol) and a total of 60 mL DCM according to the general procedure (method A) (R$_f$ = 0.72 in DCM) yielding a colorless oil (0.30 g, 42%). ^{1}H NMR (300 MHz, CDCl$_3$) δ (ppm) 12.21 (s, 1H), 7.51 – 7.42 (m, 2H), 7.25 – 7.14 (m, 2H), 5.74 (d, *J* = 7.6 Hz, 1H), 4.87 (p, *J* = 7.1 Hz, 1H), 2.31 (s, 3H), 1.49 (d, *J* = 7.1 Hz, 3H), 1.46 (s, 9H). ^{13}C NMR (75 MHz, CDCl$_3$) δ (ppm) 168.38, 161.21, 151.21, 142.81, 131.93, 127.81, 121.24, 82.86, 49.46, 28.15, 22.45, 14.51. HRMS (ESI-MS): *m/z* [M+H$^+$] calculated for C$_{16}$H$_{23}$BrN$_3$O$_3$S$^+$: 416.0638, found 416.0638; C$_{16}$H$_{22}$BrN$_3$O$_3$S (416.33).

N'-*tert*-Butoxycarbonyl-*S*-methyl-*N*-(1-(4-methoxyphenyl)ethyl)carbamoylisothiourea (3.064)

The reaction was carried out with 15% phosgene in toluene (2.36 mL, 3.31 mmol), **3.024** (0.50 g, 3.31 mmol), DIPEA (1.73 mL, 9.92 mmol), **3.008** (1.26 g, 6.62 mmol) and a total of 100 mL DCM according to the general procedure (method A) (R$_f$ = 0.36 in DCM) yielding a colorless oil (0.71 g, 58%). ^{1}H NMR (300 MHz, CDCl$_3$) δ (ppm) 12.31 (s, 1H), 7.29 – 7.21 (m, 2H), 6.90 – 6.81 (m, 2H), 5.85 (d, *J* = 7.9 Hz, 1H), 4.87 (p, *J* = 7.1 Hz, 1H), 3.77 (s, 3H), 2.28 (s, 3H), 1.48 (d, *J* = 6.9 Hz, 3H), 1.45 (s, 9H). ^{13}C NMR (75 MHz, CDCl$_3$) δ (ppm) 167.72, 161.01, 158.79, 151.11, 135.52, 127.17, 114.04, 82.57, 55.28, 49.17, 28.03, 22.17, 14.31. HRMS (ESI-MS): *m/z* [M+H$^+$] calculated for C$_{17}$H$_{26}$N$_3$O$_4$S$^+$: 368.1639, found 368.1640; C$_{17}$H$_{25}$N$_3$O$_4$S (367.46).

N'-*tert*-Butoxycarbonyl-*S*-methyl-*N*-(1-(4-trifluoromethoxyphenyl)ethyl)carbamoylisothiourea (3.065)

The reaction was carried out with 15% phosgene in toluene (1.19 mL, 1.66 mmol), **3.025**-HCl (0.40 g, 1.66 mmol), DIPEA (0.87 mL, 4.98 mmol), **3.008** (0.63 g, 3.32 mmol) and a total of 60 mL DCM according to the general procedure (method A)

(R$_f$ = 0.80 in DCM) yielding a colorless oil (0.43 g, 62%). ^{1}H NMR (300 MHz, CDCl$_3$) δ (ppm) 12.22 (s, 1H), 7.37 – 7.32 (m, 2H), 7.21 – 7.14 (m, 2H), 5.87 (d, *J* = 7.7 Hz, 1H), 4.92 (p, *J* = 7.1 Hz, 1H), 2.30 (s, 3H), 1.49 (d, *J* = 7.0 Hz, 3H), 1.45 (s, 9H). ^{13}C NMR (75 MHz, CDCl$_3$) δ (ppm) 168.28, 161.09, 151.04, 148.25, 142.32, 127.33, 121.19, 120.46 (d, *J* = 257.0 Hz), 82.74, 49.16, 27.98, 22.31, 14.32. HRMS (ESI-MS): *m/z* [M+H$^+$] calculated for C$_{17}$H$_{23}$F$_3$N$_3$O$_4$S$^+$: 422.1356, found 422.1359; C$_{17}$H$_{22}$F$_3$N$_3$O$_4$S (421.44).

N'-***tert***-Butoxycarbonyl-*S*-methyl-*N*-(1-(2-fluorophenyl)ethyl)carbamoylisothiourea (3.066)

The reaction was carried out with 15% phosgene in toluene (3.08 mL, 4.31 mmol), **3.026** (0.60 g, 4.31 mmol), DIPEA (2.20 mL, 12.93 mmol), **3.008** (1.64 g, 8.62 mmol) and a total of 100 mL DCM according to the general procedure (method A) (R$_f$ = 0.72 in DCM) yielding a yellow oil (0.93 g, 61%). ^{1}H NMR (400 MHz, CDCl$_3$) δ (ppm) 12.40 (s, 1H), 7.48 – 7.17 (m, 4H), 6.13 (s, 1H), 5.28 (p, *J* = 7.1 Hz, 1H), 2.47 (s, 3H), 1.67 (d, *J* = 7.0 Hz, 3H), 1.60 (s, 9H). ^{13}C NMR (101 MHz, CDCl$_3$) δ (ppm) 168.11, 160.85, 160.49 (d, *J* = 246.0 Hz), 151.06, 130.41 (d, *J* = 13.3 Hz), 128.89 (d, *J* = 8.3 Hz), 127.56 (d, *J* = 4.8 Hz), 124.33 (d, *J* = 3.5 Hz), 115.89 (d, *J* = 21.7 Hz), 82.65, 45.72, 28.01, 21.62, 14.36. HRMS (ESI-MS): *m/z* [M+H$^+$] calculated for C$_{16}$H$_{23}$FN$_3$O$_3$S$^+$: 356.1439, found 356.1445; C$_{16}$H$_{22}$FN$_3$O$_3$S (355.43).

N'-***tert***-Butoxycarbonyl-*S*-methyl-*N*-(1-(3-fluorophenyl)ethyl)carbamoylisothiourea (3.067)

The reaction was carried out with 15% phosgene in toluene (3.08 mL, 4.31 mmol), **3.027**-HCl (0.60 g, 4.31 mmol), DIPEA (2.20 mL, 12.93 mmol), **3.008** (1.64 g, 8.62 mmol) and a total of 100 mL DCM according to the general procedure (method A) (R$_f$ = 0.76 in DCM) yielding a colorless oil (0.77 g, 51%). ^{1}H NMR (400 MHz, CDCl$_3$) δ (ppm) 12.40 (s, 1H), 7.48 – 7.02 (m, 4H), 6.16 (d, *J* = 7.8 Hz, 1H), 5.06 (p, *J* = 7.1 Hz, 1H), 2.44 (s, 3H), 1.61 (d, *J* = 7.5 Hz, 2H), 1.60 (s, 9H). ^{13}C NMR (101 MHz, CDCl$_3$) δ (ppm) 162.96 (d, *J* = 246.2 Hz), 161.64, 161.01, 150.93, 146.32 (d, *J* = 6.6 Hz), 130.14 (d, *J* = 8.2 Hz), 121.55 (d, *J* = 2.8 Hz), 114.04 (d, *J* = 21.1 Hz), 112.80 (d, *J* = 21.8 Hz), 82.55, 53.14, 27.89, 22.15, 14.42. HRMS (ESI-MS): *m/z* [M+H$^+$] calculated for C$_{16}$H$_{23}$FN$_3$O$_3$S$^+$: 356.1439, found 356.1445; C$_{16}$H$_{22}$FN$_3$O$_3$S (355.43).

N'-tert-Butoxycarbonyl-S-methyl-N-(1-(2-furanyl)methyl)carbamoylisothiourea (3.068)

The reaction was carried out with 15% phosgene in toluene (4.41 mL, 6.18 mmol), furfurylamine (**3.028**, 0.60 g, 6.18 mmol), DIPEA (3.15 mL, 18.53 mmol), **3.008** (2.35 g, 12.36 mmol) and a total of 100 mL DCM according to the general procedure (method A) (R$_f$ = 0.74 in DCM) yielding a yellow oil (0.56 g, 29%). ^{1}H NMR (400 MHz, CDCl$_3$) δ (ppm) 12.15 (s, 1H), 7.25 (d, J = 10.3 Hz, 1H), 6.24 – 6.12 (m, 2H), 5.77 (s, 1H), 4.30 (d, J = 5.9 Hz, 2H), 2.20 (s, 3H), 1.37 (s, 9H). ^{13}C NMR (101 MHz, CDCl$_3$) δ (ppm) 168.47, 161.59, 151.45, 142.44, 110.55, 107.51, 82.91, 37.26, 28.16, 14.51. HRMS (ESI-MS): m/z [M+H$^+$] calculated for C$_{13}$H$_{20}$N$_3$O$_4$S$^+$: 314.1169, found 314.1174; C$_{13}$H$_{19}$N$_3$O$_4$S (313.37).

N'-tert-Butoxycarbonyl-S-methyl-N-(1-(2-furanyl)ethyl)carbamoylisothiourea (3.069)

The reaction was carried out with 15% phosgene in toluene (2.89 mL, 4.05 mmol), **3.029** (0.45 g, 4.05 mmol), DIPEA (2.10 mL, 12.15 mmol), **3.008** (1.54 g, 8.10 mmol) and a total of 100 mL DCM according to the general procedure (method A) (R$_f$ = 0.60 in DCM) yielding a colorless oil (0.36 g, 27%). ^{1}H NMR (400 MHz, CDCl$_3$) δ (ppm) 12.20 (s, 1H), 7.27 – 7.23 (m, 1H), 6.23 – 6.09 (m, 2H), 5.71 (s, 1H), 4.94 (p, J = 7.1 Hz, 1H), 2.21 (s, 3H), 1.43 (d, J = 7.0 Hz, 3H), 1.38 (s, 9H). ^{13}C NMR (101 MHz, CDCl$_3$) δ (ppm) 168.25, 161.70, 155.41, 151.03, 141.95, 110.16, 105.48, 53.24, 43.64, 28.03, 19.58, 14.35. HRMS (ESI-MS): m/z [M+H$^+$] calculated for C$_{14}$H$_{22}$N$_3$O$_4$S$^+$: 328.1326, found 328.1334; C$_{14}$H$_{21}$N$_3$O$_4$S (327.40).

N'-tert-Butoxycarbonyl-S-methyl-N-(1-(thiophen-2-yl)ethyl)carbamoylisothiourea (3.070)

The reaction was carried out with 15% phosgene in toluene (1.85 mL, 2.59 mmol), **3.030** (0.33 g, 2.59 mmol), DIPEA (1.35 mL, 7.78 mmol), **3.008** (0.99 g, 5.19 mmol) and a total of 60 mL DCM according to the general procedure (method A) (R$_f$ = 0.62 in DCM) yielding a colorless oil (0.29 g, 33%). ^{1}H NMR (400 MHz, CDCl$_3$) δ (ppm) 12.31 (s, 1H), 7.23 – 7.18 (m, 1H), 7.03 – 6.91 (m, 2H), 5.91 (s, 1H), 5.22 (p, J = 7.3 Hz, 1H), 2.41 (s, 3H), 1.62 (d, J = 6.9 Hz, 3H), 1.48 (s, 9H). ^{13}C NMR (101 MHz, CDCl$_3$) δ (ppm) 173.09, 161.85, 151.10, 147.24, 126.97, 124.44, 124.02, 53.39, 45.60, 28.12, 22.57,

14.61. HRMS (ESI-MS): *m/z* [M+H$^+$] calculated for C$_{14}$H$_{22}$N$_3$O$_3$S$_2^+$: 344.1097, found 344.1097; C$_{14}$H$_{21}$N$_3$O$_3$S$_2$ (343.46).

N'-*tert*-Butoxycarbonyl-*S*-methyl-*N*-(2-phenylethyl)carbamoylisothiourea (3.071) *(Synthesized by Sabrina Biselli and Claudia Honisch)*

The title compound was prepared from phenethylisocyanate (**3.039**, 258 mg, 1.75 mmol), **3.008** (500 mg, 2.63 mmol) and NEt$_3$ (0.55 mL, 3.94 mmol) according to the general procedure (method B) (EtOAc/PE 0/100-15/85 in 35 min, R$_f$ = 0.73 in EtOAc/PE 1/3) yielding a white solid (0.43 g, 73%), mp 102 – 104 °C. ^{1}H NMR (400 MHz, CDCl$_3$): δ (ppm) 12.32 (br s, 1H), 7.34 – 7.17 (m, 5H), 3.52 – 3.47 (m, 2H), 2.86 (t, *J* = 7.2 Hz, 2H), 2.29 (s, 3H), 1.49 (s, 9H). ^{13}C NMR (100 MHz, CDCl$_3$): δ (ppm) 168.90, 161.70, 151.10, 138.80, 128.80, 128.60, 126.50, 82.80, 41.40, 35.90, 28.10, 14.40. HRMS (ESI-MS): *m/z* [M+H$^+$] calculated for C$_{16}$H$_{24}$N$_3$O$_3$S$^+$: 338.1533, found 338.1546; C$_{16}$H$_{23}$N$_3$O$_3$S (337.44).

N'-*tert*-Butoxycarbonyl-*S*-methyl-*N*-(2,2-diphenylethyl)carbamoylisothiourea (3.072) *(Synthesized by Steffen Pockes)*

The reaction was carried out with 15% phosgene in toluene (1.22 mL, 1.71 mmol), 2,2-diphenylethan-1-amine (**3.031**, 0.34 g, 1.71 mmol), DIPEA (0.92 mL, 5.12 mmol), **3.008** (0.65 g, 3.42 mmol) and a total of 60 mL DCM according to the general procedure (method A) (R$_f$ = 0.60 in DCM) yielding a colorless foamlike solid (0.34 g, 48%). ^{1}H NMR (300 MHz, CDCl$_3$) δ (ppm) 12.27 (br s, 1H), 7.39 – 7.17 (m, 10H), 5.54 (br s, 1H), 4.22 (t, *J* = 7.8 Hz, 1H), 3.88 (dd, *J* = 7.9, 6.1 Hz, 2H), 2.23 (s, 3H), 1.49 (s, 9H). ^{13}C NMR (75 MHz, CDCl$_3$) δ (ppm) 167.75, 161.75, 151.10, 141.90, 128.76, 128.08, 126.85, 82.73, 50.76, 44.61, 28.06, 14.34. HRMS (ESI-MS): *m/z* [M+H$^+$] calculated for C$_{22}$H$_{28}$N$_3$O$_3$S$^+$: 414.1846, found 414.1852; C$_{22}$H$_{27}$N$_3$O$_3$S (413.54).

N'-*tert*-Butoxycarbonyl-*S*-methyl-*N*-(2-cyclohexylpropyl)carbamoylisothiourea (3.073) *(Synthesized by Sabrina Biselli)*

3.073 was prepared from 3-cyclohexyl butanoic acid (**3.040**, 150 mg, 0.88 mmol), oxalyl chloride (168 mg, 1.32 mmol), sodium azide (137 mg, 2.11 mmol), **3.008** (167 mg, 0.88 mmol) and NEt$_3$ (0.61 mL, 4.41 mmol) according to general procedure (method C) (R$_f$ = 0.81 in EtOAc/PE 1/3) yielding a colorless oil (210 mg, 67%). ^{1}H NMR (300 MHz, CDCl$_3$): δ (ppm) 12.43 (br s, 1H), 3.30 – 3.22 (m, 1H), 3.09-2.99 (m, 1H),

2.37 (br s, 3H), 1.76 – 1.62 (m, 6H), 1.48 (s, 9H), 1.30 – 0.97 (m, 6H), 0.89 (d, J = 6.9 Hz, 3H). ^{13}C NMR (100 MHz, CDCl$_3$): δ (ppm) 167.20, 162.20, 151.30, 82.60, 44.10, 40.60, 38.70, 30.90, 28.60, 28.10, 26.80, 26.74, 26.67, 14.50, 14.40. HRMS (ESI-MS): m/z [M+H$^+$] calculated for C$_{17}$H$_{32}$N$_3$O$_3$S$^+$: 358.2159, found 358.2199; C$_{17}$H$_{31}$N$_3$O$_3$S (357.51).

(*R*)-*N'*-*tert*-Butoxycarbonyl-*S*-methyl-*N*-(2-phenylpropyl)carbamoylisothiourea (3.074) *(Synthesized by Steffen Pockes)*

The reaction was carried out with 15% phosgene in toluene (1.22 mL, 1.71 mmol), (*R*)-2-phenylpropan-1-amine (**3.032**, 0.23 g, 1.71 mmol), DIPEA (0.92 mL, 5.12 mmol), **3.008** (0.65 g, 3.42 mmol) and a total of 60 mL DCM according to the general procedure (method A) (R$_f$ = 0.53 in DCM) yielding a colorless foamlike solid (0.48 g, 80%). ^{1}H NMR (300 MHz, CDCl$_3$) δ (ppm) 12.28 (br s, 1H), 7.37 – 7.18 (m, 5H), 5.53 (br s, 1H), 3.57 – 3.21 (m, 2H), 3.05 - 2.93 (m, 1H), 2.33 (s, 3H), 1.50 (s, 9H), 1.30 (d, J = 7.1 Hz, 3H). ^{13}C NMR (75 MHz, CDCl$_3$) δ (ppm) 170.10, 162.40, 151.07, 144.09, 128.69, 127.21, 126.70, 83.35, 46.96, 39.90, 28.02, 19.30, 14.34. HRMS (ESI-MS): m/z [M+H$^+$] calculated for C$_{17}$H$_{26}$N$_3$O$_3$S$^+$: 352.1689, found 352.1697; C$_{17}$H$_{25}$N$_3$O$_3$S (351.47).

(*S*)-*N'*-*tert*-Butoxycarbonyl-*S*-methyl-*N*-(2-phenylpropyl)carbamoylisothiourea (3.075) *(Synthesized by Steffen Pockes)*

The reaction was carried out with 15% phosgene in toluene (1.22 mL, 1.71 mmol), (*S*)-2-phenylpropan-1-amine (**3.033**, 0.23 g, 1.71 mmol), DIPEA (0.92 mL, 5.12 mmol), **3.008** (0.65 g, 3.42 mmol) and a total of 60 mL DCM according to the general procedure (method A) (R$_f$ = 0.53 in DCM) yielding a colorless foamlike solid (0.42 g, 70%). ^{1}H NMR (300 MHz, CDCl$_3$) δ (ppm) 12.29 (br s, 1H), 7.37 – 7.19 (m, 5H), 5.48 (br s, 1H), 3.58 – 3.23 (m, 2H), 3.05 – 2.91 (m, 1H), 2.25 (s, 3H), 1.48 (s, 9H), 1.30 (d, J = 7.1 Hz, 3H). ^{13}C NMR (75 MHz, CDCl$_3$) δ (ppm) 167.53, 161.87, 151.12, 144.10, 128.70, 127.21, 126.70, 82.64, 46.95, 39.91, 28.05, 19.31, 14.31. HRMS (ESI-MS): m/z [M+H$^+$] calculated for C$_{17}$H$_{26}$N$_3$O$_3$S$^+$: 352.1689, found 352.1694; C$_{17}$H$_{25}$N$_3$O$_3$S (351.47).

N'-*tert*-Butoxycarbonyl-*S*-methyl-*N*-(2-phenylbutyl)carbamoylisothiourea (3.076) *(Synthesized by Sabrina Biselli)*

3.076 was prepared from 3-phenyl pentanoic acid (**3.041**, 150 mg, 0.84 mmol), oxalyl chloride (160 mg, 1.26 mmol), sodium azide (131 mg, 2.02 mmol), **3.008** (160 mg, 0.84 mmol) and NEt₃ (0.59 mL, 4.21 mmol) according to general procedure (method C) (R$_f$ = 0.71 in EtOAc/PE 1/3) yielding a colorless oil (190 mg, 62%). ^{1}H NMR (300 MHz, CDCl₃): δ (ppm) 12.53 (br s, 1H), 7.36 – 7.15 (m, 5H), 3.65 – 3.56 (m, 1H), 3.33 – 3.25 (m, 1H), 2.76 – 2.66 (m, 1H), 2.37 (br s, 3H), 1.85 – 1.48 (m, 11H), 0.82 (t, *J* = 7.4 Hz, 3H). ^{13}C NMR (100 MHz, CDCl₃): δ (ppm) 167.50, 162.00, 151.30, 142.60, 128.80, 128.00, 126.80, 82.70, 47.80, 45.70, 28.20, 26.80, 14.40, 12.00. HRMS (ESI-MS): *m/z* [M+H$^+$] calculated for $C_{18}H_{28}N_3O_3S^+$: 366.1846, found 366.1895; $C_{18}H_{27}N_3O_3S$ (365.49).

N'-*tert*-Butoxycarbonyl-*S*-methyl-*N*-(3-methyl-2-phenylbutyl)carbamoylisothiourea (3.077) *(Synthesized by Sabrina Biselli)*

3.077 was prepared from 4-methyl-3-phenyl pentanoic acid (**3.042**, 150 mg, 0.78 mmol), oxalyl chloride (149 mg, 1.17 mmol), sodium azide (122 mg, 1.87 mmol), **3.008** (148 mg, 0.78 mmol) and NEt₃ (0.54 mL, 3.90 mmol) according to general procedure (method C) (R$_f$ = 0.81 in EtOAc/PE 1/3) yielding a colorless oil (130 mg, 44%). ^{1}H NMR (300 MHz, CDCl₃): δ (ppm) 12.36 (br s, 1H), 7.35 – 7.10 (m, 5H), 3.88 – 3.79 (m, 1H), 3.37 – 3.25 (m, 1H), 2.58 – 2.50 (m, 1H), 2.24 (s, 3H), 1.97 – 1.85 (m, 1H), 1.48 (s, 9H), 1.02 (d, *J* = 6.7 Hz, 3H), 0.75 (d, *J* = 6.7 Hz, 3H). ^{13}C NMR (100 MHz, CDCl₃): δ (ppm) 167.70, 161.40, 151.00, 141.60, 128.54, 128.48, 126.70, 82.80, 52.60, 43.10, 31.50, 28.00, 20.90, 20.50, 14.40. HRMS (ESI-MS): *m/z* [M+H$^+$] calculated for $C_{19}H_{30}N_3O_3S^+$: 380.2002, found 380.2034; $C_{19}H_{29}N_3O_3S$ (379.52).

N'-*tert*-Butoxycarbonyl-*S*-methyl-*N*-(2-(4-prop-2-ylphenyl)propyl)carbamoylisothiourea (3.078) *(Synthesized by Sabrina Biselli)*

3.078 was prepared from 3-(4-prop-2-ylphenyl) butanoic acid (**3.043**, 150 mg, 0.73 mmol), oxalyl chloride (138 mg, 1.09 mmol), sodium azide (114 mg, 1.75 mmol), **3.008** (138 mg, 0.73 mmol) and NEt₃ (0.51 mL, 3.64 mmol) according to general procedure (method C) (R$_f$ = 0.74 in EtOAc/PE 1/3) yielding a colorless oil (220 mg, 77%). ^{1}H NMR (300 MHz, CDCl₃): δ (ppm) 12.37 (br s, 1H), 7.21 – 7.12 (m, 4H), 3.53 – 3.44 (m, 1H), 3.33 – 3.24 (m, 1H), 2.99 – 2.85 (m, 2H), 2.29 (br s, 3H), 1.48 (s, 9H), 1.30 – 1.24 (m,

9H). ^{13}C NMR (100 MHz, CDCl₃): δ (ppm) 167.50, 162.10, 151.20, 147.30, 141.50, 127.20, 126.80, 82.70, 47.10, 39.60, 33.80, 28.23, 28.15, 24.10, 19.40, 14.40. HRMS (ESI-MS): *m/z* [M+H$^+$] calculated for $C_{20}H_{32}N_3O_3S^+$: 394.2159, found 394.2159; $C_{20}H_{31}N_3O_3S$ (393.55).

N'-*tert*-Butoxycarbonyl-*S*-methyl-*N*-(3-cyclohexyl-2-metylpropyl)carbamoylisothiourea (3.079) *(Synthesized by Sabrina Biselli)*

3.079 was prepared from 4-cyclohexyl-3-metyl butanoic acid (**3.044**, 150 mg, 0.76 mmol), oxalyl chloride (144 mg, 1.13 mmol), sodium azide (118 mg, 1.82 mmol), **3.008** (144 mg, 0.76 mmol) and NEt₃ (0.53 mL, 3.78 mmol) according to general procedure (method C) (R_f = 0.72 in EtOAc/PE 1/3) yielding a colorless oil (110 mg, 38%). ^{1}H NMR (300 MHz, CDCl₃): δ (ppm) 13.08 (br s, 1H), 3.24 – 2.97 (m, 2H), 2.68 (br s, 2H), 1.83 – 1.49 (m, 16H), 1.34 – 1.14 (m, 5H), 1.06 – 0.99 (m, 1H), 0.95 – 0.79 (m, 5H). ^{13}C NMR (75 MHz, CDCl₃): δ (ppm) 168.2, 162.0, 150.9, 83.6, 46.6, 42.4, 34.8, 34.2, 32.9, 30.3, 28.0, 26.7, 26.4, 26.3, 17.9, 14.6. HRMS (ESI-MS): *m/z* [M+H$^+$] calculated for $C_{18}H_{34}N_3O_3S^+$: 372.2315, found 372.2321; $C_{18}H_{33}N_3O_3S$ (371.54).

N'-*tert*-Butoxycarbonyl-*S*-methyl-*N*-(2-metyl-3-(4-methylphenyl)propyl)carbamoylisothiourea (3.080) *(Synthesized by Sabrina Biselli)*

3.080 was prepared from 3-methyl 4-(4-methylphenyl) butanoic acid (**3.045**, 100 mg, 0.52 mmol), oxalyl chloride (99 mg, 0.75 mmol), sodium azide (85 mg, 1.30 mmol), **3.008** (100 mg, 0.52 mmol) and NEt₃ (0.36 mL, 2.60 mmol) according to general procedure (method C) (R_f = 0.80 in EtOAc/PE 1/3) yielding a colorless oil (140 mg, 71%). ^{1}H NMR (400 MHz, CDCl₃): δ (ppm) 12.36 (br s, 1H), 7.10 – 7.04 (m, 4H), 3.22 – 3.08 (m, 2H), 2.68 – 2.63 (m, 1H), 2.44 – 2.39 (m, 1H), 2.33 – 2.31 (m, 6H), 2.04 – 1.92 (m, 1H), 1.48 (s, 9H), 0.92 (d, *J* = 6.5 Hz, 3H). ^{13}C NMR (75 MHz, CDCl₃): δ (ppm) 167.20, 162.00, 151.20, 137.10, 135.50, 129.00, 128.90, 82.60, 46.00, 40.80, 35.70, 28.00, 21.00, 17.70, 14.30. HRMS (ESI-MS): *m/z* [M+H$^+$] calculated for $C_{19}H_{30}N_3O_3S^+$: 380.2002, found 380.2009; $C_{19}H_{29}N_3O_3S$ (379.52).

N'-tert-Butoxycarbonyl-S-methyl-N-(2-metyl-4-phenylbutyl)carbamoylisothiourea (3.081) *(Synthesized by Sabrina Biselli)*

3.081 was prepared from 3-methyl 5-phenyl pentanoic acid (**3.046**, 150 mg, 0.78 mmol), oxalyl chloride (149 mg, 1.17 mmol), sodium azide (122 mg, 1.87 mmol), **3.008** (148 mg, 0.78 mmol) and NEt$_3$ (0.54 mL, 3.90 mmol) according to general procedure (method C) (R$_f$ = 0.66 in EtOAc/PE 1/3) yielding a colorless oil (220 mg, 74%). ^{1}H NMR (300 MHz, CDCl$_3$): δ (ppm) 12.40 (br s, 1H), 7.31 – 7.15 (m, 5H), 3.25 – 3.05 (m, 2H), 2.77 – 2.55 (m, 2H), 2.35 (br s, 3H), 1.78 – 1.62 (m, 2H), 1.51 – 1.43 (m, 10H), 1.01 (d, *J* = 6.6 Hz, 3H). ^{13}C NMR (100 MHz, CDCl$_3$): δ (ppm) 167.40, 162.20, 151.30, 142.50, 128.49, 128.46, 125.90, 82.70, 46.10, 36.30, 33.40, 33.30, 28.20, 17.70, 14.40. HRMS (ESI-MS): *m/z* [M+H$^+$] calculated for C$_{19}$H$_{30}$N$_3$O$_3$S$^+$: 380.2002, found 380.2025; C$_{19}$H$_{29}$N$_3$O$_3$S (379.52).

N'-tert-Butoxycarbonyl-S-methyl-N-(2-metyl-5-phenylpentyl)carbamoylisothiourea (3.082) *(Synthesized by Katharina Tropmann)*

3.082 was prepared from 3-methyl 6-phenyl hexanoic acid (**3.047**, 200 mg, 0.97 mmol), oxalyl chloride (185 mg, 1.45 mmol), sodium azide (151 mg, 2.33 mmol), **3.008** (184 mg, 0.97 mmol) and NEt$_3$ (0.67 mL, 4.85 mmol) according to general procedure (method C) (R$_f$ = 0.40 in EtOAc/PE 1/9) yielding a white foam-like solid (300 mg, 79%). ^{1}H NMR (300 MHz, CDCl$_3$) δ (ppm) 12.33 (s, 1H), 7.32 – 7.12 (m, 5H), 5.56 (t, *J* = 6.3 Hz, 1H), 3.24 – 2.95 (m, 2H), 2.70 – 2.49 (m, 2H), 2.30 (s, 3H), 1.83 – 1.54 (m, 3H), 1.53 – 1.04 (m, 11H), 0.92 (d, *J* = 6.7 Hz, 3H). ^{13}C NMR (75 MHz, CDCl$_3$) δ (ppm) 167.37, 162.20, 151.29, 142.57, 128.50, 128.41, 125.84, 82.67, 46.26, 36.20, 34.04, 33.52, 28.92, 28.17, 17.73, 14.42. HRMS (ESI-MS): *m/z* [M+H$^+$] calculated for C$_{20}$H$_{32}$N$_3$O$_3$S$^+$: 394.2159, found 394.2167; C$_{20}$H$_{31}$N$_3$O$_3$S (393.55).

3.5.1.6 Synthesis and Analytical Data of the Isothiocyanates 3.083-3.088

A solution of the respective amine (**3.014**-**3.016** or **3.031**-**3.033**, 1 eq) in DCM was added to a saturated solution of NaHCO$_3$ at rt. Subsequently, thiophosgene (1.1 eq) was added dropwise and the reaction was stirred vigorously for 30 min at rt. The organic layer was washed with H$_2$O and brine and dried over Na$_2$SO$_4$. The solvent was removed under reduced pressure and the crude product was purified with column chromatography (EtOAc/PE 5/95).

(Isothiocyanatomethylene)dibenzene (3.083) *(Synthesized by Steffen Pockes)*

The product was prepared from diphenylmethanamine (**3.014**, 0.31 g, 1.71 mmol) and thiophosgene (144 µL, 1.88 mmol) in DCM (20 mL) and a saturated solution of NaHCO$_3$ (20 mL) according to the general procedure (R$_f$ = 0.55 in EtOAc/PE 5/95). The desired compound **3.083** was isolated as an orange oil (0.37 g, 96%). ^{1}H NMR (300 MHz, CDCl$_3$) δ (ppm) 7.43 – 7.29 (m, 10H), 6.00 (s, 1H). ^{13}C NMR (75 MHz, CDCl$_3$) δ (ppm) 139.21, 130.11, 128.97, 128.36, 126.63, 64.61. MS (APCI-MS): *m/z* [M+H$^+$-H$_2$] 224.1434; C$_{14}$H$_{11}$NS (225.31).

(R)-(1-Isothiocyanatoethyl)benzene (3.084) *(Synthesized by Steffen Pockes)*

The product was prepared from (*R*)-1-phenylethan-1-amine (**3.015**, 0.21 g, 1.71 mmol) and thiophosgene (144 µL, 1.88 mmol) in DCM (20 mL) and a saturated solution of NaHCO$_3$ (20 mL) according to the general procedure (R$_f$ = 0.63 in EtOAc/PE 5/95). The desired compound **3.084** was isolated as an orange oil (0.17 g, 61%). ^{1}H NMR (300 MHz, CDCl$_3$) δ (ppm) 7.44 – 7.29 (m, 5H), 4.92 (q, *J* = 6.8 Hz, 1H), 1.68 (d, *J* = 6.8 Hz, 3H). ^{13}C NMR (75 MHz, CDCl$_3$) δ (ppm) 140.18, 132.30, 128.95, 128.25, 125.46, 57.07, 25.03. HRMS (EI-MS): *m/z* [M$^{•+}$] calculated for C$_9$H$_9$NS$^{•+}$: 163.0450, found 163.0454; C$_9$H$_9$NS (163.24).

(S)-(1-Isothiocyanatoethyl)benzene (3.085) *(Synthesized by Steffen Pockes)*

The product was prepared from (*S*)-1-phenylethan-1-amine (**3.016**, 0.21 g, 1.71 mmol) and thiophosgene (144 µL, 1.88 mmol) in DCM (20 mL) and a saturated solution of NaHCO$_3$ (20 mL) according to the general procedure (R$_f$ = 0.62 in EtOAc/PE 5/95). The desired compound **3.085** was isolated as an orange oil (0.06 g, 21%). ^{1}H NMR (300 MHz, CDCl$_3$) δ (ppm) 7.45 – 7.28 (m, 5H), 4.92 (q, *J* = 6.8 Hz, 1H), 1.68 (d, *J* = 6.8 Hz, 3H). ^{13}C NMR (75 MHz, CDCl$_3$) δ (ppm) 140.18, 132.06, 128.94, 128.25, 125.46, 57.07, 25.03. HRMS (EI-MS): *m/z* [M$^{•+}$] calculated for C$_9$H$_9$NS$^{•+}$: 163.0450, found 163.0454; C$_9$H$_9$NS (163.24).

(2-Isothiocyanatoethane-1,1-diyl)dibenzene (3.086) *(Synthesized by Steffen Pockes)*

The product was prepared from 2,2-diphenylethan-1-amine (**3.031**, 0.34 g, 1.71 mmol) and thiophosgene (144 µL, 1.88 mmol) in DCM (20 mL) and a saturated solution of NaHCO$_3$ (20 mL) according to the general procedure (R$_f$ = 0.52 in EtOAc/PE 5/95).

The desired compound **3.086** was isolated as an orange oil (0.40 g, 98%). ^{1}H NMR (300 MHz, CDCl$_3$) δ (ppm) 7.42 – 7.19 (m, 10H), 4.38 (t, *J* = 7.5 Hz, 1H), 4.09 (d, *J* = 7.5 Hz, 2H). ^{13}C NMR (75 MHz, CDCl$_3$) δ (ppm) 140.29, 131.82, 128.90, 127.98, 127.40, 51.43, 49.39. HRMS (EI-MS): *m/z* [M$^{•+}$] calculated for C$_{15}$H$_{13}$NS$^{•+}$: 239.0763, found 239.0756; C$_{15}$H$_{13}$NS (239.34).

(*R*)-(1-Isothiocyanatopropan-2-yl)benzene (3.087) *(Synthesized by Steffen Pockes)*

The product was prepared from (*R*)-2-phenylpropan-1-amine (**3.032**, 0.23 g, 1.71 mmol) and thiophosgene (144 µL, 1.88 mmol) in DCM (20 mL) and a saturated solution of NaHCO$_3$ (20 mL) according to the general procedure (R$_f$ = 0.58 in EtOAc/PE 5/95). The desired compound **3.087** was isolated as an orange oil (0.18 g, 59%). ^{1}H NMR (300 MHz, CDCl$_3$) δ (ppm) 7.42 – 7.17 (m, 5H), 3.72 – 3.54 (m, 2H), 3.20 – 3.08 (m, 1H), 1.40 (d, *J* = 7.0 Hz, 3H). ^{13}C NMR (75 MHz, CDCl$_3$) δ (ppm) 142.13, 130.68, 128.83, 127.34, 127.09, 51.96, 40.63, 18.47. HRMS (EI-MS): *m/z* [M$^{•+}$] calculated for C$_{10}$H$_{11}$NS$^{•+}$: 177.0607, found 177.0611; C$_{10}$H$_{11}$NS (177.27).

(*S*)-(1-Isothiocyanatopropan-2-yl)benzene (3.088) *(Synthesized by Steffen Pockes)*

The product was prepared from (*S*)-2-phenylpropan-1-amine (**3.033**, 0.23 g, 1.71 mmol) and thiophosgene (144 µL, 1.88 mmol) in DCM (20 mL) and a saturated solution of NaHCO$_3$ (20 mL) according to the general procedure (R$_f$ = 0.58 in EtOAc/PE 5/95). The desired compound **3.088** was isolated as an orange oil (0.25 g, 82%). ^{1}H NMR (300 MHz, CDCl$_3$) δ (ppm) 7.47 – 7.17 (m, 5H), 3.75 – 3.52 (m, 2H), 3.19 – 3.08 (m, 1H), 1.40 (d, *J* = 6.9 Hz, 3H). ^{13}C NMR (75 MHz, CDCl$_3$) δ (ppm) 142.12, 130.73, 128.83, 127.34, 127.09, 51.96, 40.63, 18.46. HRMS (EI-MS): *m/z* [M$^{•+}$] calculated for C$_{10}$H$_{11}$NS$^{•+}$: 177.0607, found 177.0607; C$_{10}$H$_{11}$NS (177.27).

3.5.1.7 Synthesis and Analytical Data for the Guanidinylation Reaction of 3.089-3.123 and 3.130-3.137

The general procedure for the synthesis of **3.089**-**3.123** and **3.130**-**3.137** is described in the literature.[299,460] The precursor amine **3.009a** was synthesized as described by Kraus et al. (2009)[302] For the synthesis of precursor amines **3.009b**, **3.011**, and **3.012** see in the Schemes 3.04 and 3.05 (chapter **3.5.1.3**). The compounds **3.089-3.094**, **3.112**, **3.114**, **3.117-3.123**, and **3.130-3.137** were directly Boc- or Trt-deprotected as described in the general procedure for the preparation of the title compounds without

analytical characterization of the Boc-/Trt-protected intermediates. The used amounts of the respective substrates and reagents are described in the characterization of **3.138**-**3.143**, **3.161**, **3.163**, **3.166-3.172**, and **3.179-3.186**, respectively.

1-(*tert*-Butoxycarbonylamino((3-(2-*tert*-butoxycarbonylamino-4-methylthiazol-5-yl)propyl)amino)methylene)-3-(diphenylmethyl)urea (3.095) *(Synthesized by Steffen Pockes)*

Compound **3.095** was prepared from **3.009a** (0.14 g, 0.50 mmol), **3.054** (0.21 g, 0.50 mmol), HgCl$_2$ (0.14 g, 0.50 mmol), and NEt$_3$ (0.21 mL, 1.50 mmol) in DCM (10 mL) conforming to the general procedure (R$_f$ = 0.59 in DCM/MeOH/NH$_3$ 99/1/0.1) yielding a yellow oil (0.12 g, 39%). ^{1}H NMR (300 MHz, CDCl$_3$) δ (ppm) 12.06 (br s, 1H), 10.45 (br s, 1H), 8.16 (br s, 1H), 7.37 – 7.17 (m, 10H), 6.04 (d, *J* = 7.6 Hz, 1H), 5.94 (br s, 1H), 3.36 (q, *J* = 6.3 Hz, 2H), 2.71 (t, *J* = 7.3 Hz, 2H), 2.21 (s, 3H), 1.87 (p, *J* = 7.1 Hz, 2H), 1.51 (s, 9H), 1.44 (s, 9H). ^{13}C NMR (75 MHz, CDCl$_3$) δ (ppm) 163.83, 157.55, 154.66, 153.40, 152.72, 142.35, 142.02, 128.61, 127.41, 127.23, 123.17, 82.50, 82.20, 58.06, 39.69, 30.78, 28.28, 28.06, 23.31, 14.51. HRMS (ESI-MS): *m/z* [M+H$^+$] calculated for C$_{32}$H$_{43}$N$_6$O$_5$S$^+$: 623.3010, found 623.3023; C$_{32}$H$_{42}$N$_6$O$_5$S (622.79).

(*R*)-1-(*tert*-Butoxycarbonylamino((3-(2-*tert*-butoxycarbonylamino-4-methylthiazol-5-yl)propyl)amino)methylene)-3-(1-phenylethyl)urea (3.096) *(Synthesized by Steffen Pockes)*

Compound **3.096** was prepared from **3.009a** (1.29 g, 4.75 mmol), **3.055** (1.60 g, 4.75 mmol), HgCl$_2$ (1.29 g, 4.75 mmol), and NEt$_3$ (1.98 mL, 14.25 mmol) in DCM (50 mL) conforming to the general procedure (R$_f$ = 0.45 in DCM/MeOH/NH$_3$ 99/1/0.1) yielding a yellow oil (2.02 g, 76%). ^{1}H NMR (300 MHz, CDCl$_3$) δ (ppm) 12.08 (br s, 1H), 10.33 (br s, 1H), 8.12 (br s, 1H), 7.42 – 7.13 (m, 5H), 5.59 (br s, 1H), 4.91 (p, *J* = 7.1 Hz, 1H), 3.35 (q, *J* = 6.6 Hz, 2H), 2.71 (t, *J* = 7.3 Hz, 2H), 2.23 (s, 3H), 1.87 (p, *J* = 7.2 Hz, 2H), 1.51 (s, 9H), 1.47 (d, *J* = 7.0 Hz, 3H), 1.44 (s, 9H). ^{13}C NMR (75 MHz, CDCl$_3$) δ (ppm) 163.84, 157.50, 154.45, 153.42, 152.69, 144.52, 142.00, 128.57, 126.95, 125.92, 123.25, 82.45, 82.22, 49.57, 39.61, 30.76, 28.27, 28.06, 23.27, 22.81, 14.54. HRMS (ESI-MS): *m/z* [M+H$^+$] calculated for C$_{27}$H$_{41}$N$_6$O$_5$S$^+$: 561.2854, found 561.2863; C$_{27}$H$_{40}$N$_6$O$_5$S (560.71).

(*S*)-1-(*tert*-Butoxycarbonylamino((3-(2-*tert*-butoxycarbonylamino-4-methylthiazol-5-yl)propyl)amino)methylene)-3-(1-phenylethyl)urea (3.097)

(Synthesized by Steffen Pockes)

Compound **3.097** was prepared from **3.009a** (0.14 g, 0.50 mmol), **3.056** (0.17 g, 0.50 mmol), HgCl$_2$ (0.14 g, 0.50 mmol), and NEt$_3$ (0.21 mL, 1.50 mmol) in DCM (10 mL) conforming to the general procedure (R$_f$ = 0.45 in DCM/MeOH/NH$_3$ 99/1/0.1) yielding a yellow oil (0.22 g, 78%). ^{1}H NMR (300 MHz, CDCl$_3$) δ (ppm) 12.09 (br s, 1H), 11.02 (br s, 1H), 8.11 (t, *J* = 5.7 Hz, 1H), 7.39 – 7.13 (m, 5H), 5.65 (d, *J* = 7.7 Hz, 1H), 4.90 (p, *J* = 7.1 Hz, 1H), 3.34 (q, *J* = 6.6 Hz, 2H), 2.70 (t, *J* = 7.3 Hz, 2H), 2.23 (s, 3H), 1.87 (p, *J* = 7.2 Hz, 2H), 1.51 (s, 9H), 1.46 (d, *J* = 7.2 Hz, 3H), 1.44 (s, 9H). ^{13}C NMR (75 MHz, CDCl$_3$) δ (ppm) 163.86, 157.97, 154.48, 153.43, 152.91, 144.55, 141.94, 128.56, 126.94, 125.91, 123.07, 82.38, 82.10, 49.55, 39.56, 30.76, 28.29, 28.06, 23.26, 22.80, 14.51. HRMS (ESI-MS): *m/z* [M+H$^+$] calculated for C$_{27}$H$_{41}$N$_6$O$_5$S$^+$: 561.2854, found 561.2855; C$_{27}$H$_{40}$N$_6$O$_5$S (560.71).

1-(*tert*-Butoxycarbonylamino((3-(2-*tert*-butoxycarbonylamino-4-methylthiazol-5-yl)propyl)amino)methylene)-3-(2,2,2-trifluoro-1-phenylethyl)urea (3.098)

Compound **3.098** was prepared from **3.009a** (0.25 g, 0.92 mmol), **3.057** (0.30 g, 0.92 mmol), HgCl$_2$ (0.25 g, 0.92 mmol), and NEt$_3$ (0.38 mL, 2.75 mmol) in DCM (10 mL) conforming to the general procedure (R$_f$ = 0.14 in DCM/MeOH/NH$_3$ 99/1/0.1) yielding a colorless oil (0.36 g, 86%). ^{1}H NMR (400 MHz, CDCl$_3$) δ (ppm) 11.81 (s, 1H), 9.61 (s, 1H), 8.24 (t, *J* = 5.6 Hz, 1H), 7.43 – 7.33 (m, 5H), 5.87 (d, *J* = 9.8 Hz, 1H), 5.51 (p, *J* = 8.3 Hz, 1H), 3.37 (q, *J* = 6.6 Hz, 2H), 2.71 (t, *J* = 7.2 Hz, 2H), 2.21 (s, 3H), 1.87 (p, *J* = 7.1 Hz, 2H), 1.51 (s, 9H), 1.46 (s, 9H). ^{13}C NMR (101 MHz, CDCl$_3$) δ (ppm) 163.58, 157.14, 155.14, 153.24, 152.41, 141.96, 133.74, 128.93, 128.81, 127.93, 126.97 (d, *J* = 149.8 Hz),123.23, 82.86, 55.34 (q, *J* = 32.1 Hz), 39.69, 30.68, 28.21, 28.03, 23.25, 14.46. HRMS (ESI-MS): *m/z* [M+H$^+$] calculated for C$_{27}$H$_{38}$F$_3$N$_6$O$_5$S$^+$: 615.2571, found 615.2583; C$_{27}$H$_{37}$F$_3$N$_6$O$_5$S (614.69).

1-(*tert*-Butoxycarbonylamino((3-(2-*tert*-butoxycarbonylamino-4-methylthiazol-5-yl)propyl)amino)methylene)-3-(1-(phenyl)propyl)urea (3.099)

Compound **3.099** was prepared from **3.009a** (0.14 g, 0.50 mmol), **3.058** (0.18 g, 0.50 mmol), HgCl$_2$ (0.14 g, 0.50 mmol), and NEt$_3$ (0.21 mL, 1.50 mmol) in DCM (10 mL) conforming to the general procedure (R$_f$ = 0.14 in DCM/MeOH/NH$_3$ 99/1/0.1)

yielding a colorless oil (60 mg, 21%). ^{1}H NMR (300 MHz, CDCl$_3$) δ (ppm) 12.09 (s, 1H), 10.47 (s, 1H), 8.11 (s, 1H), 7.27 – 7.07 (m, 4H), 5.61 (s, 1H), 4.65 (q, *J* = 7.5 Hz, 1H), 3.34 (t, *J* = 6.4 Hz, 2H), 2.70 (t, *J* = 7.3 Hz, 2H), 2.23 (s, 3H), 1.90 – 1.83 (m, 2H), 1.81 – 1.75 (m, 2H), 1.51 (s, 9H), 1.48 (d, *J* = 2.0 Hz, 3H), 1.43 (s, 9H), 0.85 (t, *J* = 6.7 Hz, 3H). ^{13}C NMR (75 MHz, CDCl$_3$) δ (ppm) 164.06, 157.59, 154.42, 153.42, 152.75, 143.38, 141.97, 128.49, 126.94, 126.44, 123.20, 82.16, 55.82, 39.56, 30.77, 29.91, 28.26, 28.05, 23.24, 14.52, 10.95. HRMS (ESI-MS): *m/z* [M+H$^+$] calculated for C$_{28}$H$_{43}$N$_6$O$_5$S$^+$: 575.3010, found 575.3021; C$_{28}$H$_{42}$N$_6$O$_5$S (574.74).

1-(*tert*-Butoxycarbonylamino((3-(2-*tert*-butoxycarbonylamino-4-methylthiazol-5-yl)propyl)amino)methylene)-3-(1-(phenyl)isobutyl)urea (3.100)

Compound **3.100** was prepared from **3.009a** (0.17 g, 0.61 mmol), **3.059** (0.30 g, 0.61 mmol), HgCl$_2$ (0.17 g, 0.61 mmol), and NEt$_3$ (0.26 mL, 1.84 mmol) in DCM (10 mL) conforming to the general procedure (R$_f$ = 0.21 in DCM/MeOH/NH$_3$ 99/1/0.1) yielding a colorless oil (0.27 g, 89%). ^{1}H NMR (300 MHz, CDCl$_3$) δ (ppm) 12.09 (s, 1H), 10.30 (s, 1H), 8.08 (t, *J* = 5.5 Hz, 1H), 7.35 – 7.13 (m, 5H), 5.62 (d, *J* = 8.9 Hz, 1H), 4.61 – 4.47 (m, 1H), 3.46 – 3.30 (m, 2H), 2.71 (t, *J* = 7.3 Hz, 2H), 2.24 (s, 3H), 2.10 – 1.95 (m, 1H), 1.87 (p, *J* = 7.2 Hz, 2H), 1.51 (s, 9H), 1.42 (s, 9H), 0.96 (d, *J* = 6.7 Hz, 3H), 0.83 (d, *J* = 6.8 Hz, 4H). ^{13}C NMR (75 MHz, CDCl$_3$) δ (ppm) 164.31, 157.44, 154.40, 153.43, 142.63, 142.01, 128.29, 126.89, 126.78, 123.31, 82.29, 59.94, 39.51, 33.74, 30.80, 28.28, 28.06, 23.26, 19.92, 18.84, 14.55. HRMS (ESI-MS): *m/z* [M+H$^+$] calculated for C$_{29}$H$_{45}$N$_6$O$_5$S$^+$: 589.3167, found 589.3177; C$_{29}$H$_{44}$N$_6$O$_5$S (588.77).

1-(*tert*-Butoxycarbonylamino((3-(2-*tert*-butoxycarbonylamino-4-methylthiazol-5-yl)propyl)amino)methylene)-3-(1-(*p*-tolyl)ethyl)urea (3.101)

Compound **3.101** was prepared from **3.009a** (0.14 g, 0.50 mmol), **3.060** (0.18 g, 0.50 mmol), HgCl$_2$ (0.14 g, 0.50 mmol), and NEt$_3$ (0.21 mL, 1.50 mmol) in DCM (10 mL) conforming to the general procedure (R$_f$ = 0.16 in DCM/MeOH/NH$_3$ 99/1/0.1) yielding a colorless oil (0.10 g, 35%). ^{1}H NMR (300 MHz, CDCl$_3$) δ (ppm) 12.10 (s, 1H), 10.72 (s, 1H), 8.09 (t, *J* = 5.5 Hz, 1H), 7.22 (d, *J* = 8.1 Hz, 2H), 7.12 (d, *J* = 8.1 Hz, 2H), 5.60 (d, *J* = 7.8 Hz, 1H), 4.86 (p, *J* = 7.0 Hz, 1H), 3.37 – 3.29 (m, 2H), 2.70 (t, *J* = 7.3 Hz, 2H), 2.31 (s, 3H), 2.23 (s, 3H), 1.86 (p, *J* = 7.2 Hz, 2H), 1.51 (s, 9H), 1.48 (d, *J* = 2.2 Hz, 3H), 1.44 (s, 9H). ^{13}C NMR (75 MHz, CDCl$_3$) δ (ppm) 163.87, 157.78, 154.44, 153.44, 152.83, 141.93, 141.60, 136.47, 129.23, 125.83, 123.14, 82.34, 49.32, 39.55,

30.76, 23.27, 21.06, 14.50. HRMS (ESI-MS): *m/z* [M+H$^+$] calculated for C$_{28}$H$_{43}$N$_6$O$_5$S$^+$: 575.3010, found 575.3017; C$_{28}$H$_{42}$N$_6$O$_5$S (574.74).

1-(*tert*-Butoxycarbonylamino((3-(2-*tert*-butoxycarbonylamino-4-methylthiazol-5-yl)propyl)amino)methylene)-3-(1-(4-fluorophenyl)ethyl)urea (3.102)

Compound **3.102** was prepared from **3.009a** (0.14 g, 0.50 mmol), **3.061** (0.18 g, 0.50 mmol), HgCl$_2$ (0.14 g, 0.50 mmol), and NEt$_3$ (0.21 mL, 1.50 mmol) in DCM (10 mL) conforming to the general procedure (R$_f$ = 0.12 in DCM/MeOH/NH$_3$ 99/1/0.1) yielding a colorless oil (60 mg, 21%). ^{1}H NMR (300 MHz, CDCl$_3$) δ (ppm) 12.04 (s, 1H), 10.51 (s, 1H), 8.14 (s, 1H), 7.30 – 7.25 (m, 2H), 7.02 – 6.95 (m, 2H), 5.65 (s, 1H), 4.87 (p, *J* = 7.1 Hz, 1H), 3.33 (t, *J* = 6.7 Hz, 2H), 2.70 (t, *J* = 7.3 Hz, 2H), 2.21 (s, 3H), 1.86 (p, *J* = 7.1 Hz, 2H), 1.50 (s, 9H), 1.44 (s, 3H), 1.43 (s, 9H). ^{13}C NMR (75 MHz, CDCl$_3$) δ (ppm) 163.79, 161.74 (d, *J* = 244.4 Hz), 157.61, 154.50, 153.37, 141.93, 140.37, 129.91, 127.42 (d, *J* = 8.0 Hz), 123.12, 115.27 (d, *J* = 21.3 Hz), 82.47, 48.93, 39.56, 30.72, 28.25, 28.04, 23.22, 22.87, 14.51. HRMS (ESI-MS): *m/z* [M+H$^+$] calculated for C$_{27}$H$_{40}$FN$_6$O$_5$S$^+$: 579.2759, found 579.2769; C$_{27}$H$_{39}$FN$_6$O$_5$S (578.70).

1-(*tert*-Butoxycarbonylamino((3-(2-*tert*-butoxycarbonylamino-4-methylthiazol-5-yl)propyl)amino)methylene)-3-(1-(4-chlorophenyl)ethyl)urea (3.103)

Compound **3.103** was prepared from **3.009a** (0.14 g, 0.50 mmol), **3.062** (0.19 g, 0.50 mmol), HgCl$_2$ (0.14 g, 0.50 mmol), and NEt$_3$ (0.21 mL, 1.50 mmol) in DCM (10 mL) conforming to the general procedure (R$_f$ = 0.12 in DCM/MeOH/NH$_3$ 99/1/0.1) yielding a colorless oil (0.11 g, 37%). ^{1}H NMR (300 MHz, CDCl$_3$) δ (ppm) 12.04 (s, 1H), 9.95 (s, 1H), 8.19 (s, 1H), 7.30 – 7.08 (m, 4H), 5.63 (s, 1H), 4.90 (p, *J* = 7.1 Hz, 1H), 3.38 (t, *J* = 6.8 Hz, 2H), 2.75 (t, *J* = 7.2 Hz, 2H), 2.26 (s, 3H), 1.91 (p, *J* = 7.1 Hz, 2H), 1.55 (s, 9H), 1.51 (d, *J* = 4.4 Hz, 3H), 1.47 (s, 9H). ^{13}C NMR (75 MHz, CDCl$_3$) δ (ppm) 161.30, 157.24, 154.51, 153.36, 146.55, 143.25, 142.00, 132.51, 128.77, 128.65, 127.39, 127.26, 123.24, 82.26, 49.08, 32.75, 30.73, 23.23, 22.81, 14.55. HRMS (ESI-MS): *m/z* [M+H$^+$] calculated for C$_{27}$H$_{40}$ClN$_6$O$_5$S$^+$: 595.2464, found 595.2475; C$_{27}$H$_{39}$ClN$_6$O$_5$S (595.16).

1-(*tert*-Butoxycarbonylamino((3-(2-*tert*-butoxycarbonylamino-4-methylthiazol-5-yl)propyl)amino)methylene)-3-(1-(4-bromophenyl)ethyl)urea (3.104)

Compound **3.104** was prepared from **3.009a** (0.14 g, 0.50 mmol), **3.063** (0.21 g, 0.50 mmol), HgCl$_2$ (0.14 g, 0.50 mmol), and NEt$_3$ (0.21 mL, 1.50 mmol) in DCM (10 mL) conforming to the general procedure (R$_f$ = 0.14 in DCM/MeOH/NH$_3$ 99/1/0.1) yielding a colorless oil (70 mg, 22%). ^{1}H NMR (300 MHz, CDCl$_3$) δ (ppm) 11.98 (s, 1H), 10.03 (s, 1H), 8.14 (s, 1H), 7.45 – 7.40 (m, 2H), 7.23 – 7.18 (m, 2H), 5.60 (s, 1H), 4.83 – 4.68 (m, 1H), 3.33 (d, *J* = 6.7 Hz, 2H), 2.70 (t, *J* = 7.2 Hz, 2H), 2.21 (s, 3H), 1.86 (p, *J* = 7.1 Hz, 2H), 1.50 (s, 9H), 1.44 (d, *J* = 2.1 Hz, 3H), 1.42 (s, 9H). ^{13}C NMR (75 MHz, CDCl$_3$) δ (ppm) 162.68, 157.36, 154.53, 153.35, 152.62, 143.80, 141.96, 131.67, 131.58, 127.67, 127.63, 123.21, 120.61, 82.54, 50.72, 39.59, 30.72, 28.25, 28.04, 23.22, 22.75, 14.53. HRMS (ESI-MS): *m/z* [M+H$^+$] calculated for C$_{27}$H$_{40}$BrN$_6$O$_5$S$^+$: 639.1959, found 639.1960; C$_{27}$H$_{39}$BrN$_6$O$_5$S (639.61).

1-(*tert*-Butoxycarbonylamino((3-(2-*tert*-butoxycarbonylamino-4-methylthiazol-5-yl)propyl)amino)methylene)-3-(1-(4-methoxyphenyl)ethyl)urea (3.105)

Compound **3.105** was prepared from **3.009a** (0.16 g, 0.60 mmol), **3.064** (0.22 g, 0.60 mmol), HgCl$_2$ (0.16 g, 0.60 mmol), and NEt$_3$ (0.25 mL, 1.80 mmol) in DCM (10 mL) conforming to the general procedure (R$_f$ = 0.22 in DCM/MeOH/NH$_3$ 99/1/0.1) yielding a colorless oil (0.22 g, 62%). ^{1}H NMR (300 MHz, CDCl$_3$) δ (ppm) 12.09 (s, 1H), 10.60 (s, 1H), 8.09 (t, *J* = 5.5 Hz, 1H), 7.29 – 7.18 (m, 2H), 6.89 – 6.79 (m, 2H), 5.53 (d, *J* = 7.8 Hz, 1H), 4.85 (p, *J* = 7.0 Hz, 1H), 3.77 (s, 3H), 3.33 (q, *J* = 6.8 Hz, 2H), 2.69 (t, *J* = 7.3 Hz, 2H), 2.22 (s, 3H), 1.86 (p, *J* = 7.1 Hz, 2H), 1.50 (s, 9H), 1.46 (d, *J* = 4.6 Hz, 3H), 1.43 (d, *J* = 1.8 Hz, 9H). ^{13}C NMR (75 MHz, CDCl$_3$) δ (ppm) 163.87, 158.50, 157.66, 154.42, 153.43, 152.77, 141.95, 136.69, 127.04, 123.18, 113.90, 82.35, 82.18, 55.27, 48.95, 39.55, 30.76, 28.28, 28.07, 23.28, 22.76, 14.52. HRMS (ESI-MS): *m/z* [M+H$^+$] calculated for C$_{28}$H$_{43}$N$_6$O$_6$S$^+$: 591.2959, found 591.2966; C$_{28}$H$_{42}$N$_6$O$_6$S (590.29).

1-(*tert*-Butoxycarbonylamino((3-(2-*tert*-butoxycarbonylamino-4-methylthiazol-5-yl)propyl)amino)methylene)-3-(1-(4-trifluoromethoxyphenyl)ethyl)urea (3.106)

Compound **3.106** was prepared from **3.009a** (0.21 g, 0.79 mmol), **3.065** (0.33 g, 0.79 mmol), HgCl$_2$ (0.21 g, 0.79 mmol), and NEt$_3$ (0.33 mL, 2.37 mmol) in DCM (10 mL) conforming to the general procedure (R$_f$ = 0.22 in DCM/MeOH/NH$_3$ 99/1/0.1) yielding a colorless oil (0.26 g, 61%). ^{1}H NMR (300 MHz, CDCl$_3$) δ (ppm) 11.99 (s, 1H),

10.71 (s, 1H), 8.14 (t, J = 5.5 Hz, 1H), 7.39 – 7.09 (m, 4H), 5.61 (d, J = 7.7 Hz, 1H), 4.88 – 4.75 (m, 1H), 3.39 – 3.30 (m, 2H), 2.70 (t, J = 7.2 Hz, 2H), 2.23 (s, 3H), 1.88 (m, 2H), 1.49 (s, 9H), 1.46 (d, J = 3.0 Hz, 3H), 1.43 (s, 9H). ^{13}C NMR (75 MHz, CDCl₃) δ (ppm) 163.91, 157.76, 154.59, 153.39, 152.82, 147.98, 143.48, 141.96, 134.97, 127.21, 123.13, 121.07, 120.46 (d, J = 254.6 Hz), 82.51, 48.96, 39.55, 30.73, 28.25, 28.04, 23.22, 22.86, 14.51. HRMS (ESI-MS): m/z [M+H$^+$] calculated for C₂₈H₄₀F₃N₆O₆S$^+$: 645.2677, found 645.2691; C₂₈H₃₉F₃N₆O₆S (644.71).

1-(*tert*-Butoxycarbonylamino((3-(2-*tert*-butoxycarbonylamino-4-methylthiazol-5-yl)propyl)amino)methylene)-3-(1-(2-fluorophenyl)ethyl)urea (3.107)

Compound **3.107** was prepared from **3.009a** (0.25 g, 0.93 mmol), **3.066** (0.33 g, 0.93 mmol), HgCl₂ (0.25 g, 0.93 mmol), and NEt₃ (0.39 mL, 2.79 mmol) in DCM (10 mL) conforming to the general procedure (R$_f$ = 0.12 in DCM/MeOH/NH₃ 99/1/0.1) yielding a colorless oil (0.19 g, 33%). ^{1}H NMR (400 MHz, CDCl₃) δ (ppm) 12.02 (d, J = 6.0 Hz, 1H), 10.38 (s, 1H), 8.14 (s, 1H), 7.37 – 6.88 (m, 4H), 5.75 (s, 1H), 5.23 – 5.07 (m, 1H), 3.41 – 3.31 (m, 2H), 2.71 (t, J = 7.3 Hz, 2H), 2.22 (s, 3H), 1.87 (p, J = 7.1 Hz, 2H), 1.50 (s, 9H), 1.47 (d, J = 7.2 Hz, 3H), 1.43 (s, 9H). ^{13}C NMR (101 MHz, CDCl₃) δ (ppm) 164.27, 160.36 (d, J = 245.7 Hz), 157.63, 154.52, 153.38, 152.68, 141.86, 131.44 (d, J = 13.5 Hz), 128.41 (d, J = 8.1 Hz), 127.36 (d, J = 4.9 Hz), 124.20 (d, J = 3.4 Hz), 123.18, 115.65 (d, J = 21.7 Hz), 82.53 (d, J = 2.0 Hz), 82.17, 45.12, 39.65, 30.75, 28.25, 28.04, 23.97, 23.26, 14.47. HRMS (ESI-MS): m/z [M+H$^+$] calculated for C₂₈H₄₀FN₆O₅S$^+$: 579.2759, found 579.2768; C₂₇H₃₉FN₆O₅S (578.70).

1-(*tert*-Butoxycarbonylamino((3-(2-*tert*-butoxycarbonylamino-4-methylthiazol-5-yl)propyl)amino)methylene)-3-(1-(3-fluorophenyl)ethyl)urea (3.108)

Compound **3.108** was prepared from **3.009a** (0.32 g, 1.19 mmol), **3.067** (0.42 g, 1.19 mmol), HgCl₂ (0.32 g, 1.19 mmol), and NEt₃ (0.50 mL, 3.58 mmol) in DCM (10 mL) conforming to the general procedure (R$_f$ = 0.12 in DCM/MeOH/NH₃ 99/1/0.1) yielding a colorless oil (0.21 g, 36%). ^{1}H NMR (400 MHz, CDCl₃) δ (ppm) 12.02 (s, 1H), 10.25 (s, 1H), 8.18 (s, 1H), 7.32 – 6.84 (m, 4H), 5.67 (s, 1H), 4.89 (p, J = 7.1 Hz, 1H), 3.43 – 3.30 (m, 2H), 2.71 (t, J = 7.3 Hz, 2H), 2.22 (s, 3H), 1.88 (p, J = 7.1 Hz, 2H), 1.50 (s, 9H), 1.46 (d, J = 3.5 Hz, 3H), 1.44 (s, 9H). ^{13}C NMR (101 MHz, CDCl₃) δ (ppm) 163.03 (d, J = 245.7 Hz), 157.54, 154.57, 153.36, 147.43 (d, J = 6.5 Hz), 141.88, 130.02 (d, J = 8.2 Hz), 123.17, 121.49 (d, J = 2.7 Hz), 113.73 (d, J = 21.2 Hz), 112.79

(d, J = 21.8 Hz), 82.61, 82.20, 49.22, 41.01, 30.73, 28.24, 28.04, 23.22, 22.74, 14.47. HRMS (ESI-MS): m/z [M+H$^+$] calculated for $C_{27}H_{40}FN_6O_5S^+$: 579.2759, found 579.2775; $C_{27}H_{39}FN_6O_5S$ (578.70).

1-(*tert*-Butoxycarbonylamino((3-(2-*tert*-butoxycarbonylamino-4-methylthiazol-5-yl)propyl)amino)methylene)-3-(1-(2-furanyl)methyl)urea (3.109)

Compound **3.109** was prepared from **3.009a** (0.30 g, 1.12 mmol), **3.068** (0.35 g, 1.12 mmol), HgCl$_2$ (0.30 g, 1.12 mmol), and NEt$_3$ (0.47 mL, 3.35 mmol) in DCM (10 mL) conforming to the general procedure (R$_f$ = 0.12 in DCM/MeOH/NH$_3$ 99/1/0.1) yielding a yellow oil (0.47 g, 89%). ^{1}H NMR (400 MHz, CDCl$_3$) δ (ppm) 12.00 (d, J = 16.2 Hz, 1H), 10.31 (s, 1H), 8.08 (t, J = 5.6 Hz, 1H), 7.29 – 7.22 (m, 1H), 6.26 – 6.04 (m, 2H), 5.75 (s, 1H), 4.31 (d, J = 6.0 Hz, 2H), 3.27 (q, J = 6.4 Hz, 2H), 2.63 (t, J = 7.2 Hz, 2H), 2.14 (s, 3H), 1.80 (p, J = 7.2 Hz, 2H), 1.44 (s, 9H), 1.40 (s, 9H). ^{13}C NMR (101 MHz, CDCl$_3$) δ (ppm) 164.35, 157.75, 154.58, 153.38, 152.68, 152.55, 141.82, 141.71, 123.10, 110.25, 106.62, 82.49, 39.54, 37.09, 30.61, 28.22, 28.05, 23.16, 14.38. HRMS (ESI-MS): m/z [M+H$^+$] calculated for $C_{24}H_{37}N_6O_6S^+$: 537.2490, found 537.2498; $C_{24}H_{36}N_6O_6S$ (536.65).

1-(*tert*-Butoxycarbonylamino((3-(2-*tert*-butoxycarbonylamino-4-methylthiazol-5-yl)propyl)amino)methylene)-3-(1-(2-furanyl)ethyl)urea (3.110)

Compound **3.110** was prepared from **3.009a** (0.25 g, 0.92 mmol), **3.069** (0.30 g, 0.92 mmol), HgCl$_2$ (0.25 g, 0.92 mmol), and NEt$_3$ (0.38 mL, 2.75 mmol) in DCM (10 mL) conforming to the general procedure (R$_f$ = 0.14 in DCM/MeOH/NH$_3$ 99/1/0.1) yielding a colorless oil (0.36 g, 86%). ^{1}H NMR (400 MHz, CDCl$_3$) δ (ppm) 12.06 (s, 1H), 9.85 (d, J = 134.2 Hz, 1H), 8.10 (s, 1H), 7.29 – 7.20 (m, 1H), 6.24 – 6.17 (m, 1H), 6.10 (d, J = 3.2 Hz, 1H), 5.59 (s, 1H), 4.98 (p, 1H), 3.35 – 3.21 (m, 2H), 2.63 (t, J = 7.3 Hz, 2H), 2.13 (s, 3H), 1.81 (q, J = 7.2 Hz, 2H), 1.45 (s, 9H), 1.42 (d, J = 7.2 Hz, 3H), 1.40 (s, 9H). ^{13}C NMR (101 MHz, CDCl$_3$) δ (ppm) 163.54, 157.60, 156.43, 154.60, 153.37, 152.52, 141.63, 141.58, 123.17, 110.02, 104.93, 82.77, 43.46, 30.70, 29.69, 28.21, 28.04, 23.24, 17.53, 14.35. HRMS (ESI-MS): m/z [M+H$^+$] calculated for $C_{25}H_{39}N_6O_6S^+$: 551.2646, found 551.2652; $C_{25}H_{38}N_6O_6S$ (550.68).

1-(*tert*-Butoxycarbonylamino((3-(2-*tert*-butoxycarbonylamino-4-methylthiazol-5-yl)propyl)amino)methylene)-3-(1-(thiophen-2-yl)ethyl)urea (3.111)

Compound **3.111** was prepared from **3.009a** (0.20 g, 0.73 mmol), **3.070** (0.25 g, 0.73 mmol), HgCl$_2$ (0.20 g, 0.73 mmol), and NEt$_3$ (0.30 mL, 2.18 mmol) in DCM (10 mL) conforming to the general procedure (R$_f$ = 0.12 in DCM/MeOH/NH$_3$ 99/1/0.1) yielding a colorless oil (0.27 g, 64%). ^{1}H NMR (400 MHz, CDCl$_3$) δ (ppm) 12.06 (d, *J* = 13.9 Hz, 1H), 9.60 (d, *J* = 268.9 Hz, 1H), 8.22 (d, *J* = 31.4 Hz, 1H), 7.18 – 7.12 (m, 1H), 7.01 – 6.85 (m, 2H), 5.77 – 5.56 (m, 1H), 5.20 (m, 1H), 3.45 – 3.26 (m, 2H), 2.69 (t, *J* = 7.3 Hz, 2H), 2.19 (s, 3H), 1.86 (p, *J* = 7.1 Hz, 2H), 1.57 (d, *J* = 6.9 Hz, 3H), 1.50 (s, 9H), 1.46 (s, 9H). ^{13}C NMR (101 MHz, CDCl$_3$) δ (ppm) 157.45, 154.58, 153.36, 152.48, 148.41, 141.72, 126.68, 123.82, 123.38, 123.21, 82.83, 45.28, 30.72, 29.70, 28.23, 28.05, 23.24, 20.90, 14.40. HRMS (ESI-MS): *m/z* [M+H$^+$] calculated for C$_{25}$H$_{39}$N$_6$O$_5$S$_2^+$: 567.2418, found 567.2422; C$_{25}$H$_{38}$N$_6$O$_5$S$_2$ (566.74).

1-(*tert*-Butoxycarbonylamino((3-(2-*tert*-butoxycarbonylamino-4-methylthiazol-5-yl)propyl)amino)methylene)-3-(2,2-diphenylethyl)urea (3.113) *(Synthesized by Steffen Pockes)*

Compound **3.113** was prepared from **3.009a** (0.14 g, 0.50 mmol), **3.072** (0.21 g, 0.50 mmol), HgCl$_2$ (0.14 g, 0.50 mmol), and NEt$_3$ (0.21 mL, 1.50 mmol) in DCM (10 mL) conforming to the general procedure (R$_f$ = 0.75 in DCM/MeOH/NH$_3$ 99/1/0.1) yielding a yellow oil (0.26 g, 82%). ^{1}H NMR (300 MHz, CDCl$_3$) δ (ppm) 12.09 (br s, 1H), 10.10 (br s, 1H), 8.09 (br s, 1H), 7.35 – 7.14 (m, 10H), 5.32 (br s, 1H), 4.21 (t, *J* = 7.8 Hz, 1H), 3.84 (dd, *J* = 7.8, 6.0 Hz, 2H), 3.28 (q, *J* = 6.5 Hz, 2H), 2.66 (t, *J* = 7.4 Hz, 2H), 2.20 (s, 3H), 1.81 (p, *J* = 7.4 Hz, 2H), 1.52 (s, 9H), 1.47 (s, 9H). ^{13}C NMR (75 MHz, CDCl$_3$) δ (ppm) 166.20, 159.89, 157.28, 154.25, 153.39, 142.36, 141.96, 128.61, 128.16, 126.61, 123.31, 82.55, 82.23, 50.97, 44.56, 39.65, 30.75, 28.29, 28.09, 23.27, 14.52. HRMS (ESI-MS): *m/z* [M+H$^+$] calculated for C$_{33}$H$_{45}$N$_6$O$_5$S$^+$: 637.3167, found 637.3174; C$_{33}$H$_{44}$N$_6$O$_5$S (636.81).

(*R*)-1-(*tert*-Butoxycarbonylamino((3-(2-*tert*-butoxycarbonylamino-4-methylthiazol-5-yl)propyl)amino)methylene)-3-(2-phenylpropyl)urea (3.115) *(Synthesized by Steffen Pockes)*

Compound **3.115** was prepared from **3.009a** (0.14 g, 0.50 mmol), **3.074** (0.18 g, 0.50 mmol), HgCl$_2$ (0.14 g, 0.50 mmol), and NEt$_3$ (0.21 mL, 1.50 mmol) in DCM

(10 mL) conforming to the general procedure (R$_f$ = 0.47 in DCM/MeOH/NH$_3$ 99/1/0.1) yielding a yellow oil (0.16 g, 56%). ^{1}H NMR (300 MHz, CDCl$_3$) δ (ppm) 12.13 (br s, 1H), 10.90 (br s, 1H), 8.07 (t, *J* = 5.5 Hz, 1H), 7.40 – 7.06 (m, 5H), 5.33 (br s, 1H), 3.52 – 3.15 (m, 4H), 3.00 – 2.90 (m, 1H), 2.74 – 2.62 (m, 2H), 2.22 (s, 3H), 1.83 (p, *J* = 7.4 Hz, 2H), 1.51 (s, 9H), 1.46 (s, 9H), 1.27 (d, *J* = 6.9 Hz, 3H). ^{13}C NMR (75 MHz, CDCl$_3$) δ (ppm) 164.68, 157.88, 154.25, 153.43, 152.88, 144.67, 141.87, 128.53, 127.26, 126.42, 123.08, 82.37, 82.06, 46.92, 40.10, 39.52, 30.73, 28.29, 28.08, 23.23, 19.33, 14.51. HRMS (ESI-MS): *m/z* [M+H$^+$] calculated for C$_{28}$H$_{43}$N$_6$O$_5$S$^+$: 575.3010, found 575.3016; C$_{28}$H$_{42}$N$_6$O$_5$S (574.74).

(*S*)-1-(*tert*-Butoxycarbonylamino((3-(2-*tert*-butoxycarbonylamino-4-methylthiazol-5-yl)propyl)amino)methylene)-3-(2-phenylpropyl)urea (3.116)

(Synthesized by Steffen Pockes)

Compound **3.116** was prepared from **3.009a** (0.14 g, 0.50 mmol), **3.075** (0.18 g, 0.50 mmol), HgCl$_2$ (0.14 g, 0.50 mmol), and NEt$_3$ (0.21 mL, 1.50 mmol) in DCM (10 mL) conforming to the general procedure (R$_f$ = 0.48 in DCM/MeOH/NH$_3$ 99/1/0.1) yielding a yellow oil (0.16 g, 90%). ^{1}H NMR (300 MHz, CDCl$_3$) δ (ppm) 12.14 (br s, 1H), 11.03 (br s, 1H), 8.06 (t, *J* = 5.5 Hz, 1H), 7.36 – 7.11 (m, 5H), 5.33 (t, *J* = 6.3 Hz, 1H), 3.53 – 3.17 (m, 4H), 3.00 – 2.91 (m, 1H), 2.67 (t, *J* = 7.3 Hz, 2H), 2.23 (s, 3H), 1.83 (p, *J* = 7.1 Hz, 2H), 1.51 (s, 9H), 1.46 (s, 9H), 1.27 (d, *J* = 6.9 Hz, 3H). ^{13}C NMR (75 MHz, CDCl$_3$) δ (ppm) 164.73, 157.95, 154.26, 153.43, 152.91, 144.68, 141.86, 128.53, 127.26, 126.43, 123.10, 82.35, 82.07, 46.92, 40.11, 39.50, 30.74, 28.30, 28.08, 23.23, 19.34, 14.49. HRMS (ESI-MS): *m/z* [M+H$^+$] calculated for C$_{28}$H$_{43}$N$_6$O$_5$S$^+$: 575.3010, found 575.3012; C$_{28}$H$_{42}$N$_6$O$_5$S (574.74).

3.5.1.8 Synthesis and Analytical Data of the Thiocarbamoylation 3.124-3.129

The Boc-protected guanidine **3.010** (1 eq; synthesized as described by Kraus et al.[302] and the respective isothiocyanate **3.083**-**3.088** (1 eq) were dissolved in DCM and refluxed for 3-4 days. After the reaction was complete (TLC monitoring), the solvent was evaporated, and the crude product was purified by column chromatography (DCM/MeOH 100/0-98/2). The NMR peaks in the ^{1}H and ^{13}C NMR are split due to thione-thiol tautomerism, as already described in the literature.[460] For ^{1}H NMR each pair of peaks was integrated jointly. For ^{13}C NMR just one peak series was taken and described.

1-(*tert*-Butoxycarbonylamino((3-(2-*tert*-butoxycarbonylamino-4-methylthiazol-5-yl)propyl)amino)methylene)-3-(diphenylmethyl)thiourea (3.124) *(Synthesized by Steffen Pockes)*

The title compound was prepared from **3.010** (0.12 g, 0.28 mmol) and **3.083** (0.06 g, 0.28 mmol) in DCM (10 mL) according to the general procedure (R_f = 0.50 in DCM/MeOH 99/1). **3.124** was yielded as a yellow oil (0.07 g, 39%). ^{1}H NMR (300 MHz, CDCl$_3$) δ (ppm) 13.08 (s, 1H), 8.50 (t, *J* = 5.7 Hz, 1H), 7.39 – 7.16 (m, 10H), 6.82 (d, *J* = 6.5 Hz, 1H), 6.24 (d, *J* = 6.4 Hz, 1H), 5.15 – 4.98 (m, 1H), 3.05 (q, *J* = 6.6 Hz, 2H), 2.46 (t, *J* = 7.3 Hz, 2H), 2.18 (s, 3H), 1.97 – 1.74 (m, 2H), 1.52 (s, 9H), 1.48 (s, 9H). ^{13}C NMR (75 MHz, CDCl$_3$) δ (ppm) 183.56, 157.72, 155.08, 153.99, 153.39, 152.73, 141.47, 128.65, 127.83, 127.42, 122.93, 83.39, 82.28, 62.05, 39.69, 30.36, 28.30, 28.03, 23.12, 14.49. HRMS (ESI-MS): *m/z* [M+H$^+$] calculated for C$_{32}$H$_{43}$N$_6$O$_4$S$_2^+$: 639.2782, found 639.2791; C$_{32}$H$_{42}$N$_6$O$_4$S$_2$ (638.85).

(*R*)-1-(*tert*-Butoxycarbonylamino((3-(2-*tert*-butoxycarbonylamino-4-methylthiazol-5-yl)propyl)amino)methylene)-3-(1-phenylethyl)thiourea (3.125) *(Synthesized by Steffen Pockes)*

The title compound was prepared from **3.010** (0.12 g, 0.28 mmol) and **3.084** (0.05 g, 0.28 mmol) in DCM (10 mL) according to the general procedure (R_f = 0.48 in DCM/MeOH 99/1). **3.125** was yielded as a yellow oil (50 mg, 31%). ^{1}H NMR (300 MHz, CDCl$_3$) δ (ppm) 13.00 (s, 1H), 10.48 (br s, 1H), 8.48 (t, *J* = 5.7 Hz, 1H), 7.38 – 7.26 (m, 5H), 6.65 (d, *J* = 7.0 Hz, 1H), 5.16 (q, *J* = 7.0 Hz, 1H), 3.21 – 3.06 (m, 2H), 2.55 (q, *J* = 7.5 Hz, 2H), 2.19 (s, 3H), 1.91 – 1.79 (m, 2H), 1.51 (s, 9H), 1.51 (s, 3H), 1.47 (s, 9H). ^{13}C NMR (75 MHz, CDCl$_3$) δ (ppm) 183.54, 157.65, 154.85, 153.71, 153.40, 152.74, 143.87, 128.52, 126.47, 125.61, 122.91, 83.30, 82.29, 53.28, 39.69, 30.46, 29.72, 28.29, 28.03, 22.73, 14.49. HRMS (ESI-MS): *m/z* [M+H$^+$] calculated for C$_{27}$H$_{41}$N$_6$O$_4$S$_2^+$: 577.2625, found 577.2631; C$_{27}$H$_{40}$N$_6$O$_4$S$_2$ (576.78).

(*S*)-1-(*tert*-Butoxycarbonylamino((3-(2-*tert*-butoxycarbonylamino-4-methylthiazol-5-yl)propyl)amino)methylene)-3-(1-phenylethyl)thiourea (3.126) *(Synthesized by Steffen Pockes)*

The title compound was prepared from **3.010** (0.12 g, 0.28 mmol) and **3.085** (0.05 g, 0.28 mmol) in DCM (10 mL) according to the general procedure (R_f = 0.48 in DCM/MeOH 99/1). **3.126** was yielded as a yellow oil (0.08 g, 51%). ^{1}H NMR (300 MHz,

CDCl$_3$) δ (ppm) 13.00 (s, 1H), 10.41 (s, 1H), 8.48 (t, J = 5.7 Hz, 1H), 7.39 – 7.25 (m, 5H), 6.67 (d, J = 6.9 Hz, 1H), 5.16 (q, J = 7.0 Hz, 1H), 3.25 – 3.05 (m, 2H), 2.55 (q, J = 7.5 Hz, 2H), 2.19 (s, 3H), 1.98 – 1.72 (m, 2H), 1.51 (s, 9H), 1.50 (s, 3H), 1.47 (s, 9H). ^{13}C NMR (75 MHz, CDCl$_3$) δ (ppm) 183.53, 157.84, 154.84, 153.71, 153.40, 152.79, 143.88, 128.52, 126.47, 125.61, 122.85, 83.29, 82.25, 53.28, 39.68, 30.46, 29.71, 28.29, 28.02, 22.72, 14.48. HRMS (ESI-MS): m/z [M+H$^+$] calculated for C$_{27}$H$_{41}$N$_6$O$_4$S$_2^+$: 577.2625, found 577.2625; C$_{27}$H$_{40}$N$_6$O$_4$S$_2$ (576.78).

1-(*tert*-Butoxycarbonylamino((3-(2-*tert*-butoxycarbonylamino-4-methylthiazol-5-yl)propyl)amino)methylene)-3-(2,2-diphenylethyl)thiourea (3.127) *(Synthesized by Steffen Pockes)*

The title compound was prepared from **3.010** (0.12 g, 0.28 mmol) and **3.086** (0.07 g, 0.28 mmol) in DCM (10 mL) according to the general procedure (R$_f$ = 0.51 in DCM/MeOH 99/1). **3.127** was yielded as a yellow oil (0.10 g, 55%). ^{1}H NMR (400 MHz, CDCl$_3$) δ (ppm) 13.02 (s, 1H), 10.47 (br s, 1H), 8.41 (t, J = 5.6 Hz, 1H), 7.34 – 7.13 (m, 10H), 6.52 (t, J = 5.8 Hz, 1H), 4.45 – 4.28 (m, 1H), 4.20 – 4.00 (m, 2H), 3.38 – 3.20 (m, 2H), 2.63 – 2.53 (m, 2H), 2.15 (s, 3H), 1.87 – 1.73 (m, 2H), 1.50 (s, 9H), 1.48 (d, J = 1.7 Hz, 9H). ^{13}C NMR (101 MHz, CDCl$_3$) δ (ppm) 184.51, 157.73, 154.87, 153.56, 153.44, 152.74, 142.02, 128.79, 127.95, 126.86, 122.84, 83.34, 82.97, 49.66, 39.95, 39.53, 30.57, 28.30, 28.05, 23.22, 14.45. HRMS (ESI-MS): m/z [M+H$^+$] calculated for C$_{33}$H$_{45}$N$_6$O$_4$S$_2^+$: 653.2948, found 653.2948; C$_{33}$H$_{44}$N$_6$O$_4$S$_2$ (652.87).

(*R*)-1-(*tert*-Butoxycarbonylamino((3-(2-*tert*-butoxycarbonylamino-4-methylthiazol-5-yl)propyl)amino)methylene)-3-(2-phenylpropyl)thiourea (3.128) *(Synthesized by Steffen Pockes)*

The title compound was prepared from **3.010** (0.12 g, 0.28 mmol) and **3.087** (0.05 g, 0.28 mmol) in DCM (10 mL) according to the general procedure (R$_f$ = 0.50 in DCM/MeOH 99/1). **3.128** was yielded as a yellow oil (0.07 g, 43%). ^{1}H NMR (300 MHz, CDCl$_3$) δ (ppm) 13.02 (s, 1H), 10.86 (br s, 1H), 8.42 (t, J = 5.6 Hz, 1H), 7.36 – 7.12 (m, 5H), 6.52 (t, J = 6.0 Hz, 1H), 3.93 – 3.57 (m, 2H), 3.50 – 3.37 (m, 2H), 3.05 (q, J = 7.1 Hz, 1H), 2.68 (m, 2H), 2.21 (s, 3H), 1.87 (m, 2H), 1.51 (s, 9H), 1.49 (s, 9H), 1.24 (s, 3H). ^{13}C NMR (75 MHz, CDCl$_3$) δ (ppm) 184.50, 157.91, 154.69, 153.47, 152.80, 143.91, 141.89, 128.72, 127.08, 126.73, 122.75, 83.26, 82.93, 50.52, 39.64, 30.62,

29.74, 28.30, 28.05, 23.32, 19.30, 14.50. HRMS (ESI-MS): *m/z* [M+H$^+$] calculated for C$_{28}$H$_{43}$N$_6$O$_4$S$_2$$^+$: 591.2782, found 591.2777; C$_{28}$H$_{42}$N$_6$O$_4$S$_2$ (590.80).

(*S*)-1-(*tert*-Butoxycarbonylamino((3-(2-*tert*-butoxycarbonylamino-4-methylthiazol-5-yl)propyl)amino)methylene)-3-(2-phenylpropyl)thiourea (3.129) *(Synthesized by Steffen Pockes)*

The title compound was prepared from **3.010** (0.12 g, 0.28 mmol) and **3.088** (0.05 g, 0.28 mmol) in DCM (10 mL) according to the general procedure (R$_f$ = 0.50 in DCM/MeOH 99/1). **3.129** was yielded as a yellow oil (0.05 g, 30%). ^{1}H NMR (300 MHz, CDCl$_3$) δ (ppm) 13.02 (s, 1H), 10.51 (br s, 1H), 8.42 (t, *J* = 5.6 Hz, 1H), 7.37 – 7.13 (m, 5H), 6.51 (t, *J* = 6.0 Hz, 1H), 3.92 – 3.57 (m, 2H), 3.50 – 3.38 (m, 2H), 3.19 – 2.91 (m, 1H), 2.73 – 2.62 (m, 2H), 2.21 (s, 3H), 1.97 – 1.76 (m, 2H), 1.52 (s, 9H), 1.49 (s, 9H), 1.25 (s, 3H). ^{13}C NMR (75 MHz, CDCl$_3$) δ (ppm) 184.51, 157.81, 154.70, 153.49, 152.77, 143.90, 142.07, 128.73, 127.09, 126.73, 122.78, 83.27, 82.93, 50.52, 39.64, 30.57, 29.72, 28.29, 28.05, 23.33, 19.31, 14.51. HRMS (ESI-MS): *m/z* [M+H$^+$] calculated for C$_{28}$H$_{43}$N$_6$O$_4$S$_2$$^+$: 591.2782, found 591.2747; C$_{28}$H$_{42}$N$_6$O$_4$S$_2$ (590.80).

3.5.1.9 Synthesis and Analytical Data of the Carbamoylguanidine-type Ligands 3.138-3.186

The general procedure for the synthesis of **3.138**-**3.186** by Boc-/Trt-deprotection is described in the literature.[299,389,460] All compounds, with the exception of **3.149** and **3.155**, were purified by preparative HPLC (MeCN/0.05 or 0.1% aqueous TFA and obtained as di-trifluoroacetates (method A). **3.149** and **3.155** were purified as follows: The crude product was subjected to column chromatography under basic conditions (DCM/MeOH/NH$_3$ 90/10/0.1). The free base was dissolved in 2-3 mL dioxane and precipitated after the dropwise addition of 2 N HCl in diethyl ether. The resulting dihydrochloride was separated and washed with diethyl ether (3 x 5 mL) (method B).

1-(Amino((3-(2-amino-4-methylthiazol-5-yl)propyl)amino)methylene)-3-(1-propyl)urea dihydrotrifluoroacetate (3.138) *(Synthesized by Claudia Honisch)*

3.089 was prepared from **3.009a** (0.15 g, 0.54 mmol), **3.048** (0.15 g, 0.54 mmol), HgCl$_2$ (0.29 g, 1.08 mmol), and NEt$_3$ (0.23 mL, 1.62 mmol) in DCM (25 mL) conforming to the general procedure for the guanidinylation reaction. Subsequently, **3.0138** was prepared from the Boc-protected intermediate **3.089** in DCM (4.0 mL) and TFA

(1.0 mL) according to the general procedure (method A) and obtained as a colorless foamlike solid (140 mg, 49%): RP-HPLC: 99%, (t$_R$ = 10.92, k = 2.80). ^{1}H NMR (600 MHz, DMSO-d$_6$, di-trifluoroacetate): δ (ppm) 10.22 (br s, 1H), 8.99 (br s, 1H), 8.87 (br s, 2H), 8.49 (br s, 2H), 7.49 (br s, 1H), 3.26 – 3.22 (m, 2H), 3.07 – 3.04 (m, 2H), 2.59 (t, J = 7.5 Hz, 2H), 2.07 (s, 3H), 1.72 (p, J = 7.2 Hz, 2H), 1.48 – 1.42 (m, 2H), 0.85 (t, J = 7.4 Hz, 3H). ^{13}C NMR (150 MHz, DMSO-d$_6$, di-trifluoroacetate): δ (ppm) 167.60, 153.80, 153.70, 132.60, 116.30, 40.90, 39.30, 28.90, 22.20, 22.00, 11.60, 11.10. HRMS (ESI-MS): m/z [M+H$^+$] calculated for C$_{12}$H$_{23}$N$_6$OS$^+$: 299.1649, found 299.1651; C$_{12}$H$_{22}$N$_6$OS x C$_4$H$_2$F$_6$O$_4$ (526.21).

1-(Amino((3-(2-amino-4-methylthiazol-5-yl)propyl)amino)methylene)-3-(1-pentyl)urea dihydrotrifluoroacetate (3.139) *(Synthesized by Katharina Tropmann)*

3.090 was prepared from **3.009a** (0.05 g, 0.17 mmol), **3.049** (0.05 g, 0.17 mmol), HgCl$_2$ (0.09 g, 0.34 mmol), and NEt$_3$ (0.07 mL, 0.51 mmol) in DCM (25 mL) conforming to the general procedure for the guanidinylation reaction. Subsequently, **3.139** was prepared from the Boc-protected intermediate **3.090** in DCM (4.0 mL) and TFA (1.0 mL) according to the general procedure (method A) and obtained as a colorless foamlike solid (140 mg, 49%): RP-HPLC: 99%, (t$_R$ = 11.14, k = 2.47). ^{1}H NMR (600 MHz, DMSO-d$_6$, di-trifluoroacetate) δ (ppm) 10.46 (s, 1H), 9.40 – 8.79 (m, 3H), 8.52 (s, 2H), 7.48 (s, 1H), 3.24 (q, J = 6.6 Hz, 2H), 3.09 (q, J = 6.6 Hz, 2H), 2.59 (t, J = 7.5 Hz, 2H), 2.08 (s, 3H), 1.73 (p, J = 7.3 Hz, 2H), 1.43 (p, J = 7.2 Hz, 2H), 1.32 – 1.19 (m, 4H), 0.86 (t, J = 7.1 Hz, 3H). ^{13}C NMR (151 MHz, DMSO-d$_6$, di-trifluoroacetate) δ (ppm) 167.82, 159.12 (q, J = 32.4 Hz, TFA), 153.83, 153.69, 131.95, 116.89 (q, J = 298.1 Hz, TFA), 116.28, 39.93, 39.16, 28.82, 28.59, 28.37, 21.98, 21.74, 13.86, 11.44. HRMS (ESI-MS): m/z [M+H$^+$] calculated for C$_{14}$H$_{27}$N$_6$OS$^+$: 327.1962; found 327.1964; C$_{14}$H$_{26}$N$_6$OS x C$_4$H$_2$F$_6$O$_4$ (554.51).

1-(Amino((3-(2-amino-4-methylthiazol-5-yl)propyl)amino)methylene)-3-(1-hexyl)urea dihydrotrifluoroacetate (3.140) *(Synthesized by Claudia Honisch)*

3.091 was prepared from **3.009a** (0.15 g, 0.47 mmol), **3.050** (0.15 g, 0.47 mmol), HgCl$_2$ (0.26 g, 0.94 mmol), and NEt$_3$ (0.20 mL, 1.41 mmol) in DCM (25 mL) conforming to the general procedure for the guanidinylation reaction. Subsequently, **3.140** was prepared from the Boc-protected intermediate **3.091** in DCM (4.0 mL) and TFA (1.0 mL)

according to the general procedure (method A) and obtained as a colorless foamlike solid (50 mg, 19%): RP-HPLC: 99%, (t$_R$ = 16.70, k = 4.80). ^{1}H NMR (600 MHz, DMSO-d$_6$, di-trifluoroacetate): δ (ppm) 10.39 (br s, 1H), 9.00 (br s, 1H), 8.73 (br s,2H), 8.50 (br s, 2H), 7.49 (br s, 1H), 6.57 (br s, 1H), 3.25 – 3.22 (m, 2H), 3.09 – 3.06 (m, 2H), 2.58 (t, J = 7.4 Hz, 2H), 2.05 (s, 3H), 1.71 (p, J = 7.3 Hz, 2H), 1.43 – 1.39 (m, 2H), 1.28 – 1.24 (m, 6H), 0.86 – 0.84 (m, 3H). ^{13}C NMR (150 MHz, DMSO-d$_6$, di-trifluoroacetate): δ (ppm) 167.40, 153.80, 153.70, 133.50, 116.30, 39.50, 39.30, 30.80, 29.00, 28.80, 25.80, 22.03, 21.98, 13.80, 11.80. HRMS (ESI-MS): m/z [M+H$^+$] calculated for C$_{15}$H$_{29}$N$_6$OS$^+$: 341.2118, found 341.2127; C$_{15}$H$_{28}$N$_6$OS x C$_4$H$_2$F$_6$O$_4$ (568.54).

1-(Amino((3-(2-amino-4-methylthiazol-5-yl)propyl)amino)methylene)-3-cyclohexylurea dihydrotrifluoroacetate (3.141) *(Synthesized by Claudia Honisch)*

3.092 was prepared from **3.009a** (0.13 g, 0.47 mmol), **3.051** (0.15 g, 0.47 mmol), HgCl$_2$ (0.26 g, 0.94 mmol), and NEt$_3$ (0.20 mL, 1.41 mmol) in DCM (25 mL) conforming to the general procedure for the guanidinylation reaction. Subsequently, **3.141** was prepared from the Boc-protected intermediate **3.092** in DCM (4.0 mL) and TFA (1.0 mL) according to the general procedure (method A) and obtained as a colorless foamlike solid (99 mg, 37%): RP-HPLC: 99%, (t$_R$ = 14.55, k = 4.00). ^{1}H NMR (600 MHz, DMSO-d$_6$, di-trifluoroacetate): δ (ppm) 10.06 (br s, 1H), 9.12 (br s, 2H), 8.96 (br s, 1H), 8.47 (br s, 2H), 7.47 (br s, 1H), 3.46 – 3.44 (m, 1H), 3.23 (q, J = 6.3 Hz, 2H), 2.59 (t, J = 7.5 Hz, 2H), 2.08 (s, 3H), 1.77 – 1.63 (m, 6H), 1.54 – 1.51 (m, 1H), 1.32 – 1.11 (m, 5H). ^{13}C NMR (150 MHz, DMSO-d$_6$, di-trifluoroacetate): δ (ppm) 167.90, 153.70, 152.80, 131.40, 116.30, 48.30, 38.70, 32.00, 28.70, 24.90, 24.10, 21.90, 11.30. HRMS (ESI-MS): m/z [M+H$^+$] calculated for C$_{15}$H$_{27}$N$_6$OS$^+$: 339.1962, found 339.1970; C$_{15}$H$_{26}$N$_6$OS x C$_4$H$_2$F$_6$O$_4$ (566.52).

1-(Amino((3-(2-amino-4-methylthiazol-5-yl)propyl)amino)methylene)-3-phenylurea dihydrotrifluoroacetate (3.142) *(Synthesized by Claudia Honisch)*

3.093 was prepared from **3.009a** (0.09 g, 0.32 mmol), **3.052** (0.10 g, 0.32 mmol), HgCl$_2$ (0.17 g, 0.64 mmol), and NEt$_3$ (0.13 mL, 0.96 mmol) in DCM (25 mL) conforming to the general procedure for the guanidinylation reaction. Subsequently, **3.142** was prepared from the Boc-protected intermediate **3.093** in DCM (4.0 mL) and TFA (1.0 mL)

according to the general procedure (method A) and obtained as a colorless foamlike solid (63 mg, 38%): RP-HPLC: 99%, (t$_R$ = 14.75, k = 4.09). ^{1}H NMR (600 MHz, DMSO-d$_6$, di-trifluoroacetate): δ (ppm) 10.47 (br s, 1H), 9.05 (br s, 2H), 8.93 (br s, 1H), 8.56 (br s, 2H), 7.45 – 7.43 (m, 2H), 7.36 – 7.32 (m, 2H), 7.12 – 7.08 (m, 1H), 3.28 (q, J = 6.5 Hz, 2H), 2.61 (t, J = 7.5 Hz, 2H), 2.09 (s, 3H), 1.75 (p, J = 7.2 Hz, 2H). ^{13}C NMR (150 MHz, DMSO-d$_6$, di-trifluoroacetate): δ (ppm) 167.80, 153.40, 153.36, 137.50, 133.80, 129.00, 123.90, 119.60, 116.30, 39.70, 28.70, 21.90, 11.40. HRMS (ESI-MS): m/z [M+H$^+$] calculated for C$_{15}$H$_{21}$N$_6$OS$^+$: 333.1492, found 333.1496; C$_{15}$H$_{20}$N$_6$OS x C$_4$H$_2$F$_6$O$_4$ (560.48).

1-(Amino((3-(2-amino-4-methylthiazol-5-yl)propyl)amino)methylene)-3-benzylurea dihydrotrifluoroacetate (3.143) *(Synthesized by Claudia Honisch)*

3.094 was prepared from **3.009a** (0.13 g, 0.47 mmol), **3.053** (0.15 g, 0.47 mmol), HgCl$_2$ (0.26 g, 0.94 mmol), and NEt$_3$ (0.20 mL, 1.41 mmol) in DCM (25 mL) conforming to the general procedure for the guanidinylation reaction. Subsequently, **3.143** was prepared from the Boc-protected intermediate **3.094** in DCM (4.0 mL) and TFA (1.0 mL) according to the general procedure (method A) and obtained as a colorless foamlike solid (49 mg, 18%): RP-HPLC: 97%, (t$_R$ = 14.89, k = 4.10). ^{1}H NMR (600 MHz, DMSO-d$_6$, di-trifluoroacetate): δ (ppm) 10.35 (br s, 1H), 9.10 (br s, 2H), 9.01 (br s, 1H), 8.52 (br s, 2H), 7.98 (br s, 1H), 7.32 – 7.35 (m, 2H), 7.25 – 7.28 (m, 3H), 4.30 (d, J = 5.8 Hz, 2H), 3.23 (q, J = 6.7 Hz, 2H), 2.58 (t, J = 7.5 Hz, 2H), 2.07 (s, 3H), 1.72 (p, J = 7.2 Hz, 2H). ^{13}C NMR (150 MHz, DMSO-d$_6$, di-trifluoroacetate): δ (ppm) 167.80, 153.80, 153.70, 138.60, 131.60, 128.40, 127.20, 127.10, 116.30, 42.70, 40.00, 28.70, 21.90, 11.30. HRMS (ESI-MS): m/z [M+H$^+$] calculated for C$_{16}$H$_{23}$N$_6$OS$^+$: 347.1649, found 347.1653; C$_{16}$H$_{22}$N$_6$OS x C$_4$H$_2$F$_6$O$_4$ (574.50).

1-(Amino((3-(2-amino-4-methylthiazol-5-yl)propyl)amino)methylene)-3-benzhydrylurea dihydrotrifluoroacetate (3.144) *(Synthesized by Steffen Pockes)*

3.144 was prepared from **3.095** (0.12 g, 0.19 mmol) in DCM (4.0 mL) and TFA (1.0 mL) according to the general procedure (method A) and obtained as a colorless foamlike solid (60 mg, 49%): RP-HPLC: 99%, (t$_R$ = 14.69, k = 3.65). ^{1}H NMR (300 MHz, CD$_3$OD, di-trifluoroacetate) δ (ppm) 7.43 – 7.22 (m, 10H), 6.06 (s, 1H), 3.34 – 3.32 (m, 2H), 2.69 (t, J = 7.6 Hz, 2H), 2.15 (s, 3H), 1.88 (p, J = 7.2 Hz, 2H). ^{13}C NMR (75 MHz,

CD$_3$OD, di-trifluoroacetate) δ (ppm) 170.36, 155.91, 154.47, 142.72, 132.69, 129.75, 128.66, 128.40, 118.40, 59.02, 41.50, 29.91, 23.57, 11.48. HRMS (ESI-MS): *m/z* [M+H$^+$] calculated for C$_{22}$H$_{27}$N$_6$OS$^+$: 423.1962, found 423.1958; C$_{22}$H$_{26}$N$_6$OS x C$_4$H$_2$F$_6$O$_4$ (650.60).

(*R*)-1-(Amino((3-(2-amino-4-methylthiazol-5-yl)propyl)amino)methylene)-3-(1-phenylethyl)urea dihydrotrifluoroacetate (3.145) *(Synthesized by Steffen Pockes)*
3.145 was prepared from **3.096** (2.02 g, 3.60 mmol) in DCM (16.0 mL) and TFA (4.0 mL) according to the general procedure (method A) and obtained as a colorless foamlike solid (210 mg, 74%): RP-HPLC: 99%, (t$_R$ = 11.14, *k* = 2.53), ee = 99%, [α]^{20}$_D$ +26.54 (*c* 0.31, MeOH). ^{1}H NMR (300 MHz, CD$_3$OD, di-trifluoroacetate) δ (ppm) 7.59 – 6.96 (m, 5H), 4.88 – 4.84 (m, 1H), 3.34 – 3.25 (m, 2H), 2.69 (t, *J* = 7.5 Hz, 2H), 2.16 (s, 3H), 1.87 (p, *J* = 7.1 Hz, 2H), 1.47 (d, *J* = 7.0 Hz, 3H). ^{13}C NMR (75 MHz, CD$_3$OD, di-trifluoroacetate) δ (ppm) 170.38, 155.99, 154.73, 144.89, 132.62, 129.68, 128.38, 127.03, 118.40, 51.17, 41.44, 29.89, 23.58, 22.70, 11.45. HRMS (ESI-MS): *m/z* [M+H$^+$] calculated for C$_{17}$H$_{25}$N$_6$OS$^+$: 361.1805, found 361.1802; C$_{17}$H$_{24}$N$_6$OS x C$_4$H$_2$F$_6$O$_4$ (588.53).

(*S*)-1-(Amino((3-(2-amino-4-methylthiazol-5-yl)propyl)amino)methylene)-3-(1-phenylethyl)urea dihydrotrifluoroacetate (3.146) *(Synthesized by Steffen Pockes)*
3.146 was prepared from **3.097** (0.22 g, 0.39 mmol) in DCM (4.0 mL) and TFA (1.0 mL) according to the general procedure (method A) and obtained as a colorless foamlike solid (190 mg, 82%): RP-HPLC: 99%, (t$_R$ = 11.08, *k* = 2.51), ee = 99%, [α]^{20}$_D$ -24.24 (*c* 0.30, MeOH). ^{1}H NMR (300 MHz, CD$_3$OD, di-trifluoroacetate) δ (ppm) 7.39 – 7.18 (m, 5H), 4.88 (s, 1H), 3.30 – 3.27 (m, 2H), 2.69 (t, *J* = 7.6 Hz, 2H), 2.15 (s, 3H), 1.87 (p, *J* = 7.2 Hz, 2H), 1.47 (d, *J* = 7.0 Hz, 3H). ^{13}C NMR (75 MHz, CD$_3$OD, di-trifluoroacetate) δ (ppm) 170.39, 156.00, 154.73, 144.89, 132.61, 129.67, 128.38, 127.03, 118.40, 51.17, 41.44, 29.87, 23.58, 22.69, 11.44. HRMS (ESI-MS): *m/z* [M+H$^+$] calculated for C$_{17}$H$_{25}$N$_6$OS$^+$: 361.1805, found 361.1807; C$_{17}$H$_{24}$N$_6$OS x C$_4$H$_2$F$_6$O$_4$ (588.53).

1-(Amino((3-(2-amino-4-methylthiazol-5-yl)propyl)amino)methylene)-3-(2,2,2-trifluoro-1-phenylethyl)urea dihydrotrifluoroacetate (3.147)
3.147 was prepared from **3.098** (0.10 g, 0.12 mmol) in DCM (8.0 mL) and TFA (2.0 mL) according to the general procedure (method A) and obtained as a colorless foamlike

solid (23 mg, 29%): RP-HPLC: 96%, (t$_R$ = 10.78, k = 3.04). ^{1}H NMR (300 MHz, CD$_3$OD, di-trifluoroacetate) δ (ppm) 7.52 – 7.34 (m, 5H), 5.57 (q, J = 8.0 Hz, 1H), 3.32 (t, J = 6.9 Hz, 2H), 2.67 (t, J = 7.6 Hz, 2H), 2.14 (s, 3H), 1.95 – 1.78 (m, 2H). ^{13}C NMR (75 MHz, CD$_3$OD, di-trifluoroacetate) δ (ppm) 168.90, 153.59, 132.36, 131.18, 129.07, 128.54, 127.86, 125.21 (d, J = 171.5 Hz), 122.63, 116.91, 54.89 (q, J = 31.0 Hz), 40.15, 28.38, 22.11, 10.00. HRMS (ESI-MS): m/z [M+H$^+$] calculated for C$_{17}$H$_{22}$F$_3$N$_6$OS$^+$: 415.1522, found 415.1523; C$_{17}$H$_{21}$F$_3$N$_6$OS x C$_4$H$_2$F$_6$O$_4$ (642.50).

1-(Amino((3-(2-amino-4-methylthiazol-5-yl)propyl)amino)methylene)-3-(1-phenylpropyl)urea dihydrotrifluoroacetate (3.148)

3.148 was prepared from **3.099** (60 mg, 0.10 mmol) in DCM (8.0 mL) and TFA (2.0 mL) according to the general procedure (method A) and obtained as a colorless foamlike solid (33 mg, 52%): RP-HPLC: 99%, (t$_R$ = 10.06, k = 2.77). ^{1}H NMR (300 MHz, CD$_3$OD, di-trifluoroacetate) δ (ppm) 7.34 – 7.14 (m, 5H), 4.60 (t, J = 7.4 Hz, 1H), 3.28 – 3.25 (m, 2H), 2.64 (t, J = 7.6 Hz, 2H), 2.11 (s, 3H), 1.92 – 1.77 (m, 2H), 1.82 – 1.64 (m, 2H), 0.86 (t, J = 7.4 Hz, 3H). ^{13}C NMR (75 MHz, CD$_3$OD, di-trifluoroacetate) δ (ppm) 170.30, 155.91, 151.26, 143.69, 132.55, 129.54, 128.33, 127.53, 118.30, 57.35, 41.36, 30.50, 29.83, 23.50, 11.39, 11.16. HRMS (ESI-MS): m/z [M+H$^+$] calculated for C$_{18}$H$_{27}$N$_6$OS$^+$: 375.1962, found 375.1961; C$_{18}$H$_{26}$N$_6$OS x C$_4$H$_2$F$_6$O$_4$ (602.55).

1-(Amino((3-(2-amino-4-methylthiazol-5-yl)propyl)amino)methylene)-3-(1-phenylisobutyl)urea dihydrochloride(3.149)

3.149 was prepared from **3.100** (0.27 g, 0.45 mmol) in DCM (8.0 mL) and TFA (2.0 mL) according to the general procedure (method B) and obtained as a colorless foamlike solid (33 mg, 52%): RP-HPLC: 97%, (t$_R$ = 13.44, k = 3.72). ^{1}H NMR (300 MHz, CD$_3$OD, di-hydrochloride) δ (ppm) 7.46 – 7.13 (m, 5H), 4.57 – 4.44 (m, 1H), 3.40 – 3.31 (m, 2H), 2.71 (t, J = 7.6 Hz, 2H), 2.17 (s, 3H), 2.11 – 1.99 (m, 1H), 1.87 (p, J = 7.2 Hz, 2H), 1.17 (t, J = 7.0 Hz, 2H), 0.99 (d, J = 6.7 Hz, 2H), 0.82 (d, J = 6.7 Hz, 3H). ^{13}C NMR (75 MHz, CD$_3$OD, di-hydrochloride) δ (ppm) 170.25, 168.72, 153.47, 141.34, 131.03, 127.99, 126.89, 126.75, 117.11, 60.49, 40.16, 33.42, 22.12, 18.80, 17.83, 14.09, 10.23. HRMS (ESI-MS): m/z [M+H$^+$] calculated for C$_{19}$H$_{29}$N$_6$OS$^+$: 389.2118, found 389.2123; C$_{19}$H$_{28}$N$_6$OS x H$_2$Cl$_2$ (461.45).

1-(Amino((3-(2-amino-4-methylthiazol-5-yl)propyl)amino)methylene)-3-(1-(*p*-tolyl)ethyl)urea dihydrotrifluoroacetate (3.150)

3.150 was prepared from **3.101** (0.10 g, 0.17 mmol) in DCM (8.0 mL) and TFA (2.0 mL) according to the general procedure (method A) and obtained as a colorless foamlike solid (48 mg, 46%): RP-HPLC: 96%, (t_R = 10.11, k = 2.79). ^{1}H NMR (300 MHz, CD$_3$OD, di-trifluoroacetate) δ (ppm) 7.15 (d, J = 8.2 Hz, 2H), 7.08 (d, J = 8.0 Hz, 2H), 4.83 – 4.76 (m, 1H), 2.64 (t, J = 7.5 Hz, 2H), 2.25 (s, 3H), 2.11 (s, 3H), 1.89 – 1.77 (m, 2H), 1.40 (d, J = 7.0 Hz, 3H). ^{13}C NMR (75 MHz, CD$_3$OD, di-trifluoroacetate) δ (ppm) 170.30, 155.91, 141.74, 138.03, 136.39, 132.57, 130.16, 126.91, 118.31, 50.81, 41.37, 29.82, 23.52, 22.63, 21.07, 11.41. HRMS (ESI-MS): *m/z* [M+H$^+$] calculated for C$_{18}$H$_{27}$N$_6$OS$^+$: 375.1962, found 375.1962; C$_{18}$H$_{26}$N$_6$OS x C$_4$H$_2$F$_6$O$_4$ (602.55).

1-(Amino((3-(2-amino-4-methylthiazol-5-yl)propyl)amino)methylene)-3-(1-(4-fluorophenyl)ethyl)urea dihydrotrifluoroacetate (3.151)

3.151 was prepared from **3.102** (60 mg, 0.10 mmol) in DCM (8.0 mL) and TFA (2.0 mL) according to the general procedure (method A) and obtained as a colorless foamlike solid (41 mg, 65%): RP-HPLC: 97%, (t_R = 9.53, k = 2.57). ^{1}H NMR (300 MHz, CD$_3$OD, di-trifluoroacetate) δ (ppm) 7.40 – 7.27 (m, 2H), 7.11 – 6.97 (m, 2H), 2.69 (t, J = 7.5 Hz, 2H), 2.16 (s, 3H), 1.95 – 1.79 (m, 2H), 1.46 (d, J = 7.1 Hz, 3H). ^{13}C NMR (75 MHz, CD$_3$OD, di-trifluoroacetate) δ (ppm) 170.36, 163.41 (d, J = 244.0 Hz), 155.97, 154.72, 140.94, 132.61, 128.98 (d, J = 8.2 Hz), 118.37, 116.21 (d, J = 21.6 Hz), 50.52, 41.43, 29.87, 23.57, 22.59, 11.44. HRMS (ESI-MS): *m/z* [M+H$^+$] calculated for C$_{17}$H$_{24}$FN$_6$OS$^+$: 379.1711, found 379.1711; C$_{17}$H$_{23}$FN$_6$OS x C$_4$H$_2$F$_6$O$_4$ (606.52).

1-(Amino((3-(2-amino-4-methylthiazol-5-yl)propyl)amino)methylene)-3-(1-(4-chlorophenyl)ethyl)urea dihydrotrifluoroacetate (3.152)

3.152 was prepared from **3.103** (0.11 g, 0.19 mmol) in DCM (8.0 mL) and TFA (2.0 mL) according to the general procedure (method A) and obtained as a colorless foamlike solid (24 mg, 21%): RP-HPLC: 96%, (t_R = 10.47, k = 2.92). ^{1}H NMR (300 MHz, CD$_3$OD, di-trifluoroacetate) δ (ppm) 7.29 (s, 4H), 2.66 (t, J = 7.5 Hz, 2H), 2.13 (s, 3H), 1.93 – 1.76 (m, 2H), 1.44 (d, J = 7.0 Hz, 3H). ^{13}C NMR (75 MHz, CD$_3$OD, di-trifluoroacetate) δ (ppm) 170.34, 162.62, 143.81, 136.43, 134.00, 132.65, 129.67, 128.76, 118.39, 50.62, 41.44, 29.88, 23.58, 22.47, 11.46. HRMS (ESI-MS): *m/z* [M+H$^+$]

calculated for C$_{17}$H$_{24}$ClN$_6$OS$^+$: 395.1415, found 395.1416; C$_{17}$H$_{23}$ClN$_6$OS x C$_4$H$_2$F$_6$O$_4$ (622.97).

1-(Amino((3-(2-amino-4-methylthiazol-5-yl)propyl)amino)methylene)-3-(1-(4-bromophenyl)ethyl)urea dihydrotrifluoroacetate (3.153)

3.153 was prepared from **3.104** (70 mg, 0.11 mmol) in DCM (8.0 mL) and TFA (2.0 mL) according to the general procedure (method A) and obtained as a colorless foamlike solid (24 mg, 34%): RP-HPLC: 96%, (t$_R$ = 10.72, *k* = 3.01). ^{1}H NMR (300 MHz, CD$_3$OD, di-trifluoroacetate) δ (ppm) 7.44 (d, *J* = 8.4 Hz, 2H), 7.23 (d, *J* = 8.4 Hz, 2H), 2.66 (t, *J* = 7.6 Hz, 2H), 2.12 (s, 3H), 1.92 – 1.76 (m, 2H), 1.43 (d, *J* = 7.0 Hz, 3H). ^{13}C NMR (75 MHz, CD$_3$OD, di-trifluoroacetate) δ (ppm) 271.53, 234.74, 218.12, 170.35, 144.32, 132.68, 129.10, 121.91, 118.39, 50.68, 41.44, 29.87, 23.58, 22.43, 11.45. HRMS (ESI-MS): *m/z* [M+H$^+$] calculated for C$_{17}$H$_{24}$BrN$_6$OS$^+$: 439.0910, found 439.0912; C$_{17}$H$_{23}$BrN$_6$OS x C$_4$H$_2$F$_6$O$_4$ (667.42).

1-(Amino((3-(2-amino-4-methylthiazol-5-yl)propyl)amino)methylene)-3-(1-(4-methoxyphenyl)ethyl)urea dihydrotrifluoroacetate (3.154)

3.154 was prepared from **3.105** (0.22 g, 0.37 mmol) in DCM (8.0 mL) and TFA (2.0 mL) according to the general procedure (method A) and obtained as a colorless foamlike solid (12 mg, 5%): RP-HPLC: 97%, (t$_R$ = 9.18, *k* = 2.44). ^{1}H NMR (300 MHz, CD$_3$OD, di-trifluoroacetate) δ (ppm) 7.28 – 7.20 (m, 2H), 6.91 – 6.82 (m, 2H), 3.76 (s, 3H), 2.70 (t, *J* = 7.5 Hz, 2H), 2.16 (s, 3H), 1.95 – 1.81 (m, 2H), 1.45 (d, *J* = 7.0 Hz, 3H). ^{13}C NMR (75 MHz, CD$_3$OD, di-trifluoroacetate) δ (ppm) 168.49, 158.97, 154.21, 153.00, 145.90, 134.98, 126.79, 118.79, 113.50, 54.28, 49.10, 39.97, 28.43, 22.12, 21.13, 10.00. HRMS (ESI-MS): *m/z* [M+H$^+$] calculated for C$_{18}$H$_{27}$N$_6$O$_2$S$^+$: 391.1911, found 391.1921; C$_{18}$H$_{26}$N$_6$O$_2$S x C$_4$H$_2$F$_6$O$_4$ (618.55).

1-(Amino((3-(2-amino-4-methylthiazol-5-yl)propyl)amino)methylene)-3-(1-(4-trifluoromethoxyphenyl)ethyl)urea dihydrochloride (3.155)

3.155 was prepared from **3.106** (0.25 g, 0.39 mmol) in DCM (8.0 mL) and TFA (2.0 mL) according to the general procedure (method B) and obtained as a colorless foamlike solid (180 mg, 90%): RP-HPLC: 95%, (t$_R$ = 11.42, *k* = 3.28). ^{1}H NMR (300 MHz, CD$_3$OD, di-hydrochloride) δ (ppm) 7.45 (m, 2H), 7.23 (d, *J* = 8.0 Hz, 2H), 3.35 (m, 2H), 2.72 (t, *J* = 7.5 Hz, 2H), 2.17 (d, *J* = 3.6 Hz, 3H), 1.87 (p, *J* = 7.0 Hz, 2H), 1.54 – 1.44

(m, 3H). ^{13}C NMR (75 MHz, CD$_3$OD, di-hydrochloride) δ (ppm) 168.72, 154.28, 153.00, 148.09, 142.74, 131.03, 127.47, 120.79, 120.49 (d, J = 255.3 Hz), 117.11, 49.24, 40.21, 28.56, 22.15, 21.27, 10.25. HRMS (ESI-MS): m/z [M+H$^+$] calculated for C$_{18}$H$_{24}$F$_3$N$_6$O$_2$S$^+$: 445.1628, found 445.1630; C$_{18}$H$_{23}$F$_3$N$_6$O$_2$S x H$_2$Cl$_2$ (517.39).

1-(Amino((3-(2-amino-4-methylthiazol-5-yl)propyl)amino)methylene)-3-(1-(2-fluorophenyl)ethyl)urea dihydrotrifluoroacetate (3.156)

3.156 was prepared from **3.107** (0.19 g, 0.32 mmol) in DCM (8.0 mL) and TFA (2.0 mL) according to the general procedure (method A) and obtained as a colorless foamlike solid (94 mg, 48%): RP-HPLC: 99%, (t$_R$ = 9.46, k = 2.54). ^{1}H NMR (400 MHz, CD$_3$OD, di-trifluoroacetate) δ (ppm) 7.39 – 7.03 (m, 4H), 5.16 (q, J = 7.0 Hz, 1H), 2.69 (t, J = 7.6 Hz, 2H), 1.93 – 1.81 (m, 2H), 1.48 (d, J = 7.0 Hz, 3H). ^{13}C NMR (101 MHz, CD$_3$OD, di-trifluoroacetate) δ (ppm) 168.93, 160.06 (d, J = 244.9 Hz), 154.52, 153.22, 131.18, 130.28 (d, J = 13.5 Hz), 128.75 (d, J = 8.4 Hz), 126.98 (d, J = 4.1 Hz), 124.17 (d, J = 3.5 Hz), 116.93, 115.05 (d, J = 22.0 Hz), 44.42, 40.00, 28.42, 22.12, 20.23, 10.00. HRMS (ESI-MS): m/z [M+H$^+$] calculated for C$_{17}$H$_{24}$FN$_6$OS$^+$: 379.1711, found 379.1710; C$_{17}$H$_{23}$FN$_6$OS x C$_4$H$_2$F$_6$O$_4$ (606.52).

1-(Amino((3-(2-amino-4-methylthiazol-5-yl)propyl)amino)methylene)-3-(1-(3-fluorophenyl)ethyl)urea dihydrotrifluoroacetate (3.157)

3.157 was prepared from **3.108** (0.21 g, 0.36 mmol) in DCM (8.0 mL) and TFA (2.0 mL) according to the general procedure (method A) and obtained as a colorless foamlike solid (100 mg, 45%): RP-HPLC: 99%, (t$_R$ = 9.50, k = 2.56). ^{1}H NMR (400 MHz, CD$_3$OD, di-trifluoroacetate) δ (ppm) 7.38 – 7.28 (m, 1H), 7.16 – 6.94 (m, 3H), 4.91 (q, 1H), 2.69 (t, J = 7.6 Hz, 2H), 2.15 (s, 3H), 1.94 – 1.81 (m, 2H), 1.47 (d, J = 7.0 Hz, 3H). ^{13}C NMR (101 MHz, CD$_3$OD, di-trifluoroacetate) δ (ppm) 168.92, 162.98 (d, J = 244.6 Hz), 162.07 (q, J = 34.6 Hz, TFA), 154.54, 153.34, 146.50 (d, J = 6.8 Hz), 131.26, 129.98 (d, J = 8.2 Hz), 121.44 (d, J = 2.9 Hz), 116.95, 116.59 (q, J = 291.7 Hz, TFA), 113.50 (d, J = 21.3 Hz), 112.42 (d, J = 22.2 Hz), 49.34 (d, J = 1.2 Hz), 48.03, 40.00, 28.43, 22.13, 21.03, 10.02. ^{19}F NMR (377 MHz, CD$_3$OD, di-trifluoroacetate) δ (ppm) -75.42 (TFA), -113.47. HRMS (ESI-MS): m/z [M+H$^+$] calculated for C$_{17}$H$_{24}$FN$_6$OS$^+$: 379.1711, found 379.1711; C$_{17}$H$_{23}$FN$_6$OS x C$_4$H$_2$F$_6$O$_4$ (606.52).

1-(Amino((3-(2-amino-4-methylthiazol-5-yl)propyl)amino)methylene)-3-(1-(2-furanyl)methyl)urea dihydrotrifluoroacetate (3.158)

3.158 was prepared from **3.109** (0.14 g, 0.26 mmol) in DCM (8.0 mL) and TFA (2.0 mL) according to the general procedure (method A) and obtained as a colorless foamlike solid (29 mg, 19%): RP-HPLC: 99%, (t$_R$ = 7.16, *k* = 1.68). ^{1}H NMR (400 MHz, CD$_3$OD, di-trifluoroacetate) δ (ppm) 7.46 – 7.40 (m, 2H), 6.36 – 6.27 (m, 2H), 4.38 (s, 2H), 3.34 (t, 3H), 2.72 (t, *J* = 7.5 Hz, 3H), 2.18 (s, 3H), 1.90 (p, *J* = 7.1 Hz, 2H). ^{13}C NMR (101 MHz, CD$_3$OD, di-trifluoroacetate) δ (ppm) 168.93, 154.54, 151.17, 142.13, 131.21, 116.98, 110.00, 107.02, 40.05, 36.04, 28.44, 22.17, 10.02. HRMS (ESI-MS): *m/z* [M+H$^+$] calculated for C$_{14}$H$_{20}$N$_6$O$_2$S$^+$: 337.1441, found 337.1442; C$_{14}$H$_{21}$N$_6$O$_2$S x C$_4$H$_2$F$_6$O$_4$ (564.46).

1-(Amino((3-(2-amino-4-methylthiazol-5-yl)propyl)amino)methylene)-3-(1-(2-furanyl)ethyl)urea dihydrotrifluoroacetate (3.159)

3.159 was prepared from **3.110** (0.22 g, 0.39 mmol) in DCM (8.0 mL) and TFA (2.0 mL) according to the general procedure (method A) and obtained as a colorless foamlike solid (17 mg, 8%): RP-HPLC: 99%, (t$_R$ = 8.24, *k* = 2.09). ^{1}H NMR (300 MHz, CD$_3$OD, di-trifluoroacetate) δ (ppm) 7.40 – 7.38 (m, 1H), 6.33 – 6.21 (m, 2H), 4.98 (q, *J* = 7.1 Hz, 1H), 3.30 (t, *J* = 6.6 Hz, 2H), 2.68 (t, *J* = 7.5 Hz, 2H), 2.15 (s, 3H), 1.95 – 1.78 (m, 2H), 1.47 (d, *J* = 7.0 Hz, 3H). ^{13}C NMR (75 MHz, CD$_3$OD, di-trifluoroacetate) δ (ppm) 168.90, 154.94, 154.50, 141.83, 131.17, 118.53, 116.95, 109.82, 105.23, 43.41, 40.04, 28.43, 22.15, 18.15, 10.01. HRMS (ESI-MS): *m/z* [M+H$^+$] calculated for C$_{15}$H$_{23}$N$_6$O$_2$S$^+$: 351.1598, found 351.1600; C$_{15}$H$_{22}$N$_6$O$_2$S x C$_4$H$_2$F$_6$O$_4$ (578.49).

1-(Amino((3-(2-amino-4-methylthiazol-5-yl)propyl)amino)methylene)-3-(1-(thiophen-2-yl)ethyl)urea dihydrotrifluoroacetate (3.160)

3.160 was prepared from **3.111** (0.21 g, 0.36 mmol) in DCM (8.0 mL) and TFA (2.0 mL) according to the general procedure (method A) and obtained as a colorless foamlike solid (11 mg, 5%): RP-HPLC: 99%, (t$_R$ = 8.80, *k* = 2.30). ^{1}H NMR (400 MHz, CD$_3$OD, di-trifluoroacetate) δ (ppm) 7.30 (dd, *J* = 5.1, 1.2 Hz, 1H), 7.05 – 6.95 (m, 2H), 5.22 (q, 1H), 3.34 (t, *J* = 6.8 Hz, 2H), 2.73 (t, *J* = 7.6 Hz, 2H), 2.19 (s, 3H), 1.96 – 1.86 (m, 2H), 1.60 (d, *J* = 6.9 Hz, 3H). ^{13}C NMR (75 MHz, CD$_3$OD, di-trifluoroacetate) δ (ppm) 168.92, 167.26, 154.53, 146.63, 131.16, 126.34, 123.83, 123.61, 116.90, 45.17, 40.02, 28.43,

22.14, 21.16, 10.02. HRMS (ESI-MS): *m/z* [M+H$^+$] calculated for C$_{15}$H$_{23}$N$_6$OS$_2^+$: 367.1369, found 367.1367; C$_{15}$H$_{22}$N$_6$OS$_2$ x C$_4$H$_2$F$_6$O$_4$ (594.55).

1-(Amino((3-(2-amino-4-methylthiazol-5-yl)propyl)amino)methylene)-3-(2-phenylethyl)urea dihydrotrifluoroacetate (3.161) *(Synthesized by Claudia Honisch)*

3.112 was prepared from **3.009a** (0.12 g, 0.44 mmol), **3.071** (0.15 g, 0.44 mmol), HgCl$_2$ (0.24 g, 0.89 mmol) and NEt$_3$ (0.18 mL, 1.33 mmol) in DCM (25 mL) conforming to the general procedure for the guanidinylation reaction. Subsequently, **3.161** was prepared from the Boc-protected intermediate **3.112** in DCM (4.0 mL) and TFA (1.0 mL) according to the general procedure (method A) and obtained as a colorless foamlike solid (110 mg, 42%): RP-HPLC: 99%, (t$_R$ = 15.00, *k* = 4.20). ^{1}H NMR (600 MHz, DMSO-d$_6$, di-trifluoroacetate): δ (ppm) 10.29 (br s, 1H), 9.04 (br s, 3H), 8.52 (br s, 2H), 7.60 (br s, 1H), 7.30 – 7.28 (m, 2H), 7.22 – 7.19 (m, 3H), 3.33 – 3.32 (m, 2H), 3.24 (br s, 2H), 2.75 (t, *J* = 7.2 Hz, 2H), 2.60 – 2.58 (m, 2H), 2.08 (s, 3H), 1.71 (p, *J* = 7.1 Hz, 2H). ^{13}C NMR (150 MHz, DMSO-d$_6$, di-trifluoroacetate): δ (ppm) 167.70, 153.70, 153.60, 138.90, 131.70, 128.60, 128.40, 126.20, 116.30, 40.70, 40.00, 35.00, 28.80, 21.90, 11.50. HRMS (ESI-MS): *m/z* [M+H$^+$] calculated for C$_{17}$H$_{25}$N$_6$OS$^+$: 361.1805, found 361.1812; C$_{17}$H$_{24}$N$_6$OS x C$_4$H$_2$F$_6$O$_4$ (588.53).

1-(Amino((3-(2-amino-4-methylthiazol-5-yl)propyl)amino)methylene)-3-(2,2-diphenylethyl)urea dihydrotrifluoroacetate (3.162) *(Synthesized by Steffen Pockes)*

3.162 was prepared from **3.113** (0.26 g, 0.41 mmol) in DCM (4.0 mL) and TFA (1.0 mL) according to the general procedure (method A) and obtained as a colorless foamlike solid (210 mg, 74%): RP-HPLC: 99%, (t$_R$ = 15.04, *k* = 3.76). ^{1}H NMR (300 MHz, CD$_3$OD, di-trifluoroacetate) δ (ppm) 7.36 – 7.12 (m, 10H), 4.26 (t, *J* = 8.1 Hz, 1H), 3.84 (d, *J* = 8.1 Hz, 2H), 3.30 – 3.25 (m, 2H), 2.68 (t, *J* = 7.6 Hz, 2H), 2.16 (s, 3H), 1.86 (p, *J* = 7.1 Hz, 2H). ^{13}C NMR (75 MHz, CD$_3$OD, di-trifluoroacetate) δ (ppm) 170.37, 155.85, 155.50, 143.40, 132.63, 129.73, 129.16, 127.86, 118.39, 51.99, 45.26, 41.41, 29.89, 23.57, 11.48. HRMS (ESI-MS): *m/z* [M+H$^+$] calculated for C$_{23}$H$_{29}$N$_6$OS$^+$: 437.2118, found 437.2120; C$_{23}$H$_{28}$N$_6$OS x C$_4$H$_2$F$_6$O$_4$ (664.62).

1-(Amino((3-(2-amino-4-methylthiazol-5-yl)propyl)amino)methylene)-3-(2-cyclohexylpropyl)urea dihydrotrifluoroacetate (3.163) *(Synthesized by Sabrina Biselli)*

3.114 was prepared from **3.009a** (0.07 g, 0.25 mmol), **3.073** (0.09 g, 0.25 mmol), HgCl$_2$ (0.14 g, 0.50 mmol), and NEt$_3$ (0.10 mL, 0.76 mmol) in DCM (25 mL) conforming to the general procedure for the guanidinylation reaction. Subsequently, **3.163** was prepared from the Boc-protected intermediate **3.114** in DCM (4.0 mL) and TFA (1.0 mL) according to the general procedure (method A) and obtained as a colorless foamlike solid (80 mg, 53%): RP-HPLC: 99%, (t$_R$ = 18.61, k = 5.42). ^{1}H NMR (600 MHz, DMSO-d$_6$, di-trifluoroacetate): δ (ppm) 13.55 (br s, 1H), 10.34 (br s, 1H), 9.07 – 8.98 (m, 3H), 8.49 (br s, 2H), 7.44 (br s, 1H), 3.25 – 3.22 (m, 2H), 3.14 – 3.10 (m, 1H), 2.94 – 2.90 (m, 1H), 2.60 – 2.58 (m, 2H), 2.07 (s, 3H), 1.74 – 1.67 (m, 4H), 1.61 – 1.55 (m, 3H), 1.47 – 1.43 (m, 1H), 1.22 – 0.90 (m, 6H), 0.78 (d, J = 6.8 Hz, 3H). ^{13}C NMR (150 MHz, DMSO-d$_6$, di-trifluoroacetate): δ (ppm) 167.81, 153.72, 153.68, 131.75, 116.28, 42.85, 40.05, 39.30, 37.77, 30.27, 28.80, 27.90, 26.23, 26.16, 26.05, 21.96, 14.03, 11.40. HRMS (ESI-MS): *m/z* [M+H$^+$] calculated for C$_{18}$H$_{33}$N$_6$OS$^+$: 381.2431, found 381.2436; C$_{18}$H$_{32}$N$_6$OS x C$_4$H$_2$F$_6$O$_4$ (608.61).

(*R*)-1-(Amino((3-(2-amino-4-methylthiazol-5-yl)propyl)amino)methylene)-3-(2-phenylpropyl)urea dihydrotrifluoroacetate (3.164) *(Synthesized by Steffen Pockes)*

3.164 was prepared from **3.115** (0.16 g, 0.28 mmol) in DCM (4.0 mL) and TFA (1.0 mL) according to the general procedure (method A) and obtained as a colorless foamlike solid (90 mg, 54%): RP-HPLC: 99%, (t$_R$ = 12.20, k = 2.86), ee = 99%, [α]$^{20}_D$ +25.82 (*c* 0.28, MeOH). ^{1}H NMR (300 MHz, CD$_3$OD, di-trifluoroacetate) δ (ppm) 7.35 – 7.12 (m, 5H), 3.36 (d, J = 7.4 Hz, 2H), 3.31 – 3.27 (m, 2H), 3.01 - 2.91 (m, 1H), 2.69 (t, J = 7.5 Hz, 2H), 2.16 (s, 3H), 1.87 (p, J = 7.1 Hz, 2H), 1.26 (d, J = 7.0 Hz, 3H). ^{13}C NMR (75 MHz, CD$_3$OD, di-trifluoroacetate) δ (ppm) 170.40, 155.94, 155.52, 145.43, 132.60, 129.67, 128.30, 127.72, 118.37, 47.64, 41.41, 41.01, 29.89, 23.59, 19.57, 11.47. HRMS (ESI-MS): *m/z* [M+H$^+$] calculated for C$_{18}$H$_{27}$N$_6$OS$^+$: 375.1962, found 375.1966; C$_{18}$H$_{26}$N$_6$OS x C$_4$H$_2$F$_6$O$_4$ (602.55).

(S)-1-(Amino((3-(2-amino-4-methylthiazol-5-yl)propyl)amino)methylene)-3-(2-phenylpropyl)urea dihydrotrifluoroacetate (3.165) *(Synthesized by Steffen Pockes)*

3.165 was prepared from **3.116** (0.26 g, 0.45 mmol) in DCM (4.0 mL) and TFA (1.0 mL) according to the general procedure (method A) and obtained as a colorless foamlike solid (230 mg, 84%): RP-HPLC: 99%, (t$_R$ = 12.16, *k* = 2.85), ee = 99%, [α]^{20}$_D$ -21.71 (*c* 0.33, MeOH). ^{1}H NMR (300 MHz, CD$_3$OD, di-trifluoroacetate) δ (ppm) 7.60 – 7.03 (m, 5H), 3.39 – 3.34 (m, 2H), 3.34 – 3.25 (m, 2H), 3.02 - 2.92 (m, 1H), 2.70 (t, *J* = 7.5 Hz, 2H), 2.17 (s, 3H), 1.87 (p, *J* = 7.1 Hz, 2H), 1.26 (d, *J* = 7.0 Hz, 3H). ^{13}C NMR (75 MHz, CD$_3$OD, di-trifluoroacetate) δ (ppm) 170.40, 163.31, 162.83, 145.43, 132.61, 129.68, 128.30, 127.73, 118.40, 47.63, 41.41, 41.02, 29.90, 23.59, 19.58, 11.46. HRMS (ESI-MS): *m/z* [M+H$^+$] calculated for C$_{18}$H$_{27}$N$_6$OS$^+$: 375.1962, found 375.1968; C$_{18}$H$_{26}$N$_6$OS x C$_4$H$_2$F$_6$O$_4$ (602.55).

1-(Amino((3-(2-amino-4-methylthiazol-5-yl)propyl)amino)methylene)-3-(2-phenylbutyl)urea dihydrotrifluoroacetate (3.166) *(Synthesized by Sabrina Biselli)*

3.117 was prepared from **3.009a** (0.07 g, 0.25 mmol), **3.076** (0.09 g, 0.25 mmol), HgCl$_2$ (0.14 g, 0.50 mmol), and NEt$_3$ (0.10 mL, 0.76 mmol) in DCM (25 mL) conforming to the general procedure for the guanidinylation reaction. Subsequently, **3.166** was prepared from the Boc-protected intermediate **3.117** in DCM (4.0 mL) and TFA (1.0 mL) according to the general procedure (method A) and obtained as a colorless foamlike solid (80 mg, 52%): RP-HPLC: 98%, (t$_R$ = 16.71, *k* = 4.76). ^{1}H NMR (600 MHz, DMSO-d$_6$, di-trifluoroacetate): δ (ppm) 10.37 (br s, 1H), 9.08 (br s, 2H), 8.98 (br s, 1H), 8.50 (br s, 2H), 7.31 – 7.28 (m, 3H), 7.21 – 7.18 (m, 3H), 3.38 – 3.34 (m, 1H), 3.29 – 3.20 (m, 3H), 2.67 – 2.62 (m, 1H), 2.58 – 2.56 (m, 2H), 2.06 (s, 3H), 1.73 – 1.64 (m, 3H), 1.54 – 1.46 (m, 1H), 0.71 (t, *J* = 7.3 Hz, 3H). ^{13}C NMR (150 MHz, DMSO-d$_6$, di-trifluoroacetate): δ (ppm) 167.80, 153.69, 153.67, 142.50, 132.00, 128.40, 127.70, 126.40, 116.30, 46.70, 44.60, 39.40, 28.80, 25.80, 22.00, 11.70, 11.40. HRMS (ESI-MS): *m/z* [M+H$^+$] calculated for C$_{19}$H$_{29}$N$_6$OS$^+$: 389.2118, found 389.2118; C$_{19}$H$_{28}$N$_6$OS x C$_4$H$_2$F$_6$O$_4$ (616.58).

1-(Amino((3-(2-amino-4-methylthiazol-5-yl)propyl)amino)methylene)-3-(3-methyl-2-phenylbutyl)urea dihydrotrifluoroacetate (3.167) *(Synthesized by Sabrina Biselli)*

3.118 was prepared from **3.009a** (0.06 g, 0.24 mmol), **3.077** (0.09 g, 0.24 mmol), HgCl$_2$ (0.13 g, 0.47 mmol), and NEt$_3$ (0.10 mL, 0.71 mmol) in DCM (25 mL) conforming to the general procedure for the guanidinylation reaction. Subsequently, **3.167** was prepared from the Boc-protected intermediate **3.118** in DCM (4.0 mL) and TFA (1.0 mL) according to the general procedure (method A) and obtained as a colorless foamlike solid (40 mg, 26%): RP-HPLC: 99%, (t_R = 18.31, k = 5.31). ^{1}H NMR (600 MHz, DMSO-d$_6$, di-trifluoroacetate): δ (ppm) 10.08 (br s, 1H), 9.16 (br s, 2H), 8.93 (br s, 1H), 8.45 (br s, 2H), 7.30 – 7.28 (m, 2H), 7.22 – 7.19 (m, 1H), 7.16 – 7.11 (m, 3H), 3.60 – 3.56 (m, 1H), 3.36 – 3.31 (m, 1H), 3.20 – 3.19 (m, 2H), 2.57 – 2.52 (m, 3H), 2.06 (s, 3H), 1.88 – 1.83 (m, 1H), 1.69 (p, J = 7.2 Hz, 2H), 0.91 (d, J = 6.7 Hz, 3H), 0.66 (d, J = 6.7 Hz, 3H). ^{13}C NMR (150 MHz, DMSO-d$_6$, di-trifluoroacetate): δ (ppm) 167.79, 153.50, 141.39, 131.37, 128.43, 128.09, 126.35, 116.24, 51.50, 41.95, 39.95, 30.38, 28.70, 21.90, 20.70, 19.99, 11.27. HRMS (ESI-MS): *m/z* [M+H$^+$] calculated for C$_{20}$H$_{31}$N$_6$OS$^+$: 403.2275, found 403.2282; C$_{20}$H$_{30}$N$_6$OS x C$_4$H$_2$F$_6$O$_4$ (630.61).

1-(Amino((3-(2-amino-4-methylthiazol-5-yl)propyl)amino)methylene)-3-(2-(4-prop-2-ylphenyl)propyl)urea dihydrotrifluoroacetate (3.168) *(Synthesized by Sabrina Biselli)*

3.119 was prepared from **3.009a** (0.06 g, 0.23 mmol), **3.078** (0.09 g, 0.23 mmol), HgCl$_2$ (0.12 g, 0.46 mmol), and NEt$_3$ (0.09 mL, 0.69 mmol) in DCM (25 mL) conforming to the general procedure for the guanidinylation reaction. Subsequently, **3.168** was prepared from the Boc-protected intermediate **3.119** in DCM (4.0 mL) and TFA (1.0 mL) according to the general procedure (method A) and obtained as a colorless foamlike solid (80 mg, 54%): RP-HPLC: 96%, (t_R = 19.33, k = 5.67). ^{1}H NMR (600 MHz, DMSO-d$_6$, di-trifluoroacetate): δ (ppm) 10.36 (br s, 1H), 9.23 (br s, 2H), 9.01 (br s, 1H), 8.51 (br s, 2H), 7.38 (br s, 1H), 7.18 – 7.14 (m, 4H), 3.25 – 3.22 (m, 4H), 2.89 – 2.82 (m, 2H), 2.61 – 2.58 (m, 2H), 2.08 (s, 3H), 1.72 (p, J = 7.1 Hz, 2H), 1.18 – 1.16 (m, 9H). ^{13}C NMR (150 MHz, DMSO-d$_6$, di-trifluoroacetate): δ (ppm) 168.00, 153.71, 153.68, 146.40, 141.50, 131.30, 127.00, 126.30, 116.30, 46.00, 38.70, 38.60, 33.00, 28.70, 23.90, 21.90, 19.10, 11.20. HRMS (ESI-MS): *m/z* [M+H$^+$] calculated for C$_{21}$H$_{33}$N$_6$OS$^+$: 417.2431, found 417.2435; C$_{21}$H$_{32}$N$_6$OS x C$_4$H$_2$F$_6$O$_4$ (644.64).

1-(Amino((3-(2-amino-4-methylthiazol-5-yl)propyl)amino)methylene)-3-(3-cyclohexyl-2-methylpropyl)urea dihydrotrifluoroacetate (3.169) *(Synthesized by Sabrina Biselli)*

3.120 was prepared from **3.009a** (0.06 g, 0.22 mmol), **3.079** (0.08 g, 0.22 mmol), HgCl$_2$ (0.12 g, 0.43 mmol), and NEt$_3$ (0.09 mL, 0.65 mmol) in DCM (25 mL) conforming to the general procedure for the guanidinylation reaction. Subsequently, **3.169** was prepared from the Boc-protected intermediate **3.120** in DCM (4.0 mL) and TFA (1.0 mL) according to the general procedure (method A) and obtained as a colorless foamlike solid (110 mg, 54%): RP-HPLC: 99%, (t$_R$ = 20.10, *k* = 5.93). ^{1}H NMR (600 MHz, DMSO-d$_6$, di-trifluoroacetate): δ (ppm) 10.42 (br s, 1H), 9.06 – 9.00 (m, 3H), 8.51 (br s, 2H), 7.47 (br s,1H), 3.26 – 3.23 (m, 2H), 3.06 – 3.02 (m, 1H), 2.89 – 2.84 (m, 1H), 2.61 – 2.58 (m, 2H), 2.08 (s, 3H), 1.75 – 1.59 (m, 8H), 1.31 – 1.26 (m, 1H), 1.23 – 1.07 (m, 4H), 0.97 – 0.93 (m, 1H), 0.88 – 0.73 (m, 5H). ^{13}C NMR (150 MHz, DMSO-d$_6$, di-trifluoroacetate): δ (ppm) 167.80, 153.78, 153.77, 131.90, 116.30, 45.30, 41.70, 39.00, 34.20, 33.50, 32.50, 29.60, 28.80, 26.20, 25.80, 25.70, 22.00, 17.70, 11.40. HRMS (ESI-MS): *m/z* [M+H$^+$] calculated for C$_{19}$H$_{35}$N$_6$OS$^+$: 395.2588, found 395.2590; C$_{19}$H$_{34}$N$_6$OS x C$_4$H$_2$F$_6$O$_4$ (622.63).

1-(Amino((3-(2-amino-4-methylthiazol-5-yl)propyl)amino)methylene)-3-(2-methyl-3-(4-methylphenyl)propyl)urea dihydrotrifluoroacetate (3.170) *(Synthesized by Sabrina Biselli)*

3.121 was prepared from **3.009a** (0.06 g, 0.22 mmol), **3.080** (0.08 g, 0.22 mmol), HgCl$_2$ (0.12 g, 0.43 mmol), and NEt$_3$ (0.09 mL, 0.65 mmol) in DCM (25 mL) conforming to the general procedure for the guanidinylation reaction. Subsequently, **3.170** was prepared from the Boc-protected intermediate **3.121** in DCM (4.0 mL) and TFA (1.0 mL) according to the general procedure (method A) and obtained as a colorless foamlike solid (30 mg, 22%): RP-HPLC: 98%, (t$_R$ = 20.21, *k* = 5.97). ^{1}H NMR (600 MHz, DMSO-d$_6$, di-trifluoroacetate): δ (ppm) 10.49 (br s, 1H), 9.14 (br s, 2H), 8.99 (br s, 1H), 8.51 (br s, 2H), 7.53 (br s, 1H), 7.07 – 7.07 (m, 4H), 3.23 (q, *J* = 6.5 Hz, 2H), 3.09 – 3.05 (m, 1H), 2.93 – 2.89 (m, 1H), 2.60 – 2.55 (m, 3H), 2.31 – 2.28 (m, 1H), 2.25 (s, 3H), 2.07 (s, 3H), 1.88 – 1.82 (m, 1H), 1.72 (p, *J* = 7.2 Hz, 2H), 0.78 (d, *J* = 6.7 Hz, 3H). ^{13}C NMR (150 MHz, DMSO-d$_6$, di-trifluoroacetate): δ (ppm) 167.88, 153.78, 136.95, 134.70, 131.61, 128.76, 128.75, 116.26, 44.61, 40.93, 38.87, 34.86, 28.79,

21.94, 20.58, 17.04, 11.33. HRMS (ESI-MS): *m/z* [M+H$^+$] calculated for $C_{20}H_{31}N_6OS^+$: 403.2275, found 403.2277; $C_{20}H_{30}N_6OS \times C_4H_2F_6O_4$ (630.61).

1-(Amino((3-(2-amino-4-methylthiazol-5-yl)propyl)amino)methylene)-3-(2-methyl-4-phenylbutyl)urea dihydrotrifluoroacetate (3.171) *(Synthesized by Sabrina Biselli)*

3.122 was prepared from **3.009a** (0.06 g, 0.24 mmol), **3.081** (0.09 g, 0.24 mmol), HgCl$_2$ (0.13 g, 0.47 mmol), and NEt$_3$ (0.10 mL, 0.71 mmol) in DCM (25 mL) conforming to the general procedure for the guanidinylation reaction. Subsequently, **3.171** was prepared from the Boc-protected intermediate **3.122** in DCM (4.0 mL) and TFA (1.0 mL) according to the general procedure (method A) and obtained as a colorless foamlike solid (30 mg, 20%): RP-HPLC: 99%, (t_R = 18.49, *k* = 5.38). ^{1}H NMR (600 MHz, DMSO-d$_6$, di-trifluoroacetate): δ (ppm) 10.32 (br s, 1H), 8.98 (br s, 1H), 8.82 (br s, 2H), 8.49 (br s, 2H), 7.51(br s, 1H), 7.26 – 7.24 (m, 2H), 7.19 – 7.14 (m, 3H), 3.21 – 3.25 (m, 2H), 3.09 – 3.05 (m, 1H), 3.01 – 2.96 (m, 1H), 2.65 – 2.51 (m, 4H), 2.05 (s, 3H), 1.71 (p, *J* = 7.2 Hz, 2H), 1.63 – 1.56 (m, 2H), 1.39 – 1.33 (m, 1H), 0.89 (d, *J* = 6.5 Hz, 3H). ^{13}C NMR (150 MHz, DMSO-d$_6$, di-trifluoroacetate): δ (ppm) 167.50, 153.80, 153.70, 142.20, 132.90, 128.23, 128.20, 125.60, 116.30, 44.80, 39.80, 35.60, 32.50, 32.40, 28.90, 22.00, 17.20, 11.70. HRMS (ESI-MS): *m/z* [M+H$^+$] calculated for $C_{20}H_{31}N_6OS^+$: 403.2275, found 403.2277; $C_{20}H_{30}N_6OS \times C_4H_2F_6O_4$ (630.61).

1-(Amino((3-(2-amino-4-methylthiazol-5-yl)propyl)amino)methylene)-3-(2-methyl-5-phenylpentyl)urea dihydrotrifluoroacetate (3.172) *(Synthesized by Katharina Tropmann)*

3.123 was prepared from **3.009b** (0.04 g, 0.09 mmol), **3.082** (0.04 g, 0.09 mmol), HgCl$_2$ (0.05 g, 0.18 mmol), and NEt$_3$ (0.04 mL, 0.27 mmol) in DCM (25 mL) conforming to the general procedure for the guanidinylation reaction. Subsequently, **3.172** was prepared from the Boc-/Trt-protected intermediate **3.123** DCM (4.0 mL) and TFA (1.0 mL) according to the general procedure (method A) and obtained as a colorless foamlike solid (5 mg, 9%): RP-HPLC: 98%, (t_R = 15.64, *k* = 3.87). ^{1}H NMR (600 MHz, DMSO-d$_6$, di-trifluoroacetate): δ (ppm) 10.20 (s, 1H), 8.97 (s, 3H), 8.48 (s, 2H), 7.48 (s, 1H), 7.27 – 7.23 (m, 2H), 7.19 – 7.12 (m, 3H), 3.23 (q, *J* = 6.6 Hz, 2H), 3.07 – 2.99 (m, 1H), 2.94 – 2.86 (m, 1H), 2.62 – 2.51 (m, 4H), 2.07 (s, 3H), 1.72 (p, *J* = 7.3 Hz, 2H), 1.65 – 1.47 (m, 3H), 1.36 – 1.26 (m, 1H), 1.14 – 1.03 (m, 1H), 0.83 (d, *J* = 6.7 Hz, 3H). ^{13}C NMR

(150 MHz, DMSO-d$_6$, di-trifluoroacetate): δ (ppm) 167.67, 158.81 (q, J = 35.8 Hz, TFA), 153.73, 142.13, 128.22 (2C), 128.21 (2C), 125.62, 116.79 (q, J = 298.5 Hz, TFA), 116.30, 44.90, 40.06, 35.32, 33.21, 32.62, 28.86, 28.32, 22.00, 17.40, 11.54. HRMS (ESI-MS): m/z [M+H$^+$] calculated for C$_{21}$H$_{33}$N$_6$OS$^+$: 417.2431, found 417.2435; C$_{21}$H$_{32}$N$_6$OS x C$_4$H$_2$F$_6$O$_4$ (644.64).

1-(Amino((3-(2-amino-4-methylthiazol-5-yl)propyl)amino)methylene)-3-benzhydrylthiourea dihydrotrifluoroacetate (3.173) *(Synthesized by Steffen Pockes)*

3.173 was prepared from **3.124** (0.07 g, 0.11 mmol) in DCM (4.0 mL) and TFA (1.0 mL) according to the general procedure (method A) and obtained as a colorless solid (50 mg, 68%), mp 82-85 °C, RP-HPLC: 98%, (t$_R$ = 17.49, k = 4.53). ^{1}H NMR (300 MHz, CD$_3$OD, di-trifluoroacetate) δ (ppm) 7.43 – 7.17 (m, 10H), 6.64 (s, 1H), 3.37 (t, J = 6.6 Hz, 2H), 2.74 (t, J = 7.6 Hz, 2H), 2.17 (s, 3H), 1.92 (p, J = 6.9 Hz, 2H). ^{13}C NMR (75 MHz, CD$_3$OD, di-trifluoroacetate) δ (ppm) 179.62, 170.36, 155.97, 141.57, 132.70, 129.82, 128.88, 128.67, 118.35, 62.73, 41.82, 29.72, 23.72, 11.54. HRMS (ESI-MS): m/z [M+H$^+$] calculated for C$_{22}$H$_{27}$N$_6$S$_2$$^+$: 439.1733, found 439.1735; C$_{22}$H$_{26}$N$_6$S$_2$ x C$_4$H$_2$F$_6$O$_4$ (666.66).

(*R*)-1-(Amino((3-(2-amino-4-methylthiazol-5-yl)propyl)amino)methylene)-3-(1-phenylethyl)thiourea dihydrotrifluoroacetate (3.174) *(Synthesized by Steffen Pockes)*

3.174 was prepared from **3.125** (0.05 g, 0.09 mmol) in DCM (4.0 mL) and TFA (1.0 mL) according to the general procedure and obtained as a colorless solid (30 mg, 57%), mp 75-78 °C, RP-HPLC: 95%, (t$_R$ = 14.18, k = 3.49), ee = 99%, [α]$^{20}_D$ +20.30 (*c* 0.34, MeOH). ^{1}H NMR (300 MHz, CD$_3$OD, di-trifluoroacetate) δ (ppm) 7.42 – 7.19 (m, 5H), 5.45 (q, J = 7.5, 7.0 Hz, 1H), 3.36 (t, J = 6.7 Hz, 2H), 2.74 (t, J = 7.6 Hz, 2H), 2.17 (s, 3H), 1.91 (p, J = 6.9 Hz, 2H), 1.54 (d, J = 7.0 Hz, 3H). ^{13}C NMR (75 MHz, CD$_3$OD, di-trifluoroacetate) δ (ppm) 179.76, 170.37, 156.02, 143.45, 132.68, 129.70, 128.58, 127.48, 118.35, 54.90, 41.74, 29.71, 23.71, 21.84, 11.53. HRMS (ESI-MS): m/z [M+H$^+$] calculated for C$_{17}$H$_{25}$N$_6$S$_2$$^+$: 377.1577, found 377.1578; C$_{17}$H$_{24}$N$_6$S$_2$ x C$_4$H$_2$F$_6$O$_4$ (604.59).

(*S*)-1-(Amino((3-(2-amino-4-methylthiazol-5-yl)propyl)amino)methylene)-3-(1-phenylethyl)thiourea dihydrotrifluoroacetate (3.175) *(Synthesized by Steffen Pockes)*

3.175 was prepared from **3.126** (0.08 g, 0.14 mmol) in DCM (4.0 mL) and TFA (1.0 mL) according to the general procedure (method A) and obtained as a colorless solid (50 mg, 60%), mp 71-75 °C, RP-HPLC: 99%, (t$_R$ = 14.10, *k* = 3.46), ee = 99%, [α]$^{20}_D$ -17.27 (*c* 0.28, MeOH). ^{1}H NMR (300 MHz, CD$_3$OD, di-trifluoroacetate) δ (ppm) 7.40 – 7.18 (m, 5H), 5.45 (q, *J* = 7.4 Hz, 1H), 3.36 (t, *J* = 6.7 Hz, 2H), 2.74 (t, *J* = 7.6 Hz, 2H), 2.16 (s, 3H), 1.91 (p, *J* = 6.9 Hz, 2H), 1.54 (d, *J* = 7.0 Hz, 3H). ^{13}C NMR (75 MHz, CD$_3$OD, di-trifluoroacetate) δ (ppm) 179.11, 170.37, 156.03, 143.47, 132.67, 129.70, 128.57, 127.48, 118.34, 54.90, 41.73, 29.71, 23.71, 21.86, 11.53. HRMS (ESI-MS): *m/z* [M+H$^+$] calculated for C$_{17}$H$_{25}$N$_6$S$_2^+$: 377.1577, found 377.1577; C$_{17}$H$_{24}$N$_6$S$_2$ x C$_4$H$_2$F$_6$O$_4$ (604.59).

1-(Amino((3-(2-amino-4-methylthiazol-5-yl)propyl)amino)methylene)-3-(2,2-diphenylethyl)thiourea dihydrotrifluoroacetate (3.176) *(Synthesized by Steffen Pockes)*

3.176 was prepared from **3.127** (0.10 g, 0.15 mmol) in DCM (4.0 mL) and TFA (1.0 mL) according to the general procedure (method A) and obtained as a colorless solid (60 mg, 58%), mp 81-83 °C, RP-HPLC: 99%, (t$_R$ = 17.91, *k* = 4.67). ^{1}H NMR (300 MHz, CD$_3$OD, di-trifluoroacetate) δ (ppm) 7.32 – 7.18 (m, 10H), 4.52 (t, *J* = 8.1 Hz, 1H), 4.17 (d, *J* = 8.1 Hz, 2H), 3.34 (t, *J* = 6.8 Hz, 2H), 2.73 (t, *J* = 7.6 Hz, 2H), 2.17 (s, 3H), 1.89 (p, *J* = 7.0 Hz, 2H). ^{13}C NMR (75 MHz, CD$_3$OD, di-trifluoroacetate) δ (ppm) 180.14, 170.35, 155.83, 143.04, 132.63, 129.80, 129.15, 128.00, 118.35, 50.27, 49.57, 41.77, 29.71, 23.71, 11.57. HRMS (ESI-MS): *m/z* [M+H$^+$] calculated for C$_{23}$H$_{29}$N$_6$S$_2^+$: 453.1890, found 453.1891; C$_{23}$H$_{28}$N$_6$S$_2$ x C$_4$H$_2$F$_6$O$_4$ (680.69).

(*R*)-1-(Amino((3-(2-amino-4-methylthiazol-5-yl)propyl)amino)methylene)-3-(2-phenylpropyl)thiourea dihydrotrifluoroacetate (3.177) *(Synthesized by Steffen Pockes)*

3.177 was prepared from **3.128** (0.07 g, 0.12 mmol) in DCM (4.0 mL) and TFA (1.0 mL) according to the general procedure (method A) and obtained as a colorless solid (60 mg, 82%), mp 124-128 °C, RP-HPLC: 99%, (t$_R$ = 15.46, *k* = 3.89), ee = 96%, [α]$^{20}_D$ +37.06 (*c* 0.29, MeOH). ^{1}H NMR (300 MHz, CD$_3$OD, di-trifluoroacetate) δ (ppm) 7.34

– 7.16 (m, 5H), 3.79 – 3.64 (m, 2H), 3.35 (t, *J* = 6.6 Hz, 2H), 3.25 – 3.15 (m, 1H), 2.74 (t, *J* = 7.5 Hz, 2H), 2.17 (s, 3H), 1.91 (p, *J* = 6.8 Hz, 2H), 1.29 (d, *J* = 7.0 Hz, 3H). ^{13}C NMR (75 MHz, CD$_3$OD, di-trifluoroacetate) δ (ppm) 180.13, 170.38, 155.95, 145.08, 132.69, 129.75, 128.24, 127.88, 118.34, 51.95, 41.71, 39.52, 29.70, 23.73, 19.70, 11.54. HRMS (ESI-MS): *m/z* [M+H$^+$] calculated for C$_{18}$H$_{27}$N$_6$S$_2^+$: 391.1733, found 391.1737; C$_{18}$H$_{26}$N$_6$S$_2$ x C$_4$H$_2$F$_6$O$_4$ (618.61).

(*S*)-1-(Amino((3-(2-amino-4-methylthiazol-5-yl)propyl)amino)methylene)-3-(2-phenylpropyl)thiourea dihydrotrifluoroacetate (3.178) *(Synthesized by Steffen Pockes)*

3.178 was prepared from **3.129** (0.05 g, 0.08 mmol) in DCM (4.0 mL) and TFA (1.0 mL) according to the general procedure (method A) and obtained as a colorless solid (50 mg, 96%), mp 124-128 °C, RP-HPLC: 99%, (t$_R$ = 15.43, *k* = 3.88), ee = 96%, [α]$^{20}_D$ -25.49 (*c* 0.31, MeOH). ^{1}H NMR (300 MHz, CD$_3$OD, di-trifluoroacetate) δ (ppm) 7.49 – 7.04 (m, 5H), 3.79 – 3.62 (m, 2H), 3.35 (t, *J* = 6.7 Hz, 2H), 3.24 – 3.16 (m, 1H), 2.74 (t, *J* = 7.5 Hz, 2H), 2.17 (s, 3H), 1.91 (p, *J* = 6.8 Hz, 2H), 1.30 (d, *J* = 7.0 Hz, 3H). ^{13}C NMR (75 MHz, CD$_3$OD, di-trifluoroacetate) δ (ppm) 180.13, 170.38, 155.95, 145.08, 132.70, 129.75, 128.24, 127.88, 118.36, 51.95, 41.72, 39.52, 29.70, 23.73, 19.72, 11.55. HRMS (ESI-MS): *m/z* [M+H$^+$] calculated for C$_{18}$H$_{27}$N$_6$S$_2^+$: 391.1733, found 391.1736; C$_{18}$H$_{26}$N$_6$S$_2$ x C$_4$H$_2$F$_6$O$_4$ (618.61).

1-(Amino((3-(2-aminothiazol-4-yl)phenyl)amino)methylene)-3-(1-propyl)urea dihydrotrifluoroacetate (3.179) *(Synthesized by Sabrina Biselli)*

3.130 was prepared from **3.011** (0.06 g, 0.29 mmol), **3.048** (0.08 g, 0.29 mmol), HgCl$_2$ (0.16 g, 0.58 mmol), and NEt$_3$ (0.12 mL, 0.87 mmol) in DCM (25 mL) conforming to the general procedure for the guanidinylation reaction. Subsequently, **3.179** was prepared from the Boc-protected intermediate **3.130** in DCM (4.0 mL) and TFA (1.0 mL) according to the general procedure (method A) and obtained as a colorless foamlike solid (40 mg, 25%): RP-HPLC: 99%, (t$_R$ = 13.87, *k* = 3.78). ^{1}H NMR (600 MHz, DMSO-d$_6$, di-trifluoroacetate): δ (ppm) 10.74 (s, 1H), 10.15 (s, 1H), 8.97 (br s, 1H), 8.62 (br s, 1H), 7.80 – 7.78 (m, 1H), 7.73 – 7.72 (m, 1H), 7.60 (t, 1H, *J* = 5.56 Hz), 7.49 (t, *J* = 7.74 Hz, 1H), 7.24 – 7.23 (m, 1H), 7.15 (s, 1H), 3.10 – 3.06 (m, 2H), 1.49 – 1.43 (m, 2H), 0.86 (t, *J* = 7.50 Hz, 3H). ^{13}C NMR (150 MHz, DMSO-d$_6$, di-trifluoroacetate): δ (ppm) 168.70, 153.60, 153.50, 147.00, 135.50, 134.00, 130.10, 124.84, 124.81,

123.00, 103.00, 41.00, 22.20, 11.20. HRMS (ESI-MS): *m/z* [M+H$^+$] calculated for C$_{14}$H$_{19}$N$_6$OS$^+$: 319.1336, found 319.1346; C$_{14}$H$_{18}$N$_6$OS x C$_4$H$_2$F$_6$O$_4$ (546.45).

1-(Amino((3-(2-aminothiazol-4-yl)phenyl)amino)methylene)-3-(1-hexyl)urea dihydrotrifluoroacetate (3.180) *(Synthesized by Sabrina Biselli)*

3.131 was prepared from **3.011** (0.05 g, 0.28 mmol), **3.050** (0.09 g, 0.28 mmol), HgCl$_2$ (0.15 g, 0.57 mmol), and NEt$_3$ (0.12 mL, 0.85 mmol) in DCM (25 mL) conforming to the general procedure for the guanidinylation reaction. Subsequently**, 3.180** was prepared from the Boc-protected intermediate **3.131** in DCM (4.0 mL) and TFA (1.0 mL) according to the general procedure (method A) and obtained as a colorless foamlike solid (60 mg, 36%): RP-HPLC: 99%, (t$_R$ = 19.25, *k* = 5.64). ^{1}H NMR (600 MHz, DMSO-d$_6$, di-trifluoroacetate): δ (ppm) 10.80 (s, 1H), 10.26 (s, 1H), 8.97 (br s, 1H), 8.65 (br s, 1H), 7.79 (d, *J* = 7.9 Hz, 1H), 7.73 (m, 1H), 7.59 (t, *J* = 5.5 Hz, 1H), 7.49 (t, *J* = 7.9 Hz, 1H), 7.24 – 7.23 (m, 1H), 7.15 (s, 1H), 3.13 – 3.09 (m, 2H), 1.44 – 1.41 (m, 2H), 1.30 – 1.22 (m, 6H), 0.87 – 0.84 (m, 3H). ^{13}C NMR (150 MHz, DMSO-d$_6$, di-trifluoroacetate): δ (ppm) 168.70, 153.57, 153.43, 147.00, 135.46, 134.01, 130.10, 124.79, 124.75, 122.93, 102.94, 39.14, 30.86, 28.80, 25.86, 22.01, 13.87. HRMS (ESI-MS): *m/z* [M+H$^+$] calculated for C$_{17}$H$_{25}$N$_6$OS$^+$: 361.1805, found 361.1813; C$_{17}$H$_{24}$N$_6$OS x C$_4$H$_2$F$_6$O$_4$ (588.53).

1-(Amino((3-(2-aminothiazol-4-yl)phenyl)amino)methylene)-3-cyclohexylurea dihydrotrifluoroacetate (3.181) *(Synthesized by Sabrina Biselli)*

3.132 was prepared from **3.011** (0.06 g, 0.29 mmol), **3.051** (0.09 g, 0.29 mmol), HgCl$_2$ (0.16 g, 0.58 mmol), and NEt$_3$ (0.12 mL, 0.87 mmol) in DCM (25 mL) conforming to the general procedure for the guanidinylation reaction. Subsequently, **3.181** was prepared from the Boc-protected intermediate **3.132** in DCM (4.0 mL) and TFA (1.0 mL) according to the general procedure (method A) and obtained as a colorless foamlike solid (70 mg, 41%): RP-HPLC: 99%, (t$_R$ = 16.34, *k* = 4.60). ^{1}H NMR (600 MHz, DMSO-d$_6$, di-trifluoroacetate): δ (ppm) 10.74 (s, 1H), 9.93 (s, 1H), 8.96 (br s, 1H), 8.65 (br s, 1H), 7.81 – 7.79 (m, 1H), 7.73 (m, 1H), 7.59 (d, *J* = 7.6 Hz, 1H), 7.50 (t, *J* = 7.9 Hz, 1H), 7.25 – 7.23 (m, 1H), 7.15 (s, 1H), 3.51 – 3.45 (m, 1H), 1.80 – 1.77 (m, 2H), 1.66 – 1.63 (m, 2H), 1.54 – 1.51 (m, 1H), 1.32 – 1.14 (m, 5H). ^{13}C NMR (150 MHz, DMSO-d$_6$, di-trifluoroacetate): δ (ppm) 169.20, 154.10, 153.10, 147.40, 136.00, 134.40, 130.60, 125.50, 125.30, 123.60, 103.50, 32.50, 48.90, 25.40, 24.60. HRMS

(ESI-MS): *m/z* [M+H$^+$] calculated for $C_{17}H_{23}N_6OS^+$: 359.1649, found 359.1649; $C_{17}H_{22}N_6OS \times C_4H_2F_6O_4$ (586.51).

1-(Amino((3-(2-aminothiazol-4-yl)phenyl)amino)methylene)-3-phenylurea dihydrotrifluoroacetate (3.182) *(Synthesized by Sabrina Biselli)*

3.133 was prepared from **3.011** (0.05 g, 0.26 mmol), **3.052** (0.08 g, 0.26 mmol), HgCl$_2$ (0.14 g, 0.52 mmol), and NEt$_3$ (0.11 mL, 0.78 mmol) in DCM (25 mL) conforming to the general procedure for the guanidinylation reaction. Subsequently, **3.182** was prepared from the Boc-protected intermediate **3.133** in DCM (4.0 mL) and TFA (1.0 mL) according to the general procedure (method A) and obtained as a colorless foamlike solid (27 mg, 18%): RP-HPLC: 99%, (t_R = 16.20, *k* = 4.59). ^{1}H NMR (600 MHz, DMSO-d$_6$, di-trifluoroacetate): δ (ppm) 10.70 (s, 1H), 10.10 (br s, 1H), 9.92 (s, 1H), 8.92 – 8.76 (m, 3H), 7.83 – 7.81 (m, 1H), 7.78 – 7.77 (m, 1H), 7.51 (t, *J* = 7.8 Hz, 1H), 7.46 – 7.45 (m, 2H), 7.37 – 7.34 (m, 2H), 7.28 – 7.26 (m, 1H), 7.14 – 7.10 (m, 2H). ^{13}C NMR (150 MHz, DMSO-d$_6$, di-trifluoroacetate): δ (ppm) 168.50, 153.30, 151.10, 148.00, 137.30, 136.10, 134.00, 130.10, 129.10, 124.80, 124.60, 124.00, 122.90, 119.50, 102.90. HRMS (ESI-MS): *m/z* [M+H$^+$] calculated for $C_{17}H_{17}N_6OS^+$: 353.1179, found 353.1180; $C_{17}H_{16}N_6OS \times C_4H_2F_6O_4$ (580.46).

1-(Amino((3-(2-aminothiazol-4-yl)phenyl)amino)methylene)-3-(1-phenylmethyl)urea dihydrotrifluoroacetate (3.183) *(Synthesized by Sabrina Biselli)*

3.134 was prepared from **3.011** (0.05 g, 0.26 mmol), **3.053** (0.09 g, 0.26 mmol), HgCl$_2$ (0.14 g, 0.52 mmol), and NEt$_3$ (0.11 mL, 0.78 mmol) in DCM (25 mL) conforming to the general procedure for the guanidinylation reaction. Subsequently, **3.183** was prepared from the Boc-protected intermediate **3.134** in DCM (4.0 mL) and TFA (1.0 mL) according to the general procedure (method A) and obtained as a colorless foamlike solid (90 mg, 58%): RP-HPLC: 99%, (t_R = 16.57, *k* = 4.71). ^{1}H NMR (600 MHz, DMSO-d$_6$, di-trifluoroacetate): δ (ppm) 7.77 – 7.75 (m, 1H), 7.72 – 7.71 (m, 1H), 7.60 (t, *J* = 7.8 Hz, 1H), 7.41 – 7.40 (m, 1H), 7.35 – 7.32 (m, 4H), 7.28 – 7.25 (m, 1H), 4.41 (s, 2H). ^{13}C NMR (150 MHz, DMSO-d$_6$, di-trifluoroacetate): δ (ppm) 172.60, 155.90, 155.30, 142.10, 139.40, 135.40, 133.30, 132.30, 129.70, 128.60, 128.50, 127.90, 127.10, 124.80, 104.70, 44.60. HRMS (ESI-MS): *m/z* [M+H$^+$] calculated for $C_{18}H_{19}N_6OS^+$: 367.1336, found 367.1341; $C_{18}H_{18}N_6OS \times C_4H_2F_6O_4$ (594.49).

1-(Amino((3-(2-aminothiazol-4-yl)phenyl)amino)methylene)-3-(2-phenylethyl)urea dihydrotrifluoroacetate (3.184) *(Synthesized by Sabrina Biselli)*

3.135 was prepared from **3.011** (0.05 g, 0.26 mmol), **3.071** (0.09 g, 0.26 mmol), HgCl$_2$ (0.14 g, 0.52 mmol), and NEt$_3$ (0.11 mL, 0.78 mmol) in DCM (25 mL) conforming to the general procedure for the guanidinylation reaction. Subsequently, **3.184** was prepared from the Boc-protected intermediate **3.135** in DCM (4.0 mL) and TFA (1.0 mL) according to the general procedure (method A) and obtained as a colorless foamlike solid (50 mg, 32%): RP-HPLC: 99%, (t$_R$ = 17.32, *k* = 4.97). ^{1}H NMR (600 MHz, DMSO-d$_6$, di-trifluoroacetate): δ (ppm) 10.67 (s, 1H), 10.06 (s, 1H), 8.96 (br s, 1H), 8.62 (br s, 1H), 7.80 – 7.79 (m, 1H), 7.73 – 7.72 (m, 1H), 7.58 (t, *J* = 5.6 Hz, 1H), 7.48 (t, *J* = 7.9 Hz, 1H), 7.31 – 7.29 (m, 2H), 7.23 – 7.20 (m, 4H), 7.13 (s, 1H), 3.39 – 3.36 (m, 2H), 2.77 (t, *J* = 7.2 Hz, 2H). ^{13}C NMR (150 MHz, DMSO-d$_6$, di-trifluoroacetate): δ (ppm) 168.50, 153.44, 153.40, 147.60, 138.80, 135.9, 133.90, 130.10, 128.70, 128.40, 126.30, 124.80, 124.70, 122.90, 102.90, 40.70, 34.90. HRMS (ESI-MS): *m/z* [M+H$^+$] calculated for C$_{19}$H$_{21}$N$_6$OS$^+$: 381.1492, found 381.1493; C$_{19}$H$_{20}$N$_6$OS x C$_4$H$_2$F$_6$O$_4$ (608.52).

1-(Amino((2-amino-4,5,6,7-tetrahydrobenzo[*d*]thiazol-6-yl)amino)methylene)-3-(1-hexyl)urea dihydrotrifluoroacetate (3.185) *(Synthesized by Sabrina Biselli)*

3.136 was prepared from **3.012** (0.07 g, 0.44 mmol), **3.050** (0.14 g, 0.44 mmol), HgCl$_2$ (0.24 g, 0.88 mmol), and NEt$_3$ (0.18 mL, 1.32 mmol) in DCM (25 mL) conforming to the general procedure for the guanidinylation reaction. Subsequently, **3.185** was prepared from the Boc-protected intermediate **3.136** in DCM (4.0 mL) and TFA (1.0 mL) according to the general procedure (method A) and obtained as a colorless foamlike solid (46 mg, 18%): RP-HPLC: 95%, (t$_R$ = 17.10, *k* = 4.90). ^{1}H NMR (600 MHz, DMSO-d$_6$, di-trifluoroacetate): δ (ppm) 10.17 (s, 1H), 9.07 (s,1H), 8.67 (br s, 4H), 7.50 (s, 1H), 4.05 – 4.04 (m, 1H), 3.09 – 3.06 (m, 2H), 2.89 – 2.86 (m, 1H), 2.60 – 2.51 (m, 3H), 1.97 – 1.83 (m, 2H), 1.42 – 1.39 (m, 2H), 1.29 – 1.24 (m, 6H), 0.86 – 0.84 (m, 3H). ^{13}C NMR (150 MHz, DMSO-d$_6$, di-trifluoroacetate): δ (ppm) 168.90, 154.20, 153.70, 136.50, 112.00, 46.90, 39.49, 31.30, 29.30, 28.40, 26.80, 26.30, 22.50, 21.70, 14.30. HRMS (ESI-MS): *m/z* [M+H$^+$] calculated for C$_{15}$H$_{27}$N$_6$OS$^+$: 339.1962, found 339.1962; C$_{15}$H$_{26}$N$_6$OS x C$_4$H$_2$F$_6$O$_4$ (566.52).

1-(Amino((2-amino-4,5,6,7-tetrahydrobenzo[*d*]thiazol-6-yl)amino)methylene)-3-(1-phenylmethyl)urea dihydrotrifluoroacetate (3.186) *(Synthesized by Sabrina Biselli)*

3.137 was prepared from **3.012** (0.10 g, 0.59 mmol), **3.053** (0.19 g, 0.59 mmol), HgCl$_2$ (0.32 g, 1.18 mmol), and NEt$_3$ (0.25 mL, 1.77 mmol) in DCM (25 mL) conforming to the general procedure for the guanidinylation reaction. Subsequently, **3.186** was prepared from the Boc-protected intermediate **3.137** in DCM (4.0 mL) and TFA (1.0 mL) according to the general procedure (method A) and obtained as a colorless foamlike solid (16 mg, 5%): RP-HPLC: 97%, (t$_R$ = 14.40, *k* = 3.97). ^{1}H NMR (600 MHz, DMSO-d$_6$, di-trifluoroacetate): δ (ppm) 10.36 (br s, 1H), 9.07 (br s, 1H), 8.74 (br s, 4H), 8.02 (br s, 1H), 7.34 – 7.32 (m, 2H), 7.28 – 7.24 (m, 3H), 4.30 (d, *J* = 5.7 Hz, 2H), 4.05 – 4.03 (m, 1H), 2.89 – 2.86 (m, 1H), 2.60 – 2.53 (m, 3H), 1.97 – 1.95 (m, 1H), 1.89 – 1.83 (m, 1H). ^{13}C NMR (150 MHz, DMSO-d$_6$, di-trifluoroacetate): δ (ppm) 168.45, 153.86, 153.18, 140.09, 138.57, 128.38, 127.17, 127.08, 111.51, 46.40, 42.73, 27.86, 26.25, 21.15. HRMS (ESI-MS): *m/z* [M+H$^+$] calculated for C$_{16}$H$_{21}$N$_6$OS$^+$: 345.1492, found 345.1485; C$_{16}$H$_{20}$N$_6$OS x C$_4$H$_2$F$_6$O$_4$ (572.49).

3.5.1.10   Synthesis and Analytical Data of Carbamoylguanidines 3.213 and 3.216
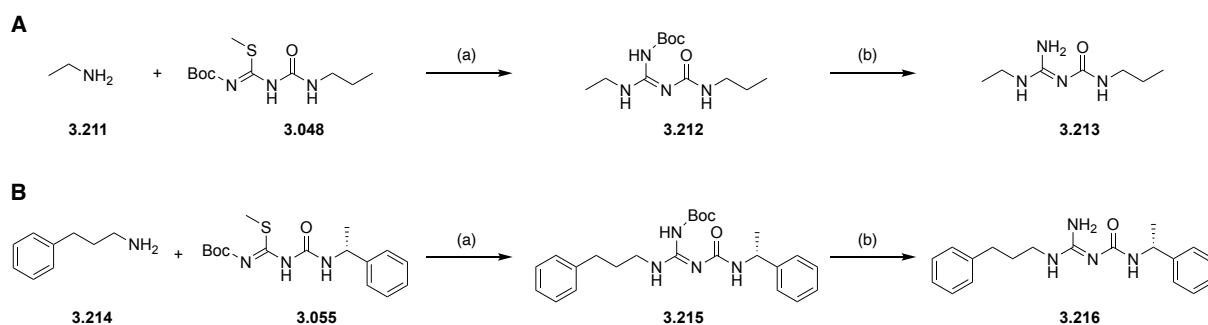
Scheme 3.07. Synthesis of carbamoylguanidines **3.213** (**A**) and **3.216** (**B**). Reagents and conditions: (a) HgCl$_2$, NEt$_3$, DCM, (Ar-atmosphere), rt, overnight; (b) 5-6 N HCl, 2-propanol, rt, overnight.

1-(*tert*-Butoxycarbonylamino(ethylamino)methylene)-3-(1-propyl)urea (3.212)

Compound **3.212** was prepared from **3.211** (0.23 g, 3.90 mmol), **3.048** (1.02 g, 3.90 mmol), HgCl$_2$ (1.06 g, 3.90 mmol), and NEt$_3$ (1.62 mL, 11.70 mmol) in DCM (30 mL) conforming to the general procedure for the guanidinylation reaction (R$_f$ = 0.63 in DCM/MeOH/NH$_3$ 99/1/0.1) yielding a colorless oil (0.74 g, 70%). ^{1}H NMR (300 MHz, CDCl$_3$) δ (ppm) 12.15 (s, 1H), 7.98 (s, 1H), 5.22 (d, *J* = 6.3 Hz, 1H), 3.35 – 3.13 (m,

4H), 1.55 (q, J = 7.3 Hz, 2H), 1.43 (s, 9H), 1.10 (t, J = 7.2 Hz, 3H), 0.91 (t, J = 7.4 Hz, 3H). ^{13}C NMR (75 MHz, CDCl$_3$) δ (ppm) 164.83, 154.28, 153.51, 82.25, 42.39, 34.81, 28.15, 22.45, 15.24, 11.55. HRMS (ESI-MS): m/z [M+H$^+$] calculated for C$_{12}$H$_{25}$N$_4$O$_3^+$: 273.1921, found 273.1927; C$_{12}$H$_{24}$N$_4$O$_3$ (272.35).

(*R*)-1-(*tert*-Butoxycarbonylamino(3-phenylpropylamino)methylene)-3-(1-phenylethyl)urea (3.215)

Compound **3.215** was prepared from **3.214** (0.16 g, 1.19 mmol), **3.055** (0.40 g, 1.19 mmol), HgCl$_2$ (0.32 g, 1.19 mmol), and NEt$_3$ (0.50 mL, 3.57 mmol) in DCM (30 mL) conforming to the general procedure for the guanidinylation reaction (R$_f$ = 0.80 in DCM/MeOH/NH$_3$ 99/1/0.1) yielding a colorless oil (0.35 g, 70%). ^{1}H NMR (300 MHz, CDCl$_3$) δ (ppm) 12.06 (s, 1H), 8.09 (t, J = 5.6 Hz, 1H), 7.37 – 7.15 (m, 10H), 5.43 (d, J = 7.8 Hz, 1H), 4.91 (p, J = 7.0 Hz, 1H), 3.33 (q, J = 5.9 Hz, 2H), 2.67 (t, J = 7.6 Hz, 2H), 1.90 (p, J = 7.5 Hz, 2H), 1.48 (d, J = 7.0 Hz, 3H), 1.45 (s, 9H). ^{13}C NMR (75 MHz, CDCl$_3$) δ (ppm) 164.06, 154.49, 153.54, 144.58, 141.50, 128.69, 128.57, 128.49, 127.11, 126.06, 126.03, 82.44, 49.62, 40.04, 33.18, 30.76, 28.20, 22.88. HRMS (ESI-MS): m/z [M+H$^+$] calculated for C$_{24}$H$_{33}$N$_4$O$_3^+$: 425.2547, found 425.2554; C$_{24}$H$_{32}$N$_4$O$_3$ (424.55).

1-(Amino(ethylamino)methylene)-3-(1-propyl)urea hydrochloride (3.213)

Compound **3.212** (660 mg, 2.42 mmol) was stirred in 5-6 N HCl in 2-propanol (25 mL) at rt overnight. The solvent was evaporated under reduced pressure and the resulting hydrochloride was washed with diethyl ether (3 x 5 mL). **3.213**-HCl was yielded as a colorless hygroscopic solid (490 mg, 90%): RP-HPLC: 99%, (t$_R$ = 9.28, k = 1.93). ^{1}H NMR (300 MHz, CD$_3$OD, hydrochloride) δ (ppm) 3.27 – 3.17 (m, 4H), 1.75 – 1.56 (m, 2H), 1.14 (t, J = 7.2 Hz, 3H), 0.99 (t, J = 7.4 Hz, 3H). ^{13}C NMR (75 MHz, CD$_3$OD, hydrochloride) δ (ppm) 154.29, 153.73, 42.70, 34.34, 21.32, 13.54, 9.96. HRMS (ESI-MS): m/z [M+H$^+$] calculated for C$_7$H$_{17}$N$_4$O$^+$: 173.1397, found 173.1397; C$_7$H$_{16}$N$_4$O x HCl (224.53).

(*R*)-1-(Amino(3-phenylpropylamino)methylene)-3-(1-phenylethyl)urea hydrochloride (3.216)

Compound **3.215** (300 mg, 0.71 mmol) was stirred in 5-6 N HCl in 2-propanol (10 mL) at rt overnight. The solvent was evaporated under reduced pressure and the resulting

hydrochloride was washed with diethyl ether (3 x 5 mL). **3.216**-HCl was yielded as a colorless solid (250 mg, 98%): RP-HPLC: 99%, (t_R = 17.63, k = 4.58). ^{1}H NMR (300 MHz, CD$_3$OD, hydrochloride) δ (ppm) 7.38 – 7.12 (m, 10H), 4.90 (q, J = 7.1 Hz, 1H), 3.26 (t, J = 7.0 Hz, 2H), 2.70 (t, J = 7.9 Hz, 2H), 1.93 (m, 2H), 1.48 (d, J = 7.0 Hz, 3H). ^{13}C NMR (75 MHz, CD$_3$OD, hydrochloride) δ (ppm) 154.18, 153.29, 143.23, 140.63, 128.26, 128.16, 128.02, 127.00, 125.81, 125.63, 49.74, 40.55, 32.23, 29.55, 21.28. HRMS (ESI-MS): m/z [M+H$^+$] calculated for C$_{19}$H$_{25}$N$_4$O$^+$: 325.2023, found 325.2028; C$_{19}$H$_{24}$N$_4$O x HCl (360.89).

3.5.1.11 Synthesis of the Guanidinylating Reagents 3.235-3.237

The guanidinylating reagents **3.235**[417] and **3.236**-**3.237**[299] were synthesized as published previously.

3.5.1.12 Synthesis and Analytical Data of the Heteroaromatic Building Blocks 3.225-3.234

The heteroaromatic building blocks **3.225**[298], **3.227**[423] , **3.229**[302], and **3.230**[421,422] were synthesized as published previously.

3.5.1.12.1 Preparation of the Heteroaromatic Building Block 3.226

The oxazole building block **3.226** was synthesized from urea and *N*-protected α-bromo-ω-amino ketone (**3.279**; cf. Scheme 3.08). The *N*-protected α-bromo-ω-amino ketone **3.279** was synthesized as published previously.[302] The ring-closure reaction was carried out with urea in DMF (comp. **3.280**). After the replacement of the formyl group by a Boc-group (**3.281**), the phthalimide residue was cleaved by hydrazinolysis to give *tert*-butyl (5-(3-aminopropyl)-4-methyloxazol-2-yl)carbamate (**3.226**). The detailed experimental procedures and analytical data for compounds **3.280**, **3.281** and **3.226** have already been published and can be found in Tropmann et al. (2021)[461] and Tropmann (PhD thesis, 2021)[284].
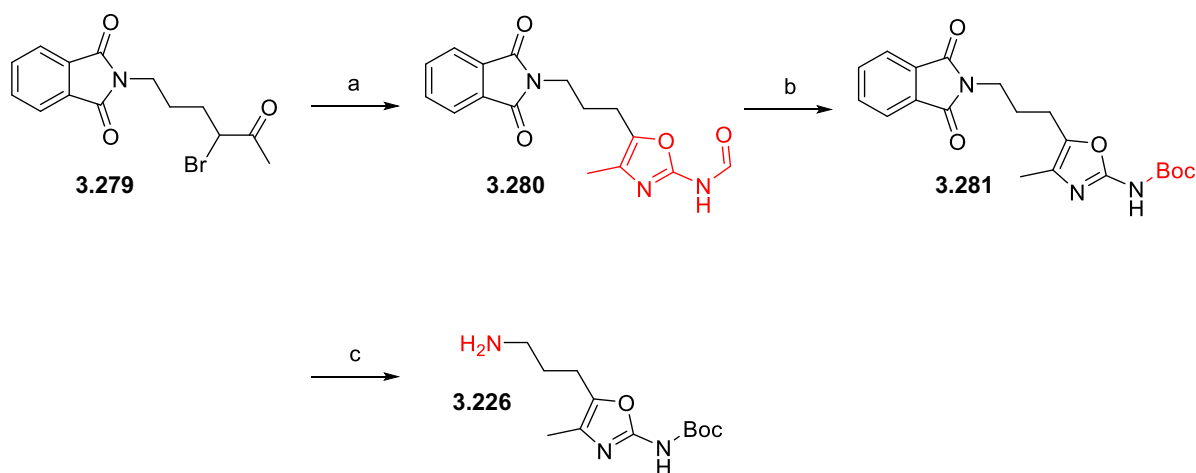
Scheme 3.08. Synthesis of *tert*-butyl (5-(3-aminopropyl)-4-methyloxazol-2-yl)carbamate (**3.226**). Reagents and conditions: (a) urea, DMF, 100 °C, 3 h, 6%; (b) Boc$_2$O, NEt$_3$, DMAP (cat.), chloroform, rt, 48 h, 43%; (c) N$_2$H$_4$ x H$_2$O, EtOH, rt, 48 h, 80%.

3.5.1.12.2 Preparation of the Heteroaromatic Building Block 3.228

Procedure A: The preparation of amine **3.228** was accomplished by a slightly modified procedure of the original synthesis (cf. Scheme 3.09).[462] γ-Aminobutyric acid (GABA, **3.282**) was converted to the corresponding phthalimide derivative **3.283** with phthalic anhydride in DMF under reflux.[463] The corresponding acyl chloride **3.284** was subsequently obtained by reaction of **3.283** with SOCl$_2$ in CH$_2$Cl$_2$.[464] Acylation of thiosemicarbazide with the acyl chloride **3.284** in the presence of pyridine afforded compound **3.285**, which was cyclized in concentrated H$_2$SO$_4$ and gave the thiadiazole **3.286**.[462] In the next step, thiadiazole **3.286** was Boc-protected and after hydrazinolysis of intermediate **3.287** the amine **3.228** was obtained. The detailed experimental procedures and analytical data for compounds **3.283-3.287** and **3.228** have already been published and can be found in Tropmann et al. (2021)[461] and Tropmann (PhD thesis, 2021)[284].
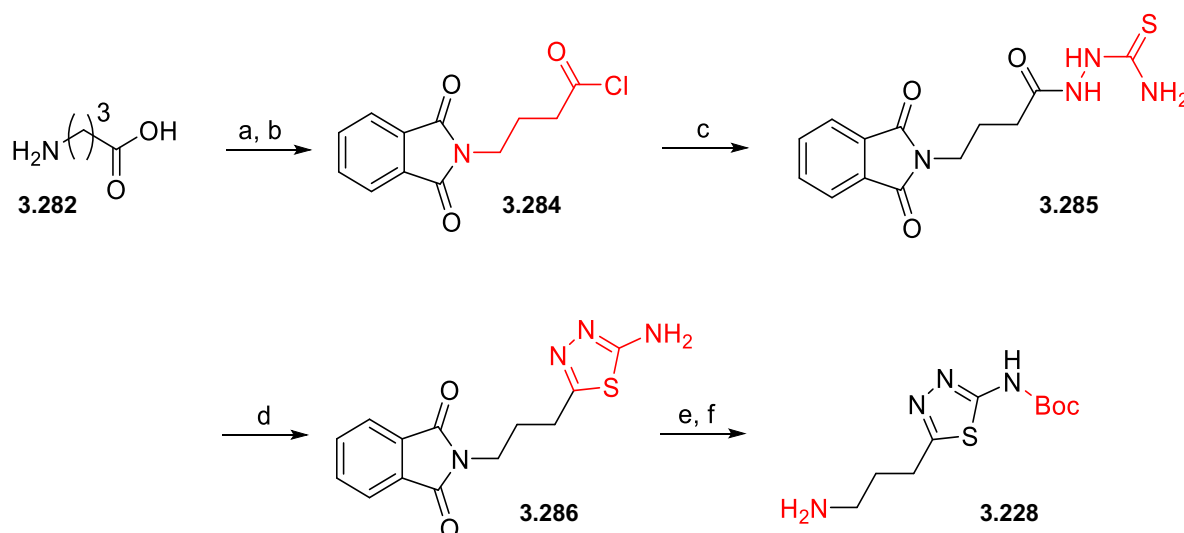
Scheme 3.09. Synthesis of *tert*-butyl (5-(3-aminopropyl)-1,3,4-thiadiazol-2-yl)carbamate (**3.228**).[462–464] Reagents and conditions: (a) phthalic anhydride, 170 °C, 5 h, 88%; (b) SOCl$_2$, CH$_2$Cl$_2$, reflux, 5 h, quant.; (c) thiosemicarbazide, pyridine, 0 °C, 3 h, 37%; (d) H$_2$SO$_4$, 100 °C, 15 min, 78%; (e) Boc$_2$O, NEt$_3$, DMAP (cat.), chloroform, rt, 16 h, 12%; (f) N$_2$H$_4$ x H$_2$O, EtOH, reflux, 2 h, quant..

Procedure B: An alternative synthetic route B for amine **3.228** was developed (cf. Scheme 3.10) because synthetic route A consists of 6 steps and provides a very low overall yield (3% over 6 steps). The synthesis route B consists of 4 steps and provides an overall yield of 6%. The synthesis of the amine **3.228** started with the cyclocondensation of the 2-bromobutanoic acid **3.288** with thiosemicarbazide in fuming hydrochloric acid. This reaction occurs according to the mechanism published

elsewhere.[465] In the same step, the bromide in 2-bromobutanoic acid was exchanged by chloride. After Boc-protection of the aromatic amine group (comp. **3.290**), the alkyl chloride was converted to the corresponding azide in an S$_N$2 reaction in DMF (comp. **3.291**). In the last step, the azide was reduced to the corresponding amine **3.228** by a Staudinger reaction.[466]
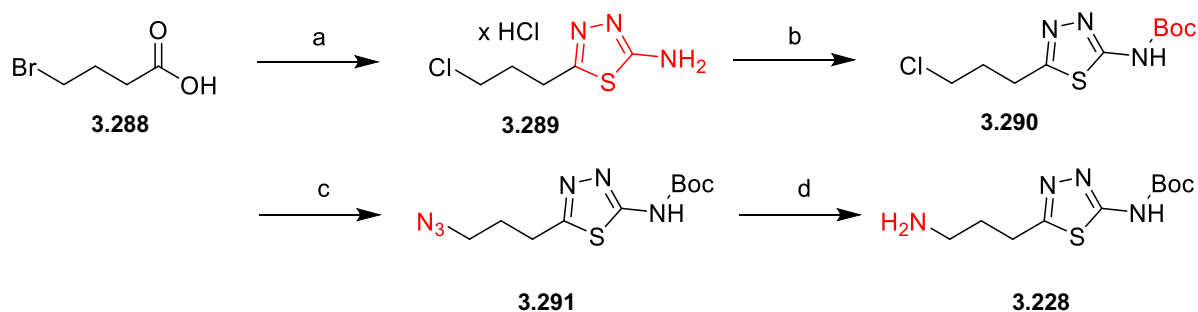
Scheme 3.10. Synthesis of *tert*-butyl (5-(3-aminopropyl)-1,3,4-thiadiazol-2-yl)carbamate (**3.228**). Reagents and conditions: (a) thiosemicarbazide, HCl (37% in H$_2$O), reflux, 5 h, 83%; (b) Boc$_2$O, NEt$_3$, DMAP (cat.), CH$_2$Cl$_2$, rt, 24 h, 23%; (c) NaN$_3$, DMF, 75 °C, overnight; (d) PPh$_3$, THF, 45 °C, 5 h; H$_2$O, 45 °C, overnight, 34% over 2 steps.

5-(3-Chloropropyl)-1,3,4-thiadiazole-2-amine hydrochloride (3.289)

To a solution of 4-bromobutanoic acid (**3.288**, 1.73 g, 10.36 mmol, 1.18 eq) in 5 mL HCl (37% in H$_2$O) thiosemicarbazide (0.80 g, 8.78 mmol, 1 eq) was added. The mixture was heated under reflux for 5 h. After cooling, the solvent was removed in vacuum. The white residue was washed with diethyl ether (3 x 20 mL), yielding 1.56 g (83%) of a white solid. The product was used without any further purification. HRMS (ESI-MS): *m/z* [M+H$^+$] calculated for C$_5$H$_9$ClN$_3$S$^+$: 178.0200, found: 178.0199; C$_5$H$_8$ClN$_3$S x HCl (214.11).

tert-Butyl (5-(3-chloropropyl)-1,3,4-thiadiazol-2-yl)carbamate (3.290).

3.289 (1.56 g, 7.29 mmol, 1 eq), NEt$_3$ (2.23 mL, 16.03 mmol, 2.2 eq), and DMAP (40 mg, cat.) were dissolved in 150 mL CH$_2$Cl$_2$. Boc$_2$O (1.59 g, 7.29 mmol, 1 eq) was slowly added to this solution over a period of 1 h. After the addition was complete, the reaction mixture was stirred at rt for 24 h. The organic phase was washed with 0.1 N HCl, brine, and water. The organic layer was dried over Na$_2$SO$_4$ and the solvent was removed in vacuum. The residue was purified by column chromatography (PE/EtOAc 1:1), to give 467 mg (23%) of a white solid. R$_f$ = 0.45 (PE/EtOAc 1:1). ^{1}H-NMR (400 MHz, CDCl$_3$) δ 3.64 (t, *J* = 6.4 Hz, 2H), 3.14 (t, *J* = 7.2 Hz, 2H), 2.29–2.22 (m,

2H), 1.54 (s, 9H). ^{13}C-NMR (101 MHz, CDCl$_3$) δ 162.33, 162.21, 152.58, 82.98, 43.59, 31.40, 28.11 (3C), 26.81. HRMS (ESI-MS): *m/z* [M+H$^+$] calculated for C$_{10}$H$_{17}$ClN$_3$O$_2$S$^+$: 278.0725, found: 278.0727; C$_{10}$H$_{16}$ClN$_3$O$_2$S (277.77).

tert-Butyl (5-(3-aminopropyl)-1,3,4-thiadiazol-2-yl)carbamate (3.228)

3.290 (407 mg, 1.47 mmol, 1 eq) was dissolved in DMF (20 mL). NaN$_3$ (95.3 mg, 1.47 mmol, 1 eq, caution – NaN$_3$ is toxic and may explode when shocked, heated, or treated with acid) was added. The reaction mixture was heated to 75 °C and stirred overnight. The mixture was concentrated in vacuum and taken up in CH$_2$Cl$_2$ (20 mL). The organic layer was washed with water, dried over Na$_2$SO$_4$, and then concentrated in vacuum resulting in *tert*-butyl (5-(3-azidopropyl)-1,3,4-thiadiazol-2-yl) carbamate (**3.291**). HRMS (ESI-MS): *m/z* [M+H$^+$] calculated for C$_{10}$H$_{17}$N$_6$O$_2$S$^+$: 285.1128, found: 285.1131. MF: C$_{10}$H$_{16}$N$_6$O$_2$S. MW: 284.34. The residue was dissolved in THF (20 mL). Triphenylphosphine (PPh$_3$, 577 mg, 2.20 mmol, 1.5 eq) was added to the solution. The mixture was heated to 45 °C. After 5 hours of continuous stirring, water (20 mL) was added to the solution and the mixture was further stirred at 45 °C overnight. The mixture was concentrated in vacuum and the residue was purified by column chromatography (DCM/MeOH 90:10 → DCM/MeOH/25% NH$_3$ in H$_2$O 50:50:1) yielding 130 mg (34%) of a colorless oil. R$_f$ = 0.21 (DCM/MeOH/25% NH$_3$ in H$_2$O 50:50:1). ^{1}H-NMR (300 MHz, CD$_3$OD) δ 2.95 (t, *J* = 7.6 Hz, 2H), 2.69 (t, 2H), 1.95–1.78 (m, 2H), 1.44 (s, 9H). ^{13}C-NMR (101 MHz, CD$_3$OD): δ 164.18, 163.25, 154.49, 81.32, 39.99, 31.37, 27.11 (3C), 26.56. HRMS (ESI-MS): *m/z* [M+H$^+$] calculated for C$_{10}$H$_{19}$N$_4$O$_2$S$^+$: 259.1223, found: 259.1225; C$_{10}$H$_{18}$N$_4$O$_2$S (258.34).

3.5.1.12.3 Preparation of the Heteroaromatic Building Block 3.231

The preparation of the amine **3.231** (cf. Scheme 3.11) started with 3-chloropropan-1-ol (**3.292**). In the first step, the chloride in **3.292** was replaced by azide in an S$_N$2 reaction. The so formed azide **3.293** was converted in the next step with *N,N*-dimethylpropargylamine in a copper-catalyzed click-reaction to the 1,2,3-triazole **3.294**. To transform the primary alcohol into an amine, a Mitsunobu reaction using phthalimide, PPh$_3$ and diisopropyl azodicarboxylate (DIAD) was performed to obtain the *N*-substituted phthalimide **3.295**.[467] In the last step, the amine was liberated from the phthalimide by hydrazinolysis yielding compound **3.231**.
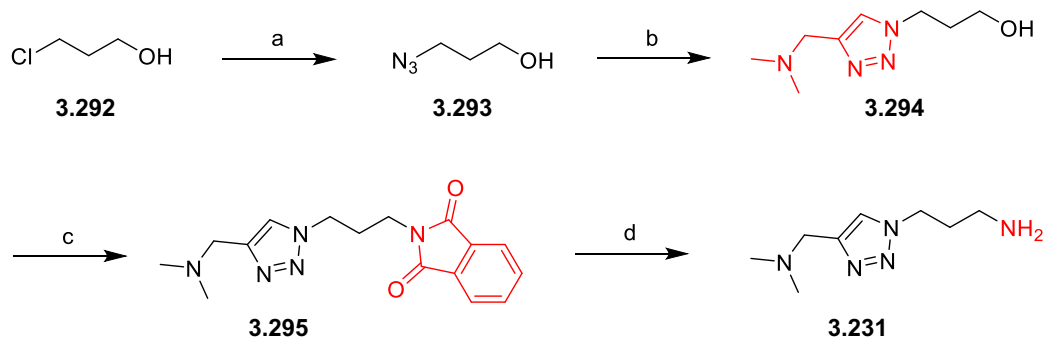
Scheme 3.11. Synthesis of 3-(4-((dimethylamino)methyl)-1*H*-1,2,3-triazol-1-yl)propan-1-amine (**3.231**). Reagents and conditions: (a) NaN$_3$, DMF, 70 °C 16 h, 98%; (b) *N,N*-dimethylpropargylamine, sodium ascorbate, CuSO$_4$ x H$_2$O, H$_2$O/*tert*-butanol (1:1), rt, 16 h, 68%; (c) phthalimide, PPh$_3$, DIAD, THF, 0 °C to rt, overnight, 32%; (d) N$_2$H$_4$ x H$_2$O, *n*-butanol, rt, overnight, 100%.

3-Azidopropan-1-ol (3.293)[468]

3-Chloropropan-1-ol (**3.292**, 1.0 g, 10.58 mmol, 1 eq) and NaN$_3$ (1.03 g, 15.84 mmol, 1.5 eq, caution – NaN$_3$ is toxic and may explode when shocked, heated, or treated with acid) were dissolved in DMF (30 mL). The mixture was stirred at 70 °C for 16 h. After cooling to room temperature, water (100 mL) was added to the reaction mixture. The product was extracted with CH$_2$Cl$_2$. The organic layers were combined, washed 3-times with 0.1 M HCl, dried over Na$_2$SO$_4$ and evaporated to dryness under reduced pressure to afford the product as a yellowish liquid (1.05 g, 98%). Note for this molecule, (C+O)/N = 1.3, thus this compound should be handled with caution and stored in solution below rt and in the dark. R$_f$ = 0.69 (PE/EtOAc 1:1). ^{1}H-NMR (300 MHz, CDCl$_3$) δ 3.72 (t, *J* = 6.0 Hz, 2H), 3.43 (t, *J* = 6.6 Hz, 2H), 2.23 (s, 1H), 1.81 (t, *J* = 6.1 Hz, 2H). ^{13}C-NMR (75 MHz, CDCl$_3$) δ 59.79, 48.46, 31.44. NMR data matches the literature reference.[469–471] Due to its structure, low weight and volatility, no HRMS could be performed on this compound. C$_3$H$_7$N$_3$O (101.11).

3-(4-((Dimethylamino)methyl)-1*H*-1,2,3-triazol-1-yl)propan-1-ol (3.294)

3.293 (810 mg, 8.01 mmol, 1 eq), sodium ascorbate (159 mg, 0.80 mmol, 0.1 eq), and diisopropyl azodicarboxylate (DIAD, 666 mg, 8.01 mmol, 1 eq) were dissolved in H$_2$O/*tert*-butanol (60 mL, 1:1). The flask was set under argon atmosphere and CuSO$_4$ x H$_2$O (40 mg, 0.16 mmol, 0.02 eq) was added. After stirring the mixture at rt for 16 h, the solvent was evaporated under reduced pressure. The obtained residue was purified by column chromatography (DCM/MeOH/25% NH$_3$ in H$_2$O 50:50:1), which resulted in 1 g (68%) of an orange oil. R$_f$ = 0.4 (DCM/MeOH/25% NH$_3$ in H$_2$O 50:50:1).

^{1}H-NMR (300 MHz, CD$_3$OD) δ 7.97 (s, 1H), 4.53 (t, *J* = 7.0 Hz, 2H), 3.71 (s, 2H), 3.56 (t, *J* = 6.1 Hz, 2H), 2.32 (s, 6H), 2.19–2.03 (m, 2H). ^{13}C-NMR (75 MHz, CD$_3$OD) δ 142.46, 124.43, 57.87, 52.76, 46.93, 43.36 (2C), 32.67. HRMS (ESI-MS): *m/z* [M+H$^+$] calculated for C$_8$H$_{17}$N$_4$O$^+$: 185.1397, found: 185.1394; C$_8$H$_{16}$N$_4$O (184.24).

2-(3-(4-((Dimethylamino)methyl)-1*H*-1,2,3-triazol-1-yl)propyl)isoindoline-1,3-dion (3.295)

3.294 (950 mg, 5.16 mmol, 1 eq) was dissolved in THF (70 mL). The flask was set under argon atmosphere and cooled to 0 °C by using an ice-bath. Phthalimide (1.14 g, 7.73 mmol, 1.5 eq) and triphenylphosphine (2.03 g, 7.73 mmol, 1.5 eq) were added to the mixture. Diisopropyl azodicarboxylate (2.23 mL, 11.34 mmol, 2.2 eq) dissolved in THF (30 mL) was added dropwise over a period of 1.5 h to the solution. The ice-bath was removed, and the mixture was stirred overnight. The solvent was removed under reduced pressure and the residue was purified by column chromatography (DCM/MeOH/25% NH$_3$ in H$_2$O 50:50:1), which resulted in 510 mg (32%) of a colorless oil. R$_f$ = 0.75 (DCM/MeOH/25% NH$_3$ in H$_2$O 50:50:1). ^{1}H-NMR (300 MHz, CDCl$_3$) δ 7.69–7.62 (m, 2H), 7.61–7.53 (m, 2H), 4.27 (t, *J* = 7.0 Hz, 2H), 3.57 (t, *J* = 6.6 Hz, 2H), 3.49 (d, *J* = 7.1 Hz, 2H), 2.27–2.14 (m, 2H), 2.13 (s, 6H). ^{13}C-NMR (75 MHz, CDCl$_3$) δ 168.18 (2C), 144.11, 134.16 (2C), 131.71 (2C), 123.37 (2C), 123.24, 53.85, 47.67, 44.67 (2C), 34.91, 29.26. HRMS (ESI-MS): *m/z* [M+H$^+$] calculated for C$_{16}$H$_{20}$N$_5$O$_2$$^+$: 314.1612, found: 314.1617; C$_{16}$H$_{19}$N$_5$O$_2$ (313.36).

3-(4-((Dimethylamino)methyl)-1*H*-1,2,3-triazol-1-yl)propan-1-amine (3.231)

3.295 (510 mg, 1.63 mmol, 1 eq) was dissolved in *n*-butanol (30 mL), N$_2$H$_4$ x H$_2$O (395 μL, 8.14 mmol, 5 eq) was added and the solution was stirred at rt overnight. The mixture was cooled to 0 °C, the produced white precipitate was removed by filtration and the solvent was evaporated under reduced pressure. The residue was purified by column chromatography (DCM/MeOH 100:10 → DCM/MeOH/25% NH$_3$ in H$_2$O), which resulted in 298 mg (100%) of a white solid. R$_f$ = 0.45 (DCM/MeOH 100:10). ^{1}H-NMR (300 MHz, CD$_3$OD) δ 8.24 (s, 1H), 4.58 (t, *J* = 6.8 Hz, 2H), 3.95 (s, 2H), 2.98–2.91 (m, 2H), 2.51 (s, 6H), 2.33 (d, *J* = 7.7 Hz, 2H). ^{13}C-NMR (75 MHz, CD$_3$OD) δ 140.89, 125.65, 52.20, 47.05, 42.73 (2C), 36.55, 27.82. HRMS (ESI-MS): *m/z* [M+H$^+$] calculated for C$_8$H$_{18}$N$_5$$^+$: 184.1557, found: 184.1557; C$_8$H$_{17}$N$_5$ (183.26).

3.5.1.12.4 Synthesis and Analytical Data of the Heteroaromatic Building Block 3.232

The rigidized thiazole building block **3.232** was synthesized, as shown in Scheme 3.12. **3.297** could be directly obtained by refluxing *N*-anilinothiourea (**3.296**) and α-chloroacetone in MeOH under neutral conditions, according to Lee et al.[472]. The HCl generated in the first step acts as an acid catalyst for a [5,5]-shift of *N*-phenyl-*N*`-[2-(4-methyl)thiazolyl]hydrazine.[472] The subsequent selective protection of the 2-aminothiazole in **3.297** with di-*tert*-butyl dicarbonate gave amine **3.232**. The detailed experimental procedures and analytical data for compounds **3.297** and **3.232** have already been published and can be found in Tropmann et al. (2021)[461] and Tropmann (PhD thesis, 2021)[284].
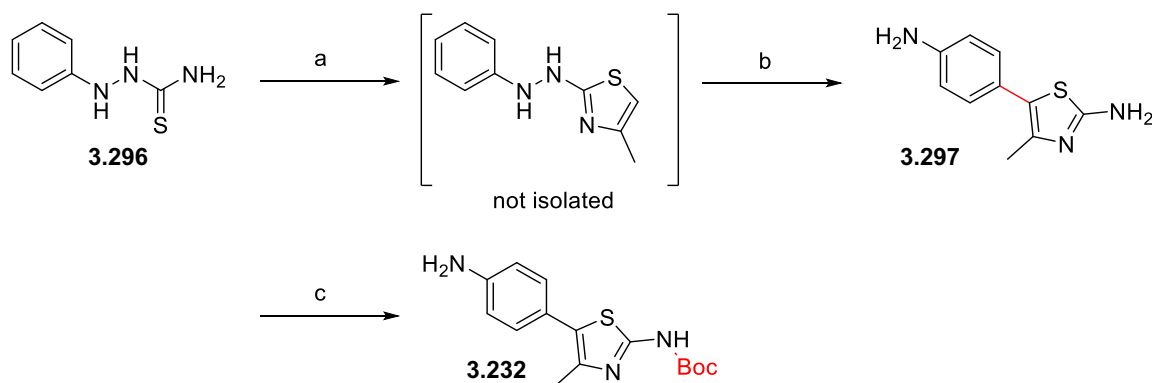
Scheme 3.12. Synthesis of *tert*-butyl (5-(4-aminophenyl)-4-methylthiazol-2-yl)carbamate (**3.232**).[472] Reagents and conditions: (a/b) chloroacetone, MeOH, reflux, 32 h, 49%; (c) Boc₂O, NEt₃, DMAP (cat.), chloroform, 30%, 0 °C to rt, 16 h.

3.5.1.12.5 Synthesis and Analytical Data of the Heteroaromatic Building Block 3.233

3.233 was synthesized in a multistep sequence (cf. Scheme 3.13). In the first, step 1-iodo-3-nitrobenzene (**3.298**) was used as starting material in a palladium-catalyzed cross-coupling to yield **3.299**. After bromination of the benzylic position (comp. **3.300**), cyclization with thiourea in DMF yielded **3.301**. Reduction of the nitro group and the subsequent deformylation and Boc protection yielded the target amine **3.233**. The detailed experimental procedures and analytical data for compounds **3.298**-**3.302** and **3.233** have already been published and can be found in Tropmann et al. (2021)[461] and Tropmann (PhD thesis, 2021)[284].
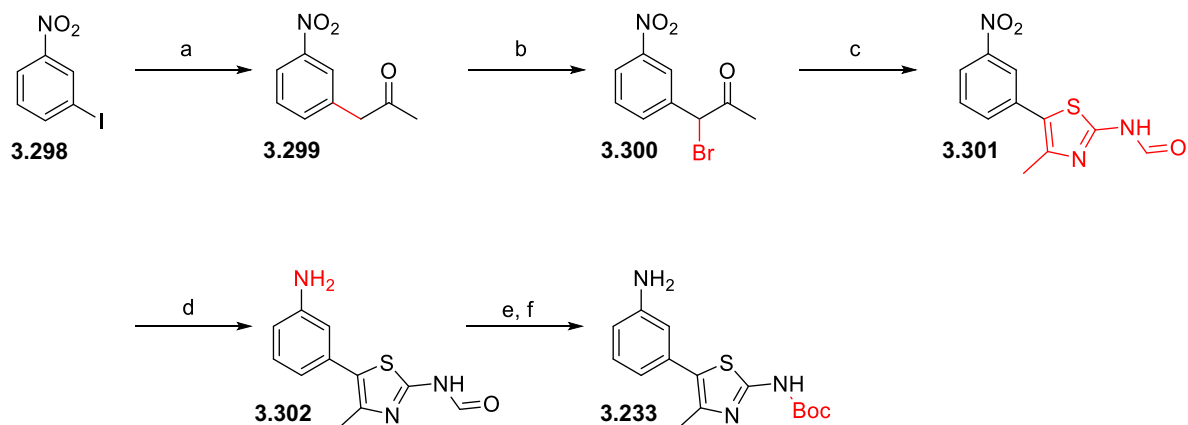
Scheme 3.13. Synthesis of *tert*-butyl (5-(3-aminophenyl)-4-methylthiazol-2-yl)carbamate (**3.233**).[303,473–475] Reagents and conditions: (a) Pd(OAc)₂, PPh₃, Cs₂CO₃, 4-hydroxy-4-methylpentan-2-one, toluene, 120 °C, 5 h, 40%; (b) Br₂, diethyl ether, rt, overnight, 68%; (c) thiourea, DMF, 100 °C, 4 h, 79%; (d) Fe, NH₄Cl, EtOH/H₂O, 90 °C, 4 h, 70%; (e) 1 N HCl in MeOH, MeOH, rt, 48 h, quant.; (f) Boc₂O, NEt₃, DMAP (cat.), chloroform, rt, overnight, 17%.

3.5.1.12.6 Synthesis and Analytical Data of the Heteroaromatic Building Block 3.234

The synthesis of the bromo ketone **3.308** (cf. Scheme 3.14) started with the preparation of **3.306** by reductive cyanation of 1,4-cyclohexanedione monoethylene acetal (**3.304**) with tosylmethylisocyanide (TosMIC) and subsequent reduction of the nitrile **3.305** with lithium aluminum hydride. After protection of the amino group of **3.306** as phthalimide, cleavage of the 1,3-dioxolane ring with hydrochloric acid gave **3.307**. The ketone **3.307** was α-brominated (comp. **3.308**). The condensation of the bromo ketone **3.308** with thiourea led to compound **3.309**. Finally, 2-aminothiazole **3.309** was trityl protected and after hydrazinolysis of the intermediate **3.310** the rigid amine **3.234** was obtained. The detailed experimental procedures and analytical data for compounds **3.304**-**3.310** and **3.234** have already been published and can be found in Tropmann et al. (2021)[461] and Tropmann (PhD thesis, 2021)[284].
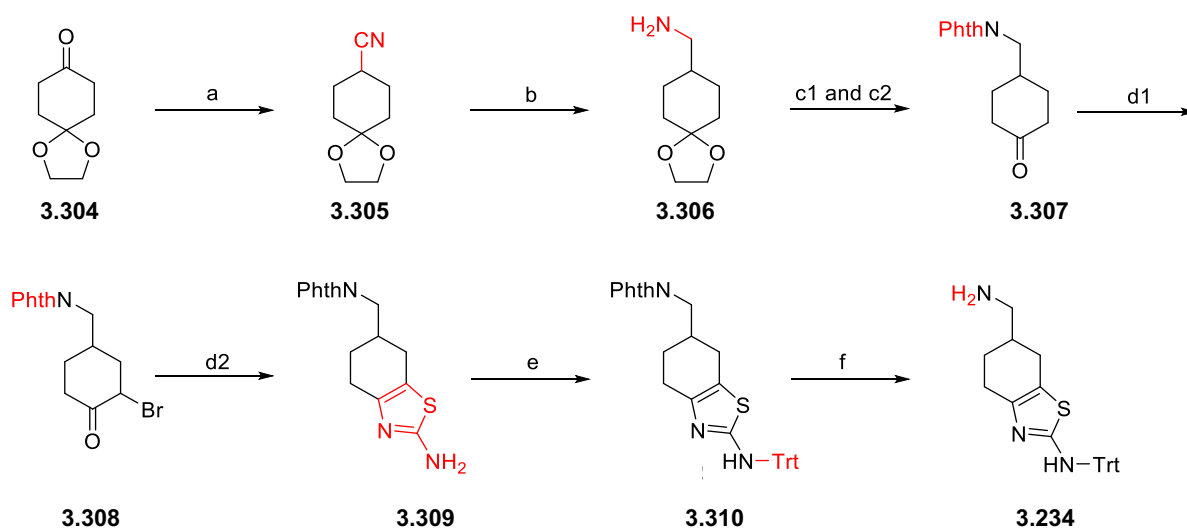
Scheme 3.14. Synthesis of 6-(aminomethyl)-*N*-trityl-4,5,6,7-tetrahydrobenzo[*d*]thiazol-2-amine (**3.234**).[476,477] Reagents and conditions: (a) TosMIC, *t*-BuOK, DME/EtOH, 0 °C, 1 h, then rt, 2 h, 75%; (b) LiAlH$_4$, THF, reflux, 2 h, then rt, 12 h, 99%; (c) 1) phthalanhydride, 135 °C, 30 min, 2) 1 M HCl, 135 °C, 2 h, 32% over two steps; (d) 1) Br$_2$, CH$_2$Cl$_2$, reflux, 1 h, 99%, 2) thiourea, EtOH, reflux, 2 h, 37%; (f) Trt-Cl, NEt$_3$, MeCN, rt, 16 h, 50%; (g) N$_2$H$_4$ x H$_2$O, EtOH, rt, 16 h, 100%.

3.5.1.13 Synthesis and Analytical Data of the Acylhydrazides 3.316 and 3.317

The 1,3,4-oxadiazole derivatives **3.245** and **3.266** were synthesized from carboxybenzyl (Cbz)–protected GABA **3.311** (cf. Scheme 3.15). The carboxyl group of **3.311** was activated using 1-ethyl-3-(3-dimethylaminopropyl)carbodiimide hydrochloride (EDC x HCl) and subsequently coupled with *tert*-butyl carbazate (comp. **3.312**). The Cbz group was removed using hydrogen and Pd/C. The exposed primary amine **3.313** was reacted with the guanidinylating reagents **3.050** or **3.080** in the presence of HgCl$_2$ and NEt$_3$, giving the N^G-carbamoylguanidines **3.314** or **3.315**. These were treated with TFA to remove the Boc-protecting group (comp. **3.316** and **3.317**). The formation of the heterocycle (comp. **3.245** and **3.266**) was performed using cyanogen bromide and KHCO$_3$ in a H$_2$O/EtOH mixture (for details, see chapter **3.5.1.15**). The detailed experimental procedures and analytical data for compounds **3.311-3.313**, **3.316**, and **3.317** have already been published and can be found in Tropmann et al. (2021)[461] and Tropmann (PhD thesis, 2021)[284].
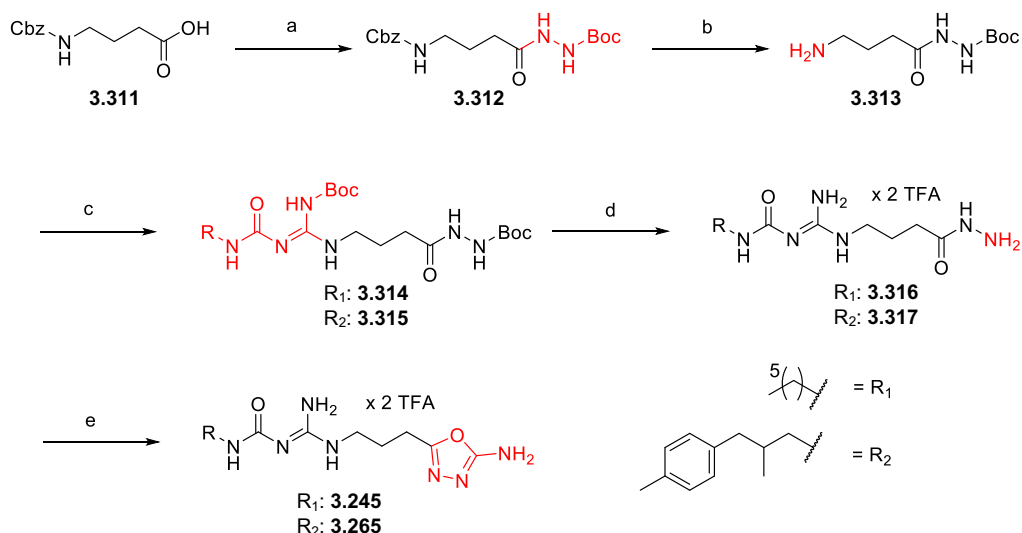
Scheme 3.15. Synthesis of 1,3,4-oxadiazole derivatives **3.245** and **3.266**.[478–481] Reagents and conditions: (a) *tert*-butyl carbazate, EDC x HCl, DIPEA, CH_2Cl_2, rt, 24 h, 20%; (b) Pd/C, H_2 (10 bar), THF/MeOH, rt, 4 h, quant.; (c) **3.050** or **3.080**, $HgCl_2$, NEt_3, CH_2Cl_2, rt, overnight, **3.314**: 46% and **3.315**: 89%; (d) TFA, CH_2Cl_2, rt, 4-6 h, **3.316**: 94% and **3.317**: 17%; (e) BrCN, $KHCO_3$, H_2O/EtOH, 60 °C, 2 h, **3.245**: 6.1% and **3.266**: 61%. Experimental details for **3.245** and **3.266** are demonstrated in chapter **3.5.1.15**.

3.5.1.14 Synthesis and Analytical Data of the Carbamoylguanidine-type Ligands 3.238-3.244, 3.246-3.265, and 3.267-3.278

The reaction was performed in analogy to the published procedure for bivalent carbamoylguanidine-type ligands.[299] In this general procedure, mercuric chloride ($HgCl_2$) is used as a reagent, which is very toxic and potentially carcinogenic. It should be used only in a well-ventilated fume hood after reading the safety precautions and wearing proper lab safety equipment (gloves, safety googles, and lab coat). Future synthetic work should consider replacements for $HgCl_2$. The guanidinylating reagents **3.049**-**3.051**, **3.053**, **3.055**, **3.067**, **3.073**, **3.080**, **3.082**, and **3.235**-**3.237** (1-1.1 eq) and 1-2 eq of the respective amines **3.225**-**3.234** were dissolved in CH_2Cl_2 (3-20 mL). NEt_3 (2.5-3 eq) and $HgCl_2$ (1.1-2 eq) were added to the mixture and stirring was continued for 4-48 h. The precipitate was removed by filtration through Celite 545 or centrifugation (4000 x *g*, 5 min). In the case of **3.260**-**3.264** the reaction was quenched with 7 N NH_3 (5 mL) in MeOH prior to filtration. The solvent was removed in vacuum. The crude product was purified by flash or column chromatography on silica gel (gradient: 0-20 min: petroleum ether/ethyl acetate (PE/EtOAc) 100:0-50:50, SF 8-12 g, gradient: CH_2Cl_2/MeOH 90:10 to CH_2Cl_2/MeOH/25% NH_3 in H_2O 50:50:1, or isocratic: CH_2Cl_2/7 N NH_3 in MeOH 99:1) and dried in vacuum. The isolated Boc-/Trt-protected intermediates were characterized by LC-MS (data are shown in Table 3.16).

Subsequently, the deprotection was performed by stirring the respective compound with 30-70% TFA in CH$_2$Cl$_2$ (5-14 mL) for 7-18 h. The obtained carbamoylguanidines (**3.238-3.244**, **3.246-3.260**, **3.263**, **3.265**, and **3.267-3.278**) were purified by preparative HPLC. In case of **3.261**-**3.262** and **3.264**, the HCl salts were synthesized according to the following procedure. After deprotection with TFA, the ligands were purified by column chromatography (isocratic: CH$_2$Cl$_2$/7 N NH$_3$ in MeOH 90:10), yielding the free base. The free base was dissolved in 1,4-dioxane (10 mL) and 1-2 N HCl (5 mL) in diethyl ether (Et$_2$O) was added dropwise so that the HCl salt precipitated. The suspension was concentrated in vacuum and the solid was washed with Et$_2$O (3 x 15 mL). After removing the solvent in vacuum, compounds **3.261**-**3.262** and **3.264** were obtained as HCl salts. The detailed experimental procedures and analytical data for compounds **3.238**-**3.244**, **3.246**-**3.259**, **3.265**, and **3.267**-**3.278** have already been published and can be found in Tropmann et al. (2021)[461] and Tropmann (PhD thesis, 2021)[284].

1-(Amino{[3-(1*H*-imidazol-4-yl)propyl]amino}methylene)-3-((*R*)-(1-phenylethyl))urea dihydrotrifluoroacetate (3.260)

3.260 was prepared from **3.225** (327 mg, 0.89 mmol, 1 eq), **3.055** (300 mg, 0.89 mmol, 1 eq), HgCl$_2$ (265 mg, 0.98 mmol, 1.1 eq) and NEt$_3$ (372 µL, 2.67 mmol, 3 eq) according to the general procedure yielding 429.1 mg (73%) of Trt-/Boc-protected intermediate. 306 mg thereof were deprotected in the next step yielding **3.260** as a white, foamlike and hygroscopic solid after purification by preparative HPLC (129.7 mg, 51%). RP-HPLC: > 99%, (t_R = 8.3 min, k = 2.11). ^{1}H-NMR (300 MHz, CD$_3$OD) δ 8.75 (d, *J* = 1.4 Hz, 1H), 7.35–7.18 (m, 6H), 4.94–4.85 (m, 1H), 3.38–3.29 (m, 2H), 2.81 (t, *J* = 7.3 Hz, 2H), 2.00 (p, *J* = 7.4 Hz, 2H), 1.47 (d, *J* = 7.0 Hz, 3H). ^{13}C-NMR (75 MHz, CD$_3$OD) δ 161.87 (q, *J* = 34.4 Hz, TFA), 154.56, 153.29, 143.49, 133.46, 132.86, 128.72 (2C), 126.89, 125.56 (2C), 116.7 (q, *J* = 288.2 Hz, TFA), 114.97, 49.71, 39.99, 26.73, 21.29, 21.10. HRMS (ESI-MS): *m/z* [M+H$^+$] calculated for C$_{16}$H$_{23}$N$_6$O$^+$: 315.1928, found: 315.1932; C$_{16}$H$_{22}$N$_6$O x C$_4$H$_2$F$_6$O$_4$ (542.44).

1-(Amino{[3-(5-amino-1,3,4-thiadiazol-2-yl)propyl]amino}methylene)-3-((*R*)-(1-phenylethyl))urea dihydrochloride (3.261)

3.261 was prepared from **3.228** (407 mg, 1.47 mmol, 1 eq), **3.055** (494 mg, 1.47 mmol, 1 eq), HgCl$_2$ (438 mg, 1.61 mmol, 1.1 eq), and NEt$_3$ (613 µL, 4.40 mmol, 3 eq)

according to the general procedure yielding the product as a white, foamlike and hygroscopic solid (50 mg, 8%). RP-HPLC: > 99%, (t_R = 9.3 min, k = 2.48). ^{1}H-NMR (300 MHz, CD$_3$OD) δ 7.37–7.20 (m, 5H), 4.89–4.85 (m, 1H), 3.49–3.35 (m, 2H), 3.02 (t, J = 7.2 Hz, 2H), 2.09 (p, J = 6.8 Hz, 2H), 1.47 (d, J = 6.9 Hz, 3H). ^{13}C-NMR (75 MHz, CD$_3$OD) δ 143.33, 128.26 (2C), 126.97, 125.65 (2C), 49.80, 40.08, 26.80, 26.63, 21.44, 4 C-signals are missing due to the low concentration of the sample. HRMS (ESI-MS): m/z [M+H$^+$] calculated for C$_{15}$H$_{22}$N$_7$OS$^+$: 348.1601, found: 348.1605; C$_{15}$H$_{21}$N$_7$OS x H$_2$Cl$_2$ (420.36).

1-(Amino{[3-(1*H*-1,2,4-triazol-5-yl)propyl]amino}methylene)-3-((*R*)-(1-phenylethyl))urea dihydrochloride (3.262)

3.262 was prepared from **3.230** (420 mg, 1.14 mmol, 1 eq), **3.055** (423 mg, 1.25 mmol, 1.1 eq), HgCl$_2$ (340 mg, 1.25 mmol, 1.1 eq), and NEt$_3$ (474 µL, 3.42 mmol, 3 eq) according to the general procedure yielding 560 mg (75%) of Trt-/Boc-protected intermediate. 540 mg thereof were deprotected in the next step yielding **3.262** as a white, foamlike and hygroscopic solid after purification by preparative HPLC (200 mg, 63%). RP-HPLC: > 99%, (t_R = 9.1 min, k = 2.41). ^{1}H NMR (300 MHz, CD$_3$OD) δ 9.27 (s, 1H), 7.41–7.19 (m, 5H), 4.88 (q, J = 6.8 Hz, 1H), 3.56–3.37 (m, 2H), 3.21–3.01 (m, 2H), 2.15 (p, J = 7.3 Hz, 2H), 1.46 (d, J = 7.0 Hz, 3H). ^{13}C-NMR (75 MHz, CD$_3$OD) δ 155.98, 155.71, 154.19, 144.64, 143.46, 129.56 (2C), 128.27, 126.95 (2C), 51.11, 41.42, 26.36, 22.97, 22.84. HRMS (ESI-MS): m/z [M+H$^+$] calculated for C$_{15}$H$_{22}$N$_7$O$^+$: 316,1880, found: 316.1883; C$_{15}$H$_{21}$N$_7$O x H$_2$Cl$_2$ (388.3).

1-(Amino{[3-(4-((dimethylamino)methyl)-1*H*-1,2,3-triazol-1-yl)propyl]amino}methylene)-3-((*R*)-(1-phenylethyl))urea trihydrotrifluoroacetate (3.263)

3.263 was prepared from **3.231** (298 mg, 1.63 mmol, 1 eq), **3.055** (549 mg, 1.63 mmol, 1 eq), HgCl$_2$ (486 mg, 1.79 mmol, 1.1 eq), and NEt$_3$ (680 µL, 4.88 mmol, 3 eq) according to the general procedure yielding the product as a white, foamlike and hygroscopic solid (50 mg, 5%). RP-HPLC: 98%, (t_R = 8.3 min, k = 2.11). ^{1}H-NMR (300 MHz, CD$_3$OD) δ 8.22 (s, 1H), 7.36–7.20 (m, 5H), 4.90–4.85 (m, 1H), 4.55 (t, J = 6.7 Hz, 2H), 4.42 (s, 2H), 3.34 (t, J = 6.7 Hz, 2H), 2.88 (s, 6H), 2.25 (p, J = 6.9 Hz, 2H), 1.47 (d, J = 7.0 Hz, 3H). ^{13}C-NMR (75 MHz, CD$_3$OD) δ 156.03, 144.86, 138.09, 129.63 (2C), 128.33, 128.05, 126.97 (2C), 52.42, 51.09, 48.65, 42.92 (2C), 39.51,

29.69, 22.70, 1 C-signal is missing due to the low concentration of the sample. HRMS (ESI-MS): *m/z* [M+H$^+$] calculated for C$_{18}$H$_{29}$N$_8$O$^+$: 373.2459, found: 373.2463; C$_{18}$H$_{28}$N$_8$O x C$_6$H$_3$F$_9$O$_6$ (714.55).

1-(Amino{[3-(5-amino-1,3,4-thiadiazol-2-yl)propyl]amino}methylene)-3-(1-(3-fluorophenyl)ethyl)urea dihydrochloride (3.264)

3.264 was prepared from **3.228** (130 mg, 0.50 mmol, 1 eq), **3.067** (179 mg, 0.50 mmol, 1 eq), HgCl$_2$ (150 mg, 0.55 mmol, 1.1 eq), and NEt$_3$ (211 μL, 1.51 mmol, 3 eq) according to the general procedure yielding the product as a white, foamlike and hygroscopic solid (70 mg, 32%). RP-HPLC: > 99%, (*t*$_R$ = 9.8 min, *k* = 2.67). ^{1}H-NMR (300 MHz, CD$_3$OD) δ 7.40-7.29 (m, 1H), 7.20–7.06 (m, 2H), 7.02–6.92 (m, 1H), 4.91–4.86 (m, 1H), 3.46-3.38 (m, 2H), 3.03 (t, *J* = 7.4 Hz, 2H), 2.08 (p, *J* = 7.1 Hz, 2H), 1.47 (d, *J* = 7.0 Hz, 3H). ^{13}C-NMR (75 MHz, CD$_3$OD) δ 172.03, 164.29 (d, *J* = 244.2 Hz), 159.72, 155.61, 154.34, 147.72 (d, *J* = 7.0 Hz), 131.41 (d, *J* = 8.2 Hz), 122.88 (d, *J* = 2.7 Hz), 114.92 (d, *J* = 21.3 Hz), 113.81 (d, *J* = 22.2 Hz), 50.76, 41.44, 28.22, 27.50, 22.63. HRMS (ESI-MS): *m/z* [M+H$^+$] calculated for C$_{15}$H$_{21}$FN$_7$OS$^+$: 366.1507, found: 366.1509; C$_{15}$H$_{20}$FN$_7$OS x H$_2$Cl$_2$ (438.35).

3.5.1.15 Synthesis and Analytical Data of the Oxadiazole Derivatives 3.245 and 3.266

The oxadiazole heterocycle was formed according to a previously published procedure.[482] Cyanogen bromine (CNBr) is used as a reagent in this procedure, which is acutely toxic and potentially carcinogenic. It should be used only in a well-ventilated fume hood after reading the safety precautions and wearing proper lab safety equipment (gloves, safety googles, and lab coat). Future synthetic work should consider replacements for CNBr. The respective acylhydrazine (1 eq, for details regarding compounds **3.316** and **3.317** see chapter **3.5.1.13**) was dissolved in a mixture of H$_2$O/ethanol (EtOH, 1:1 or 2:3 (v/v), 1-2 mL) and KHCO$_3$ (3.2 eq) was added. After the addition of BrCN (3 M in CH$_2$Cl$_2$, 1 eq), the reaction mixture was heated at 60 °C for 2 h. The reaction mixture was cooled to rt and stirred for an additional hour. EtOH was removed in vacuum and the residue was purified by preparative HPLC. The detailed experimental procedures and analytical data for compounds **3.245** and **3.266** have already been published and can be found in Tropmann et al. (2021)[461] and Tropmann (PhD thesis, 2021)[284].

3.5.1.16 Chemical Stability of Compounds 3.141, 3.142, 3.161, and Related Acylguanidines

Analytical HPLC analysis was performed with an Agilent HPLC 1290 Infinity System, composed of a 1260 DAL VL variable wavelength detector, a 1290 TCC thermostated column compartment, a 1290 sampler, and a 1290 binary pump (Agilent Technologies, Santa Clara, USA). A Kinetex XB-C18 100A (2.6 µm, 100 x 3 mm, Phenomenex, Aschaffenburg, Germany) served as a column. Mixtures of MeCN (A) and 0.05% aqueous TFA (B) were used as mobile phases. Helium degassing, 25 °C, a flow rate of 0.5 mL/min and a detection wavelength of 220 nm were used throughout. The samples for stability testing were prepared from stock solutions (10 mM in 20 mM HCl) by dilution to 100 µM with PBS (pH 7.4). For the duration of the experiment, the samples were stored in the dark at room temperature. After 0 h, 72 h, and 7 days an aliquot (20 µL) was further diluted with a mixture of 1% aqueous TFA/Millipore water/MeCN 6/3/1 (20 µL). The injection volume was 20 µL. The following linear gradient was applied: 0-15 min: A/B 5:95-35:65, 18-23 min: 95:5.

In order to compare the chemical stability of the monovalent thiazole containing carbamoylguanidines with the corresponding acylguanidines (cf. Figure 3.028), compounds **3.141**, **3.142**, and **3.161** as well as the acylguanidines UR-BIT22[483], UR-BIT23[302], and UR-BIT29[302] were dissolved in phosphate-buffered saline (PBS, pH 7.4) and incubated at rt for 7 days. Whereas the carbamoylated guanidines remained stable over this period of time (Figures 3.029-3.031), decomposition of the acylated guanidines could be observed in all samples (Figures 3.032-3.034). After 7 days, approximately 62% of the acylguanidine UR-BIT23[302], 51% of UR-BIT29[302], and 33% of UR-BIT22[483] were decomposed. The formation of a decomposition product (t_R = 1.97 min) could be observed over a period 7 days (cf. Figures 3.032-3.034).
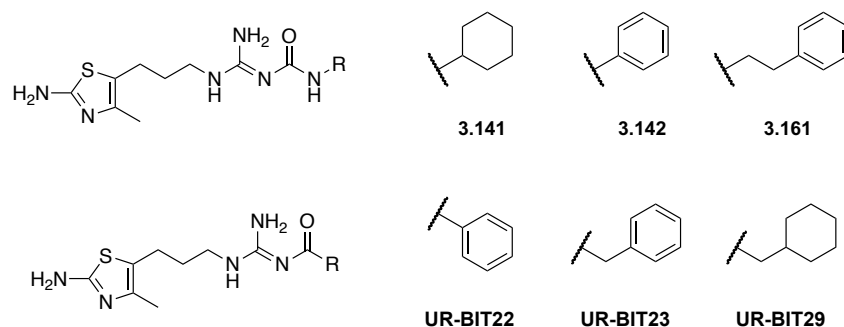
Figure 3.028. Selected structures of carbamoylguanidines (**3.141**, **3.142**, and **3.161**) and acylguanidines (UR-BIT22[483], UR-BIT23[302], and UR-BIT29[302]) used for the chemical stability test.
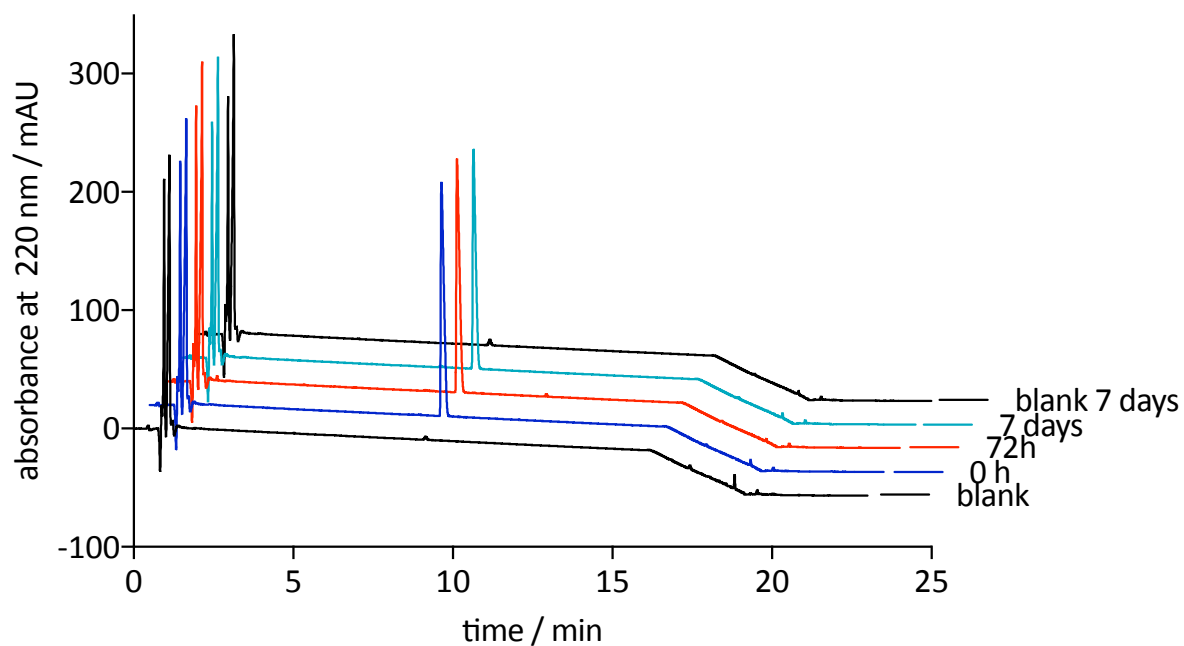
Figure 3.029. RP-HPLC stability test of **3.141** after incubation in PBS (pH 7.4) at room temperature for 7 days.
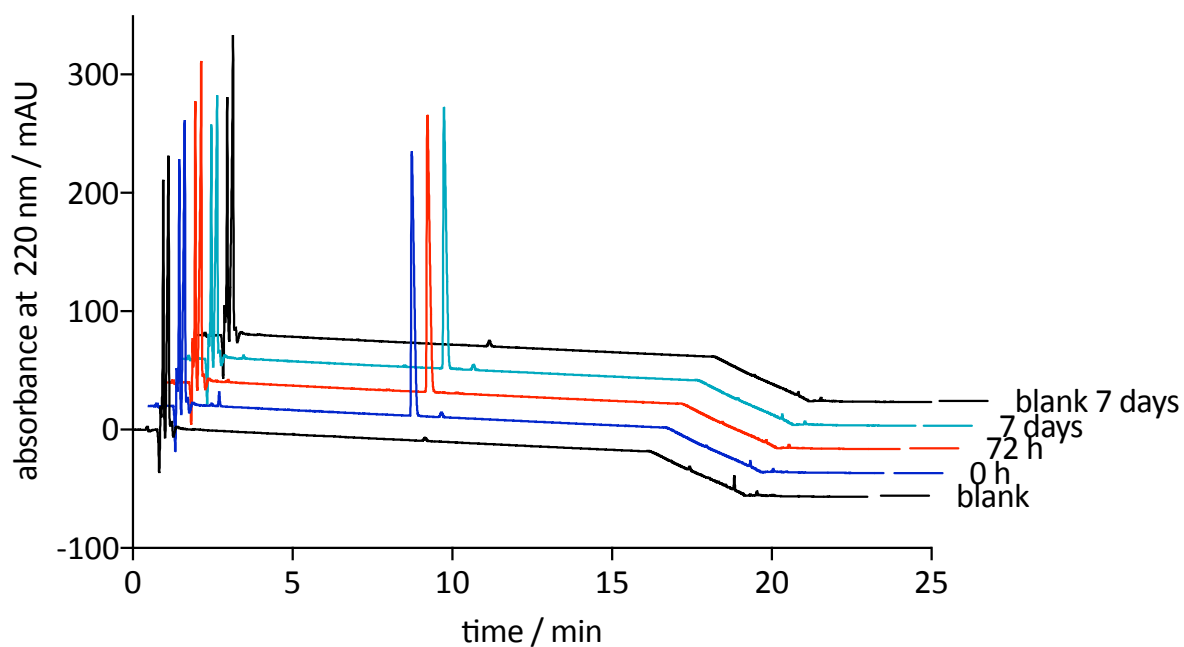
Figure 3.030. RP-HPLC stability test of **3.142** after incubation in PBS (pH 7.4) at room temperature for 7 days.
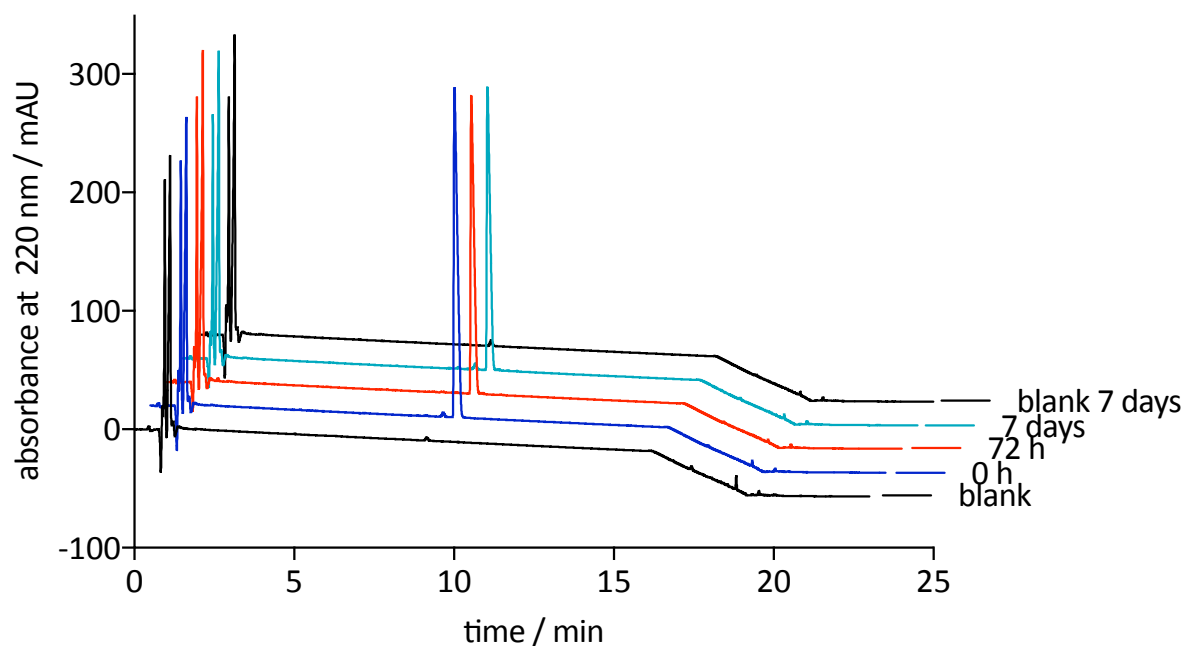
Figure 3.031. RP-HPLC stability test of **3.161** after incubation in PBS (pH 7.4) at room temperature for 7 days.
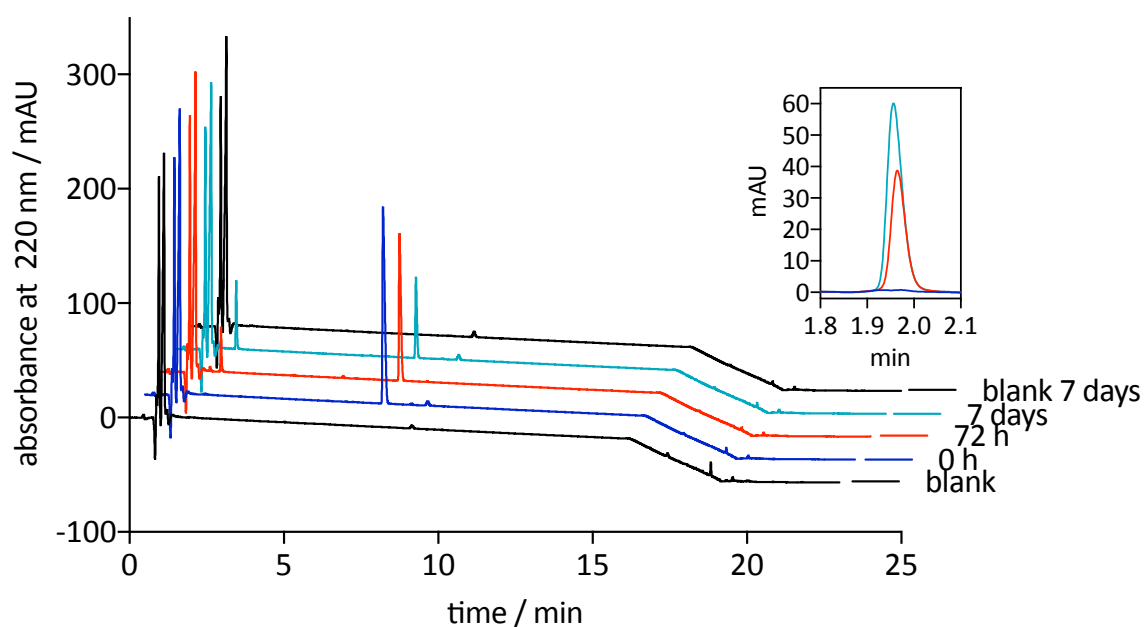
Figure 3.032. RP-HPLC stability test of UR-BIT22[483] after incubation in PBS (pH 7.4) at room temperature for 7 days.
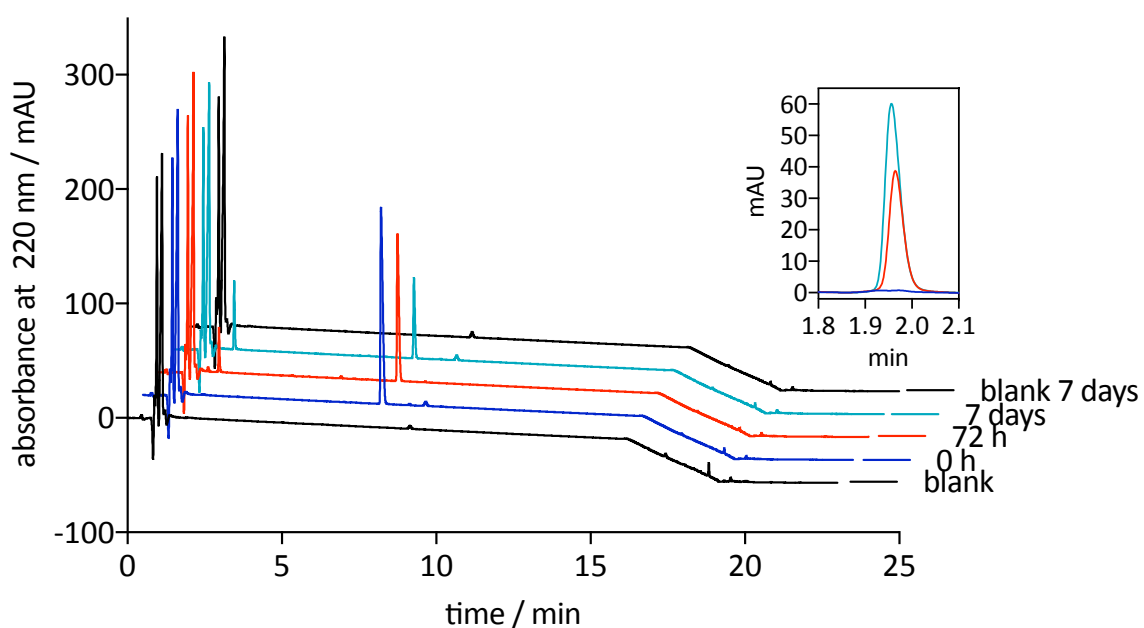
Figure 3.033. RP-HPLC stability test of UR-BIT23[302] after incubation in PBS (pH 7.4) at room temperature for 7 days.
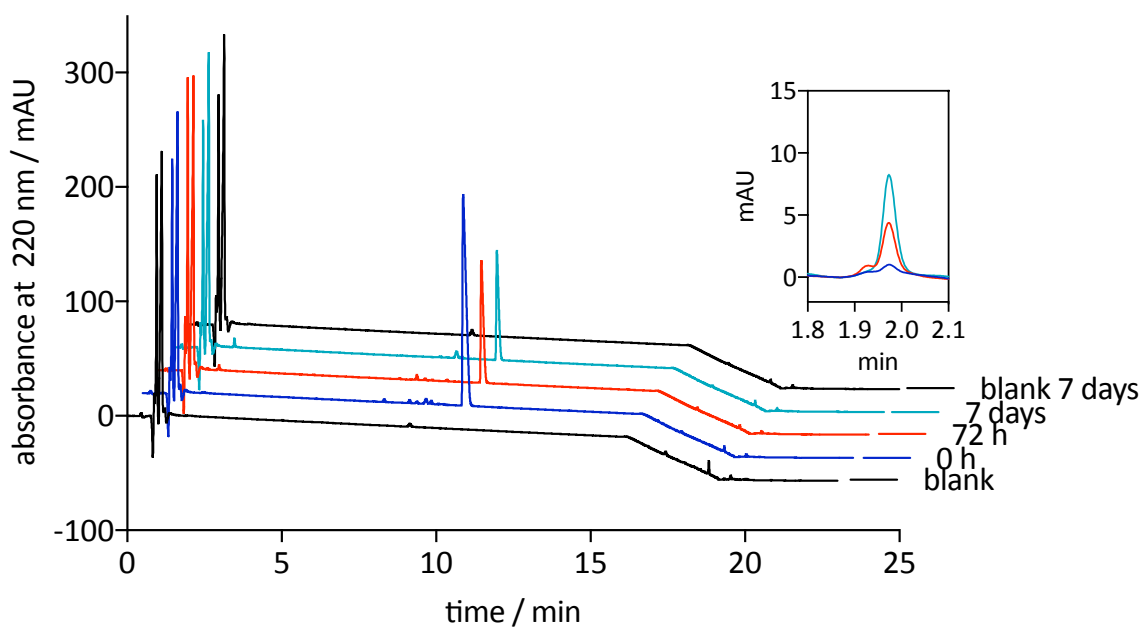
Figure 3.034. RP-HPLC stability test of UR-BIT29[302] after incubation in PBS (pH 7.4) at room temperature for 7 days.

3.5.1.17 Enantiomeric Purity of 3.145, 3.146, 3.164, 3.165, 3.174, 3.175, 3.177, and 3.178

All compounds were di-trifluoroacetates, prepared as 1 mM stock solutions and were sterile filtered with PTFE filter (25 mm, 0.2 µm, Phenomenex, Aschaffenburg, Germany). As a solvent, a mixture of Millipore water and DMSO (95:5) was chosen. Analytical HPLC analysis was performed on a system from Merck Hitachi, composed of a D-6000 interface, a L-6200A pump, an AS2000A autosampler, and a L-4000 UV-VIS detector (Darmstadt, Germany). For the analyses of the enantiomeric purity, an Eurocel 01 (250 x 4.6 mm, 5 µm, Knauer, Berlin, Germany, t_0 = 3.47 min) column was used for carbamoylguanidines (**3.145**, **3.146**, **3.164**, and **3.165**, Figure 3.035) and a ChiraDex (250 x 4.6 mm, 5µm, Merck, Darmstadt, Germany, t_0 = 3.55 min) column for thiocarbamoylguanidines (**3.174**, **3.175**, **3.177**, and **3.178**, Figure 3.036) with a flow rate of 1.0 mL/min. The mobile phase used was 0.1% diethylamine in Millipore water and MeCN for the Eurocel 01 column and an ammonium formate solution (100 mM, pH 3.2) and MeCN for the ChiraDex column. UV detection was performed at 265 nm (second UV maximum of carbamoylguanidines besides 220 nm), since the solvent additives diethylamine and ammonium formate absorb at 220 nm. For all HPLC measurements a sufficient degassing of the eluents with helium was necessary in advance. The purity of the samples was indicated by the percentage of area peaks (λ_{UV} = 265 nm). In the following, the performed methods are described:

Solvent A: MeCN; Solvent B: H$_2$O + 0.1% diethylamine; Solvent C: ammonium formate solution (100 mM, pH 3.2).

Method A, solvent (A/B): 0-25 min: 35/65, 25-26 min: 35/65 - 90/10, 26-35 min: 90/10. flow = 1.0 mL/min.

Method B, solvent (A/C): 0-40 min: 10/90, 40-41 min: 10/90 - 90/10, 41-45 min: 90/10. flow = 1.0 mL/min.
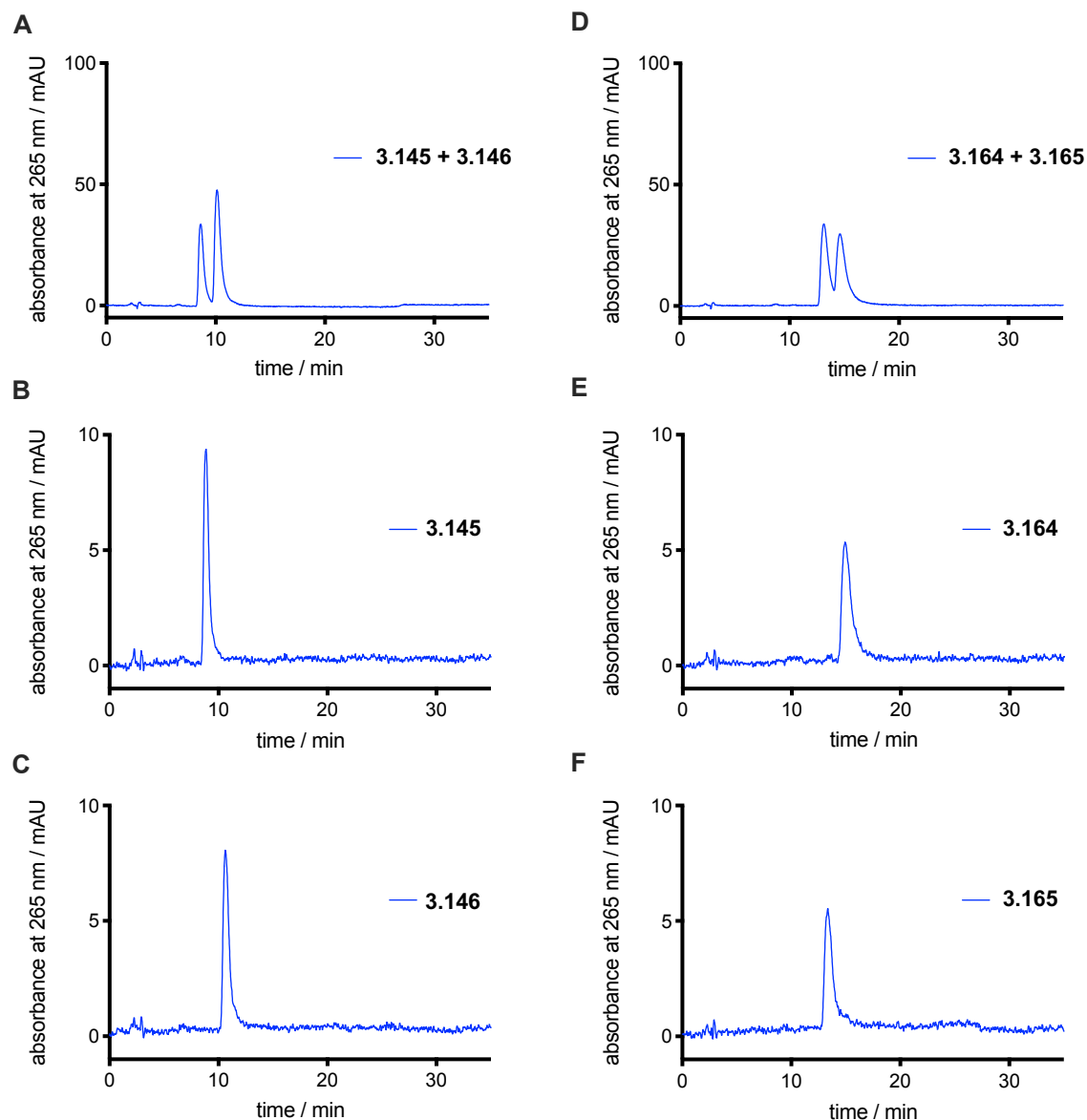
Figure 3.035. HPLC chromatograms of the enantiomers **3.145/3.146** and **3.164/3.165** using a Eurocel 01 column from Knauer (λ_{UV} = 265 nm, method A). (**A**) Spike run of **3.145** and **3.146** (ratio: 2/3); (**B**) enantiomeric purity run of **3.145** (ee = 99%, t_R = 8.85 min, k = 1.55); (**C**) enantiomeric purity run of **3.146** (ee = 99%, t_R = 10.64 min, k = 2.07); (**D**) spike run of **3.164** and **3.165** (ratio: 1:1); (**E**) enantiomeric purity run of **3.164** (ee = 99%, t_R = 14.89 min, k = 3.29); (**F**) enantiomeric purity run of **3.165** (ee = 99%, t_R = 13.35 min, k = 2.85).
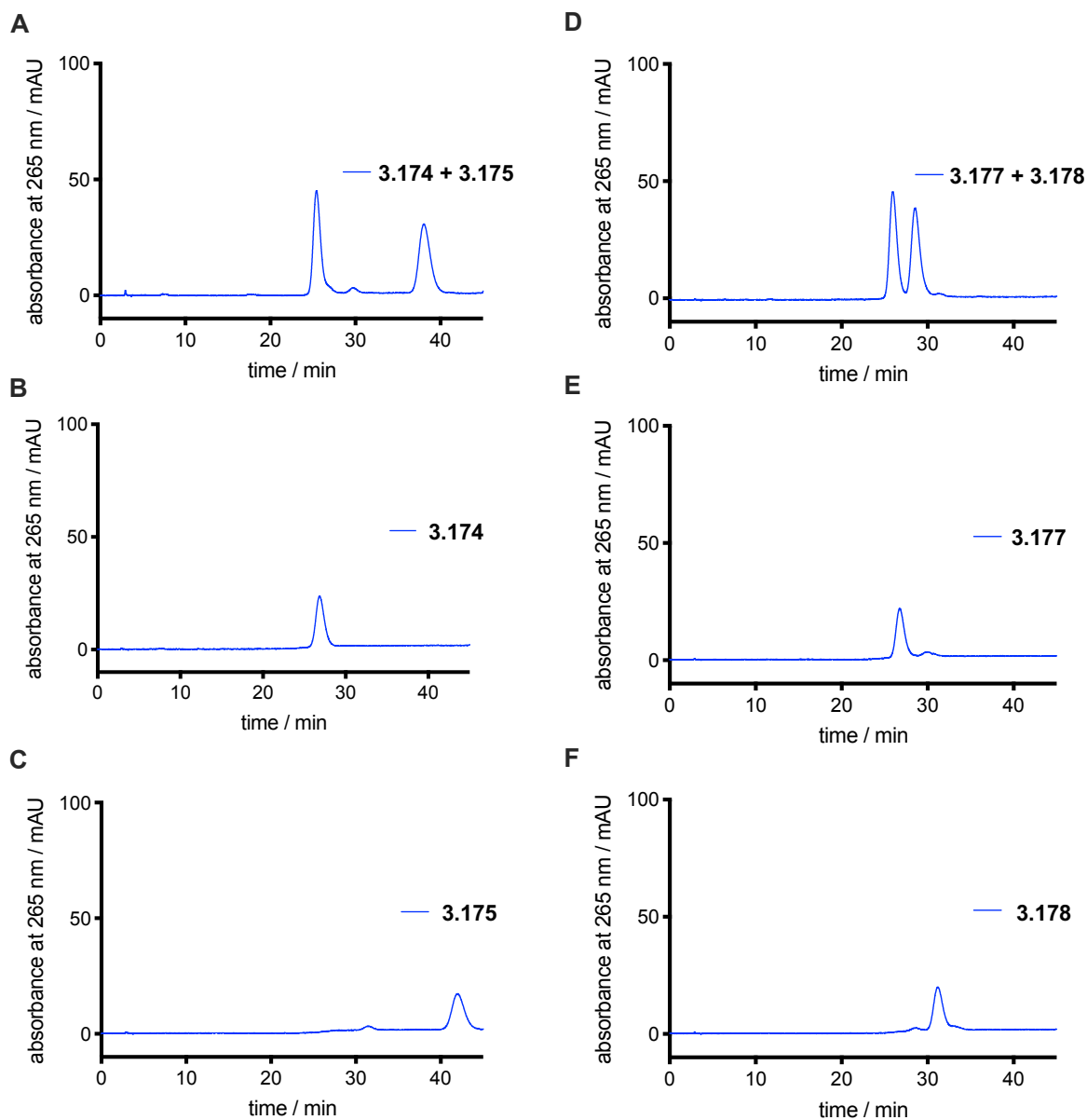
Figure 3.036. HPLC chromatograms of the enantiomers **3.174/3.175** and **3.177/3.178** using a ChiraDex column from Merck (λ_{UV} = 265 nm, method B). (**A**) Spike run of **3.174** and **3.175** (ratio: 1/1); (**B**) enantiomeric purity run of **3.174** (ee = 99%, t$_R$ = 26.81 min, k = 6.55); (**C**) enantiomeric purity run of **3.175** (ee = 99%, t$_R$ = 41.89 min, k = 10.80); (**D**) spike run of **3.177** and **3.178** (ratio: 1:1); (**E**) enantiomeric purity run of **3.177** (ee = 96%, t$_R$ = 26.75 min, k = 6.54); (**F**) enantiomeric purity run of **3.178** (ee = 96%, t$_R$ = 31.19 min, k = 7.79).

3.5.1.18   Determination of pK_a Values of 3.145, 3.213, 3.216-3.218, and 3.322

General Procedure

Method A: The corresponding hydrochloride was dissolved in 15-20 mL Millipore water or 15 mL EtOH 96%. The pH measurement was performed with a glass electrode (Schott pH-Combination Electrode BlueLine 12 pH, Schott, Mainz, Germany), which was calibrated before each measurement with calibration solutions: pH= 4, 7, and 9 ± 0.02 (Roticalipure, Carl Roth, Karlsruhe, Germany). Titration was performed with a 10 mL precision burette (Brand, Wertheim, Germany) using 0.01 M or 0.1 M NaOH (Merck, Darmstadt, Germany). The pK_a values were determined by using the half-equivalence point method (cf. Figures 3.037-3.039).

Method B: The free base was dissolved in 15 mL EtOH 96%. The pH measurement was performed with a glass electrode (Schott pH-Combination Electrode BlueLine 12 pH, Schott, Mainz, Germany), which was calibrated before each measurement (calibration solutions: pH = 4, 7, and 9 ± 0.02). Titration was performed with 1 M HCl (Merck, Darmstadt, Germany). A defined volume of 5 μL was added successively with a piston pipette (Eppendorf, Hamburg, Germany). The pK_a values were determined by using the half-equivalence point method.

(*R*)-1-(Amino((3-(2-amino-4-methylthiazol-5-yl)propyl)amino)methylene)-3-(1-phenylethyl)urea (3.145)

The pK_a values were determined according to the general procedure (method B). 36.92 mg-57.50 mg of **3.145** were dissolved in 15 mL EtOH 96% and titrated with 1 M HCl.

1-(Amino(ethylamino)methylene)-3-propylurea hydrochloride (3.213)

The pK_a values were determined according to the general procedure (method A). 39.09 mg-41.13 mg of **3.213**-HCl were dissolved in 15 mL EtOH 96% and titrated with 0.1 M NaOH.

(*R*)-1-(Amino((3-phenylpropyl)amino)methylene)-3-(1-phenylethyl)urea hydrochloride (3.216)

The pK_a values were determined according to the general procedure (method A). 73.25 mg-85.31 mg of **3.216**-HCl were dissolved in 15 mL Millipore water and titrated with 0.1 M NaOH.

2-Amino-4-methylthiazole hydrochloride (3.217)

The pK_a values were determined according to the general procedure (method A). 9.97 mg-10.20 mg of **3.217**-HCl were dissolved in 20 mL Millipore water and titrated with 0.01 M NaOH.

Figure 3.037. A) Representative titration curve of 2-amino-4-methylthiazole hydrochloride (**3.217**) with 0.01 M NaOH. **B**) The first derivative, ΔpH/ΔV, of the titration curve. **C**) The second derivative, Δ(ΔpH/ΔV)/ΔV, which is the derivative of the first derivative. End point is taken as *zero crossing* of the second derivative. Ve: volume of titrant at equivalence point.

2-Amino-4,5-dimethylthiazole hydrochloride (3.218)

The pK_a values were determined according to the general procedure (method A). 10.00 mg-10.30 mg of **3.218**-HCl were dissolved in 20 mL Millipore water and titrated with 0.01 M NaOH.
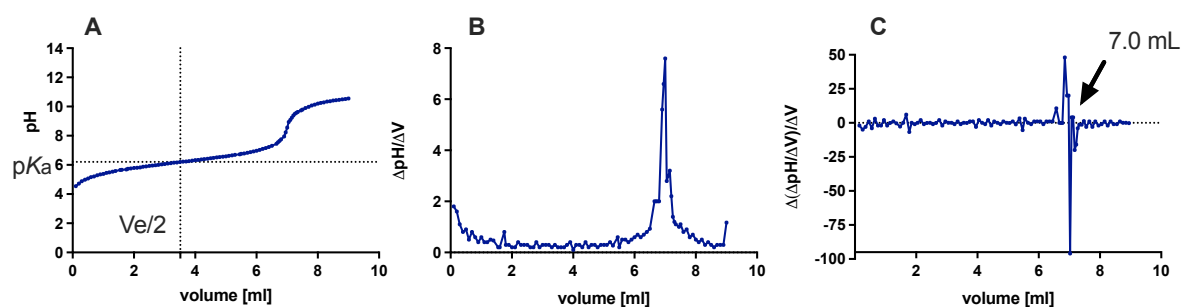
Figure 3.038. A) Representative titration curve of 2-amino-4,5-dimethylthiazole hydrochloride (**3.218**) with 0.01 M NaOH. **B**) The first derivative, ΔpH/ΔV, of the titration curve. **C**) The second derivative, Δ(ΔpH/ΔV)/ΔV, which is the derivative of the first derivative. End point is taken as *zero crossing* of the second derivative. Ve: volume of titrant at equivalence point.

2-Amino-5-methyl-1,3,4-thiadiazole hydrochloride (3.322)
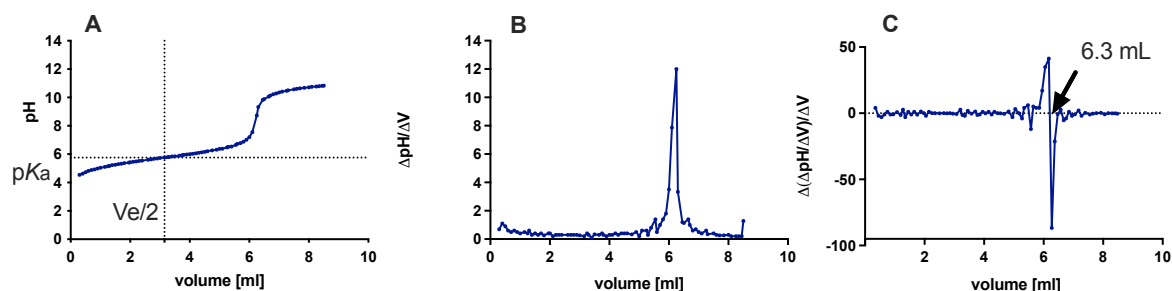
The pK_a values were determined according to the general procedure (method A). 9.6 mg-10.1 mg of **3.322**-HCl were dissolved in 20 mL Millipore water and titrated with 0.01 M NaOH.
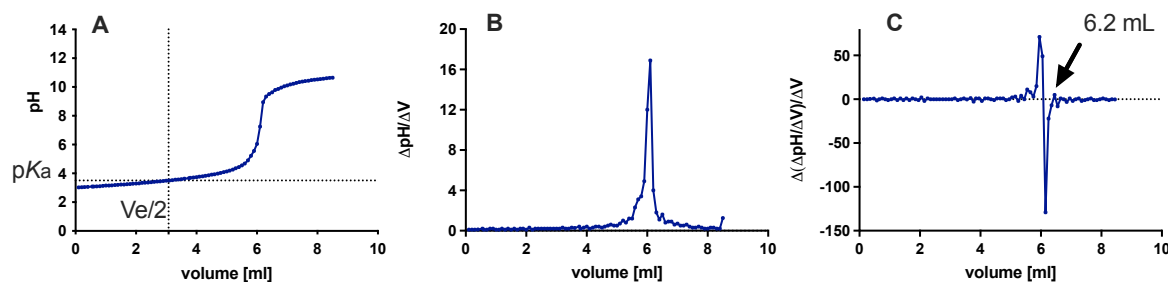
Figure 3.039. A) Representative titration curve of 2-amino-5-methyl-1,3,4-thiadiazole hydrochloride (**3.322**) with 0.01 M NaOH. **B**) The first derivative, ΔpH/ΔV, of the titration curve. **C**) The second derivative, Δ(ΔpH/ΔV)/ΔV, which is the derivative of the first derivative. End point is taken as *zero crossing* of the second derivative. Ve: volume of titrant at equivalence point.

3.5.2 Biology

3.5.2.1 Cell Culture

Cells were cultured in 75 cm^2 flasks (Sarstedt, Nümbrecht, Germany) in a humidified atmosphere (95% air, 5% CO$_2$) at 37 °C. HEK293T-CRE-Luc-hD$_{2long}$R cells[404], HEK293T NlucN-mGs/gpH$_2$R-NlucC cells[417], HEK293T-ARRB2-H$_2$R cells[187], HEK293T ElucN-βarr2 hD$_{2long}$R-ElucC cells[404], and HEK293T ElucN-βarr2 hD$_3$R-ElucC cells[404] were cultured as described previously and regularly monitored for mycoplasma infection using the Venor GeM Mycoplasma Detection Kit (Minerva Biolabs, Berlin, Germany).

3.5.2.2 Radioligand Binding Assays

3.5.2.2.1 Histamine H$_{1-4}$ Receptors

Radioligand competition binding experiments using membranes of Sf9 insect cells co-expressing hH$_1$R and RGS4, expressing hH$_2$R-G$_{sαS}$, co-expressing hH$_3$R, Gα$_{i2}$ and Gβ$_1$γ$_2$ or co-expressing hH$_4$R, Gα$_{i2}$ and Gβ$_1$γ$_2$ were performed according to published protocols.[299,389] The following radioligands were used: [^{3}H]mepyramine (hH$_1$R, specific activity: 20 Ci/mmol, Hartmann Analytics, Braunschweig, Germany or specific activity: 75-87 Ci/mmol, Novandi Chemistry AB, Södertälje, Sweden), [^{3}H]UR-DE257[390] (hH$_2$R, specific activity: 63.0 Ci/mmol, was synthesized in our laboratories), [^{3}H]*N^α*-methylhistamine (specific activity: 85.3 Ci/mmol, Hartmann Analytics) or [^{3}H]UR-PI294[391] (hH$_3$R, specific activity: 41.8 Ci/mmol, was synthesized in our laboratories) and [^{3}H]histamine (hH$_4$R, specific activity: 25 Ci/mmol Hartmann Analytics).

Modifications were made as follows: the washing steps were performed with PBS (8 g NaCl, 0.2 g KCl, 1.0 g Na$_2$HPO$_4$ x 2 H$_2$O, 0.15 g NaH$_2$PO$_4$ x H$_2$O, 0.1 g KH$_2$PO$_4$ in 1 L Millipore H$_2$O; pH 7.4; 4 °C) instead of binding buffer.

3.5.2.2.2 Dopamine D$_{1-5}$ Receptors

The competition binding experiments were performed on homogenates of HEK293T-CRE-Luc-hD$_x$R (x = 1, 2long, 3 or 5) or HEK293TElucN-βarr2 hD$_{4.4}$R-ELuc cells using [^{3}H]N-methylspiperone (hD$_{2long/3/4.4}$R, specific activity: 77 Ci/mmol, Novandi Chemistry AB) or [^{3}H]SCH23390 (hD$_{1/5}$R, specific activity: 81 Ci/mmol, Novandi Chemistry AB) using the previously published protocol.[404] Generation and cell culture of HEK293T-CRE-Luc cells, expressing the hD$_1$-, hD$_{2long}$-, hD$_3$- or hD$_{4.4}$ receptors as well as general procedure for the homogenate preparation have been described in the same publication.[404] The HEK293T-CRE-Luc cell line stably expressing the hD$_5$R was generated in an analogous manner as published for hD$_1$R, hD$_{2long}$R, hD$_3$R or hD$_{4.4}$R.[404] In brief: 2 µg of the pIRESneo3 SP-FLAG-hD$_5$R vector (generated in an analogous manner as described for hD$_1$R, hD$_{2long}$R, hD$_3$R, and hD$_{4.4}$R[404]) were used and selection was achieved in the presence of 600 µg/mL of G418. The preparation of cell homogenates was performed as previously described[404] with the following modification: after centrifugation (6 °C, 50,000 x g, 15 min) and resuspension of the remaining pellet in Tris-MgSO$_4$ buffer[404] homogenization was performed with a Potter homogenizer (10 times, ice-cooled) instead of a syringe and needle. Competition binding experiments with hD$_1$ and hD$_5$ receptors were performed by incubating homogenates in binding buffer[404] at a final concentration of 0.3 µg (hD$_1$R) or 0.4 µg (hD$_5$R) protein/well together with [^{3}H]SCH23390 (hD$_1$R (K_d = 0.23 nM) and hD$_5$R (K_d = 0.2 nM): c = 0.4 nM) and increasing concentrations of the competing ligands (**3.139**, **3.239**, **3.255**, and **3.262**) for 120 min at room temperature. Binding studies at hD$_{2long}$R, hD$_3$R, and hD$_{4.4}$R were performed in binding buffer[404] at a concentration of 0.3 µg (hD$_{2long}$R), 0.7 µg (hD$_3$R) or 0.5-1.0 µg (hD$_{4.4}$R) protein/well together with [^{3}H]N-methylspiperone (hD$_{2long}$R (K_d = 0.0149 nM): c = 0.05 nM; hD$_3$R (K_d = 0.0258 nM): c = 0.05 nM; hD$_{4.4}$R (K_d = 0.078 nM): c = 0.1 nM) and varying concentrations of the competing ligands (**3.139**, **3.239**-**3.240**, **3.254**, **3.251**, **3.255**-**3.256**, **3.261**-**3.262**, **3.264**-**3.265**, **3.267**, **3.271**, and/or **3.277**) for 60 min in case of hD$_{2long}$R and hD$_3$R and 140 min in case of the hD$_{4.4}$R at room temperature. Non-specific binding was determined in the presence of 2 µM (+)-butaclamol (Sigma, Taufkirchen, Germany,

hD_1R, $hD_{2long}R$, hD_3R) or nemonapride (Tocris Bioscience, Bristol, United Kingdom, $hD_{4.4}R$).

3.5.2.2.3 Muscarinic Acetylcholine M_{1-5} Receptors

Binding studies at human muscarinic receptors (stably expressed in CHO-hM$_x$R cells, x = 1-5) were performed using previously described radioligand competition binding assays.[430] Binding affinities towards the human adrenoceptors α_{1A}, α_{2A}, β_1, and β_2 as well as to the human serotonin receptor 5-HT$_{1A}$ and the human opioid receptor µOR were determined as described previously.[431,432] In brief, membranes were prepared from HEK293T cells each transiently transfected with appropriate cDNAs (cDNA of α_{1A}, β_2, and 5-HT$_{1A}$ from cDNA Resource Center, Bloomsberg, PA, for α_{2A}: gift from the D. Yang, Chinese University of Hong-Kong, Shenzhen, China, for µOR: gift from the Ernest Gallo Clinic and Research Center, UCSF, CA, for β_1: gift from the R. Sunahara, UCSD, CA). Receptor density (B$_{max}$ value) and specific binding affinities (K_D value) for α_{1A} were determined as 6500 fmol/mg, and 0.25 nM, respectively ([³H]prazosin (specific activity 84 Ci/mmol, PerkinElmer, Rodgau, Germany) at a concentration of 0.4 nM), for α_{2A}: 1800 fmol/mg, and 0.60 nM, respectively ([³H]RX82102 (spec. act. 52 Ci/mmol, Novandi Chemistry AB) at 0.5 nM), for β_1: 3500 fmol/mg, and 0.075 nM, respectively ([³H]CGP12177 (spec. act. 52 Ci/mmol, PerkinElmer) at 0.2 nM), for β_2: 2000 fmol/mg, and 0.070 nM, respectively ([³H]CGP12177 at 0.2 nM), for 5-HT$_{1A}$: 1100 fmol/mg, and 0.080 nM, respectively ([³H]WAY600135 (spec. act. 80 Ci/mmol, Biotrend, Cologne, Germany) at 0.2 nM), and µOR: 1700 fmol/mg, and 0.090 nM, respectively ([³H]diprenorphine (spec. act. 31 Ci/mmol, PerkinElmer) at 0.3 nM). Competition binding experiments with α_{1A}, and 5-HT$_{1A}$ were performed by incubating membranes in buffer A (50 mM Tris, 5 mM MgCl$_2$, 0.1 mM EDTA, 5 µg/mL bacitracin and 5 µg/mL soybean trypsin inhibitor at pH 7.4) at a final protein concentration of 1 µg/well, and 6 µg/well together with the radioligand and varying concentrations of the competing ligands for 60 minutes at 37 °C. Binding at α_{2A}, and µOR were done in buffer B (50 mM Tris at pH 7.4) at a protein concentration of 10 µg/well, and 6 µg/well, respectively and for β_1 and β_2 in buffer C (25 mM HEPES, 5 mM MgCl$_2$, 1 mM EDTA, and 0.01% BSA at pH 7.4) at a protein concentration of 2 µg/well, and 4 µg/well, respectively. Non-specific binding was determined in the presence of 10 µM of prazosin (α_{1A}), RX821002 (α_{2A}), CGP12177 (β_1, and β_2), WAY600135 (5-HT$_{1A}$), and naloxone (µOR). The protein concentration was established using the method of

Lowry.[484] The resulting competition curves were analyzed by nonlinear regression using the algorithms implemented in PRISM 6.0 (GraphPad Software, San Diego, CA) to provide an IC$_{50}$ value, which was subsequently transformed into the K_i value employing the equation of Cheng and Prusoff.[156]

3.5.2.3 [^{35}S]GTPγS Binding Assay

The [^{35}S]GTPγS binding assay was performed using membranes of Sf9 insect cells expressing the hH$_2$R-G$_{sαS}$ fusion protein as described in detail by Kagermeier et al.[299] [^{35}S]GTPγS was from PerkinElmer Life Science (Boston, USA) or Hartmann Analytics.

3.5.2.4 β-Arrestin Recruitment Assay

The β-arrestin recruitment assays using HEK293T-β-Arr2-hH$_2$R cells[394,395], HEK293T ElucN-βarr2 hD$_{2long}$R-ELucC cells[404] or HEK293T ElucN-βarr2 hD$_3$R-ELucC cells[404] were performed as described previously.

3.5.2.5 Mini-G Protein Recruitment Assay

The mini-G protein recruitment assay at the hH$_2$R or gpH$_2$R was performed using HEK293T NlucN-mGs/hH$_2$R-NlucC[425] or HEK293T NlucN-mGs/gpH$_2$R-NlucC[417] cells as previously described in detail. Furimazine was from Promega (Mannheim, Germany).

3.5.2.6 Histamine H$_2$ Receptor Assay on the Isolated Guinea Pig Right Atrium (Spontaneously Beating)

This functional assay was performed as previously described in detail.[389]

3.5.2.7 Transgenic Mice

The investigation conforms to the *Guide for the Care and Use of Laboratory Animals* (National Research Council Committee for the Update of the Guide for the Care and Use of Laboratory Animals, 2011). Animals were maintained and handled according to approved protocols of the animal welfare committee of the University of Halle-Wittenberg, Germany. The plasmid, containing the human H$_2$ receptor cDNA

(GenBank accession number AY136744), was kindly provided by R. Seifert (Institute of Pharmacology, Hannover Medical School, Hannover, Germany). Generation of the transgenic mice with cardiomyocyte-specific expression of the human H$_2$R was performed by the TRAM unit of the Westfälische Wilhelms-Universität, Münster, Germany, and has been described before.[439] Genotypes were identified by polymerase chain reaction analyses of tail tip DNA using the following primers: 5′-ACCCTTACCCCACATAGACC-3′ and 5′-AGCAGGTCAGTGATAGCCAA-3′. The polymerase chain reaction was performed using the Ampliqon Taq DNA polymerase (Biomol, Hamburg, Germany) according to the manufacturer's instructions. For the experiments, 3–6-month-old H$_2$-TG mice and WT littermates (age-matched) of both sexes (evenly distributed) were used.

3.5.2.8 Preparations of Right and Left Mice Atria

Mice were anesthetized by intraperitoneal injection of pentobarbital sodium (50 mg kg^{-1}), and hearts were excised. Right and left atria were dissected from isolated H$_2$-TG and WT mice hearts and mounted in an organ bath. Left atrial preparations were continuously electrically stimulated (field stimulation) with each impulse consisting of 1 Hz, with a voltage of 10–15% above threshold and 5 ms duration. Right atrial preparations were allowed to contract spontaneously. The bathing solution contained (in mM) NaCl 119.8, KCl 5.4, CaCl$_2$ 1.8, MgCl$_2$ 1.05, NaH$_2$PO$_4$ 0.42, NaHCO$_3$ 22.6, Na$_2$EDTA 0.05, ascorbic acid 0.28, and glucose 5.0, continuously gassed with 95% O$_2$ and 5% CO$_2$ and maintained at 35°C resulting in a pH of 7.4. Signals detected via an isometric force transducer were amplified and continuously recorded. UR-Po563, UR-MB-158, or UR-MB-159 was cumulatively applied to the organ bath. After three changes of the buffer in the organ bath of the indicated experiments, famotidine was applied (1 μM in the organ bath), and then cumulative addition of UR-Po563, UR-MB-158, or UR-MB-159 to the organ bath was repeated. This was done to assess the ability of famotidine to antagonize the contractile effects of the respective agonist in the organ bath.

3.5.2.9 Langendorff-Perfused Hearts Preparations

Heart preparations were used as described previously.[485] Mice were anesthetized intraperitoneally with pentobarbital sodium (50 mg kg^{-1}) and treated with 1.5 units of

heparin. The hearts were removed from the opened chest, immediately attached by the aorta to a 20-gauge cannula, and perfused retrogradely under constant flow of 2 mL min^{-1} with oxygenized buffer solution (37°C) containing (in mM) NaCl 119.8, KCl 5.4, CaCl$_2$ 1.8, MgCl$_2$ 1.05, NaH$_2$PO$_4$ 0.42, NaHCO$_3$ 22.6, Na$_2$EDTA 0.05, ascorbic acid 0.28, and glucose 5.0 in an isolated heart system. The heart preparations were allowed to equilibrate for 30 minutes before measurements. The developed force was measured with a hook applied to the apex cordis that was connected via a return pulley to a force transducer. The data were recorded using a Power-Lab system (ADInstruments, Oxford, UK). Ventricular contractions were measured and monitored continuously. The beating rate and the first derivative of the developed force (+dF/dt and -dF/dt) were calculated electronically using the chart software (ADInstruments, Oxford, UK).

3.5.2.10 Human Atrium Preparations

Human atrial preparations were used as previously described.[442] Right atrial samples were obtained from patients who underwent cardiac bypass surgery because of a three-vessel coronary artery disease. From these right atrial samples, we cut small trabeculae carneae and handled them exactly like mouse atrial samples. In brief, they were mounted in organ baths, attached to an isometric force transducer, and stimulated electrically at 1 Hz, and the buffer had the same composition as described above. The samples were freeze clamped in liquid nitrogen after the experiment to stop all biochemical reactions and to maintain the phosphorylation state of the proteins of interest. From some atrial samples, small cardiac strips were prepared and incubated in 1.5 mL reaction tubes, drugs were added, and then cardiac strips were rapidly frozen. These procedures have been reported in detail before.[486,487] Here, five atrial preparations from three patients could be used. The patient characteristics are described as follows: age, 52–72 years old; sex, male; New York Heart Association class, III–IV; Canadian Cardiovascular Society angina grading scale, III; left ventricular ejection fraction, 40–60%; further diagnoses were arterial hypertension, hypercholesterolemia, and diabetes (two of three); and medications included anticoagulants, platelet aggregation inhibitors, β-adrenoceptor antagonists, calcium channel blockers (dihydropyridines), angiotensin converting enzyme inhibitors or angiotensin receptor blockers, diuretics, proton-pump inhibitors, metformin, or insulin. The study complied with the Declaration of Helsinki and was approved by the Ethics

Committee of the University of Halle-Wittenberg (hm-bü 04.08.2005). All patients gave informed consent.

3.5.2.11 Echocardiography

Echocardiography in spontaneously breathing mice was performed under anesthesia with 1.5% isoflurane.[488] We injected the dihydrochloride salts of UR-Po563, UR-MB-158, or UR-MB-159 (dissolved in water) or famotidine as 100 µL of a 1 mM stock solution into the peritoneum of H$_2$-TG or WT mice. First famotidine was injected, and five minutes later UR-Po563, UR-MB-158, or UR-MB-159. This was done to offer enough time for the H$_2$R antagonist famotidine to occupy the cardiac H$_2$R. After five additional minutes the left ventricle was assessed using B-mode to obtain an overall view. The recording was then changed to M-mode to quantify the function of the left ventricle by measuring the ejection fraction of the left ventricle using the software supplied by the manufacturer (Vevo 2100, Visual Sonic, Toronto, Canada).

3.5.3 Data Processing

Compound purities were calculated as the percentage peak area of the analyzed compound by UV detection at 220 nm. Retention factors (k) were calculated from retention times (t_R) according to $k = (t_R - t_0)/t_0$, t_0 = dead time. Data from radioligand competition binding assays (hH$_{1-4}$[389] and hD$_{2long/3}$[404] receptors), from [^{35}S]GTPγS binding assay[389], from mini-G protein (hH$_2$R[425], gpH$_2$R[417]) or β-arrestin2 (hH$_2$[187,395] and hD$_{2long/3}$[425] receptors) recruitment assays, and from H$_2$R assay on isolated guinea pig right atrium[389] were processed as reported previously.

3.5.4 Nomenclature

Due to their importance as lead compounds (structurally or pharmacologically), the following compounds receive a special compound code: **3.139** = UR-KAT523, **3.140** = UR-CH20, **3.143** = UR-CH22, **3.145** = UR-Po563, **3.157** = UR-MB-69, **3.170** = UR-SB257, **3.172** = UR-KAT527, **3.239** = UR-KAT505, **3.240** = UR-KAT583, **3.255** = UR-KAT533, **3.261** = UR-MB-158, **3.262** = UR-MB-159, and **3.264** = UR-MB-165.

3.6 Supplementary Material

3.6.1 NMR Spectra of Representative Target Compounds 3.139, 3.144, 3.145, 3.157, 3.159, 3.163, 3.167, 3.170, 3.174, 3.180, 3.186, and 3.238-3.278
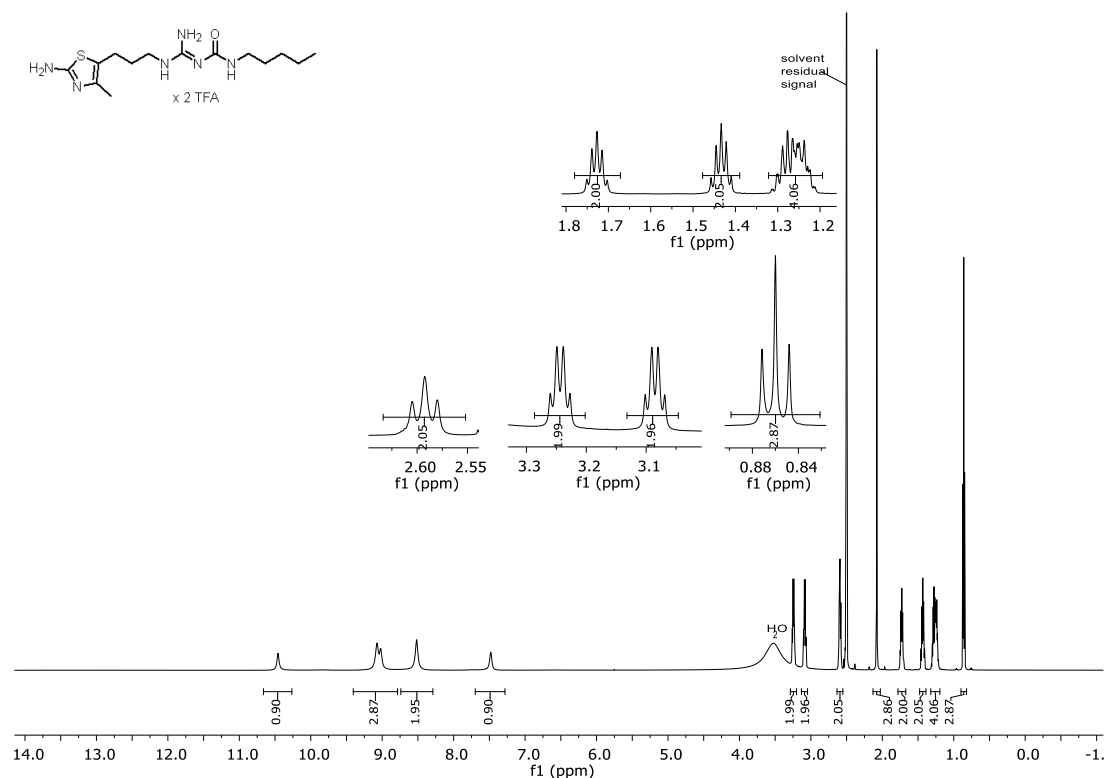
Figure 3.040. ^{1}H NMR spectrum (600 MHz, DMSO-d$_6$) of compound **3.139**.
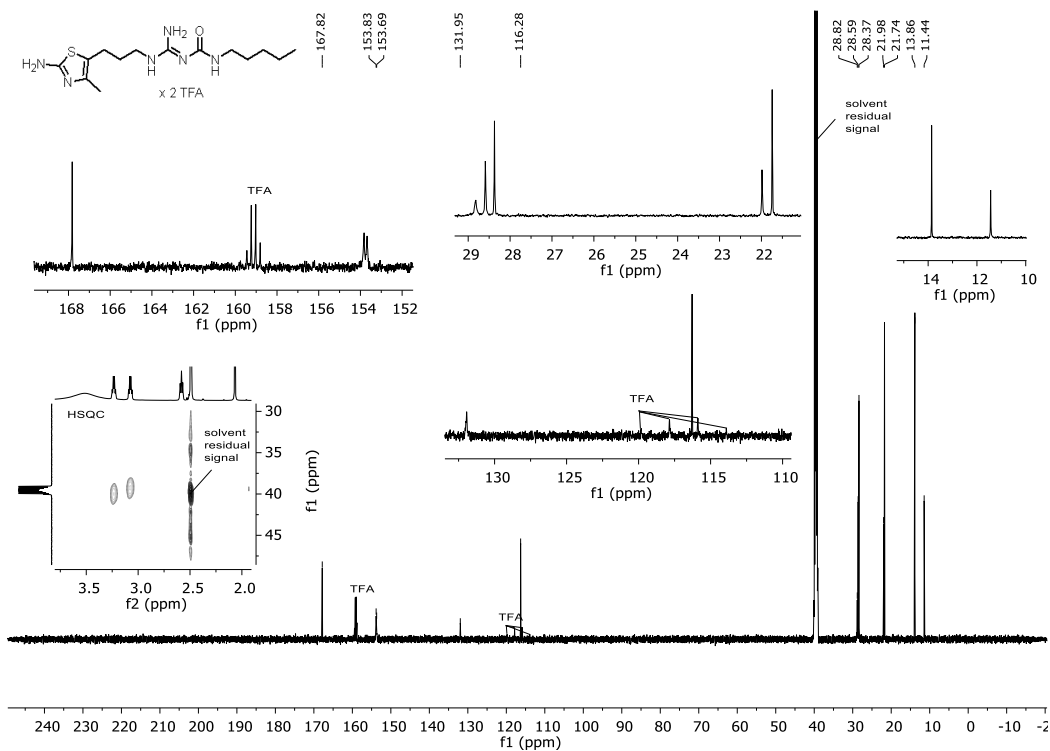
Figure 3.041. ^{13}C NMR spectrum (151 MHz, DMSO-d$_6$) of compound **3.139**.

497
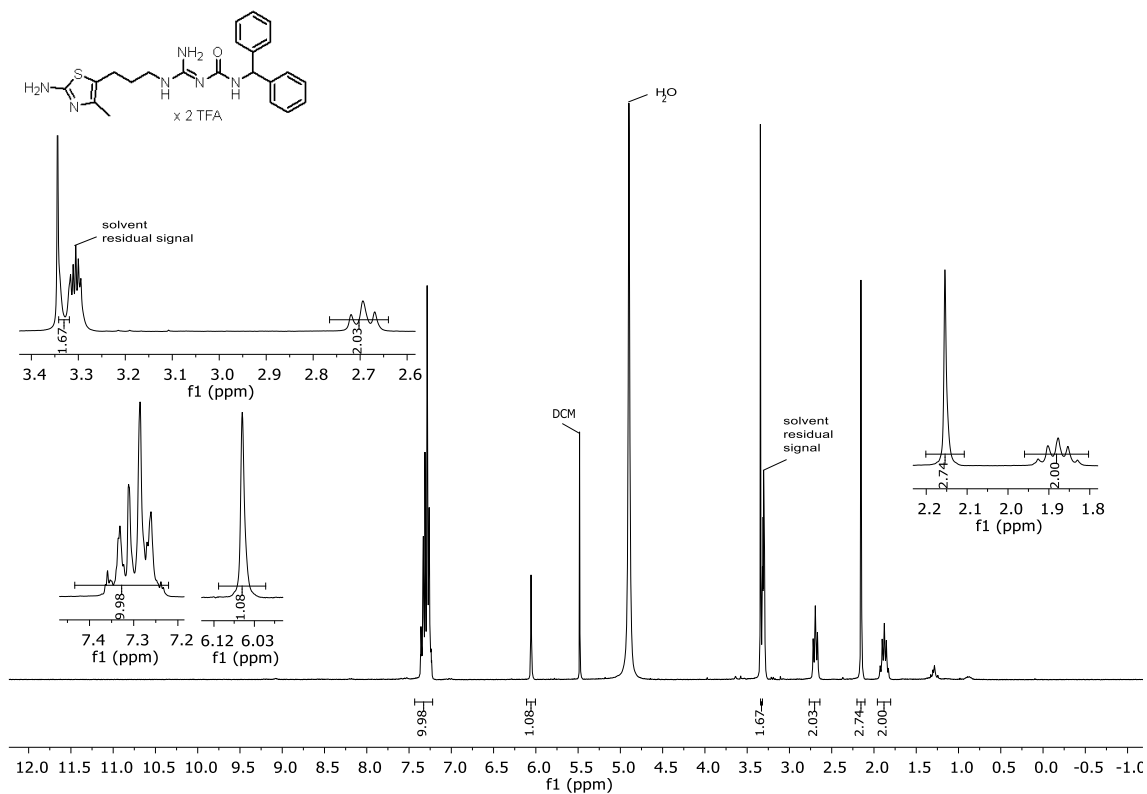
Figure 3.042. ^{1}H NMR spectrum (300 MHz, CD$_3$OD) of compound **3.144**.
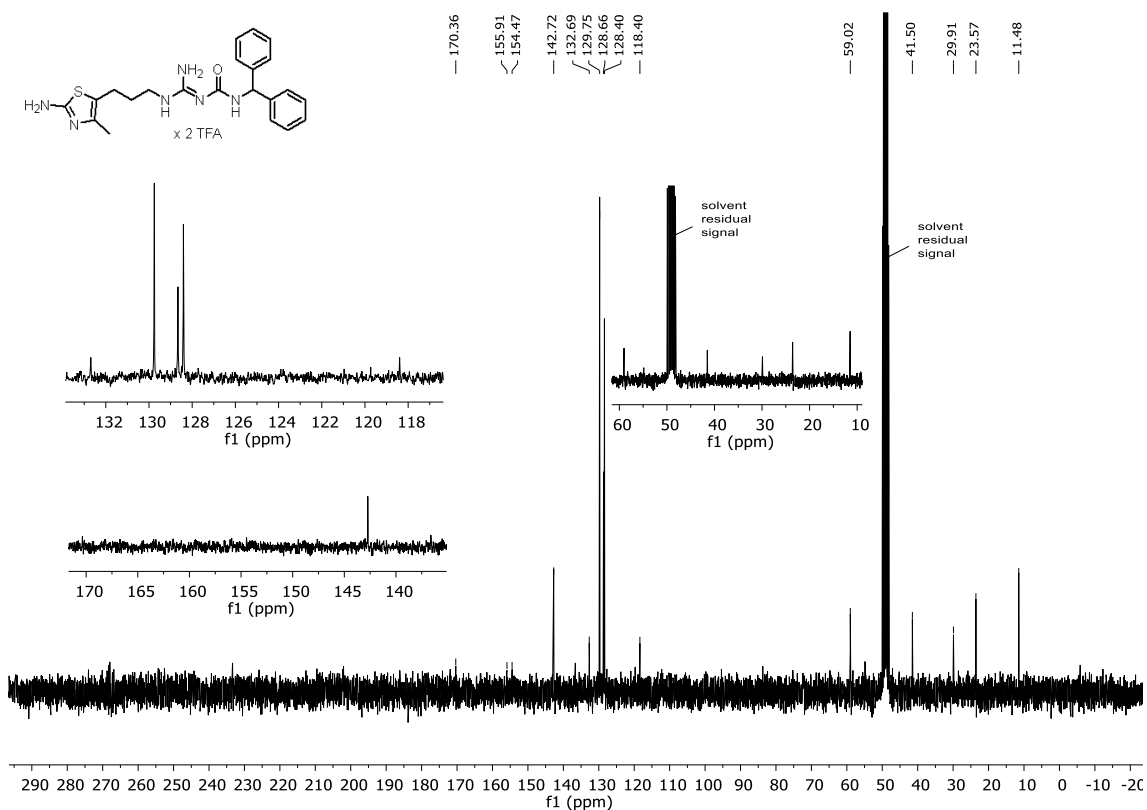
Figure 3.043. ^{13}C NMR spectrum (75 MHz, CD$_3$OD) of compound **3.144**.

498
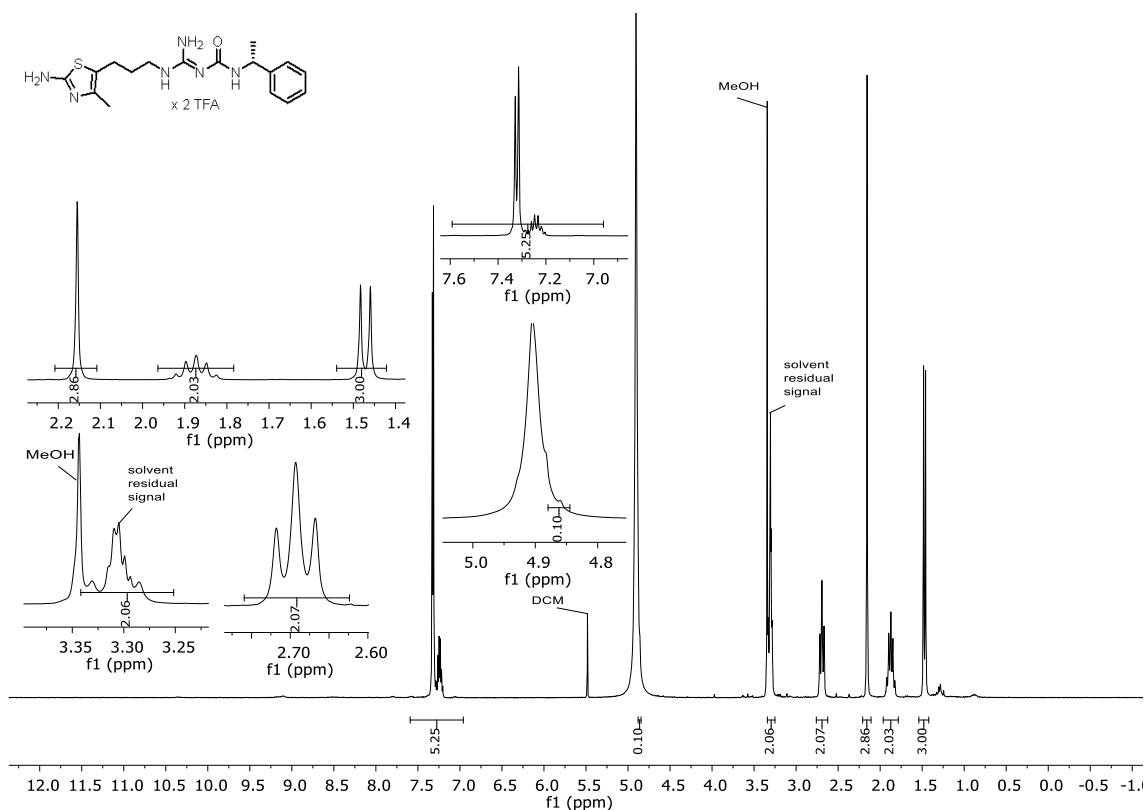
Figure 3.044. ¹H NMR spectrum (300 MHz, CD₃OD) of compound **3.145**.
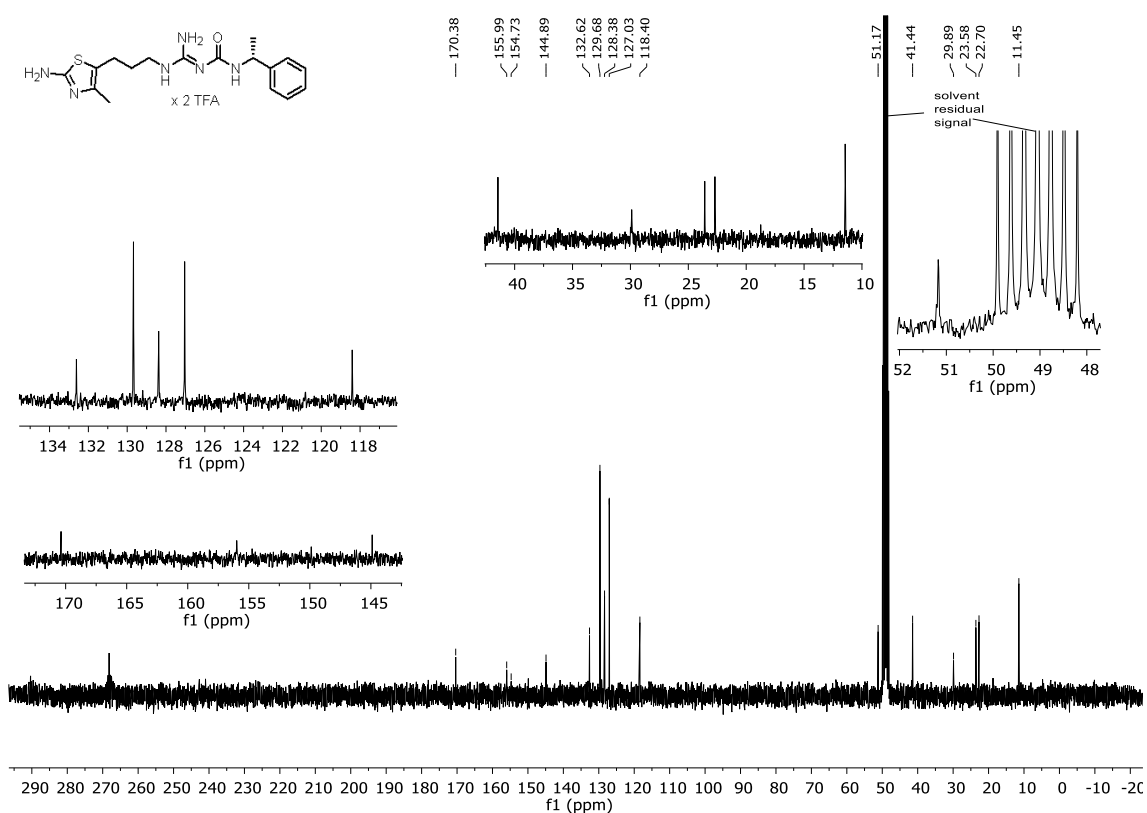
Figure 3.045. ¹³C NMR spectrum (75 MHz, CD₃OD) of compound **3.145**.
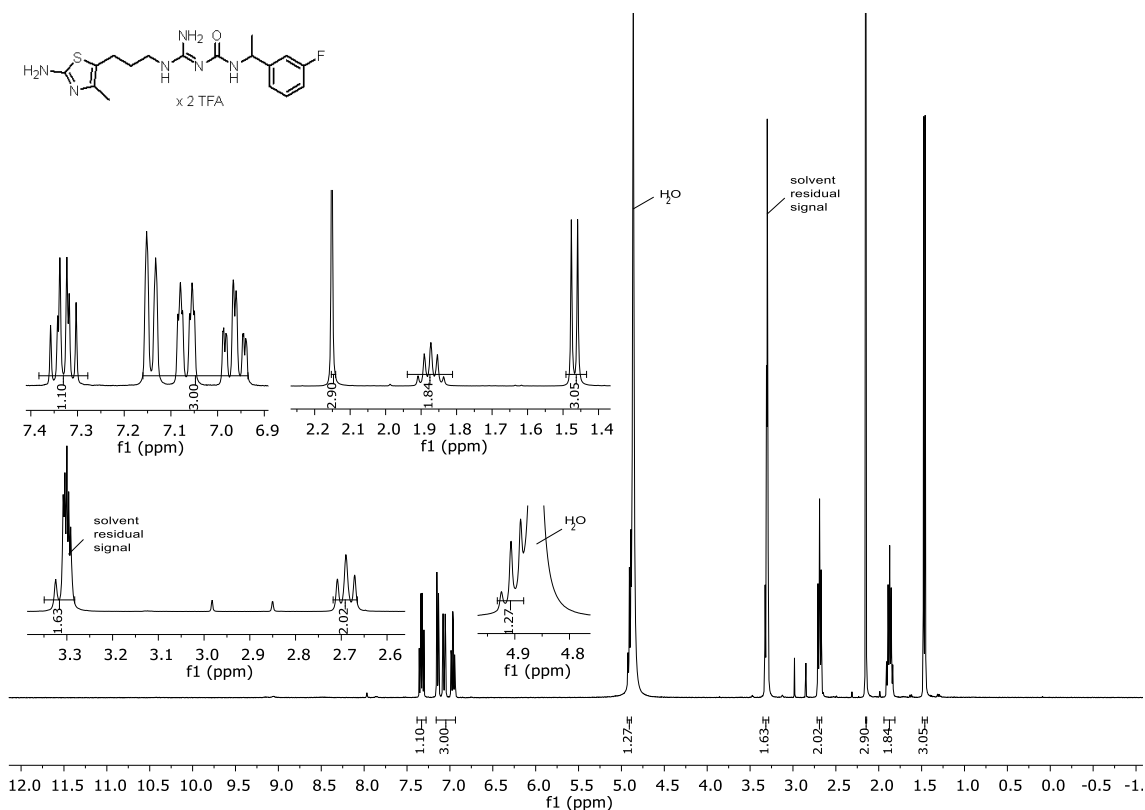
Figure 3.046. ^{1}H NMR spectrum (400 MHz, CD$_3$OD) of compound **3.157**.
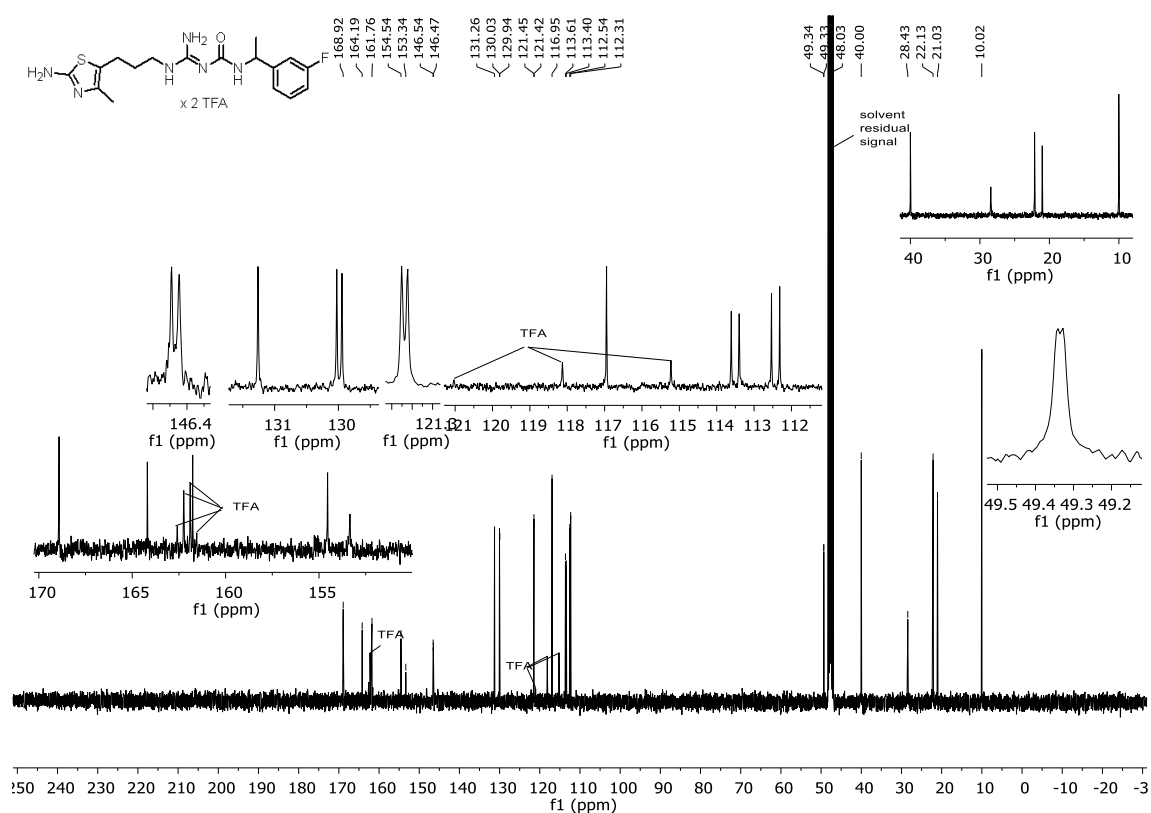
Figure 3.047. ^{13}C NMR spectrum (101 MHz, CD$_3$OD) of compound **3.157**.

500
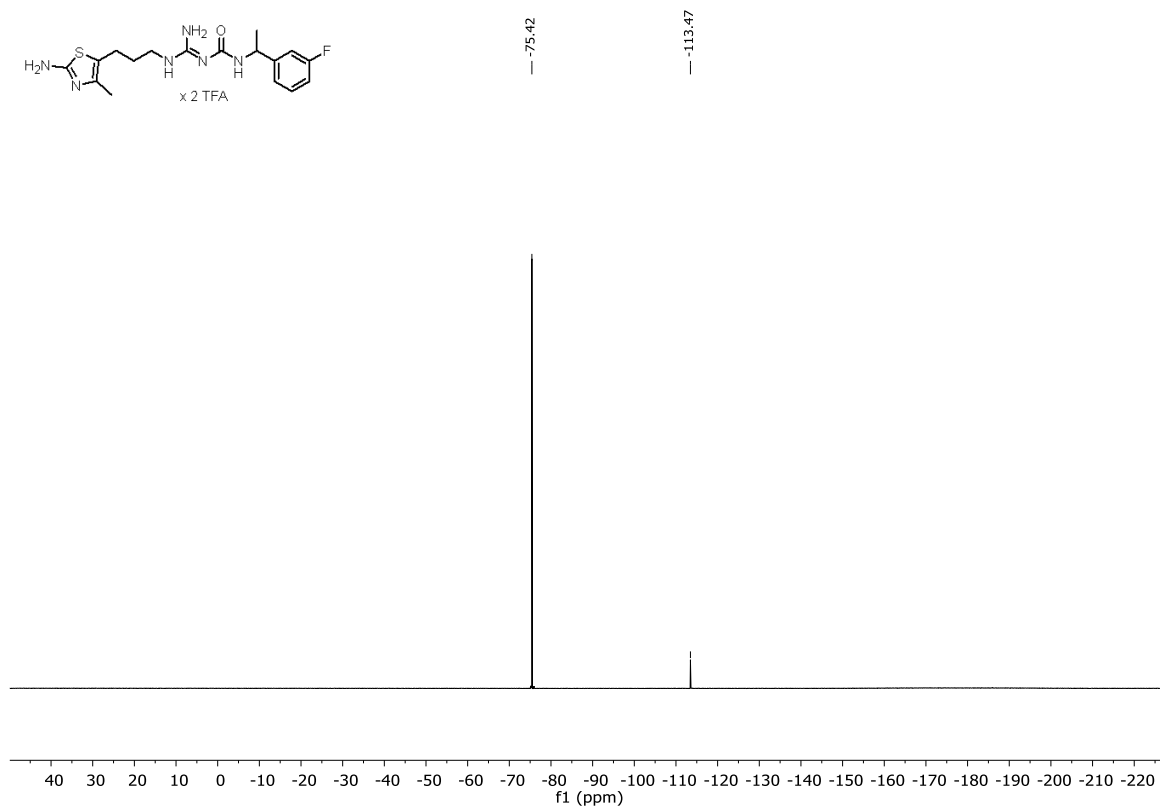
Figure 3.048. ^{19}F NMR spectrum (377 MHz, CD$_3$OD) of compound **3.157**.
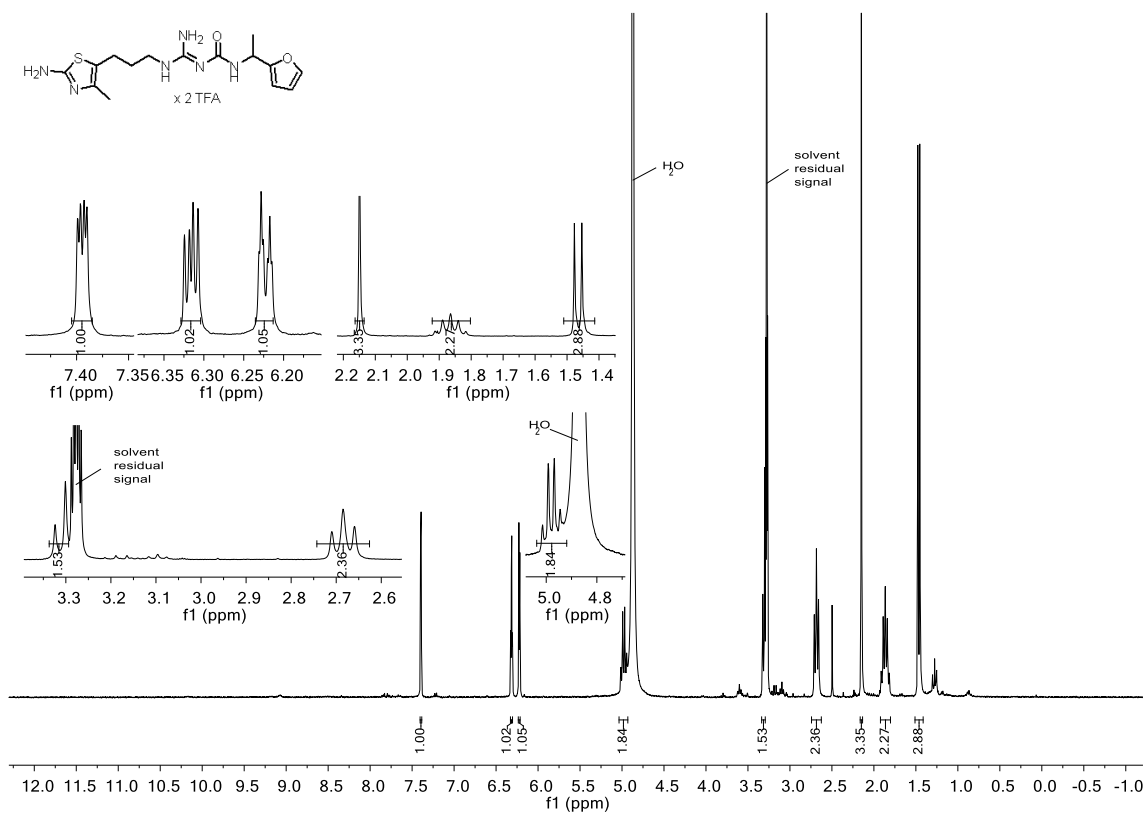
Figure 3.049. ^{1}H NMR spectrum (300 MHz, CD$_3$OD) of compound **3.159**.
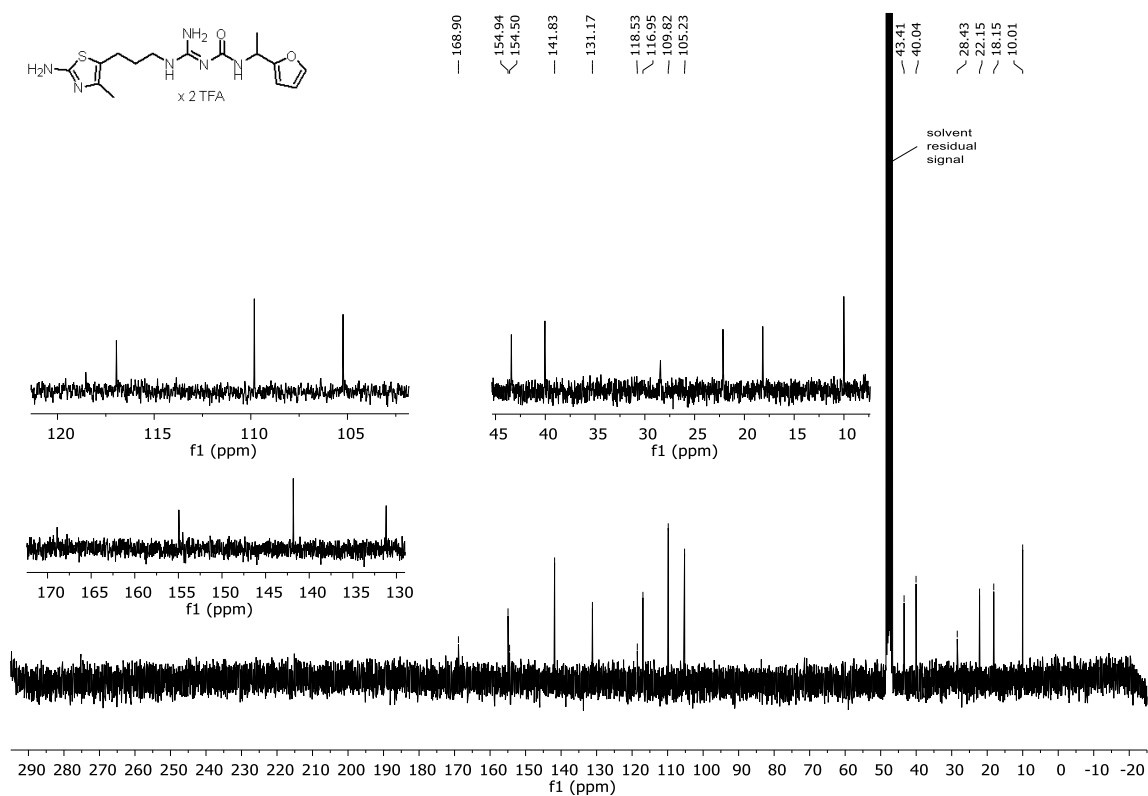
Figure 3.050. ^{13}C NMR spectrum (75 MHz, CD₃OD) of compound **3.159**.
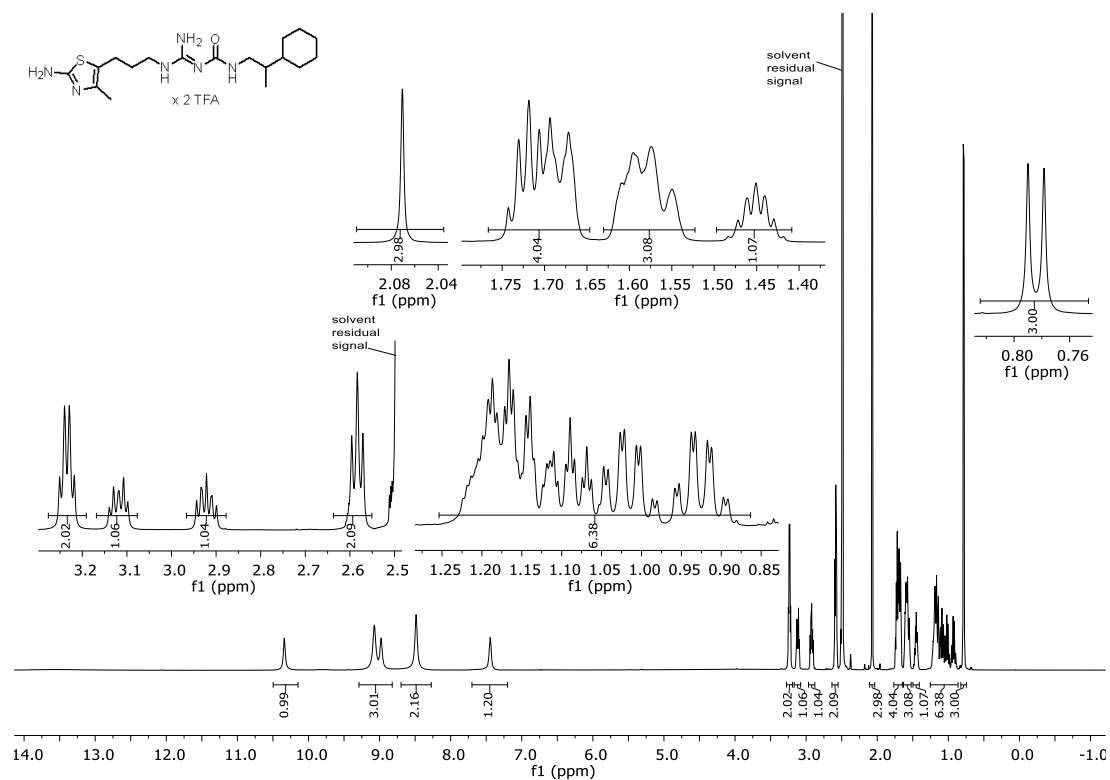
Figure 3.051. ^{1}H NMR spectrum (600 MHz, DMSO-d₆) of compound **3.163**.

502
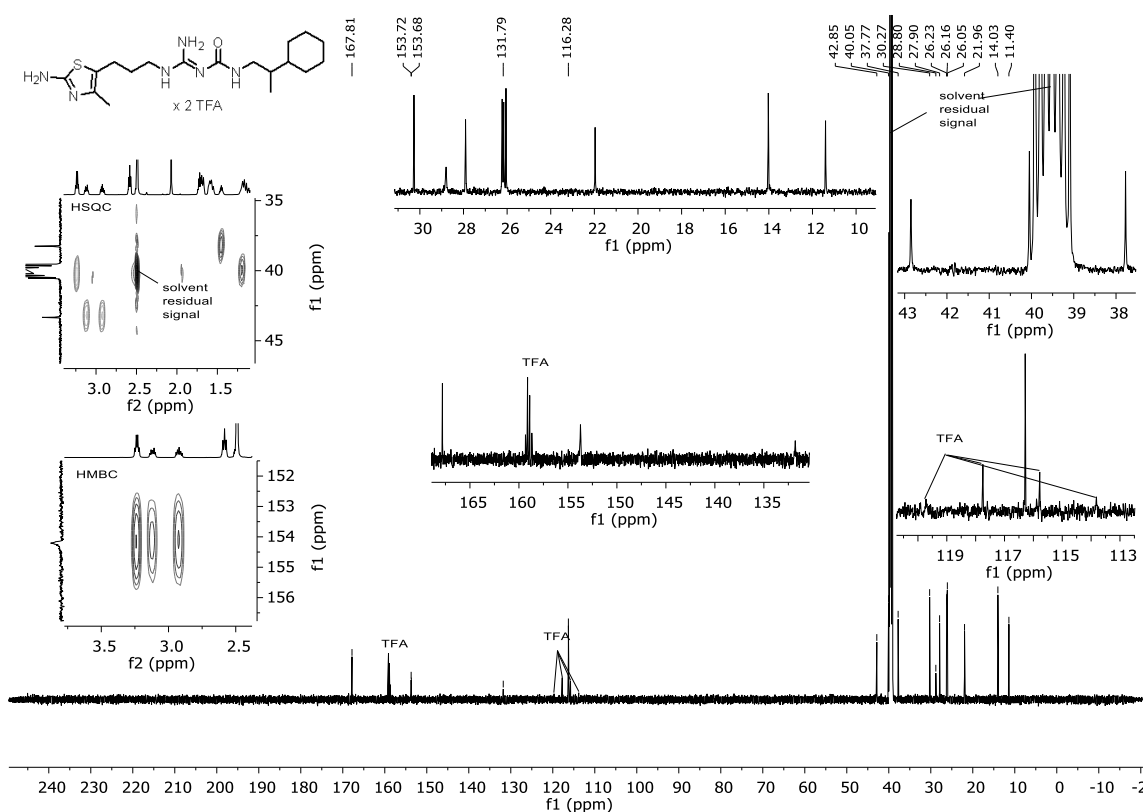
Figure 3.052. ^{13}C NMR spectrum (600 MHz, DMSO-d_6) of compound **3.163**.
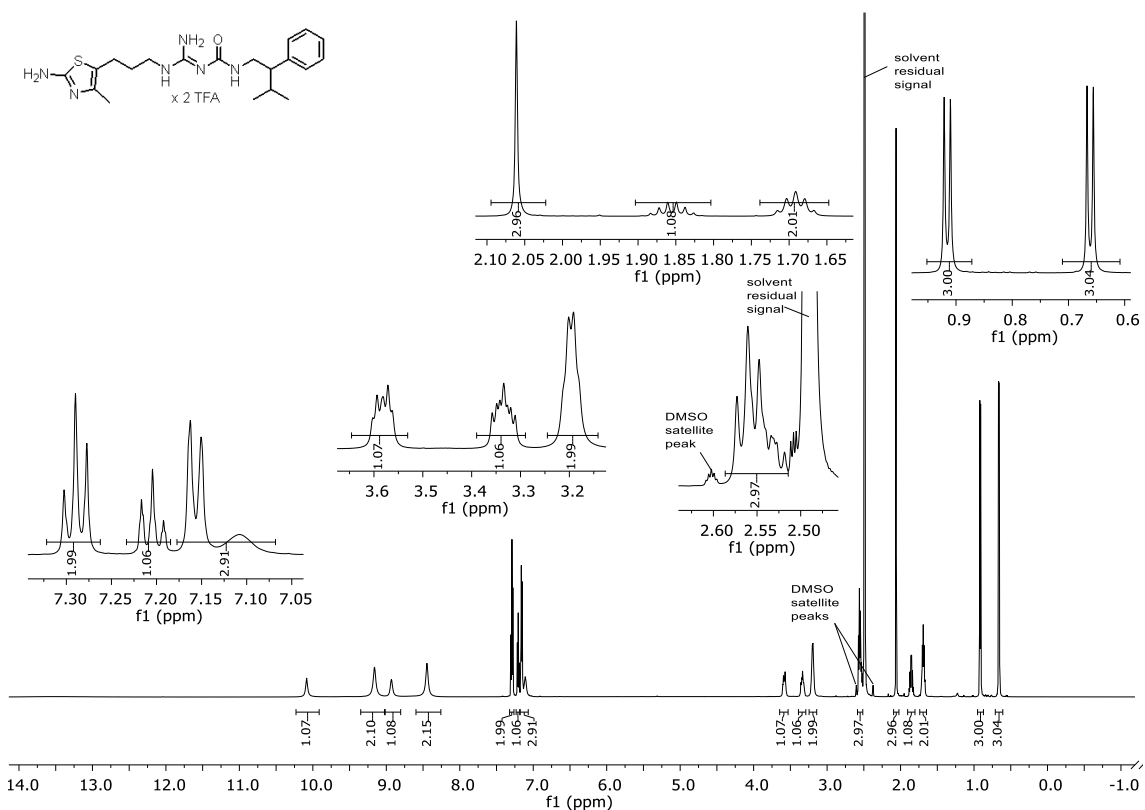
Figure 3.053. ^{1}H NMR spectrum (600 MHz, DMSO-d_6) of compound **3.167**.

503
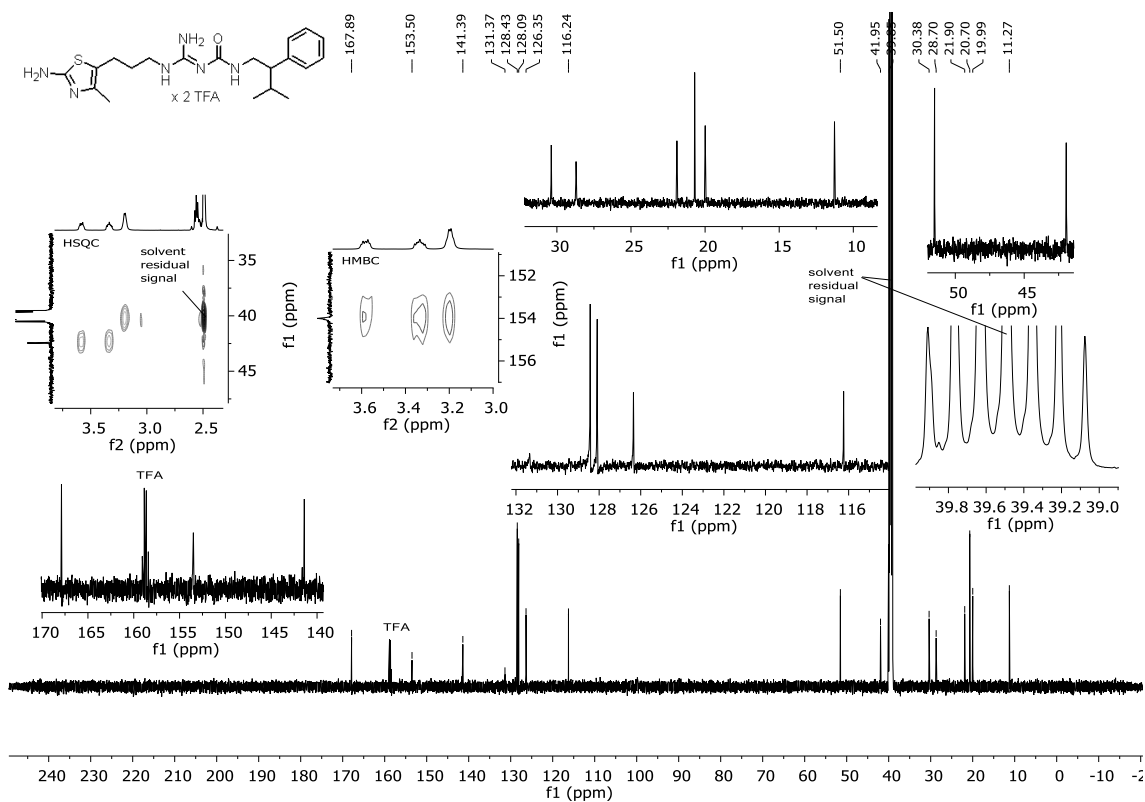
Figure 3.054. ^{13}C NMR spectrum (600 MHz, DMSO-d_6) of compound **3.167**.
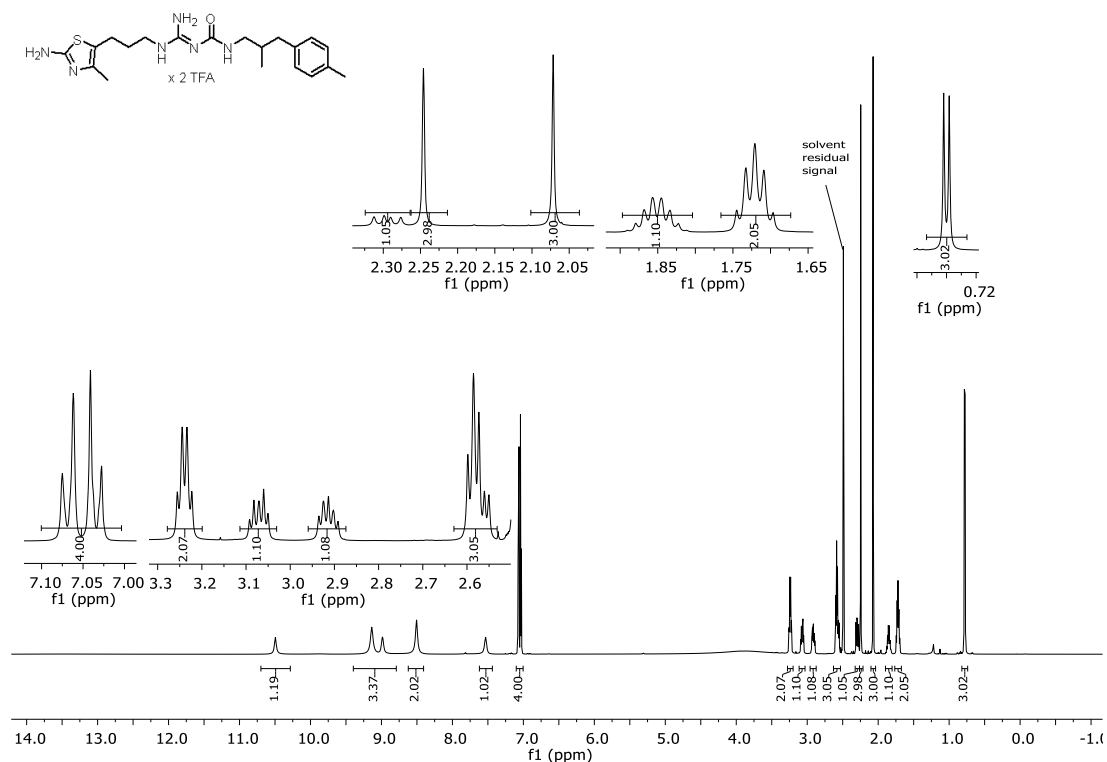
Figure 3.055. ^1H NMR spectrum (600 MHz, DMSO-d_6) of compound **3.170**.
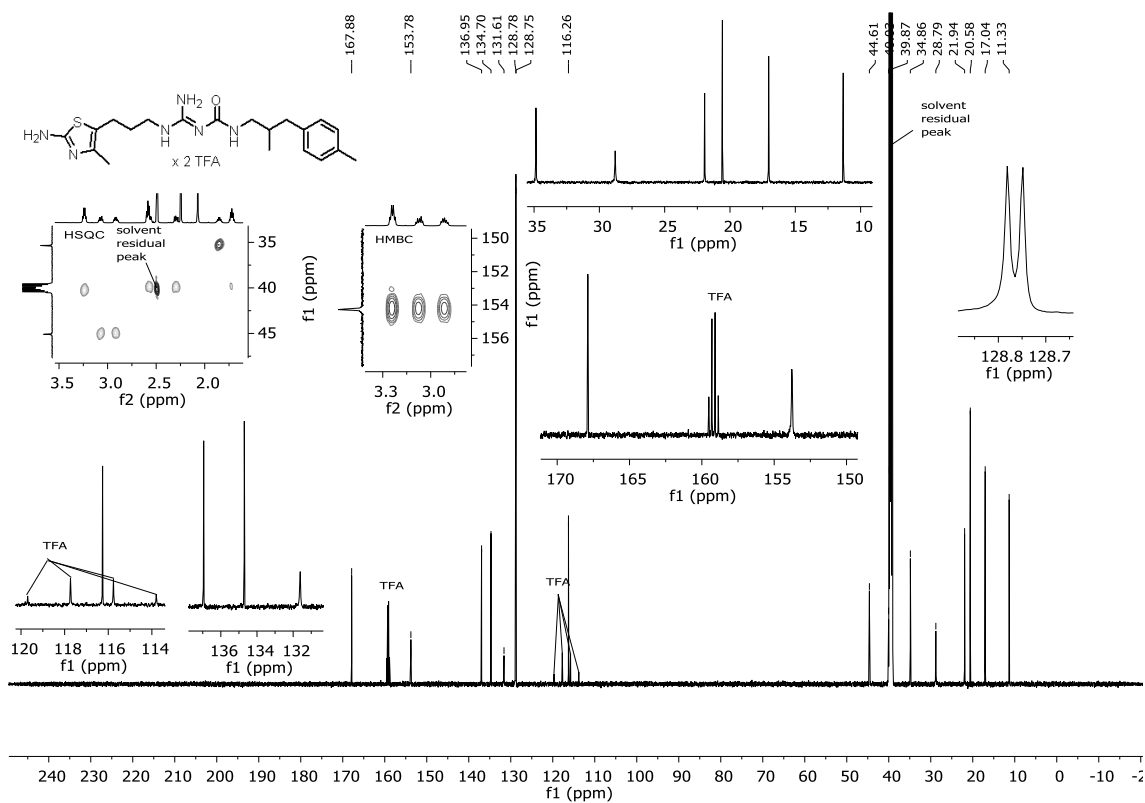
Figure 3.056. ¹³C NMR spectrum (600 MHz, DMSO-d₆) of compound **3.170**.
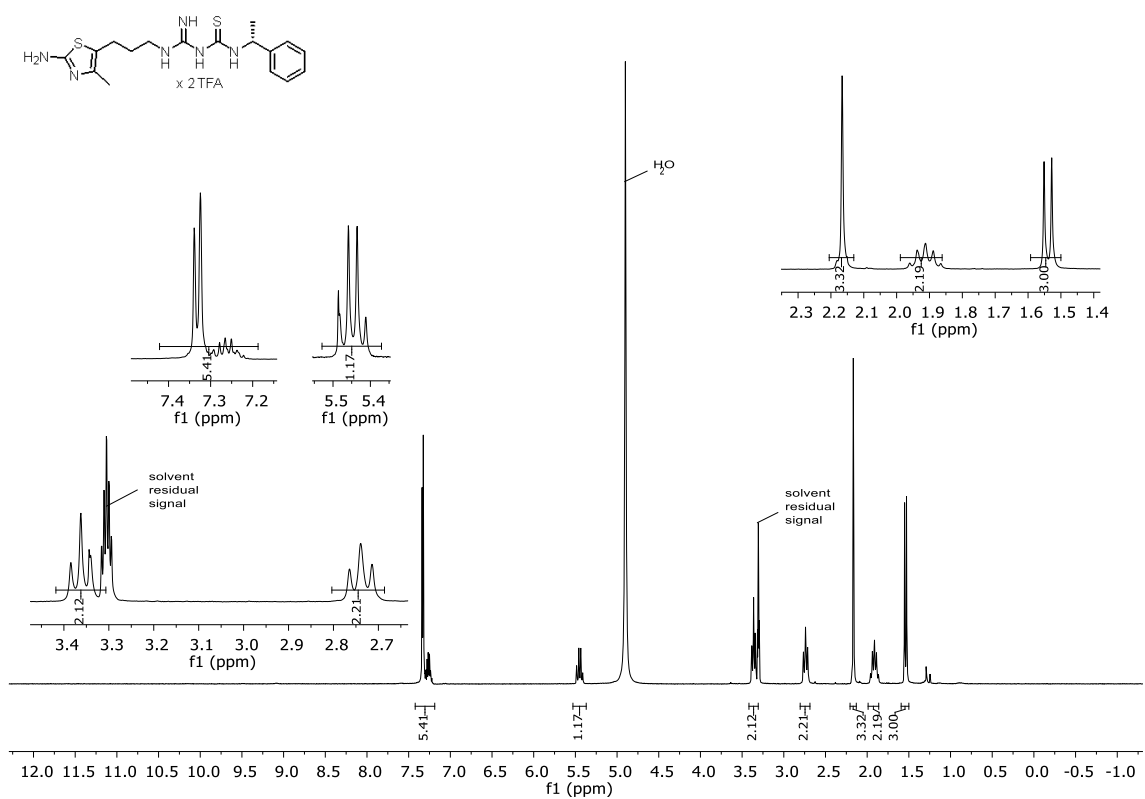
Figure 3.057. ¹H NMR spectrum (300 MHz, CD₃OD) of compound **3.174**.

505
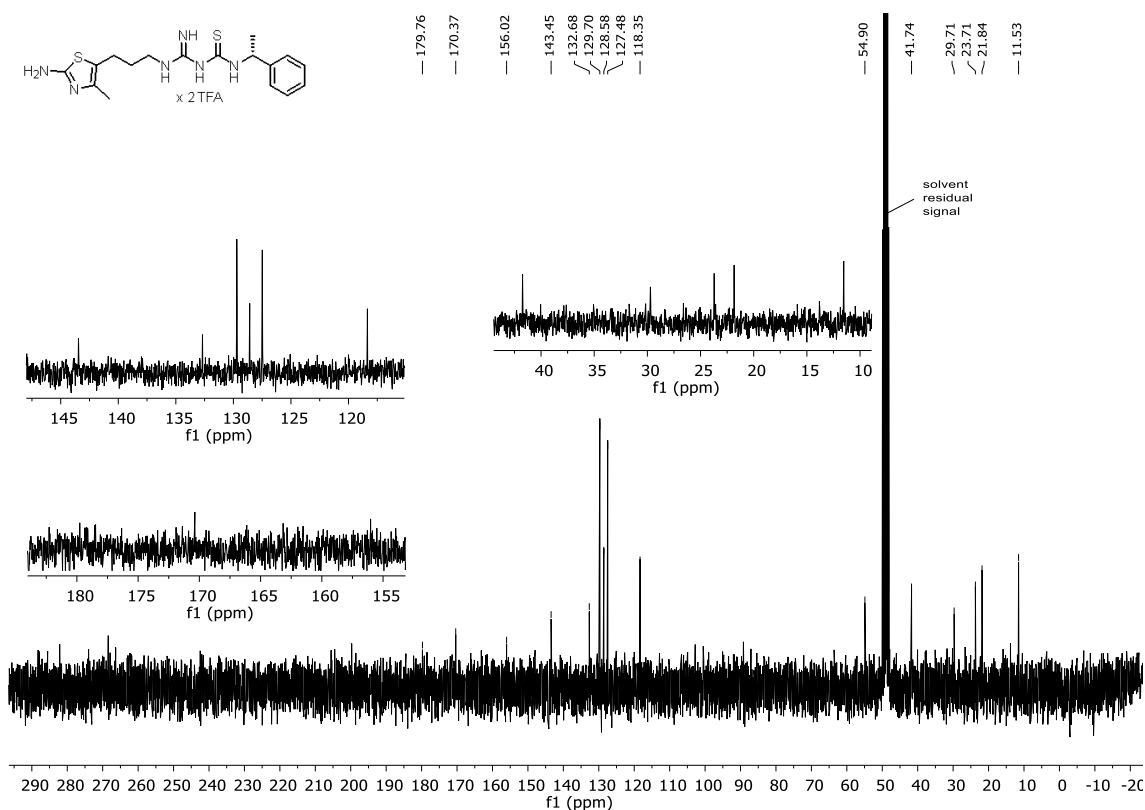
Figure 3.058. ^{13}C NMR spectrum (75 MHz, CD$_3$OD) of compound **3.174**.
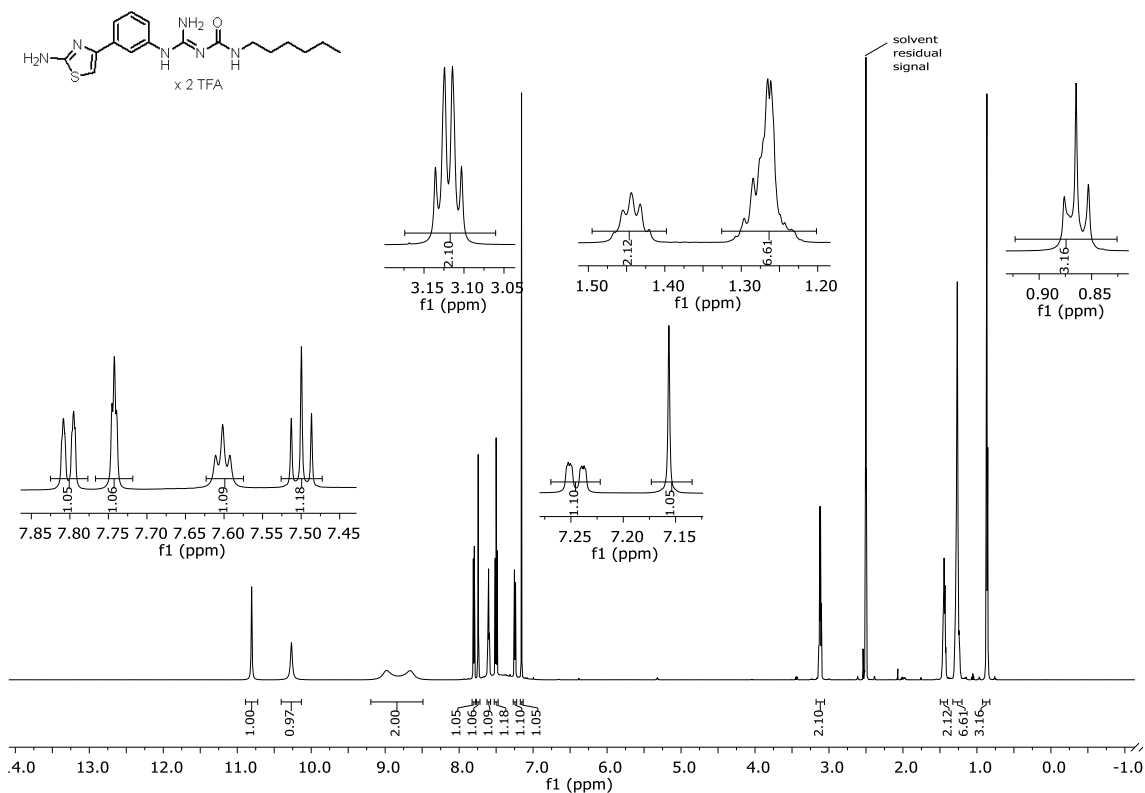
Figure 3.059. ^{1}H NMR spectrum (600 MHz, DMSO-d$_6$) of compound **3.180**.

506
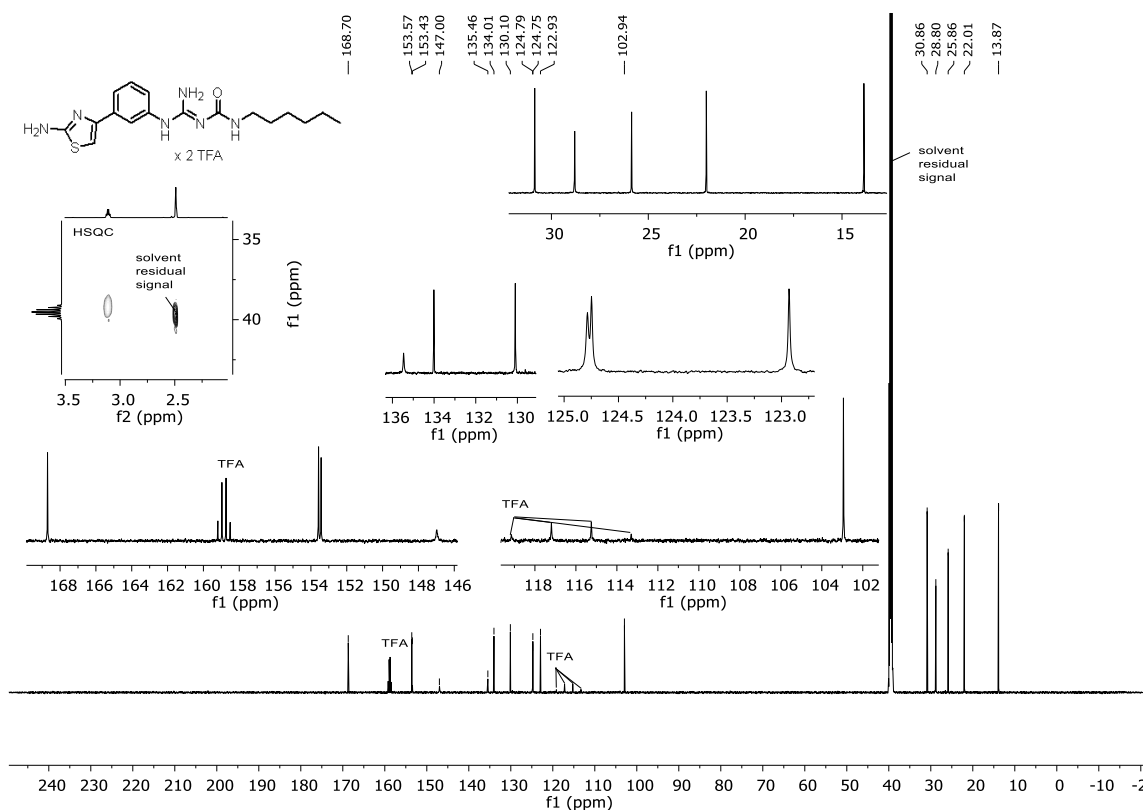
Figure 3.060. ^{13}C NMR spectrum (600 MHz, DMSO-d$_6$) of compound **3.180**.
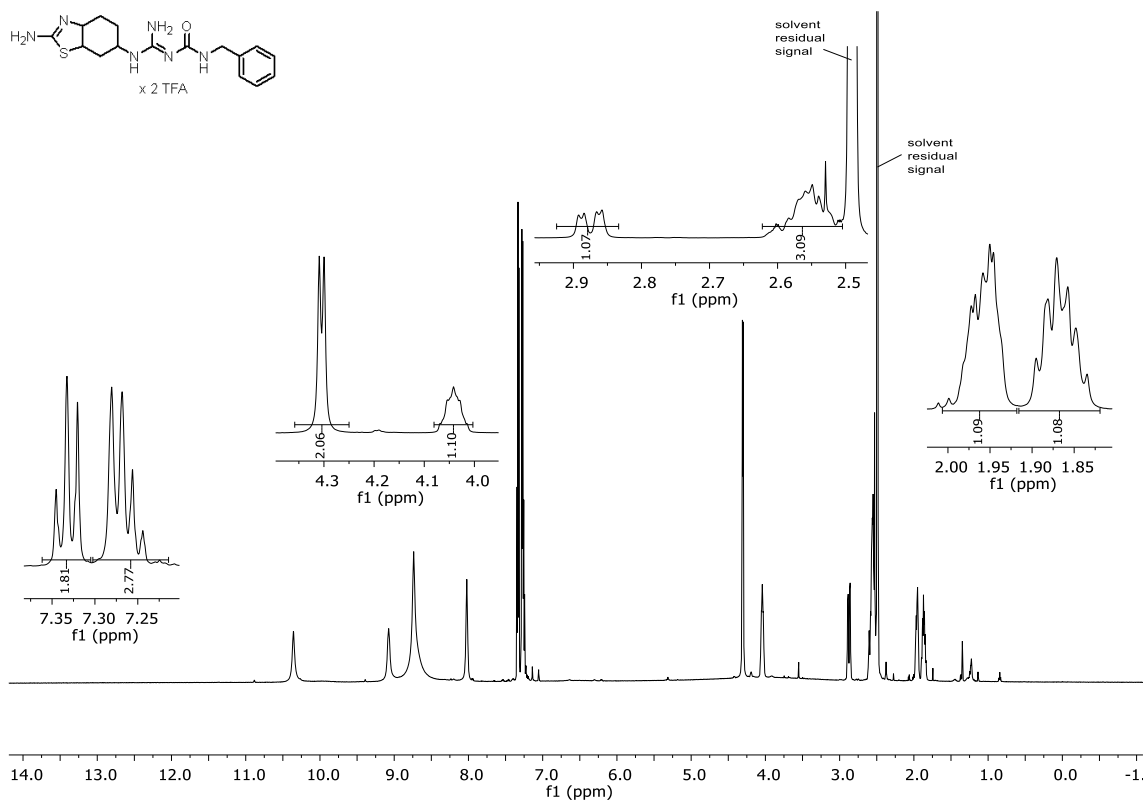
Figure 3.061. ^{1}H NMR spectrum (600 MHz, DMSO-d$_6$) of compound **3.186**.

507
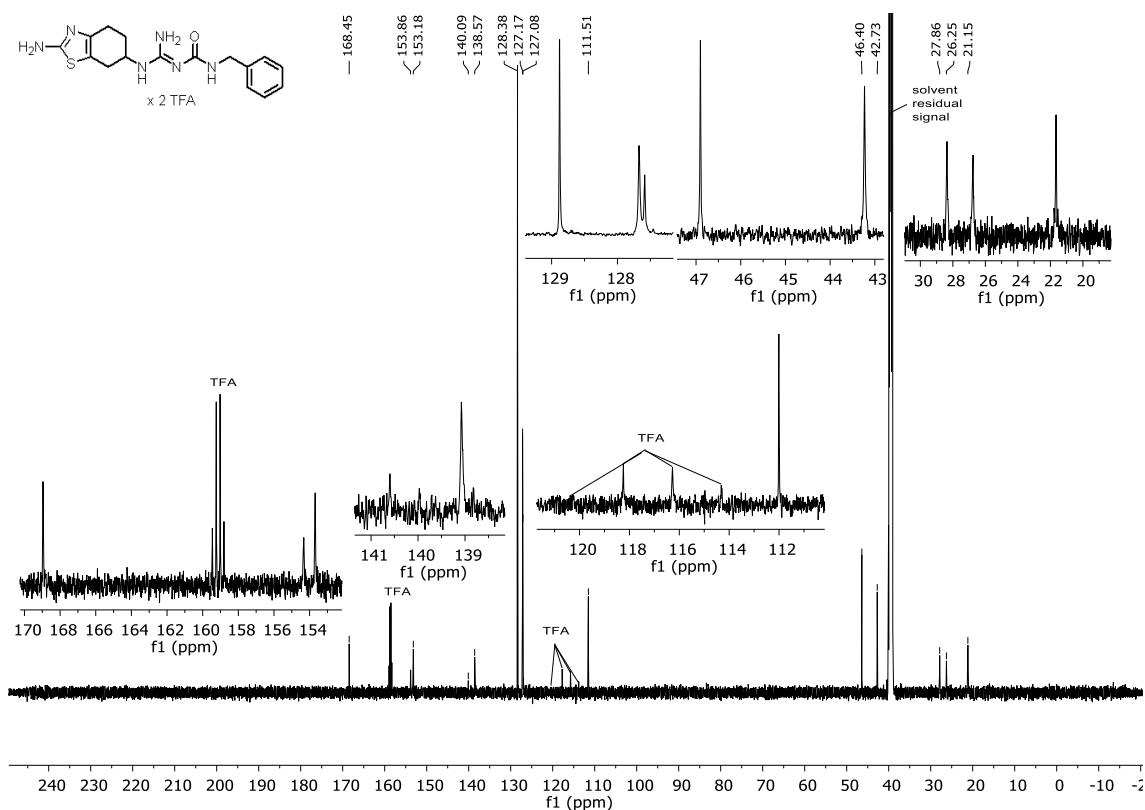
Figure 3.062. ^{13}C NMR spectrum (600 MHz, DMSO-d$_6$) of compound **3.186**.
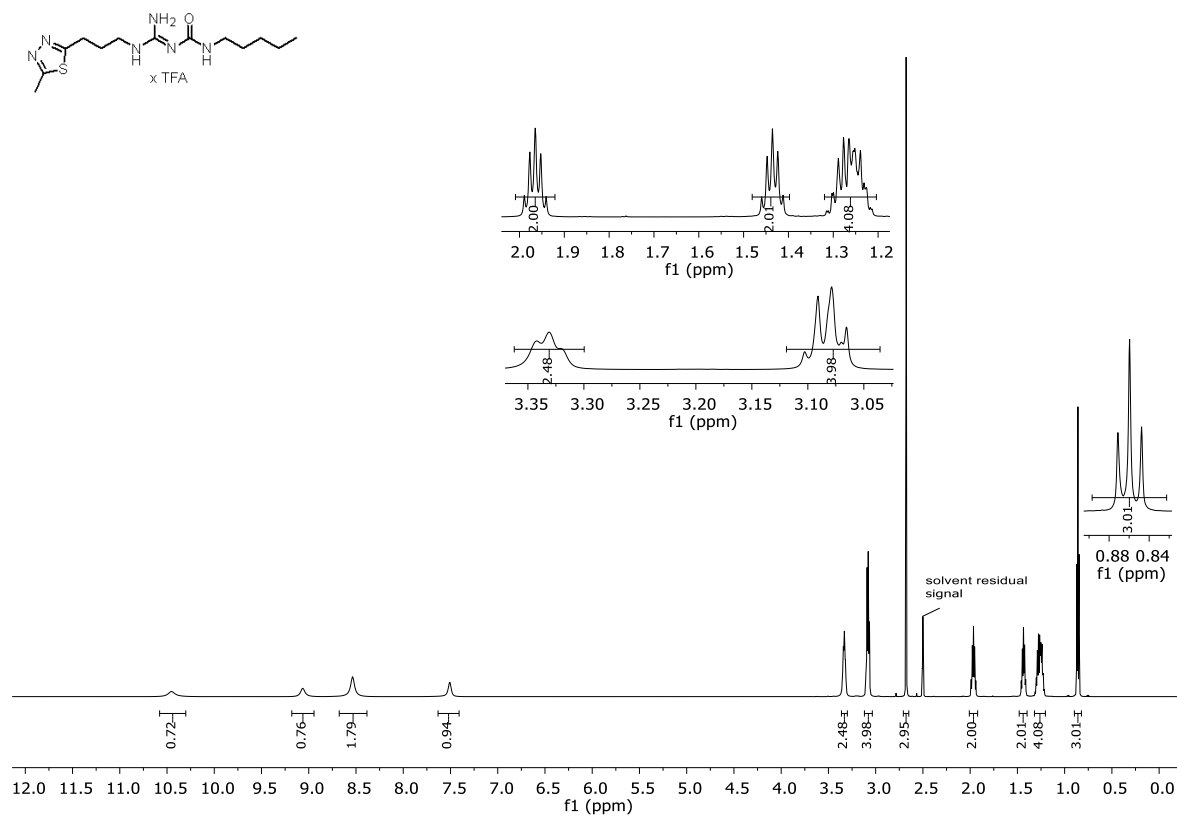
Figure 3.063. ^{1}H-NMR spectrum (600 MHz, DMSO-d$_6$) of compound **3.238**.

508
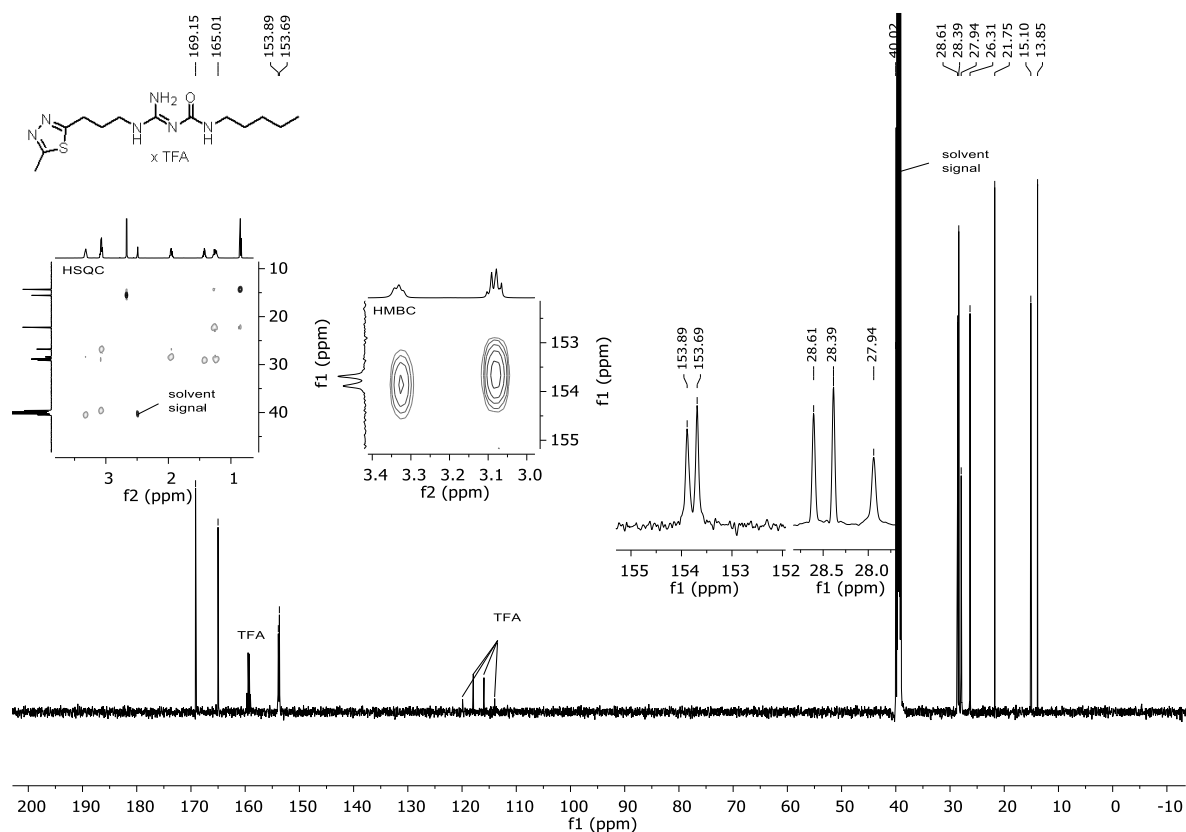
Figure 3.064. ^{13}C-NMR spectrum (151 MHz, DMSO-d$_6$) of compound **3.238**.
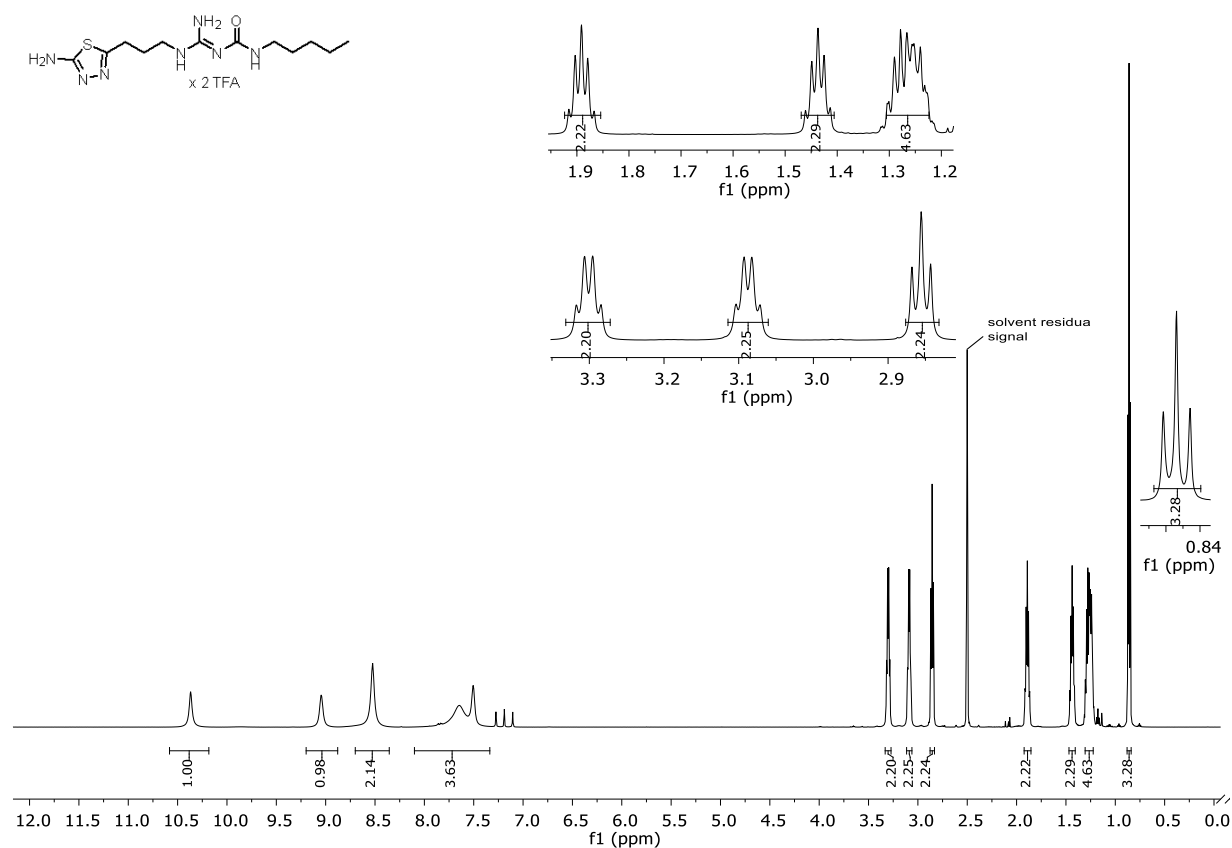
Figure 3.065. ^{1}H-NMR spectrum (600 MHz, DMSO-d$_6$) of compound **3.239**.
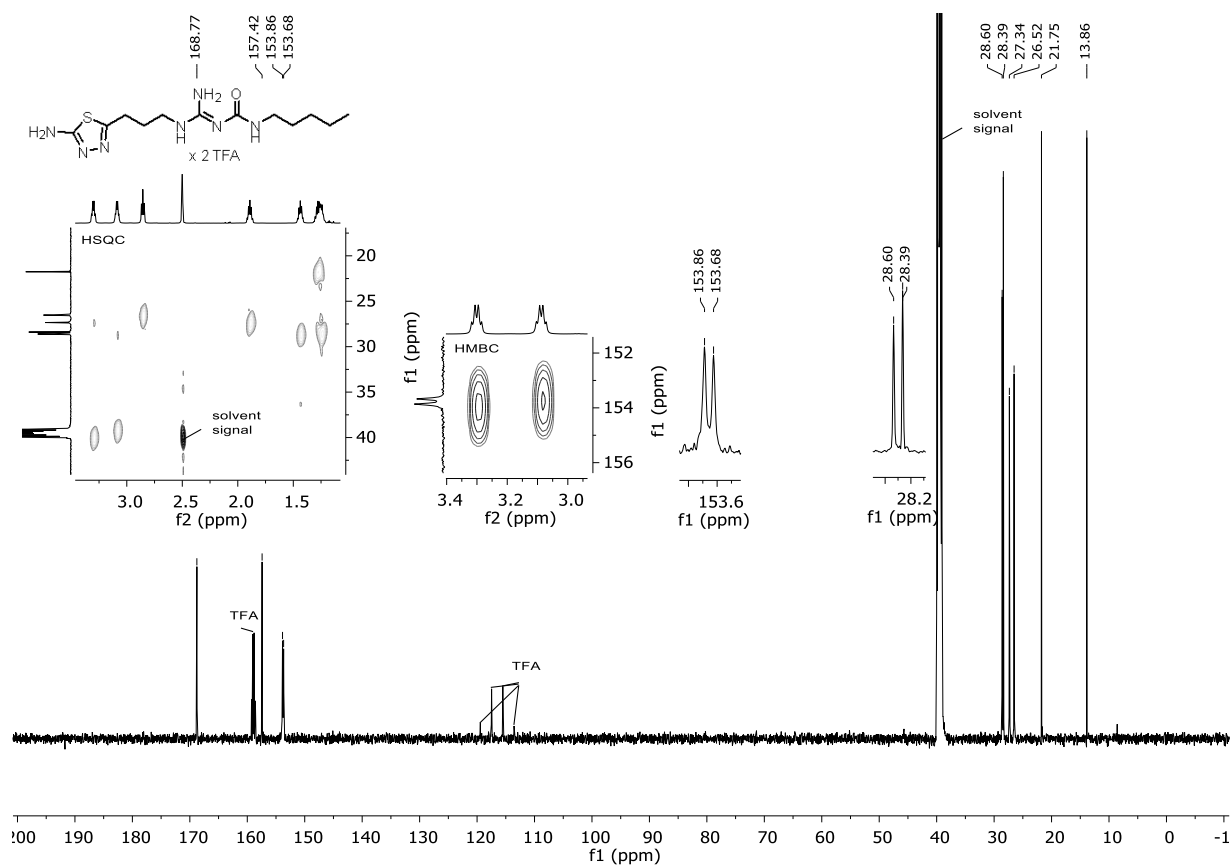
Figure 3.066. ^{13}C-NMR spectrum (151 MHz, DMSO-d$_6$) of compound **3.239**.
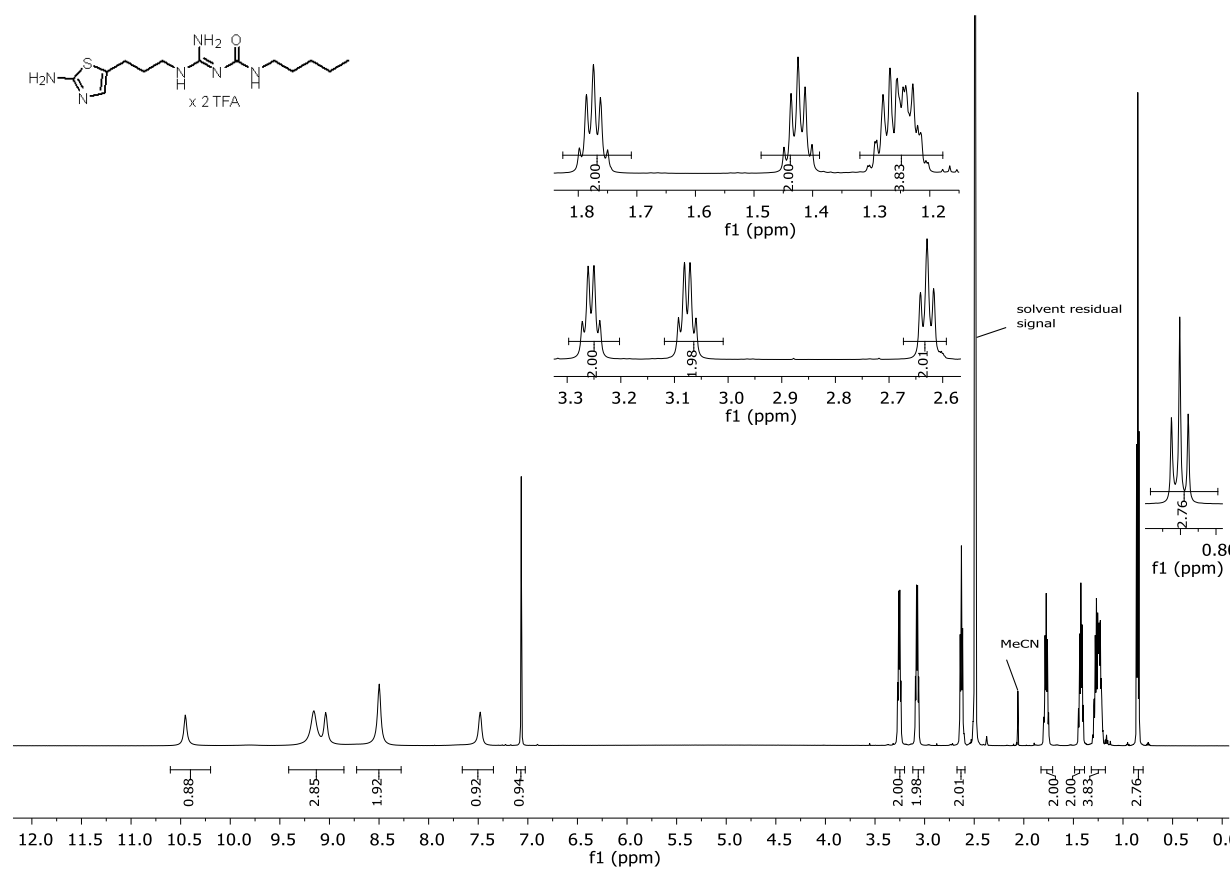
Figure 3.067. ^{1}H-NMR spectrum (600 MHz, DMSO-d$_6$) of compound **3.240**.
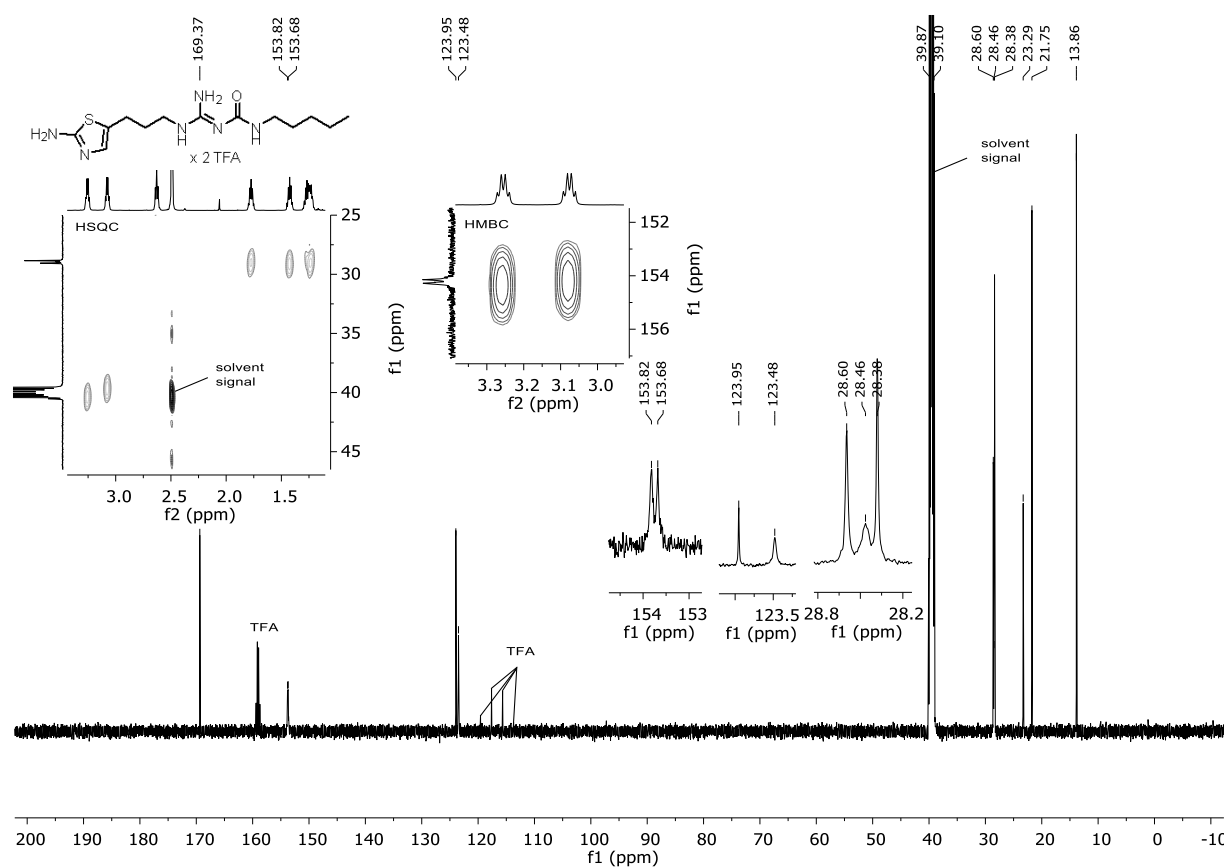
Figure 3.068. ^{13}C-NMR spectrum (151 MHz, DMSO-d₆) of compound **3.240**.
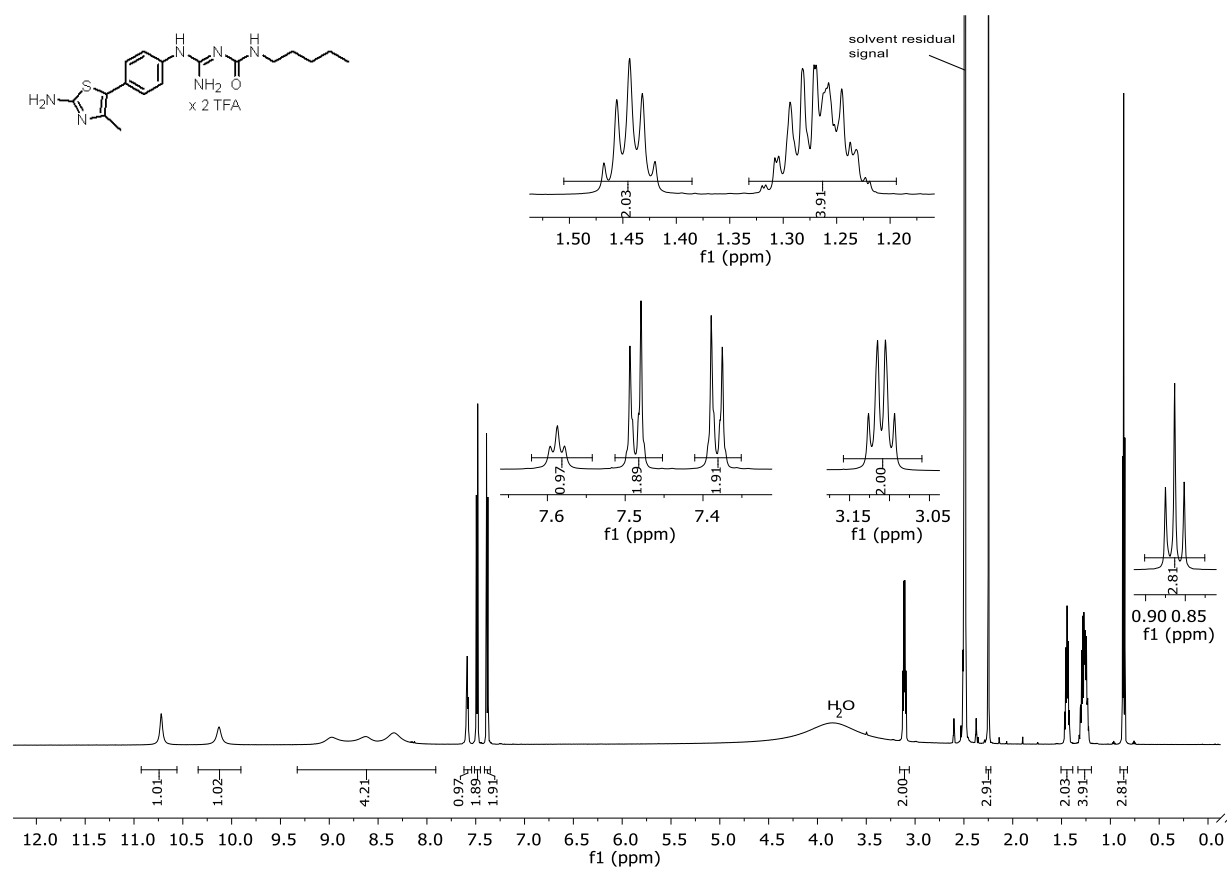
Figure 3.069. ^{1}H-NMR spectrum (600 MHz, DMSO-d₆) of compound **3.241**.
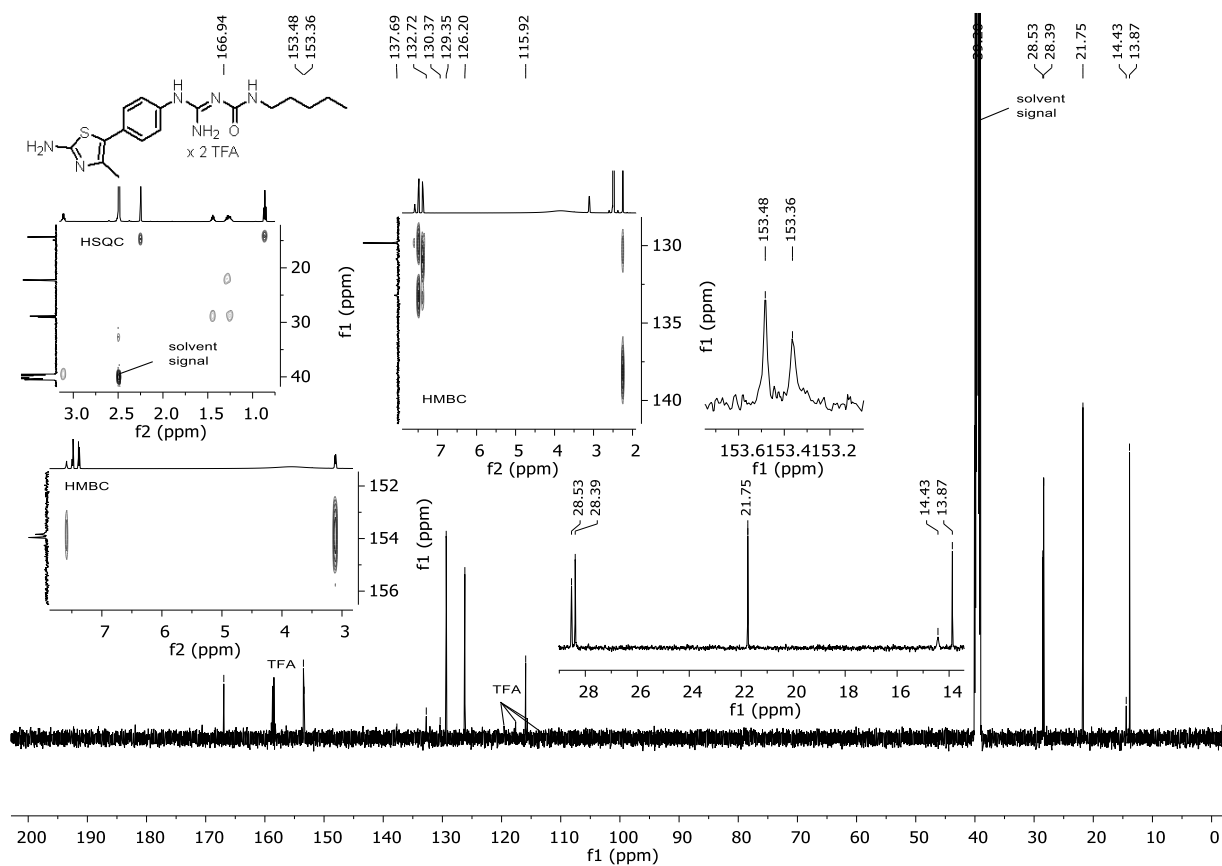
Figure 3.070. ^{13}C-NMR spectrum (151 MHz, DMSO-d₆) of compound **3.241**.
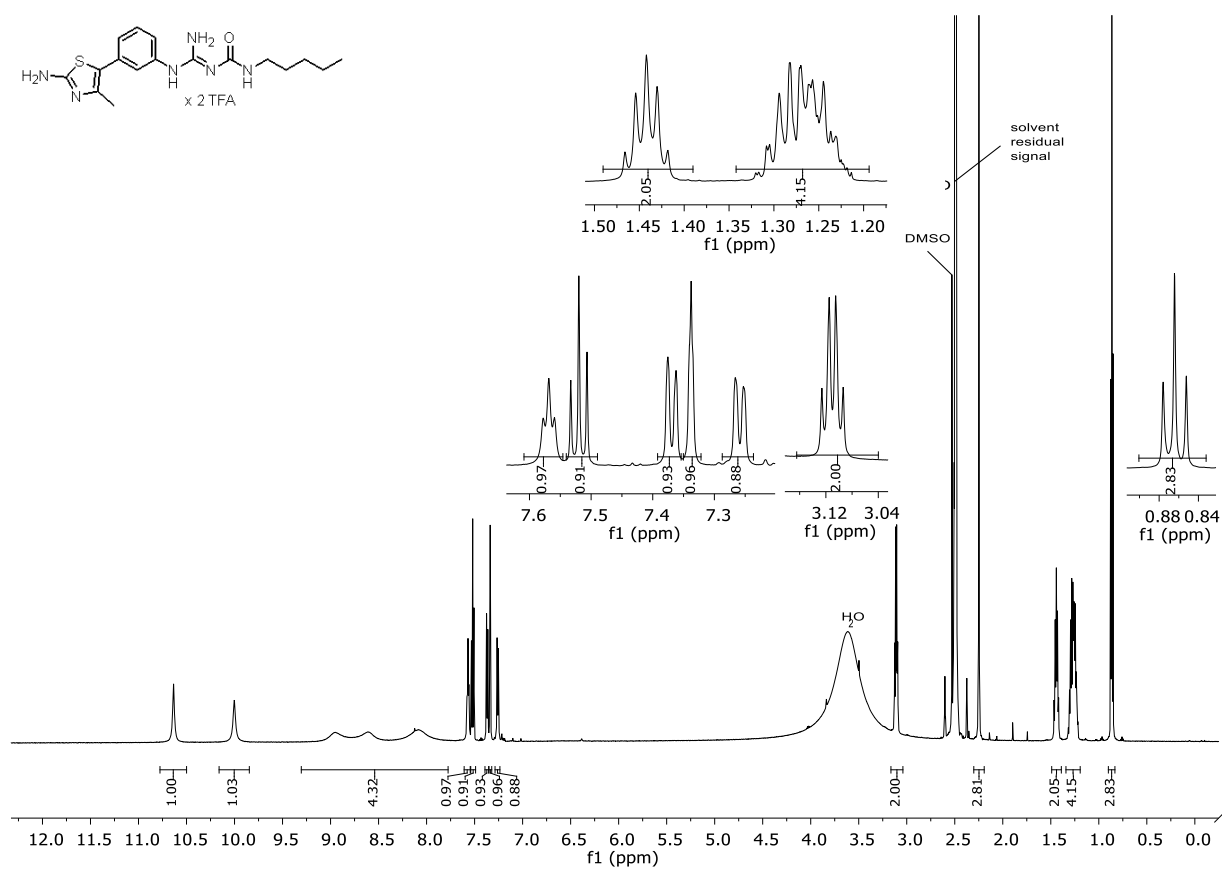
Figure 3.071. ^{1}H-NMR spectrum (600 MHz, DMSO-d₆) of compound **3.242**.
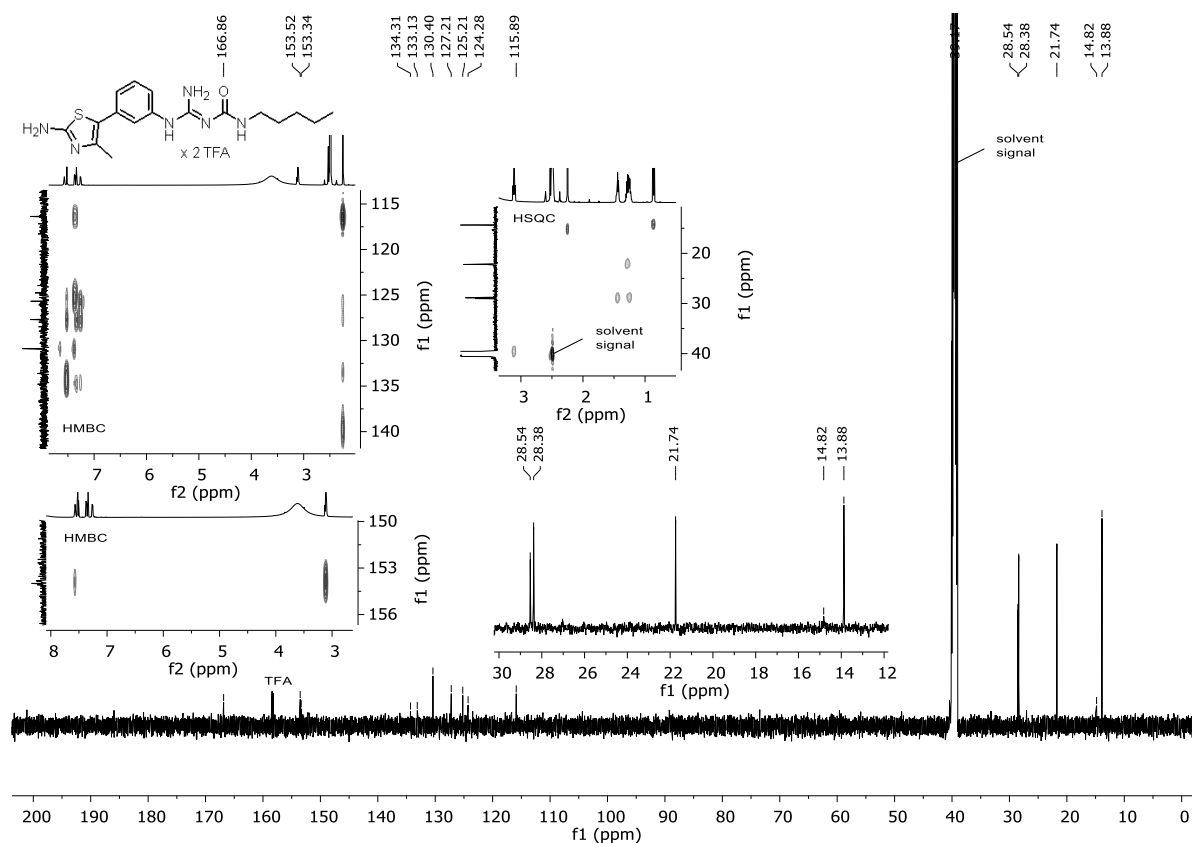
Figure 3.072. ^{13}C-NMR spectrum (151 MHz, DMSO-d$_6$) of compound **3.242**.
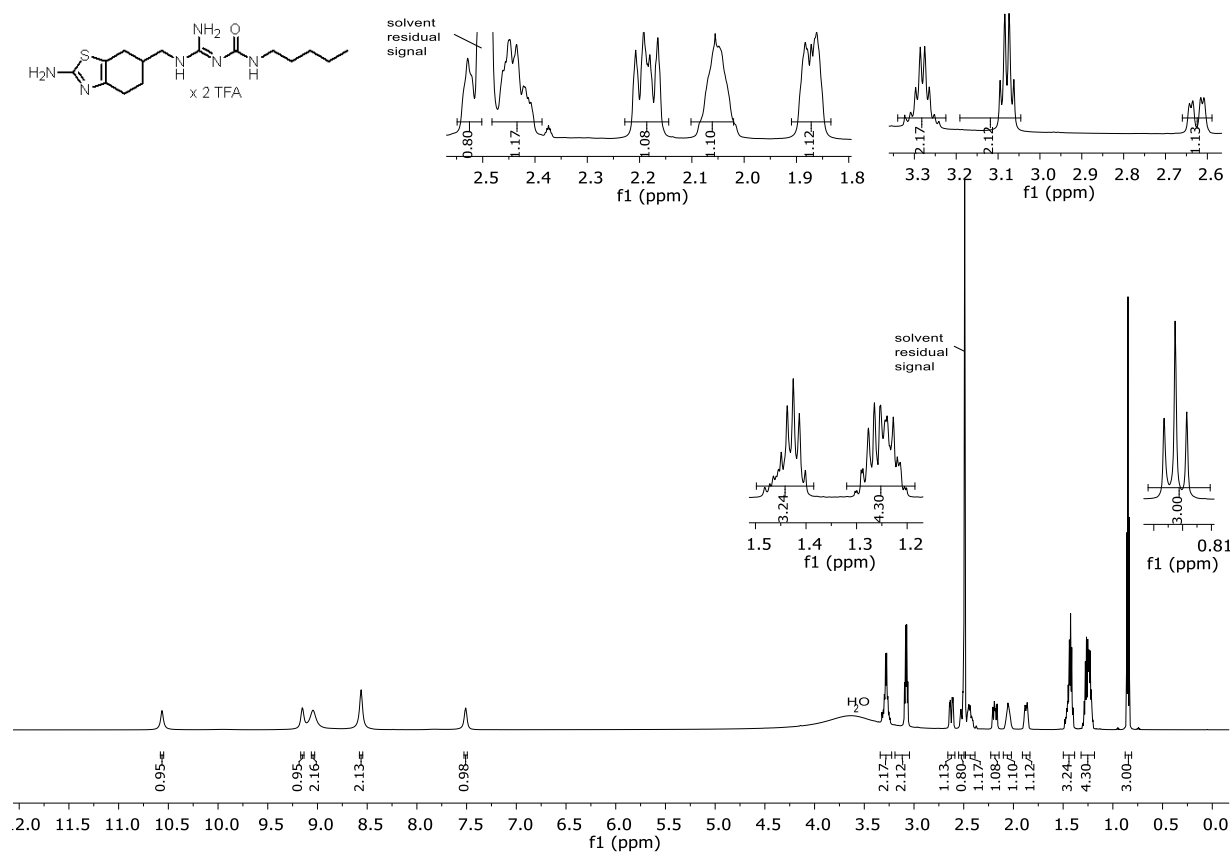
Figure 3.073. ^{1}H-NMR spectrum (600 MHz, DMSO-d$_6$) of compound **3.243**.

513
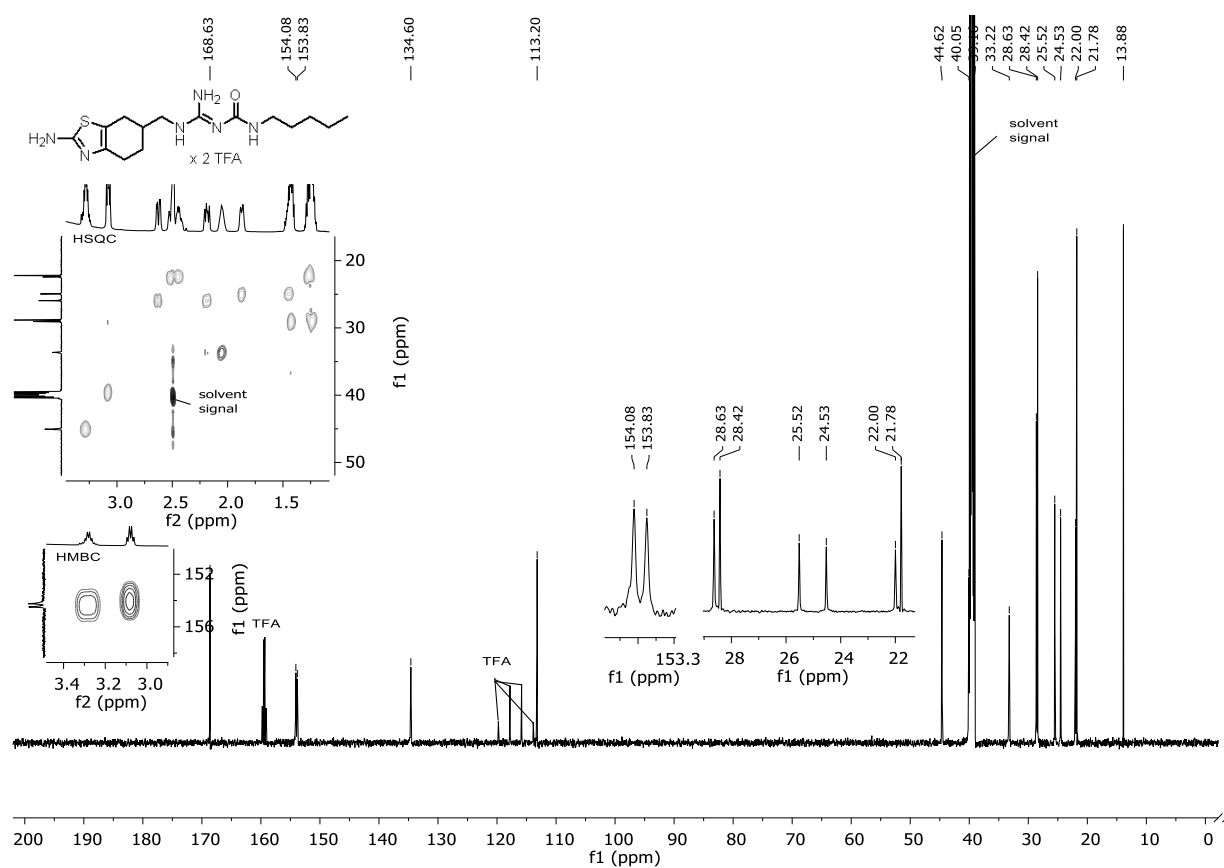
Figure 3.074. ^{13}C-NMR spectrum (151 MHz, DMSO-d₆) of compound **3.243**.
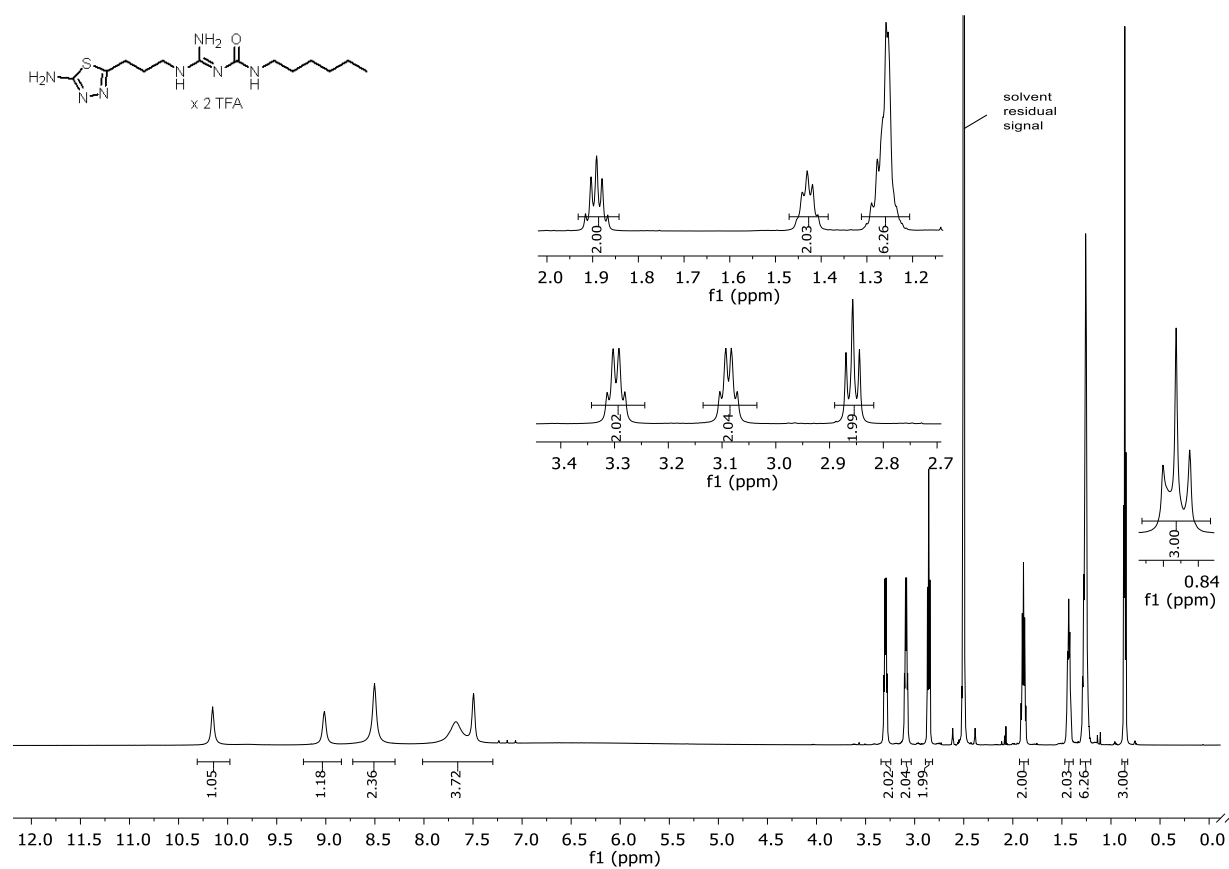
Figure 3.075. ^{1}H-NMR spectrum (600 MHz, DMSO-d₆) of compound **3.244**.
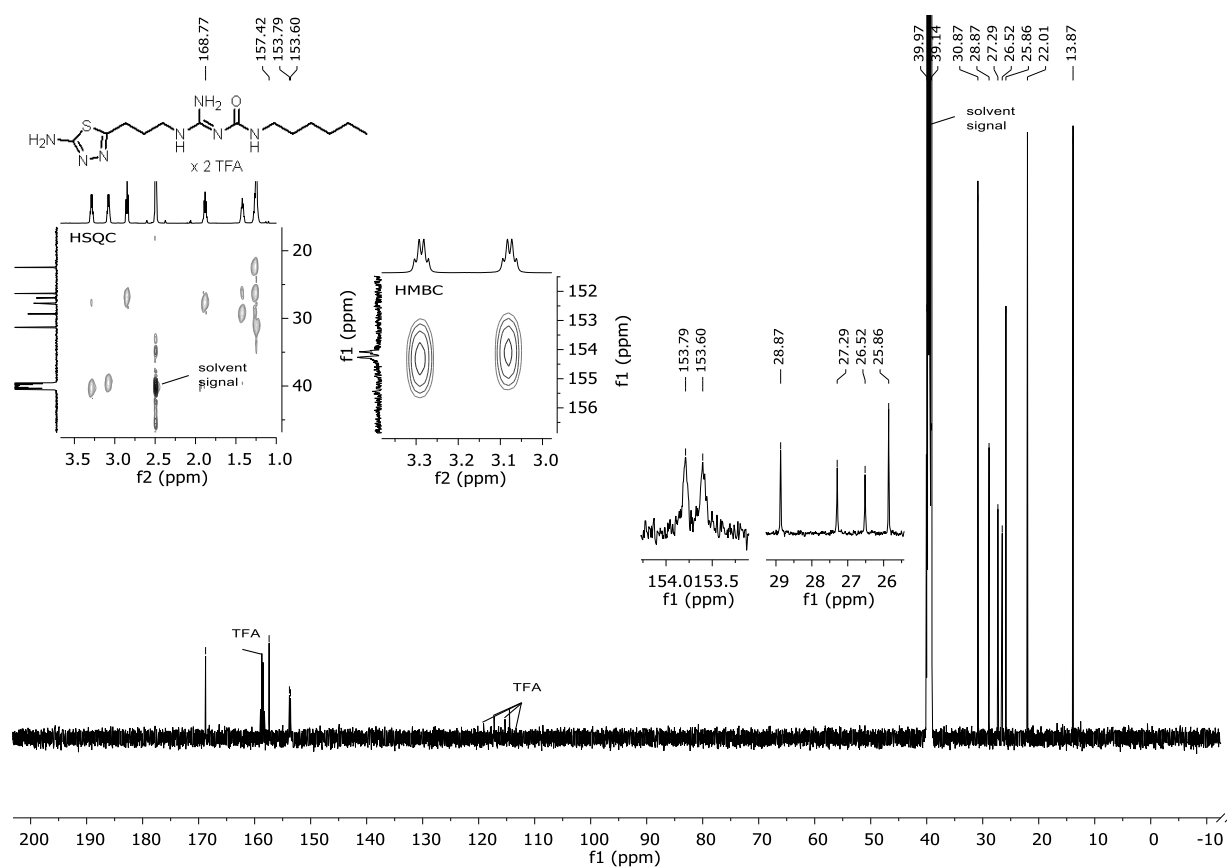
Figure 3.076. ^{13}C-NMR spectrum (151 MHz, DMSO-d$_6$) of compound **3.244**.
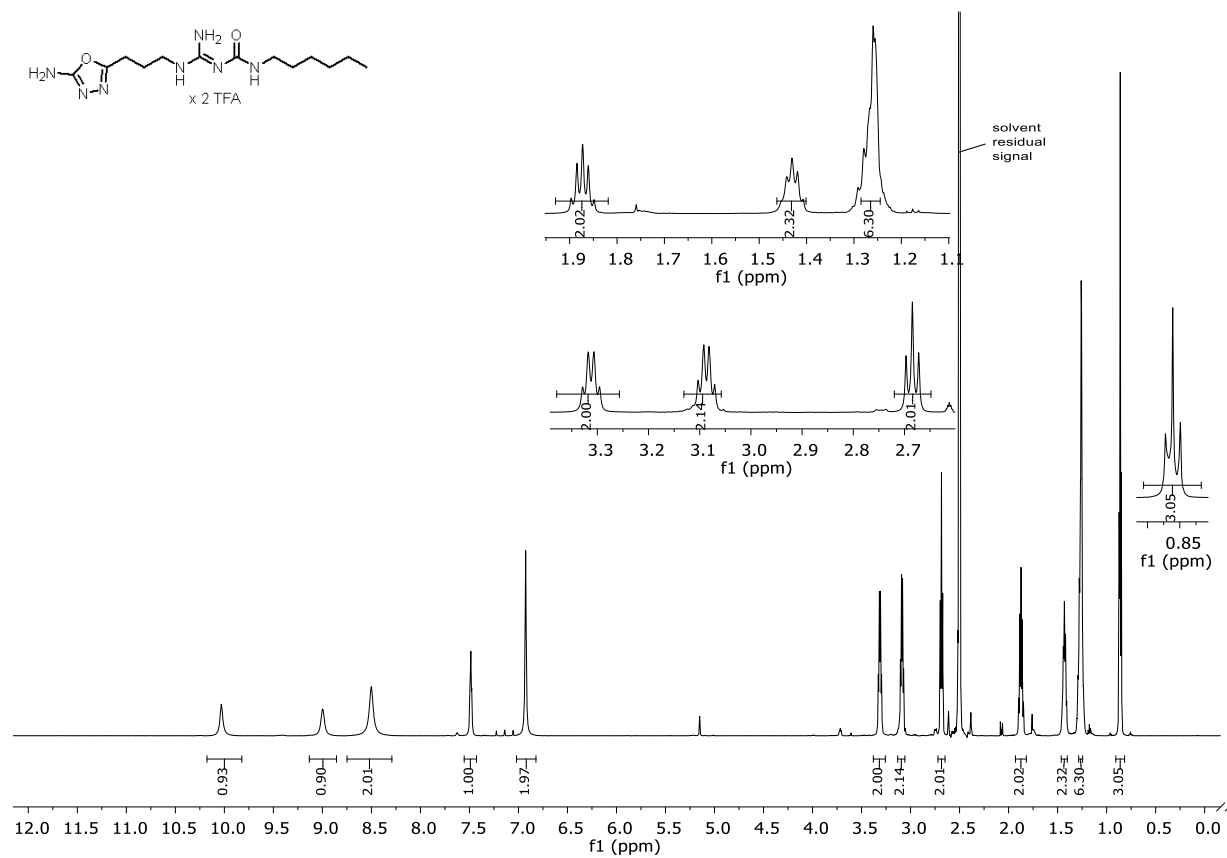
Figure 3.077. ^{1}H-NMR spectrum (600 MHz, DMSO-d$_6$) of compound **3.245**.

515
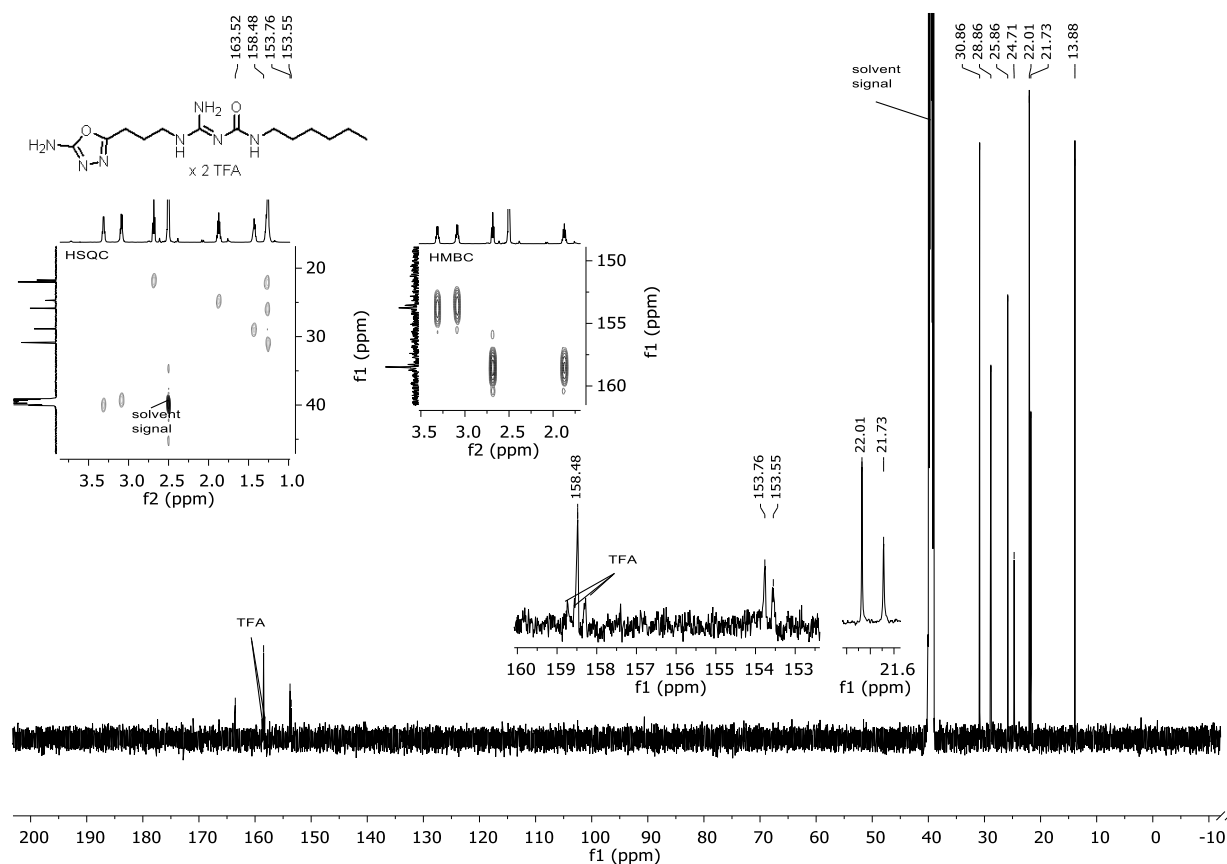
Figure 3.078. ^{13}C-NMR spectrum (151 MHz, DMSO-d_6) of compound **3.245**.
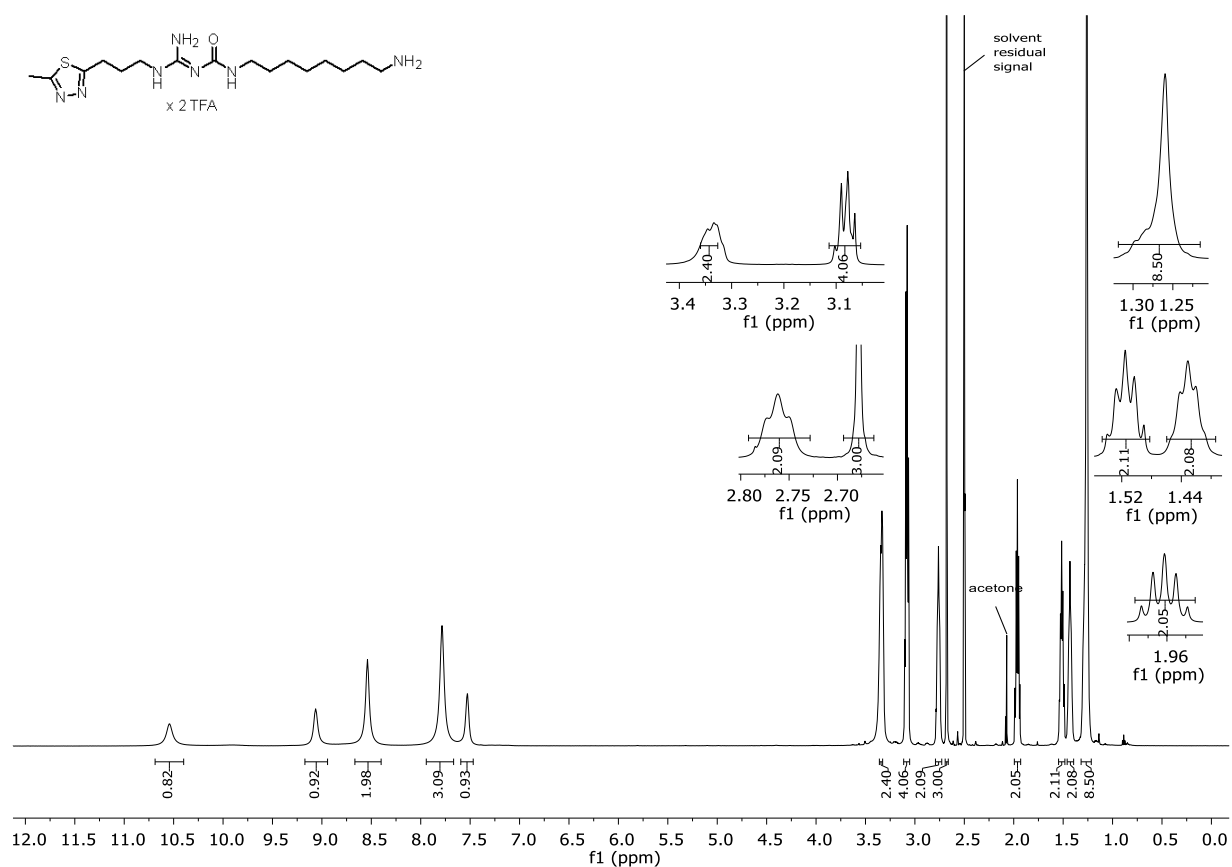
Figure 3.079. ^{1}H-NMR spectrum (600 MHz, DMSO-d_6) of compound **3.246**.
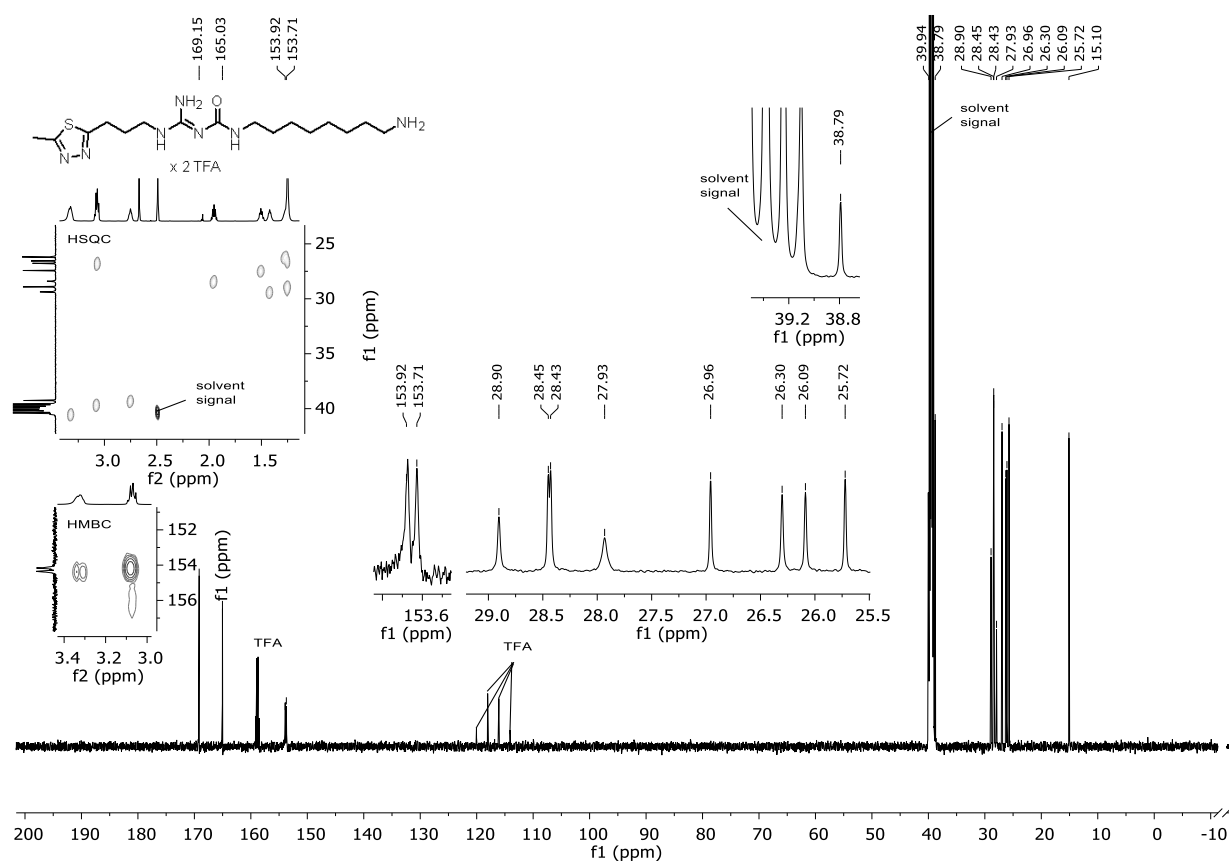
Figure 3.080. ^{13}C-NMR spectrum (151 MHz, DMSO-d$_6$) of compound **3.246**.
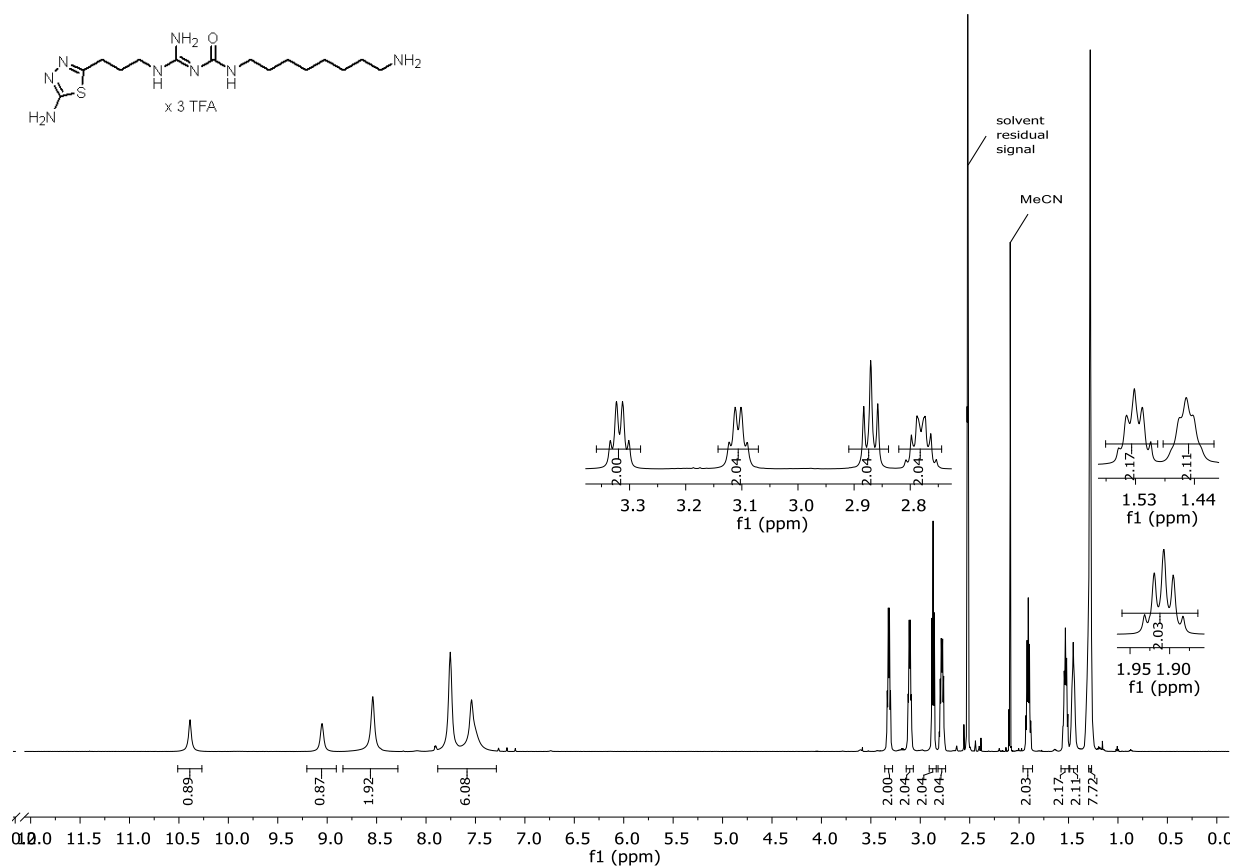
Figure 3.081. ^{1}H-NMR spectrum (600 MHz, DMSO-d$_6$) of compound **3.247**.

517
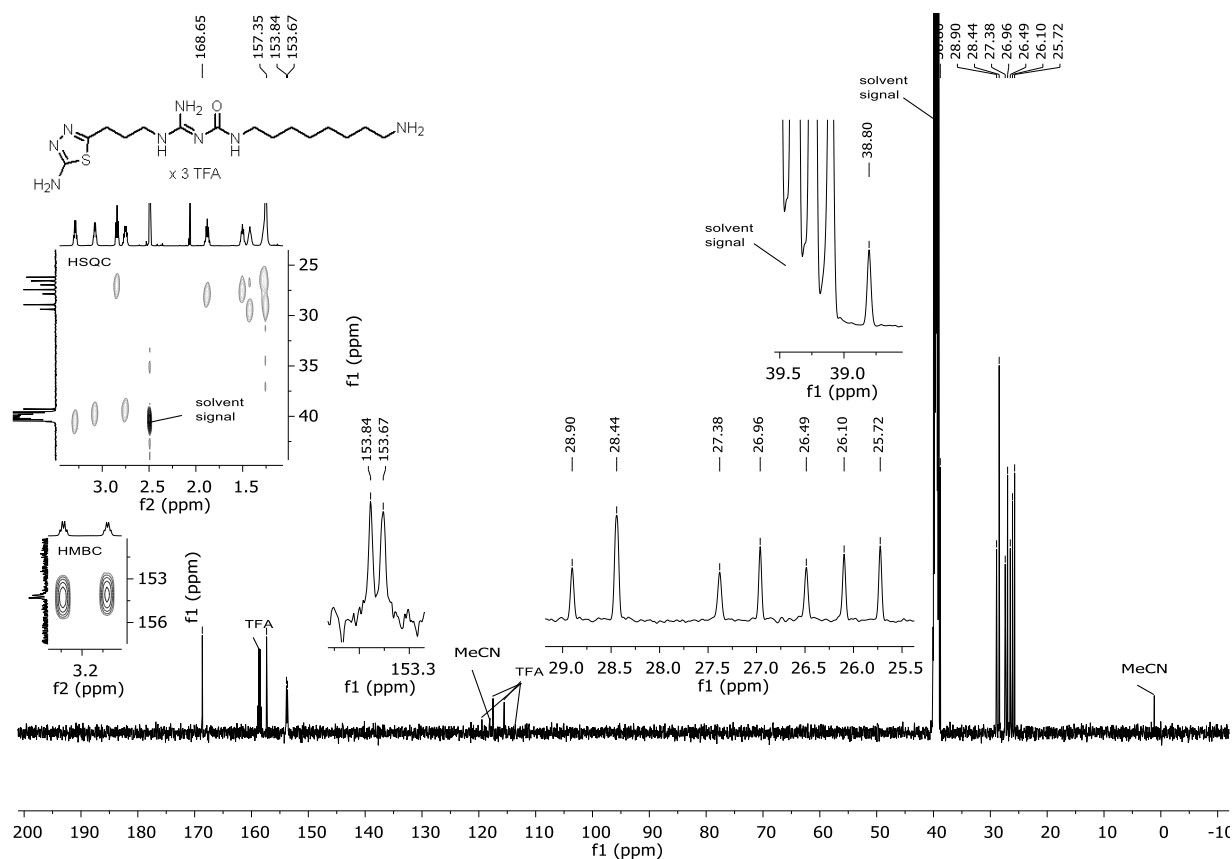
Figure 3.082. ^{13}C-NMR spectrum (151 MHz, DMSO-d$_6$) of compound **3.247**.
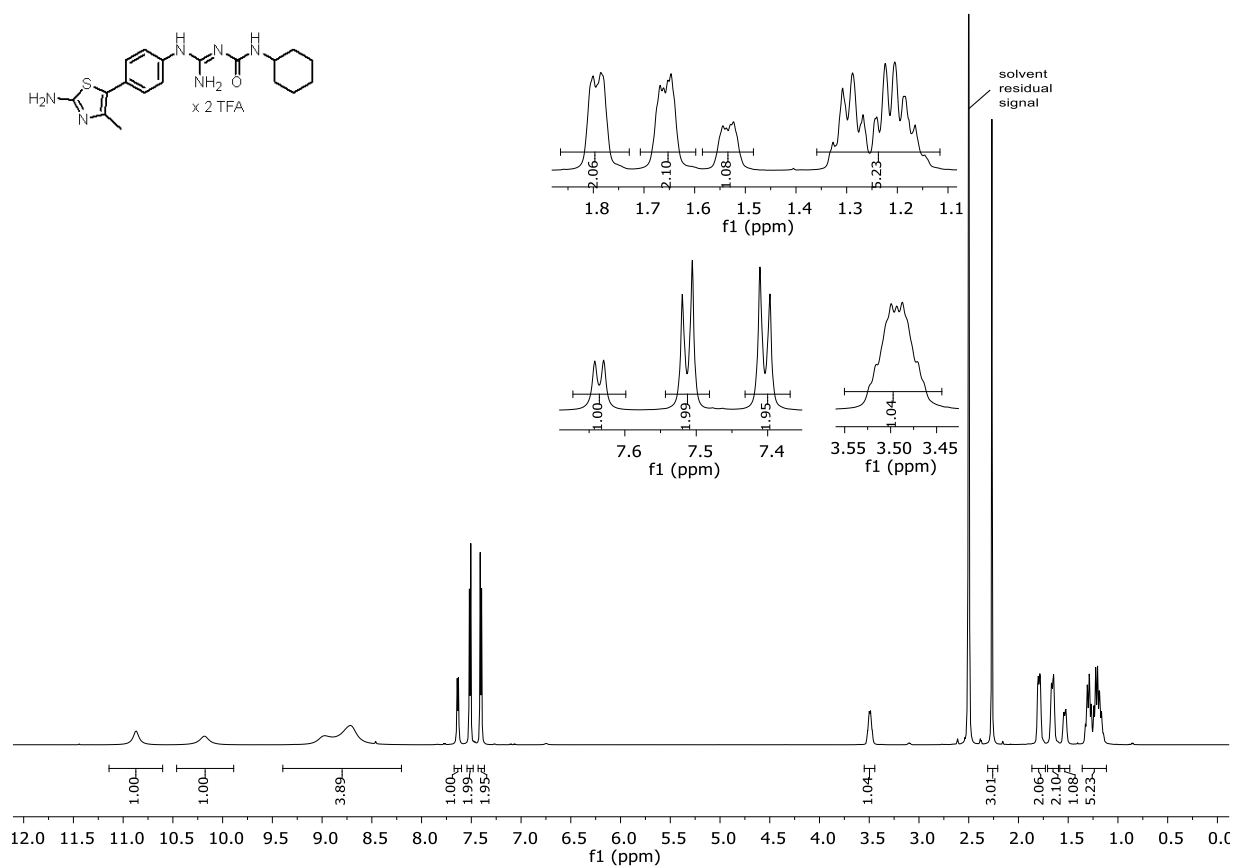
Figure 3.083. ^{1}H-NMR spectrum (600 MHz, DMSO-d$_6$) of compound **3.248**.

518
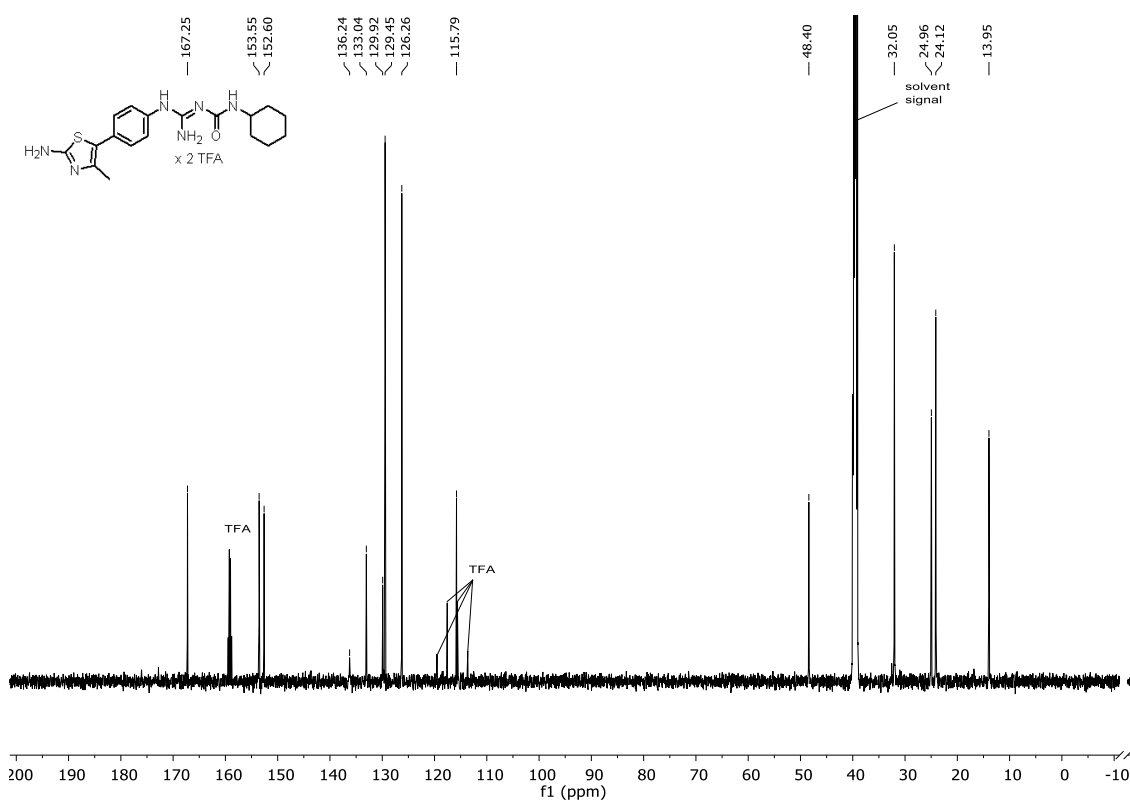
Figure 3.084. ^{13}C-NMR spectrum (151 MHz, DMSO-d$_6$) of compound **3.248**.
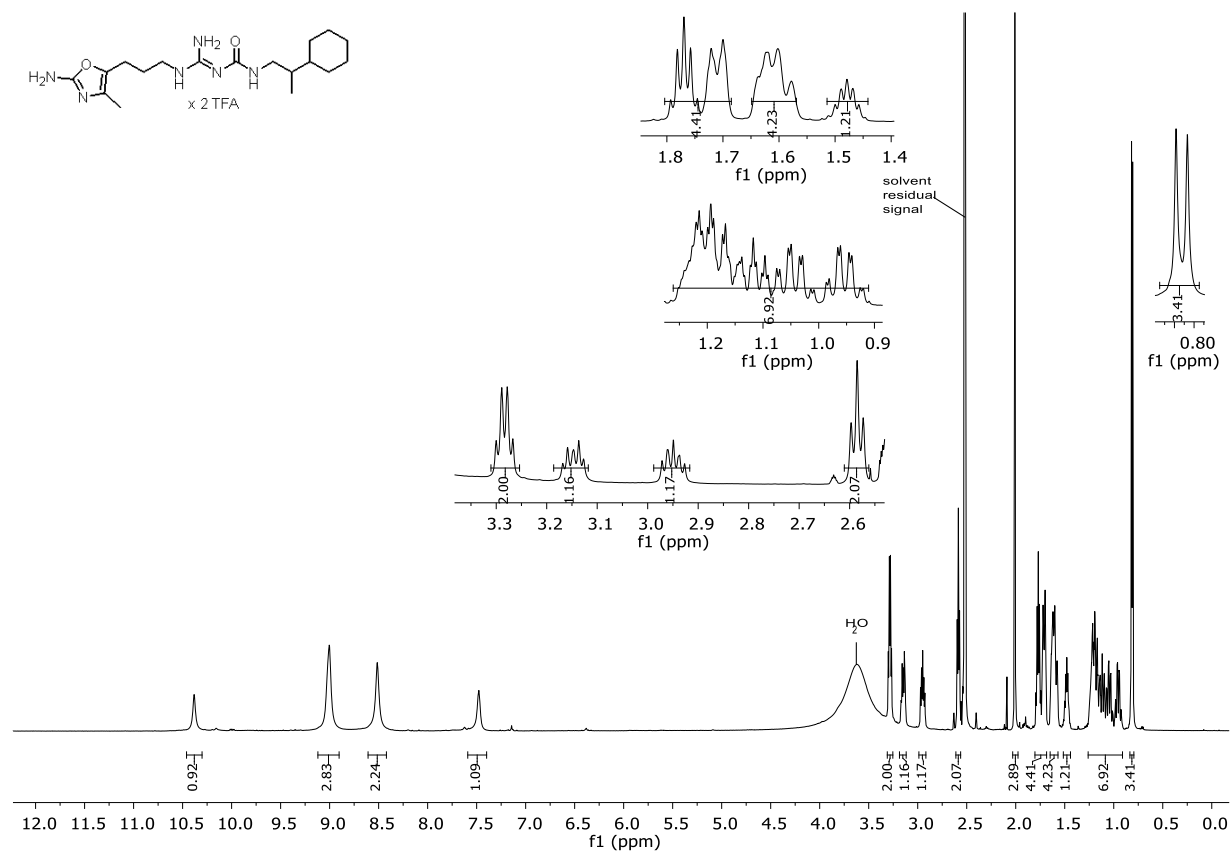
Figure 3.085. ^{1}H-NMR spectrum (600 MHz, DMSO-d$_6$) of compound **3.249**.

519
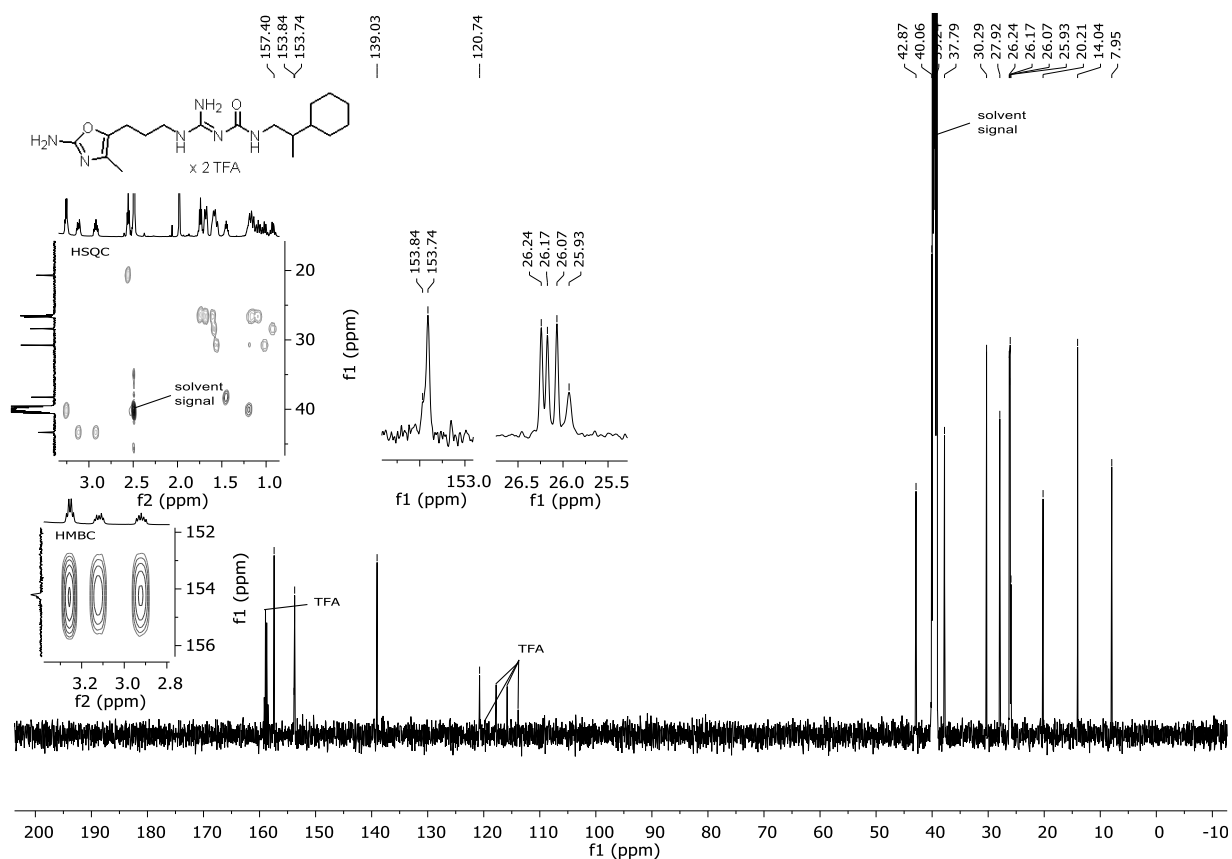
Figure 3.086. ^{13}C-NMR spectrum (151 MHz, DMSO-d$_6$) of compound **3.249**.
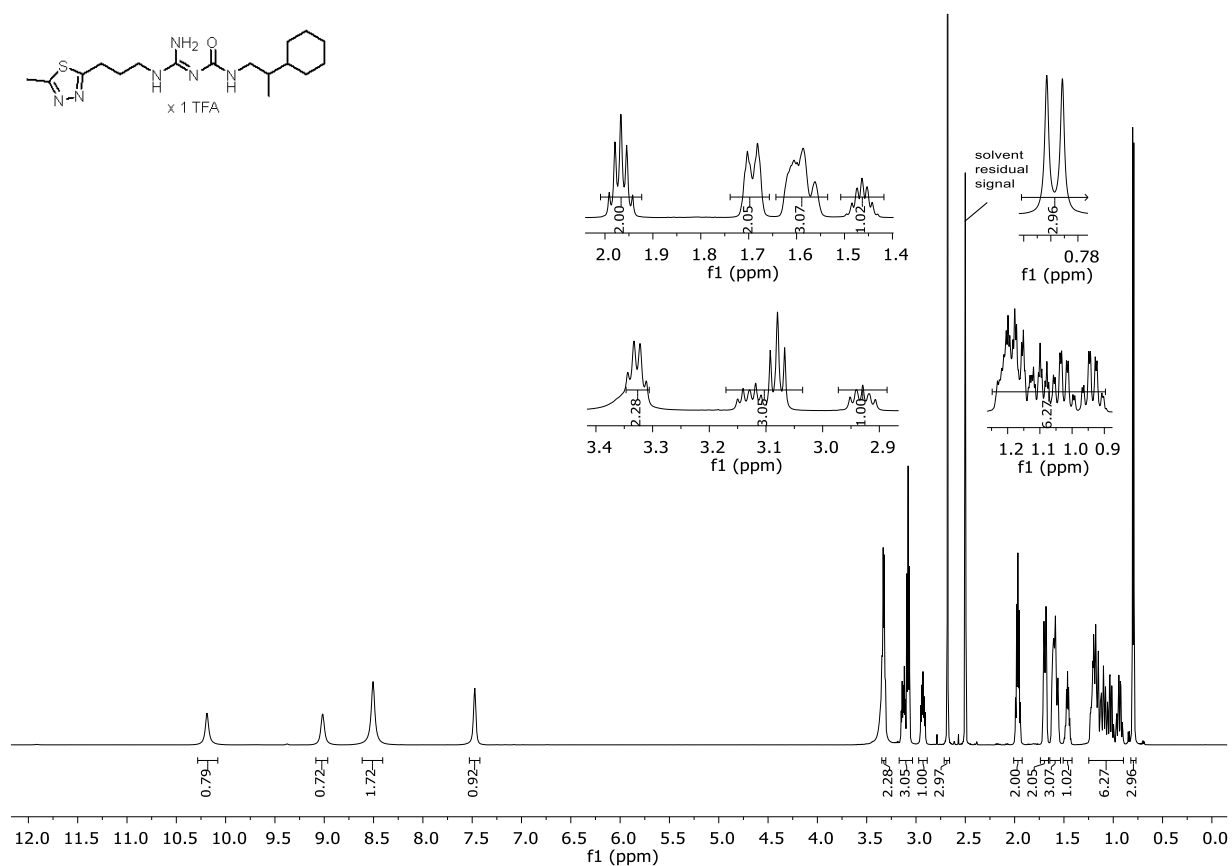
Figure 3.087. ^{1}H-NMR spectrum (600 MHz, DMSO-d$_6$) of compound **3.250**.
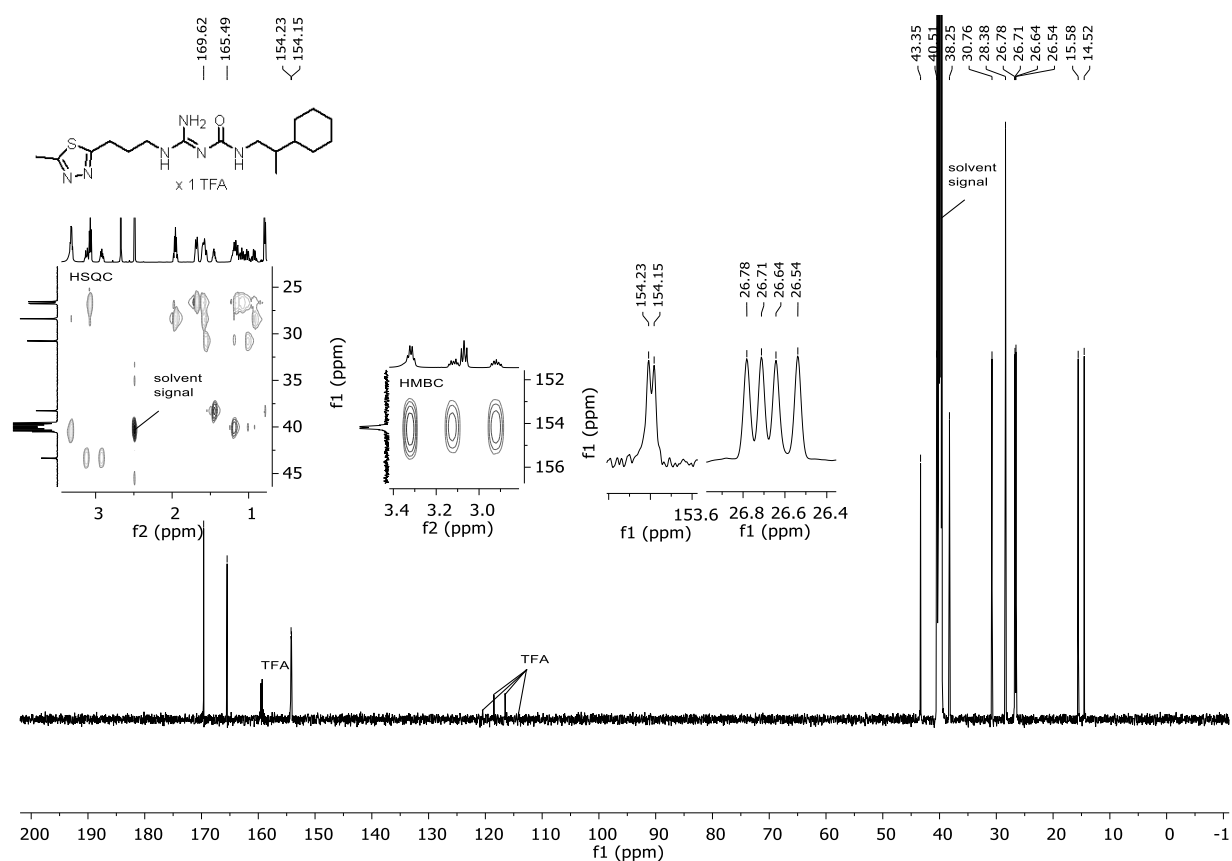
Figure 3.088. ^{13}C-NMR spectrum (151 MHz, DMSO-d$_6$) of compound **3.250**.
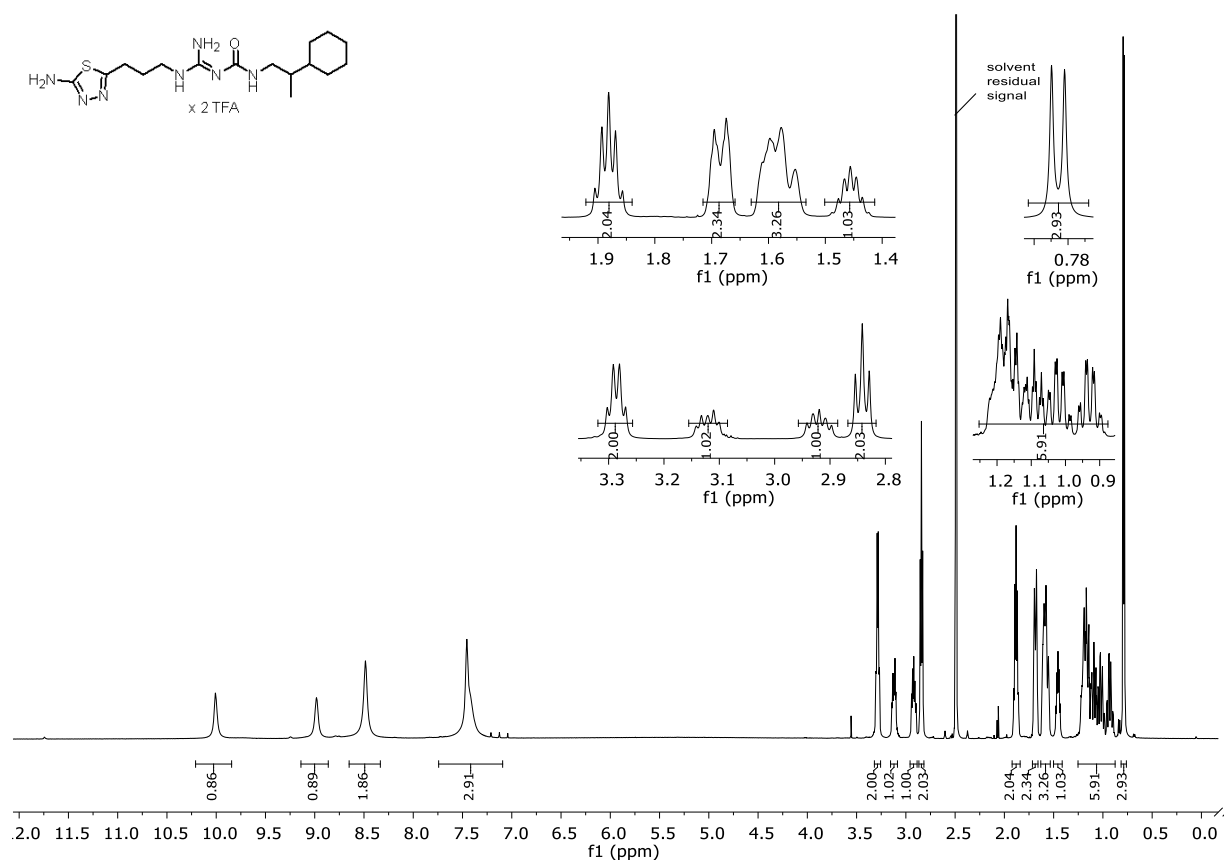
Figure 3.089. ^{1}H-NMR spectrum (600 MHz, DMSO-d$_6$) of compound **3.251**.

521
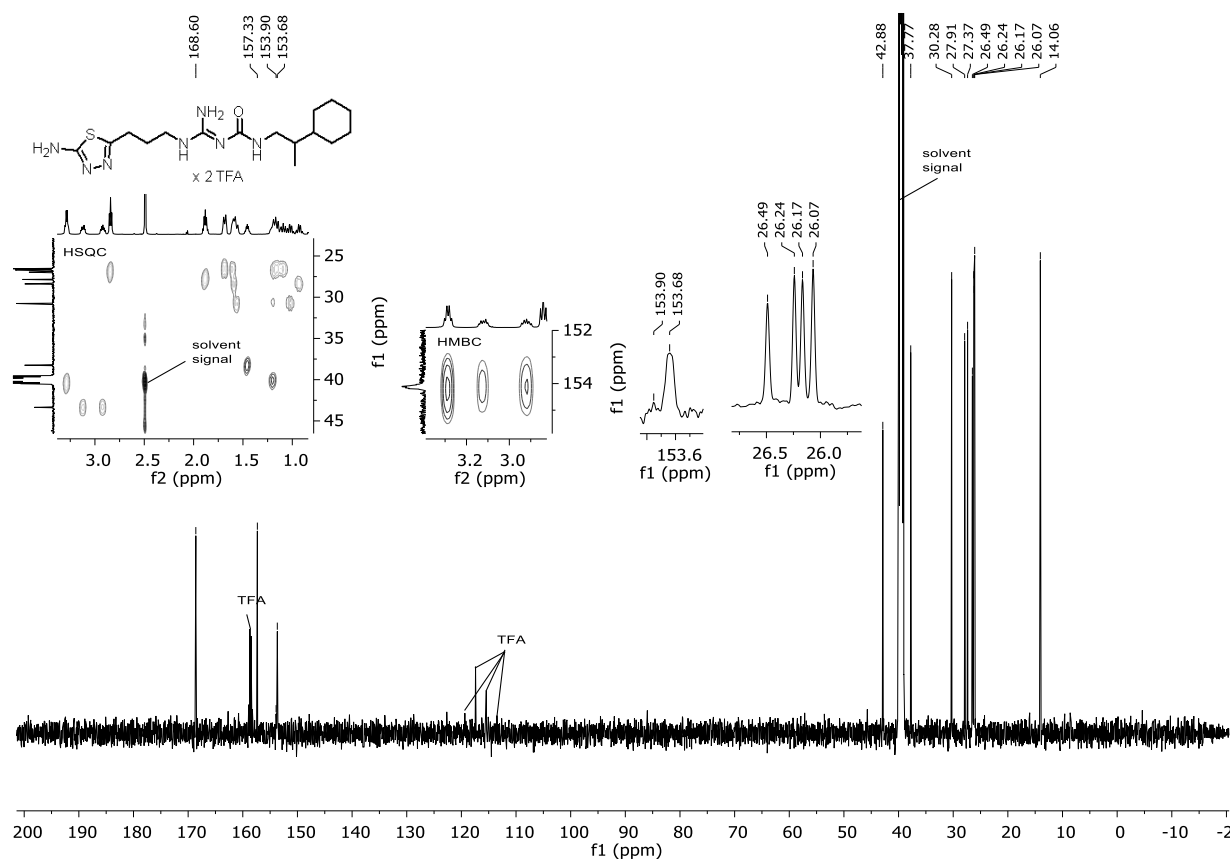
Figure 3.090. ^{13}C-NMR spectrum (151 MHz, DMSO-d$_6$) of compound **3.251**.
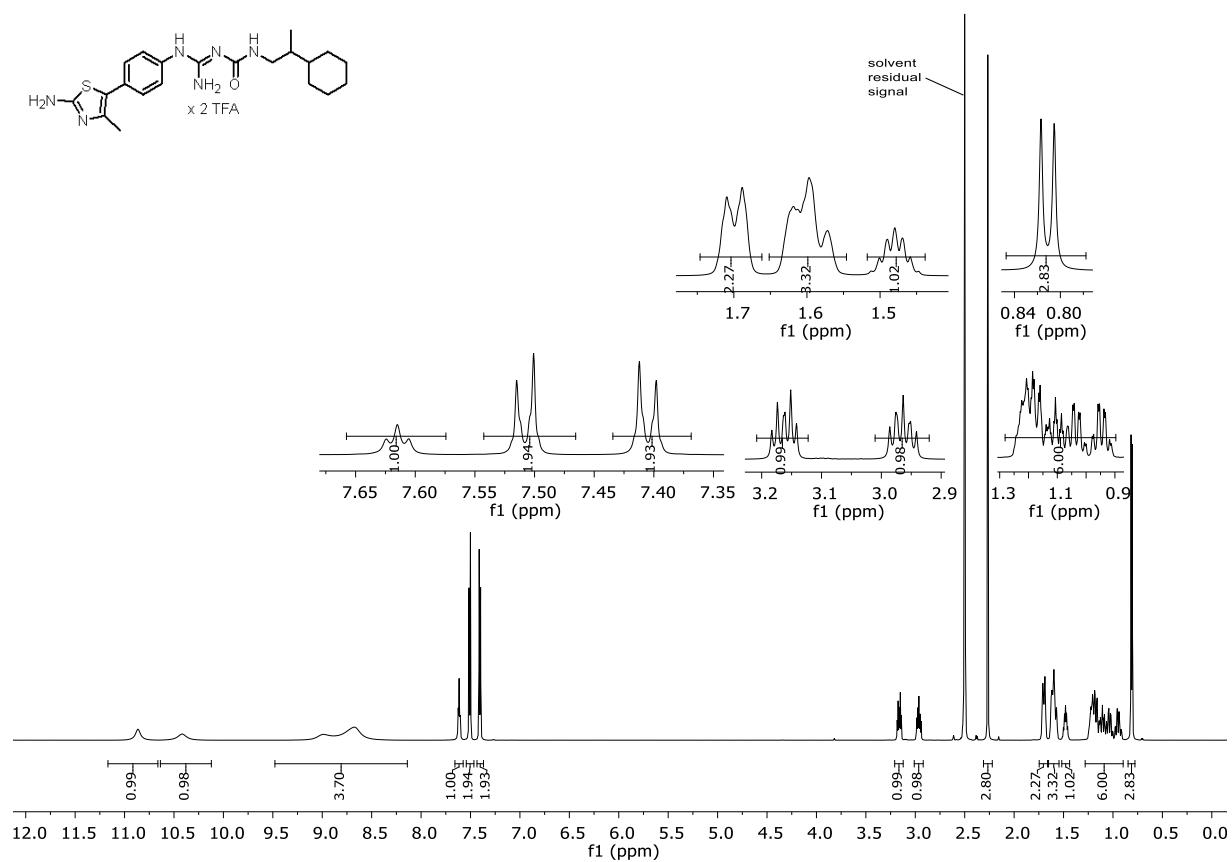
Figure 3.091. ^{1}H-NMR spectrum (600 MHz, DMSO-d$_6$) of compound **3.252**.
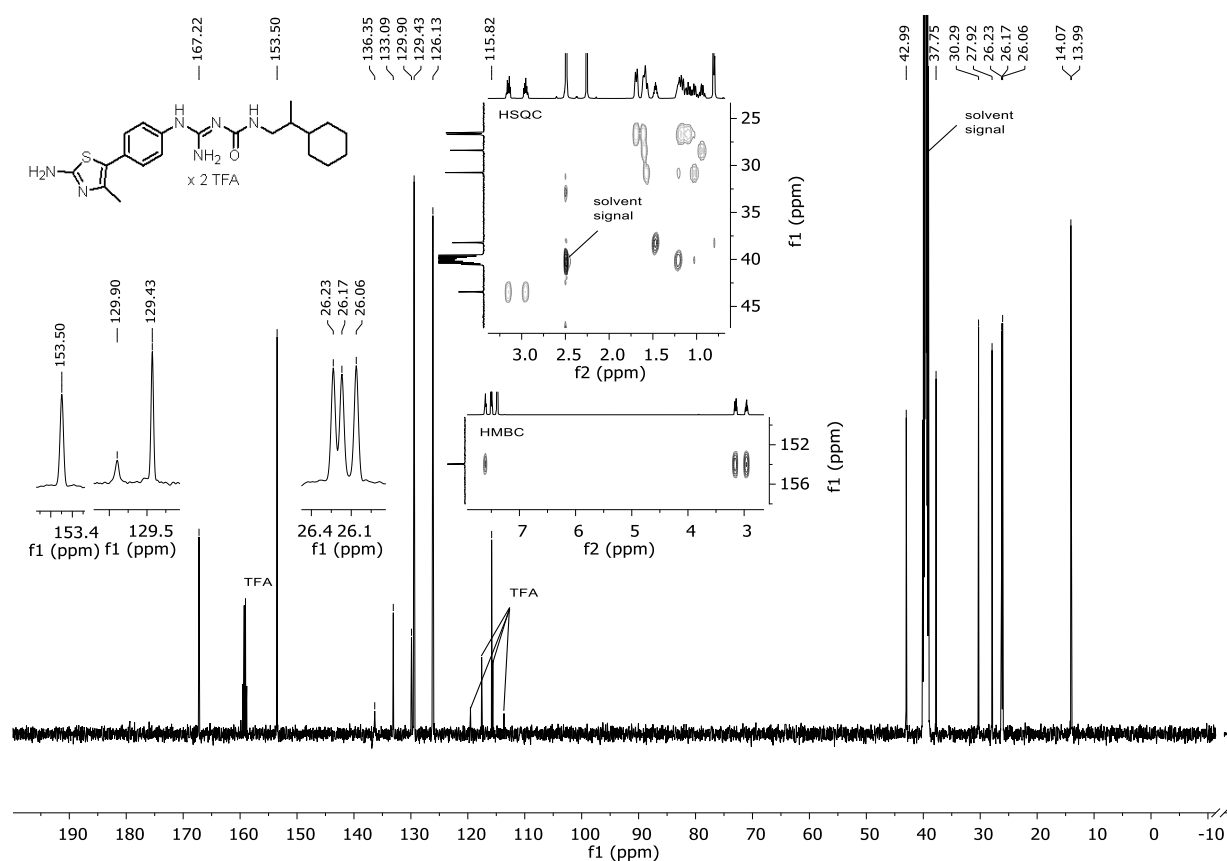
Figure 3.092. ^{13}C-NMR spectrum (151 MHz, DMSO-d$_6$) of compound **3.252**.
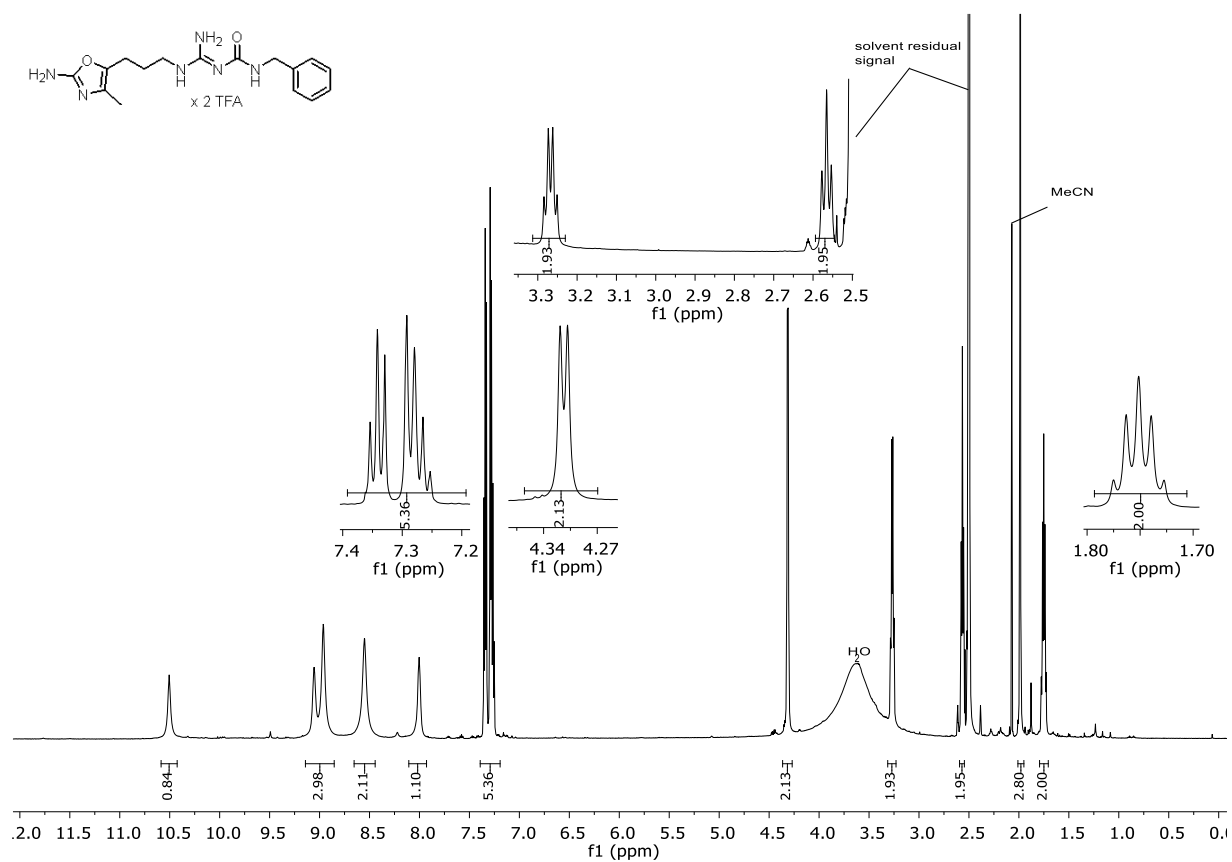
Figure 3.093. ^{1}H-NMR spectrum (600 MHz, DMSO-d$_6$) of compound **3.253**.

523
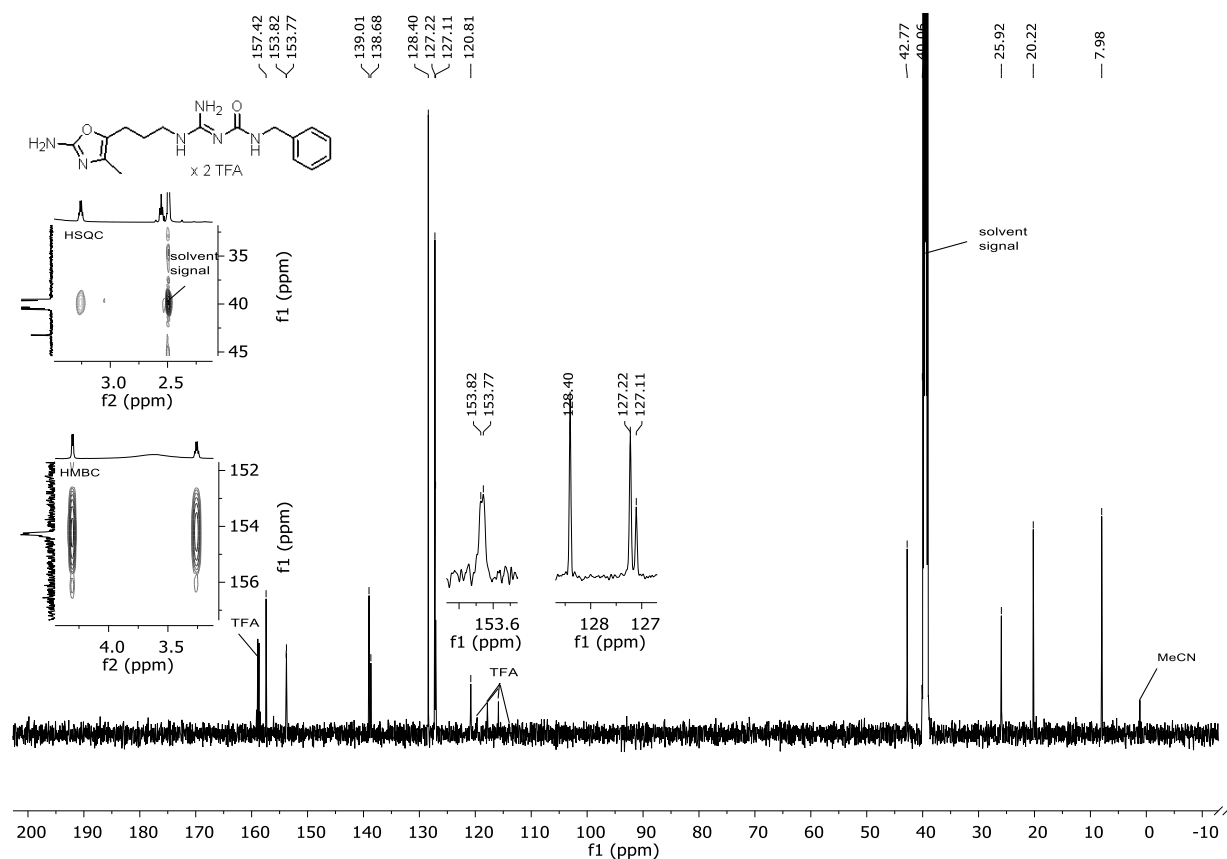
Figure 3.094. ^{13}C-NMR spectrum (151 MHz, DMSO-d$_6$) of compound **3.253**.
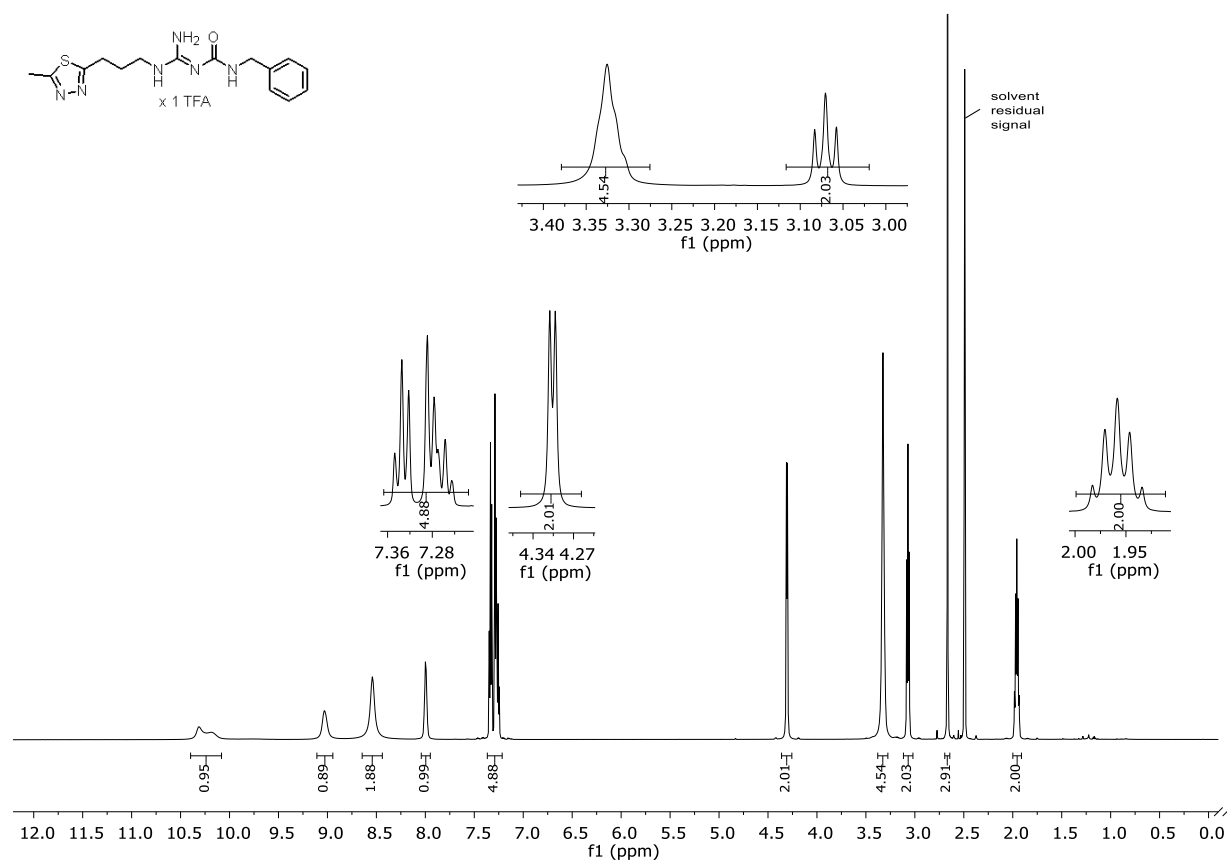
Figure 3.095. ^{1}H-NMR spectrum (600 MHz, DMSO-d$_6$) of compound **3.254**.
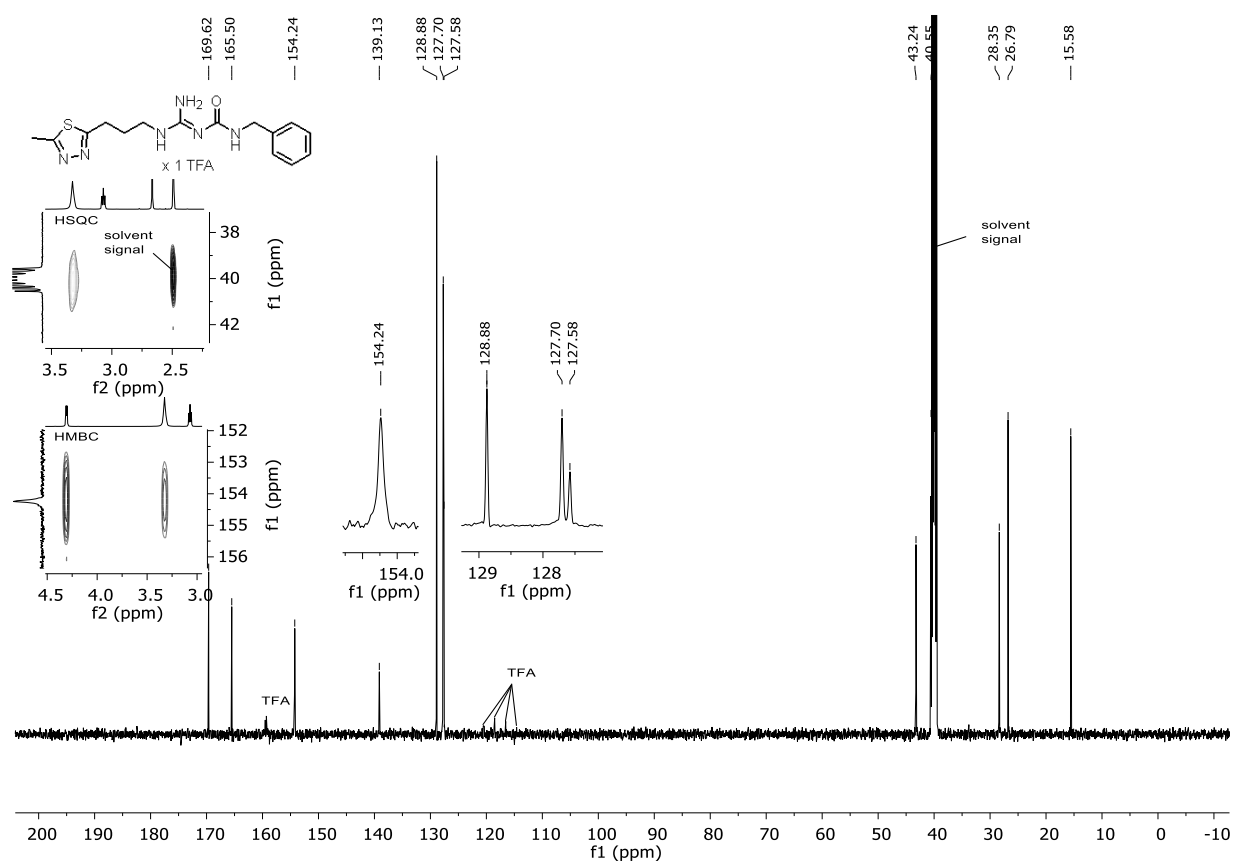
Figure 3.096. ^{13}C-NMR spectrum (151 MHz, DMSO-d$_6$) of compound **3.254**.
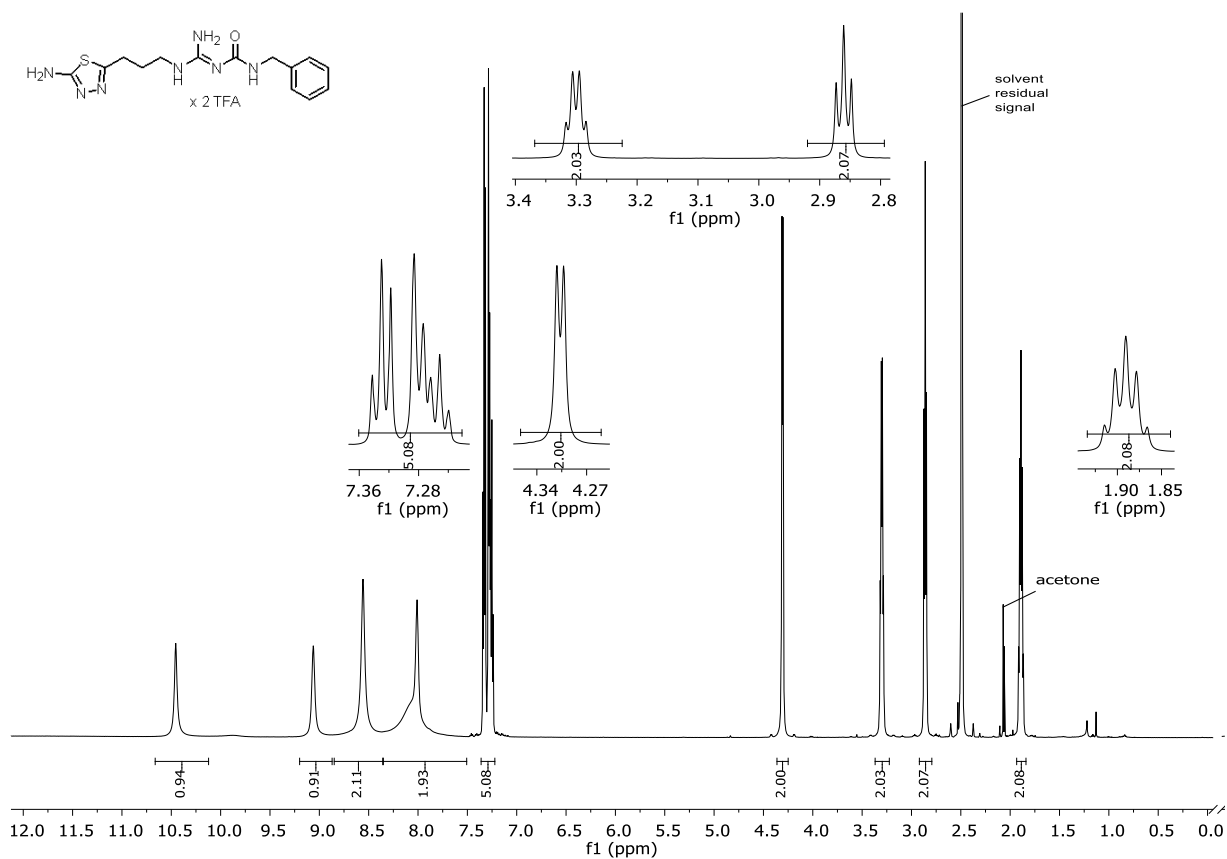
Figure 3.097. ^{1}H-NMR spectrum (600 MHz, DMSO-d$_6$) of compound **3.255**.
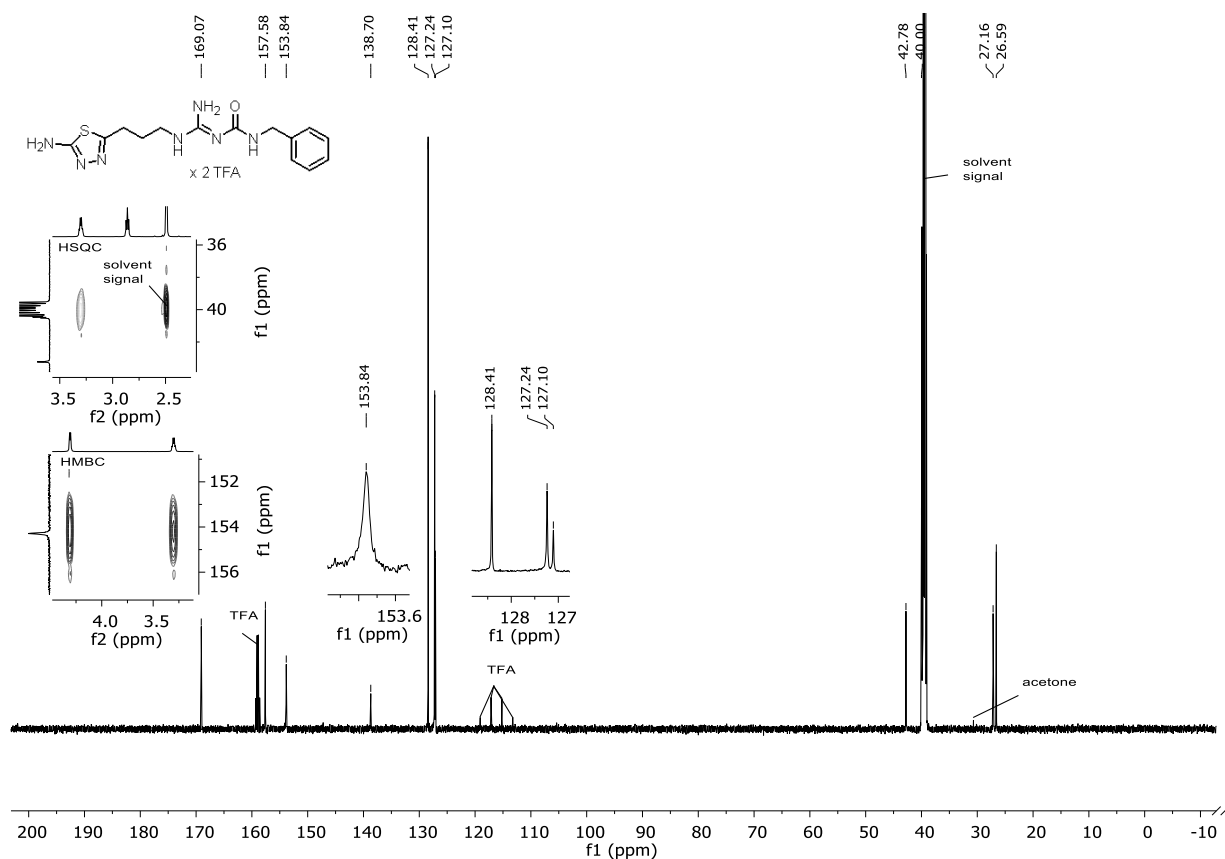
Figure 3.098. ^{13}C-NMR spectrum (151 MHz, DMSO-d$_6$) of compound **3.255**.
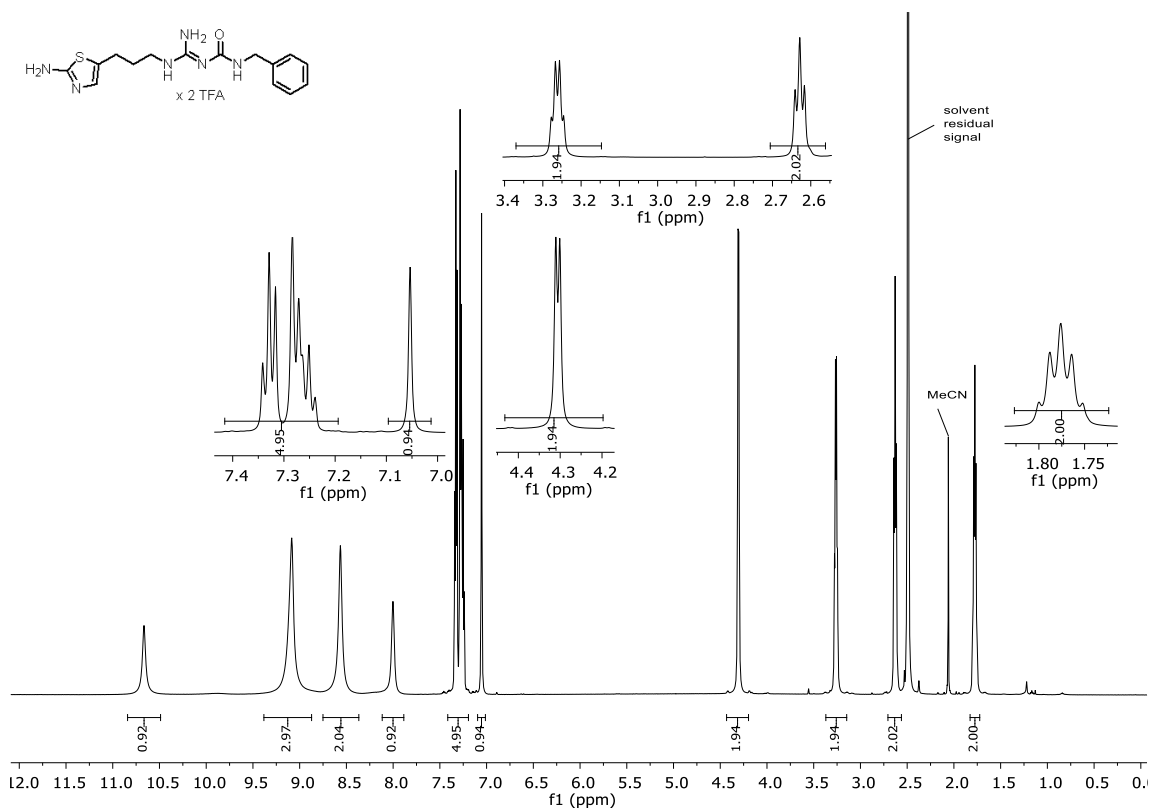
Figure 3.099. ^{1}H-NMR spectrum (600 MHz, DMSO-d$_6$) of compound **3.256**.
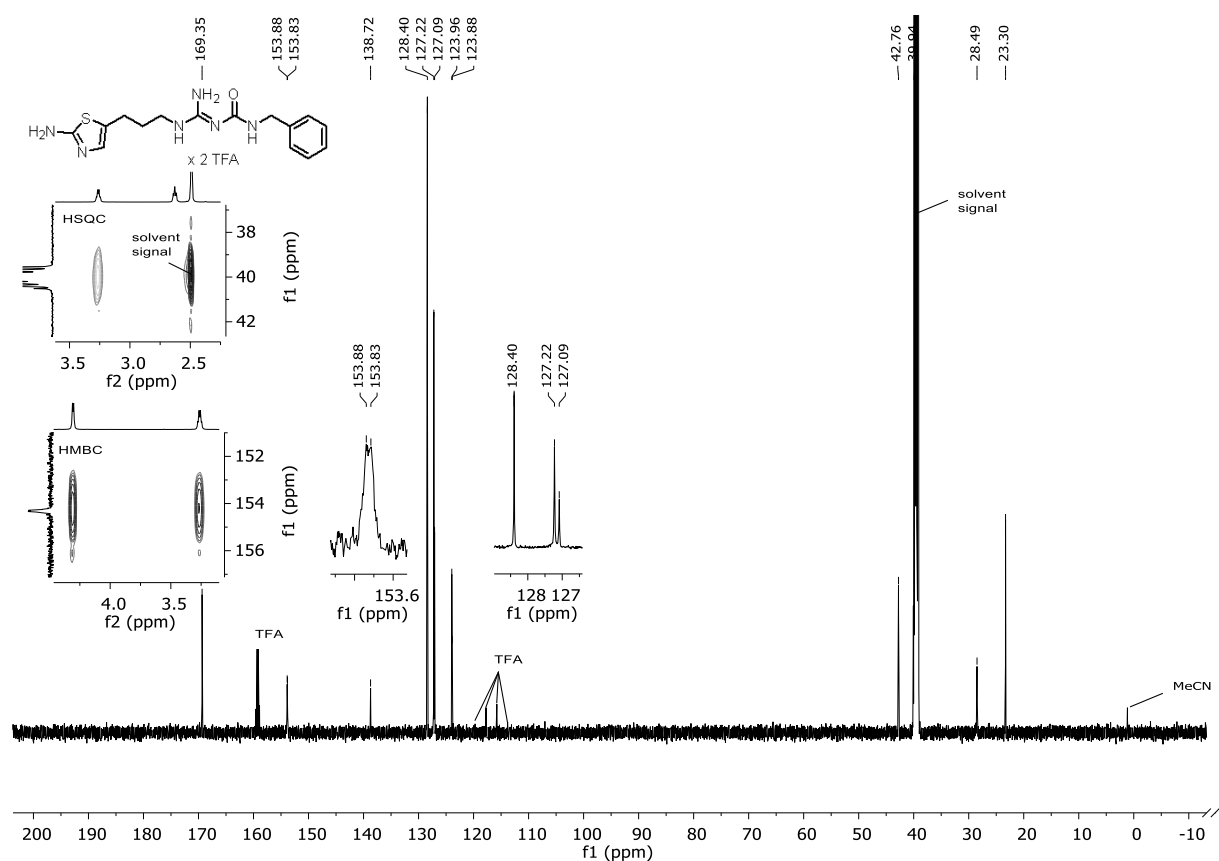
Figure 3.100. ^{13}C-NMR spectrum (151 MHz, DMSO-d$_6$) of compound **3.256**.
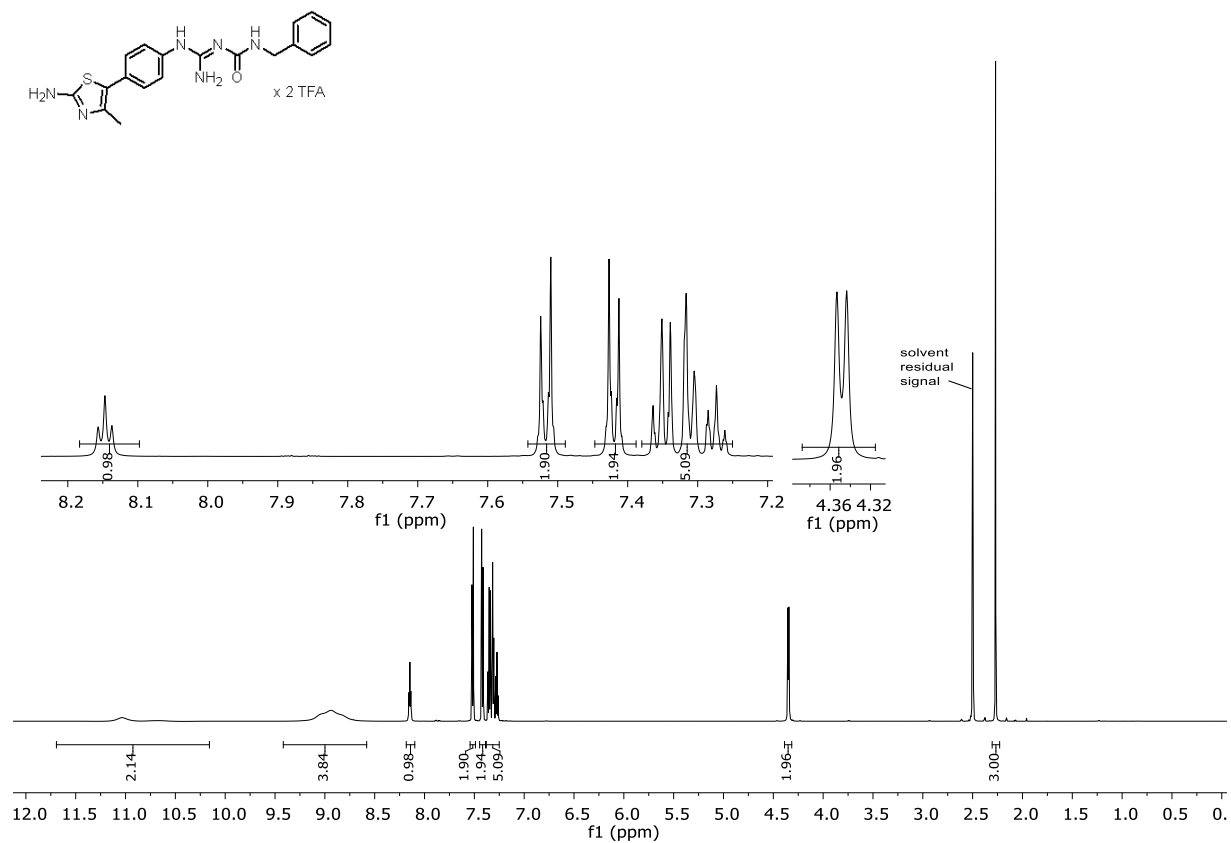
Figure 3.101. ^{1}H-NMR spectrum (600 MHz, DMSO-d$_6$) of compound **3.257**.
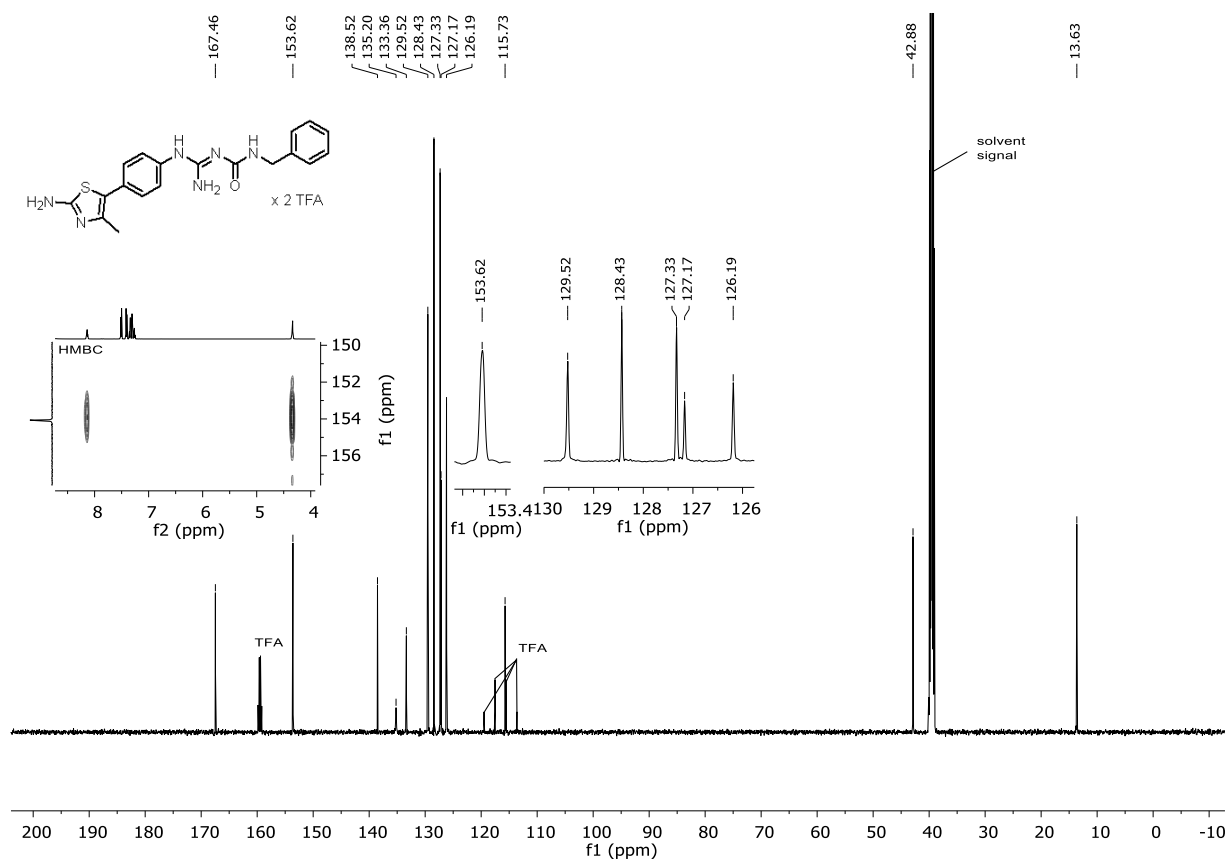
Figure 3.102. ^{13}C-NMR spectrum (151 MHz, DMSO-d$_6$) of compound **3.257**.
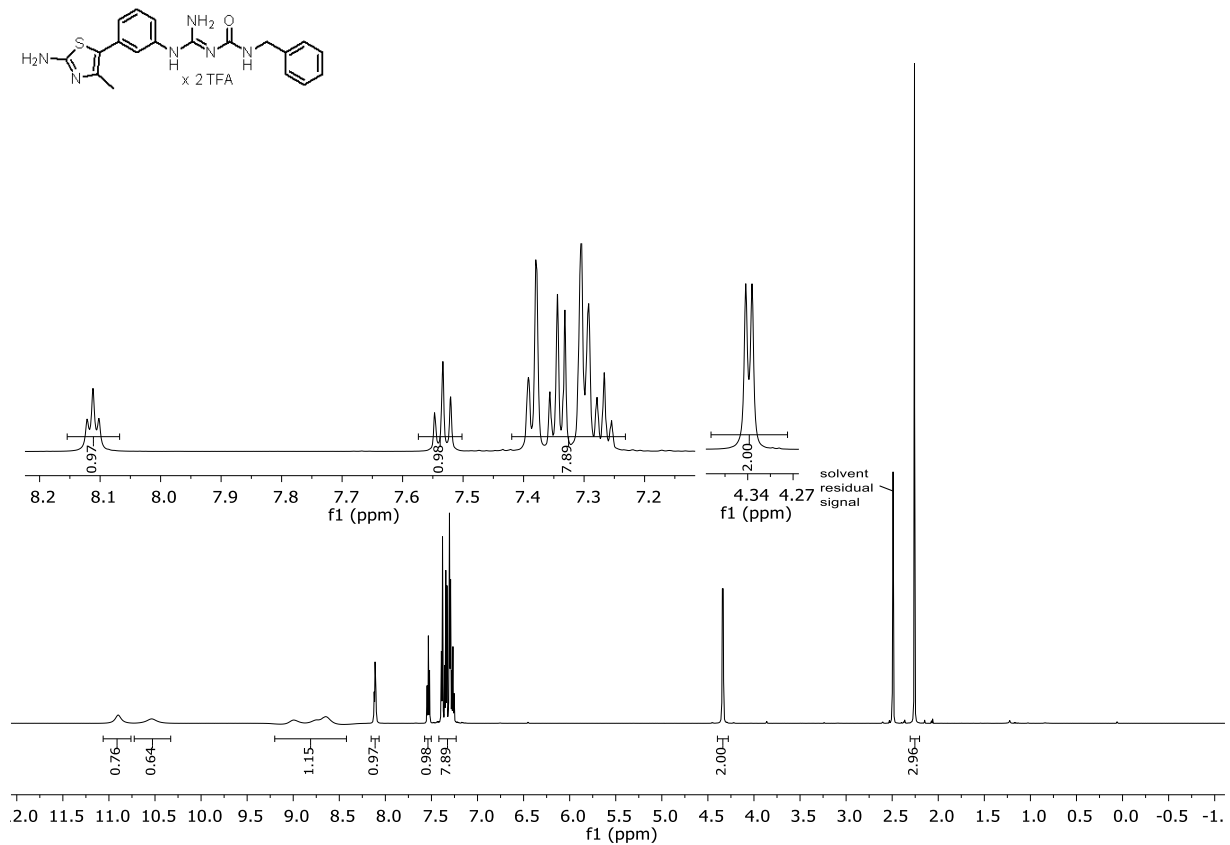
Figure 3.103. ^{1}H-NMR spectrum (600 MHz, DMSO-d$_6$) of compound **3.258**.
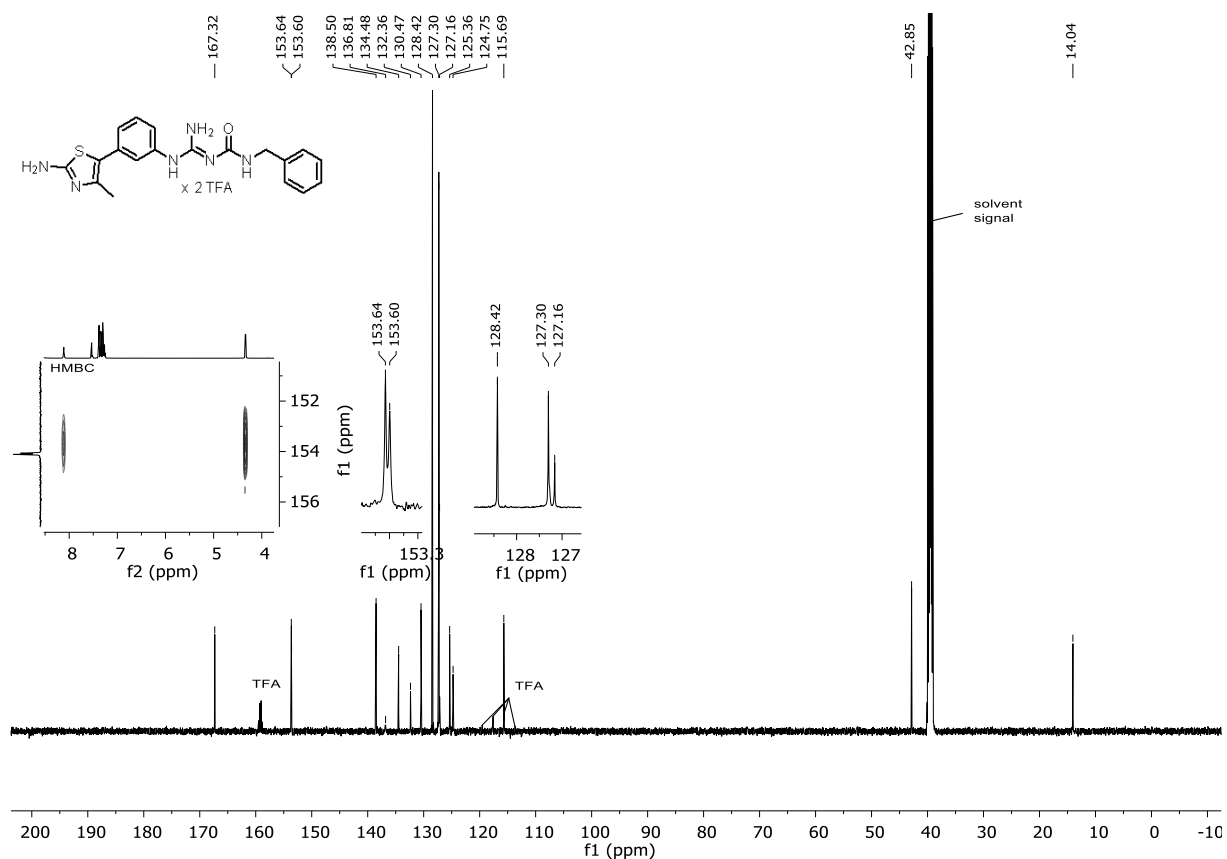
Figure 3.104. ^{13}C-NMR spectrum (151 MHz, DMSO-d$_6$) of compound **3.258**.
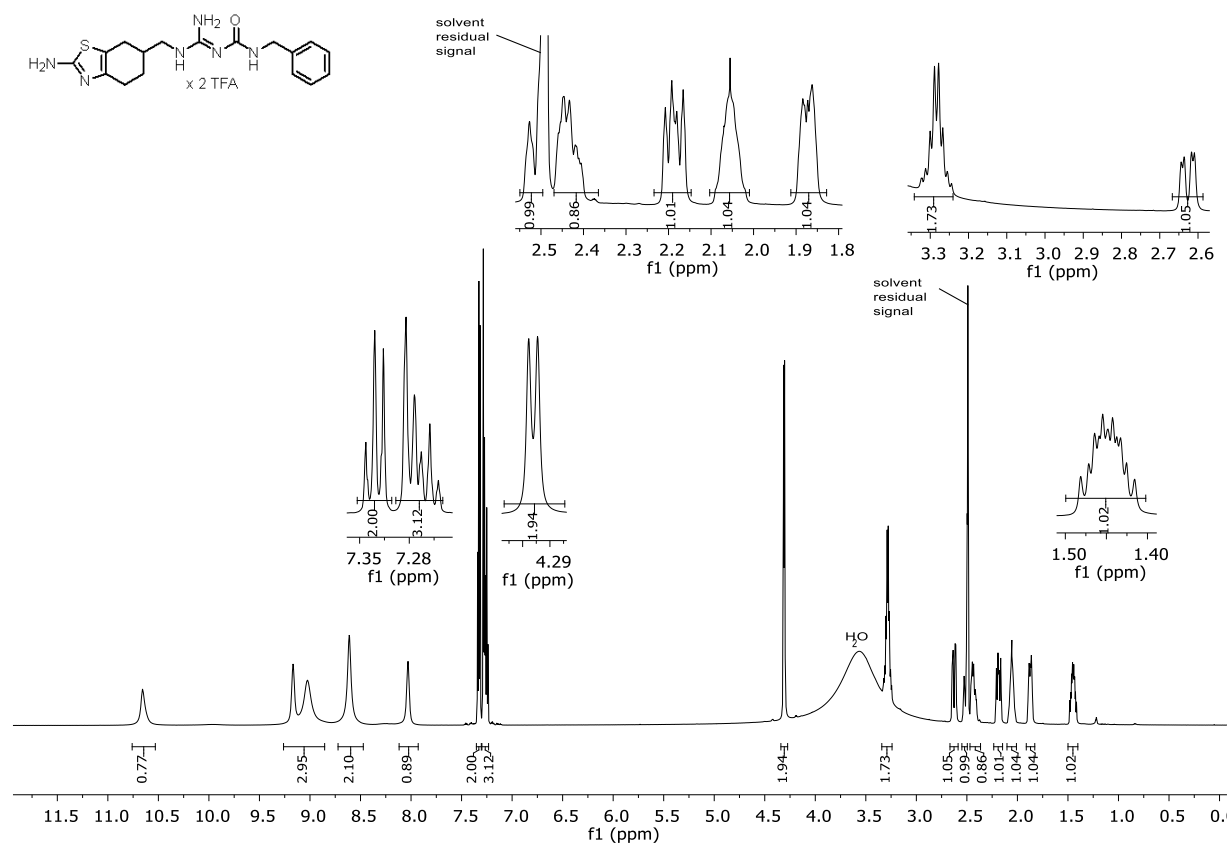
Figure 3.105. ^{1}H-NMR spectrum (600 MHz, DMSO-d$_6$) of compound **3.259**.
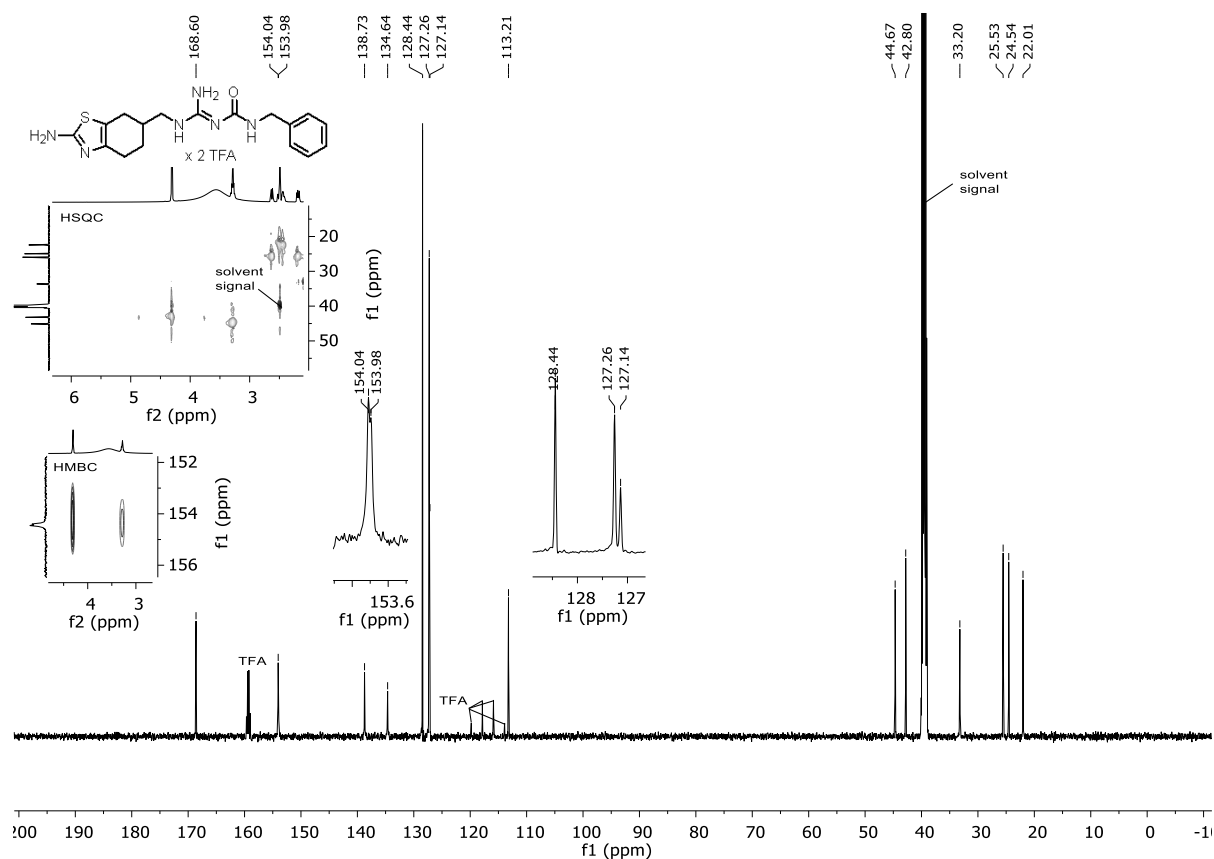
Figure 3.106. ^{13}C-NMR spectrum (151 MHz, DMSO-d$_6$) of compound **3.259**.
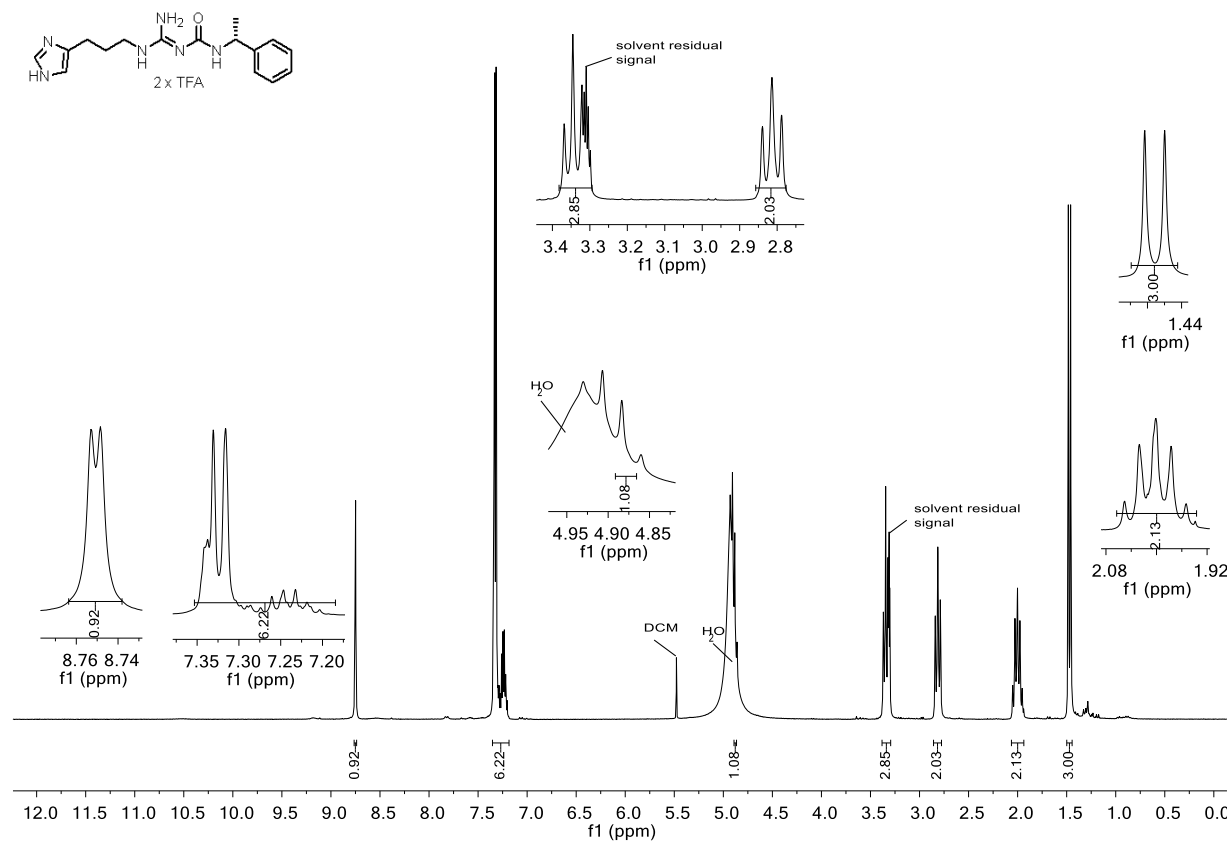
Figure 3.107. ^{1}H-NMR spectrum (300 MHz, CD$_3$OD) of compound **3.260**.
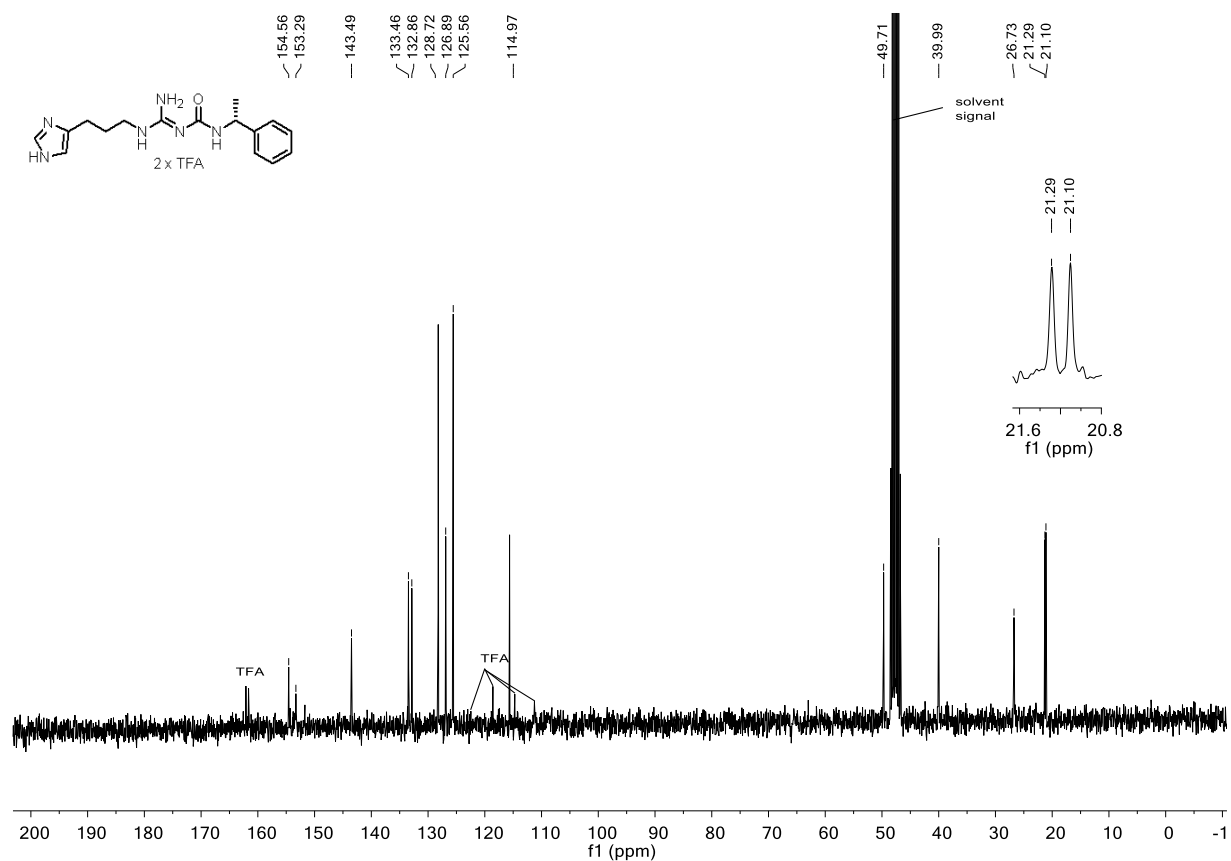
Figure 3.108. ^{13}C-NMR spectrum (75 MHz, CD$_3$OD) of compound **3.260**.
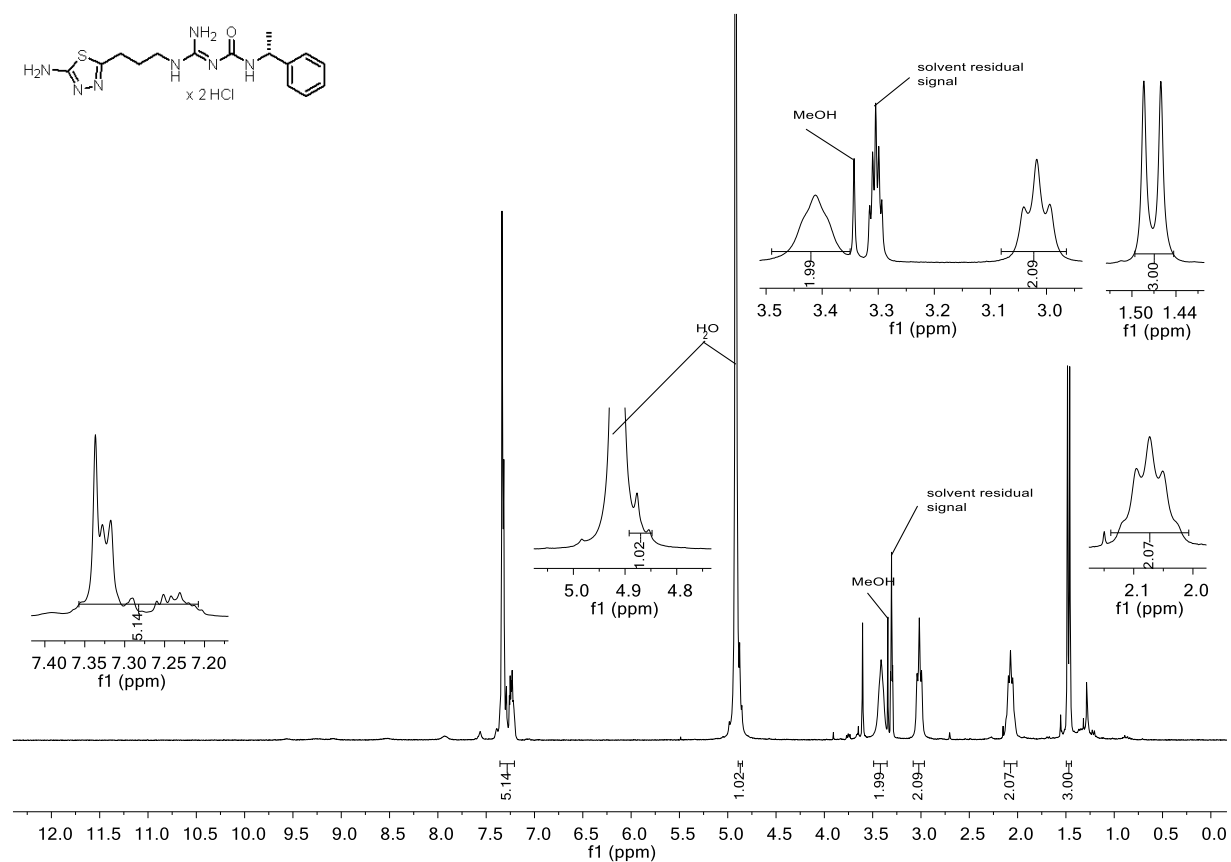
Figure 3.109. ^{1}H-NMR spectrum (300 MHz, CD$_3$OD) of compound **3.261**.

531
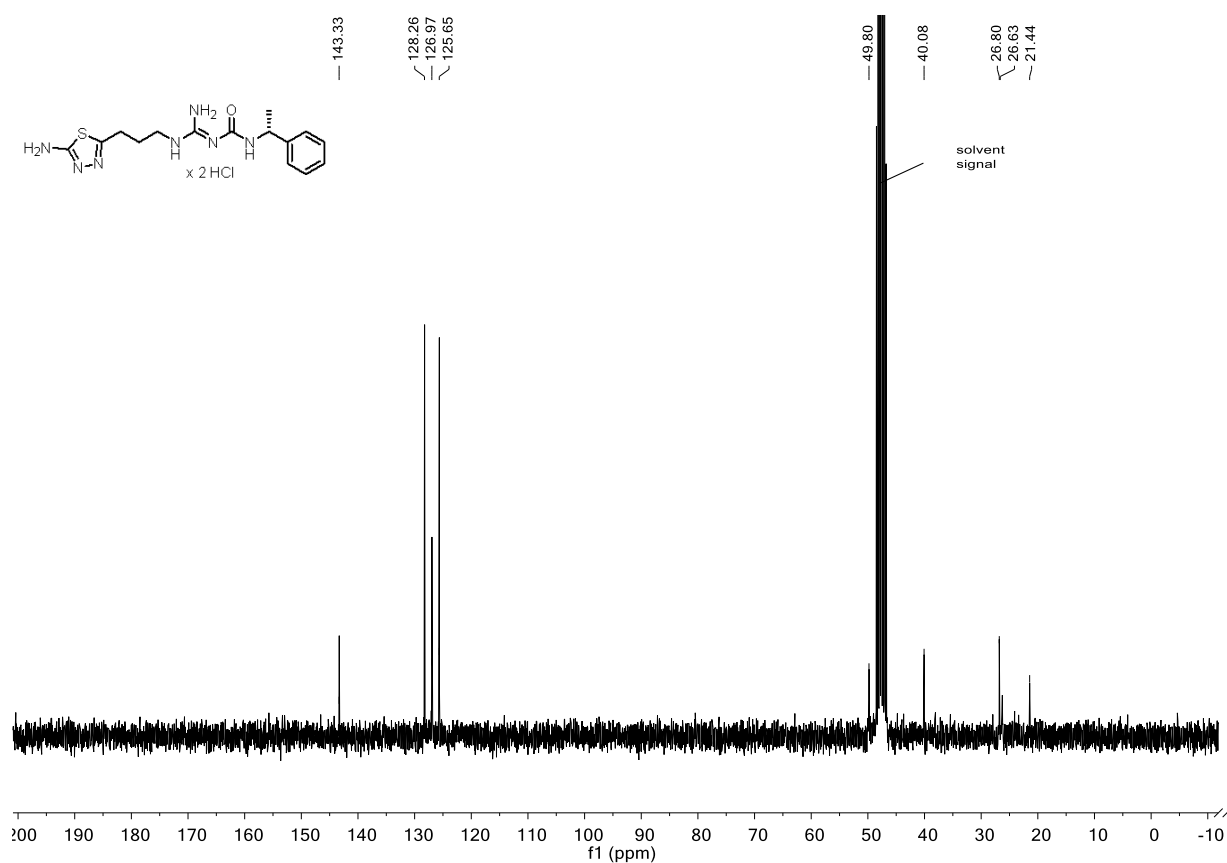
Figure 3.110. ^{13}C-NMR spectrum (75 MHz, CD₃OD) of compound **3.261**.
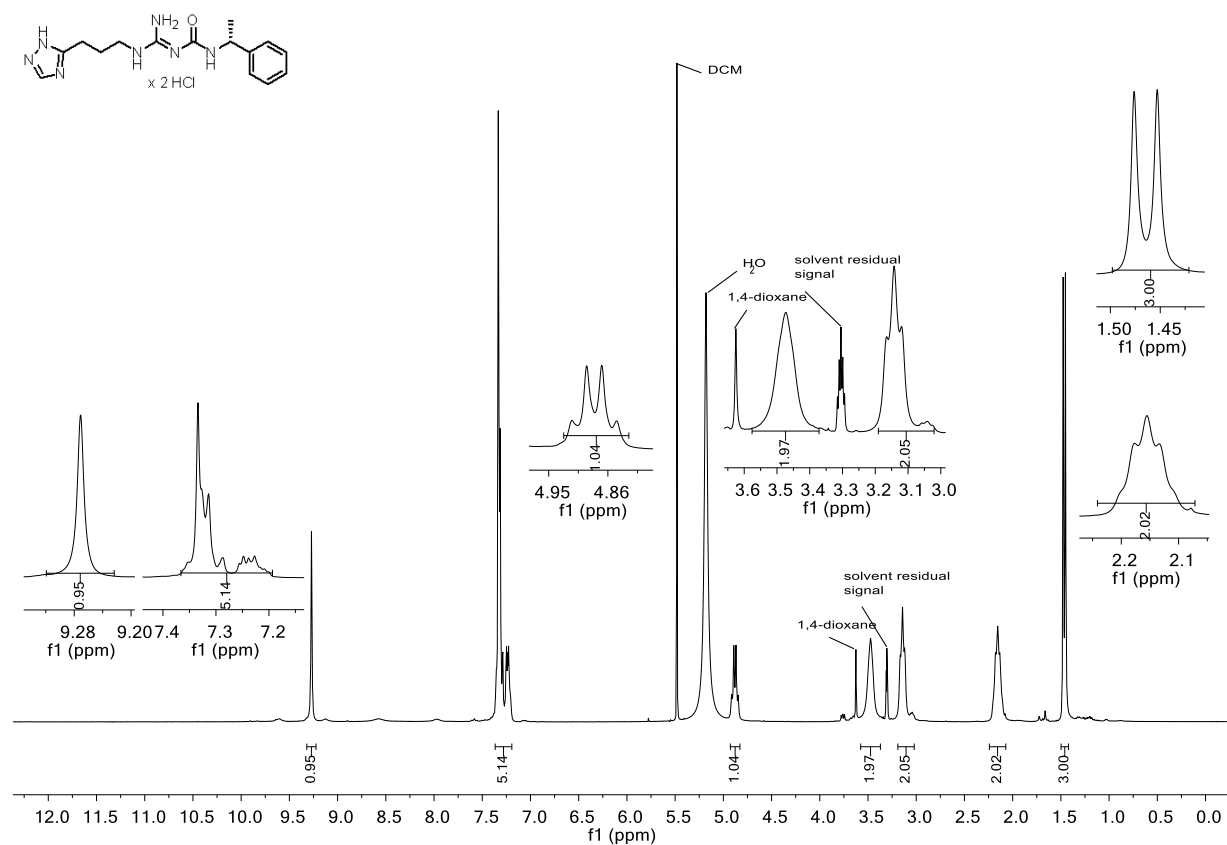
Figure 3.111. ^{1}H-NMR spectrum (300 MHz, CD₃OD) of compound **3.262**.
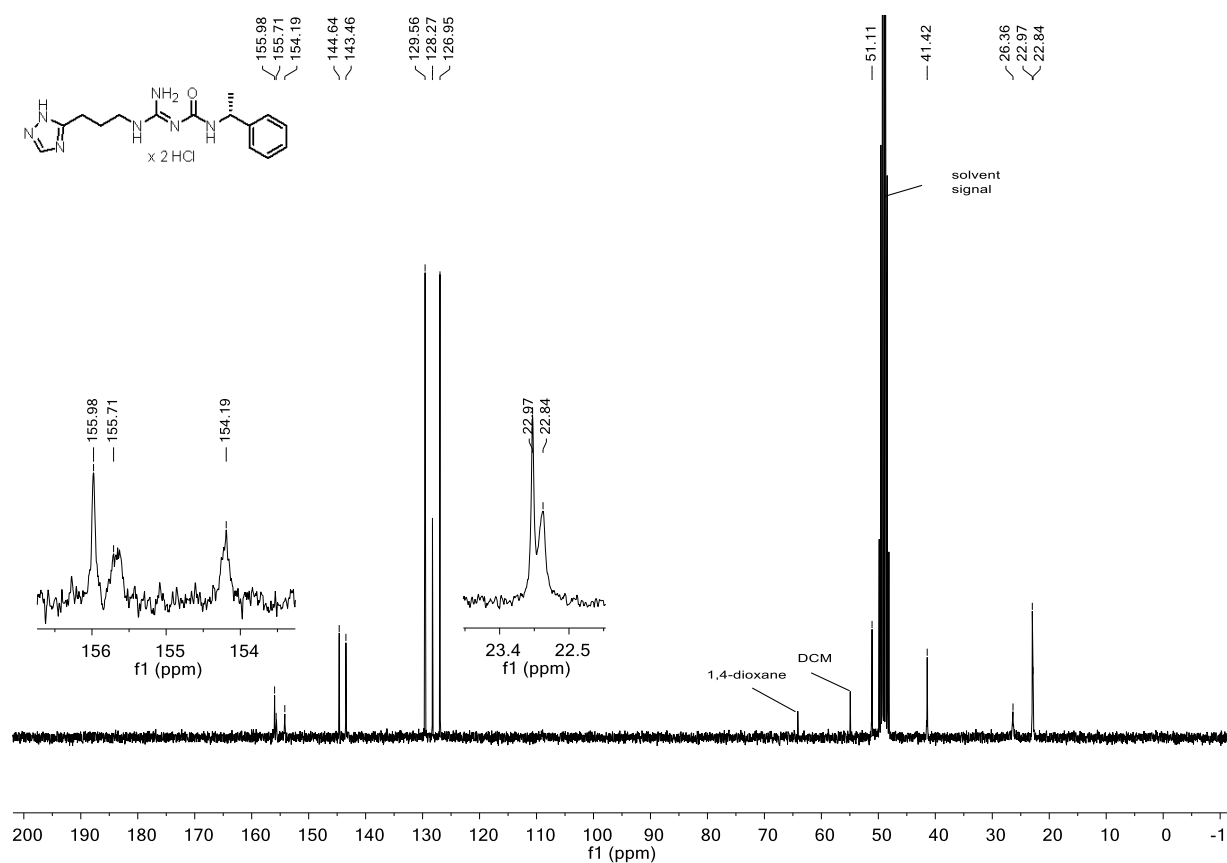
Figure 3.112. ^{13}C-NMR spectrum (75 MHz, CD$_3$OD) of compound **3.262**.
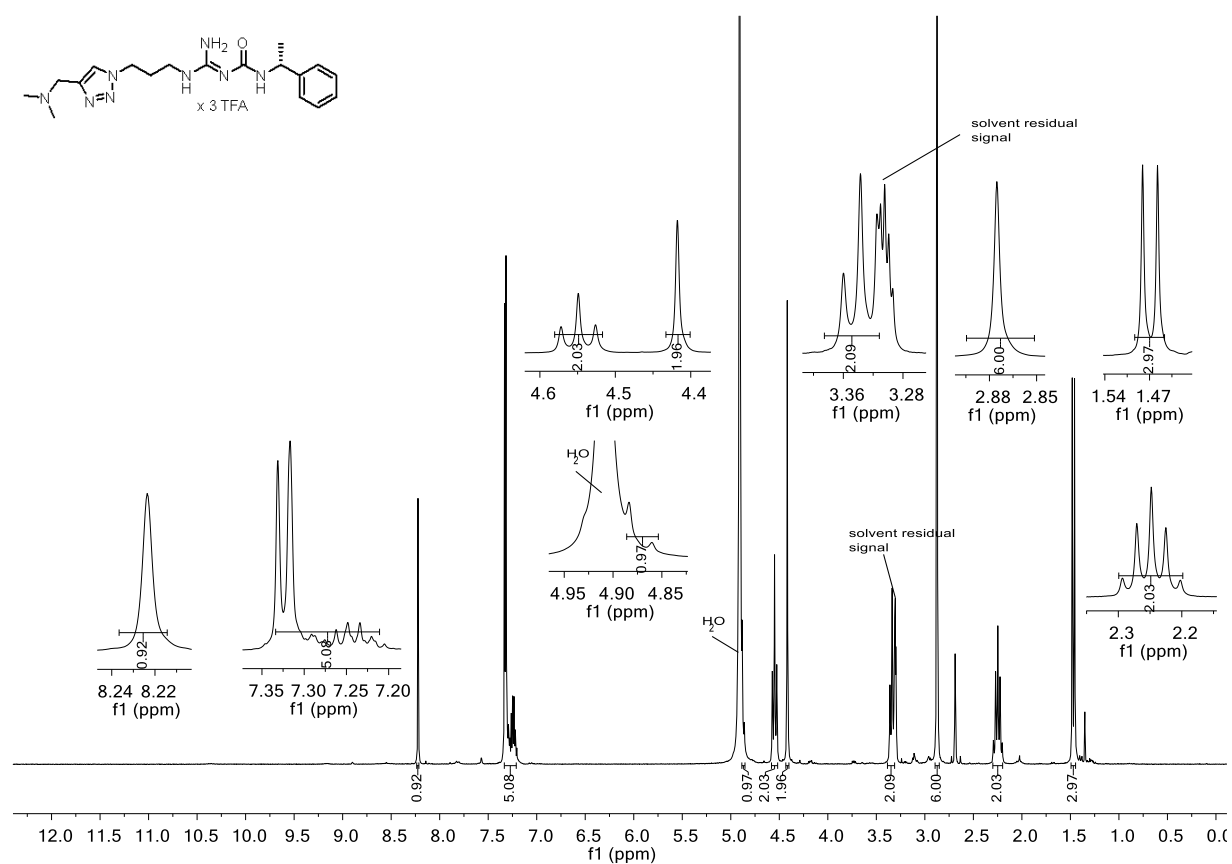
Figure 3.113. ^{1}H-NMR spectrum (300 MHz, CD$_3$OD) of compound **3.263**.
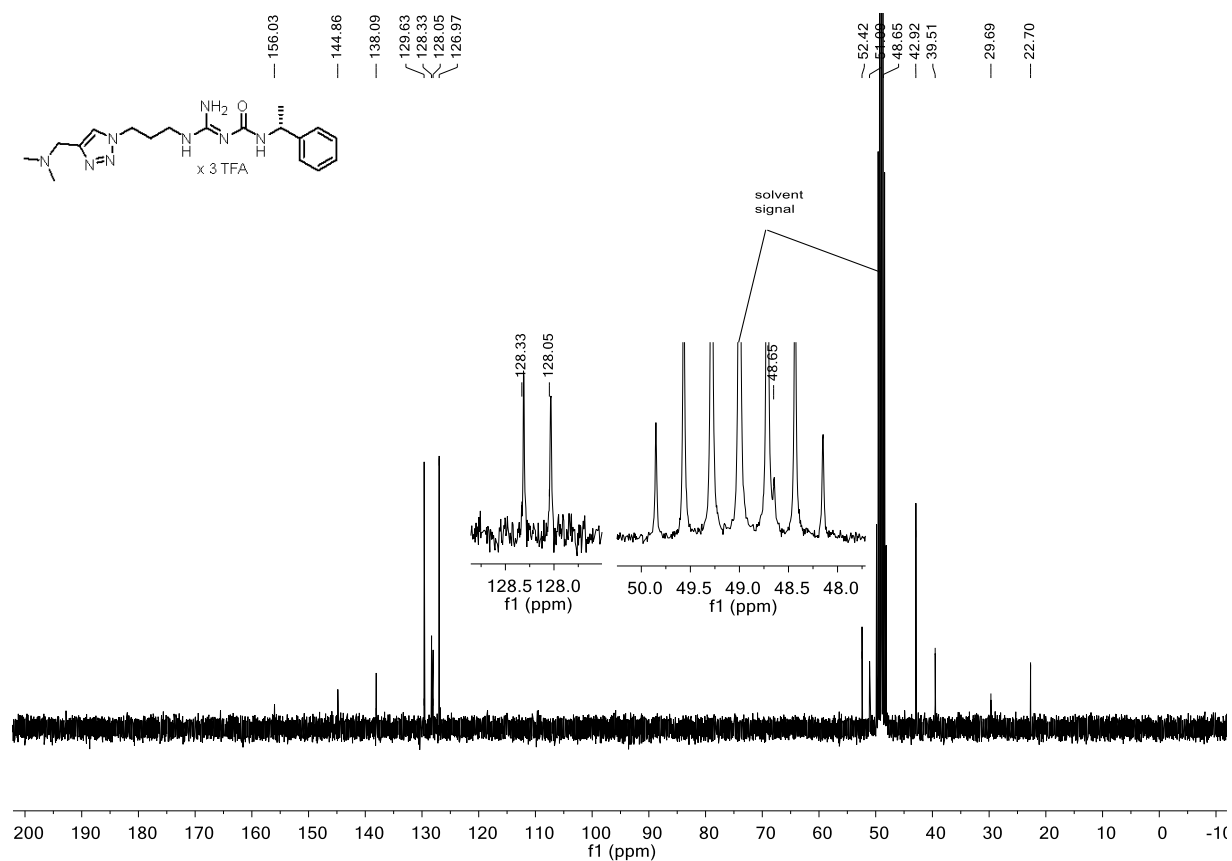
Figure 3.114. ^{13}C-NMR spectrum (75 MHz, CD$_3$OD) of compound **3.263**.
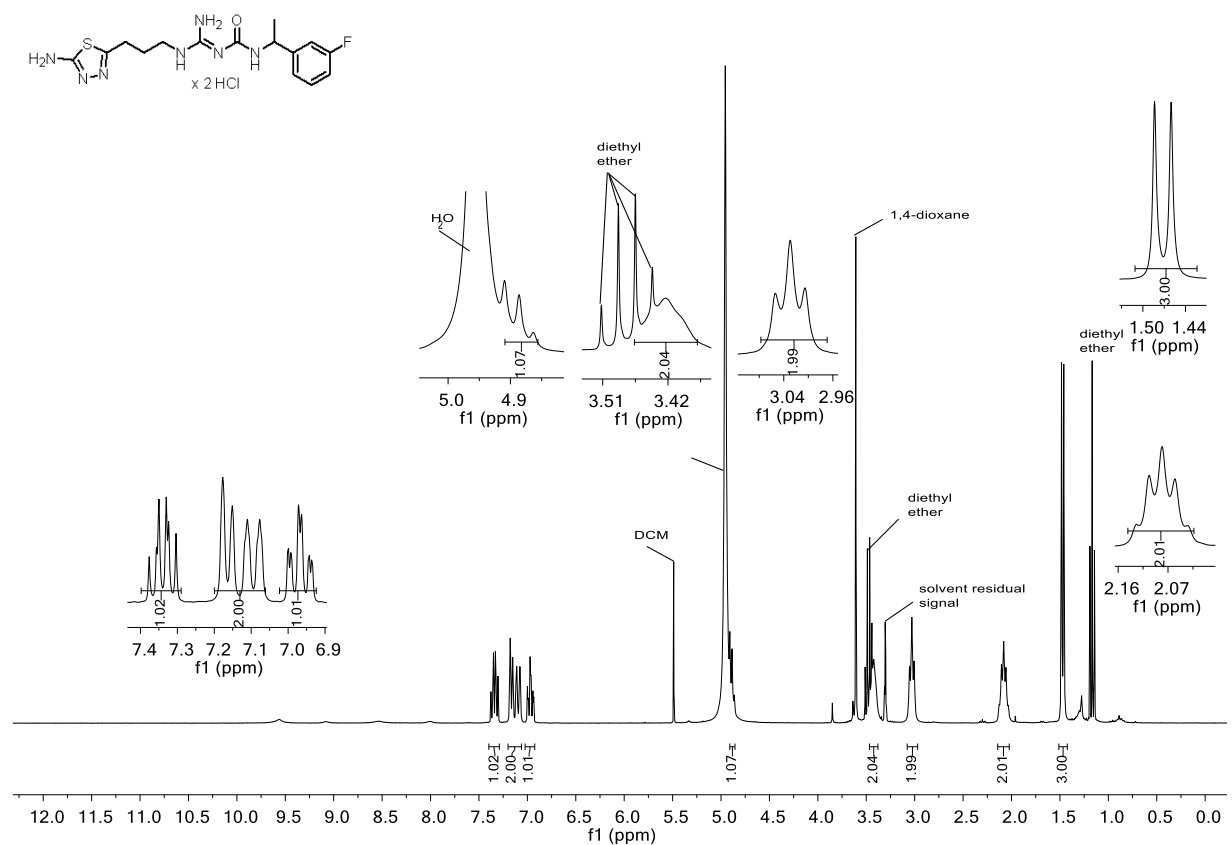
Figure 3.115. ^{1}H-NMR spectrum (300 MHz, CD$_3$OD) of compound **3.264**.

534
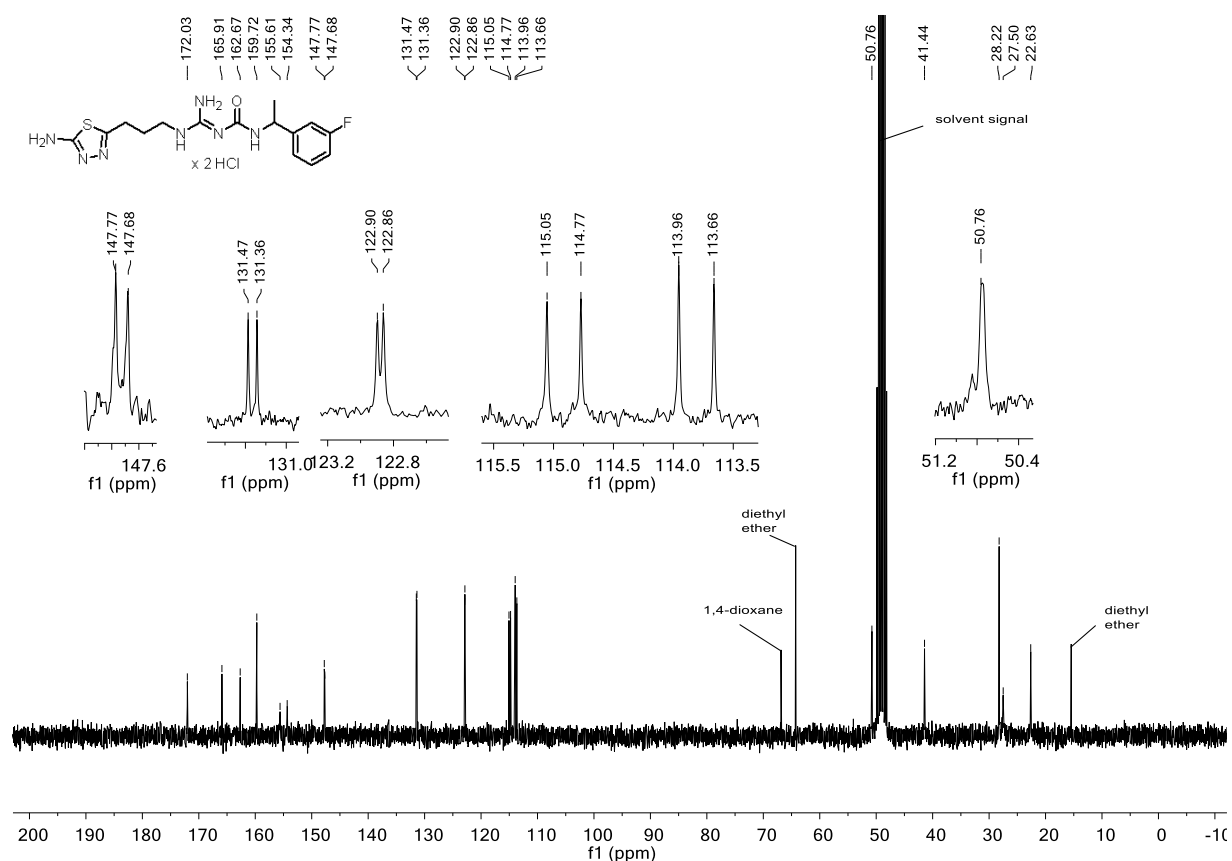
Figure 3.116. ¹³C-NMR spectrum (75 MHz, CD₃OD) of compound **3.264**.
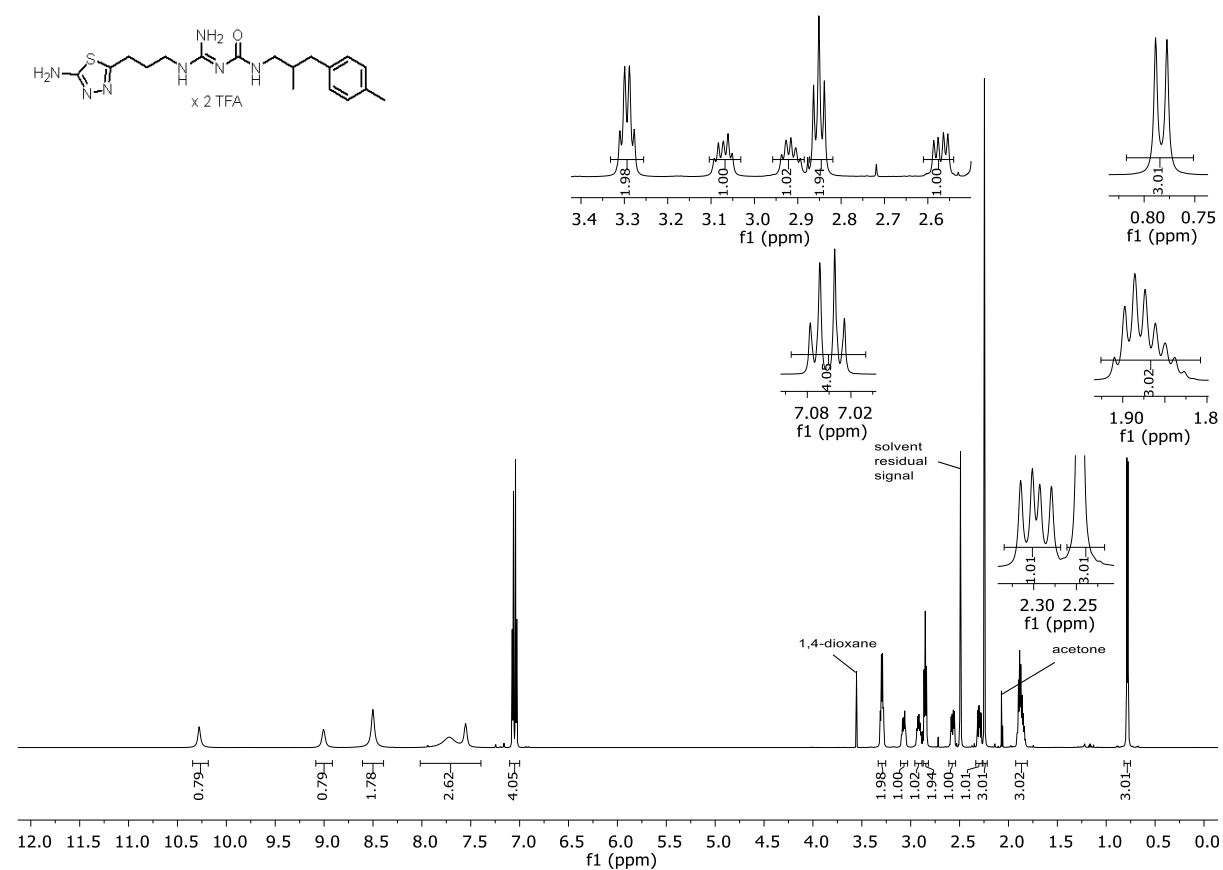
Figure 3.117. ¹H-NMR spectrum (600 MHz, DMSO-d₆) of compound **3.265**.
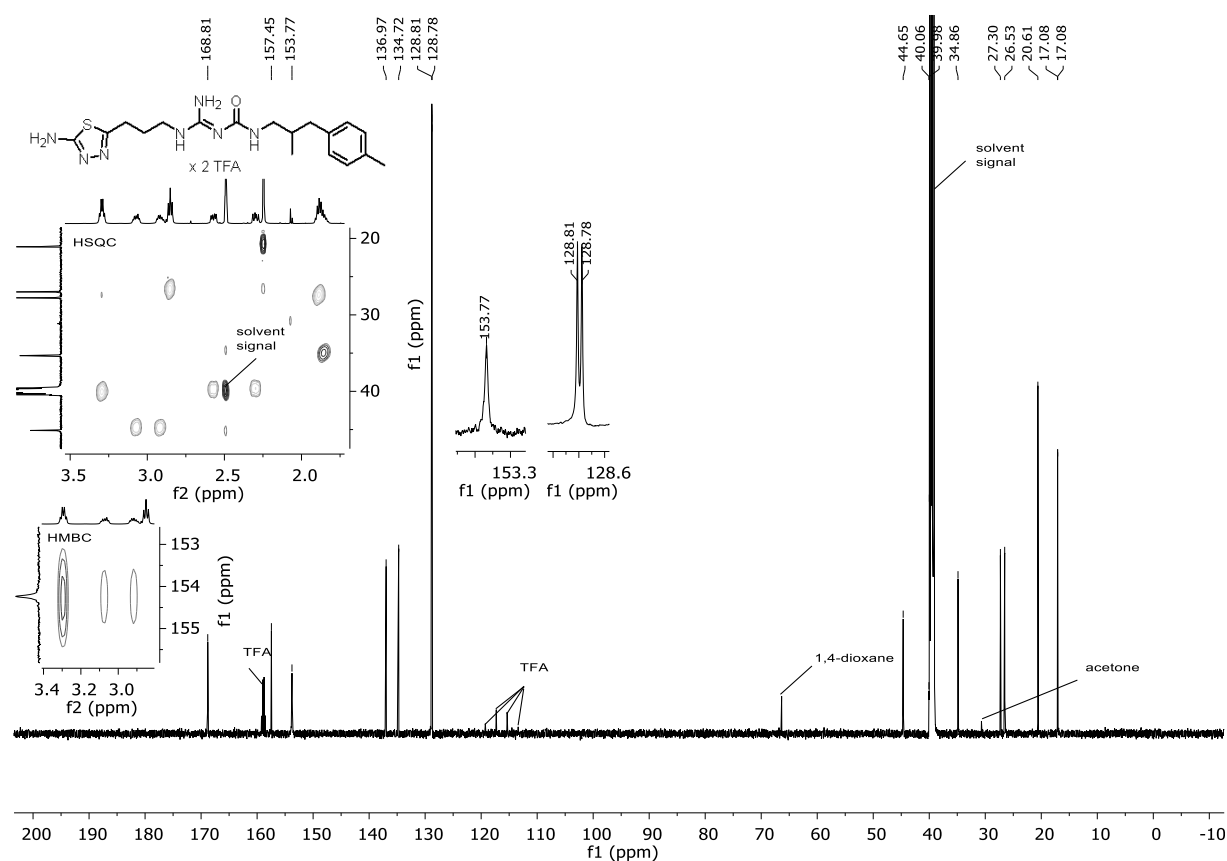
Figure 3.118. ^{13}C-NMR spectrum (151 MHz, DMSO-d$_6$) of compound **3.265**.
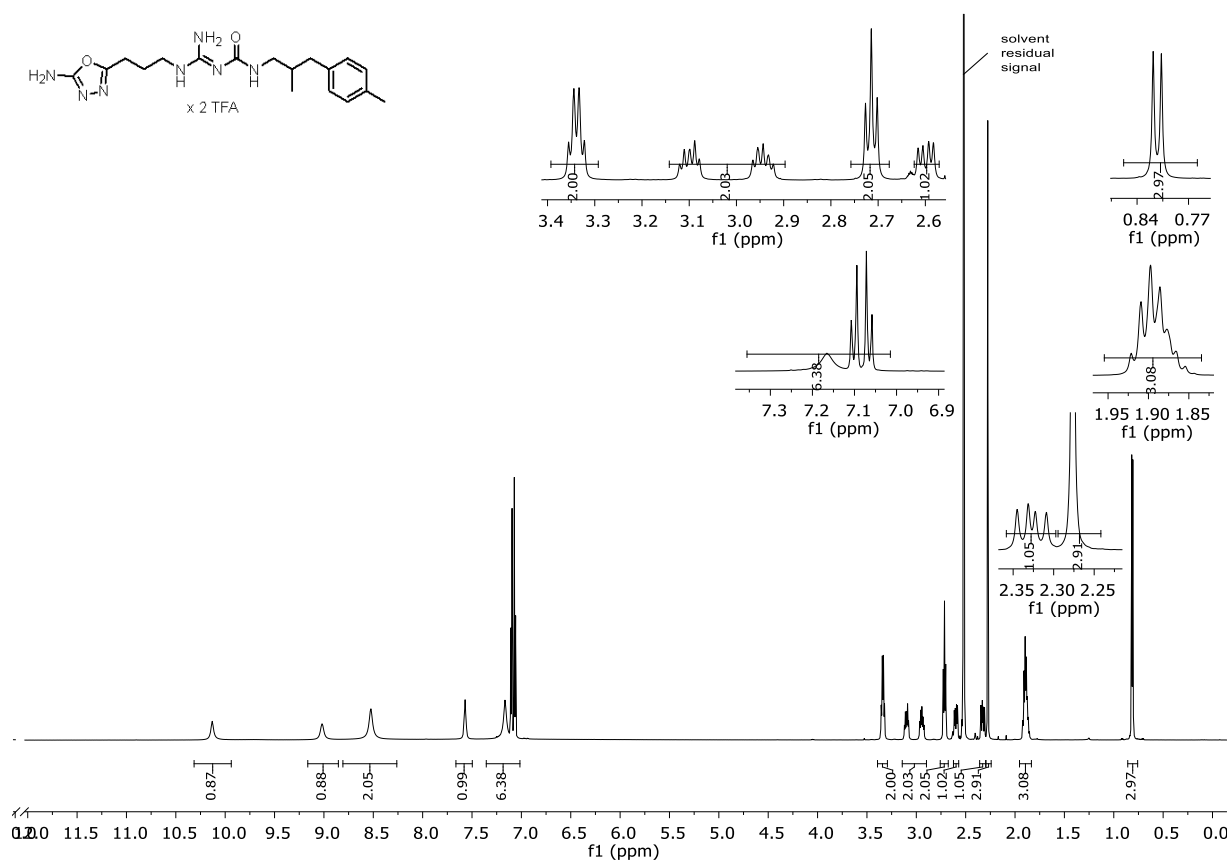
Figure 3.119. ^{1}H-NMR spectrum (600 MHz, DMSO-d$_6$) of compound **3.266**.

536
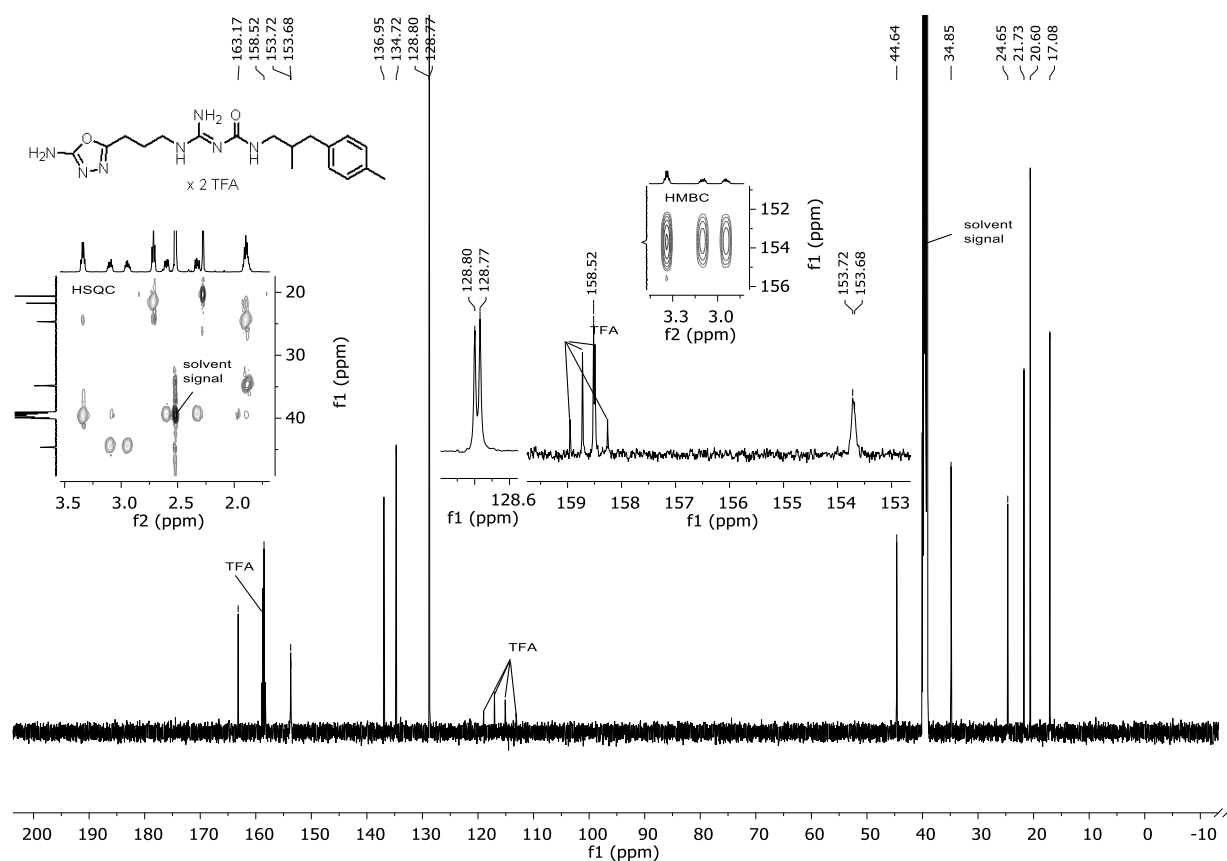
Figure 3.120. ^{13}C-NMR spectrum (151 MHz, DMSO-d$_6$) of compound **3.266**.
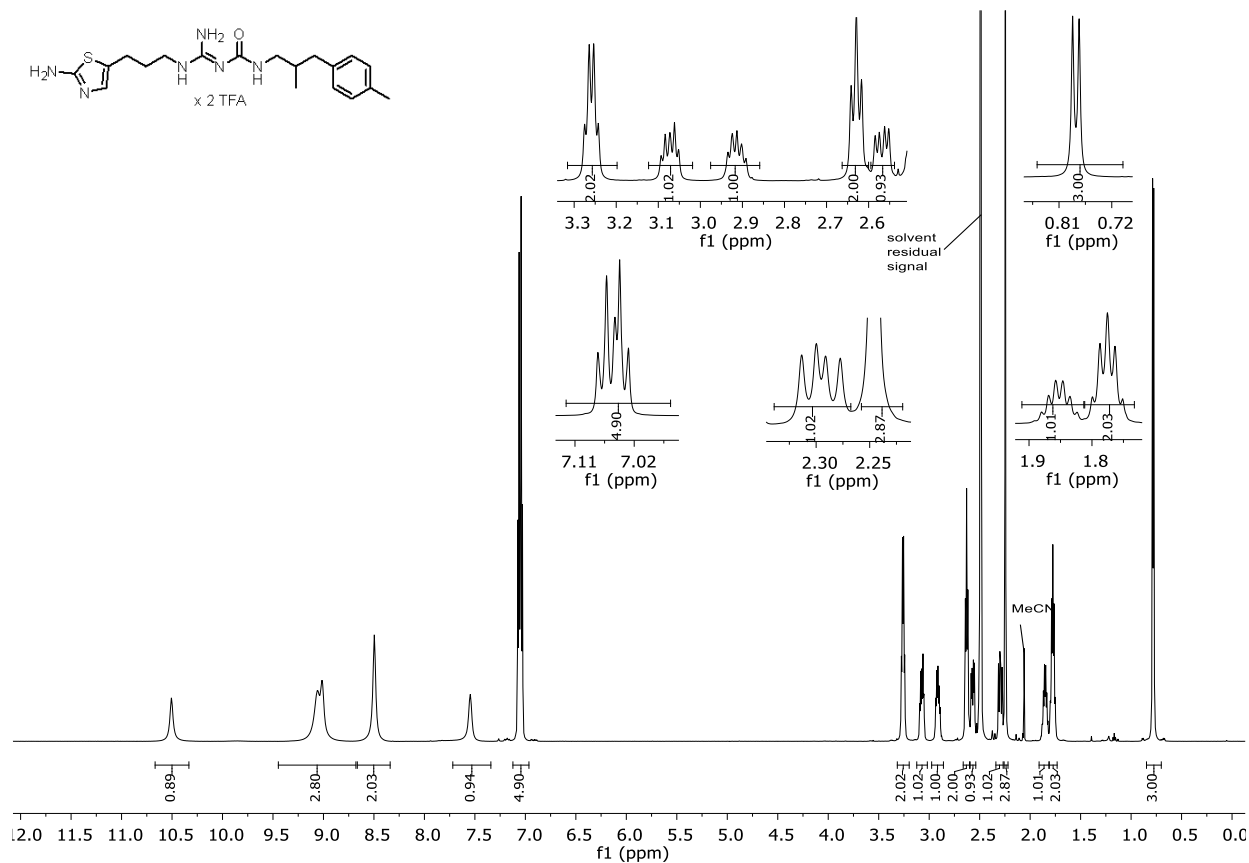
Figure 3.121. ^{1}H-NMR spectrum (600 MHz, DMSO-d$_6$) of compound **3.267**.

537
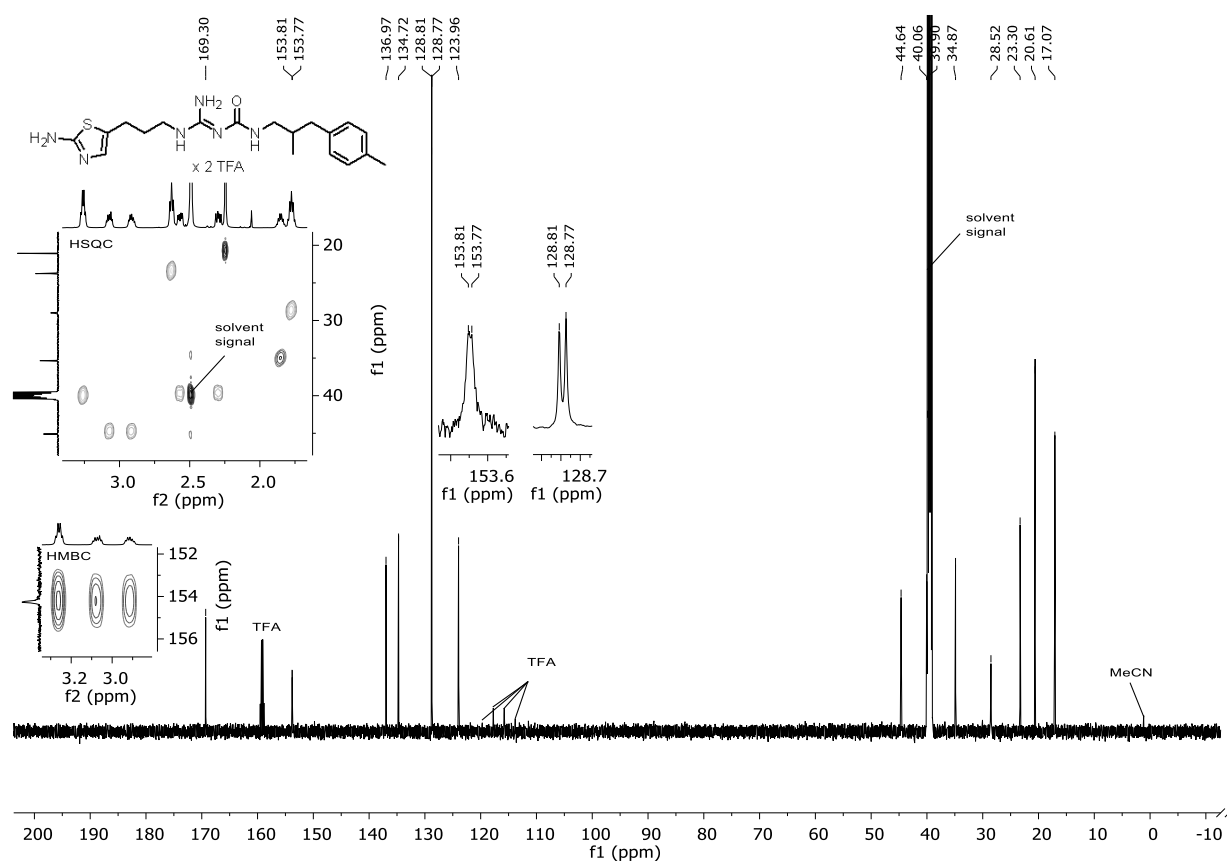
Figure 3.122. ^{13}C-NMR spectrum (151 MHz, DMSO-d$_6$) of compound **3.267**.
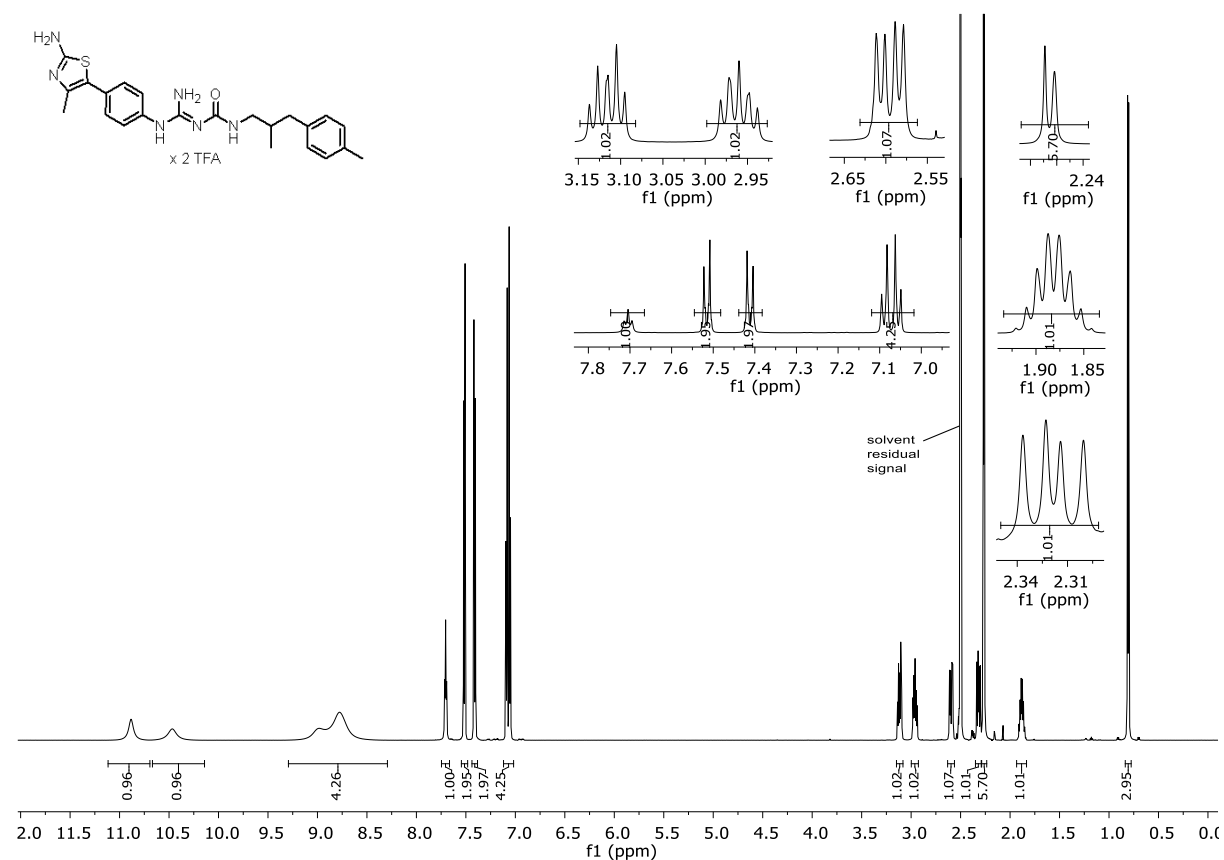
Figure 3.123. ^{1}H-NMR spectrum (600 MHz, DMSO-d$_6$) of compound **3.268**.

538
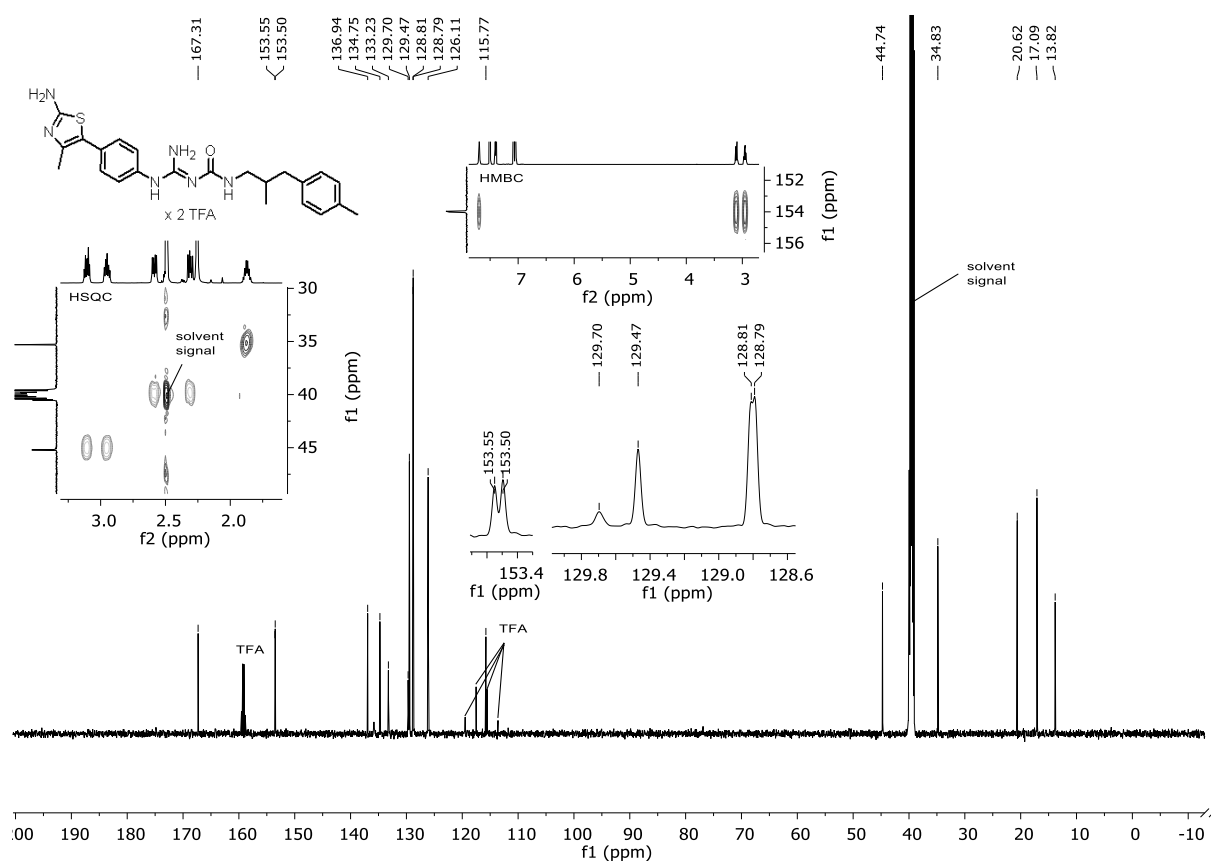
Figure 3.124. ^{13}C-NMR spectrum (151 MHz, DMSO-d$_6$) of compound **3.268**.
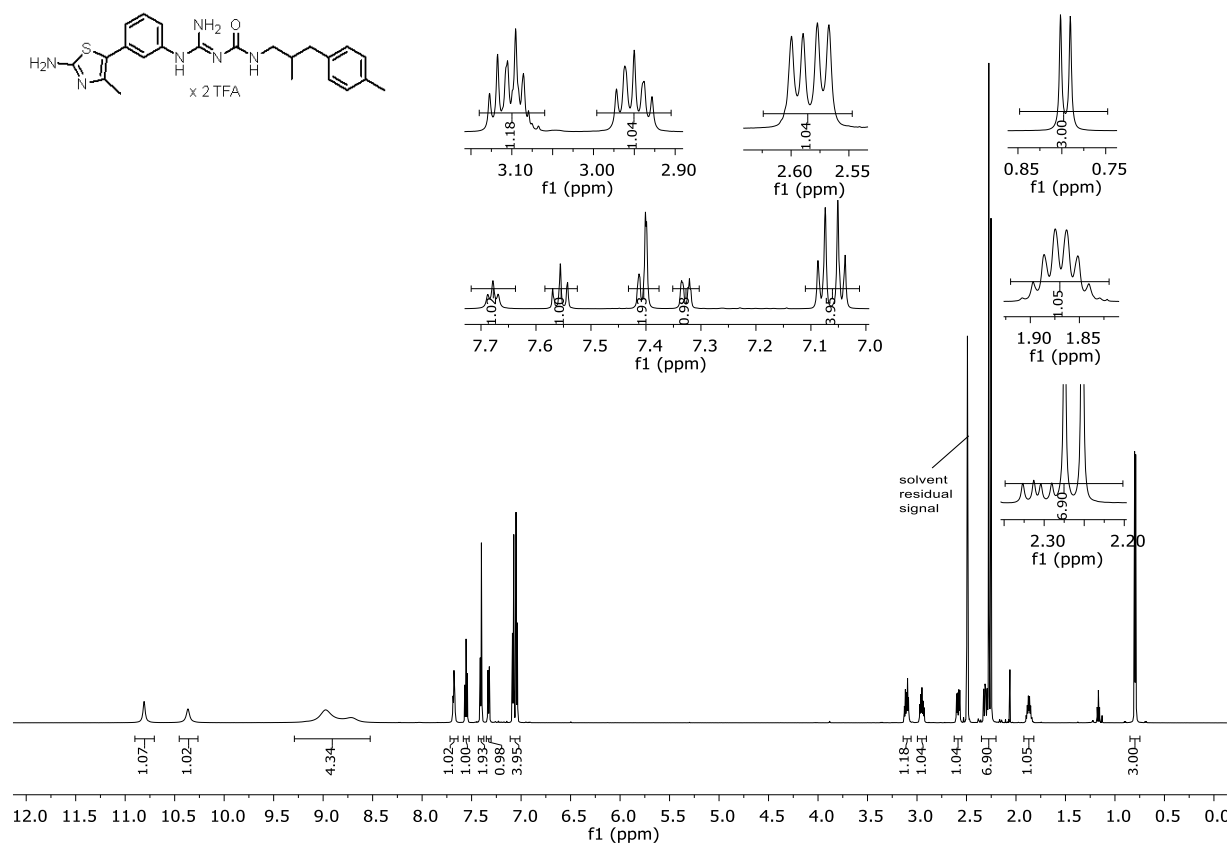
Figure 3.125. ^{1}H-NMR spectrum (600 MHz, DMSO-d$_6$) of compound **3.269**.
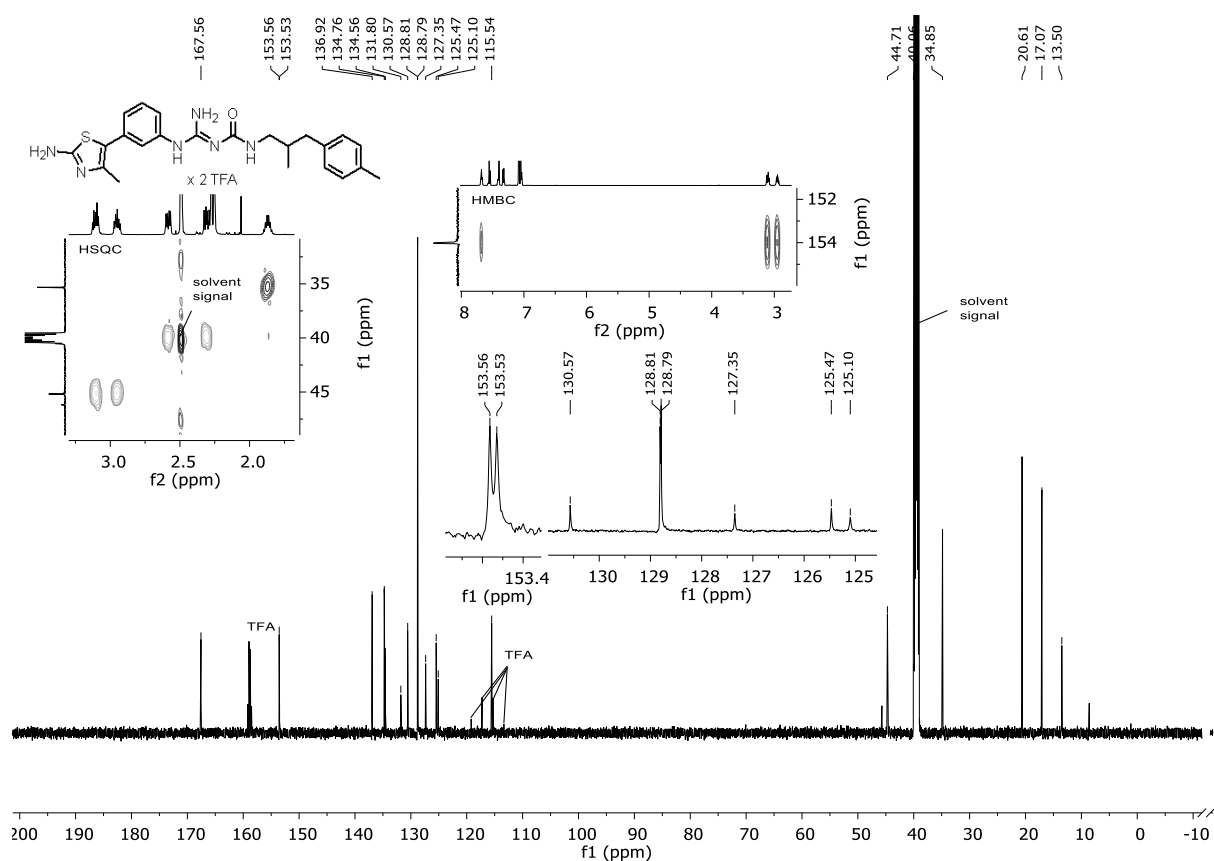
Figure 3.126. ^{13}C-NMR spectrum (151 MHz, DMSO-d$_6$) of compound **3.269**.
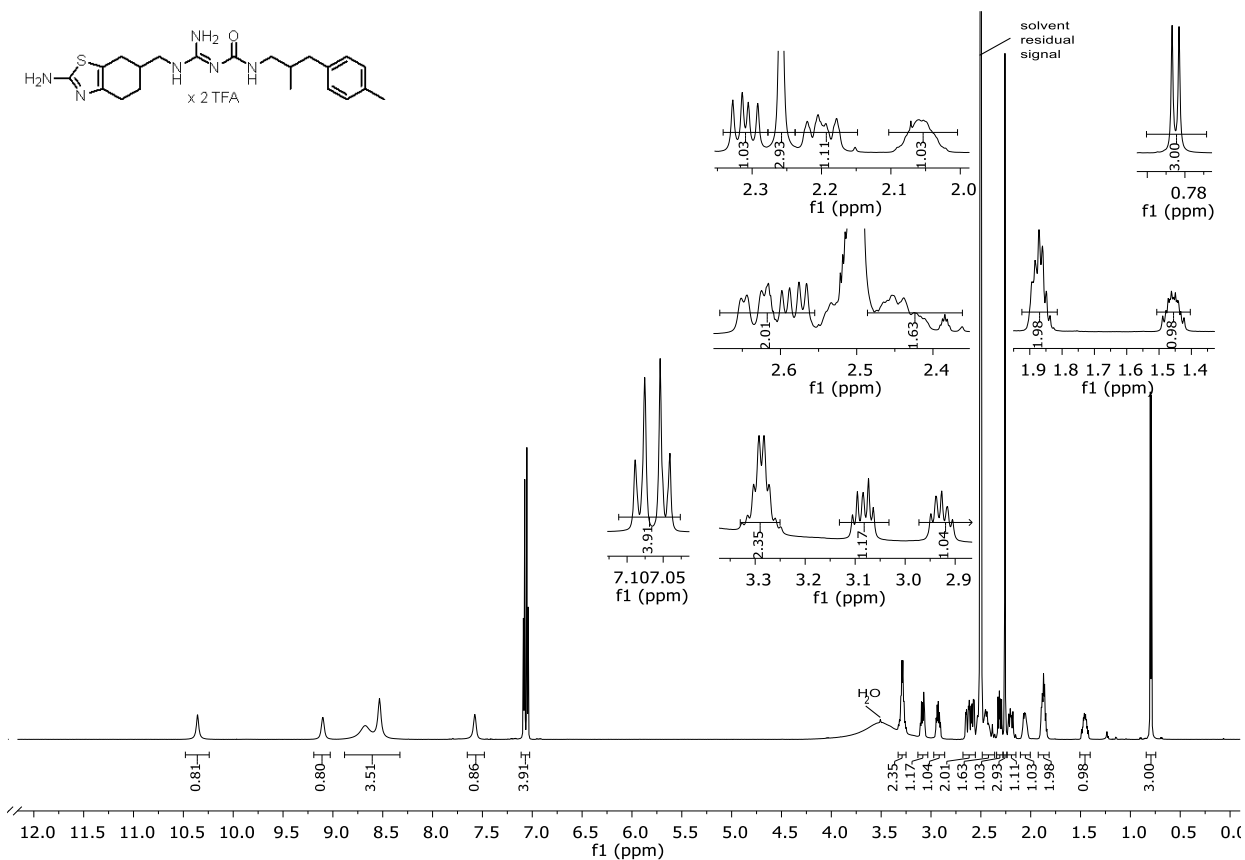
Figure 3.127. ^{1}H-NMR spectrum (600 MHz, DMSO-d$_6$) of compound **3.270**.

540
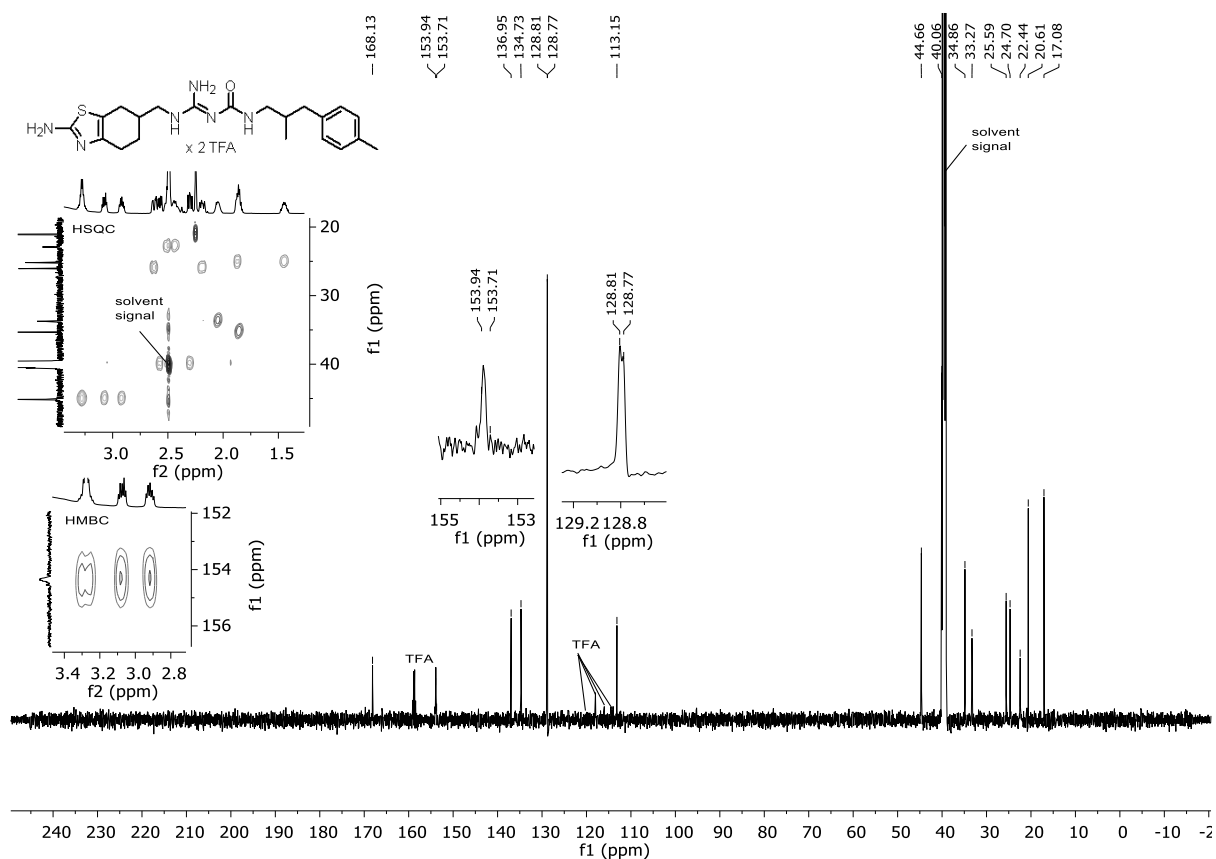
Figure 3.128. ^{13}C-NMR spectrum (151 MHz, DMSO-d$_6$) of compound **3.270**.
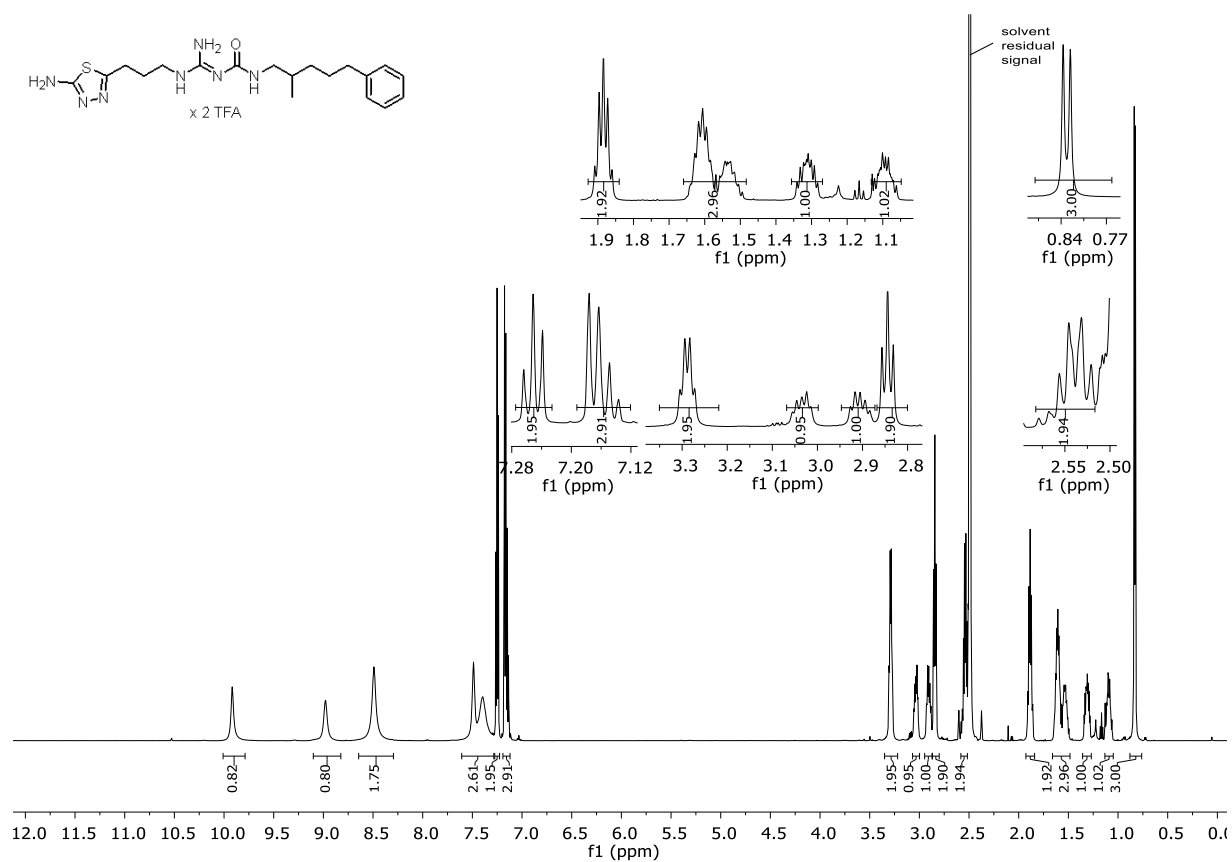
Figure 3.129. ^{1}H-NMR spectrum (600 MHz, DMSO-d$_6$) of compound **3.271**.

541
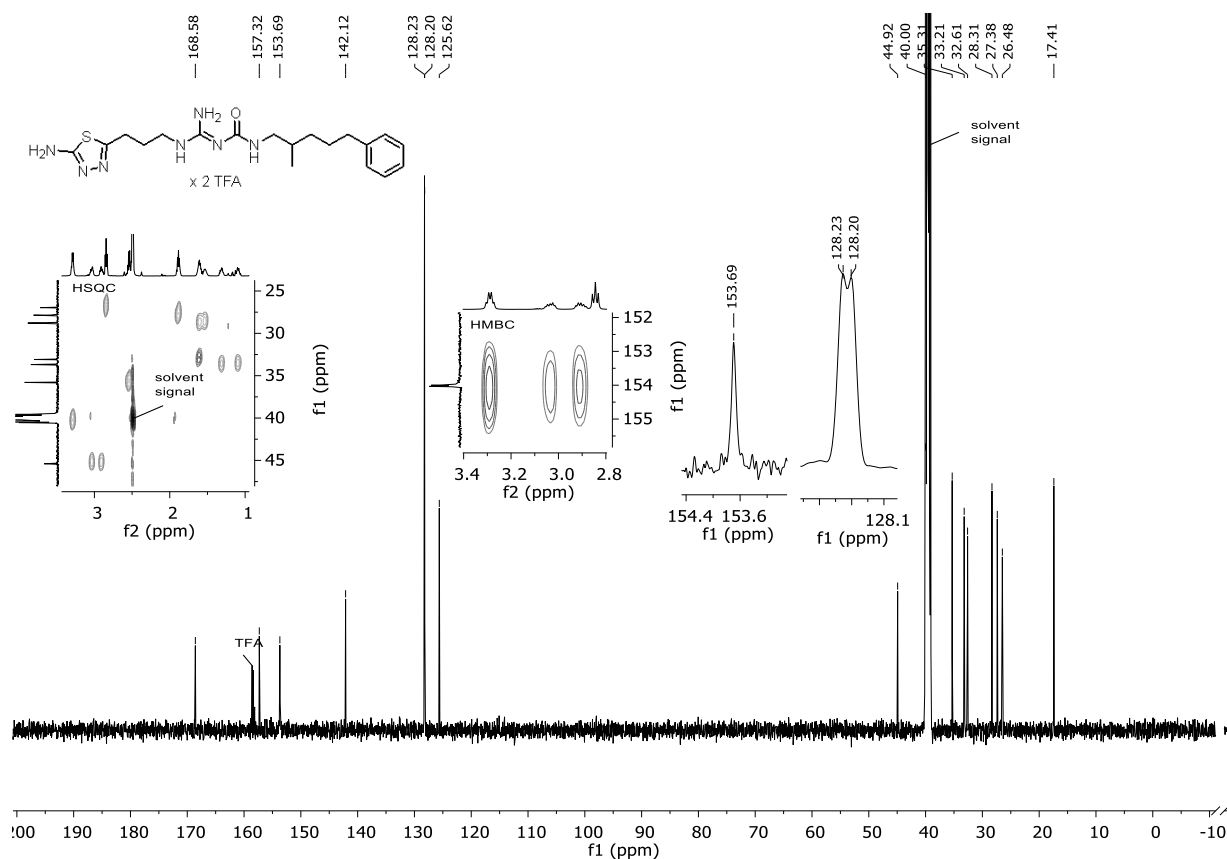
Figure 3.130. ^{13}C-NMR spectrum (151 MHz, DMSO-d$_6$) of compound **3.271**.
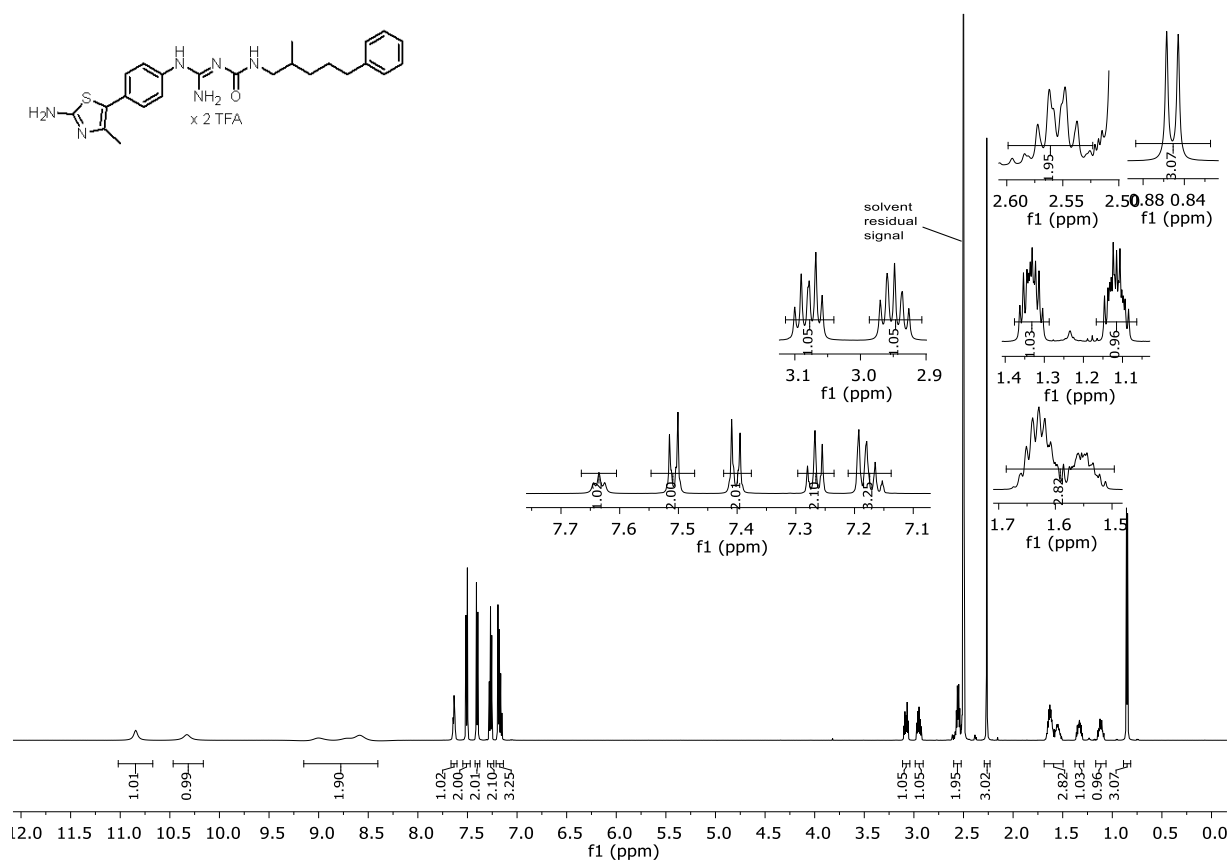
Figure 3.131. ^{1}H-NMR spectrum (600 MHz, DMSO-d$_6$) of compound **3.272**.
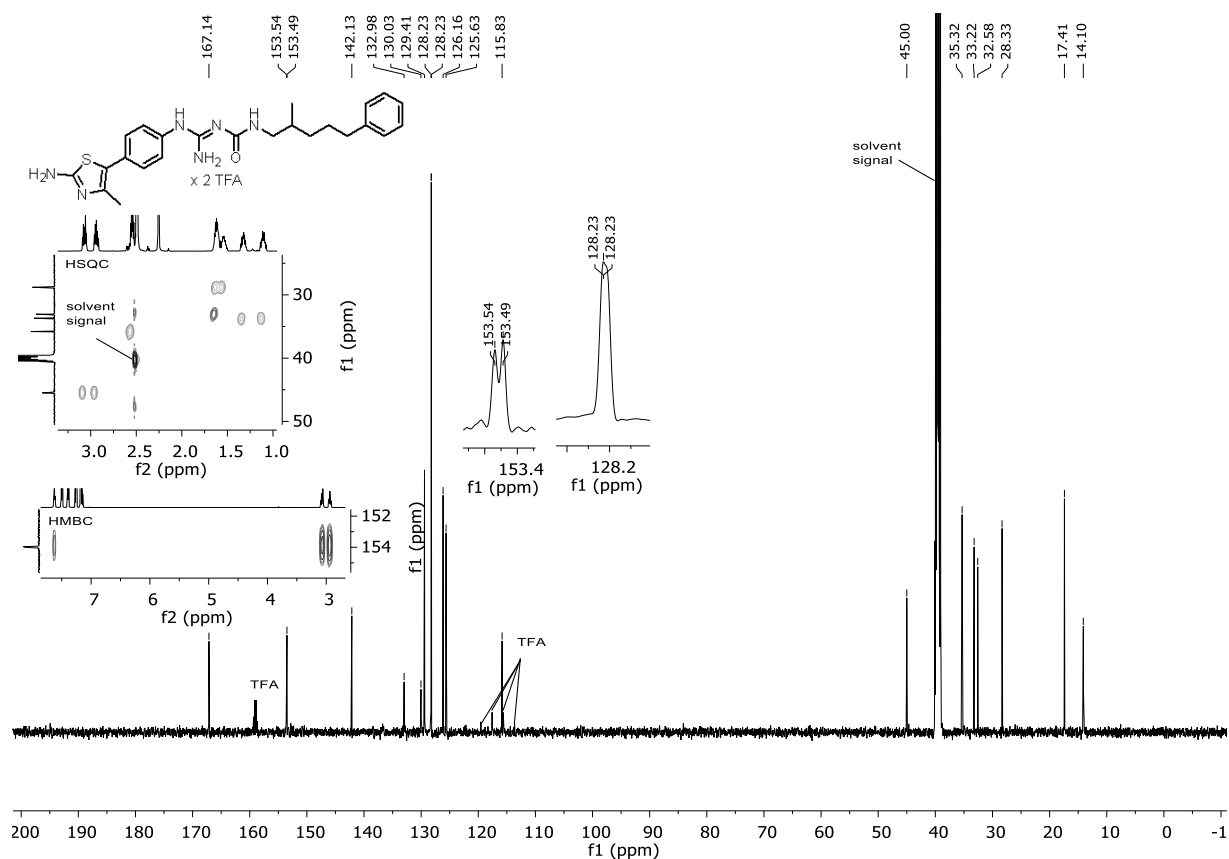
Figure 3.132. ^{13}C-NMR spectrum (151 MHz, DMSO-d$_6$) of compound **3.272**.
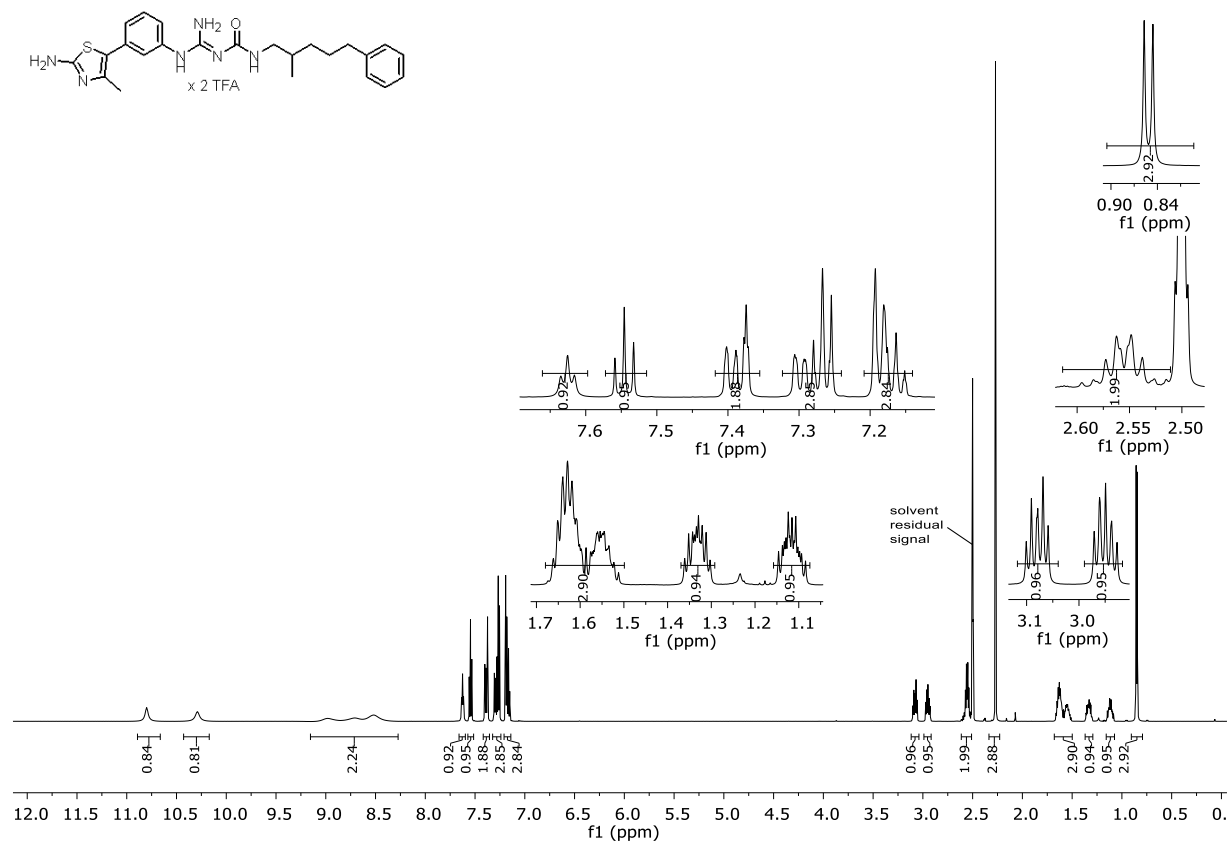
Figure 3.133. ^{1}H-NMR spectrum (600 MHz, DMSO-d$_6$) of compound **3.273**.

543
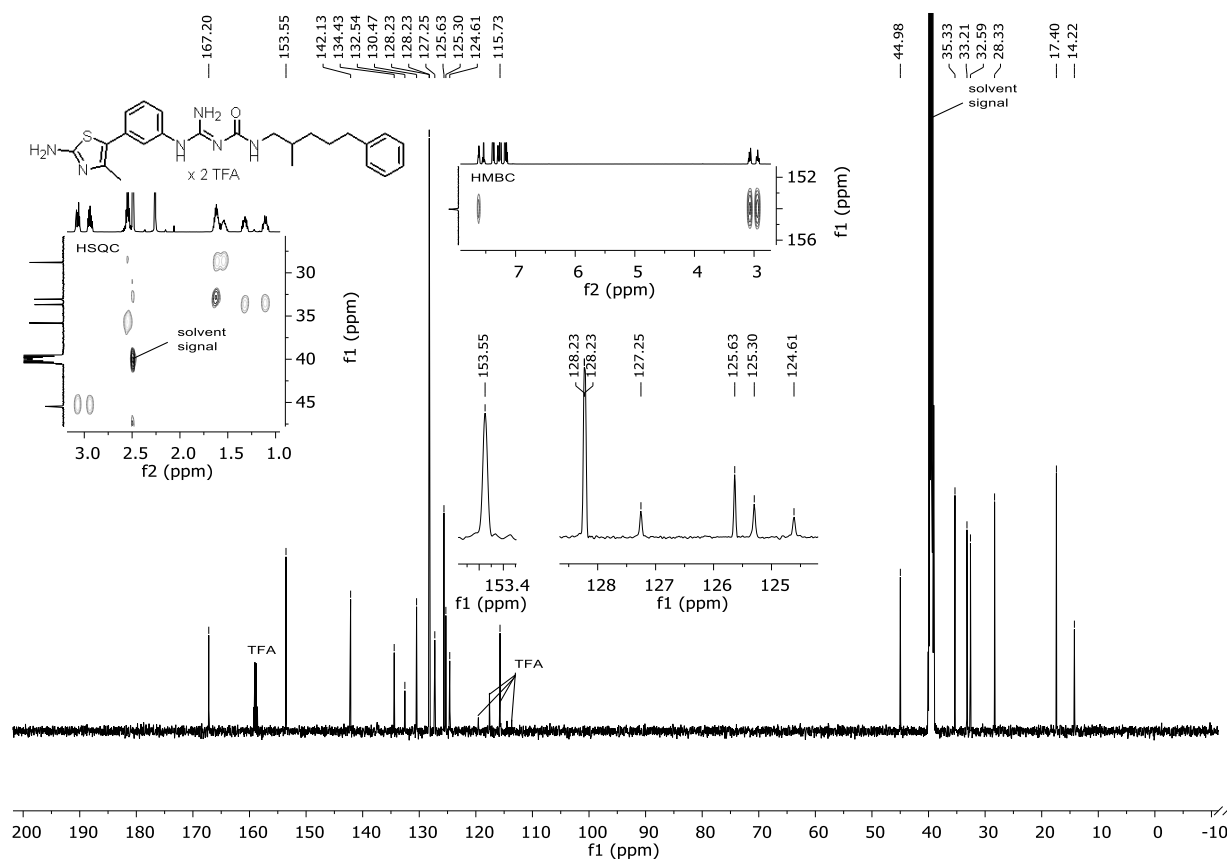
Figure 3.134. ^{13}C-NMR spectrum (151 MHz, DMSO-d$_6$) of compound **3.273**.
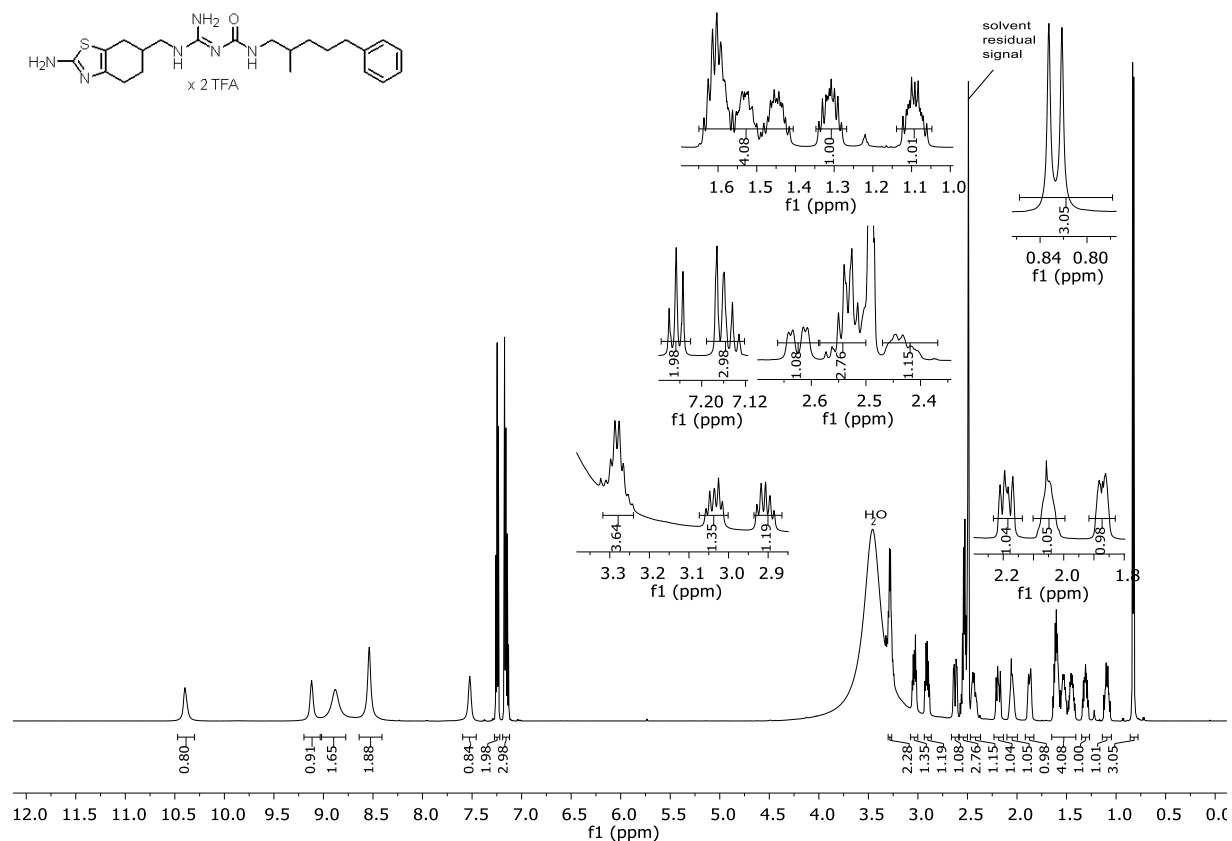
Figure 3.135. ^{1}H-NMR spectrum (600 MHz, DMSO-d$_6$) of compound **3.274**.

544
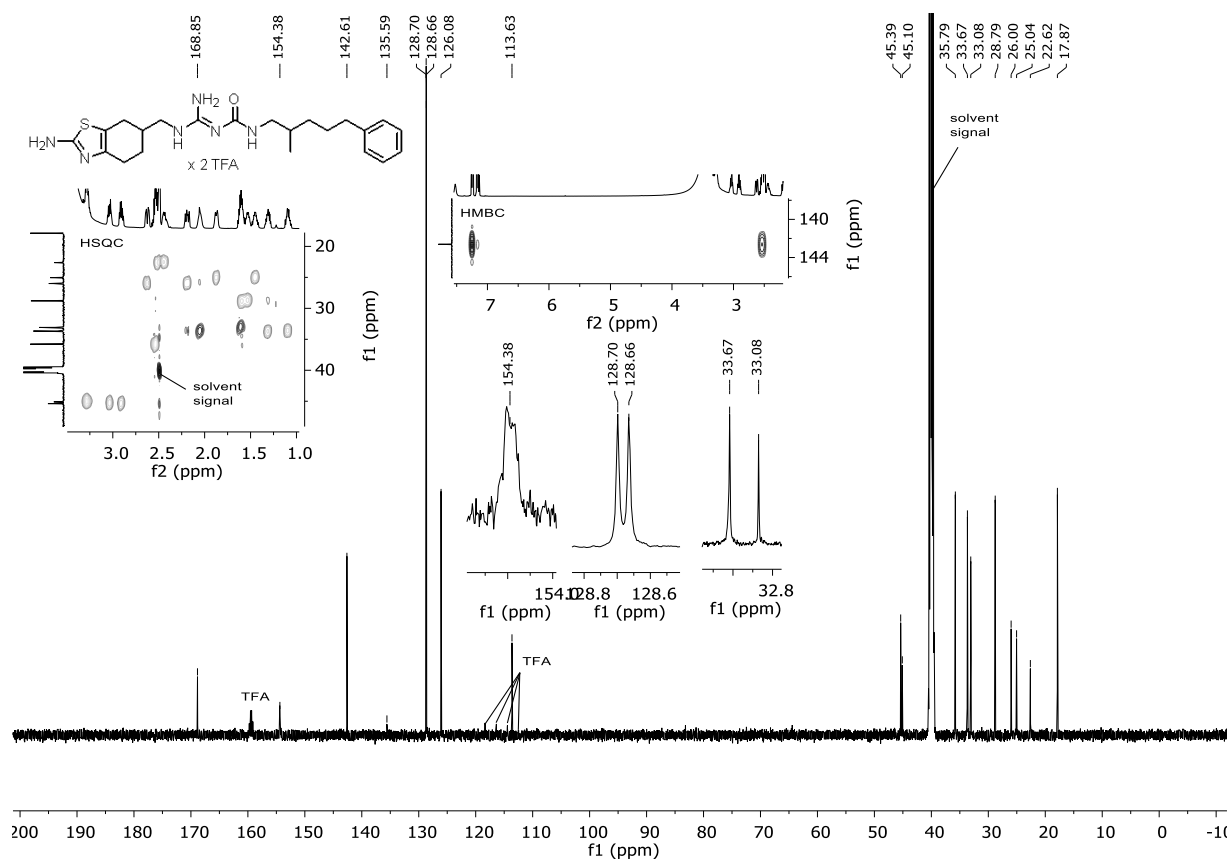
Figure 3.136. ^{13}C-NMR spectrum (151 MHz, DMSO-d$_6$) of compound **3.274**.
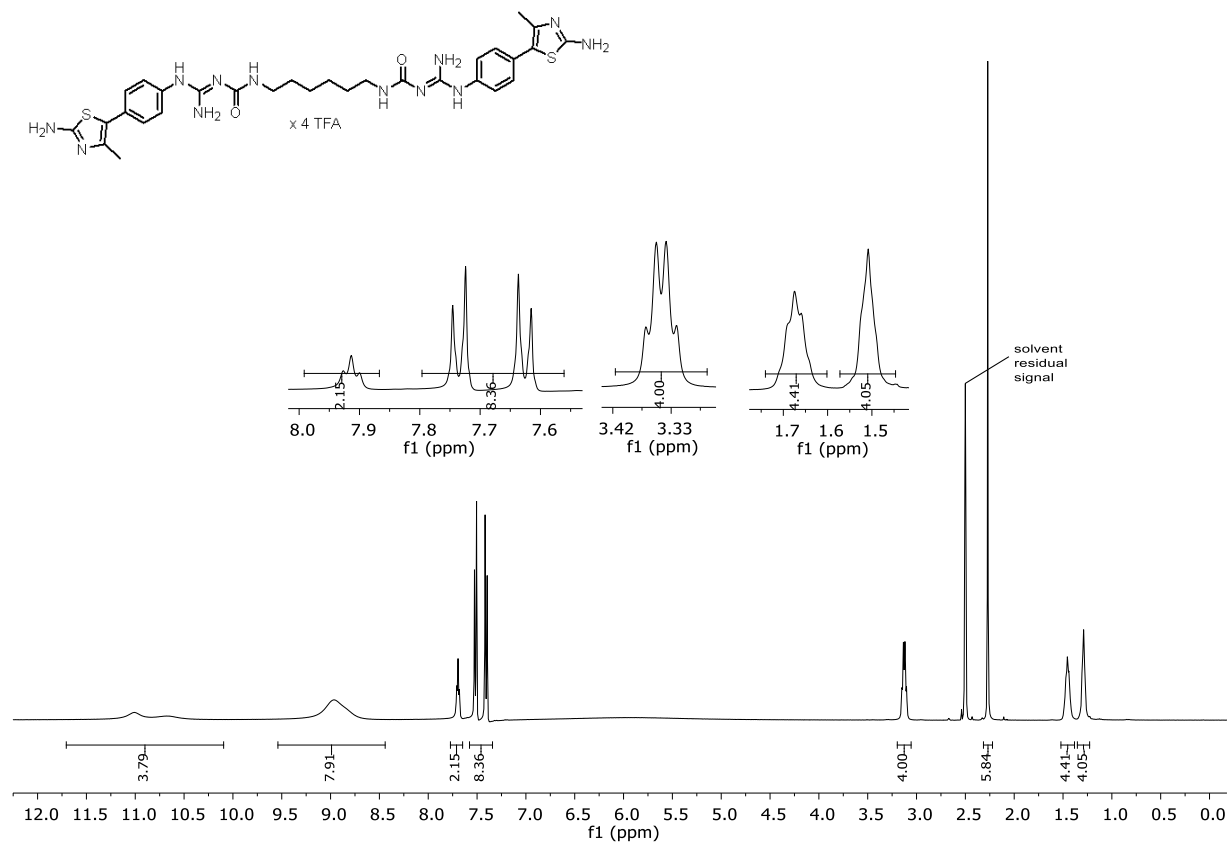
Figure 3.137. ^{1}H-NMR spectrum (600 MHz, DMSO-d$_6$) of compound **3.275**.
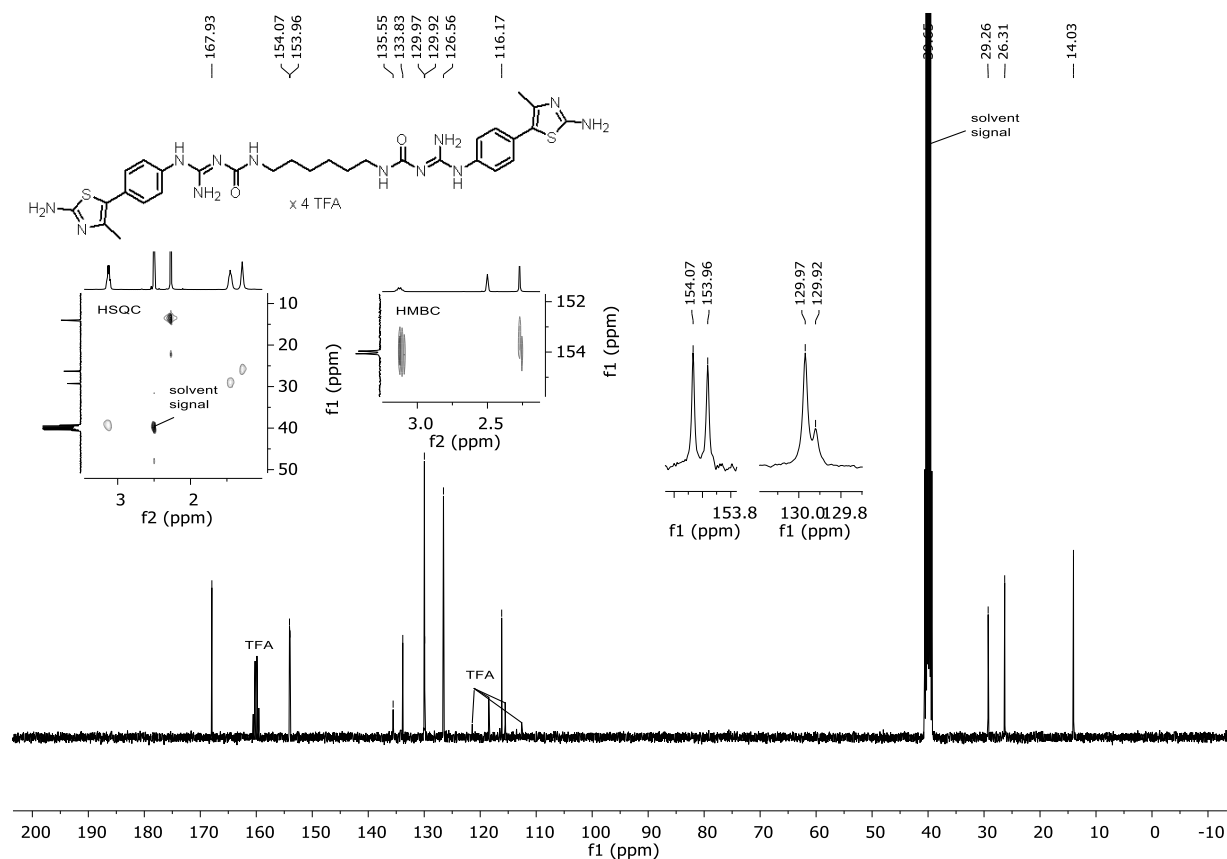
Figure 3.138. ^{13}C-NMR spectrum (151 MHz, DMSO-d$_6$) of compound **3.275**.
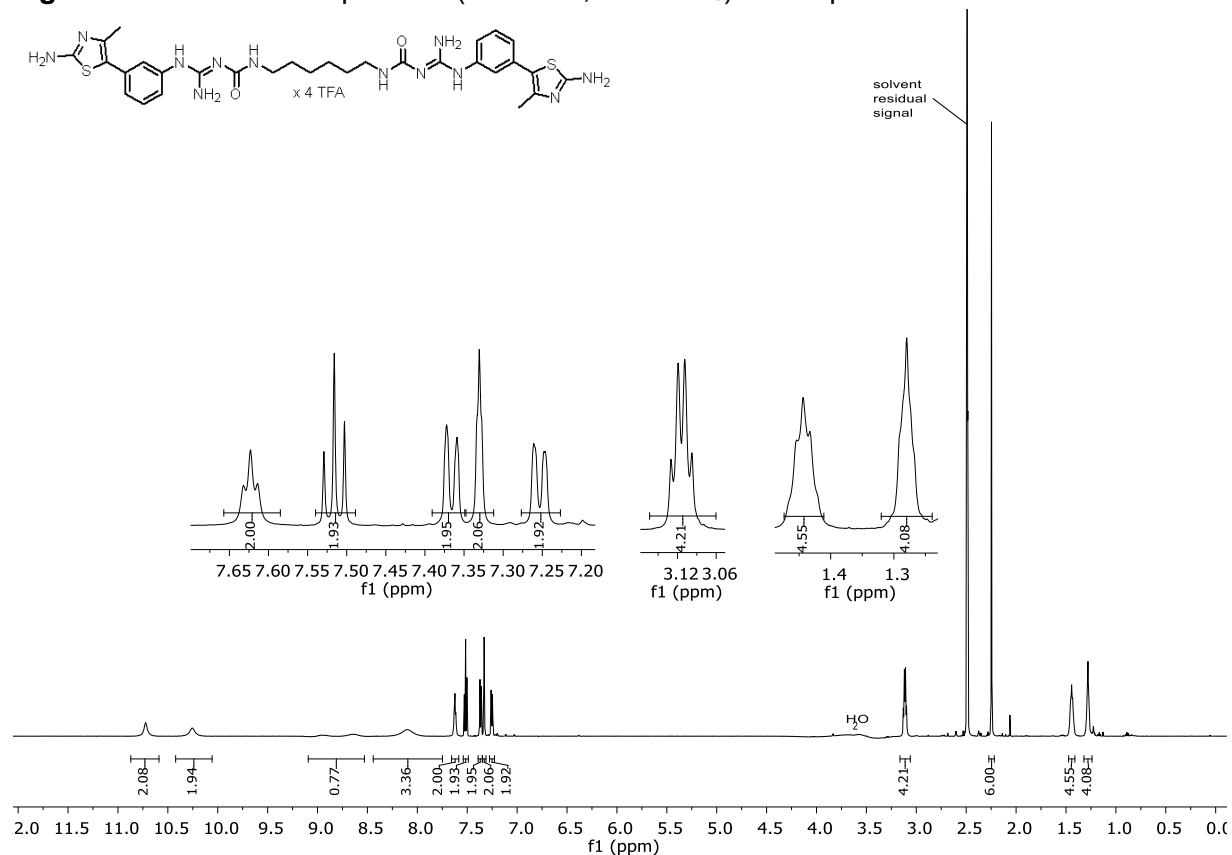
Figure 3.139. ^{1}H-NMR spectrum (600 MHz, DMSO-d$_6$) of compound **3.276**.

546
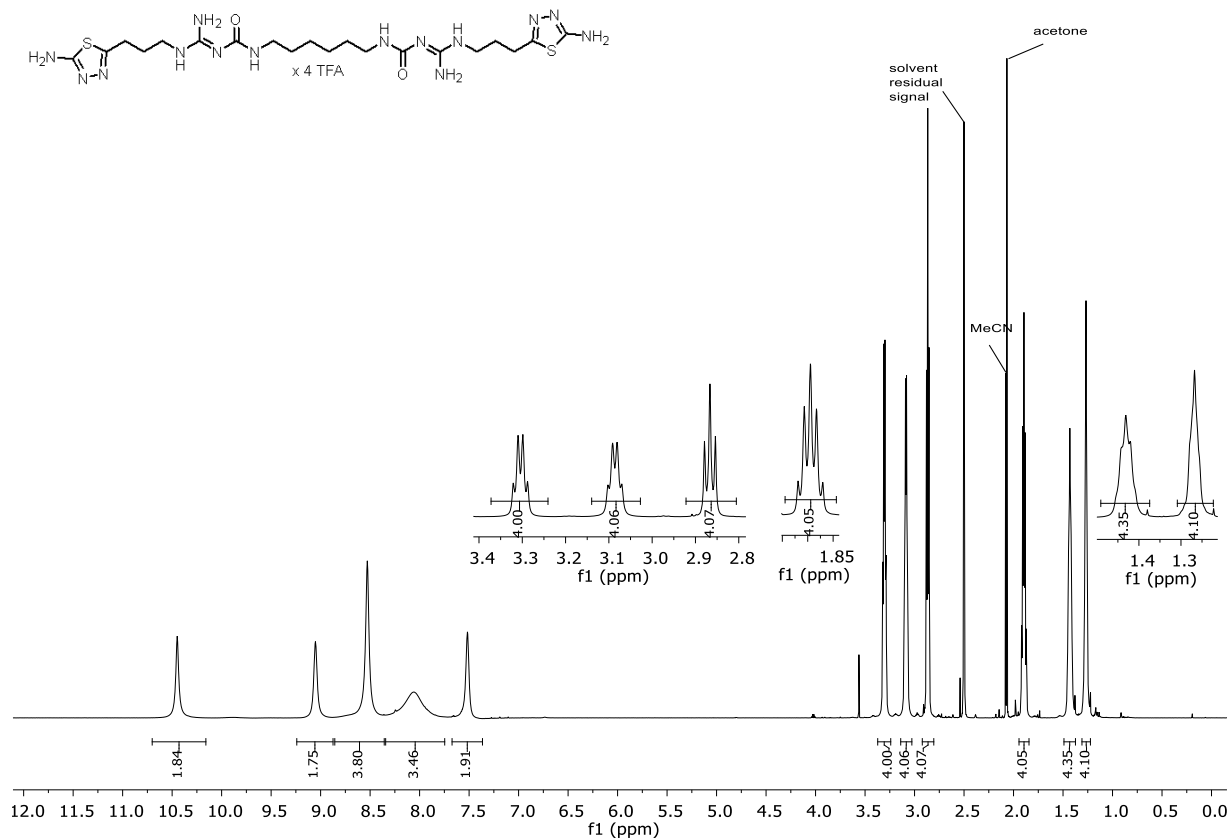
Figure 3.140. ^{1}H-NMR spectrum (600 MHz, DMSO-d$_6$) of compound **3.277**.
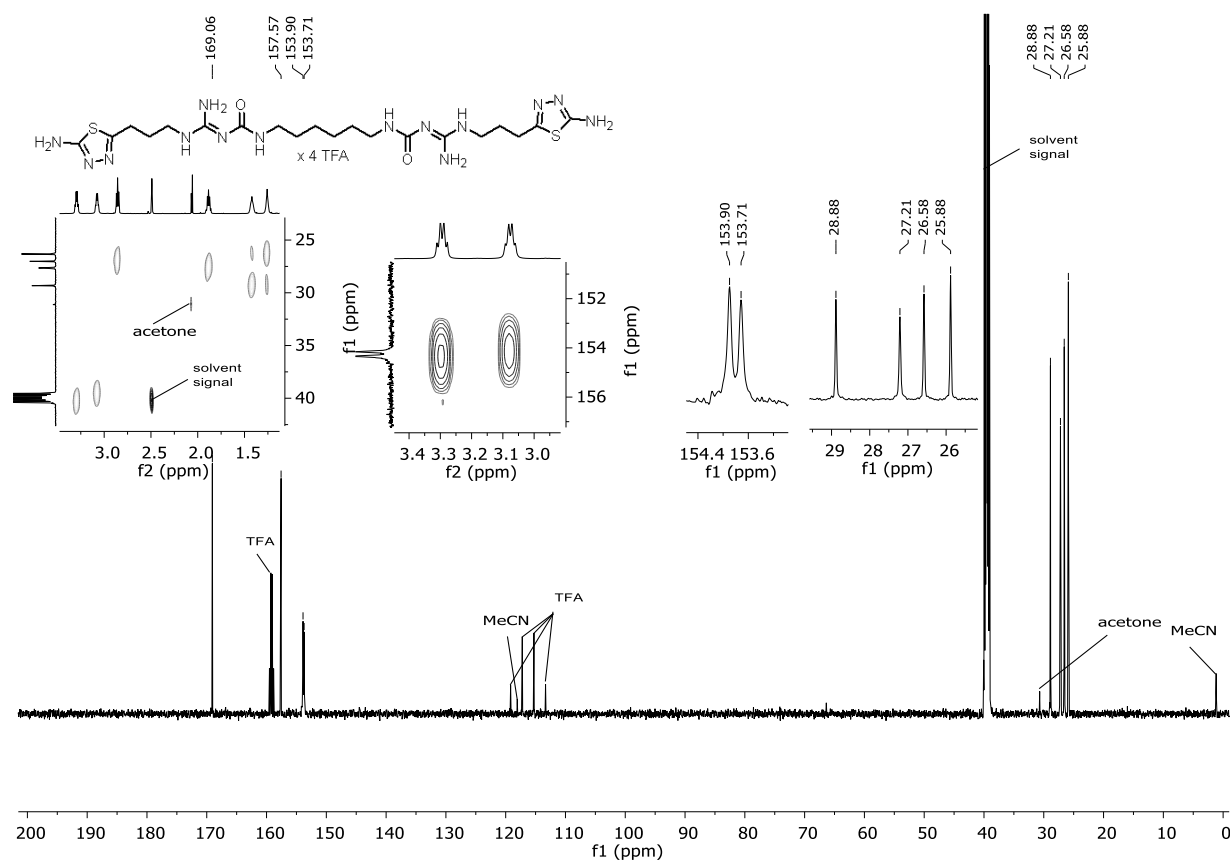
Figure 3.141. ^{13}C-NMR spectrum (151 MHz, DMSO-d$_6$) of compound **3.277**.
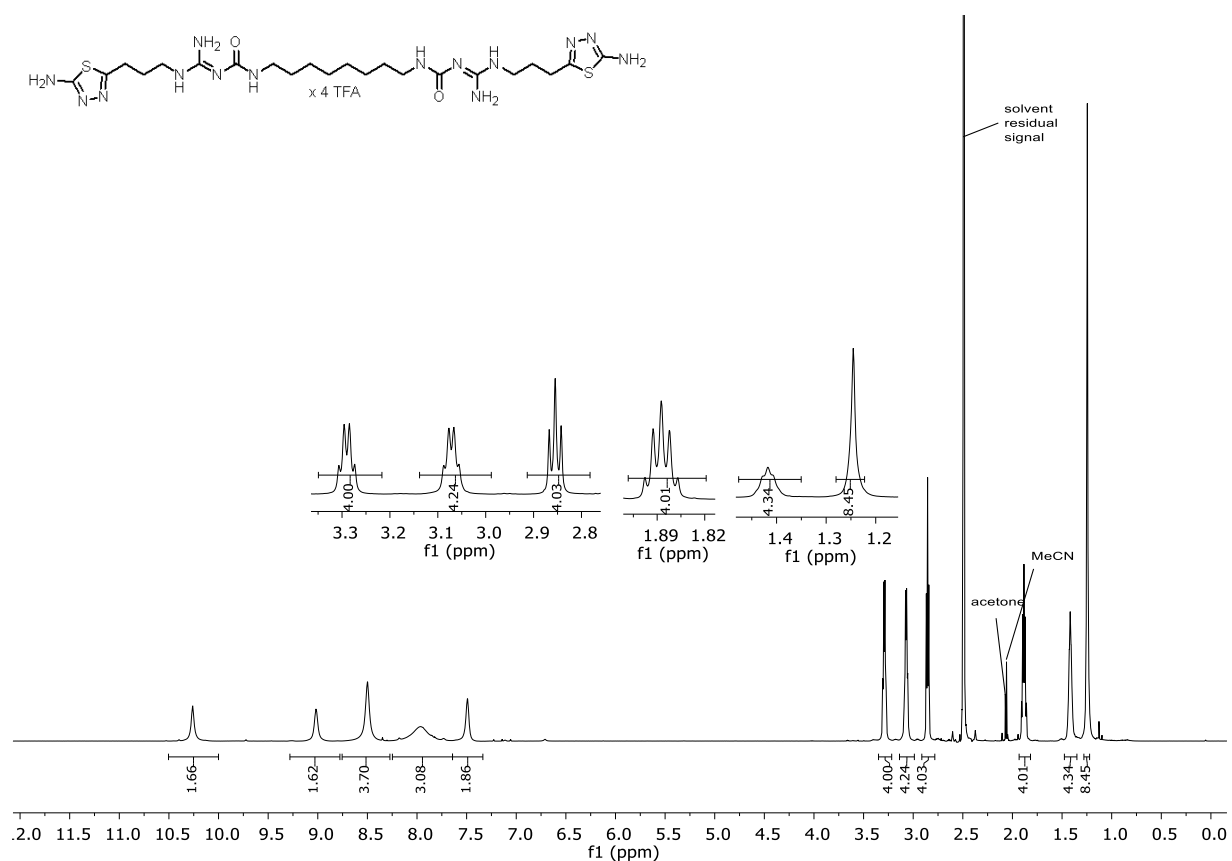
Figure 3.142. ^{1}H-NMR spectrum (600 MHz, DMSO-d$_6$) of compound **3.278**.
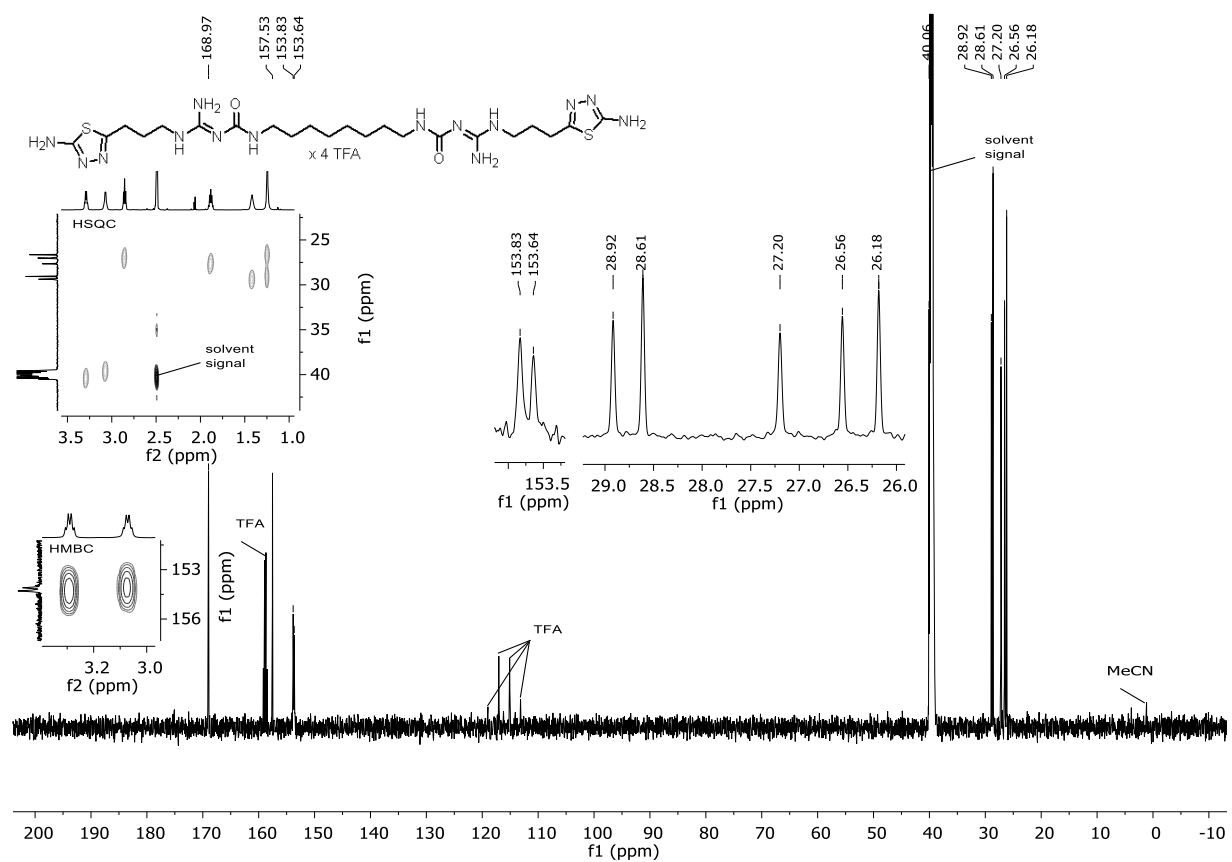
Figure 3.143. ^{13}C-NMR spectrum (151 MHz, DMSO-d$_6$) of compound **3.278**.

3.6.2 RP-HPLC Purity Control of Compounds 3.138-3.186 and 3.238-3.278
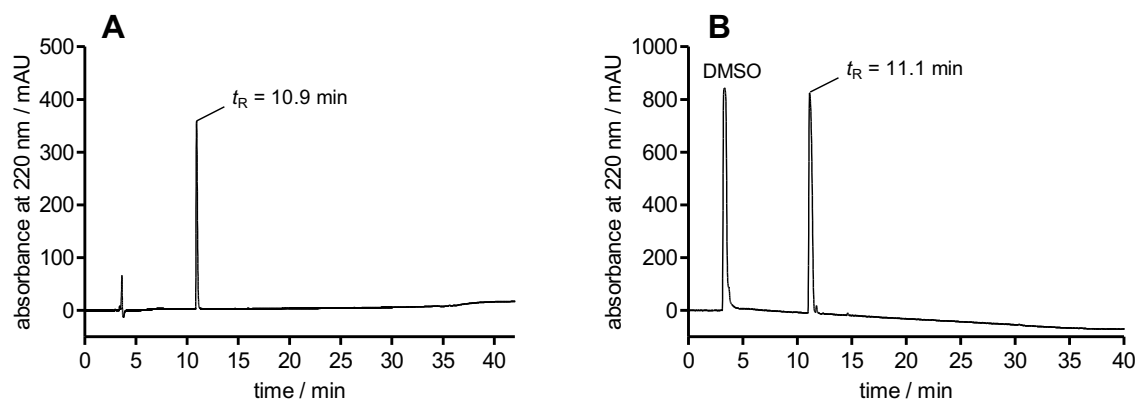
Figure 3.144. RP-HPLC analysis (purity control) of compound **3.138** (A) (99%, 220 nm) and compound **3.139** (B) (99%, 220 nm).
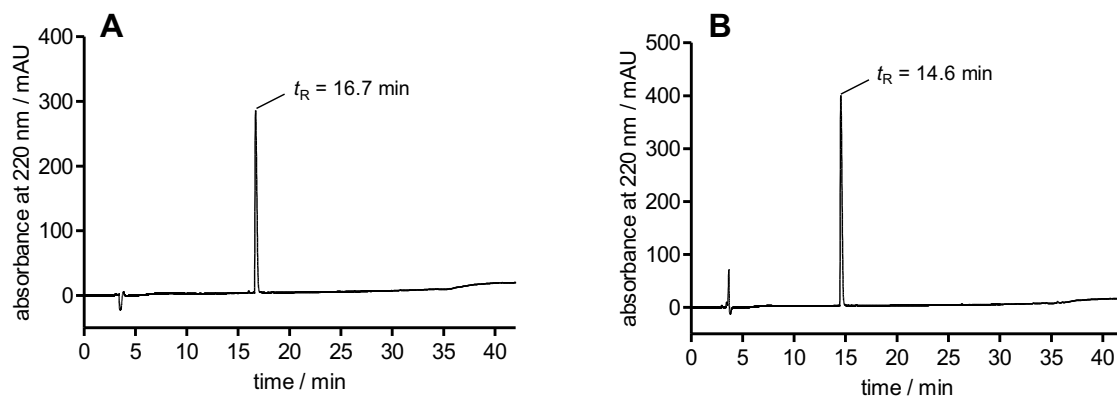
Figure 3.145. RP-HPLC analysis (purity control) of compound **3.140** (A) (99%, 220 nm) and compound **3.141** (B) (99%, 220nm)
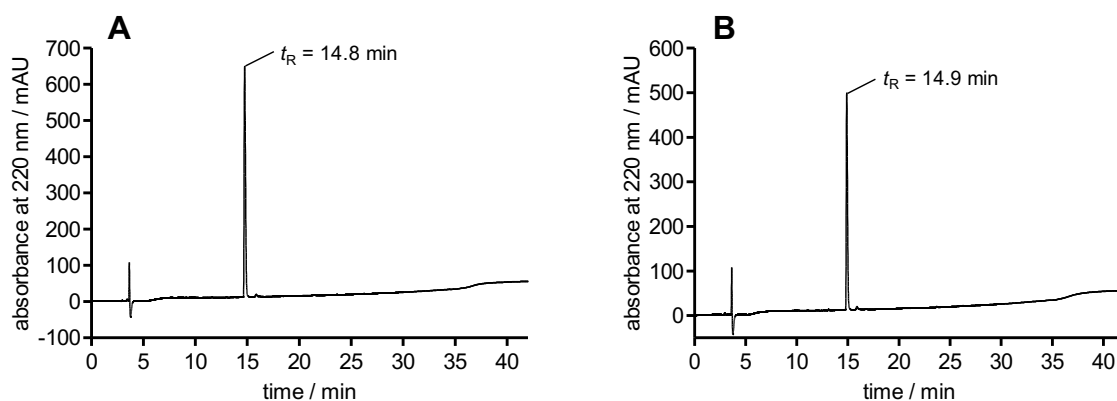
Figure 3.146. RP-HPLC analysis (purity control) of compound **3.142** (A) (99%, 220 nm) and compound **3.143** (B) (97%, 220 nm).
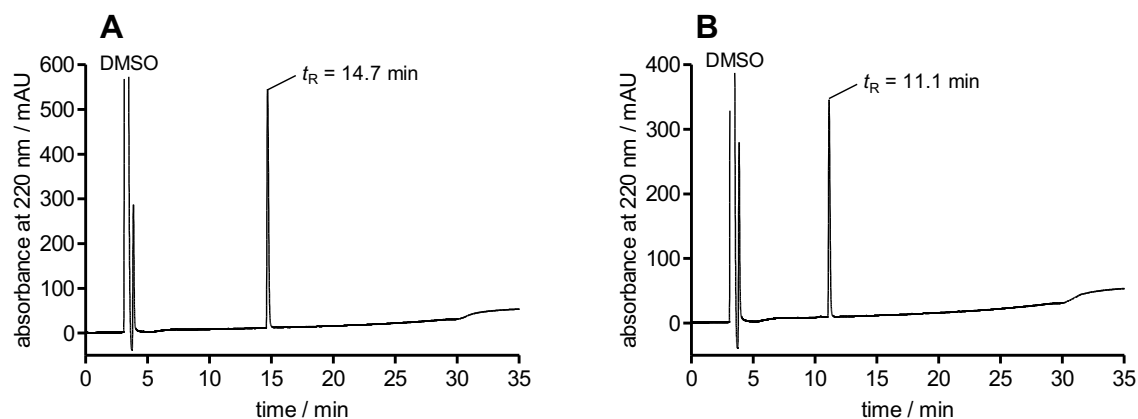
Figure 3.147. RP-HPLC analysis (purity control) of compound **3.144** (A) (99%, 220 nm) and compound **3.145** (B) (99%, 220 nm).
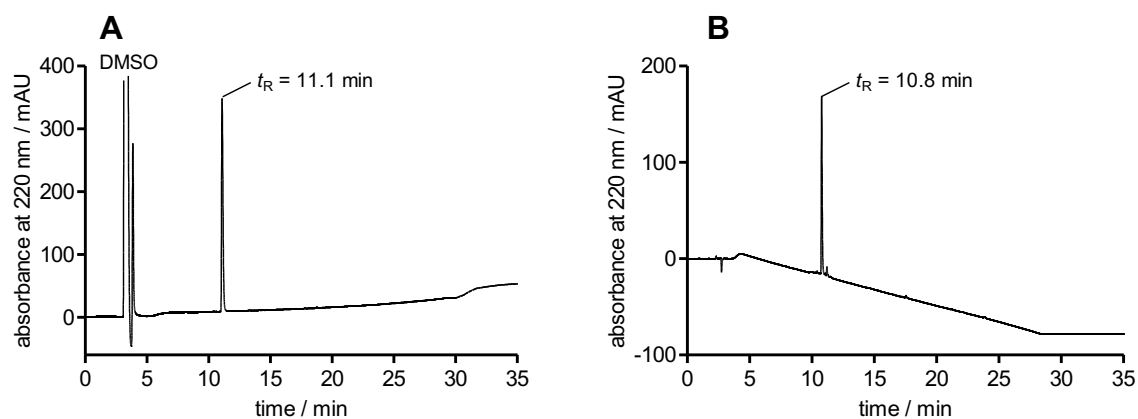
Figure 3.148. RP-HPLC analysis (purity control) of compound **3.146** (A) (99%, 220 nm) and compound **3.147** (B) (96%, 220 nm).
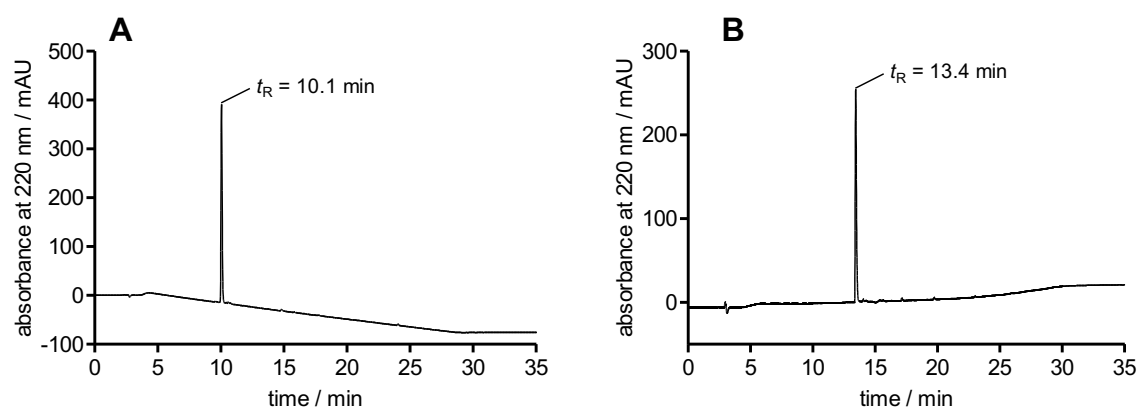
Figure 3.149. RP-HPLC analysis (purity control) of compound **3.148** (99%, 220 nm) and compound **3.149** (B) (97%, 220 nm).
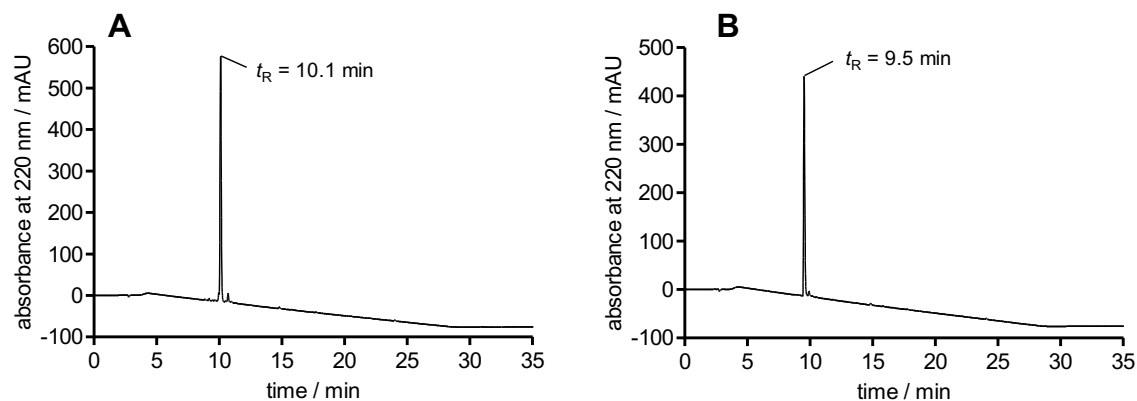
Figure 3.150. RP-HPLC analysis (purity control) of compound **3.150** (96%, 220 nm) and of compound **3.151** (B) (97%, 220 nm).
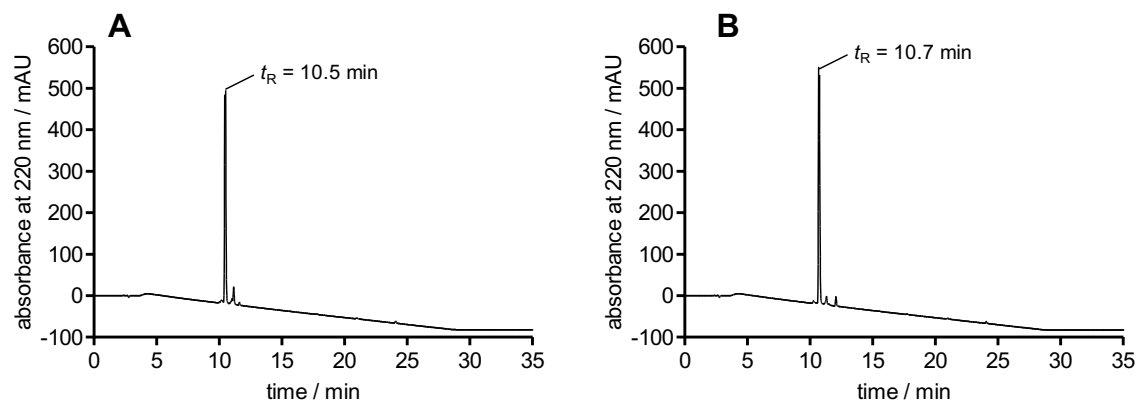
Figure 3.151. RP-HPLC analysis (purity control) of compound **3.152** (A) (96%, 220 nm) and compound **3.153** (B) (96%, 220 nm).
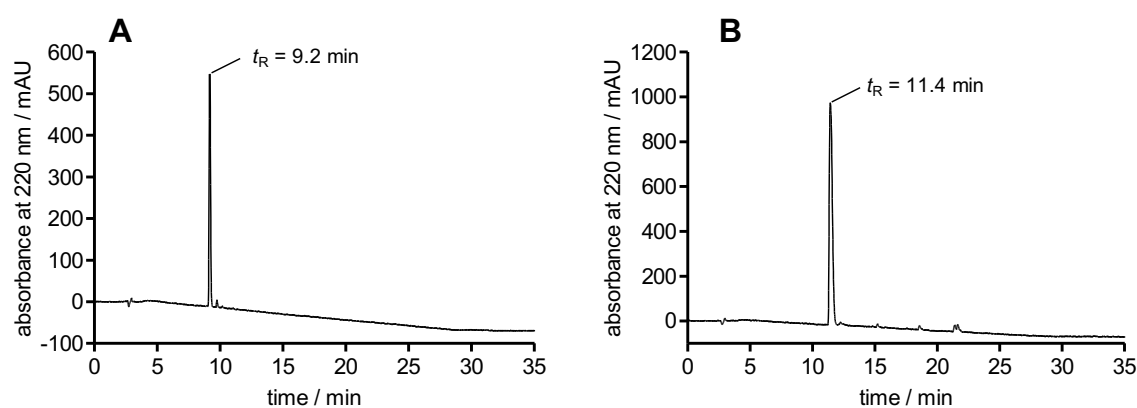
Figure 3.152. RP-HPLC analysis (purity control) of compound **3.154** (A) (97%, 220 nm) and compound **3.155** (B) (95%, 220 nm).
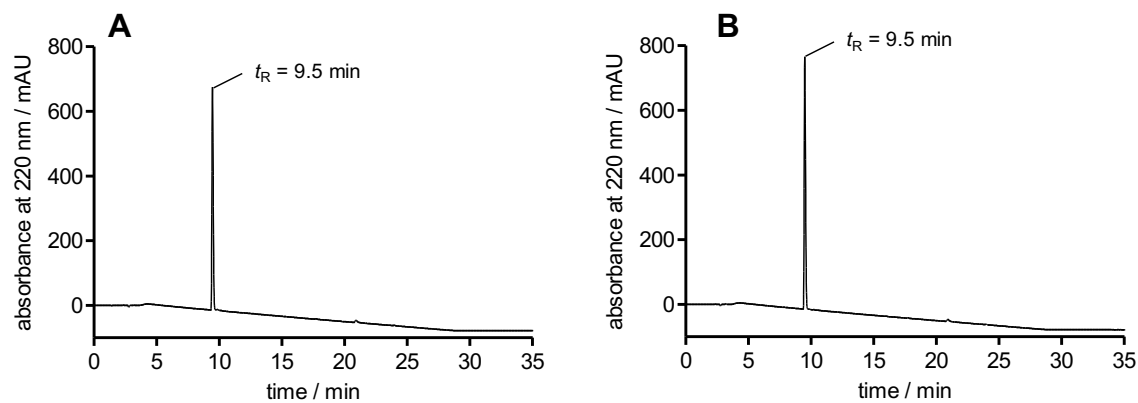
Figure 3.153. RP-HPLC analysis (purity control) of compound **3.156** (A) (99%, 220 nm) and compound **3.157** (B) (99%, 220 nm).
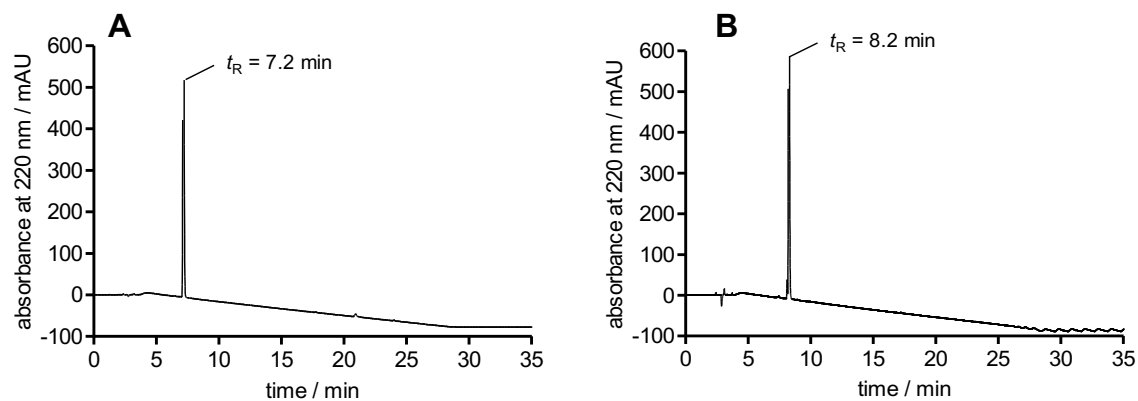
Figure 3.154. RP-HPLC analysis (purity control) of compound **3.158** (A) (99%, 220 nm) and compound **3.159** (B) (99%, 220 nm).
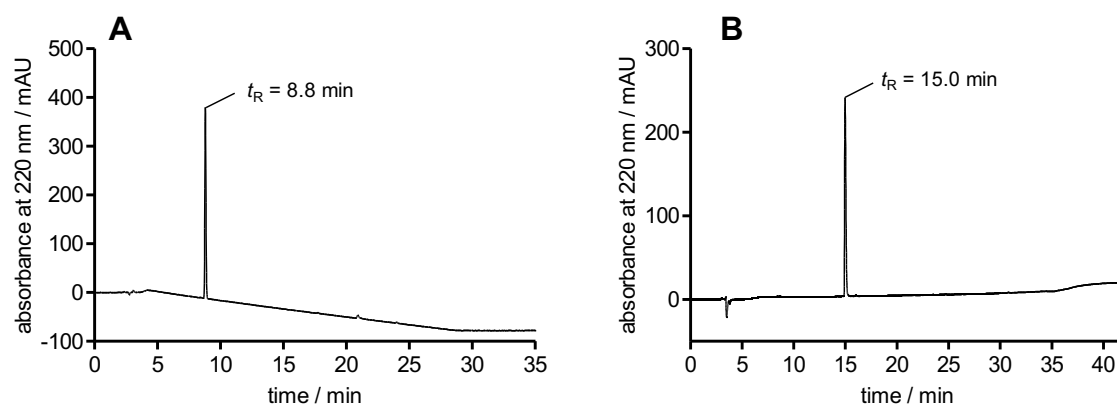
Figure 3.155. RP-HPLC analysis (purity control) of compound **3.160** (A) (99%, 220 nm) and compound **3.161** (B) (99%, 220 nm).
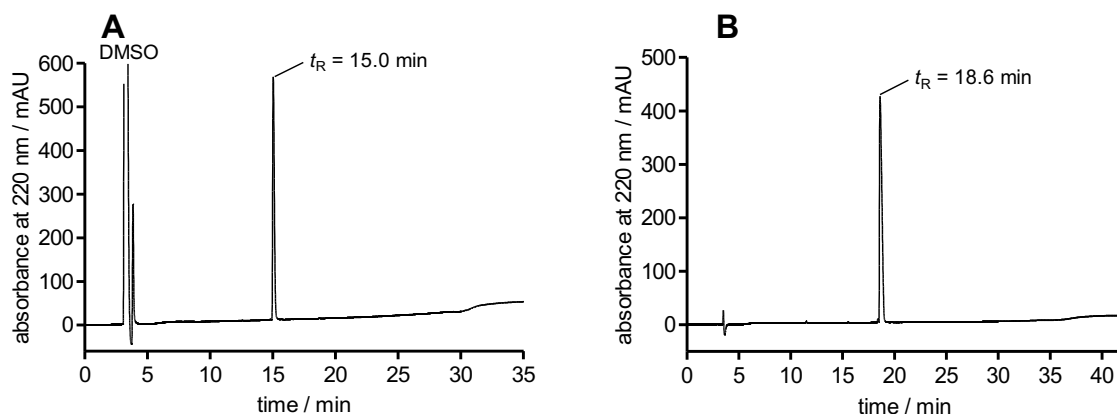
Figure 3.156. RP-HPLC analysis (purity control) of compound **3.162** (A) (99%, 220 nm) and compound **3.163** (B) (99%, 220 nm).
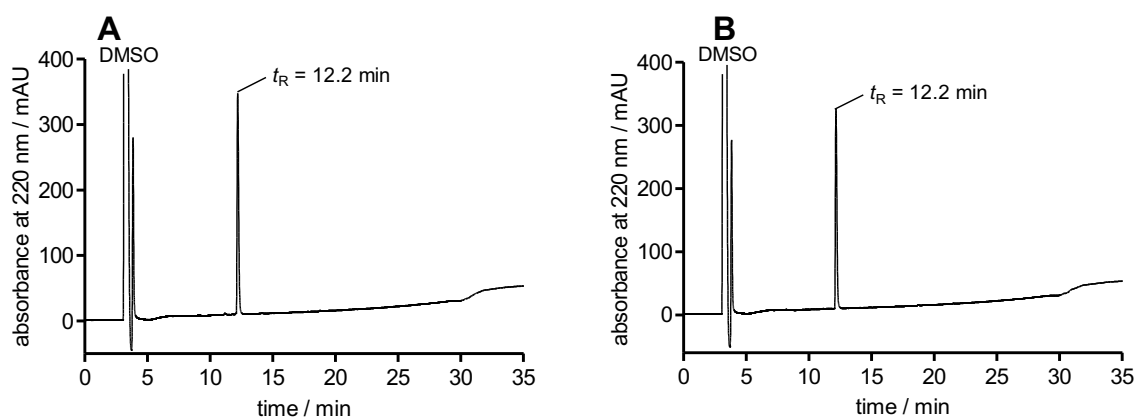
Figure 3.157. RP-HPLC analysis (purity control) of compound **3.164** (A) (99%, 220 nm) and compound **3.165** (B) (99%, 220 nm).
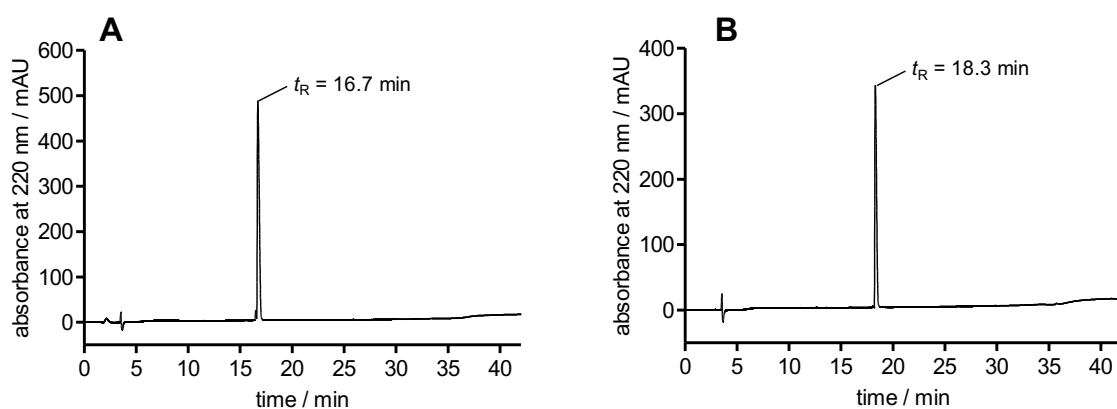
Figure 3.158. RP-HPLC analysis (purity control) of compound **3.166** (A) (98%, 220 nm) and compound **3.167** (B) (99%, 220 nm).
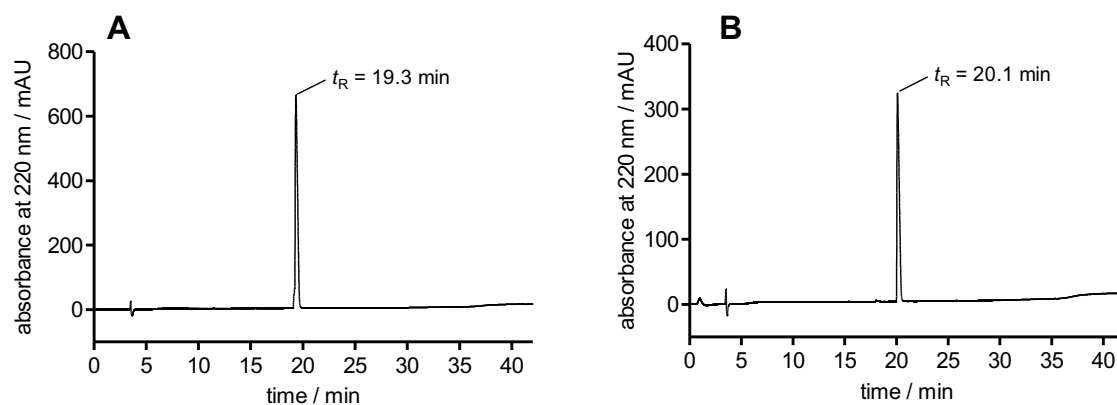
Figure 3.159. RP-HPLC analysis (purity control) of compound **3.168** (A) (96%, 220 nm) and compound **3.169** (B) (99%, 220 nm).
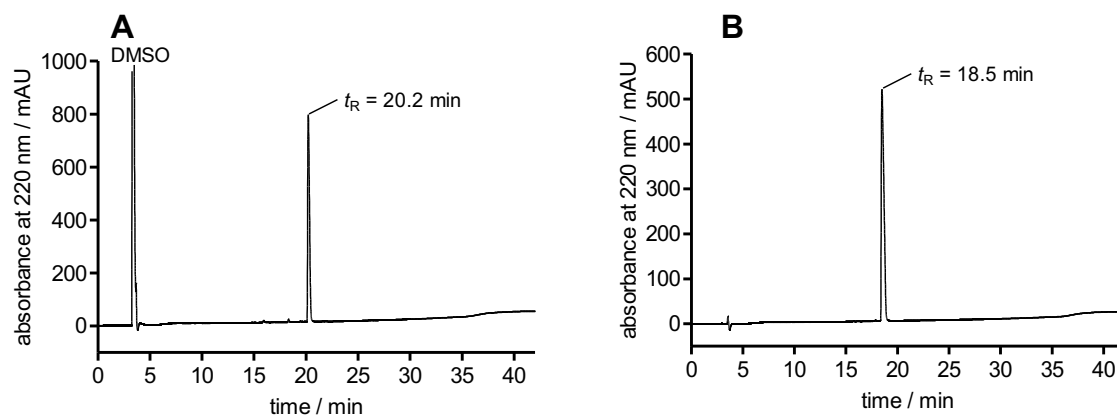
Figure 3.160. RP-HPLC analysis (purity control) of compound **3.170** (A) (98%, 220 nm) and compound **3.171** (B) (99%, 220 nm).
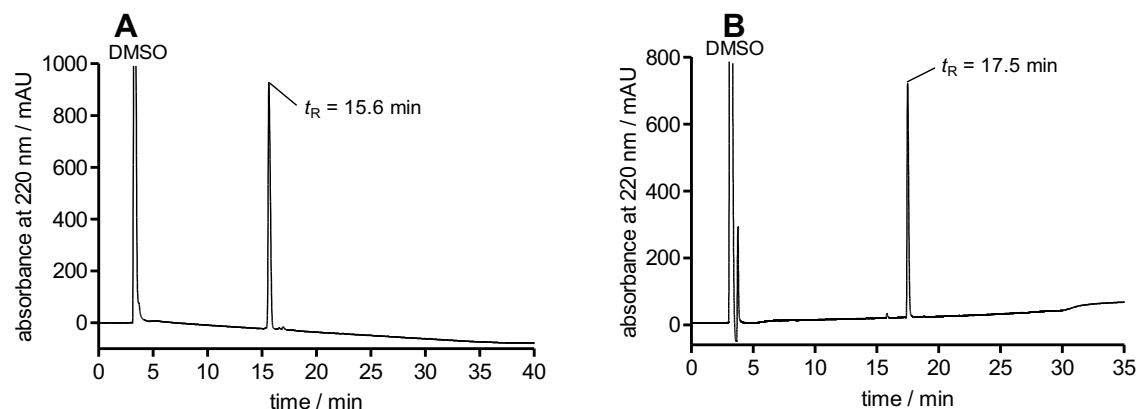
Figure 3.161. RP-HPLC analysis (purity control) of compound **3.172** (A) (98%, 220 nm) and compound **3.173** (B) (98%, 220 nm).
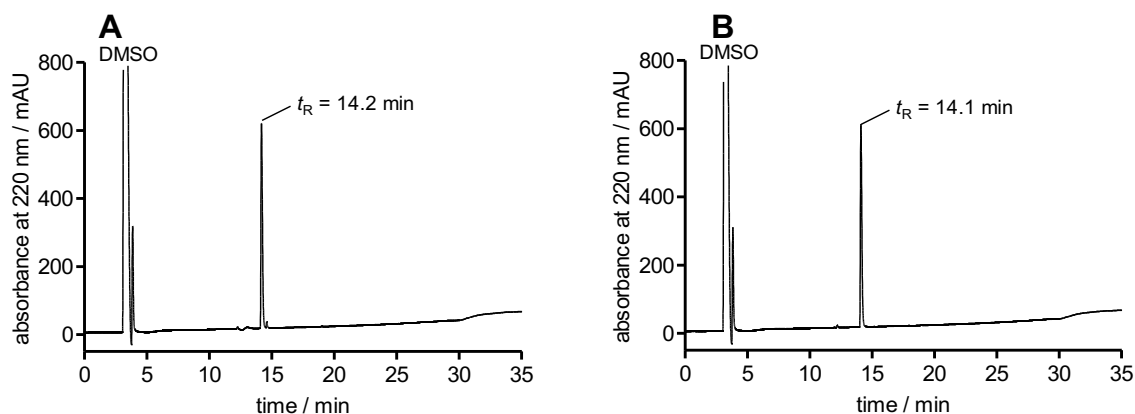
Figure 3.162. RP-HPLC analysis (purity control) of compound **3.174** (A) (95%, 220 nm) and compound **3.175** (B) (99%, 220 nm).
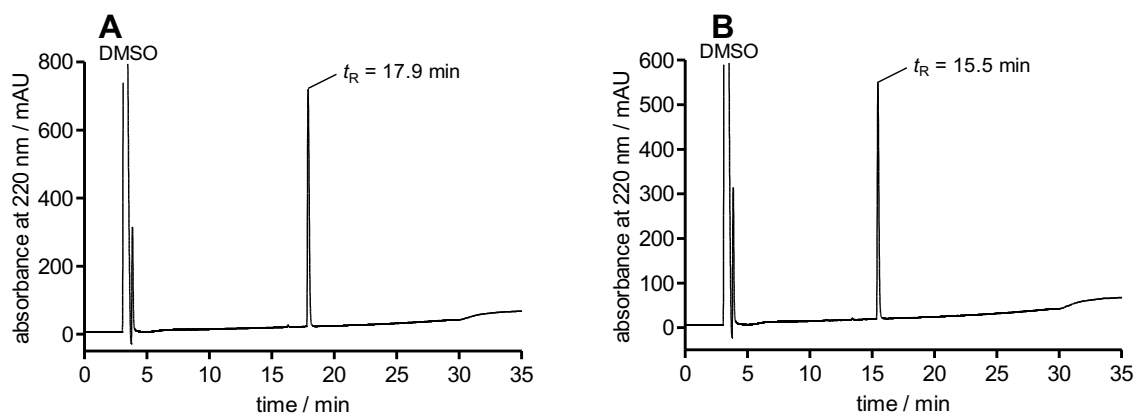
Figure 3.163. RP-HPLC analysis (purity control) of compound **3.176** (A) (99%, 220 nm) and compound **3.177** (B) (99%, 220 nm).
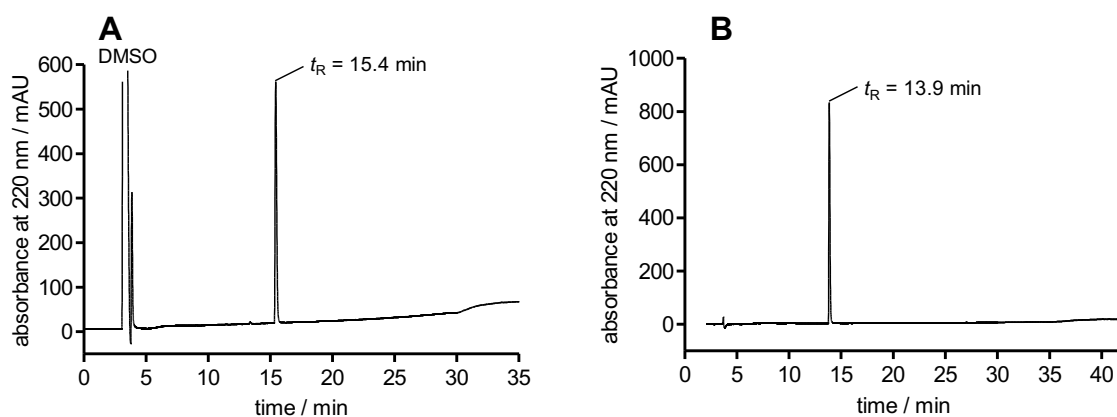
Figure 3.164. RP-HPLC analysis (purity control) of compound **3.178** (A) (99%, 220 nm) and compound **3.179** (B) (99%, 220 nm).
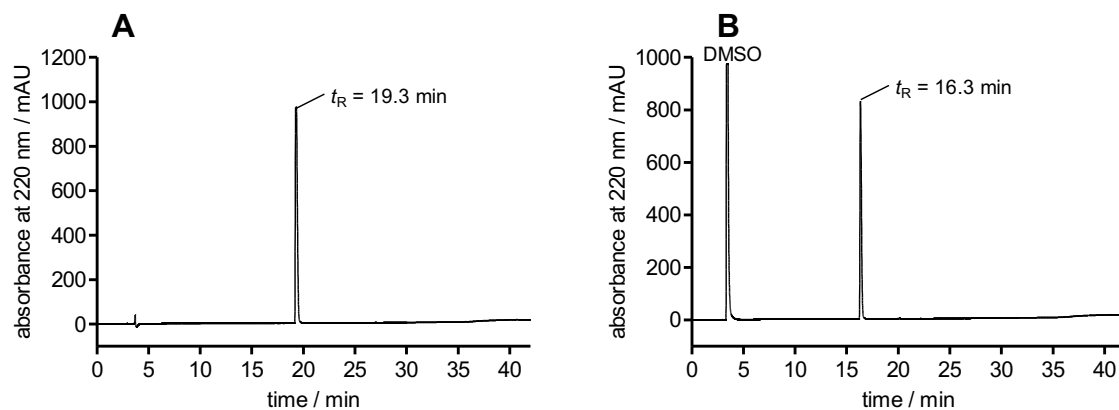
Figure 3.165. RP-HPLC analysis (purity control) of compound **3.180** (A) (99%, 220 nm) and compound **3.181** (B) (99%, 220 nm).
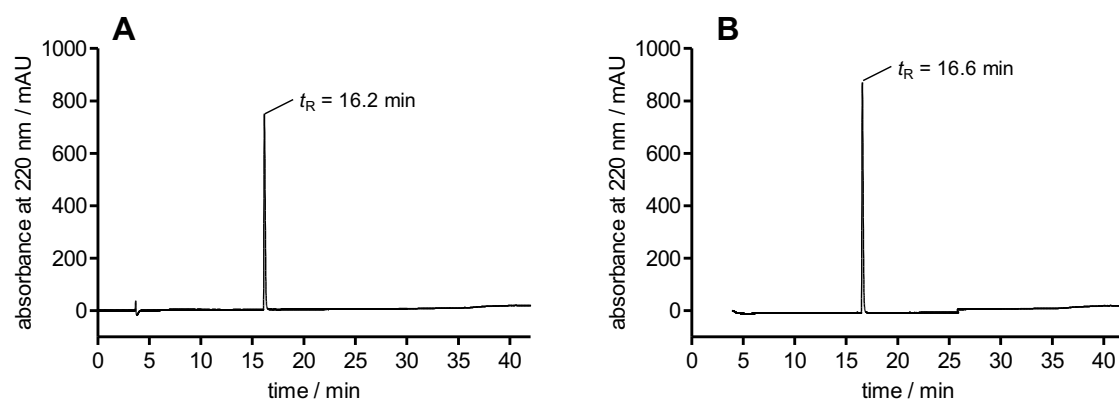
Figure 3.166. RP-HPLC analysis (purity control) of compound **3.182** (A) (99%, 220 nm) and compound **3.183** (B) (99%, 220 nm).
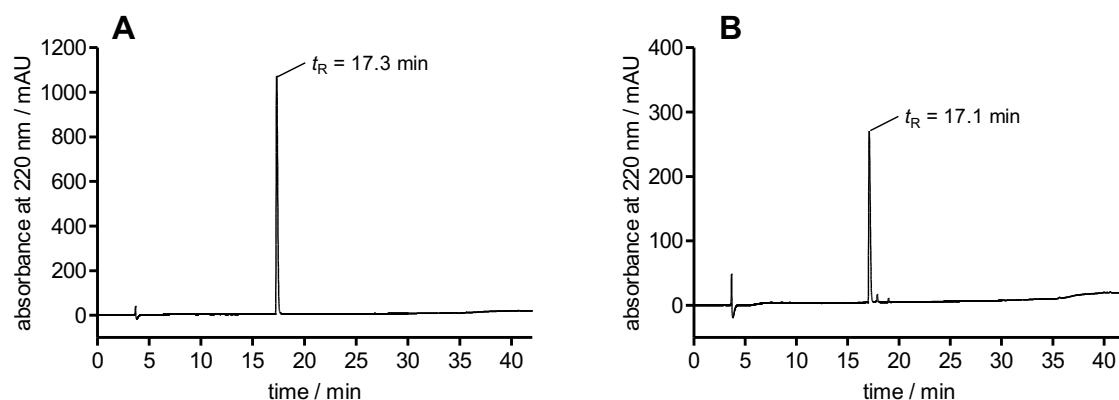
Figure 3.167. RP-HPLC analysis (purity control) of compound **3.184** (A) (99%, 220 nm) and compound **3.185** (B) (95%, 220 nm).
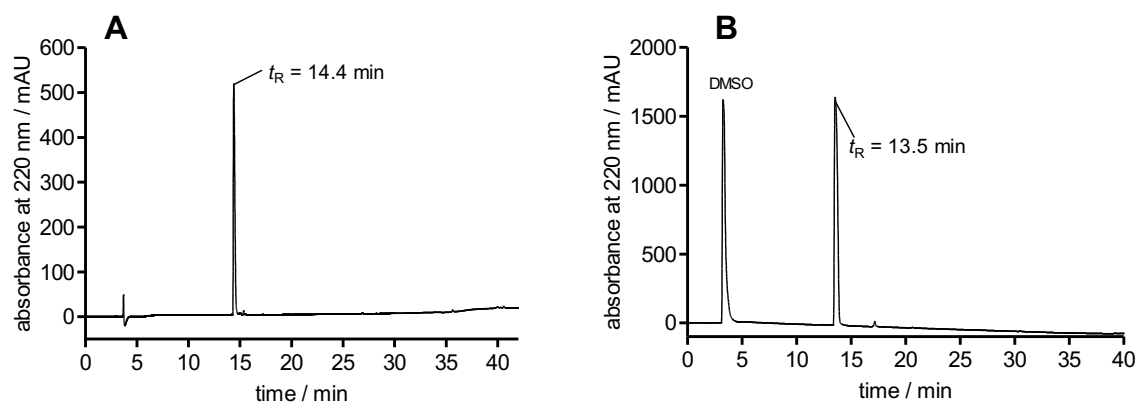
Figure 3.168. RP-HPLC analysis (purity control) of compound **3.186** (A) (97%, 220 nm) and compound **3.238** (B) (98%, 220 nm).
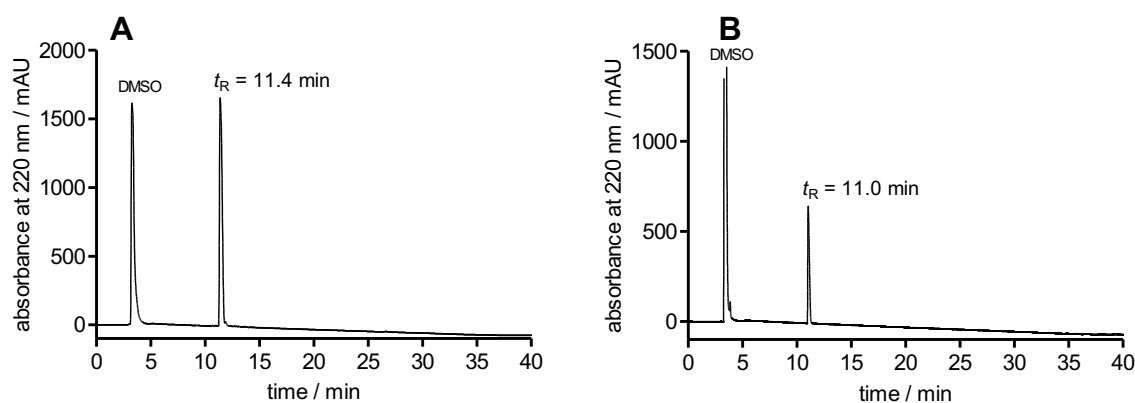
Figure 3.169. RP-HPLC analysis (purity control) of compound **3.239** (A) (99%, 220 nm) and compound **3.240** (B) (99%, 220 nm).
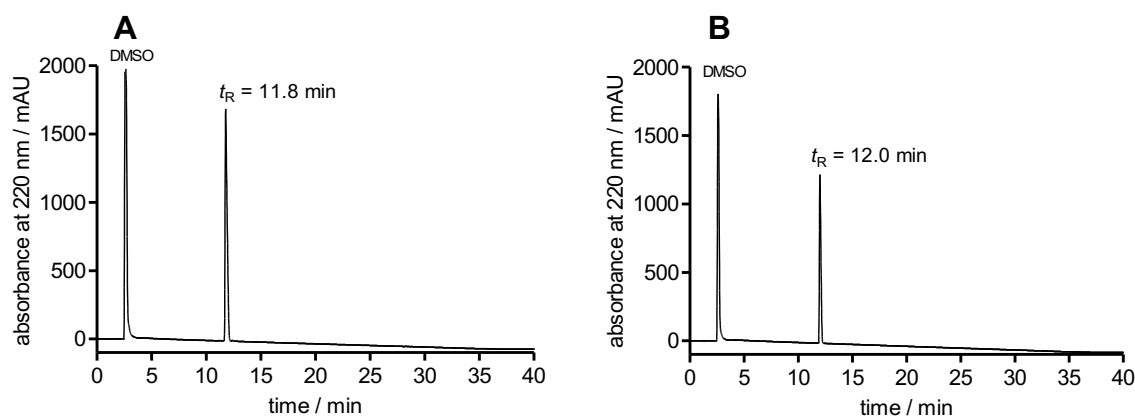
Figure 3.170. RP-HPLC analysis (purity control) of compound **3.241** (A) (> 99%, 220 nm) and compound **3.242** (B) (> 99%, 220 nm).
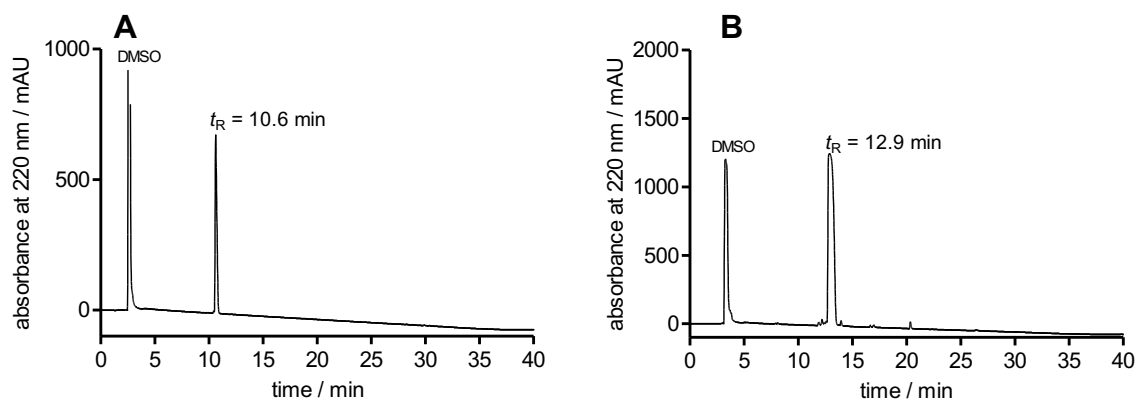
Figure 3.171. RP-HPLC analysis (purity control) of compound **3.243** (A) (> 99%, 220 nm) and compound **3.244** (B) (96%, 220 nm).
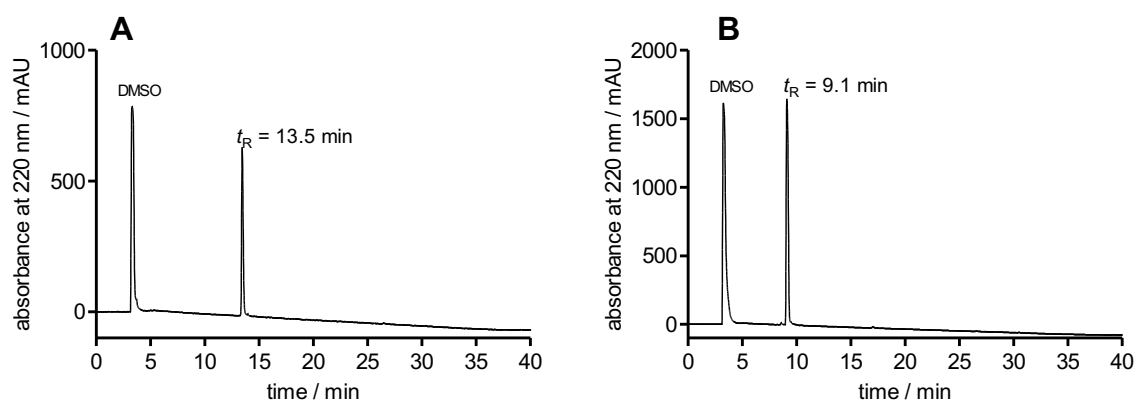
Figure 3.172. RP-HPLC analysis (purity control) of compound **3.245** (A) (99%, 220 nm) and compound **3.246** (B) (97%, 220 nm).
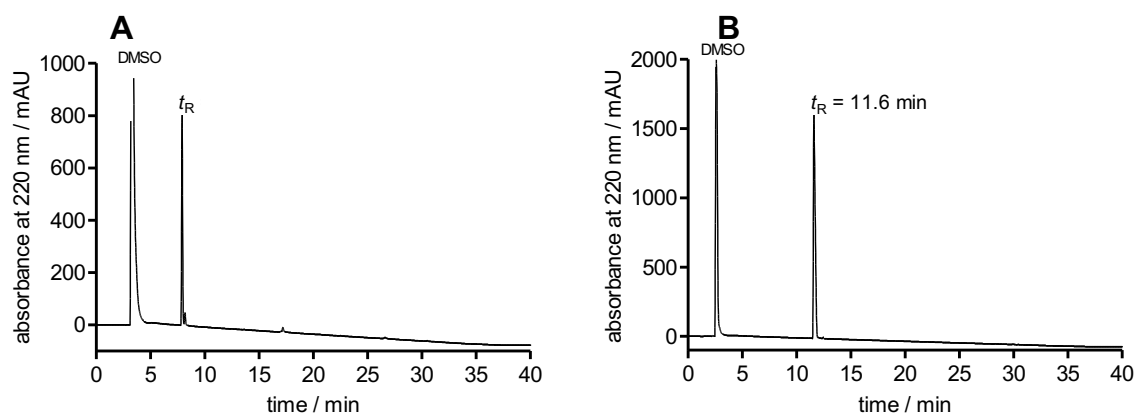
Figure 3.173. RP-HPLC analysis (purity control) of compound **3.247** (A) (96%, 220 nm) and compound **3.248** (B) (> 99%, 220 nm).
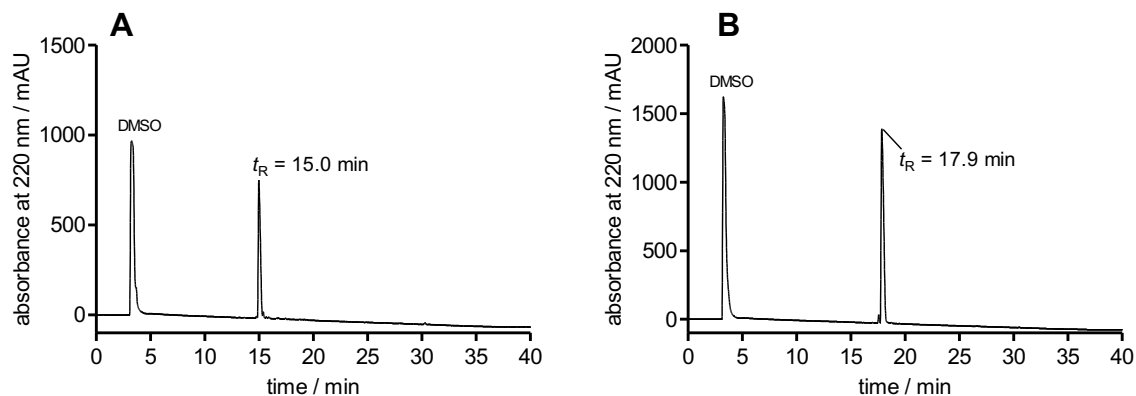
Figure 3.174. RP-HPLC analysis (purity control) of compound **3.249** (A) (97%, 220 nm) and compound **3.250** (B) (97%, 220 nm).
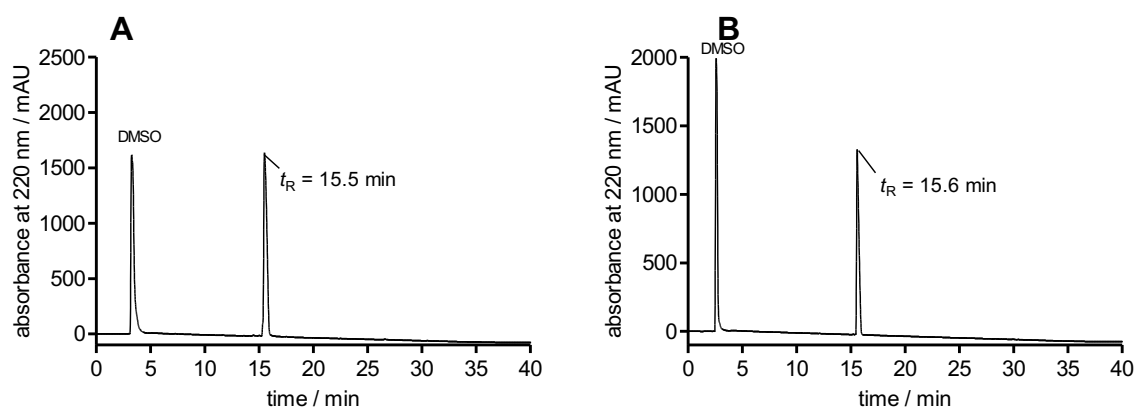
Figure 3.175. RP-HPLC analysis (purity control) of compound **3.251** (A) (99%, 220 nm) and compound **3.252** (B) (> 99%, 220 nm).
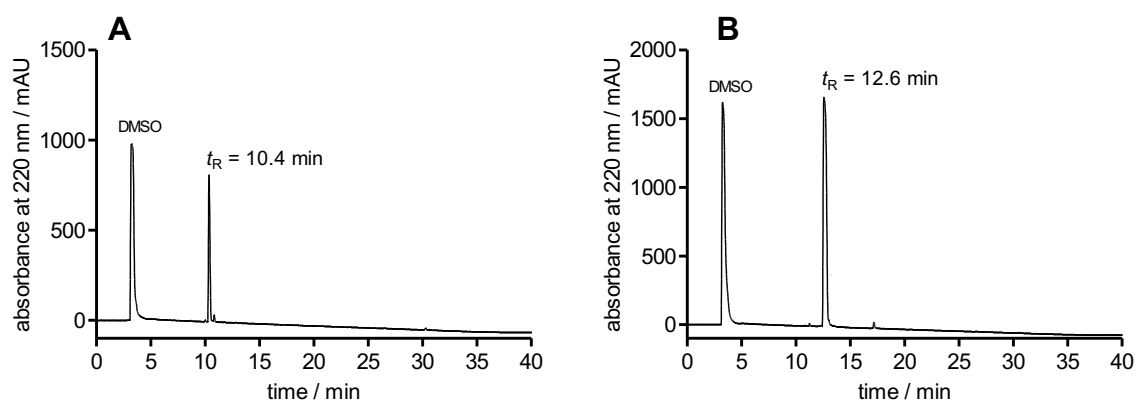
Figure 3.176. RP-HPLC analysis (purity control) of compound **3.253** (A) (96%, 220 nm) and compound **3.254** (B) (98%, 220 nm).
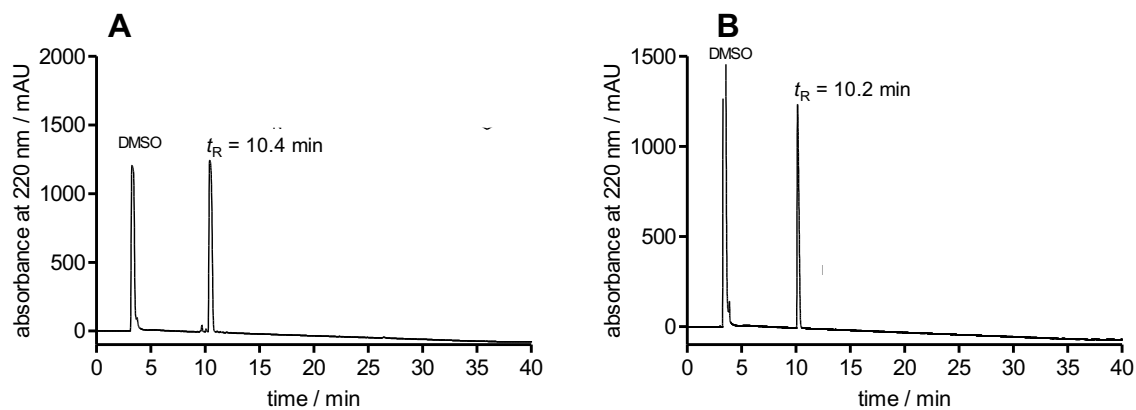
Figure 3.177. RP-HPLC analysis (purity control) of compound **3.255** (A) (98%, 220 nm) and compound **3.256** (B) (> 99%, 220 nm).
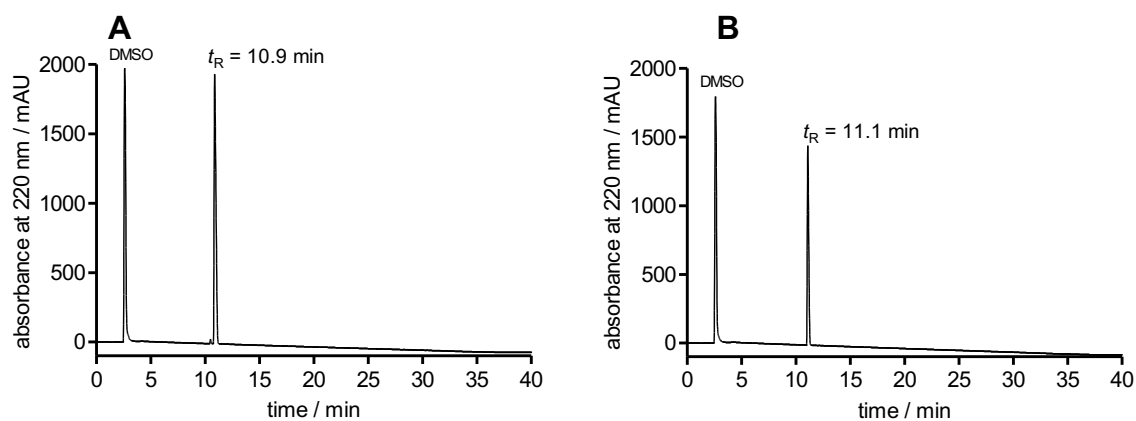
Figure 3.178. RP-HPLC analysis (purity control) of compound **3.257** (A) (99%, 220 nm) and compound **3.258** (B) (> 99%, 220 nm).
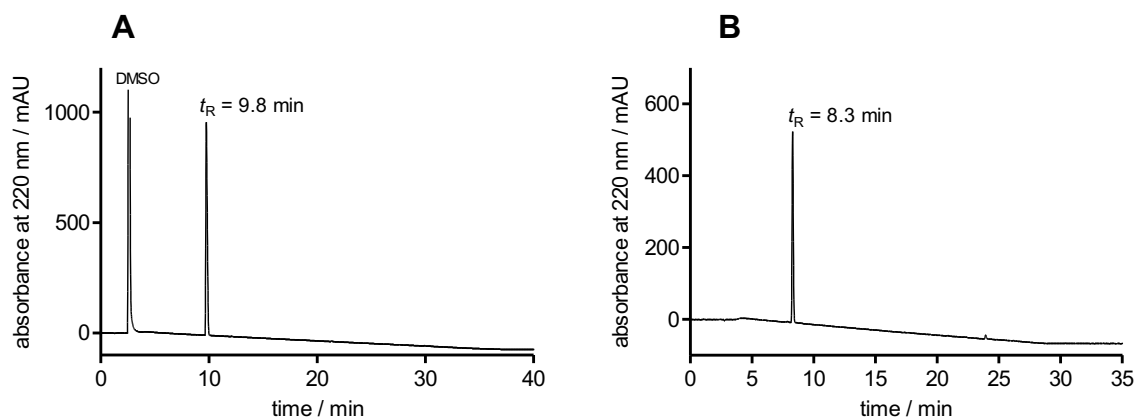
Figure 3.179. RP-HPLC analysis (purity control) of compound **3.259** (A) (> 99%, 220 nm) and compound **3.260** (B) (> 99%, 220 nm).
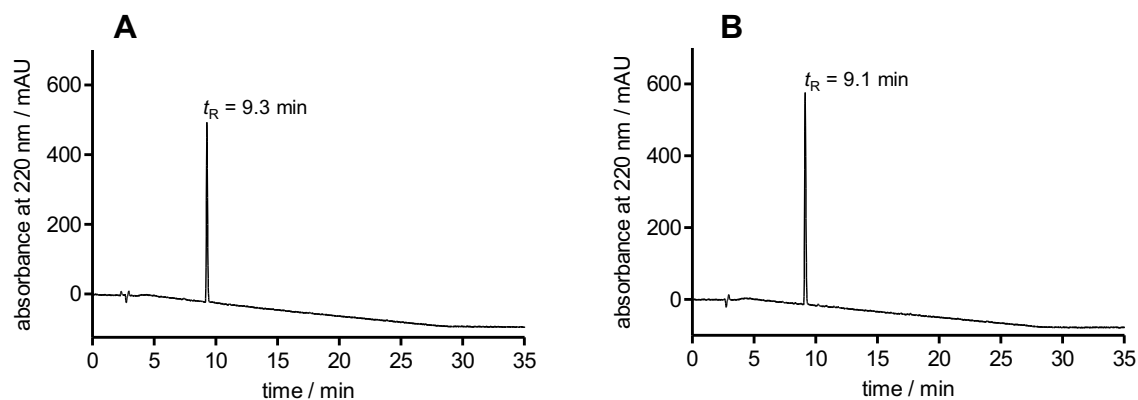
Figure 3.180. RP-HPLC analysis (purity control) of compound **3.261** (A) (> 99%, 220 nm) and compound **3.262** (B) (> 99%, 220 nm).
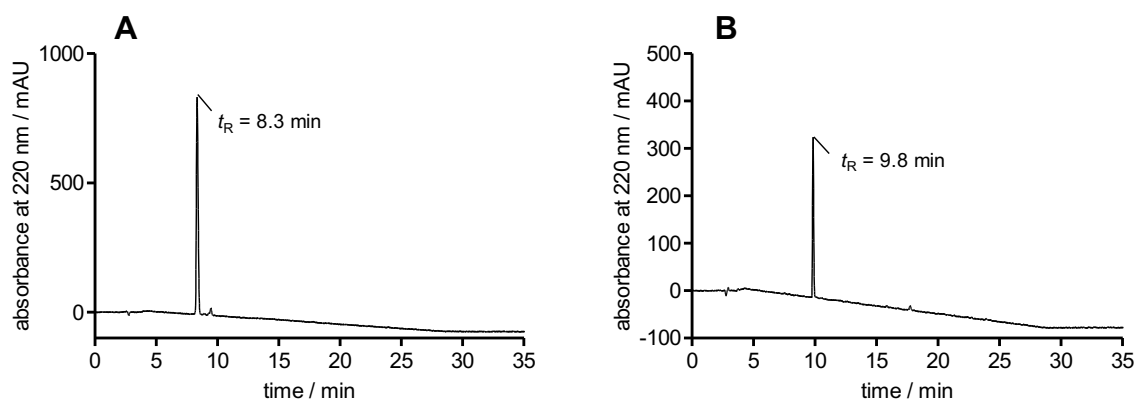
Figure 3.181. RP-HPLC analysis (purity control) of compound **3.263** (A) (98%, 220 nm) and compound **3.264** (B) (> 99%, 220 nm).
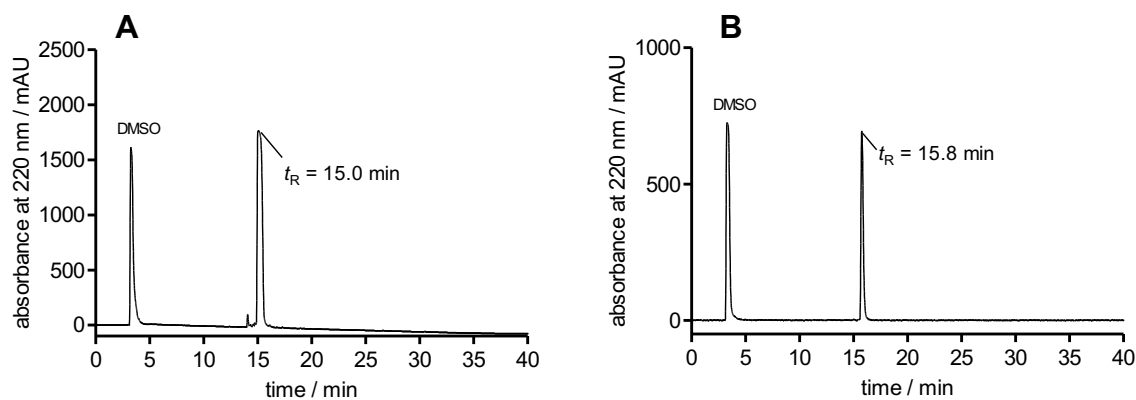
Figure 3.182. RP-HPLC analysis (purity control) of compound **3.265** (A) (98%, 220 nm) and compound **3.266** (B) (> 99%, 220 nm).
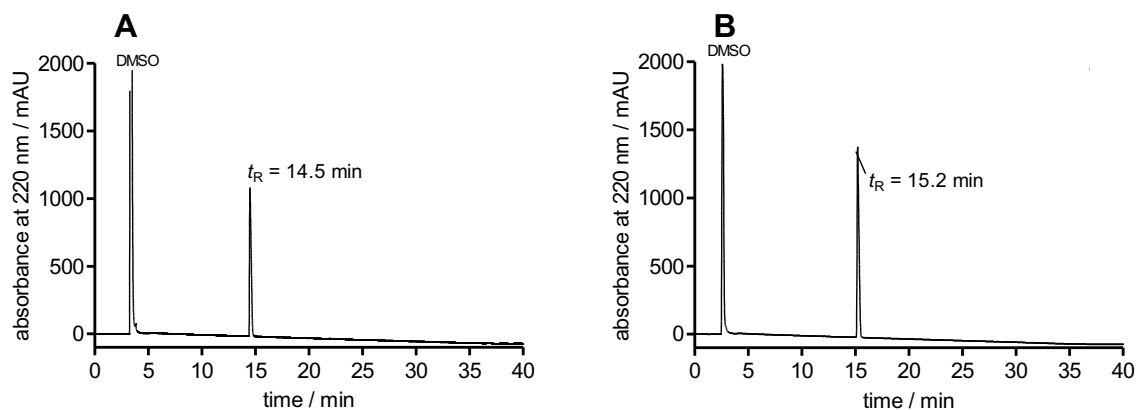
Figure 3.183. RP-HPLC analysis (purity control) of compound **3.267** (A) (99%, 220 nm) and compound **3.268** (B) (> 99%, 220 nm).
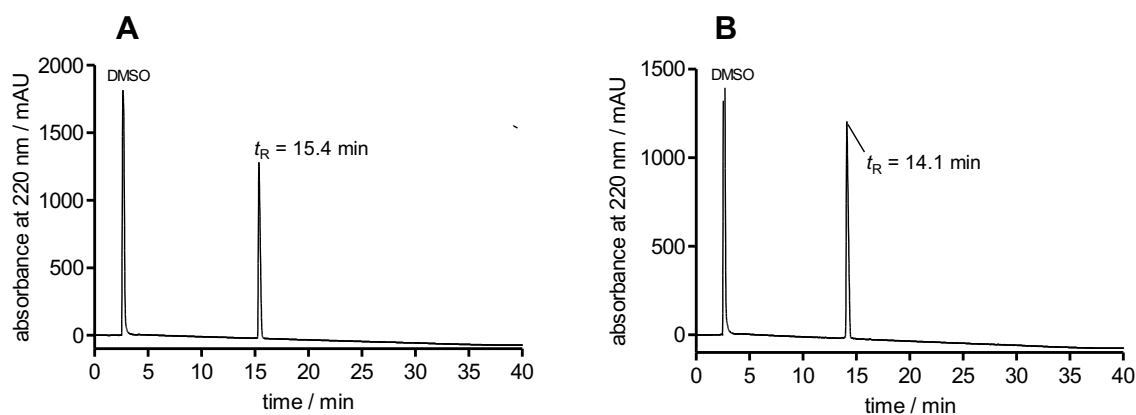
Figure 3.184. RP-HPLC analysis (purity control) of compound **3.269** (A) (> 99%, 220 nm) and compound **3.270** (B) (99%, 220 nm).
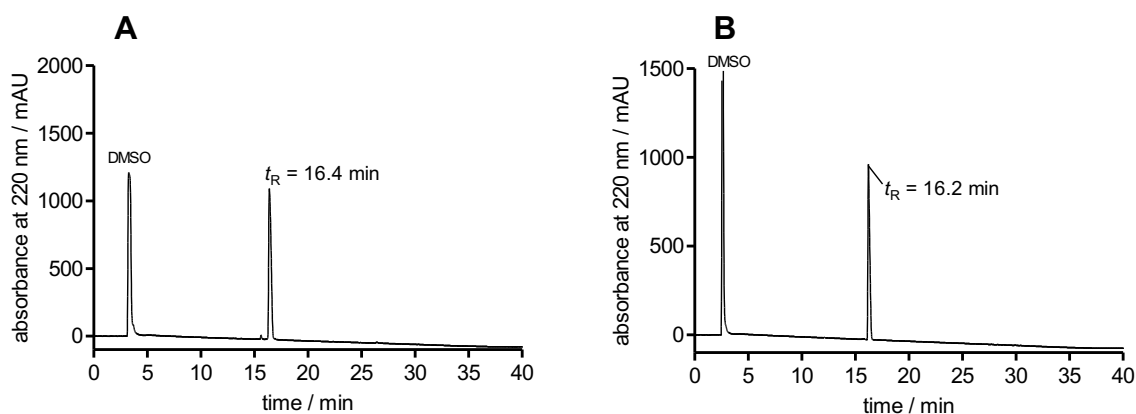
Figure 3.185. RP-HPLC analysis (purity control) of compound **3.271** (A) (97%, 220 nm) and compound **3.272** (B) (> 99%, 220 nm).
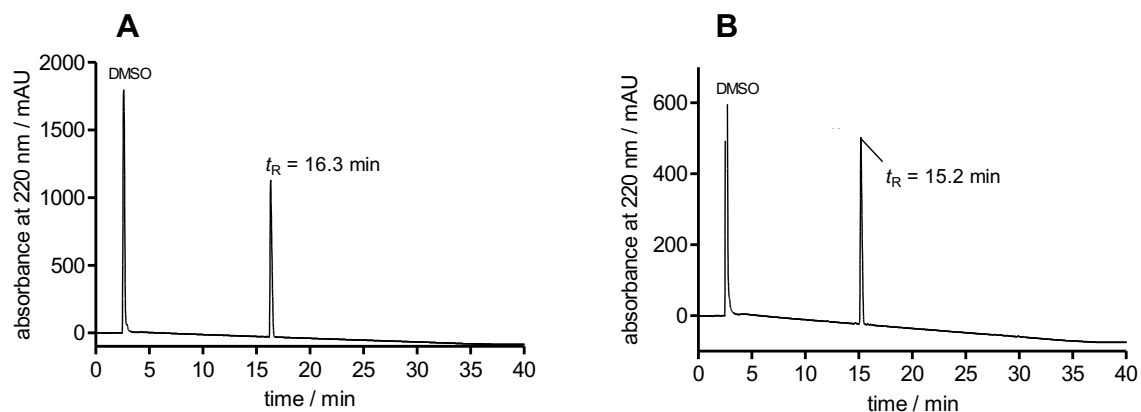
Figure 3.186. RP-HPLC analysis (purity control) of compound **3.273** (A) (99%, 220 nm) and compound **3.274** (B) (> 99%, 220 nm).
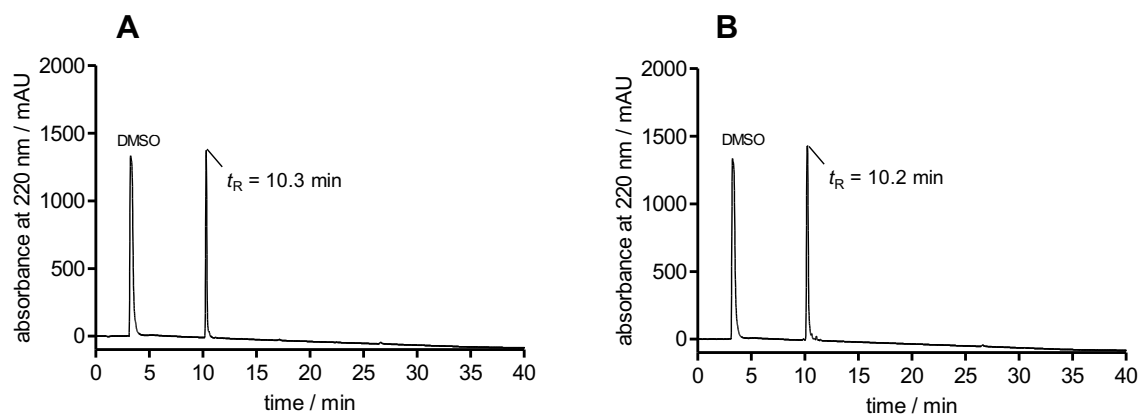
Figure 3.187. RP-HPLC analysis (purity control) of compound **3.275** (A) (98%, 220 nm) and compound **3.276** (B) (98%, 220 nm).
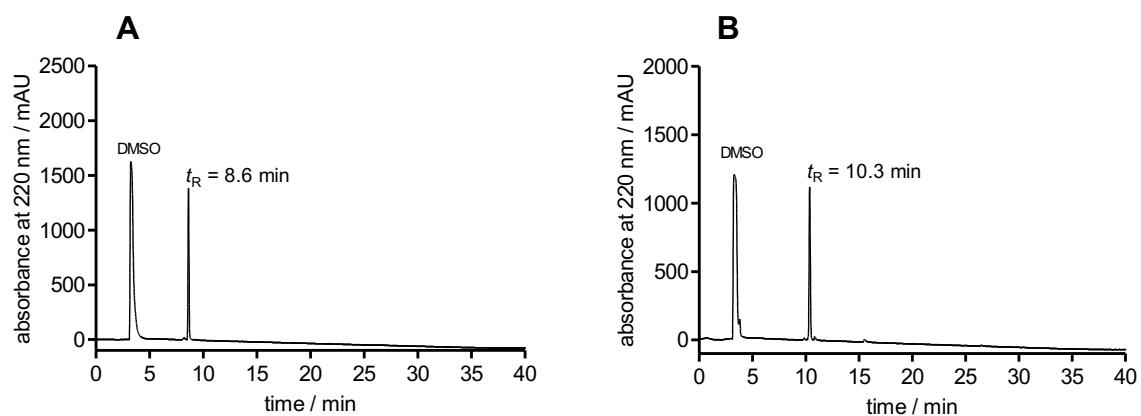
Figure 3.188. RP-HPLC analysis (purity control) of compound **3.277** (A) (96%, 220 nm) and compound **3.278** (B) (96%, 220 nm).

3.6.3 Titration Curves of the pK_a Determination of Compounds 3.145, 3.213 and 3.216
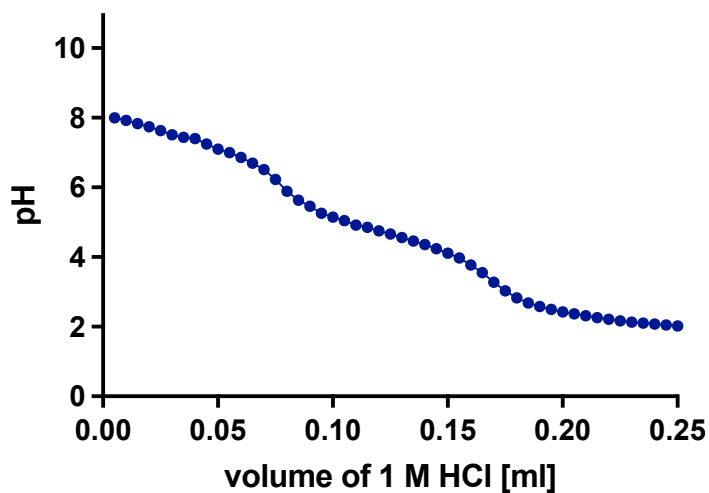
Figure 3.189. Representative pK_a titration curve of **3.145** using 1 M HCl.
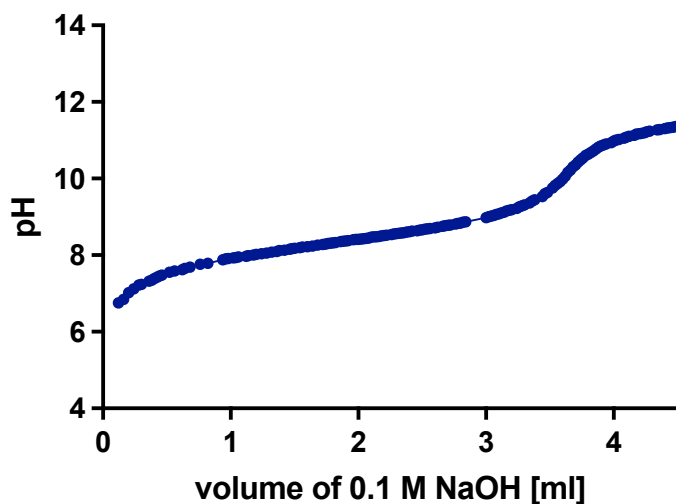
Figure 3.190. Representative pK_a titration curve of **3.213** using 0.1 M NaOH.
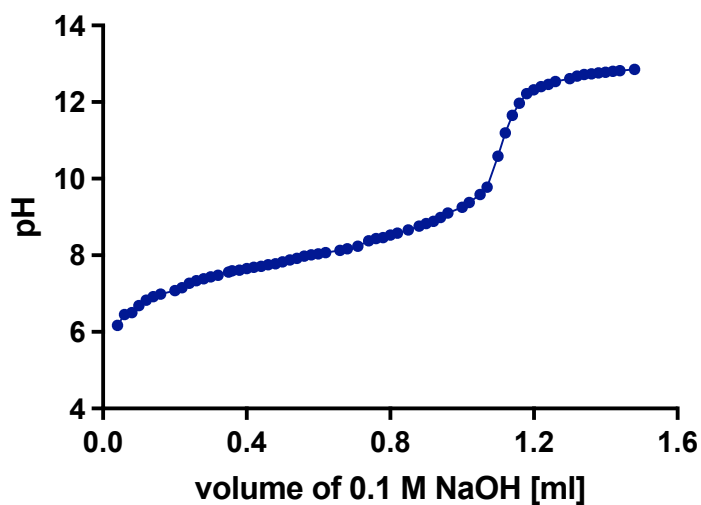
Figure 3.191. Representative pK_a titration curve of **3.216** using 0.1 M NaOH.

3.6.4 MS (ESI) Data of the Boc-/Trt-protected Intermediates 3.238-3.244, 3.246-3.265, and 3.267-3.278

Table 3.16. MS (ESI) data of Boc-/Trt-protected intermediates.

Comp.	MW	Structure	Calculated for [M+H]$^+$	Found
Boc-**3.238**	C$_{18}$H$_{32}$N$_6$O$_3$S		413.2329	413.2361
di-Boc-**3.239**	C$_{22}$H$_{39}$N$_7$O$_5$S		514.2806	514.2826
di-Boc-**3.240**	C$_{23}$H$_{40}$N$_6$O$_5$S		513.2854	513.2876
di-Boc-**3.241**	C$_{27}$H$_{40}$N$_6$O$_5$S		561.2854	561.2911
di-Boc-**3.242**	C$_{27}$H$_{40}$N$_6$O$_5$S		561.2854	561.2890
Boc-/Trt-**3.243**	C$_{39}$H$_{48}$N$_6$O$_3$S		681.3581	681.3588
di-Boc-**3.244**	C$_{23}$H$_{41}$N$_7$O$_5$S		528.2963	528.2973
di-Boc-**3.246**	C$_{26}$H$_{47}$N$_7$O$_5$S		570.3432	570.3430
tri-Boc-**3.247**	C$_{30}$H$_{54}$N$_8$O$_7$S		671.3909	671.3938
di-Boc-**3.248**	C$_{28}$H$_{40}$N$_6$O$_5$S		573.2854	573.2905
di-Boc-**3.249**	C$_{28}$H$_{48}$N$_6$O$_6$		565.3708	565.3714
Boc-**3.250**	C$_{22}$H$_{38}$N$_6$O$_3$S		467.2799	467.2846
di-Boc-**3.251**	C$_{26}$H$_{45}$N$_7$O$_5$S		568.3276	568.3319
Boc-/Trt-**3.252**	C$_{31}$H$_{46}$N$_6$O$_5$S		615.3323	615.3333
di-Boc-**3.253**	C$_{26}$H$_{38}$N$_6$O$_6$		531.2926	531.2932
Boc-**3.254**	C$_{20}$H$_{28}$N$_6$O$_3$S		433.2016	433.2028

Table 3.16. (continued)
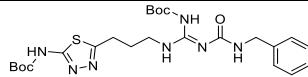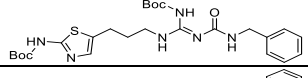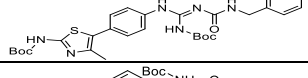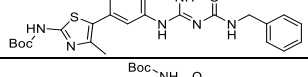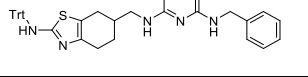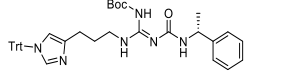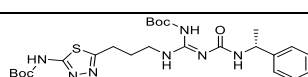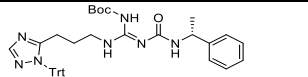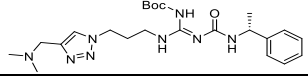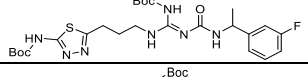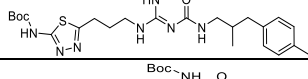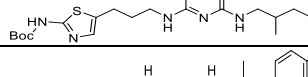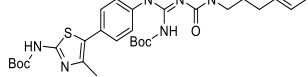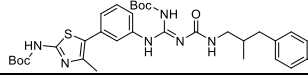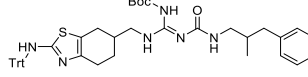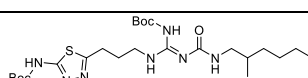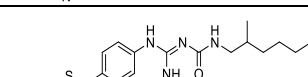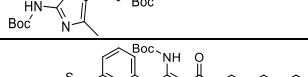
Comp.	MW	Structure	Calculated for [M+H]$^+$	Found
di-Boc-**3.255**	C$_{24}$H$_{35}$N$_7$O$_5$S		534.2493	534.2515
di-Boc-**3.256**	C$_{25}$H$_{36}$N$_6$O$_5$S		533.2541	533.2558
di-Boc-**3.257**	C$_{29}$H$_{36}$N$_6$O$_5$S		581.2541	581.2574
di-Boc-**3.258**	C$_{29}$H$_{36}$N$_6$O$_5$S		581.2541	581.2570
Boc-/Trt-**3.259**	C$_{41}$H$_{44}$N$_6$O$_3$S		701.3268	701.3277
Boc-/Trt-**3.260**	C$_{40}$H$_{44}$N$_6$O$_3$		657.3548	656.3554
di-Boc-**3.261**	C$_{25}$H$_{37}$N$_7$O$_5$S		548.2650	548.2659
Trt-**3.262**	C$_{39}$H$_{43}$N$_7$O$_3$		658.3500	658.3512
Boc-**3.263**	C$_{23}$H$_{36}$N$_8$O$_3$		473.2983	473.2988
di-Boc-**3.264**	C$_{25}$H$_{36}$FN$_7$O$_5$S		566.2555	566.2565
di-Boc-**3.265**	C$_{28}$H$_{43}$N$_7$O$_5$S		590.3119	590.3175
di-Boc-**3.267**	C$_{29}$H$_{44}$N$_6$O$_5$S		589.3167	589.3181
di-Boc-**3.268**	C$_{33}$H$_{44}$N$_6$O$_5$S		637.3167	637.3198
di-Boc-**3.269**	C$_{33}$H$_{44}$N$_6$O$_5$S		637.3167	637.3179
Boc-/Trt-**3.270**	C$_{45}$H$_{52}$N$_6$O$_3$S		757.3894	757.3905
di-Boc-**3.271**	C$_{29}$H$_{45}$N$_7$O$_5$S		604.3276	604.3289
di-Boc-**3.272**	C$_{34}$H$_{46}$N$_6$O$_5$S		651.3323	651.3366
di-Boc-**3.273**	C$_{34}$H$_{46}$N$_6$O$_5$S		651.3323	651.3348

Table 3.16. (continued)

Comp.	MW	Structure	Calculated for [M+H]$^+$	Found
Boc-/Trt-**3.274**	C$_{46}$H$_{54}$N$_6$O$_3$S		771.4051	771.4067
tetra-Boc-**3.275**	C$_{50}$H$_{70}$N$_{12}$O$_{10}$S$_2$		1063.4852	1063.4876
tetra-Boc-**3.276**	C$_{50}$H$_{70}$N$_{12}$O$_{10}$S$_2$		1063.4852	1063.4841
tetra-Boc-**3.277**	C$_{40}$H$_{68}$N$_{14}$O$_{10}$S$_2$		969.4757	969.4770
tetra-Boc-**3.278**	C$_{42}$H$_{72}$N$_{14}$O$_{10}$S$_2$		997.5070	997.5083

3.6.5 Concentration-response Curves of Compound 3.139, 3.145, and 3.157-3.159 on the Guinea Pig Right Atrium Assay
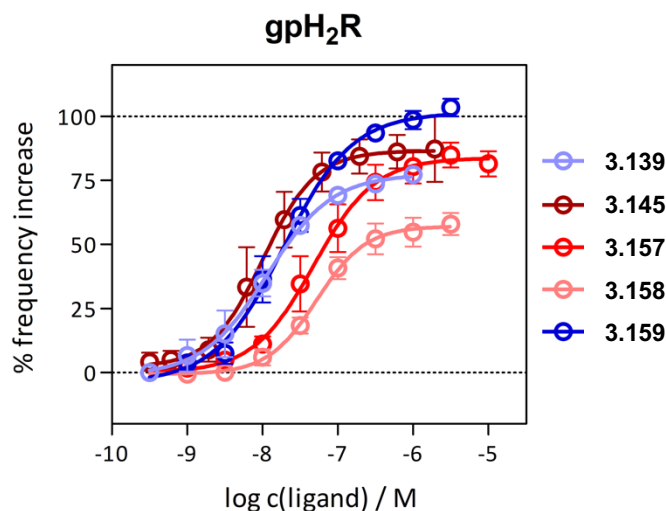
Figure 3.192. Concentration-response curves of representative carbamoylguanidines determined on the guinea pig right atrium. Data represent mean values ± SEM of 3 independent experiments.

3.6.6 Concentration-response Curves of Compound 3.139, 3.145, 3.157, 3.159 and 3.163 Obtained Using β-arrestin2 at hH$_2$R, hD$_{2long}$R, and hD$_3$R
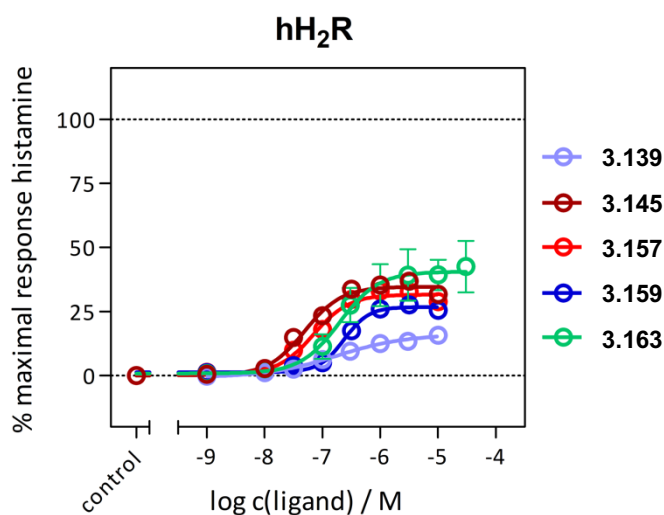
Figure 3.193. Concentration-response curves of representative carbamoylated guanidines on hH$_2$R determined by β-arrestin2 recruitment assay on HEK293T-β-Arr2-hH$_2$R cells[187], stably expressing the hH$_2$R-ElucC and βArr2-ElucN fusion constructs. Data represent mean values ± SEM of 3-4 independent experiments, each performed in duplicate or triplicate.
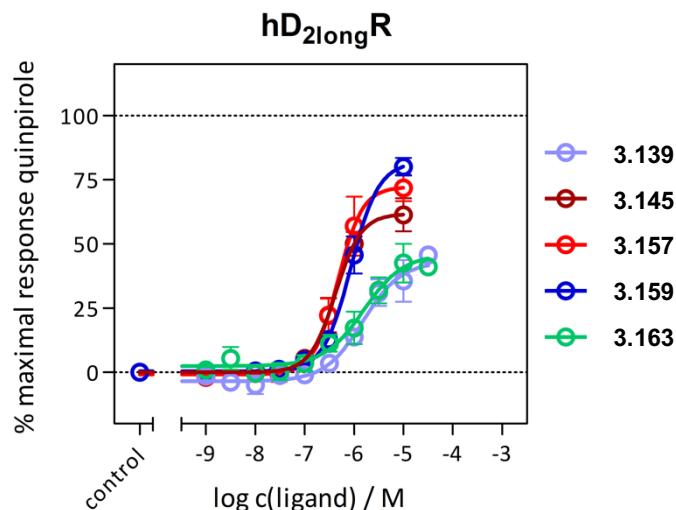
Figure 3.194. Concentration-response curves of representative carbamoylated guanidines on hD$_{2long}$R determined by β-arrestin2 recruitment assay on HEK293T ElucN-βarr2 hD$_{2long}$R-ELucC cells[404], stably expressing the hD$_{2long}$R-ElucC and βarr2-ElucN fusion constructs. Data represent mean values ± SEM of 3 independent experiments, each performed in triplicate.
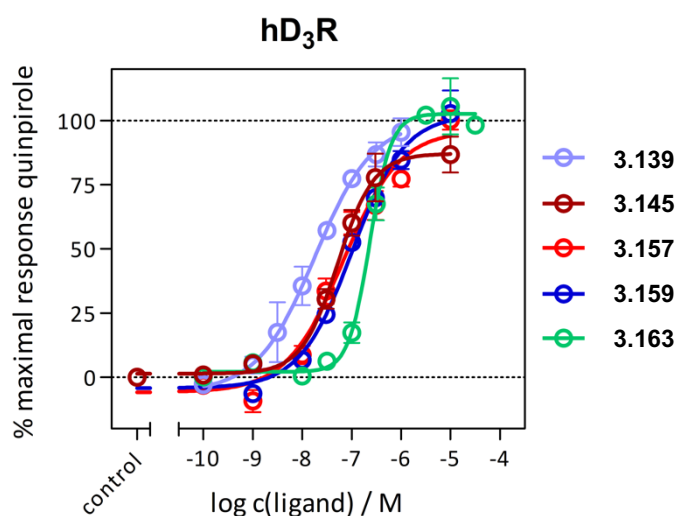
Figure 3.195. Concentration-response curves of representative carbamoylated guanidines on hD$_3$R determined by β-arrestin2 recruitment assay on HEK293T ElucN-βarr2 hD$_3$R-ELucC cells[404], stably expressing the hD$_3$R-ElucC and βarr2-ElucN fusion constructs. Data represent mean values ± SEM of 3 independent experiments, each performed in triplicate.

3.6.7 Radioligand Displacement Curves of Compound 3.139, 3.145, 3.157-3.159, and 3.163 at hH₁R, hH₂R, hH₃R, and hH₄R
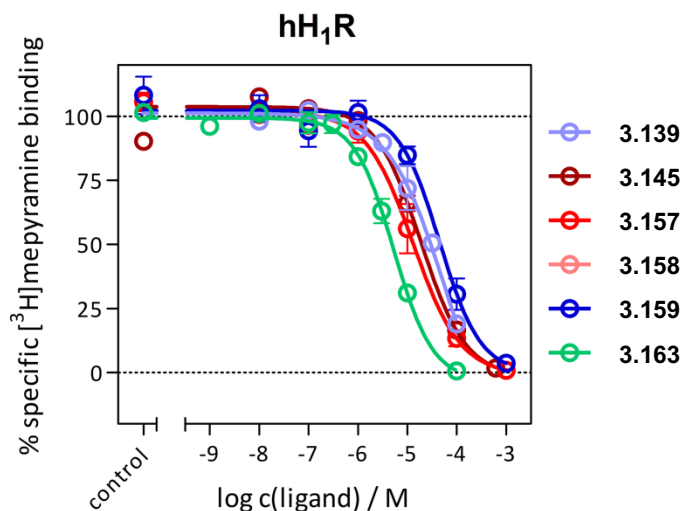
Figure 3.196. Displacement of the radioligand [³H]mepyramine (c = 5 nM, K_d = 4.5 nM) by increasing concentrations of the respective ligand determined on membrane preparations of Sf9 insect cells co-expressing the hH₁R and RGS4 proteins. Data represent mean values ± SEM of 3 independent experiments, each performed in triplicate.
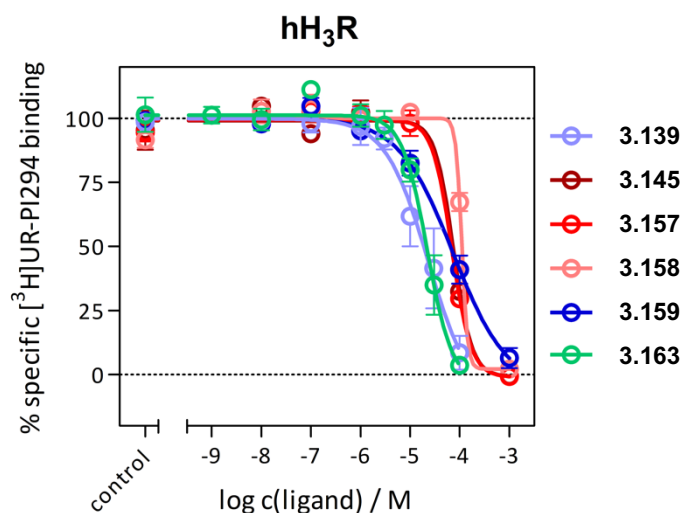
Figure 3.197. Displacement of the radioligand [³H]UR-PI294[391] (c = 2 nM, K_d = 1.1 nM) by increasing concentrations of the respective ligand determined on membrane preparations of Sf9 insect cells co-expressing the hH₃R, $G_{\alpha i2}$, and $G_{\beta 1\gamma 2}$ proteins. Data represent mean values ± SEM of 3 independent experiments, each performed in triplicate.
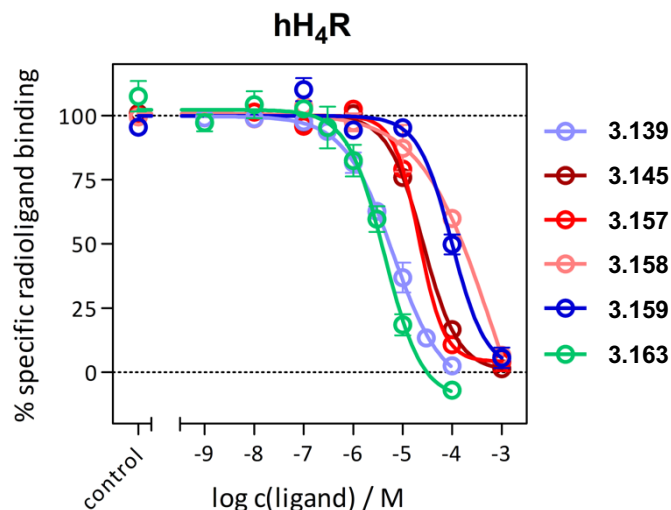
Figure 3.198. Displacement of the radioligand [^{3}H]histamine (c = 10 nM, K_d = 15.9 nM) or ^{f}[^{3}H]UR-PI294^{391} (compound **3.163**, c = 5 nM, K_d = 5.1 nM) by increasing concentrations of the respective ligand determined on membrane preparations of Sf9 insect cells co-expressing the hH$_4$R, G$_{\alpha i2}$, and G$_{\beta 1\gamma 2}$ proteins. Data represent mean values ± SEM of 3 independent experiments, each performed in triplicate.

3.6.8 Radioligand Displacement Curves of compound 3.139, 3.145, 3.157, 3.159, and 3.163 at hD$_{2long}$R
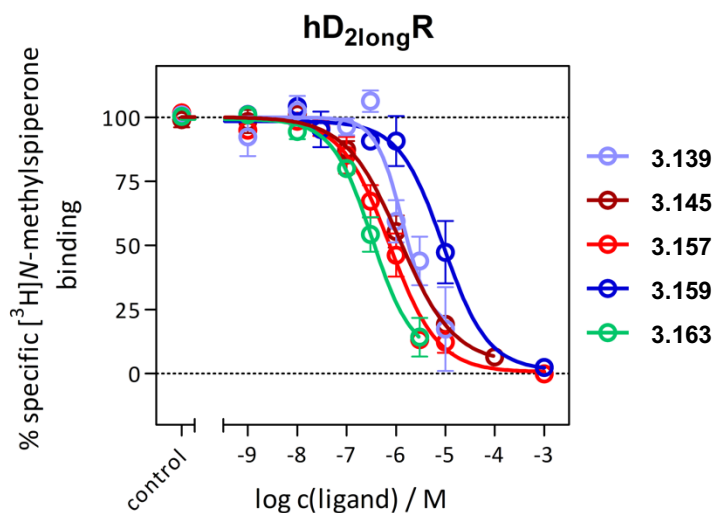
Figure 3.199. Displacement of the radioligand [^{3}H]N-methylspiperone (c = 0.05 nM, K_d = 0.0149 nM) by increasing concentrations of the respective ligand at homogenates of HEK293T-CRE-Luc-hD$_{2long}$R cells^{404}. Data represent mean values ± SEM of 3 independent experiments, each performed in triplicate.

3.6.9 Concentration-response Curves of Compound 3.005, 3.139, 3.239, 3.240, 3.244, 3.251, 3.255, 3.256, 3.261, 3.262, 3.264, 3.265, 3.267, 3.271, and 3.277 Obtained Using mini-G protein Recruitment Assay at hH$_2$R and gpH$_2$R
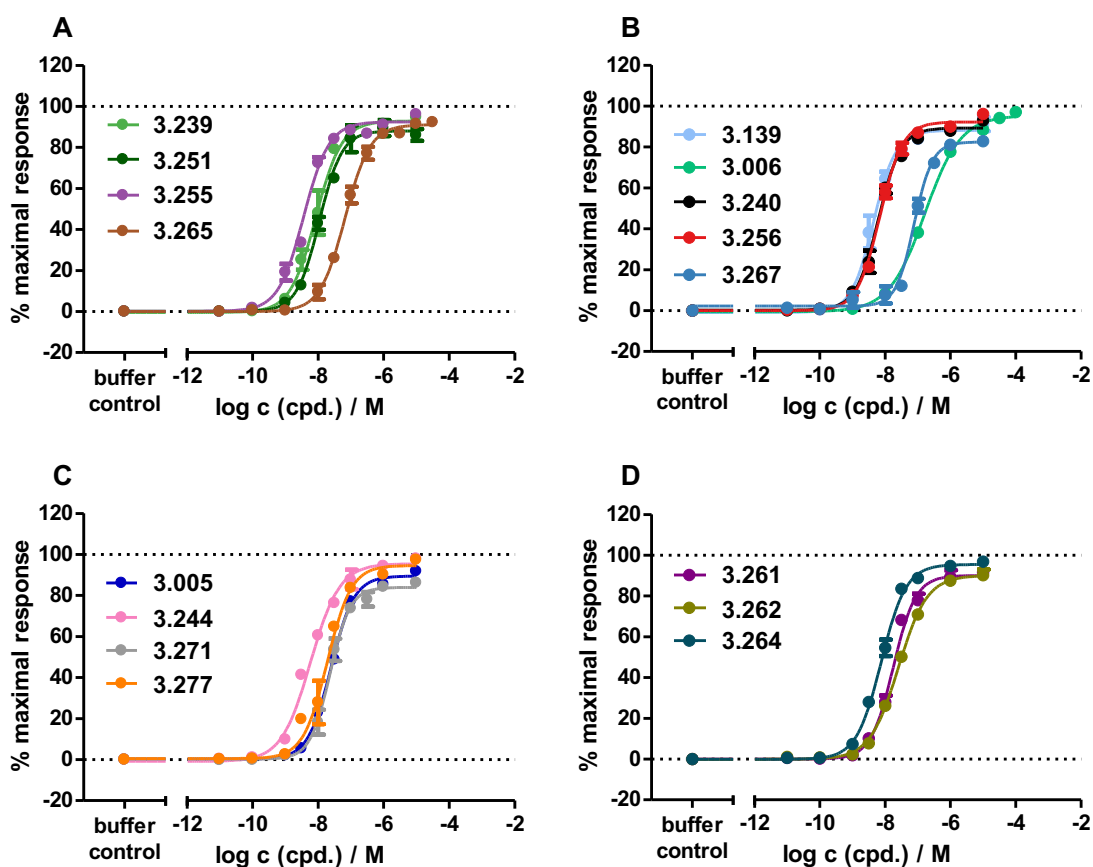
Figure 3.200. Concentration-response curves of comp. **3.005**[299], **3.139**[304,416], **3.006**, **3.239, 3.240**, **3.244**, **3.251**, **3.255**, **3.256**, **3.261**, **3.262**, **3.264**, **3.265**, **3.267**, **3.271**, and **3.277** at hH$_2$R in the mini-G protein recruitment assay using HEK293T NlucN-mGs/hH$_2$R-NlucC cells[425] (**A**: **3.239**, **3.251**, **3.255,** and **3.265**; **B**: **3.139**[304,416], **3.006**, **3.240**, **3.256**, and **3.267**; **C**: **3.005**[299], **3.244**, **3.271**, and **3.277**; **D**: **3.261**, **3.262**, and **3.264**). The response was normalized to the maximal effect induced by 100 µM histamine (100%) and buffer control (0%). Data represent mean values ± SEM from at least three independent experiments (performed in triplicate).
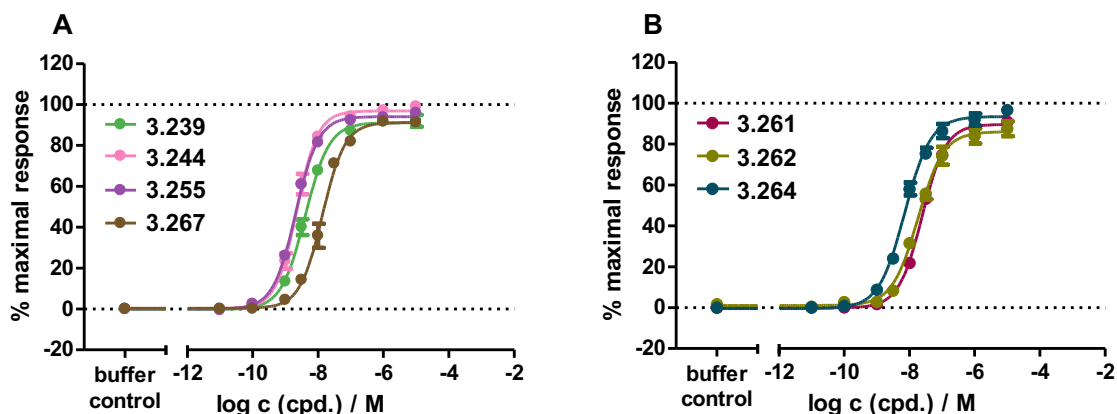
Figure 3.201. Concentration-response curves of comp. **3.239**, **3.244**, **3.255**, **3.261**, **3.262**, **3.264,** and **3.267** at gpH$_2$R in the mini-G protein recruitment assay using HEK293T NlucN-mGs/gpH$_2$R-NlucC cells[417] (**A**: **3.239**, **3.244**, **3.255**, and **3.267**; **B**: **3.261**, **3.262**, and **3.264**). The response was normalized to the maximal effect induced by 100 μM histamine (maximal response: 100%) and buffer control (maximal response: 0%). Data represent mean values ± SEM from at least three independent experiments (performed in triplicate).

3.6.10 Concentration-response Curves of Compound 3.005, 3.239, 3.240, 3.244, 3.251, 3.255, 3.256, 3.261, 3.262, 3.264, 3.265, 3.267, 3.271, and 3.277 Obtained Using β-arrestin2 at hH$_2$R, hD$_{2long}$R, and hD$_3$R
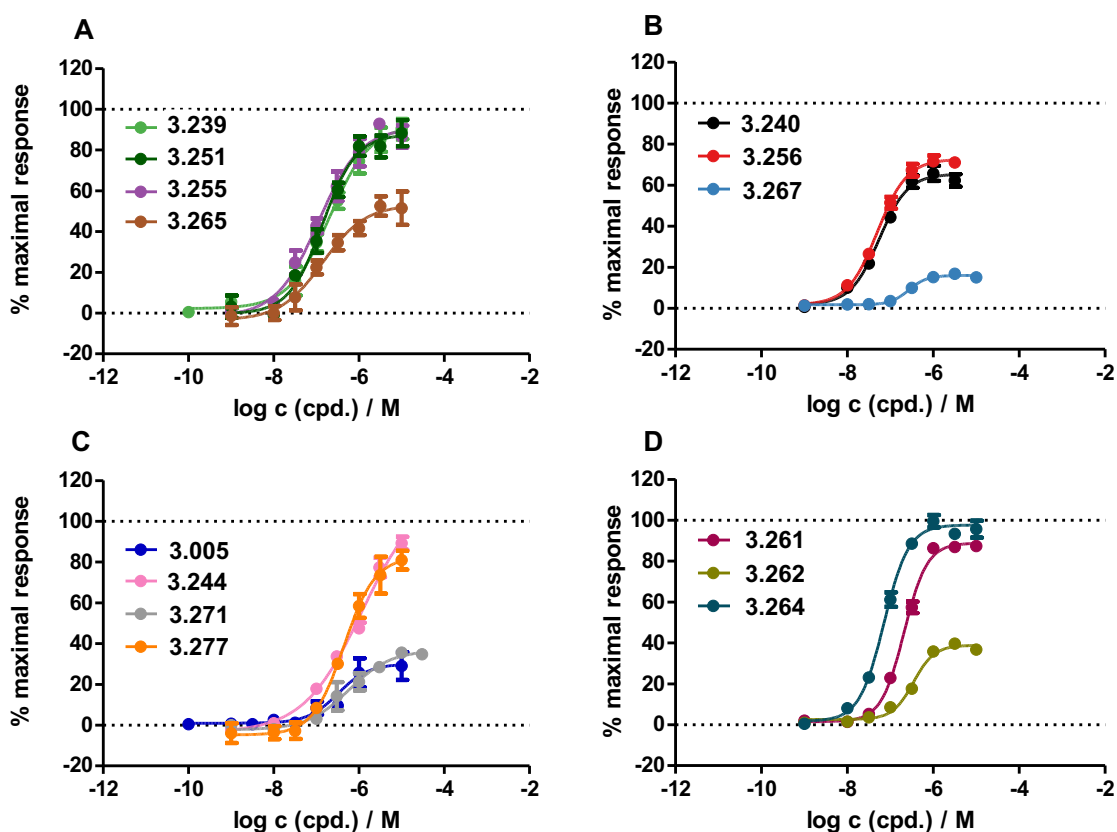
Figure 3.202. Concentration-response curves of comp. **3.005**[299], **3.239**, **3.240**, **3.244**, **3.251**, **3.255, 3.256**, **3.261**, **3.262**, **3.264**, **3.265**, **3.267**, **3.271**, and **3.277** at hH$_2$R in the β-arrestin2 recruitment assay using HEK293T-ARRB2-H$_2$R cells[187] (**A**: **3.239**, **3.251**, **3.255,** and **3.265**; **B**:

3.240, **3.256**, and **3.267**; **C**: **3.005**[299], **3.244**, **3.271**, and **3.277**; **D**: **3.261**, **3.262**, and **3.264**). The response was normalized to the maximal effect induced by 100 µM histamine (maximal response: 100%) and buffer control (maximal response: 0%). Data represent mean values ± SEM from at least three independent experiments (performed in triplicate).
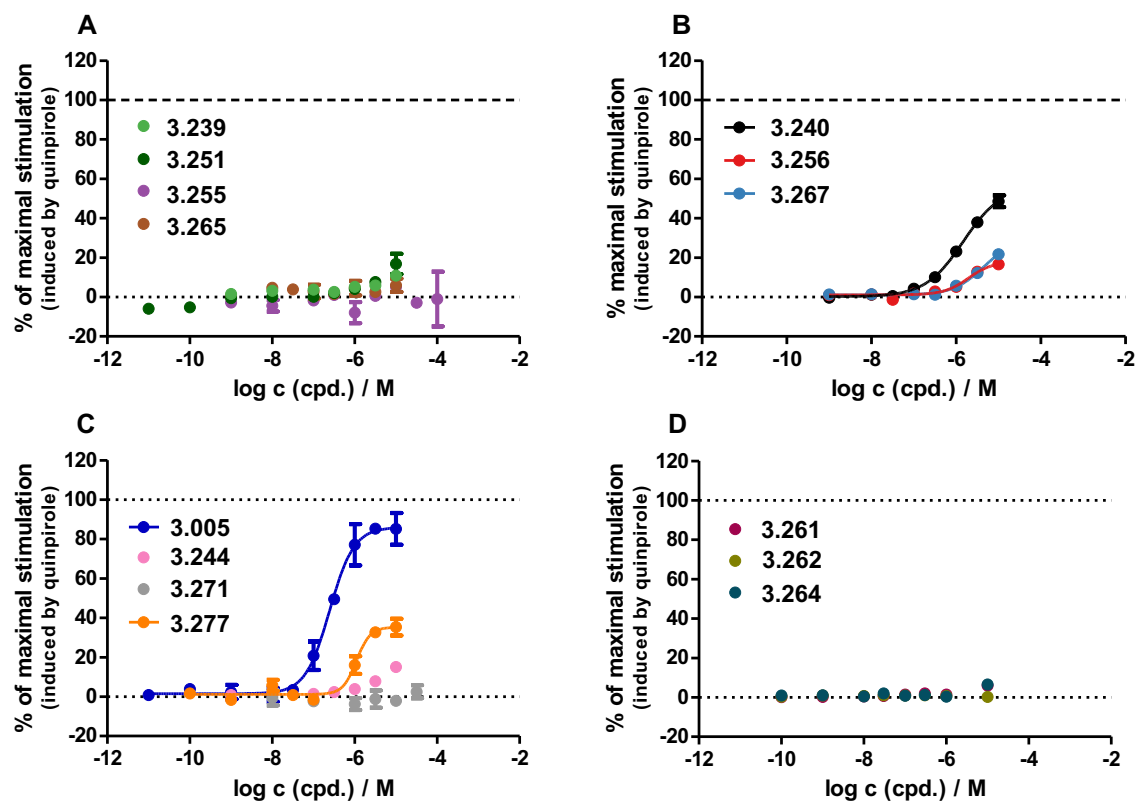
Figure 3.203. Concentration-response curves of comp. **3.005**[299], **3.239, 3.240, 3.244, 3.251, 3.255, 3.256, 3.261, 3.262, 3.264, 3.265, 3.267, 3.271**, and **3.277** at hD$_{2long}$R in the β-arrestin2 recruitment assay using HEK293T ElucN-βarr2 hD$_{2long}$R-ElucC cells[404] (**A**: **3.239, 3.251, 3.255**, and **3.265**; **B**: **3.240, 3.256**, and **3.267**; **C**: **3.005**[299], **3.244, 3.271**, and **3.277**; **D**: **3.261, 3.262**, and **3.264**). The response was normalized to the maximal effect induced by 10 µM quinpirole (maximal response: 100%) and buffer control (maximal response: 0%). Data represent mean values ± SEM from at least three independent experiments (performed in triplicate). The four-parameter logistic fits of the data from individual experiments failed in case of **3.239, 3.244, 3.251, 3.255, 3.261, 3.262, 3.264, 3.265**, and **3.271**.
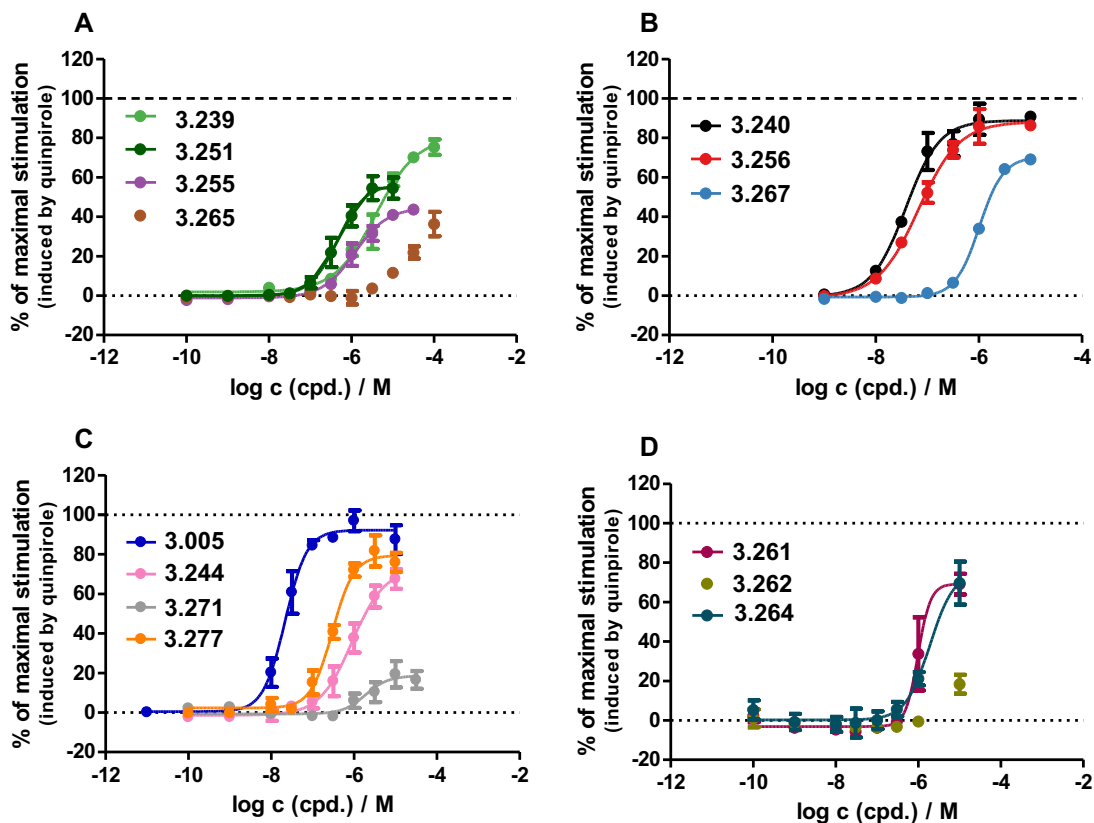
Figure 3.204. Concentration-response curves of comp. **3.005**[299], **3.239**-**3.240**, **3.244**, **3.251**, **3.255**-**3.256**, **3.261**-**3.262**, **3.264**-**3.265**, **3.267**, **3.271**, and **3.277** at hD$_3$R in the β-arrestin2 recruitment assay using HEK293T ElucN-βarr2 hD$_3$R-ElucC cells[404] (**A**: **3.239**, **3.251**, **3.255**, and **3.265**; **B**: **3.240**, **3.256**, and **3.267**; **C**: **3.005**[299], **3.244**, **3.271**, and **3.277**; **C**: **3.261**-**3.262** and **3.264**). The response was normalized to the maximal effect induced by 10 μM quinpirole (maximal response: 100%) and buffer control (maximal response: 0%). Data represent mean values ± SEM from at least three independent experiments (performed in triplicate). The four-parameter logistic fits of the data from individual experiments failed in case of **3.262** and **3.265**.

3.6.11 Radioligand Displacement Curves of Compound 3.239, 3.240, 3.244, 3.251, 3.255, 3.261, 3.262, 3.264, 3.265, 3.267, 3.271, and 3.277 at hH$_1$R, hH$_2$R, hH$_3$R, and hH$_4$R
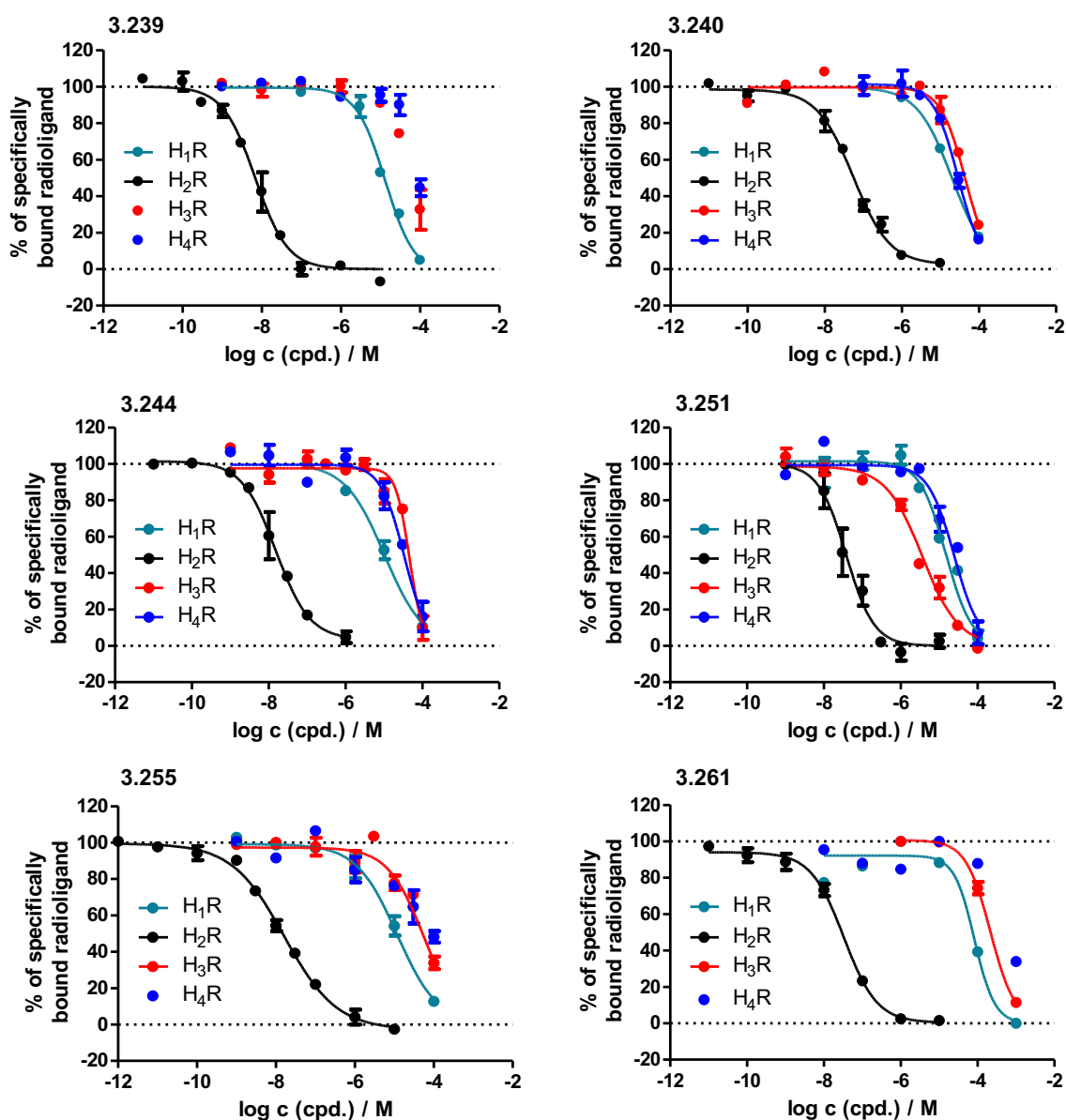
Figure 3.205. Displacement curves obtained from competition binding experiments with [^{3}H]mepyramine (hH$_1$R, c = 5 nM, K_d = 4.5 nM), [^{3}H]UR-DE257[390] (hH$_2$R, c = 20 nM, K_d = 11.2 nM), [^{3}H]UR-PI294[391] (hH$_3$R, c = 2 nM, K_d = 3 nM) or [^{3}H]**3.001** (hH$_4$R, c =15 nM, K_d = 16 nM) and **3.239**, **3.240**, **3.244**, **3.251**, **3.255**, and **3.261** at membranes of Sf9 cells expressing the hH$_1$R + RGS4, the hH$_2$R-G$_{s\alpha S}$ fusion protein, the hH$_3$R + G$_{\alpha i2}$ + G$_{\beta 1\gamma 2}$ or the hH$_4$R + G$_{\alpha i2}$ + G$_{\beta 1\gamma 2}$. Data represent mean values ± SEM from at least three independent experiments (performed in triplicate).
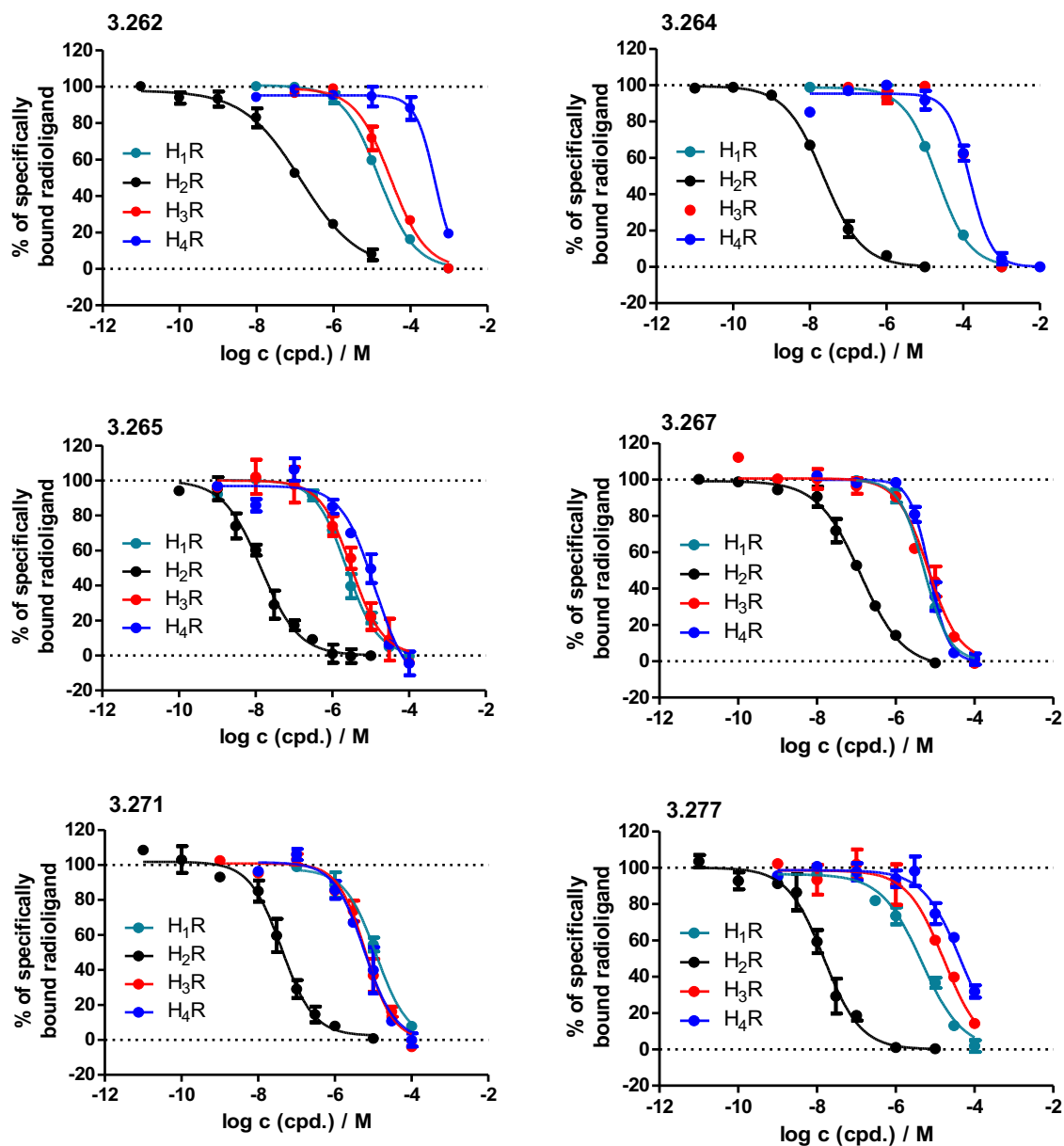
Figure 3.206 Displacement curves obtained from competition binding experiments with [^{3}H]mepyramine (hH$_1$R, c = 5 nM, K_d = 4.5 nM), [^{3}H]UR-DE257[390] (hH$_2$R, c = 20 nM, K_d = 11.2 nM), [^{3}H]UR-PI294[391] (hH$_3$R, c = 2 nM, K_d = 3 nM) or [^{3}H]**3.001** (hH$_4$R, c =15 nM, K_d = 16 nM) and **3.262**, **3.264**, **3.265**, **3.267**, **3.271**, and **3.277** at membranes of Sf9 cells expressing the hH$_1$R + RGS4, the hH$_2$R-G$_{s\alpha S}$ fusion protein, the hH$_3$R + G$_{\alpha i2}$ + G$_{\beta 1\gamma 2}$ or the hH$_4$R + G$_{\alpha i2}$ + G$_{\beta 1\gamma 2}$. Data represent mean values ± SEM from at least three independent experiments (performed in triplicate).

3.6.12 Radioligand Displacement Curves of Compound 3.239, 3.240, 3.244, 3.251, 3.255, 3.256, 3.261, 3.262, 3.264, 3.265, 3.267, 3.271, and 3.277 at hD$_{2long}$R and hD$_3$R
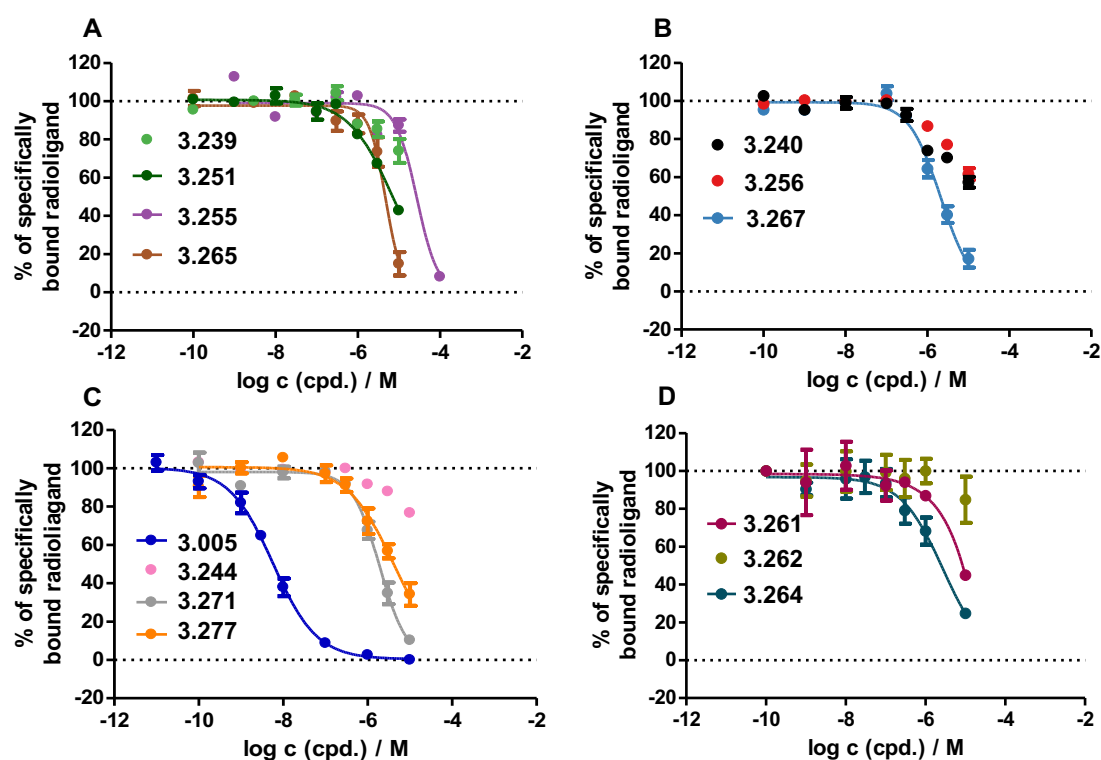
Figure 3.207. Displacement curves obtained from competition binding experiments with [^{3}H]N-methylspiperone (c = 0.5 nM, K_d = 0.014 nM) and **3.005**[299], **3.239**, **3.240**, **3.244**, **3.251**, **3.255**, **3.256**, **3.261**, **3.262**, **3.264**, **3.265**, **3.267**, **3.271**, and **3.277** on homogenates of HEK293T-CRE-Luc-hD$_{2long}$R cells[404] (**A**: **3.239**, **3.251**, **3.255,** and **3.265**; **B**: **3.240**, **3.256**, and **3.267**; **C**: **3.005**[299], **3.244**, **3.271**, and **3.277**; **D**: **3.261**, **3.262**, and **3.264**). Data represent mean values ± SEM from at least three independent experiments (each performed in triplicate).
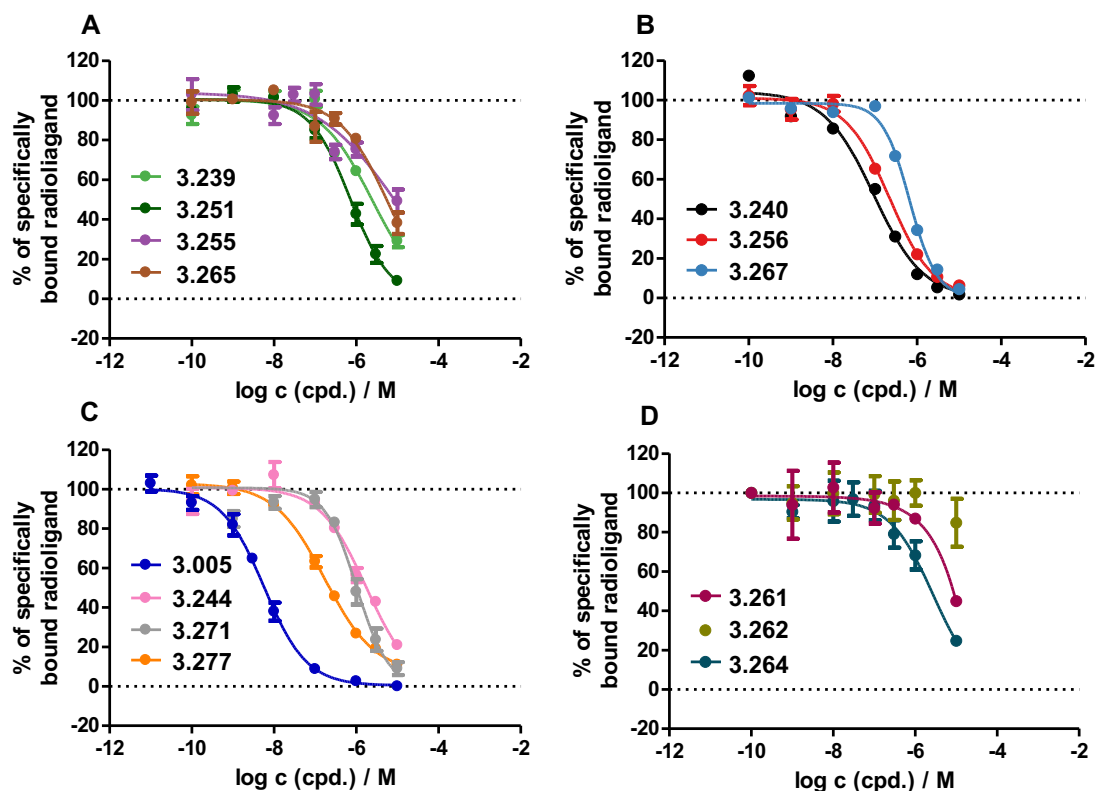
Figure 3.208. Displacement curves obtained from competition binding experiments with [^{3}H]*N*-methylspiperone (c = 0.5 nM, K_d = 0.026 nM) and **3.005**[299], **3.239**, **3.240**, **3.244**, **3.251**, **3.255**, **3.256**, **3.261**, **3.262**, **3.264**, **3.265**, **3.267**, **3.271**, and **3.277** on homogenates of HEK293T-CRE-Luc-hD$_3$R cells[404] (**A**: **3.239**, **3.251**, **3.255**, and **3.265**; **B**: **3.240**, **3.256,** and **3.267**; **C**: **3.005**[299], **3.244**, **3.271**, and **3.277**; **D**: **3.261**, **3.262**, and **3.264**). Data represent mean values ± SEM from at least three independent experiments (each performed in triplicate).

3.6.13 Investigation of β-Arrestin2 and mGs Recruitment at HEK293T-hH₂R Cells for 3.238, 3.241-3.243, 3.245-3.250, 3.252-3.254, 3.257-3.260, 3.263, 3.266, 3.268-3.270, 3.272-3.276, and 3.278

Table 3.17. Potencies and efficacies of the tested carbamoylated guanidines in the β-arrestin2 and mini-G protein recruitment assay at the hH₂R.[a]

Comp.	β-arrestin2 recruitment[b]			mGs recruitment[c]		
	pEC$_{50}$ or (pK_b)[d]	E$_{max}$[e]	N	pEC$_{50}$ or (pK_b)[d]	E$_{max}$[e]	N
3.140[304,416]	7.07 ± 0.02[304,416]	0.28 ± 0.03[304,416]	3	8.04 ± 0.04	0.87 ± 0.01	3
3.143[304,416]	7.00 ± 0.08[304,416]	0.33 ± 0.03[304,416]	3	8.14 ± 0.03	0.89 ± 0.01	3
3.145[304]	7.34 ± 0.11[304]	0.34 ± 0.03[304]	4	8.04 ± 0.01	0.88 ± 0.01	3
3.157[304]	7.19 ± 0.11[304]	0.30 ± 0.01[304]	4	8.07 ± 0.01	0.89 ± 0.01	3
3.163[304,416]	6.65 ± 0.09[304,416]	0.40 ± 0.06[304,416]	3	7.52 ± 0.11	0.84 ± 0.01	3
3.170[304,416]	6.9 ± 0.1[304,416]	0.10 ± 0.01[304,416]	3	7.43 ± 0.02	0.73 ± 0.02	3
3.172[304]	5.60 ± 0.11[304]	0.13 ± 0.02[304]	4	7.28 ± 0.09	0.76 ± 0.04	3
3.238	(5.70 ± 0.18)	n.a.	4	5.61 ± 0.02	0.62 ± 0.01	3
3.241	(7.27 ± 0.05)	n.a.	3	(6.96 ± 0.03)	n.a.	3
3.242	(7.27 ± 0.11)	n.a.	3	7.25 ± 0.10	0.43 ± 0.01	3
3.243**	(7.81 ± 0.13)	n.a.	3	7.24 ± 0.05	0.74 ± 0.04	3
3.245	5.78 ± 0.05	0.61 ± 0.02	5	7.00 ± 0.04	0.93 ± 0.02	3
3.246	(5.51 ± 0.10)	n.a.	4	< 5	0.34 ± 0.06*	4
3.247	6.70 ± 0.14	0.87 ± 0.04	5	8.13 ± 0.05	0.93 ± 0.01	3
3.248	(6.65 ± 0.08)	n.a.	3	(6.79 ± 0.02)	-0.04 ± 0.01*	3
3.249	(7.05 ± 0.04)	n.a.	3	7.08 ± 0.05	0.49 ± 0.02	3
3.250	(6.13 ± 0.12)	n.a.	4	5.97 ± 0.02	0.19 ± 0.01	3
3.252	(6.87 ± 0.10)	n.a.	4	(6.79 ± 0.03)	-0.12 ± 0.02*	3
3.253	(6.89 ± 0.20)	n.a.	4	7.24 ± 0.07	0.86 ± 0.02	3
3.254	(5.43 ± 0.14)	n.a.	4	5.63 ± 0.07	0.71 ± 0.02	3
3.257	(7.81 ± 0.11)	n.a.	5	7.30 ± 0.04	0.08 ± 0.01	3
3.258	(7.13 ± 0.10)	n.a.	3	7.16 ± 0.10	0.67 ± 0.02	4
3.259**	(7.35 ± 0.08)	n.a.	3	7.19 ± 0.05	0.73 ± 0.02	3
3.260***	7.13 ± 0.04	0.72 ± 0.06	3	8.17 ± 0.01	0.93 ± 0.01	3
3.263***	(< 5)	n.a.	3	< 5	n.a."	3
3.266	(6.31 ± 0.14)	n.a.	4	6.58 ± 0.05	0.74 ± 0.02	3
3.268	(6.80 ± 0.06)	n.a.	4	(6.73 ± 0.05)	-0.07 ± 0.01*	3
3.269	(7.32 ± 0.10)	n.a.	4	(7.09 ± 0.01)	-0.08 ± 0.01*	3
3.270**	(7.39 ± 0.07)	n.a.	4	(6.96 ± 0.03)	0.02 ± 0.01*	3
3.272	(6.57 ± 0.03)	n.a.	3	(6.86 ± 0.03)	-0.08 ± 0.01*	3
3.273	(7.02 ± 0.11)	n.a.	3	(7.31 ± 0.01)	-0.05 ± 0.01*	3
3.274**	(7.30 ± 0.11)	n.a.	3	6.69 ± 0.04 (6.96 ± 0.03)	-0.04 ± 0.01	3
3.275	(7.86 ± 0.12)	n.a.	4	6.13 ± 0.12	0.44 ± 0.05	4
3.276	(7.10 ± 0.04)	n.a.	3	6.59 ± 0.12	0.19 ± 0.02	3
3.278	6.66 ± 0.03	0.81 ± 0.07	4	8.06 ± 0.02	0.94 ± 0.01	3

[a]Data represent mean values ± SEM from N independent experiments, each performed in triplicate. [b]β-arrestin2 recruitment assay was performed using HEK293T-ARRB2-H₂R cells.[187,395] [c]mini-G protein recruitment assay was performed using HEK293T NlucN-mGs/hH₂R-NlucC cells.[425] [d]pK_b = -logK_b. K_b values were calculated from the IC$_{50}$ values according to the Cheng-Prusoff equation.[156] The K_b values of antagonists or inverse agonists were determined in the antagonist mode versus histamine (8 µM histamine for the β-arrestin2

recruitment assay or 1 µM histamine for the mini-G protein recruitment assay). [e]The response in both assays was normalized to the maximal effect induced by 100 µM histamine (E$_{max}$ = 1.00) and buffer control (E$_{max}$ = 0.00). n.a.: not applicable, silent antagonist. ": inactive as agonist as well as antagonist. *E$_{max}$ at c = 10 µM.**Selected compounds were investigated for functional activity in the [^{35}S]GTPγS binding assay at the hH$_2$R-G$_{s\alpha S}$ fusion protein[299]. The response was normalized to the maximal effect induced by histamine (E$_{max}$ = 1.00) and buffer control (E$_{max}$ = 0.00). The pIC$_{50}$ values of antagonists or inverse agonists were determined in the antagonist mode versus histamine (c = 1 µM, EC$_{50}$ = 5.85 ± 0.06) and converted to the corresponding K_b values by using the Cheng-Prusoff equation[156], pK_b = -logK_b. The obtained results were in good agreement with the mGs-results. **3.243**: pEC$_{50}$ = 7.23 ± 0.10, E$_{max}$ = 0.31 ± 0.05; **3.259**: pEC$_{50}$ = 6.91 ± 0.07, E$_{max}$ = 0.26 ± 0.03; **3.270**: pK_b = 6.79 ± 0.13; E$_{max}$ = n.a.; **3.274**: pK_b = 6.96 ± 0.03; E$_{max}$ = n.a.. ***Compounds **3.260** and **3.263** were also investigated on isolated spontaneously beating guinea pig right atrium[389]: **3.260**: pEC$_{50}$ = 8.88 ± 0.12, E$_{max}$ = 1.14 ± 0.17; **3.263**: not active, E$_{max}$ = 0.

3.6.14 Bias Analysis for 3.138, 3.140-3.143, 3.161, 3.163, 3.166-3.171, 3.185, and 3.186 Using the Data obtained from [^{35}S]GTPγS Binding Assay and β-Arrestin2 Recruitment Assay
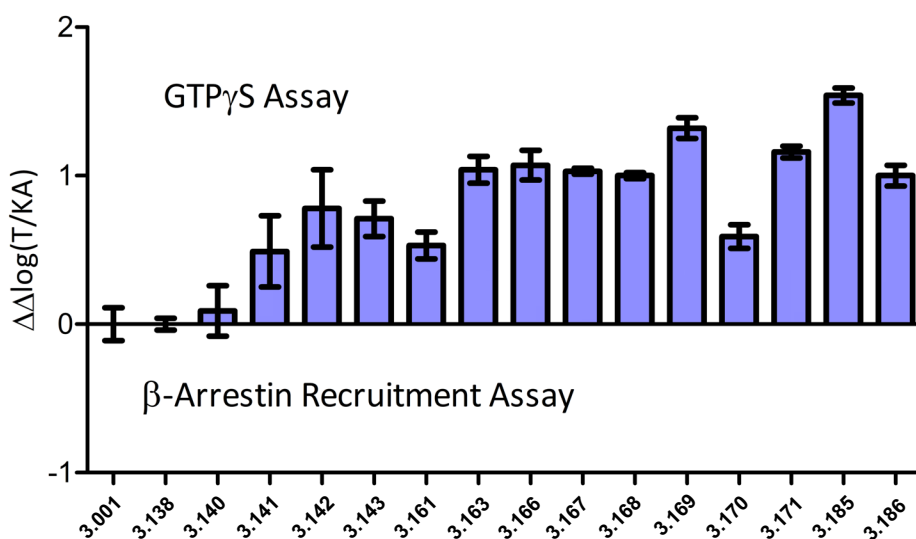
Figure 3.209. Bias analysis of **3.138**, **3.140-3.143**, **3.161**, **3.163**, **3.166-3.171**, **3.185**, and **3.186** using the potencies and efficacies obtained from GTPγS binding assay and β-arrestin2 recruitment assay at the hH$_2$R, as described by van der Westhuizen et al.[489], using histamine (**3.001**) as reference agonist. A ΔΔlog (τ/KA) ratio = 0 indicate a balanced bias profile, while a ΔΔlog (τ/KA) ratio ≠ 0 indicates a preference for one signal pathway over the other. Data represent mean ± SEM of 2-4 independent experiments performed in duplicates or triplicates.

A bias analysis was performed for **3.138**, **3.140-3.143**, **3.161**, **3.163**, **3.166-3.171**, **3.185**, and **3.186** using the potencies and efficacies obtained from GTPγS binding assay and β-arrestin2 recruitment assay at the hH$_2$R (Figure 3.209). The analysis was based on the operational model of agonism[490–492] as described by van der Westhuizen

et al.[489] using histamine (**3.001**) as reference agonist. The (partial) agonists **3.141**-**3.143**, **3.161**, **3.163**, **3.166**-**3.171**, **3.185**, and **3.186** exhibited some functional bias towards the G-protein activation pathway ($\Delta\Delta\log(\tau/KA) > 0$), whereas **3.138** and **3**.**140** showed a balanced bias profile ($\Delta\Delta\log(\tau/KA) \sim 0$). This is in agreement with the findings for acylguanidines and bivalent carbamoylguanidines.[187]

3.6.15 Bias Analysis for 3.005, 3.139, 3.140, 3.163, 3.143, 3.145, 3.157, 3.170, 3.172, 3.239-3.240, 3.244-3.245, 3.247, 3.251, 3.255-3.256, 3.260-3.262, 3.264-3.265, 3.267, 3.271, and 3.277-3.278 Using the Data Obtained from Mini-G Protein Recruitment Assay and β-Arrestin2 Recruitment Assay
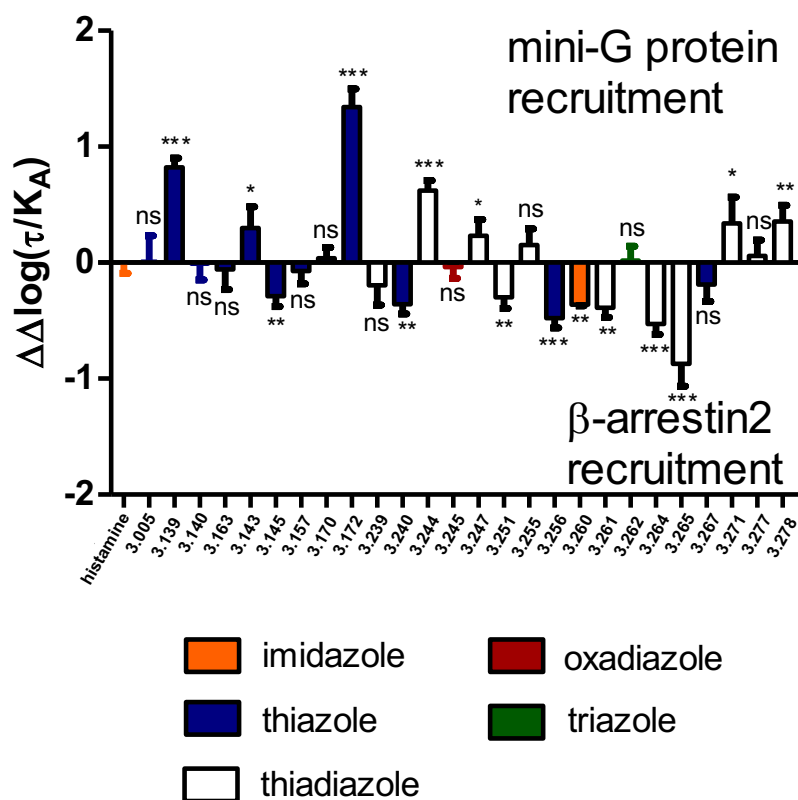
Figure 3.210. Bias analysis for histamine (His), **3.005**[299], **3.139**[304], **3.140**[304,416], **3.163**[304,416], **3.143**[304,416], **3.145**[304], **3.157**[304], **3.170**[304,416], **3.172**[304], **3.239**-**3.240**, **3.244**-**3.245**, **3.247**, **3.251**, **3.255**-**3.256**, **3.260**-**3.262**, **3.264**-**3.265**, **3.267**, **3.271**, and **3.277**-**3.278** was performed as described by van der Westhuizen at al.[489], using histamine (**3.001**) as reference agonist. A $\Delta\Delta\log(\tau/K_A)$ ratio = 0 indicate an equal activation of the G protein- and β-arrestin2 pathways, while a $\Delta\Delta\log(\tau/K_A)$ ratio ≠ 0 indicates a preference for one signal pathway over the other. Data represent mean ± SEM of 3-6 independent experiments performed in duplicates or triplicates. Data were analyzed in a pairwise manner using a two-tailed unpaired student's t-test to determine the significance of the ligand biases (ns: not significant, ***$p < 0.001$; **$p < 0.01$,*$p < 0.05$, as described by van der Westhuizen et al.[489].

A bias analysis was performed for **3.005**[299], **3.139**[304], **3.140**[304,416], **3.163**[304,416], **3.143**[304,416], **3.145**[304], **3.157**[304], **3.170**[304,416], **3.172**[304], **3.239**-**3.240**, **3.244**-**3.245**, **3.247**, **3.251**, **3.255**-**3.256**, **3.260**-**3.262**, **3.264**-**3.265**, **3.267**, **3.271**, and **3.277**-**3.278** using the potencies and efficacies obtained from mini-G protein recruitment assay and β-arrestin2 recruitment assay at the hH$_2$R (cf. Figure 3.210). The analysis was based on the operational model of agonism[490–492] as described by van der Westhuizen et al.[489] using histamine (**3.001**) as reference agonist. According to the present bias analysis some of the tested ligands possess a significant preference for the G protein (mGs) and some others a preference for the β-arrestin2 pathway (Figure 3.210). Unfortunately, no trend was determined, which could be unambiguously assigned to a specific structure-pathway bias.

3.6.16 Bioavailability Radars
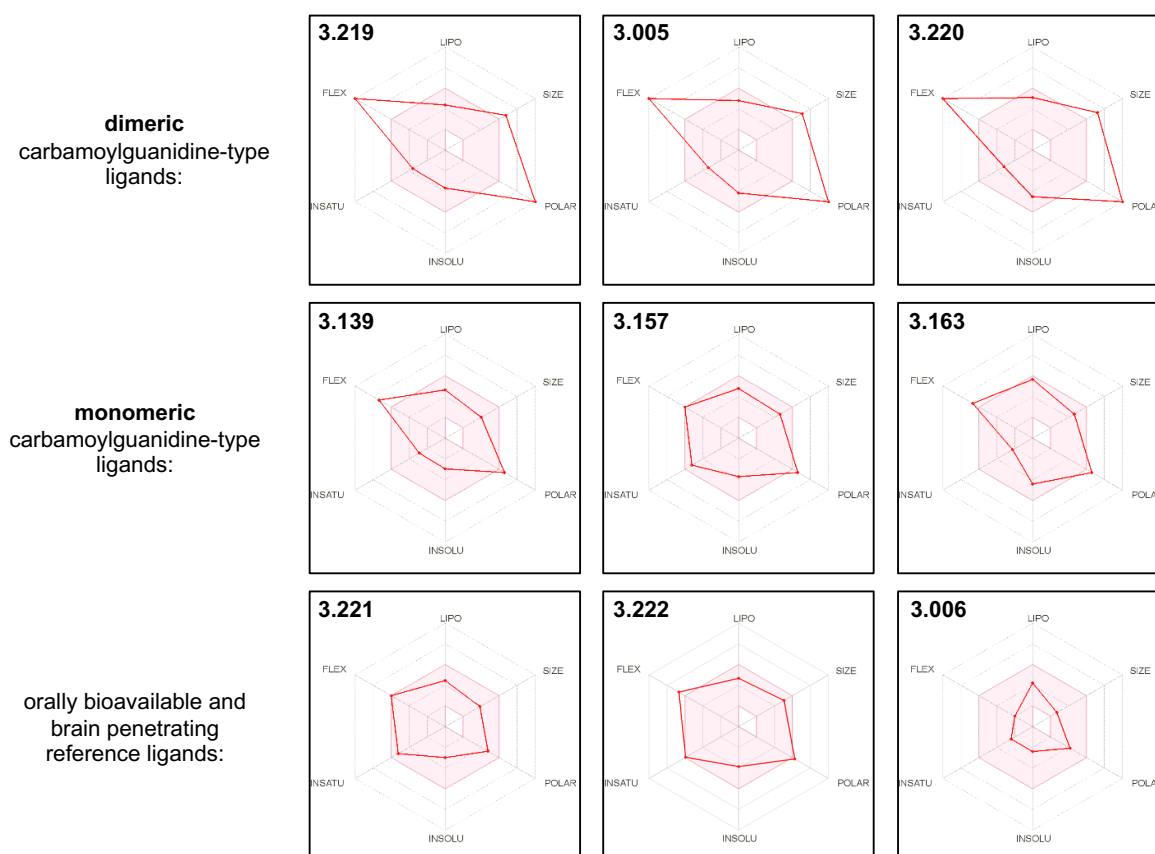
Figure 3.211. Bioavailability radars of **3.005**-**3.006**, **3.139**, **3.157**, **3.163**, and **3.219**-**3.222** obtained using SwissADME web tool[129]. Six parameters namely flexibility (FLEX, < 10 rotatable bonds), lipophilicity (LIPO, -0.7 ≤ logP (XLOGP[132]) ≤ 6), size (SIZE, 150 ≤ MW ≤ 500), polarity (POLAR, 20 ≤ TPSA ≤ 130;), solubility (INSOLU, logS (ESOL[136]) < -6) and saturation (INSATU, sp^3 hybridized carbons / total carbon count ≥ 0.25) and their critical limits are depicted in the bioavailability radar. Ranges of optimal values are depicted as a pink area. The red radar of

the compound must be fully encompassed by the pink area to consider it as drug-like and orally bioavailable. Any deviation signifies a suboptimal property for oral bioavailability.

Monomeric ligands **3.139**, **3.157**, and **3.163** fitted better in the bioavailability radar[129] than the dimeric ligands **3.005**, **3.219**, and **3.220** (cf. Figure 3.211). Compounds **3.139**, **3.157**, and **3.163** showed suitable lipophilicity, size, solubility, saturation, and flexibility (in case of **3.157**) but suboptimal polarity and flexibility (in case of **3.139** and **3.163**) (cf. Figure 3.211).

Chapter 4

Development of Fluorescent AF64394 Analogues Enables Real-time Binding Studies for the Orphan Class A GPCR GPR3

4 Development of Fluorescent AF64394 Analogues Enables Real-time Binding Studies for the Orphan Class A GPCR GPR3
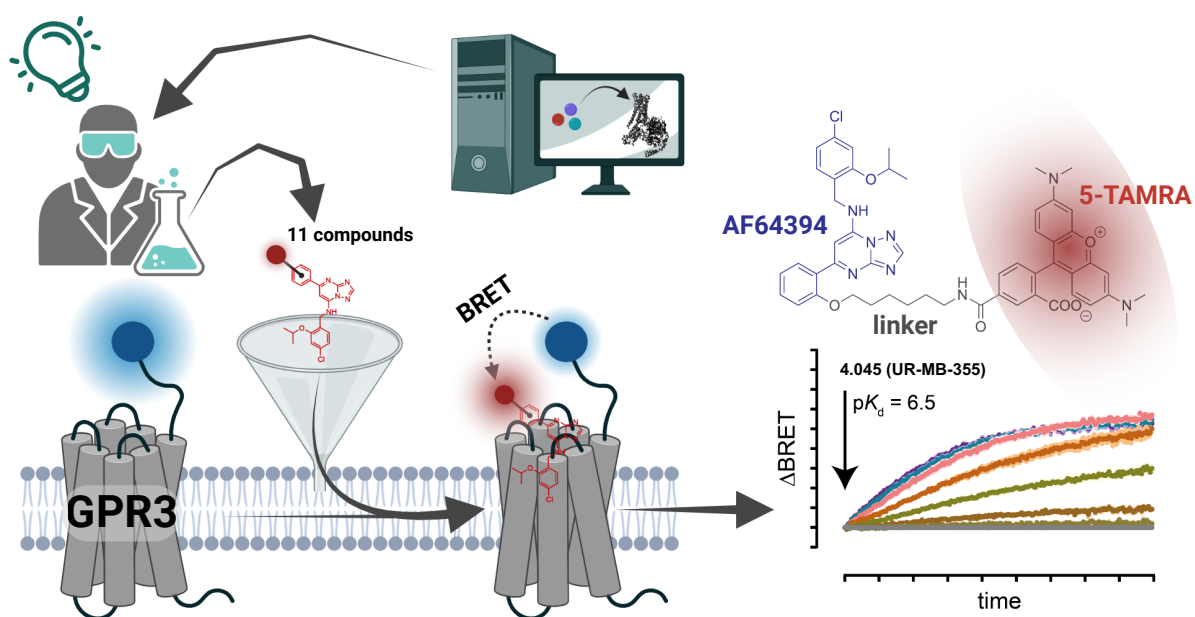
The orphan G protein-coupled receptor (oGPCR) GPR3 represents a potential drug target for the treatment of, e.g., Alzheimer's disease and metabolic disorders. However, the limited toolbox of pharmacological assays has hampered the development of advanced ligands. This study aims the development of a signaling pathway-independent readout of compound-GPR3 interaction that is based on luciferase-tagged GPR3 and fluorescently labeled ligands. From computational binding pose predictions of the most potent currently available GPR3 ligand, a series of fluorescent AF64394 analogs were designed and synthesized and assessed their suitability for BRET-based binding studies. The best ligand, **4.045** (UR-MB-355), bound to GPR3 and the closely related receptors GPR6 and GPR12 with similar nanomolar affinity. Co-incubation studies with the GPR3 agonist DPI further revealed positive allosteric modulation of **4.045** binding. These insights provide new cues for the pharmacological manipulation of GPR3 activity. Furthermore, this novel binding assay will foster the development of future drugs acting through these pharmacologically attractive oGPCRs.

Results of this chapter have been submitted for publication in the Journal of Medicinal Chemistry:

Author contributions:

H. S., **S.P.**, and **P.K.** resources; **H.S.** and **S.P.** conceptualization; **H.S.**, **M.B.**, and **A.S.** formal analysis; **M.B., H.S.**, **A.S.** investigation; **M.B.** synthesized compound **4.045**-**4.055** and the corresponding precursor compounds therefore; **M.B.**, **S.P.**, and **H.S.** writing–original draft; **M.B.**, **S.P.**, and **H.S.** visualization; **H.S.**, **S.P.**, and **P.K.** funding acquisition; **M.B.**, **S.P.**, **H.S.**, **A.S.**, and **P.K.** writing–review and editing; **P.K.**, **H.S.**, and **S.P.** supervision; **H.S.**, and **S.P.** project administration.

4.1 Introduction

The orphan class A G protein-coupled receptor (GPCR) GPR3 is a transmembrane (TM) protein that was first described in 1994 and is encoded by the *GPR3* gene.[493] GPR3 is predominantly expressed in the brain, but it is also detected in the testis, ovary, eye, and other peripheral organs.[494,495] Expression of GPR3 results in constitutive stimulation of adenylate cyclase (AC) and, thus, elevated levels of the second messenger cAMP.[494] GPR3, together with GPR6 and GPR12, is part of a cluster of class A orphan GPCRs that is phylogenetically related to lipid receptors such as $CB_{1/2}$, $LPAR_{1-5}$, $S1PR_{1-5}$, and melanocortin receptors.[496–498] Besides constitutive activation of heterotrimeric G_s by all three orphan GPCRs, GPR3 and GPR12 have also been suggested to activate inhibitory G proteins of the $G_{i/o}$ family in a ligand-independent manner.[496,499,500]

Physiologically, GPR3 is involved in a variety of central and peripheral processes. For instance, GPR3 maintains meiotic arrest in oocytes by keeping increased levels of cAMP and agonists of this receptor could therefore provide clues to treat reproductive disorders.[501,502] Likewise, advanced GPR3 agonists could represent promising drugs against metabolic disorders because upregulated expression of the receptor in adipocytes drives energy expenditure and amplifies the physiological response to caloric excess.[503] In the central nervous system, GPR3/6/12 – and GPR3 in particular – are associated with neurite outgrowth, neuronal cell survival, and axonal regeneration.[504–507] Furthermore, GPR3 mediates the formation of amyloid-beta peptides in neurons by interacting with β-arrestin2 and stimulating γ-secretase activity, hinting at the therapeutic potential for tackling Alzheimer's disease with GPR3 antagonists or inverse agonists.[508–510]

Although a couple of ligands for the GPR3/6/12 cluster have been described, GPR3 is still considered orphan. Sphingosine-1-phosphate (S1P, cf. Figure 4.001), originally put forth as the endogenous GPR3 agonist,[496] did not elicit a response in later β-arrestin recruitment and cAMP-based studies.[511,512] Instead, diphenyleneiodonium chloride (DPI, cf. Figure 4.001) was identified as a synthetic agonist of GPR3.[512] Although GPR3 and GPR6 were claimed to be novel molecular targets for cannabidiol (CBD, cf. Figure 4.001),[513,514] the inhibitory effect of CBD on pro-inflammatory cytokine production was independent of GPR3 expression.[515] In 2014, a small molecule screen

against GPR3 identified the first compound that inhibits GPR3 function with nanomolar potency, the inverse agonist AF64394 (cf. Figure 4.001).[516] The activity of AF64394 on GPR3 was also recently confirmed in an attempt to develop an HTS-compatible cAMP-based GPR3 assay.[517]

The limited number of available GPR3 ligands and their – in part – contradicting reported activities (see examples for S1P and CBD mentioned above) indicate the need for advanced pharmacological assays detecting compound:GPR3 interaction. Due to the fact that the endogenous ligand for GPR3 is still unknown, the overall portfolio of intracellular signaling pathways promoted by GPR3 remains elusive. Thus, assays detecting compound-GPR3 interaction should preferentially be independent of distinct intracellular signaling pathways. However, all previous GPR3 ligand discovery studies relied on either measuring changes in cAMP or GPR3-arrestin interaction.[496,512,516,517]

Conformational GPCR biosensors that have been optimized for microtiter plate assay formats,[518–522] as well as direct ligand binding assays based on fluorescence anisotropy or bioluminescence resonance energy transfer (BRET), provide such signaling pathway-independent readouts of compound-receptor engagement.[523–526] The technique of NanoBRET binding assays, relying on fluorescently labeled ligands and NanoLuciferase (Nluc)-tagged proteins has gained great importance in recent years as it represents an attractive alternative to radioligand binding assays. It offers the important advantages of monitoring binding kinetics in real-time on living cells, working under non-radioactive conditions and has been successfully adapted for numerous GPCRs.[527–537]

In the present study, a NanoBRET-based GPR3 ligand binding assay was developed by designing, synthesizing, and pharmacologically validating a panel of fluorescently-labeled GPR3 ligands. This assay provides the first signaling pathway-independent readout of compound-GPR3 interaction and enabled to discover an allosteric modulatory crosstalk between an AF64394-based fluorescent GPR3 ligand and DPI.
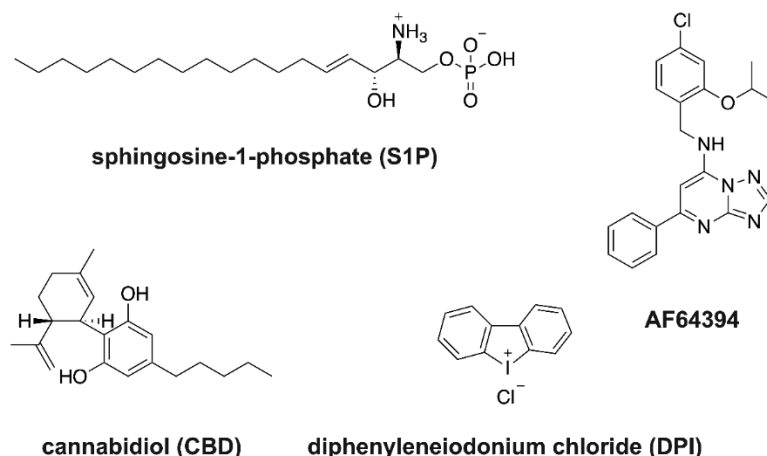
Figure 4.001. Chemical structures of sphingosine-1-phosphate (S1P), cannabidiol (CBD), diphenyleneiodonium chloride (DPI), and AF64394.

4.2 Design Rationale

This study reports the development of a BRET-based binding assay for the orphan receptor GPR3[496–498] and the synthesis of eleven fluorescent ligands that are based on either 5-TAMRA or DY-549P1 fluorophores and AF64394 as the pharmacophore scaffold. Previous molecular docking studies of a close analog of AF64394 to GPR3 suggested that the phenyl ring of AF64394 points towards the extracellular space from the receptor's binding pocket.[538] Based on these studies, this moiety was considered the optimal attachment point for a linker to introduce the fluorescent dye. The interpretation of the docking poses by Bharathi and Roy indicated that an *ortho* attachment of the linker is most promising to prevent clashes with the receptor.[538] However, to allow for a valid statement about SAR, fluorescent ligands with linkages at *ortho*, *meta*, and *para* positions of the phenyl ring were designed. Beside an alkylic linker, PEG-based linkers were chosen due to their improved water solubility, chemical stability, and reduced interaction with the cell membrane.[539]

To ensure that the pose of the fluorescent versions of AF64394 and the pose of the molecule depicted in ref. 538 (where the isopropopoxy and chlorine substituents are positioned in *meta*/*meta* instead of *ortho*/*para* on the benzyl ring) are indeed consistent, it was decided to repeat the docking calculations. To account for the linked fluorophores, close analogs of AF64394 with a methoxy group in *ortho*, *meta*, or *para* position on the phenyl ring were docked (cf. Figure 4.002A) to inactive and active models of GPR3. In this docking calculations the full-length linkers were not considered, as the extraordinary flexibility of this part would essentially lead to random conformations and poses. The docking calculations of AF64394, including linker

surrogates to the inactive model of GPR3, yielded poses that were similar to the ones obtained by Bharathi et al. (2021)[538] (cf. Figure 4.002B). In the pose of this study, the distance between the secondary amine and the backbone carbonyl of Val187 is larger than for a typical hydrogen bond – even after minimization of the ligand and the pocket – although the nitrogen does point toward the backbone of Val187. The phenyl moiety carrying the linkers is oriented towards the outside of the receptor binding site, consistent with expectation.
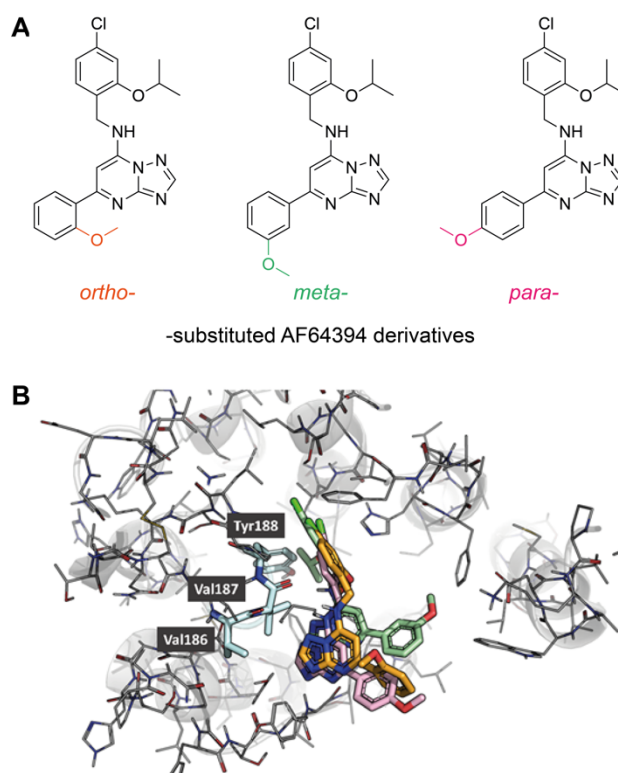
Figure 4.002. Docking poses of AF64394 derivatives to the inactive-state model of GPR3. (**A**) Chemical 2D structures of docked AF64394 derivatives with methoxy substituents in *ortho-*, *meta-* or *para-*position of the phenyl ring. (**B**) Top view of the docking poses of the three molecules when docked to the 7yxa-based GPR3 model. Orange: ortho-, green: meta- and pink: para-substituted AF64394 derivative.

In this study linkers of different lengths (C$_6$-alkyl, four or six polyethylene glycole units) were employed in order to meet the optimal distance between fluorophore and pharmacophore. The optimal linker length is distinct for every GPCR and depends on the distance between the ligand binding pocket and the receptor's extracellular N-terminus. Likewise, the structural flexibility of the employed linker can aid in avoiding unfavorable clashes of the receptor and the fluorescent ligand and can thus have a decisive influence on the affinity of the fluorescent ligand.

The selection of the fluorophore depends on the desired application, i.e., the measurement principle of the assay system. In this case, the chosen fluorophore should be an appropriate BRET acceptor for the energy donor Nluc. 5-TAMRA has been successfully employed as the energy acceptor in numerous NanoBRET studies[524,532,536,537] and was therefore chosen here for the development of AF64394-based fluorescent ligands of GPR3. Additionally, due to the similarity of its excitation and emission spectra, DY-549P1, as an alternative chromophore, was tested.

4.3 Results
4.3.1 Chemistry

The synthesis of the fluorescent ligands can be divided into three parts and is shown in Schemes 4.01-4.03, starting with the synthesis of the linker building blocks **4.003**, **4.006**, and **4.007** (cf. Scheme 4.01). For the synthesis of the PEG linkers (cf. Scheme 4.01A), it was started with the reaction of tetraethylene glycol (PEG-4) or hexaethylene glycol (PEG-6) with methanesulfonyl chloride to yield the corresponding methyl sulfonates **4.001** and **4.004**. Reaction with potassium phthalimide yielded phthalimides **4.002** and **4.005**. This functionality served as a protecting group for the primary amine needed later to introduce the fluorophore. The terminal alcohol group of **4.002** and **4.005** was brominated in a nucleophilic substitution reaction using triphenylphosphine and *N*-bromosuccinimide to yield the PEG linker building blocks **4.003** and **4.006**. In addition, in a one-step synthesis with 1,6-dibromohexane and potassium phthalimide, the alkyl linker building block **4.007** was also prepared in a substitution reaction (cf. Scheme 4.01B).
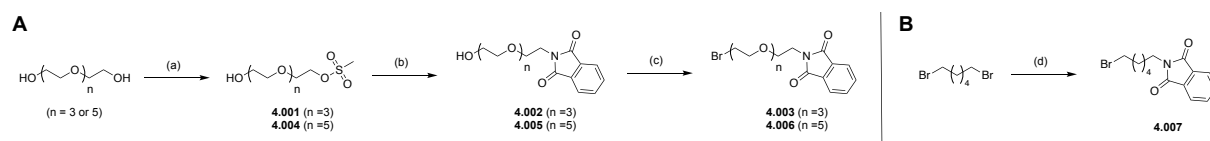
Scheme 4.01. Synthesis of the linker building blocks **4.003**, **4.006**, and **4.007**. Reagents and conditions: (**A**) (a) methanesulfonyl chloride, NEt$_3$, DCM, 0 °C, 10 h → rt, overnight, 35%/44%; (b) potassium phthalimide, DMF, 80 °C, overnight, 66%/100%; (c) triphenylphosphine, *N*-bromosuccinimide, DCM, 0 °C, 2 h, 69%/64%; (**B**) (d) potassium phthalimide, DMF, 40 °C, 24 h, 91%.

Due to the implementation of a linker structure via a phenolic group, the AF64394-like pharmacophore had to be prepared in a way contrary to the described syntheses.[516] Starting from 4-chloro-2-fluorobenzonitrile, the first step was to insert the isopropoxy side chain with the help of the strong non-nucleophilic base KHMDS for the northern

part of the molecule (**4.008**), followed by reduction of the nitrile function to the primary amine **4.009** (cf. Scheme 4.02A).[540] In the reaction to **4.009**, a slight tendency towards chlorine elimination was observed by MS. The synthesis for the southern part of the molecule (cf. Scheme 4.02B) was started from 2-, 3- or 4-hydroxy acetophenone, respectively, to allow linker attachment in *ortho*, *meta*, and *para* positions. In a first step, the phenolic group required for this was benzyl-protected using benzyl bromide to afford **4.010**-**4.012**. The subsequent conversion to β-keto ester compounds **4.013**-**4.015** was carried out using sodium hydride and diethyl carbonate.[541] With the help of 3-amino-1,2,4-triazole under acidic conditions, the formation of the essential [1,2,4]triazolo[1,5-*a*]pyrimidine bicycle and compounds **4.016**-**4.018** subsequently occurred. After chlorination with POCl$_3$, the 7-chloro-[1,2,4]triazolo[1,5-*a*]pyrimidines **4.019**-**4.021** were ready for simple chloride displacement using **4.009** to afford **4.022**-**4.024**. Benzyl deprotection to **4.025**-**4.027** and subsequent Boc protection of the amino function yielded AF64394 analogs **4.028**-**4.030** ready for linker introduction.

These precursors were subsequently converted to **4.031**-**4.037** with linkers **4.003**, **4.006**, or **4.007** (cf. Scheme 4.01), respectively, introducing alkyl- and PEG-based side chains of different lengths (cf. Scheme 4.03). Subsequent hydrazinolysis resulted not only in cleavage of the phthalimide protecting group but, unexpectedly, also of the Boc-protecting group, yielding primary amines **4.038**-**4.044**. In the final step, in a nucleophilic substitution reaction of the primary amines **4.038**-**4.044**, the fluorophores could be introduced using the 5-TAMRA NHS ester and DY-549P1 NHS ester, respectively, yielding the fluorescent ligands **4.045**-**4.055**. The fluorescent ligands were further tested for purity (cf. Figures 4.021-4.031, chapter **4.6.2**) and chemical stability (cf. Figures 4.032-4.035, chapter **4.6.3**) in aqueous solution or DMSO and showed no degradation within an incubation period of 104 days. The fluorescence properties of **4.045**-**4.055** (in DMSO) were determined by recording the excitation and emission spectra shown in shown in Figure 4.037 (chapter **4.6.5**). The 5-TAMRA-labeled ligands exhibited an excitation maximum at around 564 nm and an emission maximum at around 599 nm, while the DY-549P1-labeled ligands showed maxima at around 568 nm and 591 nm, respectively (cf. Table 4.03, chapter **4.6.5**).

A

B

Scheme 4.02. Synthesis of the AF64394 analogs **4.028**-**4.030** as precursor. Reagents and conditions: (**A**) (a) isopropanol, KHMDS (0.5 M), THF, 0 °C to rt, overnight, 99%; (b) LiAlH$_4$, THF, 0 °C, 87%; (**B**) (c) benzyl bromide, K$_2$CO$_3$, rt, 4 h, 100%/100%/100%; (d) NaH, diethyl carbonate, DMF, argon, 0 °C to rt, 8 h, 63%/45%/66%; (e) 3-amino-1,2,4-triazole, HOAc, argon, 110 °C, 16 h, 31%/21%/19%; (f) POCl$_3$, 105 °C, 1 h, 58%/69%/63%; (g) **4.009**, NEt$_3$, DCM, argon, rt, 2 d, 35%/100%/64%; (h) H$_2$ (1 atm), Pd/C, MeOH, reflux, TLC monitoring, 91%/87%/62%; (i) Boc$_2$O, NEt$_3$, DMAP (cat.), CHCl$_3$, 0 °C, overnight, 64%/77%/80%.

No.	X	R	substitution	No.	X	R	substitution
4.028	-	-	ortho	4.042	B	-	meta
4.029	-	-	meta	4.043	B	-	para
4.030	-	-	para	4.044	C	-	ortho
4.031	A	-	ortho	4.045	A	D	ortho
4.032	A	-	meta	4.046	A	D	meta
4.033	A	-	para	4.047	A	D	para
4.034	B	-	ortho	4.048	B	D	ortho
4.035	B	-	meta	4.049	B	D	meta
4.036	B	-	para	4.050	B	D	para
4.037	C	-	ortho	4.051	C	D	ortho
4.038	A	-	ortho	4.052	B	E	ortho
4.039	A	-	meta	4.053	B	E	meta
4.040	A	-	para	4.054	B	E	para
4.041	B	-	ortho	4.055	C	E	ortho

Scheme 4.03. Synthesis of the fluorescent ligands **4.045**-**4.055**. Reagents and conditions: (a) **4.003**, **4.006**, or **4.007**, K_2CO_3, DMF, 40 °C, 5-6 d, 83%/91%/51%/27%/37%/41%/85%; (b) N_2H_4 x H_2O, *n*-butanol, rt, 16 h, 5%/9%/16%/36%/8%/20%/36%; (c) 1. 5-TAMRA NHS ester or DY-549P1 NHS ester, NEt_3, DMF, rt, 3 h; 2. 10% aq. TFA, rt, 15 min, 42%/18%/65%/86%/59%/88%/66%/ 84%/100%/97%/100%.

4.3.2 Pharmacological Characterization

To assess the suitability of synthesized fluorescent AF64394 analogs for BRET-based binding studies to GPR3 (cf. Figure 4.003A), a HEK293-based cell line was developed stably expressing N-terminally Nluc-tagged GPR3. The luminescence emission spectra obtained with this cell line showed the characteristic intensity peak around 460 nm (cf. Figure 4.037, chapter **4.6.5**).

Stimulation of these cells with the eleven fluorescent AF64394 analogs (cf Figure 4.003B-L) revealed time- and concentration-dependent increases in BRET for seven compounds: **4.046**, **4.049**, **4.047**, **4.050**, **4.045**, **4.048**, and **4.051**. Of note, none of the compounds bearing the DY-549P1 fluorophore (**4.052**-**4.055**) showed increasing BRET ratios. In contrast, all 5-TAMRA-labeled compounds induced significant increases in BRET at 30 µM or lower concentrations. The time courses of **4.049** and **4.050** (Figure 4.003C, F) suggested low ligand affinities since no BRET response was obtained below 10 µM.
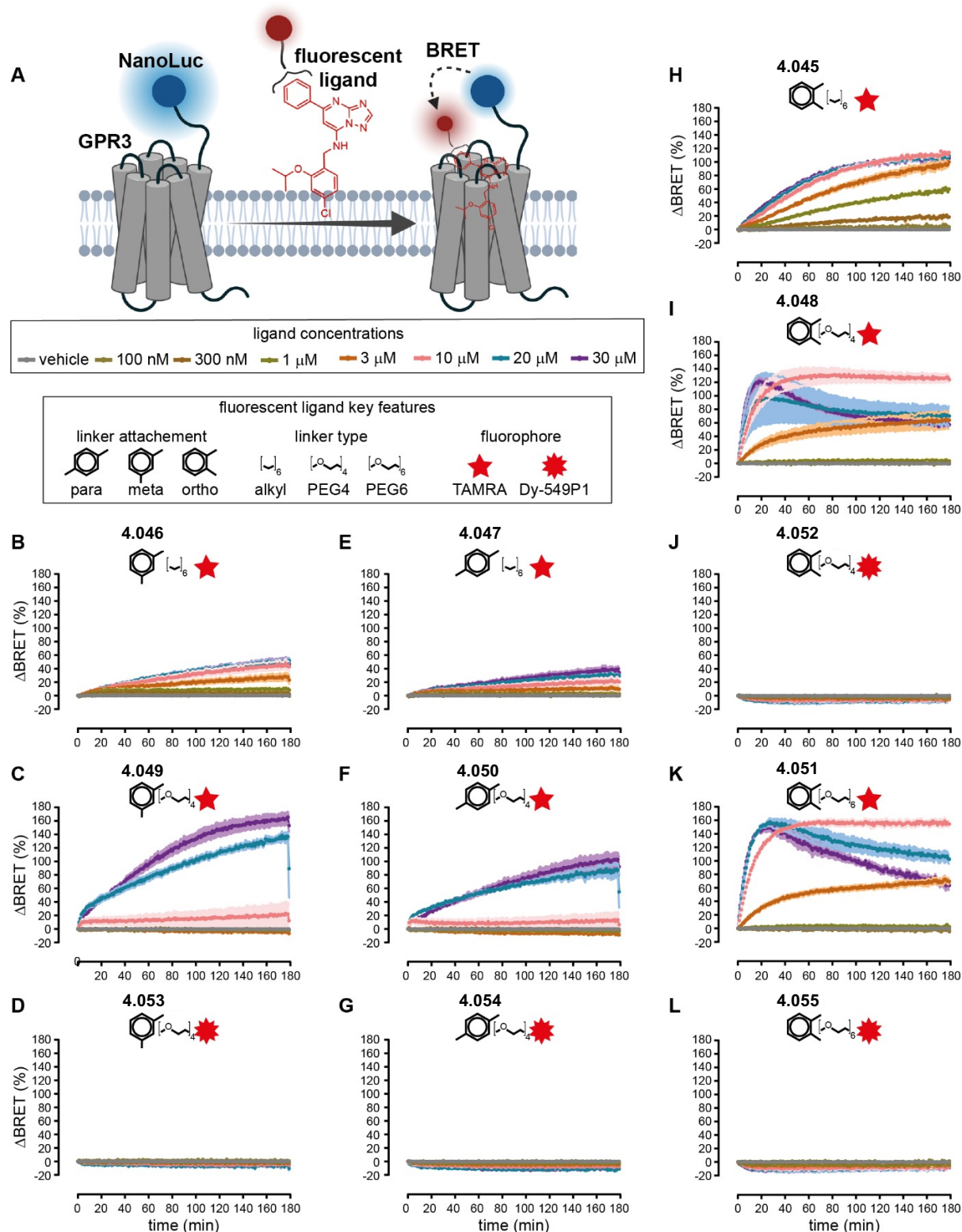
Figure 4.003. NanoBRET saturation binding time courses of fluorescent AF64394 analogs. (**A**) Scheme of the assay principle. (**B-L**) NanoBRET time courses of *meta-* (**B-D**), *para-* (**E-G**) and *ortho*-labeled (**H-L**) fluorescent AF64394 analogs. The indicated fluorescent compound was added to cells stably expressing Nluc-GPR3 before recording the first time point. Data represent mean ± SEM of three independent experiments. Experiments have been conducted with HEK293A cells stably expressing Nluc-GPR3.

To obtain a tentative estimation of the binding affinities of the five remaining 5-TAMRA-labeled compounds (**4.045**, **4.046**, **4.047**, **4.048**, and **4.051**), their half maximal effective concentrations were analyzed at the peak of the BRET response recorded in these total binding experiments in which no unspecific binding control was included (cf. Figure 4.004A, Table 4.01). These calculations suggested the lowest affinity for compound **4.047** with an alkylic linker in *para* position, while **4.046** (alkylic linker in *meta*), **4.048** (PEG-4 linker in *ortho*), and **4.051** (PEG-6 linker in *ortho*) all had very similar pEC_{50} values indicating binding affinity in the low micromolar range. Compound **4.045** (UR-MB-355), composed of the AF64394 pharmacophore, an alkylic linker in the ortho position of the phenyl ring, and TAMRA revealed the highest affinity for binding to stably expressed Nluc-GPR3. The kinetic determination of **4.045**'s dissociation constant (based on the BRET time course data shown in Figure 4.003H) further confirmed the nanomolar affinity of this fluorescent GPR3 ligand (cf. Figure 4.004B) and, therefore, this analog of AF64394 was selected for subsequent pharmacological characterization. In the docking poses of this study the methoxy-substituted phenyl ring points toward the extracellular part of the pocket. However, the resolution of docking calculations does not allow to pinpoint exactly why the ortho-substituted **4.045** shows the highest affinity.

To confirm the specificity of the obtained BRET increase, increasing concentrations of **4.045** were incubated for three hours with HEK293A cells transiently transfected with four different N-terminally Nluc-labeled GPCR constructs, which had been validated in previous BRET-based ligand binding studies[32,44] and compared the resulting BRET ratios to those obtained with HEK293A cells transiently expressing Nluc-GPR3. Here, the BRET ratios obtained with the Nluc-labeled constructs of the muscarinic acetylcholine receptor M1 (M_1R), of the β-adrenergic receptors β_1AR and β_2AR, and of the type-1 angiotensin II receptor (AT_1R) resembled a linear concentration-response correlation. Only the data obtained with Nluc-GPR3 showed an exponential increase in BRET with increasing ligand concentrations, confirming the specificity of the BRET response observed with **4.045** and its selectivity for GPR3 over other class A GPCRs (cf. Figure 4.004C).

Next, it was determined whether **4.045** preserves the inverse agonistic activity of its parent compound, AF64394. Therefore, cyclic AMP response element (*CRE*) reporter gene activity was quantified in cell transiently transfected with wildtype GPR3 or empty vector (pcDNA) (cf. Figure 4.004D). The elevated *CRE* response in vehicle-treated

pcDNA- vs. GPR3-transfected cells is in accordance with the high level of constitutive GPR3 activity leading to ligand-independent activation of the G_s-adenylyl cyclase-cAMP signaling cascade. Notably, *CRE* activity in GPR3-transfected cells was not only significantly reduced in the presence of 10 µM AF64394 but also due to incubation with 10 µM **4.045**. These results demonstrate that **4.045** still acts as a (partial) inverse agonist on GPR3. Furthermore, this finding indicates that labeling AF64394 in the *ortho* position of its phenyl ring with 5-TAMRA via an alkylic linker does not abolish ligand efficacy at GPR3.
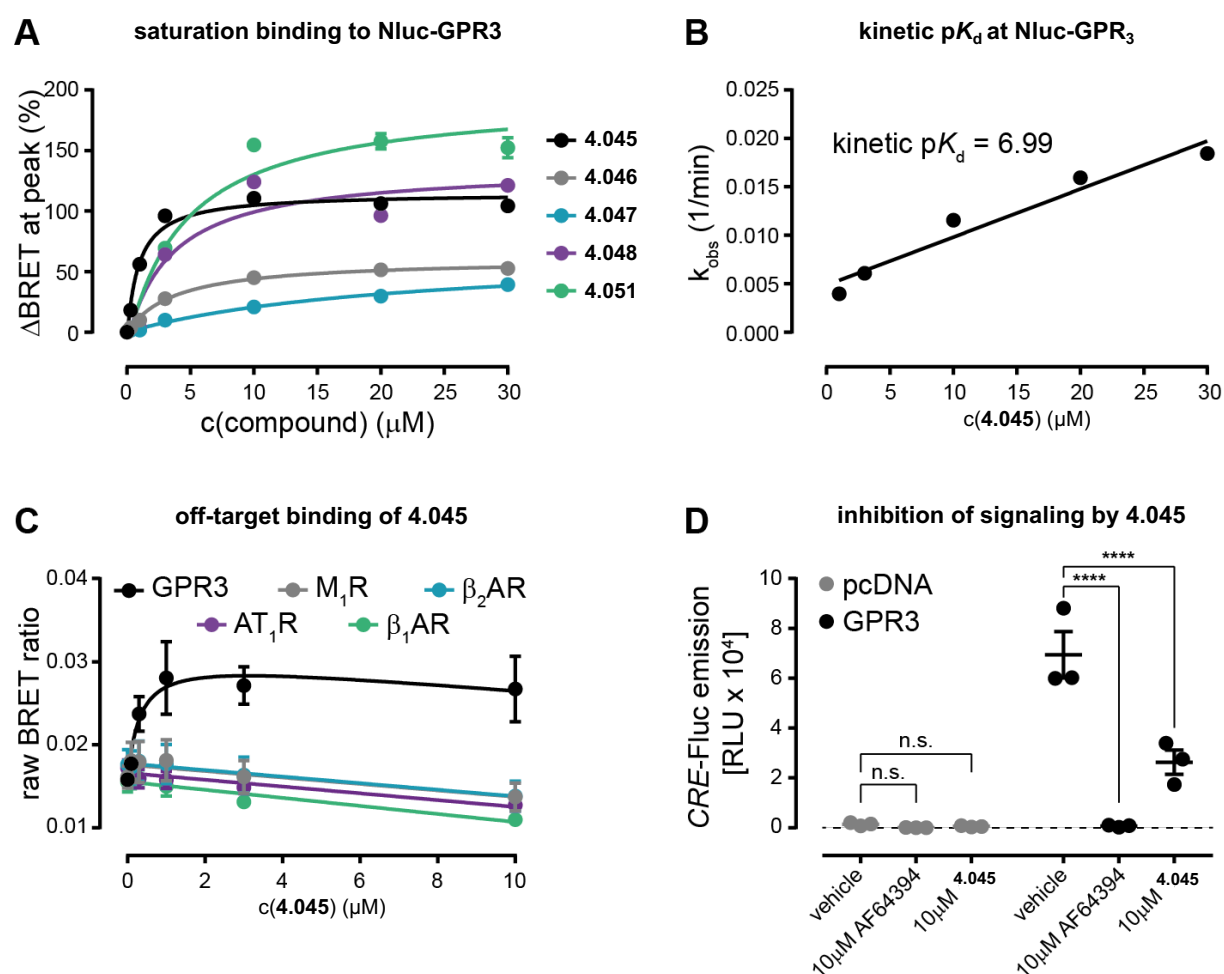
Figure 4.004. Characterization of **4.045**. (**A**) Concentration-response curves of five fluorescent AF64394 analogs (**4.045**-**4.048** and **4.051**) binding to Nluc-GPR3. (**B**) Kinetic K_d determination of **4.045** for binding to Nluc-GPR3. (**C**) Concentration-response curves of **4.045** for binding to transiently expressed Nluc-GPCR constructs. (**D**) Functional characterization of **4.045** in a luminescence-based CRE reporter gene assay. Data represent mean ± SEM of three independent experiments conducted in stably Nluc-GPR3 (**A**, **B**) or transiently transfected HEK293A cells. Linear vs. exponential correlation of the data in **C** was tested using the Extra-sum-of-squares F-test ($p < 0.05$). Significance in **D** was assessed using the Two-way-ANOVA followed by Dunnett's multiple comparison (****$p < 0.0001$).

Following the confirmation that **4.045** specifically binds to GPR3, the suitability of this fluorescent GPR3 ligand was probed for the investigation of ligand binding to the closely related class A orphan GPCRs GPR6 and GPR12 and quantified the affinity of **4.045** by including Nluc-β_1AR, allowing the correction of unspecific binding. Upon transient transfection of either Nluc-GPR3, -GPR6, or -GRP12 and incubation with increasing concentrations of **4.045**, very similar exponential concentration-response correlations for all three orphan GPCRs were obtained (cf. Figure 4.005A). Statistical comparison of the computed K_d values indicated that **4.045** exhibits a similar binding affinity for GPR3, GPR6, and GPR12 (cf. Table 4.01). Of note, the pK_d value measured in these (only specific) saturation binding experiments (mean $pK_d \pm SEM = 6.52 \pm 0.09$) was very similar to that obtained from the kinetic pK_d (6.99) calculations (cf. Figure 4.004B).

Ultimately, it was aimed to investigate whether the developed NanoBRET binding assay is suitable to assess in a signaling pathway-independent manner whether unlabeled compounds, that, e.g., ranked high in a virtual docking screen or were active in a cAMP-based screening campaign, interact with GPR3 *in vitro*. Therefore, competition binding experiments were conducted, in which the stable Nluc-GPR3 cell line was co-incubated with 1 µM **4.045**, along with increasing concentrations of either AF64394 or DPI.

The experiments with AF64394 revealed a modest (~5%), yet competitor concentration-dependent decrease in BRET between **4.045** and Nluc-GPR3 (cf. Figure 4.005B). The measured inhibitory constant allowed, for the first time, to calculate the affinity of AF64394 to GPR3 ($pK_i = 6.53 \pm 0.20$). This affinity is almost identical to that of its fluorescently labeled analog **4.045** ($pK_d = 6.52 \pm 0.09$, see above), indicating that the design strategy based on attaching the alkylic linker with TAMRA to the ortho position of the phenyl ring of AF64394 had no negative effect on ligand affinity towards GPR3.

Surprisingly, the co-incubation experiments with DPI revealed a concentration-dependent increase in **4.045** binding to Nluc-GPR3 (cf. Figure 4.005C) and the obtained potency of DPI in modulating this binding event (mean $pEC_{50} \pm SEM = 5.85 \pm 0.09$) was very similar to its potency in GPR3-mediated cAMP signaling[20]. These findings indicate that DPI has a positive allosteric modulatory effect on the binding of fluorescent AF64394 to GPR3.
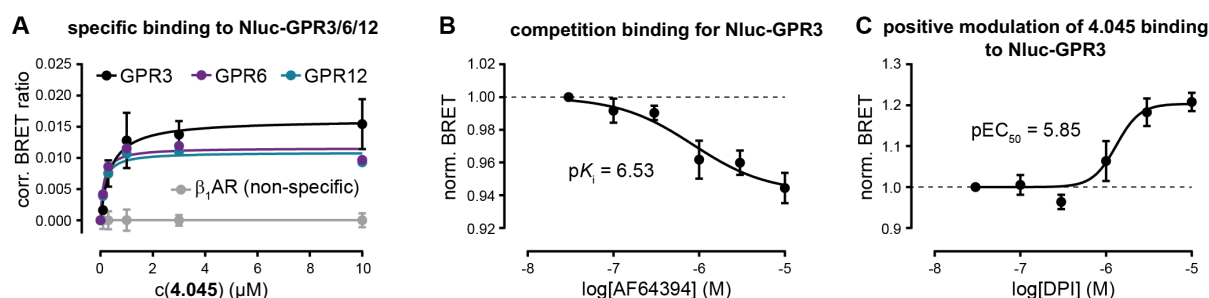
Figure 4.005. Application of **4.045** for NanoBRET binding studies with GPR3/6/12. (**A**) Concentration-response curves of **4.045** for binding to transiently expressed Nluc-GPR3, Nluc-GPR6, Nluc-GPR12, and Nluc-β_1AR after three hours of ligand incubation. The raw BRET ratios obtained with Nluc-β_1AR were averaged and deducted from raw BRET ratios obtained with Nluc-β_1AR and Nluc-GPR3/6/12 in order to correct for non-specific effects. Extra-sum-of-squares F-test revealed no statistical difference between the K_d values obtained with Nluc-GPR3, -GPR6 or -GPR12 ($p < 0.05$). (**B**) Concentration-response curve of AF64394 inhibiting BRET between Nluc-GPR3 and 1 µM **4.045**. (**C**) Concentration-response curve of DPI enhancing BRET between Nluc-GPR3 and 1 µM **4.045**. Data represent mean ± SEM of three (**A**), four (**B**), or six (**C**) independent experiments conducted in HEK293A cells transiently (**A**) or cells stably expressing (**B**, **C**) the indicated Nluc-GPCR construct.

Table 4.01. Binding affinities of fluorescent AF64394 derivatives

compound	pEC_{50} at Nluc-GPR3 (total binding)[a]		pK_d at GPR3/6/12 or (pK_i at GPR3) (specific binding)	
	mean ± SEM	N	mean ± SEM	N
4.045	6.05 ± 0.03	3	6.52 ± 0.09[n.s.] / 7.18 ± 0.04[n.s.] / 7.12 ± 0.04[n.s.]	3 / 3 / 3
4.046	5.35 ± 0.07	3	n.d.	
4.047	4.96 ± 0.26	3	n.d.	
4.048	5.47 ± 0.07	3	n.d.	
4.049	< 5	3	n.d.	
4.050	< 5	3	n.d.	
4.051	5.35 ±0.04	3	n.d.	
4.052	< 4.5	3	n.d.	
4.053	< 4.5	3	n.d.	
4.054	< 4.5	3	n.d.	
4.055	< 4.5	3	n.d.	
AF64394	n.d.		(6.53 ± 0.20)[b]	4
DPI	5.85 ± 0.09[b]	6	n.d.	

[a]: Values are derived from the total binding data shown in Figure 4.003A; [b]: Values derived from co-incubation, total binding experiments with 1 µM **4.045**. [n.s.]: No statistical difference between pK_d values as determined by Extra-sum-of-squares F-test. Values are derived from specific binding experiments using Nluc-β_1AR as a negative control shown in Figure 4.005A. Data shown are mean values ± SEM of N independent experiments.

4.4 Discussion and Conclusion

Orphan GPCRs provide an immense potential for drug discovery but represent challenging targets for pharmacological research. The search for novel ligands of these receptors is often hampered by a limited toolset of appropriate screening assays because the receptor's complete signaling portfolio remains elusive for lack of known endogenous agonists. Thus, signaling pathway-independent readouts of compound-receptor interaction (e.g., ligand binding assays or conformational GPCR biosensors) provide many advantages due to the unbiased nature of the detection principle. GPR3/6/12, in particular, suffer from a very limited assay toolbox. All GPR3-targeting small molecule screens have been conducted with either cAMP- or β-arrestin-based methods,[512–514,516,517] although it is still unknown whether GPR3 also stimulates distinct intracellular signaling pathways upon activation.

This study describes the development of a signaling-pathway independent technique to assess compound-GPR3 interaction in real-time and in living cells. Starting from the most potent currently available GPR3 ligand a series of eleven fluorescent analogs of AF64394 was designed and synthesized for BRET-based ligand binding studies to Nluc-tagged GPR3. In line with computational predictions of AF64394's binding pose in GPR3, the attachment of a linker with a 5-TAMRA fluorophore to the ligand's phenyl ring was tolerated, best in the *ortho* variant with an alkylic linker, compound **4.045**, which exhibits nanomolar affinity for Nluc-GPR3. Compared to attachments of the same linker-fluorophore combination in *meta* (**4.046**) or *para* position (**4.047**), **4.045** showed a 4- and 24-fold higher binding affinity, respectively. Interestingly, replacing the alkylic linker in **4.045** with a PEG-4 (**4.048**) or PEG-6 (**4.051**) led to a similar 4- to 5-fold reduction in affinity indicating that hydrophilic substituents in this position hamper ligand engagement with GPR3 or enhance the dissociation rates of these compounds. Conversely – and in agreement with this hypothesis – competition experiments showed only very modest displacement of **4.045** by AF64394 from GPR3. This suggests that the structural modifications in **4.045** serve as a lipophilic anchor that slows down the dissociation of this fluorescent ligand from GPR3.

An interesting observation from the docking calculations was that using a GPR3 model built based on an active structure did not deliver the same pose as shown in Figure 4.002B, but one where the phenyl ring carrying the extension points deeper inside the helix bundle in the receptor (cf. Figure 4.036, chapter **4.6.4**). Such a pose is

incompatible with the attachment of linkers and emphasizes the importance of choosing a conformational state of the receptor that is compatible with the pharmacological effect of the ligand to be docked (agonist, antagonist, or inverse agonist).

Compound **4.045** further exhibits similar, high nanomolar affinity to Nluc-GPR6 and -GPR12. This is in accordance with the high sequence similarity of these three orphan GPCRs (about 60%[497]) but surprising in view of the reported about 100-fold reduced potency of AF64394 at GPR6 and GPR12[516]. This discrepancy suggests that the attachment of lipophilic moieties in *ortho* position of the phenyl ring of AF64394 enhances binding to GPR6 and GPR12 and reduces ligand selectivity for GPR3 over GPR6/12.

From a pharmacological and drug discovery perspective, probably the most intriguing finding of this study is the enhanced binding of **4.045** upon co-incubation with DPI. Thus far, nothing is known about multiple ligand binding sites in GPR3 and previous characterization attempts of the orthosteric binding pocket were solely based on computational predictions.[538,542] In these *in silico* studies, DPI and AF64394 were docked into the same – supposedly – orthosteric binding pocket of GPR3. These results, however, suggest that (i) the AF64394-based ligand **4.045** and DPI engage different sites at this receptor and that (ii) DPI binding to GPR3 has a positive effect on **4.045**:GPR3 interaction. Given its planar three-dimensional structure, it can be hypothesized that DPI could bind to the outer surface of the transmembrane core by engaging one of the shallow groves recently described to compose the allosteric pocketome in GPCRs.[543]

Future studies should aim at exploring these allosteric mechanisms in GPR3 and its related orphan GPCRs GPR6 and GPR12 by combining this new NanoBRET binding assay with readouts for signaling, site-directed mutagenesis in GPR3/6/12, and blind docking (i.e., without a pre-specified binding site). These insights could then be taken further to design drug-like orthosteric ligands and allosteric modulators for GPR3/6/12 which could ultimately aid in the development of future therapies against Alzheimer's disease or metabolic disorders.

4.5 Experimental Part
4.5.1 Chemistry
4.5.1.1 General Experimental Conditions

Unless otherwise stated, chemicals and solvents were procured from commercial suppliers and used as received. All the solvents were of analytical grade or distilled prior to use. Anhydrous solvents were stored over molecular sieve under protective gas. The fluorescent dye 5-TAMRA NHS ester was purchased from Lumiprobe (Hannover, Germany). The fluorescent dye DY-549P1 NHS ester was purchased from Dyomics (Jena, Germany). Tetraethylene glycol, *N*-bromosuccinimide, and diethyl carbonate were purchased from Alfa Aesar (Kandel, Germany). Hexaethylene glycole, di-*tert*-butyl dicarbonate, and trifluoroacetic acid were purchased from abcr (Karlsrube, Germany). 1,6-Dibromohexane, benzyl bromide, and 4-dimethylamino pyridine were purchased from Acros Organics (Geel, Belgium). Acetic acid, isopropanol, triethylamine, methanesulfonyl chloride,1-butanol, 0.5 M potassium bis(trimethylsilyl)amide solution in toluene, sodium hydride, phosphorylchloride, and hydrazine monohydrate were purchased from Sigma-Aldrich (Taufkirchen, Germany). Dichloromethane, methanol, tetrahydrofuran, dimethylformamide, diethyl ether, chloroform, ethyl acetate, and potassium carbonate were purchased from Fisher Scientific Chemicals (Schwerte, Germany). Potassium phthalimide, 4-chloro-2-fluorobenzonitrile, 2-hydroxy acetophenone, 3-hydroxy acetophenone, 4-hydroxy acetophenone, and 3-amino-1,2,4-triazole were purchased from TCI (Eschborn, Germany). Triphenylphosphine, lithium aluminium hydride, and 1M hydrochloric acid were purchased from Merck (Darmstadt, Germany). Acetonitrile was purchased from VWR Chemicals (Darmstadt, Germany), sodium sulfate and ammonia solution 25% from Carl Roth (Karlsruhe, Germany). Deuterated solvents for nuclear magnetic resonance (NMR) spectroscopy were purchased from Deutero (Kastellaun, Germany). For the preparation of buffers and HPLC eluents Millipore-grade water was used. Column chromatography was carried out using silica gel 60 (0.040-0.063 mm, Merck (Darmstadt, Germany)). Reactions were monitored by thin layer chromatography (TLC) on silica gel 60 F254 aluminium sheets (Merck) and compounds were detected under UV light at 254 nm by potassium permanganate or ninhydrin staining (0.8 g ninhydrin, 200 mL *n*-butanol, 6 mL acetic acid). NMR spectra (^{1}H NMR and ^{13}C NMR, ^{19}F NMR, DEPT, 2D NMR) were recorded on a Bruker Avance-300 (7.05 T, [1]H: 300 MHz, [13]C: 75.5 MHz, [19]F: 188), Avance-400 (9.40 T, [1]H: 400 MHz, [13]C: 100.6 MHz,

[19]F: 282), or Avance-600 (14.1 T; [1]H: 600 MHz, [13]C: 150.9 MHz; cryogenic probe) NMR spectrometer (Bruker, Karlsruhe, Germany). Multiplicities are specified with the following abbreviations: s (singlet), d (doublet), t (triplet), q (quartet), p (pentet), m (multiplet), br (broad), as well as combinations thereof. High-resolution mass spectrometry (HRMS) was performed on an AccuTOF GCX GC/MS system (Jeol, Peabody, MA, USA) using an EI source or a Q-TOF 6540 UHD LC or GC/MS system (Agilent Technologies, Santa Clara, USA) using an ESI (in case of LC coupling) or an APCI (in case of GC coupling) source. Preparative HPLC was performed with a system from Knauer (Berlin, Germany) consisting of two K-1800 pumps and a K-2001 detector or with a Prep 150 LC system from Waters (Eschborn, Germany) consisting of a 2545 binary gradient module, a 2489 UV/visible detector and a fraction collector III. The following columns were used: Nucleodur 100-5 C18 (5 µm, 250 x 21 mm, Macherey-Nagel, Düren, Germany), a Kinetex XB-C18 100A (5 µm, 250 x 21.2 mm, Phenomenex, Aschaffenburg, Germany), and a Gemini-NX C18 (5 µm, 250 mm x 21 mm; Phenomenex). Solvent flow rates of either 15-20 mL/min (Nucleodur, Kinetex and Gemini columns) or 30 mL/min (Interchim column) at rt were employed. A detection wavelength of 220 nm and mixtures of acetonitrile (MeCN) and 0.05-0.1% aqueous TFA were used as mobile phases. MeCN was removed from the eluates under reduced pressure prior to freeze-drying (Christ Alpha 2-4 LD freeze dryer (Martin Christ, Osterode am Harz, Germany) or ScanVac CoolSafe 4-15L freeze dryer from Labogene (LMS, Brigachtal, Germany), both equipped with a RZ 6 rotary vane vacuum pump (Vacuubrand, Wertheim, Germany)). Analytical purity and stability control was performed on a 1100 HPLC system from Agilent Technologies equipped with an Instant Pilot controller, a G1312A binary pump, a G1329A ALS autosampler, a G1379A vacuum degasser, a G1316A column compartment, and a G1315B diode array detector (DAD). The column was a Phenomenex Kinetex XB-C18 column (250 x 4.6 mm, 5 µm) (Phenomenex, Aschaffenburg, Germany) or a Phenomenex Gemini NX-C18 column (250 x 4.6 mm, 5 µm). The oven temperature during HPLC analysis was 30 °C. As a mobile phase, mixtures of MeCN/aqueous TFA or MeCN/aqueous NH_3 were used. Absorbance was detected at 220 nm and 543 nm or 560 nm. The injection volume was 20-80 µL at compound concentrations of 1 mM. The following linear gradient was applied: MeCN/TFA (0.05%) (v/v) 0 min: 10:90, 25 min: 95:5, 35 min: 95:5 (compound **4.045**-**4.051**) or MeCN/NH_3 (0.05%) (v/v) 0 min: 10:90, 25 min: 95:5, 35 min: 95:5 (compound **4.052**-**4.055**); flow rate: 1.0 mL/min, t_0 (Kinetex XB-C18) =

2.75 min, t_0 (Gemini NX-C18) = 3.00 min (t_0 = dead time). Retention (capacity) factors k were calculated from the retention times t_R according to $k = (t_R - t_0)/t_0$. The dead time was experimentally determined by injecting a sample of unretained thiourea (200 μM, 10 μL) and recording of the retention time. The purities of the compounds were calculated by the percentage peak area of the chromatograms.

4.5.1.2 Compound Characterization

Compounds **4.045**-**4.055** were characterized using the following methods: HRMS, ^{1}H NMR spectroscopy, ^{13}C NMR spectroscopy, and 2D NMR spectroscopy (see chapter **4.6.1**, Figures 4.006-4.020). The purities of the target compounds **4.045**-**4.055** used for pharmacological investigation were ≥ 95% (chromatograms are shown in chapter **4.6.2**, Figures 4.021-4.031). For biological testing, the target compounds (trifluoroacetate or ammonium salts) were dissolved in DMSO to get a final concentration of 10 mM.

4.5.1.3 Synthesis and Analytical Data of Linker 4.003, 4.006, and 4.007

2-(2-(2-(2-Hydroxyethoxy)ethoxy)ethoxy)ethyl methanesulfonate (4.001)[544]
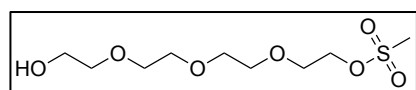
The reaction was carried out by solving tetraethylene glycol (PEG-4) (5.60 g, 28.83 mmol, 1 eq) and triethylamine (4.02 mL, 28.83 mmol, 1 eq) in 100 mL dichloromethane. The mixture was cooled to 0 °C by using an ice bath. Subsequently, methanesulfonyl chloride (2.23 mL, 28.83 mmol, 1 eq) in 300 mL dichloromethane was added dropwise over a period of 10 hours. After addition, the ice bath was removed, and stirring was continued overnight. Evaporation of the solvent and purification by column chromatography (DCM/Methanol 98/2-95/5) resulted in a yellowish oil (2.76 g, 35%).^{1}H NMR (300 MHz, CDCl₃) δ 4.31 – 4.22 (m, 2H), 3.69 – 3.43 (m, 14H), 3.05 (bs, 1H), 2.97 (s, 3H). ^{13}C NMR (75 MHz, CDCl₃) δ 72.45, 70.45, 70.32, 70.17, 69.40, 68.87, 61.45, 37.49. *m/z* [M+H^{+}] calculated for $C_9H_{21}O_7S^+$: 273.1003, found 273.1005; $C_9H_{20}O_7S$ (272.31).

2-(2-(2-(2-(2-Hydroxyethoxy)ethoxy)ethoxy)ethyl)isoindoline-1,3-dione (4.002)[545]
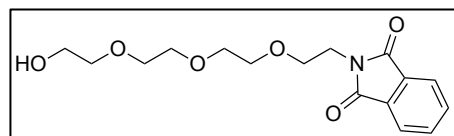
Potassium phthalimide (2.12 g, 11.46 mmol, 1.2 eq) and **4.001** (2.60 g, 9.55 mmol, 1 eq) were dissolved in 200 mL anhydrous DMF. The mixture was heated to 80 °C, and stirring was continued overnight. Subsequently, the solvent was removed

under reduced pressure, and the crude product was purified by column chromatography (DCM/Methanol 95/5), yielding a colorless oil (2.05 g, 66%). ^{1}H NMR (300 MHz, CDCl$_3$) δ 7.86 – 7.79 (m, 2H), 7.73 – 7.66 (m, 2H), 3.88 (t, J = 5.8 Hz, 2H), 3.76 – 3.52 (m, 14H), 2.64 (s, 1H). ^{13}C NMR (75 MHz, CDCl$_3$) δ 168.32, 133.95, 132.14, 123.50, 72.49, 70.66, 70.53, 70.34, 70.10, 67.97, 61.74, 37.28. HRMS (ESI-MS) m/z: [M+H$^+$] calculated for C$_{16}$H$_{22}$NO$_6^+$: 324.1442, found 324.1446; C$_{16}$H$_{21}$NO$_6$ (323.35).

2-(2-(2-(2-(2-Bromoethoxy)ethoxy)ethoxy)ethyl)isoindoline-1,3-dione (4.003)[546]
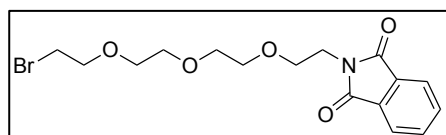
4.002 (2.05 g, 6.34 mmol, 1 eq) was dissolved in 200 mL dichloromethane and cooled by an ice bath to 0 °C. Subsequently, triphenylphosphine (2.00 g, 7.61 mmol, 1.2 eq) in 50 mL dichloromethane was quickly dropped into the solution. After 15 minutes, N-bromosuccinimide (1.35 g, 7.61 mmol, 1.2 eq) was added. The mixture was now stirred at 0 °C for 2 h. The eeaction progress was monitored by TLC (R$_f$ = 0.85, DCM/Methanol 95/5). Evaporation of the solvent and purification by column chromatography (DCM/Methanol 95/5) of the resuide resulted in a colorless oil (1.70 g, 69%). ^{1}H NMR (300 MHz, CDCl$_3$) δ 7.82 – 7.73 (m, 2H), 7.70 – 7.63 (m, 2H), 3.84 (t, J = 5.8 Hz, 2H), 3.75 – 3.66 (m, 4H), 3.63 – 3.52 (m, 8H), 3.39 (t, J = 6.3 Hz, 2H). ^{13}C NMR (75 MHz, CDCl$_3$) δ 168.20, 133.95, 132.09, 123.20, 71.13, 70.59, 70.45, 70.09, 67.89, 37.25, 30.42. m/z [M+H$^+$] calculated for C$_{16}$H$_{21}$BrNO$_5^+$: 386.0596, found 386.0598; C$_{16}$H$_{20}$BrNO$_5$ (386.24).

17-Hydroxy-3,6,9,12,15-pentaoxaheptadecyl methanesulfonate (4.004)[547]
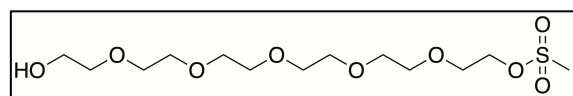
The reaction was carried out by solving hexaethylene glycole (PEG-6) (5.60 g, 19.83 mmol, 1 eq) and triethylamine (2.77 mL, 19.83 mmol, 1 eq) in 100 mL dichloromethane. The mixture was cooled to 0 °C by using an ice bath. Subsequently, methanesulfonyl chloride (1.53 mL, 19.83 mmol, 1 eq) in 300 mL dichloromethane was added dropwise over a period of 10 hours. After addition, the ice bath was removed, and stirring was continued overnight. Evaporation of the solvent and purification by column chromatography (DCM/Methanol 98/2-95/5) resulted in a yellowish oil (3.14 g, 44%). ^{1}H NMR (300 MHz, CDCl$_3$) δ 4.41 – 4.35 (m, 2H), 3.80 – 3.56 (m, 22H), 3.08 (s, 3H), 2.69 (bs, 1H). ^{13}C NMR (75 MHz, CDCl$_3$) δ 72.54, 70.62, 70.58, 70.55, 70.53, 70.32, 69.39, 69.03, 61.74, 37.76. m/z [M+H$^+$] calculated for C$_{13}$H$_{29}$O$_9$S$^+$: 361.1527, found 361.1531; C$_{13}$H$_{28}$O$_9$S (360.42).

2-(17-Hydroxy-3,6,9,12,15-pentaoxaheptadecyl)isoindoline-1,3-dione   (4.005)[548]
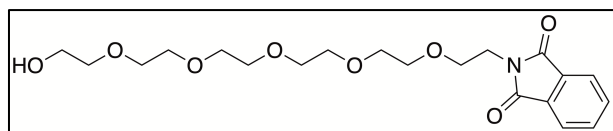
Potassium phthalimide (1.86 g, 10.02 mmol, 1.2 eq) and **4.004** (3.01 g, 8.35 mmol, 1 eq) were dissolved in 200 mL anhydrous DMF. The mixture was heated to 80 °C, and stirring was continued overnight. Subsequently the solvent was removed under reduced pressure, and the crude product was purified by column chromatography (DCM/Methanol 95/5), yielding a colorless oil (3.44 g, 100%). ^{1}H NMR (300 MHz, CDCl$_3$) δ 7.87 – 7.78 (m, 2H), 7.75 – 7.65 (m, 2H), 3.88 (t, J = 5.7 Hz, 2H), 3.76 – 3.54 (m, 22H), 2.69 (s, 1H). ^{13}C NMR (75 MHz, CDCl$_3$) δ 168.29, 133.95, 132.15, 123.25, 72.54, 70.61, 70.55, 70.52, 70.35, 70.07, 67.92, 61.75, 37.26. m/z [M+H$^+$] calculated for C$_{20}$H$_{30}$NO$_8^+$: 412.1966, found 412.1970; C$_{20}$H$_{29}$NO$_8$ (411.45).

2-(17-Bromo-3,6,9,12,15-pentaoxaheptadecyl)isoindoline-1,3-dione (4.006)
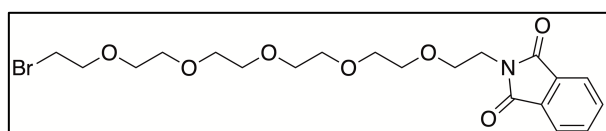
4.005 (3.44 g, 8.36 mmol, 1 eq) was dissolved in 200 mL dichloromethane and cooled by an ice bath to 0 °C. Subsequently, triphenylphosphine (2.63 g, 10.03 mmol, 1.2 eq) in 50 mL dichloromethane was quickly dropped into the solution. After 15 minutes, *N*-bromosuccinimide (1.79 g, 10.03 mmol, 1.2 eq) was added. The mixture was now stirred at 0 °C for 2 h. The reaction progress was monitored by TLC (R$_f$ = 0.85, DCM/Methanol 95/5). Evaporation of the solvent and purification by column chromatography (DCM/Methanol 95/5) of the resuide resulted in a colorless oil (2.55 g, 64%). ^{1}H NMR (300 MHz, CDCl$_3$) δ 7.84 – 7.78 (m, 2H), 7.73 – 7.66 (m, 2H), 3.87 (t, J = 0.7 Hz, 2H), 3.78 (t, J = 6.3 Hz, 2H), 3.71 (t, J = 6.0 Hz, 2H), 3.67 – 3.52 (m, 16H), 3.44 (t, J = 6.3 Hz, 2H). ^{13}C NMR (75 MHz, CDCl$_3$) δ 168.25, 133.95, 132.14, 123.24, 71.20, 70.64, 70.62, 70.59, 70.55, 70.53, 70.08, 67.91, 37.25, 30.39. m/z [M+H$^+$] calculated for C$_{20}$H$_{29}$BrNO$_7^+$: 474.1122, found 474.1120; C$_{20}$H$_{28}$BrNO$_7$ (474.35).

2-(6-Bromohexyl)isoindoline-1,3-dione (4.007)[549]
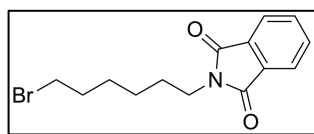
Potassium phthalimide (3.72 g, 20.09 mmol, 1 eq) and 1,6-dibromohexane (24.50 g, 100.42 mmol, 5 eq) were dissolved in 20 mL anhydrous DMF. The mixture was heated to 40 °C, and stirring was continued for 24 hours. The reaction progress was monitored by TLC (R_f = 0.80, EtOAc/PE 1/3). Subsequently the solvent was removed under reduced pressure, and the crude product was purified by column chromatography (EtOAc/PE 1/20-1/3), yielding a colorless oil (5.68 g, 91%). ^{1}H NMR (300 MHz, CDCl$_3$) δ 7.83 – 7.70 (m, 2H), 7.69 – 7.57 (m, 2H), 3.60 (t, J = 7.2 Hz, 2H), 3.31 (t, J = 6.8 Hz, 2H), 1.77 (p, J = 6.6 Hz, 2H), 1.61 (p, J = 7.6 Hz, 2H), 1.48 – 1.20 (m, 4H). ^{13}C NMR (75 MHz, CDCl$_3$) δ 167.37, 132.87, 131.08, 122.14, 36.78, 32.72, 31.56, 27.38, 26.67, 24.98. HRMS (ESI-MS) m/z: [M+H$^+$] calculated for C$_{14}$H$_{17}$BrNO$_2^+$: 310.0437, found 310.0439; C$_{14}$H$_{16}$BrNO$_2$ (310.19).

4.5.1.4 Synthesis and Analytical Data 4-Chloro-2-isopropoxyphenylmethanamine

4-Chloro-2-isopropoxybenzonitrile (4.008)
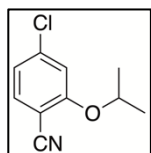
4-Chloro-2-fluorobenzonitrile (3.00g, 19.29 mmol, 1 eq) was dissolved in 30 mL THF. Subsequently, isopropanol (1.78 mL, 23.14 mmol, 1.2 eq) was added to the solution, and the mixture was cooled to 0 °C. 0.5 M potassium bis(trimethylsilyl)amide solution in toluene (KHMDS) (46.28 mL, 23.14 mmol, 1.2 eq) was added dropwise to the stirring solution. After completion, the ice bath was removed, and stirring was continued overnight. Subsequently, the reaction was quenched with 50 mL of water, and the product was extracted with ethyl acetate. The organic layer was washed with brine and dried over Na$_2$SO$_4$. The concentration of the organic solvent yielded 4-chloro-2-isopropoxybenzonitrile as a yellow solid (3.73 g, 99%). The product was used without further purification. ^{1}H NMR (300 MHz, CDCl$_3$) δ 7.43 – 7.39 (m, 1H), 6.94 – 6.88 (m, 2H), 4.58 (hept, J = 6.1 Hz, 1H), 1.36 (d, J = 6.1 Hz, 6H). ^{13}C NMR (75 MHz, CDCl$_3$) δ 160.42, 140.32, 134.48, 120.98, 114.33, 101.56, 72.54, 21.73. HRMS (EI-MS) m/z: [M$^{•+}$] calculated for C$_{10}$H$_{10}$ClNO$^{•+}$: 195.0450, found 195.0448; C$_{10}$H$_{10}$ClNO (195.65).

4-Chloro-2-isopropoxyphenylmethanamine (4.009)[550]
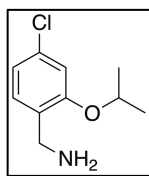
4.008 (3.73 g, 19.06 mmol, 1 eq) was dissolved in THF and cooled to 0 °C. Subsequently, lithium aluminum hydride (LiAlH$_4$) (2.89 g, 76.26 mmol, 4 eq) was added stepwise to the solution. The progress of the reaction was monitored with TLC (R$_f$ (**4.009**) = 0.00, R$_f$ (**4.008**) = 0.80, EtOAc/PE 1/6). After completion, the solution was poured into ice water, and the product was extracted with ethyl acetate. The organic layer was washed with water, dried over Na$_2$SO$_4$, and concentrated under reduced pressure, yielding the title compound as a yellowish oil (3.33 g, 87%). The product was used without further purification. ^{1}H NMR (300 MHz, CDCl$_3$) δ 7.21 – 7.09 (m, 1H), 6.91 – 6.81 (m, 2H), 4.64 – 4.48 (m, 1H), 3.74 (s, 2H), 1.58 (bs, 2H), 1.35 (d, J = 6.0 Hz, 6H). ^{13}C NMR (75 MHz, CDCl$_3$) δ 156.28, 133.04, 131.33, 129.35, 120.16, 113.08, 70.35, 42.38, 22.06. HRMS (ESI-MS) m/z: [M+H$^+$] calculated for C$_{10}$H$_{15}$ClNO$^+$: 200.0837, found 200.0837; C$_{10}$H$_{14}$ClNO (199.68).

4.5.1.5 Synthesis and Analytical Data of Precursors 4.038-4.044

General procedure A

The corresponding hydroxy acetophenone (1 eq) was dissolved in 100 mL DMF. Potassium carbonate (3 eq) and benzyl bromide (1.5 eq) was added to the solution. After addition, the mixture was stirred for 4 h hours at rt. Subsequently, the reaction was quenched with water (50 mL) and acidified with 1 M hydrochloric acid. The product was extracted with diethyl ether (3 x 100 mL). The combined organic layers were washed with 1M hydrochloric acid and dried over Na$_2$SO$_4$ and the solvent was removed under reduced pressure. The product was used in the next step without further purification.

1-(2-(Benzyloxy)phenyl)ethan-1-one (4.010)[551]
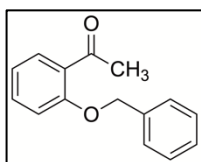
The title compound was synthesized from 2-hydroxy acetophenone (4.42 g, 32.49 mmol, 1 eq), benzyl bromide (8.33 g, 5.79 mL, 48.74 mmol, 1.5 eq), and potassium carbonate (13.47 g, 97.48 mmol, 3 eq) in DMF according to the general procedure A (R$_f$ = 0.50 in EtOAc/PE 1/8) yielding a colorless oil (7.35 g, 100%). ^{1}H NMR (300 MHz, CDCl$_3$) δ 7.81 – 7.73 (m, 1H), 7.48 – 7.37 (m, 6H), 7.07 – 6.98 (m, 2H), 5.17 (s, 2H), 2.62 (s, 3H). ^{13}C NMR (75 MHz, CDCl$_3$) δ 199.86, 158.04, 136.26, 133.59, 130.48, 128.73, 128.26, 127.59, 120.92, 112.89,

70.72, 32.11. HRMS (EI-MS) *m/z*: [M$^{\bullet+}$] calculated for C$_{15}$H$_{14}$O$_2$$^{\bullet+}$: 226.09883, found 226.09916; C$_{15}$H$_{14}$O$_2$ (226.28).

1-(3-(Benzyloxy)phenyl)ethan-1-one (4.011)[552]

The title compound was synthesized from 3-hydroxy acetophenone (4.42 g, 32.49 mmol, 1 eq), benzyl bromide (8.33 g, 5.79 mL, 48.74 mmol, 1.5 eq), and potassium carbonate (13.47 g, 97.48 mmol, 3 eq) in DMF according to the general procedure (R$_f$ = 0.66 in EtOAc/PE 1/4) yielding a colorless solid (7.35 g, 100%). ^{1}H NMR (300 MHz, CDCl$_3$) δ 7.62 – 7.55 (m, 2H), 7.49 – 7.36 (m, 6H), 7.22 – 7.17 (m, 1H), 5.12 (s, 2H), 2.59 (s, 3H). ^{13}C NMR (75 MHz, CDCl$_3$) δ 197.91, 159.00, 138.53, 136.56, 129.70, 128.70, 128.19, 127.62, 121.38, 120.31, 113.61, 70.19, 26.79. HRMS (ESI-MS): *m/z* [M$^{\bullet+}$] calculated for C$_{15}$H$_{14}$O$_2$$^{\bullet+}$: 226.09883, found 226.09908; C$_{15}$H$_{14}$O$_2$ (226.28).
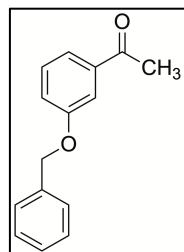
1-(4-(Benzyloxy)phenyl)ethan-1-one (4.012)[553]
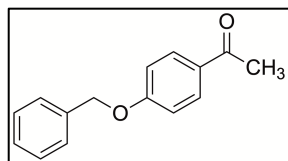
The title compound was synthesized from 4-hydroxy acetophenone (4.42 g, 32.49 mmol, 1 eq), benzyl bromide (8.33 g, 5.79 mL, 48.74 mmol, 1.5 eq), and potassium carbonate (13.47 g, 97.48 mmol, 3 eq) in DMF according to the general procedure (R$_f$ = 0.66 in EtOAc/PE 1/4) yielding a colorless solid (7.35 g, 100%). ^{1}H NMR (300 MHz, CDCl$_3$) δ 7.97 – 7.90 (m, 2H), 7.46 – 7.29 (m, 5H), 7.05 – 6.95 (m, 2H), 5.10 (s, 2H), 2.53 (s, 3H). ^{1}H NMR (300 MHz, CDCl$_3$) δ 7.96, 7.96, 7.95, 7.94, 7.93, 7.93, 7.92, 7.91, 7.45, 7.44, 7.44, 7.42, 7.42, 7.41, 7.40, 7.40, 7.40, 7.39, 7.38, 7.37, 7.37, 7.37, 7.36, 7.35, 7.34, 7.33, 7.33, 7.32, 7.32, 7.31, 7.31, 7.30, 7.30, 7.03, 7.02, 7.01, 6.99, 6.99, 6.98, 5.10, 2.53. HRMS (ESI-MS): *m/z* [M$^{\bullet+}$] calculated for C$_{15}$H$_{14}$O$_2$$^{\bullet+}$: 226.09883, found 226.09829; C$_{15}$H$_{14}$O$_2$ (226.28).

General procedure B

Sodium hydride (5 eq) was suspended in 20 mL DMF. The flask was flooded with argon and cooled to 0 °C by using an ice bath. The corresponding benzyl-protected hydroxy acetophenone (**4.010**-**4.012**, 1 eq) was dissolved in 180 mL DMF and slowly added to the suspension over a period of 1 hour. After completion, stirring was continued for approximately 15 minutes until no more gas was released. Then diethyl carbonate (5 eq) was added dropwise over a period of 1 hour. After the addition, the ice bath was

removed, and the mixture was stirred for another 6 hours at rt. The synthesis was stopped by adding 50 mL of 1 M hydrochloric acid. The product was isolated by extraction with diethyl ether. The combined organic layers were washed with 1M hydrochloric acid and dried over Na_2SO_4. The crude product was purified by column chromatography (EtOAc/PE 1/5 or EtOAc/PE 1/6). For compounds **4.013**-**4.015** a keto-enol tautomerism could be observed in the NMR because especially for the three CH_2 and the CH_3 groups double peaks were clearly visible. In the aromatic region, a clear distinction of the double peaks was not possible. The splitting is indicated accordingly in the NMR data.

Ethyl 3-(2-(benzyloxy)phenyl)-3-oxopropanoate (4.013)[554]

The β-ketoester **4.013** was prepared from **4.010** (7.35 g, 32.48 mmol, 1 eq), sodium hydride (6.50 g, 162.41 mmol, 5 eq), and diethyl carbonate (19.19 g, 20.53 mL, 162.41 mmol, 5 eq) in DMF according to the general procedure B (R_f = 0.8, EtOAc/PE 1/6) yielding a yellowish oil (6.06 g, 63%). ^{1}H NMR (300 MHz, $CDCl_3$) δ 12.74 (s, 0.1H (enol form)), 7.90 – 7.82 (m, 1H), 7.49 – 7.27 (m, 6H), 7.07 – 6.92 (m, 2H), 6.13 (s, 0.1H (enol form)), 5.15 (s, 2H), 4.22 (q, J = 7.1 Hz, 0.2H (keto-enol tautomerism)), 4.08 (q, J = 7.1 Hz, 1.8H (keto-enol tautomerism)), 3.99 (s, 1.8H (keto form)), 1.30 (t, J = 7.1 Hz, 0.3H (keto-enol tautomerism)), 1.17 (t, J = 7.1 Hz, 2.7H (keto-enol tautomerism)). ^{13}C NMR (75 MHz, $CDCl_3$) δ 193.54, 168.08, 158.21, 135.94, 134.52, 131.11, 128.79, 128.37, 127.60, 126.98, 121.07, 112.98, 92.63, 70.73, 60.90, 50.52, 14.08. HRMS (ESI-MS) *m/z*: [M+H$^+$] calculated for $C_{18}H_{19}O_4^+$: 299.1278, found 299.1281; $C_{18}H_{18}O_4$ (298.34).

Ethyl 3-(3-(benzyloxy)phenyl)-3-oxopropanoate (4.014)[555]

The β-ketoester **4.014** was prepared from **4.011** (7.35 g, 32.48 mmol, 1 eq), sodium hydride (6.50 g, 162.41 mmol, 5 eq), and diethyl carbonate (19.19 g, 20.53 mL, 162.41 mmol, 5 eq) in DMF according to the general procedure B (R_f = 0.5, EtOAc/PE 1/5) yielding a yellowish oil (4.35 g, 45%). ^{1}H NMR (300 MHz, $CDCl_3$) δ 12.63 (s, 0.2H (enol form)), 7.62 – 7.03 (m, 9H), 5.67 (s, 0.2H (enol form), 5.09 (s, 2H), 4.33 – 4.17 (m, 1.6H (keto-enol tautomerism)), 4.13 (q, J = 7.1 Hz, 0.4H (keto-enol tautomerism)), 3.97 (s, 1.6H (keto form)), 1.34 (t, J = 7.1 Hz, 0.6H), 1.26 (t, J = 7.1 Hz, 2.4H (keto-enol tautomerism)). ^{13}C NMR (75 MHz, $CDCl_3$) δ 192.35, 167.52, 159.09,

137.39, 136.41, 129.88, 128.70, 128.21, 127.60, 121.43, 121.02, 113.71, 87.71, 70.20, 70.10, 61.50, 60.42, 46.10, 14.36, 14.15. HRMS (ESI-MS) *m/z*: [M+H$^+$] calculated for $C_{18}H_{19}O_4^+$: 299.1278, found 299.1280; $C_{18}H_{18}O_4$ (298.34).

Ethyl 3-(4-(benzyloxy)phenyl)-3-oxopropanoate (4.015)[556]

The β-ketoester **4.015** was prepared from **4.012** (7.35 g, 32.48 mmol, 1 eq), sodium hydride (6.50 g, 162.41 mmol, 5 eq), and diethyl carbonate (19.19 g, 20.53 mL, 162.41 mmol, 5 eq) in DMF according to the general procedure B (R_f = 0.5, EtOAc/PE 1/5) yielding a yellowish solid (6.40 g, 66%). ^{1}H NMR (300 MHz, CDCl$_3$) δ 12.75 (s, 0.2H (enol form)), 7.90 – 7.65 (m, 2H), 7.40 – 7.25 (m, 5H), 6.99 – 6.90 (m, 2H), 5.57 (s, 0.2H (enol form)), 5.01 (s, 2H), 4.27 – 4.11 (m, 1.6H (keto-enol tautomerism)), 4.11 – 4.02 (m, 0.4H (keto-enol tautomerism)), 3.88 (s, 1.6H (keto form)), 1.27 (t, *J* = 7.1 Hz, 0.6H (keto-enol tautomerism)), 1.20 (t, *J* = 7.1 Hz, 2.4H (keto-enol tautomerism)). ^{13}C NMR (75 MHz, CDCl$_3$) δ 193.54, 168.08, 158.21, 135.94, 134.52, 131.11, 128.79, 128.37, 127.60, 126.98, 121.07, 112.98, 92.63, 70.73, 60.90, 50.52, 14.08. HRMS (ESI-MS) *m/z*: [M+H$^+$] calculated for $C_{18}H_{19}O_4^+$: 299.1278, found 299.1282; $C_{18}H_{18}O4$ (298.34).

General procedure C

The corresponding β-ketoester (**4.013-4.015**, 1 eq) and 3-amino-1,2,4-triazole (1 eq) were weighed into a flask. The flask was set under an argon atmosphere and the compounds were dissolved in 10 mL acetic acid. The mixture was stirred for 16 hours at 110 °C. The reaction was stopped by adding 30 mL of water. The product was extracted with diethyl ether and the crude product was obtained by concentrating the organic phase under reduced pressure. The residue was suspended in 4 mL methanol and then centrifuged. The supernatant was tipped off. In total, the residue was washed three times with methanol.

5-(2-(Benzyloxy)phenyl)-[1,2,4]triazolo[1,5-*a*]pyrimidin-7(4*H*)-one (4.016)

The title compound was synthesized from **4.013** (6.06 g, 20.31 mmol, 1 eq) and 3-amino-1,2,4-triazole (1.71 g, 20.31 mmol, 1eq) in acetic acid according to the general procedure C (R_f = 0.85 in DCM/Methanol 95/5) yielding **4.016** as a white solid (2.0 g, 31%). ^{1}H NMR (300 MHz, DMSO-d_6) δ 8.29 (s, 1H), 7.59 – 7.50 (m, 2H), 7.47 – 7.39 (m, 2H), 7.37 – 7.24 (m, 4H), 7.12 (t, *J* = 8.0 Hz, 1H), 6.09 (s, 1H), 5.20 (s, 2H). ^{13}C NMR (75 MHz, DMSO-d_6) δ 156.43, 156.07, 151.02, 137.11, 132.75, 130.95, 128.85, 128.28, 127.74, 122.35, 121.39, 113.82, 100.26, 70.27. HRMS (ESI-MS) *m/z*: [M+H$^+$] calculated for $C_{18}H_{15}N_4O_2^+$: 319.1190, found 319.1192; $C_{18}H_{14}N_4O_2$ (318.34).

5-(3-(Benzyloxy)phenyl)-[1,2,4]triazolo[1,5-*a*]pyrimidin-7(4*H*)-one (4.017)

The title compound was synthesized from **4.014** (4.06 g, 13.61 mmol, 1 eq) and 3-amino- 1,2,4-triazole (1.14 g, 13.61 mmol, 1eq) in acetic acid according to the general procedure C (R_f = 0.85 in DCM/Methanol 95/5) yielding **4.017** as a white solid (910 mg, 21%). ^{1}H NMR (300 MHz, DMSO-d_6) δ 13.60 (bs, 1H), 8.42 (s, 1H), 7.61 – 7.53 (m, 1H), 7.50 – 7.31 (m, 7H), 7.24 – 7.14 (m, 1H), 6.42 (s, 1H), 5.25 – 5.14 (m, 2H). ^{13}C NMR (75 MHz, DMSO-d_6) δ 206.47, 194.29, 159.04, 156.48, 151.23, 137.24, 130.55, 128.92, 128.37, 128.21, 128.18, 120.40, 118.27, 113.88, 98.10, 69.93. HRMS (ESI-MS) *m/z*: [M+H$^+$] calculated for $C_{18}H_{15}N_4O_2^+$: 319.1190, 319.1193; $C_{18}H_{14}N_4O_2$ (318.34).

5-(4-(Benzyloxy)phenyl)-[1,2,4]triazolo[1,5-*a*]pyrimidin-7(4*H*)-one (4.018)

The title compound was synthesized from **4.015** (2.15 g, 7.19 mmol, 1 eq) and 3-amino- 1,2,4-triazole (0.61 g, 7.19 mmol, 1eq) in acetic acid according to the general procedure C (R_f = 0.85 in DCM/Methanol 95/5) yielding **4.018** as a white solid (430 mg, 19%). ^{1}H NMR (300 MHz, DMSO-d_6) δ 13.47 (bs, 1H), 8.37 (s, 1H), 7.99 – 7.81 (m, 2H), 7.50 – 7.32 (m, 5H), 7.21 – 7.07 (m, 2H), 6.31 (s, 1H), 5.28 – 5.13 (m, 2H). ^{13}C NMR (75 MHz, DMSO-d_6) δ 206.48, 192.42, 161.08, 156.48, 137.08, 129.59, 128.96, 128.43, 128.27, 128.21, 118.15, 115.60, 96.74, 69.86. HRMS (ESI-MS) *m/z*: [M+H$^+$] calculated for $C_{18}H_{15}N_4O_2^+$: 319.1190, found 319.1201; $C_{18}H_{14}N_4O_2$ (318.34).

General procedure D

The synthesis was performed by solving **4.016**, **4.017**, or **4.018** (1 eq) in 3 mL phosphoryl chloride and the mixture was heated to 105 °C for 1 hour. Subsequently, the solvent was evaporated and the crude product was purified by column chromatography (EtOAc/PE 1/1).

5-(2-(Benzyloxy)phenyl)-7-chloro-[1,2,4]triazolo[1,5-*a*]pyrimidine (4.019)

4.019 was prepared from **4.016** (1300 mg, 4.08 mmol, 1 eq) in phosphoryl chloride according to the general procedure D (R_f = 0.75, DCM/Methanol 98/2) yielding a yellowish oil (800 mg, 58%). ^{1}H NMR (300 MHz, CDCl$_3$) δ 8.53 (s, 1H), 8.17 (dd, *J* = 7.8, 1.8 Hz, 1H), 8.04 (s, 1H), 7.42 – 7.06 (m, 9H), 5.20 (s, 2H). ^{13}C NMR (75 MHz, CDCl$_3$) δ 161.02, 156.99, 156.17, 155.82, 138.11, 135.93, 132.97, 131.99, 128.79, 128.38, 127.40, 125.30, 121.85, 113.09, 112.61, 71.02. HRMS (ESI-MS) *m/z*: [M+H^{+}] calculated for C$_{18}$H$_{14}$ClN$_4$O[+]: 337.0851, found 337.0851; C$_{18}$H$_{13}$ClN$_4$O (336.78).

5-(3-(Benzyloxy)phenyl)-7-chloro-[1,2,4]triazolo[1,5-*a*]pyrimidine (4.020)

4.020 was prepared from **4.017** (900 mg, 2.83 mmol, 1 eq) in phosphoryl chloride according to the general procedure D (R_f = 0.50, DCM/Methanol 98/2) yielding a yellow solid (660 mg, 69%). ^{1}H NMR (300 MHz, CDCl$_3$) δ 8.55 (s, 1H), 7.88 (t, *J* = 2.1 Hz, 1H), 7.75 – 7.59 (m, 2H), 7.50 – 7.30 (m, 6H), 7.19 – 7.11 (m, 1H), 5.15 (s, 2H). ^{13}C NMR (75 MHz, CDCl$_3$) δ 161.50, 159.50, 156.57, 155.95, 139.64, 136.64, 136.49, 130.21, 128.66, 128.15, 127.56, 120.42, 119.10, 113.63, 108.03, 70.26. HRMS (ESI-MS) *m/z*: [M+H^{+}] calculated for C$_{18}$H$_{14}$ClN$_4$O[+]: 337.0851, found 337.0861; C$_{18}$H$_{13}$ClN$_4$O (336.78).

5-(4-(Benzyloxy)phenyl)-7-chloro-[1,2,4]triazolo[1,5-*a*]pyrimidine (4.021)

4.021 was prepared from **4.018** (700 mg, 2.20 mmol, 1 eq) in phosphoryl chloride according to the general procedure D (R_f = 0.50, DCM/Methanol 98/2) yielding a yellow solid (470 mg, 63%). ^{1}H NMR (300 MHz, CDCl$_3$) δ 8.50 (s, 1H), 8.19 – 8.06 (m, 1H), 7.65 – 6.99 (m, 9H), 5.14 (d, *J* = 9.1 Hz, 2H). ^{13}C NMR (75 MHz, CDCl$_3$) δ

162.01, 161.27, 156.35, 139.32, 136.17, 131.45, 129.69, 128.77, 128.71, 128.27, 127.52, 120.87, 115.43, 108.78, 107.30, 70.21. HRMS (ESI-MS) *m/z*: [M+H$^+$] calculated for C$_{18}$H$_{14}$ClN$_4$O$^+$: 337.0851, found 337.0852; C$_{18}$H$_{13}$ClN$_4$O (336.78).

General procedure E

A solution of **4.019**, **4.020**, or **4.021** (1 eq), 4-chloro-2-isopropoxyphenylmethanamine (**4.009**) (3 eq), and triethylamine (2.4 eq) was dissolved in 20 mL dichloromethane. The reaction was performed under argon atmosphere and stirred at rt for 2 days. The monitoring of the reaction progress was carried out by TLC (EtOAc/PE 1/1). The solvent was removed by evaporation and the crude product was purified by column chromatography (EtOAc/PE 1/1-2/1).

5-(2-(Benzyloxy)phenyl)-*N*-(4-chloro-2-isopropoxybenzyl)-[1,2,4]triazolo[1,5-a]pyrimidin-7-amine (4.022)

Synthesis of **4.022** was performed with **4.019** (388 mg, 1.15 mmol, 1 eq), (4-chloro-2-isopropoxyphenyl)methanamine (**4.009**) (690 mg, 3.46 mmol, 3 eq), and triethylamine (280 mg, 383 µl, 2.77 mmol, 2.4 eq) in dichloromethane according to the general procedure E (R$_f$ = 0.45, EtOAc/PE 1/1), yielding a yellow oil (200 mg, 35%). ^{1}H NMR (300 MHz, CDCl$_3$) δ 8.32 (s, 1H), 7.83 – 7.77 (m, 1H), 7.66 – 7.57 (m, 1H), 7.43 – 6.87 (m, 11H), 6.62 (d, *J* = 15.5 Hz, 1H), 5.14 (s, 2H), 4.72 – 4.53 (m, 3H), 1.36 (d, *J* = 1.9 Hz, 6H). ^{13}C NMR (75 MHz, CDCl$_3$) δ 160.85, 158.12, 155.24, 154.74, 153.91, 146.48, 138.32, 135.76, 133.94, 128.96, 128.62, 128.37, 127.55, 126.98, 126.55, 123.52, 122.19, 119.42, 119.14, 116.31, 112.33, 84.33, 69.11, 39.90, 20.93. HRMS (ESI-MS) m/z: [M+H$^+$] calculated for C$_{28}$H$_{27}$ClN$_5$O$_2$$^+$: 500.1848, found 500.1850; C$_{28}$H$_{26}$ClN$_5$O$_2$ (500.00).
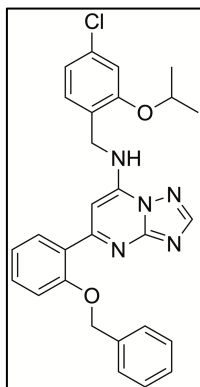
5-(3-(Benzyloxy)phenyl)-*N*-(4-chloro-2-isopropoxybenzyl)-[1,2,4]triazolo[1,5-a]pyrimidin-7-amine (4.023)
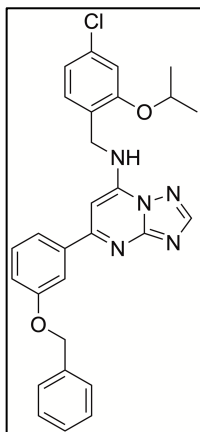
Synthesis of **4.023** was performed with **4.020** (470 mg, 1.40 mmol, 1 eq), (4-chloro-2- isopropoxyphenyl)methanamine (**4.009**) (836 mg, 4.19 mmol, 3 eq), and triethylamine (339 mg, 467 µL, 3.35 mmol, 2.4 eq) in dichloromethane according to the general procedure E (R_f = 0.45, EtOAc/PE 1/1), yielding a yellow oil (700 mg, 100%). ^{1}H NMR (300 MHz, CDCl$_3$) δ 8.33 – 8.31 (m, 1H), 7.84 – 7.79 (m, 1H), 7.69 – 7.60 (m, 1H), 7.51 – 7.05 (m, 9H), 6.97 – 6.87 (m, 2H), 6.63 (d, *J* = 14.7 Hz, 1H), 5.15 (s, 2H), 4.75 – 4.54 (m, 3H), 1.37 (d, *J* = 0.6 Hz, 6H). ^{13}C NMR (101 MHz, CDCl$_3$) δ 161.90, 159.20, 156.36, 155.75, 155.00, 147.49, 139.42, 136.82, 135.11, 130.04, 129.70, 129.48, 128.61, 128.04, 127.59, 124.53, 123.17, 120.48, 120.19, 117.41, 113.41, 85.27, 70.21, 42.08, 21.99. HRMS (ESI-MS) *m/z*: [M+H$^+$] calculated for C$_{28}$H$_{27}$ClN$_5$O$_2^+$: 500.1848, found 500.1860; C$_{28}$H$_{26}$ClN$_5$O$_2$ (500.00).

5-(4-(Benzyloxy)phenyl)-*N*-(4-chloro-2-isopropoxybenzyl)-[1,2,4]triazolo[1,5-a]pyrimidin-7-amine (4.024)
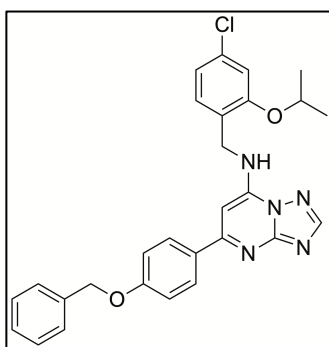
Synthesis of **4.024** was performed with **4.021** (470 mg, 1.40 mmol, 1 eq), (4-chloro-2- isopropoxyphenyl)methanamine (**4.009**) (836 mg, 4.19 mmol, 3 eq), and triethylamine (339 mg, 467 µL, 3.35 mmol, 2.4 eq) in dichloromethane according to the general procedure E (R_f = 0.30, EtOAc/PE 1/1), yielding a yellow oil (450 mg, 64%). ^{1}H NMR (300 MHz, CDCl$_3$) δ 8.28 (s, 1H), 8.05 – 7.97 (m, 2H), 7.42 – 6.81 (m, 11H), 6.53 (d, *J* = 17.3 Hz, 1H), 5.06 (s, 2H), 4.68 – 4.49 (m, 3H), 1.34 (d, *J* = 3.3 Hz, 6H). ^{13}C NMR (75 MHz, CDCl$_3$) δ 161.57, 160.80, 156.26, 155.80, 154.75, 147.49, 136.58, 134.78, 130.46, 129.96, 129.36, 129.19, 128.64, 128.10, 127.50, 124.82, 123.57, 120.48, 114.85, 113.38, 112.84, 84.54, 70.03, 41.70, 22.01. HRMS (ESI-MS) *m/z*: [M+H$^+$] calculated for C$_{28}$H$_{27}$ClN$_5$O$_2^+$: 500.1848, found 500.1850; C$_{28}$H$_{26}$ClN$_5$O$_2$ (500.00).

General procedure F

The cleavage of the benzyl protecting group was performed by palladium-on-carbon (Pd/C)-catalyzed hydrogenation. Pd/C (10%) was added to a solution of **4.022**, **4.023**, or **4.024** in 25 mL methanol. Subsequently, the mixture was heated to reflux under continuous stirring. The permanent TLC monitoring (EtOAc/PE 2/1 or EtOAc/PE 3/1) of the reaction progress is crucial because chlorine is also eliminated from the aromatic ring during hydrogenation, which should be prevented as far as possible. After complete cleavage of the protecting group, the mixture was allowed to cool to room temperature. Afterward, the catalyst was removed by filtration over celite, and the solvent was evaporated. The crude product was used without further purification.

2-(7-((4-Chloro-2-isopropoxybenzyl)amino)-[1,2,4]triazolo[1,5-a]pyrimidin-5-yl)phenol (4.025)
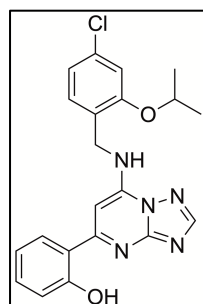
Compound **4.025** was obtained by catalyzed hydrogenation of **4.022** (200 mg, 0.400 mmol, 1 eq) in methanol according to the general procedure F (R_f = 0.40, EtOAc/PE 3/1), yielding a yellow solid (150 mg, 91%). ^{1}H NMR (300 MHz, DMSO-d_6) δ 9.02 (t, J = 6.4 Hz, 1H), 8.61 (s, 1H), 8.06 – 7.96 (m, 1H), 7.23 – 6.79 (m, 7H), 4.77 – 4.65 (m, 3H), 1.26 (d, J = 6.1 Hz, 6H). ^{13}C NMR (75 MHz, DMSO-d_6) δ 159.72, 156.38, 155.56, 154.49, 153.89, 148.79, 133.16, 130.40, 129.27, 129.20, 128.96, 126.25, 125.42, 119.43, 118.94, 118.47, 113.86, 85.34, 70.43, 22.31. HRMS (ESI-MS) *m/z*: [M+H$^+$] calculated for $C_{21}H_{21}ClN_5O_2^+$: 410.1378, found 410.1382; $C_{21}H_{20}ClN_5O_2$ (409.87).

3-(7-((4-Chloro-2-isopropoxybenzyl)amino)-[1,2,4]triazolo[1,5-*a*]pyrimidin-5-yl)phenol (4.026)
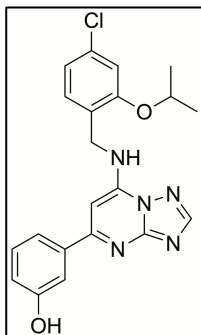
Compound **4.026** was obtained by catalyzed hydrogenation of **4.023** (670 mg, 1.340 mmol, 1eq) in methanol according to the general procedure F (R_f = 0.25, EtOAc/PE 2/1), yielding a yellow solid (480 mg, 87%). ^{1}H NMR (300 MHz, CDCl$_3$) δ 8.37 (s, 1H), 8.02 (s, 1H), 7.76 (s, 1H), 7.38 – 7.26 (m, 2H), 7.21 – 7.07 (m, 2H), 6.99 – 6.88 (m, 2H), 6.79 – 6.59 (m, 1H), 4.72 – 4.53 (m, 3H), 1.35 (d, *J* = 6.0 Hz, 6H). ^{13}C NMR (101 MHz, CDCl$_3$) δ 162.79, 157.53, 156.19, 155.64, 151.99, 147.52, 137.45, 134.78, 129.99, 129.59, 129.39, 124.37, 123.17, 120.54, 118.68, 115.05, 112.76, 87.69, 70.37, 22.10. HRMS (ESI-MS) *m/z*: [M+H$^+$] calculated for C$_{21}$H$_{21}$ClN$_5$O$_2^+$: 410.1378, found 410.1389; C$_{21}$H$_{20}$ClN$_5$O$_2$ (409.87).

4-(7-((4-Chloro-2-isopropoxybenzyl)amino)-[1,2,4]triazolo[1,5-*a*]pyrimidin-5-yl)phenol (4.027)
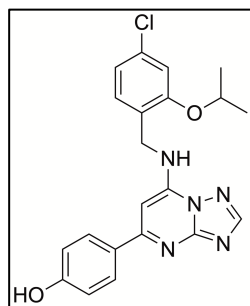
Compound **4.027** was obtained by catalyzed hydrogenation of **4.024** (450 mg, 0.900 mmol, 1 eq) in methanol according to the general procedure F (R_f = 0.25, EtOAc/PE 2/1), yielding a yellow solid (230 mg, 62%). ^{1}H NMR (300 MHz, DMSO-d$_6$) δ 8.64 – 8.51 (m, 1H), 8.46 (s, 1H), 8.02 – 7.94 (m, 1H), 7.36 – 6.67 (m, 7H), 4.88 – 4.47 (m, 3H), 1.34 – 1.22 (m, 6H). ^{13}C NMR (75 MHz, DMSO-d$_6$) δ 160.27, 156.33, 155.81, 155.52, 154.77, 148.23, 133.26, 130.25, 129.44, 129.07, 128.61, 126.67, 125.85, 120.81, 120.65, 115.86, 113.95, 84.51, 71.06, 22.33. HRMS (ESI-MS) *m/z*: [M+H$^+$] calculated for C$_{21}$H$_{21}$ClN$_5$O$_2^+$: 410.1378, found 410.1385; C$_{21}$H$_{20}$ClN$_5$O$_2$ (409.87).

General procedure G

The Boc-protection of the secondary aromatic amines was performed by solving **4.025**, **4.026**, or **4.027** (1 eq), triethylamine (1.1 eq) and catalytic amounts of 4-dimethylamino pyridine (DMAP) in chloroform. After cooling the mixture to 0 °C di-*tert*-butyl dicarbonate (1.1 eq) in chloroform was slowly added via a dropping funnel. After complete addition the ice bath was removed and the mixture was stirred continuously

overnight. Subsequently, the solvent was removed and the crude product was purified by column chromatography (EtOAc/PE 2/1).

tert-Butyl (4-chloro-2-isopropoxybenzyl)(5-(2-hydroxyphenyl)-[1,2,4]triazolo[1,5-a]pyrimidin-7-yl)carbamate (4.028)
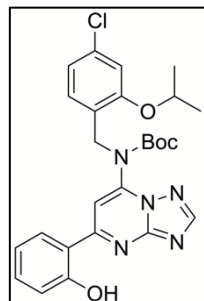
The respective N-Boc protected aromatic amine was obtained from **4.025** (140 mg, 0.342 mmol, 1 eq), DMAP (cat.), triethylamine (38 mg, 53 µL, 0.376 mmol, 1.1 eq), and di-*tert*-butyldicarbonat (82 mg, 0.376 mmol, 1.1 eq) in a total of 50 mL chloroform according to the general procedure G (R_f = 0.75, EtOAc/PE 2/1), yielding a colorless oil (122 mg, 64%). ^{1}H NMR (300 MHz, CDCl$_3$) δ 8.33 – 8.29 (m, 1H), 7.94 – 7.85 (m, 1H), 7.49 – 7.41 (m, 1H), 7.33 – 7.17 (m, 3H), 6.94 – 6.83 (m, 2H), 6.67 (d, J = 13.6 Hz, 1H), 4.71 – 4.51 (m, 3H), 1.42 (s, 9H), 1.34 (d, J = 1.3 Hz, 6H). ^{13}C NMR (75 MHz, CDCl$_3$) δ 160.18, 156.30, 155.79, 155.49, 154.90, 151.34, 147.38, 134.98, 131.82, 131.04, 130.83, 130.04, 129.47, 126.36, 124.41, 123.05, 120.38, 112.58, 88.37, 83.81, 42.72, 27.59, 22.07. HRMS (ESI-MS) *m/z*: [M+H$^+$] calculated for C$_{26}$H$_{29}$ClN$_5$O$_4$$^+$: 510.1903, found 510.1909; C$_{26}$H$_{28}$ClN$_5$O$_4$ (509.99).

tert-Butyl (4-chloro-2-isopropoxybenzyl)(5-(3-hydroxyphenyl)-[1,2,4]triazolo[1,5-a]pyrimidin-7-yl)carbamate (4.029)

The respective N-Boc protected aromatic amine was obtained from **4.026** (480 mg, 1.171 mmol, 1 eq), DMAP (cat.), triethylamine (130 mg, 181 µL, 1.1 eq), and di-*tert*- butyldicarbonat (281 mg, 1.288 mmol, 1.1 eq) in a total of 50 mL chloroform according to the general procedure G (R_f = 0.78, EtOAc/PE 2/1), yielding a colorless oil (460 mg, 77%). ^{1}H NMR (300 MHz, CDCl$_3$) δ 8.32 – 8.29 (m, 1H), 7.99 – 7.87 (m, 2H), 7.46 (t, J = 0.8 Hz, 1H), 7.33 – 7.23 (m, 2H), 6.96 – 6.87 (m, 2H), 6.60 (d, J = 16.6 Hz, 1H), 4.71 – 4.55 (m, 3H), 1.57 (s, 9H), 1.36 (d, J = 0.7 Hz, 6H). ^{13}C NMR (75 MHz, CDCl$_3$) δ 160.90, 156.31, 155.80, 155.72, 155.00, 151.44, 147.68, 139.55, 130.03, 129.73, 129.62, 129.46, 124.93, 124.46, 123.31, 120.70, 120.44, 112.79, 85.26, 83.77, 42.67, 27.75, 22.14. HRMS (ESI-MS) *m/z*: [M+H$^+$] calculated for C$_{26}$H$_{29}$ClN$_5$O$_4$$^+$: 510.1903, found 510.1910; C$_{26}$H$_{28}$ClN$_5$O$_4$ (509.99).
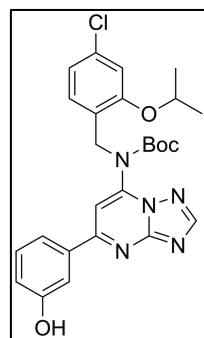
tert-Butyl (4-chloro-2-isopropoxybenzyl)(5-(4-hydroxyphenyl)-[1,2,4]triazolo[1,5-a]pyrimidin-7-yl)carbamate (4.030)
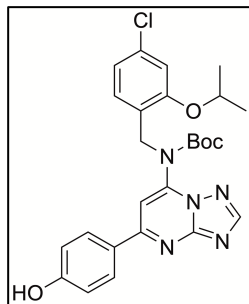
The respective N-Boc protected aromatic amine was obtained from **4.027** (200 mg, 0.488 mmol, 1 eq), DMAP (cat.), triethylamine (54 mg, 75 µL, 0.537 mmol, 1.1 eq), and di-*tert*-butyldicarbonat (117 mg, 0.537 mmol, 1.1 eq) in a total of 50 mL chloroform according to the general procedure G (R_f= 0.78, EtOAc/PE 2/1), yielding a colorless oil (200 mg, 80%). ^{1}H NMR (300 MHz, CDCl$_3$) δ 8.31 (s, 1H), 8.11 – 8.04 (m, 2H), 7.32 – 7.18 (m, 3H), 6.95 – 6.88 (m, 2H), 6.58 (d, *J* = 16.6 Hz, 1H), 4.72 – 4.53 (m, 3H), 1.56 (s, 9H), 1.35 (d, *J* = 6.0 Hz, 6H). ^{13}C NMR (75 MHz, CDCl$_3$) δ 161.19, 156.33, 155.70, 154.94, 152.88, 151.47, 147.57, 135.33, 130.01, 129.73, 129.45, 128.88, 124.50, 123.16, 121.50, 120.50, 113.44, 85.08, 83.93, 42.04, 27.72, 22.00. HRMS (ESI-MS) *m/z*: [M+H$^+$] calculated for C$_{26}$H$_{29}$ClN$_5$O$_4^+$: 510.1903, found 510.1906; C$_{26}$H$_{28}$ClN$_5$O$_4$ (509.99).

General procedure H

The coupling of the respective linkers (**4.003**, **4.006**, or **4.007**) with the pharmacophores **4.028**, **4.029**, or **4.030** was performed by a nucleophilic substitution reaction in DMF. **4.028, 4.029**, or **4.030** (1 eq) and **4.003**, **4.006**, or **4.007** (5 eq), and potassium carbonate (5 eq) were dissolved in DMF. The mixture was stirred continuously at 40 °C for 5-6 days. Monitoring of the reaction was constantly performed by TLC (EtOAc/PE 1/1 or EtOAc/PE 2/1). After completion, the solvent was removed under reduced pressure and the crude product was purified by column chromatography (DCM/Methanol 99/1-95/5 (**method A**) or EtOAc/PE 2/1- 6/1 (**method B**)).

tert-Butyl (4-chloro-2-isopropoxybenzyl)(5-(2-((6-(1,3-dioxoisoindolin-2-yl)hexyl)oxy)phenyl)-[1,2,4]triazolo[1,5-*a*]pyrimidin-7-yl)carbamate (4.031)
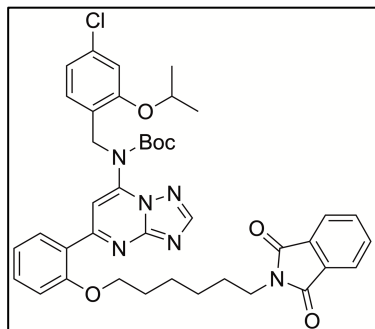
The synthesis of **4.031** was carried out with **4.028** (150 mg, 0.294 mmol, 1 eq), **4.007** (456 mg, 1.471 mmol, 5 eq) and potassium carbonate (110 mg, 0.794 mmol, 5 eq) in 10 mL DMF according to the general procedure H (method A) (R_f = 0.20 (EtOAc/PE 1/1), yielding a colorless oil (180 mg, 83%). ^{1}H NMR (300 MHz, CDCl$_3$) δ 8.34 (s, 1H), 7.93 – 7.88 (m, 1H), 7.86 – 7.80 (m, 2H), 7.75 – 7.67 (m, 2H), 7.49 – 7.41 (m, 1H), 7.39 – 7.32 (m, 1H), 7.25 – 7.20 (m, 1H), 7.09 (d, J = 8.6 Hz, 1H), 6.88 – 6.81 (m, 2H), 6.57 (s, 1H), 5.17 (s, 2H), 4.56 – 4.41 (m, 1H), 3.75 – 3.62 (m, 4H), 1.82 – 1.59 (m, 4H), 1.39 (s, 13H), 1.14 (d, J = 6.0 Hz, 6H). ^{13}C NMR (75 MHz, CDCl$_3$) δ 168.45, 159.46, 156.42, 153.85, 151.18, 149.84, 148.77, 134.44, 133.96, 132.12, 131.52, 131.06, 130.88, 129.88, 126.39, 123.44, 123.22, 123.06, 120.36, 113.22, 93.94, 83.81, 70.53, 50.90, 49.56, 37.78, 28.50, 27.56, 26.45, 26.34, 21.70. HRMS (ESI-MS) *m/z*: [M+H$^+$] calculated for C$_{40}$H$_{44}$ClN$_6$O$_6$$^+$: 739.3005, found 739.3010; C$_{40}$H$_{43}$ClN$_6$O$_6$ (739.27).

tert-Butyl (4-chloro-2-isopropoxybenzyl)(5-(3-((6-(1,3-dioxoisoindolin-2-yl)hexyl)oxy)phenyl)-[1,2,4]triazolo[1,5-*a*]pyrimidin-7-yl)carbamate (4.032)

The synthesis of **4.032** was carried out with **4.029** (90 mg, 0.177 mmol, 1 eq), **4.007** (274 mg, 0.882 mmol, 5 eq) and potassium carbonate (122 mg, 0.882 mmol, 5 eq) in 10 mL DMF according to the general procedure H (method A) (R_f = 0.20 (EtOAc/PE 1/1), yielding a colorless oil (118 mg, 91%). ^{1}H NMR (300 MHz, CDCl$_3$) δ 8.35 (s, 1H), 8.00 – 7.91 (m, 2H), 7.88 – 7.78 (m, 2H), 7.76 – 7.65 (m, 2H), 7.49 (t, J = 7.9 Hz, 1H), 7.35 – 7.27 (m, 2H), 6.97 – 6.90 (m, 2H), 6.65 (d, J = 15.7 Hz, 1H), 4.73 – 4.57 (m, 3H), 3.88 – 3.38 (m, 4H), 2.22 – 1.63 (m, 8H), 1.58 (s, 9H), 1.38 (d, J = 6.1 Hz, 6H). ^{13}C NMR (75 MHz, CDCl$_3$) δ 168.08, 160.03, 157.36, 154.51, 152.90, 151.89, 149.51, 137.50, 133.90, 131.94, 131.62, 129.83, 129.68, 129.61, 129.55, 123.20, 122.67, 120.47, 118.14, 112.78, 93.89, 83.85, 70.25, 51.40, 48.07, 35.10, 28.41, 27.76, 25.53, 25.30, 22.15. HRMS (ESI-MS) *m/z*: [M+H$^+$] calculated for C$_{40}$H$_{44}$ClN$_6$O$_6$$^+$: 739.3005, found 739.3012; C$_{40}$H$_{43}$ClN$_6$O$_6$ (739.27).
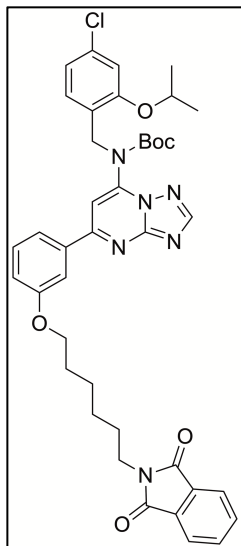
***tert*-Butyl (4-chloro-2-isopropoxybenzyl)(5-(4-((6-(1,3-dioxoisoindolin-2-yl)hexyl)oxy)phenyl)-[1,2,4]triazolo[1,5-a]pyrimidin-7-yl)carbamate (4.033)**
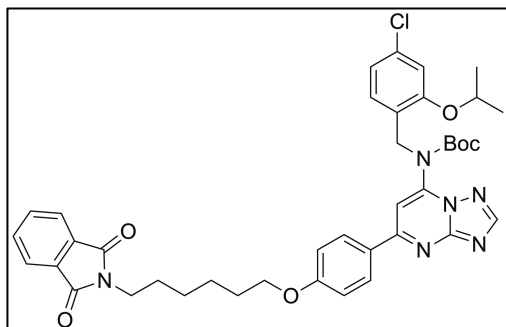
The synthesis of **4.033** was carried out with 30 (80 mg, 0.159 mmol, 1 eq), **4.007** (246 mg, 0.794 mmol, 5 eq) and potassium carbonate (110 mg, 0.794 mmol, 5 eq) in 10 mL DMF according to the general procedure H (method A) (R_f = 0.20 (EtOAc/PE 1/1), yielding a colorless oil (60 mg, 51%). HRMS (ESI-MS) *m/z*: [M+H$^+$] calculated for $C_{40}H_{44}ClN_6O_6^+$: 739.3005, found 739.3009; $C_{40}H_{43}ClN_6O_6$ (739.27).

***tert*-Butyl (4-chloro-2-isopropoxybenzyl)(5-(2-(2-(2-(2-(1,3-dioxoisoindolin-2-yl)ethoxy)ethoxy)ethoxy)ethoxy)phenyl)-[1,2,4]triazolo[1,5-*a*]pyrimidin-7-yl)carbamate (4.034)**
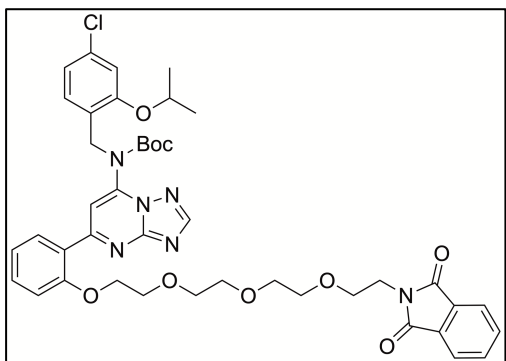
The synthesis of **4.034** was carried out with **4.028** (90 mg, 0.176 mmol, 1 eq), **4.003** (341 mg, 0.882 mmol, 5 eq) and potassium carbonate (122 mg, 0.882 mmol, 5 eq) in 10 mL DMF according to the general procedure H (method B) (R_f = 0.25 (EtOAc/PE 2/1), yielding a colorless oil (39 mg, 27%). ^{1}H NMR (400 MHz, CDCl$_3$) δ 8.31 (s, 1H), 7.86 – 7.82 (m, 1H), 7.82 – 7.78 (m, 2H), 7.69 – 7.65 (m, 2H), 7.46 – 7.40 (m, 1H), 7.34 – 7.28 (m, 1H), 7.23 – 7.09 (m, 2H), 6.87 – 6.81 (m, 2H), 6.63 (d, *J* = 4.1 Hz, 1H), 5.15 (d, *J* = 11.8 Hz, 2H), 4.56 – 4.43 (m, 1H), 4.11 – 4.03 (m, 2H), 3.85 (t, *J* = 5.9 Hz, 2H), 3.68 (t, *J* = 5.9 Hz, 2H), 3.60 – 3.46 (m, 10H), 1.41 (s, 9H), 1.16 (d, *J* = 1.5 Hz, 6H). ^{13}C NMR (75 MHz, CDCl$_3$) δ 168.22, 159.51, 156.34, 155.79, 154.09, 151.27, 148.73, 133.94, 132.09, 131.54, 130.95, 130.83, 129.71, 128.95, 126.27, 124.46, 123.21, 123.09, 120.26, 113.15, 94.10, 83.73, 70.57, 70.03, 69.81, 67.89, 37.21, 29.72, 27.55, 21.89. HRMS (ESI-MS) *m/z*: [M+H$^+$] calculated for $C_{42}H_{48}ClN_6O_9^+$: 815.3166, found 815.3173; $C_{42}H_{47}ClN_6O_9$ (815.32).

tert-Butyl (4-chloro-2-isopropoxybenzyl)(5-(3-(2-(2-(2-(2-(1,3-dioxoisoindolin-2-yl)ethoxy)ethoxy)ethoxy)ethoxy)phenyl)-[1,2,4]triazolo[1,5-*a*]pyrimidin-7-yl)carbamate (4.035)
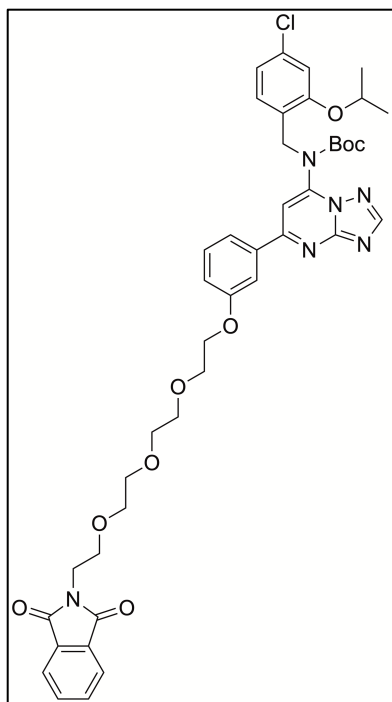
The synthesis of **4.035** was carried out with **4.029** (82 mg, 0.161 mmol, 1 eq), **4.003** (311 mg, 0.804 mmol, 5 eq) and potassium carbonate (111 mg, 0.804 mmol, 5 eq) in 10 mL DMF according to the general procedure H (method B) (R_f = 0.25 (EtOAc/PE 2/1), yielding a colorless oil (49 mg, 37%). ^{1}H NMR (400 MHz, CDCl$_3$) δ 8.35 – 8.30 (m, 1H), 7.89 – 7.84 (m, 2H), 7.82 – 7.77 (m, 2H), 7.70 – 7.65 (m, 2H), 7.47 – 7.39 (m, 1H), 7.25 – 7.19 (m, 2H), 6.90 – 6.83 (m, 2H), 6.68 (d, J = 8.2 Hz, 1H), 5.11 (d, J = 10.3 Hz, 2H), 4.61 – 4.48 (m, 1H), 4.27 – 4.06 (m, 2H), 3.87 – 3.78 (m, 4H), 3.67 (t, J = 5.9 Hz, 2H), 3.58 – 3.47 (m, 8H), 1.56 (s, 9H), 1.21 (d, J = 6.0 Hz, 6H). ^{13}C NMR (101 MHz, CDCl$_3$) δ 168.21, 160.24, 156.25, 155.67, 151.70, 151.45, 150.45, 139.16, 133.91, 132.10, 129.53, 129.12, 128.78, 124.87, 124.41, 123.40, 123.19, 120.70, 120.48, 112.85, 91.43, 83.69, 70.66, 70.61, 70.56, 70.26, 70.05, 67.90, 40.87, 37.24, 29.70, 27.73, 21.99. HRMS (ESI-MS) *m/z*: [M+H$^+$] calculated for C$_{42}$H$_{48}$ClN$_6$O$_9^+$: 815.3166, found 815.3172.; C$_{42}$H$_{47}$ClN$_6$O$_9$ (815.32)

tert-Butyl (4-chloro-2-isopropoxybenzyl)(5-(4-(2-(2-(2-(2-(1,3-dioxoisoindolin-2-yl)ethoxy)ethoxy)ethoxy)ethoxy)phenyl)-[1,2,4]triazolo[1,5-*a*]pyrimidin-7-yl)carbamate (4.036)
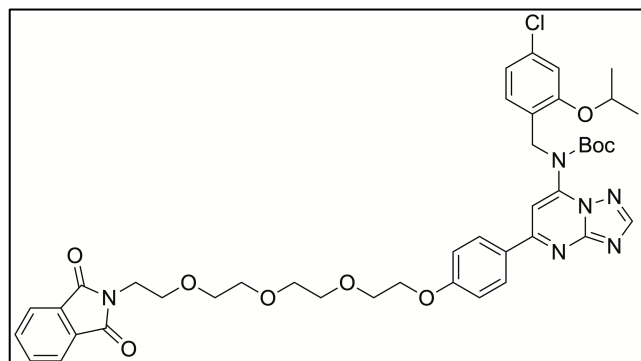
The synthesis of **4.036** was carried out with **4.030** (80 mg, 0.157 mmol, 1 eq), **4.003** (303 mg, 0.784 mmol, 5 eq) and potassium carbonate (108 mg, 0.784 mmol, 5 eq) in 10 mL DMF according to the general procedure H (method B) (R_f = 0.25 (EtOAc/PE 2/1), yielding a colorless oil (52 mg, 41%). ^{1}H NMR (300 MHz, CDCl$_3$) δ 8.30 (s, 1H), 8.08 – 8.00 (m, 2H), 7.81 – 7.76 (m, 2H), 7.69 – 7.64 (m, 2H), 7.27 – 7.18 (m, 2H), 6.91 – 6.81 (m, 2H), 6.63 (d, J = 3.3 Hz, 1H), 5.10 (d, J = 6.4 Hz, 2H), 4.61 – 4.44 (m, 1H), 4.25 – 4.12

(m, 2H), 3.87 – 3.78 (m, 4H), 3.67 (t, J = 5.8 Hz, 2H), 3.59 – 3.44 (m, 8H), 1.55 (s, 9H), 1.20 (d, J = 6.0 Hz, 6H). ^{13}C NMR (75 MHz, CDCl$_3$) δ 168.23, 160.40, 156.22, 155.64, 152.84, 151.43, 150.34, 134.41, 133.93, 132.08, 129.57, 128.83, 125.62, 125.06, 124.41, 123.20, 121.44, 120.47, 118.67, 113.35, 91.01, 83.88, 70.67, 70.61, 70.56, 70.05, 67.91, 50.90, 40.89, 37.22, 29.72, 27.70, 23.89. HRMS (ESI-MS) m/z: [M+H$^+$] calculated for C$_{42}$H$_{48}$ClN$_6$O$_9^+$: 815.3166, found 815.3187; C$_{42}$H$_{47}$ClN$_6$O$_9$ (815.32).

tert-Butyl (4-chloro-2-isopropoxybenzyl)(5-(2-((17-(1,3-dioxoisoindolin-2-yl)-3,6,9,12,15-pentaoxaheptadecyl)oxy)phenyl)-[1,2,4]triazolo[1,5-*a*]pyrimidin-7-yl)carbamate (4.037)
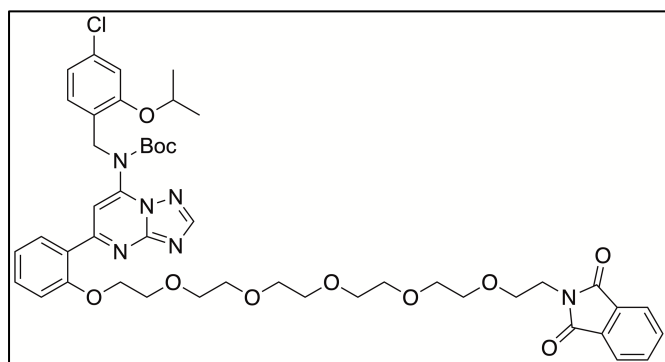
The synthesis of **4.037** was carried out with **4.030** (200 mg, 0.392 mmol, 1 eq), **4.006** (930 mg, 1.961 mmol, 5 eq) and potassium carbonate (271 mg, 1.961 mmol, 5 eq) in 10 mL DMF according to the general procedure H (method B) (R$_f$ = 0.25 (EtOAc/PE 2/1), yielding a colorless oil (300 mg, 85%). ^{1}H NMR (300 MHz, CDCl$_3$) δ 8.37 (s, 1H), 7.91 – 7.86 (m, 1H), 7.85 – 7.81 (m, 2H), 7.73 – 7.69 (m, 2H), 7.50 – 7.43 (m, 1H), 7.38 – 7.31 (m, 1H), 7.26 – 7.22 (m, 1H), 7.12 (d, J = 8.6 Hz, 1H), 6.87 – 6.83 (m, 2H), 6.70 (s, 1H), 5.15 (s, 2H), 4.57 – 4.43 (m, 1H), 4.09 (t, J = 5.3 Hz, 2H), 3.89 (t, J = 5.9 Hz, 2H), 3.82 (t, J = 5.4 Hz, 2H), 3.72 (t, J = 5.8 Hz, 2H), 3.66 – 3.50 (m, 16H), 1.42 (s, 9H), 1.17 (d, J = 6.0 Hz, 6H). ^{13}C NMR (75 MHz, CDCl$_3$) δ 168.15, 159.29, 157.76, 155.76, 154.13, 151.19, 150.19, 133.93, 132.04, 131.69, 130.89, 130.67, 129.74, 128.93, 126.23, 124.48, 123.15, 123.06, 120.22, 112.57, 93.92, 83.61, 70.63, 70.48, 70.00, 69.74, 67.83, 51.08, 50.38, 37.18, 27.52, 21.85. HRMS (ESI-MS) m/z: [M+H$^+$] calculated for C$_{46}$H$_{56}$ClN$_6$O$_{11}^+$: 903.3690, found 903.3704; C$_{46}$H$_{55}$ClN$_6$O$_{11}$ (903.43).

General procedure I

The corresponding phthalimides (**4.031-4.037**) were deprotected by hydrazinolysis. Therefore, **4.031-4.037** (1 eq) and hydrazine monohydrate (5 eq) were dissolved in 1-butanol. The mixture was stirred at rt for 16 hours. After cooling the mixture to 0 °C using an ice bath, the precipitated phthalhydrazide was filtered off over celite. The

solvent was evaporated and purification was performed with preparative HPLC (MeCN/0.1% aqueous NH_3 or MeCN/0.5% aqueous TFA).

5-(2-((6-Aminohexyl)oxy)phenyl)-*N*-(4-chloro-2-isopropoxybenzyl)-[1,2,4]triazolo[1,5-*a*]pyrimidin-7-amine dihydrotrifluoroacetate (4.038)
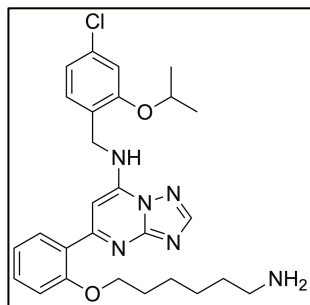
The title compound was synthesized from **4.031** (150 mg, 0.203 mmol, 1 eq) and hydrazine monohydrate (50.79 mg, 49 µL, 1.015 mmol, 5 eq) in 5 mL 1-butanol according to the general procedure I (R_f = 0.15 in DCM/Methanol/NH_3 conc. 50/50/1) yielding a colorless oil (7.92 mg, 5%). ^{1}H NMR (300 MHz, CD$_3$OD) δ 8.44 (s, 1H), 7.83 (d, *J* = 7.8 Hz, 1H), 7.41 – 7.25 (m, 2H), 7.06 – 6.85 (m, 5H), 5.28 (s, 2H), 4.64 – 4.52 (m, 1H), 3.89 (t, *J* = 7.5 Hz, 2H), 2.89 (t, *J* = 7.8 Hz, 2H), 1.89 – 1.75 (m, 2H), 1.70 – 1.58 (m, 2H), 1.48 – 1.39 (m, 4H), 1.06 (d, *J* = 6.0 Hz, 6H). ^{13}C NMR (75 MHz, CD$_3$OD) δ 160.94, 159.38, 156.63, 155.86, 151.32, 150.46, 132.74, 129.23, 129.19, 127.92, 124.21, 120.94, 120.10, 119.11, 118.17, 117.84, 112.66, 90.74, 69.54, 51.11, 39.18, 27.47, 27.10, 25.85, 25.75, 20.70. HRMS (ESI-MS) *m/z*: [M+H$^+$] calculated for $C_{27}H_{34}ClN_6O_2^+$: 509.2426, found 509.2433; $C_{27}H_{33}ClN_6O_2$ x $C_4H_2F_6O_4$ (737.10).

5-(3-((6-Aminohexyl)oxy)phenyl)-*N*-(4-chloro-2-isopropoxybenzyl)-[1,2,4]triazolo[1,5-*a*]pyrimidin-7-amine (4.039)
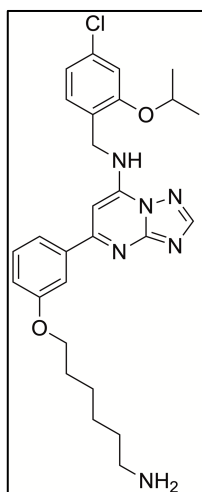
The title compound was synthesized from **4.032** (118 mg, 0.160 mmol, 1 eq) and hydrazine monohydrate (39.85 mg, 39 µL, 0.798 mmol, 5 eq) in 4 mL 1-butanol according to the general procedure I (R_f = 0.15 in DCM/Methanol/NH_3 conc. 50/50/1) yielding a colorless oil (11 mg, 9%). ^{1}H NMR (300 MHz, CD$_3$OD) δ 8.34 (s, 1H), 7.49 – 7.39 (m, 2H), 7.32 – 7.23 (m, 2H), 7.01 – 6.82 (m, 3H), 6.68 (s, 1H), 5.26 (s, 2H), 4.61 – 4.45 (m, 1H), 3.79 (t, *J* = 7.6 Hz, 2H), 2.66 (t, *J* = 7.1 Hz, 2H), 1.82 – 1.68 (m, 2H), 1.52 – 1.44 (m, 2H), 1.43 – 1.30 (m, 4H), 1.05 – 0.99 (m, 6H). ^{13}C NMR (75 MHz, CDCl$_3$) δ 160.53, 159.96, 156.58, 155.81, 154.31, 152.71, 133.66, 132.98, 131.03, 130.52, 128.84, 124.35, 123.77, 122.28, 120.58, 120.18, 118.14, 95.61, 73.16, 54.47, 36.31, 31.08, 30.21, 26.73, 24.54, 21.40. HRMS (ESI-MS) *m/z*: [M+H$^+$] calculated for $C_{27}H_{34}ClN_6O_2^+$: 509.2426, found 509.2428; $C_{27}H_{33}ClN_6O_2$ (509.05).

## 5-(4-((6-Aminohexyl)oxy)phenyl)-*N*-(4-chloro-2-isopropoxybenzyl)-[1,2,4]triazolo[1,5-*a*]pyrimidin-7-amine (4.040)
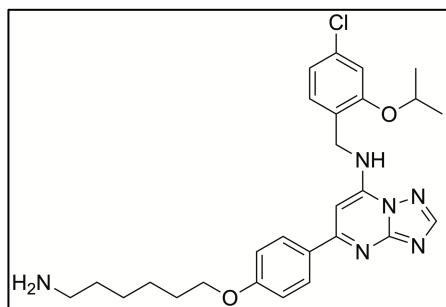
The title compound was synthesized from **4.033** (36 mg, 0.049 mmol, 1 eq) and hydrazine monohydrate (12.26 mg, 12 µL, 0.245 mmol, 5 eq) in 4 mL 1-butanol according to the general procedure I (R_f = 0.15 in DCM/Methanol/NH$_3$ conc. 50/50/1) yielding a colorless oil (3.9 mg, 16%). ^{1}H NMR (300 MHz, CD$_3$OD) δ 8.32 (s, 1H), 7.96 – 7.89 (m, 2H), 7.28 (d, *J* = 8.2 Hz, 1H), 6.99 (d, *J* = 2.1 Hz, 1H), 6.93 – 6.85 (m, 3H), 6.69 (s, 1H), 5.23 (s, 2H), 4.57 – 4.49 (m, 1H), 3.83 (t, *J* = 7.4 Hz, 2H), 2.86 (t, *J* = 7.3 Hz, 2H), 1.86 – 1.72 (m, 2H), 1.68 – 1.56 (m, 2H), 1.41 (q, *J* = 4.1 Hz, 4H), 1.02 (d, *J* = 6.0 Hz, 6H). HRMS (ESI-MS) *m/z*: [M+H$^+$] calculated for C$_{27}$H$_{34}$ClN$_6$O$_2^+$: 509.2426, found 509.2432; C$_{27}$H$_{33}$ClN$_6$O$_2$ (509.05).

5-(2-(2-(2-(2-Aminoethoxy)ethoxy)ethoxy)ethoxy)phenyl)-*N*-(4-chloro-2-isopropoxybenzyl)-[1,2,4]triazolo[1,5-*a*]pyrimidin-7-amine (4.041)
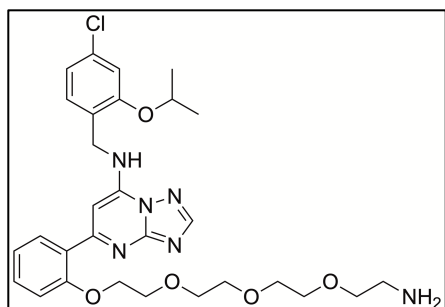
The title compound was synthesized from **4.034** (39.00 mg, 0.048 mmol, 1 eq) and hydrazine monohydrate (11.97 mg, 12 µL, 0.239 mmol, 5 eq) in 4 mL 1-butanol according to the general procedure I (R_f = 0.35 in DCM/Methanol/NH$_3$ conc. 50/50/1) yielding a colorless oil (11.7 mg, 36%). ^{1}H NMR (300 MHz, CD$_3$OD) δ 8.36 (s, 1H), 7.87 (d, *J* = 7.9 Hz, 1H), 7.40 – 7.31 (m, 2H), 7.07 (s, 1H), 7.02 (d, *J* = 1.9 Hz, 1H), 6.98 – 6.89 (m, 3H), 5.28 (s, 2H), 4.67 – 4.55 (m, 1H), 4.24 (t, *J* = 5.1 Hz, 2H), 3.80 (t, *J* = 5.1 Hz, 2H), 3.58 – 3.53 (m, 2H), 3.51 – 3.43 (m, 8H), 2.83 (t, *J* = 5.2 Hz, 2H), 1.12 (d, *J* = 6.0 Hz, 6H). ^{13}C NMR (75 MHz, CD$_3$OD) δ 159.92, 156.90, 156.45, 155.39, 152.60, 151.03, 133.28, 132.69, 127.64, 124.67, 120.08, 118.97, 118.08, 112.72, 90.26, 70.29, 70.20, 70.09, 69.56, 69.20, 51.22, 49.44, 39.98, 20.73. HRMS (ESI-MS) m/z: [M+H$^+$] calculated for C$_{29}$H$_{38}$ClN$_6$O$_5^+$: 585.2587, found 585.2584; C$_{29}$H$_{37}$ClN$_6$O$_5$ (585.10).

5-(3-(2-(2-(2-(2-Aminoethoxy)ethoxy)ethoxy)ethoxy)phenyl)-*N*-(4-chloro-2-isopropoxybenzyl)-[1,2,4]triazolo[1,5-*a*]pyrimidin-7-amine (4.042)

The title compound was synthesized from **4.035** (49.10 mg, 0.060 mmol, 1 eq) and hydrazine monohydrate (15.07 mg, 15 µL, 0.301 mmol, 5 eq) in 4 mL 1-butanol according to the general procedure I (R_f = 0.35 in DCM/Methanol/NH$_3$ conc. 50/50/1) yielding a colorless oil (2.9 mg, 8%). ^{1}H NMR (300 MHz, CD$_3$OD) δ 8.35 (s, 1H), 7.52 – 7.43 (m, 2H), 7.35 – 7.27 (m, 2H), 7.01 (d, J = 2.0 Hz, 1H), 6.95 – 6.88 (m, 3H), 5.24 (s, 2H), 4.67 – 4.51 (m, 1H), 4.22 (t, J = 5.1 Hz, 2H), 3.79 (t, J = 5.0 Hz, 2H), 3.57 – 3.51 (m, 2H), 3.50 – 3.41 (m, 8H), 2.87 (t, J = 5.0 Hz, 2H), 1.09 (d, J = 6.0 Hz, 6H). HRMS (ESI-MS) *m/z*: [M+H$^+$] calculated for C$_{29}$H$_{38}$ClN$_6$O$_5^+$: 585.2587, found 585.2595; C$_{29}$H$_{37}$ClN$_6$O$_5$ (585.10).

5-(4-(2-(2-(2-(2-Aminoethoxy)ethoxy)ethoxy)ethoxy)phenyl)-*N*-(4-chloro-2-isopropoxybenzyl)-[1,2,4]triazolo[1,5-*a*]pyrimidin-7-amine (4.043)
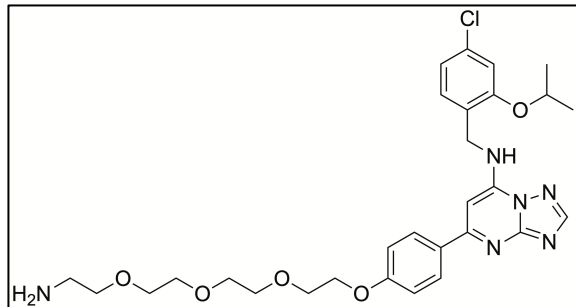
The title compound was synthesized from **4.036** (51.00 mg, 0.063 mmol, 1 eq) and hydrazine monohydrate (15.66 mg, 15 µL, 0.313 mmol, 5 eq) in 4 mL 1-butanol according to the general procedure I (R_f = 0.35 in DCM/Methanol/NH$_3$ conc. 50/50/1) yielding a colorless oil (8.6 mg, 20%). ^{1}H NMR (400 MHz, CD$_3$OD) δ 8.28 (s, 1H), 7.96 – 7.90 (m, 2H), 7.30 (d, J = 8.1 Hz, 1H), 6.99 (d, J = 1.9 Hz, 1H), 6.92 – 6.82 (m, 4H), 5.22 (s, 2H), 4.63 – 4.52 (m, 1H), 4.16 (t, J = 5.1 Hz, 2H), 3.77 (t, J = 5.1 Hz, 2H), 3.57 – 3.51 (m, 2H), 3.50 – 3.38 (m, 8H), 2.74 (t, J = 5.3 Hz, 2H), 1.09 (d, J = 6.0 Hz, 6H). ^{13}C NMR (101 MHz, CD$_3$OD) δ 161.62, 161.16, 157.56, 156.56, 152.68, 150.78, 134.23, 130.51, 128.97, 127.84, 124.10, 119.93, 115.54, 113.02, 91.13, 71.03, 70.33, 70.24, 70.14, 69.81, 69.18, 50.54, 50.33, 40.39, 20.54. HRMS (ESI-MS) *m/z*: [M+H$^+$] calculated for C$_{29}$H$_{38}$ClN$_6$O$_5^+$: 585.2587, found 585.2591; C$_{29}$H$_{37}$ClN$_6$O$_5$ (585.10).

5-(2-((17-Amino-3,6,9,12,15-pentaoxaheptadecyl)oxy)phenyl)-*N*-(2-isopropoxybenzyl)-[1,2,4]triazolo[1,5-*a*]pyrimidin-7-amine (4.044)
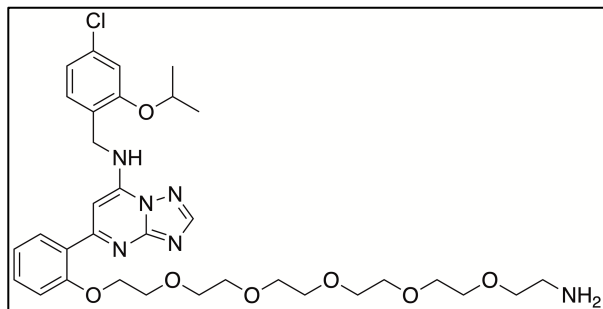
The title compound was synthesized from **4.037** (300.00 mg, 0.332 mmol, 1 eq) and hydrazine monohydrate (83.12 mg, 81 µL, 1.660 mmol, 5 eq) in 10 mL 1-butanol according to the general procedure I (R_f = 0.35 in DCM/Methanol/NH$_3$ conc. 50/50/1) yielding a colorless oil (37.0 mg, 36%). ^{1}H NMR (300 MHz, CD$_3$OD) δ 8.34 (s, 1H), 7.84 (dd, *J* = 8.1, 1.6 Hz, 1H), 7.39 – 7.27 (m, 2H), 7.08 – 6.84 (m, 5H), 5.28 (s, 2H), 4.66 – 4.52 (m, 1H), 4.20 (t, *J* = 5.1 Hz, 2H), 3.80 (t, *J* = 5.1 Hz, 2H), 3.58 – 3.42 (m, 18H), 2.80 (t, *J* = 5.3 Hz, 2H), 1.12 (d, *J* = 6.1 Hz, 6H). ^{13}C NMR (75 MHz, CD$_3$OD) δ 161.50, 159.99, 156.51, 155.38, 152.74, 151.09, 134.30, 132.66, 130.43, 127.71, 123.82, 120.04, 119.00, 118.12, 117.94, 113.08, 90.17, 70.85, 70.32, 70.22, 70.12, 70.06, 70.04, 69.98, 69.76, 69.24, 50.98, 50.76, 40.37, 20.59. HRMS (ESI-MS) *m/z*: [M+H$^+$] calculated for C$_{33}$H$_{46}$ClN$_6$O$_7^+$: 673.3111, found 673.3124; C$_{33}$H$_{45}$ClN$_6$O$_7$ (673.21).

4.5.1.6 Synthesis and Analytical Data of Fluorescence Ligands 4.045-4.055

General procedure J

The corresponding fluorophore (5-TAMRA NHS ester (1 eq) or DY-549P1 NHS ester (1 eq)) was weighed into an Eppendorf reaction vessel. The amine precursors (**4.038-4.044**, var. eq) and triethylamine (11 eq) were dissolved in DMF (100 µL) and added to the vessel. The solution was vigorously shaken for 3 hours at rt in the dark. Subsequently the reaction was stopped by adding 10% aqueous TFA (100 µL) and purified by preparative HPLC (MeCN/0.05% aqueous TFA (**Method A**) or MeCN/0.1% aqueous NH$_3$ (**Method B**)). Due to the insufficient amount (< 0.5 mg) of DY-549P1 fluorescent ligands **4.052-4.055** NMR could not be measured. The identity was confirmed by HRMS.

2-(3,6-Bis(dimethylamino)xanthylium-9-yl)-5-((6-(2-(7-((4-chloro-2-isopropoxybenzyl)amino)-[1,2,4]triazolo[1,5-*a*]pyrimidin-5-yl)phenoxy)hexyl)carbamoyl)benzoate hydrotrifluoroacetate (4.045)
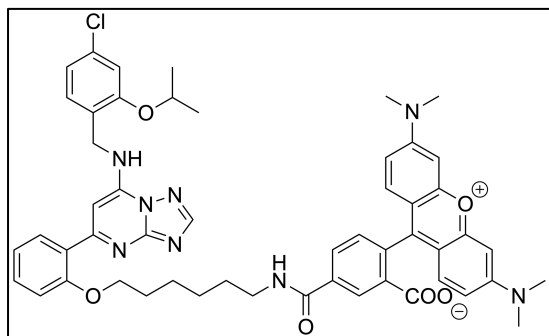
The title compound was prepared from precursor **4.038** (3.96 mg, 0.0054 mmol, 1.3 eq), 5-TAMRA NHS ester (2.23 mg, 0.0042 mmol, 1 eq) and triethylamine (6.19 µL, 0.0465 mmol, 11 eq) according to the general procedure J (using method A for purification) yielding a fluffy purple solid (1.83 mg, 42%).

RP-HPLC: 97% (t_R = 18.31 min, k = 5.10). ^{1}H NMR (400 MHz, CD$_3$OD) δ 8.74 (d, J = 1.8 Hz, 1H), 8.38 (s, 1H), 8.20 (dd, J = 7.9, 1.9 Hz, 1H), 7.83 (d, J = 8.1 Hz, 1H), 7.47 (d, J = 8.0 Hz, 1H), 7.36 – 7.28 (m, 2H), 7.12 – 6.96 (m, 7H), 6.94 – 6.88 (m, 4H), 5.32 (s, 2H), 4.62 – 4.52 (m, 1H), 3.88 (t, J = 7.7 Hz, 2H), 3.46 (t, J = 6.6 Hz, 2H), 3.30 (s*, 12H, concealed), 1.87 – 1.79 (m, 2H), 1.72 – 1.65 (m, 2H), 1.52 – 1.46 (m, 4H), 1.05 (d, J = 6.0 Hz, 6H). HRMS (ESI-MS) *m/z*: [M+H$^+$] calculated for C$_{52}$H$_{54}$ClN$_8$O$_6^+$: 921.3849, found 921.3848; C$_{52}$H$_{53}$ClN$_8$O$_6$ x C$_2$HF$_3$O$_2$ (1035.52).

2-(3,6-Bis(dimethylamino)xanthylium-9-yl)-5-((6-(3-(7-((4-chloro-2-isopropoxybenzyl)amino)-[1,2,4]triazolo[1,5-*a*]pyrimidin-5-yl)phenoxy)hexyl)carbamoyl)benzoate hydrotrifluoroacetate (4.046)
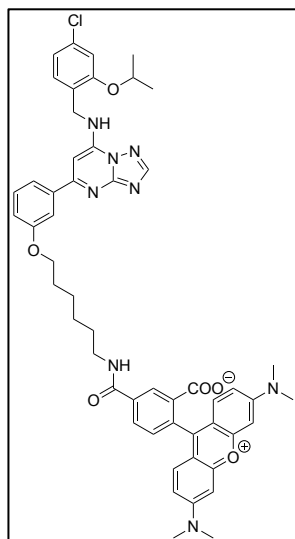
The title compound was prepared from precursor **4.039** (5.40 mg, 0.0106 mmol, 1.5 eq), 5-TAMRA NHS ester (3.73 mg, 0.0071 mmol, 1 eq) and triethylamine (10.36 µL, 0.0778 mmol, 11 eq) according to the general procedure J (using method A for purification) yielding a fluffy purple solid (1.993 mg, 18%). RP-HPLC: 97% (t_R = 17.08 min, k = 4.69). ^{1}H NMR (400 MHz, CD$_3$OD) δ 8.73 (d, J = 1.7 Hz, 1H), 8.34 (s, 1H), 8.19 (dd, J = 7.9, 1.8 Hz, 1H), 7.49 – 7.40 (m, 3H), 7.31 – 7.24 (m, J = 8.6 Hz, 2H), 7.13 – 6.95 (m, 7H), 6.92 – 6.86 (m, J = 7.2, 5.4, 2.2 Hz, 2H), 6.70 (s, 1H), 5.28 (s, 2H), 4.59 – 4.51 (m, 1H), 3.85 (t, 2H), 3.48 – 3.43 (m, 2H), 3.30 (s*, 12H, concealed), 1.86 – 1.78 (m, 2H), 1.71 – 1.65 (m, 2H), 1.52 – 1.45 (m, 4H), 1.02 (d, J = 6.0 Hz, 6H). HRMS (ESI-MS) *m/z*: [M+H$^+$]

calculated for $C_{52}H_{54}ClN_8O_6^+$: 921.3850, found 921.3849; $C_{52}H_{53}ClN_8O_6$ x $C_2HF_3O_2$ (1035.52).

2-(3,6-Bis(dimethylamino)xanthylium-9-yl)-5-((6-(4-(7-((4-chloro-2-isopropoxybenzyl)amino)-[1,2,4]triazolo[1,5-*a*]pyrimidin-5-yl)phenoxy)hexyl)carbamoyl)benzoate hydrotrifluoroacetate (4.047)
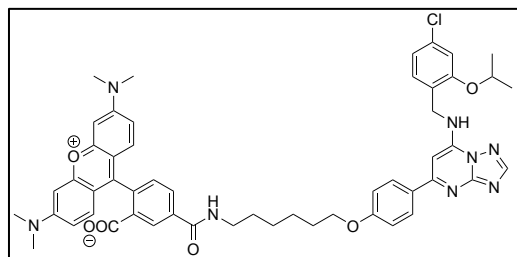
The title compound was prepared from precursor **4.040** (0.65 mg, 0.0013 mmol, 1.4 eq), 5-TAMRA NHS ester (0.50 mg, 0.0009 mmol, 1 eq) and triethylamine (1.39 µL, 0.0104 mmol, 11 eq) according to the general procedure J (using method A for purification) yielding a fluffy purple solid (0.635 mg, 65%). RP-HPLC: > 99% (t_R = 15.87 min, k = 4.29). ^{1}H NMR (400 MHz, CD$_3$OD) δ 8.74 (s, 1H), 8.22 – 8.17 (m, 1H), 7.91 (d, J = 8.7 Hz, 2H), 7.47 (d, J = 7.9 Hz, 1H), 7.28 (d, J = 8.1 Hz, 1H), 7.11 (d, 2H), 7.05 – 6.97 (m, 5H), 6.91 – 6.84 (m, 4H), 6.70 (s, 1H), 5.26 (s, 2H), 4.57 – 4.51 (m, 1H), 3.83 (t, J = 7.7 Hz, 2H), 3.47 (m, 2H), 3.30 (s*, 12H, concealed), 1.85 – 1.77 (m, 2H), 1.71 – 1.66 (m, 2H), 1.50 – 1.45 (m, 4H), 1.02 (d, J = 6.0 Hz, 6H). HRMS (ESI-MS) *m/z*: [M+H$^+$] calculated for $C_{52}H_{54}ClN_8O_6^+$: 921.3850, found 921.3849; $C_{52}H_{53}ClN_8O_6$ x $C_2HF_3O_2$ (1035.52).

2-(3,6-Bis(dimethylamino)xanthylium-9-yl)-5-((2-(2-(2-(2-(7-((4-chloro-2-isopropoxybenzyl)amino)-[1,2,4]triazolo[1,5-*a*]pyrimidin-5-yl)phenoxy)ethoxy)ethoxy)ethoxy)ethyl)carbamoyl)benzoate hydrotrifluoroacetate (4.048)
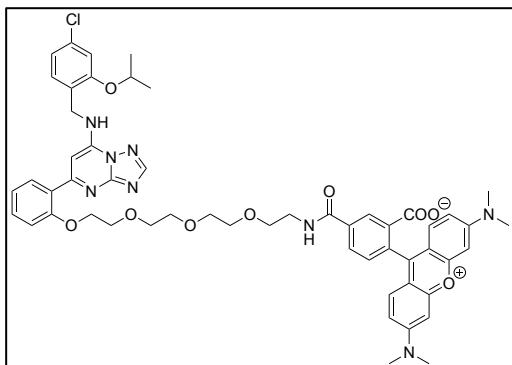
The title compound was prepared from precursor **4.041** (1.92 mg, 0.0050 mmol, 3 eq), 5- TAMRA NHS ester (0.60 mg, 0.0011 mmol, 1 eq) and triethylamine (1.67 µL, 0.0125 mmol, 11 eq) according to the general procedure J (using method A for purification), yielding a fluffy purple solid (1.091 mg, 86%). RP-HPLC: > 99% (t_R= 16.95 min, k = 4.65). ^{1}H NMR (400 MHz, CD$_3$OD) δ 8.71 (d, J = 1.8 Hz, 1H), 8.24 – 8.19 (m, 2H), 7.75 (dd, J = 8.2, 1.6 Hz, 1H), 7.40 (d, J = 7.9 Hz, 1H), 7.31 – 7.26 (m, 1H), 7.23 (d, J = 8.2 Hz, 1H), 6.99 (d, J = 9.4 Hz, 2H), 6.95 (d, J = 1.9 Hz, 1H), 6.91 –

6.80 (m, 8H), 5.23 (s, 2H), 4.56 – 4.48 (m, 1H), 4.06 (t, J = 5.3 Hz, 2H), 3.71 (t, J = 5.2 Hz, 2H), 3.63 – 3.56 (m, 4H), 3.54 – 3.48 (m, 8H), 3.22 (s, 12H), 1.02 (d, J = 6.0 Hz, 6H). HRMS (ESI-MS) m/z: [M+H$^+$] calculated for $C_{54}H_{58}ClN_8O_9^+$: 997.4010, found 997.4006; $C_{54}H_{57}ClN_8O_9$ x $C_2HF_3O_2$ (1111.57).

2-(3,6-Bis(dimethylamino)xanthylium-9-yl)-5-((2-(2-(2-(2-(3-(7-((4-chloro-2-isopropoxybenzyl)amino)-[1,2,4]triazolo[1,5-*a*]pyrimidin-5-yl)phenoxy)ethoxy)ethoxy)ethoxy)ethyl)carbamoyl)benzoate hydrotrifluoroacetate (4.049)
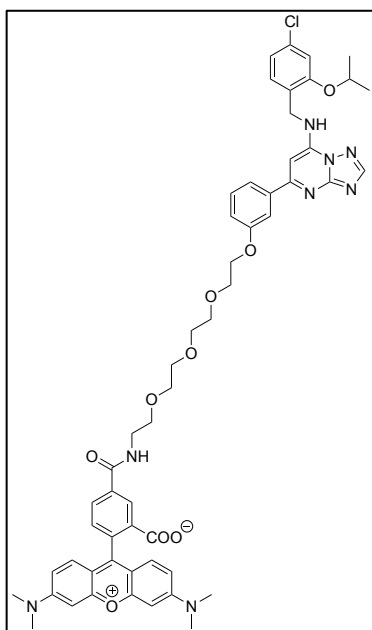
The title compound was prepared from precursor **4.042** (1.35 mg, 0.0023 mmol, 1 eq), 5- TAMRA NHS ester (1.22 mg, 0.0023 mmol, 1 eq) and triethylamine (3.38 µL, 0.0254 mmol, 11 eq) according to the general procedure J (using method A for purification) yielding a fluffy purple solid (1.508 mg, 59%). RP-HPLC: > 99% (t$_R$ = 15.20 min, k = 4.07). ^{1}H NMR (400 MHz, CD$_3$OD) δ 8.70 (s, 1H), 8.25 (s, 1H), 8.19 (d, J = 7.6 Hz, 1H), 7.44 – 7.38 (m, 3H), 7.27 – 7.21 (m, 2H), 7.06 (d, J = 9.6 Hz, 2H), 6.99 – 6.83 (m, 7H), 6.79 (s, 1H), 5.22 (s, 2H), 4.60 – 4.51 (m, 1H), 4.08 (t, J = 5.3 Hz, 2H), 3.74 (t, J = 5.2 Hz, 2H), 3.68 – 3.60 (m, 4H), 3.58 – 3.50 (m, 8H), 3.24 (s, 12H), 1.04 (d, J = 6.0 Hz, 6H).

HRMS (ESI-MS) m/z: [M+H$^+$] calculated for $C_{54}H_{58}ClN_8O_9^+$: 997.4010, found 997.4020; $C_{54}H_{57}ClN_8O_9$ x $C_2HF_3O_2$ (1111.57).

2-(3,6-Bis(dimethylamino)xanthylium-9-yl)-5-((2-(2-(2-(2-(4-(7-((4-chloro-2-isopropoxybenzyl)amino)-[1,2,4]triazolo[1,5-*a*]pyrimidin-5-yl)phenoxy)ethoxy)ethoxy)ethoxy)ethyl)carbamoyl)benzoate hydrotrifluoroacetate (4.050)
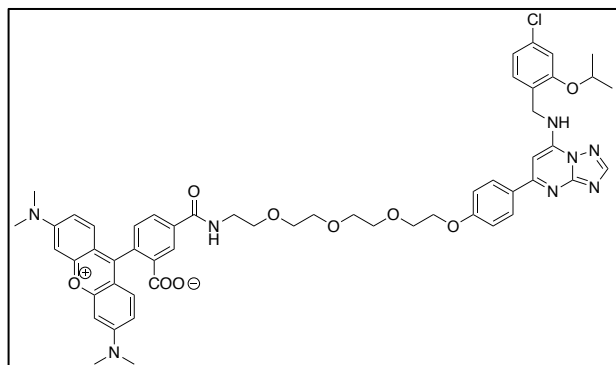
The title compound was prepared from precursor **4.043** (2.90 mg, 0.0050 mmol, 2.2 eq), 5-TAMRA NHS ester (1.20 mg, 0.0023 mmol, 1 eq) and triethylamine (3.33 μL, 0.0250 mmol, 11 eq) according to the general procedure J (using method A for purification), yielding a fluffy purple solid (2.231 mg, 88%). RP-HPLC: > 99% (t_R = 15.22 min, k = 4.07). ^{1}H NMR (400 MHz, CD$_3$OD) δ 8.75 (d, *J* = 1.8 Hz, 1H), 8.24 (dd, *J* = 7.9, 1.8 Hz, 1H), 7.89 (d, 2H), 7.45 (d, *J* = 7.9 Hz, 1H), 7.25 (d, J = 8.1 Hz, 1H), 7.04 (d, J = 9.4 Hz, 2H), 6.99 – 6.76 (m, 10H), 5.21 (s, 2H), 4.60 – 4.50 (m, 1H), 4.04 (t, J = 5.3 Hz, 2H), 3.74 (t, J = 5.2 Hz, 2H), 3.68 – 3.61 (m, 4H), 3.58 – 3.53 (m, 8H), 3.25 (s, 12H), 1.05 (d, *J* = 6.0 Hz, 6H). HRMS (ESI-MS) *m/z*: [M+H$^+$] calculated for C$_{54}$H$_{58}$ClN$_8$O$_9$$^+$: 997.4010, found 997.4012; C$_{54}$H$_{57}$ClN$_8$O$_9$ x C$_2$HF$_3$O$_2$ (1111.57).

2-(3,6-bis(Dimethylamino)xanthylium-9-yl)-5-((17-(2-(7-((4-chloro-2-isopropoxybenzyl)amino)-[1,2,4]triazolo[1,5-*a*]pyrimidin-5-yl)phenoxy)-3,6,9,12,15-pentaoxaheptadecyl)carbamoyl)benzoat hydrotrifluoroacetate (4.051)
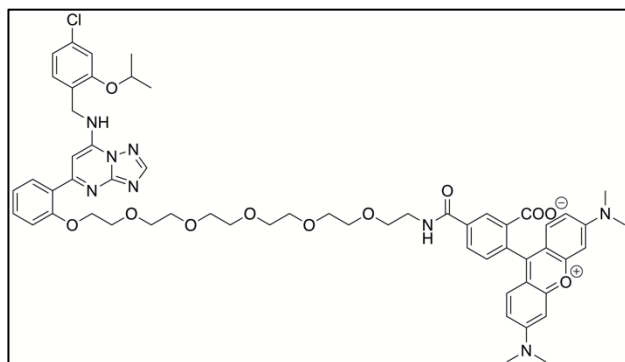
The title compound was prepared from precursor 44 (18.60 mg, 0.0365 mmol, 3.1 eq), 5-TAMRA NHS ester (6.20 mg, 0.0118 mmol, 1 eq) and triethylamine (17.21 μL, 0.1293 mmol, 11 eq) according to the general procedure J (using method A for purification) yielding a fluffy purple solid (9.34 mg, 66%). RP-HPLC: 98% (t_R = 16.80 min, k = 4.60). ^{1}H NMR (400 MHz, CD$_3$OD) δ 8.82 (d, *J* = 1.8 Hz, 1H), 8.40 (s, 1H), 8.32 (dd, *J* = 7.9, 1.9 Hz, 1H), 7.85 (d, *J* = 8.0 Hz, 1H), 7.52 (d, *J* = 7.9 Hz, 1H), 7.39 – 7.30 (m, 2H), 7.11 (d, *J* = 1.0 Hz, 2H), 7.04 (s, 2H), 7.01 – 6.88 (m, 7H), 5.31 (s, 2H), 4.68 – 4.57 (m, 1H), 4.16

(t, J = 5.1 Hz, 2H), 3.80 (t, J = 5.1 Hz, 2H), 3.76 – 3.49 (m, 20H), 3.30 (s, 12H), 1.15 (d, J = 6.0 Hz, 6H). ^{13}C NMR (101 MHz, CD$_3$OD) δ 166.74, 165.93, 161.35, 159.82, 157.49, 157.41, 156.53, 152.31, 151.06, 136.64, 136.28, 134.37, 132.73, 131.44, 131.01, 130.57, 130.43, 130.03, 127.80, 123.72, 120.06, 119.06, 118.08, 114.08, 113.24, 113.14, 96.04, 90.39, 70.39, 70.31, 70.23, 70.19, 70.11, 70.03, 69.93, 69.09, 51.05, 50.73, 39.89, 39.52, 20.59. HRMS (ESI-MS) m/z: [M+H$^+$] calculated for C$_{58}$H$_{66}$ClN$_8$O$_{11}^+$: 1085.4534, found 1085.4548; C$_{58}$H$_{65}$ClN$_8$O$_{11}$ x C$_2$HF$_3$O$_2$ (1199.68).

Triammonium   2-((*E*)-3-((*E*)-1-(1-(2-(7-((4-chloro-2-isopropoxybenzyl)amino)-[1,2,4]triazolo[1,5-*a*]pyrimidin-5-yl)phenoxy)-13-oxo-3,6,9-trioxa-12-azaoctadecan-18-yl)-3-methyl-5-sulfo-3-(3-sulfopropyl)indolin-2-ylidene)prop-1-en-1-yl)-1-(2-methoxyethyl)-3-methyl-5-sulfo-3-(3-sulfopropyl)-3*H*-indol-1-ium (4.052)
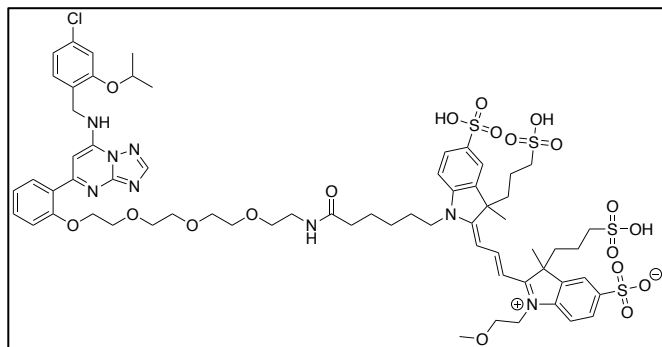
The title compound was prepared from precursor **4.041** (8.06 mg, 0.0138 mmol, 71.6 eq), DY-549P1 NHS ester (0.20 mg, 0.0002 mmol, 1 eq) and triethylamine (0.28 µL, 0.0021 mmol, 11 eq) according to the general procedure J (using method B for purification) yielding a fluffy purple solid (0.25 mg, 84%). RP-HPLC: > 99% (t$_R$ = 6.44 min, k = 1.34). HRMS (ESI-MS) m/z: [M+H$^+$] calculated for C$_{65}$H$_{84}$ClN$_8$O$_{19}$S$_4^+$: 1443.4419, found 1443.4405; C$_{65}$H$_{83}$ClN$_8$O$_{19}$S$_4$ x 3 NH$_3$ (1495.20).

Triammonium 2-((*E*)-3-((*E*)-1-(1-(3-(7-((4-chloro-2-isopropoxybenzyl)amino)-[1,2,4]triazolo[1,5-*a*]pyrimidin-5-yl)phenoxy)-13-oxo-3,6,9-trioxa-12-azaoctadecan-18-yl)-3-methyl-5-sulfo-3-(3-sulfopropyl)indolin-2-ylidene)prop-1-en-1-yl)-1-(2-methoxyethyl)-3-methyl-5-sulfo-3-(3-sulfopropyl)-3*H*-indol-1-ium (4.053)
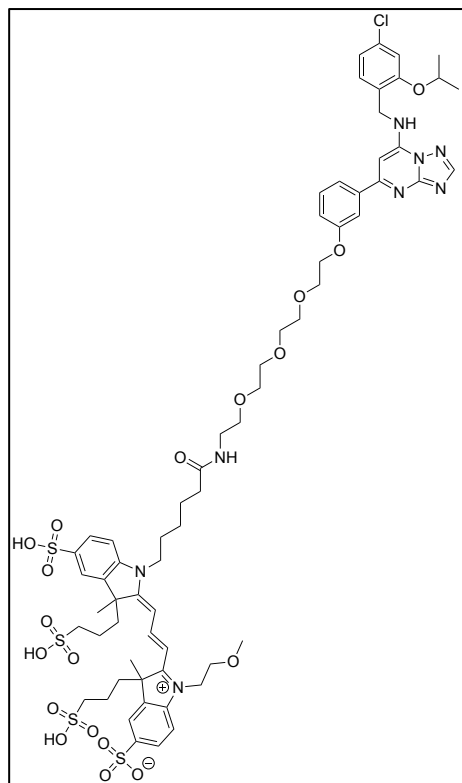
The title compound was prepared from precursor **4.042** (0.58 mg, 0.0010 mmol, 5.2 eq), DY-549P1 NHS ester (0.20 mg, 0.0002 mmol, 1 eq) and triethylamine (0.28 µL, 0.0021 mmol, 11 eq) according to the general procedure J (using method B for purification) yielding a fluffy purple solid (0.299 mg, 100%). RP-HPLC: > 99% (t_R = 5.70 min, k = 0.9). HRMS (ESI-MS) *m/z*: [M-2H]$^{2-}$ calculated for $C_{65}H_{81}ClN_8O_{19}S_4{}^{2-}$: 720.2100, found 720.2114; $C_{65}H_{83}ClN_8O_{19}S_4$ x 3 NH$_3$ (1495.20).

Triammonium 2-((*E*)-3-((*E*)-1-(1-(4-(7-((4-chloro-2-isopropoxybenzyl)amino)-[1,2,4]triazolo[1,5-*a*]pyrimidin-5-yl)phenoxy)-13-oxo-3,6,9-trioxa-12-azaoctadecan-18-yl)-3-methyl-5-sulfo-3-(3-sulfopropyl)indolin-2-ylidene)prop-1-en-1-yl)-1-(2-methoxyethyl)-3-methyl-5-sulfo-3-(3-sulfopropyl)-3*H*-indol-1-ium (4.054)
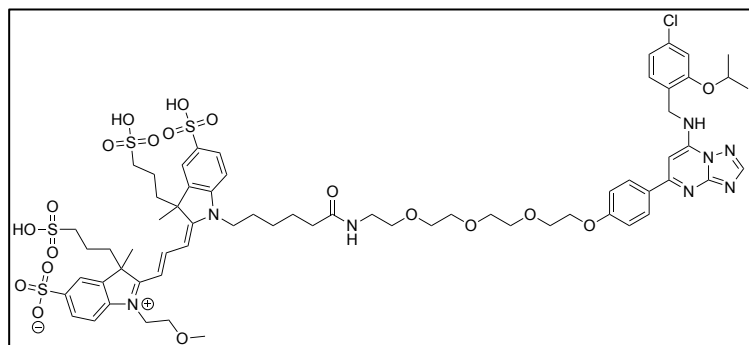
The title compound was prepared from precursor **4.043** (0.45 mg, 0.0008 mmol, 4 eq), DY-549P1 NHS ester (0.20 mg, 0.0002 mmol, 1 eq) and triethylamine (0.28 µL, 0.0021 mmol, 11 eq) according to the general procedure J (using method B for purification) yielding a fluffy purple solid

(0.290 mg, 97%). RP-HPLC: > 99% (t_R = 4.92 min, k = 0.64). HRMS (ESI-MS) *m/z*: [M-2H]$^{2-}$ calculated for $C_{65}H_{81}ClN_8O_{19}S_4^{2-}$: 720.2100, found 720.2109; $C_{65}H_{83}ClN_8O_{19}S_4$ x 3 NH$_3$ (1495.20).

Triammonium 2-((E)-3-((E)-1-(1-(2-(7-((4-chloro-2-isopropoxybenzyl)amino)-[1,2,4]triazolo[1,5-*a*]pyrimidin-5-yl)phenoxy)-19-oxo-3,6,9,12,15-pentaoxa-18-azatetracosan-24-yl)-3-methyl-5-sulfo-3-(3-sulfopropyl)indolin-2-ylidene)prop-1-en-1-yl)-1-(2-methoxyethyl)-3-methyl-5-sulfo-3-(3-sulfopropyl)-3*H*-indol-1-ium (4.055)
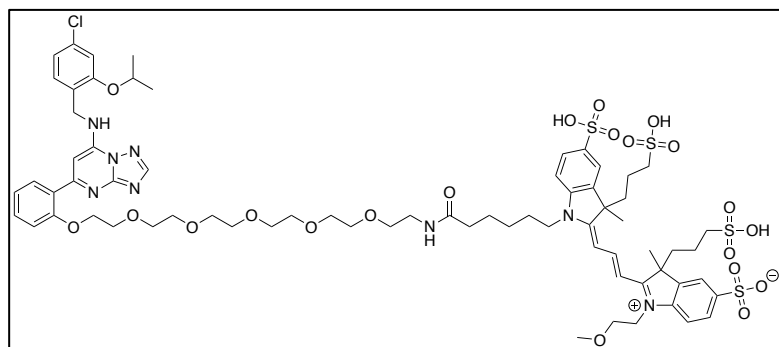
The title compound was prepared from precursor **4.044** (2.09 mg, 0.0027 mmol, 14 eq), DY-549P1 NHS ester (0.20 mg, 0.0002 mmol, 1 eq) and triethylamine (0.28 µL, 0.0021 mmol, 11 eq) according to the general procedure J (using method B for purification), yielding a fluffy purple solid (0.317 mg, 100%). RP-HPLC: > 99% (t_R = 6.64 min, k = 1.41). HRMS (ESI-MS) *m/z*: [M+H$^+$] calculated for $C_{69}H_{92}ClN_8O_{21}S_4^+$: 1531.4943, found 1531.4935; $C_{69}H_{91}ClN_8O_{21}S_4$ x 3 NH$_3$ (1583.31).

4.5.1.7 Recording of Fluorescence Excitation and Emission Spectra of 5-TAMRA- and DY-549P1-labeled AF64394 Analogs

The fluorescent compounds were diluted in DMSO to a concentration of 20 µM. 100 µL of each ligand preparation or DMSO (blank) was added to a well of a black 96-well plate and the excitation and emission spectra were recorded using a CLARIOstar plate reader with the following measurement settings: Excitation scan: emission wavelength 610-10 nm; Excitation range 500 – 585 nm with 1 nm increments; Gain 800. Emission scan: excitation wavelength 522 nm; emission range 550 – 650 nm with 1 nm increments; Gain 800.

4.5.1.8 Homology Modelling

Templates were chosen based on the alignment in GPCRdb.[557] Accordingly, sphingosine-1-phosphate receptor 5 (S1P$_5$) with 31% identity and 46% similarity to GPR3 was chosen as a template. Homology modelling was performed in MODELLER.[558] Two models, one active based on 7ew1, and one inactive based on 7yxa, were built. Five hundred model variants were generated based on each template and to find representative models, they were clustered in Chimera[559]. The best five representative models were selected, and their quality was investigated by considering DOPE (discrete optimized protein energy) score, MODELLER objective function value, RMSD (compared to the template) and normalized DOPE values (z-score). Model statistics are provided in the Supplementary Information (cf. Table 4.02, chapter **4.6.4**).

4.5.1.9 Docking Calculations

The 3D structures of the small molecules in db2 format were generated in tldr.docking.org using the newBuild3D module. Docking calculations were performed in DOCK3.7[560]. The obtained poses were then minimized using a variant of MMFF94 (Merck Molecular force field), MMFF94x[561], in the Molecular Operating Environment (MOE) software[562]. In the minimization step, the ligand and the surrounding binding pocket residues were subjected to minimization. PyMOL (The PyMOL Molecular Graphics System, Version 2.0, Schrödinger, LLC) was used for visualization of the poses.

4.5.2 Biology
4.5.2.1 Plasmids and Molecular Cloning

The expression plasmids encoding N-terminally HA-tagged GPR3 (cat. no. #GPR003TN00), GPR6 (cat. no. #GPR0060000), and N-terminally HA-tagged GPR12 (cat. no. #GPR012TN00) all encoded on a pcDNA3.1+ vector were obtained from the cDNA resource center (cdna.org). The Nluc insert was amplified with overhangs from α_{2A}AR-Nluc/HaloTag[518] and inserted between the HA-tag sequence and GPR3 using prolonged overlap extension PCR. Nluc-GPR6 and Nluc-GPR12 were cloned using restriction enzyme digestion and ligation. Nluc-AT$_1$R, Nluc-β_1AR, Nluc-β_2AR, and Nluc-M$_1$R were described previously.[536] Plasmid encoding CRE-Fluc (pGL4.29[luc2P/CRE/Hygro]) was obtained from Promega. All constructs were verified by sequencing (Eurofins genomics).

4.5.2.2 Reagents

Poly-D-lysine was obtained from Sigma Aldrich (Merck KGaA). Dulbecco's Modified Eagle's Medium (DMEM) and G-418 (Geneticin) were from Gibco. Diphenyleneiodonium chloride (DPI) and AF64394 were purchased from Tocris (Bio-Techne). The Nluc substrates furimazine (cat. no. N1572) and vivazine (cat. no. N2581) were from Promega (Madison). White-wall, white-bottomed 96-well and black-wall, black bottomed 96-well microtiter plates were from Brand.

4.5.2.3 Cell Culture

HEK293A were used for experiment upon transient transfection and grown in Dulbecco's modified Eagle's medium (DMEM) supplemented with 2 mM glutamine, 10% fetal calf serum, streptomycin (0.1 mg/mL), and penicillin (100 U/mL) at 37 °C with 5% CO$_2$. For the generation of stable Nluc-GPR3 cells, HEK293A cells grown in T75 flasks were transfected at a confluence of 40–50% with 1 µg of DNA. To select for stably expressing cells, transfected cells were cultured with 2000 µg/mL of G-418 and maintained in fully supplemented DMEM containing 500 µg/mL G-418. Absence of *mycoplasma* contamination was routinely confirmed by PCR.

4.5.2.4 Transient Transfection and Plating

Resuspended cells (300,000 cells/mL) were transfected in suspension with a total of 1 µg DNA/mL suspension using Lipofectamine 2000 (Thermo Fisher Scientific; 2 µL Lipofectamine 2000 per µg DNA). For reporter gene experiments, resuspended cells were transfected with 500 ng pcDNA or wildtype GPR3 along with 500 ng *CRE*-Fluc plasmid per mL cell suspension. Cells mixed with the transfection reagents were seeded onto poly-D-lysine–precoated, white 96-well plates and grown for 48 h at 37 °C with 5% CO_2. Stable Nluc-GPR3 expressing cells were seeded 24 h prior to the experiment at a density of 800,000 cells/mL into white 96-well plates.

4.5.2.5 Recording of Nluc-GPR3 Luminescence Spectrum

HEK293A cells stably expressing Nluc-GPR3 were seeded as described above. Luminescence emission was recorded between 400 and 700 nm with 2 nm resolution in Hank's balanced salt solution (HBSS) upon addition of 1:1000 furimazine dilution. All experiments were conducted using a CLARIOstar plate reader (BMG, Ortenberg, Germany) and spectra were normalized to the donor emission peak.

4.5.2.6 NanoBRET-based Ligand Binding Experiments

HEK293A transiently or stably expressing the indicated Nluc-GPCR constructs were grown for 48 or 24 h, respectively, and washed once with HBSS. For time-course saturation binding experiments cells were then incubated with 1/100 vivazine solution (in HBSS) for 2 h, stimulated with fluorescent compounds or vehicle control and the BRET ratios were recorded using a Spark multimode reader (Tecan, Männedorf, Switzerland) for 180 minutes with a temporal resolution of one data point per minute. For endpoint BRET measurements fluorescent compounds were incubated with or without competitor (AF64394) / modulator (DPI) for 3 h in HBSS. Following this incubation period, 1/1000 furimazine (in HBSS) was added to the wells and three BRET reads were recorded and averaged. All experiments were conducted at 37 °C. Nluc emission intensity was quantified between 430 and 530 nm with an integration time of 50 ms. TAMRA and DY-549P1 emission were quantified between 565 and 620 nm with an integration time of 50 ms.

4.5.2.7 CRE Reporter Gene Assay

Transfected cells grown in 96-well plates were washed with 100 μL of HBSS 24 h after transfection and incubated for another 24 h in fetal bovine serum (FBS)–free, fully supplemented DMEM containing either vehicle control, 10 μM AF64394 or 10 μM **4.045**. The day of the experiment, cells were washed with HBSS and lysed in 30 μL of Promega's dual luciferase passive lysis buffer (15 min, room temperature). Then, 30 μL of luciferase assay reagent (LARII) was added to each well and *CRE*–dependent firefly luciferase (Fluc) intensity was measured at 37 °C using a CLARIOstar microplate reader (580/80 nm; 800 ms integration time).

4.5.3 Data Analysis

BRET ratios were defined as acceptor emission/donor emission. The first BRET ratio of a time-course experiments was defined as BRET (Ratio$_{basal}$). To quantify ligand-induced changes ΔBRET was calculated for each well as a percent over basal ([(Ratio$_{stim}$ − Ratio$_{basal}$)/Ratio$_{basal}$] × 100). Subsequently, the average ΔBRET of vehicle control was subtracted. Data from BRET experiments were fitted using a three-parameter fit. Linear vs. exponential correlation for the data obtained from off-target binding experiments (cf. Figure 4.004C) was tested using the Extra-sum-of-squares F-test ($p < 0.05$). For competition experiments of **4.045** with AF64394 or DPI, the preferred model (three vs. four parameter log[agonist] vs. response fit) was determined using an Extra-sum-of-squares F-test. Based on the outcome of this test, a three-parameter fit was used to fit the competition data with AF64394 (cf. Figure 4.005B) and a four-parameter fit (variable hill slope) was used to fit the modulation of **4.045** binding by DPI (cf. Figure 4.005C). Data shown are mean values ± SEM of N independent experiments. Reporter gene experiments were analyzed by plotting the raw intensity in the Fluc emission channel and statistical significance was tested using Two-way-ANOVA followed by Dunnett's multiple comparison (****$p < 0.0001$). Data were analyzed using Prism 5.0 software (GraphPad, San Diego, CA, USA).

4.6   Supplementary Material
4.6.1   NMR Spectra of Compounds 4.038-4.044 and 4.045-4.051
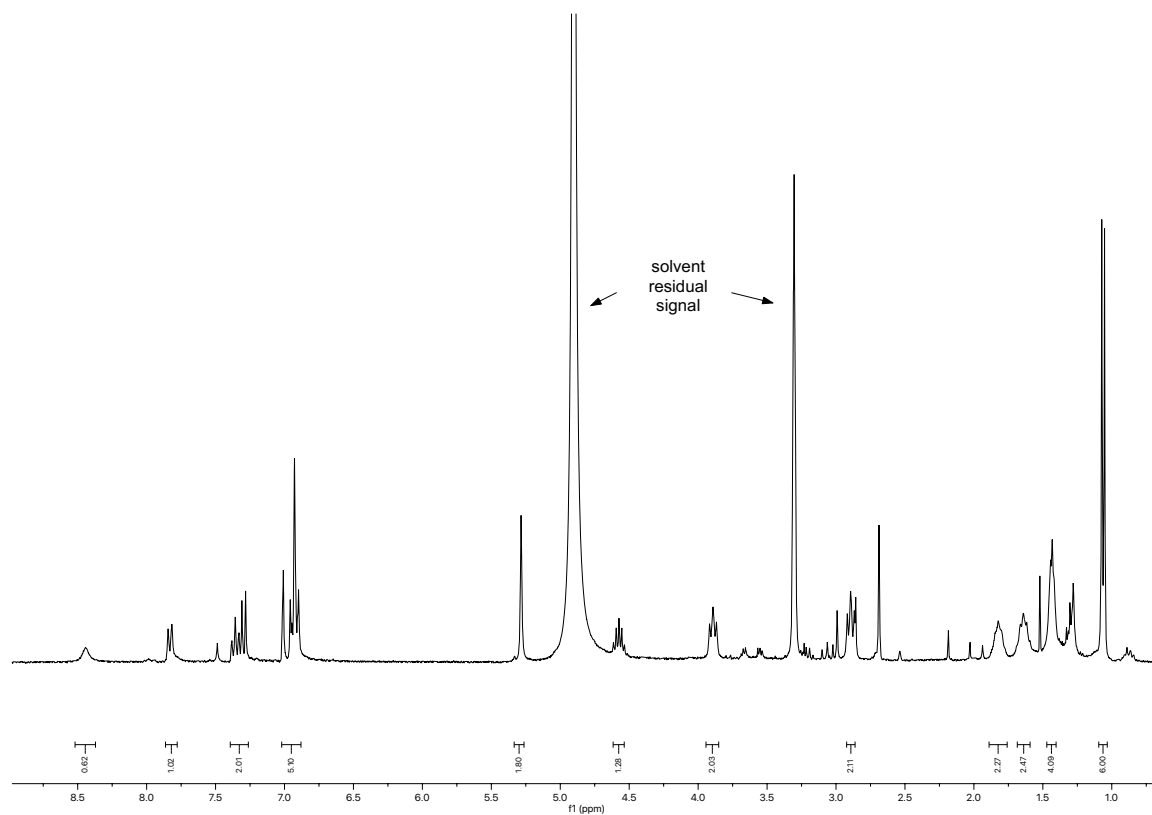
Figure 4.006. ^{1}H NMR spectrum (300 MHz, CD$_3$OD) of compound **4.038**.
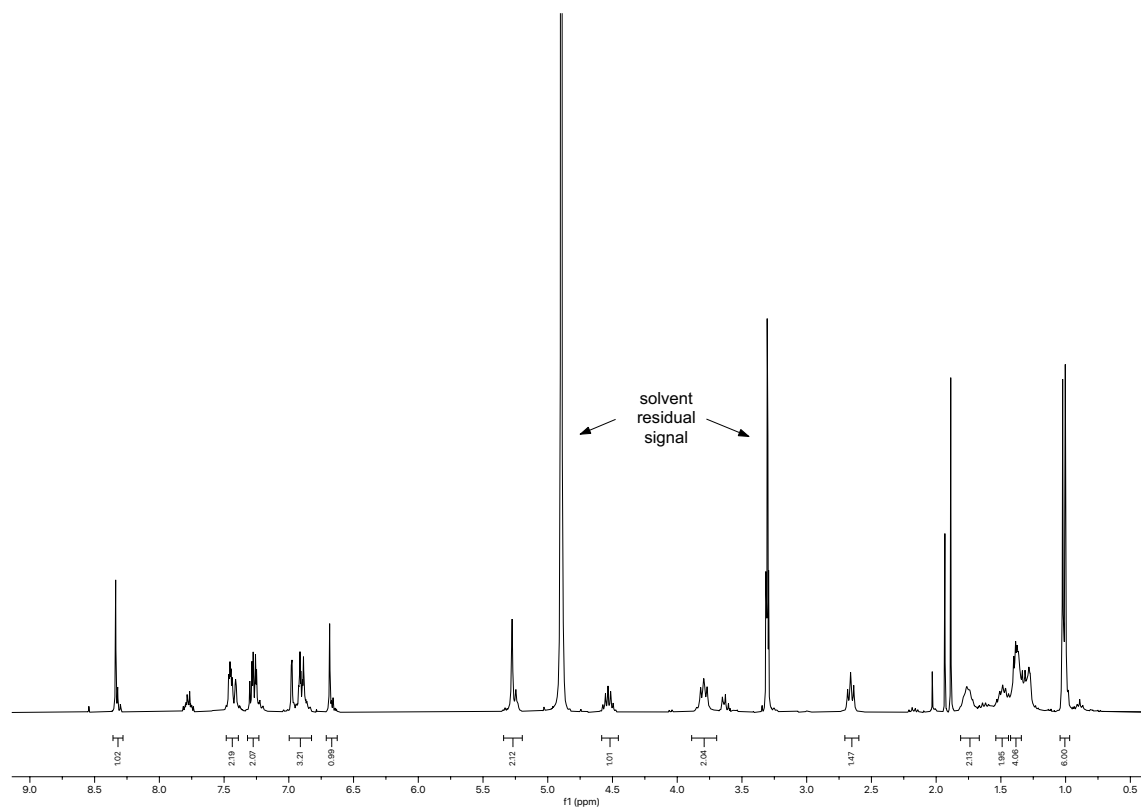
Figure 4.007. ^{1}H NMR spectrum (300 MHz, CD$_3$OD) of compound **4.039**.
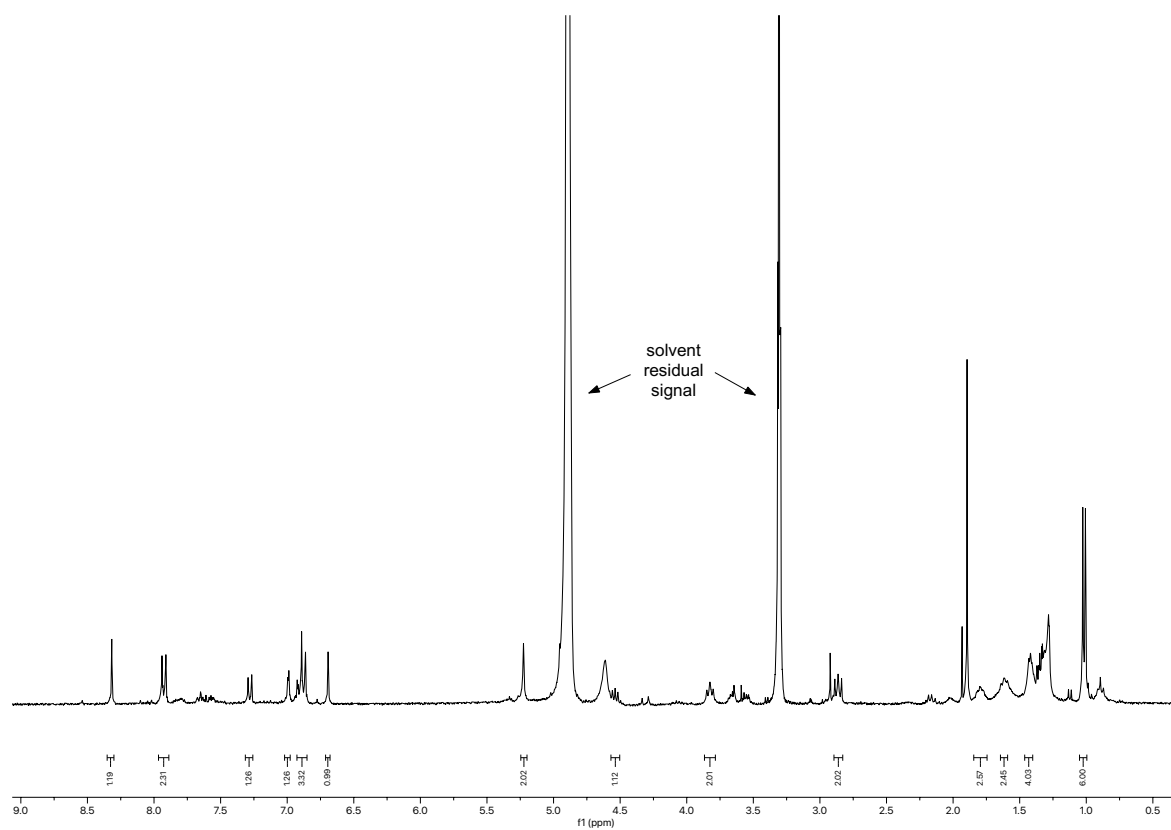
Figure 4.008. ^{1}H NMR spectrum (300 MHz, CD$_3$OD) of compound **4.040**.
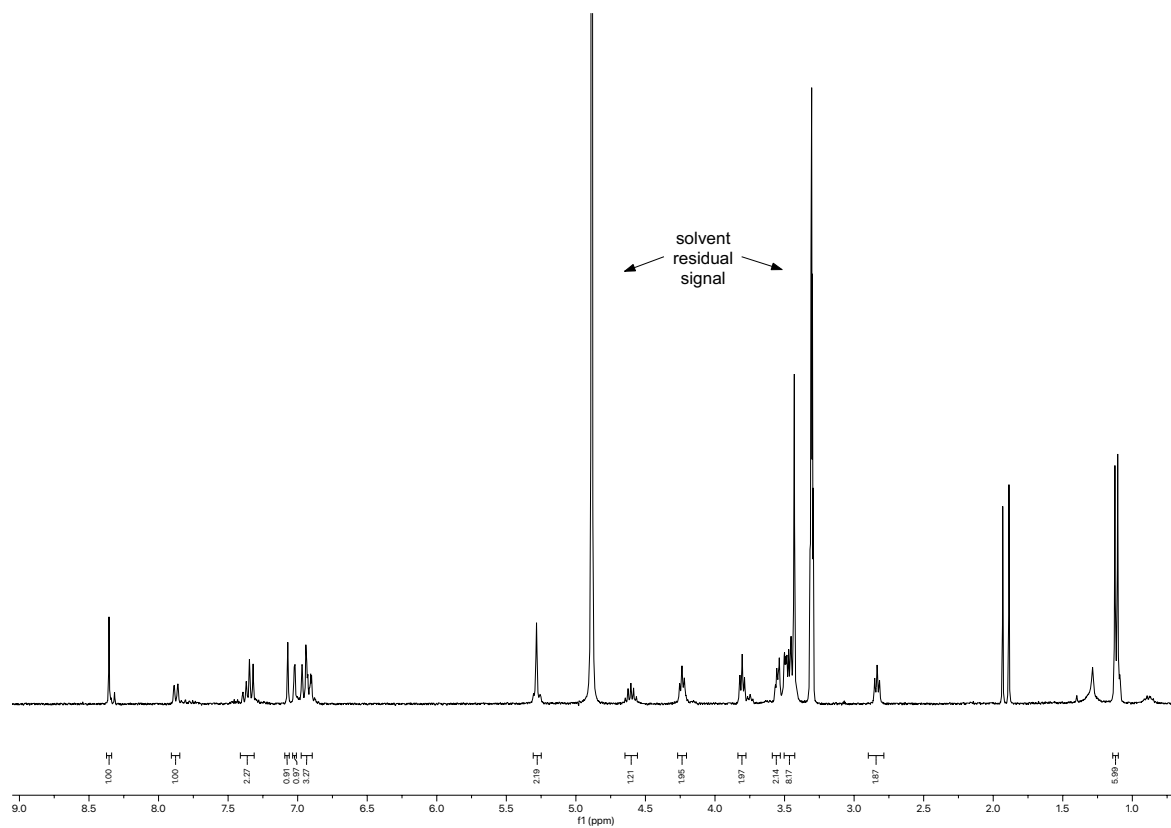
Figure 4.009. ^{1}H NMR spectrum (300 MHz, CD$_3$OD) of compound **4.041**.
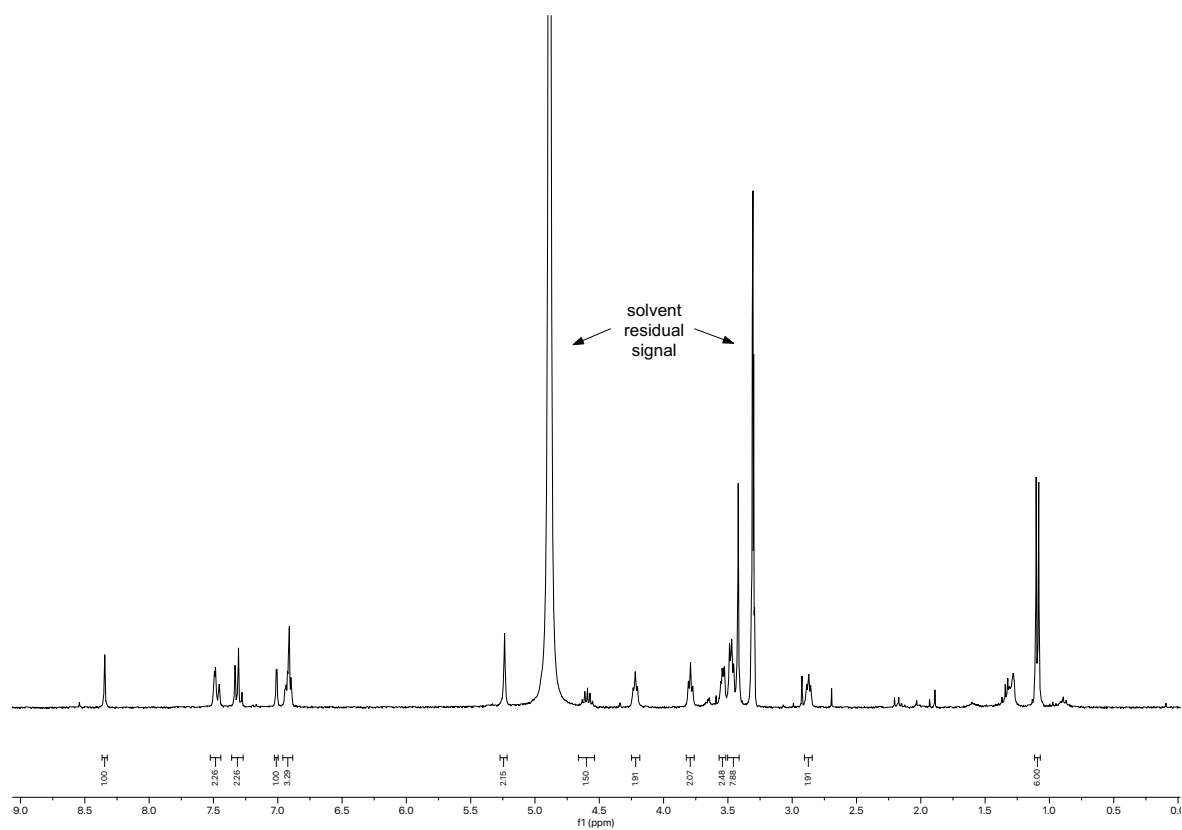
Figure 4.010. ^{1}H NMR spectrum (300 MHz, CD$_3$OD) of compound **4.042**.
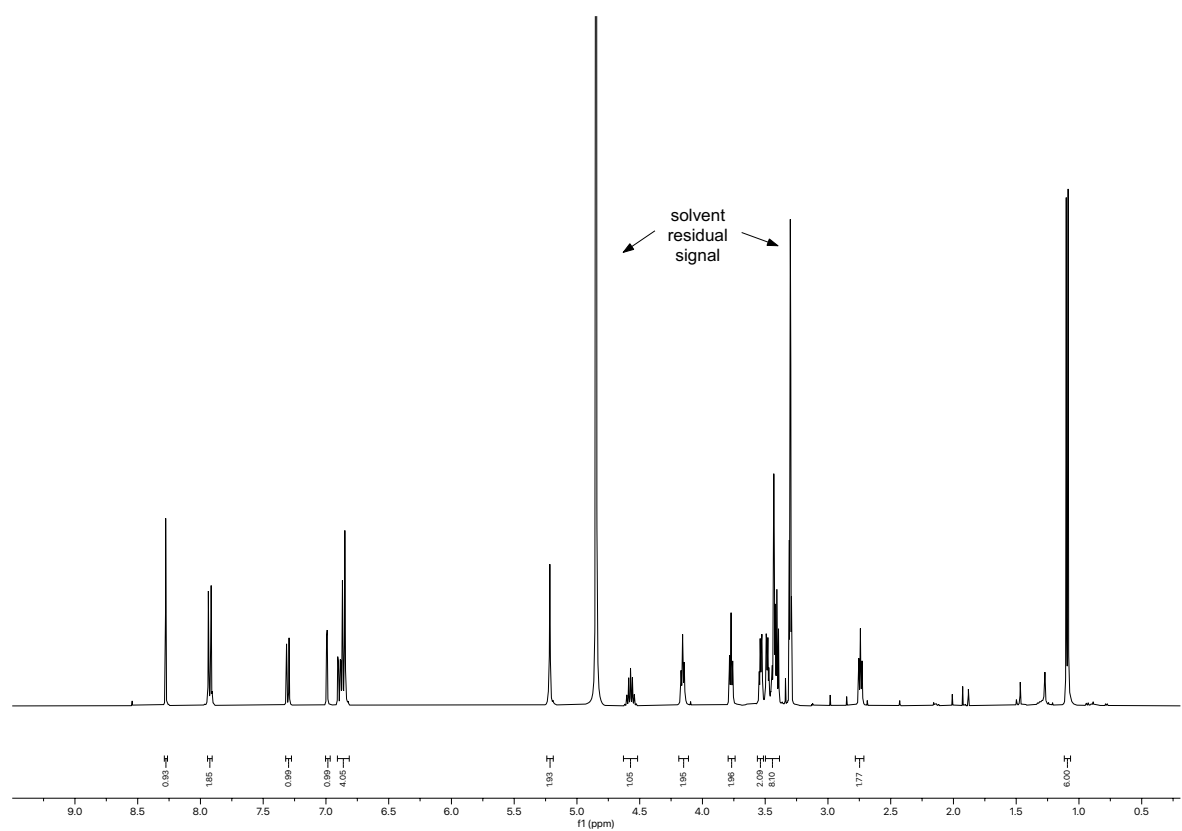
Figure 4.011. ^{1}H NMR spectrum (400 MHz, CD$_3$OD) of compound **4.043**.
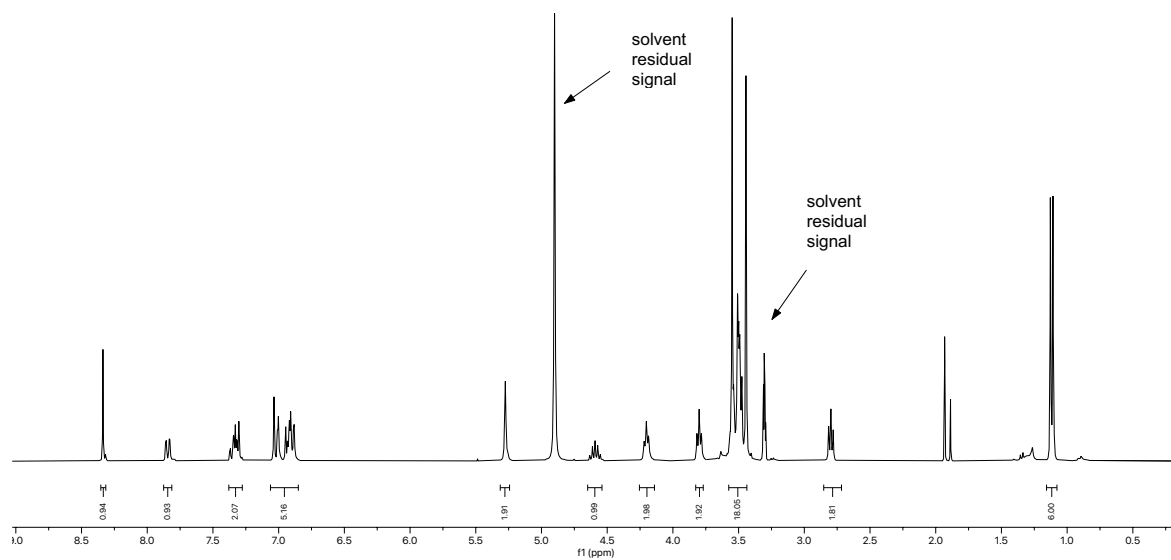
Figure 4.012. ^{1}H NMR spectrum (300 MHz, CD$_3$OD) of compound **4.044**.
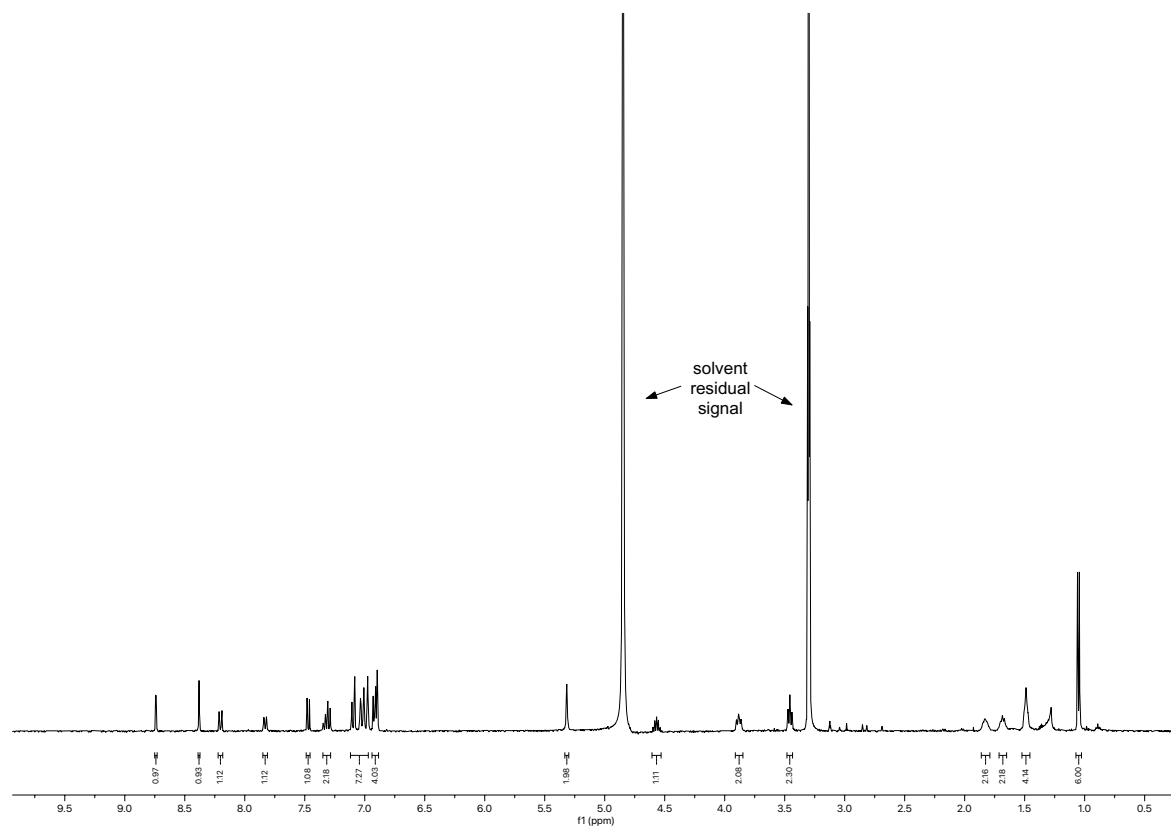
Figure 4.013. ^{1}H NMR spectrum (400 MHz, CD$_3$OD) of compound **4.045**.
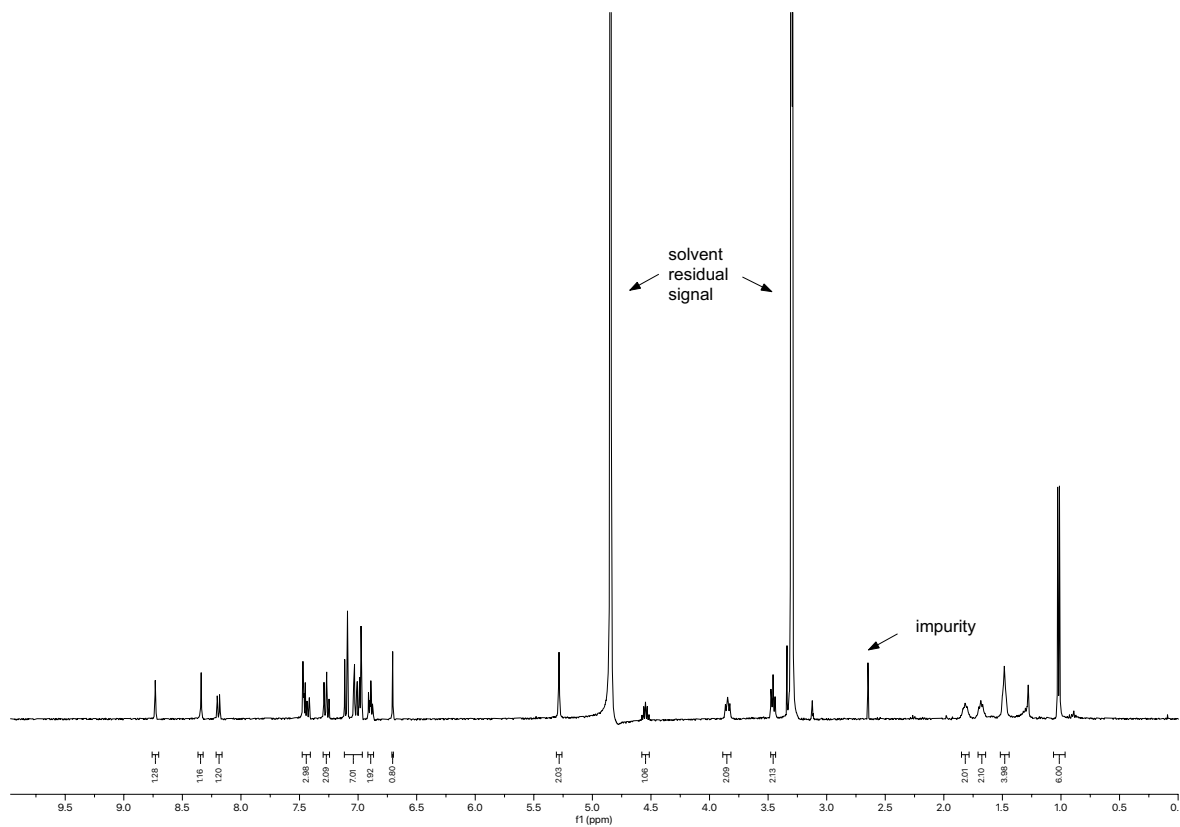
Figure 4.014. ^{1}H NMR spectrum (400 MHz, CD$_3$OD) of compound **4.046**.
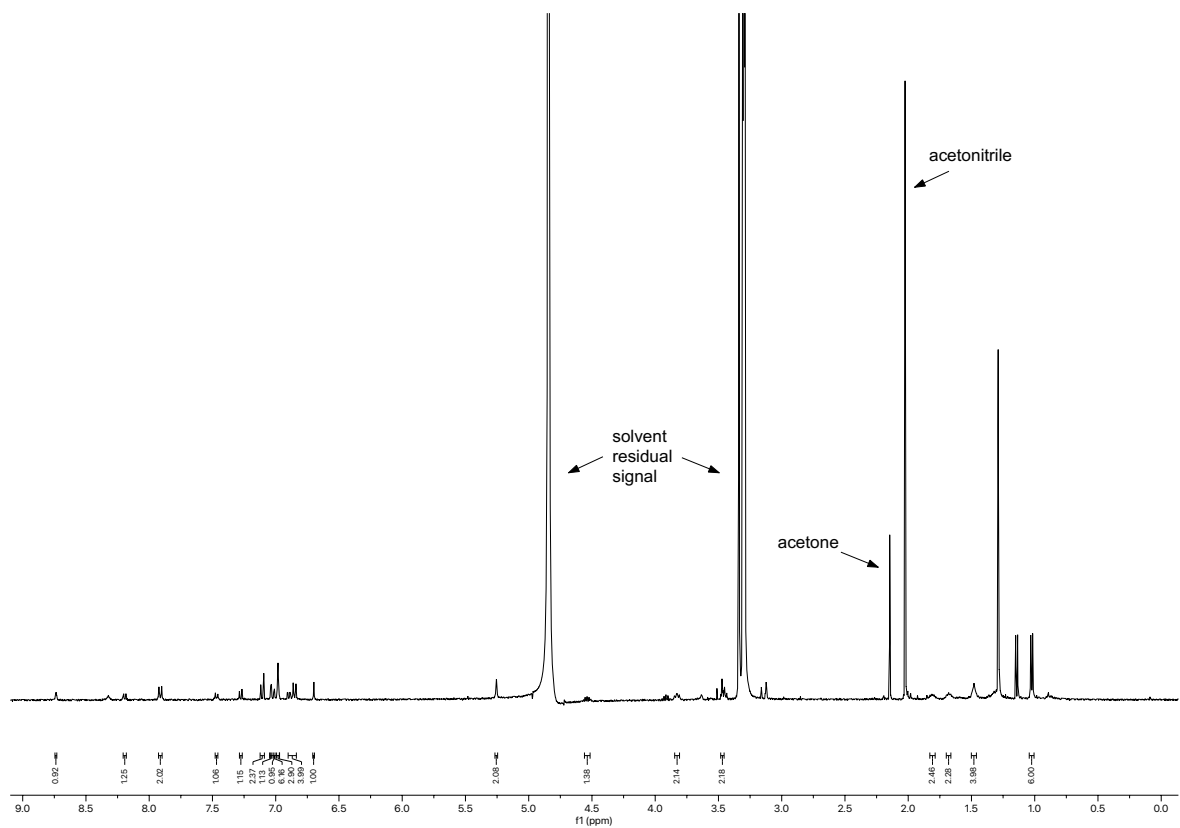
Figure 4.015. ^{1}H NMR spectrum (400 MHz, CD$_3$OD) of compound **4.047**.

644
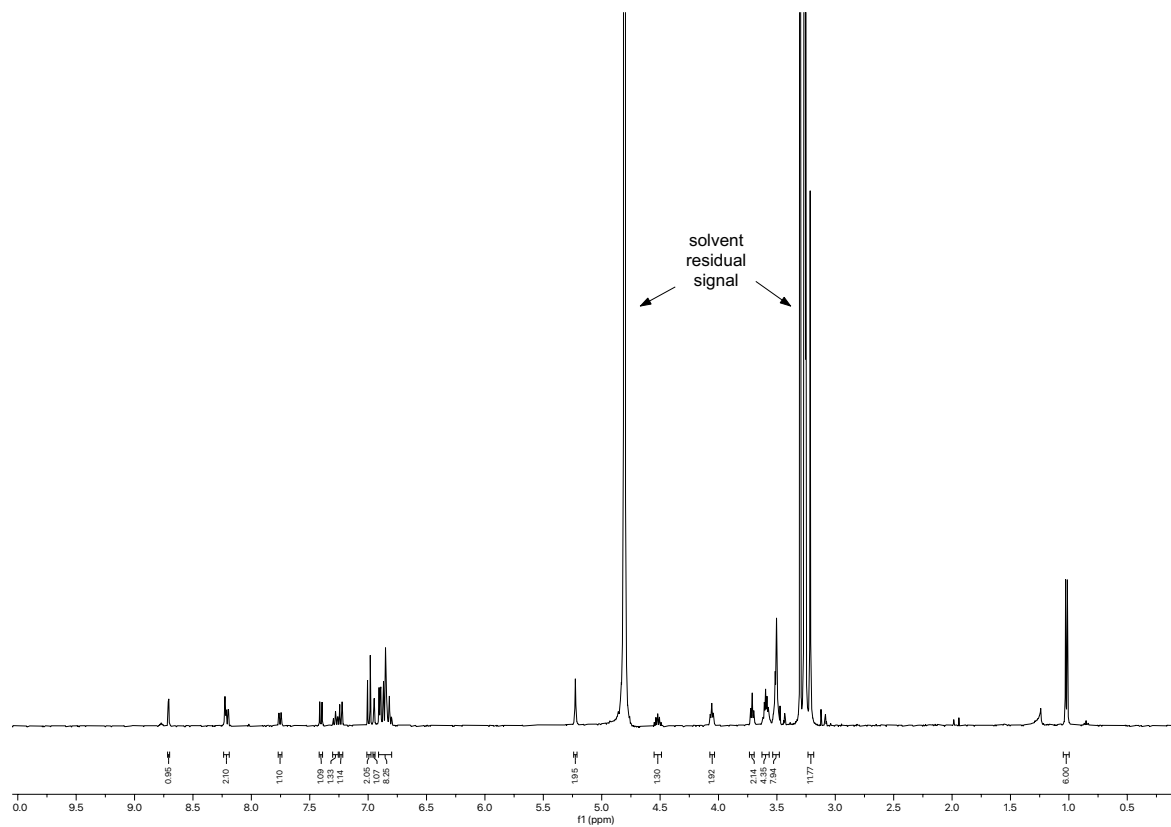
Figure 4.016. ^{1}H NMR spectrum (400 MHz, CD$_3$OD) of compound **4.048**.
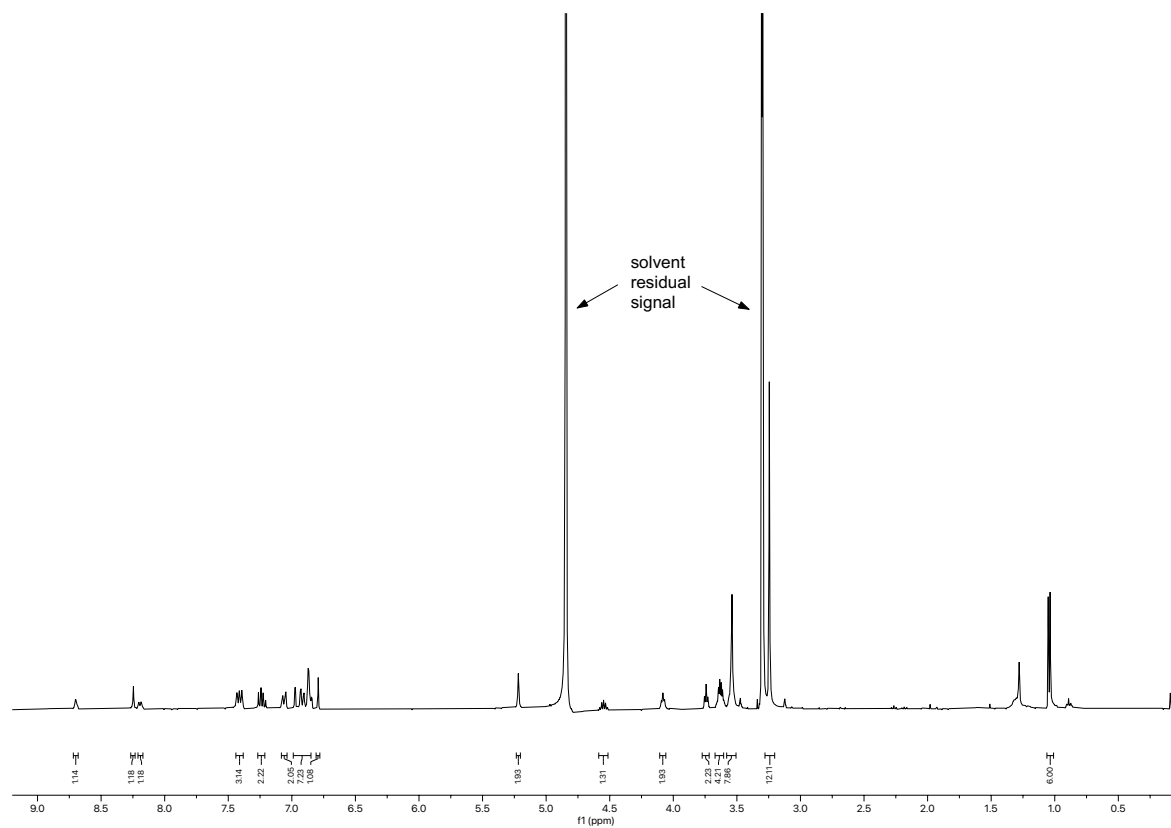
Figure 4.017. ^{1}H NMR spectrum (400 MHz, CD$_3$OD) of compound **4.049**.
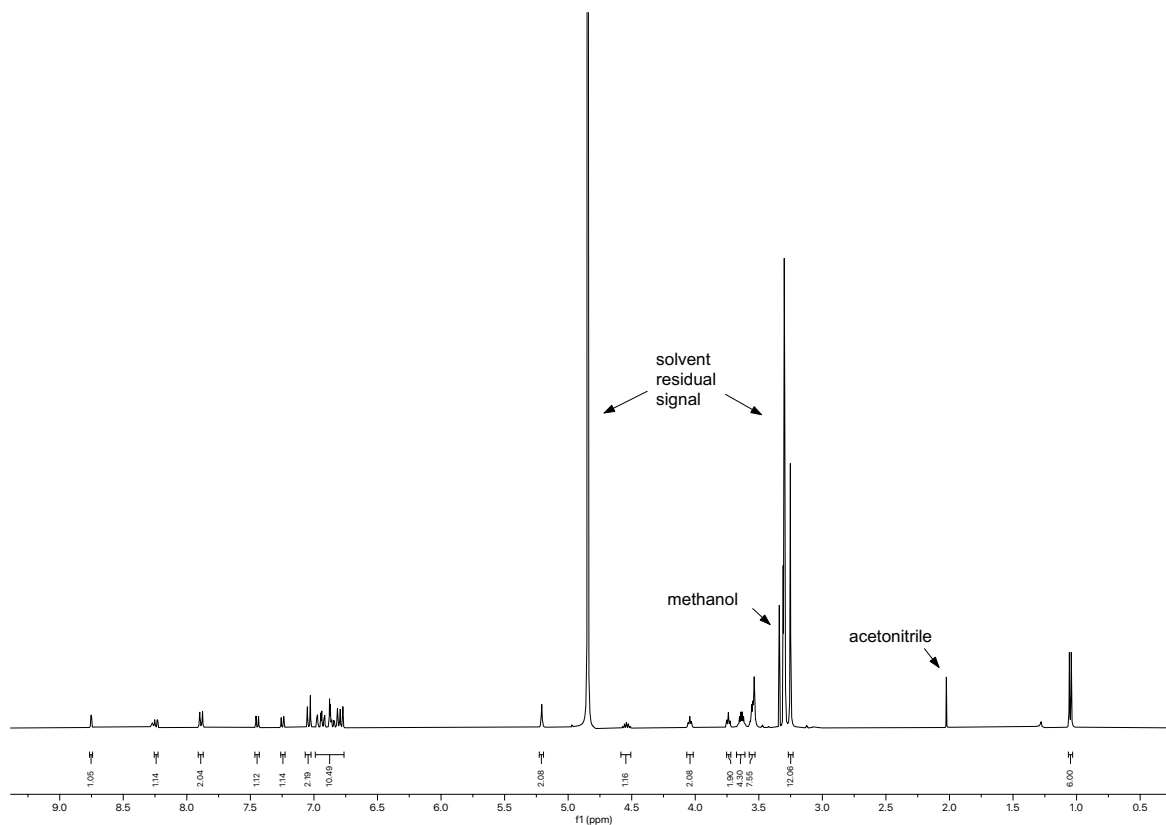
Figure 4.018. [^1]H NMR spectrum (400 MHz, CD$_3$OD) of compound **4.050**.
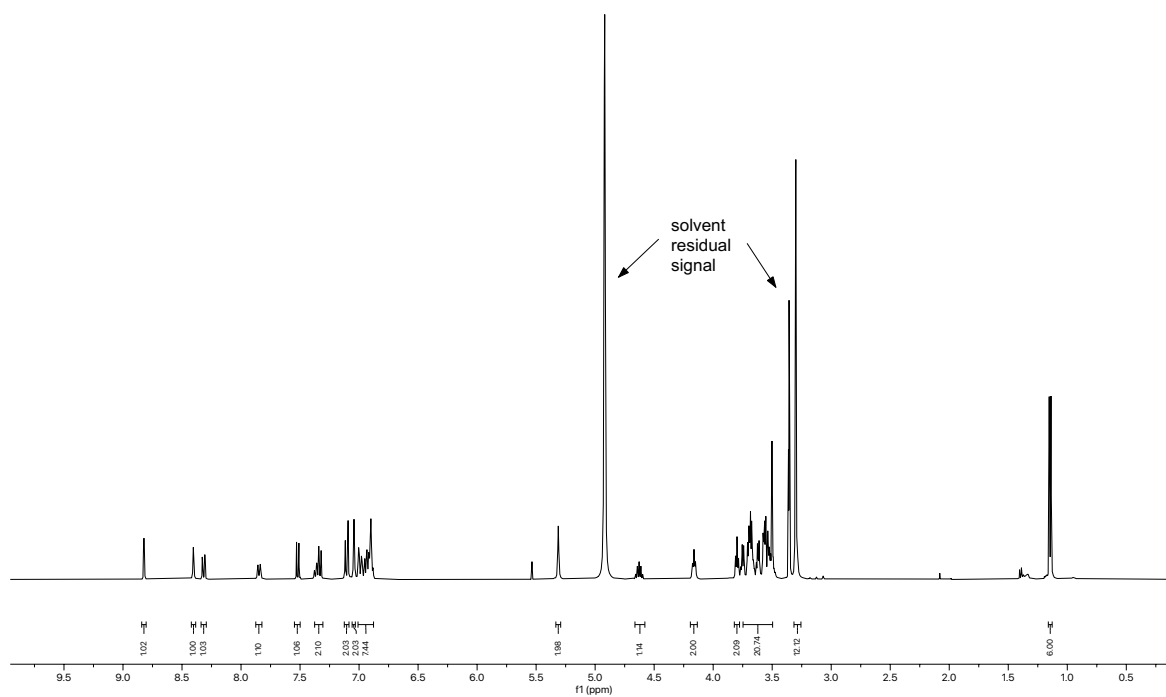
Figure 4.019. [^1]H NMR spectrum (400 MHz, CD$_3$OD) of compound **4.051**.

646
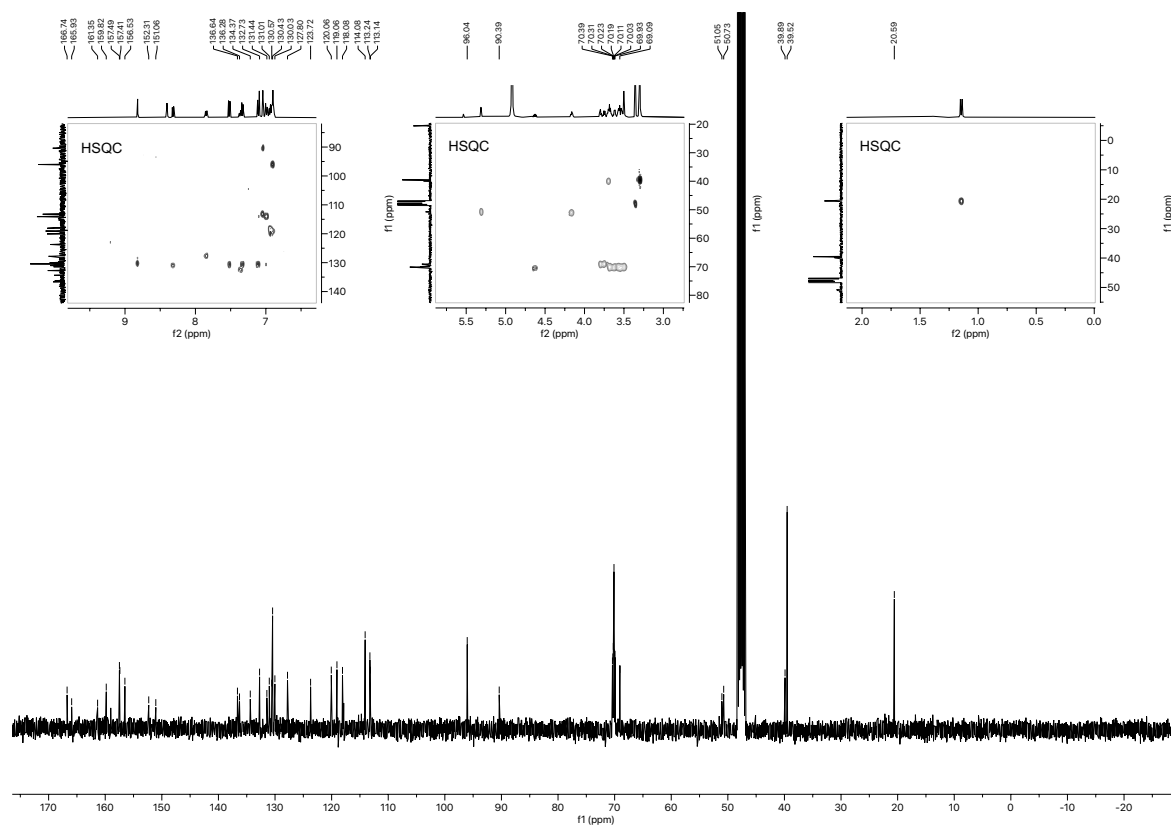
Figure 4.020. ^{13}C NMR spectrum (101 MHz, CD$_3$OD) of compound **4.051**.

4.6.2 RP-HPLC Purity Control of Compounds 4.045-4.055
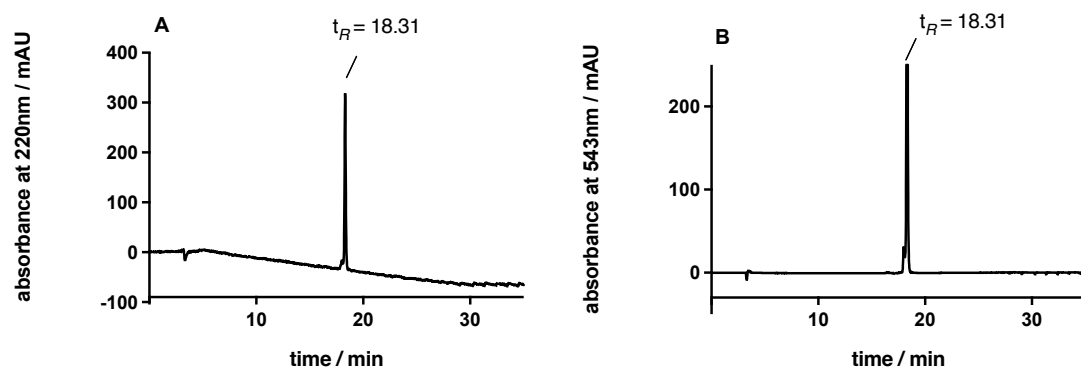
Figure 4.021. RP-HPLC analysis (purity control) of compound **4.045** (A) (97%, 220 nm) and compound **4.045** (B) (97%, 543 nm).
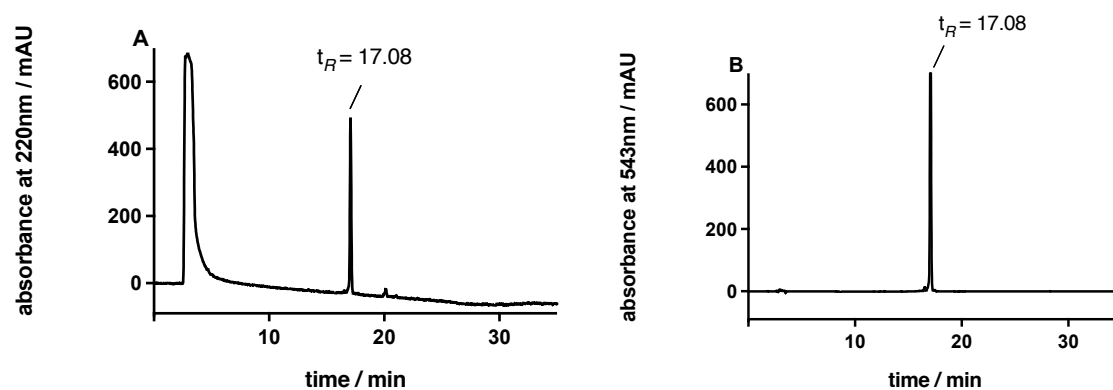
Figure 4.022. RP-HPLC analysis (purity control) of compound **4.046** (A) (97%, 220 nm) and compound **4.046** (B) (97%, 543 nm).
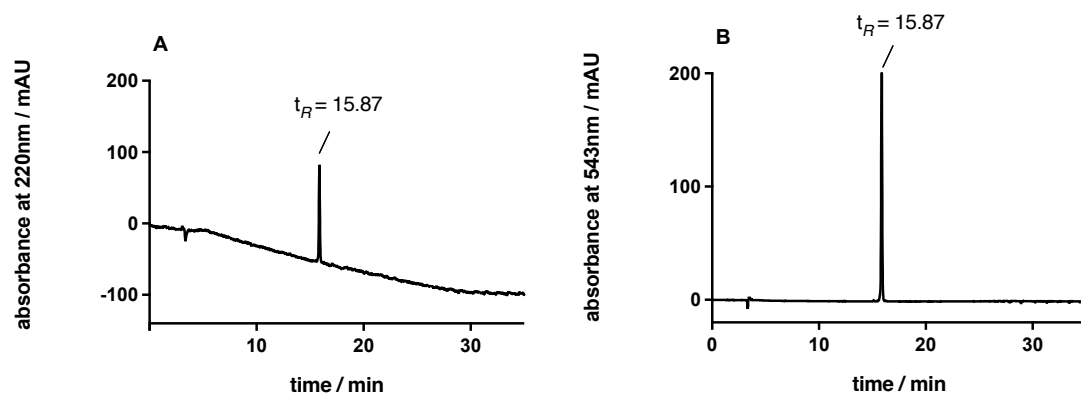
Figure 4.023. RP-HPLC analysis (purity control) of compound **4.047** (A) (> 99%, 220 nm) and compound **4.047** (B) (> 99%, 543 nm).
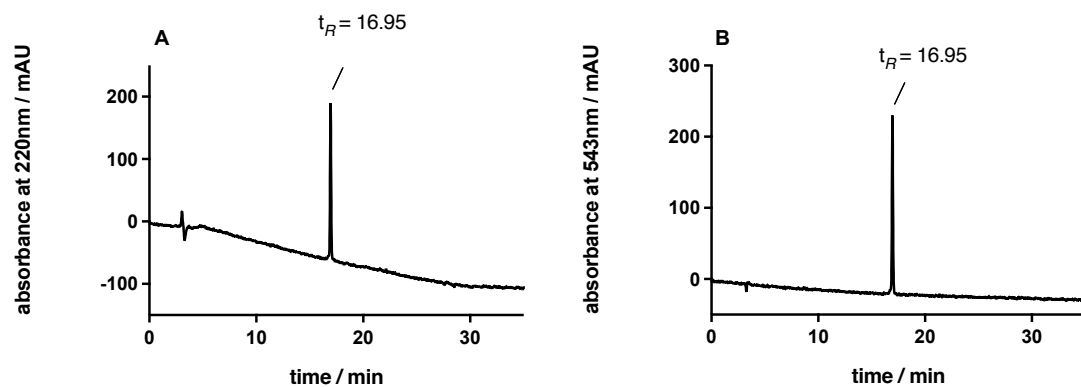
Figure 4.024. RP-HPLC analysis (purity control) of compound **4.048** (A) (> 99%, 220 nm) and compound **4.048** (B) (> 99%, 543 nm).
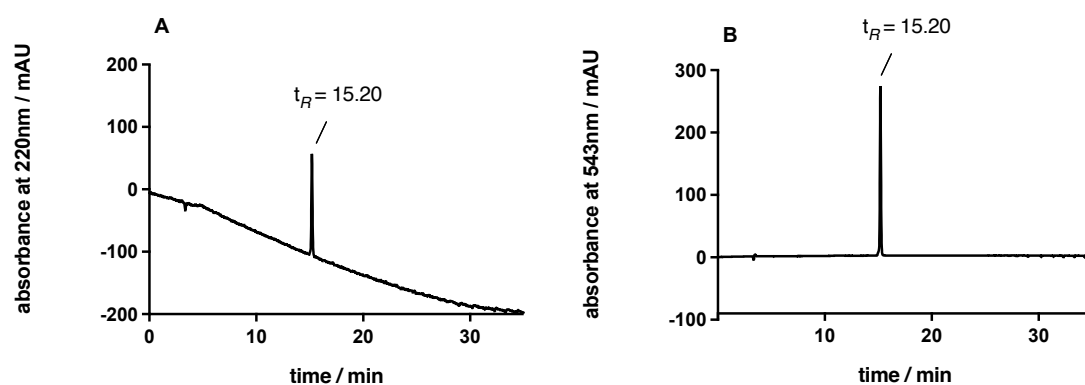
Figure 4.025. RP-HPLC analysis (purity control) of compound **4.049** (A) (> 99%, 220 nm) and compound **4.049** (B) (> 99%, 543 nm).
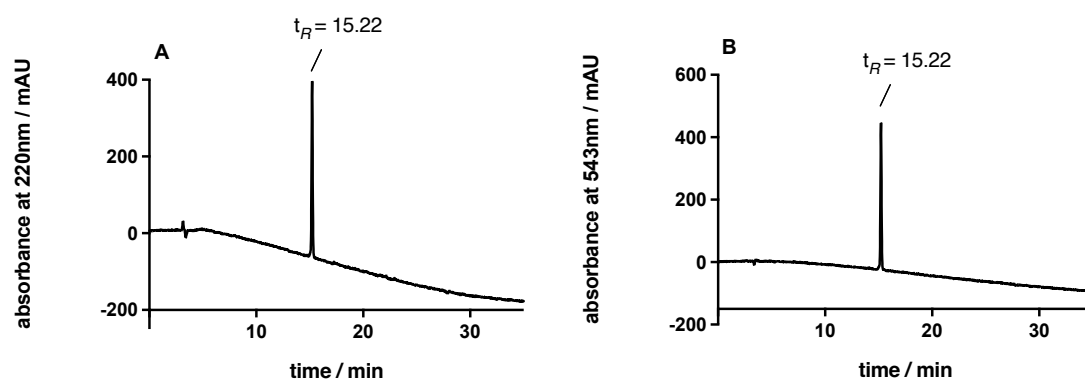
Figure 4.026. RP-HPLC analysis (purity control) of compound **4.050** (A) (> 99%, 220 nm) and compound **4.050** (B) (> 99%, 543 nm).
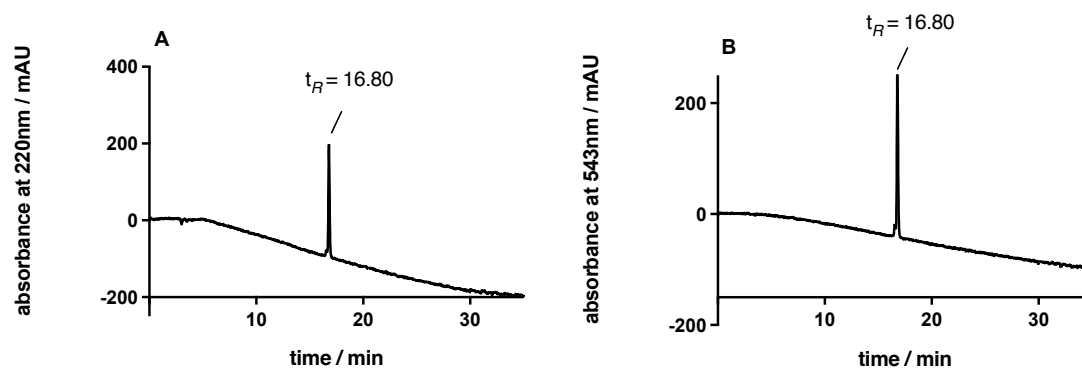
Figure 4.027. RP-HPLC analysis (purity control) of compound **4.051** (A) (98%, 220 nm) and compound **4.051** (B) (98%, 543 nm).
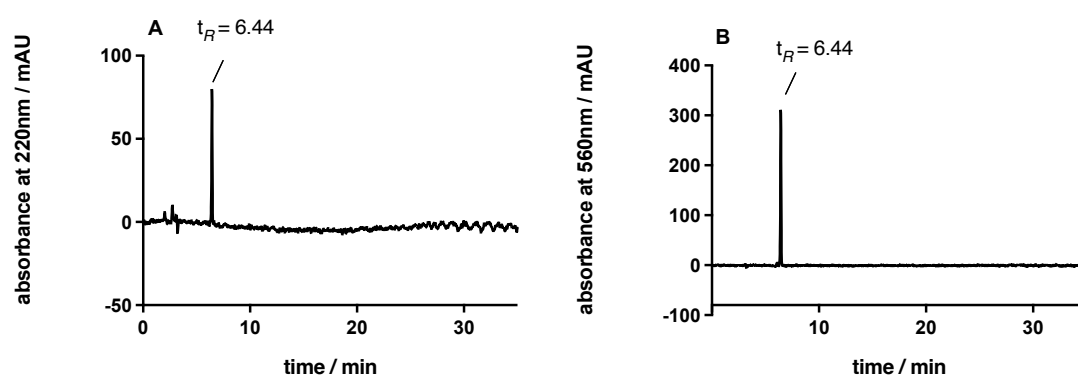
Figure 4.028. RP-HPLC analysis (purity control) of compound **4.052** (A) (> 99%, 220 nm) and compound **4.052** (B) (> 99%, 560 nm).
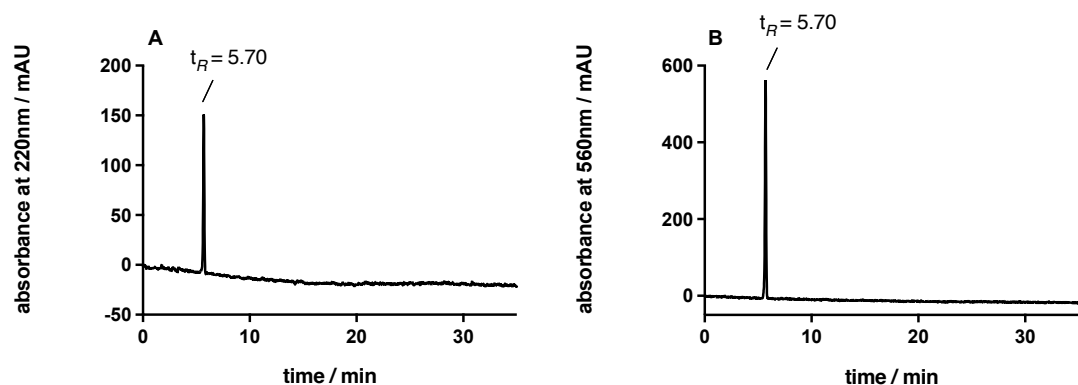
Figure 4.029. RP-HPLC analysis (purity control) of compound **4.053** (A) (> 99%, 220 nm) and compound **4.053** (B) (> 99%, 560 nm).
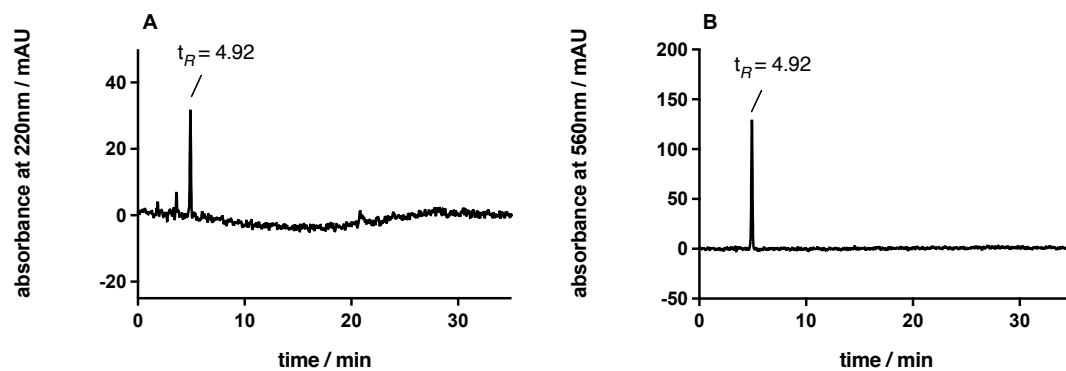
Figure 4.030. RP-HPLC analysis (purity control) of compound **4.054** (A) (> 99%, 220 nm) and compound **4.054** (B) (> 99%, 560 nm).
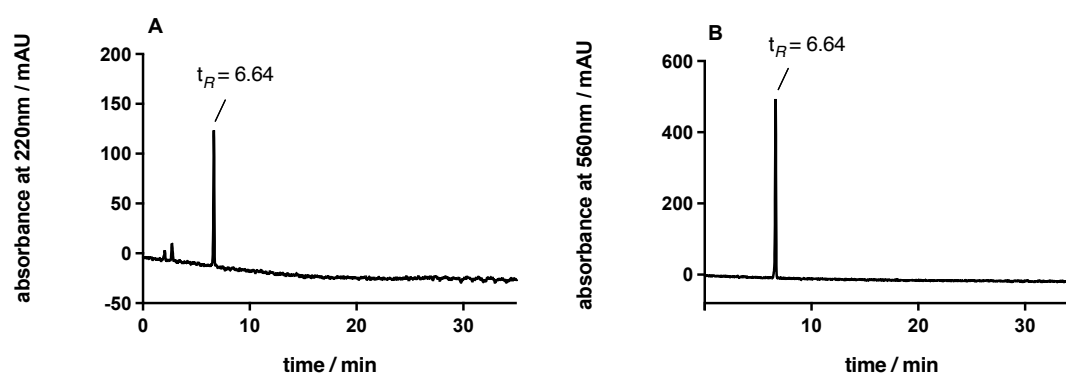
Figure 4.031. RP-HPLC analysis (purity control) of compound **4.055** (A) (> 99%, 220 nm) and compound **4.055** (B) (> 99%, 560 nm).

4.6.3 RP-HPLC Stability Control of Compound 4.046 and 4.048
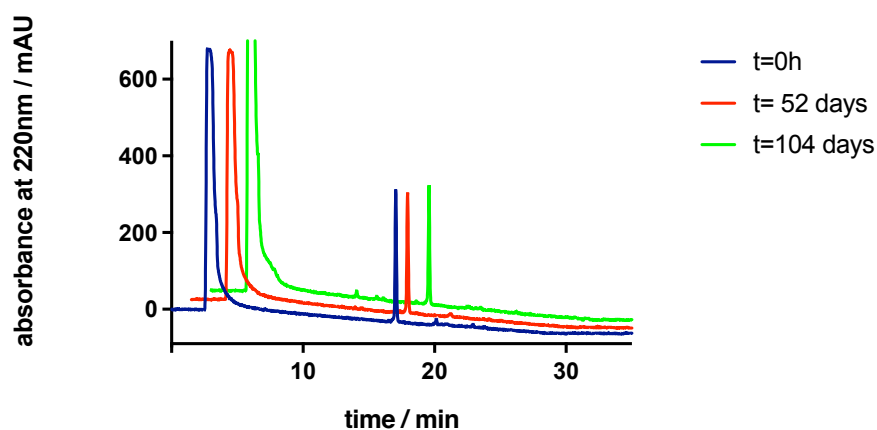
Figure 4.032. RP-HPLC analysis (stability control, 220 nm) of **4.046** at rt for 104 days in DMSO.
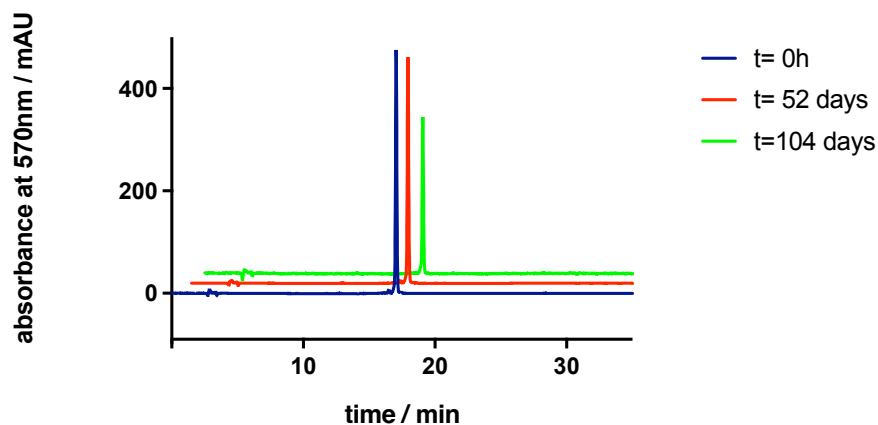
Figure 4.033. RP-HPLC analysis (stability control, 540 nm) of **4.046** at rt for 104 days in DMSO.
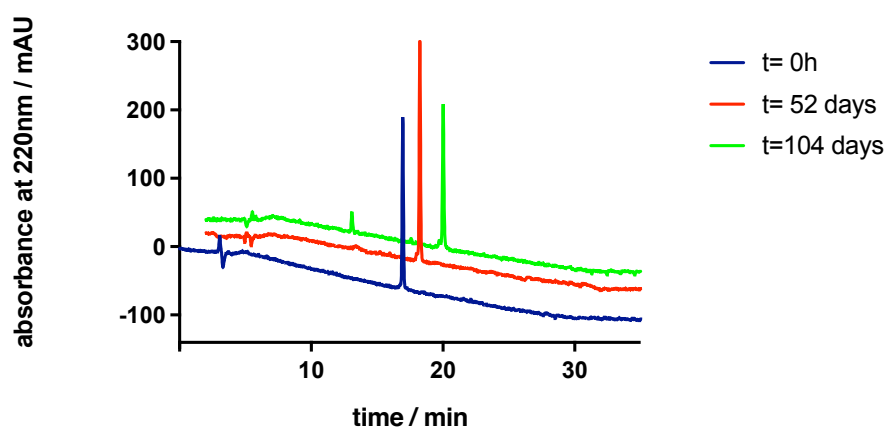
Figure 4.034. RP-HPLC analysis (stability control, 220 nm) of **4.048** at rt for 104 days in aqueous solution.
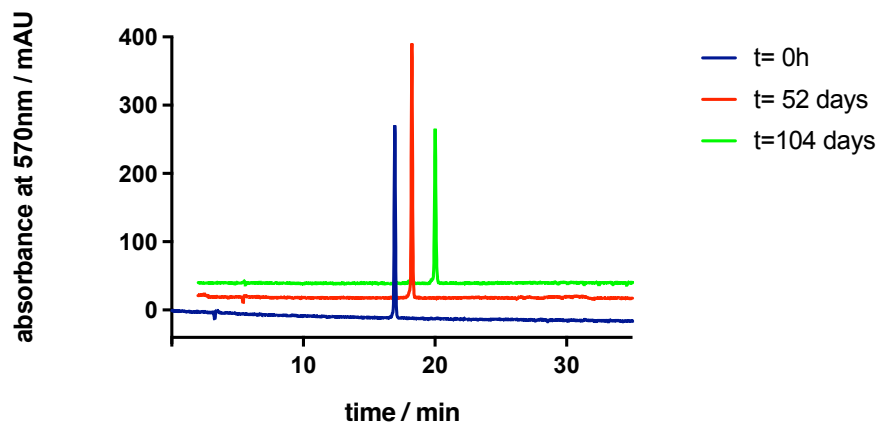
Figure 4.035. RP-HPLC analysis (stability control, 540 nm) of **4.048** at rt for 104 days in aqueous solution.

4.6.4 Computational Chemistry

Table 4.02. Model statistics. Model representative colored in gray were used in the docking calculations.

Template	#Cluster	Representative model	#Models	DOPE	MODELLER objective function	Normalized z-score	RMSD
7ew1							
	0	B99990353.pdb	221	-30928.842	2148.2905	0.987	1.15
	1	B99990068.pdb	41	-30854.664	1603.4868	1.006	1.17
	2	B99990011.pdb	34	-31040.699	1660.6511	0.958	1.21
	3	B99990373.pdb	31	-30775.529	1785.2535	1.026	1.13
	4	B99990157.pdb	22	-30620.879	1741.6594	1.066	1.2
7yxa							
	0	B99990364.pdb	155	-35546.75	1798.2273	0.287	1.95
	1	B99990146.pdb	65	-35827.797	1795.4095	0.219	1.39
	2	B99990473.pdb	47	-35724.945	1794.1129	0.244	1.88
	3	B99990165.pdb	25	-35637.68	1760.5212	0.265	1.79
	4	B99990427.pdb	25	-35887.918	1844.0547	0.205	1.97
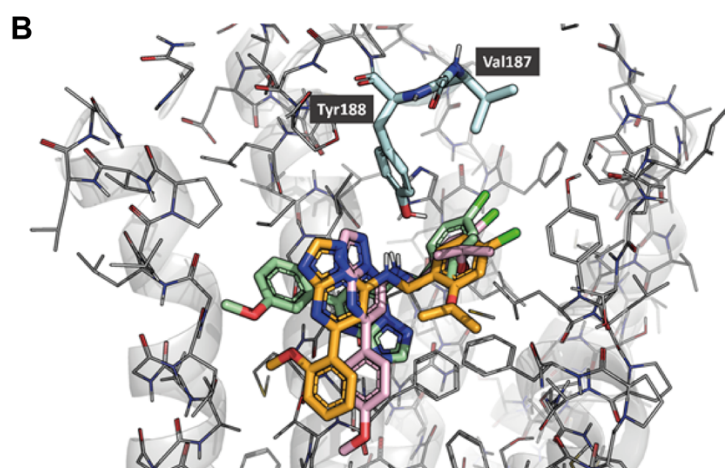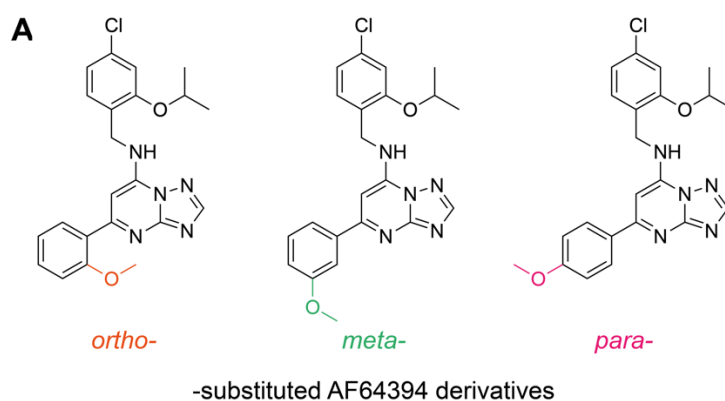
Figure 4.036. Docking poses of AF64394 derivatives to the active-state model of GPR3. **A)** Chemical 2D structures of docked AF64394 derivatives with methoxy substituents in *ortho*-, *meta*- or *para*-position of the phenyl ring. **B)** Side view of the docking poses of the three molecules when docked to the 7ew1-based GPR3 model. Orange: ortho- , green: meta- and pink: para-substituted AF64394 derivative.

4.6.5 Fluorescence Properties
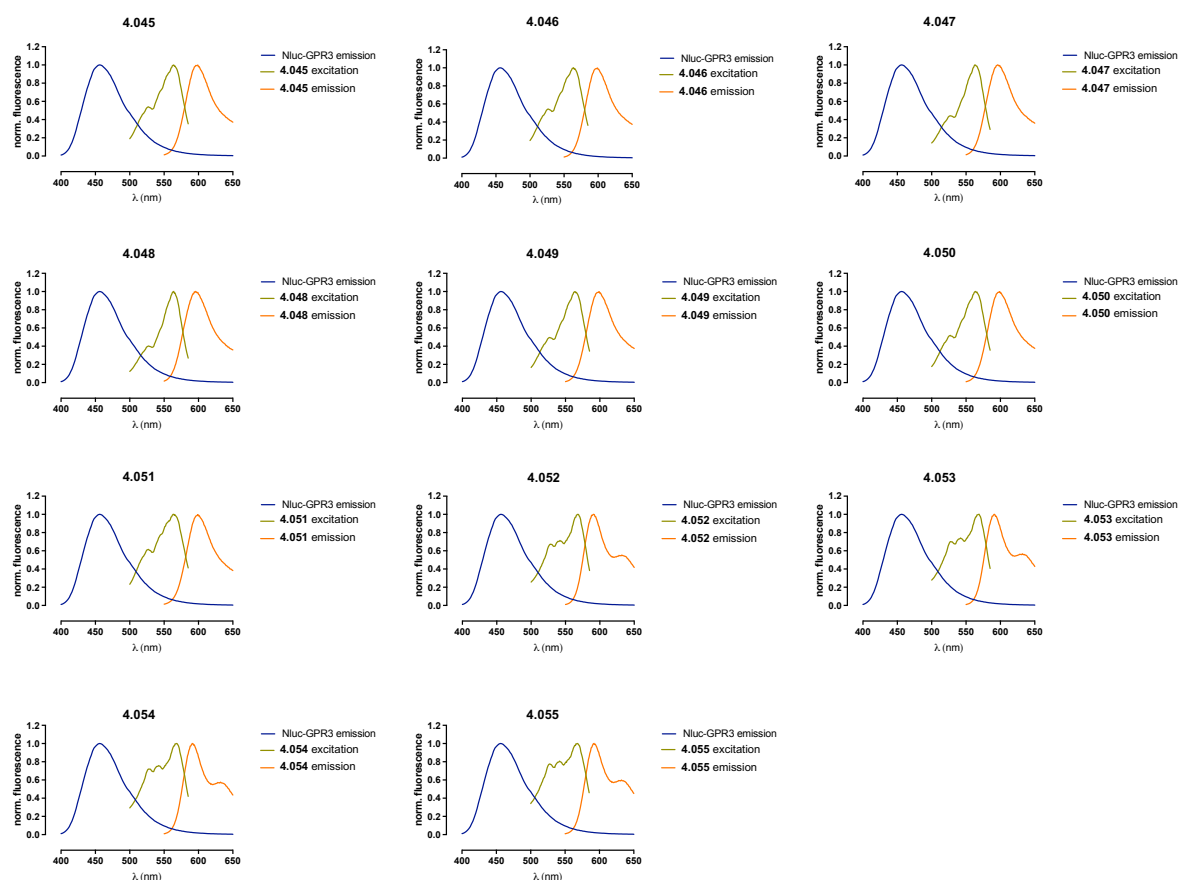
Figure 4.037. Corrected excitation and emission spectra of **4.045-4.055** overlayed with the bioluminescence emission spectrum of NLuc-GPR3 ($\lambda_{em,max}$ = 456 nm). Spectra of **4.045-4.055** were recorded in DMSO.

Table 4.03. Excitation/emission maxima of **4.045-4.055** determined in DMSO.

Comp.	$\lambda_{exc,max}/\lambda_{em,max}$ (nm)	Comp.	$\lambda_{exc,max}/\lambda_{em,max}$ (nm)
4.045	564 / 599	**4.051**	564 / 599
4.046	564 / 599	**4.052**	568 / 591
4.047	563 / 596	**4.053**	569 / 591
4.048	564 / 596	**4.054**	568 / 591
4.049	564 / 599	**4.055**	568 / 592
4.050	564 / 599		

Chapter 5

Abbreviations

5   Abbreviations

5-HT$_{1A}$	serotonin 1A receptor
5-TAMRA	5-carboxy-tetramethylrhodamin
α$_{1A}$	adrenoreceptor α1A
α$_{2A}$	adrenoreceptor α2A
β$_1$	adrenoceptor β1
β$_2$	adrenoceptor β2
βarr2 or ARRB2	β-arrestin2 gene/protein
δ	chemical shift in ppm
μOR	μ opioid receptor
Aβ	amyloid β
AADC	aromatic L-amino acid decarboxylase
AC	adenylate cyclase
ACSF	artificial cerebrospinal fluid
AD	Alzheimer's disease
ADHD	attention deficit hyperactivity disorder
Apaf-1	Apoptotic Protease-activating Factor 1
APCI	atmospheric pressure chemical ionization
APP	amyloid precursor protein
Ar	argon
AT1R	angiotensin II receptor type 1
ATP	adenosine triphosphate
AU	absorption units
BB	building block
BBB	blood-brain barrier
BH	bases
Boc	*tert*-butoxycarbonyl
Boc$_2$O	di-*tert*-butyl dicarbonate
BRET	bioluminescence resonance energy transfer
BSA	bovine serum albumin
c	molar concentration
CaM	calmodulin
CaMK	Ca^{2+}/calmodulin-dependent protein kinase
cAMP	cyclic adenosine monophosphate
CARD	caspase recruitment domain
Casp	caspase
cat.	catalyst
CBD	cannabidiol
CDCl$_3$	deuterated chloroform;
CDI	1,1'-carbonyldiimidazole
cf.	confer/conferatur
CHAPS	3-[(3-cholamidopropyl)dimethylammonio]-1-propanesulfonate
CH$_2$Cl$_2$	dichloromethane
CNS	central nervous system
Comp.	compound
CREB	cAMP-response element-binding protein
CRE-Luc	cAMP-response element driven transcriptional luciferase reporter
CRG	covalent reactive group
DAD	diode array detector
DAG	diglyceride or diacylglycerol
DAO	diamine oxidase
DED	death effector domain
DIC	*N,N'*-diisopropylcarbodiimide
DIPEA	*N,N*-diisopropylethylamine

DISC	death-inducing signaling complex
DIV	days in vitro
DMAP	4-dimethylamino pyridine
DMEM	Dulbecco's Modified Eagle's Medium
DMF	dimethylformamide
DMSO	dimethyl sulfoxide
DMSO-d$_6$	deuterated DMSO
DPI	diphenyleneiodonium chloride
D$_x$R	dopamine receptor subtype x
DTT	dithiothreitol
EBSS	Earle's Balanced Salt Solution
ECL	enterochromaffin-like
EDCI	1-ethyl-3-(3-dimethylaminopropyl)carbodiimid
e.g.	exempli gratia
EI	electron ionization
EL	extracellular loop
Eluc	Emerald luciferase
ElucC	C-terminal Eluc fragment
ElucN	N-terminal Eluc fragment
E$_{max}$	maximal inducible receptor response referenced to a standard compound
ENS	enteric nervous system
eq.	equivalent
ER	endoplasmic reticulum
ESI	electrospray ionization
Et$_2$O	diethyl ether
EtOAc	ethyl acetate
EtOH	ethanol
FAAH	fatty acid amide hydrolase
FADD	Fas-associated death domain
FBS	fetal bovine serum
FDA	US Food and Drug Administration
FTD	Frontotemporal dementia
FTDP-17	Frontotemporal dementia with parkinsonism-17
g	gram(s) or number of times the gravitational force
GABA	γ-aminobutyric acid
GDP	guanosine diphosphate
GI	gastrointestinal
gp	guinea pig
GPCRs	G-protein-coupled receptors
GRKs	G protein-coupled receptor kinases
GTP	guanosine triphosphate
GTPγS	guanosine 5′-O-[γ-thio]phosphate)
h	human
HA	proton donor
HATU	1-[Bis(dimethylamin)methylen]-1H-1,2,3-triazol[4,5-b]pyridinium-3-oxid-hexafluorophosphat
HBA	H-bond acceptors
HBD	H-bond donors
HBSS	Hank's balanced salt solution
HD	Huntington disease
HDC	L-histidine decarboxylase
HEK293T	human embryonic kidney 293T cells
HEPES	4-(2-hydroxyethyl)-1-piperazineethanesulfonic acid
Het	heterocycle
HFIP	hexafluoroisopropanol

HNMT	histamine *N*-methyltransferase
HOBt	1-hydroxybenzotriazole
H_1R	histamine H_1 receptor
H_2R	histamine H_2 receptor
H_3R	histamine H_3 receptor
H_4R	histamine H_4 receptor
HRMS	high-resolution mass spectrometry
HRP	horseradish peroxidase
HTS	high-throughput screening
IL	intracellular loop
IP	immunoprecipitation
IP_3	inositol trisphosphate
IPTG	isopropyl-*β*-D- thiogalactopyranoside
IUPHAR	The International Union of Basic and Clinical Pharmacology
J	coupling constant (NMR)
k	retention (or capacity) factor (HPLC)
K_a	acid dissociation constant
K_b	dissociation constant obtained from a functional assay
K_d	dissociation constant obtained from a saturation binding experiment
KHMDS	potassium bis(trimethylsilyl)amide
K_i	dissociation constant obtained from a competition binding experiment
LB	Luria Broth
LBD	Lewy body dementia
LC	liquid chromatography
$LiAlH_4$	lithium aluminum hydride
MAP	Mitogen-activated protein
MAPK	Mitogen-activated protein (MAP) kinase
MAP2K	Mitogen-activated protein (MAP) kinase kinase
MAP3K	Mitogen-activated Protein (MAP) kinase kinase kinase
MCI	mild cognitive impairment
MeCN	acetonitrile
MeOH	methanol
mEPSCs	miniature excitatory synaptic currents
MES	2-(*N*-morpholino)ethanesulfonic acid
mG or mini-G	engineered minimal G protein
mGs	engineered guanosine triphosphate hydrolase domain of $G_{αs}$ subunit (long splice variant)
MOE	molecular operating environment
MOMP	mitochondrial outer membrane permeabilization
MPTP	1-methyl-4-phenyl-1,2,3,6-tetrahydropyridin
MS	mass spectrometry
MW	molecular weight
M_xR	muscarinic receptor subtype x
m/z	mass-to-charge ratio
NEt_3	triethylamine
NFTs	neurofibrillary tangles
NHS	*N*-hydroxysuccinimide
Nluc	NanoLuc luciferase
NlucC	C-terminal Nluc fragment
NlucN	N-terminal Nluc fragment
NMP	*N*-methyl-2-pyrrolidone
NMR	nuclear magnetic resonance
Nuc	nucleophiles
oGPCR	orphan G protein-coupled receptor

PD	Parkinson's disease
Pd/C	palladium-on-carbon
PE	petroleum ether
pEC_{50}	negative logarithm of the half-maximum activity concentration
PEG	polyethylene glycol
PLA_2	phospholipase A_2
PLC	phospholipase C
PLP	pyridoxal phosphate
pK_a	negative logarithm of the K_a in M
PKA	protein kinase A
pK_b	negative logarithm of the K_b in M
PKC	protein kinase C
PKD	protein kinase D
pK_i	negative logarithm of the K_i in M
ppm	parts per million
PTMs	post-translational modifications
Q-TOF	quadrupole time of flight
r	rats
R	residue
RGCs	retinal ganglion cells
RGS	regulators of G protein signaling
Rho-GEF	Rho guanine nucleotide exchange factors
Rho-GTP	Rho-family GTPases
Ro5	Lipinski's rule of five
ROS	reactive oxygen species
RP-HPLC	reversed-phase HPLC
S1P	sphingosine-1-phosphate
$S1P_5$	sphingosine-1-phosphate receptor 5
SAR	structure−activity relationship
SD	standard deviation
SEM	standard error of the mean
SFC	supercritical fluid chromatography
SPPS	solid-phase peptide synthesis
t_0	dead time
tBid	truncated Bid
TFA	trifluoroacetic acid
TLC	thin layer chromatography
TM	transmembrane
TPSA	topological polar surface area
t_R	retention time
Trt	trityl
UHD	ultrahigh definition
WB	western blot
XO	xanthine oxidase

Chapter 6

References

6   References

(1)   Alzheimer, A. Über Eine Eigenartige Erkrankung Der Hirnrinde. *Allg. Z. Psychiat. Psych.-Gerichtl. Med.* **1907**, *64*, 146-148.

(2)   Vaz, M.; Silvestre, S. Alzheimer's Disease: Recent Treatment Strategies. *European Journal of Pharmacology* **2020**, *887*, 173554.

(3)   *World Health Organization. Dementia.* https://www.who.int/news-room/fact-sheets/detail/dementia (accessed 2023-01-09).

(4)   Evans, D. A.; Funkenstein, H. H.; Albert, M. S.; Scherr, P. A.; Cook, N. R.; Chown, M. J.; Hebert, L. E.; Hennekens, C. H.; Taylor, J. O. Prevalence of Alzheimer's Disease in a Community Population of Older Persons. Higher than Previously Reported. *JAMA* **1989**, *262* (18), 2551-2556.

(5)   Smith, M. A. Alzheimer Disease. *International review of neurobiology* **1998**, *42*, 1-54.

(6)   Yiannopoulou, K. G.; Papageorgiou, S. G. Current and Future Treatments for Alzheimer's Disease. *Therapeutic advances in neurological disorders* **2013**, *6* (1), 19-33.

(7)   Fish, P. V.; Steadman, D.; Bayle, E. D.; Whiting, P. New Approaches for the Treatment of Alzheimer's Disease. *Bioorganic & Medicinal Chemistry Letters* **2019**, *29* (2), 125-133.

(8)   Hardy, J. A.; Higgins, G. A. Alzheimer's Disease: The Amyloid Cascade Hypothesis. *Science* **1992**, *256* (5054), 184-185.

(9)   Golde, T. E. The Aβ Hypothesis: Leading Us to Rationally-designed Therapeutic Strategies for the Treatment or Prevention of Alzheimer Disease. *Brain pathology* **2005**, *15* (1), 84-87.

(10)   Padda, I. S.; Parmar, M. Aducanumab. In *StatPearls [Internet]*; StatPearls Publishing, **2021**.

(11)   Mahase, E. Three FDA Advisory Panel Members Resign over Approval of Alzheimer's Drug. *BMJ* **2021**, n1503.

(12)   *FDA approves Alzheimer's drug lecanemab amid safety concerns.* https://www.nature.com/articles/d41586-023-00030-3 (accessed 2023-01-10).

(13)   Thambisetty, M.; Howard, R. Lecanemab Trial in AD Brings Hope but Requires Greater Clarity. *Nature Reviews Neurology* **2023**, 1-2.

(14)   Castellani, R. J.; Rolston, R. K.; Smith, M. A. Alzheimer Disease. *Disease-a-month: DM* **2010**, *56* (9), 484.

(15)   El Kadmiri, N.; Said, N.; Slassi, I.; El Moutawakil, B.; Nadifi, S. Biomarkers for Alzheimer Disease: Classical and Novel Candidates' Review. *Neuroscience* **2018**, *370*, 181-190.

(16)   Neurath, H. Evolution of Proteolytic Enzymes. *Science* **1984**, *224* (4647), 350-357.

(17)   Neurath, H.; Walsh, K. A. Role of Proteolytic Enzymes in Biological Regulation (a Review). *Proc. Natl. Acad. Sci. U.S.A.* **1976**, *73* (11), 3825-3832.

(18)   Neurath, H.; Walsh, K. A.; Winter, W. P. Evolution of Structure and Function of Proteases: Amino Acid Sequences of Proteolytic Enzymes Reflect Phylogenetic Relationships. *Science* **1967**, *158* (3809), 1638-1644.

(19)   Rawlings, N. D.; Barrett, A. J.; Bateman, A. Asparagine Peptide Lyases. *Journal of Biological Chemistry* **2011**, *286* (44), 38321-38328.

(20)   Seemüller, E.; Lupas, A.; Stock, D.; Lowe, J.; Huber, R.; Baumeister, W. Proteasome from Thermoplasma Acidophilum: A Threonine Proteas. *Science* **1995**, *268* (5210), 579-582.

(21)   Huber, E. M.; Heinemeyer, W.; Li, X.; Arendt, C. S.; Hochstrasser, M.; Groll, M. A Unified Mechanism for Proteolysis and Autocatalytic Activation in the 20S Proteasome. *Nature Communications* **2016**, *7* (1), 10900.

(22)   Fujinaga, M.; Cherney, M. M.; Oyama, H.; Oda, K.; James, M. N. G. The Molecular Structure and Catalytic Mechanism of a Novel Carboxyl Peptidase from Scytalidium Lignicolum. *Proceedings of the National Academy of Sciences,* **2004**, *101*, 3364-3369.

(23)   Van Opdenbosch, N.; Lamkanfi, M. Caspases in Cell Death, Inflammation, and Disease. *Immunity* **2019**, *50* (6), 1352-1364.

(24)   Kurokawa, M.; Kornbluth, S. Caspases and Kinases in a Death Grip. *Cell* **2009**, *138* (5), 838-854.

(25)   Bouchier-Hayes, L. The Role of Caspase-2 in Stress-Induced Apoptosis. *Journal of*

Cellular and Molecular Medicine **2010**, *14* (6a), 1212-1224.

(26)   Lamkanfi, M. Alice in Caspase Land. A Phylogenetic Analysis of Caspases from Worm to Man. *Cell death differ.* **2002**, *9* (4), 358-361.

(27)   Sakamaki, K.; Satou, Y. Caspases: Evolutionary Aspects of Their Functions in Vertebrates. *Journal of Fish Biology* **2009**, *74* (4), 727-753.

(28)   Ramirez, M. L. G.; Salvesen, G. S. A Primer on Caspase Mechanisms. *Seminars in Cell & Developmental Biology* **2018**, *82*, 79-85.

(29)   Shi, Y. Mechanisms of Caspase Activation and Inhibition during Apoptosis. *Molecular Cell* **2002**, *9* (3), 459-470.

(30)   Tang, Y.; Wells, J. A.; Arkin, M. R. Structural and Enzymatic Insights into Caspase-2 Protein Substrate Recognition and Catalysis*. *Journal of Biological Chemistry* **2011**, *286* (39), 34147-34154.

(31)   Li, J.; Yuan, J. Caspases in Apoptosis and Beyond. *Oncogene* **2008**, *27* (48), 6194-6206.

(32)   Fuentes-Prior, P.; Salvesen, G. S. The Protein Structures That Shape Caspase Activity, Specificity, Activation and Inhibition. *Biochemical Journal* **2004**, *384* (2), 201-232.

(33)   Poreba, M.; Groborz, K.; Navarro, M.; Snipas, S. J.; Drag, M.; Salvesen, G. S. Caspase Selective Reagents for Diagnosing Apoptotic Mechanisms. *Cell Death & Differentiation* **2019**, *26* (2), 229-244.

(34)   Boatright, K. M.; Salvesen, G. S. Mechanisms of Caspase Activation. *Current Opinion in Cell Biology* **2003**, *15* (6), 725-731.

(35)   Chipuk, J. E.; Green, D. R. How Do BCL-2 Proteins Induce Mitochondrial Outer Membrane Permeabilization? *Trends in Cell Biology* **2008**, *18* (4), 157-164.

(36)   Kumar, S. Caspase 2 in Apoptosis, the DNA Damage Response and Tumour Suppression: Enigma No More? *Nature Reviews Cancer* **2009**, *9* (12), 897-903.

(37)   Bouchier-Hayes, L.; Green, D. R. Caspase-2: The Orphan Caspase. *Cell Death Differ* **2012**, *19* (1), 51-57.

(38)   Cheung, H. H.; Lynn Kelly, N.; Liston, P.; Korneluk, R. G. Involvement of Caspase-2 and Caspase-9 in Endoplasmic Reticulum Stress-Induced Apoptosis: A Role for the IAPs. *Experimental Cell Research* **2006**, *312* (12), 2347-2357.

(39)   Manzl, C.; Peintner, L.; Krumschnabel, G.; Bock, F.; Labi, V.; Drach, M.; Newbold, A.; Johnstone, R.; Villunger, A. PIDDosome-Independent Tumor Suppression by Caspase-2. *Cell Death Differ* **2012**, *19* (10), 1722-1732.

(40)   Vakifahmetoglu-Norberg, H.; Zhivotovsky, B. The Unpredictable Caspase-2: What Can It Do? *Trends in Cell Biology* **2010**, *20* (3), 150-159.

(41)   Miles, M. A.; Kitevska-Ilioski, T.; Hawkins, C. J. Old and Novel Functions of Caspase-2. In *International Review of Cell and Molecular Biology*; Elsevier **2017**, 332, 155-212.

(42)   Vakifahmetoglu-Norberg, H.; Norberg, E.; Perdomo, A. B.; Olsson, M.; Ciccosanti, F.; Orrenius, S.; Fimia, G. M.; Piacentini, M.; Zhivotovsky, B. Caspase-2 Promotes Cytoskeleton Protein Degradation during Apoptotic Cell Death. *Cell Death & Disease* **2013**, *4* (12), e940-e940.

(43)   Julien, O.; Zhuang, M.; Wiita, A. P.; O'Donoghue, A. J.; Knudsen, G. M.; Craik, C. S.; Wells, J. A. Quantitative MS-Based Enzymology of Caspases Reveals Distinct Protein Substrate Specificities, Hierarchies, and Cellular Roles. *Proc. Natl. Acad. Sci. U.S.A.* **2016**, *113* (14).

(44)   Truscott, M.; Denault, J.-B.; Goulet, B.; Leduy, L.; Salvesen, G. S.; Nepveu, A. Carboxyl-Terminal Proteolytic Processing of CUX1 by a Caspase Enables Transcriptional Activation in Proliferating Cells. *Journal of Biological Chemistry* **2007**, *282* (41), 30216-30226.

(45)   Mancini, M.; Machamer, C. E.; Roy, S.; Nicholson, D. W.; Thornberry, N. A.; Casciola-Rosen, L. A.; Rosen, A. Caspase-2 Is Localized at the Golgi Complex and Cleaves Golgin-160 during Apoptosis. *The Journal of cell biology* **2000**, *149* (3), 603-612.

(46)   Guo, Y.; Srinivasula, S. M.; Druilhe, A.; Fernandes-Alnemri, T.; Alnemri, E. S. Caspase-2 Induces Apoptosis by Releasing Proapoptotic Proteins from Mitochondria. *Journal of Biological Chemistry* **2002**, *277* (16), 13430-13437.

(47)   Kitevska, T.; Roberts, S. J.; Pantaki-Eimany, D.; Boyd, S. E.; Scott, F. L.; Hawkins, C. J. Analysis of the Minimal Specificity of Caspase-2 and Identification of Ac-VDTTD-AFC as a

Caspase-2-Selective Peptide Substrate. *Bioscience Reports* **2014**, *34* (2), e00100.

(48)   Wejda, M.; Impens, F.; Takahashi, N.; Van Damme, P.; Gevaert, K.; Vandenabeele, P. Degradomics Reveals That Cleavage Specificity Profiles of Caspase-2 and Effector Caspases Are Alike. *Journal of Biological Chemistry* **2012**, *287* (41), 33983-33995.

(49)   Oliver, T. G.; Meylan, E.; Chang, G. P.; Xue, W.; Burke, J. R.; Humpton, T. J.; Hubbard, D.; Bhutkar, A.; Jacks, T. Caspase-2-Mediated Cleavage of Mdm2 Creates a P53-Induced Positive Feedback Loop. *Molecular Cell* **2011**, *43* (1), 57-71.

(50)   Brown-Suedel, A. N.; Bouchier-Hayes, L. Caspase-2 Substrates: To Apoptosis, Cell Cycle Control, and Beyond. *Front. Cell Dev. Biol.* **2020**, *8*, 610022.

(51)   Zhao, X.; Kotilinek, L. A.; Smith, B.; Hlynialuk, C.; Zahs, K.; Ramsden, M.; Cleary, J.; Ashe, K. H. Caspase-2 Cleavage of Tau Reversibly Impairs Memory. *Nat Med* **2016**, *22* (11), 1268-1276.

(52)   Kitevska, T.; Spencer, D. M. S.; Hawkins, C. J. Caspase-2: Controversial Killer or Checkpoint Controller? *Apoptosis* **2009**, *14* (7), 829-848.

(53)   Kumar, S. Caspase 2 in Apoptosis, the DNA Damage Response and Tumour Suppression: Enigma No More? *Nature Reviews Cancer* **2009**, *9* (12), 897-903.

(54)   Krumschnabel, G.; Sohm, B.; Bock, F.; Manzl, C.; Villunger, A. The Enigma of Caspase-2: The Laymen's View. *Cell Death & Differentiation* **2009**, *16* (2), 195-207.

(55)   Krumschnabel, G.; Manzl, C.; Villunger, A. Caspase-2: Killer, Savior and Safeguard— Emerging Versatile Roles for an Ill-Defined Caspase. *Oncogene* **2009**, *28* (35), 3093–3096.

(56)   Troy, C. M.; Ribe, E. M. Caspase-2: Vestigial Remnant or Master Regulator? *Sci. Signal.* **2008**, *1* (38), pe42-pe42.

(57)   Kumar, S. Caspase Function in Programmed Cell Death. *Cell Death & Differentiation* **2007**, *14* (1), 32-43.

(58)   Machado, M. V.; Michelotti, G. A.; Jewell, M. L.; Pereira, T. A.; Xie, G.; Premont, R. T.; Diehl, A. M. Caspase-2 Promotes Obesity, the Metabolic Syndrome and Nonalcoholic Fatty Liver Disease. *Cell Death Dis* **2016**, *7* (2), e2096-e2096.

(59)   Ahmed, Z.; Kalinski, H.; Berry, M.; Almasieh, M.; Ashush, H.; Slager, N.; Brafman, A.; Spivak, I.; Prasad, N.; Mett, I.; Shalom, E.; Alpert, E.; Di Polo, A.; Feinstein, E.; Logan, A. Ocular Neuroprotection by SiRNA Targeting Caspase-2. *Cell Death Dis* **2011**, *2* (6), e173-e173.

(60)   Ho, L. H.; Read, S. H.; Dorstyn, L.; Lambrusco, L.; Kumar, S. Caspase-2 Is Required for Cell Death Induced by Cytoskeletal Disruption. *Oncogene* **2008**, *27* (24), 3393-3404.

(61)   Carlsson, Y.; Wang, X.; Schwendimann, L.; Rousset, C. I.; Jacotot, E.; Gressens, P.; Thoresen, M.; Mallard, C.; Hagberg, H. Combined Effect of Hypothermia and Caspase-2 Gene Deficiency on Neonatal Hypoxic–Ischemic Brain Injury. *Pediatric Research* **2012**, *71* (5), 566–572.

(62)   Pozueta, J.; Lefort, R.; Ribe, E. M.; Troy, C. M.; Arancio, O.; Shelanski, M. Caspase-2 Is Required for Dendritic Spine and Behavioural Alterations in J20 APP Transgenic Mice. *Nature Communications* **2013**, *4* (1), 1939.

(63)   Carroll, J. B.; Southwell, A. L.; Graham, R. K.; Lerch, J. P.; Ehrnhoefer, D. E.; Cao, L.-P.; Zhang, W.-N.; Deng, Y.; Bissada, N.; Henkelman, R.; Hayden, M. R. Mice Lacking Caspase-2 Are Protected from Behavioral Changes, but Not Pathology, in the YAC128 Model of Huntington Disease. *Mol Neurodegeneration* **2011**, *6* (1), 59.

(64)   Carlsson, Y.; Schwendimann, L.; Vontell, R.; Rousset, C. I.; Wang, X.; Lebon, S.; Charriaut-Marlangue, C.; Supramaniam, V.; Hagberg, H.; Gressens, P. Genetic Inhibition of Caspase-2 Reduces Hypoxic-ischemic and Excitotoxic Neonatal Brain Injury. *Annals of neurology* **2011**, *70* (5), 781-789.

(65)   Tiwari, M.; Lopez-Cruzan, M.; Morgan, W. W.; Herman, B. Loss of Caspase-2-Dependent Apoptosis Induces Autophagy after Mitochondrial Oxidative Stress in Primary Cultures of Young Adult Cortical Neurons. *Journal of Biological Chemistry* **2011**, *286* (10), 8493-8506.

(66)   Tiwari, M.; Herman, B.; Morgan, W. W. A Knockout of the Caspase 2 Gene Produces Increased Resistance of the Nigrostriatal Dopaminergic Pathway to MPTP-Induced Toxicity. *Experimental Neurology* **2011**, *229* (2), 421-428.

(67)   Venkatesh, A.; Ma, S.; Le, Y. Z.; Hall, M. N.; Rüegg, M. A.; Punzo, C. Activated

MTORC1 Promotes Long-Term Cone Survival in Retinitis Pigmentosa Mice. *J. Clin. Invest.* **2015**, *125* (4), 1446-1458.

(68)   Dorstyn, L.; Puccini, J.; Nikolic, A.; Shalini, S.; Wilson, C. H.; Norris, M. D.; Haber, M.; Kumar, S. An Unexpected Role for Caspase-2 in Neuroblastoma. *Cell Death Dis* **2014**, *5* (8), e1383-e1383.

(69)   Zhang, Y.; Padalecki, S.; Chaudhuri, A.; Dewaal, E.; Goins, B.; Grubbs, B.; Ikeno, Y.; Richardson, A.; Mundy, G.; Herman, B. Caspase-2 Deficiency Enhances Aging-Related Traits in Mice. *Mechanisms of Ageing and Development* **2007**, *128* (2), 213-221.

(70)   Di Donato, N.; Jean, Y. Y.; Maga, A. M.; Krewson, B. D.; Shupp, A. B.; Avrutsky, M. I.; Roy, A.; Collins, S.; Olds, C.; Willert, R. A.; Czaja, A. M.; Johnson, R.; Stover, J. A.; Gottlieb, S.; Bartholdi, D.; Rauch, A.; Goldstein, A.; Boyd-Kyle, V.; Aldinger, K. A.; Mirzaa, G. M.; Nissen, A.; Brigatti, K. W.; Puffenberger, E. G.; Millen, K. J.; Strauss, K. A.; Dobyns, W. B.; Troy, C. M.; Jinks, R. N. Mutations in CRADD Result in Reduced Caspase-2-Mediated Neuronal Apoptosis and Cause Megalencephaly with a Rare Lissencephaly Variant. *The American Journal of Human Genetics* **2016**, *99* (5), 1117-1129.

(71)   Kumar, S.; Kinoshita, M.; Noda, M.; Copeland, N. G.; Jenkins, N. A. Induction of Apoptosis by the Mouse Nedd2 Gene, Which Encodes a Protein Similar to the Product of the Caenorhabditis Elegans Cell Death Gene Ced-3 and the Mammalian IL-1 Beta-Converting Enzyme. *Genes Dev* **1994**, *8* (14), 1613-1626.

(72)   Xu, Z.-X.; Tan, J.-W.; Xu, H.; Hill, C. J.; Ostrovskaya, O.; Martemyanov, K. A.; Xu, B. Caspase-2 Promotes AMPA Receptor Internalization and Cognitive Flexibility via MTORC2-AKT-GSK3β Signaling. *Nat Commun* **2019**, *10* (1), 3622.

(73)   Liu, P.; Smith, B. R.; Huang, E. S.; Mahesh, A.; Vonsattel, J. P. G.; Petersen, A. J.; Gomez-Pastor, R.; Ashe, K. H. A Soluble Truncated Tau Species Related to Cognitive Dysfunction and Caspase-2 Is Elevated in the Brain of Huntington's Disease Patients. *acta neuropathol commun* **2019**, *7* (1), 111.

(74)   Liu, P.; Smith, B. R.; Montonye, M. L.; Kemper, L. J.; Leinonen-Wright, K.; Nelson, K. M.; Higgins, L.; Guerrero, C. R.; Markowski, T. W.; Zhao, X.; Petersen, A. J.; Knopman, D. S.; Petersen, R. C.; Ashe, K. H. A Soluble Truncated Tau Species Related to Cognitive Dysfunction Is Elevated in the Brain of Cognitively Impaired Human Individuals. *Sci Rep* **2020**, *10* (1), 3869.

(75)   Smith, B. R.; Nelson, K. M.; Kemper, L. J.; Leinonen-Wright, K.; Petersen, A.; Keene, C. D.; Ashe, K. H. A Soluble Tau Fragment Generated by Caspase-2 Is Associated with Dementia in Lewy Body Disease. *acta neuropathol commun* **2019**, *7* (1), 124.

(76)   Menkes-Caspi, N.; Yamin, H. G.; Kellner, V.; Spires-Jones, T. L.; Cohen, D.; Stern, E. A. Pathological Tau Disrupts Ongoing Network Activity. *Neuron* **2015**, *85* (5), 959-966.

(77)   SantaCruz, K.; Lewis, J.; Spires, T.; Paulson, J.; Kotilinek, L.; Ingelsson, M.; Guimaraes, A.; DeTure, M.; Ramsden, M.; McGowan, E.; Forster, C.; Yue, M.; Orne, J.; Janus, C.; Mariash, A.; Kuskowski, M.; Hyman, B.; Hutton, M.; Ashe, K. H. Tau Suppression in a Neurodegenerative Mouse Model Improves Memory Function. **2005**, *309*, 7.

(78)   Avila, J.; Lucas, J. J.; Pérez, M.; Hernández, F. Role of Tau Protein in Both Physiological and Pathological Conditions. *Physiological Reviews* **2004**, *84* (2), 361-384.

(79)   Gong, C.-X.; Liu, F.; Grundke-Iqbal, I.; Iqbal, K. Post-Translational Modifications of Tau Protein in Alzheimer's Disease. *J Neural Transm* **2005**, *112* (6), 813-838.

(80)   Hoover, B. R.; Reed, M. N.; Su, J.; Penrod, R. D.; Kotilinek, L. A.; Grant, M. K.; Pitstick, R.; Carlson, G. A.; Lanier, L. M.; Yuan, L.-L.; Ashe, K. H.; Liao, D. Tau Mislocalization to Dendritic Spines Mediates Synaptic Dysfunction Independently of Neurodegeneration. *Neuron* **2010**, *68* (6), 1067-1081.

(81)   Šimić, G.; Babić Leko, M.; Wray, S.; Harrington, C.; Delalle, I.; Jovanov-Milošević, N.; Bažadona, D.; Buée, L.; de Silva, R.; Di Giovanni, G.; Wischik, C.; Hof, P. Tau Protein Hyperphosphorylation and Aggregation in Alzheimer's Disease and Other Tauopathies, and Possible Neuroprotective Strategies. *Biomolecules* **2016**, *6* (1), 6.

(82)   Pockes, S.; Walters, M. A.; Ashe, K. H. Targeting Caspase-2 Interactions with Tau in Alzheimer's Disease and Related Dementias. *Translational Research* **2023**, *254*, 34-40.

(83)   Troy, C. M.; Jean, Y. Y. Caspases: Therapeutic Targets in Neurologic Disease. *Neurotherapeutics* **2015**, *12* (1), 42-48.

(84)   Vigneswara, V.; Ahmed, Z. The Role of Caspase-2 in Regulating Cell Fate. *Cells* **2020**, *9* (5), 1259.

(85)   Ellis, H. Genetic Control of Programmed Cell Death in the Nematode C. Elegans. *Cell* **1986**, *44* (6), 817-829.

(86)   Tiwari, M.; Sharma, L. K.; Vanegas, D.; Callaway, D. A.; Bai, Y.; Lechleiter, J. D.; Herman, B. A Nonapoptotic Role for CASP2/Caspase 2: Modulation of Autophagy. *Autophagy* **2014**, *10* (6), 1054-1070.

(87)   Sohn, D.; Budach, W.; Jänicke, R. U. Caspase-2 Is Required for DNA Damage-Induced Expression of the CDK Inhibitor P21WAF1/CIP1. *Cell Death Differ* **2011**, *18* (10), 1664-1674.

(88)   Fujiwara, K.; Daido, S.; Yamamoto, A.; Kobayashi, R.; Yokoyama, T.; Aoki, H.; Iwado, E.; Shinojima, N.; Kondo, Y.; Kondo, S. Pivotal Role of the Cyclin-Dependent Kinase Inhibitor P21WAF1/CIP1 in Apoptosis and Autophagy. *Journal of Biological Chemistry* **2008**, *283* (1), 388-397.

(89)   Capparelli, C.; Chiavarina, B.; Whitaker-Menezes, D.; Pestell, T. G.; Pestell, R. G.; Hulit, J.; Andò, S.; Howell, A.; Martinez-Outschoorn, U. E.; Sotgia, F.; Lisanti, M. P. CDK Inhibitors (P16/P19/P21) Induce Senescence and Autophagy in Cancer-Associated Fibroblasts, "Fueling" Tumor Growth via Paracrine Interactions, without an Increase in Neo-Angiogenesis. *Cell Cycle* **2012**, *11* (19), 3599-3610.

(90)   Poreba, M.; Strozyk, A.; Salvesen, G. S.; Drag, M. Caspase Substrates and Inhibitors. *Cold Spring Harbor Perspectives in Biology* **2013**, *5* (8), a008680-a008680.

(91)   Chéreau, D.; Kodandapani, L.; Tomaselli, K. J.; Spada, A. P.; Wu, J. C. Structural and Functional Analysis of Caspase Active Sites. *Biochemistry* **2003**, *42* (14), 4151-4160.

(92)   Maillard, M. C.; Brookfield, F. A.; Courtney, S. M.; Eustache, F. M.; Gemkow, M. J.; Handel, R. K.; Johnson, L. C.; Johnson, P. D.; Kerry, M. A.; Krieger, F.; Meniconi, M.; Muñoz-Sanjuán, I.; Palfrey, J. J.; Park, H.; Schaertl, S.; Taylor, M. G.; Weddell, D.; Dominguez, C. Exploiting Differences in Caspase-2 and -3 S2 Subsites for Selectivity: Structure-Based Design, Solid-Phase Synthesis and in Vitro Activity of Novel Substrate-Based Caspase-2 Inhibitors. *Bioorganic & Medicinal Chemistry* **2011**, *19* (19), 5833-5851.

(93)   Poreba, M.; Rut, W.; Groborz, K.; Snipas, S. J.; Salvesen, G. S.; Drag, M. Potent and Selective Caspase-2 Inhibitor Prevents MDM-2 Cleavage in Reversine-Treated Colon Cancer Cells. *Cell Death & Differentiation* **2019**, *26* (12), 2695-2709.

(94)   Schweizer, A.; Briand, C.; Grütter, M. G. Crystal Structure of Caspase-2, Apical Initiator of the Intrinsic Apoptotic Pathway. *Journal of Biological Chemistry* **2003**, *278* (43), 42441-42447.

(95)   McStay, G. P.; Salvesen, G. S.; Green, D. R. Overlapping Cleavage Motif Selectivity of Caspases: Implications for Analysis of Apoptotic Pathways. *Cell Death Differ* **2008**, *15* (2), 322-331.

(96)   Julien, O.; Wells, J. A. Caspases and Their Substrates. *Cell Death Differ* **2017**, *24* (8), 1380-1389.

(97)   Toulmond, S.; Tang, K.; Bureau, Y.; Ashdown, H.; Degen, S.; O'Donnell, R.; Tam, J.; Han, Y.; Colucci, J.; Giroux, A.; Zhu, Y.; Boucher, M.; Pikounis, B.; Xanthoudakis, S.; Roy, S.; Rigby, M.; Zamboni, R.; Robertson, G. S.; Ng, G. Y. K.; Nicholson, D. W.; Flückiger, J.-P. Neuroprotective Effects of M826, a Reversible Caspase-3 Inhibitor, in the Rat Malonate Model of Huntington's Disease: Neuroprotection by Reversible Caspase-3 Inhibition. *British Journal of Pharmacology* **2004**, *141* (4), 689-697.

(98)   Boxer, M. B.; Quinn, A. M.; Shen, M.; Jadhav, A.; Leister, W.; Simeonov, A.; Auld, D. S.; Thomas, C. J. A Highly Potent and Selective Caspase 1 Inhibitor That Utilizes a Key 3-Cyanopropanoic Acid Moiety. *ChemMedChem* **2010**, *5* (5), 730-738.

(99)   Chauvier, D.; Renolleau, S.; Holifanjaniaina, S.; Ankri, S.; Bezault, M.; Schwendimann, L.; Rousset, C.; Casimir, R.; Hoebeke, J.; Smirnova, M.; Debret, G.; Trichet, A.-P.; Carlsson, Y.; Wang, X.; Bernard, E.; Hébert, M.; Rauzier, J.-M.; Matecki, S.; Lacampagne, A.; Rustin, P.; Mariani, J.; Hagberg, H.; Gressens, P.; Charriaut-Marlangue, C.; Jacotot, E. Targeting Neonatal Ischemic Brain Injury with a Pentapeptide-Based Irreversible Caspase Inhibitor. *Cell Death Dis* **2011**, *2* (9), e203-e203.

(100)   Fang, B.; Boross, P. I.; Tozser, J.; Weber, I. T. Structural and Kinetic Analysis of Caspase-3 Reveals Role for S5 Binding Site in Substrate Recognition. *Journal of Molecular*

Biology **2006**, *360* (3), 654-666.

(101)   Marlowe, C. K.; Scarborough, R. M.; Laibelman, A. M.; Sinha, U.; Zhu, B.-Y. Inhibitors of Factor Xa. US5721214A, February 24, **1998**.

(102)   Black, C.; Grimm, E. L.; Isabel, E.; Renaud, J. Nicotinyl Aspartyl Ketones as Inhibitors of Caspase-3. WO2001027085A1, April 19, **2001**.

(103)   Lipinski, C. A.; Lombardo, F.; Dominy, B. W.; Feeney, P. J. Experimental and Computational Approaches to Estimate Solubility and Permeability in Drug Discovery and Development Settings. *Advanced Drug Delivery Reviews* **1997**, *23* (1), 3-25.

(104)   Pérez, M. J.; Vergara-Pulgar, K.; Jara, C.; Cabezas-Opazo, F.; Quintanilla, R. A. Caspase-Cleaved Tau Impairs Mitochondrial Dynamics in Alzheimer's Disease. *Molecular Neurobiology* **2018**, *55* (2), 1004-1018.

(105)   Singh, G.; Liu, P.; Yao, K. R.; Strasser, J. M.; Hlynialuk, C.; Leinonen-Wright, K.; Teravskis, P. J.; Choquette, J. M.; Ikramuddin, J.; Bresinsky, M.; Nelson, K. M.; Liao, D.; Ashe, K. H.; Walters, M. A.; Pockes, S. Caspase-2 Inhibitor Blocks Tau Truncation and Restores Excitatory Neurotransmission in Neurons Modeling FTDP-17 Tauopathy. *ACS Chem. Neurosci.* **2022**, *13* (10), 1549-1557.

(106)   Metcalf, B.; Chuang, C.; Dufu, K.; Patel, M. P.; Silva-Garcia, A.; Johnson, C.; Lu, Q.; Partridge, J. R.; Patskovska, L.; Patskovsky, Y.; Almo, S. C.; Jacobson, M. P.; Hua, L.; Xu, Q.; Gwaltney, S. L.; Yee, C.; Harris, J.; Morgan, B. P.; James, J.; Xu, D.; Hutchaleelaha, A.; Paulvannan, K.; Oksenberg, D.; Li, Z. Discovery of GBT440, an Orally Bioavailable R-State Stabilizer of Sickle Cell Hemoglobin. *ACS Med. Chem. Lett.* **2017**, *8* (3), 321-326.

(107)   Owen, D. R.; Allerton, C. M. N.; Anderson, A. S.; Aschenbrenner, L.; Avery, M.; Berritt, S.; Boras, B.; Cardin, R. D.; Carlo, A.; Coffman, K. J.; Dantonio, A.; Di, L.; Eng, H.; Ferre, R.; Gajiwala, K. S.; Gibson, S. A.; Greasley, S. E.; Hurst, B. L.; Kadar, E. P.; Kalgutkar, A. S.; Lee, J. C.; Lee, J.; Liu, W.; Mason, S. W.; Noell, S.; Novak, J. J.; Obach, R. S.; Ogilvie, K.; Patel, N. C.; Pettersson, M.; Rai, D. K.; Reese, M. R.; Sammons, M. F.; Sathish, J. G.; Singh, R. S. P.; Steppan, C. M.; Stewart, A. E.; Tuttle, J. B.; Updyke, L.; Verhoest, P. R.; Wei, L.; Yang, Q.; Zhu, Y. An Oral SARS-CoV-2 Mpro Inhibitor Clinical Candidate for the Treatment of COVID-19. **2021**, *374* (6575), 1586-1593.

(108)   Bommarius, A. S.; Schwarm, M.; Drauz, K. Biocatalysis to Amino Acid-Based Chiral Pharmaceuticals—Examples and Perspectives. *Journal of Molecular Catalysis B: Enzymatic* **1998**, *5* (1-4), 1-11.

(109)   Lossos, A.; Reches, A.; Gal, A.; Newman, J. P.; Soffer, D.; Gomori, J. M.; Boher, M.; Ekstein, D.; Biran, I.; Meiner, Z.; Abramsky, O.; Rosenmann, H. Frontotemporal Dementia and Parkinsonism with the P301S Tau Gene Mutation in a Jewish Family. *Journal of Neurology* **2003**, *250* (6), 733-740.

(110)   Bugiani, O.; Murrell, J. R.; Giaccone, G.; Hasegawa, M.; Ghigo, G.; Tabaton, M.; Morbin, M.; Primavera, A.; Carella, F.; Solaro, C.; Grisoli, M.; Savoiardo, M.; Spillantini, M. G.; Tagliavini, F.; Goedert, M.; Ghetti, B. Frontotemporal Dementia and Corticobasal Degeneration in a Family with a P301S Mutation in Tau. *J Neuropathol Exp Neurol* **1999**, *58* (6), 667-677.

(111)   Teravskis, P. J.; Covelo, A.; Miller, E. C.; Singh, B.; Martell-Martínez, H. A.; Benneyworth, M. A.; Gallardo, C.; Oxnard, B. R.; Araque, A.; Lee, M. K.; Liao, D. A53T Mutant Alpha-Synuclein Induces Tau-Dependent Postsynaptic Impairment Independently of Neurodegenerative Changes. *J. Neurosci.* **2018**, *38* (45), 9754-9767.

(112)   Singh, B.; Covelo, A.; Martell-Martínez, H.; Nanclares, C.; Sherman, M. A.; Okematti, E.; Meints, J.; Teravskis, P. J.; Gallardo, C.; Savonenko, A. V.; Benneyworth, M. A.; Lesné, S. E.; Liao, D.; Araque, A.; Lee, M. K. Tau Is Required for Progressive Synaptic and Memory Deficits in a Transgenic Mouse Model of α-Synucleinopathy. *Acta Neuropathologica* **2019**, *138* (4), 551-574.

(113)   Miller, E. C.; Teravskis, P. J.; Dummer, B. W.; Zhao, X.; Huganir, R. L.; Liao, D. Tau Phosphorylation and Tau Mislocalization Mediate Soluble Aβ Oligomer-Induced AMPA Glutamate Receptor Signaling Deficits. *Eur J Neurosci* **2014**, *39* (7), 1214-1224.

(114)   Braun, N. J.; Yao, K. R.; Alford, P. W.; Liao, D. Mechanical Injuries of Neurons Induce Tau Mislocalization to Dendritic Spines and Tau-Dependent Synaptic Dysfunction. *Proc. Natl. Acad. Sci. U.S.A.* **2020**, *117* (46), 29069-29079.

(115)   Takeuchi, H.; Iba, M.; Inoue, H.; Higuchi, M.; Takao, K.; Tsukita, K.; Karatsu, Y.;

Iwamoto, Y.; Miyakawa, T.; Suhara, T.; Trojanowski, J. Q.; Lee, V. M.-Y.; Takahashi, R. P301S Mutant Human Tau Transgenic Mice Manifest Early Symptoms of Human Tauopathies with Dementia and Altered Sensorimotor Gating. *PLoS ONE* **2011**, *6* (6), e21050.

(116)   Yoshiyama, Y.; Higuchi, M.; Zhang, B.; Huang, S.-M.; Iwata, N.; Saido, T. C.; Maeda, J.; Suhara, T.; Trojanowski, J. Q.; Lee, V. M.-Y. Synapse Loss and Microglial Activation Precede Tangles in a P301S Tauopathy Mouse Model. *Neuron* **2007**, *53* (3), 337-351.

(117)   Fang, B.; Fu, G.; Agniswamy, J.; Harrison, R. W.; Weber, I. T. Caspase-3 Binds Diverse P4 Residues in Peptides as Revealed by Crystallography and Structural Modeling. *Apoptosis* **2009**, *14* (5), 741-752.

(118)   Agniswamy, J.; Fang, B.; Weber, I. T. Plasticity of S2-S4 Specificity Pockets of Executioner Caspase-7 Revealed by Structural and Kinetic Analysis: Plasticity of Caspase-7 Specificity Pockets. *FEBS Journal* **2007**, *274* (18), 4752-4765.

(119)   Agniswamy, J.; Fang, B.; Weber, I. T. Conformational Similarity in the Activation of Caspase-3 and -7 Revealed by the Unliganded and Inhibited Structures of Caspase-7. **2009**, *14*, 1135-1144.

(120)   Teravskis, P. J.; Ashe, K. H.; Liao, D. The Accumulation of Tau in Postsynaptic Structures: A Common Feature in Multiple Neurodegenerative Diseases? *Neuroscientist* **2020**, *26* (5-6), 503-520.

(121)   Tracy, T. E.; Gan, L. Tau-Mediated Synaptic and Neuronal Dysfunction in Neurodegenerative Disease. *Current Opinion in Neurobiology* **2018**, *51*, 134-138.

(122)   Zhu, K.; Borrelli, K. W.; Greenwood, J. R.; Day, T.; Abel, R.; Farid, R. S.; Harder, E. Docking Covalent Inhibitors: A Parameter Free Approach to Pose Prediction and Scoring. *Journal of chemical information and modeling* **2014**, *54* (7), 1932-1940.

(123)   Toledo Warshaviak, D.; Golan, G.; Borrelli, K. W.; Zhu, K.; Kalid, O. Structure-Based Virtual Screening Approach for Discovery of Covalently Bound Ligands. *Journal of chemical information and modeling* **2014**, *54* (7), 1941-1950.

(124)   Banks, W. A. From Blood–Brain Barrier to Blood–Brain Interface: New Opportunities for CNS Drug Delivery. *Nat Rev Drug Discov* **2016**, *15* (4), 275-292.

(125)   Pardridge, W. M. The Blood-Brain Barrier: Bottleneck in Brain Drug Development. **2005**, *2* (1), 12.

(126)   Wager, T. T.; Hou, X.; Verhoest, P. R.; Villalobos, A. Central Nervous System Multiparameter Optimization Desirability: Application in Drug Discovery. *ACS Chem. Neurosci.* **2016**, *7* (6), 767-775.

(127)   Wager, T. T.; Hou, X.; Verhoest, P. R.; Villalobos, A. Moving beyond Rules: The Development of a Central Nervous System Multiparameter Optimization (CNS MPO) Approach To Enable Alignment of Druglike Properties. *ACS Publications*. **2010**, 1, 6, 435-449.

(128)   Arvanitis, C. D.; Ferraro, G. B.; Jain, R. K. The Blood–Brain Barrier and Blood–Tumour Barrier in Brain Tumours and Metastases. *Nat Rev Cancer* **2020**, *20* (1), 26-41.

(129)   Daina, A.; Michielin, O.; Zoete, V. SwissADME: A Free Web Tool to Evaluate Pharmacokinetics, Drug-Likeness and Medicinal Chemistry Friendliness of Small Molecules. *Sci Rep* **2017**, *7* (1), 42717.

(130)   Pajouhesh, H.; Lenz, G. R. Medicinal Chemical Properties of Successful Central Nervous System Drugs. *Neurotherapeutics* **2005**, *2* (4), 541-553.

(131)   Daina, A.; Michielin, O.; Zoete, V. ILOGP: A Simple, Robust, and Efficient Description of *n* -Octanol/Water Partition Coefficient for Drug Design Using the GB/SA Approach. *J. Chem. Inf. Model.* **2014**, *54* (12), 3284-3301.

(132)   Cheng, T.; Zhao, Y.; Li, X.; Lin, F.; Xu, Y.; Zhang, X.; Li, Y.; Wang, R.; Lai, L. Computation of Octanol− Water Partition Coefficients by Guiding an Additive Model with Knowledge. *Journal of chemical information and modeling* **2007**, *47* (6), 2140-2148.

(133)   Wildman, S. A.; Crippen, G. M. Prediction of Physicochemical Parameters by Atomic Contributions. *J. Chem. Inf. Comput. Sci.* **1999**, *39* (5), 868-873.

(134)   Moriguchi, I.; Hirono, S.; Liu, Q.; Nakagome, I.; Matsushita, Y. Simple Method of Calculating Octanol/Water Partition Coefficient. *Chemical & Pharmaceutical Bulletin* **1992**, *40* (1), 127-130.

(135)   Moriguchi, I.; Hirono, S.; Nakagome, I.; Hirano, H. Comparison of Reliability of Log P Values for Drugs Calculated by Several Methods. *Chemical & Pharmaceutical Bulletin* **1994**,

42 (4), 976-978.

(136)   Delaney, J. S. ESOL: Estimating Aqueous Solubility Directly from Molecular Structure. *J. Chem. Inf. Comput. Sci.* **2004**, *44* (3), 1000-1005.

(137)   Csizmadia, F.; Tsantili-Kakoulidou, A.; Panderi, I.; Darvas, F. Prediction of Distribution Coefficient from Structure. 1. Estimation Method. *Journal of Pharmaceutical Sciences* **1997**, *86* (7), 865-871.

(138)   Anand, S. A. A.; Loganathan, C.; Thomas, N. S.; Saravanan, K.; Alphonsa, A. T.; Kabilan, S. Synthesis, Structure Prediction, Pharmacokinetic Properties, Molecular Docking and Antitumor Activities of Some Novel Thiazinone Derivatives. *New J. Chem.* **2015**, *39* (9), 7120-7129.

(139)   Martin, Y. C. A Bioavailability Score. *J. Med. Chem.* **2005**, *48* (9), 3164-3170.

(140)   Ghose, A. K.; Viswanadhan, V. N.; Wendoloski, J. J. A Knowledge-Based Approach in Designing Combinatorial or Medicinal Chemistry Libraries for Drug Discovery. 1. A Qualitative and Quantitative Characterization of Known Drug Databases. *J Comb Chem* **1999**, *1* (1), 55-68.

(141)   Ferrara, S. J.; Scanlan, T. S. A CNS-Targeting Prodrug Strategy for Nuclear Receptor Modulators. *J. Med. Chem.* **2020**, *63* (17), 9742-9751.

(142)   Meinig, J. M.; Ferrara, S. J.; Banerji, T.; Banerji, T.; Sanford-Crane, H. S.; Bourdette, D.; Scanlan, T. S. Targeting Fatty-Acid Amide Hydrolase with Prodrugs for CNS-Selective Therapy. *ACS Chem. Neurosci.* **2017**, *8* (11), 2468-2476.

(143)   Meinig, J. M.; Ferrara, S. J.; Banerji, T.; Banerji, T.; Sanford-Crane, H. S.; Bourdette, D.; Scanlan, T. S. Structure–Activity Relationships of Central Nervous System Penetration by Fatty Acid Amide Hydrolase (FAAH)-Targeted Thyromimetic Prodrugs. *ACS Med. Chem. Lett.* **2019**, *10* (1), 111-116.

(144)   McKinney, M. K.; Cravatt, B. F. Structure and Function of Fatty Acid Amide Hydrolase. *Annu. Rev. Biochem.* **2005**, *74* (1), 411-432.

(145)   Ueda, N.; Puffenbarger, R. A.; Yamamoto, S.; Deutsch, D. G. The Fatty Acid Amide Hydrolase (FAAH). *Chemistry and Physics of Lipids* **2000**, *108* (1), 107-121.

(146)   Sureshbabu, V. V.; Naik, S. A.; Nagendra, G. Synthesis of Boc-Amino Tetrazoles Derived from α-Amino Acids. *Synthetic Communications* **2009**, *39* (3), 395-406.

(147)   Choong, I. C.; Lew, W.; Lee, D.; Pham, P.; Burdett, M. T.; Lam, J. W.; Wiesmann, C.; Luong, T. N.; Fahr, B.; DeLano, W. L.; McDowell, R. S.; Allen, D. A.; Erlanson, D. A.; Gordon, E. M.; O'Brien, T. Identification of Potent and Selective Small-Molecule Inhibitors of Caspase-3 through the Use of Extended Tethering and Structure-Based Drug Design. *J. Med. Chem.* **2002**, 45 (23), 5005-5022

(148)   Cserjan-Puschmann, M.; Lingg, N.; Engele, P.; Kröß, C.; Loibl, J.; Fischer, A.; Bacher, F.; Frank, A.-C.; Öhlknecht, C.; Brocard, C.; Oostenbrink, C.; Berkemeyer, M.; Schneider, R.; Striedner, G.; Jungbauer, A. Production of Circularly Permuted Caspase-2 for Affinity Fusion-Tag Removal: Cloning, Expression in Escherichia Coli, Purification, and Characterization. *Biomolecules* **2020**, *10* (12), 1592.

(149)   Denault, J.; Salvesen, G. S. Expression, Purification, and Characterization of Caspases. *Current Protocols in Protein Science* **2002**, *30* (1), 21.13.1-21.13.15.

(150)   Liu, W.; Lin, H.; He, X.; Chen, L.; Dai, Y.; Jia, W.; Xue, X.; Tao, J.; Chen, L. Neurogranin as a Cognitive Biomarker in Cerebrospinal Fluid and Blood Exosomes for Alzheimer's Disease and Mild Cognitive Impairment. *Transl Psychiatry* **2020**, *10* (1), 125.

(151)   Roos, K.; Wu, C.; Damm, W.; Reboul, M.; Stevenson, J. M.; Lu, C.; Dahlgren, M. K.; Mondal, S.; Chen, W.; Wang, L.; Abel, R.; Friesner, R. A.; Harder, E. D. OPLS3e: Extending Force Field Coverage for Drug-Like Small Molecules. *J. Chem. Theory Comput.* **2019**, *15* (3), 1863-1874.

(152)   Walters, J.; Schipper, J. L.; Swartz, P.; Mattos, C.; Clark, A. C. Allosteric Modulation of Caspase 3 through Mutagenesis. *Bioscience Reports* **2012**, *32* (4), 401-411.

(153)   Vonrhein, C.; Flensburg, C.; Keller, P.; Sharff, A.; Smart, O.; Paciorek, W.; Womack, T.; Bricogne, G. Data Processing and Analysis with the *AutoPROC* Toolbox. *Acta Crystallogr D Biol Crystallogr* **2011**, *67* (4), 293-302.

(154)   Adams, P. D.; Afonine, P. V.; Bunkóczi, G.; Chen, V. B.; Davis, I. W.; Echols, N.; Headd, J. J.; Hung, L.-W.; Kapral, G. J.; Grosse-Kunstleve, R. W.; McCoy, A. J.; Moriarty, N. W.;

Oeffner, R.; Read, R. J.; Richardson, D. C.; Richardson, J. S.; Terwilliger, T. C.; Zwart, P. H. *PHENIX* : A Comprehensive Python-Based System for Macromolecular Structure Solution. *Acta Crystallogr D Biol Crystallogr* **2010**, *66* (2), 213-221.

(155)   Emsley, P.; Lohkamp, B.; Scott, W. G.; Cowtan, K. Features and Development of *Coot*. *Acta Crystallogr D Biol Crystallogr* **2010**, *66* (4), 486-501.

(156)   Cheng, Y.-C.; Prusoff, W. H. Relationship between the Inhibition Constant (Ki) and the Concentration of Inhibitor Which Causes 50 per Cent Inhibition (I50) of an Enzymatic Reaction. *Biochemical pharmacology* **1973**, *22* (23), 3099-3108.

(157)   Lagerström, M. C.; Schiöth, H. B. Structural Diversity of G Protein-Coupled Receptors and Significance for Drug Discovery. *Nature reviews Drug discovery* **2008**, *7* (4), 339-357.

(158)   Fredriksson, R.; Lagerström, M. C.; Lundin, L.-G.; Schiöth, H. B. The G-Protein-Coupled Receptors in the Human Genome Form Five Main Families. Phylogenetic Analysis, Paralogon Groups, and Fingerprints. *Molecular pharmacology* **2003**, *63* (6), 1256-1272.

(159)   Wacker, D.; Stevens, R. C.; Roth, B. L. How Ligands Illuminate GPCR Molecular Pharmacology. *Cell* **2017**, *170* (3), 414-427.

(160)   Hauser, A. S.; Attwood, M. M.; Rask-Andersen, M.; Schiöth, H. B.; Gloriam, D. E. Trends in GPCR Drug Discovery: New Agents, Targets and Indications. *Nat Rev Drug Discov* **2017**, *16* (12), 829-842.

(161)   Fang, Y.; Lahiri, J.; Picard, L. G Protein-Coupled Receptor Microarrays for Drug Discovery. *Drug discovery today* **2003**, *8* (16), 755-761.

(162)   Vassilatis, D. K.; Hohmann, J. G.; Zeng, H.; Li, F.; Ranchalis, J. E.; Mortrud, M. T.; Brown, A.; Rodriguez, S. S.; Weller, J. R.; Wright, A. C. The G Protein-Coupled Receptor Repertoires of Human and Mouse. *Proceedings of the National Academy of Sciences* **2003**, *100* (8), 4903-4908.

(163)   Kristiansen, K. Molecular Mechanisms of Ligand Binding, Signaling, and Regulation within the Superfamily of G-Protein-Coupled Receptors: Molecular Modeling and Mutagenesis Approaches to Receptor Structure and Function. *Pharmacology & therapeutics* **2004**, *103* (1), 21-80.

(164)   Pándy-Szekeres, G.; Munk, C.; Tsonkov, T. M.; Mordalski, S.; Harpsøe, K.; Hauser, A. S.; Bojarski, A. J.; Gloriam, D. E. GPCRdb in 2018: Adding GPCR Structure Models and Ligands. *Nucleic acids research* **2018**, *46* (D1), D440-D446.

(165)   Laschet, C.; Dupuis, N.; Hanson, J. The G Protein-Coupled Receptors Deorphanization Landscape. *Biochem Pharmacol* **2018**, *153*, 62-74.

(166)   Hu, G.-M.; Mai, T.-L.; Chen, C.-M. Visualizing the GPCR Network: Classification and Evolution. *Sci Rep* **2017**, *7* (1), 15495.

(167)   Kolakowski Jr, L. F. GCRDb: A G-Protein-Coupled Receptor Database. *Receptors & channels* **1993**, *2* (1), 1-7.

(168)   *G protein-coupled receptors. IUPHAR/BPS Guide to PHARMACOLOGY*. IUPHAR/BPS Guide to PHARMACOLOGY. https://www.guidetopharmacology.org/GRAC/FamilyDisplayForward?familyId=694, (accessed 2023-02-27)

(169)   Turku, A.; Schihada, H.; Kozielewicz, P.; Bowin, C.-F.; Schulte, G. Residue 6.43 Defines Receptor Function in Class F GPCRs. *Nat Commun* **2021**, *12* (1), 3919.

(170)   Schulte, G.; Kozielewicz, P. Structural Insight into Class F Receptors – What Have We Learnt Regarding Agonist-induced Activation? *Basic Clin Pharmacol Toxicol* **2020**, *126* (S6), 17–24.

(171)   Katritch, V.; Cherezov, V.; Stevens, R. C. Diversity and Modularity of G Protein-Coupled Receptor Structures. *Trends Pharmacol Sci* **2012**, *33* (1), 17-27.

(172)   Rosenbaum, D. M.; Rasmussen, S. G.; Kobilka, B. K. The Structure and Function of G-Protein-Coupled Receptors. *Nature* **2009**, *459* (7245), 356-363.

(173)   Pockes, S. Synthese Und Pharmakologische Charakterisierung von Heteroarylpropylguanidin-Derivaten an Histamin-Rezeptorsubtypen: Struktur-Wirkungsbeziehungen Mono-Und Bivalenter Liganden. PhD Thesis, **2015**.

(174)   Ji, T. H.; Grossmann, M.; Ji, I. G Protein-Coupled Receptors I. Diversity of Receptor-Ligand Interactions. *Journal of Biological Chemistry* **1998**, *273* (28), 17299-17302.

(175)   Kobilka, B. K. G Protein Coupled Receptor Structure and Activation. *Biochimica et*

Biophysica Acta (BBA)-Biomembranes **2007**, *1768* (4), 794-807.

(176)   Stevens, R. C.; Cherezov, V.; Katritch, V.; Abagyan, R.; Kuhn, P.; Rosen, H.; Wüthrich, K. The GPCR Network: A Large-Scale Collaboration to Determine Human GPCR Structure and Function. *Nature Reviews Drug Discovery* **2013**, *12* (1), 25-34.

(177)   Gilman, A. G. G Proteins: Transducers of Receptor-Generated Signals. *Annual review of biochemistry* **1987**, *56* (1), 615-649.

(178)   Offermanns, S. G-Proteins as Transducers in Transmembrane Signalling. *Progress in biophysics and molecular biology* **2003**, *83* (2), 101-130.

(179)   Smrcka, A. V. G Protein Bγ Subunits: Central Mediators of G Protein-Coupled Receptor Signaling. *Cell Mol Life Sci* **2008**, *65* (14), 2191-2214.

(180)   Milligan, G.; Kostenis, E. Heterotrimeric G-proteins: A Short History. *British journal of pharmacology* **2006**, *147* (S1), S46-S55.

(181)   Igel, P. Synthesis and Structure-Activity Relationships of NG-Acylated Arylalkylguanidines and Related Compounds as Histamine Receptor Ligands: Searching for Selective H_4R Agonists. PhD Thesis, University of Regensburg, **2008**.

(182)   Geyer, R. Hetarylalkyl(Aryl)Cyanoguanidines as Histamine H_4 Receptor Ligands: Synthesis, Chiral Separation, Pharmacological Characterization, Structure-activity and -selectivity Relationships. PhD Thesis, University of Regensburg, **2011**.

(183)   Mannhold, R.; Kubinyi, H.; Folkers, G.; Seifert, R.; Wieland, T. G Protein-Coupled Receptors as Drug Targets: Analysis of Activation and Constitutive Activity; John Wiley & Sons, **2006**; Vol. 24.

(184)   Ross, E. M.; Wilkie, T. M. GTPase-Activating Proteins for Heterotrimeric G Proteins: Regulators of G Protein Signaling (RGS) and RGS-like Proteins. *Annual review of biochemistry* **2000**, *69* (1), 795-827.

(185)   De Vries, L.; Zheng, B.; Fischer, T.; Elenko, E.; Farquhar, M. G. The Regulator of G Protein Signaling Family. *Annual review of pharmacology and toxicology* **2000**, *40* (1), 235-271.

(186)   Neubig, R. R.; Siderovski, D. P. Regulators of G-Protein Signalling as New Central Nervous System Drug Targets. *Nature Reviews Drug Discovery* **2002**, *1* (3), 187-197.

(187)   Felixberger, J. Luciferase Complementation for the Determination of Arrestin Recruitment: Investigations at Histamine and NPY Receptors. PhD Thesis, University of Regensburg, **2014**.

(188)   Sassone-Corsi, P. The Cyclic AMP Pathway. *Cold Spring Harb Perspect Biol* **2012**, *4* (12), a011148.

(189)   Taskén, K.; Skålhegg, B. S.; Taskén, K. A.; Solberg, R.; Knutsen, H. K.; Levy, F. O.; Sandberg, M.; Orstavik, S.; Larsen, T.; Johansen, A. K.; Vang, T.; Schrader, H. P.; Reinton, N. T.; Torgersen, K. M.; Hansson, V.; Jahnsen, T. Structure, Function, and Regulation of Human CAMP-Dependent Protein Kinases. *Adv Second Messenger Phosphoprotein Res* **1997**, *31*, 191-204.

(190)   Luttrell, L. M. Reviews in Molecular Biology and Biotechnology: Transmembrane Signaling by G Protein-Coupled Receptors. *Molecular Biotechnology* **2008**, *39* (3), 239-264.

(191)   Sunahara, R. K.; Dessauer, C. W.; Gilman, A. G. Complexity and Diversity of Mammalian Adenylyl Cyclases. *Annu Rev Pharmacol Toxicol* **1996**, *36*, 461-480.

(192)   Morris, A. J.; Scarlata, S. Regulation of Effectors by G-Protein Alpha- and Beta Gamma-Subunits. Recent Insights from Studies of the Phospholipase c-Beta Isoenzymes. *Biochem Pharmacol* **1997**, *54* (4), 429-435.

(193)   Parys, J. B.; De Smedt, H. Inositol 1,4,5-Trisphosphate and Its Receptors. *Adv Exp Med Biol* **2012**, *740*, 255-279.

(194)   Berridge, M. J.; Lipp, P.; Bootman, M. D. The Versatility and Universality of Calcium Signalling. *Nat Rev Mol Cell Biol* **2000**, *1* (1), 11-21.

(195)   Yang, C.; Kazanietz, M. G. Divergence and Complexities in DAG Signaling: Looking beyond PKC. *Trends Pharmacol Sci* **2003**, *24* (11), 602-608.

(196)   Carrasco, S.; Mérida, I. Diacylglycerol, When Simplicity Becomes Complex. *Trends Biochem Sci* **2007**, *32* (1), 27-36.

(197)   Kurose, H. Gα12 and Gα13 as Key Regulatory Mediator in Signal Transduction. *Life Sciences* **2003**, *74* (2), 155-161.

671

(198)   Downes, G. B.; Gautam, N. The G Protein Subunit Gene Families. *Genomics* **1999**, *62* (3), 544-552.

(199)   Cabrera-Vera, T. M.; Vanhauwe, J.; Thomas, T. O.; Medkova, M.; Preininger, A.; Mazzoni, M. R.; Hamm, H. E. Insights into G Protein Structure, Function, and Regulation. *Endocrine reviews* **2003**, *24* (6), 765-781.

(200)   Kuehn, H. Light-Regulated Binding of Rhodopsin Kinase and Other Proteins to Cattle Photoreceptor Membranes. *Biochemistry* **1978**, *17* (21), 4389-4395.

(201)   Rajagopal, S.; Rajagopal, K.; Lefkowitz, R. J. Teaching Old Receptors New Tricks: Biasing Seven-Transmembrane Receptors. *Nature reviews Drug discovery* **2010**, *9* (5), 373-386.

(202)   Lefkowitz, R. J.; Whalen, E. J. β-Arrestins: Traffic Cops of Cell Signaling. *Current opinion in cell biology* **2004**, *16* (2), 162-168.

(203)   Lohse, M. J.; Hoffmann, C. Arrestin Interactions with G Protein-Coupled Receptors. *Handb Exp Pharmacol* **2014**, *219*, 15-56.

(204)   Gurevich, V. V.; Gurevich, E. V. The Structural Basis of Arrestin-Mediated Regulation of G-Protein-Coupled Receptors. *Pharmacol Ther* **2006**, *110* (3), 465-502.

(205)   Tobin, A. B. G-Protein-Coupled Receptor Phosphorylation: Where, When and by Whom. *Br J Pharmacol* **2008**, *153* (1), 167-176.

(206)   Patwardhan, A.; Cheng, N.; Trejo, J. Post-Translational Modifications of G Protein-Coupled Receptors Control Cellular Signaling Dynamics in Space and Time. *Pharmacol Rev* **2021**, *73* (1), 120-151.

(207)   Shenoy, S. K.; Lefkowitz, R. J. Multifaceted Roles of Beta-Arrestins in the Regulation of Seven-Membrane-Spanning Receptor Trafficking and Signalling. *Biochem J* **2003**, *375* (3), 503-515.

(208)   Lohse, M. J.; Klenk, C. Blocking Them All: β-Arrestins Inhibit Cellular Signaling. *Molecular Cell* **2008**, *31* (5), 619-621.

(209)   Kendall, R. T.; Luttrell, L. M. Diversity in Arrestin Function. *Cell Mol Life Sci* **2009**, *66* (18), 2953-2973.

(210)   Marchese, A.; Chen, C.; Kim, Y.-M.; Benovic, J. L. The Ins and Outs of G Protein-Coupled Receptor Trafficking. *Trends Biochem Sci* **2003**, *28* (7), 369-376.

(211)   Moore, C. A. C.; Milano, S. K.; Benovic, J. L. Regulation of Receptor Trafficking by GRKs and Arrestins. *Annu Rev Physiol* **2007**, *69*, 451-482.

(212)   Tian, X.; Kang, D. S.; Benovic, J. L. β-Arrestins and G Protein-Coupled Receptor Trafficking. *Handb Exp Pharmacol* **2014**, *219*, 173-186.

(213)   Jean-Charles, P.-Y.; Kaur, S.; Shenoy, S. K. G Protein-Coupled Receptor Signaling Through β-Arrestin-Dependent Mechanisms. *J Cardiovasc Pharmacol* **2017**, *70* (3), 142-158.

(214)   Song, X.; Coffa, S.; Fu, H.; Gurevich, V. V. How Does Arrestin Assemble MAPKs into a Signaling Complex? *J Biol Chem* **2009**, *284* (1), 685-695.

(215)   Gao, H.; Sun, Y.; Wu, Y.; Luan, B.; Wang, Y.; Qu, B.; Pei, G. Identification of Beta-Arrestin2 as a G Protein-Coupled Receptor-Stimulated Regulator of NF-KappaB Pathways. *Mol Cell* **2004**, *14* (3), 303-317.

(216)   Witherow, D. S.; Garrison, T. R.; Miller, W. E.; Lefkowitz, R. J. Beta-Arrestin Inhibits NF-KappaB Activity by Means of Its Interaction with the NF-KappaB Inhibitor IkappaBalpha. *Proc Natl Acad Sci U S A* **2004**, *101* (23), 8603-8607.

(217)   Shenoy, S. K.; McDonald, P. H.; Kohout, T. A.; Lefkowitz, R. J. Regulation of Receptor Fate by Ubiquitination of Activated Beta 2-Adrenergic Receptor and Beta-Arrestin. *Science* **2001**, *294* (5545), 1307-1313.

(218)   Wang, P.; Gao, H.; Ni, Y.; Wang, B.; Wu, Y.; Ji, L.; Qin, L.; Ma, L.; Pei, G. Beta-Arrestin 2 Functions as a G-Protein-Coupled Receptor-Activated Regulator of Oncoprotein Mdm2. *J Biol Chem* **2003**, *278* (8), 6363-6370.

(219)   Ma, L.; Pei, G. β-Arrestin Signaling and Regulation of Transcription. *Journal of Cell Science* **2007**, *120* (2), 213-218.

(220)   Kang, J.; Shi, Y.; Xiang, B.; Qu, B.; Su, W.; Zhu, M.; Zhang, M.; Bao, G.; Wang, F.; Zhang, X.; Yang, R.; Fan, F.; Chen, X.; Pei, G.; Ma, L. A Nuclear Function of Beta-Arrestin1 in GPCR Signaling: Regulation of Histone Acetylation and Gene Transcription. *Cell* **2005**, *123* (5), 833-847.

(221)   Shonberg, J.; Lopez, L.; Scammells, P. J.; Christopoulos, A.; Capuano, B.; Lane, J. R. Biased Agonism at G Protein-Coupled Receptors: The Promise and the Challenges-A Medicinal Chemistry Perspective. *Med. Res. Rev.* **2014**, *34* (6), 1286-1330.

(222)   Leff, P. The Two-State Model of Receptor Activation. *Trends in pharmacological sciences* **1995**, *16* (3), 89–97.

(223)   Kenakin, T. Drug Efficacy at G Protein-Coupled Receptors. *Annual review of pharmacology and toxicology* **2002**, *42* (1), 349-379.

(224)   Kenakin, T. Efficacy at G-Protein-Coupled Receptors. *Nature Reviews Drug Discovery* **2002**, *1* (2), 103–110.

(225)   Windaus, A.; Vogt, W. Synthesis of Imidazolylethylamine. *Ber Dtsch Chem Ges* **1907**, *40*, 3685–3691.

(226)   Barger, G.; Dale, H. H. CCLXV.—4-β-Aminoethylglyoxaline (β-Iminazolylethylamine) and the Other Active Principles of Ergot. *Journal of the Chemical Society, Transactions* **1910**, *97*, 2592-2595.

(227)   Dale, H. H.; Laidlaw, P. P. The Physiological Action of β-Iminazolylethylamine. *The Journal of Physiology* **1910**, *41* (5), 318.

(228)   Black, J. W.; Ganellin, C. R. Naming of Substituted Histamines. *Experientia* **1974**, *30* (1), 111-113.

(229)   Paiva, T. B.; Tominaga, M.; Paiva, A. C. Ionization of Histamine, N-Acetylhistamine, and Their Iodinated Derivatives. *J. Med. Chem.* **1970**, *13* (4), 689-692.

(230)   Aures, D.; Håkanson, R.; Schauer, A. Histidine Decarboxylase and DOPA Decarboxylase in the Rat Stomach. Properties and Cellular Localization. *European journal of pharmacology* **1968**, *3* (3), 217-234.

(231)   Schayer, R. W. The Origin and Fate of Histamine in the Body. In *Ciba Foundation Symposium-Histamine*; Chichester, UK: John Wiley & Sons, Ltd., **1956**, 183-188.

(232)   Beaven, M. A. Factors Regulating Availability of Histamine at Tissue Receptors. *Pharmacology of histamine receptors* **1982**, 103-145.

(233)   Parsons, M. E.; Ganellin, C. R. Histamine and Its Receptors. *British journal of pharmacology* **2006**, *147* (1), 127-135.

(234)   Yanai, K.; Tashiro, M. The Physiological and Pathophysiological Roles of Neuronal Histamine: An Insight from Human Positron Emission Tomography Studies. *Pharmacology & Therapeutics* **2007**, *113* (1), 1-15.

(235)   Riley, J.; West, G. Histamine in Tissue Mast Cells. *The Journal of physiology* **1952**, *117* (4), 72-73.

(236)   Saxena, S. P.; Brandes, L. J.; Becker, A. B.; Simons, K. J.; LaBella, F. S.; Gerrard, J. M. Histamine Is an Intracellular Messenger Mediating Platelet Aggregation. *Science* **1989**, *243* (4898), 1596-1599.

(237)   Håkanson, R.; Larsson, L. I.; Sundler, F. Endocrine-like Cells in Rat Stomach: Effects of 6-Hydroxydopa on Amine Stores and Amino Acid Decarboxylase Activities. A Chemical, Fluorescence Histochemical and Electron Microscopic Study. *J Pharmacol Exp Ther* **1974**, *191* (1), 92-101.

(238)   Karnushina, I. L.; Palacios, J. M.; Barbin, G.; Dux, E.; Joó, F.; Schwartz, J. C. Studies on a Capillary-Rich Fraction Isolated from Brain: Histaminic Components and Characterization of the Histamine Receptors Linked to Adenylate Cyclase. *J Neurochem* **1980**, *34* (5), 1201-1208.

(239)   Schwartz, J.-C.; Pollard, H.; Quach, T. T. Histamine as a Neurotransmitter in Mammalian Brain: Neurochemical Evidence. *Journal of neurochemistry* **1980**, *35* (1), 26-33.

(240)   Mössner, J.; Caca, K. Developments in the Inhibition of Gastric Acid Secretion. *European journal of clinical investigation* **2005**, *35* (8), 469-475.

(241)   Thurmond, R. L.; Gelfand, E. W.; Dunford, P. J. The Role of Histamine H_1 and H_4 Receptors in Allergic Inflammation: The Search for New Antihistamines. *Nature Reviews Drug Discovery* **2008**, *7* (1), 41-53.

(242)   Passani, M. B.; Giannoni, P.; Bucherelli, C.; Baldi, E.; Blandina, P. Histamine in the Brain: Beyond Sleep and Memory. *Biochemical pharmacology* **2007**, *73* (8), 1113-1122.

(243)   Knigge, U.; Warberg, J. The Role of Histamine in the Neuroendocrine Regulation of Pituitary Hormone Secretion. *Acta Endocrinol (Copenh)* **1991**, *124* (6), 609-619.

(244) Hill, S. J.; Ganellin, C. R.; Timmerman, H.; Schwartz, J. C.; Shankley, N. P.; Young, J. M.; Schunack, W.; Levi, R.; Haas, H. L. International Union of Pharmacology. XIII. Classification of Histamine Receptors. *Pharmacological reviews* **1997**, *49* (3), 253-278.

(245) Hough, L. B. Genomics Meets Histamine Receptors: New Subtypes, New Receptors. *Molecular Pharmacology* **2001**, *59* (3), 415-419.

(246) Ash, A. S. F.; Schild, H. O. Receptors Mediating Some Actions of Histamine. *British journal of pharmacology and chemotherapy* **1966**, *27* (2), 427-439.

(247) Black, J. W.; Duncan, W. A. M.; Durant, C. J.; Ganellin, C. R.; Parsons, E. M. Definition and Antagonism of Histamine H_2-Receptors. *Nature* **1972**, *236*, 385-390.

(248) Arrang, J.-M.; Garbarg, M.; Schwartz, J.-C. Auto-Inhibition of Brain Histamine Release Mediated by a Novel Class (H_3) of Histamine Receptor. *Nature* **1983**, *302* (5911), 832-837.

(249) Oda, T.; Morikawa, N.; Saito, Y.; Masuho, Y.; Matsumoto, S. Molecular Cloning and Characterization of a Novel Type of Histamine Receptor Preferentially Expressed in Leukocytes. *Journal of Biological Chemistry* **2000**, *275* (47), 36781-36786.

(250) Nakamura, T.; Itadani, H.; Hidaka, Y.; Ohta, M.; Tanaka, K. Molecular Cloning and Characterization of a New Human Histamine Receptor, HH_4R. *Biochemical and biophysical research communications* **2000**, *279* (2), 615-620.

(251) Liu, C.; Ma, X.-J.; Jiang, X.; Wilson, S. J.; Hofstra, C. L.; Blevitt, J.; Pyati, J.; Li, X.; Chai, W.; Carruthers, N. Cloning and Pharmacological Characterization of a Fourth Histamine Receptor (H_4) Expressed in Bone Marrow. *Molecular pharmacology* **2001**, *59* (3), 420-426.

(252) Morse, K. L.; Behan, J.; Laz, T. M.; West, R. E.; Greenfeder, S. A.; Anthes, J. C.; Umland, S.; Wan, Y.; Hipkin, R. W.; Gonsiorek, W. Cloning and Characterization of a Novel Human Histamine Receptor. *Journal of Pharmacology and Experimental Therapeutics* **2001**, *296* (3), 1058-1066.

(253) Nguyen, T.; Shapiro, D. A.; George, S. R.; Setola, V.; Lee, D. K.; Cheng, R.; Rauser, L.; Lee, S. P.; Lynch, K. R.; Roth, B. L. Discovery of a Novel Member of the Histamine Receptor Family. *Molecular pharmacology* **2001**, *59* (3), 427-433.

(254) Zhu, Y.; Michalovich, D.; Wu, H.-L.; Tan, K. B.; Dytko, G. M.; Mannan, I. J.; Boyce, R.; Alston, J.; Tierney, L. A.; Li, X.; Herrity, N. C.; Vawter, L.; Sarau, H. M.; Ames, R. S.; Davenport, C. M.; Hieble, J. P.; Wilson, S.; Bergsma, D. J.; Fitzgerald, L. R. Cloning, Expression, and Pharmacological Characterization of a Novel Human Histamine Receptor. *Molecular Pharmacology* **2001**, *59* (3), 434-441.

(255) Hill, S. J. Distribution, Properties, and Functional Characteristics of Three Classes of Histamine Receptor. *Pharmacological Reviews* **1990**, *42* (1), 45-83.

(256) Leurs, R.; Smit, M. J.; Timmerman, H. Molecular Pharmacological Aspects of Histamine Receptors. *Pharmacology & therapeutics* **1995**, *66* (3), 413-463.

(257) Debacker, M. D.; Gommeren, W.; Moereels, H.; Nobels, G.; Vangompel, P.; Leysen, J. E.; Luyten, W. H. Genomic Cloning, Heterologous Expression and Pharmacological Characterization of a Human Histamine H_1 Receptor. *Biochemical and biophysical research communications* **1993**, *197* (3), 1601-1608.

(258) Monti, J. M. Involvement of Histamine in the Control of the Waking State. *Life sciences* **1993**, *53* (17), 1331-1338.

(259) Malmberg-Aiello, P.; Ipponi, A.; Bartolini, A.; Schunack, W. Antiamnesic Effect of Metoprine and of Selective Histamine H_1 Receptor Agonists in a Modified Mouse Passive Avoidance Test. *Neuroscience letters* **2000**, *288* (1), 1-4.

(260) Chen, Z.; Sugimoto, Y.; Kamei, C. Effects of Intracerebroventricular Injection of Histamine and Its Related Compounds on Rectal Temperature in Mice. *Methods and findings in experimental and clinical pharmacology* **1995**, *17* (10), 669-675.

(261) Mobarakeh, J. I.; Sakurada, S.; Katsuyama, S.; Kutsuwa, M.; Kuramasu, A.; Lin, Z. Y.; Watanabe, T.; Hashimoto, Y.; Watanabe, T.; Yanai, K. Role of Histamine H_1 Receptor in Pain Perception: A Study of the Receptor Gene Knockout Mice. *European journal of pharmacology* **2000**, *391* (1), 81-89.

(262) Monti, J. M.; Jantos, H.; Leschke, C.; Elz, S.; Schunack, W. The Selective Histamine H_1-Receptor Agonist 2-(3-Trifluoromethylphenyl) Histamine Increases Waking in the Rat. *European Neuropsychopharmacology* **1994**, *4* (4), 459-462.

(263) Nakazato, E.; Yamamoto, T.; Ohno, M.; Watanabe, S. Cholinergic and Glutamatergic

Activation Reverses Working Memory Failure by Hippocampal Histamine H_1 Receptor Blockade in Rats. *Life Sciences* **2000**, *67* (10), 1139-1147.

(264)   Matsumoto, T.; Kanaide, H.; Nishimura, J.; Shogakiuchi, Y.; Kobayashi, S.; Nakamura, M. Histamine Activates H_1-Receptors to Induce Cytosolic Free Calcium Transients in Cultured Vascular Smooth Muscle Cells from Rat Aorta. *Biochemical and biophysical research communications* **1986**, *135* (1), 172-177.

(265)   Kotlikoff, M. I.; Murray, R. K.; Reynolds, E. E. Histamine-Induced Calcium Release and Phorbol Antagonism in Cultured Airway Smooth Muscle Cells. *American Journal of Physiology-Cell Physiology* **1987**, *253* (4), 561-566.

(266)   Toda, N. Endothelium-dependent Relaxation Induced by Angiotensin II and Histamine in Isolated Arteries of Dog. *British journal of pharmacology* **1984**, *81* (2), 301-307.

(267)   Van De Voorde, J.; Leusen, I. Role of the Endothelium in the Vasodilator Response of Rat Thoracic Aorta to Histamine. *European journal of pharmacology* **1983**, *87* (1), 113-120.

(268)   Majno, G.; Palade, G. E. Studies on Inflammation: I. The Effect of Histamine and Serotonin on Vascular Permeability: An Electron Microscopic Study. *The Journal of Cell Biology* **1961**, *11* (3), 571-605.

(269)   Majno, G.; Shea, S. M.; Leventhal, M. Endothelial Contraction Induced by Histamine-Type Mediators: An Electron Microscopic Study. *The Journal of cell biology* **1969**, *42* (3), 647-672.

(270)   Killackey, J. J.; Johnston, M. G.; Movat, H. Z. Increased Permeability of Microcarrier-Cultured Endothelial Monolayers in Response to Histamine and Thrombin. A Model for the in Vitro Study of Increased Vasopermeability. *The American journal of pathology* **1986**, *122* (1), 50.

(271)   Barak, N. Betahistine: What's New on the Agenda? *Expert opinion on investigational drugs* **2008**, *17* (5), 795-804.

(272)   Menghin, S.; Pertz, H. H.; Kramer, K.; Seifert, R.; Schunack, W.; Elz, S. N α-Imidazolylalkyl and Pyridylalkyl Derivatives of Histaprodifen: Synthesis and in Vitro Evaluation of Highly Potent Histamine H_1-Receptor Agonists. *J. Med. Chem.* **2003**, *46* (25), 5458-5470.

(273)   Bakker, R. A.; Leurs, R. Constitutively Active Histamine Receptors. *G Protein-Coupled Receptors as Drug Targets: Analysis of Activation and Constitutive Activity, Volume 24* **2005**, 195-222.

(274)   Gantz, I.; Munzert, G.; Tashiro, T.; Schäffer, M.; Wang, L.; DelValle, J.; Yamada, T. Molecular Cloning of the Human Histamine H_2 Receptor. *Biochemical and biophysical research communications* **1991**, *178* (3), 1386-1392.

(275)   Haas, H.; Panula, P. The Role of Histamine and the Tuberomamillary Nucleus in the Nervous System. *Nature Reviews Neuroscience* **2003**, *4* (2), 121-130.

(276)   Johnson, C. L.; Weinstein, H.; Green, J. P. Studies on Histamine H_2 Receptors Coupled to Cardiac Adenylate Cyclase: Blockade by H_2 and H_1 Receptor Antagonists. *Molecular pharmacology* **1979**, *16* (2), 417-428.

(277)   Verma, S. C.; McNeill, J. H. The Effect of Histamine, Isoproterenol and Tyramine on Rat Uterine Cyclic AMP. *Research communications in chemical pathology and pharmacology* **1976**, *13* (1), 55-64.

(278)   Eyre, P.; Chand, N. Histamine Receptor Mechanisms of the Lung. In *Pharmacology of histamine receptors*; Elsevier, **1982**, 298-322.

(279)   Ottosson, A.; Jansen, I.; Edvinsson, L. Characterization of Histamine Receptors in Isolated Human Cerebral Arteries. *British journal of pharmacology* **1988**, *94* (3), 901-907.

(280)   Inui, J.; Imamura, H. Restoration by Histamine of the Calcium-Dependent Electrical and Mechanical Response in the Guinea-Pig Papillary Muscle Partially Depolarized by Potassium. *Naunyn-Schmiedeberg's archives of pharmacology* **1976**, *294* (3), 261-269.

(281)   Levi, R.; Owen, D.; Trzeciakowski, J. Actions of Histamine on the Heart and Vasculature. *Pharmacology of Histamine Receptors* **1982**, 236-297.

(282)   Reinhardt, D.; Ritter, E. Hypothermia-Induced Potentiation of Histamine H_2-Receptor-Mediated Relaxation and Cyclic AMP Increase in the Isolated Mesenteric Artery of the Rabbit. *Agents and actions* **1979**, *9* (1), 9-14.

(283)   Dai, H.; Kaneko, K.; Kato, H.; Fujii, S.; Jing, Y.; Xu, A.; Sakurai, E.; Kato, M.; Okamura, N.; Kuramasu, A. Selective Cognitive Dysfunction in Mice Lacking Histamine H_1 and H_2

Receptors. *Neuroscience research* **2007**, *57* (2), 306-313.

(284) Tropmann, K. A Step Forward to Unravel Open Histamine H$_2$ Receptor Questions: Synthesis and Biological Evaluation of Novel H$_2$R Ligands Including Radio- and Fluorescence-Labeled Pharmacological Tools. PhD Thesis, University of Regensburg, **2021**.

(285) Mobarakeh, J. I.; Takahashi, K.; Sakurada, S.; Nishino, S.; Watanabe, H.; Kato, M.; Naghdi, N.; Yanai, K. Enhanced Antinociception by Intracerebroventricularly Administered Orexin A in Histamine H$_1$ or H$_2$ Receptor Gene Knockout Mice. *Pain* **2005**, *118* (1-2), 254-262.

(286) Mobarakeh, J. I.; Takahashi, K.; Sakurada, S.; Kuramasu, A.; Yanai, K. Enhanced Antinociceptive Effects of Morphine in Histamine H$_2$ Receptor Gene Knockout Mice. *Neuropharmacology* **2006**, *51* (3), 612-622.

(287) Durant, G. J.; Emmett, J. C.; Ganellin, C. R.; Roe, A. M.; Slater, R. A. Potential Histamine H$_2$-Receptor Antagonists. 3. Methylhistamines. *J. Med. Chem.* **1976**, *19* (7), 923-928.

(288) Durant, G. J.; Ganellin, C. R.; Parsons, M. E. Chemical Differentiation of Histamine H$_1$- and H$_2$-Receptor Agonists. *J. Med. Chem.* **1975**, *18* (9), 905-909.

(289) Durant, G. J.; Ganellin, C. R.; Parsons, M. E. Dimaprit,[S-[3-(N, N-Dimethylamino) Propyl] Isothiourea]. A Highly Specific Histamine H$_2$-Receptor Agonist. Part 2. Structure-Activity Considerations. *Agents and actions* **1994**, *43* (3-4), 139-143.

(290) Parsons, M. E.; Owen, D. A. A.; Ganellin, C. R.; Durant, G. J. Dimaprit—[S-[3-(N, N-Dimethylamino) Propyl] Isothiourea]—A Highly Specific Histamine H$_2$-Receptor Agonist. Part 1, Pharmacology. *Agents and actions* **1994**, *43* (3-4), 132-138.

(291) Eriks, J. C.; van der Goot, H.; Sterk, G. J.; Timmerman, H. Histamine H$_2$-Receptor Agonists. Synthesis, in Vitro Pharmacology, and Qualitative Structure-Activity Relationships of Substituted 4- and 5-(2-Aminoethyl)Thiazoles. *J Med Chem* **1992**, *35* (17), 3239-3246.

(292) van der Goot, H.; Eriks, J. C.; Leurs, R.; Timmerman, H. Amselamine, a New Selective Histamine H$_2$-Receptor Agonist. *Bioorganic & Medicinal Chemistry Letters* **1994**, *4* (16), 1913–1916.

(293) Parsons, M. E.; Blakemore, R. C.; Durant, G. J.; Ganellin, C. R.; Rasmussen, A. C. 3-[4(5)-Imidazolyl] Propylguanidine (SK&F 91486)-a Partial Agonist at Histamine H$_2$-Receptors. *Inflammation Research* **1975**, *5* (5), 464-464.

(294) Durant, G. J.; Duncan, W. A. M.; Ganellin, C. R.; Parsons, M. E.; Blakemore, R. C.; Rasmussen, A. C. Impromidine (SK&F 92676) Is a Very Potent and Specific Agonist for Histamine H$_2$ Receptors. *Nature* **1978**, *276* (5686), 403-405.

(295) Buschauer, A. Synthesis and in Vitro Pharmacology of Arpromidine and Related Phenyl(Pyridylalkyl)Guanidines, a Potential New Class of Positive Inotropic Drugs. *J. Med. Chem.* **1989**, *32* (8), 1963-1970.

(296) Baumann, G.; Permanetter, B.; Wirtzfeld, A. Possible Value of H$_2$-Receptor Agonists for Treatment of Catecholamine-Insensitive Congestive Heart Failure. *Pharmacology & therapeutics* **1984**, *24* (2), 165-177.

(297) Manallack, D. T. The pK_a Distribution of Drugs: Application to Drug Discovery. *Perspectives in Medicinal Chemistry* **2007**, *1*, 1177391X0700100003.

(298) Ghorai, P.; Kraus, A.; Keller, M.; Götte, C.; Igel, P.; Schneider, E.; Schnell, D.; Bernhardt, G.; Dove, S.; Zabel, M.; others. Acylguanidines as Bioisosteres of Guanidines: N G-Acylated Imidazolylpropylguanidines, a New Class of Histamine H$_2$ Receptor Agonists. *J. Med. Chem.* **2008**, *51* (22), 7193-7204.

(299) Kagermeier, N.; Werner, K.; Keller, M.; Baumeister, P.; Bernhardt, G.; Seifert, R.; Buschauer, A. Dimeric Carbamoylguanidine-Type Histamine H$_2$ Receptor Ligands: A New Class of Potent and Selective Agonists. *Bioorganic & Medicinal Chemistry* **2015**, *23* (14), 3957-3969.

(300) Keller, M.; Pop, N.; Hutzler, C.; Beck-Sickinger, A. G.; Bernhardt, G.; Buschauer, A. Guanidine− Acylguanidine Bioisosteric Approach in the Design of Radioligands: Synthesis of a Tritium-Labeled N G-Propionylargininamide ([^{3}H]-UR-MK114) as a Highly Potent and Selective Neuropeptide Y Y1 Receptor Antagonist. *J. Med. Chem.* **2008**, *51* (24), 8168-8172.

(301) Ghorai, P. Arpromidine-Related Acylguanidines: Synthesis and Structure-Activity Relationships of a New Class of Guanidine-Type Histamine H$_2$ Receptor Agonists with Reduced Basicity. PhD Thesis, **2006**.

(302) Kraus, A.; Ghorai, P.; Birnkammer, T.; Schnell, D.; Elz, S.; Seifert, R.; Dove, S.; Bernhardt, G.; Buschauer, A. NG-Acylated Aminothiazolylpropylguanidines as Potent and Selective Histamine H_2 Receptor Agonists. *ChemMedChem* **2009**, *4* (2), 232-240.

(303) Kraus, A. Highly Potent, Selective Acylguanidine-Type Histamine H_2 Receptor Agonists: Synthesis and Structure-Activity Relationships. PhD Thesis, **2008**.

(304) Biselli, S.; Bresinsky, M.; Tropmann, K.; Forster, L.; Honisch, C.; Buschauer, A.; Bernhardt, G.; Pockes, S. Pharmacological Characterization of a New Series of Carbamoylguanidines Reveals Potent Agonism at the H_2R and D_3R. *European Journal of Medicinal Chemistry* **2021**, *214*, 113190.

(305) Van Der Goot, H.; Timmerman, H. Selective Ligands as Tools to Study Histamine Receptors. *European journal of medicinal chemistry* **2000**, *35* (1), 5-20.

(306) Freston, J. W. Cimetidine in the Treatment of Gastric Ulcer: Review and Commentary. *Gastroenterology* **1978**, *74* (2), 426-430.

(307) Freston, J. W. Management of Peptic Ulcers: Emerging Issues. *World journal of surgery* **2000**, *24* (3), 250-255.

(308) Schwartz, J.-C. The Histamine H_3 Receptor: From Discovery to Clinical Trials with Pitolisant. *British journal of pharmacology* **2011**, *163* (4), 713-721.

(309) Schwartz, J.-C. Histamine as a Transmitter in Brain. *Life Sciences* **1975**, *17* (4), 503-517.

(310) Arrang, J.-M.; Garbarg, M.; Lancelo, J.-C.; Lecomte, J.-M.; Pollard, H.; Robba, M.; Schunack, W.; Schwartz, J.-C. Highly Potent and Selective Ligands for Histamine H_3-Receptors. *Nature* **1987**, *327* (6118), 117-123.

(311) Lovenberg, T. W.; Roland, B. L.; Wilson, S. J.; Jiang, X.; Pyati, J.; Huvar, A.; Jackson, M. R.; Erlander, M. G. Cloning and Functional Expression of the Human Histamine H_3 Receptor. *Molecular pharmacology* **1999**, *55* (6), 1101-1107.

(312) Cogé, F.; Guénin, S.-P.; Rique, H.; Boutin, J. A.; Galizzi, J.-P. Structure and Expression of the Human Histamine H_4-Receptor Gene. *Biochemical and biophysical research communications* **2001**, *284* (2), 301-309.

(313) Rouleau, A.; Ligneau, X.; Tardivel-Lacombe, J.; Morisset, S.; Gbahou, F.; Schwartz, J.-C.; Arrang, J.-M. Histamine H_3-receptor-mediated [^{35}S]GTPγ[S] Binding: Evidence for Constitutive Activity of the Recombinant and Native Rat and Human H_3 Receptors. *British journal of pharmacology* **2002**, *135* (2), 383-392.

(314) Clark, E. A.; Hill, S. J. Sensitivity of Histamine H_3 Receptor Agonist-Stimulated [^{35}S] GTPγ[S] Binding to Pertussis Toxin. *European journal of pharmacology* **1996**, *296* (2), 223-225.

(315) Leurs, R.; Bakker, R. A.; Timmerman, H.; de Esch, I. J. The Histamine H_3 Receptor: From Gene Cloning to H_3 Receptor Drugs. *Nature Reviews Drug Discovery* **2005**, *4* (2), 107-120.

(316) Berlin, M.; Boyce, C. W.; de Lera Ruiz, M. Histamine H_3 Receptor as a Drug Discovery Target. *J. Med. Chem.* **2010**, *54* (1), 26-53.

(317) Wijtmans, M.; Leurs, R.; Esch, I. de. Histamine H_3 Receptor Ligands Break Ground in a Remarkable Plethora of Therapeutic Areas. *Expert Opinion on Investigational Drugs*, **2007**, *16* (7), 967-985.

(318) Martinez-Mir, M. I.; Pollard, H.; Moreau, J.; Arrang, J. M.; Ruat, M.; Traiffort, E.; Schwartz, J. C.; Palacios, J. M. Three Histamine Receptors (H_1, H_2 and H_3) Visualized in the Brain of Human and Non-Human Primates. *Brain research* **1990**, *526* (2), 322-327.

(319) Arrang, J.-M.; Devaux, B.; Chodkiewicz, J.-P.; Schwartz, J.-C. H_3-Receptors Control Histamine Release in Human Brain. *J Neurochem* **1988**, *51* (1), 105-108.

(320) Arrang, J. M.; Garbarg, M.; Schwartz, J. C. Autoinhibition of Histamine Synthesis Mediated by Presynaptic H_3-Receptors. *Neuroscience* **1987**, *23* (1), 149-157.

(321) Schlicker, E.; Fink, K.; Detzner, M.; Göthert, M. Histamine Inhibits Dopamine Release in the Mouse Striatum via Presynaptic H_3 Receptors. *Journal of Neural Transmission/General Section JNT* **1993**, *93* (1), 1-10.

(322) Schlicker, E.; Betz, R.; Göthert, M. Histamine H_3 Receptor-Mediated Inhibition of Serotonin Release in the Rat Brain Cortex. *Naunyn-Schmiedeberg's archives of pharmacology* **1988**, *337* (5), 588-590.

(323)   Schlicker, E.; Fink, K.; Hinterthaner, M.; Göthert, M. Inhibition of Noradrenaline Release in the Rat Brain Cortex via Presynaptic H_3 Receptors. *Naunyn-Schmiedeberg's archives of pharmacology* **1989**, *340* (6), 633-638.

(324)   Clapham, J. I.; Kilpatrick, G. J. Histamine H_3 Receptors Modulate the Release of [^{3}H]-Acetylcholine from Slices of Rat Entorhinal Cortex: Evidence for the Possible Existence of H_3 Receptor Subtypes. *British journal of pharmacology* **1992**, *107* (4), 919.

(325)   Garcia, M.; Floran, B.; Arias-Montano, J. A.; Young, J. M.; Aceves, J. Histamine H_3 Receptor Activation Selectively Inhibits Dopamine D_1 Receptor-Dependent [^{3}H] GABA Release from Depolarization-Stimulated Slices of Rat Substantia Nigra Pars Reticulata. *Neuroscience* **1997**, *80* (1), 241-249.

(326)   Leurs, R.; Blandina, P.; Tedford, C.; Timmerman, H. Therapeutic Potential of Histamine H_3 Receptor Agonists and Antagonists. *Trends in pharmacological sciences* **1998**, *19* (5), 177-184.

(327)   Bakker, R. A. Histamine H_3-Receptor Isoforms. *Inflammation Research* **2004**, *53* (10), 509-516.

(328)   Bongers, G.; Bakker, R. A.; Leurs, R. Molecular Aspects of the Histamine H_3 Receptor. *Biochemical pharmacology* **2007**, *73* (8), 1195-1204.

(329)   Lin, J. Physiological Review Article: Brain Structures and Mechanisms Involved in the Control of Cortical Activation and Wakefulness, with Emphasis on the Posterior Hypothalamus and Histaminergic Neurons. *Sleep medicine reviews* **2000**, *4* (5), 471-503.

(330)   Cannon, K. E.; Nalwalk, J. W.; Stadel, R.; Ge, P.; Lawson, D.; Silos-Santiago, I.; Hough, L. B. Activation of Spinal Histamine H_3 Receptors Inhibits Mechanical Nociception. *European journal of pharmacology* **2003**, *470* (3), 139-147.

(331)   Toshio, M.; Moskowitz, M. A.; Zhihong, H. UK-14,304, R(-)-α-Methyl-Histamine and SMS 201-995 Block Plasma Protein Leakage within Dura Mater by Prejunctional Mechanisms. *European journal of pharmacology* **1992**, *224* (2–3), 145-150.

(332)   Ichinose, M.; Belvisi, M.; Barnes, P. Histamine H_3-Receptors Inhibit Neurogenic Microvascular Leakage in Airways. *Journal of Applied Physiology* **1990**, *68* (1), 21-25.

(333)   Millán-Guerrero, R. O.; Pineda-Lucatero, A. G.; Hernández-Benjamín, T.; Tene, C. E.; Pacheco, M. F. Nα-Methylhistamine Safety and Efficacy in Migraine Prophylaxis: Phase I and Phase II Studies. *Headache: The Journal of Head and Face Pain* **2003**, *43* (4), 389-394.

(334)   Van der Goot, H.; Schepers, M. J. P.; Sterk, G. J.; Timmerman, H. Isothiourea Analogues of Histamine as Potent Agonists or Antagonists of the Histamine H_3-Receptor. *European journal of medicinal chemistry* **1992**, *27* (5), 511-517.

(335)   Schwartz, J.-C. The Histamine H_3 Receptor: From Discovery to Clinical Trials with Pitolisant. *British journal of pharmacology* **2011**, *163* (4), 713-721.

(336)   Bonaventure, P.; Letavic, M.; Dugovic, C.; Wilson, S.; Aluisio, L.; Pudiak, C.; Lord, B.; Mazur, C.; Kamme, F.; Nishino, S.; Carruthers, N.; Lovenberg, T. Histamine H_3 Receptor Antagonists: From Target Identification to Drug Leads. *Biochem Pharmacol* **2007**, *73* (8), 1084–1096.

(337)   Syed, Y. Y. Pitolisant: First Global Approval. *Drugs* **2016**, *76* (13), 1313–1318.

(338)   Wang, J.; Li, X.; Yang, S.; Wang, T.; Xu, Z.; Xu, J.; Gao, H.; Chen, G. Pitolisant versus Placebo for Excessive Daytime Sleepiness in Narcolepsy and Obstructive Sleep Apnea: A Meta-Analysis from Randomized Controlled Trials. *Pharmacological Research* **2021**, *167*, 105522.

(339)   Pullen, L. C.; Picone, M.; Tan, L.; Johnston, C.; Stark, H. Cognitive Improvements in Children with Prader-Willi Syndrome Following Pitolisant Treatment—Patient Reports. *The Journal of Pediatric Pharmacology and Therapeutics* **2019**, *24* (2), 166–171.

(340)   Parmentier, R.; Anaclet, C.; Guhennec, C.; Brousseau, E.; Bricout, D.; Giboulot, T.; Bozyczko-Coyne, D.; Spiegel, K.; Ohtsu, H.; Williams, M. The Brain H_3-Receptor as a Novel Therapeutic Target for Vigilance and Sleep–Wake Disorders. *Biochemical pharmacology* **2007**, *73* (8), 1157-1171.

(341)   Sander, K.; Kottke, T.; Stark, H. Histamine H_3 Receptor Antagonists Go to Clinics. *Biological and Pharmaceutical Bulletin* **2008**, *31* (12), 2163-2181.

(342)   Gemkow, M. J.; Davenport, A. J.; Harich, S.; Ellenbroek, B. A.; Cesura, A.; Hallett, D. The Histamine H_3 Receptor as a Therapeutic Drug Target for CNS Disorders. *Drug discovery*

today **2009**, *14* (9), 509-515.

(343)   Leurs, R.; Vischer, H. F.; Wijtmans, M.; de Esch, I. J. En Route to New Blockbuster Anti-Histamines: Surveying the Offspring of the Expanding Histamine Receptor Family. *Trends in pharmacological sciences* **2011**, *32* (4), 250-257.

(344)   Raible, D. G.; Lenahan, T.; Fayvilevich, Y.; Kosinski, R.; Schulman, E. S. Pharmacologic Characterization of a Novel Histamine Receptor on Human Eosinophils. *American journal of respiratory and critical care medicine* **1994**, *149* (6), 1506-1511.

(345)   Raible, D. G.; Schulman, E. S.; DiMuzio, J.; Cardillo, R.; Post, T. J. Mast Cell Mediators Prostaglandin-D2 and Histamine Activate Human Eosinophils. *The Journal of Immunology* **1992**, *148* (11), 3536-3542.

(346)   Hofstra, C. L.; Desai, P. J.; Thurmond, R. L.; Fung-Leung, W.-P. Histamine H_4 Receptor Mediates Chemotaxis and Calcium Mobilization of Mast Cells. *Journal of Pharmacology and Experimental Therapeutics* **2003**, *305* (3), 1212-1221.

(347)   de Esch, I. J.; Thurmond, R. L.; Jongejan, A.; Leurs, R. The Histamine H_4 Receptor as a New Therapeutic Target for Inflammation. *Trends in pharmacological sciences* **2005**, *26* (9), 462-469.

(348)   Seifert, R.; Schneider, E. H.; Dove, S.; Brunskole, I.; Neumann, D.; Strasser, A.; Buschauer, A. Paradoxical Stimulatory Effects of the "Standard" Histamine H_4-Receptor Antagonist JNJ7777120: The H_4 Receptor Joins the Club of 7 Transmembrane Domain Receptors Exhibiting Functional Selectivity. *Molecular pharmacology* **2011**, *79* (4), 631-638.

(349)   Nijmeijer, S.; Vischer, H. F.; Rosethorne, E. M.; Charlton, S. J.; Leurs, R. Analysis of Multiple Histamine H_4 Receptor Compound Classes Uncovers Gαi Protein-and β-Arrestin2-Biased Ligands. *Molecular pharmacology* **2012**, *82* (6), 1174-1182.

(350)   Schneider, E. H.; Schnell, D.; Papa, D.; Seifert, R. High Constitutive Activity and a G-Protein-Independent High-Affinity State of the Human Histamine H_4-Receptor[†]. *Biochemistry* **2009**, *48* (6), 1424-1438.

(351)   Wifling, D.; Pfleger, C.; Kaindl, J.; Ibrahim, P.; Kling, R. C.; Buschauer, A.; Gohlke, H.; Clark, T. Basal Histamine H_4 Receptor Activation: Agonist Mimicry by the Diphenylalanine Motif. *Chemistry–A European Journal* **2019**, *25* (64), 14613-14624.

(352)   Gantner, F.; Sakai, K.; Tusche, M. W.; Cruikshank, W. W.; Center, D. M.; Bacon, K. B. Histamine H_4 and H_2 Receptors Control Histamine-Induced Interleukin-16 Release from Human CD8+ T Cells. *Journal of Pharmacology and Experimental Therapeutics* **2002**, *303* (1), 300-307.

(353)   Leurs, R.; Chazot, P. L.; Shenton, F. C.; Lim, H. D.; De Esch, I. J. Molecular and Biochemical Pharmacology of the Histamine H_4 Receptor. *British journal of pharmacology* **2009**, *157* (1), 14-23.

(354)   Dunford, P. J.; O'Donnell, N.; Riley, J. P.; Williams, K. N.; Karlsson, L.; Thurmond, R. L. The Histamine H_4 Receptor Mediates Allergic Airway Inflammation by Regulating the Activation of CD4+ T Cells. *The Journal of immunology* **2006**, *176* (11), 7062-7070.

(355)   Zhang, M.; Venable, J. D.; Thurmond, R. L. The Histamine H_4 Receptor in Autoimmune Disease. *Expert opinion on investigational drugs* **2006**, *15* (11), 1443-1452.

(356)   G Bhatt, H.; K Agrawal, Y.; G Raval, H.; Manna, K.; R Desai, P. Histamine H_4 Receptor: A Novel Therapeutic Target for Immune and Allergic Responses. *Mini Reviews in Medicinal Chemistry* **2010**, *10* (14), 1293-1308.

(357)   Dunford, P. J.; Holgate, S. T. The Role of Histamine in Asthma. *Histamine in Inflammation* **2010**, *709*, 53–66.

(358)   Mommert, S.; Gschwandtner, M.; Gutzmer, R.; Werfel, T. The Role of the Histamine H_4 Receptor in Atopic Dermatitis. *Current allergy and asthma reports* **2011**, *11* (1), 21-28.

(359)   Hashimoto, T.; Harusawa, S.; Araki, L.; Zuiderveld, O. P.; Smit, M. J.; Imazu, T.; Takashima, S.; Yamamoto, Y.; Sakamoto, Y.; Kurihara, T. A Selective Human H_4-Receptor Agonist: (-)-2-Cyano-1-methyl-3-{(2R,5R)-5-[1H-imidazol-4(5)-yl]tetrahydrofuran-2-yl}methylguanidine. *J. Med. Chem.* **2003**, *46* (14), 3162-3165.

(360)   Lim, H. D.; van Rijn, R. M.; Ling, P.; Bakker, R. A.; Thurmond, R. L.; Leurs, R. Evaluation of Histamine H_1-, H_2-, and H_3-Receptor Ligands at the Human Histamine H_4 Receptor: Identification of 4-Methylhistamine as the First Potent and Selective H_4 Receptor Agonist. *Journal of Pharmacology and Experimental Therapeutics* **2005**, *314* (3), 1310-1321.

(361) Igel, P.; Dove, S.; Buschauer, A. Histamine H$_4$ Receptor Agonists. *Bioorganic & Medicinal Chemistry Letters* **2010**, *20* (24), 7191-7199.

(362) Igel, P.; Geyer, R.; Strasser, A.; Dove, S.; Seifert, R.; Buschauer, A. Synthesis and Structure− Activity Relationships of Cyanoguanidine-Type and Structurally Related Histamine H$_4$ Receptor Agonists §. *Journal of medicinal chemistry* **2009**, *52* (20), 6297-6313.

(363) Thurmond, R. L.; Desai, P. J.; Dunford, P. J.; Fung-Leung, W.-P.; Hofstra, C. L.; Jiang, W.; Nguyen, S.; Riley, J. P.; Sun, S.; Williams, K. N.; others. A Potent and Selective Histamine H$_4$ Receptor Antagonist with Anti-Inflammatory Properties. *Journal of Pharmacology and Experimental Therapeutics* **2004**, *309* (1), 404-413.

(364) Coruzzi, G.; Adami, M.; Guaita, E.; de Esch, I. J.; Leurs, R. Antiinflammatory and Antinociceptive Effects of the Selective Histamine H$_4$-Receptor Antagonists JNJ7777120 and VUF6002 in a Rat Model of Carrageenan-Induced Acute Inflammation. *European journal of pharmacology* **2007**, *563* (1–3), 240-244.

(365) Dunford, P. J.; Williams, K. N.; Desai, P. J.; Karlsson, L.; McQueen, D.; Thurmond, R. L. Histamine H$_4$ Receptor Antagonists Are Superior to Traditional Antihistamines in the Attenuation of Experimental Pruritus. *Journal of allergy and clinical immunology* **2007**, *119* (1), 176-183.

(366) Jablonowski, J. A.; Grice, C. A.; Chai, W.; Dvorak, C. A.; Venable, J. D.; Kwok, A. K.; Ly, K. S.; Wei, J.; Baker, S. M.; Desai, P. J. The First Potent and Selective Non-Imidazole Human Histamine H$_4$ Receptor Antagonists. *Journal of medicinal chemistry* **2003**, *46* (19), 3957-3960.

(367) Altenbach, R. J.; Adair, R. M.; Bettencourt, B. M.; Black, L. A.; Fix-Stenzel, S. R.; Gopalakrishnan, S. M.; Hsieh, G. C.; Liu, H.; Marsh, K. C.; McPherson, M. J. Structure− Activity Studies on a Series of a 2-Aminopyrimidine-Containing Histamine H$_4$ Receptor Ligands. *Journal of medicinal chemistry* **2008**, *51* (20), 6571-6580.

(368) Cowart, M. D.; Altenbach, R. J.; Liu, H.; Hsieh, G. C.; Drizin, I.; Milicic, I.; Miller, T. R.; Witte, D. G.; Wishart, N.; Fix-Stenzel, S. R.; McPherson, M. J.; Adair, R. M.; Wetter, J. M.; Bettencourt, B. M.; Marsh, K. C.; Sullivan, J. P.; Honore, P.; Esbenshade, T. A.; Brioni, J. D. Rotationally Constrained 2,4-Diamino-5,6-Disubstituted Pyrimidines: A New Class of Histamine H$_4$ Receptor Antagonists with Improved Druglikeness and in Vivo Efficacy in Pain and Inflammation Models. *J. Med. Chem.* **2008**, *51* (20), 6547-6557.

(369) Smits, R. A.; Lim, H. D.; Hanzer, A.; Zuiderveld, O. P.; Guaita, E.; Adami, M.; Coruzzi, G.; Leurs, R.; de Esch, I. J. Fragment Based Design of New H$_4$ Receptor− Ligands with Anti-Inflammatory Properties in Vivo. *J. Med. Chem.* **2008**, *51* (8), 2457-2467.

(370) Smits, R. A.; de Esch, I. J.; Zuiderveld, O. P.; Broeker, J.; Sansuk, K.; Guaita, E.; Coruzzi, G.; Adami, M.; Haaksma, E.; Leurs, R. Discovery of Quinazolines as Histamine H$_4$ Receptor Inverse Agonists Using a Scaffold Hopping Approach. *J. Med. Chem.* **2008**, *51* (24), 7855-7865.

(371) Khan, N.; Saad, A.; Nurulain, S. M.; Darras, F. H.; Decker, M.; Sadek, B. The Dual-Acting H$_3$ Receptor Antagonist and AChE Inhibitor UW-MD-71 Dose-Dependently Enhances Memory Retrieval and Reverses Dizocilpine-Induced Memory Impairment in Rats. *Behav Brain Res* **2016**, *297*, 155-164.

(372) Darras, F. H.; Pockes, S.; Huang, G.; Wehle, S.; Strasser, A.; Wittmann, H.-J.; Nimczick, M.; Sotriffer, C. A.; Decker, M. Synthesis, Biological Evaluation, and Computational Studies of Tri-and Tetracyclic Nitrogen-Bridgehead Compounds as Potent Dual-Acting AChE Inhibitors and hH$_3$ Receptor Antagonists. *ACS chemical neuroscience* **2014**, *5* (3), 225-242.

(373) Sadek, B.; Khan, N.; Darras, F. H.; Pockes, S.; Decker, M. The Dual-Acting AChE Inhibitor and H$_3$ Receptor Antagonist UW-MD-72 Reverses Amnesia Induced by Scopolamine or Dizocilpine in Passive Avoidance Paradigm in Rats. *Physiology & Behavior* **2016**, *165*, 383–391.

(374) Panula, P.; Chazot, P. L.; Cowart, M.; Gutzmer, R.; Leurs, R.; Liu, W. L. S.; Stark, H.; Thurmond, R. L.; Haas, H. L. International Union of Basic and Clinical Pharmacology. XCVIII. Histamine Receptors. *Pharmacol Rev* **2015**, *67* (3), 601-655.

(375) Foord, S. M.; Bonner, T. I.; Neubig, R. R.; Rosser, E. M.; Pin, J.-P.; Davenport, A. P.; Spedding, M.; Harmar, A. J. International Union of Pharmacology. XLVI. G Protein-Coupled Receptor List. *Pharmacological reviews* **2005**, *57* (2), 279-288.

(376) Traiffort, E.; Pollard, H.; Moreau, J.; Ruat, M.; Schwartz, J. C.; Martinez-Mir, M. I.; Palacios, J. M. Pharmacological Characterization and Autoradiographic Localization of Histamine H_2 Receptors in Human Brain Identified with [^{125}I]Iodoaminopotentidine. *J Neurochem* **1992**, *59* (1), 290-299.

(377) Dove, S.; Elz, S.; Seifert, R.; Buschauer, A. Structure-Activity Relationships of Histamine H_2 Receptor Ligands. *Mini reviews in medicinal chemistry* **2004**, *4* (9), 941-954.

(378) Birnkammer, T.; Spickenreither, A.; Brunskole, I.; Lopuch, M.; Kagermeier, N.; Bernhardt, G.; Dove, S.; Seifert, R.; Elz, S.; Buschauer, A. The Bivalent Ligand Approach Leads to Highly Potent and Selective Acylguanidine-Type Histamine H_2 Receptor Agonists. *J. Med. Chem.* **2012**, *55* (3), 1147-1160.

(379) Shultz, M. D. Two Decades under the Influence of the Rule of Five and the Changing Properties of Approved Oral Drugs. *J. Med. Chem.* **2019**, *62* (4), 1701-1714.

(380) Bennett, J. P.; Piercey, M. F. Pramipexole-a New Dopamine Agonist for the Treatment of Parkinson's Disease. *J Neurol Sci* **1999**, *163* (1), 25-31.

(381) Morrell, A.; Placzek, M. S.; Steffen, J. D.; Antony, S.; Agama, K.; Pommier, Y.; Cushman, M. Investigation of the Lactam Side Chain Length Necessary for Optimal Indenoisoquinoline Topoisomerase I Inhibition and Cytotoxicity in Human Cancer Cell Cultures. *J Med Chem* **2007**, *50* (9), 2040-2048.

(382) Johnson, M.; Antonio, T.; Reith, M. E. A.; Dutta, A. K. Structure–Activity Relationship Study of N^6-(2-(4-(1H-Indol-5-yl)piperazin-1-yl)ethyl)-N^6-propyl-4,5,6,7-tetrahydrobenzo[*d*]thiazole-2,6-diamine Analogues: Development of Highly Selective D_3 Dopamine Receptor Agonists along with a Highly Potent D_2/D_3 Agonist and Their Pharmacological Characterization. *J. Med. Chem.* **2012**, *55* (12), 5826-5840.

(383) Li, Z.; Mayer, R. J.; Ofial, A. R.; Mayr, H. From Carbodiimides to Carbon Dioxide: Quantification of the Electrophilic Reactivities of Heteroallenes. *J. Am. Chem. Soc.* **2020**, *142* (18), 8383-8402.

(384) Gabryszewski, M.; Kulig, J.; Lenarcik, B. Stability and Structure of Transition Metal Complexes with Azoles in Aqueous Solutions Part 24 Comparison of Complex Forming Ability of Methylthiazoles and Aminothiazoles. *Polish Journal of Chemistry* **1982**, *56* (1), 55-60.

(385) Forlani, L.; Tocke, A. L.; Del Vecchio, E.; Lakhdar, S.; Goumont, R.; Terrier, F. Assessing the Nitrogen and Carbon Nucleophilicities of 2-Aminothiazoles through Coupling with Superelectrophilic 4,6-Dinitrobenzofuroxan. *J Org Chem* **2006**, *71* (15), 5527-5537.

(386) Al-Attas, A. S.; Habeeb, M. M.; Al-Raimi, D. S. Spectrophotometric Determination of Some Amino Heterocyclic Donors through Charge Transfer Complex Formation with Chloranilic Acid in Acetonitrile. *Journal of Molecular Liquids* **2009**, *148* (2–3), 58-66.

(387) Nagano, M.; Tobitsuka, J.; Matsui, T.; Oyamada, K. Studies on Organic Sulfur Compounds. VIII. The Reaction of Alkoxycarbonyl Isothiocyanates and 2-Aminothiazole. *Chemical and Pharmaceutical Bulletin* **1972**, *20* (12), 2618-2625.

(388) Okura, T.; Ito, R.; Ishiguro, N.; Tamai, I.; Deguchi, Y. Blood-Brain Barrier Transport of Pramipexole, a Dopamine D_2 Agonist. *Life Sci* **2007**, *80* (17), 1564-1571.

(389) Pockes, S.; Wifling, D.; Keller, M.; Buschauer, A.; Elz, S. Highly Potent, Stable, and Selective Dimeric Hetarylpropylguanidine-Type Histamine H_2 Receptor Agonists. *ACS Omega* **2018**, *3* (3), 2865-2882.

(390) Baumeister, P.; Erdmann, D.; Biselli, S.; Kagermeier, N.; Elz, S.; Bernhardt, G.; Buschauer, A. [^{3}H]UR-DE257: Development of a Tritium-Labeled Squaramide-Type Selective Histamine H_2 Receptor Antagonist. *ChemMedChem* **2015**, *10* (1), 83-93.

(391) Igel, P.; Schnell, D.; Bernhardt, G.; Seifert, R.; Buschauer, A. Tritium-Labeled N^1-[3-(1 H-Imidazol-4-Yl)Propyl]-N^2-Propionylguanidine ([^{3}H]UR-PI294), a High-Affinity Histamine H_3 and H_4 Receptor Radioligand. *ChemMedChem* **2009**, *4* (2), 225-231.

(392) Elz, S.; Kramer, K.; Pertz, H. H.; Detert, H.; ter Laak, A. M.; Kühne, R.; Schunack, W. Histaprodifens: Synthesis, Pharmacological in Vitro Evaluation, and Molecular Modeling of a New Class of Highly Active and Selective Histamine H_1-Receptor Agonists†. *J. Med. Chem.* **2000**, *43* (6), 1071-1084.

(393) Kelley, M. T.; Bürckstümmer, T.; Wenzel-Seifert, K.; Dove, S.; Buschauer, A.; Seifert, R. Distinct Interaction of Human and Guinea Pig Histamine H_2-Receptor with Guanidine-Type Agonists. *Molecular pharmacology* **2001**, *60* (6), 1210-1225.

(394)   Biselli, S.; Alencastre, I.; Tropmann, K.; Erdmann, D.; Chen, M.; Littmann, T.; Maia, A. F.; Gomez-Lazaro, M.; Tanaka, M.; Ozawa, T.; Keller, M.; Lamghari, M.; Buschauer, A.; Bernhardt, G. Fluorescent H_2 Receptor Squaramide-Type Antagonists: Synthesis, Characterization, and Applications. *ACS Med. Chem. Lett.* **2020**, *11* (8), 1521-1528.

(395)   Grätz, L.; Tropmann, K.; Bresinsky, M.; Müller, C.; Bernhardt, G.; Pockes, S. NanoBRET Binding Assay for Histamine H_2 Receptor Ligands Using Live Recombinant HEK293T Cells. *Scientific Reports* **2020**, *10* (1), 13288.

(396)   Hornigold, D. C.; Mistry, R.; Raymond, P. D.; Blank, J. L.; Challiss, R. A. J. Evidence for Cross-Talk between M_2 and M_3 Muscarinic Acetylcholine Receptors in the Regulation of Second Messenger and Extracellular Signal-Regulated Kinase Signalling Pathways in Chinese Hamster Ovary Cells. *Br J Pharmacol* **2003**, *138* (7), 1340-1350.

(397)   Chidiac, P.; Nouet, S.; Bouvier, M. Agonist-Induced Modulation of Inverse Agonist Efficacy at the Beta 2-Adrenergic Receptor. *Mol Pharmacol* **1996**, *50* (3), 662-669.

(398)   Newman-Tancredi, A.; Cussac, D.; Marini, L.; Millan, M. J. Antibody Capture Assay Reveals Bell-Shaped Concentration-Response Isotherms for h5-HT_{1A} Receptor-Mediated Galpha(I3) Activation: Conformational Selection by High-Efficacy Agonists, and Relationship to Trafficking of Receptor Signaling. *Mol Pharmacol* **2002**, *62* (3), 590-601.

(399)   Moriguchi, T.; Matsuura, H.; Itakura, Y.; Katsuki, H.; Saito, H.; Nishiyama, N. Allixin, a Phytoalexin Produced by Garlic, and Its Analogues as Novel Exogenous Substances with Neurotrophic Activity. *Life Sci* **1997**, *61* (14), 1413-1420.

(400)   Zegarra-Moran, O.; Romio, L.; Folli, C.; Caci, E.; Becq, F.; Vierfond, J.-M.; Mettey, Y.; Cabrini, G.; Fanen, P.; Galietta, L. J. V. Correction of G551D-CFTR Transport Defect in Epithelial Monolayers by Genistein but Not by CPX or MPB-07. *Br J Pharmacol* **2002**, *137* (4), 504-512.

(401)   Wreggett, K. A.; Wells, J. W. Cooperativity Manifest in the Binding Properties of Purified Cardiac Muscarinic Receptors. *J Biol Chem* **1995**, *270* (38), 22488-22499.

(402)   Owen, S. C.; Doak, A. K.; Ganesh, A. N.; Nedyalkova, L.; McLaughlin, C. K.; Shoichet, B. K.; Shoichet, M. S. Colloidal Drug Formulations Can Explain "Bell-Shaped" Concentration-Response Curves. *ACS Chem Biol* **2014**, *9* (3), 777-784.

(403)   Chen, J.; Jiang, C.; Levant, B.; Li, X.; Zhao, T.; Wen, B.; Luo, R.; Sun, D.; Wang, S. Pramipexole Derivatives as Potent and Selective Dopamine D_3 Receptor Agonists with Improved Human Microsomal Stability. *ChemMedChem* **2014**, *9* (12), 2653-2660.

(404)   Forster, L.; Grätz, L.; Mönnich, D.; Bernhardt, G.; Pockes, S. A Split Luciferase Complementation Assay for the Quantification of β-Arrestin2 Recruitment to Dopamine D_2-Like Receptors. *Int. J. Mol. Sci.* **2020**, *21* (17), 6103.

(405)   Yanagisawa, I.; Hirata, Y.; Ishii, Y. Studies on Histamine H_2 Receptor Antagonists. Synthesis and Pharmacological Activities of N-Sulfamoyl and N-Sulfonyl Amidine Derivatives. *J. Med. Chem.* **1987**, *30* (10), 1787-1793.

(406)   Schneider, E. H.; Neumann, D.; Seifert, R. Modulation of Behavior by the Histaminergic System: Lessons from H_1R-and H_2R-Deficient Mice. *Neurosci Biobehav Rev* **2014**, *42*, 252-266.

(407)   Deutsch, S. I.; Rosse, R. B.; Schwartz, B. L. Histamine H_2 Receptor Antagonists in Schizophrenia. *CNS Drugs* **1997**, *8* (4), 276-284.

(408)   Farzin, D.; Hosseini, S. H.; Shafaat, A. A Randomized Double Blind Clinical Trial in Famotidine Adjuvant Therapy in Schizophrenia. **2005**, 59-62.

(409)   Johnston, T. H.; van der Meij, A.; Brotchie, J. M.; Fox, S. H. Effect of Histamine H2 Receptor Antagonism on Levodopa-Induced Dyskinesia in the MPTP-Macaque Model of Parkinson's Disease. *Mov Disord* **2010**, *25* (10), 1379-1390.

(410)   Meskanen, K.; Ekelund, H.; Laitinen, J.; Neuvonen, P. J.; Haukka, J.; Panula, P.; Ekelund, J. A Randomized Clinical Trial of Histamine 2 Receptor Antagonism in Treatment-Resistant Schizophrenia. *J Clin Psychopharmacol* **2013**, *33* (4), 472-478.

(411)   Shi, H.; Yang, X.; Zhao, H.; Zhang, S.; Zu, J.; Zhang, W.; Shen, X.; Cui, G.; Hua, F.; Yan, C. Ranitidine Reduced Levodopa-Induced Dyskinesia by Remodeling Neurochemical Changes in Hemiparkinsonian Model of Rats. *Neuropsychiatr Dis Treat* **2015**, *11*, 1331-1337.

(412)   Ahmed, M. R.; Jayakumar, M.; Ahmed, M. S.; Zamaleeva, A. I.; Tao, J.; Li, E. H.; Job, J. K.; Pittenger, C.; Ohtsu, H.; Rajadas, J. Pharmacological Antagonism of Histamine H_2R

Ameliorated L-DOPA–Induced Dyskinesia via Normalization of GRK3 and by Suppressing FosB and ERK in PD. *Neurobiology of Aging* **2019**, *81*, 177-189.

(413) Oyewumi, L. K.; Vollick, D.; Merskey, H.; Plumb, C. Famotidine as an Adjunct Treatment of Resistant Schizophrenia. *J Psychiatry Neurosci* **1994**, *19* (2), 145-150.

(414) White, J. M.; Rumbold, G. R. Behavioural Effects of Histamine and Its Antagonists: A Review. *Psychopharmacology (Berl)* **1988**, *95* (1), 1-14.

(415) Ghorai, P.; Kraus, A.; Birnkammer, T.; Geyer, R.; Bernhardt, G.; Dove, S.; Seifert, R.; Elz, S.; Buschauer, A. Chiral NG-Acylated Hetarylpropylguanidine-Type Histamine H_2 Receptor Agonists Do Not Show Significant Stereoselectivity. *Bioorganic & Medicinal Chemistry Letters* **2010**, *20* (10), 3173-3176.

(416) Biselli, S. Synthesis and Pharmacological Characterization of Subtype-Selective Ligands, Including Radio- and Fluorescence Labeled Ligands, for the Histamine H_2 Receptor. PhD Thesis, University of Regensburg, **2019**.

(417) Tropmann, K.; Höring, C.; Plank, N.; Pockes, S. Discovery of a G Protein-Biased Radioligand for the Histamine H_2 Receptor with Reversible Binding Properties. *J. Med. Chem.* **2020**, *63* (21), 13090-13102.

(418) DeVos, S. L.; Miller, T. M. Direct Intraventricular Delivery of Drugs to the Rodent Central Nervous System. *JoVE (Journal of Visualized Experiments)* **2013**, *75*, e50326.

(419) Mierau, J. Pramipexole: A Dopamine-Receptor Agonist for Treatment of Parkinson's Disease. *Clinical neuropharmacology* **1995**, *18*, 195-206.

(420) Ganellin, C. R. Chemistry and Structure-Activity Relationships of Drugs Acting at Histamine Receptors. *Pharmacology of histamine receptors* **1982**, Bristol: Wright, 10-102.

(421) Geyer, R.; Igel, P.; Kaske, M.; Elz, S.; Buschauer, A. Synthesis, SAR and Selectivity of 2-Acyl- and 2-Cyano-1-Hetarylalkyl-Guanidines at the Four Histamine Receptor Subtypes: A Bioisosteric Approach. *Med. Chem. Commun.* **2014**, *5* (1), 72-81.

(422) Geyer, R.; Kaske, M.; Baumeister, P.; Buschauer, A. Synthesis and Functional Characterization of Imbutamine Analogs as Histamine H_3 and H_4 Receptor Ligands. *Archiv der Pharmazie* **2014**, *347* (2), 77-88.

(423) Bastos, C. M.; Munoz, B.; Tait, B. Compounds, Compositions, and Methods for Increasing Cftr Activity. WO2015138909, September 17, **2015**.

(424) Kim, K. S.; Qian, L. Improved Method for the Preparation of Guanidines. *Tetrahedron Letters* **1993**, *34* (48), 7677-7680.

(425) Höring, C.; Seibel, U.; Tropmann, K.; Grätz, L.; Mönnich, D.; Pitzl, S.; Bernhardt, G.; Pockes, S.; Strasser, A. A Dynamic, Split-Luciferase-Based Mini-G Protein Sensor to Functionally Characterize Ligands at All Four Histamine Receptor Subtypes. *Int. J. Mol. Sci.* **2020**, *21* (22), 8440.

(426) Carpenter, B.; Tate, C. G. Engineering a Minimal G Protein to Facilitate Crystallisation of G Protein-Coupled Receptors in Their Active Conformation. *Protein Engineering, Design and Selection* **2016**, *29* (12), 583-594.

(427) Nehmé, R.; Carpenter, B.; Singhal, A.; Strege, A.; Edwards, P. C.; White, C. F.; Du, H.; Grisshammer, R.; Tate, C. G. Mini-G Proteins: Novel Tools for Studying GPCRs in Their Active Conformation. *PloS one* **2017**, *12* (4), e0175642.

(428) Wan, Q.; Okashah, N.; Inoue, A.; Nehmé, R.; Carpenter, B.; Tate, C. G.; Lambert, N. A. Mini G Protein Probes for Active G Protein–Coupled Receptors (GPCRs) in Live Cells. *Journal of Biological Chemistry* **2018**, *293* (19), 7466-7473.

(429) Xie, S.-X.; Ghorai, P.; Ye, Q.-Z.; Buschauer, A.; Seifert, R. Probing Ligand-Specific Histamine H_1-and H_2-Receptor Conformations with NG-Acylated Imidazolylpropylguanidines. *Journal of Pharmacology and Experimental Therapeutics* **2006**, *317* (1), 139-146.

(430) Weinhart, C. G.; Wifling, D.; Schmidt, M. F.; Neu, E.; Höring, C.; Clark, T.; Gmeiner, P.; Keller, M. Dibenzodiazepinone-Type Muscarinic Receptor Antagonists Conjugated to Basic Peptides: Impact of the Linker Moiety and Unnatural Amino Acids on M2R Selectivity. *European Journal of Medicinal Chemistry* **2021**, *213*, 113159.

(431) Huebner, H.; Haubmann, C.; Utz, W.; Gmeiner, P. Conjugated Enynes as Nonaromatic Catechol Bioisosteres: Synthesis, Binding Experiments, and Computational Studies of Novel Dopamine Receptor Agonists Recognizing Preferentially the D_3 Subtype. *J. Med. Chem.* **2000**, *43* (4), 756-762.

(432)   Hellmann, J.; Drabek, M.; Yin, J.; Gunera, J.; Pröll, T.; Kraus, F.; Langmead, C. J.; Hübner, H.; Weikert, D.; Kolb, P. Structure-Based Development of a Subtype-Selective Orexin 1 Receptor Antagonist. *Proceedings of the National Academy of Sciences* **2020**, *117* (30), 18059-18067.

(433)   Ackermann, D.; Kutscher, F. Untersuchungen Über Die Physiologische Wirkung Einer Secalebase Und Des Imidazolyläthylamins. *Z Biol* **1910**, *54*, 387-394.

(434)   Baumann, G.; Mercader, D.; Busch, U.; Felix, S. B.; Loher, U.; Ludwig, L.; Sebening, H.; Heidecke, C. D.; Hagl, S.; Sebening, F. Effects of the H_2-Receptor Agonist Impromidine in Human Myocardium from Patients with Heart Failure Due to Mitral and Aortic Valve Disease. *Journal of cardiovascular pharmacology* **1983**, *5* (4), 618-625.

(435)   Matsuda, N.; Jesmin, S.; Takahashi, Y.; Hatta, E.; Kobayashi, M.; Matsuyama, K.; Kawakami, N.; Sakuma, I.; Gando, S.; Fukui, H. Histamine H_1 and H_2 Receptor Gene and Protein Levels Are Differentially Expressed in the Hearts of Rodents and Humans. *Journal of Pharmacology and Experimental Therapeutics* **2004**, *309* (2), 786-795.

(436)   Levi, R.; Malm, J. R.; Bowman, F. O.; Rosen, M. R. The Arrhythmogenic Actions of Histamine on Human Atrial Fibers. *Circ Res* **1981**, *49* (2), 545-550.

(437)   Sanders, L.; Lynham, J. A.; Kaumann, A. J. Chronic B1-Adrenoceptor Blockade Sensitises the H_1 and H_2 Receptor Systems in Human Atrium: Role of Cyclic Nucleotides. *Naunyn-Schmiedeberg's archives of pharmacology* **1996**, *353* (6), 661-670.

(438)   Seifert, R.; Strasser, A.; Schneider, E. H.; Neumann, D.; Dove, S.; Buschauer, A. Molecular and Cellular Analysis of Human Histamine Receptor Subtypes. *Trends Pharmacol Sci* **2013**, *34* (1), 33-58.

(439)   Gergs, U.; Bernhardt, G.; Buchwalow, I. B.; Edler, H.; Fröba, J.; Keller, M.; Kirchhefer, U.; Köhler, F.; Mißlinger, N.; Wache, H.; Neumann, J. Initial Characterization of Transgenic Mice Overexpressing Human Histamine H_2 Receptors. *J Pharmacol Exp Ther* **2019**, *369* (1), 129-141.

(440)   Gergs, U.; Büxel, M. L.; Bresinsky, M.; Kirchhefer, U.; Fehse, C.; Höring, C.; Hofmann, B.; Marušáková, M.; Čináková, A.; Schwarz, R.; Pockes, S.; Neumann, J. Cardiac Effects of Novel Histamine H_2 Receptor Agonists. *J Pharmacol Exp Ther* **2021**, *379* (3), 223-234.

(441)   Gergs, U.; Kirchhefer, U.; Bergmann, F.; Künstler, B.; Mißlinger, N.; Au, B.; Mahnkopf, M.; Wache, H.; Neumann, J. Characterization of Stressed Transgenic Mice Overexpressing H_2-Histamine Receptors in the Heart. *Journal of Pharmacology and Experimental Therapeutics* **2020**, *374* (3), 479-488.

(442)   Neumann, J.; Binter, M. B.; Fehse, C.; Marušáková, M.; Büxel, M. L.; Kirchhefer, U.; Hofmann, B.; Gergs, U. Amitriptyline Functionally Antagonizes Cardiac H_2 Histamine Receptors in Transgenic Mice and Human Atria. *Naunyn-schmiedeberg's Archives of Pharmacology* **2021**, *394* (6), 1251-1262.

(443)   Neumann, J.; Grobe, J. M.; Weisgut, J.; Schwelberger, H. G.; Fogel, W. A.; Marušáková, M.; Wache, H.; Bähre, H.; Buchwalow, I. B.; Dhein, S. Histamine Can Be Formed and Degraded in the Human and Mouse Heart. *Frontiers in pharmacology* **2021**, *12*, 582916.

(444)   Gergs, U.; Weisgut, J.; Griethe, K.; Mißlinger, N.; Kirchhefer, U.; Neumann, J. Human Histamine H_2 Receptors Can Initiate Cardiac Arrhythmias in a Transgenic Mouse. *Naunyn-Schmiedeberg's archives of pharmacology* **2021**, *394* (9), 1963-1973.

(445)   Baumann, G.; Felix, S. B.; Riess, G.; Loher, U.; Ludwig, L.; Blömer, H. Effective Stimulation of Cardiac Contractility and Myocardial Metabolism by Impromidine and Dimaprit--Two New H_2-Agonistic Compounds--in the Surviving, Catecholamine-Insensitive Myocardium after Coronary Occlusion. *Journal of cardiovascular pharmacology* **1982**, *4* (4), 542-553.

(446)   Felix, S. B.; Buschauer, A.; Baumann, G. Haemodynamic Profile of New H_2-Receptor Agonists in Congestive Heart Failure. *European journal of clinical investigation* **1995**, *25* (1), 42-46.

(447)   Daina, A.; Zoete, V. A Boiled-egg to Predict Gastrointestinal Absorption and Brain Penetration of Small Molecules. *ChemMedChem* **2016**, *11* (11), 1117-1121.

(448)   Ertl, P.; Rohde, B.; Selzer, P. Fast Calculation of Molecular Polar Surface Area as a Sum of Fragment-Based Contributions and Its Application to the Prediction of Drug Transport Properties. *J. Med. Chem.* **2000**, *43* (20), 3714-3717.

(449)   Hidalgo, I. J.; Raub, T. J.; Borchardt, R. T. Characterization of the Human Colon

Carcinoma Cell Line (Caco-2) as a Model System for Intestinal Epithelial Permeability. *Gastroenterology* **1989**, *96* (2), 736-749.

(450) Sambuy, Y.; De Angelis, I.; Ranaldi, G.; Scarino, M. L.; Stammati, A.; Zucco, F. The Caco-2 Cell Line as a Model of the Intestinal Barrier: Influence of Cell and Culture-Related Factors on Caco-2 Cell Functional Characteristics. *Cell biology and toxicology* **2005**, *21* (1), 1-26.

(451) Artursson, P. E. R. Epithelial Transport of Drugs in Cell Culture. I: A Model for Studying the Passive Diffusion of Drugs over Intestinal Absorbtive (Caco-2) Cells. *Journal of pharmaceutical sciences* **1990**, *79* (6), 476-482.

(452) Artursson, P.; Karlsson, J. Correlation between Oral Drug Absorption in Humans and Apparent Drug Permeability Coefficients in Human Intestinal Epithelial (Caco-2) Cells. *Biochemical and biophysical research communications* **1991**, *175* (3), 880-885.

(453) Jones, D. F.; Oldham, K. *Antisecretory Guanidine Derivatives and Pharmaceutical Compositions Containing Them*, US4493840A, **1981**.

(454) Ran, K.; Gao, C.; Deng, H.; Lei, Q.; You, X.; Wang, N.; Shi, Y.; Liu, Z.; Wei, W.; Peng, C. Identification of Novel 2-Aminothiazole Conjugated Nitrofuran as Antitubercular and Antibacterial Agents. *Bioorganic & medicinal chemistry letters* **2016**, *26* (15), 3669–3674.

(455) Glennon, R. A.; Hong, S.-S.; Bondarev, M.; Law, H.; Dukat, M.; Rakhit, S.; Power, P.; Fan, E.; Kinneau, D.; Kamboj, R. Binding of O-Alkyl Derivatives of Serotonin at Human 5-HT1Dβ Receptors. *J. Med. Chem.* **1996**, *39* (1), 314–322.

(456) Patel, D. A.; Kumar, R.; Dwivedi, S. D. Process for Preparing (S)-Pramipexole and Its Intermediates. WO2008041240, April 10, **2008**.

(457) Griss, R.; Schneider, C.; Hurnaus, C.; Kobinger, W.; Pichler, L.; Bauer, R.; Mierau, J. Tetrahydrobenzothiazoles, their Production and Use as Intermediates and Pharmaceuticals 186087B1. Eur. Patent., July 2, **1986**.

(458) Yan-Jie, C.; Xiao-Ping, R.; Shi-Bin, S.; Jie, S.; Yan-Qing, G. Synthesis and Antibacterial Activity of Oxime Ester Derivatives from Dehydroabietic Acid. *Letters in Drug Design & Discovery* **2013**, *10* (2), 102-110.

(459) Winthrop, S.; Gavin, G. New Analeptics: 1-(Diphenylmethyl)-2-Methyl-2-Thiopseudourea Analogs. *The Journal of Organic Chemistry* **1959**, *24* (12), 1936-1939.

(460) Pockes, S.; Wifling, D.; Buschauer, A.; Elz, S. Structure-Activity Relationship of Hetarylpropylguanidines Aiming at the Development of Selective Histamine Receptor Ligands†. *ChemistryOpen* **2019**, *8* (3), 285-297.

(461) Tropmann, K.; Bresinsky, M.; Forster, L.; Mönnich, D.; Buschauer, A.; Wittmann, H.-J.; Hübner, H.; Gmeiner, P.; Pockes, S.; Strasser, A. Abolishing Dopamine D_{2long}/D_3 Receptor Affinity of Subtype-Selective Carbamoylguanidine-Type Histamine H_2 Receptor Agonists. *J. Med. Chem.* **2021**, *64* (12), 8684-8709.

(462) Supuran, C. T.; Barboiu, M.; Luca, C.; Pop, E.; Brewster, M. E.; Dinculescu, A. Carbonic Anhydrase Activators. Part 14. Syntheses of Mono and Bis Pyridinium Salt Derivatives of 2-Amino-5-(2-Aminoethyl)-and 2-Amino-5-(3-Aminopropyl)-1,3,4-Thiadiazole and Their Interaction with Isozyme II. *European journal of medicinal chemistry* **1996**, *31* (7-8), 597-606.

(463) Guénin, E.; Monteil, M.; Bouchemal, N.; Prangé, T.; Lecouvey, M. Syntheses of Phosphonic Esters of Alendronate, Pamidronate and Neridronate. *Eur. J. Org. Chem.* **2007**, *2007* (20), 3380-3391.

(464) Mizrahi, D. M.; Waner, T.; Segall, Y. α-Amino Acid Derived Bisphosphonates. Synthesis and Anti-Resorftive Activity. *Phosphorus, Sulfur, and Silicon and the Related Elements* **2001**, *173* (1), 1-25.

(465) Barbosa, G. A. D.; de Aguiar, A. P. Synthesis of 1,3,4-Thiadiazole Derivatives and Microbiological Activities: A Review. *Rev. Virtual Quim* **2019**, *11* (3), 806-848.

(466) Staudinger, H.; Meyer, J. Über Neue Organische Phosphorverbindungen III. Phosphinmethylenderivate Und Phosphinimine. *Helvetica Chimica Acta* **1919**, *2*, 635-646.

(467) Mitsunobu, O.; Yamada, M. Preparation of Esters of Carboxylic and Phosphoric Acid *via* Quaternary Phosphonium Salts. *BCSJ* **1967**, *40* (10), 2380-2382.

(468) Pak, J. K.; Hesse, M. Synthesis of Penta-N-Protected Homocaldopentamine and Its Selective Acylation. *J. Org. Chem.* **1998**, *63* (23), 8200-8204.

(469) Puodziukynaite, E.; Wang, H.-W.; Lawrence, J.; Wise, A. J.; Russell, T. P.; Barnes, M.

D.; Emrick, T. Azulene Methacrylate Polymers: Synthesis, Electronic Properties, and Solar Cell Fabrication. *J. Am. Chem. Soc.* **2014**, *136* (31), 11043-11049.

(470)   Macerata, E.; Mossini, E.; Scaravaggi, S.; Mariani, M.; Mele, A.; Panzeri, W.; Boubals, N.; Berthon, L.; Charbonnel, M.-C.; Sansone, F.; Arduini, A.; Casnati, A. Hydrophilic Clicked 2,6-Bis-Triazolyl-Pyridines Endowed with High Actinide Selectivity and Radiochemical Stability: Toward a Closed Nuclear Fuel Cycle. *J. Am. Chem. Soc.* **2016**, *138* (23), 7232-7235.

(471)   van Dongen, S. F. M.; Clerx, J.; Nørgaard, K.; Bloemberg, T. G.; Cornelissen, J. J. L. M.; Trakselis, M. A.; Nelson, S. W.; Benkovic, S. J.; Rowan, A. E.; Nolte, R. J. M. A Clamp-like Biohybrid Catalyst for DNA Oxidation. *Nat Chem* **2013**, *5* (11), 945-951.

(472)   Lee, B. W.; Lee, S. D. [5,5] Sigmatropic Shift of N-Phenyl-N′-(2-thiazolyl)hydrazines and N,N′-bis(2-Thiazolyl)hydrazines into 2-Amino-5-(p-aminophenyl)thiazoles and 5,5′-bis(2-Aminothiazole) Derivatives. *Tetrahedron Letters* **2000**, *41* (20), 3883-3886.

(473)   Zhang, S.-L.; Yu, Z.-L. C–C Activation by Retro-Aldol Reaction of Two β-Hydroxy Carbonyl Compounds: Synergy with Pd-Catalyzed Cross-Coupling To Access Mono-α-Arylated Ketones and Esters. *J. Org. Chem.* **2016**, *81* (1), 57-65.

(474)   Altman, M. D.; Andresen, B. M.; Arrington, K. L.; Childers, K. K.; Di Francesco, M. E.; Donofrio, A.; Ellis, J. M.; Fischer, C.; Guerin, D. J.; Haidle, A. M.; Kattar, S.; Knowles, S. L.; Li, C.; Lim, J.; Machacek, M. R.; Northrup, A. B.; O'Boyle, B. M.; Otte, R. D.; Petrocchi, A.; Reutershan, M. H.; Romeo, E.; Siu, T.; Taoka, B.; Trotter, W. B.; Zhou, H.; Burch, J.; Cote, B.; Dupont-Gaudet, K.; Fournier, J.-F.; Gauthier, J. Y.; Guay, D.; Robichaud, J. S.; Grimm, J.; Maddess, M. L.; Schell, A. J.; Spencer, K. B.; Woo, H. C.; Bhat, S. Aminopyrimidines as Syk Inhibitors. WO2011075515, **2011**.

(475)   Sheehan, J. C.; Yang, D.-D. H. The Use of N-Formylamino Acids in Peptide Synthesis. *Journal of the American Chemical Society* **1958**, *80* (5), 1154-1158.

(476)   Peterlin-Mašič, L.; Jurca, A.; Marinko, P.; Jančar, A.; Kikelj, D. A General Synthetic Approach to Novel Conformationally Restricted Arginine Side Chain Mimetics. *Tetrahedron* **2002**, *58* (8), 1557-1563.

(477)   Kelly, T. R.; Lebedev, R. L. Synthesis of Some Unsymmetrical Bridged Terpyridines. *J. Org. Chem.* **2002**, *67* (7), 2197-2205.

(478)   Hoggard, L. R.; Zhang, Y.; Zhang, M.; Panic, V.; Wisniewski, J. A.; Ji, H. Rational Design of Selective Small-Molecule Inhibitors for β-Catenin/B-Cell Lymphoma 9 Protein–Protein Interactions. *J. Am. Chem. Soc.* **2015**, *137* (38), 12249-12260.

(479)   Cardenal, C.; Vollrath, S. B. L.; Schepers, U.; Bräse, S. Synthesis of Functionalized Glutamine- and Asparagine-Type Peptoids : Scope and Limitations. *Helvetica chimica acta* **2012**, *95* (11), 2237-2248.

(480)   Škalamera, Đ.; Blažek Bregović, V.; Antol, I.; Bohne, C.; Basarić, N. Hydroxymethylaniline Photocages for Carboxylic Acids and Alcohols. *J. Org. Chem.* **2017**, *82* (23), 12554-12568.

(481)   Damalanka, V. C.; Kim, Y.; Alliston, K. R.; Weerawarna, P. M.; Galasiti Kankanamalage, A. C.; Lushington, G. H.; Mehzabeen, N.; Battaile, K. P.; Lovell, S.; Chang, K.-O.; Groutas, W. C. Oxadiazole-Based Cell Permeable Macrocyclic Transition State Inhibitors of Norovirus 3CL Protease. *J. Med. Chem.* **2016**, *59* (5), 1899-1913.

(482)   Bleicher, K.; Mutel, V.; Vieira, E.; Wichmann, J.; Woltering, T. J. Preparation of Carbamic Acid Derivatives and Evaluation of Their Use as Metabotropic Glutamate Receptor Ligands. WO2000063166, Chem. Abstr., October 26, **2000**.

(483)   Birnkammer, T. Highly Potent and Selective Acylguanidine-Type Histamine H_2 Receptor Agonists: Synthesis and Structure-Activity Relationships of Mono-and Bivalent Ligands. PhD Thesis, **2011**.

(484)   Lowry, O. H.; Rosebrough, N. J.; Farr, A. L.; Randall, R. J. Protein Measurement with the Folin Phenol Reagent. *Journal of Biological Chemistry* **1951**, *193* (1), 265-275.

(485)   Kirchhefer, U.; Brekle, C.; Eskandar, J.; Isensee, G.; Kučerová, D.; Müller, F. U.; Pinet, F.; Schulte, J. S.; Seidl, M. D.; Boknik, P. Cardiac Function Is Regulated by B56α-Mediated Targeting of Protein Phosphatase 2A (PP2A) to Contractile Relevant Substrates. *Journal of Biological Chemistry* **2014**, *289* (49), 33862-33873.

(486)   Gergs, U.; Neumann, J.; Simm, A.; Silber, R.-E.; Remmers, F. O.; Läer, S. Phosphorylation of Phospholamban and Troponin I through 5-HT_4 Receptors in the Isolated

Human Atrium. *Naunyn-Schmiedeberg's archives of pharmacology* **2009**, *379* (4), 349-359.

(487) Neumann, J.; Seidler, T.; Fehse, C.; Marušáková, M.; Hofmann, B.; Gergs, U. Cardiovascular Effects of Metoclopramide and Domperidone on Human 5-HT$_4$-Serotonin-Receptors in Transgenic Mice and in Human Atrial Preparations. *European Journal of Pharmacology* **2021**, *901*, 174074.

(488) Gergs, U.; Baumann, M.; Böckler, A.; Buchwalow, I. B.; Ebelt, H.; Fabritz, L.; Hauptmann, S.; Keller, N.; Kirchhof, P.; Klöckner, U. Cardiac Overexpression of the Human 5-HT$_4$ Receptor in Mice. *American Journal of Physiology-Heart and Circulatory Physiology* **2010**, *299* (3), 788-798.

(489) van der Westhuizen, E. T.; Breton, B.; Christopoulos, A.; Bouvier, M. Quantification of Ligand Bias for Clinically Relevant B2-Adrenergic Receptor Ligands: Implications for Drug Taxonomy. *Molecular pharmacology* **2014**, *85* (3), 492-509.

(490) Black, J. W.; Leff, P.; Shankley, N. P.; Wood, J. An Operational Model of Pharmacological Agonism: The Effect of E/[A] Curve Shape on Agonist Dissociation Constant Estimation. *British journal of pharmacology* **1985**, *84* (2), 561.

(491) Black, J. W.; Leff, P. Operational Models of Pharmacological Agonism. *Proceedings of the Royal society of London. Series B. Biological sciences* **1983**, *220* (1219), 141-162.

(492) Evans, B. A.; Broxton, N.; Merlin, J.; Sato, M.; Hutchinson, D. S.; Christopoulos, A.; Summers, R. J. Quantification of Functional Selectivity at the Human A1A-Adrenoceptor. *Molecular pharmacology* **2011**, *79* (2), 298-307.

(493) Marchese, A.; Docherty, J. M.; Nguyen, T.; Heiber, M.; Cheng, R.; Heng, H. H.; Tsui, L.-C.; Shi, X.; George, S. R.; O'Dowd, B. F. Cloning of Human Genes Encoding Novel G Protein-Coupled Receptors. *Genomics* **1994**, *23* (3), 609-618.

(494) Eggerickx, D.; Denef, J. F.; Labbe, O.; Hayashi, Y.; Refetoff, S.; Vassart, G.; Parmentier, M.; Libert, F. Molecular Cloning of an Orphan G-Protein-Coupled Receptor That Constitutively Activates Adenylate Cyclase. *Biochemical journal* **1995**, *309* (3), 837-843.

(495) Uhlén, M.; Fagerberg, L.; Hallström, B. M.; Lindskog, C.; Oksvold, P.; Mardinoglu, A.; Sivertsson, Å.; Kampf, C.; Sjöstedt, E.; Asplund, A.; Olsson, I.; Edlund, K.; Lundberg, E.; Navani, S.; Szigyarto, C. A.-K.; Odeberg, J.; Djureinovic, D.; Takanen, J. O.; Hober, S.; Alm, T.; Edqvist, P.-H.; Berling, H.; Tegel, H.; Mulder, J.; Rockberg, J.; Nilsson, P.; Schwenk, J. M.; Hamsten, M.; von Feilitzen, K.; Forsberg, M.; Persson, L.; Johansson, F.; Zwahlen, M.; von Heijne, G.; Nielsen, J.; Pontén, F. Proteomics. Tissue-Based Map of the Human Proteome. *Science* **2015**, *347* (6220), 1260419.

(496) Uhlenbrock, K.; Gassenhuber, H.; Kostenis, E. Sphingosine 1-Phosphate Is a Ligand of the Human Gpr3, Gpr6 and Gpr12 Family of Constitutively Active G Protein-Coupled Receptors. *Cellular signalling* **2002**, *14* (11), 941-953.

(497) Pándy-Szekeres, G.; Esguerra, M.; Hauser, A. S.; Caroli, J.; Munk, C.; Pilger, S.; Keserű, G. M.; Kooistra, A. J.; Gloriam, D. E. The G Protein Database, GproteinDb. *Nucleic acids research* **2022**, *50* (1), 518-525.

(498) Morales, P.; Isawi, I.; Reggio, P. H. Towards a Better Understanding of the Cannabinoid-Related Orphan Receptors GPR3, GPR6, and GPR12. *Drug metabolism reviews* **2018**, *50* (1), 74-93.

(499) Schihada, H.; Shekhani, R.; Schulte, G. Quantitative Assessment of Constitutive G Protein-Coupled Receptor Activity with BRET-Based G Protein Biosensors. *bioRxiv*, **2021**, 2021.02.05.429900.

(500) Martin, A. L.; Steurer, M. A.; Aronstam, R. S. Constitutive Activity among Orphan Class-A G Protein Coupled Receptors. *PloS one* **2015**, *10* (9), e0138463.

(501) Mehlmann, L. M.; Saeki, Y.; Tanaka, S.; Brennan, T. J.; Evsikov, A. V.; Pendola, F. L.; Knowles, B. B.; Eppig, J. J.; Jaffe, L. A. The Gs-Linked Receptor GPR3 Maintains Meiotic Arrest in Mammalian Oocytes. *Science* **2004**, *306* (5703), 1947-1950.

(502) Hinckley, M.; Vaccari, S.; Horner, K.; Chen, R.; Conti, M. The G-Protein-Coupled Receptors GPR3 and GPR12 Are Involved in CAMP Signaling and Maintenance of Meiotic Arrest in Rodent Oocytes. *Developmental biology* **2005**, *287* (2), 249-261.

(503) Johansen, O. S.; Ma, T.; Hansen, J. B.; Markussen, L. K.; Schreiber, R.; Reverte-Salisa, L.; Dong, H.; Christensen, D. P.; Sun, W.; Gnad, T. Lipolysis Drives Expression of the Constitutively Active Receptor GPR3 to Induce Adipose Thermogenesis. *Cell* **2021**, *184* (13),

3502-3518. e33.

(504)   Tanaka, S.; Miyagi, T.; Dohi, E.; Seki, T.; Hide, I.; Sotomaru, Y.; Saeki, Y.; Chiocca, E. A.; Matsumoto, M.; Sakai, N. Developmental Expression of GPR3 in Rodent Cerebellar Granule Neurons Is Associated with Cell Survival and Protects Neurons from Various Apoptotic Stimuli. *Neurobiology of disease* **2014**, *68*, 215-227.

(505)   Masuda, S.; Tanaka, S.; Shiraki, H.; Sotomaru, Y.; Harada, K.; Hide, I.; Kiuchi, Y.; Sakai, N. GPR3 Expression in Retinal Ganglion Cells Contributes to Neuron Survival and Accelerates Axonal Regeneration after Optic Nerve Crush in Mice. *Neurobiology of Disease* **2022**, *172*, 105811.

(506)   Tanaka, S.; Ishii, K.; Kasai, K.; Yoon, S. O.; Saeki, Y. Neural Expression of G Protein-Coupled Receptors GPR3, GPR6, and GPR12 up-Regulates Cyclic AMP Levels and Promotes Neurite Outgrowth. *Journal of Biological Chemistry* **2007**, *282* (14), 10506-10515.

(507)   Tanaka, S.; Shimada, N.; Shiraki, H.; Miyagi, T.; Harada, K.; Hide, I.; Sakai, N. GPR3 Accelerates Neurite Outgrowth and Neuronal Polarity Formation via PI3 Kinase-Mediating Signaling Pathway in Cultured Primary Neurons. *Molecular and Cellular Neuroscience* **2022**, *118*, 103691.

(508)   Thathiah, A.; Spittaels, K.; Hoffmann, M.; Staes, M.; Cohen, A.; Horré, K.; Vanbrabant, M.; Coun, F.; Baekelandt, V.; Delacourte, A.; Fischer, D. F.; Pollet, D.; De Strooper, B.; Merchiers, P. The Orphan G Protein-Coupled Receptor 3 Modulates Amyloid-Beta Peptide Generation in Neurons. *Science*, **2009**, *323*, 946-951.

(509)   Thathiah, A.; Horre, K.; Snellinx, A.; Vandewyer, E.; Huang, Y.; Ciesielska, M.; De Kloe, G.; Munck, S.; De Strooper, B. β-Arrestin 2 Regulates Aβ Generation and γ-Secretase Activity in Alzheimer's Disease. *Nature medicine* **2013**, *19* (1), 43–49.

(510)   Nelson, C. D.; Sheng, M. Gpr3 Stimulates Aβ Production via Interactions with APP and β-Arrestin2. *PLoS One* **2013**, *8* (9), e74680.

(511)   Yin, H.; Chu, A.; Li, W.; Wang, B.; Shelton, F.; Otero, F.; Nguyen, D. G.; Caldwell, J. S.; Chen, Y. A. Lipid G Protein-Coupled Receptor Ligand Identification Using β-Arrestin PathHunter^{TM} Assay. *Journal of Biological Chemistry* **2009**, *284* (18), 12328–12338.

(512)   Ye, C.; Zhang, Z.; Wang, Z.; Hua, Q.; Zhang, R.; Xie, X. Identification of a Novel Small-Molecule Agonist for Human G Protein–Coupled Receptor 3. *Journal of Pharmacology and Experimental Therapeutics* **2014**, *349* (3), 437–443.

(513)   Laun, A. S.; Song, Z.-H. GPR3 and GPR6, Novel Molecular Targets for Cannabidiol. *Biochemical and biophysical research communications* **2017**, *490* (1), 17–21.

(514)   Laun, A. S.; Shrader, S. H.; Song, Z.-H. Novel Inverse Agonists for the Orphan G Protein-Coupled Receptor 6. *Heliyon* **2018**, *4* (11), e00933.

(515)   Wu, J.; Chen, N.; Liu, Y.; Godlewski, G.; Kaplan, H. J.; Shrader, S. H.; Song, Z.-H.; Shao, H. Studies of Involvement of G-Protein Coupled Receptor-3 in Cannabidiol Effects on Inflammatory Responses of Mouse Primary Astrocytes and Microglia. *Plos one* **2021**, *16* (5), e0251677.

(516)   Jensen, T.; Elster, L.; Nielsen, S. M.; Poda, S. B.; Loechel, F.; Volbracht, C.; Klewe, I. V.; David, L.; Watson, S. P. The Identification of GPR3 Inverse Agonist AF64394; the First Small Molecule Inhibitor of GPR3 Receptor Function. *Bioorganic & medicinal chemistry letters* **2014**, *24* (22), 5195-5198.

(517)   Ayukawa, K.; Suzuki, C.; Ogasawara, H.; Kinoshita, T.; Furuno, M.; Suzuki, G. Development of a High-Throughput Screening-Compatible Assay for Discovery of GPR3 Inverse Agonists Using a CAMP Biosensor. *SLAS DISCOVERY: Advancing the Science of Drug Discovery* **2020**, *25* (3), 287-298.

(518)   Schihada, H.; Vandenabeele, S.; Zabel, U.; Frank, M.; Lohse, M. J.; Maiellaro, I. A Universal Bioluminescence Resonance Energy Transfer Sensor Design Enables High-Sensitivity Screening of GPCR Activation Dynamics. *Communications biology* **2018**, *1* (1), 1-8.

(519)   Schihada, H.; Ma, X.; Zabel, U.; Vischer, H. F.; Schulte, G.; Leurs, R.; Pockes, S.; Lohse, M. J. Development of a Conformational Histamine H$_3$ Receptor Biosensor for the Synchronous Screening of Agonists and Inverse Agonists. *ACS sensors* **2020**, *5* (6), 1734-1742.

(520)   Schihada, H.; Kowalski-Jahn, M.; Turku, A.; Schulte, G. Deconvolution of WNT-Induced

Frizzled Conformational Dynamics with Fluorescent Biosensors. *Biosensors and Bioelectronics* **2021**, *177*, 112948.

(521) Picard, L.-P.; Schönegge, A. M.; Lohse, M. J.; Bouvier, M. Bioluminescence Resonance Energy Transfer-Based Biosensors Allow Monitoring of Ligand-and Transducer-Mediated GPCR Conformational Changes. *Communications biology* **2018**, *1* (1), 1-7.

(522) Kowalski-Jahn, M.; Schihada, H.; Turku, A.; Huber, T.; Sakmar, T. P.; Schulte, G. Frizzled BRET Sensors Based on Bioorthogonal Labeling of Unnatural Amino Acids Reveal WNT-Induced Dynamics of the Cysteine-Rich Domain. *Science advances* **2021**, *7* (46), eabj7917.

(523) Stoddart, L. A.; White, C. W.; Nguyen, K.; Hill, S. J.; Pfleger, K. D. G. Fluorescence- and Bioluminescence-Based Approaches to Study GPCR Ligand Binding: Fluorescence and Bioluminescence in Ligand Binding. *British Journal of Pharmacology* **2016**, *173* (20), 3028-3037.

(524) Stoddart, L. A.; Johnstone, E. K. M.; Wheal, A. J.; Goulding, J.; Robers, M. B.; Machleidt, T.; Wood, K. V.; Hill, S. J.; Pfleger, K. D. G. Application of BRET to Monitor Ligand Binding to GPCRs. *Nature Methods* **2015**, *12* (7), 661-663.

(525) Rinken, A.; Veiksina, S.; Kopanchuk, S. Dynamics of Ligand Binding to GPCR: Residence Time of Melanocortins and Its Modulation. *Pharmacological Research* **2016**, *113*, 747-753.

(526) Tahk, M.-J.; Torp, J.; Ali, M. A.; Fishman, D.; Parts, L.; Grätz, L.; Müller, C.; Keller, M.; Veiksina, S.; Laasfeld, T. Live-Cell Microscopy or Fluorescence Anisotropy with Budded Baculoviruses—Which Way to Go with Measuring Ligand Binding to M4 Muscarinic Receptors? *Open Biology* **2022**, *12* (6), 220019.

(527) Toy, L.; Huber, M. E.; Schmidt, M. F.; Weikert, D.; Schiedel, M. Fluorescent Ligands Targeting the Intracellular Allosteric Binding Site of the Chemokine Receptor CCR2. *ACS Chemical Biology* **2022**, *17* (8), 2142-2152.

(528) Soave, M.; Briddon, S. J.; Hill, S. J.; Stoddart, L. A. Fluorescent Ligands: Bringing Light to Emerging GPCR Paradigms. *British Journal of Pharmacology* **2020**, *177* (5), 978-991.

(529) Wesslowski, J.; Kozielewicz, P.; Wang, X.; Cui, H.; Schihada, H.; Kranz, D.; Levkin, P.; Gross, J. C.; Boutros, M.; Schulte, G. EGFP-Tagged Wnt-3a Enables Functional Analysis of Wnt Trafficking and Signaling and Kinetic Assessment of Wnt Binding to Full-Length Frizzled. *Journal of Biological Chemistry* **2020**, *295* (26), 8759-8774.

(530) White, C. W.; Johnstone, E. K.; See, H. B.; Pfleger, K. D. NanoBRET Ligand Binding at a GPCR under Endogenous Promotion Facilitated by CRISPR/Cas9 Genome Editing. *Cellular signalling* **2019**, *54*, 27-34.

(531) Mocking, T. A.; Verweij, E. W.; Vischer, H. F.; Leurs, R. Homogeneous, Real-Time NanoBRET Binding Assays for the Histamine H_3 and H_4 Receptors on Living Cells. *Molecular pharmacology* **2018**, *94* (6), 1371-1381.

(532) Hoare, B. L.; Bruell, S.; Sethi, A.; Gooley, P. R.; Lew, M. J.; Hossain, M. A.; Inoue, A.; Scott, D. J.; Bathgate, R. A. Multi-Component Mechanism of H_2 Relaxin Binding to RXFP1 through NanoBRET Kinetic Analysis. *iScience* **2019**, *11*, 93–113.

(533) Alcobia, D. C.; Ziegler, A. I.; Kondrashov, A.; Comeo, E.; Mistry, S.; Kellam, B.; Chang, A.; Woolard, J.; Hill, S. J.; Sloan, E. K. Visualizing Ligand Binding to a GPCR In Vivo Using NanoBRET. *iScience* **2018**, *6*, 280-288.

(534) Bouzo-Lorenzo, M.; Stoddart, L. A.; Xia, L.; IJzerman, A. P.; Heitman, L. H.; Briddon, S. J.; Hill, S. J. A Live Cell NanoBRET Binding Assay Allows the Study of Ligand-Binding Kinetics to the Adenosine A3 Receptor. *Purinergic Signalling* **2019**, *15* (2), 139-153.

(535) Christiansen, E.; Hudson, B. D.; Hansen, A. H.; Milligan, G.; Ulven, T. Development and Characterization of a Potent Free Fatty Acid Receptor 1 (FFA1) Fluorescent Tracer. *J. Med. Chem.* **2016**, *59* (10), 4849-4858.

(536) Rosier, N.; Grätz, L.; Schihada, H.; Möller, J.; Işbilir, A.; Humphrys, L. J.; Nagl, M.; Seibel, U.; Lohse, M. J.; Pockes, S. A Versatile Sub-Nanomolar Fluorescent Ligand Enables NanoBRET Binding Studies and Single-Molecule Microscopy at the Histamine H_3 Receptor. *J. Med. Chem.* **2021**, *64* (15), 11695-11708.

(537) Grätz, L.; Tropmann, K.; Bresinsky, M.; Müller, C.; Bernhardt, G.; Pockes, S. NanoBRET Binding Assay for Histamine H_2 Receptor Ligands Using Live Recombinant

HEK293T Cells. *Scientific reports* **2020**, *10* (1), 1-10.

(538) Bharathi; Roy, K. K. Structural Basis for the Binding of a Selective Inverse Agonist AF64394 with the Human G-Protein Coupled Receptor 3 (GPR3). *J Biomol Struct Dyn* **2021**, *4* (20), 10181-10190.

(539) Kshirsagar, T.; Nakano, A. H.; Law, P.-Y.; Elde, R.; Portoghese, P. S. NTI4F: A Non-Peptide Fluorescent Probe Selective for Functional Delta Opioid Receptors. *Neuroscience Letters* **1998**, *249* (2–3), 83-86.

(540) Boettcher, A.; Buschmann, N.; Furet, P.; Groell, J.-M.; Kallen, J.; Lisztwan, J. H.; Masuya, K.; Mayr, L.; Vaupel, A. *3-Imidazolyl-Indoles for the Treatment of Proliferative Diseases*; WO2008119741A2, **2008**.

(541) Glazier, A.; Yanachkova, M.; Yanachkov, I. *Acyclovir Diester Derivatives*; US6031096A, **2000**.

(542) Capaldi, S.; Suku, E.; Antolini, M.; Di Giacobbe, M.; Giorgetti, A.; Buffelli, M. Allosteric Sodium Binding Cavity in GPR3: A Novel Player in Modulation of Aβ Production. *Scientific Reports* **2018**, *8* (1), 11102.

(543) Hedderich, J. B.; Persechino, M.; Becker, K.; Heydenreich, F. M.; Gutermuth, T.; Bouvier, M.; Bünemann, M.; Kolb, P. The Pocketome of G-Protein-Coupled Receptors Reveals Previously Untargeted Allosteric Sites. *Nature Communications* **2022**, *13* (1), 2567.

(544) Mousli, Y.; Rouvière, L.; Traboulsi, I.; Hunel, J.; Buffeteau, T.; Heuzé, K.; Vellutini, L.; Genin, E. Hydrosilylation of Azide-Containing Olefins as a Convenient Access to Azidoorganotrialkoxysilanes for Self-Assembled Monolayer Elaboration onto Silica by Spin Coating. *ChemistrySelect* **2018**, *3* (25), 7333-7339.

(545) Kim, J.; Morozumi, T.; Kurumatani, N.; Nakamura, H. Novel Chemosensor for Alkaline Earth Metal Ion Based on 9-Anthryl Aromatic Amide Using a Naphthalene as a TICT Control Site and Intramolecular Energy Transfer Donor. *Tetrahedron Letters* **2008**, *49* (12), 1984-1987.

(546) Kalyanaraman, B.; Chitambar, C. Synergistic Inhibition of Tumor Cell Proliferation Induced by Combined Treatment of Metformin Compounds and Iron Chelators. WO2018119207A1, **2018**.

(547) Kim, J. K.; Park, S.; Yoo, R. J.; Jeong, H. J.; Oh, J.; Lee, Y. J.; Park, S.; Kim, D. W. Thin PEGylated Carbon Nitrides: Water-Dispersible Organic Nanodots as Bioimaging Probes. *Chemistry–A European Journal* **2018**, *24* (14), 3506-3511.

(548) Ji, A.; Marvin, M.; Marks, K.; Anderson, D. Oligonucleotide Synthesis on Solid Support. WO2021173615A1, **2021**.

(549) Ding, C.; Liu, Y.; Wang, T.; Fu, J. Triple-Stimuli-Responsive Nanocontainers Assembled by Water-Soluble Pillar [5] Arene-Based Pseudorotaxanes for Controlled Release. *Journal of Materials Chemistry B* **2016**, *4* (16), 2819-2827.

(550) Jensen, T.; Elster, L.; Nielsen, S. M.; Poda, S. B.; Loechel, F.; Volbracht, C.; Klewe, I. V.; David, L.; Watson, S. P. The Identification of GPR3 Inverse Agonist AF64394; The First Small Molecule Inhibitor of GPR3 Receptor Function. *Bioorganic and Medicinal Chemistry Letters* **2014**, *24* (22), 5195-5198.

(551) Wu, F.; Bai, R.; Gu, Y. Synthesis of Benzofurans from Ketones and 1, 4-Benzoquinones. *Advanced Synthesis & Catalysis* **2016**, *358* (14), 2307-2316.

(552) Nagasawa, S.; Fujiki, S.; Sasano, Y.; Iwabuchi, Y. Chromium–Salen Complex/Nitroxyl Radical Cooperative Catalysis: A Combination for Aerobic Intramolecular Dearomative Coupling of Phenols. *The Journal of Organic Chemistry* **2021**, *86* (9), 6952-6968.

(553) El Bakali, J.; Klupsch, F.; Guédin, A.; Brassart, B.; Fontaine, G.; Farce, A.; Roussel, P.; Houssin, R.; Bernier, J.-L.; Chavatte, P. 2, 6-Diphenylthiazolo [3,2-*b*][1,2,4] Triazoles as Telomeric G-Quadruplex Stabilizers. *Bioorganic & medicinal chemistry letters* **2009**, *19* (13), 3434-3438.

(554) Charlton, J. L.; Lypka, G.; Sayeed, V. The Synthesis of 2-methylchromone-3-carboxylic Acid. *Journal of Heterocyclic Chemistry* **1980**, *17* (3), 593-594.

(555) Ahn, J. H.; Shin, M. S.; Jung, S. H.; Kim, J. A.; Kim, H. M.; Kim, S. H.; Kang, S. K.; Kim, K. R.; Dal Rhee, S.; Park, S. D. Synthesis and Structure–Activity Relationship of Novel Indene N-Oxide Derivatives as Potent Peroxisome Proliferator Activated Receptor γ (PPARγ) Agonists. *Bioorganic & medicinal chemistry letters* **2007**, *17* (18), 5239-5244.

(556) Jiang, Y.; Chen, X.; Zheng, Y.; Xue, Z.; Shu, C.; Yuan, W.; Zhang, X. Highly

Diasteroselective and Enantioselective Synthesis of A-Hydroxy B-Amino Acid Derivatives: Lewis Base Catalyzed Hydrosilylation of A-Acetoxy B-Enamino Esters. *Angewandte Chemie* **2011**, *123* (32), 7442-7445.

(557)   Isberg, V.; De Graaf, C.; Bortolato, A.; Cherezov, V.; Katritch, V.; Marshall, F. H.; Mordalski, S.; Pin, J.-P.; Stevens, R. C.; Vriend, G. Generic GPCR Residue Numbers–Aligning Topology Maps While Minding the Gaps. *Trends in pharmacological sciences* **2015**, *36* (1), 22-31.

(558)   Webb, B.; Sali, A. Comparative Protein Structure Modeling Using MODELLER. *Current protocols in bioinformatics* **2016**, *54* (1), 5.6. 1-5.6. 37.

(559)   Pettersen, E. F.; Goddard, T. D.; Huang, C. C.; Couch, G. S.; Greenblatt, D. M.; Meng, E. C.; Ferrin, T. E. UCSF Chimera—a Visualization System for Exploratory Research and Analysis. *Journal of computational chemistry* **2004**, *25* (13), 1605-1612.

(560)   Coleman, R. G.; Carchia, M.; Sterling, T.; Irwin, J. J.; Shoichet, B. K. Ligand Pose and Orientational Sampling in Molecular Docking. *PloS one* **2013**, *8* (10), e75992.

(561)   Halgren, T. A. Merck Molecular Force Field. I. Basis, Form, Scope, Parameterization, and Performance of MMFF94. *Journal of computational chemistry* **1996**, *17* (5-6), 490-519.

(562)   Ccgi, M. Molecular Operating Environment (MOE), 2013.08. *Chemical Computing Group Inc., Montreal* **2016**.

Ich erkläre hiermit an Eides statt, dass ich die vorliegende Arbeit ohne unzulässige Hilfe Dritter und ohne Benutzung anderer als der angegebenen Hilfsmittel angefertigt habe; die aus Quellen direkt oder indirekt übernommenen Daten und Konzepte sind unter Angabe des Literaturzitats gekennzeichnet.

Weitere Personen waren an der inhaltlich-materiellen Herstellung der vorliegenden Arbeit nicht beteiligt. Insbesondere habe ich hierfür nicht die entgeltliche Hilfe eines Promotionsberaters oder anderer Personen in Anspruch genommen. Niemand hat von mir weder unmittelbar noch mittelbar geldwerte Leistungen für Arbeiten erhalten, die im Zusammenhang mit dem Inhalt der vorgelegten Dissertation stehen.

Die Arbeit wurde bisher weder im In- noch im Ausland in gleicher oder ähnlicher Form einer anderen Prüfungsbehörde vorgelegt.

Regensburg, den   _____

                                                                              Merlin Niklas Bresinsky